Calendar of forthcoming meetings

12–16 October 2008
San Diego, CA, USA
Microtas 2008: 12th International Conference on Miniaturized Systems for Chemistry and Life Sciences. URL: www.microtas2008.org

16–17 October 2008
Lisbon, Portugal
European Biomarkers Summit 2008. URL: https://selectbiosciences.com/conferences/EBS2008

16–17 October 2008
Lisbon, Portugal
Proteomics Europe 2008. URL: https://selectbiosciences.com/conferences/PE2008

16–17 October 2008
Lisbon, Portugal
Advances in Metabolic Profiling. URL: https://selectbiosciences.com/conferences/AMP2008

2–5 November 2008
Kaohsiung, Taiwan
APCE 2008: 8th Asia-Pacific International Symposium on Micro-scale Separations and Analysis. URL: http://www.tl.ntu.edu.tw/apce2008

2–5 December 2008
Kyoto, Japan
HPLC2008 Kyoto: 33rd International Symposium on High Performance Liquid Phase Separations and Related Techniques. URL: http://anchem.mc.kyotou.ac.jp/HPLC2008Kyoto/

26–30 January 2009
Amsterdam, The Netherlands
SCM-4: 4th International Symposium on the Separation and Characterization of Natural and Synthetic Macromolecules. Contact: scm@ordibo.be; URL: http://www.ordibo.be/scm

1–4 March 2009
Agra, India
PBA2009 India: 20th International Symposium on Pharmaceutical and Biomedical Analysis. E-mail: pba2009@gmail.com

1–3 April 2009
Rome, Italy
3rd International IUPAC Symposium on Trace Elements in Food. URL: http://www.tef3-2009.it

11–15 May 2009
Frankfurt am Main, Germany
Achema 2009: 29th International Exhibition-Congress on Chemical Engineering, Environmental Protection and Biotechnology. URL: http://www.achema.de

21–25 June 2009
Denver, CO, USA
Transducers 2009: 15th International Conference on Solid-State Sensors, Actuators and Microsystems. URL: www.transducers09.org

6–10 September 2009
Innsbruck, Austria
Euroanalysis 2009. Contact: Euroanalysis 2009 Symposium Office, PCO Tyrol Congress, c/o Ina Kaehler, Rennweg 3, 6020 Innsbruck, Austria. Tel. (+43-512) 575-600; Fax: (+43-512) 575-607; E-mail: euroanalysis09@come-innsbruck.at; URL: www.euroanalysis2009.at

9–12 September 2009
Milan, Italy
RDPA 2009: 13th International Meeting on Recent Developments in Pharmaceutical Analysis. URL: www.rdpa2009.com

14–18 September 2009
Toronto, ON, Canada
SIMS XVII: 17th International Conference on Secondary Ion Mass Spectrometry. E-mail: email@simsxvii.org; URL: www.simsxvii.org/

11–14 October 2009
Orlando, FL, USA
PBA 2009: 21st International Symposium on Pharmaceutical and Biomedical Analysis

26–28 May 2010
Glasgow, UK
Biosensors 2010: The Eleventh World Congress on Biosensors.

20–23 September 2010
Antwerp, Belgium
Drug Analysis. URL: www.druganalysis.org

doi:10.1016/S0039-9140(08)00749-2

Talanta

The International Journal of Pure and Applied Analytical Chemistry

Publication information: *Talanta* (ISSN 0039-9140). For 2008, volumes 74–76 (15 issues) are scheduled for publication. Subscription prices are available upon request from the Publisher or from the Regional Sales Office nearest you or from this journal's website (http://www.elsevier.com/locate/talanta). Further information is available on this journal and other Elsevier products through Elsevier's website: (http://www.elsevier.com). Subscriptions are accepted on a prepaid basis only and are entered on a calendar year basis. Issues are sent by standard mail (surface within Europe, air delivery outside Europe). Priority rates are available upon request. Claims for missing issues should be made within six months of the date of dispatch.

Orders, claims, and journal enquiries: please contact the Regional Sales Office nearest you:
Orlando: Elsevier, Customer Service Department, 6277 Sea Harbor Drive, Orlando, FL 32887-4800, USA; phone: (877) 8397126 [toll free within the USA]; (+1) (407) 5636022 [outside the USA]; fax: (+1) (407) 3631354; e-mail: JournalCustomerService-usa@elsevier.com
Amsterdam: Elsevier, Customer Service Department, PO Box 211, 1000 AE Amsterdam, The Netherlands; phone: (+31) (20) 4853757; fax: (+31) (20) 4853432; e-mail: JournalsCustomerServiceEMEA@elsevier.com
Tokyo: Elsevier, Customer Service Department, 4F Higashi-Azabu, 1-Chome Bldg, 1-9-15 Higashi-Azabu, Minato-ku, Tokyo 106-0044, Japan; phone: (+81) (3) 5561 5037; fax: (+81) (3) 5561 5047; e-mail: JournalsCustomerServiceJapan@elsevier.com
Singapore: Elsevier, Customer Service Department, 3 Killiney Road, #08-01 Winsland House I, Singapore 239519; phone: (+65) 63490222; fax: (+65) 67331510; e-mail: JournalsCustomerServiceAPAC@elsevier.com

USA mailing notice: *Talanta* (ISSN 0039-9140) is published monthly by Elsevier B.V. (Radarweg 29, 1043 NX Amsterdam, the Netherlands). Periodical postage paid at Rahway NJ and additional mailing offices.
USA POSTMASTER: Send change of address: Talanta, Elsevier, 6277 Sea Harbor Drive, Orlando, FL 32887-4800.
AIRFREIGHT AND MAILING in USA by Mercury International Limited, 365, Blair Road, Avenel, NJ 07001. .

Talanta 77 (2008) 863–869

Contents lists available at ScienceDirect

Talanta

journal homepage: www.elsevier.com/locate/talanta

Comparison of oil spillages using mid-IR indexes and 3-way procrustes rotation, matrix-augmented principal components analysis and parallel factor analysis

J.M. Andrade*, P. Fresco, S. Muniategui, D. Prada

Department of Analytical Chemistry, University of A Coruña, Campus da Zapateira s/n E-15071 A Coruña, Spain

ARTICLE INFO

Article history:
Received 2 May 2008
Received in revised form 15 July 2008
Accepted 22 July 2008
Available online 31 July 2008

Keywords:
Oil spillage
Prestige fuel oil
ATR-mid-IR
Procrustes rotation
Matrix-augmented principal component analysis
Parallel factor analysis

ABSTRACT

Three different approaches for 3-way analyses, namely, Procrustes rotation, parallel factor analysis (PARAFAC) and matrix-augmented principal component analysis (MA-PCA), have been used to compare six different oil spillages made under controlled conditions (one of them corresponding to the heavy oil released after the sunk of the Prestige tanker off the Galician coast–NW Spain on November 2002). Each spillage was monitored during three and a half months by attenuated total reflectance (ATR) mid-IR spectroscopy. Ten characteristic band ratios were defined. Results showed that the three 3-way chemometric techniques lead to essentially the same conclusions, where from it was concluded that the most relevant pattern defining the oil weathering was related to 'total aromaticity', i.e., the total number of C=C bonds in the molecules which form the products. In addition, weathering of the samples got clearly characterized by a steady evolution on the scores (sample weights), with a clear increase after 11–14 days. Differentiation of the products (slices of the data cube) was also possible due to their intrinsic characteristics as, in general, heavy products oppose to the lightest ones.

1. Introduction

Hydrocarbon discharges and spillages to the oceans are worldwide and ubiquitous albeit not always well perceived by most citizens. Nevertheless, huge spillages from shipwrecks like those of the Erika (S. France, 1999) and Prestige (NW Spain, November 2002) fuel tankers, releasing ca. 75,000 tons in total of heavy and long-persistant fuel oils, mobilised tenths of thousands of volunteers to help the affected coastal environments and, of most importance, to push politicians to put new rules into force. Interestingly, only around 45.5% of the overall (approximately) 5,648,000 tons of hydrocarbons released annualy to the marine environment originate in big ship wrecks, being the remaining 54.5% related to industrial activities, urban run-off and diffuse airborne hydrocarbon sources [1,2].

It is therefore important to develop strategies to identify the fate of the hydrocarbons into the aquatic environment. This involves two main critical objectives, namely, to identify the source of the oil lumps (i.e. the type of hydrocarbon and, hopefully, its origin) and to predict how the hydrocarbons would evolve [3].

Intimately intertwined to environmental monitoring is the data treatment issue. After the last two major European pollution events (Erika and Prestige carriers) many administration agencies set monitoring programs with sampling seasons extended over time. This raises two interesting issues on, first, how to treat such data and, second, whether different products can be differentiated once they suffered natural weathering. Today powerful chemometric tools are available to handle these so-called N-way data sets, many of them extensively described and exemplified in the classical text from Smilde et al. [4].

These methods, despite being conceptually complex, represent a potential solution to many environmental studies carried out nowadays and are steadily applied in practical situations. Here, we do not aim to make a broad review but several studies can be mentioned just to show how different environmental problems were addressed. PARAFAC (parallel factor analysis), MA-PCA (matrix-augmented PCA) and factor analysis were used to elucidate pollution patterns in rivers with different anthropogenic inputs [5]; residues of oil spills in soils were differentiated by PARAFAC [3]; pollution sources on the lagoon of Venice were searched for [6]; and changes on water physico-chemical parameters organized in 4-way data sets were studied by PARAFAC and Tucker 3 [7]. Two recent studies reported PARAFAC studies made on spilled oils. One considered 17 diesel oil samples weathered during only 15 days and where from 3 samples were withdrawn with the aim of studying whether GC–MS data could classify the diesel oils [8]. This study reported also an strategy to select relevant variables to classify the samples. The other, analyzed a set of groundwater samples taken in the

* Corresponding author. Fax: +34 981 167065.
E-mail address: andrade@udc.es (J.M. Andrade).

0039-9140/$ – see front matter © 2008 Elsevier B.V. All rights reserved.
doi:10.1016/j.talanta.2008.07.044

subsurface of a petroleum refinery to identify main elution profiles (gel permeating chromatography) and their relevant, dominant spectra (UV–vis detection) [3].

Regarding the analytical techniques to monitor hydrocarbon weathering, a wealth of possibilities exist. Nevertheless, two quite different techniques outstand: chromatography and IR spectrometry, each with its pros and cons. The most critical advantages of IR spectrometry are speedness and user-friendship, and availability of portable field devices. On the contrary, particularly relevant species (e.g. cancerigenous or mutagenic hydrocarbon compounds) cannot be monitored easily. Nevertheless, IR yields an overall weathering picture that accounts for the general evolution of the spillages and, many times, this is enough for decision-making and preliminary scientific studies.

A set of IR band ratios (indexes) were applied to classify road paving bitumens and to evaluate reservoirs continuities and geochemical evolution of oils from individual reservoirs [9,10]. The wavenumbers yielding the quotients were intended to visualize as remarkably as possible how samples evolved on time. Briefly, they were: carbonyl index (A_{1700}/A_{tot}), sulphoxide index (A_{1030}/A_{tot}), aromaticity index (as a measure of the total amount of C=C bonds, A_{1600}/A_{tot}), aliphatic index ($A_{1450+1376}/A_{tot}$), aromatic condensation index ($A_{864+814+743}/A_{tot}$), branched chains index ($A_{1376}/A_{1450+1376}$), long chains index ($A_{724}/A_{1450+1376}$), substitution 1 (as a measure of the number of isolated CH groups in multisubstituted rings, $A_{864}/A_{864+814+743}$), substitution 2 (as a measure of the number of 2 or 3 adjacent CH groups in substituted rings, a good indication of three-substituted aromatic rings, $A_{814}/A_{864+814+743}$), and substitution 3 (as a measure of the number of 3 or 4 adjacent CH groups in substituted rings, a good indication of di- and mono-substituted rings, $A_{743}/A_{864+814+743}$). These indexes have been used in a previous paper [11] to monitor the weathering process of several commercial crude oils and fuels and to compare them to a set of samples taken on Galician beaches. There, one of the major difficulties was to organize and coordinate the many different conclusions drawn from each univariate study.

Therefore, the aim of the present paper is to determine whether 3-way data analysis techniques can aid in the simultaneous study of a set of different spilled hydrocarbons and derive final conclusions that summarize the main findings and put forward common (different) weathering patterns. Major differences with other previous related studies are that a set of typical petroleum-related hydrocarbons is weathered simultaneously under controlled spilled conditions and monitored up to almost 4 months, and that three 3-way techniques are employed to draw conclusions.

2. Background

2.1. 3-way Procrustes rotation

The so-called Procrustes rotation (PR) uses singular value decomposition (svd) to decompose a matrix into its principal components, briefly, $X_{(nxp)} = A_{(nxk)} \times B_{(kxk)} \times L'_{(kxp)} + E_{(nxp)}$, where the scores matrix is $S = A \times B$. Since PR has not been applied as widely as PARAFAC or MA-PCA, some basic fundamentals are given just to show how two subspaces can be compared. As for the other techniques summarized here, only conceptual details are given. Interested readers are encouraged to consult more specialized works (e.g., [12–14]).

PR aims to compare two or more spaces where the same variables are measured. For convenience, principal components scores subspaces are compared in order to (i) avoid unstructured and random variation that may hide the general patterns, (ii) reduce data dimensionality and (iii) because the main patterns within the datasets can be compared directly. Only the most important PCs have to be employed in a PR comparison and their number can be determined by several statistical tests (e.g., [15–17]). An important advantage over PARAFAC and MA-PCA (explained below) is that Procrustes rotation do not require the same number of samples on each subspace to be compared. This is important because it is not uncommon that a sample is missed in some sampling campaign along an environmental study extended on time.

Having determined the number of significant PCs for each sampling campaign (without lack of generality, they should be the same), say k, the k-reduced scores matrices representing each campaign can be compared by Procrustes rotation. To explain the technique, let us say that one of the data sets, X, is fixed and therefore, we want to 'move' the other data set, Y, to match X. Geometrically this is done by translating, rotating, and then stretching/shrinking it such that the sum of squared distances, M^2, between the elements of Y and the corresponding elements of X is minimized. The smaller the value of M^2 the more similar are the two configurations. A perfect match gives M^2 of zero. The first step, translation, is obtained by mean-centering X and Y. For rotation and stretching, a singular value decomposition has to be done for the product X^TY, which yields UDV^T. Rotation is then performed with the matrix product VU^T. The discrepancy between X and Y can be evaluated by different means but a good option is to calculate $M^2 = \text{trace}(XX^T + YY^T - 2D)$. Matrices U and V can be, accordingly, considered like 'consensus' scores and loadings, which describe the common patterns of the two original spaces under comparison.

Generalized Procrustes rotation (which should be applied to compare more than two subspaces) works in the same way. It compares m scores subspaces ($m = 1,\ldots, m$) by calculating a new set of factors or consensus vectors, v, that resemble all scores subspaces. Their dimension is $(1 \times p)$, since they are defined in the original p-dimensional data space. A first consensus vector, v_1, is defined so that is close to the first principal component of all M subspaces. Since a reasonable way to define "closeness" is by the cosine of the angle between the consensus vector and the other principal component, $\sum_{m=1}^{M} \cos^2 \alpha_{k,m}$ is maximized for each k (principal component). It was demonstrated [12] that the eigenvector v_1 corresponding to the largest eigenvalue of $W = \sum_{m=1}^{M} L'_m L_m$ fulfills those conditions. L_m being the $(k \times p)$ loadings matrix for data set m. Vector v_1 can be thought of as an average factor of all m first principal component scores. The deviation of this average factor from the first PC of a given set m is given by the angle $\alpha_{1,m} = \cos^{-1}((v'_1 L'_m L_m v_1)^{1/2})$. Analogously, v_2 is the consensus vector that corresponds to the second-largest eigenvalue of W. v_1 and v_2 are orthogonal, which may simplify the chemical interpretation of the consensus vector. $\alpha_{2,m}$ is a measure of the difference of the second consensus vector from the 2nd PC of set m. The process continues until k consensus vectors are obtained.

Although not specifically developed for 3-way analysis it is interesting to compare its results with other more well-established 3-way techniques. In addition, it was demonstrated recently that sample patterns can be visualized using the consensus vectors since 'consensus scores' can be derived for each original space ('slice' or sampling season) as $C = XV$ and, visualized as a 'consensus scatterplot'. Other useful plots can be set as well [18]. A natural way to organize and resume such wealth of information is to take averages, in the same way MA-PCA does (see next section). Hence, for each consensus vector, 'temporally averaged product behaviors' and 'product-averaged temporal consensus scores' can be derived.

2.2. Matrix-augmented principal component analysis

Matrix-augmented PCA (MA-PCA) constitutes a straightforward extention of traditional PCA [19] by which the 3-way data

set (samples on time–'rows'- × mid-IR indexes –'columns'- × products–'tubes or slices') is reordered into an extended matrix. This is called 'unfolding' of the slices. In our case, the unfolding was made column-wise, i.e. maintaining the IR indexes in columns. Thus, the $17 \times 10 \times 6$ data set (samples × variables × products, $n \times p \times m$) unfolds into a $(17 \times 6) \times 10$ or 102×10 matrix. Then traditional PCA yields sample-related (scores) and variable-related (loadings) information. As some information is lost during matrix augmentation it is necessary to refold the scores matrix again after the PCA [19]. Refolding each augmented scores vector, and averaging row-wise and column-wise, two vectors are obtained which contain the weathering (time evolution) and product-related information, respectively. Repeating this process for each augmented scores vector, information can be obtained on how each "weathering pattern" influences (on average) each sample/product. MA-PCA yields comparable results to standard PARAFAC [18,20].

2.3. Parallel factor analysis

Trilinear decomposition or Parallel factor analysis, PARAFAC, [4,21] can be viewed as a generalization of singular value decomposition (svd) to include the third way. To resume, in the same way as a 2-way matrix (e.g. weathered samples × IR indexes) is decomposed using svd, $X_{(n\times p)} = W_{(n\times k)} \times R_{(k\times k)} \times P'_{(k\times p)} + E_{(n\times p)}$ and, then, rearranged into two sets of vectors (scores and loadings matrices) $X_{(n\times p)} = S_{(n\times k)} \times P'_{(k\times p)} + E_{(n\times p)}$, a 3-way data array can be decomposed into three matrices $\underline{X}_{(n\times p\times m)} = A_{(i\times k)} \times B_{(p\times k)} \times C_{(m\times k)} + E_{(n\times p\times m)}$. The indexes have the same meaning as above (weathered samples, IR indexes, products, respectively) and underscore ($\underline{X}$) is used to denote 3-way data matrices (or data cubes). One of the matrices (A) is analogous to the traditional scores matrix whereas the other two are analogous to the current loadings matrix. Nevertheless, mathematically the differentiation is somewhat arbitrary and most authors consider the three matrices as weights. As for PR, PARAFAC requires that all 'slices' (here, products) are decomposed into the same number of components. This means that the same two matrices (e.g. A and B) will be used to model each slice (product) albeit with weights given by matrix C (each slice/product will have its own set of weights). It can be seen that these weights resemble very much the consensus vectors obtained by PR, despite there is a mathematical ambiguity in PARAFAC weights [4].

According to the number of 'scores' and 'loadings' (weights) each technique has to fit, PARAFAC is a more constrained solution than MA-PCA (in fact, PARAFAC has to fulfill the trilinearity requirement), which in turn is more constrained than PR. Nevertheless, their solutions should be highly similar, at least when the trilinearity requisite for PARAFAC is met.

3. Experimental

3.1. Samples

Four crude oils, namely Maya, Ashtart, Brent and Sahara Blend; a "Marine Fuel Oil" ("IFO", distributed by the Spanish Government to the scientific community as "similar" to the Prestige's oil), and the original fuel oil from the Prestige tanker were studied. According to their specific gravity, the Maya crude oil is very heavy, Ashtart is intermediate, and Brent and Sahara Blend are light crude oils. The two fuel oils were heavy residues obtained after refinery distillation processes.

Around 500 mL of each oil were released on metallic containers containing sea water and weathered under atmospheric conditions. Continuous shaking was performed using air pumps (more details about controlled spillages can be found elsewhere [11]) and aliquots were sampled at preset intervals, less spaced during the initial days than during the final ones. The organic phase was transferred to 50 mL Pyrex centrifuge tubes where approximately 1 g of anhydrous sodium sulphate (Merck, 99.0%, Damstard, Germany) was added, and centrifuged at 3000 rpm during 30 min (Seta Oil Test thermostatized centrifuge; Hermle, Germany). Whether emulsions appeared, NaCl (Panreac, 99.5%, Barcelona, Spain) and another gram of sodium sulphate were added until they broken down. To avoid excessive handling of stable emulsions, it was found satisfactory to thermostatize them at 50–60 °C (±1 °C) while centrifuging at 3000 rpm. for 30–40 min. In total, 17 samples were taken from each spilled product.

3.2. Analytical procedure

A mid-IR spectrometer (16PC PerkinElmer, beamsplitter Ge-KBr, DTGS detector, 4 cm^{-1} resolution, Beer-Norton strong apodization) with a horizontal ZnSe ATR device (12 reflections) was used throughout (50 scans, 4000–600 cm^{-1}, wavelength penetration was corrected for using proprietary functions and spectra were baseline corrected).

The ZnSe crystal and glassware were thoroughly cleaned. As the ATR plate tends to adsorb materials, fuel oil was released using kerosene; rinsed with dichloromethane (Super Purity, Romil, Cambridge, UK) and, finally, washed with temperate water and alkaline soap; MilliQ-type water was finally used. This yielded IR backgrounds without signals of hydrocarbons.

Usefulness of the IR indexes described into the introductory section (i.e., carbonyl, sulphoxide, aromaticity, aliphatic, aromatic condensation, branched chains, long chains, substitution 1, substitution 2 and substitution 3) was evaluated studying their relative standard deviation (R.S.D.). This constitutes an overall evaluation of the analytical procedure and, hence, we employed different aliquots of a Maya crude oil (without water). Five spectra were measured after five series of eight successive centrifugation–heating cycles, each (this resembled the most extreme conditions required to treat a highly weathered sample). The R.S.D.s of selected bands and indexes never exceeded 5%, which is in good agreement with literature [9,10].

4. Results and discussion

Preliminary studies showed that there were not outlying samples and that best results were obtained after autoscaling the data through the second mode (IR indexes); this is maintained hereinafter (otherwise stated). In MA-PCA, data were scaled after catenating (augmenting) the data matrices. To simplify readability, the terms 'scores' and 'loadings' will be used instead of sample-related weights and variable-related weights, respectively. Preliminary studies were made considering either a PCA for each product individually and an unfolded PCA (the 3-way matrix was unfolded to get a (samples × product) × IR indexes matrix). They revealed that two components (PCs) accounted for around 80–90% of all variance and, therefore, this seemed a good choice to set the number of factors to take into account in the 3-way studies.

4.1. Results from Procrustes rotation

Since two principal components were fine to describe each product, two components were considered also in PR. Table 1 shows that the first consensus vector (33.33% of the variance) is almost exclusively related to the total aromaticity index (i.e., the total number of C=C bonds in the compounds that form the oils) and, therefore, that it characterizes the main spread of the samples in the

Table 1
Comparison of loadings (analytical variable-way) for each 3-way methodology

	Procrustes rotation		MA-PCA		PARAFAC
	Consensus vector 1	Consensus vector 2	Factor 1	Factor 2	Factor 1
Aromaticity	−0.99	−0.04	0.99	−0.04	0.99
Alifaticity	0.01	−0.04	−0.02	−0.02	−0.01
Branched	0.01	0.05	0.01	0.05	0.00
Long chains	−0.01	−0.02	0.01	0.04	0.01
Condensation	0.01	−0.04	−0.01	−0.02	0.00
Carbonyl	−0.01	0.04	0.01	0.00	0.01
Sulphoxide	−0.01	0.03	0.00	−0.01	0.00
Substitution 1	0.03	−0.80	0.01	0.69	−0.02
Substitution 2	−0.03	0.30	0.04	0.04	0.05
Substitution 3	0.00	0.51	−0.05	−0.72	−0.03

weathering process. This reveals that (as it is generally accepted) the weathering process changes the main skeleton of the hydrocarbons through opening of the aromatic rings, introduction of alkyl chains (through reactions by radical species), etc. [22,23]. That this is the case for all products can be deduced from the very small angles (ranging from 0.7 to 1.5°) the first consensus vector forms with the first PC of the different slides (fuels and crude oils). Also, the 'temporally averaged product behaviors' (weights linked to the slides, here the six different products) in Fig. 1a shows that all products score (weight) approximately equal on this factor. Prestige fuel is the exception not because it does not show that trend but because it is much slower than for the other products.

Fig. 1b shows the 'product-averaged temporal consensus scores', i.e., how the 17 samples evolved on time on average for all six products. The sample pattern seems clearly related with time as the higher the number of the sample, the more the weathering. Despite not very clear on the first samples (as expected because the photo-oxidation and other degrading processes need some time to start and be apparent), the trend is clear after sample #9 (one week after the spillage). This is where the Prestige fuel differed from the other products because it was only after sample #11 (2 weeks of weathering) that its pattern was clear.

The 2nd consensus vector (32.4% of the overall information) is linked mainly to the substitution 1 and 3 indexes (see Table 1). The former is as a measure of the number of isolated CH groups in mul-

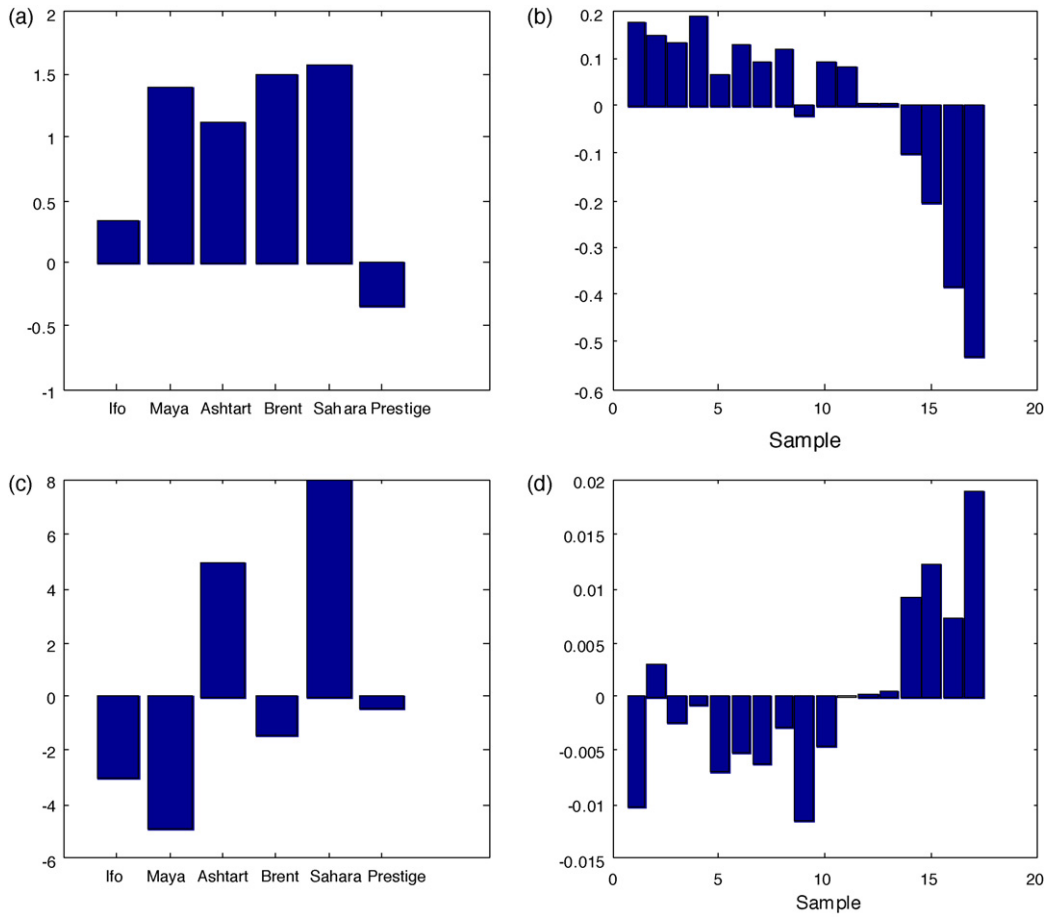

Fig. 1. 3-way Procrustes rotation, 'temporally averaged product behavior' and 'product-averaged temporal consensus scores' for consensus vectors 1 (a and b) and 2 (c and d).

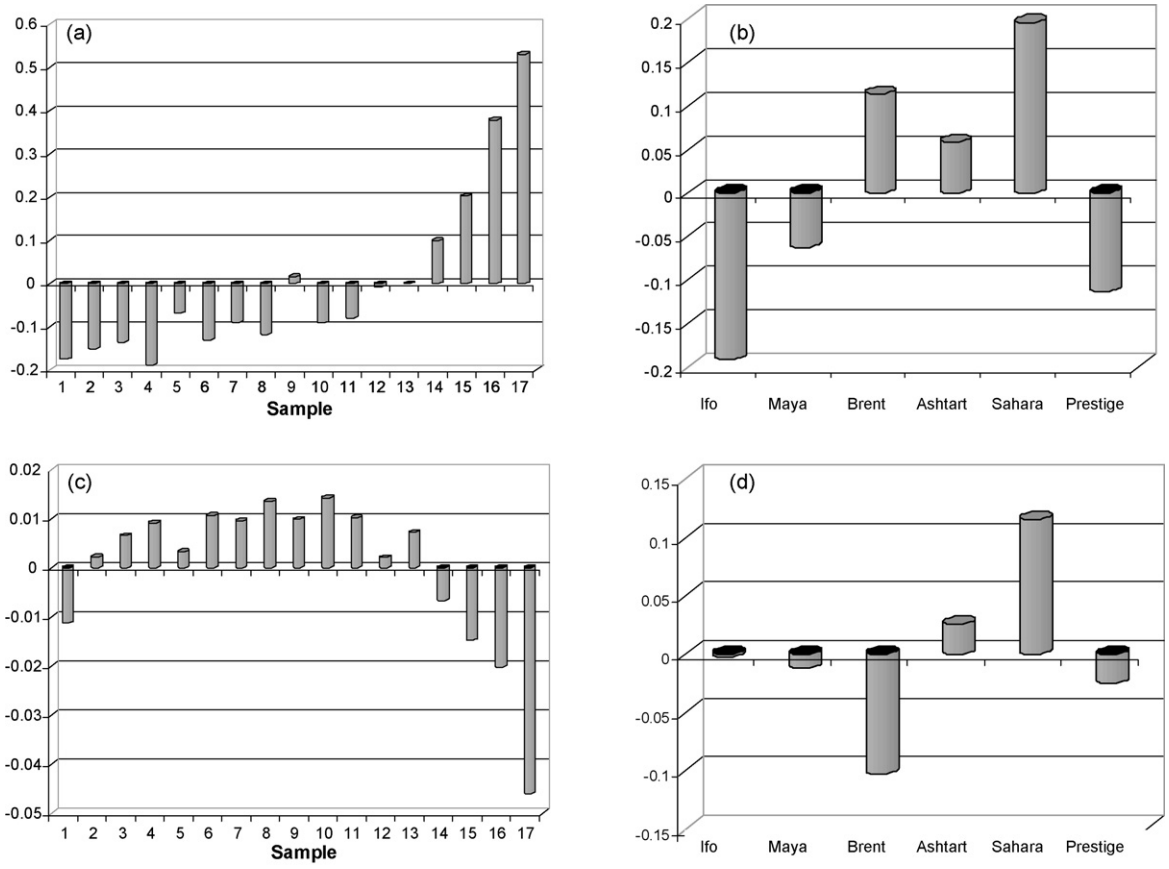

Fig. 2. Matrix-augmented PCA, and 'temporally averaged product behavior' for factors 1 (a and b) and 2 (c and d), each.

tisubstituted rings, $A_{864}/A_{864+814+743}$ whereas the latter represents the number of 3 or 4 adjacent CH groups in substituted rings, a good indication of di- and mono- substituted rings, $A_{743}/A_{864+814+743}$ [9,10]. The 2nd consensus vector was more heavily loaded by the substitution 1 index although in MA-PCA (second factor) this will not be the case (see Section 4.2). Noteworthy, the indexes show an opposite sign and, as it is the case for current loadings in common PCA this means that they vary in an opposite sense. In effect, the substitution 1 index (isolated CH groups in highly substituted aromatic rings) got reduced during ageing, mainly on light products (particularly Brent). A reason may be a steady decrease in the total amount of tetra- and/or pentasubstituted aromatic rings because of photooxidation and/or other weathering processes (see Ref. [11] for more discussions and detailed plots of the raw data).

Fig. 1c shows that two of the heaviest products (IFO and Maya oils) have a different weathering pattern. Nevertheless, the angles formed by the corresponding 2nd PC of each product and the 2nd consensus vector are 12.8°, 13.3°, 4.3°, 8.6°, 8.2° and 7.0° for IFO, Maya, Brent, Ashtart, Sahara and Prestige, respectively. This means that despite there is a common pattern, minor differences appear between the products. The most common relevant fact being that the last four weathered samples show an outstanding behavior (Fig. 1d). This occurs also for the 1st consensus vector and holds up through the following studies. There is little doubt that the longer the weathering, the larger the changes at the oil lump, and thus the more degraded the multisubstituted aromatic cycles (substitution 1 decresases), and the larger the substitution 3 index (the number of di- and tri-substituted cycles increase as a consequence of photo-oxidation and other processes).

4.2. Results with MA-PCA

Results from the column-wise augmented MA-PCA studies are shown in Figs. 2 and 3. Fig. 2 presents the 'product-averaged temporal scores' (i.e., the average behavior of the samples throughout the weathering process and through the six spillages) for the first (Fig. 2a) and second (Fig. 2c) factors. The first factor explains 94.5% of the initial variance whereas the second explains 4.7%. It seems clear that they two cope with the most relevant information of the

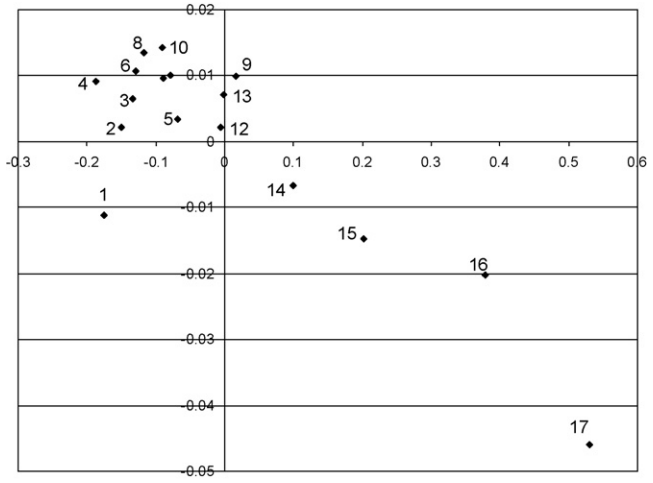

Fig. 3. Matrix-augmented PCA, PC1 vs. PC2 'product-averaged temporal scores'.

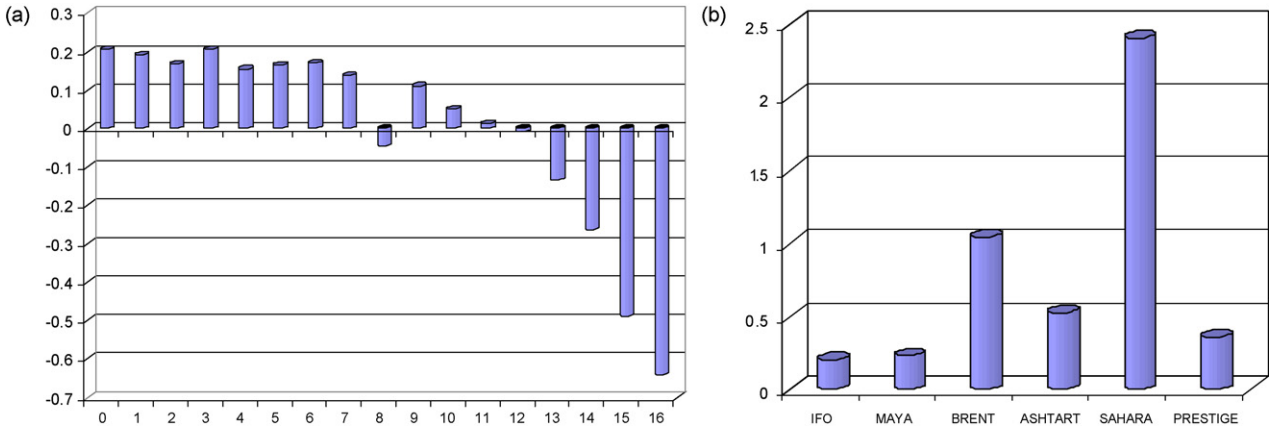

Fig. 4. PARAFAC, mode 1 (a, sample-related) and mode 2 (b, product-related) weights.

system. Fig. 2a shows a sample pattern which is clearly associated to the time evolution of the samples and that it differentiates the last four samples (from 28 to 101 days of weathering) from the initial ones. As discussed above, this is reasonable since previous studies [11] indicated that the photo-oxidation process needed some time before its evolution showed a definite pattern. In our studies, this amounted around 14 days (sample #11). The factor is almost exclusively dominated by the aromaticity index (see 'loadings' associated to the second mode, Table 1), which reflects the variation on the total amount of C=C bonds. As discussed for PR, this reveals that an important process during oil weathering implies changes on the main skeleton through opening of the aromatic rings, introduction of alkyl chains, etc.

Fig. 2b ('temporally averaged product behavior'; i.e., how the product behaves on average through all samples of the weathering process) shows that the two heaviest products (Prestige and IFO fuel oils) oppose to the lightest ones (Sahara and Brent crude oils), reflecting that the former are more resistant to weathering. This is due to their totally different nature, since the fuel oils were the final products of refinery distillation processes, with almost no volatiles and heavy and very complex structures, which are difficult to degrade. On the contrary, the crude oils were light (with large amount of volatiles) and contain many structures that dissapear because of their easy volatization, photo-oxidation, polymerization, etc. [22,23]

The second MA-PCA factor is defined by the substitution 1 and 3 indexes (Table 1). This is exactly the same behavior as that found for the Procrustes rotation decomposition and, therefore, no additional details will be given. As for the first MA-PCA factor, this yields a clear trend on the average 'scores' related to the weathering of the samples (Fig. 2c) as they become quite well ordered according to their weathering time. Again, the last four samples show a relevant difference due to their more advanced weathering.

The different behavior of the Brent crude oil (Fig. 2d) can be explained because its scores increase up to sample #9 (day 10) but, then, decrease smoothly. This was not revealed when the consensus vectors in PR were calculated, likely because of the more important participation of the substitution 3 index on MA-PCA 2 (Procrustes rotation gave more importance to the substitution 1 index). A detailed study of the samples revealed that, contrary to the substitution 1 index, the substitution 3 index (mono- and/or disubstituted rings) has a two-fold behavior as it increases for the Brent oil, Prestige and IFO fuels and it decreases for the other products. This suggests that the most complex and polysubstituted structures (substitution 1) can evolve either to trisubstituted rings (substitution 2) or to both trisubstituted and mono- and di-substituted rings (substitution 3).

Hence, a general overall conclusion for this second factor would be that it characterizes the degradation of polysubstituted aromatic structures – substitution 1 index – to less substituted ones—substitution index 3. Besides, Fig. 3 demonstrates that, on average, weathering is a bit 'random' at the beginning, probably due to the many different weathering processes that can occur (in addtion to physical phenomena like evaporation, dispersion, solubilization, etc.). However, it becomes quite definite after 7–11 days (samples 9–10) and this was monitored either by the total aromaticity and the substitution 1 and 3 indexes.

4.3. Results from PARAFAC

PARAFAC extracted only a relevant factor whose sample-related weights are depicted in Fig. 4a. They resemble the patterns of the two analyses above: a slightly undefined trend during the early stages of the weathering process, which evolved to a clear one after samples #9–10 (7–11 days). Table 1 indicates that the aromaticity index is nearly the unique relevant variable to denote such a behavior, which totally agrees with the other studies. Fig. 4b confirms that the lightest product (Sahara Blend) evolved much faster than the others (highest weight in the plot), followed by Brent, Ashart and, finally the Maya, Prestige and IFO oils. Likewise, this ordering coincides with the specific gravity of the products mentioned in Section 2.

A general finding derived from the three 3-way techniques is that the carbonyl and sulphoxide indexes, which are clearly linked to photoxidative processes [9–11,22,23], were not relevant to describe the common weathering patterns of the oils. Although this may surprise at first glance (because some products exhibited a clear evolution for both indexes, see [11] for more details), we attributed this fact to the quite different behaviors those ratios exhibited along the different products. For instance, although the carbonyl index increased abruptly for the Sahara oil just from the very first hours, it took around 11 days to change clearly for the Prestige fuel. Besides, the Ashtart oil had a variable behavior. Hence, it seems reasonable to conclude that the 3-way methods employed here extracted only the common patterns for all products (which also justifies the term 'average' employed for the scores–sample-related weights).

5. Conclusions

Results presented in this paper demonstrate that the three 3-way decomposition techniques employed here lead to essentially the same conclusions along the sample-, variable- and product-related ways. Besides, the results showed that Procrustes rotation

is a good option to address 3-way datasets because the consensus vectors constituted a quite straightforward and conceptually simple option to compare how six different hydrocarbon complex mixtures evolved on time after being spilled on the enviroment.

In the present study it was found that the total aromaticity index can be (almost exclusively) used to characterize the weathering process. Other useful indicators are the substitution 1 and 3 indexes, because they reveal details on how the number of functional substitutions into the aromatic cycles evolve.

It was also observed that other IR indexes strongly related to the specific evolution of some products; namely, the carbonyl and sulphoxide indexes, were too linked to specific products and, hence, were not relevant to extract common weathering patterns. A feasible explanation is that although they do characterize photooxidation, they depend strongly on the particular evolution of the products (more specifically, whether they are light or heavy).

Acknowledgements

The Spanish government and the European Funds for the Regional Development, FEDER-EFRD, are acknowledged by their financial support (FIT-050100-2003-4, FIT-310200-2004-106, and CIT-310200-2005-37).

References

[1] N.A. Sloan, Oil impacts on cold-water marine resources, Report Paper No. 11, Parks Canada, National Parks, 1999.
[2] www.itopf.com, May 2008.
[3] V. Gaganis, N. Pasadakis, Anal. Chim. Acta 573–574 (2006) 328.
[4] A. Smilde, R. Bro, P. Geladi, Multi-way analysis, Willey, United Kingdom, 2004.
[5] M. Felipe-Sotelo, J.M. Andrade, A. Carlosena, R. Tauler, Anal. Acta Chim. 583 (2007) 128.
[6] S. Carrer, R. Leardi, Sci. Tot. Environ. 370 (2006) 99.
[7] K.P. Singh, A. Malik, V.K. Singh, N. Basant, S. Sinha, Anal. Chim. Acta 571 (2006) 248.
[8] D. Ebrahimi, J. Li, D.B. Hibbert, J. Chromatogr. A 1166 (2007) 163.
[9] N. Pieri, J.P. Planche, J. Kister, Analysis 24 (1996) 113–122.
[10] H. Masmoudi, Y. Le Dréau, P. Piccerelle, J. Kister, Int. J. Pharm. 289 (2005) 117.
[11] P. Fresco-Rivera, R. Fernández-Varela, M.P. Gómez-Carracedo, F. Ramírez-Villalobos, D. Prada, S. Muniategui, J.M. Andrade, Talanta 74 (2007) 163.
[12] W.J. Krzanowski, Principles of Multivariate Analysis, Clarendon Press, Oxford UK, 2000.
[13] J.M. Andrade, M.P. Gómez-Carracedo, W.J. Krzanowski, M. Kubista, Chemom. Intell. Lab. Syst. 72 (2004) 123.
[14] A. Carlosena, J.M. Andrade, M. Kubista, D. Prada, Anal. Chem. 67 (1995) 2373.
[15] A. Elbergali, J. Nygren, M. Kubista, Anal. Chim. Acta 379 (1999) 143.
[16] E.R. Malinowski, Factor Analysis in Chemistry, 2nd edition, Willey, New York, 1991.
[17] H.T. Eastment, W.J. Krzanowski, Technometrics 24 (1982) 73.
[18] J.M. Andrade, M. Kubista, A. Carlosena, D. Prada, Anal. Chim. Acta 603 (2007) 20.
[19] R. Tauler, D. Barceló, E.M. Thurman, Environ. Sci. Technol. 34 (2000) 3307.
[20] M. Felipe-Sotelo, J.M. Andrade, A. Carlosena, R. Tauler, Anal. Chim. Acta 583 (2007) 128.
[21] GenEx User's Manual, MultiD, Sweden (2007) (www.multid.se).
[22] J.R. Payne, C.R. Phillips, Environ. Sci. Technol. 19 (7) (1985) 569.
[23] R.C. Prince, R.M. Garret, R.E. Bare, M.T. Grossman, T. Townsend, J.M. Suflita, K. Lee, E.H. Owens, G.A. Sergy, J.F. Braddock, J.E. Lindstrom, R.R. Lessard, Spill Sci. Technol. Bull. 8 (2) (2003) 145.

Talanta 77 (2008) 541–545

Contents lists available at ScienceDirect

Talanta

journal homepage: www.elsevier.com/locate/talanta

Automatic sequential injection liquid–liquid micro-extraction system for on-line flame atomic absorption spectrometric determination of trace metal in water samples

Aristidis N. Anthemidis *

Laboratory of Analytical Chemistry, Department of Chemistry, Aristotle University, Thessaloniki 54124, Greece

ARTICLE INFO

Article history:
Received 13 September 2007
Received in revised form 4 April 2008
Accepted 8 April 2008
Available online 20 April 2008

Keywords:
Lead
Sequential injection
Liquid–liquid extraction
Atomic absorption spectrometry

ABSTRACT

An automatic sequential injection (SI) liquid–liquid micro-extraction system incorporating a dual-conical micro-gravitational phase separator is proposed as versatile approach for on-line metal preconcentration and/or separation. Coupled to flame atomic absorption spectrometry (FAAS) the potentials of this novel schema are demonstrated for lead determination in water samples at the $\mu g\,l^{-1}$ level. The non-charged lead complex with ammonium pyrrolidine dithiocarbamate (APDC) was extracted on-line into 300 μl isobutyl methyl ketone (IBMK) through the extraction coil. The organic phase containing the extracted metal complex is collected in the upper cavity of the phase separator and then forwarded to the nebulizer. All the critical parameters were optimized and offered good performance characteristics and high preconcentration ratios. A sample consumption of 10.5 ml enabled the determination of Pb(II) in the range of 3.0–250.0 $\mu g\,l^{-1}$ with an enhancement factor of 120 and a sampling frequency of 25 h^{-1}. The detection limit and the precision were 1.4 $\mu g\,l^{-1}$ and 2.9% (at 50.0 $\mu g\,l^{-1}$ concentration level), respectively. The proposed method was evaluated by analyzing certified reference material and was applied successfully to the analysis of natural water samples.

1. Introduction

Despite its significant analytical chemical capacities for metal determination at low concentration levels, flame atomic absorption spectrometry (FAAS) often requires a suitable pretreatment step (preconcentration and/or separation) of the sample in order to facilitate the desired sensitivity and selectivity of measurement. Liquid–liquid extraction (LLE) is a widely applied and powerful pretreatment approach prior to analysis, which in batch mode procedures is labor intensive, time consuming, requires large reagent consumption, and suffers risks of sample contamination [1]. From this point of view, it is most beneficial to employ an automatic on-line procedure like flow injection (FI) or sequential injection (SI).

Since the introduction of flow injection liquid–liquid extraction (FI-LLE) as a mean for analyte preconcentration in FAAS by Nord and Karlberg [2], the applications of such systems for routine analysis are rather limited compared to other on-line preconcentration systems like solid phase extraction. This can be attributed to the complexity of the manifolds, which usually lack the ruggedness and long-term stability [3]. In addition, there are significant difficulties in organic solvents transportation using conventional FI devices. Organic solvents like isobutyl methyl ketone (IBMK), which is the most widely used in FAAS cannot be reliably pumped even with solvent resistant pump tubes. In this case displacement bottles are required, which make the manifold more complicated, while technical skills are required for their manipulations [4]. In addition there are some limitations on the aqueous to organic phase ratios of segmented stream that on-line phase separators can handle successfully [5].

Most of FI procedures use continuous unidirectional pumping of sample and reagent streams, while SI is based on using programmable bidirectional discontinuous flow as precisely coordinated and controlled by a computer. SI systems have significant advantages over FI ones in the simplicity of manifold design, robustness and versatility [6,7]. The inert devices, glass syringe, PTFE tubing and PEEK multiposition valve make the SI systems feasible to manipulate all kinds of organic solvents in micro-scale. A significant advantage of the SI system is the ability for even small volumes (down to a few tenths of microliters) metering, thanks to the use of a syringe pump [8]. Moreover, SI is more economical regarding to the sample, reagents and hence the waste production, which is a significant parameter because it is getting almost more expensive to get rid of the wastes, than to buy the chemicals. Thus,

* Fax: +30 2310 997719.
E-mail address: anthemid@chem.auth.gr.

0039-9140/$ – see front matter © 2008 Elsevier B.V. All rights reserved.
doi:10.1016/j.talanta.2008.04.017

SI technique is more suitable for on-line liquid–liquid extraction procedures.

The most critical component in on-line LLE systems is the phase separator of which various designs have been reported, such as: micro-porous membrane type [9–11] and gravitational ones [4,5,12–16]. The main drawbacks of the membrane type phase separators are: (i) insufficient separation of the phases when high segmented flow rates is required and (ii) limited lifetime of the membrane, resulting to the need of periodical change. On the other hand gravitational phase separators are more promising for large range of flow rate ratios of aqueous to organic phase and have previously been shown to be very efficient and easily operated [5,14].

In order to improve the ruggedness of FI-LLE system Tao and Fang [14] proposed the use of a gravitational phase separator with an internal conical cavity (ca. 45 μl), which is only effective for separation of low-density phase. Wang and Hansen proposed an alternative dual-conical gravitational phase separator, which facilitates the separation of both low- and high-density phase. The above phase separators have been tested coupled only with electrothermal atomic absorption spectrometry (ETAAS) for metals determination.

Hitherto, to the best of our knowledge, only one SI liquid–liquid extraction procedure with detection FAAS has been reported in the literature [17]. That procedure, instead of extraction coil and phase separator, uses a glass vial with porous ceramic plate inside, which allows solvents less dense than water to float above it.

In the present work, sequential injection is exploited for the first time as automatic and versatile approach for the implementation of liquid–liquid extraction in a simple low-cost manifold furnished with a dual-conical micro-gravitational phase separator (PS) for on-line metal flame atomic absorption spectrometric determination. In order to facilitate the on-line separation of micro-volume of a low-density organic solvent like IBMK, from a high flow rate segmented stream, a novel dual-conical micro-gravitational phase separator was designed and studied. The conical shape of the upper cavity combined with differences in density of the two phases and the hydrophobic nature of the cavity permits the continuous separation of the segmented phase.

The effectiveness and efficiency of the proposed SI-LLE system was investigated and demonstrated for lead determination, via its complexation with ammonium pyrrolidine dithiocarbamate (APDC) and extraction into isobutyl methyl ketone. The accuracy of the proposed method was tested by the analysis of certified reference material and the method was applied to the analysis of natural water samples.

2. Experimental

2.1. Apparatus

The SI manifold and its operation for on-line liquid–liquid extraction and lead determination by FAAS is depicted schematically in Fig. 1.

A FIAlab®-3000 sequential injection system (Alitea FIAlab, USA) equipped with an internally incorporated six-port multiposition valve (MV) and a syringe pump (SP, Cavro, Sunnyvale, CA) with a capacity of 1.0 ml was used. The FIAlab®-3000 system was controlled by a personal computer and the FIAlab for windows v. 5.9.245 application program, written by FIAlab instruments (http://www.flowinjection.com).

A PerkinElmer, Norwalk, Connecticut, USA (http://las.perkinelmer.com) model 5100 PC flame atomic absorption spectrometer was exploited as detection system. Lead electrodeless discharge lamp (EDL) was used as light source operated at

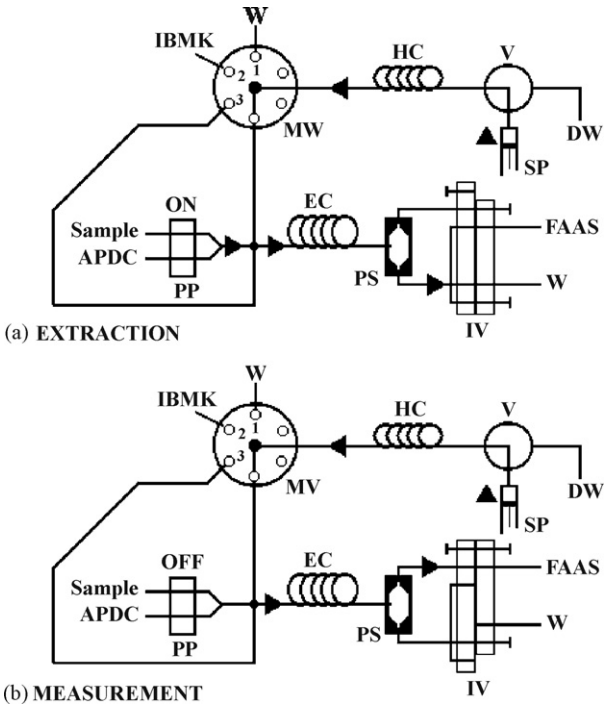

Fig. 1. SI-LLE system coupled to FAAS for lead determination. Two operation steps: (a) extraction (step 3) and (b) measurement (step 4). MV, multiposition valve; SP, syringe pump; V, syringe pump valve; PP, peristaltic pump; IV, injection valve; EC, extraction coil; HC, holding coil; PS; phase separator; DW, distilled water; W, waste.

10 W. The wavelength was set at 283.3 nm resonance line and the slit at 0.7 nm. A time-constant of 0.2 s was used for peak height evaluation. The air flow rate was set at 10.0 l min^{-1}, acetylene flow rate at 0.9 l min^{-1} and the resulting nebulizer's free uptake rate was 92 μl s^{-1}. The flame conditions were adjusted to be slightly leaner than those recommended by the manufacturer for aqueous samples, in order to compensate the effect of organic solvent isobutyl methyl ketone, which serves as an additional fuel. A flow spoiler was employed into the spray chamber for better nebulization conditions. A PerkinElmer Norwalk, Connecticut, USA model FIAS-400 flow injection analysis system was coupled to the SI system and to the FAAS for automatic processing of the whole procedure. The FIAS-400 system was controlled by a personal computer and the AA Lab. Benchtop version 7.2 software program. The FIAS-400 system consisted of two peristaltic pumps (only one, P is used for the proposed manifold) and a 5-port 2-position injection valve, IV. The connecting line between the IV and the FAAS nebulizer was a PTFE tube 20 cm long, 0.5 mm i.d.

A dual-conical micro-gravitational phase separator (Fig. 2) was incorporated within the SI system in order to accomplish the separation of organic or aqueous phases. The SP was fabricated from two "push-fit" conical (cavities of ca. 30 μl) shaped pieces of the hydrophobic material, polytetrafluoroethylene (PTFE) and one cylindrical shaped central union with perpendicular inlet bore size of 0.7 mm. The total inner volume of the PS was approximately 900 μl. The upper and lower pieces have an outlet bore size of 0.5 mm i.d. and 1.0 mm i.d., respectively. The extraction coil enters into the PS horizontally and that facilitates the fast separation and collection of organic phase free of aqueous phase in the upper conical cavity while the aqueous phase forwarded to the waste through the IV. The same PS can be used for organic solvents with either lower or higher density from water.

A VICI AG (Valco International) four-section "cross" type confluence connector made of PEEK, with 0.5 mm i.d. bore size was

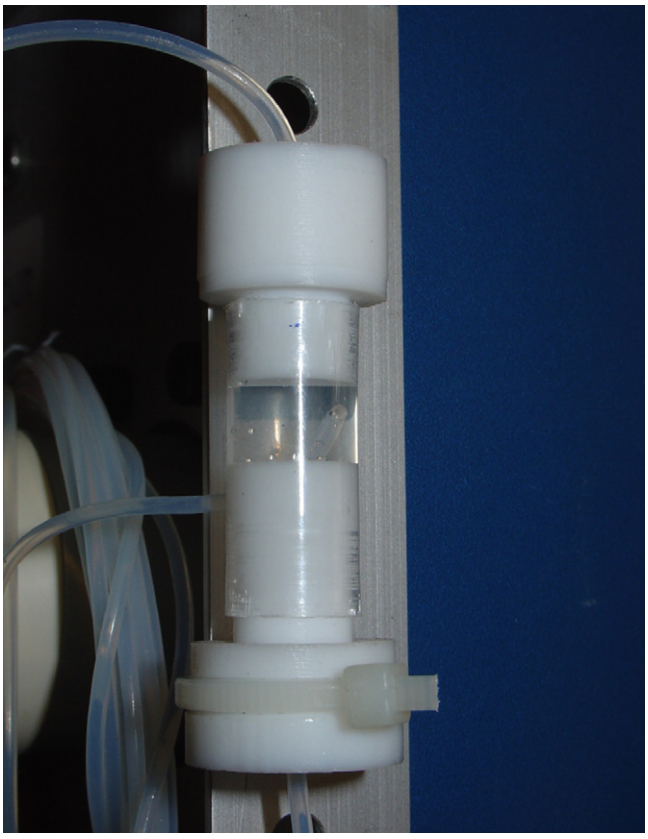

Fig. 2. Dual-conical micro-gravitational phase separator (PS).

exploited for segmentation of aqueous and organic phase. The extraction coil (EC) is advantageously made from PTFE tubing 300 cm length, 0.75 mm i.d. as a knotted reactor [15], which facilitates the dispersion of the two phases into each other so effectively that it is actually difficult to see them separately with the naked eye, that is, a very large area of interface between the two phases is generated, which in turn expedites the extraction.

An Orion EA940 pH-meter was employed for the pH measurements being defined by NIST buffers.

2.2. Reagents

All chemicals were of analytical reagent grade and were provided by Merck (Darmstadt, Germany, http://www.merck.de). Ultra-pure quality water was used throughout which was produced by a Milli-Q system (Millipore, Bedford, USA, http://www.millipore.com). Working standard solutions of lead were prepared by appropriate stepwise dilution of a 1000 mg l^{-1} stock standard solution (in HNO_3 0.5 mol l^{-1}) (Titrisol, Merck) to the required μg l^{-1} levels just before use. The pH of them was adjusted with dilute HNO_3. The chelating reagent solution was prepared daily by dissolving the appropriate amount of APDC (Merck, pro analysi) in de-ionized water and was extracted with IBMK for further purification. Isobutyl methyl ketone was previously saturated with de-ionized water.

2.3. Procedure

The operation steps of the proposed SI-LLE procedure for lead determination are summarized in Table 1.

In step 3 (Fig. 1 EXTRACTION), the sample containing the analyte is first mixed with 0.5% (m/v) APDC solution to form the metal complex and then intermixed with the extractant (300 μl IBMK) in the reaction coil (RC). Thereafter, the phases are separated in the micro-gravitational phase separator and the extractant collected in the upper cavity of the PS, while the aqueous phase was discarded to waste through the IV. In step 4 the collected IBMK is transported to the flame atomizer of FAAS detector with a flow rate of 92 μl s^{-1} for measuring the absorbance. In order to avoid a possible contamination between samples the extraction coil and the phase separator are washed during the last step. The peak height absorbance was proportional to lead concentration in the sample, and was used for all measurements. Five replicate measurements were made in all instances. The extraction was quantitative (E > 99.0%) as was estimated by sequential extraction of aqueous lead standards.

3. Results and discussion

3.1. Injection of the extractant into the atomizer

One of the major limitations of coupling continuous solvent extraction systems like FI and SI to FAAS, is the nonmatching of the uptake rate of the nebulizer, usually ranged between 66 and 133 μl s^{-1}, with the flow rate of the extractant, which is typically lower than 16 μl s^{-1}. In case the free uptake of the nebulizer exceeds that of the extractant flow, a random gaseous release of dissolved air during the delivery into the nebulizer could significantly deform the peak profile and degrade the readout precision [18]. Lower flow rate of organic solvent is necessary for higher flow rate ratios of aqueous to organic and thus higher preconcentration rates and sensitivity [5]. In this case it is more preferable to accumulate an appropriate amount of extractant in a holding coil and then to inject it into the nebulizer with a flow rate similar to the nebulizer's free uptake flow rate.

According to the proposed SI-LLE manifold, two points should be taken into account: (1) the lowest injected volume of extractant IBMK that is necessary to take the maximum absorbance, in order to reduce the reagents consumption and (2) the flow rate of the extractant that is needed for the nebulizer uptake flow rate compensation. The above considerations are achieved using the proposed dual-conical micro-gravitational phase separator.

The influence of the injected volume of the extractant into the nebulizer was examined in the range of 50–400 μl, with a fixed

Table 1
Operational sequence of the SI-LLE on-line preconcentration system for lead determination

Step	V	SP flow-rate (μl s^{-1})	MV	PP[a]	IV	SP action	Commentary
1	In	100	2	Off	Load	Aspirate 800 μl	Aspiration of water into SP
2	Out	50	2	Off	Load	Aspirate 300 μl	Aspiration of IBMK into HC
3	Out	3.0	3	On	Load	Dispense 300 μl	Extraction, collection of extract
4	Out	90	4	Off	Inject	Empty	Injection of IBMK extractant into nebulizer Absorption measurement
5	In	100	4	Off	Load	Fill	Repletion of SP with water
6	Out	100	4	Off	Load	Empty	Washing of extraction system

[a] Sample flow rate, 175 μl s^{-1}; [APDC] = 0.5% (m/v); APDC flow rate, 10 μl s^{-1}.

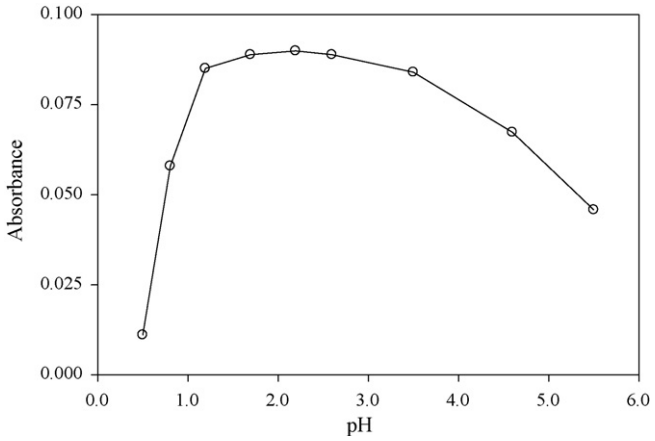

Fig. 3. Effect of sample pH on the absorbance of 90 μg l^{-1} Pb(II). Sample flow rate = 137 μl s^{-1}. All other parameters as in Table 1.

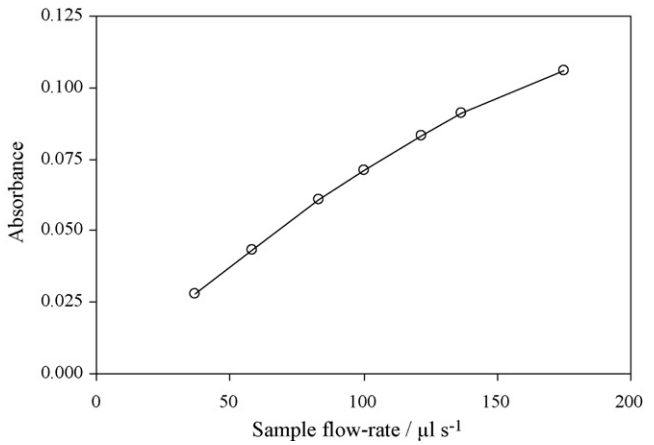

Fig. 4. Effect of sample flow rate on the absorbance of 90.0 μg l^{-1} Pb(II). IBMK flow rate = 3 μl s^{-1}; extraction coil: 300 cm length, 0.75 mm i.d. All other parameters as in Table 1.

90 μl s^{-1} flow rate using standard lead solution in IBMK without previous extraction procedure. By increasing the injected volume, the sensitivity was increased up to 100 μl and leveled off after this volume. Taking into account the extraction efficiency and in order to compensate the IBMK solubility in water, an IBMK volume of 300 μl was used for the subsequent studies.

The flow rate for transportation of the extractant (300 μl) to FAAS was studied in the range of 40–100 μl s^{-1} using standard lead solution in IBMK without previous extraction. The absorbance initially increased with the increase of the flow rate and was leveled off at 80 μl s^{-1}. Finally, feed flow rate of 90 μl s^{-1} which is similar with the free uptake flow rate (92 μl s^{-1}) of the FAAS nebulizer was selected for all measurements.

3.2. Optimization of the extraction parameters

For the optimization of the different chemical and SI parameters which will be mentioned below, the univariant method was used, utilizing a standard aqueous solution of 90 μg l^{-1} Pb(II).

The pH value of the sample solution effects significantly the Pb(II)–PDC complex formation, and also its extraction efficiency in the IBMK. Lead forms stable complexes with APDC over a wide pH range (0.1–6) [19] and can be readily extracted into IBMK. The pH of sample was studied in the range from 0.5 to 5.5 by adjusting it with dilute nitric acid or ammonia. The maximum signal was obtained within a pH range from 1.2 to 3.5 as it shown in Fig. 3. This fact shows that the method can be used directly in many aqueous samples after the common acid preservation, without any laborious precise pH adjustment. Thus, pH 2.0 was established for further study.

Ammonium pyrrolidine dithiocarbamate is the most popular dithiocarbamate agent due to the fact that its aqueous solutions are stable in acidic conditions, it operates in a broad pH range without any decomposition [20] and its complexation rate with various metals is very high. The effect of complexing reagent concentration was studied in the range of 0.1–1.0% (m/v). The absorbance was increasing for concentrations up to 0.3% (m/v) APDC, while for higher concentrations it remained constant. A concentration in excess of 0.5% (m/v) APDC was selected for subsequent studies due to the possible consumption caused by other extractable metals present in the sample.

In continuous liquid–liquid extraction systems the preconcentration factor is determined by the flow rate ratio of aqueous to organic phase, which is corresponding with the volume ratio of aqueous to organic phase in batch (off-line) extraction methods. Generally, higher ratios give higher sensitivity. However, in flow systems there are practical limits to obtain very high flow rate ratios, due to the limited range of organic phase flow rate that peristaltic pumps can handle precisely and also due to the insufficient versatility and robustness of them at very low flow rates. The problem can be solved using stepper-motor driven syringe pumps and SI systems controlled by computer. On the other hand the aqueous phase (sample + complexing reagent) flow rate cannot be very high because in this case the resulted segmented (total) flow rate would be extremely high. Too high segmented flow rate causes significant disturbance of the segmentation in the extraction coil leading to an inferior contact between the two phases and thus to a decrease of the extraction efficiency [5]. Moreover, the efficiency of the extraction procedure depends not only on the interface area but also on the time of contact.

According to the above considerations the effect of sample flow rate on the absorbance was studied in the range of 37–175 μl s^{-1}, while the APDC flow rate was fixed at 10 μl s^{-1}. The results are shown in Fig. 4. The absorbance increased with increasing the sample flow rate. Thus, a sample flow rate of 175 μl s^{-1} was adopted in order to get higher sensitivity for the proposed method.

The effect of extracting solvent (300 μl IBMK) flow rate on the absorbance was studied in the range of 1–5 μl s^{-1}, while the sample flow rate was fixed at 175 μl s^{-1}. The absorbance decreased with increasing the IBMK flow rate, while a higher standard deviation was recorded at flow rate of 1 μl s^{-1}. An IBMK flow rate of 3 μl s^{-1} was used as a compromise between the time consumption and the high sensitivity.

A selection of the appropriate extraction coil length at the used flow rates is important when maximum extraction efficiency is required. The dimensions (length and internal diameter) of the extraction coil define the time of contact (extraction time) and thus the extraction efficiency. In addition, the increase in coil length increases the extraction efficiency by providing larger contact area of the aqueous sample with a thin film of organic phase adsorbed on the inside wall of the coil, where partial transfer of analyte to the organic phase takes place [21]. The effect of the length of the extraction coil was studied in the range of 50–500 cm (0.75 mm i.d.). The absorbance was increased upon increasing coil length and reaches a maximum at length in excess of 300 cm. These results suggest that at shorter coils, the residence time of the analyte in the coil is short, resulting in incomplete extraction. A length of 300 cm was employed for the proposed method.

Table 2
Analytical characteristics of the SI-LLE on-line FAAS method for lead determination

Enhancement factor	120
Sample consumption (ml)	17.5
Sampling frequency (h^{-1})	25
Linear range ($\mu g\,l^{-1}$)	3.0–250.0
Regression equation ([Pb] in $\mu g\,l^{-1}$)	0.0012 [Pb] + 0.0021
Correlation coefficient	$r = 0.9995$
Detection limit (3s) ($\mu g\,l^{-1}$)	$c_L = 1.4$
Precision (RSD, $n = 11$; 50.0 $\mu g\,l^{-1}$) (%)	$s_r = 2.9$

Table 3
Analytical results of lead determination in natural waters by the proposed method

Sample	Added ($\mu g\,l^{-1}$)	Found[a] ($\mu g\,l^{-1}$)	Recovery (%)
Tap water	–	$<c_L$	–
	10.0	9.9 ± 0.6	99
River water	–	6.5 ± 0.5	–
	10.0	16.2 ± 0.9	97
Seawater	–	5.3 ± 0.5	–
	10.0	14.9 ± 1.2	96

[a] Mean value ± standard deviation based on three replicate measurements.

3.3. Interference studies

The effect of potential interferents encountered in natural waters on the preconcentration and determination of lead were examined using the SI-LLE manifold shown in Fig. 1, under the optimum conditions described above for 50.0 $\mu g\,l^{-1}$ Pb(II). Taking as a criterion for an interference the deviation of the recovery more than ±5%, Al(III) (10 $mg\,l^{-1}$), Cd(II) (0.5 $mg\,l^{-1}$), Co(II) (1.0 $mg\,l^{-1}$), Cr(III) (10.0 $mg\,l^{-1}$), Cr(VI) (10.0 $mg\,l^{-1}$), Cu(II) (1.0 $mg\,l^{-1}$), Fe(III) (10.0 $mg\,l^{-1}$), Hg(II) (0.5 $mg\,l^{-1}$), Mn(II) (10.0 $mg\,l^{-1}$), Ni(II) (1.0 $mg\,l^{-1}$), and Zn(II) (2.0 $mg\,l^{-1}$) do not interfere. Although APDC does not form complexes with alkali and alkaline earth metals, high concentrations of them were tested because they are usually found in high concentrations in natural waters. Na^+ and K^+ up to 2000 $mg\,l^{-1}$ and Ca^{2+}, Mg^{2+}, Ba^{2+} up to 500 $mg\,l^{-1}$ and NaCl up to 30 $g\,l^{-1}$, did not caused any significant interference.

3.4. Analytical characteristics

The analytical characteristics of the proposed SI-LLE system for lead determination with FAAS are summarized in Table 2. For a 62 flow rate ratio of aqueous to organic phase, the sampling frequency was 25 h^{-1}. The enhancement factor, calculated from the ratio of the slope obtained with the proposed method to the slope without extraction (using aqueous standards solutions in batch mode), was 120. The linear calibration graph for lead determination was 3.0–250.0 $\mu g\,l^{-1}$. The limit of detection (c_L) defined by the 3s criterion and was found to be $c_L = 1.4\,\mu g\,l^{-1}$. The relative standard deviation (RSD) which define the precision was $s_r = 2.9\%$ at 50.0 $\mu g\,l^{-1}$ Pb(II) concentration level.

The accuracy of the proposed method was tested, by determining the lead concentration of a certified reference material NIST CRM 1643d (National Institute of Standard and Technology, Trace elements in water) with a certified content of lead, $18.15 \pm 0.64\,\mu g\,l^{-1}$ and the recovery obtained was 96% ($17.42 \pm 0.8\,\mu g\,l^{-1}$, $n = 3$). The result was in good agreement with the certified value and the calculated recovery was satisfactory.

3.5. Analysis of natural waters

The proposed method was applied to the analysis of tap water river water and coastal seawater samples collected from rivers and gulfs of Northern Greece. Natural water samples were filtered through 0.45 μm membrane filters and acidified to 0.01 $mol\,l^{-1}$ HNO_3 (pH ≈ 2). The results are presented in Table 3. The obtained recovery varied from 96% to 99% showing that the performance of the method was very good in all types of natural waters.

4. Conclusions

The SI-LLE continuous extraction system with a dual-conical micro-gravitational phase separator has been evaluated and demonstrated to be promising for improving the sensitivity and selectivity of the FAAS method for routine determination of trace amounts of lead in water samples. A cost-effective simple fabricated micro-phase separator unit attached at the multiposition selection valve of the FIAlab®-3000 SI system offers an automatic on-line extraction in micro-scale by drastically reducing organic solvent volumes. The system versatility concerning the variation of the sample and organic extractant flow rate provides an expeditious way to control the sensitivity and high preconcentration factors.

It is further advantageous regarding the extraction with organic solvents denser than water like chloroform and feasibility of application to other metals determination with LLE and FAAS.

References

[1] Z. Fang, Flow Injection Atomic Absorption Spectrometry, John Wiley & Sons Ltd., West Sussex, England, 1995.
[2] L. Nord, B. Karlberg, Anal. Chim. Acta 125 (1981) 199.
[3] Z.-L. Fang, Anal. Chim. Acta 400 (1999) 233.
[4] J.-H. Wang, E.H. Hansen, Anal. Chim. Acta 456 (2002) 283.
[5] A.N. Anthemidis, G.A. Zachariadis, C.G. Farastelis, J.A. Stratis, Talanta 62 (2004) 437.
[6] J. Ruzicka, G.D. Marshall, Anal. Chim. Acta 237 (1990) 329.
[7] C.E. Lenehan, N.W. Barnett, S.W. Lewis, Analyst 127 (2002) 997.
[8] E.H. Hansen, J. Environ. Sci. Health 40 (2005) 1507.
[9] S. Motomizu, M. Oshima, Analyst 112 (1987) 295.
[10] K. Backstrom, L.-G. Danielsson, Anal. Chim. Acta 232 (1990) 301.
[11] T. Sakai, H. Harada, X. Liu, N. Ura, K. Takeyoshi, K. Sugimoto, Talanta 45 (1998) 543.
[12] S. Lin, H. Hwang, Talanta 40 (1993) 1077.
[13] S. Lin, Q. Shuai, H. Qiu, Z. Tang, Spectrochim. Acta Part B 51 (1996) 1769.
[14] G. Tao, Z. Fang, Spectrochim. Acta Part B 50 (1995) 1747.
[15] J.-H. Wang, E.H. Hansen, J. Anal. At. Spectrom. 17 (2002) 1284.
[16] A.N. Anthemidis, G.A. Zachariadis, J.A. Stratis, J. Anal. At. Spectrom. 18 (2003) 1400.
[17] R. Cerdeira de Campos Costa, A.N. Araujo, Anal. Chim. Acta 438 (2001) 227.
[18] G. Tao, Z. Fang, J. Baasner, B. Welz, Anal. Chim. Acta 481 (2003) 273.
[19] Standard Methods for the Examination of Water and Wastewater, APHA, AWWA, WEF, Washington, 19th ed., 1995.
[20] Z.-S. Liu, S.-D. Huang, Anal. Chim. Acta 267 (1992) 31.
[21] R.H. Atallah, J. Ruzicka, G.D. Christian, Anal. Chem. 59 (1987) 2909.

Talanta 77 (2008) 663–666

Contents lists available at ScienceDirect

Talanta

journal homepage: www.elsevier.com/locate/talanta

Cloud point extraction for ultra-trace Cd determination in microwave-digested biological samples by ETAAS

Pedro R. Aranda, Raúl A. Gil, Susana Moyano, Irma De Vito, Luis D. Martinez*

Área de Química Analítica, Facultad de Química, Bioquímica y Farmacia Universidad Nacional de San Luis-Instituto de Química San Luis (INQUISAL-CONICET), Chacabuco y Pedernera, CP 5700 San Luis, Argentina

ARTICLE INFO

Article history:
Received 5 May 2008
Received in revised form 5 July 2008
Accepted 7 July 2008
Available online 15 July 2008

Keywords:
Cadmium
Urine samples
Cloud point extraction
Chemical modifiers
ETAAS

ABSTRACT

Cloud point extraction (CPE) has been used for the preconcentration of cadmium, after the formation of a complex with 2-(5-bromo-2-pyridylazo)-5-(diethylamino)-phenol (5-Br-PADAP), and further determination by graphite furnace atomic absorption spectrometry (ETAAS) using polyethyleneglicolmono-*p*-nonyphenylether (PONPE 7.5) as surfactant. The chemical variables that affect the cloud point extraction were optimized. The separation of the two phases was easily accomplished by cooling the mixture in order to make more viscous the surfactant-rich phase. In order to establish the optimum conditions for the determination of Cd by ETAAS, Pd + Mg, Pt, Ir, Rh and Ru were studied as chemical modifiers. The best thermal stabilization was obtained with Pd + Mg, with a maximum pyrolysis temperature of 1100 °C. Under the optimum conditions i.e., pH 9.0, [5-Br-PADAP] = 2.0×10^{-5} mol L^{-1}, [PONPE 7.5] = 0.02% (w/v), an enhancement factor of 22-fold was reached. The lower limit of detection (LOD) obtained under the optimal conditions was 0.008 μg L^{-1}. The precision for 10 replicate determinations at 0.2 μg L^{-1} Cd was 3.5% relative standard deviation (R.S.D.). The calibration graph using the preconcentration method was linear with a correlation coefficient of 0.9984 at levels close to the detection limit up to at least 1.0 μg L^{-1}. The method was successfully applied to the determination of cadmium in urine samples and in a water standard reference material.

1. Introduction

Cadmium is one of the most toxic elements and accumulates in humans mainly in the kidneys and liver. A prolonged intake of cadmium leads to calcium regulation in biological systems, which induces cell injury and death. It also inhibits the action of zinc enzymes by substitution. Cd is also a teratogenic and carcinogenic agent [1].

Cd enters the organism primarily via the alimentary and/or respiratory tract. The sources of this metal are food, drinking water and air [2]. Due to that, trace and ultra-trace determinations of Cd in environmental and biological samples have become of increasing interest [3]. The exposure is obviously dependent upon the emission of that element and might be particularly serious in factories; 50% of inhaled Cd, for example, is absorbed and most of it is concentrated in the liver and kidneys [4].

ETAAS appears as one of the most popular analytical technique for Cd determination in a great variety of matrixes [5–9], and the conventional solution sample introduction is the most widely used method for a vast majority of samples [10].

However, the determination of trace elements in biological samples is particularly difficult because of the complexity of matrix and the usually low concentration that these elements present in such samples, requiring sensitive instrumental techniques and a preconcentration step in order to determine them [11–14].

The use of the CPE process for extraction of metals, metal chelates, biomolecules, many types of organic species and environmental clean-up procedures has been reported [15,16]. Nevertheless, the coupling of CPE to instrumental methods is not an easy challenge. The effect of the experimental parameters on the extraction and sensitivity has to be thoroughly evaluated and optimized. The optimal combination of experimental variables leads to higher extraction percentage, optimal stability, lower equilibration time and ease of phase separation.

The use of micellar systems as an alternative to other techniques of separation offers several advantages, including low cost, safety and high capacity to concentrate a wide variety of analytes distributed widely in nature, varying with high recoveries and high concentration factors. From an analytical point of view, the surfactant-rich phase can be used to separate and/or

* Corresponding author.
E-mail address: ldm@unsl.edu.ar (L.D. Martinez).

0039-9140/$ – see front matter © 2008 Elsevier B.V. All rights reserved.
doi:10.1016/j.talanta.2008.07.009

preconcentrate different analytes before their determination [15].

CPE in connection with graphite furnace atomic absorption spectrometry has been a powerful analytical technique for Cd preconcentration and determination analysis [17,18] This scheme is an efficient alternative, particularly because the organic matrix consisting in the surfactant and residual organic substances from the digested materials can be eliminated at least in part during the gradual increase in temperature prior to the atomization of the analyte.

The use of a chemical modifier, which is part of the stabilized temperature platform furnace (STPF) concept in ETAAS [19], has been the subject of several investigations since its first proposal in 1975 by Ediger [20]. The main purpose of a chemical modifier is to increase the volatility of the matrix or to thermally stabilize the analyte to higher temperatures for removal of the matrix during pyrolysis [21] without loss of the analyte. A mixture of Pd and Mg nitrates, applied in solution, has been proposed as a universal modifier since it stabilizes more than 20 analytes [22]. In addition, other chemical elements have shown modifier properties, such as the platinum element group (Pt, Pd, Ir, Rh, and Ru) or the carbide-forming elements [21–23,10].

The aim of this study was to develop an ultra-trace Cd determination method. In this way, a CPE method was proposed to be coupled to ETAAS in order to perform a sensitive cadmium determination in biological samples with minimal requirements of reagents and sample consumption after a microwave-assisted digestion which ensured accurate Cd determinations. For this purpose, cadmium was extracted as Cd-2-(5-Br-2-pyridylazo)-5-diethylaminophenol [Cd (II)-(5-Br-PADAP)] complex mediated by micelles of non-ionic surfactant PONPE 7.5.

All significant variables for CPE were studied including pH of extraction, surfactant and reagent concentration. On the other hand, all variables related to the ETAAS determination, were also studied, i.e. pyrolysis and atomization temperatures and effect of different chemical modifiers. As palladium–magnesium mixed modifier has been successfully used for the analysis of biological and environmental matrices [10], the modifier performance was tested in an organic matrix (surfactant-rich phase). Additionally, Pt as regular modifier and three permanent modifiers, e.g. Ir, Rh and Ru were tested.

The developed method was applied to the determination of trace cadmium in urine samples and in a certified reference material (QC METAL LL2).

2. Experimental

2.1. Instrumentation

The measurements were performed with a Shimadzu Model AA-6800 Atomic Absorption Spectrometer (Tokyo, Japan), equipped with a deuterium background corrector, a 6500-electrothermal atomizer and an ASC-6100 autosampler. Stabilized platform (L'Vov) graphite tubes (Shimadzu, Tokyo, Japan) were used in all experiments. Cadmium hollow-cathode lamp (Hamamatsu, Photonics K.K., Japan) was employed as radiation source. All measurements were performed using integrated absorbance (peak area). The temperature program for ETAAS analysis is shown in Table 1. The 228.8 nm Cd wavelength was used in the subsequent determinations. The background correction was made with deuterium lamp mode.

Microwave digestion was performed with a domestic microwave oven (Philco, Ushuaia, Argentina) operating at a maximum power of 700 W, equipped with a magnetron of 2450 MHz and Milestone hermetically sealed 100 mL internal volume, 1 cm wall thickness polytetrafluoroethylene (PTFE) reactors.

Table 1
Furnace temperature program for Cd determination

Stage	Temperature (°C)	Ramp (s)	Hold (s)	Argon gas flow (L min^{-1})
Drying	140	5	15	1.0
Pyrolysis	1100	5	35	1.0
	1100	–	1	0.0 (read)
Atomization	1800	–	2	0.0 (read)
Clearing	2400	–	2	1.0

2.2. Reagents

All reagents were of analytical-reagent grade and the presence of the cadmium was not detected within the working range. A stock standard solution of cadmium at a concentration of 1000 μg mL^{-1} was prepared from pure cadmium nitrate-4-hydrate (E. Merck, Darmstadt, Germany) in 0.4 mol L^{-1} HCl (E. Merck). Working standard solutions were obtained by stepwise diluting the stock standard solution. A 0.01 mol L^{-1} solution of 5-Br-PADAP (Aldrich, Milwaukee, WI, USA) and the surfactant polyethyleneglycolmono-*p*-nonyphenylether (PONPE 7.5) (Tokyo, Kasei Industries, Chuo-Ku, Tokyo, Japan) were prepared as it was described earlier [24].

The buffer solution (0.005 mol L^{-1}) was prepared dissolving sodium tetraborate (Merck, Darmstadt, Germany) and taken to 1000 mL with ultrapure water. A $NaClO_4$ (Merck, Darmstadt, Germany) solution was used in order to adjust ionic strength. Nitric acid (Fluka, Sigma–Aldrich, Seelze, Germany) used for sample pretreatment was of ultrapure reagent grade.

Mg, Ir, Pd, Pt, Rh and Ru were prepared from highest purity salts and the presence of Cd was not detected in the final solutions obtained.

All solutions containing potentially interfering ions were prepared by adding appropriate amounts of stock solutions made from Merck Titrisol or their chloride salts in 0.3 mol L^{-1} hydrochloric acid.

Ultrapure water (18.1 MΩ cm) was obtained from Barnstead EASY pure RF water system (Iowa, USA).

All solvents and reagents were of analytical-reagent grade or better, and the presence of cadmium was not detected in the working range.

2.3. Sample pre-treatment

Urine samples were collected in the morning from voluntary patients and were digested immediately as follows: 8 mL of urine were placed in a 100 mL PTFE reactor and after that, 2 mL of concentrated nitric acid and 2 mL of hydrogen peroxide were added. Then the samples were digested applying different microwave powers, i.e. MW power was held at 250 W (5 min), 250 W (5 min), 500 W (5 min), 500 W (5 min). The vessels were then removed from the oven and cooled at 20° C, after that, they were cooled and opened.

2.4. Experimental procedure

The general CPE methodology was carried out as it was described in a previous work [24].

The preconcentration procedure started with the addition of 0.5 mL of surfactant solution, 0.1 mL of 0.01 mol L^{-1} chelating solution, 1.5 mL of 8×10^{-5} mol L^{-1} metal–ion solution and 5.0 mL of

buffer solution (pH 9.0) were placed in a centrifuge tube. The mixture was diluted to 50 mL with ultrapure water.

After that the mixture was heated (70 °C during 10 min) and cooled (10 min) in order to achieve the phase separation.

The removal of the aqueous phase was carried out by simply inverting the tubes. Any residual water was removed using a Pasteur pipette. External calibration was performed by the same cloud point extraction procedure. Additionally, an internal calibration was made in selected samples. A blank submitted to the same procedure described above was measured parallel to the samples and calibration solutions.

3. Results and discussion

3.1. Graphite furnace temperature programs

A study of the best conditions for graphite furnace determination was carried out by optimization of the temperature program, i.e. ramp and hold time, and drying, pyrolysis and atomization temperatures. For this purpose, a cloud point extraction prepared from an aqueous solution containing 0.2 μg L^{-1} of Cd was employed for all experiments. To reduce the viscosity of the surfactant phase prior to ETAAS analysis, 1.0 mL of methanol acidified with 0.1 mol L^{-1} HNO_3 was added to the extract. Suitable amounts of Pd–Mg solution were co-injected with the extract directly into the graphite furnace. Additionally, in order to obtain the most suitable times and temperatures, the common way of working in graphite furnace AAS was followed. The drying temperature was selected at 140 °C, with a hold time of 15 s, which was enough to take out the solvent completely.

Pyrolysis temperatures lower than 700 °C could not be used, since matrix components were not eliminated efficiently under these conditions, and background was considerable, leading in some cases to over-correction and, as a consequence, erroneous absorption values for the analytes. The ramp time for the pyrolysis stage was carefully adjusted to allow gradual elimination of the matrix, avoiding any analyte loss by a sudden increase in temperature.

Fig. 1 shows the pyrolysis curves obtained when different regular or permanent modifiers were employed. The chemical modifiers: Ir, Pd + Mg, Pt, Rh and Ru, were tested in order to maximize the thermal stability of Cd. It is evident that the best thermal stabilization was reached when 20 μg Pd + 20 μg Mg were co-injected with the extract.

Besides the thermal stabilization reached with the mixed modifier, a further thermal stabilization could be attributed to the addition of methanol–HNO_3, since the background signal diminished considerably when this mixture was added to the extract.

The atomization stage was studied in the range of 1300–2200 °C The optimum atomization temperature was selected at 1800 °C within the temperature interval studied. In addition, a hold time of 2 s was selected for this step. Atomization temperatures for standards and samples were not different, and then the temperature of 1800 °C was considered for both.

A temperature of 2200 °C and a hold time of 2 s were selected for cleaning step.

3.2. Study of the CPE system variables

The effect of pH upon the complex formation of Hg-5-Br-PADAP was studied within the range of pH 5–12. The results are shown in Fig. 2. The complex extraction begins at pH 6.0 and starts to decrease at pH 9.7, showing a plateau at pH values between 7.5 and 9.5. Then a pH 8.5 was chosen for further experiments.

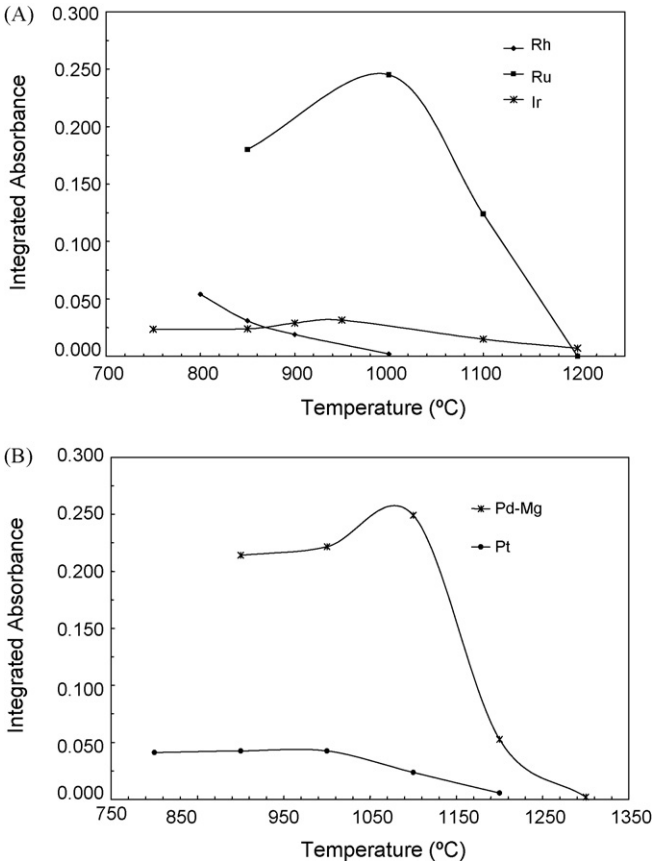

Fig. 1. Optimization of pyrolysis conditions for Cd determination in CPE extracts with methanol acidified with 0.1 mol L^{-1} HNO_3. (A) Pyrolysis curve of Cd (0.5 μg L^{-1}) with Pd + Mg or Pt regular modifiers; (B) pyrolysis curve of Cd (0.5 μg L^{-1}) with Ir, Rh or Ru permanent modifiers.

The extraction efficiency was examined as the surfactant concentration was varied within the range from 0.025 to 1.5% (v/v). Quantitative extraction was observed for a surfactant concentration higher than 0.07% (v/v). Thus, 0.2% (v/v) was chosen as optimal.

The reagent to metal ratio was studied to establish the concentration of 5-Br-PADAP necessary to achieve the best Cd recoveries. Above a reagent to metal ratio of 20:1, no variation took place in

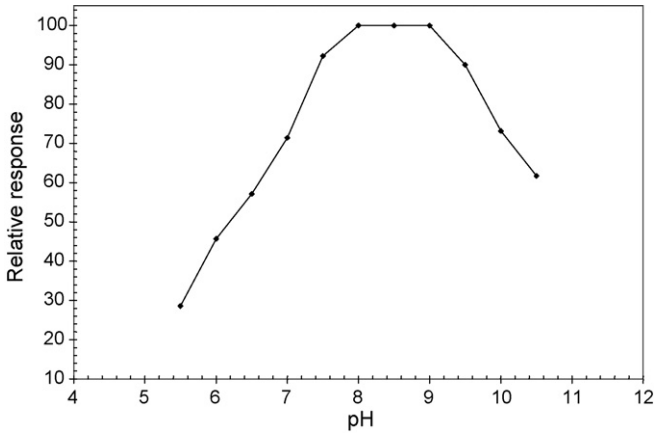

Fig. 2. Pyrolysis and atomization curves for cadmium submitted to cloud point extraction. Conditions: 1.0 mL of 0.01 mol L^{-1} HNO_3 in methanol added to micellar phase, and Pd + Mg modifier co-injected.

Table 2
Concentrations of Cd in human urine samples (95% confidence level; $n = 6$)

Cd added ($\mu g\,L^{-1}$)	Cd found ($\mu g\,L^{-1}$)	Recovery (%)[a]
0.0	1.06 ± 0.02	–
0.2	1.25 ± 0.03	95
0.4	1.45 ± 0.02	97

[a] [(Found-base)/added] × 100.

the analytical signal. However, a regent excess of 80 was selected in order to avoid interferences from foreign ions of the sample matrix.

Sodium tetraborate was chosen as buffer and its concentration was studied within the range: 5×10^{-4} to 5×10^{-2} mol L^{-1}. Additionally, the ionic strength was studied within the range: 0–1 mol L^{-1}, adjusted with $NaClO_4$. The highest extraction percentage; optimal stability; lowest equilibration time and ease of phase separation, were achieved for a sodium tetraborate concentration of 0.005 mol L^{-1} and an ionic strength up to 0.35 mol L^{-1}.

3.3. Interferences

The effects of representative potential interfering species were tested. Thus, Co^{2+}, Cu^{2+}, Hg^{2+}, Mn^{2+}, $Ni^{2+}$and Fe^{3+} could be tolerated up to at least 2000 $\mu g\,L^{-1}$. Commonly encountered matrix components such as alkali and alkaline earth elements generally do not form stable complexes under the experimental conditions, and were not CPE-extracted. The value of the reagent blank signal was not modified by the presence of the potentially interfering ions assayed. A high concentration of 5-Br-PADAP reagent was added in order to assure the complete chelation of the analyte even in the presence of interferents.

3.4. Analytical performance

The detection and quantification limits (LOD and LOQ) were established. For this reason, 10 blank extracts were performed following the overall procedure. The values obtained were 8 ng L^{-1} for LOD and 27 ng L^{-1} for LOQ (by considering 3 and 10 times the standard deviation, respectively). The precision of the method was evaluated at 0.2 $\mu g\,L^{-1}$ Cd and the value obtained as relative standard deviation (R.S.D.%) was equal to 3.5%. Finally, a sensitive enhancement factor of 22 (calculated as the ratio between the slopes of the calibration plots before and after CPE) was achieved.

3.5. Method validation

In order to evaluate the accuracy of the proposed method, Cd was determined in a standard reference material, QC METAL LL2 metals in natural water, with a cadmium content of 1.97 ± 0.11 $\mu g\,L^{-1}$. Employing the proposed method, the content of cadmium determined in this SRM was 1.90 ± 0.09 $\mu g\,L^{-1}$ (95% confidence interval; $n = 6$).

In addition, Cd was analyzed in urine samples mineralized by a microwave-assisted digestion. The obtained concentrations were in the range of 0.58–1.21 $\mu g\,L^{-1}$. Recovery studies were carried out in order to validate the results obtained in each sample. These results are shown in Table 2.

4. Conclusion

In this work, the use of micellar systems as an alternative to other techniques of separation and offers several advantages including low cost, safety and high extraction efficiency. Cadmium was determined by ETAAS in the surfactant-rich phase when Mg + Pd were used as matrix modifier. This method is a promising alternative for Cd determination which joints the advantages of the CPE with the obvious advantages of any ETAAS method, i.e. minimal reagent employment, feasibility, low cost and sensibility. Additionally, the microwave digestion makes it such a versatile method, being adequate for environmental and biological studies.

Acknowledgments

This work was supported by Consejo Nacional de Investigaciones Científicas y Técnicas (CONICET); Agencia Nacional de Promoción Científica y Tecnológica (FONCYT) (PICT-BID) and Universidad Nacional de San Luis (Argentina).

References

[1] R. Eisler, Handbook of Chemical Risk Assessment: Health Hazards to Humans, Plants and Animals, vol. 1, Lewis Publishers, New York, NY, USA, 2000 (Chapters 1 and 4).
[2] J.L. Manzoori, G. Karim-Nezhad, Anal. Chim. Acta 521 (2004) 173.
[3] L. Li, B. Hu, L. Xia, Z. Jiang, Talanta 70 (2006) 468.
[4] R. Fernandez Orsi, R. Wuilloud, J. Wuilloud, R. Olsina, L. Martinez, J. AOAC Int. 85 (2002) 1410.
[5] M.G.R. Vale, M.M. Silva, B. Welz, E.C. Lima, Spectrochim, Acta Part B 56 (2001) 1859.
[6] M. Zemberyová, J. Barteková, M. Závadská, M. Sisolákova, Talanta 71 (2007) 1661.
[7] O. Acar, Anal. Chim. Acta 545 (2005) 244.
[8] T.G. Kazi, A.R. Memon, H.I. Afridi, M.K. Jamali, M.B. Arain, N. Jalbani, R.A. Sarfraz, Sci. Total Environ. 389 (2008) 270.
[9] M. Vilar Fariñas, J. Barciela García, S. García Martín, R. Peña Crecente, C. Herrero Latorre, Anal. Chim. Acta 591 (2007) 231.
[10] J. González-Nieto, J.F. López-Sánchez, R. Rubio, Talanta 69 (2006) 1118.
[11] S. Kunnath Subramanian, Spectrochim. Acta B 51 (1996) 291.
[12] A. Taylor, S. Branch, D. Halls, M. Patriarca, M. White, J. Anal. At. Spectrom. 17 (2002) 414.
[13] A. Taylor, S. Branch, A. Fisher, D. Halls, M. White, J. Anal. At. Spectrom. 16 (2001) 421.
[14] Irma E. De Vito, Roberto A. Olsina, Julio Raba, Adriana N. Masi, Anal. Chim. Acta 501 (2004) 11.
[15] M.F. Silva, S. Cerutti, L.D. Martinez, Microchim. Acta 155 (2006) 349.
[16] F. Shemirani, N. Shokoufi, Anal. Chim. Acta 577 (2006) 238.
[17] T.A. Maranhao, D.L.G. Borges, M.A.S. da Veiga, A.J. Curtius, Spectrochim. Acta B 60 (2005) 667.
[18] C.G. Yuan, G.B. Jiang, Y.Q. Cai, B. He, J.F. Liu, At. Spectrosc. 25 (2004) 170.
[19] W. Slavin, D.C. Manning, G.R. Carnrick, At. Spectrosc. 2 (1981) 137.
[20] R.E. Ediger, At. Absorpt. Newsl. 14 (1975) 127.
[21] M.B.O. Giacomelli, J.B.B. da Silva, T.D. Saint'Pierre, A.J. Curtius, Microchem. J. 77 (2004) 151.
[22] B. Welz, G. Schlemmer, J.R. Mudakavi, J. Anal. At. Spectrom. 7 (1992) 1257.
[23] D.A. Maria, M.C. Rollemberg, J.B. Borda da Silva, At. Spectrosc. 26 (2005) 4.
[24] P.R. Aranda, R.A. Gil, S. Moyano, I.E. De Vito, L.D. Martinez, Talanta 75 (2008) 307.

Talanta 77 (2008) 695–700

Contents lists available at ScienceDirect

Talanta

journal homepage: www.elsevier.com/locate/talanta

Separation of U and Pu in spent nuclear fuel sample using anion-exchange-group-introduced porous polymer sheet for ICP-MS determination

Shiho Asai[a,*], Masaaki Magara[a], Nobuo Shinohara[a], Shinsuke Yamada[b], Masanori Nagai[b], Kazuyoshi Miyoshi[c], Kyoichi Saito[c]

[a] Division of Environment and Radiation Sciences, Japan Atomic Energy Agency, Ibaraki 319-1195, Japan
[b] INOAC Corporation, Atsuta, Nagoya 456-0054, Japan
[c] Department of Applied Chemistry and Biotechnology, Chiba University, Inage, Chiba 263-8522, Japan

ARTICLE INFO

Article history:
Received 30 March 2008
Received in revised form 4 July 2008
Accepted 4 July 2008
Available online 15 July 2008

Keywords:
Porous sheet
Graft polymerization
Anion-exchange
Decontamination factor
ICP-MS
Spent fuel

ABSTRACT

Anion-exchange porous sheets were prepared by radiation-induced graft polymerization and subsequent chemical modifications. A diethylamino (DEA) group as an anion-exchange group was introduced into the polymer chain grafted onto a porous sheet. The DEA group-introduced porous sheet was cut into disks 13 mm in diameter and 3 mm in thickness to fit an empty cylindrical cartridge (DEA cartridge). The DEA sheet had a DEA group of 3.4 mol/kg of the DEA-group-containing porous sheet and a linear velocity of 46 m/h at a permeation pressure of 0.1 MPa at 298 K. The adsorption capacity of the DEA cartridge for $FeCl_4^-$ as a model ion in equilibrium with 1 g-Fe(III)/L in 10 M HCl was 0.17 mmol-Fe(III)/DEA cartridge. No Pu leakage during the permeation of 5 mL of 10 M HCl–0.1 M HNO_3 containing Pu ionic species through the DEA cartridge was observed irrespective of the permeation rate ranging from 0.3 to 80 mL/min. A solution containing known amounts of ^{233}U, ^{240}Pu, and ^{241}Am in 10 M HCl–0.1 M HNO_3 was loaded onto the DEA cartridge. U and Pu were retained on the DEA cartridge, while Am was allowed to pass through the DEA cartridge. Subsequently, 7 M HNO_3 and 1 M HCl as eluents were permeated to elute U and Pu from the DEA cartridge, respectively. The decontamination factor of U in a Pu fraction, defined by dividing the activity of U in the feed solution by that of U in the Pu fraction, was 2.7×10^5, which is desirable for the highly accurate ICP-MS determination of Pu for samples containing both U and Pu. The method using the DEA cartridge was validated by measuring isotopic compositions and quantities of U and Pu in a spent nuclear fuel sample by double-focusing magnetic sector ICP-MS.

1. Introduction

The determination of elemental and isotopic compositions of U and Pu in spent nuclear fuels is required for the management of radioactive wastes and for the evaluation of calculation codes based on neutron flux [1,2]. The removal of interfering elements in a spent nuclear fuel sample dissolved with nitric or hydrochloric acids is indispensable for an accurate determination of U and Pu by alpha spectrometry, inductively coupled plasma-mass spectrometry (ICP-MS) [3–5], or thermal ionization mass spectrometry (TIMS) [1,6,7]. Numerous methods for the separation and purification of U and Pu have been suggested. Of these methods, the method using a column charged with ion-exchange resins has been widely employed [6,8,9]. Due to the insufficient selectivity of the ion-exchange resins, several columns were combined to separate U and Pu; therefore, these methods are tedious and time-consuming for a routine analysis.

Recently, extraction chromatographic resins, onto which highly selective organic extractants, e.g., CMPO and Aliquat 336, impregnated, have received considerable attention because they simplified the separation of actinides [10–15]. For example, Morgenstern et al. [12] demonstrated a mutual separation of U, Pu, Np, and Am using a single column charged with a uranium-selective extraction chromatographic resin (UTEVA resin). However, the diffusion of target ions to the extractant impregnated onto the interior of the resin is a rate-determining step, resulting in the low recovery of the target ions at a high flow rate through the column.

We have thus far developed functional porous polymeric membranes with high performance, by the radiation-induced graft polymerization of an epoxy-group-containing vinyl monomer and the subsequent addition of various chemicals to the epoxy group of

* Corresponding author. Tel.: +81 29 282 3668; fax: +81 29 282 3668.
E-mail address: asai.shiho@jaea.go.jp (S. Asai).

0039-9140/$ – see front matter © 2008 Elsevier B.V. All rights reserved.
doi:10.1016/j.talanta.2008.07.012

the graft chain [16]. For example, an iminodiacetate (IDA)-group-containing porous hollow-fiber membrane exhibited a high-speed collection of various metal ions [17,18]. The permeative flow of a metal solution through the pores driven by transmembrane pressure ensures the negligible diffusional mass-transfer resistance of metal ions. In other words, the time required for metal ions to diffuse to the ion-exchange group of the polymer chain grafted onto the pore is much shorter than the residence time of the metal solution to permeate across the porous membrane [17–21].

In our previous publication [21], we suggested a simple method for the separation of actinides using an anion-exchange cartridge charged with a diethylamino (DEA)-group-containing porous sheet (DEA cartridge). Decontamination factors estimated from the elution profiles of U, Pu, and Am obtained by elution chromatography were higher than 10^4 for both U and Pu fractions. However, the applicability of the DEA cartridge to the simple and accurate determination of U and Pu in a spent nuclear fuel sample has not yet been validated.

The objective of this study was twofold: (1) to evaluate the permeability and adsorptivity of the DEA cartridge and (2) to validate the applicability of the DEA cartridge to the separation of U and Pu in a spent nuclear fuel sample. We obtained DFs that are more accurate than those described in the previous publication [21] by the acquisition of detailed elution profiles and thus applied this method to the determination of a trace amount of Pu (<pg) in the spent nuclear fuel.

2. Experimental

2.1. Chemicals, standard solutions, and materials

Glycidyl methacrylate (GMA, $CH{=}CCH_3COOCH_2CHOCH_2$) was purchased from Tokyo Kasei Co. and used without further purification. An iron standard solution ($FeCl_3$ in 3% HNO_3) was acquired from Wako Pure Chemical Industries. Hydrochloric and nitric acids used for separation and ICP-MS analysis were of super-pure grade (AA-10, Tama Chemicals). Other reagents were of analytical grade. Standard solutions of ^{233}U, ^{240}Pu, and ^{241}Am were supplied by Isotope Products Laboratories (IPL), Oak Ridge National Laboratory (ORNL), and the National Institute of Standard and Technology (NIST), respectively.

A porous sheet, made of high-density polyethylene, with a thickness, porosity, and average pore size of 2 mm, 75%, and 1.0 μm, respectively, was used as a trunk polymer for grafting. This porous sheet, supplied by INOAC Corporation, was referred to as a PE sheet. For comparison, anion-exchange resin beads (MCI-GEL CA08Y) were purchased from Mitsubishi Chemical Corporation.

2.2. Preparation of anion-exchange cartridge

The anion-exchange porous sheet was prepared by the graft polymerization of GMA and the subsequent introduction of a DEA group ($-N(C_2H_5)_2$) as an anion-exchange group into the graft chain. Briefly, the preparation scheme consisted of the following three steps: the first step was the irradiation of electron beams to produce radicals, that is, the PE sheet was irradiated with electron beams at a dose of 200 kGy. The second step was the graft polymerization of GMA, that is, the electron-beam-irradiated porous sheet was immersed into 20% (v/v) GMA/methanol solution at 313 K for 7 min. The degree of GMA grafting, defined as the mass gain of the porous sheet in percentage, was set at 200%, and the resultant GMA-grafted porous sheet was referred to as a GMA sheet. The third step was the introduction of a DEA group, that is, the DEA group was introduced into the graft chain by immersing the GMA sheet in 50% (v/v) diethylamine/water at 313 K. The resultant porous sheet was referred to as a DEA sheet.

The amount of DEA group introduced was evaluated from the mass gain of the porous sheet as follows:

$$\text{Amount of DEA group introduced (mol/kg)} = (W_2 - W_1)/73/W_2 \quad (1)$$

where W_1 and W_2 are the masses of the GMA and DEA sheets, respectively. The numeral character 73 is the molecular mass of diethylamine.

The DEA sheet was cut into disks 13-mm in diameter. The resultant porous disk, DEA disk, was packed into an empty cylindrical cartridge 13 mm in diameter purchased from Varian, Inc. The DEA disk was sandwiched with prefilters on both sides of the DEA disk. The resultant cartridge was referred to as a DEA cartridge.

2.3. Properties of DEA sheet and disk

The swelling ratio in a dry state was evaluated by dividing the volume of the DEA sheet by that of the GMA sheet. The liquid permeability of the DEA disk was evaluated by measuring linear velocity (LV), defined below, at a constant permeation pressure of 0.1 MPa and 298 K with a syringe pump (Model 11 E, Harvard Apparatus)

$$\text{LV (m/h)} = \frac{\text{permeation rate of pure water}}{\text{cross-sectional area of DEA disk}} \quad (2)$$

For comparison, the LV of an anion-exchange-bead-packed column was also measured.

2.4. Determination of breakthrough characteristics and adsorptivity of DEA cartridge

$FeCl_4^-$ was selected as a model metal ion to estimate the elution chromatographic behavior of U(IV) in the hydrochloric acid medium [22]. A 1 g-Fe(III)/L iron solution dissolved in 10 M HCl was permeated upward through the DEA cartridge at a constant permeation rate of 20 mL/min with the syringe pump to determine an equilibrium adsorption capacity for $FeCl_4^-$. The effluent penetrating the upper surface of the DEA disk was continuously collected with fraction vials. The concentration of Fe of each fraction was determined by UV–Vis spectrometry. Subsequently, 0.01 M hydrochloric acid was permeated to elute $FeCl_4^-$ adsorbed onto the DEA disk.

^{240}Pu (11.9 ng) dissolved in 5 mL of 10 M HCl–0.1 M HNO_3 was fed to the DEA disk and permeated through the DEA cartridge. The permeation rate ranged from 0.3 to 80 mL/min. The total activity of each fraction of the effluent was determined using a silicon surface barrier detector (SSD) [23]. The adsorption efficiency, defined below, was calculated to evaluate the dependence of adsorptivity on permeation rate

$$\text{Adsorption efficiency (\%)} = \frac{100(\text{total activity of } ^{240}\text{Pu adsorbed on DEA cartridge})}{\text{total activity of } ^{240}\text{Pu in feed}} \quad (3)$$

2.5. Elution chromatography of actinides with DEA cartridge

A standard solution containing a prescribed amount of actinides was prepared: the masses of ^{233}U, ^{240}Pu, and ^{241}Am added to the solution were 48.0 μg (17,100 Bq), 0.965 μg (8100 Bq), and 0.797 μg (101,200 Bq), respectively.

The procedure of elution chromatography of U, Pu, and Am is shown in Fig. 1. This procedure consisted of the following four steps:

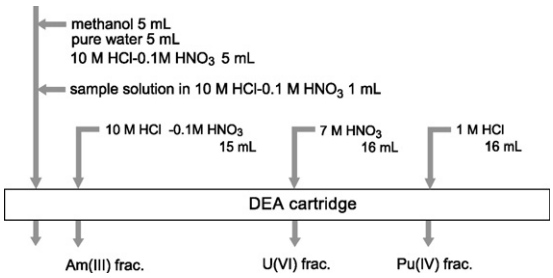

Fig. 1. Procedure for mutual separation of U(VI), Pu(IV), and Am(III) using DEA cartridge.

the first step was the adjustment of the oxidation state, that is, the standard solution containing ^{233}U, ^{240}Pu, and ^{241}Am was evaporated and then dissolved with 0.5 mL of 1 M HCl. Subsequently, the oxidation state of Pu was reduced to III with 10 μL of 1 M NH_2OH in 1 M HCl. After evaporating the solution, 1 mL of 10 M HCl–0.1 M HNO_3 was added to the residue to adjust the oxidation state of Pu to IV. The second step was the adsorption of U(VI) and Pu(IV), that is, 1 mL of the resultant solution was fed as a loading solution to the DEA cartridge. Then, the DEA cartridge was washed with 15 mL of 10 M HCl–0.1 M HNO_3 to remove Am(III) from the DEA cartridge, while U(VI) and Pu(IV) were adsorbed. The third step was the elution of U(VI), that is, 16 mL of 7 M HNO_3 was permeated through the DEA cartridge to elute U(VI), whereas Pu(IV) was retained. The fourth step was the elution of Pu(IV), that is, 16 mL of 1 M HCl was permeated to elute Pu(IV) retained to the DEA cartridge.

The effluent with a volume ranging from 0.25 to 12 mL was continuously sampled in fraction vials, and the activity of each fraction was measured using the SSD. Alpha-counting sources were prepared according to the "direct drop deposition method" proposed by Shinohara and Kohno [23]. The purity and recovery of a target nuclide of each fraction were evaluated by calculating the decontamination factor (DF) and recovery percentage defined as

$$\mathrm{DF}\ (-) = \frac{\text{activity of feed}}{\text{activity of each effluent}} \quad (4)$$

$$\text{Recovery percentage}\,(\%) = \frac{100\,(\text{activity in fraction})}{\text{activity of feed}} \quad (5)$$

The permeation rate was adjusted to a value higher than 2 mL/min with the syringe pump throughout the procedure.

2.6. Determination of U and Pu in spent nuclear fuel by elution chromatography with DEA cartridge

The procedure for the separation of actinides using the DEA cartridge was validated with a spent nuclear fuel sample solution. The spent nuclear fuel (fuel type: UO_2–GdO_3, burnup: 29.2 GWd/t) was obtained from a fuel lattice assembly of a boiling water reactor (Fukushima-daini). The fragment of the sample cut out from the rod, with a weight of approximately 300 mg, was dissolved in 7 M HNO_3. The portion of the sample solution was diluted to adjust the amounts of U and Pu to 37.08 pg-U and 0.3440 pg-Pu, respectively. The standard solution of ^{233}U (21.85 pg) and ^{242}Pu (0.17 pg) was added to calculate the concentration of each isotope in the fraction by the isotopic dilution method [24]. U, Pu, and Am were mutually separated by the procedure described in Section 2.5.

The activity concentrations of U and Pu in each fraction were determined by high-resolution ICP-MS (Element, Thermo Fisher Scientific, Inc.) The operation conditions of ICP-MS are summarized in Table 1, and mass bias correction was performed by the method reported by Magara et al. [25]. A relative error was set to be twice the standard deviation of the measurement.

Table 1
Operating conditions for ICP-MS

Frequency (MHz)	27.12
RF power (kW)	1.12–1.24
Sample gas flow rate (L/min)	1.01–1.06
Auxiliary gas flow rate (L/min)	1.03
Cooling gas flow rate (L/min)	16.0
Sampling uptake rate (L/min)	0.245
Sampling time (ms)	50
Scan per replicate	400
Number of replicates	5
Monitored isotopes	^{233}U, ^{234}U, ^{235}U, ^{236}U, ^{238}U ^{239}Pu, ^{240}Pu, ^{242}Pu

3. Results and discussion

3.1. Amount of anion-exchange group and liquid permeability of anion-exchange cartridge

The epoxy group of the polymer chain grafted onto the pore surface of the porous sheet was converted into a diethylamino (DEA) group. The time course of the amount of DEA group introduced into the poly-GMA grafted chain is shown in Fig. 2. The final amount of DEA group introduced was 3.4 mol/kg-DEA sheet at a reaction time of 90 min. The resultant amount of anion-exchange group introduced was higher than that of commercially available anion-exchange resin beads (MCI-GEL CA08Y).

The linear velocity (LV) as a function of the amount of DEA group introduced is shown in Fig. 3. The LV decreased with an increase in the amount of DEA group introduced. The mutual electrostatic repulsion of the positive charges of the DEA groups causes the graft chain to extend from the pore surface of the porous sheet toward the pore interior; therefore, the pore size of the DEA sheet decreased with an increase in the amount of DEA group introduced. The DEA sheet with an amount of DEA group introduced of 3.4 mol/kg-DEA sheet exhibited an LV of 46 m/h at 0.1 MPa comparable to the PE sheet (43 m/h). This LV value corresponded to a permeation rate of 101 mL/min through the surface area of 0.00133 m^2. The decrease in pore size was compensated by the swelling of the entire volume of the porous sheet, which was induced by the invasion of the graft chain into the matrix of the PE sheet.

The properties of the DEA disk and anion-exchange-bead-packed column used for the separation of actinides [26] are

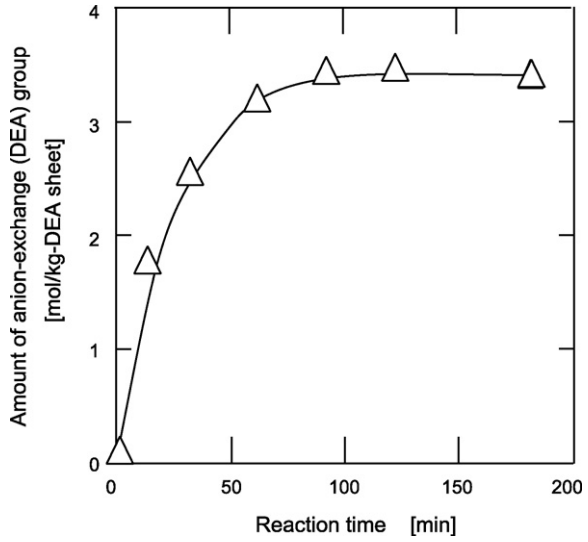

Fig. 2. Time courses of anion-exchange group (DEA group) introduced into the poly-GMA chain grafted onto the porous polymer sheet.

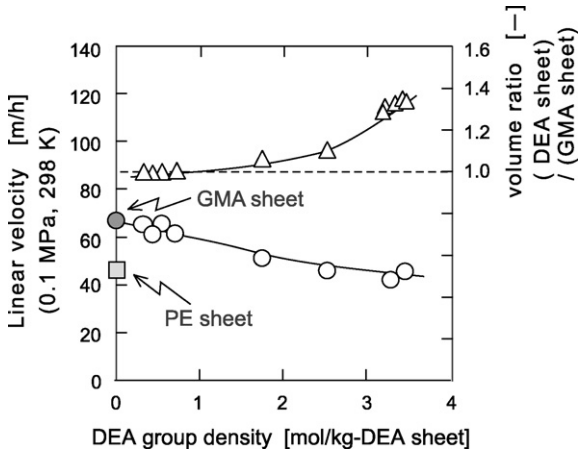

Fig. 3. Linear velocity and volume ratio as functions of amount of DEA group introduced.

compared in Table 2. The time required for pure water to permeate through the DEA cartridge driven by the gravity was shortened to 1/9 that through the anion-exchange-bead-packed column with an identical bed volume as the DEA disk.

3.2. Equilibrium adsorption capacity of DEA cartridge for Fe ions

An iron solution (1 g-Fe(III)/L in 10 M HCl) was forced to permeate through the pores of the DEA cartridge. The breakthrough curve of the DEA cartridge for Fe ions at a permeation rate of 20 mL/min, i.e., a residence time of 1.2 s of the solution across the DEA disk thickness, is shown in Fig. 4. The equilibrium adsorption capacity of the DEA disk for Fe ions, where the major ionic species of Fe(III) in 10 M HCl is $FeCl_4^-$, was calculated as 1.1 mol-Fe/kg-DEA sheet or 0.17 mmol-Fe/DEA cartridge. This value is comparable to those of conventional anion-exchange bead-packed columns.

3.3. Adsorption efficiency for Pu

^{240}Pu in 5 mL of 10 M HCl–0.1 M HNO_3 was permeated through the DEA cartridge in the permeation rate range of 0.3–80 mL/min, i.e., the residence time range of 78–0.30 s. The adsorption efficiency defined by Eq. (3) was 100% irrespective of the permeation rate, as shown in Fig. 5. This demonstrated that the higher permeation rate of the Pu solution led to the higher overall adsorption rate of Pu

Table 2
Comparison of properties of DEA cartridge and anion-exchange-bead-packed column

Adsorbent	MCI-GEL: CA08Y (strong base anion exchanger)	DEA cartridge (this study)
Structure	Styrene–divinylbenzene copolymer with trimethylammonium group	Diethylamino group-introduced polymer chain grafted onto porous sheet
Amount of anion-exchange group (mol/kg)	1.2	3.4
Bead diameter (μm)	25	–
Pore diameter (μm)	n.a.	0.15
Permeation time at gravity flow (min) (bed volume: 0.4 cm^3)	7	0.8

n.a.: not available in data supplied by manufacturer.

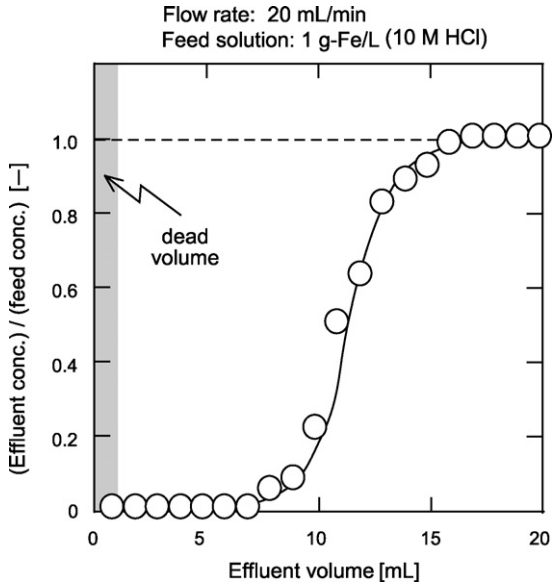

Fig. 4. Breakthrough curve of DEA cartridge during permeation of 1 g-Fe/L $FeCl_3$ solution.

onto the DEA disk owing to the negligible diffusional mass-transfer resistance of Pu ions in the pore interior to the DEA group of the polymer chain grafted onto the pore surface of the DEA disk. This adsorption characteristic of the functional-porous-disk-packed cartridge is advantageous over conventional functional-bead-packed columns in that a higher flow rate of the sample solution, i.e., a shorter processing time of analysis, is achievable.

3.4. Elution chromatographic performance of DEA cartridge for actinides

Prescribed amounts of ^{233}U, ^{240}Pu, and ^{241}Am were analyzed by elution chromatography by the procedure described in Section 2.5. The elution profiles of Am, U, and Pu, i.e., cpm corresponding to the counting rate of α-rays emitted by a target nuclide in each fraction as a function of effluent volume, are shown in Fig. 6(a). In this figure, cpm is the count rate of the α-rays detected by SSD. First, more than 99% of the amount of Am passed through the DEA cartridge during the permeation of 1 mL of the loading solution and 1 mL of 10 M HCl–0.1 M HNO_3 of a washing solution. Second,

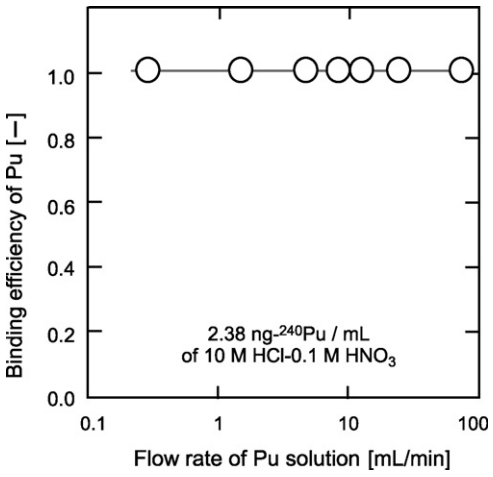

Fig. 5. Adsorption efficiency of Pu as function of flow rate.

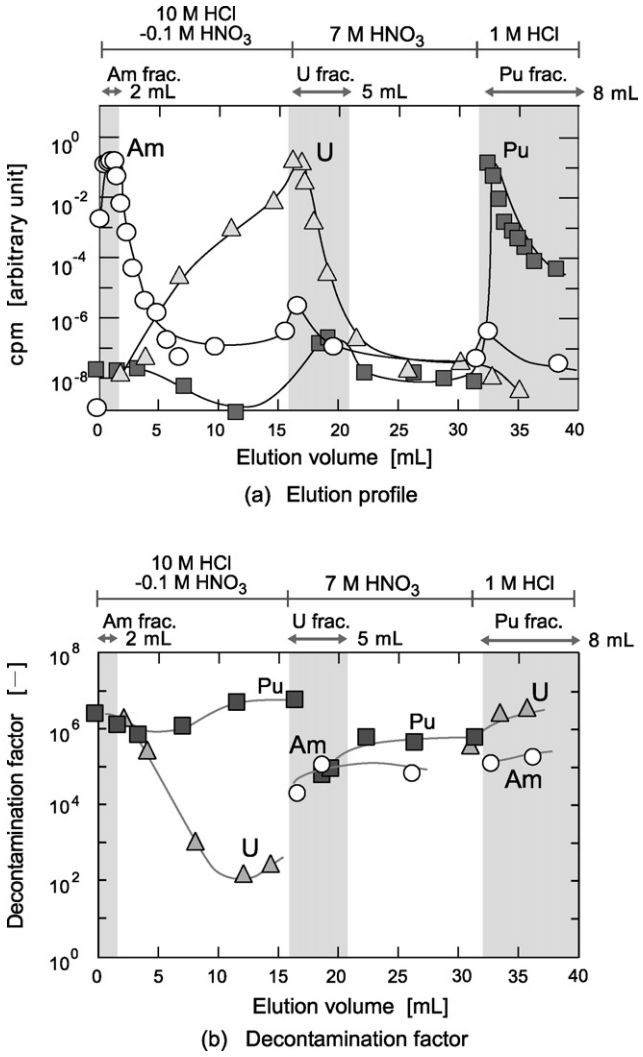

Fig. 6. Elution profiles and DFs of Am(III), U(VI), and Pu(IV) with 10 M HCl–0.1 M HNO_3, 7 M HNO_3, and 1 M HCl as respective eluents.

1% of the amount of U adsorbed onto the DEA cartridge was slightly eluted in another 14 mL of 10 M HCl–0.1 M HNO_3, whereas 99% of the amount of U was recovered by the subsequent permeation of 5 mL of 7 M HNO_3. Finally, Pu adsorbed onto the DEA cartridge was quantitatively eluted by permeating 8 mL of 1 M HCl.

DF, defined by Eq. (4), as a function of effluent volume is shown in Fig. 6(b). Two, five, and eight mL of 10 M HCl–0.1 M HNO_3, 7 M HNO_3, and 1 M HCl as eluents of Am, U, and Pu, respectively, as indicated by shaded region in Fig. 6(b), exhibited DFs ranging from 10^4 to 10^6. A DF value of 2.7×10^5 for U was observed in the Pu fraction, which is favorable for the determination of a trace amount of ^{239}Pu by ICP-MS because the isobaric interference at mass number 239 caused by the production of $^{238}U^1H^+$ arising from the sample matrix is minimized. These values demonstrated that this separation method using the DEA cartridge is applicable to the accurate determination of U, Pu, and Am in spent nuclear fuel samples.

3.5. Analysis of U and Pu in spent nuclear fuel sample with DEA cartridge

U, Pu, and Am in the solution of the spent nuclear fuel sample were separated using the DEA cartridge to validate the separation method described in Section 3.4. The isotopic abundances and elemental quantities of U and Pu in the spent nuclear fuel determined by ICP-MS are shown in Tables 3 and 4, respectively. The results agreed well with those obtained by TIMS measurement after separating U and Pu in an identical spent nuclear fuel solution using the conventional anion-exchange-bead-packed column (MCI-GEL, CA08Y) [26]. Trace amounts of U (38.16 pg) and Pu (0.34 pg) in the spent nuclear fuel were found to be successfully determined by the method suggested in this study.

Table 3
Isotopic abundances (%)[a] of U and Pu in spent nuclear fuel sample solution determined by ICP-MS

	Experimental value	Reference value
^{234}U	0.0190 ± 0.0006	0.0186
^{235}U	0.7826 ± 0.0042	0.7856
^{236}U	0.4774 ± 0.0066	0.4793
^{238}U	98.721 ± 0.009	98.7164
^{239}Pu	54.7 ± 0.2	54.75
^{240}Pu	30.7 ± 1.0	30.35

[a] Relative abundances of isotopes of an element.

Table 4
Quantities of U and Pu in spent nuclear fuel sample solution determined by ICP-MS

	Experimental value	Reference value
Total U (pg)	38.16 ± 1.70	37.08
Total Pu (pg)	0.34 ± 0.03	0.34

4. Conclusions

A rapid and accurate method for the separation of actinides using an anion-exchange porous sheet was described. A diethylamino (DEA) group as an anion-exchange group was introduced into the polymer chain grafted onto the pore surface of the porous sheet with a DEA density of 3.4 mol/kg and an equilibrium adsorption capacity of 1.1 mol-Fe(III)/kg of the DEA sheet. The resultant porous sheet was cut into disks 13 mm in diameter to fit a commercially available empty cylindrical cartridge. The time required for a liquid to permeate through the resultant DEA cartridge driven by the gravity was ninefold higher than that of the conventional column charged with the anion-exchange resin beads. Elution profiles for U, Pu, and Am observed by elution chromatography with the DEA cartridge were determined, using a standard solution containing known amounts of U, Pu, and Am, to evaluate decontamination factors. High decontamination factors indispensable for the accurate determination of the elemental quantity and isotopic abundances of U and Pu were achieved. The DEA cartridge is a promising alternative tool for actinide separation at high-speed and accuracy.

Acknowledgement

We are grateful to Nobuaki Kohno for helpful comments on the manuscript.

References

[1] F. Chartier, M. Aubert, M. Pilier, Fresenius J. Anal. Chem. 364 (1999) 320–327.
[2] J.I.G. Alonso, F. Sena, P. Arbore, M. Betti, L. r Koch, J. Anal. Atom. Spectrom. 10 (1995) 381–393.
[3] S.F. Boulyga, J.S. Becker, J. Anal. Atom. Spectrom. 17 (2002) 1143–1147.
[4] S.F. Boulyga, J.S. Becker, J.L. Matusevitchc, H.-J. Dietze, Int. J. Mass Spectrom. 203 (2000) 143–154.
[5] R.N. Taylor, T. Warneke, J.A. Milton, I.W. Croudace, P.E. Warwick, R.W. Nesbitt, J. Anal. Atom. Spectrom. 16 (2001) 279–284.
[6] K.O. Buesseler, J.E. Halverson, J. Environ. Radioactiv. 5 (1987) 425–444.
[7] E.L. Callis, R.M. Abernathey, Int. J. Mass. Spectrom. Ion. Process. 103 (1991) 93–105.

[8] N. Shinohara, N. Kohno, K. Suyama, J. Inagawa, Y. Nakahara, S. Kurosawa, K. Watanabe, S. Usuda, M. Oshima, H. Katsuta, M. Ito, Radiochim. Acta 89 (2001) 135–138.
[9] M.P.R. Montero, A.M. Sánchez, M.T.C. Vázquez, J.L.G. Murillo, Appl. Radiat. Isotopes 53 (2000) 259–264.
[10] E.P. Horwitz, M.L. Dietz, R. Chiarizia, H. Diamond, S.L. Maxwell III, M.R. Nelson, Anal. Chim. Acta 310 (1995) 63–78.
[11] K. Tagami, S. Uchida, Appl. Radiat. Isotopes 61 (2004) 255–259.
[12] A. Morgenstern, C. Apostolidis, R. Carlos-Marquez, K. Mayer, R. Molinet, Radiochim. Acta 90 (2001) 81–85.
[13] E.P. Horwitz, R. Chiarizia, M.L. Dietz, H. Diamond, D.M. Nelson, Anal. Chim. Acta 281 (1993) 361–372, TRU.
[14] M. Rodrígueza, J.L. Gascónb, J.A. Suárez, Talanta 45 (1997) 181–187.
[15] H. Lee, C.W. Lee, Talanta 54 (2001) 181–186.
[16] K. Saito, Sep. Sci. Technol. 37 (2002) 535–554.
[17] H. Yamaguchi, K. Saito, S. Furusaki, T. Sugo, I. Ichigaki, Ind. Eng. Chem. Res. 30 (1991) 2234–2237.
[18] S. Tsuneda, K. Saito, S. Furusaki, T. Sugo, J. Okamoto, J. Membr. Sci. 58 (1991) 221–234.
[19] S. Asai, K. Watanabe, T. Sugo, K. Saito, J. Chromatogr. A 1094 (2005) 158–164.
[20] S. Domon, S. Asai, K. Watanabe, T. Sugo, K. Saito, J. Membr. Sci. 262 (2005) 153–158.
[21] S. Asai, M. Magara, S. Sakurai, N. Shinohara, K. Saito, T. Sugo, J. Ion Exchange 18 (2007) 486–491.
[22] K.A. Kraus, F. Nelson, Proceedings of the First Geneva Conference, vol. 7, 1956, p. 113.
[23] N. Shinohara, N. Kohno, Appl. Radiat. Isotopes 40 (1989) 41–45.
[24] C.-S. Kim, C.-K. Kim, P. Martin, U. Sansone, J. Anal. Atom. Spectrom. 22 (2007) 827–841.
[25] M. Magara, T. Sakakibara, S. Kurosawa, M. Takahashi, S. Sakurai, Y. Hanzawa, F. Esaka, K. Watanabe, S. Usuda, J. Anal. Atom. Spectrom. 17 (2002) 1157–1160.
[26] Y. Nakahara, K. Suyama, T. Suzaki, JAERI-Tech 2000-071, 2000, pp. 95–114.

Talanta 77 (2008) 642–646

Contents lists available at ScienceDirect

Talanta

journal homepage: www.elsevier.com/locate/talanta

Evaluation of peroxide value of olive oil and antioxidant activity by luminol chemiluminescence

Siham Bezzi[a], Sofia Loupassaki[a], Christos Petrakis[a], Panagiotis Kefalas[a], Antony Calokerinos[b,*]

[a] Mediterranean Agronomic Institute of Chania, P.O. Box 85, Chania, 73100 Crete, Greece
[b] University of Athens, Department of Chemistry, Laboratory of Analytical Chemistry, Panepistimiopolis, 157 71 Athens, Greece

ARTICLE INFO

Article history:
Received 25 February 2008
Received in revised form 19 June 2008
Accepted 3 July 2008
Available online 17 July 2008

Keywords:
Olive oil
Chemiluminescence
Luminol
Peroxide value
Antioxidant activity

ABSTRACT

Three procedures are developed and investigated for the simple and fast determination of peroxide value of olive oil by luminol chemiluminescence. The procedure using hemin as catalyst in carbonate alkaline solution allows the determination of hydrogen peroxide within the range 0.014–50 μM. The method can be used for the determination of peroxide value within the range 2.00–30.0 mequiv. O_2/kg oil and results correlate very well (r^2 = 0.99) with those of the official method. All reagents are aqueous solutions and olive oil is dissolved in acetone:ethanol mixed solution and, hence, the method is using minimal amounts of organic solvents and can be successfully applied to field analysis. Antioxidant activity of five common compounds found in natural products was determined by using luminol CL with Co(II) as EDTA complex as catalyst at pH 9.00.

1. Introduction

Olive oil and other edible oils are complicated matrices and very often analytical results depend on various parameters such as adulteration. Official methods for the measurement of various quality factors such as acidity and peroxide content depend on titrations which are time consuming, laborious and erroneous. The official method for the determination of peroxide value is based on the iodometric titration of iodine, which is stoichiometrically liberated by the addition of excess of KI from oil peroxides. The method is highly empirical and accuracy depends on a variety of experimental factors, such as accurate timing and protection of the reaction mixture from light and atmospheric oxygen [1]. The reference procedure used for this analysis is accurately described by the European Community method [2]. A plethora of analytical procedures have been proposed as alternatives to the official titrimetric method for peroxide measurement. These methods include Fourier transform near-infra-red spectroscopy [3] or flow injection analysis with spectrophotometric detection [4]. Nevertheless, none of the proposed methods can be utilized as field analysers and some of them use high amounts of organic solvents.

It is well established within the literature that hydrogen peroxide and peroxides in general can be measured in aqueous media by luminol chemiluminescence (CL) [5,6] or in non-aqueous media by peroxyoxalate CL (PO-CL) [7]. PO-CL has been successfully applied to the determination of peroxide value of olive oil [8] but the reaction proceeds only in organic solvents. The use of organic solvents is considered as a drawback of the procedure since olive oil is usually consumed in conjunction with aqueous media and quality characteristics may vary from solvent to solvent. Hence it was decided to investigate whether peroxide value and other quality characteristics of olive oil can be chemiluminometrically measured in aqueous media.

Luminol was chosen as the CL reagent since it can be used in aqueous media for sensitive CL measurements and has been thoroughly investigated in a variety of applications. However, the main difficulty was to prepare a homogeneous solution of olive oil in water or in an organic solvent miscible with water. Initially, the olive oil was brought into solution by using Tween-20, Tween-80, tetradecyltrimethylammonium bromide (AmBr) and polyoxyethylene 9 lauryl ether (Polydocanol) with luminol in borate buffer (pH 9.00) in the presence of Co(II)–EDTA (procedure A). Procedure B was similar to procedure A except the oil sample was dissolved in the mixed solvent acetone:ethanol 2:1 (v/v). The same solvent was used in procedure C but the alkaline solution required for luminol was achieved by the presence of sodium carbonate and hemin was used instead of Co(II)–EDTA.

The oil substrate known as Delios S was initially used, followed by the application of the method in commercial oils. Delios S is a stable model oil mixture of triglycerides of caprylic (C-8) and

* Corresponding author.
E-mail address: calokerinos@chem.uoa.gr (A. Calokerinos).

0039-9140/$ – see front matter © 2008 Elsevier B.V. All rights reserved.
doi:10.1016/j.talanta.2008.07.019

capric (C-10) acids (70:30) which is used in the flavour industry, as well as for cosmetic and pharmaceutical skin care preparations, well-fatting emulsions and skin oils. The oil substrate has been successfully used previously for the measurement of PV value by PO-CL [8]. Furthermore, it was decided to develop a simple procedure, which would enable the successful field measurement of PV. Hence, the method was optimised for batch analysis and the final procedure can be applied in field analysers allowing estimation of the quality of olive oil by the producer.

2. Experimental

2.1. Apparatus

CL measurements were carried out using a Jenway 6200 Fluorimeter with the excitation lamp off and glass cuvettes of optical path equal to 10 mm.

2.2. Reagents

Acetonitrile, methanol, acetic acid, chloroform, *tert*-butylperbenzoate (*t*-BP, 98%, w/w), *tert*-butylhydroperoxide (*t*-BHP, 80%, w/w), cobalt(II) chloride hexahydrate, hydrogen peroxide (35%, v/v) were supplied by Merck, Germany. Ethanol, acetone, polyoxyethylene (20) and (80) sorbitan monolaurate (Tween-20 and -80), AmBr, Polydocanol, 3-aminophthalhydrazide (luminol), hemin and boric acid were supplied by Sigma, St. Louis, MO, USA while ethyl acetate (EtOAc) and 9,10-dimethylanthracene were obtained from Aldrich and Fluka Chemika, Germany, respectively. L-Ascorbic acid, β-carotene, quercetin and butylated hydroxytoluene were supplied by Sigma while α-tocopherol was supplied by Merck.

Delios S (CASR number: 73.398-61-5) is a mixture of triglycerides of vegetable medium-chain saturated fatty acids (Caprylic (C-8)/Capric (C-10) acids—70:30), was gracefully offered by Vioryl S.A., Greece.

All chemicals were of analytical grade. Aqueous solutions were prepared with doubly de-ionised water from a Labconco Water Pro^{TM} system (Kansas City, MO, USA).

2.3. Solutions

2.3.1. Borate buffer solution (pH 9.00)

Weigh 3.1 g of boric acid, dissolve in water and dilute with water to 1 L. Adjust to pH 9.00 by adding the appropriate amount of 1.00 M NaOH.

2.3.2. Co(II) (8.40×10^{-4} M)–EDTA (2.63×10^{-3} M) mixed solution

Weigh 0.500 mg of EDTA and 0.100 mg of $CoCl_2 \cdot 6H_2O$, dissolve and dilute with borate buffer (pH 9.00) solution to 500 mL. Solutions with different concentrations were prepared in a similar way.

2.3.3. Luminol solution (5.6×10^{-4} M)

Weigh 50 mg luminol, dissolve and dilute with borate buffer (pH 9.00) solution to 500 mL.

2.3.4. Luminol (7.0×10^{-4} M)–hemin (4.6×10^{-6} M) mixed solution

Weigh 3.0 mg hemin and 124 mg luminol, dissolve in 0.0100 M Na_2CO_3 and dilute with the same solution to 1 L.

2.4. Standard solutions

2.4.1. Hydrogen peroxide (100 mmol/kg) in Delios

10 g of Delios S were mixed with 5 mL of methanol and 260 μl of 5.81 M of H_2O_2 in a round bottom flask. The mixture was vigorously stirred on a rotary evaporator at room temperature for 30 min under vacuum in order to achieve homogeneous distribution of hydrogen peroxide in Delios, after removal of methanol and water. The final solution contained 100 mmol H_2O_2/kg oil (200 mequiv. O_2/kg oil). More dilute solutions were prepared in a similar way.

2.4.2. t-BP in Delios

0.0185 mL (0.100 mmol) of *tert*-butylperbenzoate (*t*-BP, 98%, w/w) are mixed with 1 g of Delios. The final solution contains 100 mmol *t*-BP/kg oil. More dilute solutions were prepared in a similar way.

2.4.3. t-BHP in methanol

112.5 mg of *tert*-butylhydroperoxide (*t*-BHP, 80%, w/w) are dissolved in 100 mL of methanol. The final solution contains 0.0100 M *t*-BHP. More dilute solutions were prepared in a similar way.

2.5. Commercial oil solutions

Weigh accurately 300 mg of oil, dissolve in 10% (w/w) Tween-20 (procedure A) or acetone: ethanol (2:1, v/v) mixed solvent (procedures B or C) and dilute to 10.00 mL. 0.500 mL of this solution were further diluted to 10.00 mL.

2.6. Measurement procedures

2.6.1. Procedure A

Mix 1.00 mL of 5.6×10^{-4} M luminol solution in borate buffer solution (pH 9.00) together with 1.00 mL of a mixed solution containing 7.3×10^{-4} M Co(II) and 2.3×10^{-3} M EDTA, inject 100 μL of sample solution in 10% (w/w) Tween-20 and record the change of emission intensity as a function of time.

2.6.2. Procedures B and C

Procedure B is similar to procedure A except the sample is dissolved in acetone:ethanol (2:1, v/v) mixed solvent and procedure C is similar to procedure B except luminol is made in carbonate buffer solution and hemin is used instead of the mixed Co(II)–EDTA solution.

3. Results and discussion

3.1. Procedure A

Procedure A involves the use of emulsifiers for preparation of homogeneous solutions of oils with the luminol-borate buffer solution.

3.1.1. Effect of emulsifier

The effect of 10% (w/w) of Tween-20, Tween-80, tetradecyltrimethylammonium bromide (AmBr) and polyoxyethylene 9 lauryl ether (Polydocanol) on the emission intensity from various concentrations of hydrogen peroxide in Delios from the luminol CL reaction in borate buffer (pH 9.00) and Co(II)–EDTA was investigated (Table 1). From the results shown in Table 1, it is obvious that %R.S.D. values are lower when Tween-20 and -80 are used. Hence, Tween-20 was chosen for all further studies since emission intensities are higher than those from Tween-80. The effect of amount of Tween-20 on the emission intensity from 100 mmoles H_2O_2/kg

Table 1
Effect of 10% (w/w) of emulsifiers on the emission intensity from various concentrations of H_2O_2 in Delios from the luminol CL reaction in borate buffer (pH 9.00) and Co(II)–EDTA

Emulsifier (mmoles H_2O_2/kg Delios)	Emission intensity ± s (n = 3) (%R.S.D.)			
	Tween-20	Tween-80	AmBr	Polydocanol
1.87	24.6 ± 0.2 (0.8)	19.1 ± 0.1 (0.5)	25.3 ± 0.1 (5.5)	26.6 ± 0.6 (2.3)
3.75	24.1 ± 0.1 (0.4)	22.3 ± 0.6 (2.7)	25.2 ± 0.6 (2.4)	26.4 ± 0.5 (1.9)
7.50	24.0 ± 0.7 (2.9)	24.4 ± 0.4 (1.6)	26.3 ± 0.7 (2.7)	32.3 ± 0.8 (2.5)
15.0	38.0 ± 0.8 (2.1)	33.3 ± 0.6 (1.8)	62.3 ± 1.7 (2.7)	43.2 ± 1.0 (2.3)
30.0	91.6 ± 1.6 (1.7)	59.9 ± 1.0 (1.7)	51.9 ± 1.6 (3.1)	127.6 ± 2.0 (1.6)

Table 2
The effect of amount of Tween-20 on the emission intensity from 100 mmol H_2O_2/kg Delios

Tween-20 (%, w/w)	Emission intensity ± s (n = 3)
7.5	329 ± 4
10	332 ± 5
11.2	334 ± 7
12.5	336 ± 6
15	346 ± 6

Delios is shown in Table 2. Ten percent (w/w) was used for all further studies as a compromise between intensity and consumption of emulsifier.

3.1.2. Effect of concentration of chemiluminogenic reactants

The effect of concentration of Co(II) and EDTA on the emission intensity from 5.6×10^{-4} M luminol in borate buffer (pH 9.00) and 100 mmol H_2O_2/kg Delios in the presence of 10% (w/w) Tween-20 is shown in Table 3. Hence, a mixed solution containing 7.3×10^{-4} M Co(II) and 2.3×10^{-3} M EDTA was used since no significant increase of emission intensity was observed at higher concentrations at the conditions used. At the optimal experimental conditions, a typical profile of emission intensity from 30 mmol H_2O_2/kg Delios versus time profile is shown in Fig. 1. All measurements were performed in borate buffer at pH 9.00, as optimized in previous work [9] and verified in this work as well.

3.2. Procedure B

Procedure B is similar to procedure A except a mixed acetone:ethanol (2:1, v/v) mixed solvent is used for preparation of homogeneous solutions of oils with luminol.

3.2.1. Effect of mixed solvent

The optimum concentrations of luminol, Co(II) and EDTA were used as in procedure A. When acetone:ethanol mixed solvent was used at 1:1 and 2:1 (v/v), the CL reaction was very fast and it was not possible to record a response similar to that shown in Fig. 1. Hence, the solvent was prepared at 2:1 (v/v) ratio.

Table 3
The effect of concentration of Co(II) and EDTA on the emission intensity from 5.6×10^{-4} M luminol in borate buffer (pH 9.00) and 100 mmol H_2O_2/kg Delios in the presence of 10% (w/w) Tween-20

Concentration (M)		Emission intensity ± s (n = 3)
Co(II)	EDTA	
2.1×10^{-4}	6.6×10^{-4}	8.4 ± 0.5
3.8×10^{-4}	1.2×10^{-3}	24.6 ± 0.1
5.2×10^{-4}	1.6×10^{-3}	58.8 ± 1.7
6.0×10^{-4}	1.9×10^{-3}	93.4 ± 5.6
6.5×10^{-4}	2.0×10^{-3}	100.7 ± 4.6
7.0×10^{-4}	2.1×10^{-3}	143.0 ± 4.0
7.1×10^{-4}	2.2×10^{-3}	148.0 ± 3.2
7.3×10^{-4}	2.3×10^{-3}	150.0 ± 1.6
7.5×10^{-4}	2.4×10^{-3}	150.0 ± 2.5

3.3. Procedure C

Procedure C involves the use of a mixed acetone:ethanol (2:1, v/v) mixed solvent for preparation of homogeneous solutions of oils with luminol in the presence of carbonate and hemin. Hemin is an iron-containing porphyrin which acts as a catalyst in the luminol CL reaction, has been previously used for the evaluation of antiradical capacity [10] and the detection of lipid oxidation by luminol CL and was used similarly [11].

3.3.1. Analytical figures of merit

By using procedure A, emission intensity, I, was linearly related to concentration of hydrogen peroxide, C, within the range 2.5–50 mmol H_2O_2/kg Delios with regression equation: $I = 2.1 \times C + 3.3$, $r^2 = 0.993$ ($n = 7$). Nevertheless, the organic peroxides t-BP and t-BHP did not show any emission intensity at the optimised conditions for hydrogen peroxide. This was attributed to incomplete dissolution and steric hindrance. Therefore, it was decided to select a variety of olive oils, determine the peroxide value (PV, mequiv. O_2/kg oil) by using the official method and construct the calibration graph of PV versus emission intensity, I. A linear regression was established between I and PV value (mequiv. O_2/kg oil) within the range 3.00–30.0 mequiv. O_2/kg oil: $I = 0.32\text{PV} - 0.12$, $r^2 = 0.98$ ($n = 7$).

By using procedure B, emission intensity was linearly related to concentration of hydrogen peroxide, C, within the range 2–200 μM with regression equation: $I = 0.09 \times C - 3.2$, $r^2 = 0.97$ ($n = 5$). It was therefore decided to construct a calibration graph of CL intensity with PV values on olive oils determined by the official method. A linear regression was established between I and PV value (mequiv. O_2/kg oil) within the range 2.00–30.0 mequiv. O_2/kg oil: $I = 0.16\text{PV} + 0.9$, $r^2 = 0.98$ ($n = 7$).

By using procedure C, emission intensity was linearly related to concentration of hydrogen peroxide, C, within the range

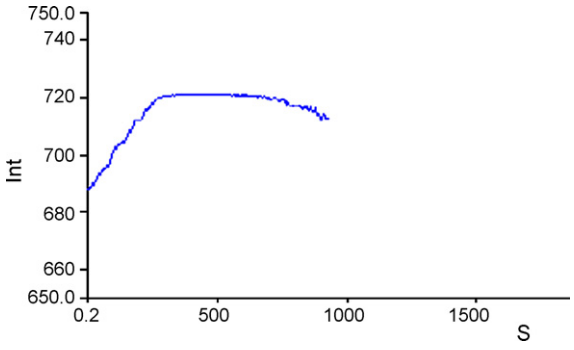

Fig. 1. Typical profile of emission intensity versus time from 30 mmol H_2O_2/kg Delios at the optimal conditions of procedure A.

Table 4
Determination of peroxide value (PV) by the official method and proposed CL methods

Oil sample	PV value (mequiv. O_2/kg oil)			
	Official method	Procedure		
		A	B	C
Extra virgin oil				
1	7.5	2.2 ± 0.7	1.9 ± 0.5	7.0 ± 0.4
2	10.3	2.4 ± 0.4	1.9 ± 0.1	7.3 ± 0.9
3	11.7	3.0 ± 0.1	2.4 ± 0.3	9.0 ± 0.3
4	8.6	2.2 ± 0.1	1.8 ± 0.4	7.1 ± 0.4
Virgin oil				
1	11.6	2.6 ± 1.2	2.2 ± 0.3	9.7 ± 0.6
2	15.2	3.2 ± 1.5	1.7 ± 0.6	11.0 ± 0.9
Refined oil				
Cotton seed oil	8.9	2.5 ± 0.2	2.2 ± 0.2	7.6 ± 0.2
sunflower	2.3	1.8 ± 0.5		
Other oils				
Lampante	6.3	2.1 ± 0.2	1.8 ± 0.6	6.0 ± 0.4
Lampante blend	27.8	4.2 ± 0.7	3.3 ± 1.1	17.1 ± 0.4

0.014–50 μM with regression equation: $I = 664 \times C - 14.0$, $r^2 = 0.990$ ($n = 7$). Under the experimental conditions for hydrogen peroxide, t-BHP was also found to generate emission linearly related to concentration within the range 0.025–2.5 μM with regression equation: $I = 130 \times C + 20.2$, $r^2 = 0.990$ ($n = 8$). Nevertheless, *t*-BP did not generate any emission. It was therefore decided to construct a calibration graph of CL intensity with PV values on olive oils determined by the official method. A linear regression was established between *I* and PV value (mequiv. O_2/kg oil) within the range 2.00–30.0 mequiv. O_2/kg oil: $I = 0.28PV + 0.02$, $r^2 = 0.990$ ($n = 7$).

3.4. Determination of peroxide value of commercial oils

By using the three procedures developed, the PV value of a variety of commercial oils was determined and the results were compared to the results of the official method (Table 4) and the corresponding regression equations and correlation coefficients of each proposed procedure with the official method are summarized in Table 5. From the results in Table 5, it becomes apparent that the best correlation between the official method and proposed method occurs with procedure C. This was expected since this procedure was capable of measuring the organic peroxides present in olive oil.

3.5. Estimation of activity of antioxidants

Luminol CL has been applied to the estimation of antioxidant activity (AA) of a variety of compounds such as quercetin, ascorbic acid and trolox [9] or for the estimation of antioxidant activity of complex matrices such as olive oil mill wastewater [12], fruits [13] and tea and herbal infusions [14]. AA can also be evaluated by differential pulse [15] or cyclic voltammetry [16] or flow injection analysis [17]. Despite the fact that the results for AA depend on parameters such as reaction medium, principle of measurement and measurement of single antioxidants or mixtures, the results are capable of estimating the antioxidant activity of compounds or natural products.

Table 5
Regression equations and correlation coefficients for the measurement of PV value by proposed CL method (PV_{CL}) and official method (PV_{off})

Procedure	PV_{CL} = slope × PV_{off} + intercept		r^2 ($n = 10$)
	Slope	Intercept	
A	0.10	1.5	0.95
B	0.078	1.3	0.91
C	0.50	3.2	0.99

Table 6
Range of concentration, slope of calibration line, antioxidant activity (IC_{50}) and scavenging activity of hydrogen peroxide (SAHP) for the five antioxidants studied by procedure B

Antioxidant	Concentration range (μM)	Slope	IC_{50} (μM)	SAHP (μM^{-1})
L-AA	0.004–0.05	141	0.0074	135
BHT	0.002–0.07	31.2	0.038	26.3
α-Tocopherol	0.005–0.12	2.23	0.31	3.22
β-Carotene	0.005–0.12	2.82	0.36	2.78
Quercetin	0.005–0.016	1.22	0.82	1.22

Procedure B was used to estimate the activity of common antioxidants in olive oil. The antioxidants selected were β-carotene, BHT, α-tocopherol, quercetin and L-ascorbic acid (L-AA). Different concentrations of each antioxidant were mixed with a 1.3×10^{-4} M H_2O_2 at the optimum concentrations of luminol, Co(II) and EDTA of procedure B and the emission intensity (*I*) was measured. The emission intensity (I_o) from 1.3×10^{-4} M H_2O_2 without any antioxidant added was also measured. By plotting I_o/I versus concentration of antioxidant, a linear regression equation is obtained. IC_{50}, defined as the concentration of antioxidant which reduces the emission intensity by 50%, was calculated from the regression equation for each antioxidant at $I_o/I = 2$. The scavenging activity of hydrogen peroxide (SAHP) defined as: $SAHP = I/IC_{50}$ was also calculated.

The range of concentration, slope of calibration line, antioxidant activity (IC_{50}) and scavenging activity of hydrogen peroxide (SAHP) for the five antioxidants studied by procedure B are shown in Table 6. From the results in Table 6, it is obvious that L-AA and BHT are the most powerful H_2O_2 scavengers followed by α-tocopherol, β-carotene while quercetin is the weakest scavenger under the given experimental conditions. The sequence of antioxidant ability, expressed as IC_{50} or SAHP, changes with the polarity of solvents used [7,9] as well as with the measurement procedure employed. Hence, more than one method is required to provide adequate information on the in vitro antioxidant activity behaviour [18].

4. Conclusions

From the three procedures proposed, procedure C can easily and reliably be used for the determination of PV of olive oil and oils, in general. The method is easy to apply and the optical instrument required is very simple. Measurement of antioxidant ability, expressed as IC_{50} or SAHP, shows that ascorbic acid and quercetin are the strongest and weakest antioxidants, respectively but the results depend on chemical and physical properties of the reaction mixture. Therefore, further interpretation with results by other methods such as cyclic voltammetry is required to increase the reliability of the conclusions.

References

[1] J.B. Rossell, J.L.R. Pritchard, Analysis of Oilseeds, Fats and Fatty Foods, Elsevier, London, 1991.
[2] Determination of the peroxide value in Commission Regulation EEC, Off. J. Eur. Commun., No. 2568r91, No. L 248 5.9.91, p. 9.
[3] H. Li, F.R. van de Voort, A.A. Ismail, R. Cox, J. Am. Oil Chem. Soc. 77 (2000) 137.
[4] P.G. Nouros, C.A. Georgiou, M. Polyssiou, Anal. Chim. Acta 389 (1999) 239.
[5] G. Merenyi, J. Lind, T.E. Eriksen, J. Biol. Chem. 5 (1990) 53.
[6] S. Baj, T. Krawczyk, Anal. Chim. Acta 585 (2007) 147.
[7] A. Arnous, C. Petrakis, D.P. Makris, P. Kefalas, J. Pharmacol. Toxicol. Methods 48 (2002) 171.
[8] V. Stepanyan, A. Arnous, C. Petrakis, P. Kefalas, A.C. Calokerinos, Talanta 65 (2005) 1056.

[9] I. Parejo, C. Codina, C. Petrakis, P. Kefalas, J. Pharmacol. Toxicol. Methods 44 (2000) 507.
[10] E.L. Bastos, P. Romoff, C.R. Eckert, W.J. Baader, J. Agric. Food Chem. 51 (2003) 7481.
[11] B. Matthäus, C. Wiezorek, K. Eichner, Fat Sci. Technol. 96 (1994) 96.
[12] D. Atanassova, P. Kefalas, E. Psillakis, Environ. Int. 31 (2005) 275.
[13] A. Termentzi, P. Kefalas, E. Kokkalou, Food Chem. 98 (2006) 599.
[14] A.K. Atoui, A. Mansouri, G. Boskou, P. Kefalas, Food Chem. 89 (2005) 27.
[15] E.I. Korotkova, O.A. Avramchik, T.M. Angelov, Y.A. Karbainov, Electrochim. Acta 51 (2005) 324.
[16] S. Martinez, L. Valek, J. Rešetić, D. Ferenec Ružić, J. Electroanal. Chem. 588 (2006) 68.
[17] D.L. Giokas, A.G. Vlessidis, N.P. Evmiridis, Anal. Chim. Acta 589 (2007) 59.
[18] E.N. Frankel, A.S. Meyer, J. Agric. Food. Sci. 80 (2000) 1925.

Talanta 77 (2008) 647–651

Contents lists available at ScienceDirect

Talanta

journal homepage: www.elsevier.com/locate/talanta

An expeditious method for determining particle size distribution by near infrared spectroscopy: Comparison of PLS2 and ANN models

Marcelo Blanco*, Anna Peguero

Departament de Química, Edifici Cn, Universitat Autònoma de Barcelona, 08193 Bellaterra, Barcelona, Spain

ARTICLE INFO

Article history:
Received 3 April 2008
Received in revised form 19 June 2008
Accepted 3 July 2008
Available online 16 July 2008

Keywords:
Particle size distribution
PLS2
ANN
NIR spectroscopy

ABSTRACT

The particle size distribution of a solid product can be crucial parameter considering its application to different kinds of processes. The influence of particle size on near infrared (NIR) spectra has been used to develop effective alternative methods to traditional ones in order to determine this parameter. In this work, we used the chemometrical techniques partial least squares 2 (PLS2) and artificial neural networks (ANNs) to simultaneously predict several variables to the rapid construction of particle size distribution curves. The PLS2 algorithm relies on linear relations between variables, while the ANN technique can model non-linear systems.

Samples were passed through sieves of different sieve opening in order to separate several size fractions that were used to construct two types of particle size distribution curves. The samples were recorded by NIR and their spectra were used with PLS2 and ANN to develop two calibration models for each. The correlation coefficients and relative standard errors of prediction (RSEP) have been used to assess the goodness of fit and accuracy of the results.

The four calibration models studied provided statistically identical results based on RSEP values. Therefore, the combined use of NIR spectroscopy and PLS2 or ANN calibration models allows determining the particle size distributions accurately. The results obtained by ANN or PLS2 are statistically similar.

1. Introduction

Many industrial products are solids consisting of particles of variable size and shape. An accurate knowledge of the physical dimensions of the particles in raw materials can be crucial with a view to ensuring proper development of a production process or the desired properties in the end product. Many industrial pharmaceutical processes involve transferring homogeneous mixtures of ingredients (active principle and excipients) to various production zones without altering their uniformity or detracting from the physical properties sought in the end product—in fact, the flowing properties of powdered solids depend strongly on their particle size and shape. Granulating powders in order to facilitate product transfer and determining particle size distribution are two frequent operations in this context. Also, the stability of a suspension depends largely on the particle size of the dispersant; ensuring such stability is crucial for purposes such as the production of plastic paints, – which typically consist of aqueous emulsions of a vinyl or acrylic resin – inks or drugs formulated as suspensions of the active principal ingredient (API) in sweetened water. Particle size distribution is also strongly influential on the quality of building mortars, where too high or too low a proportion of small particles can alter some properties such as the workability of wet mortar, its hardening time or its strength once cured. The previous examples testify to the importance of particle size in various industrial fields and of developing expeditious, reliable methods to determine it.

The determination of particle size distribution has been approached in various ways depending on the accuracy and precision required, and also of the size discrimination level to be reached. Laser diffraction analysis [1–4] is probably the most widespread choice by virtue of its affording measurements over a wide range of particle sizes (0.05–3500 μm). Scanning electron microscopy and sieving [5–6] are also widely used for this purpose. The latter provides a simple method for determining particle size distribution by passing the sample through a series of sieves of variable sieve opening and weighing the fraction retained on each sieve.

Particle size is known to influence NIR spectra [7]. Its effect has frequently been deemed undesirable or disturbing with a view to the subsequent processing of data. This has promoted its lessening or the use of some sample pretreatment (*e.g.* sieving) in order to ensure uniformity prior to recording the NIR spectrum or subjecting the spectrum to a common spectral treatment such

* Corresponding author. Tel.: +34 935811367; fax: +34 935811367.
E-mail address: marcel.blanco@uab.es (M. Blanco).

0039-9140/$ – see front matter © 2008 Elsevier B.V. All rights reserved.
doi:10.1016/j.talanta.2008.07.015

as multiplicative scatter correction (MSC), standard normal variate (SNV), detrending or derivation.

Studies on the use of NIR to determine particle size have so far focused on predicting an average particle size (whether the mass median particle size or the mean particle diameter) [1,4,8]; by contrast, few have aimed at determining particle size distribution [9,10]. O'Neil et al. [9] determined cumulative particle size distributions by applying multiple linear regression (MLR) or principal component regression (PCR) to each individual variable to be predicted and found the latter to provide the better results; in fact, PCR afforded accurate predictions of particle size from NIR data, but required constructing one calibration model per target variable. In subsequent work [10], he used a single calibration model, of the partial least squares 2 (PLS2) type, to simultaneously obtain the whole particle size distribution curve for samples of microcrystalline cellulose reference values for which had previously been determined by laser diffraction analysis.

Extracting analytically useful information from a NIR spectrum entails using a multivariate calibration technique such as those employed in the previous studies [1,4,8–10]. In this work, we used the calibration techniques PLS2 and artificial neural networks (ANNs). The PLS2 algorithm [11], which is an extension of that originally developed by Wold et al. [12] and Martens and Næs [13], calculates latent variables by aiming at the largest possible covariance between the variables X (NIR spectra) and Y (the n properties to be determined), models all Y variables simultaneously and provides a calibration model for the n properties. Simultaneously modeling all variables has the advantage that it allows a single model to be used to predict all; also, it is especially suitable when the Y variables are correlated. However, it fails to provide the best possible model for each individual variable. This algorithm requires a bilinear model.

We also used the ANN algorithm [14–16], which, unlike PLS2, assumes no linear relationship between X (the NIR spectra or latent variables) and Y (the properties to be determined). artificial neural networks are trained until they "learn" the nature of the relationship between their inputs and outputs.

The primary aim of this work was to develop a working methodology for determining particle size distribution. To this end, we comparatively examined the predictive ability of four calibration models based on two different algorithms (*viz*. PLS2, which assumes a linear relationship between NIR spectra and particle size distribution, and ANN, which assumes no linear relationship); the models were applied to size distribution curves constructed from a different number of points (*viz*. 13, including 2 unresolved maxima, and 8, with a single maximum).

2. Experimental

2.1. Samples

The sample is an aggregate, a natural product composed basically by silicon dioxide. A total of 30 samples of aggregate, with different particle size distributions were studied. All were prepared by mixing variable proportions of two types of aggregate also differing in average particle size and size distribution.

2.2. Instrumentation and software

Spectra were recorded on a Foss NIRSystems 6500 spectrophotometer equipped with a rapid content analyser (RCA) module. The instrument was governed via the software Vision v. 2.51, also from NIRSystems.

Each sample was sieved with a BA100-N Sieve Shaker from CISA (Barcelona, Spain).

PLS2 models were constructed by using The Unscrumbler v. 9.2 from Camo and the ANN models by using ANN toolbox in Matlab v. 7.0.

2.3. Reference method

An amount of *ca*. 100 g of each sample was sieved to obtain 13 fractions of different particle size. The sieve opening of the 12 sieves used was 0.050, 0.075, 0.100, 0.125, 0.150, 0.175, 0.200, 0.250, 0.300, 0.400, 0.500 and 1.000 mm, respectively. The fraction passing through all sieves (<0.050 mm in size) was also collected. Each fraction was weighed on an analytical balance in order to calculate the proportion of sample retained by each sieve with a view to constructing a particle size distribution curve.

In order to examine the predictive ability of the ensuing models (PLS2 and ANN) over resolution curve, we prepared another curve with less data points. The new reference curve was obtained by sum of the fraction weights of two consecutive sieves (*e.g.* 0.100 and 0.125 mm), in this way a new value of mass was obtained and the fraction was renamed like tighter sieve. This calculation provided eight new fractions and therefore a new Y data set, which draws a curve with minor resolution, that previous one. These new combined fractions were used to study the influence on resolution in different chemometrical models.

2.4. Recording of NIR spectra

Near infrared reflectance spectra were recorded at 2-nm intervals over the wavelength range 1100–2500 nm by placing the powdered samples in glass cells and using a ceramic plate as reference. Each spectrum was the average of 32 scans and an aliquot of each sample (3–4 g) were measured in triplicate, with turnover between recordings.

2.5. Construction of models and processing of data

Spectral data were subjected to the following treatments: standard normal variate (SNV), and first and second derivative. Both spectral derivatives were obtained by using the Savitzky–Golay algorithm with a second-order polynomial and an 11-point moving window. PLS2 models were constructed by cross-validation, using the leave-one-out method. The optimum number of PLS2 components was taken to be that minimizing the least squares difference between the reference value and the measured parameter.

Artificial neural network models were constructed from a reduced number of variables, using the scores of a PCA of the second-derivative spectra over the wavelength range 1100–2450 nm as inputs. The specific network architecture used was of the back-propagation type and subjected to supervised training on a selected body of samples (the test set). Back-propagation training involved feeding the network with an input and propagating it in order to obtain an output. The output was then compared with the correct response in order to determine the prediction error. Finally, the weight of each connection to an output unit was adjusted in the appropriate direction in order to reduce the error.

The transferred functions used with ANNs can be of the non-linear, linear and threshold types. We used a non-linear sigmoidal (*tansig*) function for the input layer and found the *puerlin* function to provide the best results for the hidden layer.

The number of nodes in the output layer coincided with that of fractions used to construct the particle size distribution curve.

The goodness of the results provided by the different models was assessed via the relative standard error (RSE):

$$\mathrm{RSE} = \sqrt{\frac{\sum_{i=1}^{n}\sum_{j=1}^{m}(Y_{ij}^{\mathrm{NIR}} - Y_{ij}^{\mathrm{REF}})^2}{\sum_{i=1}^{n}\sum_{j=1}^{m}Y_{ij}^{\mathrm{REF}^2}}} \times 100$$

3. Results and discussion

One of the primary aims of this study was to establish an effective working methodology for determining the distribution of particle sizes in powders applicable to all types of samples, whichever their nature. To this end, we used an inorganic sample, namely: an aggregate consisting largely of silica – which exhibits low absorption in the NIR region – in an average particle size similar to those of intermediate granulates in industrial drug production processes. We assessed the goodness of fit obtained as a function of the size resolution of the sieving system (7 or 12 sieves) and the linear (PLS2) or non-linear nature (back-propagation ANN) of the algorithm used to construct the models.

The first question to be answered was how the NIR spectrum would be affected by variability in particle size. Fig. 1 shows the NIR spectra for several samples with different particle size mean. As can be seen, the spectral profiles were identical in shape; however, there were substantial baseline shifts between consecutive groups of samples as a result of differences in particle size—the greater the particle size, the higher the absorption in the NIR region.

Ensuring an adequate predictive ability in a multivariate model is known to entail using a calibration set containing all possible sources of variability in the samples to be predicted; this in turn relies on appropriate selection of the samples. Spectral variability can be exposed by using principal component analysis. The scores plot of Fig. 2 shows the distribution of samples in the PCA space. As can be seen, the samples clearly clustered in two groups reflecting the same differences previously observed in the absorbance spectra (see Fig. 1), *i.e.* those in particle size between samples, the cluster on top encompassing the samples with the greater particle sizes. The samples to be included in the calibration and prediction sets, which are shown in Fig. 2, were chosen by visual inspection of the scores plot and in such a way as to ensure that both sets would include the typical spectral variability of the samples.

The wavelength ranges for application of the PLS2 models were selected in terms of the positions of the spectral bands for the aggregate (1350–1460 and 1850–2450 nm) (see Fig. 1). This allowed NIR spectral zones of low absorption or containing noise only to be excluded, and each regression model to be constructed from those zones containing useful information about the target variable.

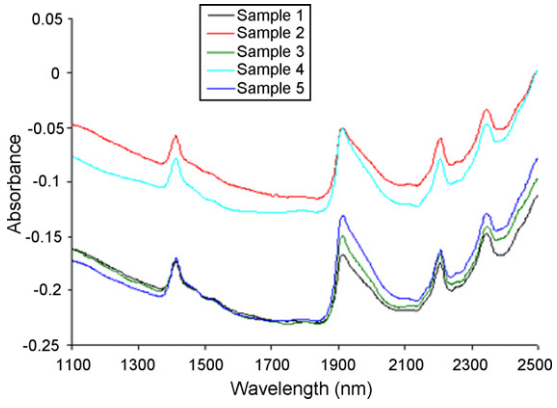

Fig. 1. NIR spectra for selected aggregate samples.

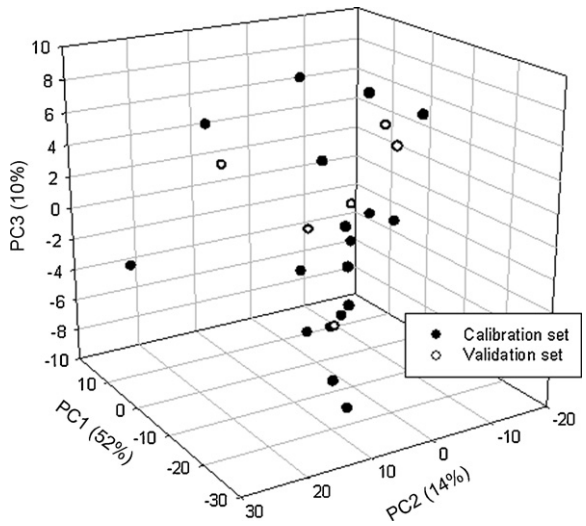

Fig. 2. PCA scores plot obtained from the second-derivative spectra for selected aggregate samples.

The usual sample pretreatments fail to completely suppress the above-described shifts resulting from differences in particle size. Also, the SNV algorithm failed to accurately classify spectra according to particle size; on the other hand, the second-derivative spectra for the sieved fractions afforded accurate classification (see Fig. 3) from all spectral bands. The spectra for the finest fractions (0 and 0.050 nm) and the coarsest one (>1 mm) could not be recorded owing to the inadequate amounts obtained after sieving.

The ability of derivative spectra to discriminate samples according to particle size led us to adopt this spectral treatment to construct the calibration models; second-derivative spectra provided even better predictions than first-derivative spectra.

We tested both PLS2 and ANN because the two afford the simultaneous quantitation of n variables. However, we discarded using PLS models, even though they were highly likely to provide better predictions than the sole PLS2 model employed since PLS models variables one by one rather than as a whole. In fact, we chose to sacrifice the predictive ability of PLS in order to be able to use a single PLS2 model to predict particle size distribution in an expeditious manner. Also, the undeniable correlation between the predictor variables further warranted using PLS2.

We constructed two PLS2 models from second-derivative spectra to obtain particle size distribution curves consisting of 7 and 12 points (sieves). The results are shown in Table 1, and the RSEC

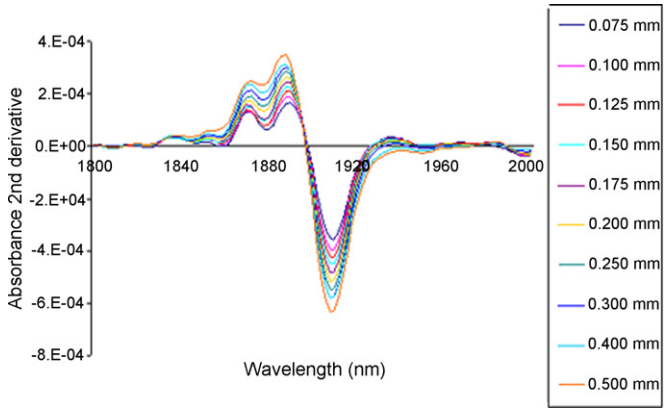

Fig. 3. Comparison of the second-derivative spectra in the 1800–2000 nm region for different particle size fractions.

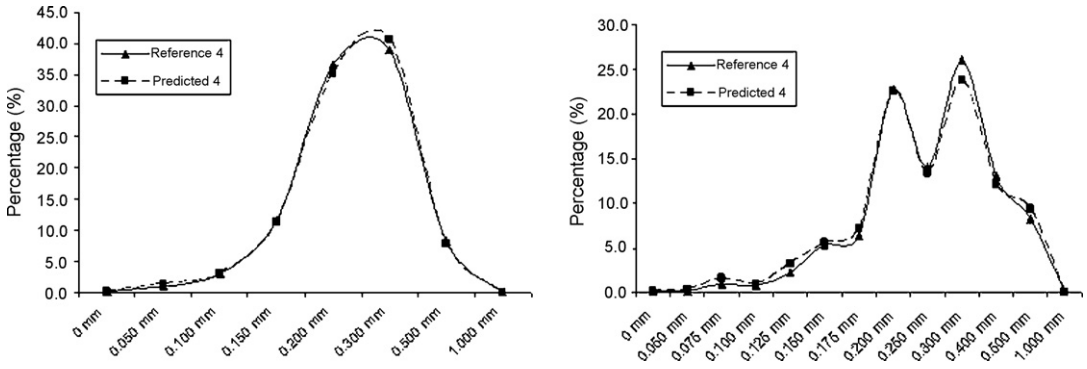

Fig. 4. Predicted particle size distribution curves for sample 4 as obtained by using PLS2 calibration models constructed from 7 (left) and 12 variables (right).

Table 1
Parameters for the best PLS2 calibration models

	Calibration	Prediction	Calibration	Prediction
Number of sieves	7		12	
Pretreatment	2nd derivative		2nd derivative	
Range (nm)	1350–1460, 1850–2450		1350–1460, 1850–2450	
PLS factors	3		8	
Samples	19	6	19	6
RSEC/*P*%	8.7	8.6	2.6	7.6

Table 2
RSEC and RSEP for the PLS2 models with 7 variables

	PC1	PC2	PC3	PC4	PC5
RSEC	11.0	10.0	**8.7**	11.3	13.0
RSEP	8.9	8.8	**8.6**	10.7	11.2

and RSEP values for the ensuing models in Tables 2 and 3 (the best results are in bold). As can be seen, the number of factors resulting in the lowest RSEP with the 7 and 12 variables model was 3 and 8, respectively. Using a greater number of factors provided no further improvement in predictive ability with any model.

A comparison of the results provided by the two PLS models reveals that determining an increased number of variables required using a more complex mathematical model and hence an also greater number of PLS factors to account for variability and also, possibly, to correct non-linearity in the system—PLS is known to correct small deviations from linearity by using models expanded with new factors. On the other hand, a comparison of the RSEP values for the two models (Table 1) reveals that both had a similar predictive ability.

Table 3
RSEC and RSEP for the PLS2 models with 12 variables

	PC6	PC7	PC8	PC9	PC10
RSEC	3.7	3.2	**2.6**	2.2	2.1
RSEP	8.3	8.1	**7.6**	7.6	7.6

Table 4
Operational parameters and figures of merit of the ANN calibration models

	Calibration	Prediction	Calibration	Prediction
Number of sieves	7		12	
Pretreatment	2nd derivative		2nd derivative	
Range (nm)	1100–2450		1100–2450	
Data reduction	PCA (3PC)		PCA (9PC)	
Input nodes	3		9	
Transfer function to input layer	Tansig		Tansig	
Hidden nodes	2		1	
Transfer function to hidden layer	Puerlin		Puerlin	
Output layer	7		12	
Samples	18	6	21	6
RSEC/P%	11.2	5.6	7.2	7.9

We then constructed two calibration models by using ANN with 7 and 12 *Y* variables, respectively. Also, we reduced the number of variables by using the scores of a PCA as inputs in order to simplify the network architecture. However, reducing the number of variables can also reduce the spectral information that can be extracted from a system; this was avoided by using a variable number of principal components from 1 to 5 with the 7 variables network and up to 12 with the 12 variables network. The best results were provided by the networks shown in Table 4.

The model containing 7 *Y* variables was used with 3 PCs, which jointly accounted for 96.5% of the total variance; by contrast, the model involving 12 variables required 9 PCs, which accounted for 98.9% of the total variance. The increased number of inputs required by the latter model was an obvious consequence of the greater complexity of the curves. The number of neurons in the input layer, that of hidden layers, and that of neurons in each hidden layer, were optimized as a function of RSEP for the respective outputs. The optimum number of neurons in the hidden layer was 2 for the 7 variables model and 1 for the 12 variables model; both networks exhibited the lowest RSEP values among all studied.

As with the PLS2 models, the architecture of the network required for the 7 variables model was simpler than that for the 12 variables model (see Table 4). The increased complexity of the particle size profile with 12 variables called for a more complex network; even so, the 2 models provided essentially similar RSEP values.

By way of example, Figs. 4 and 5 show the reference and predicted particle size distribution curves obtained with the PLS and ANN models, respectively. As can be seen, the prediction curves fitted the reference curves quite closely. The correlation coefficient proved useful with a view to comparing the reference and NIR-predicted particle size profiles obtained with each model. As can be seen from Table 5, the average correlation coefficient for all mod-

Table 5
Correlation coefficients between the reference and predicted distribution curves

Sample	PLS2		ANN	
	7 variables	12 variables	7 variables	12 variables
1	0.98	0.97	0.98	0.97
2	0.95	0.93	0.99	0.95
3	0.92	0.96	0.99	0.94
4	1.00	1.00	0.97	1.00
5	0.97	0.98	0.98	0.99
6	0.99	0.99	0.99	0.99
Average	0.97	0.97	0.98	0.97

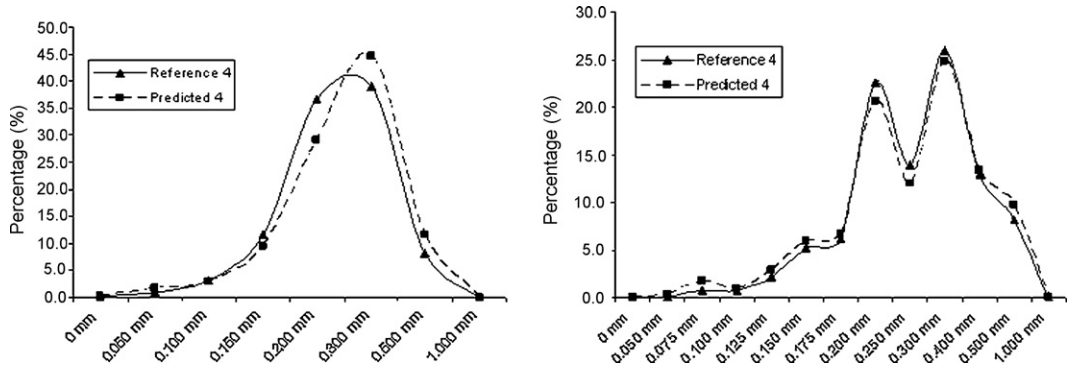

Fig. 5. Predicted particle size distribution curves for sample 4 as obtained by using ANN calibration models constructed from 7 (left) and 12 variables (right).

els was at least 0.97, which testifies to the high similarity of the reference and predicted curves. Tables 3 and 4 list the prediction errors in the particle size distribution curves obtained with the four studied models. As can be seen, RSEPs were statistically identical; also, they ranged from 5.6 to 8.6%, which is quite acceptable for the reference method used.

4. Conclusions

As confirmed in this work, NIR spectra contain information about particle size. Also, it allows particle size distribution curves essentially identical with those obtained by sieving to be constructed. Therefore, NIR spectroscopy is an effective choice for determining particle size distribution.

The four calibration models used were constructed from second-derivative spectra. Therefore, derivation not only retains the effects of particle size contained in a NIR spectrum, but also constitutes the most suitable treatment for this type of data.

Using models consisting of 7 and 12 *Y* variables revealed that an accurate prediction of particle size distribution does not depend on its particle size profile; in fact, both types of models provided similar results as regards percent error. However, the greater the number of variables required a greater number of factors to be used in PLS2 or neurons in ANN.

The PLS2 and ANN techniques approach the resolution of spectral problems differently; based on the correlation coefficients between the reference and NIR-predicted curves obtained in this work, however, they are equally effective with a view to obtaining accurate results.

Acknowledgement

The authors are grateful to Spain's MCyT for funding this research within the framework of Project CTQ2006-12923.

References

[1] A.J. O'Neil, R.D. Jee, A.C. Moffat, Analyst 123 (1998) 2297.
[2] O. Beerntsson, L.G. Danielsson, M.O. Johansson, S. Folestad, Analytica Chimica Acta 419 (2000) 45.
[3] C. Marriot, H.B. MacRitchie, X.-M. Zeng, G.P. Martin, International Journal of Pharmaceutics 326 (2006) 39.
[4] M. Otsuka, Powder Technology 141 (2004) 244.
[5] C. Washington, Particle Size Analysis in Pharmaceutics and other Industries Theory and Practice, Ellis Horwood Limited, England, 1992.
[6] ASTM D 6913 Standard Test Methods for Particle-Size Distribution (Gradation) of Soils Using Sieve Analysis.
[7] M.C. Pasikatan, J.L. Steele, C.K. Spillman, E. Haque, Journal Near Infrared Spectroscopy 9 (1998) 153.
[8] P. Frake, I. Gill, et al., Analyst 123 (1988) 2043.
[9] A.J. O'Neil, R.D. Jee, A.C. Moffat, Analyst 124 (1999) 33.
[10] A.J. O'Neil, R.D. Jee, A.C. Moffat, Analyst 128 (2003) 1326–1330.
[11] R.G. Brereton, Analyst Review 125 (2000) 2125.
[12] S. Wold, C. Albano, W.J. Dunn III, K. Esbensen, S. Hellberg, E. Johansson, M. Sjøstrøm, in: H. Martens, H. Russworm (Eds.), Food Research and Data Analysis, Applied Science Publishers, London, 1983, p.147.
[13] H. Martens, T. Næs, in: P.C. Williams, K. Norris (Eds.), Near-Infrared Technology in Agricultural and Food Industries, American Association of Cereal Chemist, St. Paul, MN, 1987, p. 57.
[14] B.J. Wythoff, Chemometrics and Intelligent Laboratories Systems 18 (1993) 115–155 (tutorial).
[15] J.R.M. Smits, W.J. Melssen, L.M.C. Buydens, G. Kateman, Chemometrics and Intelligent Laboratories Systems 22 (1994) 165–189 (tutorial).
[16] F. Despagne, D.L. Massart, The Analyst 123 (1998) 157R–178R (tutorial).

Talanta 77 (2008) 684–694

Contents lists available at ScienceDirect

Talanta

journal homepage: www.elsevier.com/locate/talanta

Determination of *S*-nitrosoglutathione and other nitrosothiols by *p*-hydroxymercurybenzoate derivatization and reverse phase chromatography coupled with chemical vapor generation atomic fluorescence detection

Emilia Bramanti[a,*], Karin Jacovozzi[a], Lucia D'Ulivo[a], Cecilia Vecoli[b], Roberto Zamboni[c], Zoltan Mester[d], Alessandro D'Ulivo[a]

[a] *Italian National Research Council-Istituto per i Processi Chimico-Fisici, Laboratory of Instrumental Analytical Chemistry, Via G. Moruzzi 1, 56124 Pisa, Italy*
[b] *Scuola Superiore Sant'Anna Piazza Martiri della Libertà, 33 56127 Pisa, Italy*
[c] *University of Pisa, Department of Chemistry and Industrial Chemistry, Via Risorgimento 35, 56127 Pisa, Italy*
[d] *Institute for National Measurement Standards, National Research Council Canada, 1200 Montreal Road, Ottawa, ON K1A 0R6, Canada*

ARTICLE INFO

Article history:
Received 1 April 2008
Received in revised form 26 June 2008
Accepted 4 July 2008
Available online 23 July 2008

Keywords:
Nitrosothiols
Nitrosoglutathione
GSNO
Ascorbic acid
Liquid chromatography
Atomic fluorescence spectrometry

ABSTRACT

S-Nitrosoglutathione (GSNO) reacts with the organic mercurial probe, *p*-hydroxymercury benzoate (PHMB, HO–Hg–(C_6H_4)–COO^-Na^+) giving the complex GS–Hg(C_6H_4)COOH (GS–PHMB). This reaction has been studied by UV measurements at 334 nm also in the presence of ascorbic acid and the product of reaction, the GS–PHMB complex, characterized by Electrospray Ionization Mass Spectrometry (ESI-MS) and by Reversed Phase Chromatography (RPLC) coupled on-line and sequentially with a UV–visible diode array detector (DAD) followed by a cold vapor generation atomic fluorescence spectrometer (CVGAFS). The simultaneous presence of PHMB and ascorbate produced a synergistic effect on GSNO decomposition rate that can be observed only above a given concentration threshold of ascorbate (ascorbate/GSNO molar ratio $\geq$ 180). The results indicated that the formation of GS–PHMB, both in the presence and the absence of ascorbic acid, does not involve the formation of free thiolic species but it takes place through a more complex mechanism. The PHMB derivatives of GSH and GSNO obtained by the present method were found to be identical by ESI-MS. GSSG did not interfere because it was not reduced and derivatized to GS–PHMB. Once complexed by the alkylating agent *N*-ethylmaleimide (NEM), GSH did not interfere with the derivatization reaction. This ensured a good selectivity of the developed PHMB derivatization system for RSNO determination. Thus, we have optimized the operating conditions for the selective reaction of PHMB with GSNO and other nitrosothiols (RSNOs) in order to determinate RSNOs in human plasma. LODc for RSNOs in plasma ultrafiltrate was 30 nM (injected concentration, 50 μL loop), the DLR ranged between 0.08 and 50 μM and the CV% was 6.5% at 300 nM concentration level. Reduced and oxidized thiols spiked to plasma did not interfere with the measurement of RSNOs. We found that the sampling procedure was critical for the recovery of endogenous and spiked RSNOs. The ultrafiltrate samples of plasma of 8 healthy humans contained 1460 ± 310 CysNO, 1000 ± 330 nM HCysNO and 320 ± 60 nM GSNO if blood was sampled in a mixture NEM/ethylendiaminotetracetic acid (EDTA)/serine–borate complex (SBC), where serine–borate complex is a potent inhibitor of γ-glutamyltransferase, an enzyme involved in the conversion of GSNO into CysGlyNO. In the absence of SBC during the sampling of blood GSNO concentration found in the ultrafiltrate was lower (at level of the determination limit in plasma ultrafiltrate, i.e. 75 nM) and the peak of CysGlyNO appeared, which corresponded to a concentration of 200 ± 60 nM (*N* = 4 blood samples).

1. Introduction

Low-molecular weight *S*-nitrosothiols (LMW-RSNO or thionitrites) are derived from the nitric oxide (NO)-mediated *S*-nitrosation of thiols and they play an important role in the transport, and metabolism of NO radical ($NO^\bullet$) [1–3]. The measurement

* Corresponding author. Tel.: +39 050 315 2293; fax: +39 050 315 2555.
E-mail address: emilia@ipcf.cnr.it (E. Bramanti).

0039-9140/$ – see front matter © 2008 Elsevier B.V. All rights reserved.
doi:10.1016/j.talanta.2008.07.020

of RSNOs in blood and plasma is still the subject of controversy [4–6].

Due to the low-molar absorptivity of the *S*-nitroso group of *S*-nitroso compounds [7] direct, quantitative UV detection of RSNO after chromatographic separation or capillary electrophoresis (CZE) has been limited to micromolar concentrations [8,9]. RSNOs have also been determined directly by using a modified planar amperometric nitric oxide sensor, with detection limit around 1 μM [10]. Alternative indirect methods can be used to determine RSNO decomposition products.

RSNOs are generally decomposed by photolytic or reductive processes. After this step, the decomposition products (generally NO• or its end oxidation product nitrite NO_2^-) are detected by various techniques (chemiluminescence, fluorimetry, electrochemical detectors, electron spin resonance, mass spectrometry, ...). The only method reported in the literature for the determination of GSNO based on the derivatization of the GS-fragment [11] deals with a multi-step procedure passing through the formation of the free thiol after reduction with β-mercaptoethanol.

The methods and the issues and artefacts affecting these methods have been extensively described recently [4,12]. Indeed, multiple factors may strongly affect the results of analysis: the choice of the system employed for the cleavage of S–NO bond (photolysis, $HgCl_2$, $HgCl_2$/V(III), KI/I_2, Cys/KI/Cu(I), Cu(I)/Cys, Cu(I)/KI/I_2, CO/Cu(I)/Cys, DTT), the type of the analyte detected (NO, nitrite, or thiol product), the detection reactant (chromophore, fluorophore or ozone) and the detection technique used [13]. Furthermore, these metabolites/analytes are generally measured in complex biological matrices (*e.g.* plasma) that require complex sample handling procedures [4,13,14]. During these procedures the analytes interact with various reactants. They may also interact with biological constituents and, in turn, the reactants may deeply modify the matrix.

All these different analytical approaches – in the absence of a reference, validated method – have yielded highly divergent plasma levels of LMW-RSNOs, often ranging in healthy subjects between low-nanomolar (<1–62 nM) and low-micromolar/micromolar concentration levels [4–6]. Although Wang et al. attempted a validation of the tri-iodide based chemiluminescence assay, which is a common employed RSNO detection technique, the actual analytical *validation* of a RSNO detection method, involving the comparison of the results obtained by two or more independent methods was not reported [15]. Finally, Hausladen et al. have recently published some results against the use of tri-iodide to assay nitrosylated species or nitrite in biological mixtures, and suggested that previous results obtained with this methodology should be reassessed [16].

Much of the chemistry of *S*-nitrosothiols is poorly elucidated [17,18]. In solution *S*-nitrosothiols have weak absorbance in the 330–350 nm region (around $10^3\ M^{-1}\ cm^{-1}$, $n_o \rightarrow \pi^*$ transition) and also at 550–600 nm (around $20\ M^{-1}\ cm^{-1}$, $n_N \rightarrow \pi^*$ transition). UV/visible spectrophotometry has been used to monitor RSNO decomposition [7].

It has long been known that *S*-nitrosothiols decompose to yield the corresponding disulfide and NO• by photochemical [19] and thermal routes [20,21], and by metal ions, principally by copper [7,22–25]. Often Cu^{2+} trace impurity that can be present in the distilled water/buffer components is enough to bring about reaction. However, it is known that the decomposition reaction is actually brought about by Cu^+ formed in the reaction medium by reduction of Cu^{2+} with thiolate or, in principle, by any reducing agent [7,26–28].

Reactivity of RSNOs is structure dependent. *S*-Nitrosothiols that can complex Cu^+ strongly bidentately, *e.g.* at a $-NH_2$ group, or a $-COO^-$ group, in addition to the nitroso group are the most reactive [29]. Among other metal ions tested in addition to Cu^{2+} (Zn^{2+}, Ca^{2+}, Mg^{2+}, Ni^{2+}, Co^{2+}, Mn^{2+}, Cr^{3+} and Fe^{3+}) only Fe^{2+}, Ag^+ and Hg^{2+} were effective in the decomposition of *S*-nitrosothiols [22,29].

It is known, that excess mercuric chloride ($HgCl_2$) gives heterolytic cleavage of the S–N bond of GSNO, giving $Hg(GS)_2$ and NO^+, the latter evolving to NO_2^- in aqueous media [29]. This reaction is the basis of Saville assay for measuring the concentration of thiols in aqueous solution [30]. Saville in 1958 reported that a number of RSNO compounds underwent facile hydrolysis to HNO_2 in the presence of mercuric, silver, or cupric salts [30]. The reaction with Hg^{2+} has subsequently been widely used in the analytical determination of thiols, and an S-bound RSNO complex was proposed as an intermediate, whose weakened S–N bond was then attacked by (nucleophilic) water molecules to form $[Hg–SR]^+$ and $[H_2ONO]^+$ [30].

Swift and Williams studied the Hg^{2+}/RSNO reaction in detail [29], finding that the Hg^{2+} reaction (as $HgCl_4^{2-}$ or $Hg(NO_3)_2$) performed in acid conditions gives $Hg(SR)_2$ and NO^+ [29]. Unfortunately, this reaction cannot be used for the chromatographic separation of $Hg(SR)_2$ because the strong excess of ionic Hg(II) necessary for RSNO decomposition adsorbs to the stationary phases of HPLC columns precluding reproducible and accurate determination of Hg(II)-thiol complexes.

Over the last 10 years we studied the interaction of inorganic mercury and the monofunctional mercury probe *p*-hydroxymercury benzoate (PHMB, $HO–Hg–(C_6H_4)–COO^-Na^+$) with reduced –SH functional groups on proteins and low-molecular weight thiolic compounds. We experienced that the replacement of inorganic Hg(II) by PHMB could overcome this problem [31–35].

In this paper we evidenced that PHMB, similarly to $HgCl_4^{2-}$ [29], decomposes RSNO giving the $RS–Hg–(C_6H_4)–COO^-$ complex (RS–PHMB). As RS–PHMB complexes can be sensitively and selectively determined by liquid chromatography coupled to mass spectrometric detectors or a mercury-specific detector [31–35] the study of this reaction is of interest for the selection of a suitable chemical derivatization method allowing a reliable determination of nitrosothiols.

We studied in detail the reaction GSNO-PHMB by UV measurements at 334 nm also in the presence of ascorbic acid and we characterized the product of reaction, the GS–PHMB complex, by Electrospray Ionization Mass Spectrometry (ESI-MS) and by Reversed Phase Chromatography (RPLC) coupled on-line and sequentially with a UV–visible diode array detector (DAD) followed by a cold vapor generation atomic fluorescence spectrometer (CVGAFS). Thus, we optimized the pre-analytical operating conditions (blood sampling) for preserving the stability of GSNO and other RSNOs (CysNO, HCysNO and CysGlyNO) in human plasma, and the analytical operating conditions for their selective determination.

2. Experimental procedures

2.1. Chemicals

Analytical reagent-grade chemicals were used without further purification. PHMB (4-(hydroxymercuric)benzoic acid, sodium salt, CAS No. 138-85-2, $HOHgC_6H_4CO_2Na$) was purchased from Sigma (Sigma–Aldrich, Chemical Co.). 1×10^{-2} M stock solution of PHMB was prepared by dissolving the sodium salt in 0.01 M NaOH in order to improve its solubility, stored at 4 °C, and diluted freshly, just before use. The precise concentrations of PHMB solutions were determined from the absorbance at 232 nm ($\varepsilon_{232} = 1.69 \times 10^4\ cm^{-1}\ M^{-1}$).

Stock solutions of GSH (G6529), cysteine (30089, Cys), homocysteine (H4628, HCys), cysteinylglycine (CysGly, Sigma C-0166),

oxidized glutathione (49740, GSSG), cistine (30199), oxidized HCys (H0501) and oxidized CysGly (C0166) (Fluka–Sigma–Aldrich, Milan, Italy) were prepared in 0.1 M phosphate buffer solution (PBS) pH 7.4, 0.5 mM ethylendiaminotetracetic acid (EDTA). In order to prevent oxidation, standard solutions of thiols were prepared daily and kept cold (4 °C) and protected from light until used. Stock solution of GSNO (N4148, CAS No. 57564-91-7, Sigma, Chemical Co., St. Louis, MO, USA) was prepared in 0.1 M PBS pH 7.4, 0.5 mM EDTA. In these experimental conditions (0.1 M PBS pH 7.4, 0.5 mM EDTA), in absence of PHMB added, GSNO standard solution was stable during the working day (9 h time tested at room temperature). EDTA prevents the possible copper-ion catalysed decomposition process of GSNO and RSNOs, in general [24]. Aliquots of stock solution were prepared and stored at −20 °C until used. The concentration of GSNO was calculated from absorbance at 334 nm using the extinction coefficient 977 M^{-1} cm^{-1} [36]. At −20 °C GSNO stock solution was stable for about 1 month.

S-Nitrosocysteine (CysNO), *S*-nitrosohomocysteine (HCysNO) and *S*-nitrosocysteinylglycine (CysGlyNO) were prepared by reacting 1 M $NaNO_2$ in H_2O with 1.1 M thiols in 0.5 M HCl, 0.5 mM EDTA, at 0 °C for 40 min [37], and used after measuring their concentration by their absorbance at 334 nm.

The buffer solutions were prepared from monobasic monohydrate sodium phosphate, dibasic anhydrous potassium phosphate (BDH Laboratory Supplies, Poole, England).

L(+)-Ascorbic acid sodium salt (11140 BioChemika, ≥99.0% NT, CAS No. 134-03-2) and *N*-ethylmaleimide (NEM, 04259 BioChemika Ultra, ≥99.0%, Fluka) were purchased from Sigma and the stock solution prepared daily in Milli-Q water.

Methanol for RPLC was purchased from Carlo Erba (Rodano, MI, Italy).

Stock solutions of $NaBH_4$ (about 6.5 M) were prepared by dissolving the solid reagent (Merck, pellets, reagent for AAS, minimum assay >96%) into 0.3% (m/v) NaOH solution. The solutions were microfiltered through a 0.45 μm membrane and stored in a refrigerator. Dilute solutions of $NaBH_4$ (0.05 M) were prepared by appropriate dilution of the stock solutions, with the total NaOH concentration maintained at 0.3% (m/v).

The 24–26% hydrazine standard solution (53847, CAS No. 10217-52-4) was purchased from Fluka Chemie and the optimized concentration (0.1 M) added to $NaBH_4$ solution containing 0.3% (m/v) of NaOH.

3.5 M HCl solutions were prepared with 37% (m/m) HCl (Carlo Erba).

A working solution of Br^-/BrO_3^- was prepared by solid reagents (Carlo Erba) (0.075 M Br^-, 0.015 M BrO_3^-) keeping an approximate Br^-/BrO_3^- 5:1 molar ratio on the basis of stoichiometry of redox reaction. Addition of a moderate excess of Br^- guaranteed a complete conversion of bromate to Br_2.

Water deionized with a Milli-Q system (Millipore, Bedford, MA, USA) was used throughout.

2.1.1. Safety considerations

PHMB is toxic. Inhalation and contact with skin and eyes should be avoided. All work should be performed in a well-ventilated fume hood.

2.2. Derivatization procedure

The decomposition reaction of GSNO by PHMB/ascorbate was studied by UV spectroscopy in 0.1 M PBS pH 7.4, 0.5 mM EDTA at 21 ± 1 °C. We made the measurements at 334 nm following the disappearance of the absorbance due to the GSNO (Beckman DU-600 spectrophotometer). Values of the rate constants are mean values of at least five determinations, and the standard error was always better than ±3.5%.

The products of the derivatization procedure were studied by RPLC–DAD–CVGAFS.

Derivatization of GSNO with PHMB was performed in 0.1 M PBS pH 7.4, 0.5 mM EDTA with or without ascorbic acid as reducing agent in the 0.5–20 mM range, as specified, by mixing the GSNO solution at the established concentration (in the 0.08–50 μM range) with PHMB solution.

In order to study the possible interference of GSH and GSSG, present in blood of healthy humans [38], mixtures of GSNO, GSSG and GSH were added to 0.1 M PBS pH 7.4, 0.5 mM EDTA or blood previously spiked with NEM, an alkylating agent employed as blocker of –SH groups, which is known to reacts in stoichiometric ratio 1:1 with GSH in less than 20 s at room temperature and pH 7.0 [39]. After the established reaction time (see Section 3) solutions were injected into the RPLC–DAD–CVGAFS system. Measurements were performed at $t = 21 \pm 1$ °C with no significant variations of the results in this temperature interval.

In quantitative determinations the incubation time of RSNO with 150 μM PHMB and 3.15 mM ascorbate was 30 min.

2.3. Calibrations

For the calibration experiments of thiols, GSH, Cys, HCys and CysGly were derivatized by diluting the stock solution in 0.1 M PBS (pH 7.43) containing a stoichiometric amount or a moderate excess of PHMB, at 25 °C. After a reaction time ≥5 min at room temperature (21 ± 1 °C), the solutions were injected in the RP chromatographic column.

For the calibration of RSNOs, RSNOs were derivatized as reported in Section 2.2 and injected in the RP chromatographic column. The yield of the derivatization was evaluated by comparing the slope of the calibration curves of RSNO with the calibration curve of the corresponding thiol.

2.4. Human blood sampling and storage

Sampling and storage are critical steps because of the occurrence of RSNO losses which can be promoted by transnitrosylation reactions, metal-mediated and enzyme-mediated decomposition. These processes can be blocked by the presence of NEM, EDTA and serine/borate complex, respectively (see Section 3).

Plasma was obtained from blood of 12 non-smoking, normotensive volunteer donors. Venous blood was collected by venipuncture using eparine as an anticoagulant. 0.5 mL of whole blood of 8 out of 12 samples were immediately spiked with 10 μL of 50 mM EDTA stock solution (1 mM final concentration of EDTA in blood), 30 μL of 0.2 M NEM stock solution (12 mM final concentration of NEM) and 50 μL of 0.1 M SBC stock solution (10 mM final concentration of serine/borate) (procedure A). Four out of 12 samples were immediately spiked with NEM/EDTA solution, but no SBC solution (procedure B).

RSNO recovery was evaluated in human whole blood by adding RSNOs after the addition of EDTA/NEM/SBC.

After low-speed centrifugation (1500 × *g*, 10 min) at room temperature, plasma samples were stored at −80 °C until analysis. Plasma can be stored at −80 °C for 4 weeks (time tested) without significant variation of the RSNO content.

Before the analysis, the plasma samples were diluted 1:1 in 0.1 M PBS pH 7.4, 0.5 mM EDTA, loaded onto the sample reservoir of an Amicon Microcon YM-3 centrifugal filter units (cut-off 10,000 Da; Millipore, Bedford, MA, USA) and centrifugated at 11.000 *g* for 90 min at 4 °C to remove proteins and high molecular weight compounds. The ultrafiltrate was treated with PHMB/ascorbate, as described in Section 3, and injected in the chromatographic system.

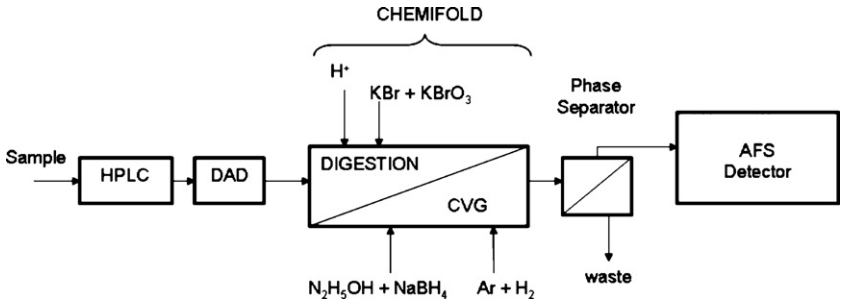

Fig. 1. Schematic flow diagram of HPLC coupled on-line with: diode array detector (DAD); chemifold for continuous flow (CF) system for on line oxidation of organic mercury to Hg^{2+} and chemical vapor generator of Hg^0; gas–liquid phase separator; atomic fluorescence detector equipped with miniaturized Ar/H_2 diffusion flame atomizer.

We verified that ultrafiltration membranes employed in this work do not cause artifactual formation of RSNO.

2.5. Apparatus

2.5.1. Chromatographic instrumentation

An HPLC gradient pump (P4000, ThermoQuest) was coupled with: a mechanical degassing system (SC1000, ThermoQuest), a Rheodyne 7125 injector (Rheodyne, Cotati, CA, USA), and a 50 μL injection loop. Sample eluted from the column passed into a diode array detector (UV6000, ThermoQuest) equipped with a 5 cm path length flow cell (10 μL), and finally into the CVGAFS detection system. This detection system (RPLC–DAD–CVGAFS) provided multi-dimensional analysis, including UV/visible absorbance and mercury-specific chromatograms, from a single injection. The instrumental set up gave a delay of retention times between the two sequential detectors of 20 s. The detection limit (LODc) for GSNO was at best 0.2 μM with DAD detection (by employing a flow cell with 5 cm path length) because of the low value of extinction coefficient, the GS–PHMB complex can be determined by CVAFS detection in the adopted operating conditions with a detection limit of 25 nM, a precision (CV%) of 6.5% at 0.3 μM concentration level, and a 0.08–50 μM linear dynamic range.

2.5.2. Chromatographic conditions

The HPLC separations were carried out by a reversed phase HPLC column Hydra RP C_{18} (Phenomenex) 250 mm × 4.6 mm (silica particle size 4 μm), equipped with a Guard Cartridge KJ0-4282 Phenomenex with an isocratic elution in 97% 0.02 M PBS pH 7.0 or 6.0, 3% methanol, flowing at 1 mL min^{-1}. The chromatographic run was complete in 13 min by using an eluent phase at pH 7.0 or 10 min at pH 6.0.

All the solutions were filtered by a 0.45 μm cellulose acetate filter (Millipore).

2.5.3. Chemical vapor generation with AFS detection

Fig. 1 shows the schematic diagram and a detailed description of the continuous flow (CF) mercury chemical vapor generator modified for on line oxidation of organic mercury to inorganic Hg(II) in a miniaturized Ar/H_2 flame. The details have been previously reported [31–35]. Reagent concentrations, reaction coil dimension, and flow rates, as well, were optimized and reported elsewhere [40].

2.5.4. ESI-MS measurements

The ESI-MS^n experiments were performed on a Finnigan LCQ DecaXP ion trap mass spectrometer (Thermo Finnigan, San Jose, CA) equipped with a commercial atmospheric pressure ESI source. The mass spectrometer parameter was optimized to obtain maximum sensitivity. The temperature of the LCQ capillary was held at 250 °C. The automatic gain control (AGC) was on. The number of scans averaged was chosen arbitrarily balancing speed of analysis and signal to noise ratio. The mass spectrometer was operated both in positive and negative ion mode. The typical sample infusion flow rate was 5 μL min^{-1}.

3. Results and discussion

3.1. Reactivity of GSNO toward PHMB: UV/visible measurements at 334 nm

In preliminary experiments the rate of the reaction between GSNO and an excess of PHMB was measured by UV–vis spectrophotometry, by following the disappearance of GSNO absorbance at 334 nm both in the absence and in the presence of ascorbic acid. The results are reported in Fig. 2. All the measurements were performed in the presence of 0.5 mM EDTA in order to prevent Cu^{2+}-dependent decomposition. It is known in literature that ascorbate accelerates *in vitro* and *in vivo* the decomposition of GSNO [7,41–43]. The decomposition of GSNO was also studied by Holmes and Williams [44] in a reaction medium containing a strong excess of ascorbate in the range of 2–20 mM. In our experiments (Fig. 2) 5 mM ascorbate did not significantly decompose GSNO within 10 min reaction time in agreement with the kinetic reported by Holmes and Williams [44] (Fig. 2, curve a). Instead, 500 μM PHMB decomposed GSNO by about 50% (Fig. 2, curve b). We observed a dramatic increase of the decomposition rate of GSNO by PHMB when 5 mM ascorbate was present (Fig. 2, curve d), while no

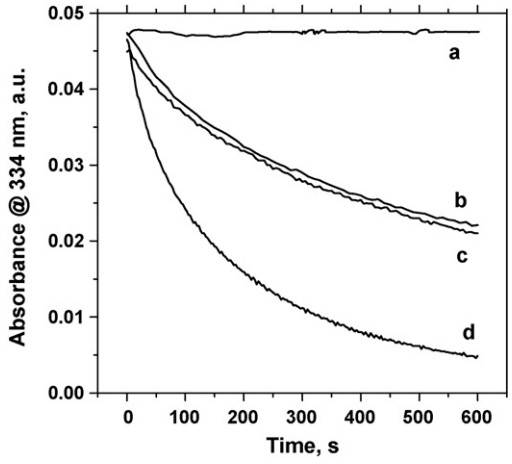

Fig. 2. Absorbance–time plots measured at 334 nm featuring the decomposition of 50 μM GSNO in 0.1 M PBS pH 7.4, 0.5 mM EDTA, at 21 °C in the presence of 5 mM ascorbate (no PHMB) (a), 500 μM PHMB (no ascorbate) (b), 0.5 mM ascorbate and 500 μM PHMB (c), 5 mM ascorbate and 500 μM PHMB (d).

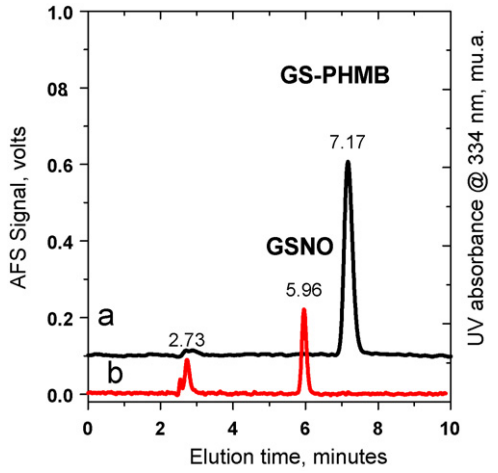

Fig. 3. (a) RPLC-CVGAFS chromatogram of 20 μM GSH, 40 μM PHMB in 0.1 M PBS pH 7.43, 0.5 mM EDTA, (b) absorbance chromatogram at 334 nm of 294 μM GSNO in 0.1 M PBS pH 7.43, 0.1 M EDTA. Chromatographic conditions: isocratic elution in 97% 0.02 M PBS pH 7.0, 3% methanol; flow rate = 1 mL min^{-1}.

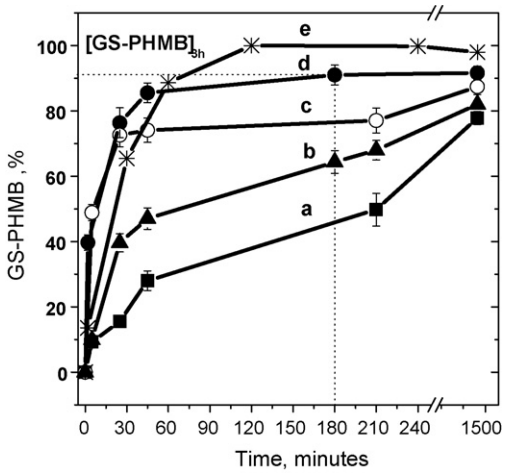

Fig. 4. Effect of GSNO:PHMB molar ratio and incubation time on the percentage of formation of the GS–PHMB complex produced by the reaction of GSNO (5 μM) with PHMB in 0.1 M PBS pH 7.4, 0.5 mM EDTA ($t = 21 \pm 1$ °C). PHMB:GSNO = 2 (curve a), 10 (curve b), 20 (curve c), 50 (curve d), PHMB:GSNO = 5 (curve e), in the presence of 5 mM ascorbate in the reaction medium.

significant effect was observed in the presence of 0.5 mM ascorbate (curve c).

PHMB decomposed GSNO much faster than ascorbate and the simultaneous presence of the two reagents at 5 mM concentration level of ascorbate clearly produced a synergistic effect on the decomposition rate of GSNO.

We observed that in the absence of ascorbate the decomposition of GSNO was complete in 10 min for PHMB/GSNO molar ratio ≥20 and for PHMB/GSNO molar ratio ≥10 with 5 mM ascorbate (data not shown for brevity).

3.2. Reactivity of GSNO toward PHMB: RPLC–DAD–CVGAFS measurements

Sulfydryl group of GSH reacts quantitatively with PHMB in stoichiometric amount of 1:2 molar excess at room temperature in 0.1 M PBS, pH 7.4, 0.5 mM EDTA in less than 2 min and the complex is stable 48 h at room temperature and for months at −20 °C [35].

Fig. 3 shows the RPLC-CVGAFS chromatograms of the GS–PHMB complex and the absorbance chromatogram of GSNO standard solution eluted in 20 mM PBS, pH 7.0, 3% MeOH. GS–PHMB complex eluted at 7.17 ± 0.1 min. In the adopted eluting conditions, GS–PHMB and GSNO were separated, the last one eluting at 5.96 ± 0.2 min. The peak eluting with the dead volume of the column was present also injecting the PHMB in the same buffer solution and it was likely due to a non-covalent complex of PHMB with EDTA. The PHMB excess eluted as a broad peak between 22 and 27 min and it did not interfere with the analysis.

By contrast, in the same conditions employed for obtaining the GS–PHMB complex from GSH (PHMB:GSNO molar ratio = 2) we found that GSNO reacted slowly with PHMB. By sequential chromatographic analysis of a GSNO/PHMB mixture over 24 h we observed the disappearance of GSNO peak in the absorbance chromatogram at 334 nm, and the correspondent appearance of the GS–PHMB peak in the CVGAFS chromatogram. After 3 h incubation at room temperature, less than 40% of GSNO was converted to the derivative eluting at 7.17 min and after 24 h it reached only the 77%.

The kinetic of this reaction was studied as a function of the molar ratio GSNO:PHMB. The effect of PHMB:GSNO molar ratios was systematically studied by choosing a GSNO concentration quantitatively detectable also by UV absorbance at 334 nm, but 10 folds lower than that employed in UV experiments. Fig. 4 shows the effect of GSNO:PHMB molar ratio and incubation time on the percentage of formation of the GS–PHMB complex produced by the reaction of GSNO with PHMB.

By increasing the molar ratio PHMB:GSNO from 2 to 50 the reaction was complete in 180 min at room temperature, giving the complete, simultaneous disappearance of GSNO peak (curve not shown in figure for brevity) and about the 90% of GSNO decomposed in form of GS–PHMB complex. The quantitative conversion of GSNO to GS–PHMB derivate was calculated on the basis of the values of peak area of GS–PHMB complex at 7.17 min and of GSNO at 5.96 min (Fig. 3), and the respective calibration curves. The percentage of formation of GS–PHMB complex was calculated on the basis of the following equation:

$$\text{GS–PHMB\%}(t) = \frac{S(t)_{\text{GS–PHMB}}/\text{slope}_{\text{GS–PHMB}}}{S^0_{\text{GSNO}}/\text{slope}_{\text{GSNO}}} \times 100 \quad (1)$$

where $S(t)_{\text{GS–PHMB}}$ was the area of GS–PHMB peak after t incubation time and S^0_{GSNO} was the GSNO peak area measured in the starting solution, before the addition of PHMB.

GSSG forming from GSNO decomposition can also be estimated from the balance of mass of GSNO:

$$[\text{GSSG}] = \frac{C_{\text{GSNO}} - ([\text{GSH}] + [\text{GSNO}])}{2} \quad (2)$$

where C_{GSNO} was the initial analytical concentration. Since we found chromatographically that GS–PHMB standard solutions were stable at room temperature for 48 h, it can be hypothesized that GS–PHMB complex or GSSG forms directly from GSNO decomposition, depending on a balance between the kinetics of reactions in the chosen operating conditions.

In Fig. 4 it is also reported the effect of 5 mM ascorbate on the derivatization reaction of GSNO by PHMB (PHMB:GSNO molar ratio = 5). As observed in the experiments described in Section 3.1, the ascorbate favourites the derivatization of GSNO by PHMB. The RPLC-CVGAFS chromatograms shown that the formation of the GS–PHMB complex was quantitative for PHMB:GSNO molar ratio = 5 after 120 min.

Both GSH and GSNO react with PHMB to give the same derivative. Thus, in the perspective of the analytical application of this derivatization reaction for the determination of GSNO also in the presence of GSH, we tested the derivatization reaction of a GSH/GSNO mixture in the presence of an alkylating agent of

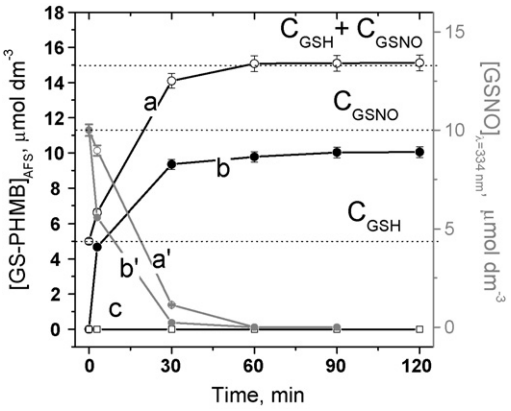

Fig. 5. Decomposition kinetic of GSNO (10 μM) with PHMB (100 μM) in 0.1 M PBS pH 7.4, 0.5 mM EDTA, 5.0 μM GSH ($t = 21 \pm 1$ °C) without NEM ((a) and (a′)) or with 0.1 mM NEM ((b) and (b′)) in the reaction medium; (c) GS–NEM complex as a function of time (5.0 μM GSH, 100 μM NEM, 100 μM PHMB in 0.1 M PBS pH 7.4, 0.5 mM EDTA, 21 ± 1 °C). (a′) and (b′) curves represent the decrease of GSNO concentration calculated from the decrease of the GSNO peak in the absorbance chromatogram at 334 nm. Dotted lines indicate the expected values of GS–PHMB concentrations corresponding to the initial analytical concentrations.

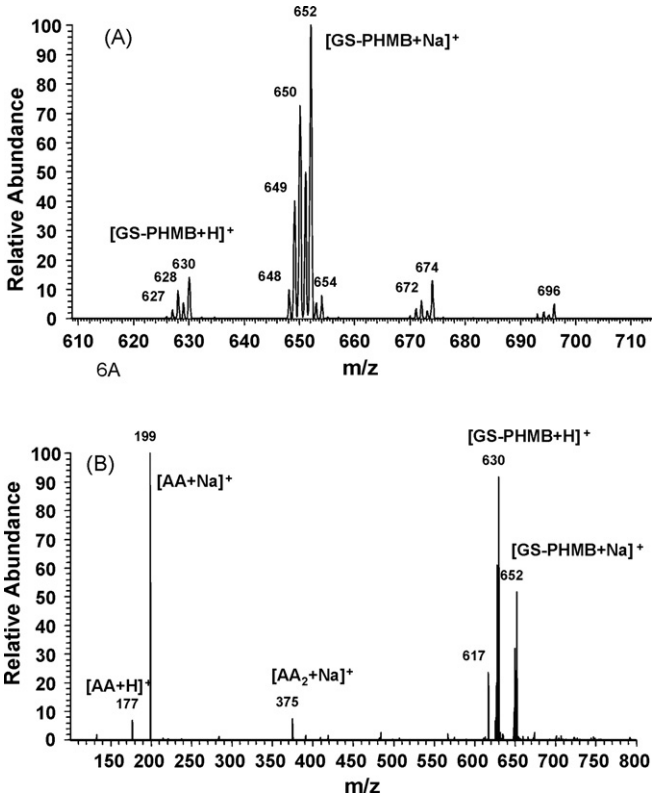

Fig. 6. (A) ESI-MS spectrum of GS–PHMB obtained by the reaction of GSH with PHMB (1:1 molar ratio, [GSH] = 125 μM) in the absence of ascorbate, showing the mercury isotopic pattern of GS–PHMB complexes. (B) ESI-MS spectrum of GS–PHMB obtained by the reaction of GSNO with PHMB (1:1 molar ratio, [GSNO] = 125 μM) with 1.25 mM ascorbate in the reaction medium. AA = ascorbic acid: AA_2 = ascorbic acid dimer.

–SH groups, the *N*-ethylmaleimide [39], in the reaction medium. RPLC–DAD–CVGAFS experiments performed in the presence of NEM showed that 0.1 mM NEM in the reaction medium containing GSNO and GSH (NEM:GSNO molar ratio = 10, NEM:GSH molar ratio = 20, Fig. 5) blocked quantitatively –SH groups and avoided GSH titration. However, the excess of NEM did not affect the reactivity of GSNO with PHMB, giving a GSNO recovery of 89 ± 4% ($N = 3$) in form of GS–PHMB complex after 120 min reaction. This percentage was not significantly different from 91 ± 4% obtained in the absence of NEM after 180 min reaction (Fig. 4). We also found that, once alkylated by NEM, the –SH groups did not react any more with PHMB at 21 °C (Fig. 5, curve c).

Since at neutral pH NEM reacts faster than PHMB with –SH groups (20 s against 90 s for completion reaction) [31,39], the results may suggest that the reaction between GSNO and PHMB did not follow a sequential mechanism S_N1 involving the formation of a free thiolic intermediate. GSNO, more likely, reacted with PHMB according to a concerted S_N2 mechanism.

An inspection of Fig. 5 showed also that the reduced thiol, complexed or not with NEM, favourites the PHMB-mediated decomposition of GSNO that is quantitative and complete in 30–60 min. Almost in the same conditions (GSNO 5 μM, PHMB/GSNO molar ratio = 10, Fig. 4, curve b), 80% of GS–PHMB complex formed only after 24 h reaction time. Although the role of thiols in nitrosothiols decomposition has been mainly ascribed to their reducing properties able to convert Cu(II) to Cu(I) [45] this result cannot be mediated by the –SH group that was alkylated, in a set of experiments, by NEM. This result could be due to the role of GSH as NO acceptor, according to the results of several authors who reported on Cys-mediated decomposition of CysNO also in the presence of metal-chelating agents [46].

RPLC–DAD–CVGAFS experiments confirmed, as well, that GSSG does not interfere with the derivatization reaction (not shown for brevity) and this can be addressed to their respective reduction potentials [47].

3.3. ESI-MS experiments

ESI-MS was employed in the study of GSNO–PHMB reaction to confirm the identity of some reaction products. In several ESI-MS experiments 1.25 mM ascorbate was employed in order to make the reaction complete in 10 min also for GSNO/PHMB molar ratios close to 1. In the absence of ascorbate the mixture GSNO/PHMB was stable in the same reaction time (10 min). Pure PHMB solution gave no detectable ESI-MS spectra, while the spectrum of GS–PHMB was well detectable (Fig. 6A). Results confirmed that the product of the GSNO + PHMB reaction was the same of GSH + PHMB reaction, i.e. GS–PHMB complex (Fig. 6A and B, respectively). The signal of GSNO in Fig. 6B was not detectable (m/z 337 due to $[GSNO + H]^+$, mass spectrum not shown for brevity), indicating that GSNO was completely decomposed. ESI-MS experiments confirmed that GSSG did not react with PHMB in the presence of ascorbate or in its absence (data not shown for brevity).

Fig. 7A shows mass spectrum of GS–NEM complex. Mass spectrum is compatible with the formation of the complex shown in Fig. 7A, according to the literature data [48]. The addition of PHMB and ascorbate to the GS–NEM solution (Fig. 7B) did not affect the GS–NEM complex, showing the peaks characteristic of GS–NEM complex at 455, 477 and 499 m/z, but no peaks characteristic of GS–PHMB complex. Mass spectrum did not change 90 min after the sample preparation confirming the absence of GS–PHMB complex in the reaction solution. These results confirmed also the data obtained by HPLC-DAD-CVGAFS (Fig. 5, curve c). Once GS–NEM is formed, PHMB is not able to decompose GS–NEM complex to form GS–PHMB.

The ESI-MS spectra shown in Fig. 8 were obtained after reaction of GSNO and PHMB in the presence of NEM and ascorbate. They indicated that the only reaction products obtained was GS–PHMB while the GS–NEM complex was not detectable. The absence of GS–NEM was a clear indication that the formation of

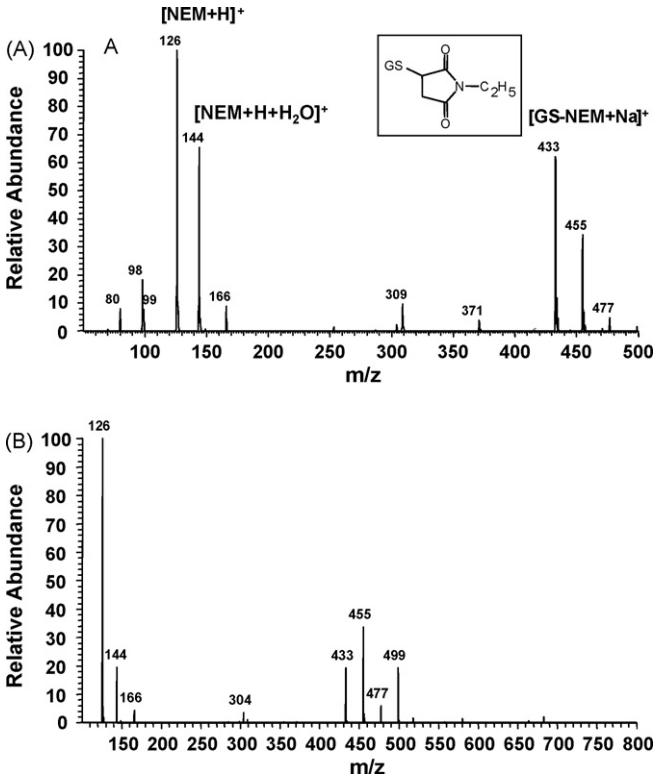

Fig. 7. (A) Mass spectrum of GS–NEM complex (5 mM NEM, 0.125 mM GSH). (B) Mass spectrum of the product of the reaction of 62.5 μM GSH, 0.63 mM NEM (NEM/GSH = 10), followed by the addition of 67 μM PHMB and 0.625 mM ascorbate. Complexation reaction has been performed at pH 8 and aliquots were treated with 40 μL formic acid to reach pH 3 before the ESI-MS analysis.

GS–PHMB did not pass through a dissociation step forming free GSH species.

The collected results suggested that the reactivity of GSNO with the monofunctional, organic mercurial probe PHMB is similar to that one reported for mercuric chloride [29]. In both cases the mercurial probes cleave the S–N bond leading to the formation of reaction products containing the S–Hg bond, $(GS)_2Hg$ and GS–PHMB for $HgCl_2$ and PHMB, respectively.

Thus, the reaction between GSNO and PHMB does not involve the formation of free thiolic species and it has the unique characteristic of directly derivatizing GSNO in a single step decomposition–derivatization process. The absence of a reaction step involving the formation of free GSH species, both in the absence and in the presence of ascorbate, represents a remarkable feature for the implementation of a derivatization method for the characterization and determination of GSNO in biological fluids.

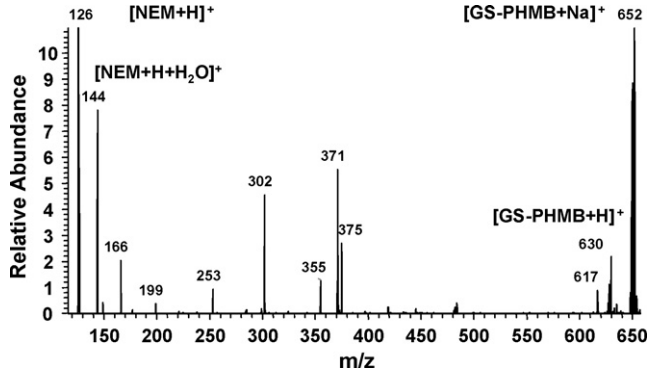

Fig. 8. Mass spectrum of the reaction product between 0.125 M GSNO and 0.1 mM PHMB in a reaction medium containing 5 mM NEM and 1.25 mM ascorbate analysed after 15 min reaction time.

3.4. Determination of GSNO, CysNO, HCysNO and CysGlyNO in human plasma: method development, validation and application

The results described in the previous section represent the fundamentals for the development of an analytical method for the determination of GSNO and other RSNOs in biological fluids. Indeed, Cys, HCys and CysGly as well as GSH form complexes with PHMB [35] and their *S*-nitrosoderivates CysNO, HCysNO and CysGlyNO are potentially detectable as thiol-PHMB complexes.

The PHMB complexes of Cys, HCys, GSH and CysGly were chromatographically separated in our experimental conditions (97% 20 mM PBS pH 6.0, 3% MeOH or 95% 20 mM PBS pH 6.0, 5% MeOH) in less than 10 min (t_R were 5.26, 7.33 and 9.3 for Cys-PHMB, HCys-PHMB, GS–PHMB and CysGly, respectively, with 3% MeOH, and 4.58, 6.03, 8.82 and 7.51 min with 5% MeOH). Thus, also CysNO, HCysNO and CysGlyNO can be selectively determined by the RPC–CVGAFS method if suitable operating conditions were found for their quantitative PHMB/ascorbate-mediated derivatization.

Therefore, we optimized the operating conditions for the derivatization of RSNOs with PHMB in the presence of NEM in the reaction medium in order to block, by alkylation, all the free –SH groups.

The optimization of the analytical operating conditions was performed by varying the concentration of PHMB and ascorbate on the basis of a central composite design (CCD, Box–Wilson design) between 0 and 1000 μM and 0.5 and 20 mM, respectively [49]. We evaluated the decomposition of a 50 μM RSNO solution by following the kinetics at 334 nm by UV spectroscopy and by determining the concentration of the RS–PHMB derivative formed by RPC–CVGAFS.

Table 1 reports the optimal conditions found by the experimental design for obtaining the maximal decomposition/derivatization (ranging between 75 and 100%) of RSNOs and the formation of the RS–PHMB complex by PHMB/ascorbate-mediated decomposition reaction.

CysNO, HCysNO and CysGlyNO required higher concentrations of ascorbate in order to avoid the formation of disulfides. We verified that in the extreme conditions studied (20 mM ascorbate and 1000 μM PHMB) GSSG and the oxidized species of Cys, HCys and CysGly were unreactive toward PHMB.

The operating conditions optimized for RSNOs derivatization in buffer summarized in Table 1 were applied to the decomposition/derivatization of RSNOs in real matrices. If we consider that, on the basis of the literature data, the maximum concentration of low-molecular weight RSNOs in plasma may be at best around 10 μM [4], on the basis of the data reported in Table 1 we chose a PHMB concentration of 150 μM ([PHMB]/[RSNO] = 15) and ascorbate concentration = 3.15 mM ([ascorbate]/[RSNO] = 315) in order to achieve the calibration curves of GSNO, HcysNO, CysNO and CysGlyNO within the range 0–5000 nM in 0.1 M PBS pH 7.4, 0.5 mM EDTA. Table 2 summarizes the results of the calibration experiments in buffer. GSNO calibration curve was also obtained in mixture with 10 μM GSH and 10 μM GSSG (concentrations by far higher than those present in plasma of healthy humans [38]) in the presence of 0.2 mM NEM without significant variations with respect to the results obtained in their absence.

3.4.1. Accuracy

In the absence of reference (certified or not certified) samples and not consolidated analytical methods for RSNOs, the accuracy of the method was evaluated by the analyte addition technique. Whole blood was spiked with GSNO, HCysNO, CysNO and CysGlyNO

Table 1
Experimental conditions for the optimal decomposition (75–100%) of RSNOs (50 μM) and the formation of the GS–PHMB complex by PHMB/ascorbate-mediated decomposition reaction in 0.1 M PBS pH 7.4, EDTA 0.5 mM, 21 °C, NEM 200 μM

RSNO	[Ascorbate] (mM)	[PHMB] (μM)	[Ascorbate]/[RSNO] ratio	[PHMB]/[RSNO] ratio
GSNO	≥9	≥500	≥180	≥10
CysNO	≥12.5	≥750	≥250	≥15
HCysNO	≥15.8	≥250	≥316	≥5
CysGlyNO	≥20	≥1000	≥400	≥20

solutions within the range 0–5000 nM. Due to the high amount of blood required for these experiments, performed in triplicate, a pool of whole blood collected in eparine and remained from routinely analysis was obtained from clinical laboratory. This sample was spiked with RSNOs only after the addition of NEM/EDTA/SBC solution (see Section 2.4). The lack of NEM/EDTA/SBC treatment in the sampling and storage step is the reason for which endogenous RSNOs were not detected in this pool sample. It was employed only for recovery tests of spiked RSNO species (see next paragraph).

Regression analysis between peak area (y) and RSNO concentration (x) spiked in blood gave linear fitting in the investigated range. The ratio of the slopes of the calibration curves in plasma ultrafiltrate and of the calibration curves in buffer gave a recovery of 97 ± 7 (R = 0.9908, N = 4) for GSNO, 98 ± 5 (R = 0.9876, N = 3) for HCysNO, 75 ± 14% (R = 0.965, N = 3) for CysNO and 73 ± 9% (R = 0.9953, N = 4) for CysGlyNO. The mean intra- and inter-assay variability in plasma ultrafiltrate in the concentration range investigated was 3 and 8% (CV), respectively. The LOQc was determined as 80 nM with a precision (CV) of 10%.

3.4.2. Interferences and selectivity

We also carefully investigated in blood possible source of interference concerning with derivatization reaction. This could be affected by those processes, which give underestimation or overestimation of the RS-fragment, which comes from RSNO. Concerning underestimation, the liberated RS-fragment from RSNO can be sequestered by reactive species other than PHMB. This possible interference is unlikely because the experiments in the presence of excess of NEM (ESI-MS and RPC–CVGAGS) indicated that the reaction does not proceed through the formation of free RSH. This minimizes the risk of underestimation. Concerning overestimation, it can arise from other low-molecular weight compounds containing the GS-fragment, Y-SG (Y = H, RS, R) present in plasma ultrafiltrate and that could be potentially broken by PHMB/ascorbate reaction to give GS–PHMB. However, the lack of peaks with the retention time of RS–PHMB derivatives in the ultrafiltrate of the unspiked pooled blood sample used for recovery experiments, suggested that neither NEM-complexed GSH nor GSSG nor RSR compounds (by analogy with NEM-complexed thiols) present in the plasma ultrafiltrate interfere with the measurement of RSNOs by this method. Furthermore, the recovery of GSNO in the ultrafiltrate sample obtained from blood treated with NEM/EDTA/SBC and spiked with the mixture 1 μM GSNO/10 μM GSH/10 μM GSSG was non-significantly different from that obtained in blood spiked only with GSNO (97 ± 7%). Thus, both S–S bond and C–S bond are not broken by PHMB/ascorbate reaction in buffer or plasma ultrafiltrate.

Table 2
Parameters of the linear regression analysis of calibration curves of GSNO, HcysNO, CysNO and CysGlyNO in 0.1 M PBS pH 7.4, EDTA 0.5 mM, 21 °C, NEM 200 μM derivatized by PHMB/ascorbate reaction and analysed by RPC–CVGAFS

RSNO[a]	Slope	R	Recovery[b]
GSNO	0.0154 ± 0.00017	0.9986	103 ± 5%
CysNO	0.0143 ± 0.00106	0.99458	90 ± 5%
HCysNO	0.0143 ± 0.00106	0.99458	95 ± 6%
CysGlyNO	0.0110 ± 0.00110	0.99458	73 ± 7%

[a] Operating conditions: 150 μM PHMB, 3.15 mM ascorbate in PBS 0.1 M pH 7.4, 0.5 mM EDTA, 0.2 mM NEM, incubation at 21 °C for 30 min.

[b] On the basis of ratio of the slope of calibration curve of RSNO decomposed/derivatized by PHMB/ascorbate and the corresponding RS–PHMB complex (0.015 ± 0.0007 slope, V min^{-1} μM^{-1}).

3.4.3. Determination of RSNOs in plasma ultrafiltrate and sampling issue

In this work we also faced the issues related to the stability of RSNOs during the sampling procedure.

CysNO and CGNO are the most labile species among RSNOs because of their structure [50]. It is known, and we also verified, that Cu(II) decomposes CysNO and CGNO in a few ms and HcysNO in minutes. The stability of CysNO, HcysNO and CGNO is guaranteed only if EDTA or diethylenetriamine-pentaacetic acid (DTPA) are present in the solution in order to complex metal and, most of all, Cu(II) [51]. However, if reduced thiols are present in the medium, like in blood/plasma, they reduce Cu(II) to Cu(I), and Cu(I) decompose also GSNO in a few seconds [50]. Therefore, the addition of NEM in blood as soon as it is sampled is mandatory (i) in order to avoid possible artifactual formation of RSNO due to transnitrosation reactions from proteins (basically nitroso-albumin) [52] and thiols (in particular GSH) present at micromolar concentration levels in plasma [38], (ii) in order to avoid RSNO losses [50].

Last, but not least, GSNO is a substrate of the enzyme γ-glutamyl-transferase (GGT) [53–55]. Thus, the following enzymatic decomposition of GSNO has to be inhibited:

$$\text{GSNO} + \text{acceptor} \xrightarrow{\text{GGT}} \text{CysGlyNO} + \gamma\text{-Glu-acceptor} \quad (1')$$

In normal subjects GGT is present in plasma at 10–50 U/L and dipeptides are the physiological acceptors of γ-Glu group. Once the more stable GSNO is converted in less stable CysGlyNO, this is easily decomposed [56]:

$$\text{CysGlyNO} \xrightarrow{\text{metals}} \text{NO} + \text{CG}_{\text{ox}} \quad (2')$$

Again, reaction (2′) is inhibited by the presence of metal-chelating agents (EDTA, DTPA).

In the previous published papers, no author controlled reaction (1′) during the sampling step.

Serine/borate complex is a potent inhibitor of reaction (1′) and we propose its use during blood sampling on the basis of the following results.

Fig. 9 shows the RPC–CVGAFS chromatograms of 4 ultrafiltrate plasma samples derivatized in the optimized conditions by 150 μM PHMB/3.15 mM ascorbate and analysed after 30 min incubation time at 21 °C. The peak broadening and the peak shape of the AF signal is due to the dead volume of the on line, post-column digestion system of PHMB derivates (oxidation coil of PHMB to Hg(II) with Br^-/BrO_3^- and reduction coil of Hg(II) to Hg^0 with $NaBH_4$/hydrazine) and stripping coil and gas–liquid separator of the AF detector (see Section 2.5.3). For P1, P3 and P5 ultrafiltrate, blood was sampled in eparine and immediately spiked with EDTA/NEM/SBC (procedure A). For P12 blood was sampled

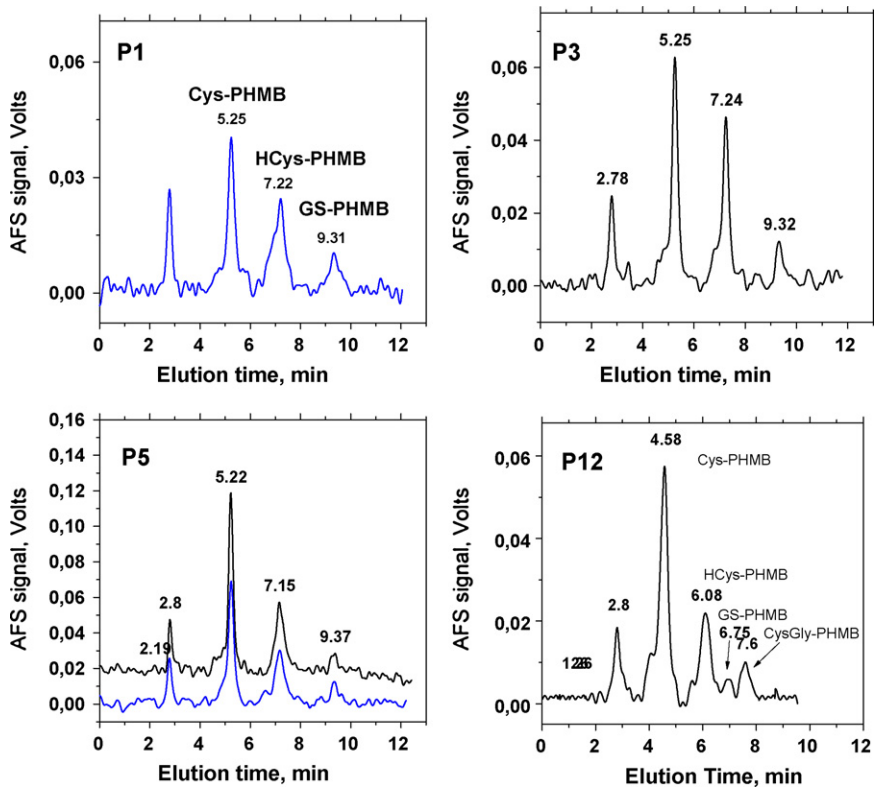

Fig. 9. RPC–CVGAFS chromatograms of ultrafiltrate plasma samples treated with 150 μM PHMB, 3.15 mM ascorbate at 21 °C for 30 min: P1, P3 and P5 blood was sampled in 12 mM NEM/0.5 mM EDTA/10 mM SBC (procedure A); P12 bloos was sampled in 12 mM NEM/0.5 mM EDTA (no SBC, procedure (B). P5 shows the chromatograms of the ultrafiltrate obtained from two distinct plasma aliquots, as example of the reproducibility of the analysis. Chromatographic conditions for P1, P3, P5: isocratic elution in 97% 20 mM PBS pH 6.0, 3% MeOH. Chromatographic conditions for P12: isocratic elution in 95% 20 mM PBS pH 6.0, 5% MeOH.

in eparine and immediately spiked with EDTA/NEM but no SBC (procedure B).

Table 3 shows the results of RSNO determination in human plasma from 12 volunteer donors, by following for 8 blood samples the procedure A and for 4 blood samples the procedure B.

The results showed that when NEM/EDTA/SBC was added immediately after blood sampling CysNO and HCysNO in plasma ultrafiltrate were 1460 ± 310 and 1000 ± 330 nM mean values, respectively. GSNO concentration was 320 ± 60 nM (mean value). CysGlyNO concentration was below the detection limit of the method. In the absence of SBC, GSNO peak decreased and the peak of CysGlyNO appeared in the RPC–CVGAFS chromatograms (Fig. 9, P12). In the absence of SBC CysNO, HCysNO, GSNO and CysGlyNO in plasma ultrafiltrate were 1850 ± 290, 1100 ± 300, 80 ± 8 and 200 ± 60 nM, respectively. The CV% of the entire procedure of analysis was around 10%. Interestingly, CysNO concentration was slightly higher in the ultrafiltrate samples obtained in the absence of SBC, which is in agreement with the

Table 3
RSNO determination in human plasma from 12 volunteer donors

Sample	[CysNO]* (nM)	[HcysNO]* (nM)	[GSNO]* (nM)	[CysGlyNO]* (nM)
Sampling with NEM/EDTA/SBC (procedure A)				
P1	1100 ± 100	900 ± 70	300 ± 30	<LOQc
P2	1000 ± 200	500 ± 40	300 ± 30	<LOQc
P3	1700 ± 170	1400 ± 100	370 ± 40	<LOQc
P4	1500 ± 340	1100 ± 190	330 ± 40	<LOQc
P5	1970 ± 340	1460 ± 120	290 ± 40	<LOQc
P6	1460 ± 200	860 ± 100	210 ± 10	<LOQc
P7	1620 ± 110	770 ± 100	330 ± 30	<LOQc
P8	1250 ± 130	940 ± 110	410 ± 40	<LOQc
Mean values ± S.D. (*N* = 8 subjects)	1460 ± 310	1000 ± 330	320 ± 60	
Sampling with NEM/EDTA (procedure B)				
P9	2100 ± 40	1300 ± 40	75 ± 10	160 ± 30
P10	1600 ± 100	1100 ± 40	<LOQc	250 ± 40
P11	2100 ± 100	1250 ± 50	80 ± 10	140 ± 20
P12	1600 ± 110	650 ± 60	90 ± 10	270 ± 10
Mean values ± S.D. (*N* = 4 subjects)	1850 ± 290	1100 ± 300	80 ± 8	200 ± 60

S.D. refers to *N* = 3 replicates.
* Values correspond to the plasmatic concentration of each RSNO, taking into account the 1:1 dilution factor of plasma.

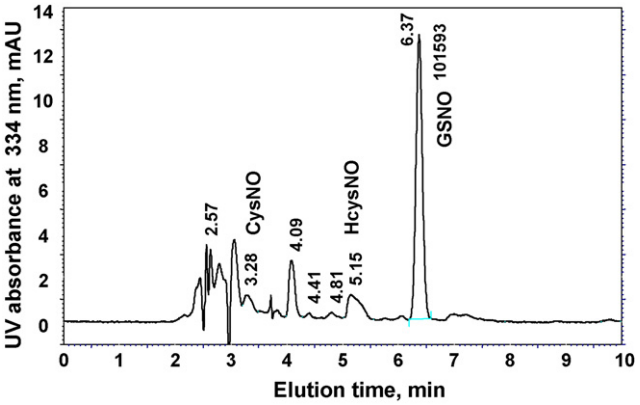

Fig. 10. UV absorbance chromatogram at 334 nm of the P2 plasma ultrafiltrate sample spiked with 20 μM GSNO.

formation of CysNO from CysGlyNO by the reaction of dipeptidases [57].

These results clearly show that the missing control of GGT activity even in normal subjects (what about in patients with GGT concentration levels >50 U/L?) gives a loss of GSNO in the pre-analytical step. This can be an additional factor, among the other discusses in the present paper, which contributes to the huge dispersion of GSNO concentrations reported in plasma by different authors.

In conclusion, only the immediate addition of the EDTA/NEM/SBC solution spiked to real samples guaranteed the stability of RSNOs. This applies both to endogenous and spiked RSNOs present in the sample. As a consequence of these results, we believe that all the work on the determination of RSNOs in human plasma has to be carefully revised, hopefully in the framework of an interlaboratory study.

The relative abundance of CysNO and HCysNO found deserves a discussion, as well.

The CysNO value found is about 20% of the total concentration of (free) reduced cysteine in human plasma [38]. HCysNO value found is about 7–20% of the total homocysteine (reduced and oxidized) in human plasma and about 20 times the concentration of reduced, free homocysteine [58]. Although there are a lot of studies on the RSH/RSSR ratio in biological fluids, nobody systematically studied if RSNOs belong to "oxidized pool" or "reduced pool" of thiols (this is in progress in our laboratory). Other authors [11] and we found [35] that GSNO belongs to "oxidized pool" and it reacts with derivatization agents only after treatment with strong reducing agents (DTT, β-mercaptoethanol).

This suggests that, once the stability of the analytes in the pre-analytical step is preserved and once we are sure that no interferences exist in the measurement, no prejudices should exist on the "high" values of HCysNO or CysNO found.

As micromolar concentrations of CysNO and HCysNO should be in principle detectable by UV detector, P2 ultrafiltrate sample, spiked with 19 μM GSNO, was also analysed by inspecting the UV absorbance chromatogram at 334 nm (Fig. 10). GSNO was added, instead, because the concentration of endogenous GSNO in P2 sample was close to the UV detection limit (0.2 μM). On the basis of the peak area of GSNO at 6.37 min and the slope of GSNO analyte addition curve in blood (10618 ± 1579 mAU at 334 nm min^{-1} μM^{-1}, $R = 0.9978$, $N = 4$) we found a GSNO concentration by UV detector of 19 μM, taking into account the 1:1 factor dilution of plasma (101% recovery). In Fig. 10 the peaks of CysNO and HcysNO at 3.28 and 5.15 min, respectively, identified by the injection of standard solutions, can be detected, but, because of the poor specificity and sensitivity of the absorbance at 334 nm, they cannot be accurately measured.

4. Conclusion

Aqueous phase reaction of PHMB with RSNOs (pH 7.4) forms the RS–Hg–(C_6H_4)–COO^- complex (RS–PHMB). The reaction is quantitative under optimized conditions, and it has the unique characteristic of directly derivatizing RSNO with a single step decomposition–derivatization process, which does not involve the formation of free thiols. RS–PHMB complexes are stable during the working day and are selectively and sensitively (LODc = 30 nM) determined by liquid chromatography coupled to mercury-specific AFS detector. The rate of formation of RS–PHMB derivative is accelerated by the presence of appropriate excess of ascorbate. Interfering reaction pathways giving RS–PHMB derivatives from free RSHs are blocked by excess of NEM, while RSSRs did not generate RS–PHMB in the presence or absence of NEM. In the presence of NEM recovery of RSNO are not significantly affected by the presence of excess of RSHs and RSSRs both in pure aqueous buffer and human plasma samples.

In the application of the analytical derivatization method to determination of RSNOs in human plasma it is of paramount importance the adoption of a sampling and storage protocol which ensures the stability of RSNOs in the pre-analytical step. The addition of EDTA, NEM and SBC prevents the degradation of RSNOs due to reaction with metal ions, transnitrosylation reactions and enzyme-mediated reactions (by GGT), respectively. This applies to both spiked and endogenous RSNOs. The speciation and determination of endogenous RSNOs in plasma is here reported for the first time in the literature.

The final consideration is on GSNO determination in plasma and on the huge variance of concentration levels reported by different authors. The trend is to address the inconsistency of results to the inaccuracy of analytical methods or protocols, while little attention has been devoted to the pre-analytical step, sampling and storage, which could be a major source of inaccuracy due to occurrence of endogenous process altering the concentration of GSNO. The results reported in this work are obtained by using a new analytical method, possessing a reasonable degree of selectivity, combined with a protocol for the stabilization of GSNO in plasma, represents a contribution to the determination of GSNO and other nitrosothiols in plasma samples.

Acknowledgements

This work has been financially supported by CNR. The authors thank M. Cempini, M. Onor, M.C. Mascherpa, C. Lanza and R. Spiniello for their technical support.

References

[1] B. Gaston, J. Reilly, J. Drazen, J. Fackler, P. Ramdev, D. Arnell, M.E. Mullins, D.J. Sugarbaker, C. Chee, D.J. Singel, J. Loscalzo, J.S. Stamler, Proc. Natl. Acad. Sci. U.S.A. 90 (1993) 10957.
[2] V.G. Kharitonov, A.R. Sundquist, V.S. Sharma, J. Biol. Chem. 270 (1995) 28158.
[3] R.M. Clancy, D. Levartovsky, J. Leszczynska-Piziak, J. Yegudin, S.B. Abramson, Proc. Natl. Acad. Sci. U.S.A. 91 (1994) 3680.
[4] D. Giustarini, A. Milzani, I. Dalle-Donne, R. Rossi, J. Chromatogr. B 851 (2007) 124.
[5] D. Giustarini, A. Milzani, R. Colombo, I. Dalle-Donne, R. Rossi, Trends Pharmacol. Sci. 25 (2004) 311.
[6] P.H. MacArthur, S. Shiva, M.T. Gladwin, J. Chromatogr. B 851 (2007) 93.
[7] D.L.H. Williams, Acc. Chem. Res. 32 (1999) 869.
[8] J.S. Stamler, J. Loscalzo, Anal. Chem. 64 (1992) 779.
[9] A.M. Leone, M. Kelm, in: M. Feelisch, J.M. Stamler (Eds.), Methods in Nitric Oxide Research, Wiley, Chichster, 1996, p. 499.
[10] W. Cha, Y. Lee, B.K. Oh, M.E. Meyerhoff, Anal. Chem. 77 (2005) 3516.

[11] D. Tsikas, J. Sandmann, S. Rossa, F.-M. Gutzki, J.C. Frohlich, Anal. Biochem. 273 (1999) 32.
[12] A. Gow, A. Doctor, J. Mannick, B. Gaston, J. Chromatogr. B 851 (2007) 140.
[13] S.C. Rogers, A. Khalatbari, P.W. Gapper, M.P. Frenneaux, P.E. James, J. Biol. Chem. 280 (2005) 26720.
[14] B.K. Yang, E.X. Vivas, C.D. Reiter, M.T. Gladwin, Free Radic. Res. 37 (2003) 1.
[15] X. Wang, N.S. Bryan, P.H. MacArthur, J. Rodriguez, M.T. Gladwin, M. Feelisch, J. Biol. Chem. 37 (2006) 26994.
[16] A. Hausladen, R. Rafikov, M. Angelo, D.J. Singel, E. Nudler, J.S. Stamler, Proc. Natl. Acad. Sci. U.S.A. 104 (2007) 2157.
[17] A.R. Butler, P. Rhodes, Anal. Biochem. 249 (1997) 1.
[18] J.S. Stamler, E.J. Toone, Curr. Opin. Chem. Biol. 6 (2002) 779.
[19] J. Barrett, L.J. Fitzgibbons, J. Glauser, R.H. Still, P.N.W. Young, Nature 211 (1966) 848.
[20] L. Field, R.V. Dilts, R. Ravichandran, P.G. Lenhert, G.E. Carnahan, J. Chem. Soc., Chem. Commun. (1978) 249.
[21] H. Rheinbolt, F. Mott, J. Prakt. Chem. 133 (1932) 328.
[22] J. McAninly, D.L.H. Williams, S.C. Askew, A.R. Butler, C. Russell, Chem. Commun. 23 (1993) 1758.
[23] P. Andrew, P. Dicks, H. Beloso, D.L.H. Williams, J. Chem. Soc. Perkin Trans. 2 (1997) 1429.
[24] D.L.H. Williams, Org. Biomol. Chem. 1 (2003) 441.
[25] J. Stuart, C. Askew, D.J. Barnett, J. McAninly, D.L.H. Williams, J. Chem. Soc., Perkin Trans. 2 (1995) 741.
[26] A.P. Dicks, H.R. Swift, D.L.H. Williams, A.R. Butler, H.H. Al-Sadoni, B.G. Cox, J. Chem. Soc., Perkin Trans. 2 (1996) 481.
[27] A.C.F. Gorren, A. Schrammel, K. Schmidt, B. Mayer, Arch. Biochem. Biophys. 330 (1996) 219.
[28] R.J. Singh, N. Hogg, J. Joseph, B. Kalyanaraman, J. Biol. Chem. 271 (1996) 18596.
[29] H.R. Swift, D.L.H. Williams, J. Chem. Soc., Perkin Trans. 2 (1997) 1933.
[30] B. Saville, Analyst 83 (1958) 670.
[31] E. Bramanti, S. Lucchesini, A. D'Ulivo, L. Lampugnani, R. Zamboni, M. Spinetti, G. Raspi, J. Anal. Atom. Spectrom. 16 (2001) 166.
[32] E. Bramanti, C. Sortino, C. Lomonte, M. Onor, R. Zamboni, G. Raspi, A. D'Ulivo, Talanta 63 (2004) 383.
[33] E. Bramanti, C. Lomonte, M. Onor, R. Zamboni, G. Raspi, A. D'Ulivo, Anal. Bioanal. Chem. 380 (2004) 310.
[34] E. Bramanti, C. Lomonte, A. Galli, M. Onor, R. Zamboni, G. Raspi, A. D'Ulivo, J. Chromatog. A 1054 (2004) 285.
[35] E. Bramanti, C. Vecoli, D. Neglia, M.P. Pellegrini, G. Raspi, R. Barsacchi, Clin. Chem. 51 (2005) 1007.
[36] K.R. Matthews, S.W.J. Kerr, J. Pharmacol. Exp. Ther. 267 (1993) 1529.
[37] A. Doctor, R. Platt, M.L. Sheram, A. Eischeid, T. McMahon, T. Maxey, J. Doherty, M. Axelrod, J. Kline, M. Gurka, A. Gow, B. Gaston, Proc. Natl. Acad. Sci. U.S.A. 102 (2005) 5709.
[38] M.A. Mansoor, A.M. Svardal, P.M. Ueland, Anal. Biochem. 200 (1992) 218.
[39] J.D. Gregory, J. Am. Chem. Soc. 77 (1955) 3922.
[40] A. D'Ulivo, E. Bramanti, L. Lampugnani, R. Zamboni, Spectrochim. Acta B 56 (2001) 1893.
[41] G. Scorza, D. Pietraforte, M. Minetti, Free Radic. Biol. Med. 22 (1997) 633.
[42] K.-I. Misato, Y. Makiko, I. Masayasu, FEBS Lett. 389 (1996) 149.
[43] A. Xu, J.A. Vita, J.F. Keaney, Hypertension 36 (2000) 291.
[44] A.J. Holmes, D.L.H. Williams, J. Chem. Soc., Perkin Trans. 2 (2000) 1639.
[45] A.P. Dicks, D.L.H. Williams, Chem. Biol. 3 (1996) 655.
[46] T. Komiyama, K. Fujimori, Bioorg. Med. Chem. Lett. 7 (1997) 175.
[47] K. Wang, W. Zhang, M. Xian, Y.-C. Hou, X.-C. Chen, J.-P. Cheng, P.G. Wang, Curr. Med. Chem. 7 (2000) 821.
[48] S. Kurono, T. Kurono, N. Komori, S. Niwayama, H. Matsumoto, Bioorg. Med. Chem. 14 (2006) 8197.
[49] D.C. Montgomery, Design and Analysis of Experiment, Wiley, London, 1976.
[50] D.R. Noble, D.L.H. Williams, Nitric Oxide 4 (2000) 392.
[51] D.H.L. Williams, Chem. Commun. (1996) 1085.
[52] O. Rafikova, R. Rafikov, E. Nudler, Proc. Natl. Acad. Sci. U.S.A. 99 (2002) 5913.
[53] S.C. Askew, A.R. Butler, F.W. Flitney, G.D. Kemp, I. Megson, Bioorg. Med. Chem. 3 (1995) 1.
[54] N. Hogg, R.J. Singh, E. Konorev, J. Joseph, B. Kalyanaraman, *S*-Nitrosoglutathione as a substrate for c-glutamyl transpeptidase, Biochem. J. 323 (1997) 477.
[55] V. Angeli, A. Tacito, A. Paolicchi, R. Barsacchi, M. Franzini, R. Baldassini, C. Vecoli, A. Pompella, E. Bramanti, *S*-Nitrosoglutathione as a substrate of gamma-Glutamyltransferase (GGT) - A Kinetic study, Arch. Biochem. Biophys. (2008), submitted for publication.
[56] H. Al-Sa'doni, A. Ferro, Clin. Sci. 98 (2000) 507.
[57] M.A. Shipp, A.T. Look, Blood 82 (1993) 1052.
[58] O. Nekrassova, N.S. Lawrence, R.G. Compton, Talanta 60 (2003) 1085.

Talanta 77 (2008) 800–803

Contents lists available at ScienceDirect

Talanta

journal homepage: www.elsevier.com/locate/talanta

Microwave enhanced alkaline digestion of silicate samples for determination of Fe_2O_3

Hong-Wei Cai [a,b], Ping Jiang [b], Ling Jin [b], Ji-Ming Hu [a,*]

[a] College of Chemistry and Molecular Sciences, Wuhan University, Wuhan 430072, PR China
[b] Department of Chemistry, Wuhan University of Technology, Wuhan 430070, PR China

ARTICLE INFO

Article history:
Received 10 January 2008
Received in revised form 11 July 2008
Accepted 16 July 2008
Available online 30 July 2008

Keywords:
Microwave alkaline digestion
Alkali metal hydroxide solution
Silicate samples
Fe_2O_3

ABSTRACT

A novel approach to the study of microwave enhanced alkaline digestion was developed for rapid digestion of silicate samples. By using alkali metal hydroxide solution as microwave digestion solvent, the feasibility and principle of digestion were discussed for the determination of Fe_2O_3 contents in quartz, kaolin, feldspar and soda-lime-silica glass. The results obtained from four standard samples and six real world samples are in good agreement with the certified values, and are comparable to the predicted results from traditional alkaline digestion method. All the above demonstrates that this new proposed method is precise, accurate and can provide a simple, fast and energy saving procedure for the determination of components in silicate samples.

1. Introduction

Silicate is an oxysalt which consists of silicic acid ion and different metal ions. It includes two kinds, one kind is crude silicate rock or mineral, and the other is artificial silicate, such as cement, glass and ceramic. They are widely used in industrial production, scientific analysis and daily life. Due to good chemical stability and the wide variety of silicates, it is very difficult to decompose the silicate samples. In routine method, first, the sample was decomposed by the acid soluble method or the alkalified melting method, and then, the chemical analysis or the instrumental analysis was used for the system analysis or the determination of one component in the sample [1].

In the acid dissolving method, the mixture of HF and H_2SO_4 is used as a solvent. After the silicate sample is decomposed, i.e. SiO_2 is transformed to SiF_4; the excessive HF must be eliminated by heating. Therefore, it takes more than 1 h for sample decomposition. In the alkalified melting method, alkalified solvent and high temperature (up to 900 °C) are used for sample decomposition. Although the decomposition efficiency of alkalified melting method is better than the former, there are still some disadvantages in this method, such as high temperature, erosion of material, electricity wastage, etc. It is necessary to develop these two traditional methods for silicate decomposition.

At present, the widely used microwave digestion method has the advantages of high speed and low energy consumption [2]. However, it is difficult to treat silicate samples by this method. As for routine microwave digestion, silicates are often digested with a mixture of concentrated HNO_3 and HF or HCl and HF. For instance, 9 mL HNO_3 and 3 mL HF were used to digest silicate samples [3], 2 mL aqua regia and 3 mL HF were adopted to digest high-Si and high-Al rocks [4] and 5 mL HNO_3, 1 mL HCl and 4 mL HF were used to digest soil [5] with microwave. It leads to decomposition or coordination compounds formed by the added HF with metal ion in the sample, such as AlF_6^{3-}, etc. Additionally, impurity will be introduced from glass-vessels eroded by HF. To avoid the influence of HF, excessive H_3BO_3 must be added, which makes the procedure more complicated and prolongs the digestion time [6–17]. Thus, it is difficult to apply in industrial production.

The caustic alkali was used to decompose corundum and quartz successfully in the airtight supercharger with PTFE lining by Dolezal [18]. At 240 °C with 30% KOH (m/v) 15 mL, it took 4 h to decompose corundum (1 g) and 5 h to decompose quartz (1 g), respectively. As the time of decomposition was too long and the airtight supercharger was developing at that time, the further work had not been carried out. NaOH solution was used to digest glass samples by Nascimento. But because the PTFE vessel was not airtight, NaOH solution was not able to dissolve real samples satisfactorily [19].

In the airtight PTFE instrument, if alkali metal hydroxide such as NaOH or KOH was used as solvent, the speeds of the polarity molecule (H_2O), OH^- and positive ion of the alkali metals get to $2.45 \times 10^9\ S^{-1}$, which leads to vibration and breakage among

* Corresponding author. Tel.: +86 27 68752439/8701; fax: +86 27 68752136.
E-mail address: jmhu@whu.edu.cn (J.-M. Hu).

0039-9140/$ – see front matter © 2008 Elsevier B.V. All rights reserved.
doi:10.1016/j.talanta.2008.07.035

the bonds, the friction and collision of the ions, and then, a great amount of thermal energy is produced rapidly. Therefore, there is more action between the solvent and the sample. On the other hand, the thermal energy from the dielectric fluid is several thousand times higher than that from the sample surface. It leads to very strong thermal convection, which constantly stirs and refreshes the surface of the sample to accelerate sample decomposition effectively. At the same time, the high temperature and high pressure in the airtight instrument can also accelerate the decomposition of sample.

In the airtight instrument, the reactions between the clay, such as Kalin and quartz in the alkaline digestion solvent are shown as follows:

$$Al_2O_3{\cdot}2SiO_2{\cdot}2H_2O\,(\text{Kaolin}) + 6NaOH = 2Na_2SiO_3 + 2NaAlO_2 + 5H_2O$$

$$SiO_2\,(\text{quartz}) + 2NaOH = Na_2SiO_3 + H_2O$$

Due to the destroyed Si–O tetrahedron in the silicate samples, the metal ions in the crystal lattice, such as Ca^{2+}, Mg^{2+}, Fe^{3+}, Al^{3+} and Ti^{4+} are dissolved into the solution. The spectroscopy method can be used to determine the content of metal ions.

To distinguish the method in which acid was used as solvent, the methods using alkali metal hydroxide as solvent were called microwave enhanced alkaline digestion method. The method with tetramethyl ammonium hydroxide as digestion could also be classified as the microwave enhanced alkaline digestion method. However, because of the alkalescence of tetramethyl ammonium hydroxide, it could not be used to digest silicate samples [20,21].

In this paper, a new technique based on alkalified solvent for microwave digestion was developed and was applied to determine the content of Fe_2O_3 in four silicate samples, i.e. quartz, kaolin, feldspar and soda-lime-silica glass. The probability and the efficiency of microwave digestion were discussed. The experimental results demonstrate that this new proposed method is precise, accurate and can provide a simple, fast and energy-saving procedure for the determination of components in silicate samples.

2. Experimental

2.1. Apparatus

MDS-2003A Microwave digestion instrument (Shanghai Sineo Microwave Chemistry Technology Co., China): The microwave output power is 800 W, the work pressure is 0.1–4.0 MPa, increment is 0.1 MPa.The instrument has the function of automatic controlling pressure and the digestion can be carried out by single pot or several pots. Midea microwave oven (Midea Co., China): The microwave output power is 700 W.There are five different temperatures for microwave heating: high, middle–high, middle–low and low temperature.

Microwave digestion pot (Shanghai Sineo Microwave Chemistry Technology Co., China): Composed of Telflon digestion inner pot and PEEK digestion outer pot. The maximum work pressure is 5.0 MPa and it has the function of automatic pressure-relief for safety protection.

722 N spectrophotometer (Shanghai 3rd Analytical Instrument Company, China).

2.2. Selection of instrument

At the beginning, 'MDS-2003A Microwave digestion instrument' was used to digest the silicate samples. The samples could be occasionally digested when the work pressure was 3.5 MPa. Even if NaOH concentration was increased to 700 g L^{-1} at the maximum work pressure of 4.0 MPa and more than 20 min digestion time, the successful digestion rate was improved to certain degree, but it does not satisfy the routine sample analysis.

As there is no microwave digestion instrument, which could afford higher pressure such as 5.0 MPa, the ordinary microwave oven was tried to digest the sample by the microwave digestion pot from the 'MDS-2003A Microwave digestion instrument' in the following experiments. Under the selected digestion parameters, it is interesting that the silicate samples were able to be digested at a rate of almost 100%. Compared with 'MDS-2003A Microwave digestion instrument', the digestion time was shortened from 10 to 3 min when the same concentrations of the solvents were used in the ordinary microwave pot.

In this work, the ordinary microwave oven along with the standard digestion pot was used to study the favorable digestion conditions.

For safety, the experiment was carried out in our reconstructed hood. In addition, the pressure in Teflon digestion inner pot could be detected and controlled from the height of the pressure plate on the digestion outer pot.

2.3. Reagents and standard material

450 g L^{-1} NaOH solution: 450 g NaOH was weighted and sufficiently dissolved in plastic bottle by adding 1 L H_2O.

100 μg mL^{-1} Fe standard solution: $NH_4Fe(SO_4)_2{\cdot}12H_2O$ (0.8634 g) was weighted in a 200 mL-beaker. After dissolving in 6 mol L^{-1} HCl (20 mL) and a little water, the solution was transferred to a volumetric flask (1 L). After diluting to the scale, it must be shaken up.

10 μg mL^{-1} Fe solution: Extract 25.00 mL Fe standard solution (100 μg mL^{-1}) into a volumetric (250 mL), dilute to the scale and shake up for usage.

10 g L^{-1} 1,10-phenanthroline solution: 10 g L^{-1} ascorbic acid solution, pH 4.3 HAc–NaAc buffer.

All reagents were of analytical grade and double distilled water was used. Four standard materials, which were confirmed by China National Technique supervision Administration, were chosen and their numbers were GBW03113 (quailz), GBW03122 (Kaolin), GBW 03116 (potassium feldspar) and GBW03117 (soda-line-silica glass).

2.4. Calibration curve

Take Fe standard solution (10 μg mL^{-1}) 0.00, 2.00, 4.00, 6.00, 8.00 and 10.00 mL in respectively the volumetric flask (50 mL), and then, 5.0 mL, 1,10-phenanthroline solution (10 g L^{-1}) and 2.0 mL HAc–NaAc buffer solution were added in each flask, and the mixtures were diluted and shaken up after 10 min placement.

At 508 nm with 1 cm cuvette, the absorbances of the solution were measured and the reagent blank was used as control. The calibration curve was plotted by using the concentration and the absorbance values.

2.5. Microwave digestion of sample and determination of Fe_2O_3 contents

The sample (0.1000 g) was weighted and put into the Teflon digestion pot. The alkalified digestion solution (5.0 mL 450 g L^{-1} NaOH) was added and stirred. The pot was covered and put into the microwave oven for sample digestion with the optimized program. Then the sample was taken out and cooled, and 10 mL HCl (1 + 1) was added slowly. The final Fe_2O_3 contents were obtained from the calibration curve.

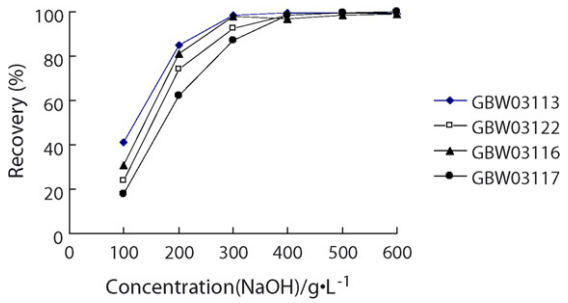

Fig. 1. Selection of microwave digestion solvent concentration (volume of solvent: 5.0 mL, time: 210 s, microwave: High).

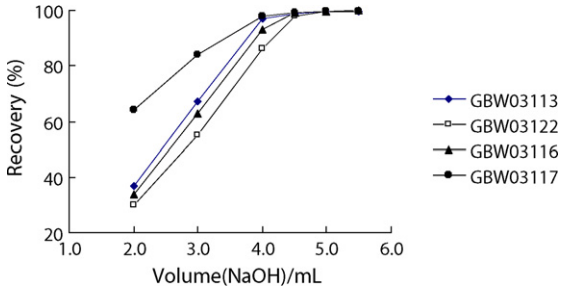

Fig. 2. Selection of microwave digestion solvent volume (concentration of NaOH: 450 g L^{-1}, time: 210 s, microwave: High).

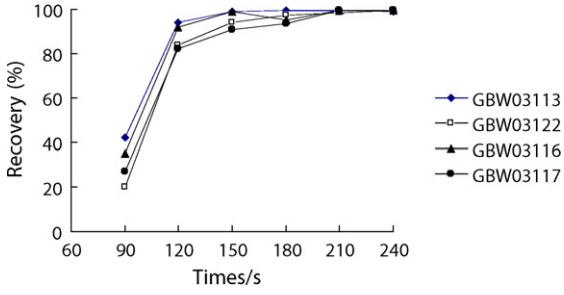

Fig. 3. Selection of microwave digestion solvent concentration (concentration of NaOH: 450 g L^{-1}, volume of solvent: 5.0 mL, microwave: High).

3. Results and discussion

3.1. Microwave digestion solvent and weight of sample

The NaOH, KOH, LiOH, Na_2CO_3, K_2CO_3, $LiBO_2$, $Na_2B_4O_7{\cdot}10H_2O$ solutions were used as solvent for digesting four silicate samples (quartz, kaolin, feldspar and soda-lime-silica glass). A clean and transparent solution was obtained when NaOH and KOH were used, but for other five solvents, only part of the sample was decomposed. So, in this work, NaOH was chosen to be the solvent because of its cheaper price as compared to KOH.

The more the samples weighted, more the digestion solution was added and longer the time for digestion was needed. The weight of silicate sample was selected to be around 0.1000 g in this research.

3.2. Concentration of solvent

Based on the determination of Fe content together with the clear and transparent solution, using the selected digestion solvent (5.0 mL NaOH) and 210 s digestion time with 0.1000 g sample, the effect of NaOH concentration was investigated. As shown in Fig. 1 and Table 1, more than 300 g L^{-1} NaOH was required to completely digest quartz and potash feldspar. However, more than 400 g L^{-1} NaOH was necessary for digesting kaolin and soda-lime-silica glass. In view of the complexity from actual samples, about 450 g L^{-1} NaOH was selected.

3.3. Volume of digestion solvent

According to the selected 450 g·L^{-1} NaOH, the effect of digestion solvent volume was studied under 210 s digestion time. When the volume of solvent rose to 4.5 mL, more than 97% recovery yield was obtained in four samples (Fig. 2). Therefore, 5.0 mL solvent was used in the following work.

3.4. Time for digestion

Using the selected digestion solvent (5.0 mL 450 g L^{-1} NaOH), the favorable digestion time was studied. It was found in Fig. 3 that more than 150 s were required for digesting quartz and potash feldspar completely, and about 180 s was needed for kaolin and soda-lime-silica glass. Therefore, 210 s was used as digestion time for the complex samples.

3.5. Selection of heating modes

In the ordinary microwave oven, there are normally five heating modes: high, mid–high, middle, mid–low and low temperatures. It was observed that the various digestion times corresponded to heating modes. In order to reduce digestion time, the high temperature mode was selected.

After detailed investigation of experimental parameters for microwave digestion, the final desired conditions for digestion of four silicate samples were determined as shown in Table 1.

3.6. Determination of Fe_2O_3 content in the certified samples

By adopting the selected digestion conditions in Table 2, the Fe_2O_3 contents in four certified samples were analyzed. As shown in Table 3, the determined values agreed well with the standard values. With 95% confidence level, the *t*-values were calculated and they were lower than the 95% probability coefficient *t*-value (2.776). It is shown that there was no significant difference between the results from the new method and the certified values. The standard deviations were 0.012, 0.009, 0.013 and 0.014, respectively. All the data strongly suggested that the developed digestion method had both high accuracy and precision.

Table 1
The effect of NaOH concentration

NaOH concentration (g L^{-1})	GBW03113	GBW03122	GBW03116	GBW03117
100	Turbidness	Turbidness	Turbidness	Turbidness
200	Turbidness	Turbidness	Turbidness	Turbidness
300	Transparence	Turbidness	Transparence	Turbidness
400	Transparence	Transparence	Transparence	Transparence
500	Transparence	Transparence	Transparence	Transparence

Table 2
Parameter of microwave digestion

Weight of sample (g)	Digestion solvent	Concentration of digestion solvent ($g\,L^{-1}$)	Volume of digestion solvent (mL)	Microwave	Time of digestion (s)
~0.1000	NaOH	450	5.0	High	210

Table 3
Determination of Fe_2O_3(%)in the standard materials ($n = 5$)

Standard materials	Standard value	Average	Standard deviation	Probability coefficient
GBW03113	0.21 ± 0.01	0.20	0.012	1.86
GBW03121	0.50 ± 0.03	0.53	0.029	2.31
GBW03116	0.19 ± 0.02	0.20	0.013	1.72
GBW03117	0.18 ± 0.01	0.17	0.014	1.60

Table 4
Determination of Fe_2O_3(%) in real samples

Real sample	High-temperature alkalified melting method	Microwave enhanced alkaline digestion method				Average
River sand	0.92	0.92	0.94	0.93	0.93	0.93
Quartz	0.12	0.11	0.12	0.11	0.10	0.11
Kaolin	0.78	0.77	0.76	0.77	0.78	0.77
Pyrophyllite	0.28	0.28	0.28	0.29	0.28	0.28
Feldspar	0.16	0.17	0.17	0.16	0.17	0.17
Soda-lime-silica glass	0.14	0.13	0.13	0.14	0.13	0.13

3.7. Determination of Fe_2O_3 content in real world samples

The new developed sample digestion method was further used to determine the Fe_2O_3 content in river sand, quartz, kaolin, pyrophyllite, feldspar and soda-lime-silica glass. As shown in Table 4, the results were also in good accord with data from the traditional high-temperature alkalified melting method. However, the microwave digestion method presents the significant advantages of being simple, time-saving, energy-saving, etc.

4. Conclusions

For the silicate sample, the digestion time was 210 s in the proposed method, which was much less than that in the traditional alkalified melting method and the acid soluble method. At the same time, the process of dissolving the clinker was avoided, and the time for treatment of the sample was shorted in the proposed method. Simultaneously, the method had significant advantages of being simple, time-saving and energy-saving, etc. It could be applied in the pretreatment and rapid analysis of silicate samples.

Compared to the microwave acid soluble method, the adding of HF was avoided. Therefore, the process to add excessive H_3BO_3 for eliminating HF could also be omitted. Additionally, the obtained solution from microwave digestion could be used to determine contents of SiO_2, Al_2O_3, CaO, MgO and TiO_2, etc. in the silicate sample, which solved the long-term problem the traditional microwave digestion technique whereby it was difficult to determine the contents of components directly in the silicate sample by using chemical analysis and photometric analysis. More research will be done in the near future.

The ordinary microwave oven had advantages of being cheap, time-saving, etc., but safety was a potential problem.

Acknowledgements

We are highly thankful to Shanghai Sineo Microwave Chemistry Technology Co. for freely providing us with MDS-2003A Microwave digestion instrument. We are also greatly thankful to Mr. Huang Xian-ting and Mr. Wang Qin-hua for their support.

References

[1] Compilation Committee of Rock and Mineral Analysis. Rocks and Minerals Analysis, vol. 1, third ed., Geological Publishing House, Beijing, 1991, p. 52.
[2] H.M. Kingston, L.B. Jassie (Eds.), Introduction to Microwave Sample Preparation Theory and Practice, American Chemical Society, Washington, 1998, p. 93.
[3] SW-846 EPA Method 3052, US Environmental Protection Agency, Washington, DC, 1995.
[4] K.L. Pruseth, S. Yadav, P. Meht, D. Pandey, J.K. Tripathi, Sci. Correspond. 89 (2005) 1668.
[5] D. McGrath, Talanta 46 (1998) 439.
[6] P. Barrett, L.J. Davidowski, J.K.W. Penaro, T.R. Copeland, Anal. Chem. 50 (1978) 1021.
[7] M. Bettinelli, G.M. Benone, S. Spezia, C. Baffi, Anal. Chim. Acta 424 (2000) 289.
[8] R.C. Richter, Dirk Link, H.M. Kingston, Anal. Chem. 73 (2001) 30.
[9] V. Sandroni, C.M.M. Smith, A. Donovan, Talanta 60 (2003) 715.
[10] J.L. Luque-Garc a, M.D. Luque de Castro, Trends Anal. Chem. 22 (2003) 90.
[11] R.T.T. Rantala, D.H. Loring, Anal. Chim. Acta 220 (1989) 263.
[12] J. Nieuwenhuize, C.H. Poley-Vos, A.H. van den Akker, W. van Delft, Analyst 116 (1991) 347.
[13] H. Matusiewicz, Anal. Chem. 66 (1994) 751.
[14] Y. Han, H.M. Kingston, R.C. Richter, C. Pirola, Des. Appl. 73 (2001) 1106.
[15] K. Swami, C.D. Judd, L. Husain, Fresenius, J. Anal. Chem. 369 (2001) 63.
[16] G. Pignalosa, N. Cabrera, A. Mollo, Spectrochim. Acta B 56 (2001) 1995.
[17] P. Kulkarni, S. Chellam, D.W. Mittlefehldt, Anal. Chim. Acta 581 (2007) 247.
[18] J. Dolezal, Anal. Chem. Acta 47 (1969) 517.
[19] P.C. Nascimento, D. Bohrer, E. Becker, L.M. Carvalho, J. Non-Cryst. Solids 351 (2005) 1312.
[20] S. Hauptkorn, J. Pavel, H. Seltner, Fresenius, J. Anal. Chem. 370 (2001) 246.
[21] H. Matusiewicz, B. Golik, Microchem. J. 76 (2004) 23.

Talanta 77 (2008) 822–826

Contents lists available at ScienceDirect

Talanta

journal homepage: www.elsevier.com/locate/talanta

Treating NIR data with orthogonal discrete wavelet transform: Predicting concentrations of a multi-component system through a small-scale calibration set

Chen-Bo Cai, Qing-Juan Han, Li-Juan Tang, Jin-Fang Nie, Li-Qun Ouyang, Ru-Qin Yu*

State Key Laboratory of Chemo/Biosensing and Chemometrics, College of Chemistry and Chemical Engineering, Hunan University, Changsha 410082, PR China

ARTICLE INFO

Article history:
Received 27 April 2008
Received in revised form 4 July 2008
Accepted 16 July 2008
Available online 31 July 2008

Keywords:
Near-infrared spectroscopy (NIR)
Discrete wavelet transform (DWT)
Correlation coefficient test (*r*-test)
Random experimental design
Partial least squares (PLS)
Multi-component
Small-scale calibration set

ABSTRACT

Through randomly arranging samples of a calibration set, treating their NIR spectra with orthogonal discrete wavelet transform, and selecting suitable variables in terms of correlation coefficient test (*r*-test), it is possible to extract features of each component in a multi-component system respectively and partial least squares (PLS) models based on these features are capable of predicting the concentration of every component. What is perhaps more important, with the proposed strategy, the predictive ability of the model is at least not impaired while the size of the calibration set can be obviously reduced. Therefore, it provides a more economical, rapid, as well as convenient approach of NIR quantitative analysis for multi-component system. In addition, all important factors and parameters related to the proposed strategy are discussed in detail.

1. Introduction

One of the most annoying burdens in NIR quantitative analysis is the demand for many calibration samples. It becomes more obvious in multi-component system, the most common situation in practice, where a calibration set with tremendous numbers of samples is usually required in order to accurately predict the amount of each component. For example, if using full experimental design, the number of calibration samples with 30 concentration levels (a moderate requirement for quantitative NIR analysis) in an one-component system is merely 30; the number of calibration samples with 30 levels for each component respectively in a two-component system is 900 (30^2); while that in a three-component system would become 27,000 (30^3). Of course, not all multi-component systems need a large-scale calibration set, in particular when concentrations of the system vary in a small range, or only a rough prediction is satisfactory so that several levels of the calibration set are enough [1–4]. But for a multi-component system with wide concentration scopes, it is impossible to make exact prediction in such a simple way because the larger the concentration interval in the calibration sets is, the more prediction error would be.

It seems that the size of calibration set could be decreased through carefully designing experiments like fraction factorial design, half-fraction factorial design, or popular orthogonal design. These methods could effectively find optimal point concerned, but may be not so helpful for solving the problem discussed above, since (1) what we need are precise predictions within the entire concentration range rather than just near a certain concentration point; (2) unlike full design, in formerly mentioned designs the fact that not all levels of one component have chance to combine with each level of another component may probably cause prediction error when the interactions among components are un-negligible and vary with concentrations; (3) even using these designs the number of experiments is often still great sometimes, for instance, in orthogonal design at least 900 (30^2) samples are demanded when each component needs 30 concentration levels.

Obviously, the number of calibration samples would become the least in the multi-component system, if the system conforms with two prerequisites simultaneously: (1) at least a part of absorption bands of each component are separate or not overlapping; (2) within the separate bands, the absorbances of every component are independent or insusceptible to the concentration variation

* Corresponding author. Tel.: +86 731 8822577; fax: +86 731 8822782.
E-mail address: rqyu@hnu.cn (R.-Q. Yu).

0039-9140/$ – see front matter © 2008 Elsevier B.V. All rights reserved.
doi:10.1016/j.talanta.2008.07.037

of all other components. For example, in a system that needs 30 concentration levels for each component, 30 calibration samples are enough no matter the system is one-component or multi-component. Unfortunately, it is untrue for most practical cases. But it is worth noting that all discussion above is limited in wavelength (or wavenumber) domain. Therefore, it is meaningful to study the feasibility of the strategy in other domains such as wavelet domain with the aim to make quantitative NIR analysis more economical, rapid, and convenient for multi-component systems.

2. Theory and algorithm

2.1. Treating NIR spectra with discrete wavelet transform (DWT)

Wavelets derive from a basis function (i.e., mother wavelet) through dilation and translation processes. DWT uses wavelets of different scales and positions to decompose a signal. Consequently, DWT can describe the feature of the signal in both time and frequency domains simultaneously. Furthermore, various mother wavelets in terms of its waveform or length make DWT more powerful and flexible to extract the feature of the signal as compared with other signal processing methods. In other words, through the DWT nearly all information of the original signal in time (or position) domain can be transformed into a series of coefficients (namely, approximation coefficients and detail coefficients) in a new time–frequency (or position-scale) space. Consequently, some features inconspicuous in the initial domain might become obvious in the new space [5,6]. It is worth noting that there is usually overlapping information among these coefficients unless the mother wavelet is discrete as well as orthogonal. This will be discussed later in detail.

The same DWT procedure can be simply implemented for a NIR spectrum as long as the time domain is replaced by the wavelength domain. Therefore, it is possible for DWT to magnify some features of the NIR spectrum as a "microscope". In fact, just because of this advantage, it has been widely applied to NIR analysis for decades as a pre-processing step to suppress noise, correct baseline, or compress database [5–11]. As for the field of multivariate calibration, there also have been a number of reports related to DWT [12–15]. But to our knowledge, little effort has been made to study the application of DWT to predicting the amount of each component in multi-component systems with a small-scale calibration set.

There are two ways to build a multivariate calibration model between the concentrations of components and the NIR signal responses. One is to reconstruct spectra with detail coefficients and approximation coefficients after denoising, correction and/or database compression, and then build a model between the reconstructed spectra and the concentrations [8]. Another way is directly to use these processed coefficients as variables, since wavelets transform a signal linearly from its original domain to a new domain without prejudice. Clearly, the latter strategy is more convenient and time-saving, and accordingly becomes more and more popular recently [5,6,12–15]. In this paper, we also selected the latter method.

2.2. Criterion for variable selection and the least sample required in a multi-component system

In the wavelet domain, all information of a NIR spectrum of a multi-component system is transformed into a series of detail and approximation coefficients. Now what we need is to determine which coefficients are related merely to the concentration of a particular component, while insusceptible to the concentration variation of all other components. Such coefficients can be used as variables to build a multivariate calibration model for predicting the concentration of this component. A variety of chemometrics methods have been developed to select variables for model construction, from stepwise regression analysis (SRA) [16], uninformative variables elimination (UVE) [17–20], genetic algorithm (GA) [12,14,20–23], simulated annealing algorithm (SAA) [24], interval partial least squares (iPLS) [25], to moving window partial least squares regression (MWPLSR) [26,27]. These methods work well in their own cases, but might be not appropriate for the case of our concern, since they mainly focused on selecting variables most relevant to one component without paying special attention to the correlation between these variables selected and other components.

For the purpose, we have tried to combine random experimental design with correlation coefficient test (r-test). In random experimental design: (1) the concentration of any component in one sample should differ from the concentrations of that component in all other samples if possible; (2) the concentration intervals of one component should be equal; (3) the concentrations of every component are randomly arranged in each sample. With this experimental design, not only could the number of experimental samples be significantly reduced, but it is possible to select suitable variables. If a detail or approximation coefficient transformed out of these samples largely correlates with the concentration of one component, while being obviously irrelevant to those of all other components, it is just the variable we are looking for. In statistics r-test is commonly used to determine the correlation between two variables. If $|r| \leq R_{0.05}\,(n-2)$, then we think the correlation between them is feeble; and if $|r| > R_{0.01}\,(n-2)$, the two variables are obviously correlated. Here, r is the correlation coefficient; R_α can be simply inferred from F-test: $R_\alpha\,(n-2) = \{F_\alpha(1,\, n-2)/[F_\alpha(1,\, n-2)+n-2]\}^{0.5}$; α is the significance level; and n is the level or dimension of the two variables.

Another crucial parameter should be decided is the appropriate number of the calibration samples. Clearly, if there are merely two concentration levels for each component, the correlation coefficient between their concentrations would always be 1 no matter how to design the samples, while if the concentration level approaches infinity, it would become zero nearly. Table 1 shows some statistical parameters of two variables whose levels are the

Table 1
Correlation coefficients between two variables (LV: level or dimension of each variable; MCC: mean of the absolute value of 1000 correlation coefficients between the two variables; CICC: 95% confidence interval for the absolute value of correlation coefficients; SDCC: standard deviation of the absolute value of correlation coefficients)

LV	2	5	10	15	20
MCC	1.0000	0.4311	0.2789	0.2196	0.1841
CICC	1.0000–1.0000	0.4142–0.4480	0.2670–0.2908	0.2096–0.2296	0.1755–0.1928
SDCC	0.0000	0.2731	0.1921	0.1616	0.1396
LV	25	30	40	50	60
MCC	0.1654	0.1479	0.1268	0.1110	0.1051
CICC	0.1580–0.1729	0.1412–0.1546	0.1209–0.1326	0.1059–0.1162	0.1001–0.1100
SDCC	0.1203	0.1081	0.0942	0.0827	0.0802

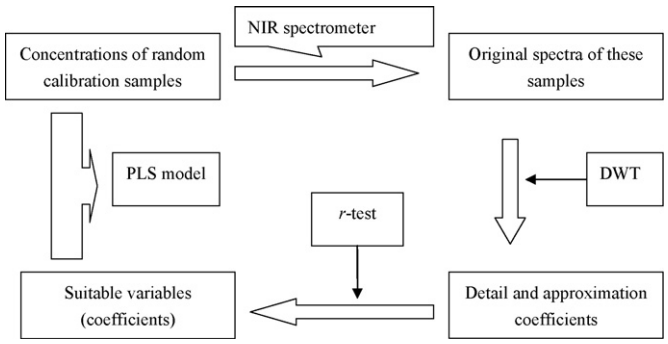

Fig. 1. An overview of steps involved in data processing.

same and arranged according to random experimental design. The data given in the table are 1000 simulations on computer. From the table, one could know that as the level increases the mean of correlation coefficients and their standard deviation decrease. Therefore, 30–50 levels are appropriate, since a larger level cannot obviously reduce the correlation coefficient and its deviation further. It means 30–50 calibration samples are also often required in our random experimental design. Such a calibration set is not too large and generally necessary even for multivariate calibration model construction in a one-component system.

2.3. Overview of data processing

Firstly, 30–50 samples are prepared as calibration set according to random experimental design, and their original spectra are all decomposed by a kind of discrete wavelets on each possible decomposition level. After discarding the detail coefficients on the first level (usually due to the noise of spectrometer) and the approximation coefficients on the last level (generally resulted from baseline drift or rotation) to save computing time, the correlation coefficients between every wavelet coefficient (including detail and approximation coefficients) and the concentration of each component are obtained, respectively. Then *r*-test is carried out to select suitable wavelet coefficients as variables for one component. And finally based on these variables and the concentration of the component, a partial least squares (PLS) model is constructed in a conventional leave-one-out cross-validation way for predicting the amount of the component in the multi-component system. It is worth noting that in the above process, denoising, baseline correction and database compression have also been implemented at the same time. The total treatment is succinctly depicted in Fig. 1.

3. Experimental

Two 2-component systems, aniline–acetone carbon tetrachloride solution and aniline–acetone water solution, have been studied. Although the two systems were prepared in laboratory rather than solutions out of industrial processes, the fact that they are all homogeneous systems made no essential differences between the formal and the latter ones, and consequently the method effective for the formal may also be effective for the latter. For each system, according to above random experimental design, 41 samples, in which the concentration of every component ranged from 0.5 to 5.0% (v/v) at intervals of 0.1125%, respectively, were prepared as a calibration set, and 15 samples within 0.5–5.0% were prepared as a prediction set. Spectra were all recorded with a Nicolet Nexus 870 FT-IR spectrometer under the same conditions, i.e., resolution of NIR: 4000 cm^{-1}; number of scans: 32; range of scans: 4000–10,000 cm^{-1}, the thickness of quartz-cell: 1 mm; and temperature: 273.15 K. In addition, all the spectra were difference spectra, namely, subtracting the spectra of solvent away from the sample spectra for obtaining the "pure" spectral effect of the solutes. For comparison, 100 aniline–acetone carbon tetrachloride solution samples ranging from 0.5 to 5.0% (v/v) at intervals of 0.5% were prepared as another calibration set in terms of full experimental design; so were the aniline–acetone water solution. Their spectra were obtained in the same way.

Algorithms required in this paper were written with MATLAB 7.0 and performed on a personal computer. The steps of the DWT were carried out using the Wavelet Toolbox 3.0 in MATLAB 7.0.

4. Results and discussion

Fig. 2 exhibits a typical spectrum of aniline-acetone carbon tetrachloride solution, in which the informative wavebands cover 4000–7000 cm^{-1} (the absorbances within about 8300–8900 cm^{-1} of second overtones is relatively lower, and not considered in the study). For comparison, the spectra of its component (aniline and acetone), and their mathematical addition are also shown in order to provide an intuitive view about interaction between aniline, acetone and/or the solvent. The fact that in some wavelengths, the spectrum 3 is far away from 4 indicates the un-negligible interaction in the system. As for water solution, besides the interaction the less informative waveband is another problem because of water. In water solution, only wavelengths ranging in 4300–4800 and 5400–6200 cm^{-1} are available, whereas other wavebands are submerged by the strong absorbance peaks of water. Therefore, DWT was carried out merely within these wavelength ranges, respectively, for carbon tetrachloride and aqueous system.

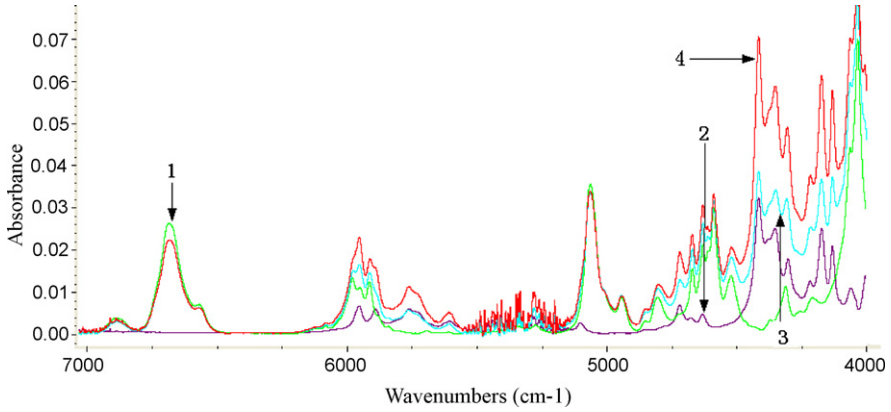

Fig. 2. Spectrum of 2% aniline (spectrum 1), 2% acetone (spectrum 2), mixture of 2% aniline and 2% acetone (spectrum 3) in carbon tetrachloride solution. Spectrum 4 is obtained by adding spectra 1 and 2. Noting: all spectra are processed with baseline correction for comparing them clearly.

Table 2
Results obtained for the aniline-acetone carbon tetrachloride system with different significance levels of *r*-test

Lower and upper of α	N of aniline	RMSEC of aniline	RMSEP of aniline	N of acetone	RMSEC of acetone	RMSEP of acetone
0.01, 0.1	39	0.0576	0.0733	40	0.0785	0.0830
0.01, 0.05	54	0.1879	0.1507	53	0.1533	0.1755
0.005, 0.05	42	0.0831	0.1031	37	0.1233	0.1374
0.005, 0.1	33	0.0354	0.0375	29	0.0479	0.0530

Table 3
Results obtained for aniline-acetone aqueous system with different significance levels of *r*-test

Lower and upper of α	N of aniline	RMSEC of aniline	RMSEP of aniline	N of acetone	RMSEC of acetone	RMSEP of acetone
0.01, 0.1	17	0.1180	0.1233	14	0.1424	0.1319
0.01, 0.05	27	0.2284	0.2450	29	0.2637	0.3011
0.005, 0.05	20	0.1033	0.0986	18	0.1079	0.1250
0.005, 0.1	12	0.1580	0.1874	9	0.2845	0.2544

Eight kinds of mother wavelet have been tried: two from the Daubechies family (db4, db6), one from the Symlet family (sym8), one from the Coiflet family (coif2), two from the biorthogonal family (bior2.2, bior3.3, bior4.4), and meyer. The results obtained with db4, db6, sym8, coif2 or meyer were roughly the same, but in general better than those obtained with bior2.2, biro3.3, and bior4.4 no matter in carbon tetrachloride or water solution in terms of root mean standard error in calibration (RMSEC) and root mean standard error in prediction (RMSEP). This is probably resulted from the overlapping information among wavelet coefficients of non-orthogonal DWT, which may cause collinear problem and consequently impair the predictive ability of multivariate calibration models followed [15]. It seems the effect of non-orthogonal DWT was overlooked and it might be the reason why the use of DWT does not provide sufficiently satisfactory results in some cases. The db4 has been selected as the mother wavelet for following studies.

In above study, the significance levels (α) of *r*-test were all 0.01 as the lower limit and 0.05 as the upper limit. Altering them would largely affect variable selection, and finally have great influence upon the performance of the PLS model followed. The effect is shown in Tables 2 and 3. Here, *N* is the number of variables (namely, wavelet coefficients) entering into constructing PLS model.

Increasing the lower limit of significance level (for example, from 0.005 to 0.01), more variables containing the information of one component would be selected for the component correctly, while some variables probably relevant to other components would be also chosen simultaneously. In contrast, increasing the upper limit of the level could prevent the variables irrelevant to one

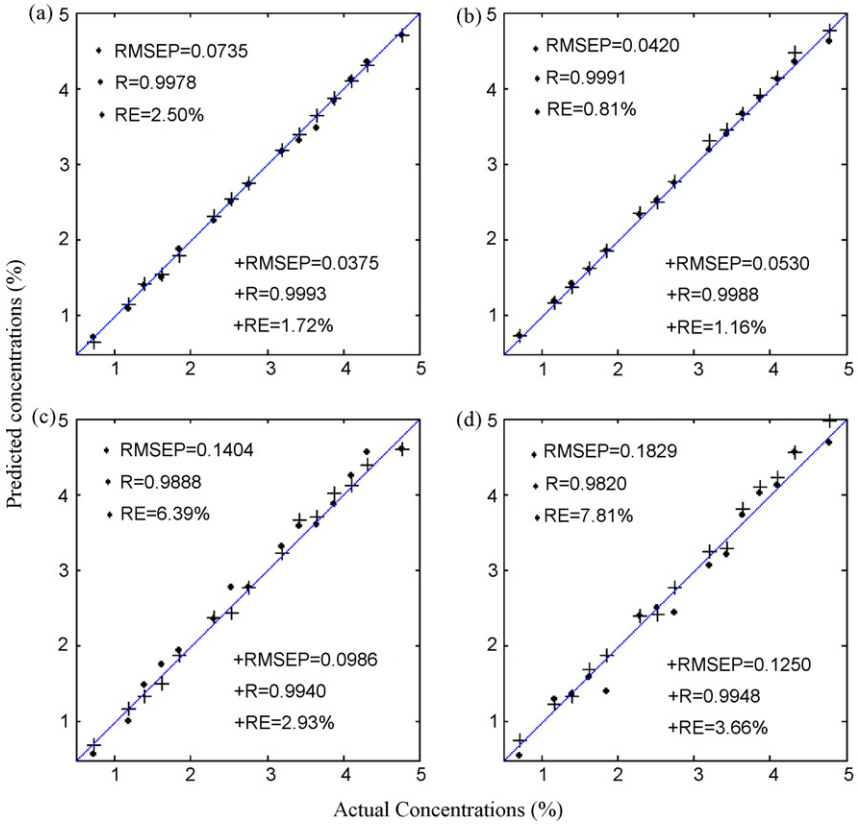

Fig. 3. Correlation plots between actual concentrations and predicted concentrations of every component in a multi-component system: (a) aniline concentrations in carbon tetrachloride system; (b) acetone concentrations in carbon tetrachloride system; (c) aniline concentrations in aqueous system; (d) acetone concentrations in aqueous system.

component, but the risk of loosing some variables containing information of the component would increase at the same time. Similar problem takes place when decreasing the upper or lower limit. This can be clearly observed from N under different significance levels. Therefore, a compromise should be taken. From Tables 2 and 3, the optimal lower and upper levels were 0.005 and 0.1 for carbon tetrachloride system, while 0.005 and 0.05 were chosen as the lower and upper limit, respectively for aqueous system. This was reasonable, since in the carbon tetrachloride system, there were more candidate variables for selection, and the stricter criterion would get rid of more ineligible candidates but still retain enough suitable ones for calibration models. However, in water solution the number of candidate variables was less, and the criterion should become looser in order to look for more suitable variables for constructing calibration model. But the looser criterion may introduce some ineligible ones, and accordingly would deteriorate the predictive ability of the multivariate calibration model.

Finally, a comparison between proposed strategy and full experimental design is shown Fig. 3. The spectra of calibration samples with the later design were processed by a convenient algorithm: after 15-point smoothing, their second-derivatives were used as variables directly to build a PLS calibration model without any other data processing. The performance of the traditional method was evaluated with the same prediction set in terms of RMSEP, determination coefficient (R^2) and relative error (RE), too.

Fig. 3 indicates that in carbon tetrachloride system, predictive ability of two methods were roughly the same, whereas in the aqueous system solution, the proposed strategy was clearly better. This was probably because the strong solvent effect of water made the system more nonlinear and needed more information to correct the nonlinearity. However, the fact that there was even less NIR information available in water solution than in carbon tetrachloride required more concentration levels to deal with this case. Therefore, the full experimental design (10 concentration levels) was more incapable of coping with this problem than the proposed strategy (41 concentration levels). The results predicted in aqueous system by the proposed strategy were not very accurate, but are enough for some cases like preliminary or in-line analysis.

5. Conclusion

It is possible for the proposed strategy to predict concentrations of each component in a multi-component system with a small-scale calibration set. In the proposed strategy, a calibration set with 30–50 samples should be prepared according to random experimental design at first, and then their NIR spectra are decomposed with orthogonal wavelets. The *r*-test is performed to select suitable wavelet coefficients as variables for constructing PLS models. The criterion for variable selection could be adjusted through changing the significance level of the *r*-test to optimize the multivariate calibration model. For the system containing less NIR information, such as aqueous system, the proposed strategy can increase the predictive ability in a way, but is not enough satisfactory in most cases, and other experimental and/or chemometrics improvement should be taken further.

References

[1] M.S.D. Nezio, M.F. Pistonesi, W.D. Fragoso, M.J.C. Pontes, H.C. Goicoechea, M.C.U. Araujo, B.S.F. Band, Microchem. J. 85 (2007) 194.
[2] H. Namkung, Y. Lee, H. Chung, Anal. Chim. Acta 606 (2008) 50.
[3] N.W. Broad, R.D. Jee, A.C. Moffat, M.J. Eaves, W.C. Mann, W. Dziki, Analyst 125 (2000) 2054.
[4] P.J. Brown, J. Chemom. 6 (1992) 151.
[5] D. Jouan-Rimbaud, B. Walczak, R.J. Poppi, O.E. Noord, D.L. Massart, Anal. Chem. 69 (1997) 4317.
[6] K. Jetter, U. Depcynski, K. Molt, A. Niemöller, Anal. Chim. Acta 420 (2000) 169.
[7] U. Depczynski, K. Jetter, K. Molt, A. Niemöller, Chemom. Intell. Lab. Syst. 49 (1999) 151.
[8] I. Esteban-Díez, J.M. González-Sáiz, C. Pizarro, Anal. Chim. Acta 515 (2004) 31.
[9] B. Walczak, D.L. Massart, Chemom. Intell. Lab. Syst. 36 (1997) 81.
[10] C.E.W. Gributs, D.H. Burns, Chemom. Intell. Lab. Syst. 83 (2006) 44.
[11] R.N.F. Santos, R.K.H. Galvão, M.C.U. Araujo, E.C. Silva, Talanta 71 (2007) 1136.
[12] I. Esteban-Díez, J.M. González-Sáiz, C. Pizarro, Anal. Chim. Acta 555 (2006) 84.
[13] Y. Wang, B. Xiang, Anal. Chim. Acta 602 (2006) 55.
[14] U. Depczynski, K. Jetter, K. Molt, Chemom. Intell. Lab. Syst. 47 (1999) 179.
[15] J. Trygg, S. Wold, Chemom. Intell. Lab. Syst. 42 (1998) 209.
[16] Z. Ramadan, X.H. Song, P.K. Hopke, M.J. Johnson, K.M. Scow, Anal. Chim. Acta 446 (2001) 231.
[17] V. Centner, D.L. Massart, O.E. Noord, S. Jong, B.M. Vandeginste, C. Sterna, Anal. Chem. 68 (1996) 3851.
[18] J. Koshoubu, T. Iwata, S. Minami, Appl. Spectrosc. 54 (2000) 148.
[19] J. Koshoubu, T. Iwata, S. Minami, Anal. Sci. 17 (2001) 319.
[20] W.S. Cai, Y.K. Li, X.G. Shao, Intell. Lab. Syst. 90 (2008) 188.
[21] M.J. Arcos, M.C. Ortiz, B. Villahoz, L.A. Sarabia, Anal. Chim. Acta 339 (1997) 63.
[22] D. Broadhurst, R. Goodacre, A. Jones, J.J. Rowland, D.B. Kell, Anal. Chim. Acta 348 (1997) 71.
[23] D. Jouan-Rimbaud, D.L. Massart, O.E. Noord, Chemom. Intell. Lab. Syst. 35 (1997) 213.
[24] J.M. Brenchley, U. Horchener, J.H. Kalivas, Appl. Spectrosc. 51 (1997) 689.
[25] L. Norgaard, A. Sauland, J. Wagner, J.P. Nielsen, L. Munck, S.B. Engelsen, Appl. Spectrosc. 54 (2000) 88A.
[26] D.D. Archibald, D.E. Akin, Vib. Spectrosc. 23 (2000) 169.
[27] J.H. Jiang, R.J. Berry, H.W. Siesler, Y. Ozaki, Anal. Chem. 74 (2002) 3555.

Talanta 77 (2008) 793–799

Contents lists available at ScienceDirect

Talanta

journal homepage: www.elsevier.com/locate/talanta

Speciation of arsenic using capillary gas chromatography with atomic emission detection

N. Campillo, R. Peñalver, P. Viñas, I. López-García, M. Hernández-Córdoba*

Department of Analytical Chemistry, Faculty of Chemistry, University of Murcia, E-30071 Murcia, Spain

ARTICLE INFO

Article history:
Received 8 May 2008
Received in revised form 2 July 2008
Accepted 11 July 2008
Available online 23 July 2008

Keywords:
Dimethylarsinic acid (DMA)
Monomethylarsonic acid (MMA)
Inorganic arsenic
Seawater
Wine
Beer
Infant foods
Gas chromatography (GC)
Atomic emission detection (AED)

ABSTRACT

A gas chromatography method with atomic emission detection (GC-AED) for the determination of dimethylarsinic acid (DMA), monomethylarsonic acid (MMA) and inorganic arsenic was optimized. The analytes were derivatized in the sample solutions with methyl thioglycolate (TGM) and the products were extracted into cyclohexane before an aliquot of this organic phase was directly injected into the chromatograph. The procedure was applied to the analysis of seawaters, wines, beers and infant foods, the last requiring an additional enzymatic reaction prior to analyte derivatization. Detection limits in seawaters and beverages were 0.05, 0.15 and 0.8 ng mL^{-1} for DMA, MMA and inorganic arsenic, respectively. In infant foods the detection limits were 1, 10 and 25 ng g^{-1} for DMA, MMA and inorganic arsenic, respectively. Inorganic arsenic was detected in some of the seawater samples and three of the wines analyzed at concentration levels in the range 1–40 ng mL^{-1}, and DMA in several of the infant foods in the range 20–80 ng g^{-1}. The method was validated by analyzing a certified reference material and by recovery studies. All the samples were also analyzed by hydride generation and atomic fluorescence spectrometry (HG-AFS), which provided data for the total arsenic content.

1. Introduction

Arsenite, arsenate, monomethylarsonate (MMA) and dimethylarsinate (DMA) are arsenic species present in the environment both naturally and as a consequence of human activities. The higher toxicity of inorganic arsenic compared with these organoarsenical compounds has been well established. On the other hand, arsenobetaine is non-toxic [1]. The evident importance of arsenic speciation has led to the publication of several reviews [2–7]. The most commonly used separation technique is high-performance liquid chromatography (HPLC), while gas chromatography (GC) is less used because non-volatile arsenic compounds have to be submitted to a prior derivatization step.

Arsenic speciation has been studied by forming a wide number of arsenic derivatives, which are then subjected to GC: trimethylsilyl derivatives [8], halogenated arsines [9], hydrides [10], dithiocarbamate derivatives [11] and thioarsenite derivatives [12], the most common forms being thioglycolic acid methylesters [13–20]. Methyl thioglycolate (TGM) permits the simultaneous determination of inorganic arsenic, as the sum of arsenite plus arsenate, and of the two alkylated arsenocompounds, MMA and DMA, which remain stable for several days in cyclohexane extracts [13].

The simultaneous determination of DMA, MMA and inorganic arsenic in the form of TGM derivatives has already been carried out in water samples [14,17], while the methodology is here adapted for beverages and infant food products, using the selective atomic emission detector. The literature contains few papers dealing with arsenic speciation in wines [21–25] and beers [26–28], and most of those that exist are based on hydride generation (HG). The maximum level of arsenic permitted in these beverages has been legally established. For example, the Office Internationale de la Vigne et du Vin has set a maximum limit of 200 ng mL^{-1} in wines [29], while Spanish legislation establishes a maximum limit of 100 ng mL^{-1} for beer, a lower value than in other countries [30,31].

The analysis of infant foods, which may contain cereals, fruits, vegetables, fish and meat, is of great importance due to the need to monitor nutrition in the first years of human life. Rice, a common ingredient of baby foods, is a bioaccumulative plant for the more toxic arsenic species, whereas seafood accumulates the non-toxic arsenobetaine [32]. Arsenic speciation in infant products [33–35] and cereals [36–39] has been studied, but not by gas chromatography.

* Corresponding author. Tel.: +34 968 367406; fax: +34 968 364148.
E-mail address: hcordoba@um.es (M. Hernández-Córdoba).

0039-9140/$ – see front matter © 2008 Elsevier B.V. All rights reserved.
doi:10.1016/j.talanta.2008.07.028

2. Experimental

2.1. Chemicals

Standard solutions of 1000 μg mL^{-1} As(III) and As(V) were supplied by Fluka (Buchs, Switzerland). Cacodylic acid [$(CH_3)_2As(O)OH$, DMA, Sigma, St. Louis, MO, USA] and sodium methylarsinate [$CH_3AsO(ONa)_2{\cdot}6H_2O$, MMA, Carlo Erba, Milan, Italy] standard solutions (1000 μg mL^{-1}) were prepared in water and kept at 4 °C in PTFE bottles. Both solid compounds were of 98% purity. Working solutions were prepared daily. High-quality water, obtained by using a Milli-Q water purification system (Millipore, Bedford, MA, USA), was used throughout.

Hydrochloric acid (37%, HCl), methyl thioglycolate (98.5%, TGM), sodium borohydride (>96%, $NaBH_4$) and the organic solvents, hexane and cyclohexane, were obtained from Fluka. 1,3-Propanedithiol and 2-mercaptoethanol were obtained from Sigma.

Streptomyces griseus (protease type XIV) and *Bacillus subtilis* (α-amylase) were obtained from Sigma and Fluka, respectively. Other reagents used were $Mg(NO_3)_2{\cdot}6H_2O$ (99.5%, Fluka), MgO (97%, Fluka), ascorbic acid (99.5%, Fluka), potassium iodide (99%, KI, Panreac, Barcelona, Spain), L-cysteine (99%, Sigma) and tetramethylammonium hydroxide (25%, TMAH, Sigma). Silicone polymer based antifoam A emulsion (Sigma) was used to avoid foam formation during the generation of hydride. Other chemicals used were obtained from Fluka.

The plasma gas and carrier gas used for GC was helium. The reagent gas for the AED was hydrogen. Nitrogen was used to purge the AED system and argon to flush the volatile hydride to the AFS. All the gases (99.999% purity) were supplied by Air Liquide (Madrid, Spain).

2.2. Instrumentation

2.2.1. GC-AED

An Agilent 6890 gas chromatograph was directly coupled by a transfer line to a G2350A microwave-induced plasma atomic emission detector (Agilent, Waldbronn, Germany). The updated G2070AA ChemStation application with G2360AA GC-AED software was used to control and automate many features of the GC and AED systems, and for data acquisition and treatment. The chromatograph was fitted with a 25 m × 0.32 mm i.d. HP-5, 5% diphenyl 95% dimethyl polysiloxane capillary column from Agilent with a low-film thickness of 0.17 μm to minimise chromatographic peak widths, thus improving the signal-to-noise ratios. The temperature programme used was as follows: from 45 to 230 °C at 20 °C min^{-1} and then to 300 °C at 50 °C min^{-1}, where it was held for 1 min. Sample volumes of 3 μL were injected into a liner of 900 μL internal volume, in the splitless mode with an injection port temperature of 200 °C. Helium was used as the carrier gas at a flow rate of 4 mL min^{-1}. Solvent venting was switched on immediately after injection and switched off 3.5 min later. The final part of the GC column was used as a transfer line to the detector. The transfer line and the cavity were set at the same temperature as recommended by the manufacturer, 250 °C. The helium make-up flow was 160 mL min^{-1}. Hydrogen at 10 psi was used as the only scavenger gas. Filter and backamount adjustment in the AED were set according to Agilent default specifications. The spectrometer was purged with nitrogen at 2.5 L min^{-1}. All compounds were quantified in the arsenic 189 nm emission line, using peak area as the analytical parameter.

2.2.2. HG-AFS

Hydride generation atomic fluorescence spectrometry was performed using a PSA Millenium Excalibur continuous flow system (PS Analytical, Orping, UK) for total arsenic quantification. Measurements were carried out using a boosted discharge hollow cathode lamp for arsenic (Photron Pty. Ltd., Australia) at the 197.3 nm line, with a 27.5 mA primary current and a 34.9 mA boost current. The delay was set at 10 s, while analysis and memory were set at 30 s.

The conditions selected for seawater and infant food analysis were: reagent flow rates of 9 mL min^{-1} for the reducing solution containing 3.5 M HCl, 1% (w/v) KI and 0.2% (w/v) ascorbic acid solution and 4.5 mL min^{-1} for the 0.7% (w/v) $NaBH_4$ solution stabilized in 0.1 M NaOH. For beverages, a flow-rate of 4 mL min^{-1} was used for the reductor reagent solution containing 0.01 M HCl, 0.1% (w/v) L-cysteine, 10^{-4}% (w/v) antifoam agent and 1.2 or 0.4% (v/v) ethanol for wines and beers, respectively. The flow-rate of the 0.6% (w/v) $NaBH_4$ solution stabilized in 10 mM NaOH [25] was 2 mL min^{-1}.

The U-shaped gas liquid separator was flushed with argon gas and the volatile hydride produced was transported by the gas stream (330 mL min^{-1}), being dried as it passed through a Perma Pure hygroscopic membrane (Farmingdale, NJ, USA) and atomised using a hydrogen diffusion flame generated from the reaction between $NaBH_4$ and HCl. Valves and T-pieces were obtained from Omnifit (Cambridge, UK).

2.2.3. Centrifugation and ultrasonication systems

Two centrifuges were used for phase separation: a Mixtasel (Selecta, Barcelona, Spain) for 100-mL volume tubes and a Hermle Z 252μ (HERMLE Labortechnik, Wehingen, Germany) for 10-mL volume tubes. An UP 200H ultrasonic probe processor (Dr. Hielscher, Teltow, Germany) was also used for the infant food samples.

2.3. Samples and reference material

Ten seawater samples were obtained from different harbours and beaches of southeast Spain, collecting 200 mL of water in polycarbonate flasks. Non-filtered samples were acidified to pH 2 [17] using concentrated hydrochloric acid in the laboratory and kept in the dark at 4 °C before analysis, which was carried out normally within 48 h of sample collection. A series of red, white and rose wines were obtained from commercial sources, to make up a total of 10 different samples. Five different alcoholic beers were also obtained from local supermarkets. The beer samples were previously degassed in an ultrasonic bath in order to improve the analytical performance of the determinations. All the flasks were washed using a 5% (v/v) nitric acid solution and rinsed with deionised water prior to use.

A total of 20 infant food samples of different varieties (9 based on cereals and/or fruits and 11 puree products containing meat, fish, vegetables and/or cereals) were supplied by a local manufacturer. The NIST-SRM 1568a Rice flour certified reference material (National Institute of Standards and Technology, Gaithersburg, MD, USA) was used for validation purposes.

2.4. Procedures

2.4.1. Arsenic speciation by GC-AED

2.4.1.1. Liquid samples (seawaters, wines and beers). To carry out the extractions, 30 mL samples were placed in 100 mL capped glass tubes containing 2 and 3 g of sodium chloride for seawaters and beverages, respectively. Concentrated HCl (30 μL) and TGM (750 μL) were added under a fume hood and the recipient was immediately sealed. The derivatization reaction was allowed to proceed at ambient temperature, while being shaken for 2 min. After adding 1 mL of cyclohexane, shaking was continued for another minute. Finally, the upper layer was used for measurements by injecting 3 μL into the GC injection port. For beverages, more efficient phase separation was achieved by centrifugating the

mixture for 2 min at 4000 rpm (an unnecessary step in the case of seawaters).

2.4.1.2. Infant food products. Four grams of solid sample were placed in a 100-mL glass centrifuge tube with 80 mg of α-amylase and 10 mL of water. The mixture was sonicated for 2 min (40% amplitude) by means of a probe directly immersed into the sample solution. Next, 400 mg of protease were added and the mixture was again treated with ultrasound for 4 min [37]. The mixture was centrifuged at 4000 rpm for 10 min and the supernatant was submitted to derivatization by adding 10 μL of concentrated HCl and 250 μL of TGM. After shaking the mixture manually for 2 min, 1 mL of cyclohexane was added, shaken for 30 s and the mixture centrifuged for 1 min at 6000 rpm, before 3 μL of the organic phase was injected into the chromatograph.

In the case of puree products, the procedure was slightly modified, and 40 mg α-amylase and 200 mg of protease were added, along with only 5 mL of water, to four grams of sample.

2.4.2. Total arsenic determination by HG-AFS

For confirmation purposes, the total arsenic content was determined, by using several slightly modified procedures previously reported in the literature [25,39].

2.4.2.1. Liquid samples (seawaters, wines and beers). 2.8 mL of concentrated HCl and 200 μL of a reducing solution of 50% (w/v) KI and 10% (w/v) ascorbic acid were added to 7 mL of seawater. A sample dilution step was carried out for beverage analysis: a 1 mL sample, previously degassed in the case of beers, was mixed with 1 mL of a 1% (w/v) solution of L-cysteine in 0.1 M HCl and 10 μL of 0.1% (w/v) antifoam solution agent before being made up to 10 mL with water [25]. L-Cysteine was selected as the pre-reducing agent in order to overcome potential interferences from the non-digested beverage samples. In all cases, the mixtures were allowed to stand for 1 h in order to reduce all arsenic species to As(III) before being analyzed.

2.4.2.2. Infant food products. Sample masses of 1 g were weighed into porcelain crucibles and treated with 2.5 mL of an ashing aid suspension of 20% (w/v) $Mg(NO_3)_2{\cdot}6H_2O$ and 2% (w/v) MgO, and 5 mL of 50% (v/v) nitric acid. The mixture was evaporated to dryness and mineralized in a muffle oven, whose temperature was gradually increased to 450 °C, which was maintained for 12 h. The white ashes were moistened with 1 mL of water and dissolved in 9 mL of 10% (v/v) HCl.

For the samples based on rice and those containing fish, which were expected to contain the highest levels of arsenic, 8.75 mL of concentrated HCl and 600 μL of the reducing solution (50% (w/v) KI and 10% (w/v) ascorbic acid) were added to 3 mL of the mineralized solution before being diluted to 30 mL with water [39]. For the rest of the samples (with presumably lower arsenic contents), 2.8 mL of concentrated HCl and 200 μL of the reducing solution were added to 7 mL of the mineralized solution. Once the reducing solution had been added, the samples were left for 1 h before being measured.

2.5. Recovery assays for the GC-AED speciation procedure

Recovery experiments were carried out using two seawaters, a red wine, a white wine and a beer, which were spiked with the analytes at three concentration levels ranging from 2 to 10 ng mL^{-1} for DMA and MMA, and from 25 to 75 ng mL^{-1} for inorganic arsenic. Five infant food samples (based on fruits, cereals, meat, fish and vegetables) were also spiked at three concentration levels in a range 10–20 ng g^{-1} for DMA, 50–100 ng g^{-1} for MMA and 100–200 ng g^{-1} for inorganic arsenic. The spiked samples were left to equilibrate at room temperature for at least 1 h before analysis.

3. Results and discussion

3.1. Derivatization and liquid–liquid extraction

The effectiveness of 1,3-propanedithiol and 2-mercaptoethanol as derivatization agents was checked. The chromatographic separations obtained in both cases were unsatisfactory and they were not considered.

The high-reducing power of TGM prevented the discrimination of pentavalent and trivalent arsenic since both species formed the same derivative. This derivatization reaction implies that inorganic arsenic, MMA and DMA are substituted by a three, two and one thioglycol side-chain, respectively. The different polarities of the reaction products provide efficient gas chromatographic separation. Preliminary experiments were carried out to select the optimal conditions for derivatization efficiency of the analytes by using an aqueous standard solution. Methyl thioglycolate and hydrochloric acid concentrations, temperature and reaction time were the parameters studied. The effect of the derivatizing reagent concentration was studied by adding 20 μL to 1 mL volumes to 10 mL of a 10% (v/v) hydrochloric solution containing 25, 50 and 100 ng mL^{-1} of DMA, MMA and inorganic arsenic, respectively. The derivatized compounds were extracted in 1 mL of cyclohexane before being injected into the GC. Signals increased up to 100 μL of TGM and then remained constant for the alkylate arsenocompounds. Maximum sensitivity was attained for inorganic arsenic when 250 μL of TGM were added and so, a concentration of 2.5% (v/v) was selected for subsequent experiments.

When the derivatization reaction was carried out under different HCl concentrations ranging between 0 and 10% (v/v), signals increased up to 0.1% (v/v) for DMA and MMA, and then remained constant. On the other hand, sensitivity for inorganic arsenic decreased for acid concentrations higher than 1% (v/v). Therefore, derivatization was carried out in the presence of a 0.1% (v/v) acid concentration.

No significant differences in sensitivity were achieved when the reaction was allowed to proceed for times ranging between 0.5 and 5 min, while being stirred. A reaction time of 2 min was finally selected to ensure that derivatization was complete in samples with high-analyte concentrations. The effect of temperature on derivatization efficiency was checked by submitting the reaction mixture to temperatures ranging from ambient to 80 °C, for 2 min using a water bath. The peak areas of the three derivatized compounds decreased as the temperature increased, reaching values of between 20 and 70% of the maximum signals obtained, corresponding to DMA and MMA, respectively. Therefore, the reaction was carried out at room temperature.

Once the conditions for the derivatizing step had been selected, the influence of changing the ionic strength of the sample was studied by adding 0–2.8 g of sodium chloride to 10 mL of the aqueous standard mixture. The sensitivity for the alkylated arsenic compounds increased up to a 10% (w/v) salt concentration and then slightly decreased. No change in sensitivity was observed for inorganic arsenic in the salt concentration range studied. Therefore, a 10% (w/v) sodium salt concentration was adopted for further experiments. For seawater samples, the salt concentration was adjusted to the selected value, taking into account their content of about 3.5% (w/v).

No differences were observed between hexane and cyclohexane when they were tested for use as extraction solvents. In both cases when extraction was carried out in wine, beer or infant food matrices, a centrifugation step was required to accelerate the sepa-

ration between phases because emulsification occurred during the extraction step. Cyclohexane was finally selected.

The sample-to-cyclohexane volume ratio was studied by extracting different volumes of an aqueous standard solution in 1 mL of cyclohexane. Best results were attained with the proportion 30:1.

It was experimentally verified that, as previously reported [40], TGM-derivatives were not suitable for preconcentration using solid-phase microextraction.

3.2. Chromatographic and AED parameters

The low-polar stationary phase, HP-5, provided good discrimination between the three derivatized analytes. The oven temperature was increased from 45 to 230 °C, thus permitting DMA and MMA to elute. As the temperature rose to 300 °C, inorganic arsenic was eluted. Separation was carried out using different constant flow-rates between 1 and 4 mL min^{-1}. The latter value was selected, since this reduced the analysis time needed and increased the sensitivity compared with lower flow-rates. Higher helium flow-rate values are not recommended by the manufacturer to preserve the stationary phase. Under the selected chromatographic conditions, analytes were eluted at retention times of 4.67, 8.03 and 10.29 min for DMA, MMA and inorganic arsenic derivatives, respectively.

The effect of the injection temperature was studied between 200 and 300 °C, by injecting 0.2 μL of a cyclohexane extract of the three derivatized analytes, in the splitless mode. The injection temperature hardly affected the sensitivity for the alkylated arsenocompounds in the range of values studied, although peak area decreased for the inorganic derivative as the temperature was increased. Lower injection temperatures were not assayed because of pressure problems in the GC front inlet. Therefore, 200 °C was selected as the optimal injection temperature. In order to increase the sensitivity of the chromatographic determination, larger volume injections were assayed. As expected, sensitivity increased for all the analytes, especially for the most volatile (DMA), in the range of volumes studied (0.2–3 μL). To improve the efficiency of sample transfer to the capillary column, different carrier gas inlet pressures (10, 20, 40 and 60 psi) were applied just before the beginning of every run, returning to the normal value after a specified amount of time. Because no differences in sensitivity and/or peak shape were observed in any of the cases, no pressure pulse was applied for further experiments. The split valve remained closed for 3.5 min before being opened, with the default split ratio (19.5:1) established by the instrument.

The detector operating parameters were studied by injecting 3 μL of the organic extract. Make-up gas flow-rate and reagent gas pressure were the parameters optimized for AED. The helium make-up flow was varied between 100 and 200 mL min^{-1}, and measured with the window purge gas flow open. Even though the greatest sensitivity was attained using the lowest flow-rate, 160 mL min^{-1} was adopted as a compromise value because the chromatographic peaks obtained with lower helium flow-rates were very broad. A hydrogen pressure of 10 psi provided maximum sensitivity.

3.3. Optimization of the infant food treatment

Optimization of the infant food treatment was carried out using a fortified sample based on rice flour and a puree product containing chicken and vegetables. A mild extraction procedure was required to maintain species integrity. Previous studies have shown that extraction of arsenic species from rice samples using 1% (w/v) tetramethylammonium hydroxide solutions provides good extraction efficiencies for the analytes studied here [37]. The oxidation of arsenite to arsenate by this alkaline reagent would not be a problem in the present procedure because both species are jointly detected as inorganic arsenic. However, a suspension was formed when TMAH solution was added to the sample, which prevented good derivatization, even when the suspension was centrifuged or filtered. The use of lower TMAH concentrations did not solve this problem. Moreover, if lower sample masses were treated, unacceptable detection limits were achieved. Therefore, the use of TMAH was discarded, and the enzymatic hydrolysis previously optimized by Cámara and co-workers [37] was selected with minor modifications. To check the performance of the procedure, sample masses of 1–4 g were submitted to enzymatic digestion, the highest sample mass being selected because it provided the lowest detection limits. Higher sample masses were not assayed because of poor homogenization in the sonication step. For puree samples, it was found that lower quantities of the enzymes than those previously used were sufficient to obtain good results. The masses of α-amylase and protease were reduced to 40 and 200 mg, respectively, and 5 mL of water were added to 4 g of sample, because of the high-moisture content of these samples.

3.4. Analytical characteristics of the method

The analytical characteristics of the method appear in Table 1. Six concentration levels were analyzed and two replicates were made. The correlation coefficients obtained demonstrated a direct proportional relationship between the amount of analyte extracted and its concentration in the sample. When the slopes of the aqueous calibration graphs (Table 1) were compared with those obtained when the standard additions method was applied to a seawater, a red wine and a beer, no significant differences were found, confirming the absence of matrix effects. Detection and quantification limits were calculated by using a signal-to-noise ratio of 3 and 10, respectively (Table 1). The repeatability was calculated by using the relative standard deviation from a series of 10 consecutive analyses of a fortified seawater and a fortified red wine, under the optimized conditions for each sample matrix (see Table 1 for the seawater sample). R.S.D. values obtained for the red wine were similar to those obtained for seawater, 5.6, 8.3 and 7.6% for DMA, MMA and inorganic arsenic, respectively.

Table 1
Analytical characteristics of the studied arsenic species using the GC-AED method for liquid samples

Analyte	Slope[a] (mL ng^{-1})	Correlation coefficient	Linearity range (ng mL^{-1})	Detection limit[b] (ng mL^{-1})	Quantification limit[c] (ng mL^{-1})	R.S.D.[d]
DMA	14.5 ± 0.40	0.9985	0.2–50	0.05 (0.15 pg)	0.17	6.0
MMA	5.85 ± 0.32	0.9998	0.5–50	0.15 (0.45 pg)	0.5	8.1
Inorganic As	1.04 ± 0.01	0.9992	2–500	0.8 (2.4 pg)	2.5	5.3

[a] Mean value ± standard deviation (n = 6).
[b] Corresponding to S/N = 3.
[c] Corresponding to S/N = 10.
[d] Calculated for concentrations 20-fold the corresponding quantification limits.

Table 2
Analytical characteristics of the studied arsenic species using the GC-AED method for infant foods

Analyte	Slope[a] (g ng^{-1})	Correlation coefficient	Linearity range (ng g^{-1})	Detection limit[b] (ng g^{-1})	Quantification limit[c] (ng g^{-1})	R.S.D.[d]
DMA	0.95 ± 0.02	0.9972	3–100	1.0	3.5	9.8
MMA	0.10 ± 0.01	0.9950	30–300	10	35	11.4
Inorganic As	0.04 ± 0.01	0.9890	50–500	25	80	14.2

[a] Mean value ± standard deviation (n = 6).
[b] Corresponding to S/N = 3.
[c] Corresponding to S/N = 10.
[d] Calculated for concentrations 20-fold the corresponding quantification limits.

When the slopes obtained using aqueous standard solutions and those obtained by means of standard addition for two different infant food products were compared, significant differences were observed. Consequently, the standard addition method was used for quantification of these samples. Table 2 shows the analytical characteristics obtained using the optimized procedure for the analysis of infant foods.

High-Fe(III) concentrations have been shown to bind arsenic fractions, inhibiting the TGM reaction. The addition of chelating agents prior to the derivatization step has been found to prevent such binding [17]. The addition of EDTA at a concentration of 0.1 M to different spiked infant food samples led to no difference in sensitivity, and so the absence of this interference was assumed in the studied samples, and no chelating agent was added.

3.5. Real samples and validation of the method

The optimized procedure was applied to 10 different seawaters, in 5 of which inorganic arsenic was detected, 3 of them providing signals near the detection limit (see Table 3). Samples 4 and 5 showed arsenic concentration levels higher than those normally found in seawaters (0.5–2 ng mL^{-1}), which can be attributed to anthropogenic inputs and/or to the geological characteristics of the area where they were collected. Inorganic arsenic was detected in three of the wine samples analyzed (Table 3), the data being in accordance with those previously reported [21,22]. On the other hand, none of the studied species was detected in the beers analyzed (Table 3).

The reliability of the optimized procedure for seawaters and beverages was checked by recovery studies for four different samples spiked at three concentration levels. Average recoveries ± standard deviations (n = 36) of 95.4 ± 6.4, 92.1 ± 7.0 and 91.7 ± 10 were obtained for DMA, MMA and inorganic arsenic, respectively, as can be seen in Table 4. Slight differences were observed between the R.S.D. values obtained for inorganic arsenic in the spiked samples and the values obtained for the organic arsenic compounds.

Table 3
Results obtained in the analysis of liquid samples

Sample	Inorganic arsenic (ng mL^{-1}) (GC-AED)[a]	Total arsenic (ng mL^{-1}) (HG-AFS)[a]
Seawater 1	1.8 ± 0.1	1.9 ± 0.05
Seawater 2	1.2 ± 0.2	1.1 ± 0.04
Seawater 3	1.0 ± 0.1	0.9 ± 0.03
Seawater 4	6.4 ± 0.3	6.5 ± 0.1
Seawater 5	39 ± 3	40.1 ± 0.1
Seawater 6	<LOD	0.24 ± 0.02
Seawater 7	<LOD	0.45 ± 0.01
Seawater 8	<LOD	0.38 ± 0.02
Seawater 9	<LOD	0.31 ± 0.01
Seawater 10	<LOD	<LOD
Red wine 1	10.2 ± 0.8	10.5 ± 0.04
Red wine 2	11.2 ± 0.6	11.4 ± 0.04
Red wine 3	3.6 ± 0.2	3.70 ± 0.02
White wine 1	<LOD	1.12 ± 0.02
Beer 1	<LOD	0.15 ± 0.01
Beer 2	<LOD	0.11 ± 0.01
Beer 3	<LOD	0.20 ± 0.02

LOD means detection limit.
[a] Mean ± standard deviation (n = 3).

Table 4
Mean recovery efficiencies and R.S.D. obtained in fortified samples by using the GC-AED method

Analyte	Recovery[a] (%)				
	Spike level (ng mL^{-1})	Seawater	Red wine	White wine	Beer
DMA	2	98.3 (7.9)	89.9 (8.8)	93.2 (7.5)	93.1 (6.7)
	5	96.4 (8.1)	99.1 (7.1)	95.1 (5.9)	92.4 (5.4)
	10	95.4 (5.6)	98.2 (6.3)	96.4 (5.9)	97.2 (6.3)
MMA	2	88.4 (9.1)	91.5 (8.8)	87.2 (8.5)	90.4 (8.3)
	5	99.6 (7.9)	92.3 (5.9)	89.2 (8.1)	88.0 (8.2)
	10	93.2 (8.6)	96.3 (7.9)	92.6 (7.2)	95.9 (5.5)
Inorganic arsenic	25	89.9 (11.1)	82.1 (12.0)	87.9 (11.5)	95.3 (13.1)
	50	90.5 (9.9)	85.9 (13.5)	95.3 (12.6)	92.7 (12.4)
	75	93.3 (10.5)	93.4 (12.4)	96.2 (10.2)	98.1 (10.1)

[a] Values in parentheses are R.S.D. values for n = 3.

The optimized procedure for infant foods was applied to the analysis of 20 samples of differing composition. MMA was not detected in any sample. In the case of cereal and fruit-based infant foods, the levels found for total arsenic varied widely (5–150 ng g^{-1}), six of the nine samples showing DMA levels in the 20–80 ng g^{-1} range. For the meat-based and vegetables-based purees, the total arsenic levels were very low (2–85 ng g^{-1}) and DMA was not detected. For the case of purees based on fish and vegetables, the total arsenic content was in the 105–280 ng g^{-1} range, only one of the samples (based on hake and rice) providing a low signal for DMA (28 ng g^{-1}). This was attributed to the fact that most of the arsenic present in fish samples was in the form of the non-toxic arsenic species, arsenobetaine [34].

Recovery studies carried out for five different infant products provided average recoveries ± standard deviations (n = 45) of 95.0 ± 5.9, 90.5 ± 8.7 and 89.3 ± 11.1 for DMA, MMA and inorganic

Table 5
Results for the analysis of NIST 1568a Rice flour

Concentration value (ng g^{-1})	DMA	MMA	Inorganic As	Total As
Found[a]	149 ± 3[b]	<LOD[b]	101 ± 5[b]	279 ± 15[c]
Certified				290 ± 30
Other data[d]	155 ± 2	9.2 ± 0.2	102 ± 2	

[a] Mean value ± standard deviation (n = 3).
[b] GC-AED procedure.
[c] HG-AFS procedure.
[d] Values obtained from Ref. [39].

arsenic, respectively. NIST 1568a Rice Flour was used to validate the proposed procedure for infant food samples. As can be observed in Table 5, the results obtained for each of the studied analytes were in accordance with those found by other authors [36,37,39] using different analytical methods for this material. Quantification of MMA was difficult because the content was near the detection limit of the applied procedure.

3.6. Total arsenic determination

Total arsenic was determined for each of the samples by HG-AFS, in order to check the data obtained for speciation. The detection limit obtained as three times the standard deviation of the ordinate divided by the slope was 20 ng L^{-1} in the case of seawaters. Table 3 shows the results obtained for seawaters, the results confirming that all the arsenic contained in these samples was present in the form of inorganic species.

The analysis of total arsenic in the beverages was carried without a previous digestion step [25], and a 1:10 dilution was sufficient to minimise the matrix effect, providing a detection limit of 0.2 ng mL^{-1} for both wines and beers. The data obtained also revealed that all the wine samples analyzed could be described as uncontaminated [24].

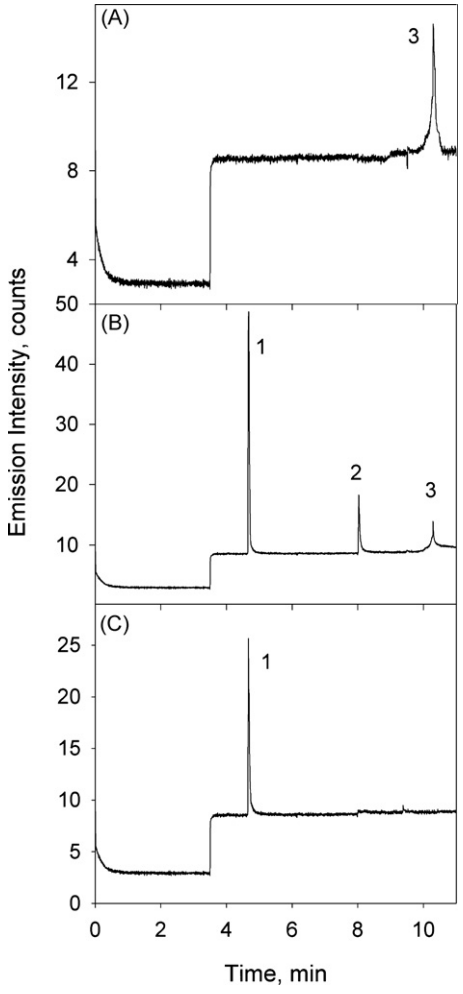

Fig. 1. GC-AED chromatograms of: (A) unfortified red wine sample 2; (B) a red wine sample free from the analytes fortified at the concentration levels of 5, 3 and 10 ng mL^{-1} for DMA, MMA and inorganic arsenic, respectively; (C) unfortified infant food based on rice, containing 80 ng g^{-1} of DMA. (1) DMA, (2) MMA and (3) inorganic arsenic.

Since the total arsenic content obtained for the NIST 1568a agreed with the certified value (Table 5), the HG-AFS procedure applied to infant foods was considered reliable. For the infant products, a 0.15 ng g^{-1} detection limit was obtained for a 1 g sample mass.

4. Conclusion

The use of the selective atomic emission detector (AED), together with the high-separation capability of capillary columns, makes gas chromatography a useful technique for arsenic speciation. Methyl thioglycolate allows the simultaneous determination of inorganic arsenic and the two alkylated arsenic compounds, DMA and MMA (Fig. 1). Since preconcentration can be carried out by a simple liquid–liquid extraction using cyclohexane, reliable results can be obtained at minimum cost and with uncomplicated sample manipulation. The sensitivity attained is perhaps not as high as desirable but it is higher than that previously reported for similar procedures based on GC-AED. In the samples analysed, namely, waters, wines, beers and infant foods, the levels of DMA, MMA and inorganic arsenic were very low.

Acknowledgements

The authors are grateful to the Spanish Ministerio de Educacion y Ciencia, MEC (Project CTQ2006-08037/BQU) and to Comunidad Autónoma de la Región de Murcia (CARM, Fundación Séneca, Project 02993/PI/05) for financial support. RP acknowledges a fellowship from MEC. The authors thank Hero España, S.A. for the kind gift of some baby food samples.

References

[1] UN International Programme on Chemical Safety, Environmental Health Criteria 224: Arsenic and Arsenic Compounds, 2001. http://www.inchem.org/documents/ehc/ehc/ehc224.htm (last accessed March 2008).
[2] M. Burguera, J.L. Burguera, Talanta 44 (1997) 1581.
[3] Z. Gong, X. Lu, M. Ma, C. Watt, X. Chris Le, Talanta 58 (2002) 77.
[4] C. B'Hymer, J.A. Caruso, J. Chromatogr. A 1045 (2004) 1.
[5] I. Ali, C.K. Jain, Int. J. Environ. Anal. Chem. 84 (2004) 947.
[6] K.A. Francesconi, D. Kuehnelt, Analyst 129 (2004) 373.
[7] D.J. Butcher, Appl. Spectrosc. Rev. 42 (2007) 1.
[8] F.T. Henry, T.M. Thorpe, J. Chromatogr. 166 (1978) 577.
[9] S. Fukui, T. Hirayama, M. Nohara, Y. Sakagami, Talanta 28 (1981) 402.
[10] U.M. Grüter, J. Kresimon, A.V. Hirner, Fresen. J. Anal. Chem. 368 (2000) 67.
[11] J. Yu, C.M. Wai, Anal. Chem. 63 (1991) 842.
[12] D.R. Killelea, J.H. Aldstadt, J. Chromatogr. A 918 (2001) 169.
[13] B. Beckermann, Anal. Chim. Acta 135 (1982) 77.
[14] K. Dix, C.J. Cappon, T.Y. Toribara, J. Chromatogr. Sci. 25 (1987) 164.
[15] H. Haraguchi, A. Takatsu, Spectrochim. Acta B 42 (1987) 235.
[16] K. Schoene, J. Steinhanses, H.-J. Bruckert, A. König, J. Chromatogr. 605 (1992) 257.
[17] F.A. Claussen, J. Chromatogr. Sci. 35 (1997) 568.
[18] Z. Mester, G. Vitányi, R. Morabito, P. Fodor, J. Chromatogr. A 832 (1999) 183.
[19] Z. Mester, G. Horváth, G. Vitányi, L. Lelik, P. Fodor, Rapid Commun. Mass Spectrom. 13 (1999) 350.
[20] Z. Mester, J. Pawliszyn, J. Chromatogr. A 873 (2000) 129.
[21] S. Wangkarn, S.A. Pergantis, J. Anal. At. Spectrom. 15 (2000) 627.
[22] E. Moreno, C. Cámara, W.T. Corns, D.W. Bryce, P.B. Stockwell, J. Autom. Meth. Manage. Chem. 22 (2000) 33.
[23] C. Herce-Pagliai, I. Moreno, G. González, M. Repetto, A.M. Cameán, Food Addit. Contam. 19 (2002) 542.
[24] K. Tašev, I. Karadjova, T. Stafilov, Microchim. Acta 149 (2005) 55.
[25] I.B. Karadjova, L. Lampugnani, M. Onor, A. D'Ulivo, D.L. Tsalev, Spectrochim. Acta B 60 (2005) 816.
[26] C. Herce-Pagliai, G. González, A.M. Cameán, M. Repetto, Food Addit. Contam. 16 (1999) 267.
[27] N.M. Melo Coelho, C. Parrilla, M.L. Cervera, A. Pastor, M. de la Guardia, Anal. Chim. Acta 482 (2003) 73.
[28] A. Martínez, A. Morales-Rubio, M.L. Cervera, M. de la Guardia, J. Anal. At. Spectrom. 16 (2001) 762.
[29] International Code of Oenological Practices, Code Sheet-Edition 2006/1, p. 238. http://www.oiv.int (last accessed March 2008).

[30] Real Decreto 53/1995, Reglamentación Técnico-Sanitaria para la Elaboración, Circulación y Comercio de la Cerveza y la Malta Líquida, B.O.E. No. 34 (09/02/1995).
[31] Food Legislation Surveys No. 6, Metallic Contaminants in Food. A Survey of International Prescribed Limits, 3rd ed., The Bristish Food Manufacturing Industries Research Association, Leatherhead, Surrey, UK, 1993.
[32] P.G. Craig, Organometallic Compounds in the Environment, John Wiley & Sons, Chichester, England, 2003.
[33] M. Pardo-Martínez, P. Viñas, A. Fisher, S.J. Hill, Anal. Chim. Acta 441 (2001) 29.
[34] P. Viñas, I. López-García, B. Merino-Meroño, N. Campillo, M. Hernández-Córdoba, Chromatographia 57 (2003) 611.
[35] N.P. Vela, D.T. Heitkemper, J.A.O.A.C. Int. 87 (2004) 244.
[36] D.T. Heitkemper, N.P. Vela, K.R. Stewart, C.S. Westphal, J. Anal. At. Spectrom. 16 (2001) 299.
[37] E. Sanz, R. Muñoz-Olivas, C. Cámara, Anal. Chim. Acta 535 (2005) 227.
[38] C. Yuan, G. Jiang, B. He, J. Anal. At. Spectrom. 20 (2005) 103.
[39] M.N. Matos Reyes, M.L. Cervera, R.C. Campos, M. de la Guardia, Spectrochim. Acta B 62 (2007) 1078.
[40] B. Szostek, J.H. Aldstadt, J. Chromatogr. A 807 (1998) 253.

Talanta 77 (2008) 751–757

Contents lists available at ScienceDirect

Talanta

journal homepage: www.elsevier.com/locate/talanta

Characterization of paper finishes by use of infrared spectroscopy in combination with canonical variate analysis

T. Canals[a,1], J.R. Riba[a], R. Cantero[a], J. Cansino[a], D. Domingo[a], H. Iturriaga[b,*]

[a] EUETII, L'Escola d'Adoberia, Universitat Politècnica de Catalunya, Igualada, Barcelona, Spain
[b] Facultat de Ciéncies, Química Analítica, Universitat Autònoma de Barcelona, E-08193 Bellaterra, Barcelona, Spain

ARTICLE INFO

Article history:
Received 29 February 2008
Received in revised form 30 June 2008
Accepted 11 July 2008
Available online 8 August 2008

Keywords:
Paper finish
Paper coating
FTIR
NIR
PCA
CVA

ABSTRACT

The finishing process used by the paper industry involves subjecting the paper surface to the action of chemicals and physical treatments in a series of operations intended to provide an end-product suitable for its intended use. In this work, we studied various paper finishes by using infrared spectra processed with appropriate chemometric techniques. To this end, we used a wide range of paper samples supplied in various finishes (coated, offset and cast-coated) by several paper manufacturers. Fourier transform middle-infrared (FTIR) spectra for the paper samples were recorded by using an ATR module, and reflectance near-infrared (NIR) spectra with the aid of a fibre-optic probe. Both techniques are fast and require no sample pretreatment.

The primary aim of this work was to develop a new methodology affording the accurate classification and identification of paper finishes in samples other than those used to construct the calibration model. To this end, we used the discriminant chemometric techniques principal component analysis (PCA) and canonical variate analysis (CVA), application of which was followed by that of the k-nearest neighbour algorithm to the samples in the prediction set. This procedure was also used to classify the coated samples into three subgroups. Both FTIR and NIR spectroscopy allowed most of the samples in the prediction sets to be accurately classified and identified.

1. Introduction

Although paper demand was anticipated to fall with the expansion of computers and the steadily growing use of electronic documents, the outcome has been quite the opposite and paper consumption has increased vastly worldwide over the past few decades [1].

The paper industry has become highly productive and competitive by reducing production costs, using highly automated continuous processes and minimizing the need for chemicals and labour. Also, the growing demands for paper products and the need to adjust processes to environmental protection requirements have brought about substantial improvements in raw materials, production technology, process control and end-product quality.

The finishing treatment is one of the key steps in the papermaking process inasmuch as it largely dictates some properties of the end-product including smoothness, opacity and brightness, and also its potential uses. Paper can be finished by chemical (surface coating, gluing) or physical means (calendering, brushing, embossing) [2,3].

The European Declaration on Paper Recycling [4] proposed measures aimed at ensuring that, by 2010, at least 66% of all paper and board used in Europe would be recycled. This would entail the strict use of specific chemicals and processes to improve the quality of finished paper.

Manufacturers require fast, efficient automatic methods to control the properties of each paper finish, as well as uniformity in the final properties of paper. Also, some clients require an effective method to check the properties and quality of the paper they purchase in order to ascertain whether it meets their requirements.

The paper industry characterizes paper finishes for quality in accordance with applicable standards based on methods which provide average values for some parameters determined from random measurements made with instrumental techniques (IR, Raman, X-ray photoelectron spectroscopies) over large areas of paper. The complex composition of finished paper makes it difficult to relate the spectral information provided by these techniques to the processes that dictate the quality of paper finishes [5].

Infrared spectroscopy has proved an essential tool for studying paper structure and pulp chemistry [6–12]. The paper industry has

* Corresponding author. Tel.: +34 935811012; fax: +34 935812379.
E-mail addresses: tcanals@euetii.upc.edu (T. Canals), hortensia.iturriaga@uab.es (H. Iturriaga).
[1] Tel.: +34 93 8035300.

0039-9140/$ – see front matter © 2008 Elsevier B.V. All rights reserved.
doi:10.1016/j.talanta.2008.07.059

long used infrared spectroscopy (FTIR and NIR) for process development and control, and also for the on-line control of specific parameters such as moisture content and grammage. Both FTIR and NIR provide large amounts of data which require chemometric processing in order to extract analytically relevant information. Chemometrics has facilitated the expeditious extraction of useful information from on-line spectral data supplied by fast-scan spectroscopic techniques; this has promoted its use for process control purposes [9,13–16].

Each type of finish gives paper characteristic physical and chemical properties; infrared spectroscopy, in combination with chemometric techniques, has been used to extract information about paper finishes [17].

The primary aim of this work was to develop an effective method for the direct, immediate classification and identification of paper finishes from FTIR or NIR spectra processed by principal component analysis (PCA), canonical variate analysis (CVA) and the k-nearest neighbour (kNN) algorithm. To this end, we used a large number of samples supplied in various finishes (coated, offset and cast-coated) by several paper manufacturers which were analyzed by FTIR and NIR with the need for no pretreatment or reagent addition. The ensuing methodology affords on-line measurements.

2. Experimental

2.1. Paper samples

We used a total of 92 samples that were split into three groups according to finish type, namely: coated (43), cast-coated (24) and offset (25). The samples were supplied by the firms Sarriópapel y Celulosa S.A. (Barcelona, Spain), Torraspapel S.A. (Barcelona, Spain) and Grup d'Impressió S.L. (Vilanova del Camí, Spain).

The industrial printing and packaging sectors are highly demanding on paper finishes and meeting their requirements entails applying various formulations to paper surfaces (*i.e.*, coating). Coating treatments usually involve the use of pigments, adhesives (binders) and additives. Pigments, which consist of insoluble minerals (kaolin, calcium carbonate, talc, titanium dioxide) in very small grain sizes, constitute the major ingredient and make paper highly smooth and microporous. Adhesives (binders) are usually starch, protein or latex products intended to fix other substances applied to paper surfaces. Finally, additives, which are available in a variety of forms including insolubilizers, plasticizers, dispersants and protectors, improve the final properties of coated paper.

Cast-coated paper is obtained by subjecting coated paper to a physical treatment known as calendering; this involves ironing the paper at a high temperature. Although this treatment is usually applied to one side only, it can be used on both—this allows high-grammage paper to be obtained by gluing two sheets on their untreated sides. Cast-coated paper can be obtained in a variety of colours and hues ranging from pale to strong, and also in metallic finishes.

Offset paper is named after the offset printing technique, which is its usual target use. This type of paper is usually made from chemical pulp, whether alone or in mixture with mechanical pulp (and also, occasionally, some recycled paper). Offset paper is subject to virtually no specific finishing treatment other than dyeing, bleaching or silking.

2.2. Data acquisition

Spectra for the 92 paper samples were obtained by FTIR and NIR, which penetrate paper surfaces to a disparate depth [13,18].

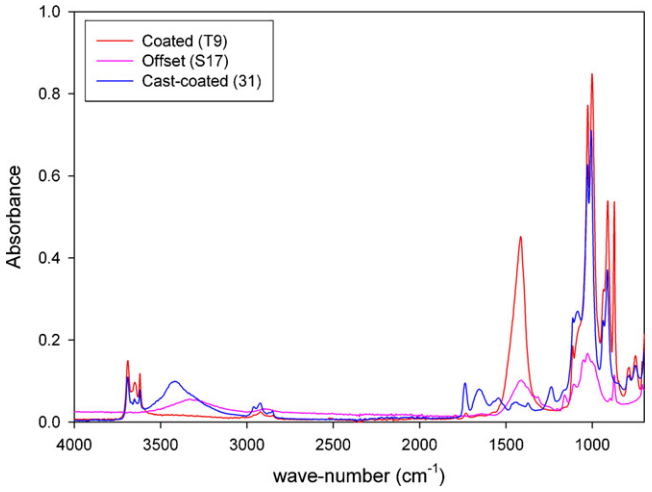

Fig. 1. FTIR absorbance spectra for three selected paper samples representing each finish type.

FTIR spectra were recorded by using an ATR cuvette over the wavenumber range 4000–650 cm^{-1}, each result being the average of four consecutive readings made on an IR Spectrum One (S/N 57458) from PerkinElmer (Beaconsfield, UK) equipped with an ATR internal reflectance module (Universal Sampling Accessory, S/N P0DL01101418).

Near-infrared reflectance spectra were obtained in the absorbance mode, using a fibre-optic probe over the wavelength range 1100–2500 nm; each measurement was the average of 32 scans. In order to consider heterogeneity in each paper sample, and ensure that the spectra would be representative of the whole sample. The fibre-optic probe was moved across the paper surface and three readings made at randomly chosen points in each measurement. The spectrum for each sample was obtained by averaging the three recordings. Spectra were obtained on a Foss NIRSystems 5000 instrument (Silver Spring, MD) equipped with a reflectance detector and an Ortiprobe fibre-optic probe.

Both NIR and MIR spectra were acquired at room temperature (25 ± 1°C).

Figs. 1 and 2 show the FTIR and NIR spectra for a selected paper sample per finish type.

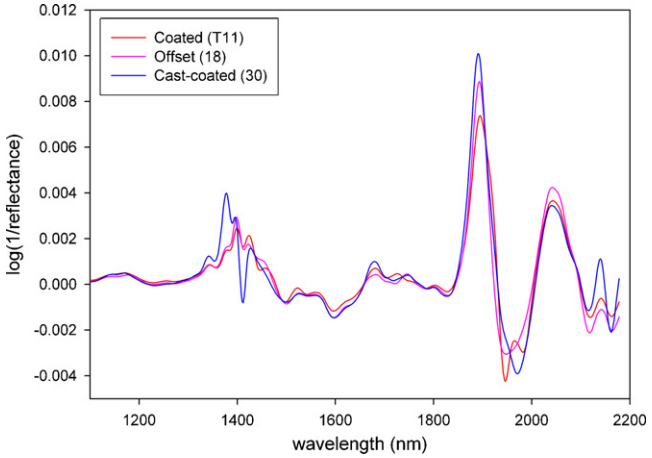

Fig. 2. First-derivative NIR spectra for three selected paper samples representing each finish type.

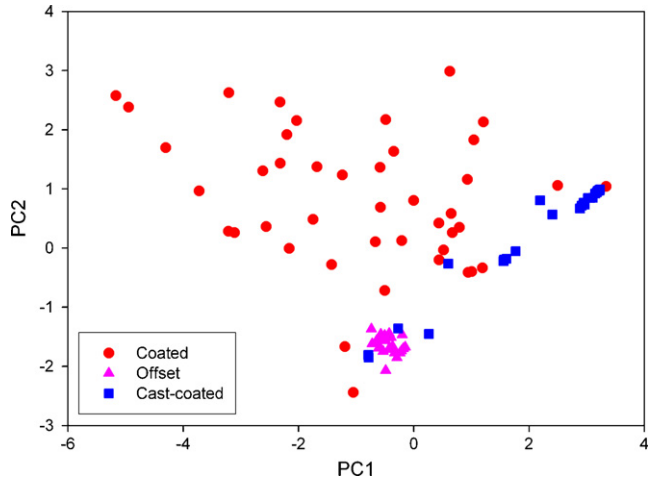

Fig. 3. PCA of the FTIR absorbance spectra for the 92 samples as done on centred data.

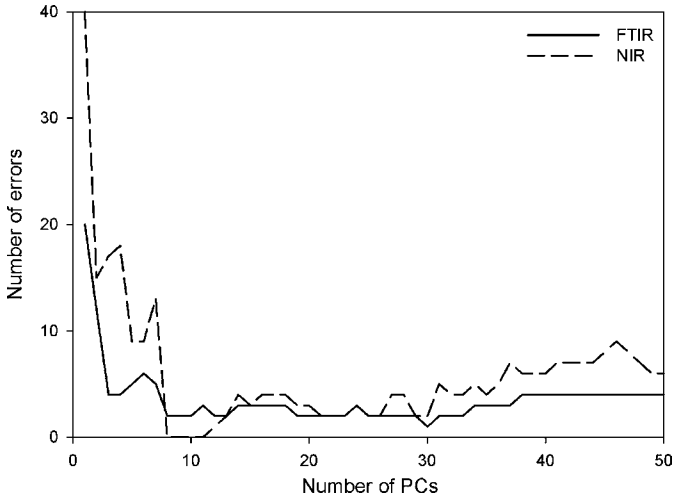

Fig. 5. Cross-validation results for the samples of the calibration set. Number of prediction errors versus the number of retained PCs for both studies, FTIR and NIR.

2.3. Multivariate statistical analysis

The information obtained from the FTIR and NIR spectra allowed the paper samples to be classified into the three above-mentioned groups by using chemometric techniques the foundation of which is outlined below.

2.3.1. Principal component analysis (PCA)

Principal component analysis [19] is an unsupervised multivariate chemometric technique widely used to simplify structure in complex information produced in various fields of knowledge such as chemistry [14–16,20], medicine, psychology or economics. The PCA technique transforms the original measured variables (spectral data obtained at different wavelengths in our case) into new variables called principal components (PCs); in this way, it provides a group of orthogonal axes that represent the directions of greatest variance of the data. PCs are linear combinations of the original measured variables. PCA allows the dimensionality of data to be reduced while retaining as much information contained in them as possible. Frequently, PCA is the first data analysis technique applied to the results as it allows patterns in measured data to be exposed.

2.3.2. Canonical variate analysis (CVA)

Canonical variate analysis is a supervised discriminant technique intended to strengthen differences between data groups. Thus, CVA estimates the directions in space that maximize the differences between groups in the original data according to a statistical criterion. Unlike PCA, which is based on regression criteria, CVA relies on discrimination criteria (separation of classes). Therefore, CVA is more suitable for classification purposes than is PCA. The mathematical foundation of CVA is described elsewhere [19,21]. The CVA algorithm projects the original data into new axes called canonical variables (CVs), which are latent variables not necessarily orthogonal to one another. The separation criterion aims at obtaining the maximum separation between classes and the minimum separation within classes.

Canonical variate analysis has the drawback that it cannot deal with data where the number of variables is greater than that of samples. This is often the case with spectroscopic data and requires reducing their dimensionality (*e.g.*, by PCA) before CVA is applied. The CVA technique is frequently used to classify samples from FT-Raman, FTIR and NIR spectral data [22–24].

The optimum number of variables to be retained for CVA (PCs in our case) can be determined in various ways and no universal

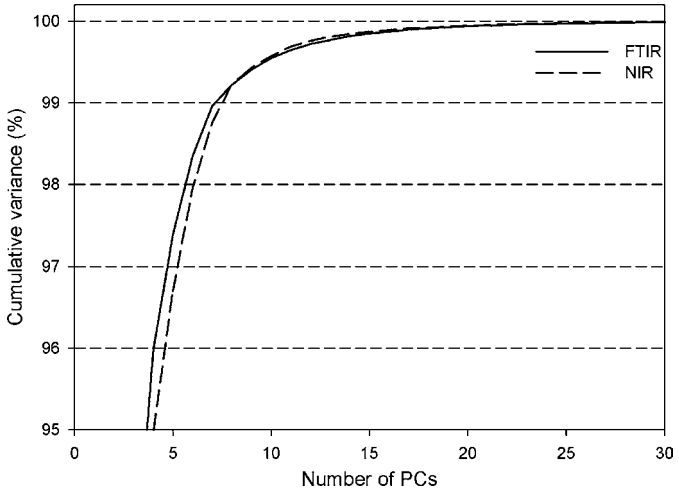

Fig. 4. Cumulative variance as a function of the number of PCs used with FTIR and NIR data.

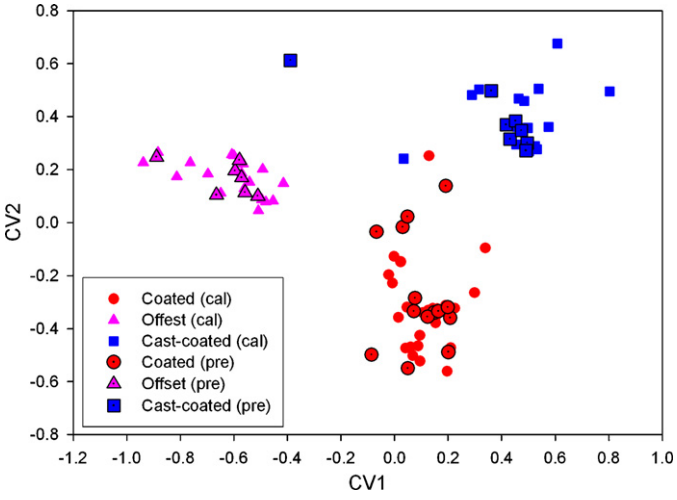

Fig. 6. CVA of the FTIR absorbance spectra for the calibration and prediction samples as done on centred data.

Table 1
Characteristics of the 92 paper samples studied and their finish and of the FTIR and NIR calibration and prediction sets

Sample	Paper type	Gram (g/m^2)	FTIR (absorbance mode) PCA + CVA (9 PCs)			NIR (first-derivative mode) PCA + CVA (8 PCs)		
			Cal. (63 s)	Pred. (29 s)	kNN success	Cal. (58 s)	Pred. (28 s)	kNN success
T1	Double-sided glossy coated art paper	115		×	Yes		×	Yes
T2	Double-sided glossy coated art paper	280	×			×		
T3	Double-sided glossy coated art paper	300	×			×		
T4	Double-sided glossy coated paper	250	×				×	Yes
T5	Double-sided lightweight glossy coated paper	125		×	Yes	×		
T6	Double-sided industrial cast-coated mechanical paper	80	×			×		
T7	Double-sided embossed linen art paper	170	×			×		
T8	Double-sided semi-matte coated art paper	135	×				×	Yes
T9	Double-sided semi-matte ivory coated art paper	135		×	Yes	×		
T10	Double-sided semi-matte coated art paper	115	×			×		
T11	Double-sided semi-matte coated paper	125	×			×		
T12	Double-sided matte coated paper	125	×				×	No
T13	Double-sided lightweight matte coated paper	112		×	Yes	×		
T14	Double-sided industrial cast-coated mechanical paper	80	×			×		
M25	Double-sided glossy coated paper	350	×				×	Yes
M26	Double-sided glossy coated paper	80		×	Yes	×		
M27	Double-sided glossy coated paper	250	×				×	Yes
M28	Double-sided glossy coated paper	170	×			×		
M29	Double-sided glossy coated paper	150	×			×		
M30	One-sided glossy coated paper	75		×	Yes	×		
M31	One-sided glossy coated paper	90	×			×		
S20	Three-layer glossy coated paper	170	×			×		
S21	Three-layer semi-matte coated paper	170		×	Yes		×	Yes
S22	Textured coated paper	150	×			×		
S23	One-sided glossy coated label paper	135		×	Yes	×		
1	Multi-layer semi-matte ivory coated offset paper	135		×	Yes	×		
2	Multi-layer semi-matte coated paper	125	×				×	Yes
3	Ecological semi-matte coated paper	135		×	Yes		×	Yes
4	Classic semi-matte coated paper	135	×			×		
5	Classic matte coated paper	125		×	Yes	×		
6	Classic matte coated bulk paper	125	×			×		
7	Lightweight matte coated paper	125		×	Yes	×		
8	Recycled lightweight matte coated paper	135	×				×	Yes
9	Lightweight semi-matte coated mechanical paper	80	×				×	Yes
10	Glossy coated illustration paper	135	×			×		
11	Multi-layer glossy coated paper	125		×	Yes		×	Yes
12	Ecological glossy coated paper	135	×				×	Yes
13	Classic glossy coated paper	125	×			×		
14	Lightweight glossy coated paper	115	×			×		
15	Glossy coated mechanical paper	80	×				×	Yes
16	One-sided classic glossy coated paper	115		×	Yes	×		
17	One-sided classic wet-strength glossy coated paper	80	×			×		
18	One-sided classic glossy grease-proof coated paper	80	×			×		
2001	Offset paper	–	×					
2002	Offset paper	–	×					
2003	Offset paper	–	×					
2004	Offset paper	–	×					
M32	Double-sided offset paper	–	×			×		
M33	Double-sided offset paper	–	×				×	Yes
M34	Double-sided offset paper	–		×	Yes	×		
M35	Double-sided offset paper	–	×			×		
M36	Yellow offset paper	–	×				×	Yes
S15	Ivory offset publishing paper	90		×	Yes	×		
S16	Premium silk cast-coated paper	120	×				×	Yes
S17	100% cotton offset paper	160	×			×		
S18	100% ecological recycled offset paper	90		×	Yes	×		
S19	Mass-dyed red offset paper	80	×			×		
19	Extra-premium white offset paper	125		×	Yes	×		
20	Premium white offset paper	90	×				×	Yes
21	Premium white offset paper	50	×			×		
22	Premium white offset paper	120		×	Yes	×		
23	Mono 2 bulk offset paper	80	×			×		
24	100% recycled white offset paper	115		×	Yes	×		
25	100% recycled white offset paper	90	×				×	Yes
26	Ivory register paper	125	×				×	Yes
27	Ivory offset paper	100		×	Yes	×		
28	Mono 2 ivory bulk offset paper	80	×			×		
29	Special unbleached white cheque paper	95	×				×	Yes
S24	Calendered cast-coated paper	200	×			×		

Table 1 (*Continued*)

Sample	Paper type	Gram (g/m^2)	FTIR (absorbance mode) PCA + CVA (9 PCs)			NIR (first-derivative mode) PCA + CVA (8 PCs)		
			Cal. (63 s)	Pred. (29 s)	kNN success	Cal. (58 s)	Pred. (28 s)	kNN success
ecv	Green cast-coated paper	250		×	Yes		×	Yes
els1	One-sided cast-coated paper	75	×			×		
e2c5	High-rigidity cast-coated paper	250		×	Yes		×	Yes
eca2	Yellow cast-coated paper	250	×			×		
ecc	Sky-blue cast-coated paper	250		×	Yes	×		
eccr	Cream cast-coated paper	250		×	No	×		
ecg	Grey cast-coated paper	250	×			×		
ecr	Pink cast-coated paper	250	×			×		
elc	One-sided cast-coated paper	125		×	Yes	×		
e2ca	Double-sided cast-coated paper	200	×			×		
e2cb	Double-sided cast-coated paper	200		×	Yes	×		
elws1	Wet-strength cast-coated paper	80	×				×	Yes
mvob	Metallic gold cast-coated paper	95	×			×		
mvpb	Metallic silver cast-coated paper	95	×				×	Yes
30	One-sided cast-coated paper	120	×				×	Yes
31	One-sided cast-coated paper	180		×	Yes	×		
32	Double-sided cast-coated paper	250		×	Yes	×		
33	One-sided semi-matte cast-coated paper	215	×			×		
34	One-sided cast-coated paper (colour 11, light chamois)	250	×				×	Yes
35	One-sided cavitated cast-coated paper (colour 05, pearl)	250	×				×	No
36	One-sided pigmented cast-coated paper with white coated back (colour 63, turquoise)	250	×			×		
37	One-sided metallized cast-coated paper (colour 86, green)	250	×					
38	One-sided metallized silver cast-coated paper	250	×					

The results provided by the kNN method with $k = 3$ and 4 are also given.

method for this purpose exists; in any case, overfitting can always be avoided by splitting samples into a training set and a test set [25].

2.3.3. *k-nearest neighbour method (kNN)*

The kNN method is a non-parametric classification method that places the objects of the prediction set in the same multi-dimensional space as those of the calibration set. The process involves determining the k-nearest neighbours of each individual object in the prediction set and assigning a score k to the nearest neighbour, $k - 1$ to the second nearest and so on until a unity score is given. Finally, the object in question is included in the class for which it exhibits the largest score. One problem with this method is that, in principle, no optimum k value other than $k = 1$ exists; this entails trying various k values and comparing the classification outputs. Some authors recommend using k values from 3 to 5 [20].

Spectra were processed by using the software The Unscrambler v. 7.5. To this end, spectral data obtained in the absorbance mode were converted into their first- and second-derivatives. A five-point moving average was obtained at each point in order to avoid diminishing the signal-to-noise ratio during differentiation. Spectral derivatives were obtained by using the Savitzky-Golay algorithm. Finally, the chemometric models required to classify the samples were generated by using three programmes developed by the authors in Matlab 7.0.

3. Results and discussion

We studied a large number of paper samples of the three above-described types. The differences in finish reflected in differences in physical and chemical properties, and also in spectral characteristics. Appropriately processing the spectral information obtained from them with a view to their accurate classification and identification according to finish required the use of effective chemometric methods.

We initially studied the behaviour of the whole body of samples and then split them into a calibration set and prediction set in order to develop the classification model. We tested various types of models and carefully examined the effects of potentially influential variables, data processing methods, wavelength ranges, spectral modes and choices of samples for explaining diversity in each paper finish group for both sets. This allowed the most suitable model for classifying and identifying paper finishes in the prediction set to be established.

Because application of the PCA technique to the FTIR and NIR data allowed no accurate classification of the paper samples in terms of finish, we used CVA, successfully, instead. Applying CVA required the prior reduction of the number of variables, which was accomplished by PCA. One important choice here is the number of variables to be retained for application of CVA in order to ensure the development of robust models while avoiding overfitting. This additionally entailed choosing the most suitable variables; with such a complex body of samples, which exhibited strong spectral overlap in a number of components, this entailed retaining as much data as needed to explain 99.9% of the total variance. To this end, we applied leave-one-out cross-validation to the calibration sets and related the number of PCs used to that of failures in sample prediction. Thus, we applied CVA to the first 9 PCs obtained from the 1676 original FTIR variables, and also to the first 8 PCs resulting from the 550 original NIR variables.

The first two canonical variables allowed the paper samples to be classified into independent groups according to finish on the basis of both FTIR and NIR data.

The kNN method allowed the numerical descriptor for the degree of membership of each prediction sample to each group defined in the calibration step to be obtained.

3.1. *Classification of paper samples from FTIR spectra*

The FTIR spectra for the 92 paper samples provided a data matrix consisting of 92 rows and 1676 columns which was used to obtain a 92×1666 first-derivative matrix and a 92×1656 second-derivative matrix.

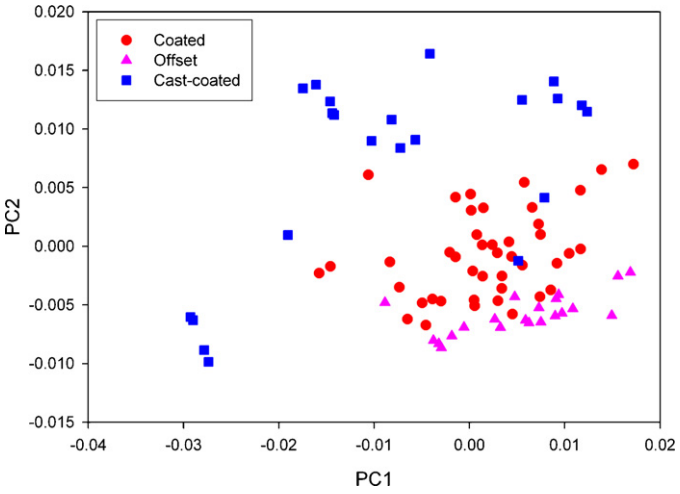

Fig. 7. PCA of the first-derivative NIR spectra for 86 samples as done on centred data.

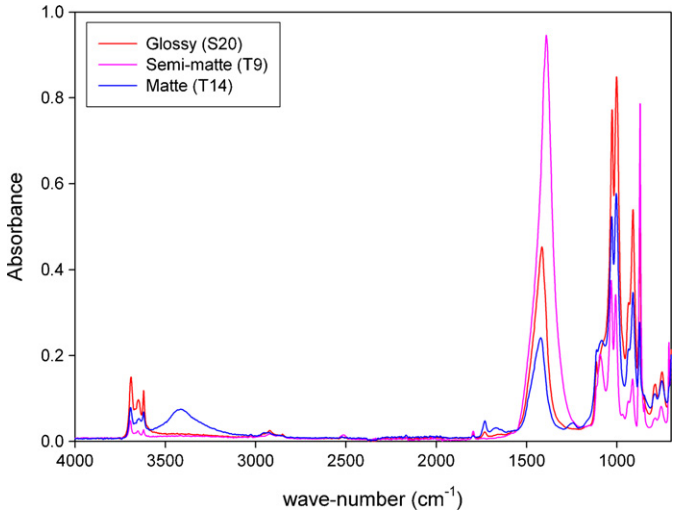

Fig. 9. FTIR spectra for samples in the three coated finish subgroups.

Fig. 3 depicts the 92 samples in the space defined by the first two PCs. As can be seen, the coated paper samples were widely scattered, the cast-coated samples partially scattered and the offset samples scarcely scattered. Other spectral modes provided similar clustering results. The strong overlap between groups of the PCA revealed the inability of this technique to discriminate FTIR spectra for differently finished paper surfaces.

In order to improve separation, we used CVA on a reduced number of variables selected by PCA. As noted earlier, preliminary tests revealed the need to retain as many PCs as needed to explain 99.9% of the total variance in the spectral data; this required applying CVA to a 36-column matrix. Fig. 4 shows the cumulative variance explained by the first few principal components.

Once the previous procedure was checked to accurately classify samples according to finish, the samples were split into a calibration set and a prediction set. To this end, 14 of the 43 coated paper samples, 7 of the 25 offset samples and 8 of the 24 cast-coated samples were randomly selected for inclusion in the prediction set, the remaining 63 being included in the calibration set.

By using the above-described procedure, PCA was applied to the 63×1676 matrix in order to reduce the number of variables. To this end, we applied leave-one-out cross-validation to the prediction results obtained from the samples in the calibration set at a variable number of PCs. Fig. 5 shows the number of prediction errors obtained as a function of that of PCs used to construct the model. Based on the results, a total of 9 PCs were retained for application of CVA to the calibration matrix (63×9) and prediction matrix (29×9). Fig. 6 shows the distribution of the calibration and prediction samples in the space defined by the canonical variables. As can be seen, the former were accurately separated and the latter classified. As can be seen from Table 1, application of the kNN method resulted in 96.6% successful identifications of the specific finishes for the 29 samples in the prediction set.

3.2. Classification of paper samples from NIR spectra

Six of the 92 samples in the NIR matrix were outliers and thus discarded; such samples were either metallized or black-coloured. Therefore, the starting matrix consisted of 86 rows and 550 columns of NIR data obtained in the absorbance mode. This matrix was used to obtain a first- and second-derivative.

Fig. 7 shows the scatter plot for the 86 samples in the space defined by the first two PCs as obtained from first-derivative spectra with centred data. As can be seen, the three finish groups overlapped with both absorbance data and their two derivatives. This

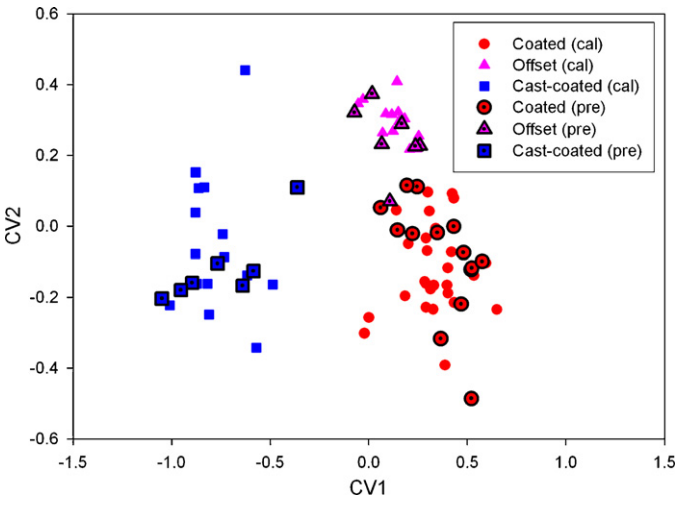

Fig. 8. CVA of first-derivative NIR spectra for the calibration and prediction samples as done on centred data.

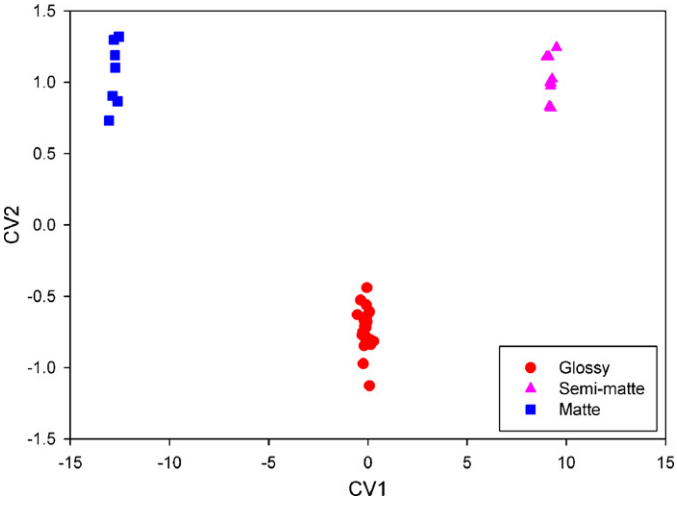

Fig. 10. Coated finish subgroups established by CVA of first-derivative FTIR spectra as done on centred data.

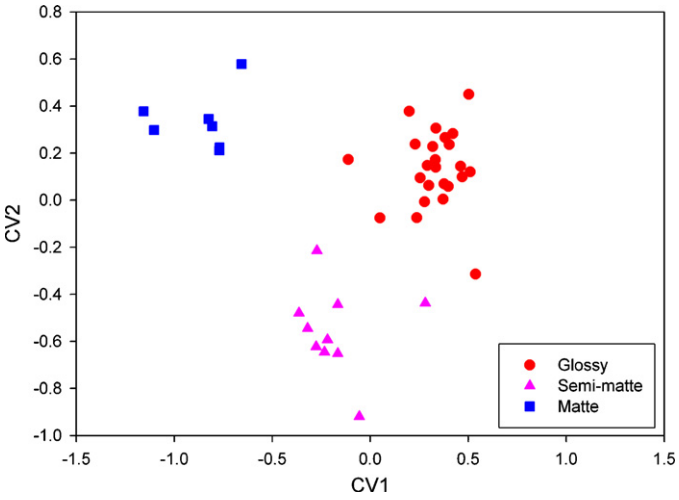

Fig. 11. Coated finish subgroups established by CVA of second-derivative NIR spectra as done on centred data.

required using an alternative discrimination method. As with FTIR data, we used CVA following reduction of variables by PCA for this purpose.

Fig. 4 shows the explained variance as a function of the number of PCs.

The next step involved selecting 14 of the 43 coated paper samples, 7 of the 21 offset samples and 7 of the 22 cast-coated samples for inclusion in the prediction set, the remaining 58 being included in the calibration set. Then, we applied leave-one-out cross-validation to the calibration set in order to select the optimum number of PCs. Fig. 5 shows the results thus obtained.

The number of variables was reduced to 8 by PCA of a 58×540 matrix. Application of CVA to the calibration matrix (58×8) and prediction matrix (28×8) provided the results of Fig. 8, calibration samples were accurately separated and prediction samples identified.

Finally, application of the kNN method confirmed that finishes were accurately identified in 92.9% of cases (see Table 1).

3.3. Coated paper subgroups

Samples in each group were not completely identical as regards finish. This led us to assess the ability of the proposed methodology to discriminate subgroups within each finish group. Because this entailed using a large number of samples, tests were performed on coated paper only, which was the largest group. The studied samples were split into three subgroups, namely: glossy, semi-matte and matte.

Fig. 9 shows the FTIR spectra for three selected samples representative of the three types of coated finishes. As before, CVA was applied to a reduced number of variables; however, the high similarly between the 41 samples in the coated paper group entailed retaining a greater number of PCs (37). Fig. 10 shows the separation obtained by applying CVA to the reduced data matrix (41×37); as can be seen, the first canonical variable allowed the samples to be accurately split into the three subgroups. However, the calibration model is less robust for the purpose of identifying samples. Improving its robustness would require expanding the sub-set with more samples.

A similar procedure was followed with the NIR spectra. A total of 25 PCs were retained for the 41 samples. Fig. 11 shows the separation obtained by applying CVA to the reduced data matrix (41×25), which, as can be seen, sufficed to accurately discriminate between subgroups. As in the previous case, however, the identification model obtained with the available number and distribution of samples was not robust enough.

4. Conclusions

The finishing treatment is the last step in the industrial production of paper and also largely responsible for many properties of the end-product. The paper industry needs effective methods to control the physical and chemical properties of the paper it produces. In this work, we developed a new methodology which affords real-time control of the characteristics of finished paper by using chemometrically processed FTIR or NIR spectral data. Once the calibration model is constructed, the spectrum for each test sample is subjected to CVA on a previously reduced number of variables in order to identify its finish.

Application of the proposed methodology to paper samples from various manufacturers afforded nearly 100% success in their classification with the kNN method, using both FTIR and NIR spectra.

Because NIR light penetrates more deeply into the paper surface than does MIR light, the information for the paper matrix overlaps with that for the finish. This requires exercising greater care in constructing calibration models in order to discard outliers and avoid overfitting.

The proposed methodology was also successfully used to classify the coated papers into three finish subgroups.

Acknowledgement

The authors are grateful to Spain's Ministry of Education and Science for funding this research within the framework of Project CTQ 2006-12923.

References

[1] R. Grae, Pulp Paper 1 (2007) 5.
[2] J.P. Casey, Pulp and Paper, John Wiley & Sons, 1983.
[3] M. Kouris, M.J. Kourek, Coating, Converting and Specialty Processes, vol. 8, Joint Textbook Committee of the Paper Industry, 1990.
[4] European Declaration on Paper Recycling 2006–2010, European Recovered Paper Council, 2006.
[5] J. Vyörykkä, A. Fogden, J. Daicic, M. Ernstsson, A.S. Jääskeläinen, Proceedings of the Advanced Coating Fundamentals Symposium, Turku, Finland, February 8–10, Tappi (Technical Association for the worldwide pulp, paper, and converting industry), 2006.
[6] J.J. Workman, Appl. Spectr. Rev. 34 (1 & 2) (1999) 1.
[7] B.B. Sitholé, Anal. Chem. 67 (1995) 87R.
[8] J.J. Workman, Appl. Spectr. Rev. 36 (2 & 3) (2001) 139.
[9] J. Pan, K.L. Nguyen, Anal. Chem. 79 (6) (2007) 2259.
[10] T. Trafela, M. Strli, J. Kolar, D.A. Lichtblau, M. Anders, D.P. Mencigar, B. Pihlar, Anal. Chem. 79 (16) (2007) 6319.
[11] S. Tsuchikawa, Appl. Spectr. Rev. 42 (1) (2007) 43.
[12] J. Havermans, H.A. Aziz, N. Fenders, Restaurator 26 (3) (2005) 172.
[13] L. Dolmatova, C. Ruckebusch, N. Dupuy, J.P. Huvenne, P. Legrand, Chemometr. Intell. Lab. Syst. 16 (1997) 125.
[14] M.T. Bona, J.M. Andrés, Talanta 74 (4) (2008) 998.
[15] J.S. Câmara, M.A. Alves, J.C. Marques, Talanta 68 (5) (2006) 1512.
[16] S. López-Feria, S. Cárdenas, J.A. García-Mesa, M. Valcárcel, Talanta 75 (4) (2008) 937.
[17] D. Anderson, Anal. Chem. 73 (2001) 2701.
[18] O. Berntssona, L.G. Danielssona, S. Molestad, Anal. Chim. Acta 364 (1–3) (1998) 243.
[19] R.A. Johnson, D.W. Wichern, Applied Multivariate Statistical Analysis, Prentice Hall, 1992.
[20] L.A. Berrueta, R.M. Alonso-Salces, K. Héberger, J. Chromatogr. A 1158 (1–2) (2007) 196.
[21] L. Nørgaard, R. Bro, F. Westad, S.B. Engelsen, J. Chemometr. 20 (8–10) (2006) 425.
[22] H. Yanga, J. Irudayarajb, M.M. Paradkar, Food Chem. 93 (1) (2005) 25.
[23] M.M. Paradkar, J. Irudayaraj, Food Chem. 76 (2) (2002) 231.
[24] M.M. Paradkar, S. Sivakesava, J. Irudayaraj, J. Sci. Food Agric. 83 (May (7)) (2003) 714.
[25] W.J. Krzanowski, Principles of Multivariate Analysis. A User's Perspective, Oxford University Press, New York, 1993.

Talanta 77 (2008) 566–570

Contents lists available at ScienceDirect

Talanta

journal homepage: www.elsevier.com/locate/talanta

Determination of pesticides fenoxycarb and permethrin by sequential injection chromatography using miniaturized monolithic column

Petr Chocholouš*, Dalibor Šatínský, Radek Sladkovský, Marie Pospíšilová, Petr Solich

Department of Analytical Chemistry, Faculty of Pharmacy in Hradec Králové, Charles University in Prague, Heyrovského 1203, 500 05 Hradec Králové, Czech Republic

ARTICLE INFO

Article history:
Received 30 October 2007
Received in revised form 1 June 2008
Accepted 10 June 2008
Available online 21 June 2008

Keywords:
Sequential injection chromatography (SIC)
Chromolith™ monolithic column
Fenoxycarb
Permethrin
Pesticides
Spectrophotometric determination

ABSTRACT

Sequential injection chromatography system equipped with miniaturized 10 mm monolithic column was used for fast simultaneous determination of two pesticides—fenoxycarb (FC) and permethrin (PM). The system was composed of a commercial sequential injection analysis (SIA) system (FIAlab® 3000, 6-port selection valve and 5.0 mL syringe pump), commercially available column Chromolith™ RP-18e (10 mm × 4.6 mm i.d.) (Merck®, Germany) and CCD UV–vis detector (USB 2000, Ocean-optics) with 1.0 cm Z-flow cell, absorbance was monitored at 225 nm. The mobile phase used for analysis was acetonitrile/water (60:40, v/v), flow rates were 0.6 mL min^{-1} for elution of fenoxycarb and 1.2 mL min^{-1} for elution of permethrin. For each analysis 4.8 mL of mobile phase was used. The chromatographic resolution between both compounds was >8 and analysis time was <6.5 min under the optimal conditions. Limits of detection were determined at 2.0 μg mL^{-1} for fenoxycarb and 1.0 μg mL^{-1} for permethrin. Samples were prepared by diluting with mobile phase and injected volume was 10 μL for each analysis. Developed method was applied to analysis of both pesticides in veterinary pharmaceutical foams and sprays ARPALIT® Neo (Aveflor, Czech Republic). SIC method was compared with validated method (HPLC, reverse phase 100 mm monolithic column, gradient elution).

1. Introduction

Chromatography is widely used in separation of mixtures in almost all branches of chemistry. Sequential injection chromatography (SIC) based on integration of very short monolithic column (10–50 mm) into flow manifold has been introduced as a new generation of flow methods analysis and extended the possibilities of sequential injection analysis (SIA). SIC technique enables determination of simple multi-compound samples by chromatography [1].

SIA, highly versatile technique based on a programmable flow [2] has been proposed by Ruzicka and Marshall as an efficient tool for automated liquid handling [3]. The "single-line" technique is based on forward and reverse movement of a piston of syringe pump, which together with a multi-position selection valve enables precise sampling of liquid chemicals into the system and propelling of the sequenced zones to the reactors and detector [4]. Automation, speed of the analysis and low consumption of sample and reagents are the most important features that favour the SIA technique for application in many fields of analysis, primarily by more complicated operations such as sample pre-treatment, derivatization reactions or monitoring of long lasting processes [5–7].

On the other hand, SIA technique itself has generally one important drawback—it generally cannot provide the separation procedure and analysis of multi-component samples. This weak point was first time solved by insertion of short monolithic column into SIA manifold, creating a technique called sequential injection chromatography [8]. The monolithic columns (formed by "sol–gel" technology from a single piece of porous silica gel) enable operation at high flow rates with lower-back pressure [9]. This feature is used for integrating these columns into a SIC manifold and for extending the possibilities of low pressure flow technique. SIC manifold was successfully applied to the analysis of relatively simple multi-component samples mainly in pharmaceutical area [1].

Coupling of monolithic columns with SIA/FIA manifolds show increasing trend in flow analysis area. Zacharis et al. have incorporated monolithic strong anion-exchanger disk (CIM®) into SIA manifold for on-line drug–protein interaction studies [10]. Multisyringe flow system with three solenoid valves coupled with Chromolith™ Flash RP-18e (25 mm × 4.6 mm i.d.) monolithic column created by González-San Miguel et al. have been used for determination of β-lactam antibiotics [11]. García-Jiménez et al. have employed Chromolith™ Guard Cartridge RP-18 endcapped (5 mm × 4.6 mm i.d.) monolithic pre-column in FIA for analysis of

* Corresponding author. Fax: +420 495 067 164.
E-mail address: petr.chocholous@faf.cuni.cz (P. Chocholouš).

0039-9140/$ – see front matter © 2008 Elsevier B.V. All rights reserved.
doi:10.1016/j.talanta.2008.06.015

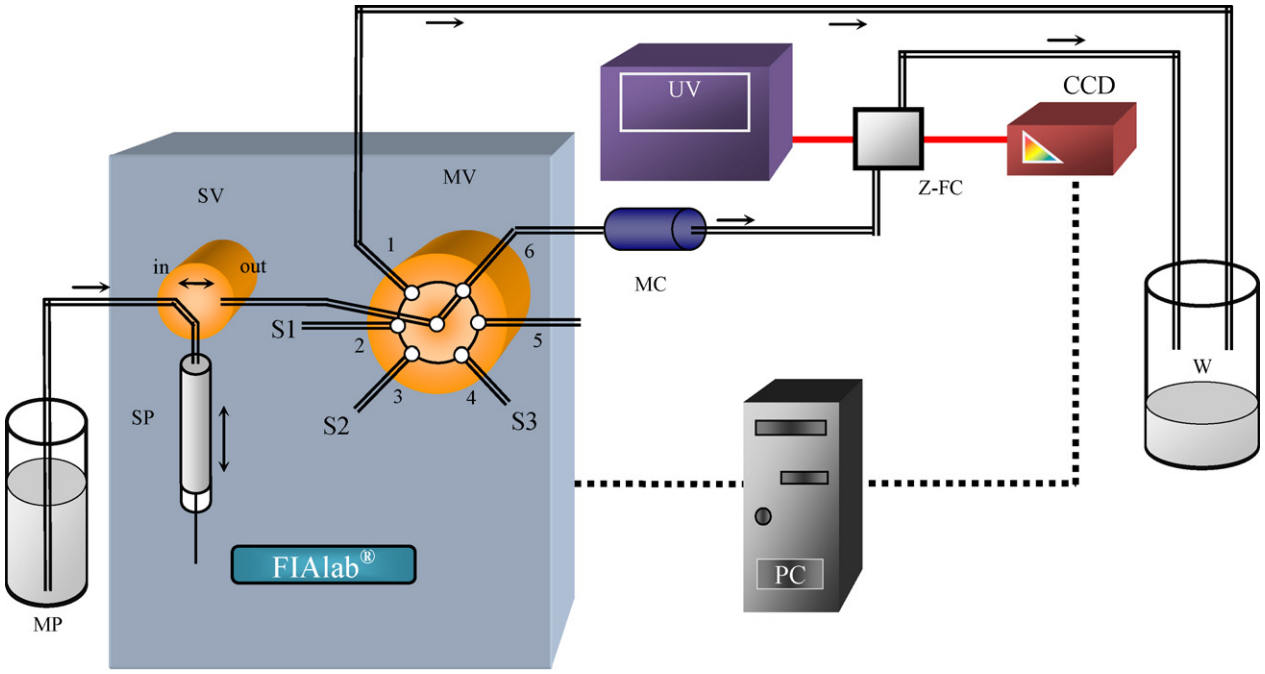

Fig. 1. Scheme of SIC set-up for determination of FC and PM. CCD: CCD UV–vis detector; MC: monolithic column; MP: mobile phase; MV: 6-port multi-position valve; PC: computer; SP: syringe pump; SV: solenoid valve; S1, S2, S3: Sample 1, 2, 3; UV: UV lamp, W: waste, Z-FC: Z-flow cell.

antioxidants, preservatives and sweeteners in food and cosmetics [12], while Claver et al. have used same system for determination of parabens in cosmetics [13]. Adcock et al. have incorporated monolithic column Chromolith™ Flash RP-18e (25 mm × 4.6 mm i.d.) with 5 mm pre-column into a hybrid FIA/HPLC manifold for determination of opiate alkaloids and biogenic amines (neurotransmitter metabolites) with chemiluminescence detection [14].

Permethrin (PM) [3-phenoxybenzyl (±) *cis*/*trans*-3-(2,2-dichlorovinyl)-2,2-dimethylcyclopropane-1-carboxylate]—a pyrethroid insecticide, is widely used throughout the world as a wide-spectrum insecticide for numerous crops and also for indoor pest control in the public health sector and housing. There are four isomeric forms: two *cis* (PMC) and two *trans* (PMT) of technical PM (the *cis* and *trans* isomers differ in the spatial arrangement of the atoms). Product formulations of PM can vary greatly in isomeric content so the sum of all forms is usually declared.

Fenoxycarb (FC) [ethyl 2-(4-phenoxyphenoxy)ethylcarbamate] is a carbamate insect growth regulator used to control a wide variety of insect pests. It is used as a fire ant bait and for flea, mosquito, and cockroach control, and can also be used to control butterflies, moths, beetles, and scale and sucking insects on olives, vines, cotton, and fruit. It is also used to control these pests on stored products, and is often formulated as a grit or corncob bait. Compared to other carbamates, FC is one of the least toxic in this chemical class.

There have been recently a number of reports in literature dealing with various analytical methods for the determination of FC [15–18] and PM [19–24], mainly by HPLC and GC methods, but there is no analytical method in literature for simultaneous determination of FC in the presence of PM.

2. Experimental

2.1. Apparatus

2.1.1. Sequential injection chromatography system

A commercially available FIAlab® 3000 instrument (FIAlab® Instruments Inc., Bellevue, USA) with a syringe pump (syringe reservoir 5.0 mL) and a 6-port selection Cheminert® valve (Valco Instrument Co., Houston, USA) was used. The manifold was equipped with fiber-optic CCD UV–vis detector USB 2000 (Ocean Optics Inc., Dunedin, USA), 10 mm Z-flow cell (Avantes, CO, USA) and UV light source D-1000-CE (Analytical Instrument Systems Inc., Flemington, USA). The whole SIC system was controlled by the program FIAlab®. Flow lines were made from 0.50 mm i.d. PTFE tubing. Samples were aspirated through the 6-port multi-position valve then delivered to the monolithic column and to the detector. Direct sample separation was performed on reversed phase C-18 monolithic column Chromolith™ RP-18e (10 mm × 4.6 mm i.d.) (Merck®, Germany). The monolithic column was placed between the multi-position valve and flow cell of the detector. Manifold set-up depicted in Fig. 1.

2.1.2. HPLC apparatus

Validated HPLC method for veterinary product samples was performed on HPLC system Shimadzu Prominence LC-20A series with DAD detector (set on 225 nm). System was equipped with the monolithic column Chromolith™ Performance RP-18e (100 mm × 4.6 mm i.d.) (Merck®, Germany). Gradient elution was under the following conditions: 0–4 min acetonitrile/water (60:40, v/v), 4–8 min acetonitrile/water (95/5, v/v) and flow rate 2.0 mL min^{-1}. The sample injection volume was 10.0 μL.

2.2. Reagents

Permethrin mixture of *cis* and *trans* isomers standard was obtained from Riedel-de-Haën (Germany, contend of 94.4% *cis*/*trans* isomers), FC standard was obtained from Riedel-de-Haën (Germany, contend of 99.9%). Acetonitrile (Chromasolv, for LC) was obtained from Sigma–Aldrich. All other used chemicals were of analytical grade quality. Millipore Milli-Q RG (Millipore s.r.o., Czech Republic) ultra pure water was used for preparing the solutions. Mobile phases were degassed by helium before use. Stock standards were dissolved in acetonitrile 80% (v/v) at concentration of 6.0 mg mL^{-1} (PM) and 1.5 mg mL^{-1} (FC), all were stored at 5 °C for

1 month. The final concentrations of the sample working standard solutions and reference standards for veterinary preparations analysis were prepared by diluting the stock solution in the mobile phase.

2.3. Method and sample preparation

2.3.1. Mobile phase

The optimal mobile phase for separation FC and PM was acetonitrile/water (60:40, v/v). Flow rates were 0.6 mL min^{-1} for elution of FC and 1.2 mL min^{-1} for elution of PM. Volume of mobile phase used for one analysis was 4.8 mL. All experiments were done at ambient temperature.

2.3.2. Solutions and sample preparation

The tested preparations were ARPALIT® Neo spray containing 470 mg of PM and 120 mg of FC in 100 g of solution, ARPALIT® Neo foam containing 480 mg of PM and 120 mg of FC in 100 g of foam and ARPALIT® Neo mechanical spray containing 470 mg of PM and 120 mg of FC in 100 g of solution (all preparations Aveflor, Czech Republic). Preparation of spray samples was done by the following procedure: 1.0 g of well-shake spray was squirt into 25.00 mL calibrated flask and filled to the mark with mobile phase, mixed and dissolved by 5 min sonication. Foam samples were prepared as follows: 2.0 g of well-shaken foam was added into small beaker with 20.0 mL of mobile phase, diluted and transferred into 50.0 mL calibrated flask and filled to the mark with mobile phase, mixed and dissolved by 5 min sonication. The comparative standard solution was same for all the analysis and it was prepared by diluting stock standard solution in 25.00 mL calibrated flask and the flask was filled to the mark with mobile phase and mixed. The final concentrations of the analytes in comparative standard solution were 240.0 μg mL^{-1} of PM and 60.0 μg mL^{-1} of FC. Standards and samples were measured in triplicate and the mean peak height values were used for data acquisition.

3. Results and discussion

3.1. Method development and optimization

In this work for the first time very short monolithic column (10 mm of length) has been used in the SIC method. The optimization of mobile phase was started with acetonitrile/water (50:50, v/v) mobile phase. The mobile phases containing acetonitrile as organic part have shown better separation of peaks and peak symmetry than methanol containing mobile phases. The optimization was focused on finding an appropriate acetonitrile/water composition to achieve a sufficient symmetry of the peaks of FC and PM together with a good separation of compounds and a short retention time. Both substances had still same chromatographic properties within changing of pH so the adjustment of mobile phase's pH was not necessary. There was not necessary to separate precisely PMC and PMT forms of PM (double-peak) because they were declared in preparations as a sum. The optimal mobile phase for the separation of FC and PM was found acetonitrile/water (60:40, v/v). Flow-rate was set to 0.6 mL min^{-1} for elution of FC; first volume of 1.2 mL and flow-rate 1.2 mL min^{-1} for elution of PM (rest volume of 3.6 mL). The sample injection volume was 10.0 μL. Detector was set into 225 nm to ensure good response of FC and PM and to prevent disturbances of additives. The proposed system enabled successful separation of target analytes in the time 6.7 min (1.6 min for aspiration of mobile phase, 0.0016 min for aspiration of sample and 2.0 plus 3.0 min for elution of analytes). Total volume of mobile phase for one analysis was 4.8 mL. The sequence of particular steps of the SIC control program for ARPALIT Neo® determination (a single cycle) is described in Table 1. Peak height evaluation was performed using the FIAlab® software.

Table 1
The sequence of particular steps of the SIC control program for ARPALIT Neo® determination (a single cycle)

Action	Unit	Parameter	
Mobile phase aspiration	Syringe pump	Flow rate (μL s^{-1})	100
		Volume, aspiration (μL)	4800
Sample aspiration	Multi-position valve	Valve port	2
	Syringe pump	Flow rate (μL s^{-1})	10
		Volume (μL)	10
Elution of FC	Multi-position valve	Valve port	6
	Syringe pump	Flow rate (μL s^{-1})	10
		Volume, dispension (μL)	1200
Elution of PM	Syringe pump	Flow rate (μL s^{-1})	20
		Volume, dispension (μL)	3600

3.2. Parameters of sequential injection chromatography process

The target compounds were successfully separated using the proposed procedure. Basic chromatographic parameters were calculated from experimental data, such as retention times, peak symmetry, number of theoretical plates and peak resolution; they are given in Table 2 in comparison to HPLC results. Since content of PM in preparations is calculated as a sum of all forms, it is not necessary to separate them completely.

3.3. Validation and analytical parameters of the method

The validation showed good results for all analytical parameters (linearity, sensitivity, repeatability, recovery, selectivity, precision and accuracy). Linearity was established with a series of working solutions prepared by diluting the stock solution with mobile phase to the final concentrations. Each concentration was injected in triplicate and the mean value of peak height was used for the calibration curve. The calibration graphs involved five experimental points for FC (concentration range 7.6, 23.1, 69.1, 138.3 and 276.5 μg mL^{-1}) and it is described by the following equation: $A = (0.0029 \pm 0.0001)\,c + (0.0256 \pm 0.0211)$ (where A is the absorbance and c the analyte concentration), the correlation coefficient was 0.995; for PM six experimental points (concentration range 3.4, 11.3, 37.8, 126.0, 252.0 and 420.0 μg mL^{-1}) and they are described by following

Table 2
Characterization of SIC process and its comparison with validated HPLC method

	Fenoxycarb		*Cis*, permethrin		*Trans*, permethrin	
	SIC	HPLC	SIC	HPLC	SIC	HPLC
Retention time (min)	0.5	1.8	3.0	7.2	3.3	7.5
Peak symmetry	3.1	1.3	1.4	1.4	1.6	1.1
Number of theoretical plates	99	1009	1149	27,855	682	37,250
Peak resolution	$R_{FC/PMC}$ = 8.75	$R_{FC/PMC}$ = 36.30	$R_{PMC/PMT}$ = 0.90	$R_{PMC/PMT}$ = 2.25		

Table 3
SIC Analytical parameters and method validation results

	Fenoxycarb	Permethrine	
		Cis	*Trans*
Calibration range, ($\mu g\,mL^{-1}$)	7.6–276.5	3.4–420.0	
Correlation coefficient	0.995	0.994	
Limit of detection, 3σ ($\mu g\,mL^{-1}$)	2.00	1.00	
Limit of quantification, ($\mu g\,mL^{-1}$)	6.00	3.00	
System precision, spray diluted 10× (%)[a]	1.22	0.60	0.56
System precision, spray diluted 20× (%)[a]	1.71	1.54	1.85
System precision, spray diluted 100× (%)[a]	1.59	2.54	1.80
Repeatability of time, t_R (%)[a]	1.50	0.90	1.03
Method precision (%)[b]	2.29	2.98	
Accuracy, spike recovery (%)[c]	98.9	97.5	

[a] Relative standard deviation (R.S.D.) values were calculated for repeated standard injections ($n = 6$).
[b] R.S.D. for repeated injections of multiple sample preparations ($n = 6$).
[c] Spiked sample solutions.

equations: $A = (0.0021 \pm 0.0001)\ c - (0.0365 \pm 0.0241)$, the correlation coefficient was 0.994. The limit of detection (LOD) was calculated by comparison of the threefold variation of signal to noise ratio (3 S/N) obtained from analysis of the standards, and the limit of quantification (LOQ) was defined as the lowest measured quantity above which the analyte can be quantified at a given statistical level of (3 LOQ). The system precision of the method was determined by preparing the standards of FC and PM at three concentration levels (spray diluted 10 times, spray diluted 20 times and spray diluted 100 times) and peak heights for each compound were determined after processing each six times. The method validation results obtained under the final conditions are shown in Table 3. To validate the precision of the method a number of six different veterinary insecticide sample solutions were used, which were prepared from the same batch and analyzed consecutively. This approach provides a means of covering the precision of the entire method, from sample preparation to data handling. The precision of the method calculated as R.S.D. of six-sample determination, including sample preparation, was 2.29% for FC and 2.98% for PM. The accuracy of the method was carried out measuring of the veterinary samples fortified with known quantity of the analytes (addition of 100% amount of FC and PM standards to veterinary preparation). Spiked sample solutions and un-spiked sample solutions were compared for recovery evaluation. The method accuracy results—mean values of the recoveries were found as 98.9% for FC and 97.5% for PM. Assay values of recoveries show that the method allows direct determination of FC and PM in commercial dosage forms in the presence of other adjuvants.

3.4. Determination in veterinary products

The novel method has been applied to the determination of FC and PM in ARPALIT® Neo spray, foam and mechanical spray. The veterinary preparations were commercially available on the Czech market. The interference effect of adjuvants (D-panthenol, tween 20, hydroxyethylcellulose, cetrimonium bromide, phenyl trimethicone) was not observed under the optimized analytical conditions. The samples were prepared just by 25-fold dilution with mobile phase. The mean values of found amount were 0.14% of FC and 0.60% of PM in foam, 0.14% of FC and 0.58% of PM in spray and 0.15% of FC and 0.59% of PM in mechanical spray (declared amount of FC 0.14–0.16% and of PM 0.57–0.63% both in spray and foam). Two packages (cans) of one batch of each kind of preparations were measured in our study. Representative sequential injection chromatogram showing successful separation of active substances of ARPALIT® Neo spray is shown in Fig. 2.

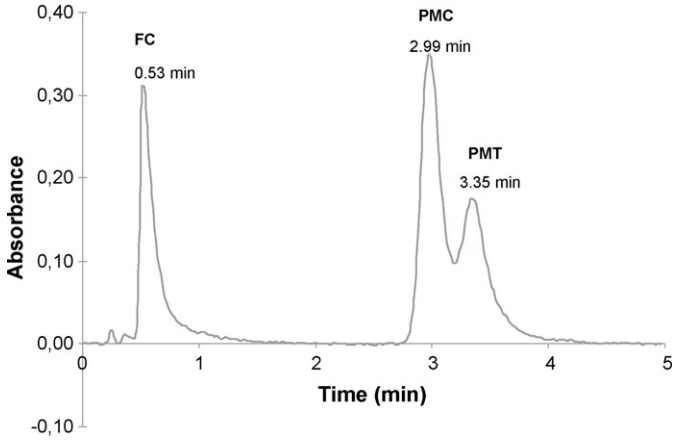

Fig. 2. SI chromatogram of the separation of active substances of ARPALIT® Neo. Mobile phase: acetonitrile/water (60:40, v/v), flow rate 0.6 mL min^{-1} for elution of FC (1.2 mL) and 1.2 mL min^{-1} for elution of PMC and PMT (*cis* and *trans* isomer) (3.6 mL); UV detection at 225 nm.

The SIC determination results were compared with validated method (HPLC)—(samples of foam: FC 0.14% and PM 0.60%; spray: FC 0.15% and PM 0.58%; mechanical spray: FC 0.15% and PM 0.59%).

4. Conclusion

Very short Chromolith™ RP-18e (10 mm × 4.6 mm i.d.) (Merck®) column was first time implemented into SIC manifold. This set-up was proved to be a convenient and efficient tool for the separation and determination of mixture of FC and PM in veterinary preparations. The assay showed good precision and accuracy and results were compared to established HPLC method. Advantage of SIC method were lower consumption of mobile phase, use of isocratic elution, shorter time of analysis, simple preparation and easy sample handling. All these features enable reduction of cost per analysis. Easy liquid manipulation not attainable by classical HPLC set-up, dimensions and portability of the SIC system provides the opportunity for possible analysis "on field".

Recent development and increasing trend of SIC practical applications resulted in commercially available SIChrom™ liquid chromatography analyzer by FIAlab® Instruments (Bellevue, WA, USA) [25]—equipped with more powerful pump (enables use of higher flow rates and longer columns) and chemical resistant Lab-On-Valve system for variable sample handling.

In summary, the SIC system provides a useful alternative to existing chromatographic methods and can be an important tool for the rapid separation and quantification of several compounds not only in analysis of pesticides in veterinary preparations.

Acknowledgements

The authors gratefully acknowledge the financial support of the Czech Science Foundation project no. 203/08/P338 and Czech Ministry of Education project no. MSM 0021620822.

References

[1] P. Chocholouš, P. Solich, D. Šatínský, Anal. Chim. Acta 600 (2007) 129.
[2] C.E. Lenehan, N.W. Barnett, S.W. Lewis, Analyst 127 (2002) 997.
[3] J. Ruzicka, G. Marshall, Anal. Chim. Acta 237 (1990) 329.
[4] T. Gübeli, G.D. Christian, J. Ruzicka, Anal. Chem. 63 (1991) 2407.
[5] R.W. Min, J. Nielsen, J. Villadsen, Anal. Chim. Acta 312 (1995) 149.
[6] X.Z. Liu, S.S. Liu, J.F. Wu, Z.L. Fang, Anal. Chim. Acta 392 (1999) 273.

[7] P. Solich, H. Sklenářová, J. Huclová, D. Šatínský, U.F. Schaefer, Anal. Chim. Acta 499 (2003) 9.
[8] D. Šatínský, P. Solich, P. Chocholouš, R. Karlíček, Anal. Chim. Acta 499 (2003) 205.
[9] H. Minakuchi, K. Nakanishi, N. Soga, N. Ishizuka, N. Tanaka, J. Chromatogr. A 762 (1997) 135.
[10] C. Zacharis, G. Theodoridis, A. Podgornik, A. Voulgaropoulos, J. Chromatogr. A 1121 (2006) 46.
[11] H.M. González-San Miguel, J.M. Alpízar-Lorenzo, V. Cerdá-Martín, Talanta 72 (2007) 296.
[12] J.F. García-Jiménez, M.C. Valencia, L.F. Capitán-Vallvey, Anal. Chim. Acta 594 (2007) 226.
[13] J.B. Claver, M.C.V. Mirón, L.F. Capitán-Vallvey, Book of abstracts XIITH International Symposium on Luminiscence Spectrometry, Lugo, Spain (2006) PO 72.
[14] J.L. Adcock, P.S. Francis, K.M. Agg, G.D. Marshall, N.W. Barnett, Anal. Chim. Acta 600 (2007) 136.
[15] M.L. Reyzer, J.S. Brodbelt, Anal. Chim. Acta 436 (2001) 11.
[16] J. Wang, Y. Xu, S. Liu, S. Jiang, C. Pan, J. Sep. Sci. 30 (2007) 3.
[17] T. Kovalczuk, M. Jech, J. Poustka, J. Hajslova, Anal. Chim. Acta 577 (2006) 8.
[18] E. Maloschik, A. Ernst, G. Hegedus, B. Darvas, A. Szekacs, Microchem. J. 85 (2007) 88.
[19] M. Natangelo, S. Tavazzi, R. Fanelli, E. Benfenati, J. Chromatogr. A 859 (1999) 193.
[20] M.M. Galera, M.D.G. Garcia, R.S. Valverde, J. Chromatogr. A 1113 (2006) 191.
[21] S. Morales-Muñoz, J.L. Luque-García, M.J. Ramos, A. Fernández-Alba, M.D. Luque de Castro, Anal. Chim. Acta 552 (2005) 50.
[22] A.W. Abu-Qare, M.B. Abou-Donia, J. Pharm. Biomed. Anal. 26 (2001) 291.
[23] E. García, A. García, C. Barbar, J. Pharm. Biomed. Anal. 24 (2001) 999.
[24] S. Oepkemeier, S. Schreiber, D. Breuer, G. Key, W. Kleiböhmer, Anal. Chim. Acta 393 (1999) 103.
[25] http://www.sichrom.com/.

Talanta 77 (2008) 710–717

Contents lists available at ScienceDirect

Talanta

journal homepage: www.elsevier.com/locate/talanta

Fabrication of an ammonia gas sensor using inkjet-printed polyaniline nanoparticles

Karl Crowley[a], Aoife Morrin[a], Aaron Hernandez[a], Eimer O'Malley[a], Philip G. Whitten[b], Gordon G. Wallace[b], Malcolm R. Smyth[a], Anthony J. Killard[a,*]

[a] School of Chemical Sciences, National Centre for Sensor Research, Dublin City University, Glasnevin, Dublin 9, Ireland
[b] ARC Centre of Excellence for Electromaterials Science, Intelligent Polymer Research Institute, University of Wollongong, Northfields Avenue, Wollongong, NSW 2522, Australia

ARTICLE INFO

Article history:
Received 14 March 2008
Received in revised form 26 June 2008
Accepted 4 July 2008
Available online 23 July 2008

Keywords:
Inkjet printing
Polyaniline nanoparticles
Gas phase ammonia analysis
Conductimetric
Interdigitated electrode array
Thermal analysis
Temperature control

ABSTRACT

This work details the fabrication and performance of a sensor for ammonia gas analysis which has been constructed via the inkjet-printed deposition of polyaniline nanoparticle films. The conducting films were assembled on interdigitated electrode arrays and characterised with respect to their layer thickness and thermal properties. The sensor was further combined with heater foils for operation at a range of temperatures. When operated in a conductimetric mode, the sensor was shown to exhibit temperature-dependent analytical performance to ammonia detection. At room temperature, the sensor responded rapidly to ammonia (t_{50} = 15 s). Sensor recovery time, response linearity and sensitivity were all significantly improved by operating the sensor at temperatures up to 80 °C. The sensor was found to have a stable logarithmic response to ammonia in the range of interest (1–100 ppm). The sensor was also insensitive to moisture in the range from 35 to 98% relative humidity. The response of the sensor to a range of common potential interferents was also studied.

1. Introduction

Ammonia is a highly toxic, polluting gas. With global production in excess of 100 million tonnes per annum, it has a wide variety of uses including the production of nitrogenous fertilizers and other nitrogenous chemicals, as well as an industrial refrigerant. Monitoring of leakage in a wide range of industrial applications is thus deeply desired. A range of devices is available for monitoring ammonia, the most established of which are electrochemical devices based on electrolytic cells. An overview of the various ammonia sensing technologies under development was detailed by Timmer et al. [1]. In brief, other ammonia sensing devices include those based on solid state sensors [2], spectroscopic techniques [3] and conducting polymers [4]. Electrolytic devices have been around for decades but generally suffer from lower detection limits and limited accuracy. A variety of solid state devices have shown promise with detection limits down to 1 ppm, though selectivity can be an issue [1]. Spectroscopic sensors range from simple, non-selective pH indicator-based sensors to complex spectrometer-based systems capable of measuring down to 1 ppb NH_3 [3]. Though powerful, these systems are generally large and costly, suited to the laboratory rather than low cost sensors. Conducting polymer-based sensors have been increasingly employed over the last few years with detection limits in the ppm region being demonstrated. However, these sensors can suffer from irreversible reactions leading to a reduction in response [1].

Polyaniline (PANI) is a highly versatile conducting polymer. Sensors composed of PANI and other conducting polymers have routinely been applied to the analysis of ammonia and other gases, such as a chip-based solution-cast PANI sensor described by Kukla et al. [5], an ammonia sensor based on a PANI-dodecylbenzenesulfonate emulsion (in chloroform) described by Wu et al. [6] and more recently, the use of a PANI-coated filter paper for a number of applications including the colorimetric detection of gaseous and aqueous ammonia [7]. PANI is an excellent material for ammonia sensing as it deprotonates the amine groups in the emeraldine salt converting it to the emeraldine base form with a corresponding drop in conductivity of several orders of magnitude. A simplified version of this reaction is given in the following equation:

$$\text{PANI}\,H^+ + NH_3 \rightleftharpoons \text{PANI} + NH_4{}^+ \quad (1)$$

The very high affinity of PANI for ammonia does have its drawbacks, particularly with regards to sensor regeneration, where long timescales of minutes or hours are required to return the sensor to

* Corresponding author. Tel.: +353 17007871; fax: +353 17007873.
E-mail address: tony.killard@dcu.ie (A.J. Killard).

0039-9140/$ – see front matter © 2008 Elsevier B.V. All rights reserved.
doi:10.1016/j.talanta.2008.07.022

its initial state. The chip-based PANI sensor described by Kukla et al. incorporated heaters that were used to run a thermal regeneration step once the electrode displayed deviation [5]. This method was used to reclaim sensor performance after exposures to lower ambient ammonia conditions. Unfortunately, even with the thermal regeneration, irreversible changes to the sensor were observed if it was exposed to high concentrations for an extended period.

A major issue for a sensor composed of PANI is the difficulty in handling or processing the polymers. Traditionally, aniline could be polymerised by either chemical or electrochemical means, both of which gave little control over the type of film formed and its morphology at both the macro- and microscales. The advent of aqueous formulations of conducting polymers and aqueous dispersions of conducting polymer nanoparticles and other nanostructured materials has opened up a new range of fabrication options [8], while also demonstrating superior functional properties for sensing and other applications [9,10].

In the past few years, inkjet printing has rapidly emerged as a means to print a wide variety of materials. Conducting polymers [11–13], metallic layers [14,15], and bio-materials [16,17] are examples of just some of the materials printed. Inkjet printing is also a means to fabricate finely patterned, thin films of conducting polymers. Previously, techniques such as spin-coating or drop-casting have been used to apply conducting polymers though these methods do not readily allow any patterning and have various levels of deposition control. A significant advantage of inkjet printing is that it is non-contact. Thus, multiple layers of varying composition can be built up without the concerns of cross-contamination or physical damage to previously printed layers. It also allows finer detailing than screen printing with feature sizes of 10 μm or less compared with the 50–100 μm possible with screen printing—which allows the fabrication of smaller, more complex devices. Wang et al. achieved even greater resolution by modifying the substrate surface energy to allow the possibility of sub-micron sized features with inkjet-printed PEDOT/PSS [18]. In addition, devices fabricated from inkjet-printed conducting polymer layers are more amenable to low cost mass production [19], compared with more conventional means of manufacture such as chemical or electrochemical polymerisation. Conducting polymers have previously been used in a variety of devices, including electrochromic displays [20], batteries and supercapacitors [21,22], fuel cells [23], antistatic layers [24] and basic electrical components have also been fabricated using these materials. Recently, an Al/PANI Schottky diode was constructed via inkjet printing and assessed for its electronic and thermoelectric properties [25]. Inkjet printing allows many of these devices to be fabricated for a fraction of the cost of equivalent silicon-based devices, allowing for much wider application in low cost/high volume applications such as RFID [19], smart packaging, disposable biomedical devices, etc.

Previously, an aqueous polyaniline–DBSA nanoparticle suspension was characterised and optimised for inkjet printing [26]. Optimal synthesis conditions resulted in polyaniline nanoparticle suspensions with an average particle diameter of ~82 nm. UV–vis analysis showed that the polyaniline was in the emeraldine salt form with a high DBS doping level. In addition, a rheological study was performed on the polyaniline nanosuspension; comparing properties such as viscosity and surface tension with commercial inkjet ink. In this paper, we describe the fabrication and application of a fully printed sensor for ammonia fabricated from an inkjet-printed film of the polyaniline–DBSA nanoparticles deposited onto screen-printed silver interdigitated electrodes. Temperature control of the sensor was provided by commercially available heater foils. The sensor was optimised for gas phase analysis and applied to the analysis of ammonia in air. Methods of enhancing recovery times and tuning the sensor response were also investigated and optimised. The effects of temperature, humidity, long term stability and effect of potential interferents were also investigated.

2. Experimental

The synthesis of the polyaniline nanoparticle suspension has been detailed previously [26,27]. In brief, 0.6 ml of freshly distilled aniline (Sigma–Aldrich), 3.4 g dodecylbenzenesulfonic acid (DBSA, TCI) and 0.36 g ammonium persulfate (APS, Sigma) were added to 40 ml deionised water and stirred for 2.5 h until a dark green viscous solution was formed. The solution was centrifuged at 5000 rpm for 30 min and then dialysed against 0.05 M sodium dodecyl sulfate (SDS) for 2 days to remove excess DBSA and APS. Electrical measurements were performed on either a CHI 1000 potentiostat (CH Instruments, Inc.) or a Palmsens (Palm Instruments BV), both controlled via a PC. Sensors were connected to the potentiostat in a two-electrode configuration (working electrode and common reference and auxiliary electrode). Current measurements were performed either using fixed potential at typically +0.1 V or by applying potential cycling (saw-tooth) waveform to the sensor between two equivalent but opposite potentials, e.g. +0.1 to −0.1 V. Headspace gas measurements were performed either in a 1.1-L or a 3-L chamber, both with sealed access points for cables. Ammonia was introduced through an additional sealed opening in both chambers. The 3-L chamber contained a fan for rapid mixing of the introduced gas and an Impulse XP Gas Detector (Zellweger Analytics) was employed within the 1.1-L chamber as a control method for ammonia analysis.

2.1. Fabrication of sensors

NanoPANI-modified interdigitated electrode arrays (nanoPANI-IDAs) were fabricated using screen printing and inkjet printing methods. The electrode patterns were designed using AutoCAD (Autodesk) and silver and carbon IDA patterns were prepared using screen printing. Screen printing was performed using a DEK model 247 and the IDA patterns were printed on 175 μm polyethylene terephthalate (PET 505, HiFi films Ltd., Dublin) substrate and cured at 150 °C for 30 min.

Inkjet printing was performed using unmodified Epson C46/C48 piezoelectric printers. Both the black and color printer cartridges were opened and the ink removed. The cartridges were rinsed thoroughly with deionised water prior to being refilled with the nanoPANI suspension. Print designs were drawn using standard Windows software (e.g. MS Word) and printing was performed through the supplied software in the standard way. The printer was first primed with standard cartridges and once good quality prints were obtained with the commercial ink, the cartridges were replaced with the nanoPANI cartridges. Priming the printer with the nanoPANI solution involved the use of cleaning cycles and ink purging features until a good quality print was achieved. These cleaning/purging cycles were controlled using the SSC Service Utility (available from http://www.ssclg.com/epsone.shtml). Following printing, the sensors were gently rinsed in deionised water before being heat cured at 75 °C for 30 min.

Sensors were also constructed by attaching polyimide-based flexible heating foils (Minco, USA) to the back of the PET substrate. Temperature was monitored through a Thermal Tab thermistor (S665PDZ40B, Minco, USA). Heater control and temperature monitoring was performed with a CT325 Temperature Controller (Minco, USA).

2.2. Electrical measurement

The electrode design chosen as suitable for gas phase analysis was the interdigitated array (IDA). IDA electrodes have been widely

used in conjunction with thin films, typically with conductimetric measurements for both characterisation and sensor applications. Zaretsky et al. presented a detailed theoretical treatment of interdigitated electrodes and developed an impedance-based continuum model that allowed the estimation of a number of parameters, including film thickness, film permittivity and conductivity [28]. Sheppard et al. utilised this model and found that cell constants calculated from an electromagnetic field model were in strong agreement with their experimental results [29]. In the case of the nanoPANI sensor, a silver IDA substrate was employed as a means of measuring the change in measured current (and hence film conductivity) as the film interacts with gaseous ammonia. Current measurements were performed using either potential step or potential cycling techniques. For unheated sensors, a small baseline drift was observed when a fixed potential (+0.1 V) was employed. Cycling the potential between two equal but opposite potentials (e.g. +0.1 and −0.1 V at 0.2 V s^{-1}) was found to minimise this drift. The result was an Ohmic plot. Processing this data involved sampling the current at a predefined potential. The sampled current data was then plotted against time, yielding a quasi-chronoamperometric plot. In heated sensors the short-term drift was not observed so a fixed potential was employed.

2.3. Thermal characterisation of nanoPANI films

Differential scanning calorimetry (DSC) was performed in a nitrogen atmosphere using a TA Instruments (USA) Q200 differential scanning calorimeter. The samples used for DSC consisted of dropcast nanoPANI dispersions (~10 mg sample size). DSC heating scans were performed at a rate of 10 °C min^{-1}, and cooling scans at a rate of 5 °C min^{-1}. Thermogravimetric analysis (TGA) was performed with a TA instruments Q500 thermogravimetric analyzer in an air atmosphere at a heating rate of 5 °C min^{-1}.

2.4. Characterisation of the effects of temperature and humidity

Heat curing and preliminary heating experiments were performed using a Mammert 400 oven. The effects of temperature and humidity were assessed by placing the electrodes in a MTCL 350 environmental chamber (Tas Ltd., UK) over a range of temperature and humidity settings, the connections made through a sealable cable port in the environmental chamber.

3. Results and discussion

3.1. Sensor fabrication

Fig. 1(a) and (b) shows the two sensors without and with the heater foil, respectively. Even with the heating foil, sensor thickness was below 1 mm. The numbers visible at the base of the electrodes (e.g. 200 × 1500 in Fig. 1(a)) refer to the digit width and digit spacing in micrometers. Varying the spacing and digit number would affect the measured current but was not found to have any effect on normalised ammonia response, i.e. the measured current response divided by the initial, baseline current (I/I_0). Fig. 1(c) shows an exploded schematic of the foil-heated sensor.

3.2. Thermal characterisation

Most chemical sensors are affected by thermal conditions, with extremes in temperature having an effect on response or lifetime. Conducting polymer-based sensors are no exception. Many thermal analyses have been performed on polyaniline compositions as differences in these materials such as dopant, synthesis method, morphology, etc., can all have an effect on the behaviour of the material and make comparisons difficult. Previously, Jurczyk et al. noted that a variety of polyaniline nanocomposites were gravimetrically stable below 200 °C, with small mass losses at lower temperatures attributable to loss of moisture [30]. Neoh et al. also observed relative stability below 200 °C for PANI–DBSA with the onset of weight loss occurring between 200 and 225 °C [31]. Chen observed a gradual decrease in mass above 100 °C for a PANI–DBSA powder, attributable to moisture loss, with an accelerated drop in mass over 250 °C which was explained as evaporation or degradation of DBSA [32].

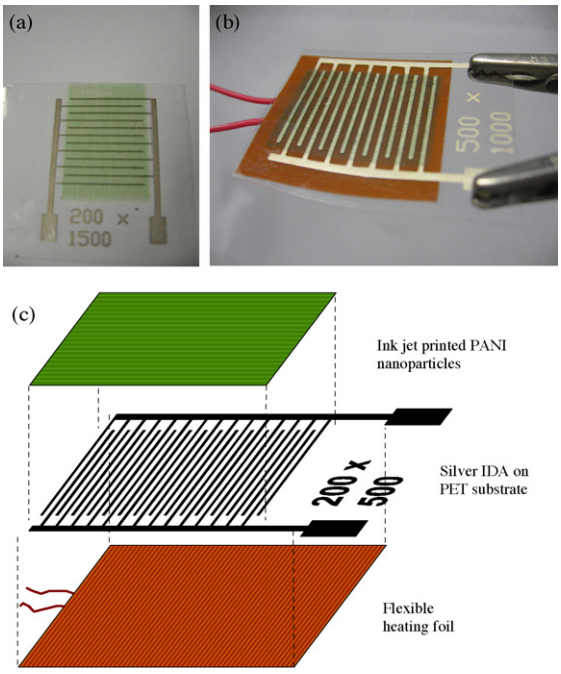

Fig. 1. Polyaniline interdigitated electrodes (nanoPANI-IDAs) shown alone (a) and with a thermofoil heater (b). Exploded schematic diagram of the nanoPANI-IDA electrode showing the different layers of the sensor (c).

As noted earlier, temperatures will affect the equilibrium of Eq. (1) in many ways. Therefore, to determine the effect of heat on the nanoPANI sensors, TGA and DSC were performed on cured (75 °C for 30 min) and uncured samples of the nanoPANI particle suspension. From the TGA plot in Fig. 2(a) it can be seen that the cured sample displays a gradual weight loss between 50 and 150 °C, over which the polymer loses approximately 8% of its initial mass. This initial mass loss is most likely due to the loss of residual moisture in the film and is similar that observed by Chen [32] and Tsotcheva et al. [33] for PANI–DBSA powder. At 150 °C the rate of loss could be seen to accelerate and then remain essentially constant over the temperature range of 150– 500 °C as the sample weight dropped to approximately 30%. In contrast, the uncured sample displays a rapid mass drop of approximately 25% as the temperature is increased to 100 °C, indicating moisture removed from the film. At temperatures above 100 °C, the uncured sample follows the same trend as the cured sample. This is clearer in the inset of Fig. 2(a) where the rate of % mass change per unit time is plotted against temperature where both samples display similar variations at temperatures greater than 100 °C. At the end of the experiment, a white residue approximately 10% of the original mass remained. In addition, the rate of weight loss was constant which implies weight loss at these temperatures was due to drying, as a change in slope and hence a change in the first differential is expected if the mechanism changes. The accelerated weight drop above 150 °C occurred at noticeably lower temperatures than observed in other studies, and

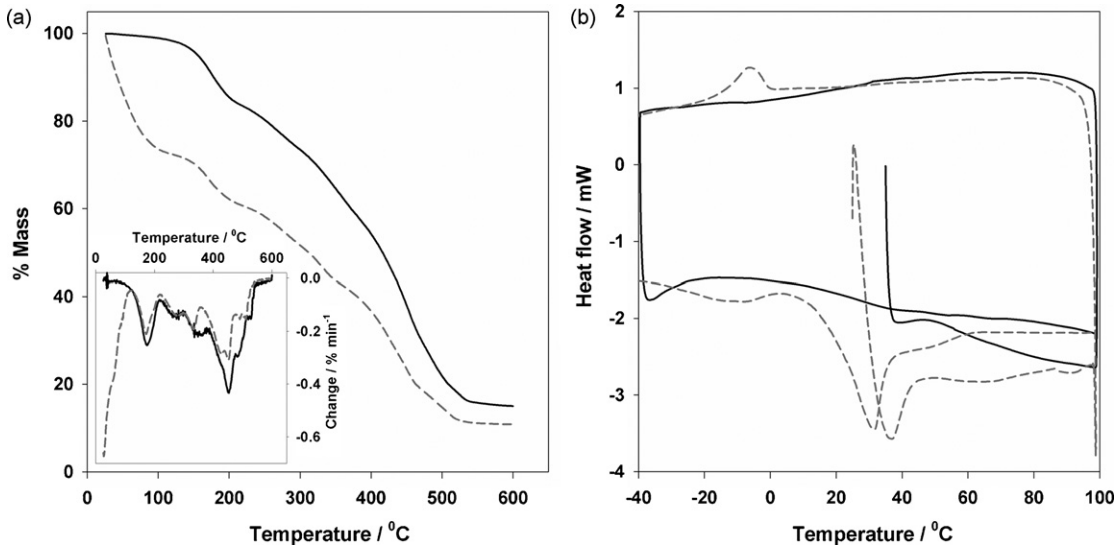

Fig. 2. Thermogravimetric analysis (a) and differential scanning calorimetry (b) of nanoPANI. TGA: sample temperature increased at a rate of 5 °C min^{-1}, inset shows rate of change of % mass against temperature. DSC: sample temperature increased at 10 °C min^{-1} and decreased at 5 °C min^{-1}. Endothermic is shown as negative heat flow. Cured sample (solid line) and uncured (dotted line).

is due to degradation of PANI–DBSA. The DSC data in Fig. 2(b) for the cured sample shows no major features over the range investigated (−40 to 100 °C) whereas the uncured sample shows distinctive peaks: at −10 °C (exothermic) and 38 °C (endothermic), shifting to 30 °C on subsequent scans. These peaks are due to crystallisation and melting of hydrated DBSA complexes [33]. Therefore, it is apparent that once a PANI film is cured, it displays no observable structural changes over the temperature range studied while uncured films show changes associated with the water present.

3.3. Effect of operating temperature on sensor behaviour

The impact of elevated temperature on the sensor performance was investigated with the assumption that an increase in temperature would have an impact on the reaction kinetics on the interaction of PANI with ammonia due to changes in the association and dissociation rate constants of the binding interaction as well as the partition coefficient of the ammonia between the solid and gaseous phases. To this end and for its potential application across a range of environmental conditions, it was vital to understand the effects of heat on the behaviour of the sensor; specifically the effect on sensor conductivity, ammonia response and lifetime. Numerous models have been proposed to explain conduction mechanisms within polyaniline and the variations in conductivity observed at different temperatures. Kulkarni et al. observed only very slight increases in conductivity for a variety of different inorganic acids over a 25–125 °C range (perchloric acid being a particular exception, showing a drop over this range) [34]. Yakuphanoglu and Şenkal found three different conductive regions for polyaniline synthesised in ionic liquid [25].

The effect of temperature on the sensor background current is given in Fig. 3. In Fig. 3(a), a nanoPANI-IDA sensor was progressively heated from room temperature to 160 °C. Initially, only a slight increase in current was observed, though at temperatures above 60 °C, this increase was much more pronounced. At temperatures between 120 and 140 °C, the rate of increase began to slow

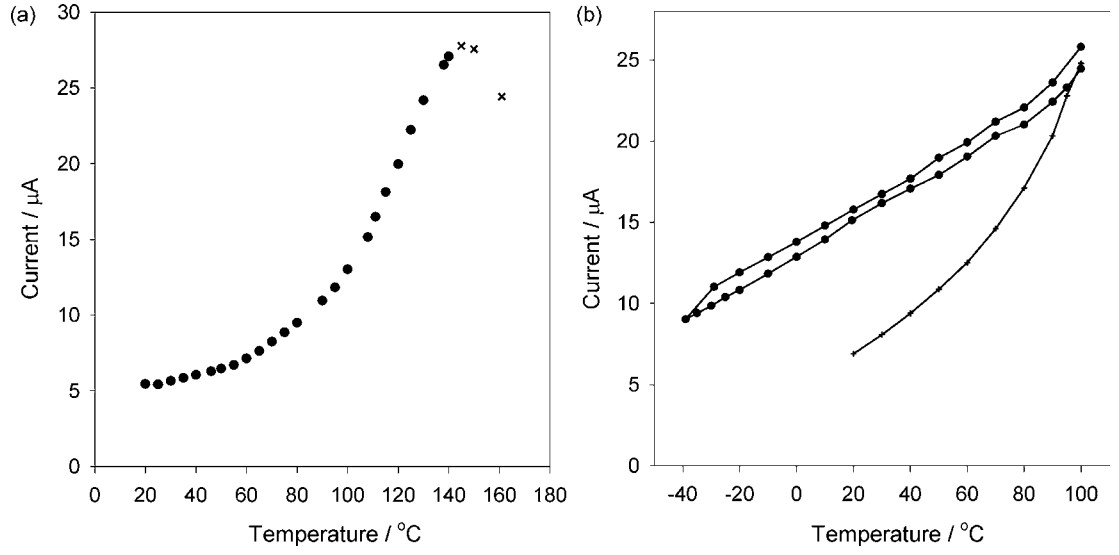

Fig. 3. Temperature effects on nanoPANI-IDA sensors under ambient atmospheric conditions. (a) Effect on background current of increasing sensor temperature from 20 to 160 °C. (b) Temperature cycling between −40 and 100 °C. Electrodes were cycled from +1 to −1 V at 2 V s^{-1}, current sampled at +1 V. Rapid degradation indicated by ×.

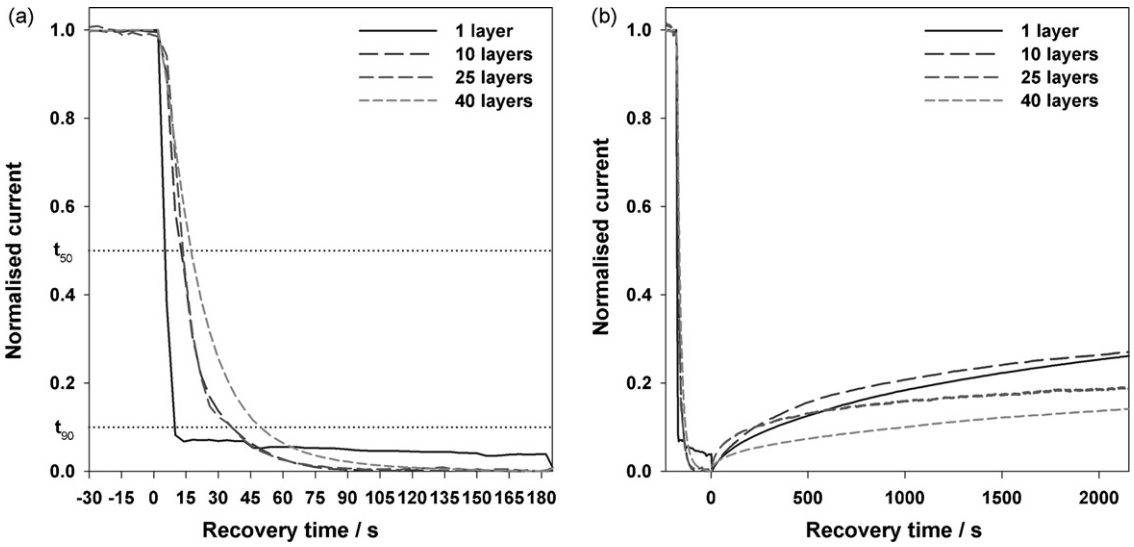

Fig. 4. Response (a) and recovery (b) of the nanoPANI-IDA on exposure to ammonia vapour at 60 ppm. Electrodes were cycled from +0.1 to −0.1 V at 0.2 V s^{-1}, current sampled at +0.1 V. 1 layer (solid), 10 layers (dashed), 25 layers (medium dashed) and 40 layers (short dashed).

before a rapid, irreversible degradation was observed above 140 °C at which point a permanent drop in measured current occurred. This rapid degradation correlates with the onset of thermal degradation implied by the accelerated rate of weight loss above these temperatures in the TGA data in Fig. 2(a).

Fig. 3(b) shows the effect of cycling the temperature between −40 and 100 °C on the background current. In the first cycle, a similar curve to that in Fig. 3(a) was obtained. However, in the subsequent two scans (corresponding to a decrease and increase in temperature, respectively) an apparently linear relationship formed over the full range. This difference in conductivity behaviour observed between the first and subsequent temperature cycles matches the heat flow changes observed for the DSC data in which also stabilised following the first cycle. The reason for this process is not clear but may relate to the removal of moisture from the film in the initial cycle as it has been found that, when left under ambient conditions, the initial thermal profile is re-established. This demonstrates that the linearity of the conductivity change of cured films between −40 and 100 °C correlates with the lack of features observed in the DSC data for the cured film in Fig. 2(b).

3.4. Effect of print thickness on ammonia response at room temperature

An important consideration in the fabrication of the sensor was the effect that the number of nanoPANI layers would have on the sensor behaviour. Thicker films would presumably result in better conductance and therefore greater measured currents. However, this may impact negatively on the response time of the sensor. In terms of production, thinner films mean less materials and faster manufacture. However, care must be taken to ensure viable and reproducible films are obtained. To this end, the relationship between nanoPANI layer thickness and electrode response to ammonia was investigated. The thickness of nanoPANI layers has been found to be approximately 170 nm per layer (for 10 layers and less) [35]. To assess the effect of increasing layer thickness on current under atmospheric conditions, a range of nanoPANI films were inkjet-printed onto the IDAs using different numbers of prints and therefore different layer thicknesses. After each print, the fresh nanoPANI layer was allowed to dry after which the current response (μA) was measured through each electrode. From 1 to 10 prints a linear response ($y = 60.4x - 67.2$) was observed as the layers were built up. Over 10 prints, the measured current began to plateau, levelling off completely over 20 prints which appeared to indicate that the nanoPANI film was moving from conductance that was limited by thickness to bulk conductance behaviour.

Film thickness may be expected to have a significant effect on the analytical response to ammonia. Response and recovery times of sensors are vitally important parameters. The Instrument Association of America (ISA) specifies that ammonia detectors should reach a minimum of 50% of response within 90 s (i.e. $t_{50} < 90$ s) on exposure to a fixed concentration of ammonia gas [36]. Likewise for recovery, a t_{50} of 90 s is specified when the detector is exposed to clean air. For the purposes of testing the sensors, t_{50} was taken as the point at which the sensor reached 50% of its final steady state value. A range of sensors of varying numbers of prints were exposed to a quantity of ammonia to ascertain the effect of film thickness.

Fig. 4 shows the response (a) and recovery (b) of the nanoPANI sensors on exposure to ammonia gas (60 ppm) in which the measured current has been normalised with respect to the initial and final readings and where time zero is taken as the moment of exposure to the ammonia vapour. From Fig. 4(a) it can be observed that all sensors displayed a rapid response to the ammonia. However, the single layer print displayed the fastest response with a t_{50} below 15 s. The thicker films (10, 25 and 40 layers) took marginally longer but still yielded t_{50} values in the region between 15 and 20 s—well below the 90 s specified in the ISA standard [36].

Fig. 4(b) shows the recovery of the sensors in air once the ammonia had been removed (time zero). In contrast to the rapid response times, the recovery was very slow in all cases with little difference observed due to film thickness. The rapid response of the electrodes coupled with slow recovery implied that under ambient conditions, the equilibrium of Eq. (1) was heavily shifted to the right, demonstrating the high affinity of nanoPANI (emeraldine salt) to ammonia. As no major variation in response time was found for the different thicknesses, in addition to the fact that larger currents were obtained for thicker films, further sensors were fabricated using 10 inkjet-printed layers, corresponding to approximately 1.7 μm layer thickness.

3.5. Quantitative analysis of ammonia at room temperature

Initial calibration testing involved ascertaining the response of the sensors to ammonia under ambient conditions. Two replicate

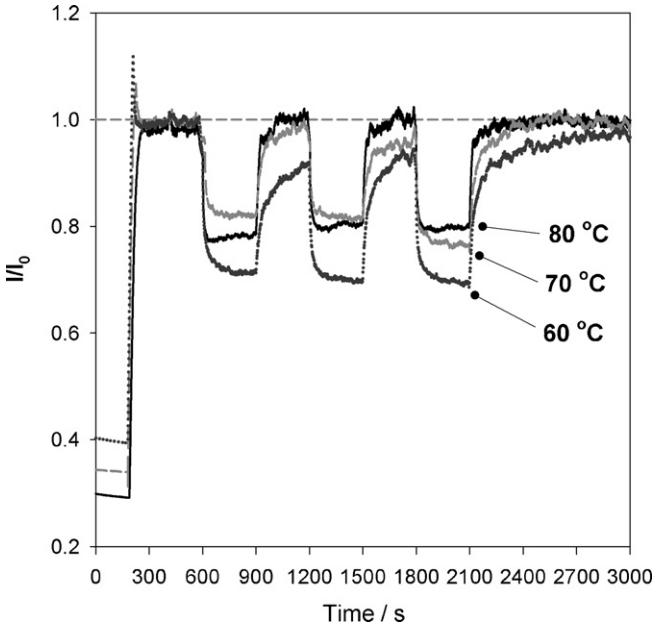

Fig. 5. Effect of heat on sensor response and recovery to the repeated application and removal of 50 ppm ammonia at 60, 70, 80 °C. +0.1 V potential applied to sensor. Currents normalised with respect to initial current (clean atmosphere).

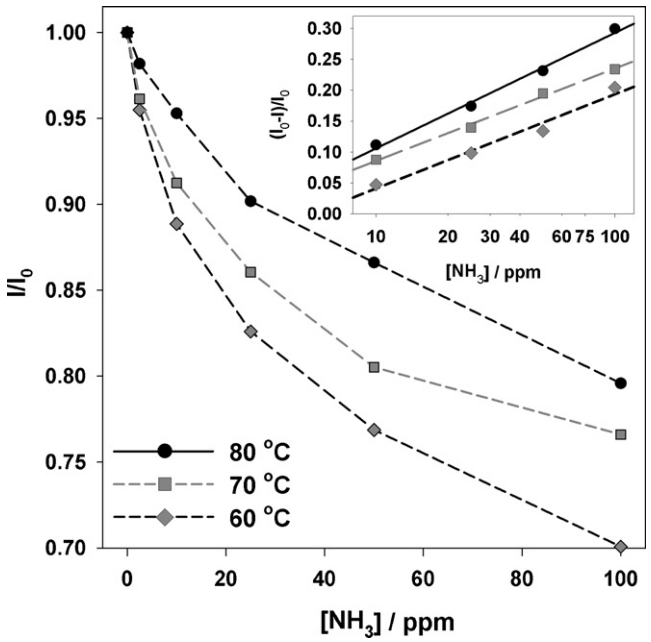

Fig. 6. Effect of operating temperature on analytical response to ammonia (I/I_0 vs. [NH_3]). Inset shows $(I_0 - I)/I_0$ vs. log[NH_3] at 60 °C, 70 °C and 80 °C. +0.1 V potential applied to sensor.

calibrations were performed on the same electrode, 35 days apart. For a sensor at room temperature, a drop in measured current by about a factor of five was observed when the sensor was exposed to ammonia at sub-10 ppm concentrations. This sharp initial drop implies that the sensor can potentially monitor ammonia concentrations well into the sub ppm region, although this region is generally outside that required for environmental health and safety applications, which was the subject of this study. Plotting normalised current, $(I - I_0)/I_0$, against the log of concentration yielded a linear fit of $y = 0.129x + 0.631$ on the first day and $y = 0.127x + 0.628$, 35 days later displaying good stability over the 5-week period tested.

In Fig. 4(b) the very slow recovery of the sensors after ammonia exposure was noted. To test the effect of temperature on the analytical response, sensors with heater foils were used (see Fig. 1(b) and (c)). These heater-sensors allowed a rapid appraisal of temperature effects on the sensor behaviour. The thin build of the sensors also allowed rapid temperature equilibration and reduced power consumption, which are also important concerns for sensors. As the application of heat shifts the equilibrium of Eq. (1) to the left, it is expected that sensitivity to ammonia will also decrease. Earlier, it was noted that the sharp initial drop in measured current between 0 and 10 ppm (440 nM L^{-1}) implied that the sensors possessed higher sensitivity than that required for environmental analytical applications (1–100 ppm, 44 nM L^{-1} to 4.4 μM L^{-1}). Therefore there was scope to trade off sensitivity for improved sensor recovery times by employing operation at elevated temperatures.

3.6. Analytical characterisation at elevated temperatures

Preliminary studies had shown that the most promising temperature region for sensor recovery was between 60 and 80 °C as temperatures below this did not result in noticeably better recovery than that obtained at room temperature conditions. Fig. 5 shows the operation of the sensor at temperatures of 60, 70 and 80 °C. The heater foil was powered on after 150 s and stabilised at its desired temperature within 60 s. An increase in the signal noise was observed once the heater was activated. This was due to the sensor temperature drifting above and below the desired temperature due to the controller being a simple on/off device and could be easily eliminated with improved control electronics. At 600 s, 50 ppm ammonia was introduced into the chamber and then vented 300 s later, this procedure being repeated twice more. As sensor temperature was increased, the recovery time was seen to decrease noticeably. At 60 °C, the recovery was still significant, with the sensor showing partial recovery after 5 min and only approaching the baseline after 15 min, following the third ammonia injection. The sensor at 70 °C displayed a noticeably faster recovery reaching the baseline at 5 min, while the sensor heated to 80 °C displayed the fastest recovery, with full recovery in approximately 2.5 min.

Fig. 6 compares the responses obtained for ammonia for heated sensors at a range of temperatures. The main plot shows the current drops measured at each temperature on a normalised scale to allow comparison, which also takes into account the increase in background current due to the elevation in temperature. Compared with the response of the unheated sensor, the sensors heated to 60, 70 and 80 °C show a much decreased initial drop due to the reduction in the signal-to-background ratio. The inset shows the same data (for 60, 70 and 80 °C) with a linear positive slope ($(I_0 - I)/I_0$ vs. log[NH_3]), where the initial value (no NH_3 present) was equal to zero.

Once again, the greater drop at lower temperatures for similar concentrations of ammonia implies that ammonia concentrations of 1 ppm should be easily detectable. Kemp et al. demonstrated that this temperature-dependent increase in response to ammonia extends well below 0 °C for polypyrrole [37]. Therefore, varying the temperature of the sensor may be a means of tuning the response to the analytical region of interest. In this case, the desired range was 1–100 ppm, and log plots could be obtained by heating the sensor element to 70 °C. Heating the sensors had the twin benefits of considerably improving the regeneration time while yielding an improved response in the region of interest. In terms of stability, heating the sensors was found to cause a gradual reduction in the sensor response over time. Three weeks of continuous heating at 70 °C resulted in a steady drop to approximately 85% of the initial

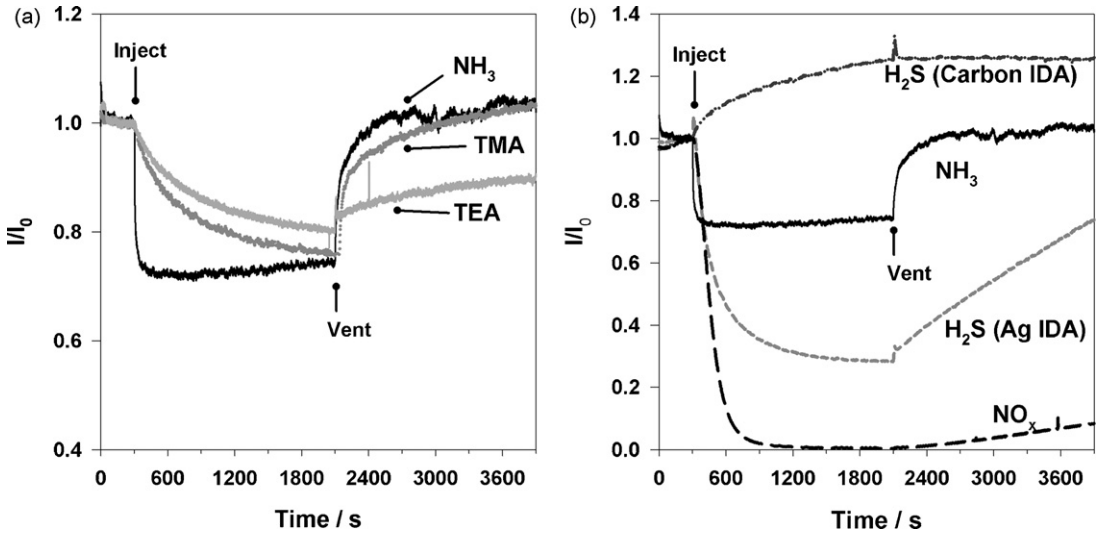

Fig. 7. Response and recovery of nanoPANI sensors (at 70 °C) to 100 ppm of different species. (a) Trimethylamine (TMA) and triethylamine (TEA). (b) Hydrogen sulfide, nanoPANI-silver IDA, hydrogen sulfide, nanoPANI carbon IDA and NO_x. In both graphs, the response to 100 ppm ammonia is given. +0.1 V potential applied to sensor.

background current. Reducing the continuously applied temperature to 50 °C resulted in stable baselines over a 2-month period (data not shown).

3.7. Effect of humidity and interferents

To ascertain the effect of humidity on the sensor response, nanoPANI-IDAs were enclosed within an environmental chamber and subjected to changes in atmospheric conditions. The effect of water vapour on the ammonia response of a sensor is difficult to determine precisely as the moisture will react with ammonia to produce ammonium hydroxide. However, the effect of humidity on the sensor background can be readily established. A number of polyaniline sensors have been found to display small but observable effects due to water vapour [38,39]. The nanoPANI sensor showed only a slight change in background response from 35 to 98% relative humidity with a mean value of 12.06 ± 0.42 μA over the range tested.

To assess the effect of potential interferents, the nanoPANI sensors were exposed to a variety of gaseous species. For the nanoPANI sensors heated to 70 °C, a wide variety of volatile organics (such as acetone, methanol, dichloromethane, etc.) were tested at 100, 1000 ppm and above, with no measurable response being obtained for any of these species at these concentrations. As the mechanism for detection in polyaniline sensors is generally based on the protonation/deprotonation of the polymer, these sensors can be prone to interference from other acidic or basic species. Carbon dioxide, carbon monoxide and acetic acid vapour were found to have little effect on the nanoPANI sensor at concentrations of 100 and 1000 ppm. However, a number of gaseous species were found to interfere with the sensor. Fig. 7 shows the nanoPANI sensor response to a variety of acidic and basic gaseous species and selectivity data of the sensor to these species, relative to ammonia, is provided in Table 1.

Fig. 7(a) compares the response of two volatile amines with that of ammonia at 100 ppm concentrations. Aliquots of these were injected at 300 s and the sensors allowed stabilise over 30 min, after which the chamber was vented with air to assess sensor recovery. In comparison with the fast ammonia response, the two volatile amines were seen to take considerably longer to reach steady state and were still not fully stable after 30 min. This could be due to the fact that the larger molecules require more time to penetrate the nanoPANI film. From Table 1 it can be seen that the sensors displayed a similar selectivity for ammonia and trimethylamine, with triethylamine response about 70% of this after 30 min exposure. Relatively rapid recovery can be observed for ammonia and trimethylamine, though triethylamine only displayed a very weak recovery over this time. Fig. 7(b) shows the results obtained for 100 ppm hydrogen sulfide and NO_x. When exposed to hydrogen sulfide, the nanoPANI sensors (on silver IDAs) displayed an unexpected drop in measured current; approximately three times that observed for ammonia. When the same test was performed for nanoPANI sensors on carbon IDAs, the measured current shows a steady increase of approximately 25%, equivalent but opposite to the ammonia response, implying that the nanoPANI is being further protonated. In a study on hydrogen sulfide sensors based on modified polyanilne, Virji et al. noted a weak response was obtained for the unmodified polyaniline in the presence of hydrogen sulfide, though this was for a 10-ppm exposure [40]. The hydrogen sulfide response observed for the nanoPANI-silver IDA electrode is clearly due the reaction between hydrogen sulfide and the silver electrode. It should be noted that use of carbon or silver IDA electrodes had little effect on the normalised response obtained for ammonia, though carbon IDA based sensors displayed an intrinsic conductivity of about two and a half orders of magnitude below nanoPANI-silver IDA sensors. The injection of 100 ppm NO_x had a very pronounced effect on measured current, with a drop of approximately 3.5 orders of magnitude. Once the system was purged with air, a very slow recovery was observed. This was found to level off at approximately 33% the initial measured current over the following 12 h. Identical results were obtained whether silver or carbon interdigitated electrodes substrates were employed and point to an effect of the gas on the nanoPANI. This effect was consistent with the effect observed for nitrogen dioxide on the emeraldine

Table 1
Response and selectivity data of the nanoPANI sensors to a variety of gaseous species (100 ppm)

Species	I/I_0	$(I_0 - I)/I_0$	Selectivity
NH_3	0.76	0.24	1
H_2S (carbon IDA)	1.25	−0.25	−1.04
H_2S (silver IDA)	0.28	0.72	2.96
NO_x	3.84E−03	1.00	4.13
Trimethylamine	0.75	0.25	1.02
Triethylamine	0.83	0.17	0.72

salt form of PANI, suggesting that the NO_2 component of the NO_x mixture is affecting this change. Elizalde-Torres et al. found that the emeraldine salt form was oxidised first to emeraldine base and then to pernigraniline (the non-conductive, fully oxidised form of PANI) by NO_2 [41]. They also noted that the desorption of NO_2 from PANI was only slowly reversible in an ambient, humid atmosphere. Current and future work involves improving the sensor selectivity to discriminate against these interfering species, possibly using selective membranes or modifications to the nanoPANI layer.

4. Conclusion

The development and optimisation of a sensor composed of an inkjet-printed polyaniline nanoparticles was demonstrated. An aqueous dispersion of the nanoPANI was deposited over a silver interdigitated array using a piezoelectric inkjet printing technique. The nanoPANI films were found to have stable thermal properties which made them amenable to operation at elevated temperatures.

The nanoPANI sensors were found to be highly responsive to gaseous ammonia with calibration plots obtained within the analytically important 1–100 ppm region. Heating the sensors was found to have the double benefit of improving recovery times and allow control of the analytical profile while the use of heater foils was established as a low cost and readily implementable means to control sensor temperature. Though the sensors displayed no interference from changes in humidity or from a range of volatile organic compounds, some cross-sensitivity to other acidic and basic species was observed.

Acknowledgement

The authors would like to thank Enterprise Ireland for funding under the Proof of Concept fund PC/06/113.

References

[1] B. Timmer, W. Olthuis, A. van den Berg, Sens. Actuators B: Chem. 107 (2005) 666.
[2] A. Dubbe, Sens. Actuators B: Chem. 88 (2003) 138.
[3] G.H. Mount, B. Rumburg, J. Havig, B. Lamb, H. Westberg, D. Yonge, K. Johnson, R. Kincaid, Atmos. Environ. 36 (2002) 1799.
[4] D. Nicolas-Debarnot, F. Poncin-Epaillard, Anal. Chim. Acta 475 (2003) 1.
[5] A.L. Kukla, Y.M. Shirshov, S.A. Piletsky, Sens. Actuators B: Chem. B37 (1996) 135.
[6] S.Z. Wu, F. Zeng, F.X. Li, Y.L. Zhu, Eur. Polym. J. 36 (2000) 679.
[7] D. Dutta, T.K. Sarma, D. Chowdhury, A. Chattopadhyay, J. Colloid Interface Sci. 283 (2005/3/1) 153.
[8] A. Morrin, F. Wilbeer, O. Ngamna, S.E. Moulton, A.J. Killard, G.G. Wallace, M.R. Smyth, Electrochem. Commun. 7 (2005) 317.
[9] H.D. Tran, R.B. Kaner, Chem. Commun. (2006) 3915.
[10] F. Masdarolomoor, P.C. Innis, S. Ashraf, R.B. Kaner, G.G. Wallace, Macromol. Rapid Commun. 27 (2006) 1995.
[11] J. Bharathan, Y. Yang, Appl. Phys. Lett. 72 (1998) 2660.
[12] B. Ballarin, A. Fraleoni-Morgera, D. Frascaro, S. Marazzita, C. Piana, L. Setti, Synth. Met. 146 (2004) 201.
[13] Y. Yoshioka, G.E. Jabbour, Synth. Met. 156 (2006) 779.
[14] H.H. Lee, K.S. Chou, K.C. Huang, Nanotechnology 16 (2005) 2436.
[15] K.J. Lee, B.H. Jun, T.H. Kim, J. Joung, Nanotechnology 17 (2006) 2424.
[16] T. Okamoto, T. Suzuki, N. Yamamoto, Nat. Biotechnol. 18 (2000) 438.
[17] T. Xu, J. Jin, C. Gregory, J.J. Hickman, T. Boland, Biomaterials 26 (2005) 93.
[18] J.Z. Wang, J. Gu, F. Zenhausem, H. Sirringhaus, Appl. Phys. Lett. 88 (2006) 133502.
[19] V. Subramanian, P.C. Chang, J.B. Lee, S.E. Molesa, S.K. Volkman, IEEE Trans. Compon. Pack. Technol. 28 (2005) 742.
[20] R.J. Mortimer, A.L. Dyer, J.R. Reynolds, Displays 27 (2006) 2.
[21] G. Wegner, Polym. Adv. Technol. 17 (2006) 705.
[22] K.S. Ryu, S.K. Jeong, J. Joo, K.M. Kim, J. Phys. Chem. B 111 (2007) 731.
[23] V. Neburchilov, J. Martin, H.J. Wang, J.J. Zhang, J. Power Sources 169 (2007) 221.
[24] G. Defieuw, R. Samijn, I. Hoogmartens, D. Vanderzande, J. Gelan, Synth. Met. 57 (1993) 3702.
[25] F. Yakuphanoglu, B.F. Senkal, J. Phys. Chem. C 111 (2007) 1840.
[26] O. Ngamna, A. Morrin, A.J. Killard, S.E. Moulton, M.R. Smyth, G.G. Wallace, Langmuir 23 (2007) 8569.
[27] S.E. Moulton, P.C. Innis, L.A.P. Kane-Maguire, O. Ngamna, G.G. Wallace, Curr. Appl. Phys. 4 (2004) 402.
[28] M.C. Zaretsky, L. Mouayad, J.R. Melcher, IEEE Trans. Electr. Insul. 23 (1988) 897.
[29] N.F. Sheppard, R.C. Tucker, C. Wu, Anal. Chem. 65 (1993) 1199.
[30] M.U. Jurczyk, A. Kumar, S. Srinivasan, E. Stefanakos, Int. J. Hydrogen Energy 32 (2007) 1010.
[31] K.G. Neoh, M.Y. Pun, E.T. Kang, K.L. Tan, Synth. Met. 73 (1995) 209.
[32] C.H. Chen, J. Polym. Res.-Taiwan 9 (2002) 195.
[33] D. Tsotcheva, T. Tsanov, L. Terlemezyan, S. Vassilev, J. Therm. Anal. Calorim. 63 (2001) 133–141.
[34] V.G. Kulkarni, L.D. Campbell, W.R. Mathew, Synth. Met. 30 (1989) 321.
[35] A. Morrin, O. Ngamna, E. O'Malley, N. Kent, S.E. Moulton, G.G. Wallace, M.R. Smyth, A.J. Killard, Electrochim. Acta 53 (2008) 5092.
[36] ISA-92.03.01-1998—Performance Requirements for Ammonia Detection Instruments (25–500 ppm), Instrument Society of America, 1998, p. 22.
[37] N.T. Kemp, A.B. Kaiser, H.J. Trodahl, B. Chapman, R.G. Buckley, A.C. Partridge, P.J.S. Foot, J. Polym. Sci. Part B: Polym. Phys. 44 (2006) 1331.
[38] G.E. Collins, L.J. Buckley, Synth. Met. 78 (1996) 93.
[39] L. Grigore, M.C. Petty, J. Mater. Sci.: Mater. Electron. 14 (2003) 389.
[40] S. Virji, J.D. Fowler, C.O. Baker, J. Huang, R.B. Kaner, B.H. Weiller, Small 6 (2005) 624.
[41] J. Elizalde-Torres, H. Hu, A. Garcia-Valenzuela, Sens. Actuators B 98 (2004) 218.

Talanta 77 (2008) 652–658

Contents lists available at ScienceDirect

Talanta

journal homepage: www.elsevier.com/locate/talanta

Adsorption versus covalent, statistically oriented and covalent, site-specific IgG immobilization on poly(vinyl alcohol)-based surfaces

Katarzyna Derwinska, Ursula Sauer, Claudia Preininger*

Austrian Research Centers GmbH – ARC, Department of Bioresources, 2444 Seibersdorf, Austria

ARTICLE INFO

Article history:
Received 16 January 2008
Received in revised form 19 June 2008
Accepted 3 July 2008
Available online 16 July 2008

Keywords:
Poly(vinyl alcohol)
IgG
Adsorption
Crosslinkers
Aminophenylboronic acid

ABSTRACT

Plain poly(vinyl alcohol) (PVA) surfaces, PVA surfaces tailored with additives (chitosan, chitosan-oligo) and PVA surfaces crosslinked with homo- or hetero-bifunctional amino-linkers (ethylenediamine, hexamethylenediamine, adipic acid dihydrazide, 3-aminophenylboronic acid) were evaluated for their ability to immobilize IgG. Immobilization strategies tested were adsorption as well as covalent, statistically oriented and covalent, site-specific binding of antibodies. The PVA surfaces were optimized with respect to the type of PVA, to PVA concentration and to glass substrate type. The resulting hydrogel surface of choice consists of 4% PVA coated onto adhesive glass. Comparison of modified and unmodified PVA surfaces revealed six surfaces which showed significantly higher loading capacity than plain PVA:PVA surfaces tailored with 2% chitosan resulted in twice greater fluorescence, whereas PVA surfaces oxidized using HIO_4 with and without further crosslinking using adipic acid dihydrazide revealed 2.6–2.8 times greater fluorescence. Yet the greatest fluorescence compared with plain PVA (up to 3.5 times as much) was achieved on PVA surfaces coupled with 3-aminophenylboronic acid activated by means of either 1% or 2.5% glutaraldehyde. Meanwhile, fluorescence signals were similar for statistically oriented IgG and IgG bound site-specifically using IgG activated with sodium meta-periodate.

1. Introduction

The choice of proper surface chemistry in protein chips is critical due to the structural complexity of proteins. The biochip surface therefore holds a central role in the protein chip development as the immobilization strategy applied influences sensitivity and specificity of the chip experiment. Strength of the binding, orientation and accessibility of the probes, density of bound probe molecules and the proportion of non-specific adsorption depend on the reaction chemistry.

Various chip surfaces have been reported [1,2] ranging from silane and gold monolayers to functional polymers and hydrogels. The latter are considered especially suitable for protein immobilization, since they provide a liquid microenviroment that can keep the proteins hydrated and stabilize the structure, which is responsible for the protein's activity [3]. The hydrogels that have been reportedly used as immobilization matrices on protein chips are: agarose [4], poly(acrylamide) [3,5,6], polyurethane [7], dextran [8] and polyethyleneglycol (PEG). For example, Dominguez et al. [9] fabricated antibody-entrapped hydrogel chambers by arraying solutions of both tetra- or octa-amine functionalized peptide-based branch macromolecules and IgG on aldehyde glass slides. In contrast to many covalent attachment methods this approach is single-step, facile and rapid, keeps the antibody hydrated and in its original conformation (no modification by crosslinkers or by surface reactive groups as a result of immobilization). A similar approach was reported by Rubina et al. [5], who used so-called hydrogel drop microchips of polyacrylamide for a quantitative immunoassay of plant and bacterial toxins. Derwinska et al. [7] developed polyurethane surfaces that compared with commercial hydrogel slides showed significantly improved loading capacity, especially at low IgG concentrations. This agrees well with Zubtsov et al. [10], who compared the chip performance of hydrogel and non-hydrogel surfaces in direct and sandwich immunoassays concluding that at the same concentration of spotted antibody hydrogel surfaces provide stronger fluorescence signals than non-hydrogel slides. This effect was attributed to the relatively large molecular size of the antibodies and the improved capacity of gel surfaces.

Widely used hydrogels in biochips are based on acrylamide and dextran, whereas PVA, by contrast, is used mainly as an encapsulation material for enzymes and cells, in drug delivery, or as blends in (bio)sensors. Photosensitive poly(vinyl alcohol-styrylpyridinium) (PVA-SbQ), for example, is cited as having been used for surface-patterning of a bio-MEMS-based cell chip using recombinant *Escherichia coli* [11], and according to [12] PVA was part of a

* Corresponding author. Tel.: +43 50550 3527; fax: +43 50550 3666.
E-mail address: claudia.preininger@arcs.ac.at (C. Preininger).

0039-9140/$ – see front matter © 2008 Elsevier B.V. All rights reserved.
doi:10.1016/j.talanta.2008.07.016

polymer blend in a glucose biosensor. In order to produce mechanically stable PVA layers, often polymer blends or co-polymers are developed and employed that combine the mechanical strength of the additive polymer blend or monomer with the biocompatibility and hydrophilicity of PVA, for example mechanically stable PVA ormosils using organically modified silicates (ormosils) for BOD biosensing in seawater [13] or polysiloxane–PVA discs fabricated through sol–gel process for binding of anti-S100 protein antibody [14]. In addition, improved hydrogel strength has also been obtained by crosslinking PVA with glutaraldehyde [14–16] or chitosan. For example, Yu et al. [15] reported on PVA functionalized poly(dimethylsiloxane) surfaces that were activated for antibody binding using glutaraldehyde, whereas Kumar et al. [17] prepared PVA membranes of different swelling index for entrapment of glucoseoxidase combining PVAs of low and high degree of polymerization together with a photolinker. Furthermore, boronic

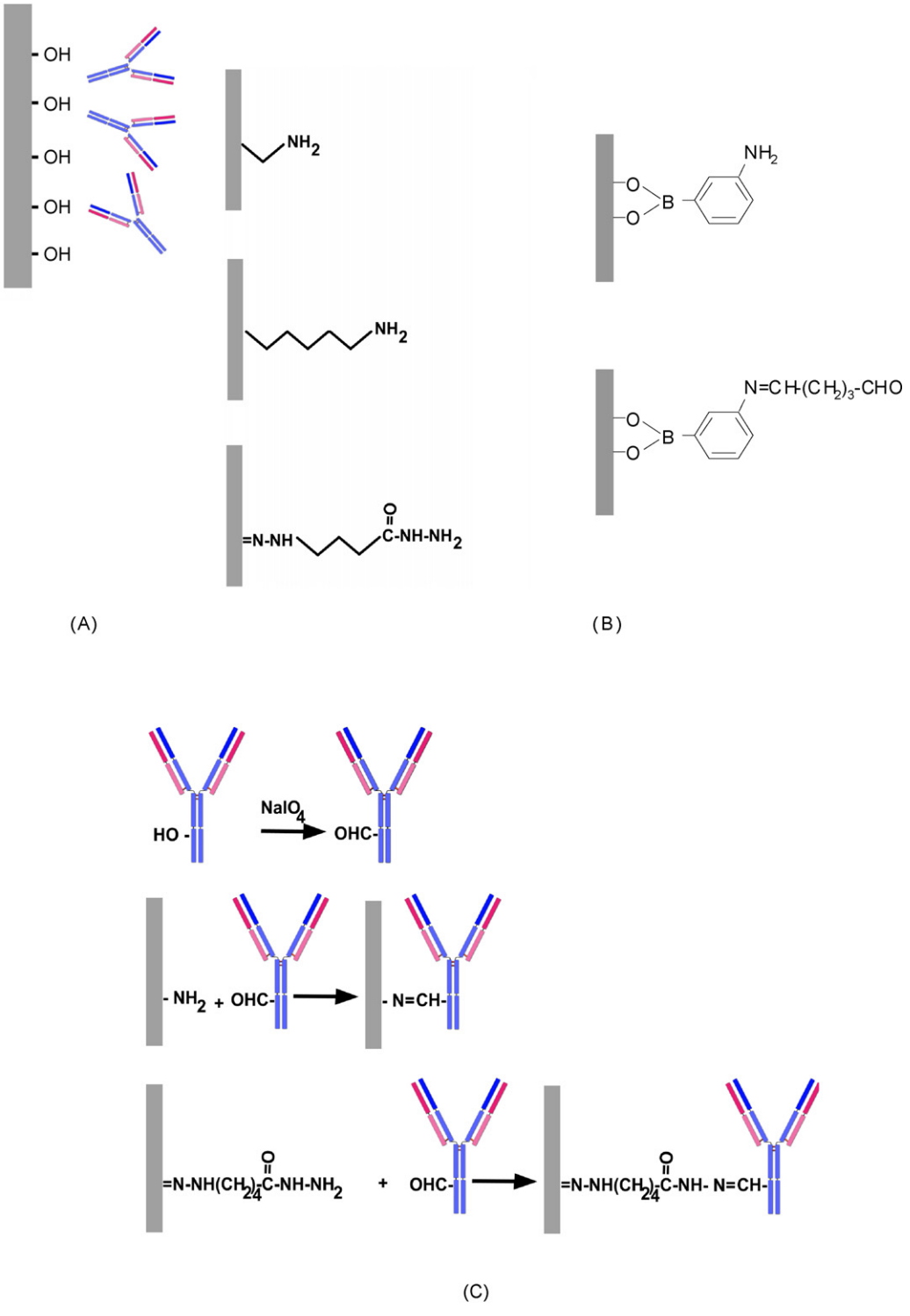

Fig. 1. Binding principle schematically shown for (A) antibody adsorption on the PVA surface, (B) covalent binding on PVA surfaces crosslinked with 2EI, HDA and ADH (left), and APBA and glutaraldehyde (right), and (C) site-specific attachment of IgG–CHO on PVA/chitosan and PVA crosslinked with ADH.

acids were reported to covalently bind to 1,2 or 1,3 diols, such as PVA which was taken advantage of in biomolecule immobilization [18] as well as sensing of glucose and polysaccharides [19].

Herein, PVA was chosen because it is one of the most hydrophilic polymers and thus can pre-eminently preserve proteins' activity due to its high water content, and furthermore prevent non-specific adsorption. To fully exploit the potential of PVA as coating material in biochips we aim to optimize layer fabrication as well as surface modification and antibody binding.

In the following, we describe first additive-functionalized and then crosslinked PVA, which we employed as an immobilization matrix for IgG and IgG activated with sodium periodate in order to evaluate: (1) the suitability of modified and unmodified PVAs in protein arrays; and (2) the effectiveness of simple, one-step IgG adsorption versus multi-step statistically oriented and site-specific covalent immobilization.

2. Materials and methods

2.1. Materials

Dodecyl sulfate sodium salt (SDS) was provided by Merck and phosphate buffered saline (PBS) by Gibco. Aminosulfobetain (ASB-14), sodium deoxycholate, cysteamine chloride, octyl-β-D-1-thioglucopyranoside, glutaraldehyde (25% in water) and 3-aminophenylboronic acid monohydrate (98%) (APBA) were from Sigma whereas 3-(decyldimethylammonio) propanesulfonate inner salt (SB3-10), 3-[(3-cholamidopropyl) dimethylammonio]-1-propanesulfonate (CHAPS), sodium *N*-dodecanoyl-*N*-methylglycinate (sarcosyl) and hexadecyltrimethylammonium bromide (CTAB) were from Fluka. Tween-20 was purchased from Fluka. Monochlortriazinyl-β-cyclodextrin sodium salt (MCT) was acquired from Wacker. All other reagents were analytical grade.

2.2. Chip fabrication and surface modification

Aqueous solutions of 1%, 4% and 10% PVA1 (Sigma-36306, Mw 146,000–186,000, hydrolysis degree 99+%), PVA2 (Sigma-341584, Mw 89,000–98,000, hydrolysis degree 99+%), PVA3 (Sigma-363103, Mw 146,000–186,000, hydrolysis degree 87–89+%), and PVA4 (Aldrich-9002895, Mw 85,000–146,000, hydrolysis degree 99+%), 4% PVA4/2% chitosan (food grade, Dalwoo) and 4% PVA4/2% oligo-chitosan (food grade, Dalwoo) were prepared and dip-coated onto either plain glass (Sigma, 8902), Silane Prep™ (Sigma, S4651) or adhesive Histobond slides (Marienfeld, no. 08 100 00) using the KSVD dip coater by KSV Instruments (velocity: 100 mm/min; retention time: 60 s; retention time between layers: 2 min). For IgG adsorption (schematically shown in Fig. 1A) the PVA slides were used without further treatment, whereas for covalent IgG immobilization adhesive glass slides were coated with 4% PVA4 and modified with bifunctional crosslinkers, such as ethylenediamine (2EI) (Fluka), hexamethylenediamine (HDA), adipic acid dihydrazide (ADH) (Aldrich), chitosan and chitosan-oligo subsequently to HIO_4 oxidation (the slides were immersed in 1% aqueous HIO_4 for 1 h and then washed twice with MiliQ water before incubating the slides in 1% crosslinker solution (pH 8) for 60 min). PVA4 slides modified with 3-aminophenylboronic acid were prepared by incubating the slides in 0.1N 3-aminophenylboronic acid monohydrate (pH 8.6) for 1 h. The slides were washed intensively in distilled water and blown dry with compressed air. Schemes of the resulting modified surfaces are presented in Fig. 1B.

2.3. Chemical modification of IgG

The carbohydrate groups of IgG were activated using sodium meta-periodate as described in [20]. Briefly, 3 mg ml^{-1} IgG in 0.1 M sodium acetate buffer (NaOAc) (pH 5.5) was incubated with sodium meta-periodate (25 mg ml^{-1} in NaOAc buffer, pH 5.5). After 1 h glycerol was added to stop the reaction. The activated antibody was then filled into microfilterfuge tubes (Microcon YM-30, Millipore) and centrifuged to separate the antibody from excess of periodate. Antibody samples were then washed twice with cold NaOAc. The activated IgG (IgG–CHO) was arrayed onto plain 4% PVA4, 4% PVA/2% chitosan and 4% PVA4 surfaces crosslinked with ADH. The binding principle is shown in Fig. 1C. The concentration of IgG–CHO was determined spectrophotometrically with respect to non-activated IgG using the NanoDrop (ND-1000, protein a 280 mode) and the loss of material due to chemical modification was calculated as percentage of the starting material.

2.4. Microarray printing

Glutaraldehyde crosslinked surfaces were prepared by spotting 1% and 2.5% glutaraldehyde in 1× PBS (pH 7.2) respectively onto PVA4/APBA surfaces prior to antibody spotting. Three replicates of 0.005–1 mg ml^{-1} rabbit IgG (technical grade, Sigma) were arrayed onto PVA-based surfaces using the OmniGrid contact spotter from GeneMachines (pin SMP3). Unless stated otherwise, 1× PBS (pH 7.2) was used as print buffer. The spot-to-spot distance was 500 μm, spot volume was 0.6 nl.

2.5. Postarraying and blocking

After arraying, the slides were incubated in a humid chamber at 4 °C overnight to complete probe immobilization. Surface blocking was performed in 1× PBS (pH 7.2)/0.1% Tween-20 to rinse off unbound protein and deactivate reactive surface groups. Finally, the slides were washed twice in 1× PBS (pH 7.2) and then blown dry using compressed air or spun dry in the centrifuge (900 rpm for 3 min).

2.6. Determination of immobilization capacity

Immobilization capacity in fmoles/mm^2 was calculated by taking the median fluorescence minus the local background of 27 replicate spots of 0.05 mg ml^{-1} dye-labelled anti-IgG before and after blocking (30 min) multiplied by spotted protein concentration and divided by molecular mass of labelled protein and square radius of the spot. 27 replicates were obtained by using three slides with nine replicates each. Thereby data F_A and F_B were determined using the same chip. The calculation was done according to formula (1) (I, immobilization capacity; F_B, fluorescence before blocking; F_A, fluorescence after blocking; M_{LP}, molecular mass of labelled protein; R, spot radius (typically 120 μm); *CLP*, concentration of spotted protein (0.05 mg ml^{-1})). The factor 1.9×10^6 is calculated from the volume of the protein solution per spot (0.6 nl/spot) and the Π.

$$I = 1.9 \times 10^6 \frac{F_A}{F_B M_{LP} R^2} C_{LP} \quad (1)$$

2.7. Direct immunoassay

Protein slides were processed with 4 ng μl^{-1} Dy633-labelled anti-Rabbit IgG (Dyomics) in 1× PBS (pH 7.2)/0.1% Tween-20 at 4 °C for 3 h, then washed twice in 1× PBS (pH 7.2) and spun dry in the centrifuge (900 rpm for 3 min).

2.8. Fluorescence detection and data analysis

Slides were stored in the dark and scanned at λ_{ex} = 635 nm and λ_{em} = 670 nm on the same day the immunoassay was performed.

Fluorescence measurements were taken using a Genepix™ 4000B non-confocal scanner from Axon Instruments. For data comparison, the photomultiplier tube (PMT) was kept constant within single experiments. All fluorescence (a.u.) data are background-corrected. Additionally, data flagged as bad, according to parameters set in the Genepix software (e.g. spot diameter 30–480 μm; signals >100 a.u. fluorescence), were filtered.

2.9. Profilometry

Layer thicknesses were measured over 2.5 mm × 2.5 mm surface areas using the Wyko NT1100 optical profiling system (Veeco) and Vision32 Veeco software. The values are mean values for two measurements.

3. Results and discussion

3.1. IgG adsorption

3.1.1. Choice of PVA

4% PVA1, −2, −3 and −4 coated onto aminosilane substrates were tested in a direct on-chip immunoassay using IgG adsorbed on the PVA-surface. The following criteria were taken into account in evaluation: fluorescence signals (a.u.), background (a.u.) and spot morphology. Fig. 2 compares the fluorescence obtained at the maximum loading concentration of IgG on PVA surfaces 1–4 (0.5 mg ml^{-1} IgG; spot volume 0.6 nl; 300 pg IgG/spot). The fluorescence signals were mean values calculated from 27 spots (three slides, nine replicates each). As is evident from Fig. 2, molecular weight (Mw) and hydrolysis degree of PVA plays an important role in the assay performance. Up to 30% stronger signals were achieved using PVA1 as compared to PVA3, despite the same molecular weight distribution. This is most likely due to the increased number of hydroxy groups available for IgG loading. The influence of molecular weight on fluorescence signals, at a hydrolysis degree of 99+%, is not entirely clear. It can nonetheless be observed that PVA2, with the lowest Mw, and PVA4, containing low and high Mw parts, produce the strongest signals. Signals for the highest Mw PVA tested (PVA1) were 40–60% weaker. PVA2, while having a narrower molecular weight distribution than PVA4, shows a similar IgG loading curve and equivalent assay performance. This indicates that the optimum molecular weight for the tested application is between 90.000 and a maximum of 146.000. PVA4 was chosen for further measurements, as the % coefficient of variation (CV) was 11%, i.e. four times lower than for PVA2.

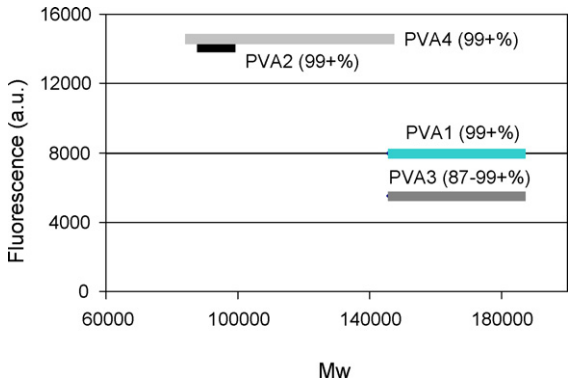

Fig. 2. Fluorescence achieved with 0.5 mg ml^{-1} IgG spotted on PVA1, PVA2, PVA3 and PVA4 surfaces. Bars indicate the distribution of Mw for the tested PVAs.

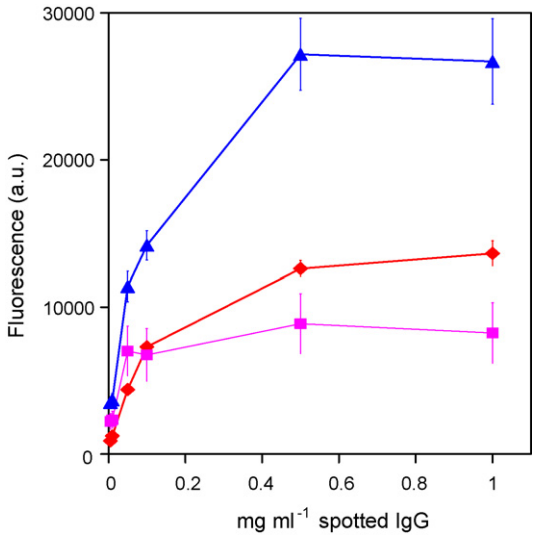

Fig. 3. Loading of 0.005–1 mg ml^{-1} IgG on (◆) plain, (■) aminosilane and (▲) adhesive glass slides covered with 4% PVA4.

3.1.2. Choice of substrate

The choice of optimal substrate is crucial for microarray surface development. The substrate should allow good polymer adherence without peeling off during the microarray experiment and display low autofluorescence at the wavelengths of interest. Three different substrates were coated with 4% PVA4 and evaluated: unmodified glass (Sa = 5.81 nm), aminosilane glass (Sa = 1.73 nm) and adhesive glass (Sa = 12.5 nm). Due to pretreatment, the latter two substrates were expected to foster stronger PVA binding, resulting in a more stable PVA-layer, as hydrogel swelling along the substrate is thereby inhibited. The best results in terms of fluorescence signal, as shown in Fig. 3, were obtained on the adhesive substrate, whereas the plain glass and the silanized glass resulted in signals that were at least 50% weaker. However, concerning the loading capacity saturation occurs at 0.5 mg ml^{-1} IgG (300 pg/spot), regardless of the substrate used. Although both aminosilane and adhesive glass provide reactive groups that are expected to bind PVA to the substrate more effectively than plain glass, substrate modification evidently had no significant effect with regard to producing stable PVA surfaces. This behaviour contrasts previous studies on poly(urethane) (PU) [7] which report comparable performance for both aminosilane and adhesive glass. An explanation for this might be found in the electrostatic interaction between PU and aminosilane. This is stronger than between aminosilane and PVA, with PVA displaying only a slight negative surface charge that decreases linearly from −2 mV at pH 5 to −6 mV at pH 9, while PU is more negatively charged, with a ζ potential that decreases linearly from −9 mV at pH 5 to −24 mV at pH 9. In the present case, the improved loading capacity on PVA-coated adhesive substrates is most likely the result of increased substrate roughness (the roughness of adhesive glass is six times greater than that of aminosilane glass). Increased roughness leads to better coverage of the substrate by PVA and to the formation of a rougher PVA layer onto which a higher amount of IgG can be adsorbed, which in turn results in stronger fluorescence signals.

3.1.3. Optimization of PVA concentration

Adhesive slides coated with aqueous solutions of 1%, 4% and 10% PVA4 were evaluated with respect to mechanical stability over incubation time (3 h) and to loading capacity, as determined in an immunoassay and by spotting labelled IgG. Fluorescence of spotted IgG processed with 4 ng μl^{-1} Dy633-labelled anti-Rabbit IgG

increases with increasing PVA concentration: when PVA concentration was increased by a factor of 4, signals were 2.5 times stronger, whereas five times stronger signals were obtained by increasing PVA concentration by a factor of 10. This is most likely due to better substrate coverage with PVA4 at higher hydrogel concentrations.

The thickness of a dip-coated film is influenced by the dipcoating velocity, especially the withdrawal speed, the viscosity of the coating solution, which is a function of the polymer concentration and the acceleration due to gravity. At constant withdrawal speed the amount of coating solution moving upwards with the substrate is larger for a more viscous solution, since the drag force is proportional to the solution viscosity. In fact, the thickness of the hydrogel layer increased significantly with increasing PVA concentration: The layer thickness (dry state) for 1% and 4% PVA as determined by profilometry was 46.5 nm and 407.5 nm, respectively. Thus, increasing the hydrogel concentration by a factor of 4, enhances the layer thickness by nine times. The fact that the increase in layer thickness is more pronounced might be related to a comparatively stronger increase in viscosity with increasing PVA concentration.

Furthermore, increasing the PVA concentration resulted in improved mechanical stability: when using 1% PVA surfaces twice as much hydrogel dissolves out in solution during incubation (3 h) than with 4% PVA surfaces. As a consequence, hydrogel layer thickness for 1% and 4% PVA is reduced by 67.7% and 38.2%, respectively. Apart from the improved mechanical stability of surfaces consisting of high PVA concentration, the immobilization capacity is drastically improved on thicker gels. This is obvious from the loading curve as well as from the immobilization capacity calculated for labelled IgG: 1% PVA4–16 fmoles mm^{-2}, 4% PVA4–91 fmoles mm^{-2}, and 10% PVA4 126 fmoles mm^{-2}. Moreover, the improved IgG loading on 4% and 10% PVA4 surfaces may be a result of increased density of OH-groups on the surface that due to their polarity promote the interactions between local dipoles existing on the interacting molecules [2]. In further experiments 4% PVA4 surfaces were employed because of the lower viscosity of solutions of 4% PVA and thus easier fabrication compared with 10% PVA.

3.1.4. Effect of print buffer composition on IgG adsorption

Adsorption is a simple, one-step immobilization method. Attachment occurs as a result of electrostatic and/or hydrophobic interaction forces. Thus, the printing solution containing additives of varying polarity and ionic charge can influence the strength of IgG adsorption by affecting the wettability of the surface, the binding kinetics and the net charge both of the surface and of the protein. Several additives ranging from 0.01% to 0.001% in 1× PBS (pH 7.2) have been tested: ASB-14, Tween-20, sarcosyl, SDS, MCT, CHAPS, CTAB, octyl-β-D-1-thioglucopyranoside, SB3-10, sodium deoxycholate, cysteamine chloride and glycerol [1,21–23]. The choice of additives was based on their widespread use in electrophoresis for the prevention of aggregation and scientific reports on improved printing solutions. In Fig. 4a fluorescence image of processed IgG spotted in various printing solutions is presented.

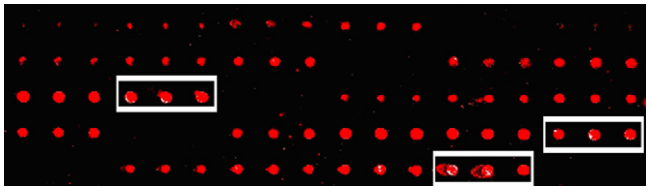

Fig. 4. Spot images of IgG spotted in various buffers based on 1× PBS (pH 7.2) (Flu: 4280, CV 29.5%). Spots in PBS containing 0.005% Tween-20 (Flu: 7600 a.u., CV 9.5%), 0.01% thioglucopyranose (Flu: 6335 a.u., CV 7.7%) and 0.01% ASB14 (Flu: 8527 a.u., CV 39%), respectively are highlighted.

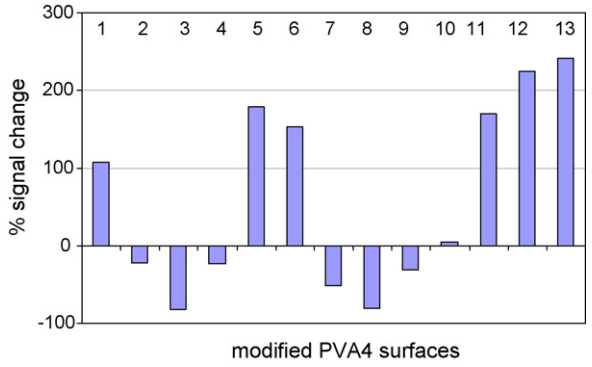

Fig. 5. Percentage signal change for 1 mg ml^{-} spotted IgG on surfaces made of PVA4 tailored with additives: (1) 2% chitosan, (2) 4% chitosan, (3) 2% chitosan-oligo, (4) 4% chitosan-oligo; and PVA4 activated with (5) periodate and further crosslinked with (6) ADA, (7) 2 EA, (8) 1, 6 HMA, (9) chitosan and (10) chitosan-oligo; and PVA4 crosslinked with (11) aminophenyl boronic acid and additionally with (12) 1%, and (13) 2.5% glutaraldehyde in comparison with unmodified 4% PVA4.

The triplicate spots of the most suitable print buffers as compared with plain PBS are highlighted. The corresponding fluorescence intensity values and coefficients of variation (%CV) are indicated in the figure caption. The use of PBS containing 0.005% Tween-20 (non-ionic), 0.01% octyl-β-D-1-thioglucopyranoside (non-ionic) and 0.01% ASB14 (anionic) resulted in 1.8, 1.5 and 2 times stronger fluorescence signals respectively than those obtained using PBS without additives. These additives, obviously provide the greatest solubilizing power and do not denature the antibody as strongly as other agents tested. As reported also by Brogan et al. [24] adjustment of additive concentration is critical, i.e. addition of 0.005% Tween-20 led to signal enhancement by 30%, whereas addition of 0.01% Tween-20 resulted in 1.5 times weaker fluorescence signals as compared to signals obtained in plain 1× PBS (pH 7.2).

3.2. Covalent IgG immobilization on modified PVA

1 mg ml^{-1} IgG in 1× PBS was spotted onto PVA surfaces, onto PVA surfaces activated with HIO_4, onto surfaces activated and crosslinked with amino-functional linkers of various lengths (2EA; HAD; DAH), and with 3-aminophenylboronic acid; and finally onto glass slides covered with PVA/chitosan and PVA/oligo-chitosan. IgG was bound to the surfaces in a statistically oriented manner, since some orientation already exists due to preferential binding between the reactive surface groups and the amino- and thiol groups of the antibody. Fig. 5 shows the percentage of signal change for each modified surface as compared with the plain PVA4 surface. As is evident from the figure, only modification with ADH, activation with HIO_4 and modification using APBA with and without glutaraldehyde led to significantly enhanced signals. Modification with ADH addresses the thiol-groups in the cystein units, whereas activated PVA can bind both amino and thiol groups present in the antibody. The greatest signal enhancement was achieved upon modification with APBA. This modification procedure is based on the well-known interaction of boronic acids with polyols, such as PVA or sugars. APBA is crosslinked to the PVA surface forming a cyclic ester between the diol group of the PVA and the boronic acid group of the crosslinker. The amino function was used for coupling IgG via its thiol groups, or its amino groups, in the latter case if glutaraldehyde was employed as an additional crosslinker. Functionalization of the chip surface by the addition of 2% chitosan results in higher loading capacity as indicated by the two times enhanced fluorescence, whereas 4% chitosan and the addition of oligochitosan led to a deterioration of the on-chip assay.

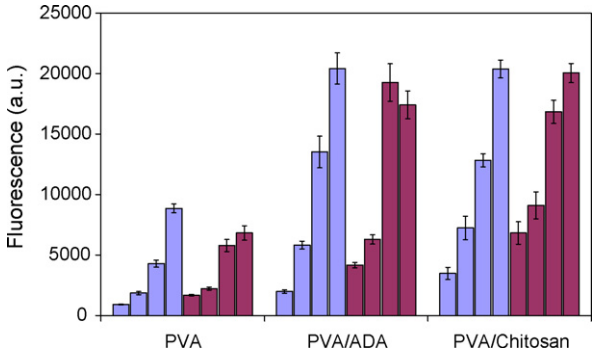

Fig. 6. Comparison of 0.1 mg ml^{-1}, 0.25 mg ml^{-1}, 0.5 mg ml^{-1} and 1 mg ml^{-1} spotted (■) IgG and (■) IgG–CHO on plain PVA4 surfaces, PVA4 crosslinked with adipic acid dihydrazide (ADH) and PVA4/chitosan surfaces.

3.3. Covalent, site-specific immobilization of modified IgG

In order to attach IgG to the surface site-specifically, IgG was activated with $NaIO_4$ by oxidation of the carbohydrate residues in the Fc fragment of the antibody and formation of reactive aldehyde groups (refer to Section 2). Three types of surfaces were employed for activated IgG immobilization: plain 4% PVA4, activated 4% PVA4 crosslinked with adipic acid dihydrazide and 4%PVA/4% Chitosan. Fig. 6 compares the fluorescence signals obtained with 0.1 mg l^{-1}, 0.25 mg l^{-1}, 0.5 mg l^{-1} and 1 mg l^{-1} spotted IgG and IgG–CHO respectively after processing with 4 ng μl^{-1} Dy633-labelled anti-Rabbit IgG. As is obvious from the figure, no improvement in loading was achieved with oriented immobilization using activated IgG. Moreover, data reproducibility did not improve either. This agrees well with Kusnezow et al. [25] who reported similar signal-to-noise ratios when using activated and non-activated antibodies as well as a loss of about 40% of antibody due to activation and purification steps (herein the loss was 33%). Moreover, Wacker et al. [26] demonstrated that direct spotting and site-specific immobilization of IgG via streptavidin–biotin attachment is similar with regard to signal intensity, assay sensitivity and assay reproducibility. By contrast, Peluso et al. [27] reported that specific orientation of capture agents (oriented IgG (biotinylated on carbohydrate on Fc domain), oriented Fab'fragments (biotinylated in hinge region)) consistently increases the analyte-binding capacity of streptavidin surfaces, with up to 10-fold improvements over surfaces with randomly oriented capture agents (randomly biotinylated IgG and Fab'fragments). This concurs strongly with Luk et al. [28] who reported measuring for ribonuclease inhibitor (RI) a four-times greater binding capacity (compared with random immobilization) in the case of RNase A immobilized with a preferred orientation. However, one has to keep in mind that there is no common opinion as to the effect of orientation on the assay performance using protein chips and that the preparation and purification of specifically activated antibodies and antibody fragments is tedious; in addition great material losses have to be accepted when applying this procedure. Clearly, in striving to achieve oriented antibodies one needs to accept the trade-off of increased costs for more starting material as well as increased effort in preparation and purification of the antibody over and against possible improvement of on-chip assay performance.

3.4. Reproducibility of fabrication and storage stability of PVA slides

PVA slides were fabricated in batches of 50 slides using the KSV dipcoater. The software controlled dipping speed was 100 mm/min for immersion and 100 mm/min for withdrawal (hold time 60 s). The slide-to-slide variation was encountered in data analysis in that not only replicate spots (nine per slide), but also replicate slides (three) were employed in each chip experiment. The inter-slide variation as described by the CV was typically 46%; the intra-slide variation was 33%.

The PVA slides were stored in the fridge to prevent them from drying out. The slides were stable for at least 2 months without deterioration of assay performance. However, when stored at room temperature for more than 3 weeks slides lost their binding ability resulting in reduced fluorescence signals. This is in contrast to Melo-Junior et al. [14], who reported a 30% activity loss in 6 months, whereas there was almost no decrease in loading capacity during the first 2 months. Furthermore, spot morphology significantly deteriorated which became evident by the deformation of spots. Spots "frayed out", most likely due to surface degradation. As spot morphology has a critical impact on data analysis, reproducibility of data declined (CV 63%).

4. Conclusions

Several immobilization chemistries were evaluated using chip surfaces based on PVA. In this, one-step IgG adsorption was optimized with regard to the type of PVA (Mw 85,000–146,000), the PVA concentration (4%) and the glass support type (adhesive). Modification of PVA surfaces improved the loading capacity significantly: addition of 2% chitosan resulted in two times stronger signals, whereas activation of PVA surfaces using periodate with or without subsequent crosslinking with adipic acid dihydrazide or slide modification using 3-phenylboronic acid led to signal improvement by a factor of up to 2.8. A minimum of a threefold increase in fluorescence was achieved with PVA surfaces modified by applying a two-step process using 3-phenylboronic acid and glutaraldehyde. Especially in sandwich immunoassays high loading of antibody is important as the assay sensitivity is directly related to the immobilization capacity. From the results presented it is clear that one- or two-step processes relying on either adsorption or covalent, statistically oriented immobilization of IgG are in any case more efficient, less tedious and result in better assay performance than covalent, site-specific immobilization using IgG with activated carbohydrate residues.

References

[1] E.W. Olle, J. Messamore, M.P. Deogracias, S.D. McClintock, T.D. Anderson, K.J. Johnson, Exp. Mol. Pathol. 79 (2005) 206–209.
[2] U. Bilitewski, Anal. Chim. Acta 568 (2006) 232–247.
[3] S.B. Brueggemeier, S.J. Kron, S.P. Palecek, Anal. Biochem. 329 (2004) 180–189.
[4] T. Sawasaki, N. Kamura, S. Matsunaga, M. Saeki, M. Tsuchimochi, R. Morishita, Y. Endo, FEBS Letters 582 (2008) 221–228.
[5] A.Y. Rubina, V.I. Dyukova, E.I. Dementieva, A.A. Stomakhin, V.A. Nesmeyanov, E.V. Grishin, A.S. Zasedatelev, Anal. Biochem. 340 (2005) 317–329.
[6] A.V. Hatch, A.E. Herr, D.J. Throckmorton, J.S. Brennan, A.K. Singh, Anal. Chem. 78 (2006) 4976–4984.
[7] K. Derwinska, L.A. Gheber, C. Preininger, Anal. Chim. Acta 592 (2007) 132–138.
[8] Y. Zhou, O. Andersson, P. Lindberg, B. Liedberg, Microchim. Acta 147 (2004) 21–30.
[9] M.M. Dominguez, M. Wathier, M.W. Grinstaff, S.E. Schaus, Anal. Chem. 79 (2007) 1064–1066.
[10] D.A. Zubtsov, E.N. Savvateeva, A.Yu. Rubina, S.V. Pan'kov, E.V. Konovalova, O.V. Moiseeva, V.R. Chechetkin, A.S. Zasedatelev, Anal. Biochem. 368 (2007) 205–213.
[11] S.K. Yoo, J.H. Lee, S.S. Yun, M.B. Gu, J.H. Lee, Biosens. Bioelectron. 22 (2007) 1586–1592.
[12] J.H. Han, J.D. Taylor, D.S. Kim, Y.S. Kim, Y.T. Kim, G.S. Cha, H. Nam, Sens. Actuators B 123 (2007) 384–390.
[13] Y. Jiang, L.L. Xiao, L. Zhao, X. Chen, X. Wang, K.Y. Wong, Talanta 70 (2006) 97–103.
[14] M.R. de Melo-Junior, L.C. Alves, F.B. dos Santos, E.I.C. Beltrao, L.B. de Carvalho Jr., React. Funct. Polym. 68 (2008) 315–320.
[15] L.B. Carvalho, A.M. Araujo, A.M.P. Almeida, W.M. Azevedo, Sens. Actuators 36 (1996) 427–430.
[16] L. Yu, C.M. Li, Q. Zhou, J.H.T. Luong, Bioconj. Chem. 18 (2007) 281–284.

[17] J. Kumar, S.F.D. 'Souza, Talanta 75 (2008) 183–188.
[18] Y. Ma, L. Qian, H. Huang, X. Yang, J. Colloid Interface Sci. 295 (2006) 583–588.
[19] J. Zhang, C.D. Geddes, J.R. Lakowicz, Anal. Biochem. 332 (2004) 253–260.
[20] L.C. Shriver-Lake, B. Donner, R. Edelstein, K. Breslin, S.K. Bhatia, F.S. Ligler, Biosens. Bioelectron. 12 (1997) 1101–1106.
[21] P. Wu, D.W. Grainger, J. Proteome Res. 5 (2006) 2956–2965.
[22] C. Preininger, U. Sauer, J. Dayteg, R. Pichler, Bioelectrochemistry 67 (2005) 155–162.
[23] S. Zampieri, A. Ghirardello, A. Doria, M. Tonello, R. Bendo, K. Rossini, P.F. Gambari, J. Immunol. Meth. 239 (2000) 1–11.
[24] K.L. Brogan, J.H. Shin, M.H. Schoenfisch, Langmuir 20 (2004) 9729–9735.
[25] W. Kusnezow, A. Jacob, A. Walijew, F. Diehl, J.D. Hoheisel, Proteomics 3 (2003) 254–264.
[26] R. Wacker, H. Schröder, C.M. Niemeyer, Anal. Biochem. 330 (2004) 281–287.
[27] P. Peluso, D.S. Wilson, D. Do, H. Tran, M. Venkatasubbaiah, D. Quincy, B. Heidecker, K. Poindexter, N. Tolani, M. Phelan, K. Witte, L.S. Jung, P. Wagner, S. Nock, Anal. Biochem. 312 (2003) 113–124.
[28] Y.Y. Luk, M.L. Tingey, K.A. Dickson, R.T. Raines, N.L. Abbott, J. Am. Chem. Soc. 126 (2004) 9024–9032.

Talanta 77 (2008) 727–732

Contents lists available at ScienceDirect

Talanta

journal homepage: www.elsevier.com/locate/talanta

Salmonella typhi determination using voltammetric amplification of nanoparticles: A highly sensitive strategy for metalloimmunoassay based on a copper-enhanced gold label

Wijitar Dungchai[a], Weena Siangproh[b], Wanpen Chaicumpa[c], Pongsri Tongtawe[d], Orawon Chailapakul[a,*]

[a] *Sensor Research Unit, Department of Chemistry, Faculty of Science, Chulalongkorn University, Patumwan, Bangkok 10330, Thailand*
[b] *Department of Chemistry, Faculty of Science, Srinakharinwirot University, Sukhumvit 23, Wattana, Bangkok 10110, Thailand*
[c] *Department of Parasitology, Faculty of Medicine, Siriraj Hospital, Mahidol University, Bangkok 10700, Thailand*
[d] *Faculty of Allied Health Sciences, Thammasat University, Pathumthani 12120, Thailand*

ARTICLE INFO

Article history:
Received 3 June 2008
Received in revised form 7 July 2008
Accepted 7 July 2008
Available online 16 July 2008

Keywords:
Electrochemical immunoassay
Gold nanoparticles
Copper-enhancer solution
Salmonella typhi

ABSTRACT

A highly sensitive electrochemical amplification immunoassay for *Salmonella typhi* (*S. typhi*) determination has been developed for the first time by using a copper-enhanced gold nanoparticle label coupled with anodic stripping voltammetry. Monoclonal antibodies for *S. typhi* were first immobilized on polystyrene microwells and then captured by *S. typhi* bacteria. After an immunoreaction occurred, a polyclonal, antibody–colloidal gold conjugate was added to bind to the *S. typhi* bacteria. Next, a copper-enhancer solution containing ascorbic acid and copper (II) sulfate was added into the polystyrene microwells. The ascorbic acid was employed to reduce the copper (II) ions to copper (0), which was subsequently deposited onto the gold nanoparticle tags. After the copper was dissolved in nitric acid, the released copper ions were detected by anodic stripping voltammetry. The amount of deposited copper was related to the amount of gold nanoparticle tag present, which was controlled by the amount *S. typhi* attached to the polyclonal antibody–colloidal gold conjugate. Therefore, the anodic stripping peak current was linearly dependent on the *S. typhi* concentration over concentration range of 1.30×10^2 cfu/mL to 2.6×10^3 cfu/mL in a logarithmic plot, with a detection limit as low as 98.9 cfu/mL. The influences of the relevant experimental variables, such as the concentration of copper and the reaction time of *S. typhi* with antibody, were investigated. We also successfully applied this method to determine the presence of *S. typhi* in human serum. Our results are a step towards developing more sensitive and reliable nanoparticle immunoassays.

1. Introduction

Typhoid fever is a serious problem for the public health of both underdeveloped and developing countries. It is a bacterial illness caused by *Salmonella typhi* (*S. typhi*), also known as *Salmonella enterica* serotype Typhi, a Gram-negative rod found only in humans. Each year, around 16 million incidences of typhoid are reported worldwide, resulting in an estimated 600,000 deaths [1,2]. The transmission of typhoid fever may occur through several pathways, such as by contact with infected individuals and by eating food or by drinking water that is contaminated with typhoid bacteria. Following ingestion, the bacteria spread from the intestine via the bloodstream to the intestinal lymph nodes and other areas of the body where they multiply. The symptoms of this illness are characterized by the sudden onset of sustained fever, severe headache, loss of appetite, and either constipation or mild diarrhea. Samples of urine or blood are used to check the presence of *S. typhi*, which is the only way to ensure that the observed illness is typhoid fever [3]. Therefore, the determination of *S. typhi* in urine or blood plays an important role in clinical research and diagnosis of typhoid fever. Furthermore, a person who recovers from typhoid fever may still become an asymptomatic carrier who can infect others. Thus, the level of *S. typhi* in the patient's urine or blood after recovery should be continuously monitored in order to control the spread of this epidemic disease. Classical methods are usually used to detect *S. typhi*, including culturing [4,5], serological methods, such as slide agglutination and the Widal test [6], and polymerase chain reaction (PCR) [7,8]. Even though these methods can provide highly sensitive results for both qualitative and quantitative analysis, they are quite labor- and time-intensive to perform due to the

* Corresponding author. Tel.: +66 2 218 7615; fax: +66 2 254 1309.
E-mail address: corawon@chula.ac.th (O. Chailapakul).

0039-9140/$ – see front matter © 2008 Elsevier B.V. All rights reserved.
doi:10.1016/j.talanta.2008.07.014

pre-enrichment, isolation, and amplification steps of the bacterial cells.

With the above-mentioned drawbacks, efforts to develop a method for *S. typhi* determination with increased sensitivity and selectivity and a reduction in analysis time have been proposed. Currently, alternative methods for biological molecular analysis are enzyme immunoassay [9,10], surface plasmon resonance [11], and electrochemical immunoassay [12–14]. In particular, the use of electrochemical immunoassay has attracted considerable interest for *S. typhi* determination because of its inherent simplicity, high sensitivity, inexpensive instrumentation, and miniaturization. Although this method has a low detection limit and could be used in the diagnosis of typhoid fever, a sensitive and rapid method for analyzing and obtaining important information about the effectiveness of therapy, follow-up treatments, the epidemic disease, and protection is still needed. With the development of nanotechnology, various nanoparticles [15,16] and nano-quantum dots [17,18] have been used as labels to enhance the sensitivity of the electrochemical immunoassay technique. Amplified electrochemical detection of biological molecules was achieved by the dissolution of the metallic nanoparticles and by recording the subsequent electrochemical stripping of the dissolved ions. Gold nanoparticles act as a class of labels with many unique features, such as optical, electronic, and catalytic properties, that have been previously explored for potential applications in biomolecular detection. Based on these advantages, colloidal gold was used as an electrochemical marker or catalytic label for nanoparticle enlargement in order to elevate the sensitivity of the bioassay.

Recently, copper, silver, and gold-enhanced colloidal gold have been reported for immunoglobin G (IgG) determination, which is the model of electrochemical immunoassay with low detection limits ranged from 1.0 ng/mL to 0.25 pg/mL [19–21]. The metal-enhanced colloidal gold electrochemical stripping metalloimmunoassay combines the high sensitivity of stripping metal analysis with the remarkable signal amplification resulting from the catalytic precipitation of metals onto the gold nanoparticles [21–23]. Among these metals, the copper-enhanced protocol is better than the other metal-enhancing protocols because the copper-enhancer solution, which contains ascorbic acid and copper sulphate, is easy to prepare and preserve. Furthermore, the copper determination by anodic stripping voltammetry is simple, and highly sensitive. Willner and co-workers also applied the catalytic deposition of copper on gold nanoparticles for NADH detection [24]. However, metal-enhanced colloidal gold has not been previously applied to the detection of bacterial cells in real samples, especially for the detection of *S. typhi*. Therefore, we have employed the electrochemical stripping metalloimmunoassay based on a copper-enhanced gold nanoparticle label for the determination of *S. typhi* in real samples for the very first time, which will be useful in the diagnosis, follow-up treatment, and controlling in advance the epidemic disease of typhoid fever.

In this work, our ultimate aim was to develop an electrochemical metalloimmunoassay based on copper-enhanced gold nanoparticle label for *S. typhi* determination in real samples with a low limit of detection, high accuracy, and fast analysis time. The details of the optimization and the excellent performance of our proposed method are presented in the following sections.

2. Experimental

2.1. Instrumentation

The stripping voltammograms were recorded using an Autolab Potentiostat 30 (Metrohm, Switzerland) with a three-electrode system. A glassy-carbon (GC) electrode (Bioanalytical System Inc., area 0.07 cm^2) was used as the working electrode. Prior to use, the GC electrode was pretreated by sequential polishing with 1 μm and 0.3 μm of alumina/water slurries on felt pads, followed by rinsing with deionized water in order to remove the alumina impurities. A platinum wire and Ag/AgCl with a salt bridge were used as the counter and reference electrodes, respectively. The electrochemical equipment was housed in a Faraday cage to reduce electronic noise.

2.2. Materials and methods

The polystyrene, 96-well, microtiter plates (high-binding ELISA plates) were purchased from Ronbio (Shanghai, China). Polyclonal and monoclonal rabbit antibodies for polysaccharides of *S. typhi* O901 and *S. typhi* were obtained from Siriraj Hospital. Hydrogen tetrachloroaurate (III) and albumin bovine serum (BSA) were obtained from the Sigma Chemical Co. (St. Louis, MO). Nitric acid (65%), sodium chloride, sodium dihydrogen phosphate, disodium hydrogen phosphate, sodium carbonate, sodium bicarbonate, sodium citrate, copper (II) sulfate, and ascorbic acid were obtained from Merck (Germany).

The coating buffer for the microwells was 0.05 M $NaHCO_3$–Na_2CO_3 (pH 9.6). The incubation and washing buffer consisted of 0.01 M NaH_2PO_4–Na_2HPO_4 (pH 7.4) and 0.15 M sodium chloride. The copper-enhancer solution was made from a 1:1 (v/v) ratio of 0.10 M ascorbic acid and 0.2 M copper (II) sulfate. All of the solutions were prepared using Milli-Q 18 MΩ water (Millipore purification system).

2.3. Preparation of the antibody–colloidal gold conjugate

2.3.1. Preparation of gold nanoparticles

The gold nanoparticles were prepared according to the method reported in Refs. [19,25] with slight modifications. Briefly, 1 mL of 1% $HAuCl_4$ solution was mixed with 100 mL of doubly distilled water and boiled under vigorous stirring. Then, 2.5 mL of 1% sodium citrate was added into solution under continuous heating and stirring for 15 min until the color of solution changed to wine red. The colloidal solution was left to cool at room temperature under stirring and was later stored in dark bottles at 4 °C. The solution of colloidal gold particles was characterized by a UV–vis spectrophotometer and a transmission electron microscope (TEM).

2.3.2. Antibody–colloidal gold conjugate

The amount of coating antibody (polyclonal rabbit antibody for polysaccharides of *S. typhi* O901) on the surface of the gold nanoparticles was optimized from 75 mg/L to 1200 mg/L. Solutions were prepared from 15,000 mg/L stock solutions of the rabbit antibody to *S. typhi*. An appropriate volume of stock solution was added into a centrifuge tube containing 2.0 mL of the colloidal gold solution. The pH solution was adjusted to 8.0 under stirring and was followed by incubation at room temperature for 1 h. The absorbance at 519 nm of these samples was recorded and plotted versus the amount of coating antibody in order to determine the optimal amount of coating antibody.

After obtaining the optimal amount of coating antibody, the antibody–colloidal gold conjugate was prepared. The optimized amount of polyclonal rabbit antibody for the polysaccharides of *S. typhi* was added to 2 mL of the colloidal gold solution. The solution was then adjusted to pH 8.0 using Na_2CO_3 and was followed by incubation at room temperature for 1 h under stirring. Next, 100 μL of 3% BSA solution was added to minimize nonspecific adsorption, and the solution was incubated under stirring for an additional hour at room temperature. The antibody–colloidal gold conjugate was centrifuged at 15,000 rpm for 10 min. The soft sediment was col-

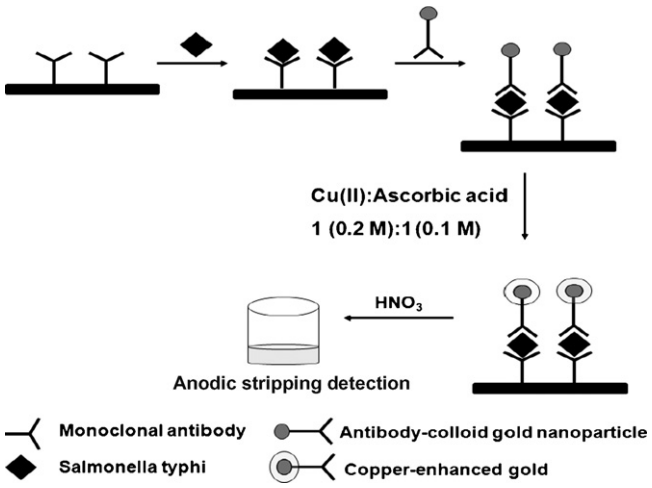

Fig. 1. Schematic diagram of the proposed *S. typhi* immunoreactions.

lected, washed and suspended in PBS solution, where the conjugate could be stored for more than 1 month at 4 °C.

2.4. Immunoassay procedure

The immunoassay procedure is shown in Fig. 1. First, 50 μL of 125 mg/L monoclonal antibody was added into the polystyrene microwells and incubated at 37 °C for 2 h. Second, the solution was removed, and the microwells were washed with PBS (pH 7.4) for four times followed by the addition of 50 μL of 1% BSA solution to block the active sites of microwells from nonspecific adsorption. The microwells were incubated at 37 °C for 2 h. The PBS (pH 7.4) washing step was repeated followed by the addition of 50 μL of *S. typhi* into the microwells. After incubating at 37 °C for 1 h followed by another PBS washing step, 50 μL of the antibody–colloidal gold conjugate was added to the solution, which was incubated at 37 °C for 1 h in order to obtain the sandwich reaction. After performing four washing steps, 100 μL of copper-enhancer solution was added to the solution, which was incubated at room temperature for 10 min. After the microwells were washed four times with doubly distilled water, 100 μL of 1 M nitric acid solution was added to dissolve copper. Finally, the solution containing the released copper ions was transferred into an electrochemical cell and diluted to 3 mL with doubly distilled water. The experiments were carried out by anodic stripping voltammetry.

3. Results and discussion

3.1. Preparation of the antibody–colloidal gold conjugate

3.1.1. Preparation of the gold nanoparticles

To characterize the gold nanoparticles, primary UV–vis spectra of the gold (III) ion and the gold nanoparticle solution were recorded. It was observed that the maximum absorbance of the gold nanoparticles occurred at a wavelength of 519 nm, which was similar to other reports [25]. This result indicated that the synthesis had yielded gold nanoparticles. From TEM measurements, the average gold nanoparticle size was 15 nm (data not shown).

3.1.2. Preparation of the antibody–colloidal gold conjugate

Using the preparation procedure for antibody–colloidal gold conjugates as mentioned above, it was found that the antibodies could bind with the gold nanoparticles. The visible spectrum of antibody–colloidal gold conjugate displayed an absorption band at 519 nm, and there were no significant changes in the absorption spectrum of the gold nanoparticles. This could be explained if gold still exhibited the characteristics of a nanosized particle after binding. However, the antibody–colloidal gold conjugate generated a higher signal when compared to those of the gold nanoparticle at the same wavelength.

The effect of the amount of coating antibody on the surface of the gold nanoparticles was examined in a range of 75–1200 mg/L. It could be seen that the absorbance increased with increasing the amount of coating antibody up to 450 mg/L. The absorbance decreased after the amount of coating antibody was higher than 450 mg/L (data not shown). This indicated that a concentration of 450 mg/L was a suitable amount of coating antibody. Moreover, it was also effective in preventing aggregation.

3.2. Determination of copper (II) ion at a glassy carbon electrode

In our proposed method, the final step of immunoassay, the copper deposited on gold nanoparticles, was dissolved in an acid solution and detected at GC electrode. The amount of copper deposited on the gold nanoparticles is directly proportional to the amount of *S. typhi*. Therefore, the sensitivity of *S. typhi* determination is related to the sensitivity of the Cu (II) ion determination. Our goal was to evaluate the performance of the electrochemical assay for the determination of the copper (II) ion using a glassy carbon electrode. Several parameters were investigated in order to obtain suitable conditions for the Cu (II) ion determination.

3.2.1. The effect of the deposition potential

The effect of the deposition potential on the stripping peak current of the Cu (II) ion was studied from −0.3 V to −0.6 V. The anodic peak currents were increased rapidly from −0.3 V to −0.45 V, and no significant differences were observed for the anodic peak current between −0.5 V and −0.6 V as shown in Fig. 2(A). Therefore, a deposition potential of −0.5 V was selected in the experiment.

3.2.2. The effect of the deposition time

The deposition time of the Cu (II) ion at a glassy carbon electrode directly affects the sensitivity of the anodic stripping analysis. For this reason, the influence of the deposition time for the detection of copper was studied, with deposition times ranging from 1 min to 8 min. As shown in Fig. 2(B), when the deposition times were increased from 1 min to 6 min, the anodic peak currents also increased, and after 6 min, the current remained constant. Therefore, 6 min was chosen as the suitable deposition time.

3.2.3. Linearity

In order to judge the possibility of applying the assay for quantitative analysis, the linearity range was examined. Under optimal conditions, a good linearity in the anodic peak current with the copper (II) concentration over a range of 0.10–100 μM was obtained with a linear correlation coefficient of 0.9950 (as shown in Fig. 2(C)). The detectable limit, which was calculated as three times the standard deviation, was 3.77×10^{-2} μM. It can therefore be concluded that anodic stripping voltammetry is a very highly sensitive method for Cu (II) ion determination, and therefore copper-enhanced gold nanoparticles can be effectively detected by this method.

3.3. Optimization of the immunoassay conditions

3.3.1. The effect of the concentration and the reaction time of copper-enhancer solution

The sensitivity of the electrochemical immunoassay based on a colloidal gold-labeled antibody can be achieved by the catalytic

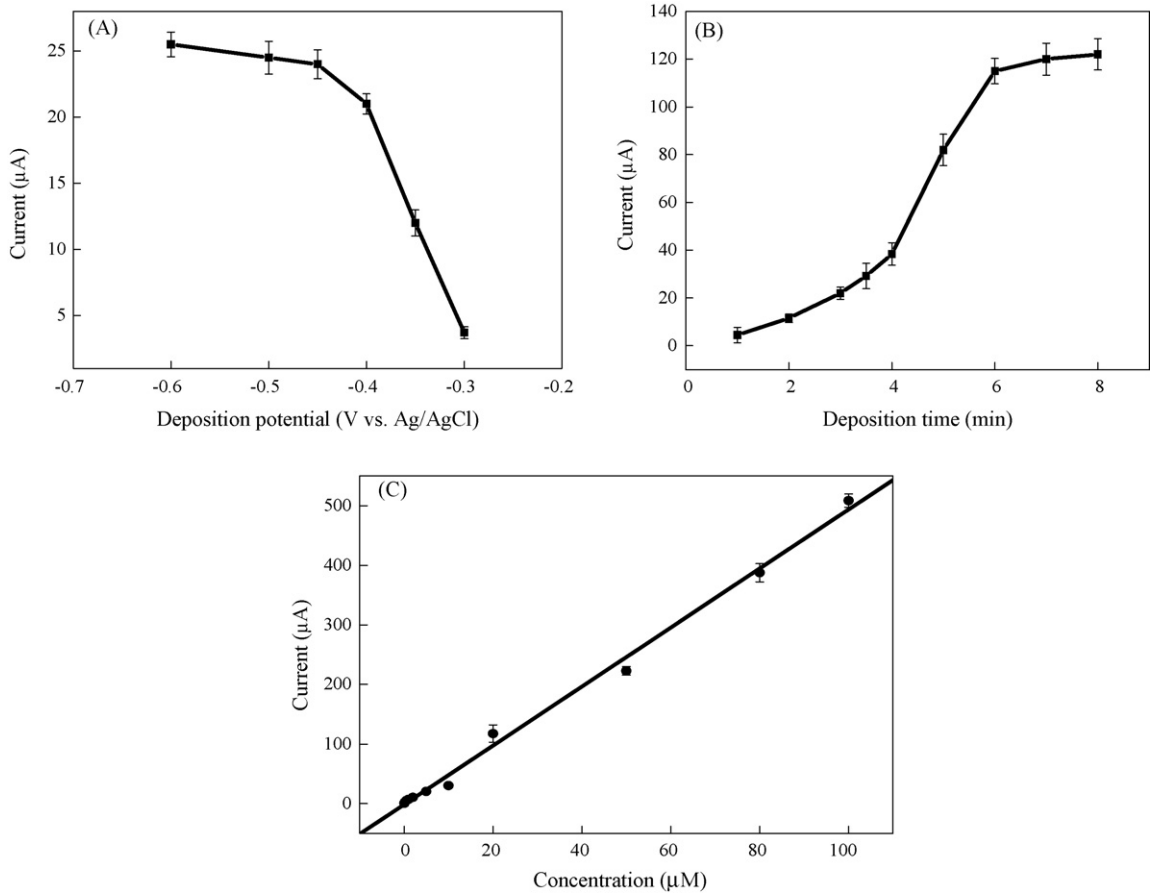

Fig. 2. (A) The effect of the deposition potential of the Cu (II) ion under a 3 min deposition time with a concentration of Cu (II) 1×10^{-5} M in a 0.1-M nitric acid solution. (B) The effect of the deposition time of Cu (II) ion under a −0.5 V deposition potential with a concentration of Cu (II) 1×10^{-5} M in a 0.1-M nitric acid solution. (C) The calibration plots of the Cu (II) ion for a −0.5 V deposition potential and for a 6 min deposition time, $n = 3$.

precipitation of copper on the gold nanoparticles. The concentration of copper would therefore affect the amount of copper metal deposited on the gold nanoparticles. The copper concentration in the copper-enhancer solution was investigated within the range of 0.10–0.40 M. The results demonstrated (Fig. 3(A)) that the anodic peak current increased with increasing copper concentration along with the background signal. Therefore, the ratio of current between the *S. typhi* and the background signal was calculated as a function of the copper concentration to determine the concentration which provided optimal sensitivity. The signal to background ratio reached a maximum value at a copper concentration of 0.10 M and signal was steady, as shown in Fig. 3(B). To assure that amount of copper is enough for detection of *S. typhi*, therefore; excess copper concentration of 0.2 M was selected for all subsequent experiments. The reaction time of the copper-enhancer solution should also be optimized, since it is related to the amount of copper metal

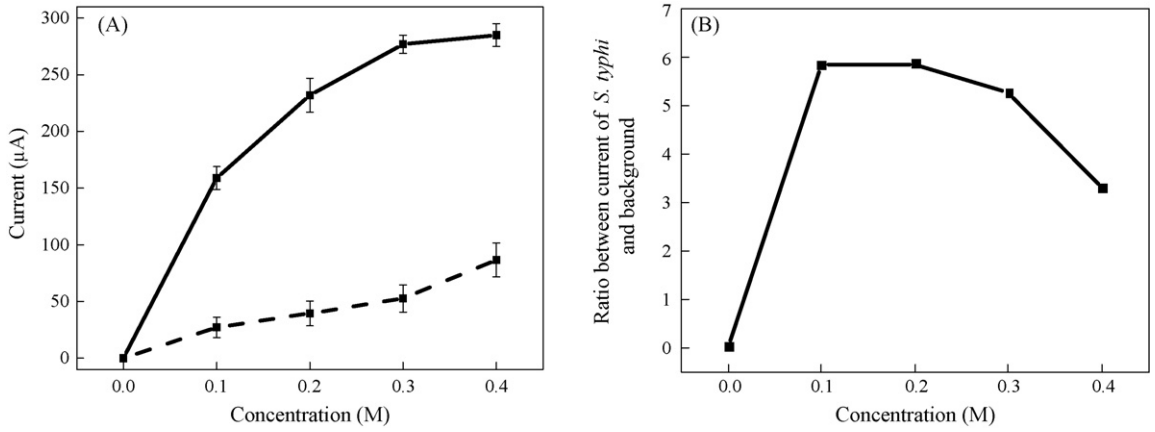

Fig. 3. (A) The effect of the copper concentration; *S. typhi* signal (solid line) and background signal (dash line) and (B) the ratio between *S. typhi* signal and the background signal. The following conditions were used: 2.6×10^3 cfu/mL of *S. typhi*, a 60 min incubation time for the *S. typhi* with the monoclonal antibody and the antibody–colloid gold conjugate, a 1:1 dilution ratio of the antibody–colloid gold conjugate, and a copper enhancement time of 10 min, $n = 3$.

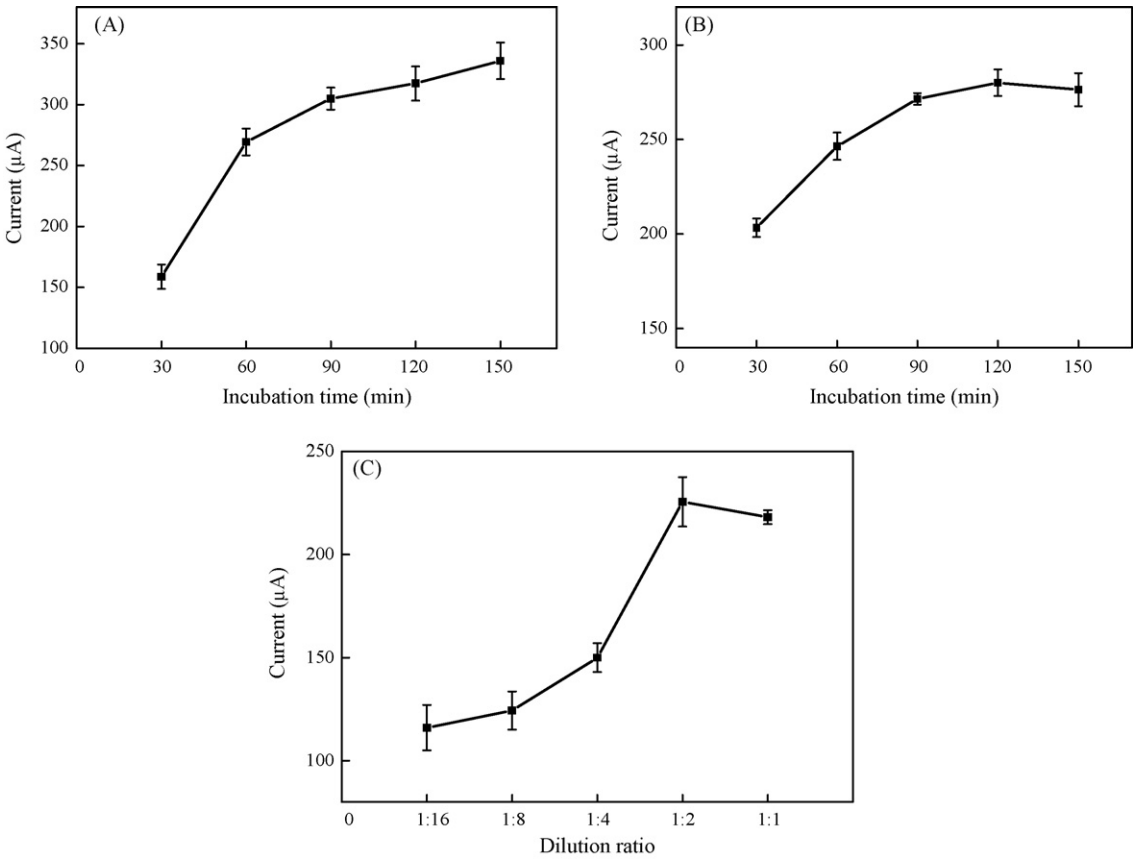

Fig. 4. The effect of the incubation time between the *S. typhi* and either (A) the monoclonal antibody or (B) the antibody–colloid gold conjugate. (C) The effects of antibody–colloidal gold conjugate dilution. The same conditions were used as those in Fig. 3, $n = 3$.

deposited on the gold nanoparticles. In this work, the reaction time was optimized over a range of 5–30 min. It was observed that the anodic peak current significantly increased with reaction time in the range of 5–10 min and then only slightly increased. However, the background also increased when the reaction time of copper-enhancer solution increased. Therefore, the ratio of the signal between the *S. typhi* and the background was calculated as a function of the reaction time of the copper-enhancer solution. A maximum of the signal with *S. typhi* to the background signal was obtained at a reaction time of 10 min, which was therefore chosen for the reaction time of copper-enhancer solution in further experiments (data not shown).

The temperature effecting the copper enhancing protocol was also investigated (data are not shown). It was observed that the background signal significantly increased when temperature increased. The *S. typhi* signal also increased with the increasing of the temperature from 4 °C to 25 °C. However, the signal began to decrease when the temperature was higher than 25 °C. Therefore, in this work, at room temperature (25 °C) was chosen to obtain the high sensitivity and the convenience for doing the experiments.

3.3.2. *The effect of the immunoassay incubation time*

The immunoreaction time between the *S. typhi* and the monoclonal antibody coated on the microwells was studied for times between 30 min and 150 min. Fig. 4(A) shows the results from the assay plotted as a function of the incubation time, and the current signal was found to increase with increasing incubation time. An incubation time of 60 min was selected since at longer incubation times, no significant changes in the signal were observed.

3.3.3. *The effect of the dilution ratio and the incubation time of the antibody–colloidal gold conjugate*

From the immunoassay procedure, *S. typhi* was bound with the antibody–colloidal gold conjugate in order that the amount of antibody–colloidal gold conjugate added would directly affect the sensitivity of the *S. typhi* detection. In addition, the amount of bound antibody–colloidal gold conjugate also depends on the diffusion rate of the nanoparticle label. The diffusion rates of the nanoparticle label are smaller than that of the free antibody due to the bigger size of the nanoparticle label. Therefore, the antibody-conjugated particle binding could be the time-limiting step in the assay unless a high concentration of nanoparticles is used. However, the minimal amount of nanoparticle labels that can maintain an acceptable sensitivity is normally used in order to reduce the assay cost. Therefore, the dilution ratio and the incubation time of antibody–colloidal gold conjugate were optimized in this experiment. The results are shown in Fig. 4(B and C). The anodic stripping peak current was increased when the dilution ratio was increased up to 1:2. Therefore, a 1:2 of dilution ratio of the antibody–colloidal gold conjugate was selected. The peak current increased rapidly with the incubation time between 30 min and 60 min and was found to remain constant for times greater than 60 min. Therefore, an incubation time of 60 min was chosen as a compromise between the analysis time and the sensitivity.

3.4. *Analytical performance*

Using the optimal conditions, the relationship between the anodic peak current of copper and the concentration of *S. typhi* is

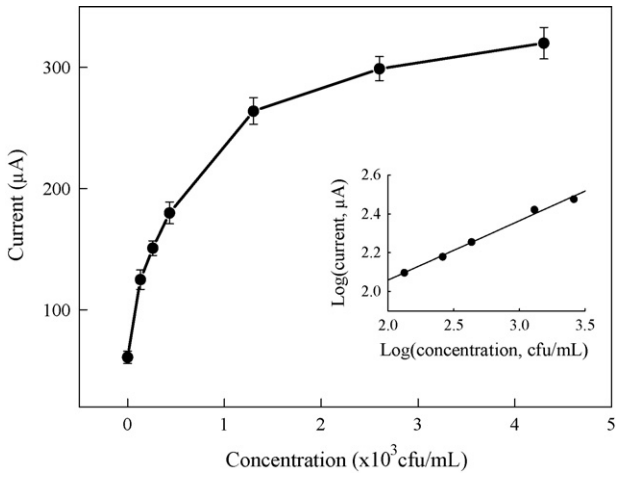

Fig. 5. The relationship between the anodic stripping peak current and concentration of *S. typhi* (with concentrations of 0 and 1.30×10^2 cfu/mL to 4.30×10^3 cfu/mL). The calibration plot for the *S. typhi* determination (1.30×10^2 cfu/mL to 2.60×10^3 cfu/mL) is shown in the insert, $n = 3$.

plotted in Fig. 5 over a concentration range of 0–4.30×10^3 cfu/mL. A linear relationship, $\log i_{pa} = 0.3053 \log C + 1.4489$, was observed with a correlation coefficient of 0.9961 for *S. typhi* concentrations between 1.30×10^2 cfu/mL and 2.6×10^3 cfu/mL. The data was plotted on a logarithmic scale in order to solve the curvature problem which resulted from the saturation of the probe binding site and particle aggregation (see insert of Fig. 5) [22]. The detection limit was estimated to be 98.9 cfu/mL (based on a criterion of three times the standard deviation with $n = 8$), which is better than both the detection limit of 1.3×10^3 cfu/mL obtained from a direct-binding optical grating coupler immunosensor [26] and the detection limit of 5×10^3 cfu/mL obtained from a phage immobilized magnetoelastic sensor [27]. The reproducibility of our proposed method was studied by analyzing concentrations of *S. typhi* of 2.60×10^2 cfu/mL and 2.60×10^3 cfu/mL, where measurements were performed eight times during the same day on a single immunoassay (intra-assay) and on three separate immunoassays over a 3 day period (inter-assay). A relative standard deviation (R.S.D.) of the immunoassay of below 14% was observed for both the intra- and inter-assays. The results are shown in Table 1.

3.5. Analytical applications

The proposed method was also applied to determine the level of *S. typhi* in human serum. In order to determine the accuracy of our method, normal human serum was spiked with different concentration of *S. typhi* and analyzed by using a calibration method without any pretreatment. Recoveries of *S. typhi* were in the range of 80–101%. The results (as shown in Table 2) demonstrated that this method can be used to efficiently determine *S. typhi* in human serum without any sample preparation.

Table 1
The reproducibility of the proposed method

Assay type	Concentration (cfu/mL)	%R.S.D.
Intra-assay ($n = 8$)	2.6×10^2	11.4
	2.6×10^3	7.7
Inter-assay ($n = 3$)	2.6×10^2	13.7
	2.6×10^3	8.4

Table 2
Results of *S. typhi* in human serum sample

Concentration (cfu/mL, $n = 3$)		Recovery (%)
Added	Found	
260	223.3 ± 28.6	85.9
433	352.1 ± 37.5	81.3
1300	1305.3 ± 115.8	100.4
2600	2541.5 ± 216.1	97.7

4. Conclusion

For the first time, we have successfully developed an electrochemical metalloimmunoassay, which is based on a copper-enhanced gold nanoparticle label, for *S. typhi* determination with high sensitivity, specificity, and reproducibility. The electrochemical stripping metalloimmunoassay combines the inherent signal amplification of stripping metal analysis with a biospecific interaction. The proposed method was also applied with satisfactory recovery results for *S. typhi* determination in human serum. The coupling of gold nanoparticles with the advantages of electrochemical stripping analysis can easily be extended for detecting other bacterial cells in real samples with high accuracy and sensitivity.

Acknowledgements

The authors would like to acknowledge the support from the Thailand Research Fund through the Royal Golden Jubilee Ph.D. Program (Grant No. PHD/39/2548), Basic Research Grant, Chulalongkorn University and The National Center of Excellence for Petroleum, Petrochemicals, and Advanced Materials.

References

[1] B. Ivanoff, M.M. Levine, P.H. Lambert, Bull. World Health Organ. 72 (1994) 957.
[2] C.M. Parry, T.T. Hien, G. Dougan, N.J. White, J.J. Farrar, New Engl. J. Med. 347 (2002) 1770.
[3] Typhoid fever, Centers for Disease Control and Prevention, Department of Health and Human Services, U.S.A., 2005, from http://www.cdc.gov/nczved/dfbmd/.
[4] J. Wain, T.S. Diep, V.A. Ho, A.M. Walsh, N.T.T. Hoa, C.M. Parry, N.J. White, J. Clin. Microbiol. 36 (1998) 1683.
[5] B. Swaminathan, P. Feng, Annu. Rev. Microbiol. 48 (1994) 401.
[6] M.L. Myron, G. Oscar, H.G. Robert, E.W. William, S.P. Rene, W. William, Am. J. Trop. Med. Hyg. 27 (1978) 795.
[7] H.S. Huang, M.M. Garcia, B.W. Brooks, K. Nielsen, S.P. Ng, Int. J. Food Microbiol. 51 (1999) 85.
[8] I. Hein, G. Flekna, M. Krassnig, M. Wagner, J. Microbiol. Methods 66 (2006) 538.
[9] W. Chaichupa, Y. Ruangkunaporn, D. Burr, M. Chongsanguan, P. Echeverria, J. Clin. Microbiol. 30 (1992) 2513.
[10] W. Chaicumpa, W. NgrenNgarmlert, T. Kalambaheti, Y. Ruangkunaporn, M. Chongsanguan, P. Tapchaisri, V. Desakorn, O. Suthienkul, Asian Pac. J. Allergy Immunol. 13 (1995) 159.
[11] S.D. Mazumdar, M. Hartmann, P. Kampfer, M. Keusgen, Biosens. Bioelectron. 22 (2007) 2040.
[12] V.K. Rao, G.P. Rai, G.S. Agarwal, S. Suresh, Anal. Chim. Acta 531 (2005) 173.
[13] S. Suye, T. Matsuura, T. Kimura, H. Zheng, T. Hori, Y. Amano, H. Katayama, Microelectron. Eng. 81 (2005) 441.
[14] T.S. Huang, Y. Tzeng, Y.K. Liu, Y.K. Chen, K.R. Walker, R. Guntupalli, C. Liu, Diamond Relat. Mater. 13 (2004) 1098.
[15] M. Dequaire, C. Degrand, B. Limoges, Anal. Chem. 72 (2000) 5521.
[16] S.B. Zhang, Z.S. Wu, M.M. Guo, G.L. Shen, R.Q. Yu, Talanta 71 (2007) 1530.
[17] H. Wu, G.D. Liu, J. Wang, Y.H. Lin, Electrochem. Commun. 9 (2007) 1573.
[18] R. Thurer, T. Vigassy, M. Hirayama, J. Wang, E. Bakker, E. Pretsch, Anal. Chem. 79 (2007) 5107.
[19] X. Mao, J.H. Jiang, Y. Luo, G.L. Shen, R.Q. Yu, Talanta 73 (2007) 420.
[20] X. Chu, X. Fu, K. Chen, G.L. Shen, R.Q. Yu, Biosens. Bioelectron. 20 (2005) 1805.
[21] K.T. Liao, H.J. Huang, Anal. Chim. Acta 538 (2005) 159.
[22] J. Wang, D.K. Xu, A.N. Kawde, R. Polsky, Anal. Chem. 73 (2001) 5576.
[23] J. Wang, R. Polsky, D. Xu, Langmuir 17 (2001) 5739.
[24] B. Shlyahovsky, E. Katz, Y. Xiao, V. Pavlov, I. Willner, Small 1 (2005) 213.
[25] C.G. Katherine, F.R. Griffith, B.H. Michael, J.N. Michael, Anal. Chem. 67 (1995) 735.
[26] N. Kim, I.S. Park, W.Y. Kim, Sens. Actuators B 121 (2007) 606.
[27] R.S. Lakshmanan, R. Guntupalli, J. Hu, V.A. Petrenko, J.M. Barbaree, B.A. Chin, Sens. Actuators B 126 (2007) 544.

Talanta 77 (2008) 858–862

Contents lists available at ScienceDirect

Talanta

journal homepage: www.elsevier.com/locate/talanta

Optimization of hydroxyl radical formation using TiO_2 as photocatalyst by response surface methodology

Sandra A.V. Eremia[a,c], Dominique Chevalier-Lucia[b], Gabriel-Lucian Radu[a], Jean-Louis Marty[c,*]

[a] Politehnica University of Bucharest, 1-7 Polizu Str., Bucharest, Romania
[b] Univeriste Montpellier II, UMR 120, cc 023, Place Eugene Bataillon, 34095 Montpellier Cedex 5, France
[c] Universite de Perpignan, IMAGES EA 4218 Centre de Phytopharmacie, 52 Avenue Paul Alduy, 66860 Perpignan Cedex, France

ARTICLE INFO

Article history:
Received 27 April 2008
Received in revised form 9 July 2008
Accepted 22 July 2008
Available online 6 August 2008

Keywords:
TiO_2 photocatalysis
Hydroxyl radical
Fluorescence probe
UV light
Experimental design

ABSTRACT

The determination of the optimum parameters for hydroxyl radicals (•OH) formation by a TiO_2 solution has been investigated by measuring the emitted fluorescence after the reaction with terephthalic acid has occurred. After UV irradiation, the terephthalic acid was transformed into 2-hydroxyterephthalic acid whose fluorescence is directly proportional to the generated •OH. Optimization of hydroxyl radicals' formation using TiO_2 as catalyst was carried out by studying the effects of irradiation time, TiO_2 concentration and terephthalic acid concentration on the production of the fluorescent HTA with an experimental design. The aim of our research was to apply response surface methodology as a chemometric method for the optimization of the reaction conditions. The combination of irradiation time, TiO_2 concentration and terephthalic acid concentration was varied at designed points of a central composite rotatable design. The three factors were found to have a significant effect upon the reaction. The optimum conditions for the reaction achievement were estimated to be 10 min for the irradiation time, 25 $\mu g\,mL^{-1}$ TiO_2 concentration and 0.1 $mmol\,L^{-1}$ terephthalic acid concentration. Afterwards, using these parameters the method was applied for the determination of the ability of several plant extract samples to scavenge the formed •OH.

1. Introduction

Oxidative stress has been one of the most studied processes for several years, as during this process there occurs an overproduction of reactive oxygen species (ROS) that lead to the cellular components malfunction and even to cell death. The oxidative stress plays an important role in the initiation step of many diseases like: atherosclerosis, Parkinson's disease, Alzheimer's disease and also in the ageing process [1–3]. The oxidative stress is caused by an imbalance between the rate of oxidative stress production and the rate of repairing or removing of the oxidative damage.

The pro-oxidant species represent highly reactive oxygen or nitrogen species (ROS or RNS), e.g., superoxide anion ($O_2^{\bullet -}$), hydroxyl radical (•OH), hydrogen peroxide H_2O_2, nitric oxide (NO) or peroxynitrite ($ONOO^-$) [4]. The ROS formed in the photocatalytic reaction of TiO_2, especially the hydroxyl radical that shows the highest reactivity, are involved in physiological phenomenon, can cause DNA damage and are able to perturb the cell components thus leading to the oxidative stress [5]. The assessment of free radicals toxicity is a subject of major interest due to the increasing degree and sources of pollution as long as the increasing occurrence of pathologies is associated to the presence of free radicals in living organisms [6–9]. In order to ensure a suitable defence of the living organisms against pathologic injuries induced by free radicals attack, there are used antioxidants. It is well known that antioxidants can answer in many ways to a different radical or oxidant sources [10], therefore, when the efficacy of an antioxidant should assessed attention should be paid to the appropriate way of scavenging the free radicals, because each type of free radical is efficiently "quenched" by a specific antioxidant. The most damaging free radical in living organisms is HO• radical. This could be produced via different pathways, like the Fenton's reaction (Scheme 1), Haber–Weiss cycle [11] or ascorbic acid transformation [12].

Inside the living organisms •OH is formed according to the Fenton's reaction (Scheme 1):

In general •OH could also be produced by (i) irradiation of terephthalic acid (TA) with 254 nm UV, (ii) irradiation with gamma rays and (iii) by the reaction between H_2O_2 and Cu^{2+} [13]. Yang and Guo produced •OH as a result of the reduction of molecular oxygen by Fe (II)–EDTA to form superoxide radical, which then transforms to hydrogen peroxide and Fe (II)–EDTA catalyses its decomposition to •OH [14].

* Corresponding author. Tel.: +33 4 68 66 22 54; fax: +33 4 68 66 22 23.
E-mail addresses: sandraeremia@gmail.com (S.A.V. Eremia), jlmarty@gala.univ-perp.fr (J.-L. Marty).

0039-9140/$ – see front matter © 2008 Elsevier B.V. All rights reserved.
doi:10.1016/j.talanta.2008.07.056

$$Fe^{2+} + H_2O_2 + H^+ \longrightarrow Fe^{3+} + OH^{\bullet} + H_2O$$

Scheme 1. Fenton's reaction.

In our case, •OH is formed by the photocatalysis of TiO_2. Ishibashi et al. produced •OH by lightening a TiO_2 film with UV light and they used coumarin and TA to measure •OH production [15,16].

Response surface methodology (RSM) was lately used in order to optimize the conditions for the photocatalytic degradation of different organic compounds found in wastewaters in the presence of TiO_2 [17–19]. The aim of the present work was to apply the response surface methodology method to a new field, estimation of radical scavenger properties against •OH generated by TiO_2 catalysis using spectrofluorimetry measurements and to optimize the method parameters.

TiO_2 was used to generate hydroxyl radicals via UV irradiation in aqueous solution, the mechanism is shown below, that subsequently should be scavenged by terephthalic acid. Compounds that are able to react with •OH and TA will compete for the scavenging of hydroxyl radicals. Therefore, the antioxidant capacity of different plant extracts was assessed by means of the scavenging ability toward •OH.

The use of TA was made due to several arguments: the measuring technique, fluorimetry (TA product in the reaction with •OH, the HTA can be easily measured using simple fluorimeters and its efficiency of production is higher than in the case of formation of other products) and the avoidance of isomer interferences, because a single isomer is formed in the reaction [20].

Response surface methodology was used in order to optimize the factors influencing the fluorescence signal that is directly proportional to the quantity of formed •OH. RSM is a method that combines mathematics and statistics in order to analyse the relationships between several variables and one or more response variables.

The parameters chosen to be optimized were irradiation time, TiO_2 and TA concentration, because these are the factors that are influencing the production of •OH and the measurement of antioxidant capacity of different compounds able to scavenge these radicals.

2. Experimental

2.1. Materials

The TiO_2 nanoparticles (Degussa P25), purchased from Germany, were suspended into aqueous solution (0.5 mg mL^{-1}) and sonicated for 15 min before use. Na_2HPO_4, Trolox, gallic acid and vitamin C were supplied by Sigma–Aldrich, while NaCl, terephthalic acid and lipoic acid from Fluka. NaH_2PO_4 was supplied by Prolabo.

Phosphate buffer saline (PBS), pH 7.4, was sodium phosphate dissolved in 10 mmol L^{-1} NaCl to a final concentration of 50 mmol L^{-1}.

Terephthalic acid was dissolved in a minimum volume of 1 mol L^{-1} NaOH, underwent sonication until complete dissolution and adjusted with PBS at a concentration of 1 mmol L^{-1}. 6-Hydroxyl-2,5,7,8-tetramethylchroman-2-carboxylic acid (Trolox), gallic acid, vitamin C and lipoic acid were dissolved in PBS (pH 7.4) at a concentration of 5 mmol L^{-1}.

The plant extract samples were dissolved in PBS at a concentration of 1 mg mL^{-1} and submitted to sonication for 15 min.

2.2. TiO_2 photocatalysis

•OH is formed by the photocatalysis of TiO_2. The P25 formulation of TiO_2 from Degussa Chemical Company is the most widely used photocatalyst. It is produced [21] at high temperature flame hydrolysis of $TiCl_4$ in the presence of hydrogen and oxygen. Afterwards the obtained TiO_2 is treated with steam in order to remove HCl.

$$TiO_2 + h\nu \longrightarrow e^-_{CB} + h^+_{VB}$$

Scheme 2. TiO_2 photocatalysis.

$$H_2O_{ads} + h^+_{VB} \longrightarrow H^+ + HO\bullet$$
$$\downarrow$$
$$H^+ + HO^-$$

Scheme 3. Reaction between the produced holes and the hydroxide ions.

$$e^-_{CB} + O_2 \longrightarrow O_2^{\bullet -}$$
$$2O_2^{\bullet -} + 2H_2O \longrightarrow 2\,OH\bullet + 2\,OH^- + O_2$$

Scheme 4. Reaction between the electrons and the molecular oxygen.

TiO_2, in the anatase form, is a photocatalyst under ultraviolet light due to the fact that it is a semiconductor with a band gap of 3.2 eV. Irradiation of TiO_2 nanoparticles with photons of energy equal to or greater than the band gap energy, results in the promotion of an electron from the valence band to the conduction band, leaving a hole behind (Scheme 2) [22].

The positive holes oxidises water to produce OH• that are known to be the most oxidising species (Scheme 3).

The electrons react with adsorbed molecular oxygen to produce superoxide anion radical, which then forms more OH• (Scheme 4). OH• generated by the TiO_2 photocatalyst are very potent oxidants [21] and are nonselective in reactivity.

2.3. Instrumental and operating conditions

Fluorescence was used to monitor the formation of HTA following the scavenging of •OH by terephthalic acid and the addition reaction on the benzene ring as shown in Scheme 5. The light source for the excitation of TiO_2 was a 15-W UV lamp (Fischer Bioblock Scientific). The excitation wavelength needed to produce the hydroxyl radicals was 365 nm. These radicals react with terephthalic acid and generate HTA that emits fluorescence at 424 nm after excitation at 315 nm. The fluorescence spectra of generated HTA were measured using a Safas Monaco fluorescence spectrophotometer.

After the optimization of reaction conditions using the experimental plan, the standard aqueous solutions and the plant extract solutions were mixed with TiO_2 (25 μg mL^{-1}) and with terephthalic acid (0.1 mmol L^{-1}) and then submitted to UV irradiation for 10 min. Immediately after the irradiation the solutions were transferred for fluorescence measurements and the antioxidant capacity

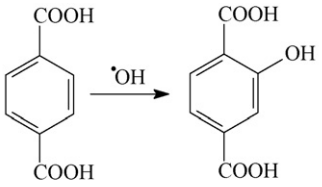

Terephthalic acid 2-Hydroxyterephthalic acid

Scheme 5. The addition of hydroxyl radical to the benzenic ring.

Table 1
Independent variables and their levels used for this study

Variables	Symbols coded	Levels				
		-1.68 ($-\alpha$)	-1	0	1	1.68 (α)
Irradiation time (min)	X_1	1.6	5.0	10.0	15.0	18.4
TiO_2 concentration ($\mu g\,mL^{-1}$)	X_2	8.18	15.00	25.00	35.00	41.83
Terephthalic acid concentration ($mmol\,L^{-1}$)	X_3	0.015	0.050	0.100	0.150	0.184

of the plant extracts is expressed as Trolox equivalents. Trolox is the water soluble vitamin E like compound, which is commonly used as reference compound when antioxidant capacity (radical scavenger properties) has to be evaluated [23,24].

2.4. Experimental design and data analysis

Response surface methodology was adopted to study the simultaneous effect of the irradiation time, TiO_2 and terephthalic acid concentrations on the fluorescence signal. Preliminary experiments were carried out to determine the experimental domain; therefore five levels of each variable were selected to cover the experimental conditions. The experiments were based on a three-factor central composite rotatable design with six star points ($\alpha = 1.68$) and five replicates of the central point. The factors selected as independent variables, their real values and corresponding codified levels are shown in Table 1. The complete design consisted of 19 and the associated responses are synthesized in Table 2. Three replications were carried out for all design points.

The variables were coded according to the equation:

$$x_i = \frac{X_i - X_0}{\Delta X_i}, \quad i = 1,\ 2,\ 3$$

where x_i is the independent variable coded value, X_i is the independent variable real value, X_0 is the independent variable real value on the centre point and ΔX_i is the step changing value.

Statistica 7.1 (Statsoft France, Maisons-Alfort, France) was used to fit the data to the second-order equations:

$$Y = b_0 + \sum_{i=1}^{3} b_i X_i + \sum_{i=1}^{3} b_{ii} X_i^2 + \sum_{i<j=1}^{3} b_{ij} X_i X_j$$

where Y is the response variable, b_0, b_i, b_{ii} and b_{ij} are intercept, linear, quadratic and interaction coefficients, respectively, X_i and X_j are independent variables.

Table 2
Response surface central composite design and experimental and predicted responses (average of three measurements excepted for the central point which was repeated 15 times at all)

Coded variables			Fluorescence intensity	
X_1	X_2	X_3	Experimental	Predicted
−1	−1	−1	16.67 ± 0.86	11.52
1	−1	1	39.56 ± 1.00	40.78
0	0	0	38.38 ± 2.09[a]	35.15
1	1	1	61.13 ± 1.51	57.62
0	1.682	0	45.06 ± 1.01	41.81
−1.682	0	0	11.74 ± 0.50	14.26
1	−1	−1	35.98 ± 3.96	31.74
0	0	−1.682	17.10 ± 0.88	18.44
−1	−1	1	18.68 ± 0.48	11.32
1	1	−1	41.95 ± 0.94	40.62
−1	1	−1	23.68 ± 0.72	20.40
0	−1.682	0	17.72 ± 1.07	20.18
−1	1	1	26.00 ± 4.62	28.16
1.682	0	0	56.98 ± 1.52	56.04
0	0	1.682	34.69 ± 2.17	32.57

[a] Average of 15 measurements.

Table 3
Coefficients of regression with standard deviation associated

Variable	Standard deviation	Coefficient
X_1	0.6338	12.4231
X_2	0.6338	6.4326
X_3	0.6338	4.1498
X_1X_1	0.6339	−0.4236
X_1X_2	0.8281	1.6596
X_1X_3	0.8281	2.3029
X_2X_2	0.6339	−1.4754
X_2X_3	0.8281	1.9887
X_3X_3	0.6339	−3.4188

$R^2 = 0.9280$; adjusted $R^2 = 0.9104$.

The fluorescence was taken as the dependent variable or the response, Y.

3. Results and discussion

3.1. Model fitting and statistical analysis

The coefficients of the independent variables in the model predicting fluorescence signal and its corresponding determination coefficient R^2 are shown in Table 3. An empirical second-order polynomial expressing the fluorescence response as a function of the independent variables was proposed by the following equation:

$$Y = 37.15 + 12.42X_1 + 6.43X_2 + 4.14X_3 - 0.42X_1^2 - 1.47X_2^2 - 3.42X_3^2 + 1.65X_1X_2 + 2.30X_1X_3 + 1.99X_2X_3 \quad (1)$$

where Y is the fluorescence and X_1, X_2 and X_3, the independent variables as described in Table 1.

The response surface model developed in this study for predicting fluorescence was adequate as indicated by the value of the determination coefficient $R^2 = 0.9280$ (a good agreement between experimental data and predicted data). Moreover, the value of adjusted determination coefficient Adj $R^2 = 0.9104$ was very high.

Analysis of variance (ANOVA) summary is shown in Table 4. The degree of significance of each factor is represented in this table by its p-value; when a factor has a p-value smaller than 0.05, it influences the fluorescence response at a confidence level of 0.95. It was observed from Table 4 that the linear effect of all the three variables, i.e., irradiation time, TiO_2 and TA concentration ($p = 0.000$)

Table 4
Variance analysis of factor effects

Variable	DF	F-value	$p > F$
X_1	1	384.1490	0.000000
X_2	1	102.9938	0.000000
X_3	1	42.8631	0.000000
X_1X_1	1	0.4464	0.507475
X_1X_2	1	3.9676	0.052474
X_1X_3	1	7.7327	0.007891
X_2X_2	1	5.4156	0.024515
X_2X_3	1	5.7668	0.020524
X_3X_3	1	29.0781	0.000002
Blocks	2	0.2891	0.750286

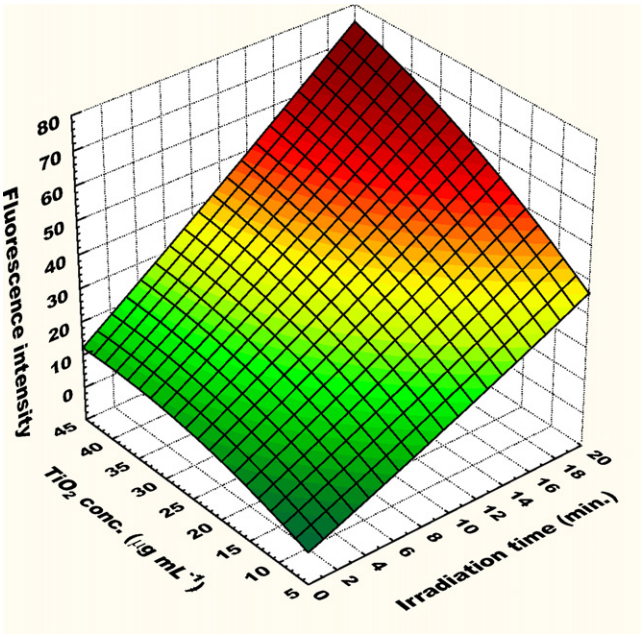

Fig. 1. Response surfaces for interaction between irradiation time (X_1) and TiO_2 concentration (X_2) with a terephthalic acid concentration fixed equal to 0.

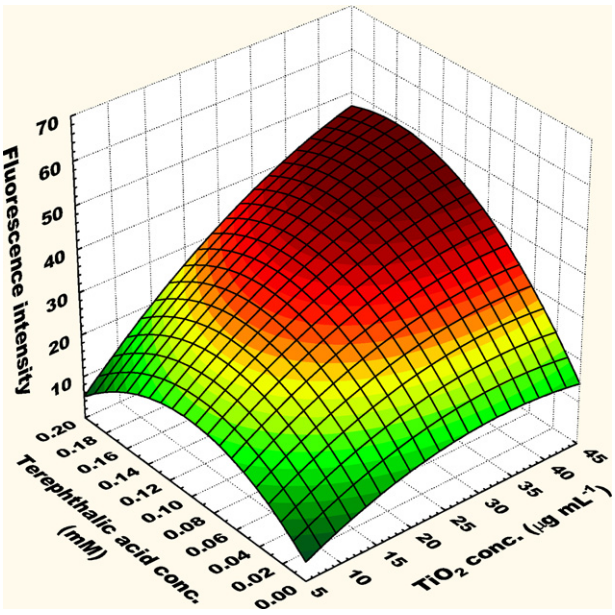

Fig. 3. Response surfaces for interaction between TiO_2 concentration (X_2) and terephthalic acid concentration (X_3) with a time fixed equal to 0.

was highly significant for fluorescence responses. The quadratic effects of TiO_2 and TA concentrations ($p < 0.05$) were also significant for this response. Two interaction effects, namely irradiation time and TA concentration and TiO_2 and TA concentrations, respectively, appeared as significant ($p < 0.05$). Besides, no significant effect was observed concerning the blocks ($p = 0.75$).

3.2. Analysis of response surfaces

The three-dimensional response surface plots were used in order to determine the interaction between the three variables. Figs. 1–3 show the relative effects of any two variables on fluorescence signal, keeping the third variable at a constant level.

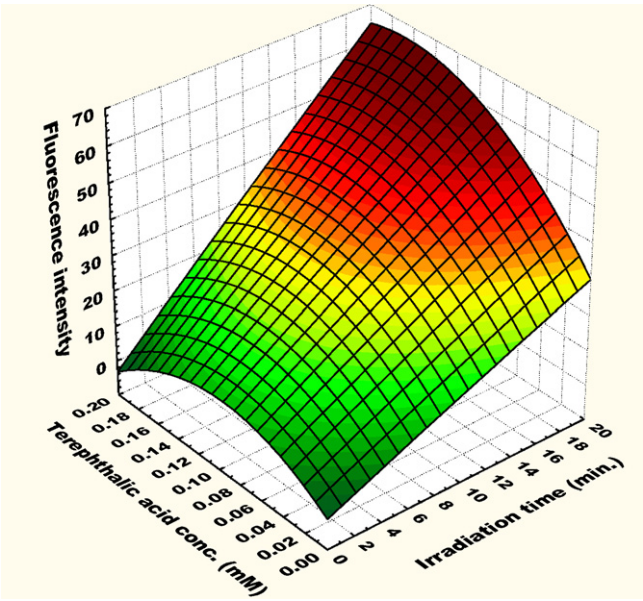

Fig. 2. Response surfaces for interaction between irradiation time (X_1) and terephthalic acid concentration (X_3) with a TiO_2 concentration fixed equal to 0.

These constant levels represent the central levels of each variable taken in the respective considered ranges. The coordinates of the central point in the highest contour level in each of these figures will correspond to the optimum conditions of the respective variables. Particularly, the response surface curves showed that the fluorescence intensity increased with the increase of time reaction, TiO_2 and terephthalic acid concentrations. Besides, the shapes of response plots indicate the nature and extend of the interactions. Prominent interactions are shown by the elliptical nature of response surfaces as in the case of irradiation time and terephthalic acid concentration and TiO_2 and terephthalic acid concentration interactions (Figs. 2 and 3). Less prominent and negligible interactions appeared with more circular response surfaces as in the case of irradiation time and TiO_2 concentration interaction (Fig. 1).

Fig. 2 shows that with the increase in terephthalic acid concentration, the fluorescence signal increases with the increase in irradiation time. Therefore, the optimum value of the two factors, the terephthalic acid concentration and irradiation time is the value of the central point, namely 0.1 mmol L^{-1} and 10 min of irradiation. These values are taken and not higher ones in order to minimize the time and reagents consumption.

Fig. 3 shows the interaction effect of TiO_2 concentration and TA concentration on the fluorescence signal. As in the case of the interaction effects of irradiation time and TA concentration, the optimum values were found to be the ones of the central point, 25 μg mL^{-1} TiO_2 and 0.1 mmol L^{-1}

3.3. Fluorimetric assay

Starting from the conclusions raised by RSM, the following conditions are necessary to obtain a significant intensity of fluorescence and to minimize time reaction and reagents amount: 10 min of reaction, 25 μg mL^{-1} TiO_2 concentration and 0.1 mmol L^{-1} terephthalic acid. The fluorimetric assay was based on measuring the fluorescence intensity of HTA formed as a result of the reaction between TA and the hydroxyl radicals produced by TiO_2 catalysis.

If another molecule known to react with •OH is introduced in the reaction, this molecule will compete in the reaction between TA and •OH and therefore a decrease of the fluorescence signal

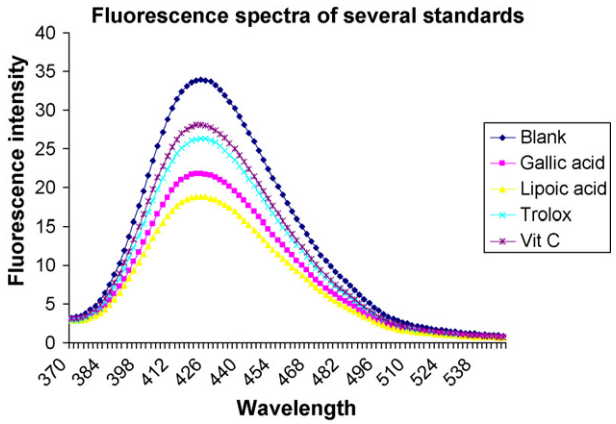

Fig. 4. Fluorescence spectra of Trolox, gallic acid, lipoic acid and vitamin C.

Table 5
Antioxidant capacity expressed as Trolox equivalents for the plant extracts

Sample	TEAC (μmol) g^{-1} sample
1 SOUPI 5	4019
2 SOUPI 5	2431
3 SOUPI 5	3304
Soybean isoflavones	
Crude	827
Purified	0
Mint flavonoids	
Crude	5428
Purified	4344

due to the decrease in the formed HTA will be obtained. Fig. 4 shows the fluorescence spectra for HTA alone and HTA in presence of several standards known to have scavenging properties against hydroxyl radical, like: vitamin C, Trolox, lipoic acid and gallic acid. As it can be noticed, the lipoic acid has the highest ability to scavenge •OH. For further measurements of the plant extracts, Trolox was used as standard and the antioxidant capacity was expressed as Trolox equivalents, as Trolox is known to be the most used reference antioxidant.

Several plant extracts – previously characterised as composition by partner that supplied the samples – known to have antioxidant properties were tested according to this method and each experiment was performed in triplicate and the antioxidant capacity was calculated according to the following relationship:

$$\text{TEAC} = n_{\text{Tr}} f \frac{F_{\text{blank}} - F_{\text{sample}}}{F_{\text{blank}} - F_{\text{Trolox}}} \frac{1}{m}$$

where n_{Tr} is the Trolox number of moles in the cell, f is the dilution factor, F_{blank} is the average fluorescence intensity measured at 424 nm for the blank, F_{sample} is the average fluorescence intensity measured at 424 nm for the real sample, F_{Trolox} is the average fluorescence intensity measured at 424 nm for Trolox and m is the mass of dry base.

The results are presented in Table 5. As could be noticed, the highest values of the antioxidant capacity were obtained in the case of the mint extracts, followed by those obtained from *Salvia officinallis* and a very low scavenging activity was found in the case of soybean isoflavone extracts, as expected. This pattern is normal due to the structure of the analysed compounds, the polyphenols and flavonoids being well known to be able to scavenge the hydroxyl radicals.

4. Conclusions

Response surface methodology, which combines factorial designs and regression analysis, represents a useful method for optimizing the experimental conditions needed for the determination of antioxidant capacity of different aqueous extracts. Out of three main factors and three potential interactions researched, irradiation time, TiO_2 concentration, terephthalic acid concentration, irradiation time × terephthalic acid concentration and TiO_2 concentration × terephthalic acid concentration were the factors and the interactions that significantly affect the fluorescence. Good agreement was found between the values predicted by the experimental design and the values obtained experimentally. The selected optimal parameters were 10 min for the irradiation time, 25 μg mL^{-1} TiO_2 concentration and 0.1 mmol L^{-1} terephthalic acid concentration. The method relies on the fluorescent signal generated by the hydroxylation of terephthalic acid with •OH formed during TiO_2 photocatalysis. It could be stressed that another advantage of the fluorescence method is that it is rapid, efficient, highly sensitive and needs only simple standards instrumentation. Moreover, once formed, the fluorescent product is stable.

Acknowledgments

This financial support of the EU through NUTRA-SNACKS project contract FOOD-2006-0230244 is gratefully acknowledged. Authors acknowledge Pisa University, Italy for providing the alcoholic extracts.

References

[1] J.K. Willcox, S.L. Ash, G.L. Catignani, Crit. Rev. Food Sci. 44 (2004) 275–295.
[2] D. Huang, B. Ou, R.L. Prior, J. Agric. Food Chem. 53 (2005) 1841–1856.
[3] K.F. Gey, Biochem. Soc. Trans. 18 (1990) 1041–1045.
[4] A. Ruffien–Ciszak, P. Gros, M. Comtat, A.M. Schmitt, E. Questel, C. Casas, D. Redoules, J. Pharm. Biomed. Anal. 40 (2006) 162–167.
[5] J. Liu, B. Su, G. Lagger, P. Tacchini, H.H. Girault, Anal. Chem. 78 (2006) 6879–6884.
[6] J.M.C. Gutteridge, Free Radical Res. Commun. 19 (1993) 141–158.
[7] B.M. Ames, M.K. Shigenaga, T.M. Hagen, Proc. Natl. Acad. Sci. U.S.A. 90 (1993) 7915–7922.
[8] A. Ghiselli, M. Serafini, F. Natella, C. Scaccini, Free Radical Biol. Med. 29 (2000) 1106–1114.
[9] M. Martínez-Cayuela, Biochimie 77 (1995) 147–161.
[10] R.L. Prior, X. Wu, K. Schaich, J. Agric. Food Chem. 53 (2005) 4290–4302.
[11] S. Xianglin, N.S. Dalal, Arch. Biochem. Biophys. 292 (1992) 323–327.
[12] D. Nowak, G. Piasecka, A. Antczak, T. Pietras, Biomed. Biochim. Acta. 50 (1991) 265–272.
[13] J.C. Barreto, G.S. Smith, N.H.P. Strobel, P.A. McQuillin, T.A. Miller, Life Sci. 56 (1994) 89–96.
[14] X.-F. Yang, X.-Q. Guo, Analyst 126 (2001) 928–932.
[15] K.-i. Ishibashi, A. Fujishima, T. Watanabe, K. Hashimoto, J. Photochem. Photobiol. A: Chem. 134 (2000) 139–142.
[16] K.-i. Ishibashi, A. Fujishima, T. Watanabe, K. Hashimoto, Electrochem. Commun. 2 (2000) 207–210.
[17] J. Fu, Q. WU, Taiyangneng Xuebao/Acta Energiae Solaris Sinica 29 (2008) 152–157.
[18] S. Merabet, D. Robert, J.-V. Weber, M. Bouhelassa, S. Benkhanouche, Environ. Chem. Lett. (in press) 1–5.
[19] V.A. Sakkas, P. Calza, C. Medana, A.E. Villioti, C. Baiocchi, E. Pelizzetti, T. Albabis, Appl. Catal. B: Environ. 77 (2007) 135–144.
[20] M. Saran, K.H. Summer, Free Radical Res. 31 (1999) 429–436.
[21] A. Mills, S. Le Hunte, J. Photochem. Photobiol. A: Chem. 108 (1997) 1–35.
[22] K. Nagaveni, M.S. Hegde, N. Ravishankar, G.N. Subbanna, G. Madras, Langmuir 20 (2004) 2900–2907.
[23] G. Cao, R.L. Prior, Method. Enzymol. 299 (1999) 50–62.
[24] C. Rice-Evans, N.J. Miller, P.G. Bolwell, P.M. Bramley, J.B. Pridham, Free Radical Res. 22 (1995) 375–383.

Talanta 77 (2008) 876–881

Contents lists available at ScienceDirect

Talanta

journal homepage: www.elsevier.com/locate/talanta

Electrochemical immunosensor designs for the determination of *Staphylococcus aureus* using 3,3-dithiodipropionic acid di(*N*-succinimidyl ester)-modified gold electrodes

Vanessa Escamilla-Gómez, Susana Campuzano, María Pedrero, José M. Pingarrón*

Dpto. Química Analítica, Facultad de CC. Químicas, Universidad Complutense de Madrid, E-28040 Madrid, Spain

ARTICLE INFO

Article history:
Received 5 May 2008
Received in revised form 16 July 2008
Accepted 22 July 2008
Available online 5 August 2008

Keywords:
S. aureus
DTSP SAM
Protein A-HRP
antiRbIgG-HRP
Screen-printed electrodes

ABSTRACT

The preparation of novel *Staphylococcus aureus* (*S. aureus*) amperometric immunosensing designs based on the covalent immobilization of RbIgG at gold electrodes using the heterobifunctional cross-linker 3,3-dithiodipropionic acid di(*N*-succinimidyl ester) (DTSP), are reported. Two different competitive immunosensing configurations have been tested and compared. In the first one, protein A-bearing *S. aureus* cells and HRP-labelled antiRbIgG compete for immobilized RbIgG binding sites, while in the second case HRP-labelled protein A was used. In both cases, the evaluation of the developed immunosensors performance was accomplished through the monitoring at 0.00 V (vs. Ag/AgCl) of the catalytic current originated after addition of hydrogen peroxide, using tetrathiafulvalene as redox mediator entrapped at the modified electrode surface by cross-linking with glutaraldehyde. Optimization of variables concerning the composition of the immunosensors as well as the detection conditions was carried out in 0.1 M NaAc/0.1 M NaCl buffer of pH 5.6. The configuration that employed antiRbIgG-HRP resulted in better analytical characteristics, with a detection limit of 1.4×10^4 cells mL^{-1} for *S. aureus* cells submitted to wall lyses by ultrasonic treatment. This immunosensor design was also evaluated using gold screen-printed electrodes in order to reduce the analysis time and cost. In this case, a limit of detection of 3.7×10^2 cells mL^{-1} and a dynamic range from 1.3×10^3 to 7.6×10^4 cells mL^{-1} was obtained. A RSD value of 10.5% was found for the responses to 9.6×10^3 *S. aureus* cells mL^{-1} obtained with seven different Au/SPEs-immunosensors. These disposable immunosensors were applied to the quantification of *S. aureus* in milk spiked at two concentration levels, 1.2×10^3 and 4.8×10^3 cells mL^{-1}, with good recoveries.

1. Introduction

Nowadays, there is a growing demand for fast, reliable, sensitive and accurate methods to detect the presence of pathogen microorganisms in environmental and food samples. The incidence of foodborne pathogens disease constitutes an increasing public health problem in many countries of the world [1]. In particular, food poisoning by *Staphylococcus aureus* (*S. aureus*), one of the major pathogens in humans, is characterized by sudden onset of symptoms including nausea, vomiting, abdominal cramps, and diarrhoea within 2–6 h after ingestion of toxin-contaminated foods [2]. Moreover, the implementation of the Hazard Analysis Critical Control Point (HACCP) system to ensure food safety through the identification and control of specific hazards has increased the demand for tests that can be completed within hours and enable processors to take quick corrective actions when necessary [3].

Immunological biosensors do not require large sample volumes or toxic solvents for analysis, and are also characterized by a minimal sample preparation, low reagent consumption, high specifity in complex matrices, and easy miniaturization and automation in portable devices [4]. Although several electrochemical immunosensors for the detection of foodborne pathogenic bacteria have been reported in literature, only a few of them were used for the quantification of *S. aureus* [5–7]. Furthermore, the application of electrochemical immunosensors to food analysis is not too extended, and most of the approaches described in literature [8–11] required a pre-enrichment step to be useful in real samples analysis [3].

Several strategies have been employed to improve stability and sensitivity of electrochemical immunosensors. Hence, physical and chemical adsorption has been proposed for preparing oriented antibody molecular layers on solid matrix surfaces [12–15]. Also, methods to minimize the distance between the transducer surface and the immobilized layer of antibodies have been proposed [16,17]. Moreover, self-assembled monolayer (SAM) technology provides a powerful tool to obtain monomolecular films of

* Corresponding author. Fax: +34 9139 44329.
E-mail address: pingarro@quim.ucm.es (J.M. Pingarrón).

0039-9140/$ – see front matter © 2008 Elsevier B.V. All rights reserved.
doi:10.1016/j.talanta.2008.07.045

biological molecules on various substrates, and has been used to prepare antibody molecular layers on solid surfaces using thiolated antibodies [18] or exploiting carboxyl–amine coupling of the antibody over the SAMs of thiol or sulphide compounds [19–23,11]. In this context, we have reported recently on electrochemical immunosensors for the determination of *S. aureus* using 3-mercaptopropionic acid (MPA)-modified gold electrodes [11,23].

In this work novel approaches for the construction of *S. aureus* amperometric immunosensors with improved analytical performance are reported. These approaches make use of the heterobifunctional cross-linker 3,3 dithiodipropionic acid di(*N*-succinimidyl ester) (DTSP), which forms spontaneously covalent adducts with gold and specifically reacts with the primary amino group of antibodies through ester groups [24], and which, to our knowledge, has not been used in the development of electrochemical immunosensors until now. RbIgG antibodies were covalently immobilized onto DTSP-modified gold electrodes, and two competitive immunosensor configurations were evaluated and compared: (a) competition for the binding sites of RbIgG between protein A-bearing *S. aureus* cells and antiRbIgG labelled with horseradish peroxidase (HRP), and (b) between protein A-bearing *S. aureus* cells and protein A labelled with HRP. Protein A can be considered as a specific product of *S. aureus* and about 99% of the bacterial strains contain this protein [2].

One important drawback of immunosensors using conventional electrodes is the need to use a new electrode for each assay because regeneration procedures are usually time-consuming, can deteriorate the binding capacity, and may lead to stability problems together with a decrease in the sensor's lifetime. In order to minimize these disadvantages, the use of low cost mass-produced screen-printed electrodes (SPEs) has recently been proposed [3]. Accordingly, in order to improve the usefulness of the most favourable approach checked in this work, its performance was also evaluated using gold SPEs (Au/SPEs). This disposable configuration was finally employed for the analysis of non-diluted milk samples spiked with known amounts of the target bacteria.

2. Experimental

2.1. Apparatus and electrodes

Amperometric measurements were carried out with an ECO Chemie Autolab PSTAT 10 potentiostat using the software package GPES 4.9 (General Purpose Electrochemical System). A P-Selecta ultrasonic bath and a P-Selecta Agimatic magnetic stirrer were also used.

A XBAS-NS-AU gold disk electrode ($\phi \sim 3$ mm) was used as electrode substrate to be modified. A BAS MF-2052 Ag/AgCl/KCl (3 mol L^{-1}) reference electrode and a Pt wire counter electrode were also employed. A 10 mL glass electrochemical cell was used in the experiments.

Gold screen-printed electrodes (Au/SPEs) purchased from DropSens were also used. The format of these SPEs includes a gold disk-shaped (12.6 mm^2) working electrode, a silver pseudo-reference electrode and a gold counter electrode, all of them screen-printed on a ceramic substrate (3.4 × 1.0 cm) and subjected to high-temperature curing.

2.2. Reagents and solutions

A 2 M KOH (Panreac) solution, prepared in deionized water, was used for the pretreatment of the gold disk electrode. A 0.5 M H_2SO_4 solution containing 10 mM KCl prepared in deionized water was used for the pretreatment of the Au/SPEs.

A 4 mM 3,3′-dithiodipropionic acid di(*N*-succidimidyl ester) (DTSP) (Fluka) solution, prepared in dimethylsulfoxide (DMSO) (Scharlau) was employed for the covalent antibody immobilization on the gold electrodes.

A 1 mg mL^{-1} IgG from rabbit serum (Sigma) solution was prepared in 150 mM NaCl. Solutions of 4 μg mL^{-1} anti-rabbit IgG (whole molecule) peroxidase conjugate (Sigma), 0.5 mg mL^{-1} protein A peroxidase-labelled (Sigma) and 2.4% (w/v) *S. aureus* cells (Sigma; 10% wet w/v of essentially non-viable *S. aureus* Cowan strain cells in 0.04 M sodium phosphate buffer, pH 7.2, 0.15 M sodium chloride containing 0.05% sodium azide) were prepared in 0.05 M phosphate buffer of pH 7.0. Moreover, a 0.5 M tetrathiafulvalene (TTF, Aldrich) solution prepared in acetone, a 25% glutaraldehyde (Scharlau) solution, and a 2% BSA solution in 0.05 M NaH_2PO_4/Na_2HPO_4 containing 0.15 M NaCl and 0.05% Tween 20 (pH 7.0) were also used.

Hydrogen peroxide (35% v/v) was purchased from Scharlau, and the substrate solutions were prepared daily in a 0.1 M acetate buffer solution containing 0.1 M NaCl, pH 5.6.

All chemicals used were of analytical-reagent grade, and water was obtained from a Millipore Milli-Q purification system. Semi-skimmed milk samples were purchased in a local supermarket.

2.3. Procedures

2.3.1. Preparation of DTSP-modified gold electrodes

Before carrying out the deposition of the DTSP monolayer, the gold disk electrode (AuE) was pretreated as described previously [25]. The Au/SPEs were pretreated by placing a 50-μL drop of a 0.5 M H_2SO_4 solution containing 10 mM KCl on the electrodes surface. Then, 10 cyclic voltammograms from 0.00 to 1.25 V were recorded at a scan rate of 100 mV s^{-1}, and the electrodes were washed with deionised water.

DTSP monolayers were formed by immersion of the clean AuE in a 4 mM DTSP solution in DMSO for 2 h or by deposition of a 50-μL drop of this solution on the Au/SPEs and allowing the reaction to proceed for 2 h. Then, the modified electrodes were rinsed with acetone and deionised water.

2.3.2. Construction of the immunosensors

RbIgG was covalently attached onto the DTSP SAM. DTSP is adsorbed onto the gold electrode surface through its disulfide groups. The terminal succinimidyl groups become then exposed to the solution allowing covalent immobilization of amine groups of the antibody.

Two 5 μL-drops of a 1 mg mL^{-1} RbIgG solution were deposited on the DTSP-modified gold electrode (waiting in between drops for drying of the previous one at ambient temperature). Once the electrode surface had dried out, it was washed for 5 min in 0.05 M phosphate buffer of pH 7.0 in order to remove non-covalently immobilized RbIgG onto the DTSP-modified gold electrode. Then, a 3-μL drop of a 0.5 M TTF solution was deposited on the RbIgG-DTSP-modified gold electrode and let to dry at ambient temperature. The mediator was immobilized by immersion of the modified electrode in a 25% glutaraldehyde solution for 1 h at 4 °C. In this way TTF was entrapped in the three-dimensional aggregate formed.

Prepared immunosensors were subsequently immersed for 5 min in a stirred 2% BSA solution in 0.05 M NaH_2PO_4/Na_2HPO_4 containing 0.15 M NaCl and 0.05% Tween 20 (pH 7.0) to prevent non-specific adsorption of antiRbIgG-HRP or protein A-HRP and *S. aureus* cells on the electrode surface.

2.3.3. Immunoassay procedures

The procedure for the competitive amperometric immunosensor which uses protein A-HRP as marker involved the following steps:

(a) The TTF-RbIgG-DTSP-AuE was incubated for 10 min at room temperature in a stirred 10-mL 0.1 M NaAc, 0.1 M NaCl (pH 5.6) solution containing an aliquot of *S. aureus* cells standard solution.
(b) The *S. aureus*-TTF-RbIgG-DTSP-AuE was immersed for 30 min at room temperature in 10 mL of a stirred solution containing 20 μL of 0.25 mg/mL prot A-HRP in a 0.1 M NaAc and 0.1 M NaCl (pH 5.6) solution.

The procedure for the competitive amperometric immunosensor which uses antiRbIgG-HRP as marker involved the following steps:

(a) The TTF-RbIgG-DTSP-modified gold electrode was immersed at room temperature during 20 min in 10 mL of a stirred 0.1 M NaAc, 0.1 M NaCl (pH 5.6) solution containing an aliquot of *S. aureus* cells standard solution.
(b) The electrode was immersed for 30 min in 10 mL of a stirred 0.1 M NaAc solution containing 0.1 M NaCl (pH 5.6) and an aliquot (1000 μL) of a 4 μg mL^{-1} antiRbIgG-HRP solution.

2.3.4. Amperometric measurements

All measurements were carried out at room temperature. They were performed in stirred solutions by applying the desired potential and allowing the steady-state current to be reached. Once prepared, the immunosensors were immersed in 10 mL of a 0.1 M NaAc/0.1 M NaCl buffer solution (pH 5.6) and the amperometric responses (E_{app} = 0.00 V vs. Ag/AgCl) to the addition of 100 μL or 50 μL of a 0.01 M H_2O_2 solution were recorded for the antiRbIgG-HRP and protein A-HRP immunosensors, respectively.

2.3.5. Staphylococcus aureus cells wall lyses

In order to partially extract protein A from the *S. aureus* cells, two experimental procedures were tested. In the first one, the appropriate portion of the standardized cells suspension, prepared in a 0.1 M NaAc/0.1 M NaCl buffer solution (pH 5.6), was heated for 30 min [7]. Then it was let to cool down to room temperature and, after blocking with BSA as described previously, the corresponding working electrode was incubated in this solution for 20 min.

The second procedure consisted of immersing the *S. aureus* cells solution prepared in a 0.1 M NaAc/0.1 M NaCl buffer solution (pH 5.6) in an ultrasonic bath during 30 min. Then the corresponding modified electrode was incubated in this solution for 20 min after blocking with BSA.

2.3.6. Milk analysis

S. aureus was determined in semi-skimmed milk samples spiked at two concentration levels, 1.2×10^3 and 4.8×10^3 cells mL^{-1}, using the antiRbIgG-HRP labelled immunosensor with DTSP-modified Au/SPEs. The spiked milk sample was immersed in an ultrasonic bath for 30 min. After blocking with BSA as described above the modified electrode was directly incubated in the stirred milk sample for 20 min.

3. Results and discussion

Fig. 1 schematizes the two amperometric immunosensor configurations developed in this work for the determination of *S. aureus*. Relative sizes of the components are not drawn on real scale in order to visualize all of them. Covalent immobilization of RbIgG onto a DTSP SAM was carried out in both cases. Two modes of monitoring the affinity reaction between protein-A bearing *S. aureus* cells and the Fc region of RbIgG [6] were evaluated and compared: (a) using antiRbIg-HRP conjugate, and (b) using protein A labelled with HRP. The competitive immunosensing approach involved competition between *S. aureus* cells and the peroxidase-labelled reagents (antiRbIgG-HRP or protein A-HRP) for the binding sites of RbIgG immobilized onto the electrode surface. In both cases, TTF was employed as mediator of the enzyme reaction with H_2O_2, and the mediator was co-immobilized onto the bioelectrode surface by cross-linking with glutaraldehyde.

Non-specific adsorption of *S. aureus* cells, antiRbIgG-HRP and protein A-HRP was shown to occur onto the TTF-DTSP-AuE. This non-specific adsorption gave rise to measurable amperometric signals in the absence of immobilized RbIgG. Therefore, blocking of electrode sites unmodified with RbIgG was necessary. This blocking was accomplished by immersing of the immunosensor in a 2% BSA solution for 5 min.

3.1. Optimization of the working variables

Optimization of variables concerning the composition of the immunosensors as well as the detection conditions were performed in 10 mL of 0.1 M NaAc/0.1 M NaCl buffer solution (pH 5.6), after additions of 100 μL or 50 μL of a 0.01 M H_2O_2 solution for the antiRbIgG-HRP and the protein A-HRP immunosensors, respectively. These enzyme substrate concentrations were high enough to ensure that the enzyme reaction rate depended only on the enzyme concentration. The applied potential was 0.00 V (vs. Ag/AgCl) and these studies were carried out for a *S. aureus* concentration level of 1.2×10^5 cells mL^{-1}.

Fig. 2 shows that the amperometric signal increased with TTF loading up to a value (1.5 μmol) after which a sharp signal decrease was produced. This behaviour can be attributed to the hindrance of the electron transfer in the presence of large amounts of TTF, which is non-conducting, on the electrode.

Concerning the influence of the amount of antibody immobilized on the electrode surface, the current measured at 0.00 V increased with the antibody loading up to 0.010 mg, after which it practically levelled off. Consequently, 0.010 mg RbIgG were used for subsequent work.

Furthermore, the antiRbIgG-HRP or protein A-HRP solution concentrations used for each one of the tested configurations, as well as the incubation time in these solutions were also evaluated. Fig. 3a shows that although the current increased with the antiRbIgG-HRP concentration in the whole range studied, at concentration values higher than 0.68 μg mL^{-1} a much higher variability in the amperometric signals (n = 5) was observed. Accordingly, a 0.68 μg mL^{-1} concentration was chosen for further work. Similar experiments for the protein A-HRP conjugate (Fig. 3b) showed a stabilization in the amperometric response for concentrations higher than 5.0×10^{-4} mg mL^{-1}, which was chosen for further studies. Regarding both incubation times (data not shown) 30 min were enough to achieve maximum signals in every case.

Since an increase in the *S. aureus* cells loading produced a decrease in the amount of antiRbIgG-HRP or protein A-HRP attached to the RbIgG immobilized onto the electrode surface, the higher the incubation time in the analyte solution, the lower amperometric signals were recorded, with a levelling off for incubation times longer than 20 min for the antiRbIgG-HRP-based immunosensor, and 10 min for the protein A-HRP-based configuration.

Finally, the influence of the applied potential on the hydrogen peroxide amperometric response in the −0.20 to +0.40 V

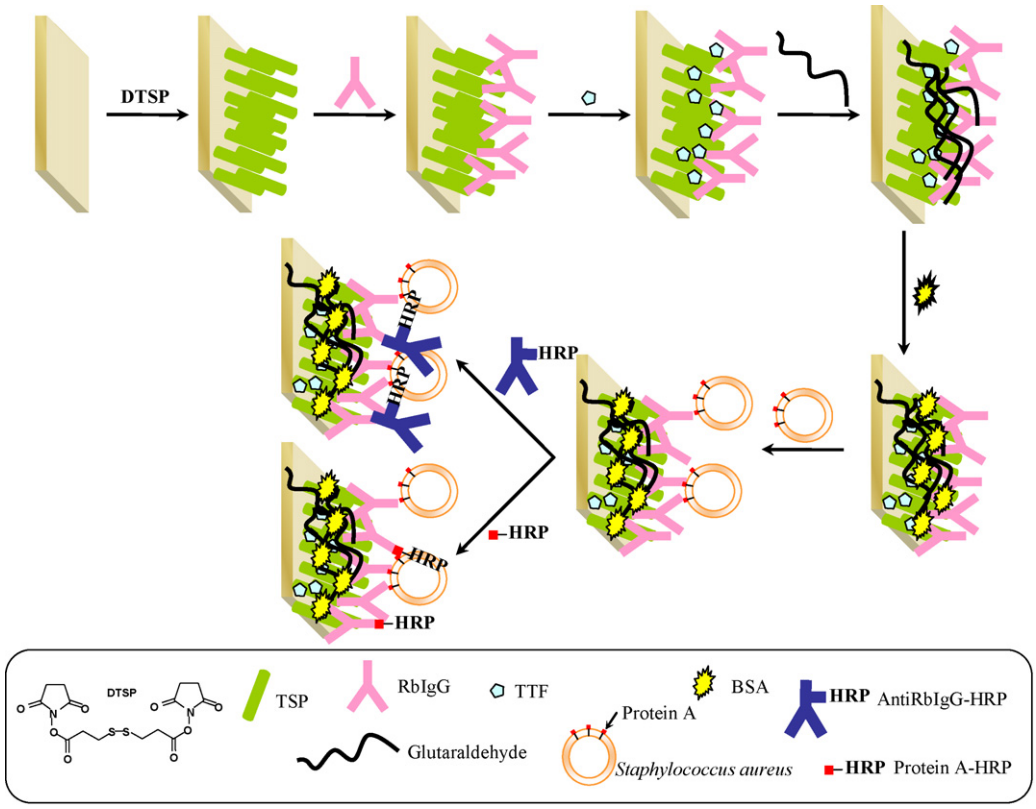

Fig. 1. Scheme showing the developed immunosensors configuration.

gave rise to similar results for both configurations with similar obtained results. The H_2O_2 cathodic current increased rapidly when the applied potential was varied from 0.40 to 0.00 V, reaching a steady state for more negative values. An applied potential value of 0.00 V was chosen for both configurations in order to accomplish a sensitive detection and also to minimize the number of potential interferents able to be reduced at the electrode surface.

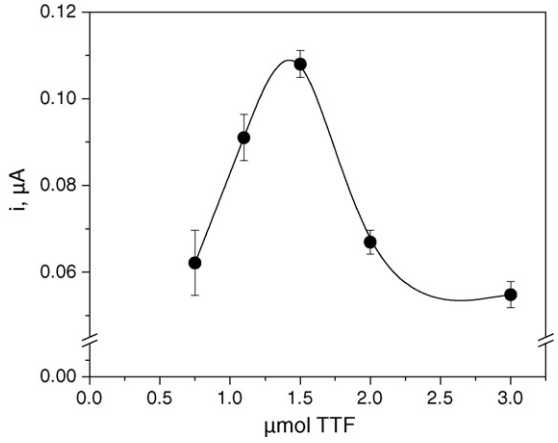

Fig. 2. Amperometric response as function of TTF loading in the antiRbIgG-HRP immunosensor configuration for 1.0×10^{-4} M hydrogen peroxide. Amount of immobilized RbIgG: 0.015 mg; *S. aureus* cells level in the incubation solution: 1.2×10^5 cells mL^{-1}; incubation time in the *S. aureus* cells solution: 20 min; antiRbIgG-HRP incubation solution concentration: 0.04 μg mL^{-1}; incubation time in the antiRbIgG-HRP solution: 10 min. Background solution: 0.1 M NaAc/0.1 M NaCl buffer solution (pH 5.6). E_{app} = 0.00 V.

3.2. Performance characteristics of the developed immunosensors

Firstly the repeatability of the measurements was evaluated by performing 10 successive amperometric measurements in stirred solutions (0.00 V) with each of the developed immunosensors, under the optimized conditions commented above. Repetitive measurements for 1.4×10^6 cells mL^{-1} were carried out with the antiRbIgG-HRP-based configuration while, in the case of the protein A-HRP configuration, the bacteria concentration level checked was of 1.92×10^7 cells mL^{-1}. Relative standard deviation (RSD) values of 7.3% and 4.1% were obtained for the measured steady state currents, respectively, indicating a good repeatability of such measurements with both types of immunosensors.

The reproducibility of the responses obtained with different immunosensors was evaluated. Results for five different antiRbIgG-HRP immunosensors and five different protein A-HRP immunosensors yielded RSD values for the signals corresponding to the *S. aureus* concentration levels mentioned above of 9.1% and 8.4%, respectively. This demonstrated that the fabrication procedure of both immunosensor designs was reliable, allowing reproducible amperometric responses to be obtained with different immunosensors constructed following the developed methodologies.

Calibration curves for *S. aureus*, expressed as the number of *S. aureus* cells per mL, were constructed for each configuration. The obtained responses were normalized according to:

$$s_n = \frac{i - i_\infty}{i_0 - i_\infty}$$

where i is the amperometric signal measured for a given analyte concentration, i_∞ is the signal measured in the presence of an excess of *S. aureus* cells, and i_0 is the blank current in the absence of bacteria. The calibration curves are displayed in Fig. 4. As expected

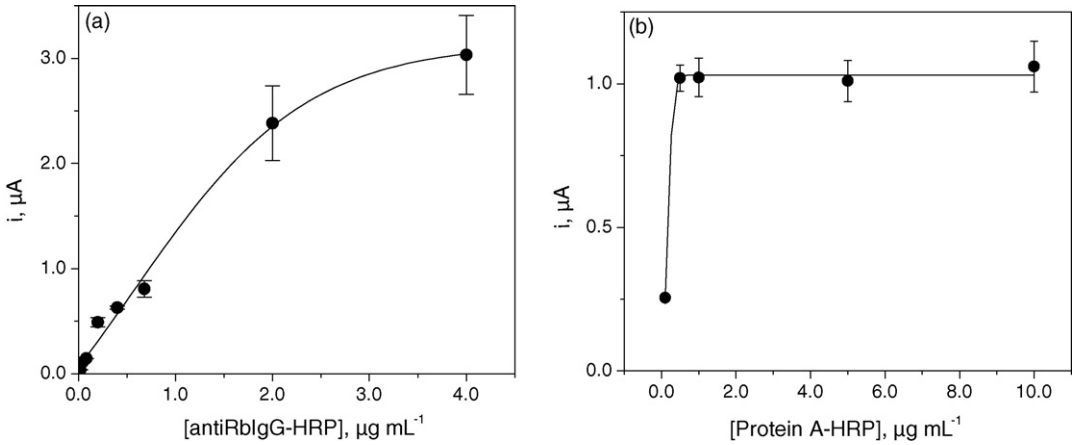

Fig. 3. Amperometric response as function of antiRbIgG-HRP (a), and protein A-HRP (b) solution concentration for 1.0×10^{-4} M (a), and 5.0×10^{-5} M (b) hydrogen peroxide. Amount of immobilized RbIgG: 0.010 mg; *S. aureus* level in the incubation solution: 1.2×10^5 cells mL^{-1} (a), and 9.6×10^5 cells mL^{-1} (b); incubation time in the *S. aureus* cells solution: 20 min; incubation time in the antiRbIgG-HRP or in the protein A-HRP solution: 10 min; other conditions as in Fig. 2.

for competitive configurations, an increase in the amount of *S. aureus* cells causes a smaller possibility of antiRbIgG-HRP or protein A-HRP to compete efficiently for the antibody binding sites, thus resulting in a decrease of the obtained amperometric signals. For the antiRbIgG-HRP-based immunosensor, the IC_{50} value corresponded to 1.5×10^6 cells mL^{-1}, and the limit of detection, calculated as the analyte concentration for which the tracer binding to the antibody was inhibited by 10%, was 3.4×10^5 cells mL^{-1}. The immunosensor showed a dynamic range (normalized signal in the 20–80% range) from 6.6×10^5 to 3.0×10^6 cells mL^{-1}. Regarding the protein A-HRP-based configuration, the IC_{50} value corresponded to 3.7×10^6 cells mL^{-1}, and the limit of detection to 2.4×10^6 cells mL^{-1}. The dynamic range was from 2.8×10^6 to 5.1×10^6 cells mL^{-1}.

As it can be seen, the antiRbIgG-HRP-based configuration allowed a lower limit of detection and a broader dynamic range to be achieved. This limit of detection is comparable with those obtained using other immunosensor designs without cell lyses treatments [11,23,26,27]. Moreover, the immunosensor can be prepared in a reasonable short time because the time needed to prepare DTSP-modified electrodes is much shorter than that required for other SAM-modified gold electrodes [28].

The sensitivity of the developed method can be improved by subjecting bacteria cells to wall lyses in order to increase the availability of protein-A-bearing cell portions, and their diffusion towards the antibodies immobilised on the sensing surface. Two cell disruption procedures involving heat [21] and ultrasonic [29] treatments were evaluated. Accordingly, *S. aureus* cells were treated as described in Section 2.3.5, and subsequently immobilized using the same procedure that for non-treated cells. The calibration graphs obtained with lysed cells are displayed in Fig. 5. Dynamic ranges from 6.8×10^4 to 7.6×10^5, and from 3.0×10^4 to 3.7×10^5 cells mL^{-1}, IC_{50} values of 1.2×10^5 and 1.1×10^5 cells mL^{-1}, and detection limits of 3.5×10^4 and 1.4×10^4 cells mL^{-1}, were obtained for cells subjected to heat treatment and ultrasonic treatment, respectively. As expected, the limits of detection achieved using both cell lyses treatments were lower (about one order of magnitude) than that obtained without cell lyses, which can be attributed to the lyses effects commented above that also lead to a lower steric hindrance. Although the preparation of lysed cells samples increased the assay time in approximately 30 min, the remarkable increase in sensitivity achieved makes this approach worth it.

3.3. *Staphylococcus aureus* immunosensors using gold screen-printed electrodes

One major drawback of the developed immunosensors is that they can only be used for a single *S. aureus* cells concentration level and a new one has to be fabricated for each concentration change or sample. As a consequence, the use of gold screen-printed electrodes was considered for *S. aureus* determination by transferring to this electrode substrate the same antibody immobilization

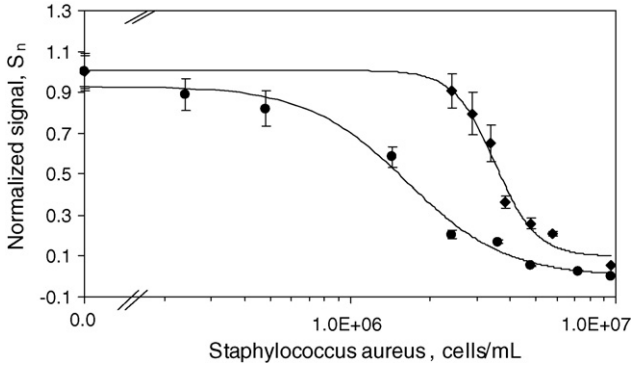

Fig. 4. Calibration curves obtained for *S. aureus* using competitive immunosensors based on: antiRbIgG-HRP (●), and protein A-HRP (♦) configurations.

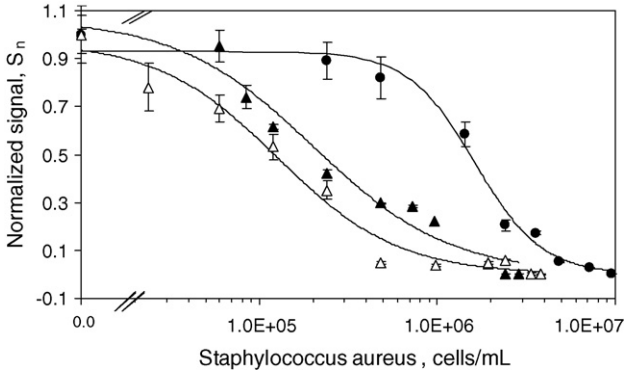

Fig. 5. Calibration curves obtained for *S. aureus* with an antiRbIgG-HRP-based immunosensor: without cells lyses treatment (●), after cells lyses by heat treatment (▲), and after cells lyses by ultrasonic treatment (△). Other conditions as in Fig. 2.

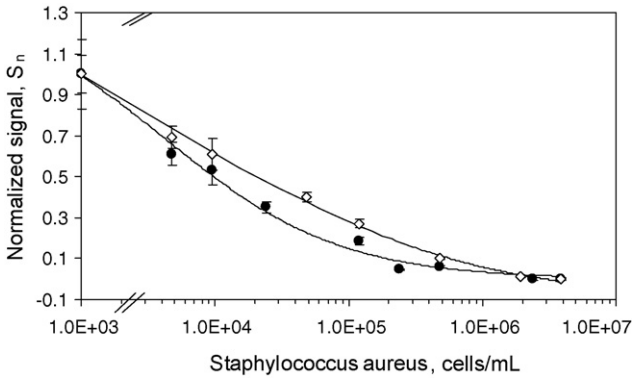

Fig. 6. Calibration curves for *S. aureus* obtained with antiRbIgG-HRP-Au/SPEs: standard solutions (●) and semi-skimmed milk samples (◊).

methodology, immunoassay fundamentals and transduction strategy optimized for the antiRbIgG-HRP configuration. This way, up to fifteen sensors could be prepared and used in each working day resulting in a much lower analysis time at a low cost. Given that the electrode surface of the Au/SPEs was bigger than that of the conventional gold disk electrodes, a higher sensitivity is now expected. Fig. 6 shows the calibration graph obtained after subjecting bacteria to ultrasonication wall lyses. The dynamic range extended from 1.3×10^3 to 7.6×10^4 cells mL^{-1}, with an IC_{50} value of 1.0×10^4 cells mL^{-1}. The limit of detection achieved was of 3.7×10^2 cells mL^{-1}, two orders of magnitude lower than that obtained with conventional gold disk electrodes. Repeatability tests for a *S. aureus* concentration level of 9.6×10^3 cells mL^{-1} resulted in a RSD value of 7.0% for 10 measurements with the same sensor. The reproducibility of the responses obtained with seven different Au/SPEs immunosensors was also tested. A RSD value for the same *S. aureus* concentration level of 10.5% was obtained, which can be considered as acceptable for this kind of disposable immunosensor.

The antiRbIgG-HRP-Au/SPEs were applied to the determination of *S. aureus* in semi-skimmed milk samples. Milk not containing bacteria was spiked at two *S. aureus* concentration levels: 1.2×10^3 and 4.8×10^3 cells mL^{-1}. The samples were subjected to the ultrasonication cell lyses procedure as specified in Section 2.3.6. Thereafter, a calibration graph for *S. aureus* cells in milk was constructed over the 1.7×10^3 to 3.8×10^6 cells mL^{-1} range following the same methodology that for standard solutions (see Fig. 6). The similarity of this calibration plot with respect to that obtained with *S. aureus* cells standards prepared in buffer solution, suggested the possibility of performing direct *S. aureus* determination in milk with no need for dilution or sample treatment. The calculated limit of detection in milk, according to the criterion mentioned previously, 3.8×10^2 cells mL^{-1}, is also similar to that obtained with standard solutions. Analysis of four milk samples spiked at the 1.2×10^3 cells mL^{-1} concentration level, and of seven milk samples spiked at the 4.8×10^3 cells mL^{-1} concentration level, yielded *S. aureus* mean contents of $(1.1 \pm 0.1) \times 10^3$ cells mL^{-1} and $(5.1 \pm 0.5) \times 10^3$ cells mL^{-1}, respectively, the confidence interval being calculated for $\alpha = 0.05$. Mean recoveries of (95 ± 12) % and of (107 ± 11) %, respectively, were obtained. The total time for the assay, once the immunosensor is prepared, is of approximately 1.5 h, which compares well with other approaches such as the one proposed by Mantzila et al. [30] in which the immunodetection is performed directly in culture samples, and 100 cfu mL^{-1} bacteria were detected with a detection time interval of 10 h. All these data show fairly well the usefulness of the disposable immunosensor design to be used in the analysis of real samples.

4. Conclusions

Amperometric immunosensors for the determination of *S. aureus* cells, making use of DTSP-SAM modified gold electrodes on where RbIgG and HRP-labelled antigens were coimmobilized showed good analytical performance. In particular, the immunosensor design involving antiRbIgG-HRP, cell wall lyses by ultrasonication, and Au/SPEs as electrochemical transducers allows a detection limit of 3.7×10^2 cells mL^{-1} to be obtained. A similar sensitivity is achieved for the detection of *S. aureus* in milk samples, which is one order of magnitude lower than the maximum allowed limit for *S. aureus* in food. Moreover, the use of disposable mass-produced SPEs-immunosensors allows the preparation and handling of 15 sensors per day, which also constitutes an important feature in the application of the developed immunosensors to the determination of *S. aureus* in real samples.

Acknowledgements

The financial support of project CTQ2006-02743BQU is gratefully acknowledged. V. Escamilla-Gómez acknowledges a pre-PhD fellowship of the Spanish Ministerio de Ciencia y Tecnología.

References

[1] L. Chen, L. Deng, L. Liu, Z. Peng, Biosens. Bioelectron. 22 (2007) 1487.
[2] S.H. Huang, Sens. Actuators B 127 (2007) 335.
[3] F. Ricci, G. Volpe, L. Micheli, G. Palleschi, Anal. Chim. Acta 605 (2007) 111.
[4] R.H. Hall, Microbes Infect. 4 (2002) 425.
[5] R.M. Baird, W.H. Lee, Int. J. Food Microbiol. 26 (1995) 15.
[6] J. Rishpon, D. Ivnitski, Biosens. Bioelectron. 12 (1997) 195.
[7] B. Mirhabibollahi, J.L. Brooks, R.G. Kroll, Appl. Microbiol. Biotechnol. 34 (1990) 242.
[8] N. Kim, I.S. Park, Biosens. Bioelectron. 18 (2003) 1101.
[9] S. Chemburu, E. Wilkins, I.A. Hamid, Biosens. Bioelectron. 21 (2005) 491.
[10] E. Delibato, G. Volpe, D. Stangalini, D. De Medici, D. Moscone, G. Palleschi, Anal. Lett. 39 (2006) 1611.
[11] V. Escamilla-Gómez, S. Campuzano, M. Pedrero, J.M. Pingarrón, Anal. Bioanal. Chem., in press, doi:10.1007/s00216-007-1810-1.
[12] G.B. Sigal, C. Bamddad, A. Barberis, J. Strominger, G.M. Whitesides, Anal. Chem. 68 (1996) 490.
[13] J. Pei, J.M. Hu, Y. Hu, Y. Zeng, J. Chem. Technol. Biotechnol. 73 (1998) 59.
[14] Y.S. Lo, N.D. Huefner, W.S. Chan, F. Stevens, J.M. Harris, T.P. Beebe, Langmuir 15 (1999) 1373.
[15] S. Kanno, Y. Yanagida, T. Haruyama, E. Kobatake, M. Aizawa, J. Biotechnol. 76 (2000) 207.
[16] T. Dubrovsky, A. Tronin, S. Dubrovskaya, S. Vakula, C. Nicolini, Sens. Actuators B 23 (1995) 1.
[17] W. Lee, B.K. Oh, Y.M. Bae, S.H. Paek, W.H. Lee, J.W. Choi, Biosens. Bioelectron. 19 (2003) 185.
[18] I.S. Park, N. Kim, Biosens. Bioelectron. 13 (1998) 1091.
[19] Y. Dong, C. Shannon, Anal. Chem. 72 (2000) 2371.
[20] I.S. Park, D.K. Kim, N. Adanyi, M. Varadi, N. Kim, Biosens. Bioelectron. 19 (2004) 667.
[21] A.D. Taylor, Q. Yu, S. Chen, J. Homola, S. Jiang, Sens. Actuators B 107 (2005) 202.
[22] A. Subramanian, J. Irudayaraj, T. Ryan, Biosens. Bioelectron. 21 (2006) 998.
[23] V. Escamilla-Gómez, S. Campuzano, M. Pedrero, J.M. Pingarrón, Electroanal. 19 (2007) 1476.
[24] K. Ataka, F. Giess, W. Knoll, R. Naumann, S. Haber-Pohlmeier, B. Richter, J. Heberle, J. Am. Chem. Soc. 126 (2004) 16199.
[25] S. Campuzano, R. Gálvez, M. Pedrero, F.J. Manuel de Villena, J.M. Pingarrón, J. Electroanal. Chem. 526 (2002) 92.
[26] B. Mirhabibollahi, J.L. Brooks, R.G. Kroll, J. App. Bacteriol. 68 (1990) 577.
[27] A. Subramanian, J. Irudayaraj, T. Ryan, Sens. Actuators B 114 (2006) 192.
[28] O.A. Loaiza, S. Campuzano, M. Pedrero, J.M. Pingarrón, Talanta 73 (2007) 838.
[29] R. Nandakumar, A.M. Gounot, B. Mattiason, J. Biotechnol. 83 (2000) 211.
[30] A.G. Mantzila, V. Maipa, M.I. Prodromidis, Anal. Chem. 80 (2008) 1169.

Talanta 77 (2008) 844–851

Contents lists available at ScienceDirect

Talanta

journal homepage: www.elsevier.com/locate/talanta

LC determination of biopterin reduced forms by UV-photogeneration of biopterin and fluorimetric detection

A. Espinosa-Mansilla, A. Muñoz de la Peña, F. Cañada-Cañada*, A. Mancha de Llanos

Department of Analytical Chemistry, University of Extremadura, Avda. Elvas, 06071 Badajoz, Spain

ARTICLE INFO

Article history:
Received 27 March 2008
Received in revised form 17 July 2008
Accepted 22 July 2008
Available online 31 July 2008

Keywords:
LC
Fluorimetric detection
Photoirradiation
Tetrahydrobiopterin (BH_4)
Biopterin (BIO)
Serum
Hyperphenylalaninemia

ABSTRACT

An off-line photoirradiation LC fluorimetric method to determine tetrahydrobiopterin (BH_4), by photogeneration of biopterin (BIO), is described, as an alternative way to the chemical oxidation procedure. To minimize the uncontrolled BH_4 oxidation, due to environmental oxygen, an antioxidant, dithiothreitol (DTT), was used. The acidity of the medium, as well as the presence of hydrogen peroxide, affects the rate of the photoreaction and the nature of the obtained fluorescent photoproducts. The best conditions were achieved by irradiation in hydrochloric acid (0.2 M) medium, in presence of 100 mM hydrogen peroxide, and using an irradiation time of 20 min. The method was tested in the analysis of serum samples containing BH_4, and recoveries between 89 and 105% were found. Also, the proposed method allows the resolution of BH_4 and BIO, in the same sample, by injection of non-irradiated and irradiated sample aliquots in the chromatographic system.

1. Introduction

In humans, tetrahydrobiopterin (BH_4) has been recognized as the most important nonconjugated pteridin. BH_4 is a cofactor of aromatic amino acid hydrosylases involved in hydroxylation reactions of phenylalanine, tyrosine and tryptophan. The participation of BH_4 in neurotransmitter metabolism regulation allows knowing some type of phenylketonuria [1]. BH_4 is linked to its ability to reduce molecular oxygen generating electrons, transformation in 4-α-hydroxytetrahydrobiopterin and then, by dehydration, in quinonoid dihydrobiopterin (qBH_2) [2]. As a consequence, BH_4 is, at least, an essential cofactor of five enzymatic reactions; for phenylalanine-4-hydroxylase (PAH), tyrosine-3-hydroxylase, and tryptophan-5-hydroxylase. It is evident its implication in the phenylalanine—tyrosine transformation (Scheme 1). The alteration of the mentioned pathway gives rise to different types of hyperphenylalaninemia [3]. An amount of phenylalanine >150 μmol/L, in human serum, is considered as pathologic. Both, patients with defects in the biosynthesis of BH_4, as well as patients with BH_4 responsive phenylalanine hydrosylase (PAH) deficiency, benefit from substitution with the synthetic cofactor. BH_4 is administered orally at doses of 2–10 mg/kg body weight, in order to keep the normal hydroxylation of phenylalanine to tyrosine in the liver.

In addition to the hydroxylation of aromatic amino acids, BH_4 serves as the cofactor for nitric oxide synthase and glyceryl-ether monooxygenase. Nitric oxide (NO) is an important signalling molecule for vascular homeostasis by the regulation of blood vessel diameter, platelet aggregation, leukocyte adhesion and smooth muscle proliferation. It is believed that NO production is reduced by decreasing BH_4 concentration during oxidative stress, since it is one of the most potent naturally occurring reducing agents [4].

The main metabolite of BH_4 is biopterin (BIO). The determination of the neopterin/biopterin (NEO/BIO) ratio in urine, along with others analytical parameters, such as phenylalanine and tyrosine content, enzymatic activities evaluation and others, are applied to establish the differential diagnostic of the hyperphenylalaninemia.

Mother's milk contains high amounts of BIO, 90-fold than in serum, that fact indicates the possibility of production of BH_4 from mammary glands [1]. A number of data point out feeble permeability of cell membrane for BH_4; blood–brain barrier seems to be relatively impermeable for BH_4, which has been documented in animal experimental models and by mild efficacy in supplementation treatment with BH_4, in patients with deficiency in this compound [5]. Chemical reduction of biopterin yields two diastereoisomers, 6*R*- and 6*S*-BH_4, being 6*R*-BH_4 the natural form of tetrahydrobiopterin. Other important pteridine ring compounds are neopterin and biopterin [6].

* Corresponding author. Tel.: +34 924 289 375; fax: +34 924 289 375.
E-mail address: floricanada@gmail.com (F. Cañada-Cañada).

0039-9140/$ – see front matter © 2008 Elsevier B.V. All rights reserved.
doi:10.1016/j.talanta.2008.07.046

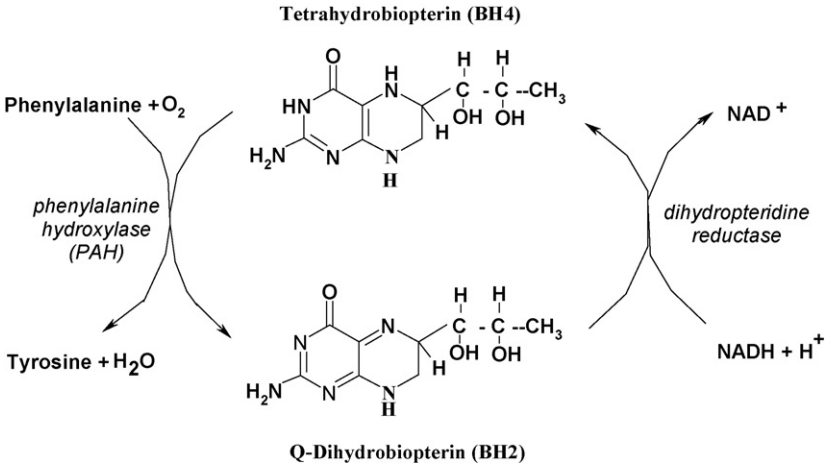

Scheme 1. Regeneration of 5,6,7,8-tetrahydrobiopterin (BH_4).

Most of the studies about the determination of BH_4 levels in plasma or urine are based on its indirect determination, by generation of biopterin, being the Fukushima method [7] widely applied. Briefly, the method consists on two steps: (1) by acid iodine oxidation the 7,8-dihydrobiopterin and BH_4 give rise to biopterin; (2) by alkaline iodine oxidation BH_4 gives rise to pterin and BH_2 undergoes to biopterin. The content of BH_4 in the original sample is calculated by difference between the amounts of biopterin obtained by acid and alkaline oxidation. It is described that the instability of BH_4 generates low content and poor repeatability in these analysis. Recently, two antioxidants have been tested, dithioerythriol (DTE) [8] and dithiothreitol (DTT) [9], in plasma. However, the presence of antioxidants could interfere in the later iodine oxidation [9].

Research studies about the photochemistry of folates, and other biologically active derivatives of pterin, indicate that the activity of the pterin heterocycle gives rise to changes of reduction degree of the original compounds. It is known that the attachment of formyl, methyl, methenyl or other one-carbon moieties to tetrahydrofolic acid affects the properties of excited molecules of folates. It is also known that photolysis of folic acid, folate derivatives and simple (non-conjugated) pterins, involves chemical bonds in the pteridine heterocycle and other portions of the molecule [10].

In previous papers, it has been observed how the photoirradiaton of some folates as folic acid, folinic acid and 5-methyltetrahydrofolic acid [11], is strongly affected by the UV irradiation. In some cases, a notable increment of the fluorescence is observed, and the generation of the corresponding oxidized pteridin appears feasible according to the spectral characteristics of the generated photoproducts. In other cases, the fluorescence disappears because a total oxidation of the molecule occurs. However, several photoproducts, with similar fluorescent characteristics, may be formed from the parent reduced forms.

With the aim of establishing the transformation in the oxidized pteridines, as an alternative way to the chemical oxidation described before, we have carried out several photoirradiation experiments accomplished with LC studies of some pteridin reduced forms. The 5,6,7,8-tetrahydrobiopterin (BH_4) and 7,8-dihydrobiopterin (BH_2) (Scheme 2) were studied as interesting biochemistry and clinical compounds. In both cases, the formation of biopterin would be desirable due to its high fluorescence quantum yield.

2. Experimental

2.1. Reagents

Pterin derivatives, as well as tetrahydro- and dihydro-derivatives, were purchased from Schircks Laboratories (Jona, Switzerland). BH_4, as dichorhydrate, was acquired as 6*R*-BH_4. All other chemicals were purchased from Sigma–Aldrich (Madrid, Spain). Stock standard solutions (90 μg mL^{-1}) of 5,6,7,8-tetrahydro-L-biopterin dihydrochloride (BH_4) and 7,8-dihydro-L-biopterin (BH_2), containing 0.1% DTT, were prepared by dissolution with ultrapure water. Exposure to direct sunlight was avoided.

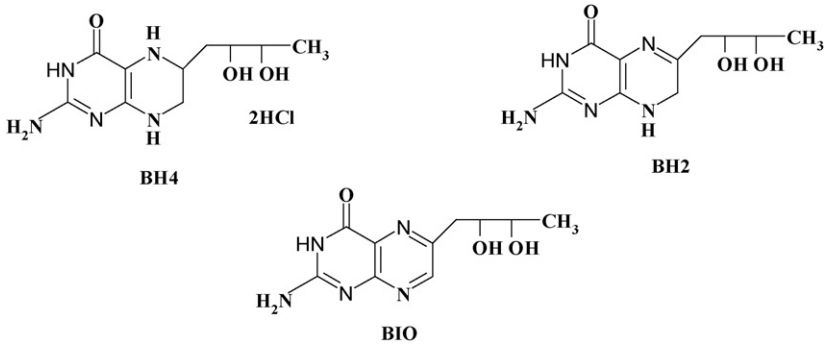

Scheme 2. Chemical structures of the analytes, BH_4, BH_2 and BIO.

2.2. Apparatus

2.2.1. Off-line photoirradiation system

An Osram 200 W HBO high-pressure mercury lamp, with an Oriel model 8500 power supply (Spectra-Physics, Newport, USA), was used for the photoreactions of BH_4 and BH_2. The photochemical set-up included a light-box consisting of a fan, a mercury lamp and a quartz lens. Both, 3 and 10 mL quartz cells were used in the irradiation process. The cells were placed in an optical bench at 30 cm from the mercury lamp. The solutions were magnetically stirred during the UV irradiation.

2.2.2. Chromatographic system

Chromatographic studies were performed on an Agilent 1100 LC High Performance Liquid Chromatograph (Agilent Technologies, Palo Alto, CA, USA), equipped with an on-line degasser, a quaternary pump, a diode array detector (DAD 61315A), and a rapid scan fluorescence detector (G1321 A), connected online. The ChemStation software was used for controlling the instrument, data acquisition and data interpretation. Chromatographic separation was achieved on an analytical column Zorbax Eclipse XDB-C18 (150 mm × 4.6 mm, 5 μm; Agilent Technology).

The LC mobile phase was formed by a mixture of citric acid buffer, 10 mM at pH 5.5/acetonitrile (99:1, v/v). The mobile phase was filtered through a 0.2-μm nylon filter and degassed before use. The flow rate was 1.0 mL min^{-1} and the injection volume was 20 μL. Before injection, samples were filtered through a Millipore Swineex syringe adapter, containing a 0.22-μm regenerated cellulose membrane filter. Detection was performed with photometric (256, 272 and 330 nm) and fluorimetric (435 nm and 444 nm; λ_{ex} = 272 nm) detectors, connected in series.

2.3. General chromatographic procedure to determine BH_4 by using off-line photoirradiation process

Into a 25.0-mL volumetric flask, aliquots of BH_4 stock standard solutions, adequate volume of hydrochloric acid to obtain a concentration of 0.2 M, hydrogen peroxide (final concentration 100 mM), and deionised water to the mark, were added. The sample was located in a 10-mL quartz cell in the photo reactor, stirred constantly, and irradiated during 20 min. When the irradiation process is finished, a 1/5 dilution was made with a citric acid buffer, 10 mM at pH 5.5, filtered through a nylon filter (0.22 μm) and then aliquots of 20 μL were injected into the chromatographic system. The BH_4 was determined by fluorimetric measurement of the photoproduct (BIO) at 444 nm, after excitation at 272 nm. Peak areas and peak heights can be used to quantify BH_4.

2.4. Procedure for determining total BIO in serum samples

Into a 25.0-mL volumetric flask, aliquots of 1.00 mL serum sample (a pool of serum taken from healthy individuals) were spiked with different amounts of the BH_4 stock solution (concentration range was between 200 and 1800 ng mL^{-1}) after that, the sample was treated in the same way described above. The total BIO was determined by fluorimetric measurement of the photoproduct (BIO) at 444 nm, after excitation at 272 nm. Peak areas were used to quantify total BIO.

3. Results and discussion

Tetrahydropteridine derivatives are absorbent compounds that show sparingly fluorescence in aqueous medium. In neutral medium, BH_4 exhibits an absorption spectrum with two maxima

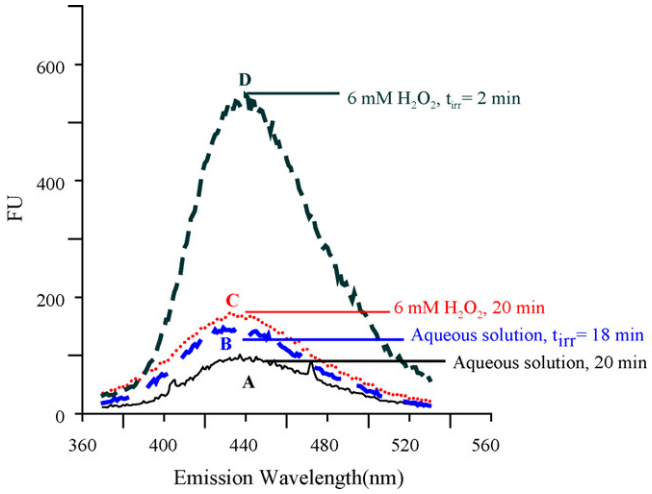

Fig. 1. Emission spectra of BH_4 aqueous solution of 15 μg mL^{-1}, pH 7 and λ_{ex} = 272 nm. (A) 20 min after preparation; (B) after irradiation during 18 min; (C) in presence of 6 mM H_2O_2, 20 min after preparation; (D) in presence of 6 mM H_2O_2 and after irradiation of 2 min.

located at 225 (the most intensive), and 300 nm. BH_2 is slightly fluorescent, due to the presence of a double bond in the pyrazinic ring conjugated with the pyrimidinic ring, and its emission wavelength is located at 444 nm, when exciting at 272 nm. It is not possible to develop an enough sensitive methodology using the native fluorescence of these compounds. BIO is an oxidized pteridine highly fluorescent, with an emission maximum at 447 nm and, because of this, an oxidation process is necessary prior to the determination of BH_4 and BH_2, to convert them in BIO. This oxidation is a rapid process, which occurs when the aqueous solution of BH_4 and BH_2 are in presence of air, during a short time.

We studied the effect of the UV irradiation in the tetrahydro- and dihydro-pteridines, with the aim of generating the oxidized pteridines, as an alternative to the chemical oxidation method.

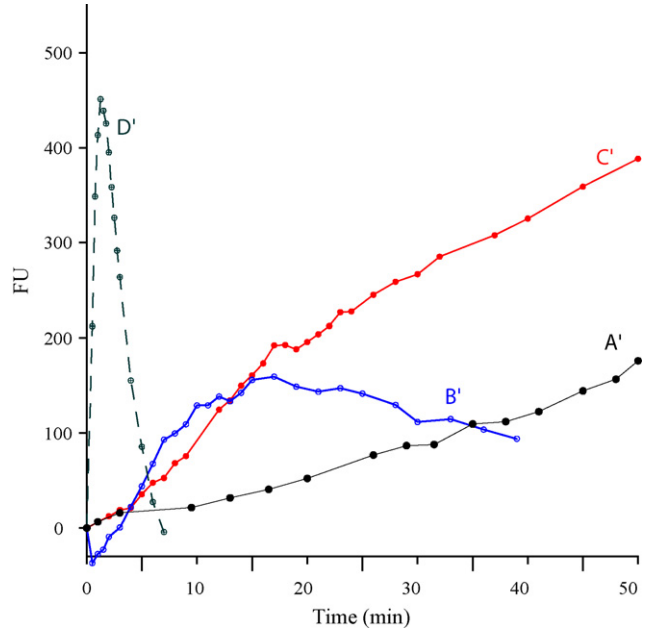

Fig. 2. Evolution of the fluorescence intensity of BH_4 aqueous solution of 15 μg mL^{-1}, pH 7 (λ_{em} = 440 nm; λ_{ex} = 272 nm). (A) Aqueous solution; (B) with irradiation; (C) in presence of 6 mM of H_2O_2; (D) in presence of 6 mM H_2O_2 and irradiation.

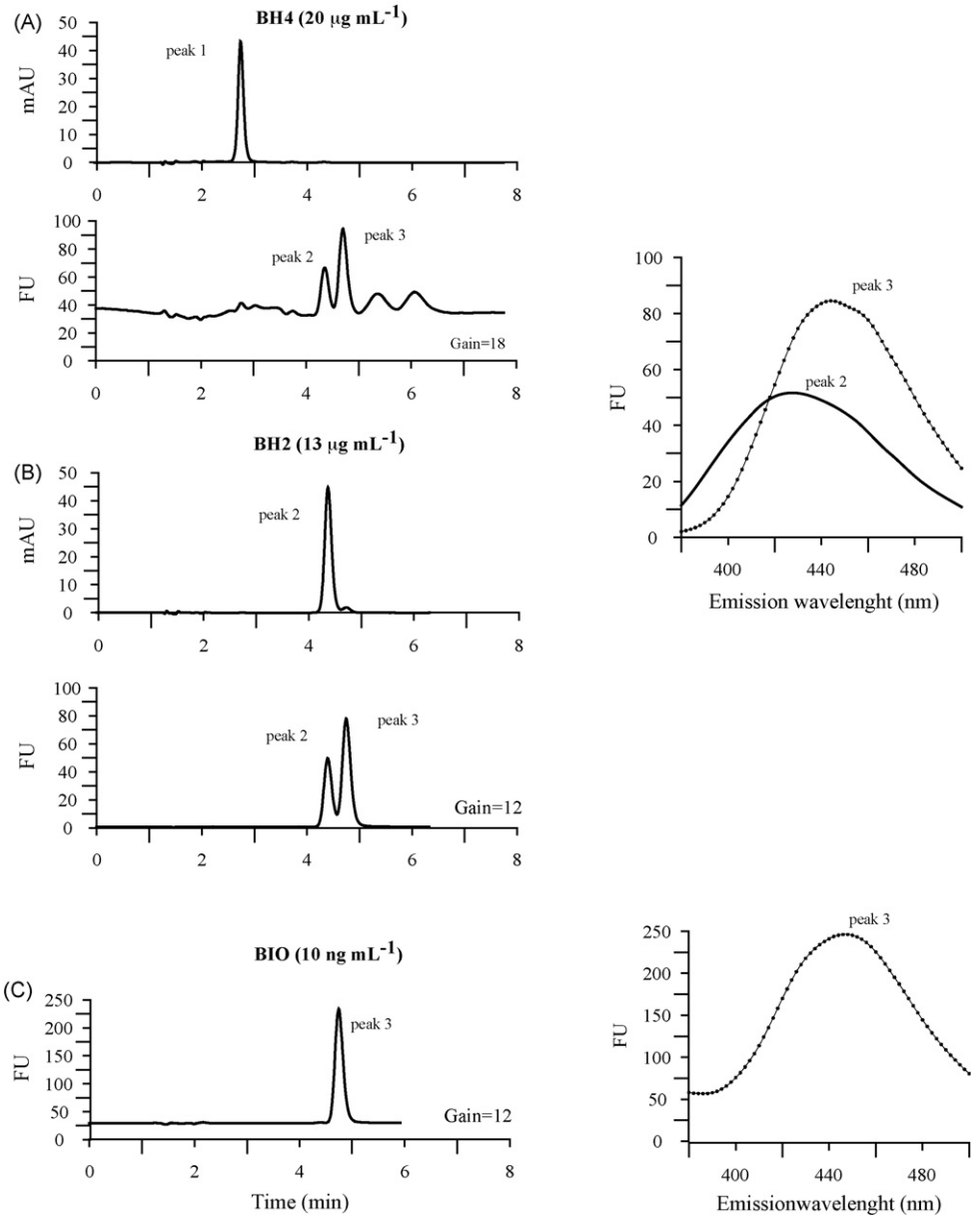

Fig. 3. Chromatograms for aqueous solution of BH_4, 20 μg mL^{-1} (A) and BH_2, 13 μg mL^{-1} (B) and dynamic emission spectra in the peaks 2 and 3. Chromatogram for an aqueous solution of BIO, 10 ng mL^{-1} (C), and dynamic emission spectra in the peak 3. λ_{ex} = 272 nm. Mobile phase: citric acid buffer 10 mM, pH 5.5/acetonitrile, 99/1.

3.1. Evolution of the fluorescent characteristic of BH_4 and BH_2 in aqueous solution

BH_4 neutral solutions are slightly fluorescent, but its fluorescence is time dependent, due to its transformation in BIO. In 20 min, well-defined emission spectra are observed, showing an emission maximum at 440 nm, by exciting at 272 nm (Fig. 1(A)). As it can be noticed in Fig. 1, the rate of this evolution is favoured by the presence of low amounts of hydrogen peroxide (C). Nevertheless, the maximum evolution rate is reached when an aqueous solution of BH_4, in presence of H_2O_2, is irradiated (D), and the highest fluorescence signal is obtained in only 2 min.

Kinetic curves, belonging to the process above described, are represented in Fig. 2(A′–D′). In the presence of H_2O_2 (C′), the equilibrium is obtained in about 80 min but, when the same BH_4 solutions are irradiated, two different processes are accelerated; the formation and the degradation of the fluorescent photoproduct (D′) and, as a result, the equilibrium is never reached. By comparing kinetic curves A′ and C′, we could conclude that the presence of H_2O_2 accelerates the conversion of BH_4 to a fluorescent product. On the other hand, comparing the kinetic curves B′ and D′, obtained by irradiation of the solutions, the presence of H_2O_2 (D′), moreover, of acting as an accelerator, also keeps the formed fluorescent intermediates for a few seconds.

A similar behaviour is observed from BH_2 aqueous solution, although the initial fluorescence of BH_2 aqueous solution is higher than that obtained from BH_4. The fluorescent spectral characteristics of the photoproducts, in both cases, are similar and, in accordance with the formation of a pteridinic ring, give rise to BIO or derivate compounds. To minimize the uncontrolled oxidation, due to environmental oxygen, it is recommended the addition of an antioxidant, as DTT, to the BH_4 and BH_2 stock solutions, and avoiding light exposure. The acidity of the medium and the presence of hydrogen peroxide affect the rate of the photoreaction and

the generated fluorescent compounds. A chromatographic monitoring of the photoreaction was developed to clarify the nature of the photoreaction in several acidity media.

3.2. Preliminary chromatographic studies

Preliminary chromatographic studies were performed in order to separate several pteridines of biochemistry importance as NEO, BIO, pterin and BH_2. Several buffer solutions were tested and the best results were obtained by using citrate buffer, 10 mM at pH 5.5. Also, several acetonitrile percentages were assayed and 1% acetonitrile was selected as optimum to obtain an adequate isocratic elution. Under these conditions, adequate separation of NEO (t_r = 2.1 min), BH_2 (t_r = 4.2 min), BIO (t_r = 4.7 min) and pterin (t_r = 5.3 min) was achieved in 6 min.

As a preliminary study the stability of BH_4 and BH_2 aqueous solutions, containing 200 ng mL^{-1}, in presence of DTT, was tested. The stock solutions of BH_4 were stable, at least, during 4 h. However, in the BH_2 aqueous solutions, BIO was always present.

The injection of samples of BH_4, BH_2 and BIO allow knowing the chromatographic profiles for the three analytes (Fig. 3). With the aim of simultaneously observing the photometric and fluorimetric signals, by using two serial detectors, and due to the low fluorescence of BH_4 and BH_2, a high amount of these analytes was injected. Hence, the possible presence of BH_2 and BIO, at trace levels, generated by the environmental oxidation of BH_4, could be monitored in the fluorimetric detector. Because of the high quantum yield of fluorescence of BIO, 10 ng mL^{-1} were enough to monitor the chromatographic profile. In Fig. 3(A), the chromatograms for the BH_4 (peak 1), BH_2 (peak 2) and BIO (peak 3) are shown. It can be observed the generation of very low amounts of BH_2 and BIO, in aqueous solution, from BH_4. Also, the higher fluorescence of BH_2 and the presence of low amounts of BIO were confirmed. In comparison with BH_4, BIO exhibits very high fluorescence. The dynamic emission spectra in the peak are also shown. On the other hand, the formation of BIO appears more favourable from BH_2.

3.3. Chromatographic monitoring of the photoreaction

Aqueous solutions of BH_4, containing 200 ng mL^{-1}, in presence and absence of H_2O_2, were injected in a chromatographic system with the aim to establish the influence of the photoirradiation process in the chromatographic profiles. The photoirradiation was tested in neutral, acid and basic media.

In neutral and basic medium, the photoirradiation process, in presence and absence of H_2O_2, give rise to several peaks, indicating the co-existence of several photoproducts in all the range of irradiation times assayed. In the first, an increasing in the peak areas is observed, and for high irradiation times, the peak areas diminish for all peaks. In Fig. 4, the chromatograms corresponding to the evolution of an aqueous solution of BH_4, in presence of 6 mM H_2O_2, at different irradiation times, are plotted. The instability and proliferation of photoproducts made of these conditions unfeasible for our purposed.

However, when the irradiation process is made in acid medium (hydrochloric acid, 0.2 M), at the beginning of the irradiation two peaks (peak 1 and peak 2) appeared, but only one was obtained for irradiation times higher than 12 min (Fig. 5). The peak 1 appears as an unstable intermediate compound and the formation of peak 2, according to the diminishing of peak 1, can be observed in Fig. 6(A). The peak 2 appears at the same retention time that the biopterin standard sample and, the emission spectra through the peak (exciting at 272 nm), shows the purity and similarity with a biopterin peak (Fig. 6(B)).

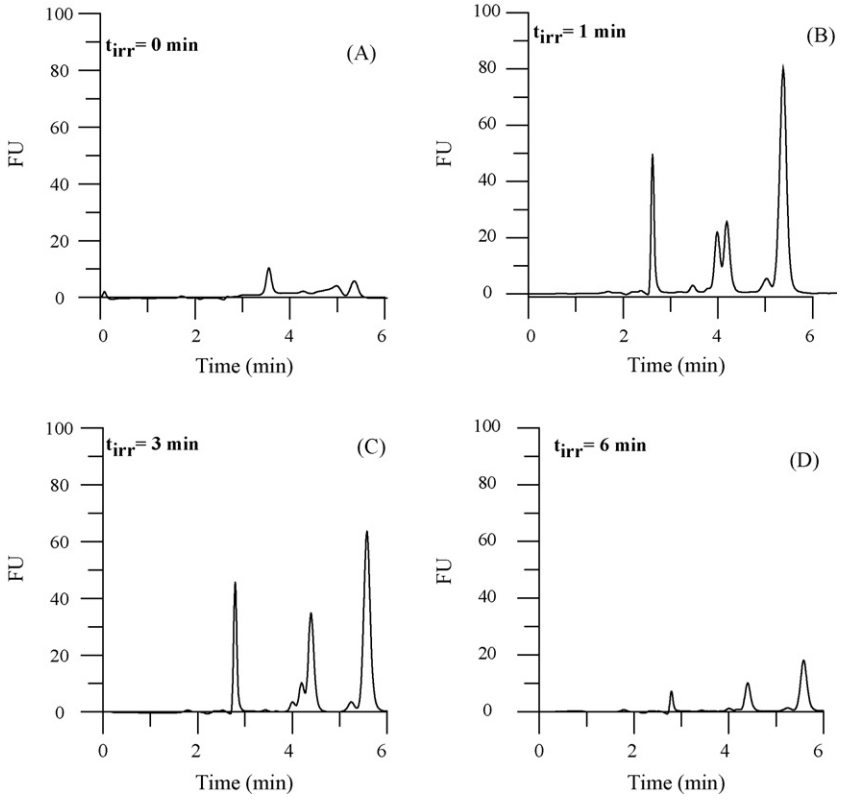

Fig. 4. Chromatograms for BH_4 solution, 1 μg mL^{-1}, 6 mM H_2O_2, after irradiation in aqueous medium (λ_{em} = 440 nm; λ_{ex} = 272 nm). A: non-irradiated; B: $t_{irradiated}$ = 1 min; C: $t_{irradiated}$ = 3 min; D: $t_{irradiated}$ = 6 min.

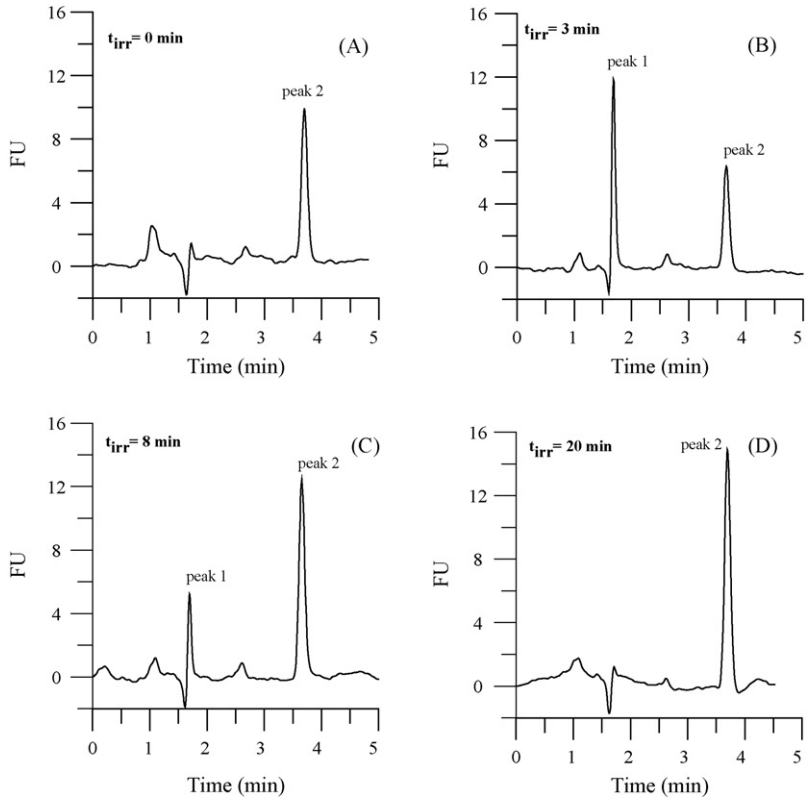

Fig. 5. Chromatograms for BH_4 solution, 200 ng mL^{-1}, 100 mM H_2O_2, after irradiation in acidic medium (0.2 M) (λ_{em} = 440 nm; λ_{ex} = 272 nm). A: non-irradiated; B: $t_{irradiated}$ = 3 min; C: $t_{irradiated}$ = 8 min; D: $t_{irradiated}$ = 20 min. Flow rate: 1.2 mL min^{-1}.

The maximum quantum yield was achieved for an irradiation time of 20 min, in presence of 100 mM H_2O_2 and, for higher amounts of H_2O_2 a decreasing of the peak area was observed.

3.4. Analytical reference parameters

Regression analysis of the mean peak area and height against concentration was performed, once the samples were irradiated in the optima conditions. The range of concentration was varied between 100 and 1200 ng mL^{-1}, for BH_4, and between 50 and 500 ng mL^{-1}, for BH_2. Each concentration was injected by triplicate. The results of the linear univariate regression analysis are summarized in Table 1, which includes the detection limits (calculated according to the criteria of Clayton et al. [12], by using the deviation values of slope and intercept of the linear calibration equation) and the determination coefficients.

3.5. Analytical parameters for calibration of BH_4 in presence of serum

The proposed method has been tested in the analysis of spiked serum samples with BH_4, and has been compared with a reference

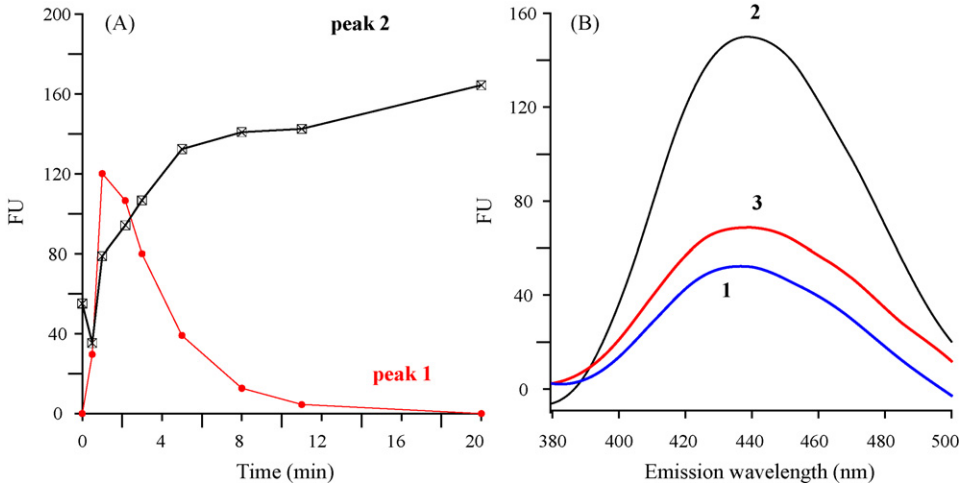

Fig. 6. Evolution of the peak heights 1 and 2 at different irradiation time (A) and dynamic emission spectra through the peak 2 at $t_{irradiated}$ = 20 min (λ_{em} = 440 nm; λ_{ex} = 272 nm) (B).

Table 1
Analytical and statistical parameters for the calibration of BH_4 and BH_2

Component	Detector	Chromatographic signal	Slope[a] (determination coefficient)	σ Slope	LOD[b] (ng mL^{-1})
BH_4	λ_{ex}=272 nm	Peak height	0.13 (0.9977)	0.01	67
	λ_{ex}=440 nm	Peak area	1.47 (0.9977)	0.03	69
BH_2	λ_{ex}=272 nm	Peak height	1.32 (0.9971)	0.02	24
	λ_{ex}=440 nm	Peak area	12.64 (0.9940)	0.31	35

[a] Expressed as FU mL ng^{-1}.
[b] LOD is the limit of detection according to the criterium of Clayton ($\alpha = \beta = 0.05$) [12].

Table 2
Results for the determination of BH_4 in presence of serum using the standard addition method

Analyte	Added[a]	Recovery (%)[b] (s)	Slope calibration[c] (determination coefficient)	
			In absence of serum	In presence of serum
BH_4	232	102 (7.5)	1.470 (0.9977)	1.423 (0.9934)
	626	90 (2.6)		
	1021	98 (6.3)		
	1415	94 (4.1)		
	1800	98 (1.2)		
			Statistical comparison ($P = 0.05$) $F_{cal} = 0.50 < F_{tab} = 2.57$ $t_{cal} = 1.32 < t_{tab} = 2.05$	

[a] Expressed as ng mL^{-1}.
[b] Mean recovery for three individual replicates for each addition.
[c] Expressed as FU mL ng^{-1}.

calibration in absence of serum. Before the injection, the serum samples were diluted 125-fold. The concentration range added was 200–1800 ng mL^{-1}. The recovery values for all additions were calculated using the peak area as analytical signal. The slopes of the calibration curves in presence of serum are similar to the reference slopes in absence of serum. The comparison of the slopes of two regression lines was performed by means of a *t*-test [13]. No significant statistical difference ($P = 0.05$) was found, when a comparison between the slopes was made. Statistical parameters for the linear regressions are summarized in Table 2. Mean recovery values were between 90 and 102%.

Regression analysis of added *versus* found concentration values in serum was applied for BH_4. The estimated intercept and slope were compared with ideal values of 0 and 1, using the elliptical joint confidence region (EJCR) test [14,15], for using both analytical signals, peak area and peak height. All plots contain the theoretical [0,1] point in the experimental ellipse (Fig. 7). This fact indicates that the security and precision of the analysis of BH_4, using the peak area and peak height, are similar. A slightly higher surface was obtained for peak height measurements.

The precision of the method was calculated by injection of nine individual replicates of serum samples, containing 300 ng mL^{-1} of BH_4, and was expressed as relative standard deviation (R.S.D.). R.S.D. were 3.5 and 6.8%, by measuring of peak area and peak height, respectively. Taking into account the R.S.D. values, the peak area was selected as optimum analytical signal, to measure BH_4, by the off-line photoirradiation HPLC proposed method. The proposed method allows calculating the total biopterin ($BH_4 + BH_2 + BIO$) concentration in the sample.

3.6. Simultaneous determination of BH_4 and BIO

As it has been described above, BH_4 and BH_2 generate BIO by photoirradiation. When aqueous solutions of BIO are irradiated in the optimized conditions, the peak area notably decreases by decomposition of the BIO. The ratio slope calibration $BIO_{irradiated}$ (b')/slope calibration $BIO_{non\text{-}irradiated}$ (b) was 0.464. Irradiated mixtures composed by BH_4 and BIO gave rise to only one chromatographic peak, corresponding to the BIO formed from BH_4, plus the amount of BIO not affected by the irradiation. Calculating the slope calibration for BH_4 (b''), the slope calibration for $BIO_{non\text{-}irradiated}$ (b) and the slope calibration for $BIO_{irradiated}$ (b'), BH_4 and BIO can be determined for each sample. Only two injections are made, one for an aliquot of problem (peak area = S) and other for an aliquot of problem previously irradiated (peak area = S_T).

Table 3
Results obtained in the determination of BH_4 AND BIO in binary mixtures

$[BH_4]^a_{added}$	$[BIO]^a_{added}$	$[BH_4]^b_{found}$ (R.S.D.)	Recovery (%)	$[BIO]^b_{found}$ (R.S.D.)	Recovery (%)
300	10	302 (0.2)	101	11.1 (1.3)	111
600	10	572 (0.7)	95	10.4 (0.2)	104
600	20	559 (1.0)	93	20.5 (1.3)	103
400	25	461 (0.2)	115	25.8 (0.8)	103
500	30	564 (0.1)	113	33.0 (0.7)	110
700	50	620 (0.7)	88	50.7 (0.5)	101
1000	50	992 (0.4)	99	45.2 (0.7)	90

[a] Expressed as ng mL^{-1}.
[b] Mean value for two individual replicates expressed as ng mL^{-1}.

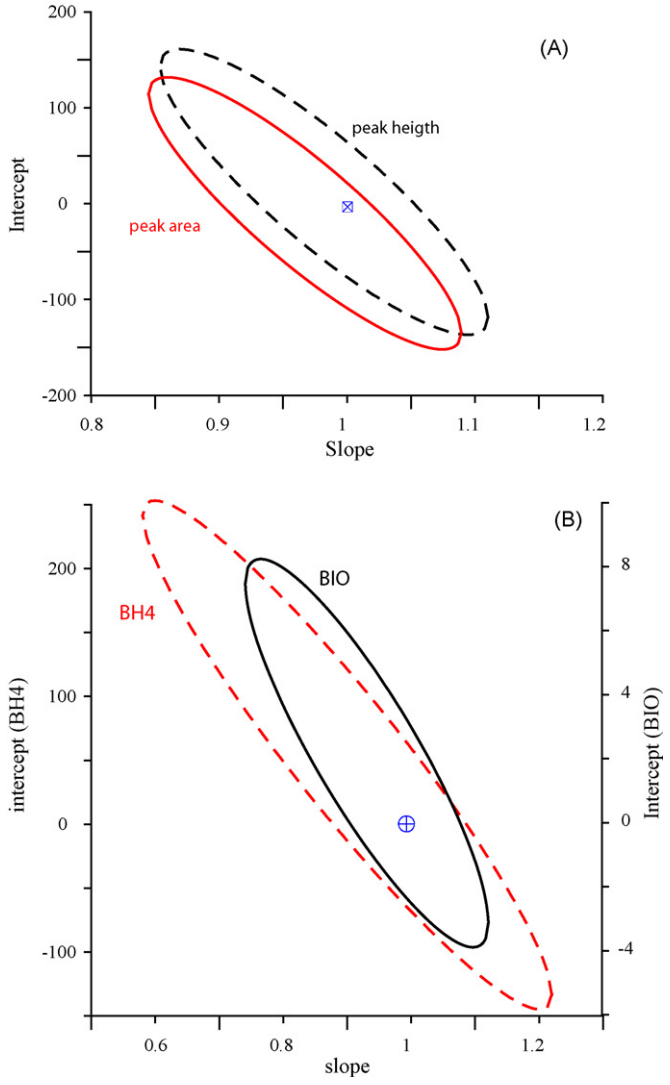

Fig. 7. Peak height and peak area EJCR plots comparison for the BH_4 proposed method (A). Found/added regression EJCR plots for the determination of BH_4 and BIO in their mixtures (B).

The signal corresponding to the amount of BIO not affected by the irradiation may be calculated as

$$S\prime = S\left(\frac{b\prime}{b}\right) = S \times 0.464$$

The signal corresponding to the initial amount of BH_4 is:

$$S_{BH_4} = ST - S\prime$$

The amount of original BIO is easily calculated from the reference calibration equation of BIO as: [BIO] = S/b; and the amount of BH_4 is calculated, in the same way, using the BH_4 calibration curve: [BH_4] = SBH_4/b''. By this method, BH_2 and BH_4 are determined together.

The concentration of BH_4 and BIO, in a test group composed by seven samples of binary mixtures of BH_4 and BIO, has been resolved in the way above indicated. The composition and results obtained are shown in Table 3. Recovery values were between 88–115% and 90–11%, for BH_4 and BIO, respectively. The elliptical joint confidence region test was applied to evaluate the security and precision of the found/predicted values, for both analytes. As it can be noticed in Fig. 7, both ellipses contain the theoretical [0,1] point, hence, the security and the precision of the determination was confirmed.

4. Conclusions

BH_4 and BH_2, by effect of the UV radiation, generate BIO and other non-identified molecular fractions. The formation of BIO is proportional to the initial BH_4 amount in the sample, and the presence of human serum does not interfere in the generation of BIO. However, the addition of DTT, as antioxidant, is recommended to prevent the spontaneous BIO generation from BH_4. The proposed off-line photoirradiation HPLC method allows the resolution of BH_4 and BIO, in a same sample, by injection of non-irradiated and irradiated aliquots. This method must be implemented to increase the sensitivity, with the aim of analyzing biological fluids from patients not pretreated with BH_4. Current, an on-line photoirradiation chromatographic system method is being developed in our laboratory to analyze BH_4 and BH_2 in presence of marker pteridines.

Acknowledgements

Financial support was provided by DGI-MCI of Spain (Project CTQ 2008-00468/BQU). Alicia Mancha de Llanos is grateful to the Consejería de Educación, Ciencia y Tecnología de la Junta de Extremadura for a fellowship (DOE 29/06/2006).

References

[1] L.J. Dhondt, M.J. Hayte, P.J. Fariaux, Pathol. Biol. 37 (1989) 283.
[2] R.C. Scriver, S. Kaufman, K.C. Risensmith, S.L.C. Woo, in: C.R. Screver (Ed.), The Metabolic and Molecular Basis of Inherited Disease, McGraw-Hill, Inc., NY, 1995, pp. 1015–1076.
[3] N. Blau, B. Thony, R.G.H. Cotton, K. Hyland, in: C.R. Scriver, A.L. Beaudet, W.S. Sly, D. Valle, B. Childs, B. Vogelstein (Eds.), The Metabolic and Molecular Bases on Inherited Disease, Eighth edition, McGraw-Hill, NY, 2001, pp. 1725–1776.
[4] S. Shimizu, M. Ishii, Y. Miyasaka, T. Wajima, T. Negoro, T. Hagiwara, Y. Kiuchi, Int. J. Biochem. Cell Biol. 37 (2005) 864.
[5] G. Bjlakovic, T. Jevtovic-Stoimenov, B. Bjelakovic, I. Stajanovic, Facta Univ. Ser.: Med. Biol. 11 (2004) 49–54.
[6] A. Espinosa-Mansilla, I. Durán Merás, F. Salinas, Chromatographia 53 (2001) 510.
[7] T. Fukushima, J.C. Nixon, Anal. Biochem. 102 (1980) 176.
[8] B. Fiege, D. Ballhausen, L. Kierat, W. Leimsbacher, D. Goriounov, B. Schircks, B. Thony, N. Blau, Mol. Genet. Metabol. 81 (2004) 45.
[9] D. Fekkes, A. Voskuilen-Kooijman, Clin. Biochem. 40 (2007) 411.
[10] T.A. Telegina, T.A. Lyudnikova, Y.L. Zemskova, E.A. Sviridov, M.S. Kritsky, Appl. Biochem. Microbiol. 41 (2005) 275.
[11] I. Durán Merás, A. Muñoz de la Peña, A. Jimenez Girón, A. Espinosa-Mansilla, F. Cañada-Cañada, A.C. Olivieri, Anal. Bioanal. Chem. 391 (2008) 827.
[12] C.A. Clayton, J.W. Hines, P.D. Elkins, Anal. Chem. 59 (1987) 2506.
[13] D.L. Massart, B.G.M. Vandeginste, L.M.C. Buydens, S. De Jong, P.J. Lewi, J. Smeyers-Verbeke, Handbook of Chemometrics and Qualimetrics: Part A, Elsevier, UK, 1997.
[14] J. Riu, F.X. Rius, Trends Anal. Chem. 16 (1997) 211.
[15] F.J. del Río, J. Riu, F.X. Rius, Anal. Chim. Acta 446 (2001) 49.

Talanta 77 (2008) 882–888

Contents lists available at ScienceDirect

Talanta

journal homepage: www.elsevier.com/locate/talanta

Ultrasonic energy as a tool in the sample treatment for polymer characterization through matrix-assisted laser desorption ionization time-of-flight mass spectrometry

L. Fernandes, R. Rial-Otero [1], M. Temtem, C. Veiga de Macedo, A. Aguiar-Ricardo, J.L. Capelo *

REQUIMTE/CQFB, Departamento de Química, Faculdade de Ciências e Tecnologia, Universidade Nova de Lisboa, 2829-516 Monte de Caparica, Portugal

ARTICLE INFO

Article history:
Received 5 May 2008
Received in revised form 15 July 2008
Accepted 22 July 2008
Available online 3 August 2008

Keywords:
Polymers
Ultrasound
Molecular mass distribution
MALDI-TOF-MS

ABSTRACT

Different ultrasonic devices including ultrasonic bath with dual frequency, sonoreactor and ultrasonic probe, were tested for their viability in the sample treatment for polymer characterization by matrix-assisted laser desorption/ionization time-of-flight mass spectrometry analysis. The effect of sonication frequency (35 kHz, 40 kHz and 130 kHz), sonication amplitude, and sonication time on the polymer's number-average molecular weight (M_n) and weight-average molecular weight (M_w) were investigated. The effect of those variables in the molecular mass distribution of three polymer standards, poly(styrene) 2000 Da and 10,000 Da and poly(ethylene glycol) 1000 Da, was evaluated. In addition, the influence of ultrasonic energy on the sample treatment as a function of the matrix-assisted laser desorption/ionization time-of-flight mass spectrometry (MALDI) matrix was also studied through two common standard matrices, dithranol and 2,5-dihydroxybenzoic acid. The results obtained show that the ultrasonic bath at 35 kHz is the best option for the purpose of fast sample treatment for polymer characterization. The M_n and M_w values obtained for this ultrasonic device and for the three polymers tested using dithranol as MALDI matrix, were not statistically different from the ones acquired with vortex mixing and also were in concordance with the values recommended by the polymer manufacturers.

1. Introduction

Synthetic polymers today find application in nearly every industry and area of life. They are used as adhesives, lubricants, structural components for many different materials, from computers to satellites. The most recent applications are found in the bioscience area, from artificial components for the human body to drug delivery.

The way in which monomers are distributed to form the structure of the polymer will dictate the polymer's properties, such as solubility, durability, resistibility, crystallinity or tensile strength.

The characterization of a polymer is mandatory to define its properties, since the monomers are distributed statistically in chains of variable lengths which originate differences in terms of polymer's physical and chemical characteristics.

Different analytical techniques can be used to define a polymer, including wide Fourier-transform infrared spectroscopy, angle X-ray scattering, scattering, small angle neutron scattering, gel permeation chromatography (GPC), Raman, small angle X-ray, nuclear magnetic resonance, polydispersity and mass spectrometry-based techniques. Furthermore, matrix-assisted laser desorption/ionization time-of-flight mass spectrometry, MALDI-TOF-MS, referred in this manuscript as MALDI, is a well-established rapid instrumental technique for polymer characterization [1,2].

Polymer characteristics that can readily be determined by MALDI include the following: (i) the number-average molecular weight, M_n, which provides an average weight of a given polymer; (ii) the weight-average molecular weight, M_w, is another form of to give the molecular weight of a polymer and is calculated as the arithmetic mean or average on the molecular weights of a certain number of molecules; (iii) the mass of repeat units; (iv) the polydispersity, PDI, which is the ratio M_w to M_n; and (v) the end-group mass structure [3,4]. Polymer distributions are typically characterized by M_n and M_w, which are calculated as follows [5]:

$$M_n = \sum \frac{M_i I_i}{I_i}$$

$$M_w = \sum \frac{M_i^2 I_i}{M_i I_i}$$

$$\mathrm{PDI} = \frac{M_w}{M_n}$$

* Corresponding author. Tel.: +351 21 294 9649; fax: +351 21 294 8550.
E-mail address: jlcapelom@dq.fct.unl.pt (J.L. Capelo).
[1] Present address: Univ Vigo, Fac Food Sci & Technol, Nutr & Bromatol Grp, Analyt & Food Chem Dept, E-32400 Orense, Spain.

0039-9140/$ – see front matter © 2008 Elsevier B.V. All rights reserved.
doi:10.1016/j.talanta.2008.07.049

where M_i and I_i are the molecular weights of the oligomeric components and their signal intensities, respectively. It is assumed a linear relationship between number of ions and signal intensity [5].

The following features can be considered the major advantages of polymer analysis by MALDI [2,6,7]:

(i) Absolute molecular weights of narrowly distributed polymers (polydispersity < 1.2) can be determined as opposed to relative molecular weights obtained by chromatographic techniques.
(ii) Analysis does not require polymer standards to assign molecular weights to oligomers.
(iii) Using submilligram amounts of sample material, the actual analysis can be accomplished in few minutes.
(iv) In addition, MALDI can determine the molecular weight independently of the polymer structure.

Therefore, the speed and information obtained by MALDI are significantly greater than with other conventional molecular-weight-determination techniques, such as gel permeation chromatography (GPC) [2,6]. The following drawbacks that can also be extended to other type of analysis by MALDI, limit widespread application of MALDI for polymer analysis [3,4,7–9]:

(i) The availability of proper matrices for specific polymers.
(ii) The availability of proper cationization reagents.
(iii) The availability of common solvents for both analyte and matrix.
(iv) The polymer distribution is affected by (1) matrix type; and (2) polymer and matrix salt concentrations used to prepare the sample.
(v) The following MALDI instrumental parameters affect polymer distribution: (1) detector voltage; (2) laser energy; (3) delay time; (4) extraction voltage; and (5) lens voltage.

In addition to the above mentioned drawbacks, it must be emphasized that the M_n and M_w of polymers determined by MALDI often differ from those moments determined by other methods of polymer characterization such as GPC, overall for polymers with high polydispersity (PDI > 1.2). As an example, when data obtained through MALDI are compared with data obtained by GPC, larger discrepancies in the values for M_n and M_w are observed for polymers of high polydispersity. On the other hand, when polymers of narrow polydispersities (PDI < 1.2) are compared, the GPC and MALDI values for M_n and M_w tend to have better agreement [4].

MALDI analysis consists of three steps: sample preparation, sample deposition on the MALDI sample plate and mass spectral analysis. Regarding sample preparation, one of the keys to a successful MALDI analysis depends primarily on uniformly mixing the matrix and the analyte. Samples are typically prepared in an analyte/matrix concentration ratio comprised between $1{:}10^3$ and $1{:}10^5$ in a suitable solvent such as water, acetone, or tetrahydrofuran. However, for high molecular weight samples much higher ratios ($1{:}8 \times 10^6$) have been used [10]. Matrices used for polymer analysis by MALDI include dithranol, 2,5-dihydroxybenzoic acid (DHB), *trans*-3-indoleacrylic acid (IAA), and 2-(4-hydroxyphenylazo) benzoic acid (HABA). These matrices are often used in conjunction with alkali metal salts (LiCl, NaCl and KCl) or silver salts such as silver trifluoroacetate (AgTFA) to form matrix-cationization agent mixtures in order to promote polymer ionization [3,4,6-8].

Concerning sample deposition on the MALDI sample plate, hand-spotting and electrospray are the techniques of choice. The aforementioned deposition methods can lead to different results as a function of the matrix used in the sample preparation process [6,7].

As far as MALDI analysis concerns, as written above, the instrumental parameters must be carefully chosen and controlled since variations can arise from those sources [4,7,8].

Ultrasonication has been used for sample treatment for analytical chemistry for decades [9,11]. Ultrasonication has also become a tool in polymer research with two main aims. On the one hand, ultrasonication has been used for long in the synthesis of polymers, as an initiator or to obtain a homogeneous distribution of the monomers. On the other hand, it has been also used to study polymer degradation mechanisms. However, one of its multiple applications, the mixing of different matrices to form more homogeneous samples, has not been systematically studied for sample preparation of polymers for MALDI characterization yet, despite of the advantages of high throughput and simplicity allowed by ultrasonication.

In this work an ultrasonic bath with dual frequency, a sonoreactor, and an ultrasonic probe, were used to study the influence frequency of sonication, amplitude of sonication and time of sonication on the M_n and M_w values, when the aforementioned devices are used in the sample treatment for mixing polymers and matrices previous to MALDI analysis. Vortex mixing was used for comparative purposes and it was considered the reference procedure for polymer/matrix homogeneization. Poly(styrene) (PS) and poly(ethylene glycol) (PEG) polymers were used as target analytes because both have been systematically studied by MALDI by numerous authors and there is a huge amount of information available in literature regarding these polymers [4,10,12,13].

2. Experimental

2.1. Chemicals, solvents, disposables and apparatus

MALDI-TOF-MS analysis was performed on the following synthetic polymers purchased from Fluka (Buchs, Switzerland): (1) a 2000-Da poly(styrene) sample (M_n = 2140, M_w = 2250 and PDI = 1.05); (2) a 10,000-Da poly(styrene) sample (M_n = 8650, M_w = 8900 and PDI = 1.03); and (3) a 1000-Da poly(ethylene glycol) sample (M_n = 970, M_w = 940 and PDI = 1.05). All of them were standards for GPC certified according to DIN, the German Institute for Standardization [14]. Matrices used in this work were dithranol and 2,5-dihydroxybenzoic acid (DHB), both with quality for MALDI-MS (>98.5%) purchased from Fluka and used as received. Silver trifluoroacetate (AgTFA) (>98%) from Fluka was used to increase the polymer ionization and to minimize the formation of adducts with Na^+ and K^+. Acetone Pestanal® grade from Fluka was used as solvent for MALDI matrices and samples.

Polymer–matrix solutions were prepared in safe-lock tubes of 0.5 ml from Eppendorf (Hamburg, Germany) and were homogenized with a vortex, model Sky Line, from ELMI (Riga, Latvia) or using the following ultrasonic devices: an ultrasonic bath with dual frequency (35 kHz and 130 kHz), model Transsonic TI-H-5, from Elma (Singen, Germany); a sonoreactor model UTR200, from dr. Hielsher (Teltow, Switzerland); and an ultrasonic probe, model UP 200S (dr. Hielscher).

2.2. Sample preparation

Stock solutions of PS and PEG were prepared by dissolving the polymer samples in acetone to a final concentration of ca. 2×10^{-4} M. MALDI matrices (dithranol and DHB) were also dissolved in acetone to a final concentration of 10 mg/ml, and AgTFA was added to the matrix solution to enhance polymer ioniza-

tion. An aliquot of 20 μl of the polymer stock solution was mixed with 20 μl of the MALDI matrix solution. Polymer–matrix mixing and homogenization was done through one of the following processes:

(i) Homogeneization in vortex for 30 s.
(ii) Homogeneization in an ultrasonic bath: 100% sonication amplitude, continuous mode, 130 kHz sonication frequency, and 120 s sonication time.
(iii) Homogeneization in an ultrasonic bath: 100% sonication amplitude, continuous mode, 35 kHz sonication frequency, and 30 s sonication time.
(iv) Homogeneization in a sonoreactor: 20% sonication amplitude, continuous mode and 10 s sonication time.
(v) Homogeneization in a sonoreactor: 20% sonication amplitude, continuous mode and 30 s sonication time.
(vi) Homogeneization with an ultrasonic probe: 20% sonication amplitude, continuous mode, and 10 s sonication time.
(vii) Homogeneization with an ultrasonic probe: 20% sonication amplitude, continuous mode, and 30 s sonication time.

Finally, the samples were hand-spotted onto the MALDI sample plate. Three replicates were done for each sample preparation mode ($n = 3$).

The sonication amplitudes and the sonication times were selected based on our expertise with ultrasonication for sample treatment [9,11]. Briefly, to avoid polymer degradation due to ultrasonication, short sonication times were generally used. For the same reason, for the sonoreactor and ultrasonic probe, both having high sonication intensity, the lower amplitude of sonication was selected.

2.3. MALDI analysis

A MALDI-TOF-MS system, model Voyager DE-PRO Biospectrometry Workstation, equipped with a nitrogen laser radiating at 337 nm and 3 ns pulse from Applied Biosystems (Foster City, USA) was used to obtain the polymer mass spectra following the instructions of the manufacturer. The polymers with molecular weight of 1000 Da and 2000 Da were analyzed in the ion reflector mode in order to enhance peak resolution. Analysis of the 10,000 Da PS sample was done in the linear mode, due to the low sensitivity obtained in the reflector mode for high molecular weight polymers. Measurements were done in the positive ion mode, with the following parameter settings: an accelerating voltage of 20 kV, a grid voltage of 77%, a guide wire of 0.01% and a mirror voltage ratio of 1.12. Delayed extraction was optimized for signal-to-noise for the necessary mass range. Matrix type has a large influence on the laser energy required to obtain a MALDI mass spectrum. As recommended by Wetzel et al. [7], for each matrix data were obtained at randomized laser energy intervals within that range, not in order of increasing or decreasing laser energy. The polymer mass spectra were collected at laser energies of 5.9–6.3 μJ/cm^2 for dithranol; and 6.9–7.1 μJ/cm^2 for DHB. The resolution of the peaks near the molecular mass, for 500 laser shots, was 6500 in the reflector mode and 600 in the linear mode.

MALDI mass spectra were obtained in a manner designed to minimize bias due to sample preparation and application. Each mass spectrum represents the accumulated data from 500 laser shots as the laser spot was moved over a sample site on a stainless steel MALDI sample plate. The mass spectra were obtained from different sites on the 100-site MALDI sample plate to reduce the possibility of bias.

2.4. Data analysis methods

M_n and M_w values were calculated from each polymer mass spectrum obtained by MALDI-MS. Polymerix (Sierra Analytics, Modesto, CA, USA) analysis software was used to integrate the M_n and M_w, and to obtain the moments and separate the different peak series. When necessary, the secondary and tertiary peaks series were used to obtain an estimate of extent of fragmentation through the polymerix program. Analysis of variance (ANOVA) was used to determine whether the measured polymer M_n and M_w were influenced by the sample treatment applied or not. The significance level of the ANOVA was chosen to be 0.05. ANOVA compares the variance at a given parameter value with the variance among parameter values to determine if there is a significant influence of the parameter on the polymer distribution. A parameter has a significant variation when the variance between parameter values is greater than a multiple (depending of the significant level) of the variance within parameter values. When significant variations were detected a multiple range test was done to determine which means were significantly different from which others. This test uses the Fisher's least significant difference (LSD) procedure to discriminate among the means. With this method, there is a 5.0% risk of calling each pair of means significantly different when the actual difference equals zero [15].

3. Results and discussion

3.1. Poly(styrene), PS, 2000 Da

3.1.1. MALDI spectra

Poly(styrene), PS, (2000 Da) was analyzed in dithranol and DHB matrices using AgTFA to enhance polymer ionization during MALDI analysis [1]. Fig. 1A shows the MALDI mass spectrum obtained for the 2000 Da PS sample, for the 35 kHz ultrasonic bath, UB, in dithranol, where peaks can be seen with mass differences of 104 Da, corresponding to the PS monomer mass (C_8H_8).

Regarding PS in dithranol (Fig. 1A) the mass spectra showed good repeatability regardless of the polymer/matrix mixing process used. A matrix made of dithranol (10 mg/ml) and AgTFA (1 mg/ml) was used. The average PS MALDI mass spectrum (500 laser shots) showed in Fig. 1A was easily obtained thought the accumulation of five spectra with a total of 100-laser shots/spectrum. In addition, no fragmentation was observed during the ionization process. Therefore, no fragmentation due to ultrasonication sample pretreatment neither to MALDI ionization was observed. These results are in agreement with previous data described in the literature [7], and can be related to the thermal stability of PS, which has a high ceiling temperature, and as such, no fragmentation is expected during a typical MALDI analysis.

Concerning PS in DHB matrix, a higher amount of AgTFA (6 mg/ml) was necessary to obtain good polymer ionization, thus confirming that the choice of the MALDI matrix is critical when performing polymer analysis by MALDI, as previously reported by different authors [3,4]. The MALDI mass spectra acquisition was more difficult than with dithranol. In fact, to achieve similar results in terms of intensity to those obtained with PS in dithranol, we needed to reduce the laser shots/spectrum ratio to 50 and also we needed to impact the laser twice in the same point of the sample spot, so the first 50 shots were discarded and the following 50 shots were accumulated. Sample preparations containing high salts concentrations often yield increased signal intensity after an initial period of low intensity at the top layer of sample spot, suggesting the formation of a layer of salt over the polymer during the sample

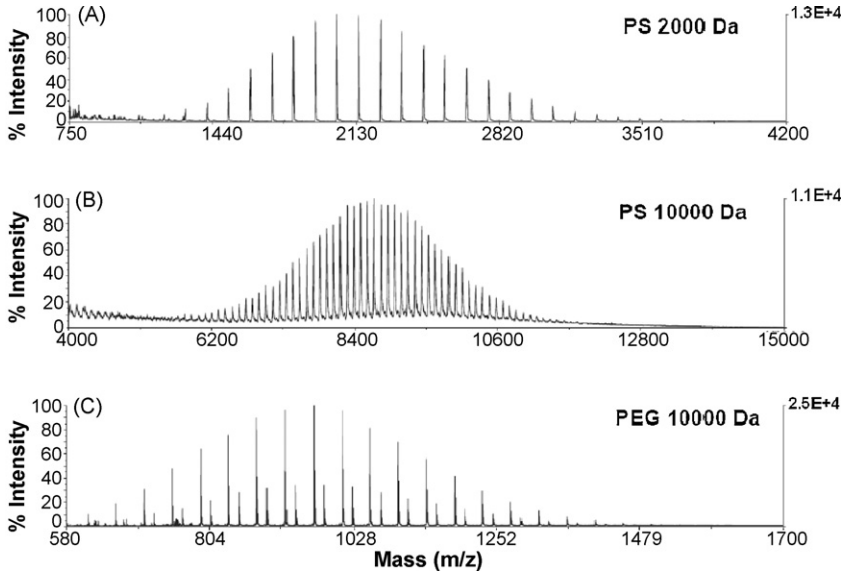

Fig. 1. MALDI mass spectra in dithranol matrix with sample treatment done with the ultrasonic bath at 35 kHz sonication frequency of poly(styrene) standard 2000 Da (A); poly(styrene) standard 10,000 Da (B) and poly(ethylene glycol) standard 10,000 Da (C).

drying in the MALDI sample plate [16]. The poor performance of the DHB as matrix for PS is directly linked with its chemical properties: the DHB is recommended for polar polymers and PS is an aromatic one. The different ultrasonic conditions tested for sample treatment did not help to improve results when DHB matrix was used.

3.1.2. Polymer characterization

As far as M_n and M_w values concerns, data regarding PS in dithranol and DHB for the seven sample treatments tested are shown in Table 1. As it can be seen, results obtained for both matrices were different. On the one hand, M_n values obtained in dithranol (ranging from 2156 Da to 2250 Da) were similar to the theoretical M_n value for this polymer recommended by the manufacturer (2140 Da). Results closest to the theoretical value were obtained with the sonoreactor for either 10 s or 30 s of sonication time. In the same way, equivalent conclusions were drawn for the M_w values. ANOVA analysis of the M_n and M_w values obtained using dithranol revealed no significant variation among the different sample treatments studied. In addition, sample sonication time, in the range studied in this work, was also found non-significant. On the other hand, as it can be seen in Table 1, M_n and M_w values obtained in DHB were ca. 200–500 Da lower than those obtained with dithranol. This finding has been previously reported in literature and can be related to analyte–matrix interactions rather than to the mixing procedure [4]. In addition, M_n and M_w values for PS 2000 Da in DHB were also lower than its recommended mass values. ANOVA analysis of the M_n and M_w values for DHB showed statistically significant differences at 95% confidence level ($P = 0.05$). To determine which means were significantly different, a multiple range test was done. In Fig. 2, a plot of the ANOVA analysis of means at 95% confidence level for the M_n and M_w values obtained for PS 2000 Da in DHB is showed. As it can be seen in this figure, statistical differences were found between the vortex mixing and the sample/matrix homogenization using the ultrasonic bath at 130 kHz for 120 s. This sample treatment displayed the lowest M_n and M_w values (1755 and 1855, respectively).

3.2. Poly(styrene) 10,000 Da

3.2.1. MALDI spectra

As described above for the PS 2000, good MALDI spectra were obtained using dithranol (10 mg/ml) and AgTFA (1 mg/ml) as matrix for the PS 10,000 Da. It must be pointed out that it was impossible to analyze this polymer with DHB even after increasing the amount

Table 1
M_n and M_w values ± standard deviations of the three polymers in dithranol and DHB matrices for each one of the seven sample treatments tested

Sample treatment	Polymer									
	PS 2000				PS 10,000		PEG 1000			
	Dithranol		DHB		Dithranol		Dithranol		DHB	
	M_n	M_w	M_n	M_w	M_n	M_w	M_n	M_w	M_n	M_w
US bath 130 HHz, 120 s	2246 ± 24	2382 ± 29	1755 ± 71	1855 ± 75	8711 ± 47	8828 ± 41	1009 ± 8	1037 ± 8	1028 ± 1	1058 ± 1
US bath 35 kHz, 30 s	2250 ± 42	2371 ± 57	1826 ± 22	1930 ± 25	8681 ± 38	8795 ± 28	1001 ± 11	1033 ± 10	1003 ± 20	1033 ± 21
US cell disruptor 10 s	2234 ± 26	2378 ± 23	1922 ± 70	2028 ± 66	8524 ± 146	8638 ± 145	1024 ± 7	1054 ± 9	997 ± 5	1031 ± 3
US cell disruptor 30 s	2245 ± 70	2392 ± 71	1876 ± 10	1993 ± 11	8625 ± 72	8743 ± 70	1024 ± 6	1053 ± 4	1010 ± 14	1045 ± 14
Sonoreactor 10 s	2156 ± 81	2312 ± 98	1921 ± 25	2029 ± 31	8726 ± 63	8837 ± 64	1014 ± 11	1043 ± 8	1029 ± 8	1058 ± 9
Sonoreactor 30 s	2176 ± 35	2313 ± 20	1954 ± 60	2059 ± 52	8646 ± 95	8757 ± 94	1029 ± 12	1056 ± 11	1039 ± 2	1069 ± 1
Vortex	2198 ± 39	2352 ± 56	1888 ± 95	2004 ± 92	8615 ± 72	8727 ± 67	1003 ± 7	1035 ± 5	1014 ± 4	1044 ± 6
Theoretical value	2140	2250	2140	2250	8650	8900	900	940	900	940

M_n and M_w values are averages of the data obtained for three samples ($n = 3$).

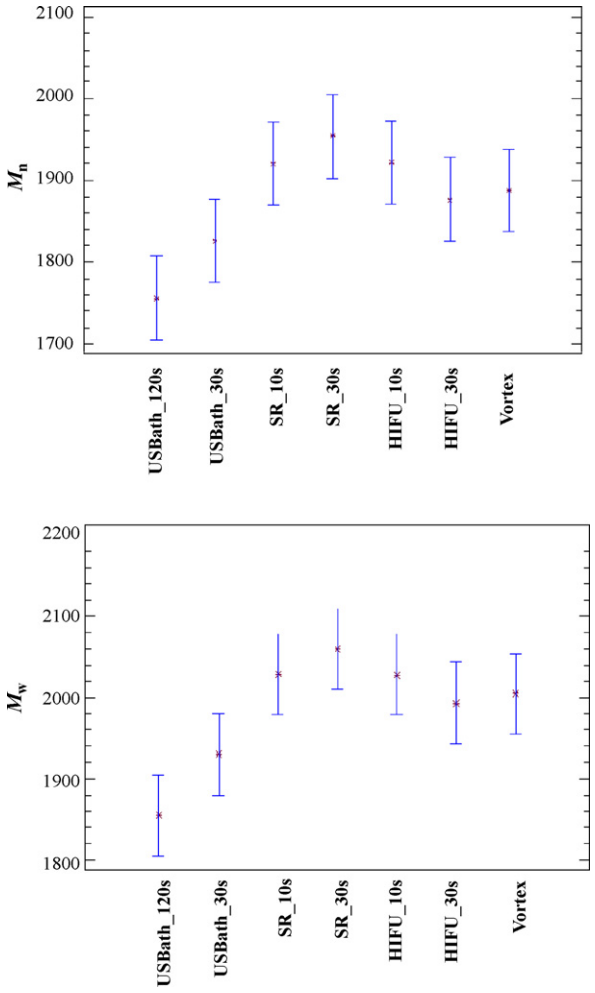

Fig. 2. Statistical analysis of means at 95% confidence level for the M_n and M_w values obtained for the poly(styrene) standard 2000 Da in DHB. LSD intervals display the least significant difference intervals for the two-factor interactions.

of silver to 6 mg/ml. The mass spectrum of PS 10,000 in dithranol is shown in Fig. 1B, where it can be seen peaks with mass differences of 104 Da, corresponding to the PS monomer mass (C_8H_8). No fragmentation peaks were noted.

3.2.2. Polymer characterization

M_n and M_w values for PS 10,000 Da in dithranol are shown in Table 1. As it can be seen in this table, M_n and M_w values were very similar to the recommended values certified by the manufacturer for this polymer (8650 Da and 8900 Da, respectively). In addition, ANOVA analysis of the M_n and M_w values revealed no significant variations as a result of the sample treatments done with the different apparatus tested (vortex, ultrasonic bath, ultrasonic cell disruptor and sonoreactor), regardless of the sonication times applied. Differences observed in the M_n values for the different sample treatments are comprised between ±1.5% of the theoretical value.

3.3. Poly(ethylene glycol), PEG, 1000 Da

3.3.1. MALDI spectra

Polyethylene glycol, PEG, was analyzed in dithranol and DHB using AgTFA (1 mg/ml). The mass spectra of PEG obtained in dithranol is shown in Fig. 1C, where it can be seen main peaks with mass differences of 44 Da, corresponding to the PEG monomer mass (C_2H_4O).

Regarding analysis done in dithranol, either for ultrasonication or vortex, a secondary peak series shifted about 16 Da to lower masses from the main series was observed (see Fig. 1C). The peak series shifted by about 16 Da to lower masses from the main series can be attributed to the fragmentation at the carbon–oxygen bond as referred in the literatures [7,13]. This fragmentation series was obtained independently of the mixing process used, thus indicating that ultrasonication was not the cause of the fragmentation. The percentage of the peak area represented by the secondary peak series was comprised between 15% and 25%. It must be stressed that there was not a link between the areas of the secondary fragmentation and the sample treatment used, thus showing that no extra fragmentation due to ultrasonication was observed.

Concerning DHB matrix, a secondary and tertiary peak series were observed shifted by about 4 Da and 16 Da, respectively, to lower masses from the main series (data not shown). Those series indicate fragmentation. The tertiary peak series shifted 16 Da can be attributed to the fragmentation at the carbon–oxygen bond as commented above. To the best of our knowledge, the secondary peak series shifted 4 Da has not been cited in literature previously. In any case, for the purposes of this study, it is unnecessary to fully characterize the fragments, since the apparent molecular mass distribution was close to the theoretical one given as reference for PEG by the manufacturer of the polymer. The pattern of fragmentation is not linked to ultrasonication since the same series of peaks were obtained after mixing the PEG and matrix with vortex. For DHB matrix the secondary peak series represented the principal contribution to the polymer distribution with an area percentage of about 50–65%, being the contribution of the main series of about 35–50% and the percentage of the tertiary series lower than 9%. Those data suggest that for DHB matrix the polymer fragmentation during the MALDI ionization process is higher than that for dithranol matrix.

The best resolution with the highest intensity was obtained for the PEG/dithranol mixture in the clear zone, situated in the outer zones of the sample spot. In this position, the matrix peaks are less intense and have no influence in the mass spectra. On the other hand, when DHB was used, the best MALDI mass spectra were obtained in the dark region of the sample spot because in the clear region more interferences of the matrix were found. This can be explained because hand-spotting usually causes large matrix crystals to form, the polymer sample being not homogeneously distributed throughout the matrix. Hand-spotted samples can have large signal variations across the sample plate; in some regions, it can be obtained large polymer signals ('sweet spots'), whilst in other regions no polymer signal is obtained [7].

3.3.2. Polymer characterization

M_n and M_w values obtained for PEG in dithranol and DHB, for all sample treatments studied are summarized in Table 1. As it can be seen in this table, results for both matrices were similar, for the same sample treatment. In addition, similar standard deviations were observed. Finally, depending on the sample treatment, a slight increment comprised between 3% and 7% for the M_n value and between 10% and 14% for the M_w value was obtained when comparing it with the recommended value given for the manufacturer.

The ANOVA analysis of M_n and M_w values obtained for PEG in dithranol and DHB revealed statistically significant differences, at 95% confidence level ($P = 0.05$), among the different sample treatments used. As consequence, a multiple range test was performed to find out which treatments were significantly different. Results

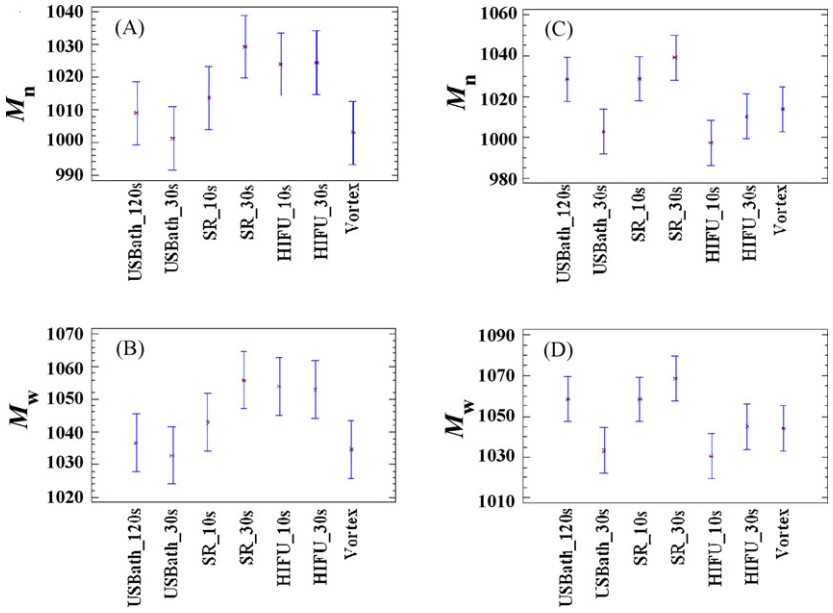

Fig. 3. Statistical analysis of means at 95% confidence level for the M_n and M_w values obtained for the poly(ethylene glycol) standard 1000 Da in dithranol (A and B) and DHB (C and D).

are given in Fig. 3, where it can be seen that

(i) For dithranol, the M_n value obtained with the vortex sample/matrix mixing was statistically different from the M_n values obtained after sample/matrix mixing with the sonoreactor with a sonication time of 30 s and the ultrasonic probe, with a sonication time of 10 s or 30 s (Fig. 3A). Similar conclusions can be obtained for the M_w values (Fig. 3B). Consequently, for this polymer and dithranol, vortex homogenization cannot be substituted for the sonoreactor or the ultrasonic probe.

(ii) For DHB, M_n and M_w values obtained for vortex and sonoreactor with a sonication time of 30 s were statistically different (Fig. 3C and D). Accordingly, for this polymer and DHB, vortex homogenization cannot be substituted for the sonoreactor.

4. Conclusions

The most promising device for sample treatment for polymer characterization by MALDI seems to be the ultrasonic bath. With this system it was assayed two different frequencies of sonication 35 kHz and 130 kHz. The homogenization process with the last frequency for the PS 2000 Da in DHB matrix during 120 s, led to low $\bar{M}_w$ and $\bar{M}_n$ values, that were found statistically different from the values obtained for the sample homogenization using vortex and from the values giving by the polymer manufacturer. Despite of this results, when UB at a sonication frequency of 35 kHz was used, the values for $\bar{M}_w$ and $\bar{M}_n$ obtained for PS and PEG in dithranol matrix were not statistically different from the ones acquired with vortex mixing or from the values recommended by the manufacturers.

As a general role, the sonoreactor and the ultrasonic probe can be also used, but firstly needs to be clearly established by comparison with a regular mixing procedure, such as vortex, that they can be used without troubles in the sample preparation of a given polymer, since in this work the applicability of such devices was shown to be dependant of a series of factors such as the type of matrix used and the sonication time employed.

For PS analysis by MALDI the DHB matrix should not be used. This matrix needs six times more Ag as cationic reagent than dithranol, for the analysis of PS 2000 Da, making necessary to discard the spectrum of the first 50 shots due to the high saline content of the mixture. In addition, it was found a high dependence on the analyte/matrix mixing procedure for this matrix. For instance, PS 2000 in DHB cannot be mixed with the ultrasonic bath at 130 kHz with a sonication time of 120 s. Moreover, when the mass of the poly(styrene) was increased from 2000 Da to 10,000 Da, analysis with DHB matrix was not possible for any of the sample mixing procedures studied, even increasing the cationic agent six times more than the amount needed for the analysis of PS 10,000 Da in dithranol.

For PEG analysis in dithranol, significant differences were found for M_n and M_w values, between vortex mixing and the sonoreactor (30 s of sonication time) and the sonication probe (10 s or 30 s of sonication time), the most intense sonication devices. When the matrix for PEG was DHB, M_n and M_w values obtained with vortex mixing were statistically different than those obtained with the sonoreactor (30 s of sonication time).

This pioneer work thus suggests that the UB with a sonication frequency of 35 kHz could be used for fast and high throughput sample treatment of polymers for their characterization. Nevertheless, this methodology needs of further confirmation and to be extended to more polymers, and for this reason more works dealing with this subject are anticipated.

Acknowledgements

R. Rial-Otero acknowledges the post-doctoral grant given by the FCT (Science and Technical Foundation) from Portugal (SFRH/BPD/23072/2005). C. Veiga de Macedo and M. Temtem acknowledge the doctoral grants SFRH/BD/19055/2004 and SFRH/BD/16908/2004, respectively, from FCT (Portugal).

References

[1] J.A. Castro, C. Koster, C. Wilkins, Rapid Commun. Mass Spectrom. 6 (1992) 239.
[2] S.F. Macha, P.A. Limbach, Curr. Opin. Solid State Mater. Sci. 6 (2002) 213.
[3] S.J. Wetzel, C.M. Guttman, K.M. Flynn, J.J. Filliben, J. Am. Soc. Mass spectrum. 17 (2006) 246.

[4] S.J. Wetzel, C.M. Guttman, J.E. Girard, Int. J. Mass Spectrom. 238 (2004) 215.
[5] J.H. Gross, Mass Spectrometry: A Text Book, Springer-Verlag, 2004, p. 425.
[6] K.J. Wu, R.W. Odom, Anal. Chem. 70 (1998) 456A.
[7] S.J. Wetzel, C.M. Guttman, K.M. Flynn, Rapid Commun. Mass Spectrom. 18 (2004) 1139.
[8] C.M. Guttman, S.J. Wetzel, J.E. Girard, W.R. Blair, B.M. Fanconi, R.J. Goldschmidt, W.E. Wallace, D.L. Van der Hart, Anal. Chem. 773 (2001) 1252.
[9] H.M. Santos, J.L. Capelo, Talanta 73 (2007) 795.
[10] D.C. Schriemer, L. Li, Anal. Chem. 68 (1996) 2721.
[11] J.L. Capelo, A.M. Mota, Curr. Anal. Chem. 1 (2005) 193.
[12] J. Axelsson, A. Hoberg, C. Waterson, P. Myatt, G.L. Shiel, J. Varney, D.M. Haddleton, P.J. Derrick, Rapid Commun. Mass Spectrom. 11 (1997) 209.
[13] R.P. Lattimer, J. Anal. Appl. Pyrol. 56 (2000) 61.
[14] German Institute for Standardization, http://www.din.de (last access December 2007).
[15] J.N. Miller, J.C. Miller, Statistics and Chemometrics for Analytical Chemistry, 4th ed., Prentice Hall, 1999 (Chapter 4).
[16] Voyager Biospectrometry Workstation, User Guide, Applied Biosystems, USA, 2001; pp. 8–67.

Talanta 77 (2008) 571–575

Contents lists available at ScienceDirect

Talanta

journal homepage: www.elsevier.com/locate/talanta

An expert flow system involving in-line prior assay for turbidimetric determination of chloride and sulphate in natural waters

Paula R. Fortes, Mário A. Feres, Elias A.G. Zagatto*

Centre for Nuclear Energy in Agriculture, University of São Paulo, P.O. Box 96, Piracicaba 13400-970, Brazil

ARTICLE INFO

Article history:
Received 16 October 2007
Received in revised form 11 March 2008
Accepted 17 March 2008
Available online 25 March 2008

Keywords:
Turbidimetry
Multi-pumping flow system
Prior assay
Expert system

ABSTRACT

A multi-pumping flow system exploiting prior assay is proposed for sequential turbidimetric determination of sulphate and chloride in natural waters. Both methods are implemented in the same manifold that provides facilities for: in-line sample clean-up with a Bio-Rex 70 mini-column with fluidized beads; addition of low amounts of sulphate or chloride ions to the reaction medium for improving supersaturation; analyte precipitation with Ba^{2+} or Ag^{+}; real-time decision on the need for next assay.

The sample is initially run for chloride determination, and the analytical signal is compared with a pre-set value. If higher, the sample is run again, now for sulphate determination. The strategy may lead to an increased sample throughput.

The proposed system is computer-controlled and presents enhanced figures of merit. About 10 samples are run per hour (about 60 measurements) and results are reproducible and unaffected by the presence of potential interfering ions at concentration levels usually found in natural waters. Accuracy was assessed against ion chromatography.

1. Introduction

In flow analysis, the result of an in-line performed prior assay can be taken into account for improving analytical strategies relying on real-time decisions [1]. The capacity of the analytical laboratory is then expanded, and the analytical results may become more reliable. As feedback mechanisms are involved [2], highly versatile flow systems are required. Multi-pumping flow systems (MPFS) [3] fulfil this requirement, as versatility is a core characteristic of them.

MPFS can be designed to behave as an expert system allowing, for instance, reduction in the number of assayed samples, simplification of the analytical procedure and/or lowering the reagent consumption.

The abilities of expert systems to perform a prior assay, interpret the gathered result and set conditions for further analytical course through concentration-oriented feedback mechanisms have been emphasised elsewhere [4]. Moreover, expert systems constitute themselves in a useful tool for screening analyses [5]. As a rule, the samples to be analysed are selected by comparing the result of the prior assay with a pre-set value. The pre-set value is inherent to the focussed problem, and a binary answer such as yes/no, absent/present, low/high is always involved.

Regarding flow analysis, in-line screening may lead to a pronounced reduction in the total number of determinations, as demonstrated in the determination of zinc and phosphate in soil extracts [6]. A 30% lessening in the number of determinations was attained because determination of zinc was carried out only when phosphate was present in concentrations higher then a pre-set value. Recently, in-line selection of the detection technique allowed better results to be obtained in the sulphite determinations in untreated water samples [7].

The aim of the present work was to develop an expert MPFS for sequential turbidimetric determination of chloride and sulphate in surface waters, involving real-time decision for selecting the samples to be run for sulphate. Both methods are implemented in the same manifold, and the need for sulphate determination depends on the chloride concentration that is in-line estimated. In-line sample clean-up is performed by letting the sample to pass through a Bio-Rex 70 cation exchanger mini-column with fluidized beads [8]. Detection limits are improved by adding low amounts of sulphate or chloride ions to the reaction medium. In order to reduce uncertain-

* Corresponding author.
E-mail address: ezagatto@cena.usp.br (E.A.G. Zagatto).

0039-9140/$ – see front matter © 2008 Elsevier B.V. All rights reserved.
doi:10.1016/j.talanta.2008.03.019

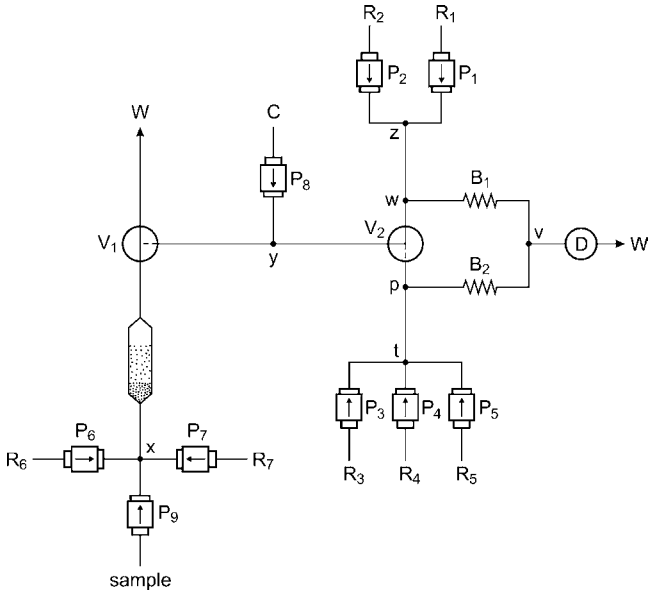

Fig. 1. Flow diagram. P_i = solenoid pumps; V_i = three-way valves; R_1 reagent: 0.01 mol L^{-1} $AgNO_3$ in 3.0 mol L^{-1} HNO_3, 1.0 mL min^{-1}; R_2 reagent: 8.0 mg L^{-1} NaCl, 1.0 mL min^{-1}; R_3 reagent: 0.16 mol L^{-1} Ba in 0.3% (v/v) Tween-80, 0.8 mL min^{-1}; R_4 reagent: 100 mg L^{-1} SO_4 in 2.0 mol L^{-1} HNO_3, 0.8 mL min^{-1}; R_5 reagent: 0.3% (w/v) EDTA in 0.2 mol L^{-1} NaOH, 0.8 mL min^{-1}; R_6 reagent: 0.1 mol L^{-1} NaOH, 1.2 mL min^{-1}; R_7: 1.5 mol L^{-1} HNO_3, 7.5 mL min^{-1}; P_8: water; B_1 and B_2 = coiled reactors (75 and 250 cm); x, y, w, z, p, t, v: confluence points; D: detector (410/800 nm).

ties of the results, the number of analytical replications is in-line defined.

2. Experimental

2.1. Samples, standards, and reagents

All solutions were prepared with analytical-grade chemicals and deionised water.

Natural water samples were collected into polyethylene bottles, preserved with 1.0 mL HNO_3 per litre, and filtered through a 0.45-μm membrane cellulose filter [9].

The stock standard solutions (1000 mg L^{-1} Cl or SO_4) were based on NaCl or $(NH_4)_2SO_4$. Working standard solutions were daily prepared in 0.014 mol L^{-1} HNO_3, covering the 0.0–20.0 mg L^{-1} range.

The following solutions were used as R_1–R_7 reagents (Fig. 1). R_1: 1.0×10^{-2} mol L^{-1} $AgNO_3$ plus 3.0 mol L^{-1} HNO_3 (weekly prepared, stored in amber bottle); R_2: 8.0 mg L^{-1} Cl; R_3: 0.15 mol L^{-1} Ba (as barium nitrate) plus 0.3% (v/v) Tween-80; R_4: 100 mg L^{-1} SO_4^{2-} plus 2.0 mol L^{-1} HNO_3; R_5: 0.3% (w/v) EDTA (disodium salt) plus 0.2 mol L^{-1} NaOH; R_6: 0.1 mol L^{-1} NaOH; R_7: 1.5 mol L^{-1} HNO_3. Water was used as C carrier stream.

The ion-exchange mini-column was prepared by packing the weakly acid cation exchanger Bio-Rex 70 (Bio-Rad, 50–100 mesh, sodium form) into a 20-mm long × 2.9-mm i.d. glass cylinder. In order to avoid resin losses during system operation, polyethylene foams were placed at both ends of the column. The resin was conditioned by passing a 1.0-mol L^{-1} HNO_3 solution (1.0 mL min^{-1}) through it for about 10 min.

2.2. Apparatus

A FIAlab-3000 flow analyser, including a model USB 2000 UV–vis Ocean Optics spectrophotometer furnished with an acrylic Z-shaped flow cell [10] (inner volume = 10 μL, optical path = 10 mm) was used. Wavelength was set as 410 nm.

The solenoid pumps (Bio-Chem Valve Inc., Boonton, NJ) with 5, 8 or 50 μL stroke volumes and the MTV-3-N1/4UKG three-way solenoid valves (Takasago Electric Inc., Nagoya, Japan) were operated through a power driver based on the PCL-711 interface card (Advantech, Cincinnati, OH) and the Quick Basic 5.0 software.

Coiled reactors and transmission lines were build-up with polyethylene tubing (i.d. = 0.8 mm) of the non-collapsible wall type.

2.3. Flow diagram

The proposed MPFS (Fig. 1) was operated according to the flowchart in Fig. 2, which emphasises the real-time decisions relying on previous measurements. Its operation is synthesized in Table 1.

The selected sample aliquot was initially handled according to the analytical procedure related to method A, here chloride. After threefold repetitive sample handling, the analytical results and uncertainties were estimated. If uncertainty was higher to an acceptable value (here 1%) the sample was run again (up to six replications). Thereafter, the averaged analytical result was compared with the pre-set threshold value. If higher, the sample was run again but aiming method B, here sulphate. If lower, next sample was run (method A).

The analytical cycle started by passing the sample through the ion-exchange mini-column with fluidized beads (P_9 pump ON). Potential interfering cations that could co-precipitate with barium sulphate [11] and organic matter that could affect formation of the silver chloride turbidity [12] were then retained. The sample excess was directed towards waste.

For chloride determination, only P_1, P_2 and P_8 pumps were switched ON. Thereafter, V_2 valve rested in the position specified in Fig. 1 during a pre-set time interval that defined the sample aliquot in terms of pump stroke volume and number of pulses [3]. During sample insertion, P_8 was switched OFF. After sample insertion, V_1 was switched back to position in Fig. 1, and P_8 was restored, thus pushing the sample selected aliquot through the analytical path related to chloride determination. At the w con-

Table 1
System operation

Step	Operation	Pump (Volume per pulse)	# Pulses	Valve position	
				V_1	V_2
1	Sampling	P_1 (5 μL) + P_2 (5 μL) + P_8 (8 μL) + P_9 (8 μL)	100	1	1
2	Sample introduction	P_1 (5 μL) + P_2 (5 μL) + P_9 (8 μL)	20	2	1
3	Reaction/column washing (phase 1)	P_1 (5 μL) + P_2 (5 μL) + P_6(8 μL) + P_8 (8 μL)	80	1	1
4	Reaction/column washing (phase 2)	P_1 (5 μL) + P_2 (5 μL) + P_8(8 μL) + P_7 (50 μL)	32	1	1
5	Sampling	P_3 (5 μL) + P_4 (5 μL) + P_8 (8 μL) + P_9 (8 μL)	100	1	2
6	Sample introduction	P_3 (5 μL) + P_4 (5 μL) + P_9 (8 μL)	60	2	2
7	Reaction/column washing (phase 1)	P_3 (5 μL) + P_4 (5 μL) + P_6 (8 μL) + P_8 (8 μL)	80	1	2
8	Column and analytical path washing (phase 2)	P_5 (5 μL) + P_7 (50 μL) + P_8 (8 μL)	32	1	2

Only P_i pumps specified below were switched ON; valve position 1 means the position specified in Fig. 1 and number 2 the alternative position.

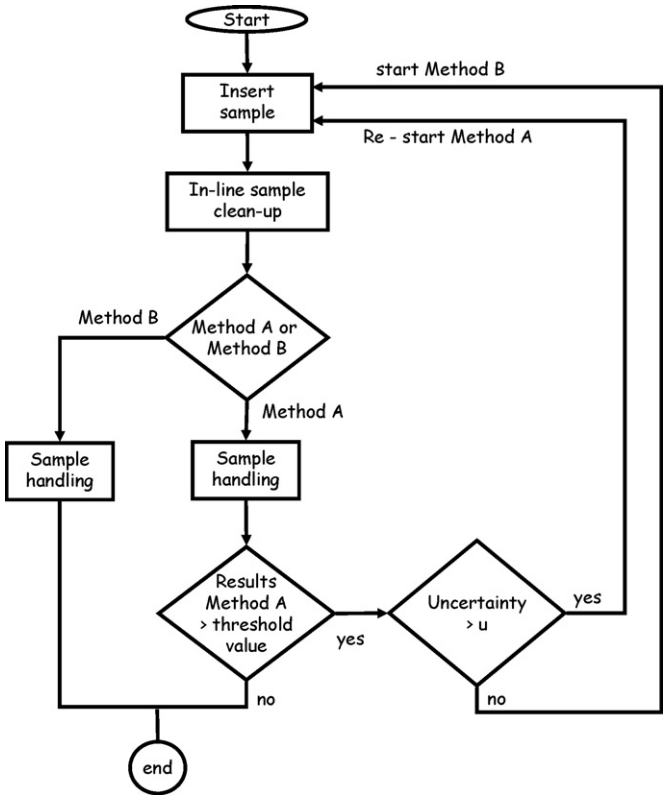

Fig. 2. Flowchart. Logical sequence of software is repeated three or six folds according to the experimental response.

fluence, the previously mixed (z confluence) R_1 and R_2 reagents were added to the sample, allowing formation of the analyte concentration-dependent turbidity inside B_1 reactor. Details of the involved chemistry are given elsewhere [12]. Passage of the sample though the detector resulted in a transient increase in turbidance, which was recorded as a peak with height proportional to chloride concentration in the sample, providing that uniform particle size and shape was attained [13]. Meantime, P_6 and P_7 were successively actuated in order to direct R_6 and R_7 streams towards the mini-column, thus eluting the retained potential interfering species towards waste and washing the mini-column. The procedure was threefold repeated and the mean analytical signal associated with the chloride determination as well as its uncertainty was analysed as above-mentioned.

For sulphate determination, V_2 valve was moved to the alternative position, and the sample merged with R_3 and R_4 reagents at the p confluence connector. Details of the reaction occurring inside B_2 reactor are discussed elsewhere [14]. Analogously to chloride, the number of replications was defined in function of the measurement repeatability. After that, P_5 pump was switched directing the R_5 reagent to wash the analytical path. Addition of alkaline EDTA solution was beneficial for this purpose. Preliminary tests emphasised that efficient washing of the manifold portions associated to sulphate determination was attained with a 0.3-w/v EDTA plus 0.2 mol L^{-1} NaOH concentrations in the R_5 reagent.

2.4. Procedure

Regarding chloride determination, influence of acidity of the reaction medium was investigated by varying the HNO_3 concentration (0.0–5.0 mol L^{-1}) in R_1 reagent. Concentrations of $AgNO_3$ (R_1 reagent) and chloride (R_2 reagent) were investigated within the 5.0×10^{-4} to 1.0×10^{-1} mol L^{-1} and 0.0–10.0 mg L^{-1} ranges, respectively. Optimization followed the one-parameter-at-a-time approach. Studies focusing on the influence of primary nucleous formation and further chloride addition to the analytical path were accomplished by varying the lengths of z–w transmission line and B_1 reactor within the 0–300 and 10–100 cm ranges, respectively. Influence of total flow rate was investigated between 2.0 and 5.0 mL min^{-1}. The sample-injected volume was varied between 80 and 240 μL (10–30 pulses).

Regarding sulphate determination, influence of concentration of R_3 reagent was investigated between the 0.12–0.30 mol L^{-1} Ba and 0.1–0.3% (w/v) Tween-80 ranges. Influence of acidity was investigated by varying the HNO_3 concentration between 0.1 and 2.0 mol L^{-1} (R_4 reagent). Additionally, concentration of added sulphate ions (R_4 reagent) was investigated between 0 and 100 mg L^{-1}. Influence of the available time for reaction development was studied by varying either the B_2 reactor length (75–200 cm) or the total flow rate (2.0–5.0 mL min^{-1}). The sample-injected volume was investigated between 320 and 800 μL.

After system dimensioning, it was applied to natural waters and the main analytical figures of merit were evaluated.

3. Results and discussion

3.1. System dimensioning

Formation of the precipitate involves nucleation and crystal growth. During the nucleation period, clusters are formed under supersaturated conditions, and the precipitate is not visible. The newly formed crystals reach a critical size beyond which the stability pattern is reversed and the particles tend to grow [15]. The number of formed crystals varies with the nature of precipitate, and depends also on several parameters amongst them the concentration of the involved solutions and presence of surfactants [11,13].

Regarding silver chloride precipitation, the colloidal particles under formation adsorb silver ions, present in large excess, being then positively charged. The stability of the colloidal suspension is therefore dependent on van der Waals and electrical double layer forces, and a tendency towards uniformity in particle size is noted. Consequently, surfactant addition (colloid protector) and/or high Ag concentrations are not needed for the turbidimetric determination of chloride. In fact, no measurable differences in recorded peak heights were noted when Tween-80 was added to the R_2 reagent. Another relevant aspect is the relatively fast turbidity formation. In the present work, no increase in turbidance was noted after stopping the sample zone at the detector, demonstrating that turbidity was fully established during the mean sample residence time in the analytical path.

Increasing the Ag concentration from 5×10^{-4} to 5.0×10^{-2} mol L^{-1} Ag in R_1 reagent improved sensitivity, but further increase (up to 5.0×10^{-3} mol L^{-1} Ag) caused a slight lessening in sensitivity, probably because of particle agglutination that led to a reduction in the available particle area for radiation scattering [16]. The Ag concentration in R_1 reagent was then selected as 1.0×10^{-2} mol L^{-1} Ag.

Addition of chloride ions permitted lower chloride concentrations to be detected, as one can perceive by analysing Fig. 3. As rate of turbidity formation was not a limiting factor in this context, the beneficial aspects arising from the Cl addition were then more related to solubility product. However, the chloride concentration in R_2 reagent could not be increased at will, in order to avoid a too high and noisy baseline. It was then set as 8.0 mg L^{-1} resulting in a stable baseline of about 0.05 turbidance.

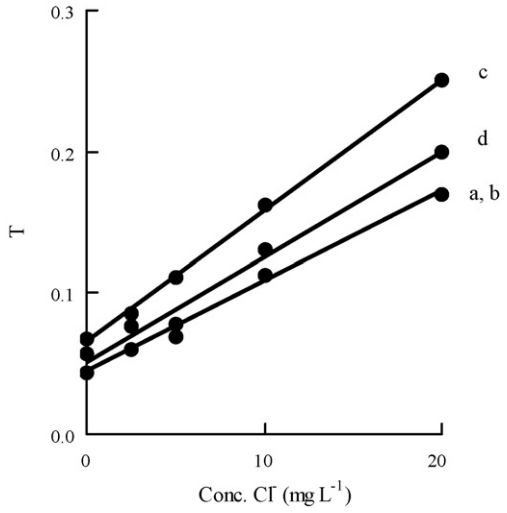

Fig. 3. Influence of chloride addition. T = turbidance; curves a, b, c, and d refer to 2.0, 4.0, 8.0 and 10.0 mg L^{-1} Cl in R_2 reagent, respectively.

In contrast to AgCl, a very large excess of barium ions is needed for a more uniform formation of the crystalline barium sulphate precipitate, as supersaturation is more relevant in relation to $BaSO_4$ formation, and improved under higher Ba concentrations. Moreover, number of clusters is increased. A surfactant should be added in order to guarantee a uniform particle size distribution, thus measurement repeatability. In fact, erratic results in the absence of a colloid protector were noted, corroborating earlier findings [13]. Addition of surfactants played a beneficial influence also in relation to system washing, as retention of barium sulphate crystals in the analytical path (mainly adsorption on the tubing inner walls) was minimised. Here, addition of 0.3% (v/v) Tween-80 surfactant in R_3 reagent was enough for attaining reproducible measurements (R.S.D. < 2%) and a baseline with a very slight drift (<0.05 turbidance per hour).

The barium concentration in R_3 reagent was also a relevant parameter. For <0.12 mol L^{-1} Ba, detection limit was not satisfactory, as suitable supersaturated conditions were not attained. Stopping the sample zone at the detector permitted one to conclude that rate of turbidity formation was too low, as the peak recorded for 5.0 mg L^{-1} SO_4 was noted only after about 2 min. Increasing the Ba concentration up to 0.20 mol L^{-1} Ba led initially to an improvement in detection limit and then to an increase in the analytical signal associated to 0.00 mg L^{-1} SO_4, whereas the slope of the analytical curve remained practically unaffected. The Ba concentration was then selected as 0.16 mol L^{-1}.

Analogously to the chloride determination, addition of sulphate ions to the reaction medium permitted lower analyte concentrations to be detected. The sulphate concentration in R_4 reagent was experimentally selected as 100 mg L^{-1} SO_4. Lower values impaired detection limit whereas higher ones led to higher signals recorded for 0.00 mg L^{-1} SO_4.

Both chloride and sulphate methods are carried out under acidic conditions in order to avoid formation of insoluble hydroxides with some potential interfering species, as well as precipitation of barium with foreign anions such as hydroxides and carbonates. Acidity was not a parameter of paramount relevance in the chloride method, and was set as 3.0 mol L^{-1} HNO_3 in R_1 reagent. Under the consequent high acidity, variations in sample acidity did not affect the analytical results. Regarding sulphate determination, acidity of the reaction medium is a relevant parameter, and could not be increased indefinitely, as the solubility of the precipitate would be higher [17] and nucleation rate and crystal growth would be impaired [14], deteriorating sensitivity. Acidity was then selected as 2.0 mol L^{-1} HNO_3 in R_4 reagent.

Length of z–w transmission line (or conversely, flow rate through it) determines the available time for interaction between added chloride and silver ions. This length was not relevant in relation to the chloride determination, as the involved nucleation is fast. On the other hand, the t–p line was kept as short as possible (10 cm), to avoid settlement of barium sulphate crystals on the tubing inner walls. With longer lines, sensitivity was improved but repeatability deteriorated in view of the erratic crystal release.

B_1 and B_2 reactor lengths were defined as 75 and 250 cm, enough for attaining good mixing conditions. Increasing B_1 length beyond this value lessened recorded peak height in view of the increased sample axial dispersion. Regarding B_2 length, sensitivity was slightly affected by increasing this parameter, as the increase in sample dispersion was compensated by the increase in the turbidity formation. This aspect was confirmed, although conversely, by varying total flow rate. As a compromise between sensitivity, detection limit and sample throughput, 3.0 and 3.2 mL min^{-1} total flow rates and 160 and 460 μL sample volumes were selected in relation to the chloride and sulphate determinations, respectively.

3.2. Figures of merit

The proposed system has been applied to large-scale analyses of natural water samples. About 10 samples are run per hour, meaning 1.88 g barium nitrate and 0.086 g silver nitrate consumed per determination. Sample throughput can be improved by reducing the number of replications or when the number of samples without requiring sulphate determination is significant. In the present situation, all samples were assayed for both analytes, as validation of the involved methods was aimed.

The system is stable, and a slight baseline drift is noted during extended (4 h) working periods. Schlieren noise is usually lower then 0.03 turbidance and can be circumvented by using the dual-wavelength strategy [18] with measurements performed simultaneously at 410 and 800 nm. The analytical curves are lin-

Table 2
Results related to analysis of samples collected near seashore

Sample	Chloride		Sulphate	
	This work	Ion chromatography [20]	This work	Ion chromatography
1	8.95 ± 0.16	9.22 ± 0.05	1.33 ± 0.02	1.33 ± 0.01
2	8.88 ± 0.11	9.40 ± 0.01	1.35 ± 0.06	1.36 ± 0.02
3	8.90 ± 0.32	9.40 ± 0.04	1.38 ± 0.01	1.44 ± 0.01
4	5.50 ± 0.67	5.56 ± 0.06	1.30 ± 0.02	1.33 ± 0.03
5	5.25 ± 0.13	5.84 ± 0.04	0.95 ± 0.01	0.96 ± 0.01
6	5.15 ± 0.03	5.27 ± 0.01	1.12 ± 0.01	1.10 ± 0.01

Data expressed in g L^{-1}. Data based on three replications. For details, see text.

ear for chloride and sulphate determinations, typical regression coefficients being estimated as 0.997 and 0.993 ($n = 5$), respectively. Detection limits based on 3σ were estimated as 0.7 mg L^{-1} Cl and 1.3 mg L^{-1} SO_4.

Implementation of both methods in a single expert system did not impair accuracy, as the main analytical characteristics were maintained. Statistical differences between the proposed procedure and ion chromatography [19] were not found at the 95% probability level.

4. Conclusions

The feasibility of implementing turbidimetric procedures in expert multi-pumping flow system was demonstrated. The system is versatile and some of the involved routines can be skipped. In fact, the number of replications can be fixed and the algorithm for selecting samples to be run for method B can be by-passed. This happened in, e.g., the analyses of sample lots from estuarine waters where both chloride and sulphate determinations were needed. As high values were expected, samples underwent a 200-fold manual dilution with water. Results are presented in Table 2 that, again, permits one to conclude that the proposed system provides accurate results. In arid regions near the sea border, the typical seawater sulphate-to-chloride concentration ratio of 0.14 [20] tends to be modified when the sample is subjected to influence of interior waters, and this is evident in Table 2.

In view of its potentialities, the proposed strategy is recommended for flow-based large-scale analyses. In fact real-time decisions based on in-line prior assays constitute themselves in a powerful tool for expanding the capacity of the laboratory with consequent benefits in the analytical quality and cost.

Acknowledgements

Partial support from CNPq and FAPESP is greatly appreciated.

References

[1] J.M.T. Carneiro, A.C.B. Dias, E.A.G. Zagatto, R.S. Honorato, Anal. Chim. Acta 455 (2002) 327.
[2] B.A. Hohne, T.H. Pierce, Expert System Applications in Chemistry, ACS Symposium Series, American Chemical Society, Washington, DC, 1989.
[3] J.L.F.C. Lima, J.L.M. Santos, A.C.B. Dias, M.F.T. Ribeiro, E.A.G. Zagatto, Talanta 64 (2004) 1091.
[4] C. Filippini, B. Sonnleitner, A. Fiechter, Anal. Chim. Acta 265 (1992) 63.
[5] M. Valcarcel, S. Cardenas, M. Gallego, Trends Anal. Chem. 18 (1999) 685.
[6] V. Grassi, A.C.B. Dias, E.A.G. Zagatto, Talanta 64 (2004) 1114.
[7] L. Ferrer, J.M. Estela, V. Cerda, Anal. Chim. Acta 573 (2006) 391.
[8] M.F.T. Ribeiro, J.L.M. Santos, J.L.F.C. Lima, A.C.B. Dias, E.A.G. Zagatto, Talanta 68 (2005) 351.
[9] L.S. Clesceri, A.E. Greenberg, A.D. Eaton (Eds.), Standard Methods for the Examination of Water and Wastewater, 20th edn, American Public Health Association, American Water Works Association, Water Environmental Federation, Washington, 1998.
[10] J. Ruzicka, Analyst 125 (2000) 1053.
[11] I.M. Kolthoff, E.B. Sandell, E.J. Meehan, S. Bruckenstein, Quantitative Chemical Analysis, 4th edn, The Macmillan Co., London, 1969.
[12] R.P. Sartini, C.C. Oliveira, E.A.G. Zagatto, Quim. Anal. 16 (1997) 233.
[13] F.J. Krug, H. Bergamin Filho, E.A.G. Zagatto, S.S. Jorgensen, Analyst 102 (1977) 503.
[14] F.J. Krug, E.A.G. Zagatto, B.F. Reis, O. Bahia Filho, A.O. Jacintho, Anal. Chim. Acta 145 (1983) 179.
[15] M.L. Salutsky, W.R. Grace, in: I.M. Kolthoff, P.J. Elving (Eds.), Treatise on Analytical Chemistry. Part 1. Theory and Practice, The Interscience Encyclopedia Inc., New York, 1959 (Chapter 18).
[16] G.W. Ewing, Instrumental Methods of Chemical Analysis, McGrow-Hill, Inc., Columbus, OH, 1969.
[17] R.A. Johnson, J.D. O'Rourke, J. Am. Chem. Soc. 76 (1954) 2124.
[18] A.C.B. Dias, E.P. Borges, E.A.G. Zagatto, P.J. Worsfold, Talanta 68 (2006) 1076.
[19] N. Gros, B. Gorenc, J. Chromatogr. B 668 (1994) 385.
[20] K. Grasshoff, Methods of Seawater Analysis, Verlag Chemie, Weinheim, New York, 1976.

Talanta 77 (2008) 461–462

Contents lists available at ScienceDirect

Talanta

journal homepage: www.elsevier.com/locate/talanta

Preface

Fourteenth International Conference on Flow Injection Analysis

The 14th International Conference on Flow Injection Analysis and Related Techniques (ICFIA 2007) was held in Berlin, Germany, 2–7 September 2007. The conference was held jointly with the Japanese Association for Flow Injection Analysis (JAFIA).

ICFIA 2007 was hosted by Wolfgang Frenzel, acting also as Program Chairman, from the Technical University Berlin and Jürgen Simon from the Freie Universität Berlin.

There were 116 participants from 30 countries representing five continents, thus creating a truly international flair in many respects. The programme consisted of 9 invited keynote lectures, representing a cross-section of leading FIA research around the globe, 32 submitted oral presentations and 108 posters.

Keynote lectures were given by Manuel Miro (University of the Balearic Islands, Spain) on application of various generations of FIA for processing solid samples, Ian McKelvie (Monash University, Melbourne, Australia) on water quality assessment using FIA techniques with emphasis on determination of nutrients and metal species in natural waters, Marcela Segundo (University of Porto, Portugal) on the role of FIA and SIA for food analysis, Kate Grudpan (Chiang Mai University, Thailand) who compared the relationships of various FI techniques to other flow methods, Olaf Elsholz (University of Applied Sciences, Hamburg, Germany) on the use of FIA in bioprocess analysis, emphasising the requirements of robustness for routine analysis, Edgar Paski (British Columbia Institute of technology, Burnaby, Canada) on the challenges of implementing ISO standards for FIA and SIA methodologies, Krystyna Pyrzynska (University of Warsaw, Poland) who reviewed separation and preconcentration techniques for trace metal analysis, Paul Worsfold (University of Plymouth, United Kingdom) giving an overview of luminescence techniques in FIA and the particular benefits that arise from this combination, and Dalibor Satinsky (Charles University, Czech Republic) who presented the current status of sequential injection chromatography.

A special half-day session was devoted to FIA/SIA developments in Japan. The session was chaired by Elo Harald Hansen, who in a brief introductory speech also highlighted the contribution of Japanese scientists to developments of FI methodologies. The six selected contributions given by Hideyuki Itabashi, Koichi Oguma, Tsutomo Nagaoka, Hideji Tanaka, Norio Teshima and Shoji Motomizu were a very impressive documentation of the current activities in Japan featuring many innovations and presenting interesting areas of application.

The submitted lectures and the poster presentations covered the enormous breadth of flow-based analytical techniques. This was well illustrated by contributions presenting instrumental developments and automation (e.g., sequential injection analysis, sequential injection chromatography, all-injection analysis, multipumping systems, microfluidic devices), various means of on-line sample preparation such as membrane separation, preconcentration and extraction, as well as a variety of novel configurations for multi-component determinations, speciation and kinetic-catalytic methods.

Several contributions of ICFIA 2007 presented novel derivatisation reactions for spectrophotometric detection but also combinations with other detection principles like fluorimetry, chemiluminescence measurements and different electroanalytical techniques. The continuous interest in atomic spectrometric methods as FIA detectors for trace metal determinations became evident from several contributions, often involving in-line preconcentration and/or matrix separation techniques. A larger number of contributions dealt with enzymatic methods and biosensors, impressively demonstrating the advantages of kinetically controlled conditions inherent to FI methodology. Hyphenated techniques such as FI-LC and FI-CE were also presented offering interesting options for both sample pretreatment and multi-analyte determinations. Several contributions focussed on theoretical aspects of FIA related to mixing conditions, calibration strategies and chemometric data evaluation.

Applications of FIA and related techniques to a large variety of sample matrices were reported, including the environmental and agricultural samples, food, and pharmaceuticals as well as clinical and biological samples. Possibilities of analysis of gases and non-aqueous samples using FI-methodology were also presented.

FIA instruments were exhibited by Hach Lange GmbH, Düsseldorf, Germany, and by Medizin- und Labortechnik Engineering GmbH, Dresden, Germany. Furthermore FIAlab Instruments (Bellevue, WA, USA) and eDAQ Company (Chalgrove, UK) displayed instrument literature and Sciware SL (Palma de Mallorca, Spain) made a live presentation of their software tools for control of flow systems and data evaluation. All these companies have sponsored ICFIA 2007 in one or the other way.

The social programme of ICFIA 2007 included a welcome reception on Sunday afternoon, a get-together party on Monday evening (which incidentally felt together with the birthday of the Conference Chairman and was hence a unique opportunity for him to celebrate this event in a very memorable way) and a full day excursion to Potsdam visiting the famous Sanssouci Castle and eventually having a cruise on the beautiful lakes of this area. The conference dinner took place on Thursday evening in the form of a buffet with a large variety of typical Berlin food specialities in the canteen of the

0039-9140/$ – see front matter
doi:10.1016/j.talanta.2008.09.012

Technical University. As the Conference Chairman I had the pleasure to present poster prizes donated by Talanta, Microchimica Acta and Analytical and Bioanalytical Chemistry and also to say *Thank You* to all persons that have contributed to the success of ICFIA 2009.

This special issue includes 24 peer reviewed papers submitted by conference attendees. They provide an excellent cross-section of the contributions of ICFIA 2007 and the current research in the field of flow-based techniques in general. I sincerely hope that going through this issue will stimulate the readers to consider FIA and related techniques even more than before to be interesting research subjects and valuable tools for problem solving.

The 15th ICFIA will be held in Nagoya, Japan, 28th September to 3rd October 2008. The conference will be jointly organised by the International Conference on Flow Injection Analysis and the Japanese Association for Flow Injection Analysis celebrating the 25th anniversary meeting of the latter association.

Wolfgang Frenzel*
Department of Environmental Technology, Technical University Berlin, Str. d. 17. Juni 135, D-10623 Berlin, Germany

* Tel.: +49 30 314 29710.
E-mail address: wolfgang.frenzel@tu-berlin.de

Available online 18 September 2008

Talanta 77 (2008) 673–678

Contents lists available at ScienceDirect

Talanta

journal homepage: www.elsevier.com/locate/talanta

Simultaneous determination of econazole nitrate, main impurities and preservatives in cream formulation by high performance liquid chromatography

Angel Arturo Gaona-Galdos*, Pedro López García, María Segunda Aurora-Prado, Maria Inês Rocha Miritello Santoro, Érika Rosa Maria Kedor-Hackmann

Department of Pharmacy, Faculty of Pharmaceutical Sciences, University of São Paulo, Av. Prof. Lineu Prestes 580, 05508-900 São Paulo, SP, Brazil

ARTICLE INFO

Article history:
Received 16 April 2008
Received in revised form 3 July 2008
Accepted 7 July 2008
Available online 15 July 2008

Keywords:
Econazole nitrate
Impurities
Preservatives
Gradient method

ABSTRACT

A reversed-phase high performance liquid chromatographic (RP-HPLC) method for determination of econazole nitrate, preservatives (methylparaben and propylparaben) and its main impurities (4-chlorobenzyl alcohol and alpha-(2,4-dichlorophenyl)-1*H*-imidazole-1-ethanol) in cream formulations, has been developed and validated. Separation was achieved on a column Bondclone® C18 (300 mm × 3.9 mm i.d., 10 μm) using a gradient method with mobile phase composed of methanol and water. The flow rate was 1.4 mL min^{-1}, temperature of the column was 25 °C and the detection was made at 220 nm. Miconazole nitrate was used as an internal standard. The total run time was less than 15 min. The analytical curves presented coefficient of correlation upper to 0.99 and detection and quantitation limits were calculated for all molecules. Excellent accuracy and precision were obtained for econazole nitrate. Recoveries varied from 97.9 to 102.3% and intra- and inter-day precisions, calculated as relative standard deviation (R.S.D.), were lower than 2.2%. Specificity, robustness and assay for econazole nitrate were also determined. The method allowed the quantitative determination of econazole nitrate, its impurities and preservatives and could be applied as a stability-indicating method for econazole nitrate in cream formulations.

1. Introduction

Most fungal infections involve superficial invasion of skin or the mucous membranes of body orifices. Some species under certain conditions are capable of invading deeper body cavities and causing systemic mycoses. Such infections may become serious and occasionally life-threatening, and are frequently difficult to treat. The treatment of systemic mycoses is becoming very important in recent years as a result of the increased incidence of opportunistic yeast infections in immunocompromised patients. The widespread use of immunosuppressants following organ transplant operations and AIDS has been major contributors to this situation [1].

The azoles represent a class of versatile antifungal agents. In general, the azoles are effective against most fungi that cause superficial infections of the skin and mucous membranes. At high concentrations the azoles are fungicidal; at low concentrations they are fungistatic. The fungicidal effect is associated with damage to the fungi cell membrane, with the loss of essential cellular constituents. The fungistatic effects of the azoles have been correlated with the inhibition of membrane-bound enzymes by low concentration of the azoles [1].

Econazole nitrate (1-[2-(4-chlorophenyl)methoxy]-2-(2,4-dichlorophenyl)ethyl)-1*H*-imidazole mononitrate (Fig. 1EN) is a potent broad-spectrum antifungal agent used topically in the treatment of skin infections. Further, results indicate that econazole could replace rifampicin/isoniazid as well as both rifampicin and isoniazid in chemotherapy of murine tuberculosis. Econazole alone or in combination with antitubercular drugs did not produce any hepatotoxicity in normal or *Mycobacterium tuberculosis*-infected mice [2,3].

Reported methods for the determination of econazole nitrate in pharmaceutical formulations include titrimetry [4], spectrophotometry [5,6], derivative spectrophotometry [7,8], high performance liquid chromatography (HPLC) [9–12], gas chromatography [13], high performance thin-layer chromatography [14] and capillary electrophoresis (CE) [15]. A variety of enantiomeric separations using HPLC and CE methods were also published [16–25]. Quantification of EN in biological samples has been developed using

* Corresponding author at: Department of Pharmacy, Faculty of Pharmaceutical Sciences, University of São Paulo, Av. Prof. Lineu Prestes 580 B-13, Butantã, 05508-900 São Paulo, SP, Brazil. Tel.: +55 11 3091 3655; fax: +55 11 3815 4418.
E-mail address: aagaona@usp.br (A.A. Gaona-Galdos).

0039-9140/$ – see front matter © 2008 Elsevier B.V. All rights reserved.
doi:10.1016/j.talanta.2008.07.010

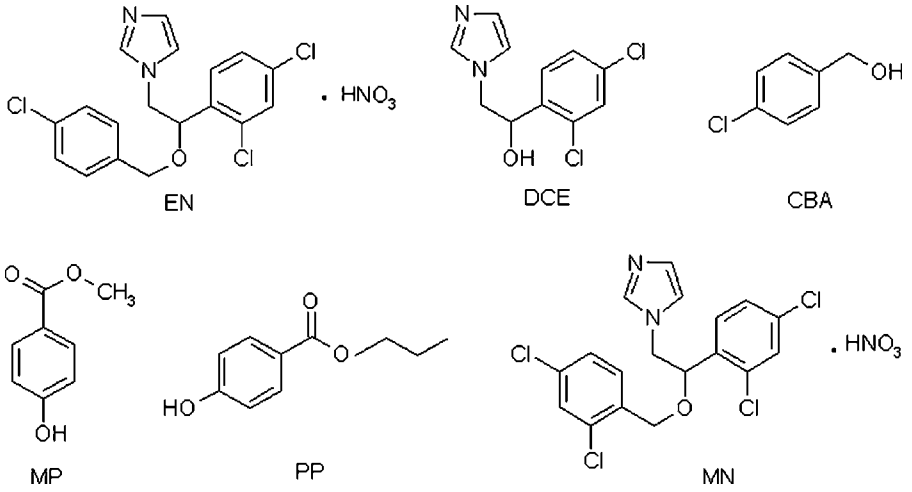

Fig. 1. Chemical structures of econazole nitrate (EN), alpha-(2,4-dichlorophenyl)-1*H*-imidazole-1-ethanol (DCE), 4-chlorobenzyl alcohol (CBA), methylparaben (MP), propylparaben (PP) and miconazole nitrate (MN).

near infrared spectrometry [26,27] and liquid chromatography [28]. A stability-indicating assay method validated for econazole nitrate is described in the literature [29], showing specificity for its degradation products (4-chlorobenzyl alcohol and alpha-(2,4-dichlorophenyl)-1*H*-imidazole-1-ethanol), as well as the inactive ingredients, but not for preservatives because they were not present in the formulation (methylparaben and propylparaben). This chromatographic separation was achieved with isocratic elution on a RP-18 column using methanol/aqueous ammonium carbonate solution/tetrahydrofurane as the mobile phase and miconazole nitrate as an internal standard. Nevertheless, this method allows only the quantitative determination of econazole nitrate.

A pharmaceutical impurity is a component that is not the chemical entity defined as the drug substance or an excipient in the drug product. For this reason the safety of pharmaceuticals is dependent not only on the intrinsic toxicological properties of the active ingredient and excipients in the drug product, but also in part upon the impurities that it may contain [30]. Therefore, identification, quantification and control of impurities in the drug substance and drug product are important in the drug development.

Preservatives would be effective at low concentrations against all possible microorganisms, nontoxic and compatible with other constituents used in the preparation. Esters of *p*-hydroxybenzoic acid (parabens) have antifungal properties. Their toxicity is generally low, owing to rapid *in vivo* hydrolysis to *p*-hydroxybenzoic acid, which is rapidly conjugated and excreted [1].

The present methodology in comparison with the methods described in the literature, shows a simple sample preparation and mobile phase composition and the last containing methanol–water without buffers. This proposed method allows the simultaneous determination of econazole nitrate, its impurities and preservatives in creams formulations with good resolution and peak symmetry.

2. Experimental

2.1. Instrumentation

The gradient HPLC method was performed on a chromatographic system, consisted of a solvent delivery pump system model LC-10AD (Shimadzu® Corporation, Japan), an auto injector fitted with 20 μL loop model SIL-10AD (Shimadzu® Corporation, Japan), an online degasification system model DGU-14A (Shimadzu® Corporation, Japan), a column thermostat oven model CTO-10AS (Shimadzu® Corporation, Japan) and an UV–VIS photodiode array detector model SPD-M10A (Shimadzu® Corporation, Japan). The output signal was monitored and integrated using CLASS VP® software v.5.91 (Shimadzu® Corporation, Japan). A reversed-phase C18 Column, Bondclone® (300 mm × 3.9 mm i.d., 10 μm) Phenomenex™ California, USA, was used for separation.

2.2. Chemicals

The reagents were of analytical grade. Methanol (HPLC grade), obtained from Merck (Darmstadt, Germany). Water was deionized and purified on a Milli-Q® water purification system (Millipore, Bedford, MA, USA) and used to prepare all solutions.

2.3. Chromatographic conditions

The mobile phase was methanol–water. The analysis was carried out in a gradient elution mode with 57% methanol at 0 min gradually increased to 72% at 6.5 min, then increased to 98% at 10 min, from 10.01 to 15 min 98% using a flow rate of 1.4 mL min^{-1} at 25 °C. Before delivering into the system the solvent was filtered through 0.45 μm, HV membrane and degassed. The chromatograms were recorded at 220 nm.

Table 1
Development of solvent gradient systems

	System 1		System 2		System 3		System 4		System 5		System 6	
	T (min)	%	*T* (min)	%	*T* (min)	%	*T* (min)	%	*T* (min)	%	*T* (min)	%
Methanol	0	55	0	55	0	55	0	55	0	57	0	57
	45	100	35	100	13	72	13	72	10	72	6.5	72
					15	90	15	90	14	97	10	98
					23	95	23	95	19	97	15	98
Flow rate (mL min^{-1})	1.0		1.2		1.2		1.4		1.4		1.4	

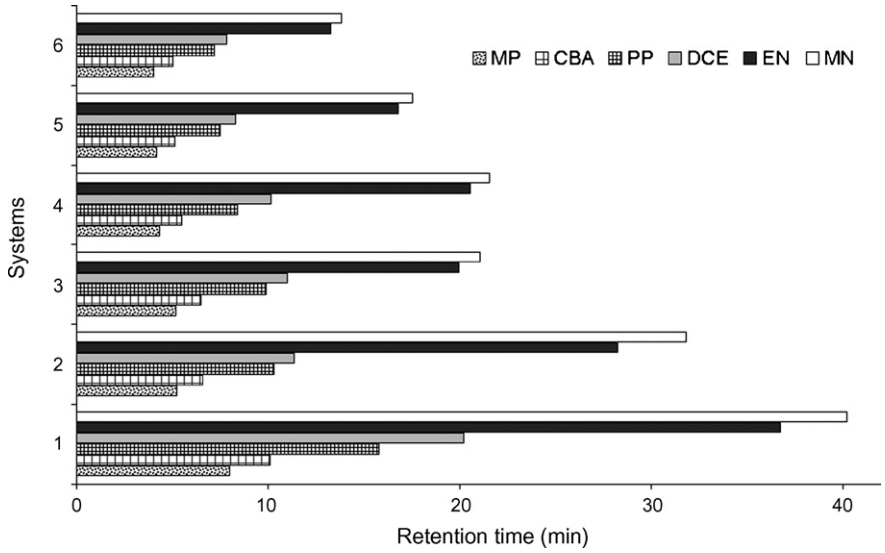

Fig. 2. Gradient developing systems for methylparaben (MP), 4-chlorobenzyl alcohol (CBA), propylparaben (PP), alpha-(2,4-dichlorophenyl)-1*H*-imidazole-1-ethanol (DCE), econazole nitrate (EN) and miconazole nitrate (MN). (Systems as in Table 1.)

2.4. Standards

Econazole nitrate (100.55% purity) (Fig. 1EN) and miconazole nitrate (100.32% purity) (Fig. 1MN) were kindly donated by Formil Química Ltda. (São Paulo, Brazil). Impurities of econazole nitrate: alpha-(2,4-dichlorophenyl)-1*H*-imidazole-1-ethanol (98% purity) (Fig. 1DCE) and 4-chlorobenzyl alcohol (99% purity) (Fig. 1CBA) were purchased from Acrõs Organics (Geel, Belgium). Preservatives: methylparaben (Fig. 1MP) and propylparaben (Fig. 1PP) were donated by Laboratório Stiefel Ltda. (São Paulo, Brazil).

2.5. Sample

The cream sample was supplied by Laboratório Stiefel Ltda. (São Paulo, Brazil) containing 1% (w/w) of econazole nitrate.

2.6. Preparation of standard and sample solutions

Standard stock solutions of econazole nitrate (1000 μg mL^{-1}), miconazole nitrate (1000 μg mL^{-1}), alpha-(2,4-dichlorophenyl)-1*H*-imidazole-1-ethanol (20 and 40 μg mL^{-1}), 4-chlorobenzyl alcohol (20 and 40 μg mL^{-1}), methylparaben (500 μg mL^{-1}) and propylparaben (200 μg mL^{-1}) were prepared in methanol. The solutions were stored under refrigeration. Working standard solutions were prepared fresh daily by diluting appropriately the stock solutions with the same solvent.

Table 2
Chromatographic parameters

Compounds	Parameters			
	t_R (min)	K	α	R_s
MP	4.03	1.47	MP/CBA = 1.40	2.31
CBA	5.00	2.06	CBA/PP = 1.65	4.92
PP	7.11	3.40	PP/DCE = 1.12	1.47
DCE	7.85	3.81	DCE/EN = 1.87	12.46
EN	13.25	7.12	EN/MN = 1.05	2.25
MN	13.83	7.48		

MP: methylparaben; CBA: 4-chlorobenzyl alcohol; PP: propylparaben; DCE: alpha-(2,4-dichlorophenyl)-1*H*-imidazole-1-ethanol; EN: econazole nitrate; MN: miconazole nitrate; t_R: retention time; α: separation factor; K: retention factor; R_s: resolution.

For the preparation of sample solution an amount equivalent to about 0.25 g of cream was accurately weighed into a 25-mL beaker and dissolved in 10 mL of a mixture of methanol–water (50:50, v/v) in a water-bath at 60 °C for 5 min. After this period, the solution was quantitatively transferred to a 25-mL volumetric flask. A 2.5-mL aliquot of the miconazole nitrate solution (1000 μg mL^{-1}, stock solution) was transferred into a 25-mL volumetric flask. Then the solution was homogenized, cooled to room temperature and the volume was completed to 25 mL with the mixture methanol–water. The sample solution was then filtered using blue strip filter paper (Schleicher & Schull, Germany). Before injection on chromatograph, the solution was filtered through a 0.22 μm filter (Millex PTFE, Millipore®). Final concentrations of econazole nitrate and miconazole nitrate solutions were 100 μg mL^{-1}.

2.7. Method validation

The method was validated according to the United States Pharmacopeia requirements [31]. The following validation charac-

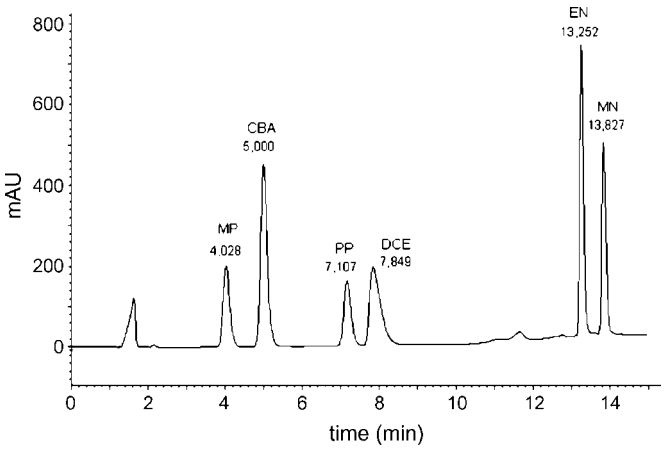

Fig. 3. Chromatogram of standard solutions. Peaks: methylparaben (MP), 4-chlorobenzyl alcohol (CBA), propylparaben (PP), alpha-(2,4-dichlorophenyl)-1*H*-imidazole-1-ethanol (DCE), econazole nitrate (EN) and miconazole nitrate (MN). Conditions: Bondclone® C18 Column, 300 mm × 3.9 mm i.d., 10 μm; mobile phase: gradient elution starting with 57%, v/v methanol–water; temperature: 25 ± 1 °C; flow rate: 1.4 mL min^{-1}; UV detection at 220 nm.

Table 3
Linearity, detection and quantitation limits determined for the proposed RP-HPLC method for all compounds

Statistical parameter	EN	MP	PP	CBA	DCE
Concentration range ($\mu g\,mL^{-1}$)	70–120	30–55	8–18	0.2–6.2	0.2–6.2
Intercept	0.0834	0.0192	0.0031	−0.0015	−0.0011
Slope	0.0101	0.0066	0.0050	0.0144	0.0086
Correlation coefficient (r^2)	0.9977	0.9977	0.9991	0.9991	0.9991
Residual S.D. of the regression line (σ)	0.0144	0.0047	0.0009	0.0015	0.0009
DL ($\mu g\,mL^{-1}$)	4.71	2.35	0.57	0.35	0.35
QL ($\mu g\,mL^{-1}$)	14.28	7.13	1.72	1.06	1.05
F	857.57	861.19	2356.78	2220.68	2278.52

EN: econazole nitrate; MP: methylparaben; PP: propylparaben; CBA: 4-chlorobenzyl alcohol; DCE: alpha-(2,4-dichlorophenyl)-1*H*-imidazole-1-ethanol; DL: detection limit; QL: quantitation limit; *F*-test tabulated$_{(0.05,1.4)}$ = 7.71.

teristics were addressed to: linearity, detection and quantitation limits, precision, accuracy, robustness, system suitability, selectivity, assay and specificity.

2.7.1. Linearity, detection and quantitation limits, precision and accuracy

Appropriate aliquots of stock solutions were transferred into 10 mL volumetric flasks and diluted to volume with methanol. Concentration range from 70 to 120 $\mu g\,mL^{-1}$ for econazole nitrate, 30–55 $\mu g\,mL^{-1}$ for methylparaben, 8–18 $\mu g\,mL^{-1}$ for propylparaben, and 0.2–6.2 $\mu g\,mL^{-1}$ for degradation products (4-chlorobenzyl alcohol and alpha-(2,4-dichlorophenyl)-1*H*-imidazole-1-ethanol) were obtained. Then, the solutions were filtered using a 0.22-μm filter (Millex PTFE, Millipore®) and injected on the HPLC instrument. Each solution was injected in triplicate. Peak area ratios (compound/miconazole nitrate) were plotted versus the respective compound concentrations.

Detection (DL) and quantitation limits (QL) were calculated from the residual standard deviation of the regression line (σ) of the analytical curve and its slope (S) in accordance with the equations DL = 3.3 (σ/S) and QL = 10 (σ/S) [32].

In order to measure repeatability of the system (while keeping the operating conditions identical), 20 consecutive injections were made using a standard solution containing 80 $\mu g\,mL^{-1}$ of econazole nitrate and 100 $\mu g\,mL^{-1}$ of miconazole nitrate (IS). The results were expressed as the percentage relative standard deviation (%R.S.D.) for peak area ratio (PAR) of econazole nitrate/miconazole nitrate and retention time of econazole nitrate.

For the determination of repeatability sample solutions were prepared at 100 $\mu g\,mL^{-1}$ of econazole nitrate and 100 $\mu g\,mL^{-1}$ of miconazole nitrate. Ten determinations were performed to establish the intra-day precision.

The intra-day precision was evaluated by injecting sample solutions prepared at lower, middle and higher concentrations of the analytical curve (80–120 $\mu g\,mL^{-1}$ econazole nitrate) containing 100 $\mu g\,mL^{-1}$ of miconazole nitrate, in 1 day. The inter-day precision was evaluated by injecting the same solutions on three consecutive days. Three determinations for each concentration were performed. Precision was expressed as the %R.S.D. for peak area ratio of econazole nitrate/miconazole nitrate.

The accuracy was calculated as the percentage recovery of a known amount of standard added to the sample. The accuracy of method was evaluated in triplicate using three concentration levels 80, 100 and 120 $\mu g\,mL^{-1}$. Econazole nitrate standard solution was added to commercial sample solution and analyzed by the proposed method.

2.7.2. Robustness

The robustness of an analytical procedure is a measure of its capacity to remain unaffected by small, but deliberate, variations in method parameters, and provides an indication of its reliability during normal usage [33]. In order to the robustness study of the proposed method, deliberate modifications in temperature–wavelength values were made. Thus, three temperatures values were selected, one below and one above of the chosen temperature. The same was made with wavelength.

2.7.3. Specificity

The specificity of the method for econazole nitrate was tested by analyzing a mixture of the inactive ingredients (placebo), the commercial samples of econazole nitrate and a mixture of standard solutions.

2.7.4. Selectivity

The selectivity of the method was established through study of retention time, separation factor, retention factor, resolution of all peaks and the absorption spectra of the eluted peaks.

3. Results and discussion

3.1. Method development

In order to develop a simple HPLC method for quantitative determination of EN, its impurities and preservatives in cream formulations, different solvent systems were evaluated (acetonitrile, methanol and isopropanol), each one in different proportions. Rate gradients and flow rates also were tested to achieve efficient separation with a satisfactory resolution in a short time of analysis. Both solvents acetonitrile and isopropanol do not provided satisfactory

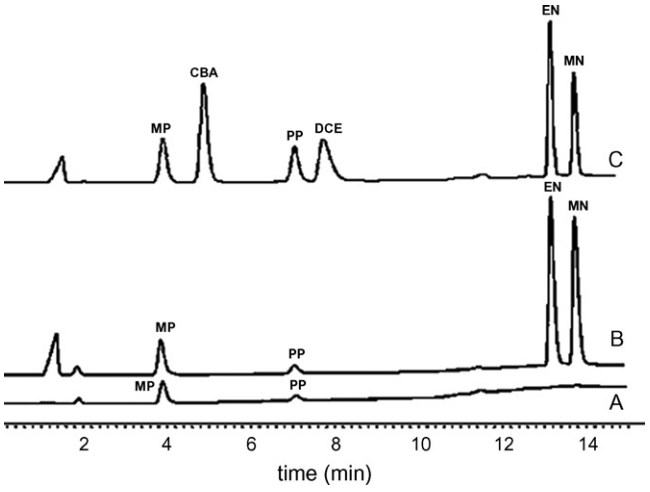

Fig. 4. Chromatograms of placebo (A), commercial sample containing econazole nitrate (B) and standard solutions(C). Conditions: Bondclone® C18 Column, 300 mm × 3.9 mm i.d., 10 μm; mobile phase: gradient elution starting with 57%, v/v methanol–water; temperature: 25 ± 1 °C; flow rate: 1.4 mL min^{-1}; UV detection at 220 nm.

chromatographic profiles (overlaps in degradation products peaks and inadequate drift).

Several gradient systems were tested with the mobile phase, methanol–water (Table 1). The optimization of the methodology had targets as an adequate analysis time, avoid a pronounced rise of drift and an adequate resolution factor of all compounds separated. To reduce time analysis it was determined the elapsed time between the increase in the composition of mobile phase and its passage through the detector. In order, to avoid the drift elevation, it was also determined the adequate time in which the percentage of methanol increases from 72 to 98% in 3.5 min, since a smaller time produced an abrupt rise in the baseline. On the other hand, a greater time does not cause significant difference. To achieve an adequate resolution between all eluted peaks, it was calculated the resolution factor, which was higher than 1.45 for all the substances. Time analysis was significantly reduced in the system 6 in comparison with the others tested systems. Fig. 2 shows the retention times for the 6 compounds in each one of the systems. The gradient developed system 6 was the one who provides the best results in time, resolution and symmetry of the peaks, as depicted in Fig. 3. Other parameters are shown in Table 2.

3.2. Method validation

Analytical curves were obtained by plotting peak area ratios (compound/IS) against the concentrations of respective substances. In all cases, straight regression lines with correlation coefficients (r) above 0.997 were obtained. F-test was applied for all calibration curves and the data provide conclusive evidence of a linear effect between concentration and instrumental response [34]. Data are summarized in Table 3.

The DL and QL were calculated using analytical curves results (Table 3). DL and QL values were obtained by injecting 20 μL of standard solutions in the chromatographic system.

Table 4
Intra- and inter-day precision of the proposed RP-HPLC method for econazole nitrate quantitative determination

	80 μg mL^{-1}	100 μg mL^{-1}	120 μg mL^{-1}
Intra-day (n = 3)			
%R.S.D.	2.20	0.81	1.56
Inter-day (n = 9)			
%R.S.D.	0.52	1.27	0.93

Injection precision was determined after injecting 20 times in the chromatographic system an econazole nitrate standard solution containing 80 μg mL^{-1}. The results obtained for PAR were, %R.S.D. 0.25 and for retention time, %R.S.D. 0.04. The values obtained demonstrate that the system is reliable for analysis.

The precision of the method was evaluated by repeatability and intermediate precision determinations. For repeatability, 10 sample solutions at 100 μg mL^{-1} were analyzed in the same day and the R.S.D. obtained was 1.74%. The intermediate precision was achieved by analyzing three different concentrations on three consecutive days. The one-way ANOVA was used to estimate the total variability within and between days. The results, which, are shown in Table 4 present good agreement.

The accuracy of the method was evaluated at three concentration levels. Triplicate determinations were made at each concentration level. The accuracy is expressed as percentage of standard recovered from sample matrix as R.S.D. The results are shown in Table 5.

For robustness determination, changes in the temperature and wavelength were evaluated. About 1.8% of difference was observed in the more critical result when the analytical parameters were modified and compared with the original conditions.

The specificity of the method was demonstrated by the absence of interference among econazole nitrate, methylparaben, propy-

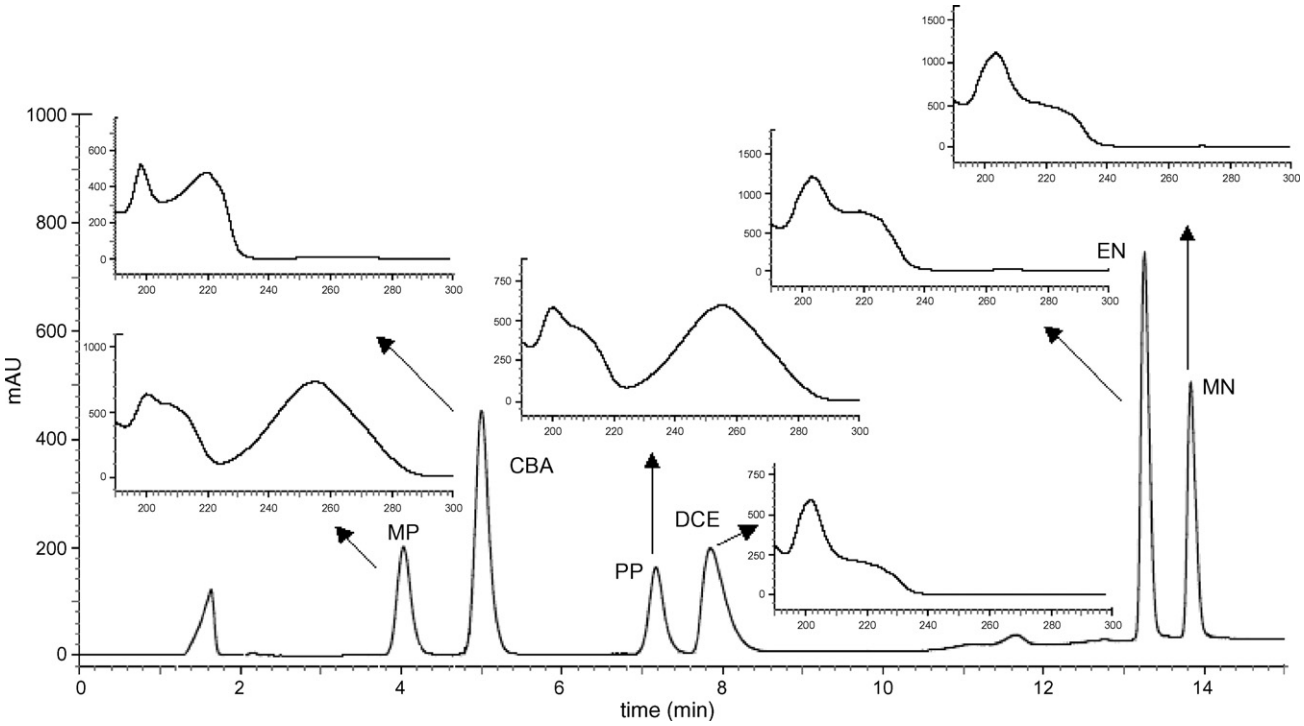

Fig. 5. Chromatogram of separation of standard solutions and spectra for all compounds. Peaks: methylparaben (MP), 4-chlorobenzyl alcohol (CBA), propylparaben (PP), alpha-(2,4-dichlorophenyl)-1*H*-imidazole-1-ethanol (DCE), econazole nitrate (EN) and miconazole nitrate (MN). Conditions: Bondclone® C18 Column, 300 mm × 3.9 mm i.d., 10 μm; mobile phase: gradient elution starting with 57%, v/v methanol–water; temperature: 25 ± 1 °C; flow rate: 1.4 mL min^{-1}; UV detection at 220 nm.

Table 5
Recovery of a standard solution of econazole nitrate added to sample and determined using the proposed HPLC method

Standard added to commercial sample[a] ($\mu g\,mL^{-1}$)	Standard found ($\mu g\,mL^{-1}$)	Recovery (%)[b]
40.00	39.15	97.88
50.00	51.13	102.26
60.00	60.68	101.13

[a] Commercial sample (econazole nitrate cream).
[b] Average of three determinations.

lparaben, alpha-(2,4-dichlorophenyl)-1*H*-imidazole-1-ethanol, 4-chlorobenzyl alcohol, miconazole nitrate and excipients in the samples, using the criteria defined in the USP 30 for assays [31]. A mixture of the inactive ingredients (placebo) (Fig. 4A), the commercial sample of econazole nitrate (Fig. 4B) and a standard mixture solution (Fig. 4C), were analyzed by the proposed methodology. As it can be observed, neither the cream excipients nor preservatives and the impurity interfere in the analysis of EN.

Two preservative substances present in the formulation and impurities of econazole nitrate were used to evaluate the selectivity of the method. Results are showed in Table 2. The absorption spectra of the eluted peaks were achieved using a photodiode array detector and then compared with those of the reference standards. The results showed equivalent spectrophotometric profiles (Fig. 5).

For the assay, a sample was analyzed in triplicate and the average obtained was 105.50%. The British Pharmacopoeia [35] established a range between 90 and 110%. The tested sample using the proposed method, presented satisfactory results.

System suitability test is an important part of liquid chromatographic method. It is used to verify if the chromatographic system is adequate and reliable. Data from 5 injections of a solution containing 80 $\mu g\,mL^{-1}$ of econazole nitrate standard solutions were analyzed. The R.S.D. was 0.09%. This result agrees with those specified in the United States Pharmacopeia [31].

4. Conclusion

The validated method is rapid and efficient, and allows the separation of econazole nitrate in the presence of its degradation products, impurities and excipients, without using buffers or pH modifier in the mobile phase.

Since it was possible to identify and quantify econazole nitrate impurities as (4-chlorobenzyl alcohol and alpha-(2,4-dichlorophenyl)-1*H*-imidazole-1-ethanol), the proposed method can be used as a stability-indicating method for this drug in pharmaceutical formulations.

Acknowledgements

The authors thank the Conselho Nacional de Desenvolvimento Cientifico e Tecnológico of Brazil (CNPq, 130652/2007-5; CNPq, 142664/2005-7) for fellowship.

References

[1] A.R. Martin, in: J.N. Delgado, W.A. Remers (Eds.), Wilson and Davold's Textbook of Organic Medicinal and Pharmaceutical Chemistry, Lippincot Williams & Wilkins, England, 1998, pp. 173–221.
[2] A. Zahoor, S. Sharma, G.K. Khuller, FEMS Microbiol. Lett. 258 (2006) 200.
[3] A. Zahoor, S. Sharma, G.K. Khuller, FEMS Microbiol. Lett. 261 (2006) 181.
[4] M. Massaccesi, Analyst 111 (1986) 987.
[5] S.R. El-Shabouri, K.M. Emara, P.Y. Khashaba, A.M. Mohamed, Anal. Lett. 31 (1998) 1367.
[6] P.Y. Khashaba, S.R. El-Shabouri, K.M. Emara, A.M. Mohamed, J. Pharm. Biomed. Anal. 22 (2000) 363.
[7] D. Bonazzi, V. Cavrini, R. Gatti, E. Boselli, M. Caboni, J. Pharm. Biomed. Anal. 18 (1998) 235.
[8] V. Cavrini, A.M. Di Pietra, R. Gatti, J. Pharm. Biomed. Anal. 7 (1989) 1535.
[9] X.-L. Yang, Z.-F. Xi, J.-F. Sheng, Chin. J. Antib. 29 (2004) 403.
[10] L. Gagliardi, D. De Orsi, P. Chimenti, R. Porra', D. Tonelli, Anal. Sci. 19 (2003) 1195.
[11] E. Kublin, T. Kaniewska, J. Pharm. Belg. 53 (1998) 208.
[12] A.M. Di Pietra, V. Andrisano, R. Gotti, V. Cavrini, J. Pharm. Biomed. Anal. 14 (1996) 1191.
[13] E. Kublin, T. Kaniewska, Chem. Anal. (Warsaw, Pol.) 41 (1996) 19.
[14] G. Popovic, M. Cakar, K. Vucicevic, S. Vladimirov, D. Agbaba, J. Planar Chromatogr. Mod. TLC 17 (2004) 109.
[15] A. Arranz, C. Echevarria, J.M. Moreda, A. Cid, J.F. Arranz, J. Chromatogr. A 871 (2000) 399.
[16] L. Toribio, M.J. Del Nozal, J.L. Bernal, C. Alonso, J.J. Jimenez, J. Chromatogr. A 1144 (2007) 255.
[17] X. Lin, C. Zhu, C. Hao, Electrophoresis 26 (2005) 3890.
[18] I. Ali, H.Y. Aboul-Enein, Biomed. Chromatogr. 17 (2003) 113.
[19] H.Y. Aboul-Enein, I. Ali, J. Pharm. Biomed. Anal. 27 (2002) 441.
[20] H.Y. Aboul-Enein, I. Ali, Anal. Bioanal. Chem. 370 (2001) 951.
[21] H.Y. Aboul-Enein, I. Ali, Chromatographia 54 (2001) 200.
[22] A. Van Eeckhaut, S. Boonkerd, M.R. Detaevernier, Y. Michotte, J. Chromatogr. A 903 (2000) 245.
[23] J.Y. Liu, Y.Y. Dong, T.S. Wang, H.W. Liu, A.J. Huang, Y.L. Sun, Z.P. Sun, Chin. Chem. Lett. 10 (1999) 39.
[24] E. Peyrin, Y.C. Guillaume, Chromatographia 49 (1999) 691.
[25] N. Morin, Y.C. Guillaume, J.C. Rouland, Chromatographia 48 (1998) 388.
[26] J.P. Medendorp, K.S. Paudel, R.A. Lodder, A.L. Stinchcomb, Pharm. Res. 24 (2007) 186.
[27] J. Medendorp, J. Yedluri, D.C. Hammell, T. Ji, R.A. Lodder, A.L. Stinchcomb, Pharm. Res. 23 (2006) 835.
[28] P. Chiap, Ph. Hubert, J. Crommen, J. Chromatogr. A 948 (2002) 151.
[29] R. Christinat, H.W. Zulliger, Arzneim. Forsch. 34 (1984) 551.
[30] A.K. Basak, A.S. Raw, L.X. Yu, Adv. Drug Delivery Rev. 59 (2007) 1.
[31] United States Pharmacopeia, 31st ed. The United States Pharmacopeial Convention, Rockville, 2008, pp. 683–687.
[32] E. McEvoy, S. Donegan, J. Power, K. Altria, J. Pharm. Biomed. Anal. 44 (2007) 137.
[33] International Conference on Harmonization (ICH) of Technical Requirements for Registration of Pharmaceuticals for Human Use, Topic Q2 (R1): Validation of Analytical Procedures: Text and Methodology, Geneva, 2005.
[34] J.O. Rawlings, S.G. Pantula, D.A. Dickey, Applied Regression Analysis, 2nd ed., Springer, 1998, pp. 16–18.
[35] British Pharmacopoeia. http://www.pharmacopeia.co.uk, 2008 (accessed 3/7/2008).

Talanta 77 (2008) 533–540

Contents lists available at ScienceDirect

Talanta

journal homepage: www.elsevier.com/locate/talanta

Underway determination of alkalinity in estuarine waters by reagent-injection gas-diffusion flow analysis

Sarah M. Gray[1], Peter S. Ellis, Michael R. Grace, Ian D. McKelvie*

Water Studies Centre, School of Chemistry, P.O. Box 23, Monash University, Clayton, Victoria 3800, Australia

ARTICLE INFO

Article history:
Received 29 October 2007
Received in revised form 11 March 2008
Accepted 17 March 2008
Available online 25 March 2008

Keywords:
Gas diffusion
Reagent-injection
Alkalinity
Spectrophotometry

ABSTRACT

The development and application of a portable, hybrid reagent-injection gas-diffusion flow analysis technique is described for the underway measurement of total alkalinity in estuarine waters. Injection of pH 4.5 buffer into a continuously flowing sample stream produced gaseous CO_2 that diffused across a microporous PTFE membrane into a weakly buffered acceptor stream containing bromothymol blue indicator. The resultant change in acceptor stream pH was detected photometrically using a super-bright LED with a multi-reflection flow cell and charge coupled device detector. This method gave a detection limit of 0.5 mg $CaCO_3$ L^{-1}, with reproducibility of 1.0% R.S.D. at 160 mg $CaCO_3$ L^{-1}, and a measurement rate of 71 injections h^{-1}. The portable FIA system was used for underway analysis of estuarine waters with salinities ranging from that of freshwater to seawater, and there was close agreement between the results obtained by underway analysis and from a reference titration method.

1. Introduction

The total alkalinity (TA) of natural waters is practically defined as the amount of base (HCO_3^-, CO_3^{2-}, OH^-) that must be titrated with acid in order to reach a pH of 4.5, the point at which hydroxyl ions and dissolved carbonate species are converted to carbonic acid [1]. In marine waters, the total alkalinity will also include other basic or weakly basic species with pK_a values of ≥4.5 that are present at detectable concentrations, such as borate and silicate [2].

Total alkalinity is historically expressed in terms of the mass equivalent of calcium carbonate, and in freshwaters total alkalinity can range from 0.05 to 500 mg $CaCO_3$ L^{-1} (1–10,000 μM) [3], while in marine systems the concentration usually lies within a narrow range of 115–130 mg $CaCO_3$ L^{-1} (2300–2600 μM) [4]. Total alkalinity is an important water quality parameter because it provides a measure of the buffering capacity of a waterbody. Acidic species from atmospheric or catchment sources, or from internal biogeochemical processes, may exceed the buffer capacity of a natural waterbody, causing measurable pH change. There have, for example, been widespread reports of the acidification of freshwater lakes in response to acid rain [5]. It is estimated that 30–40% of the anthropogenic carbon dioxide added to the atmosphere due to the burning of fossil fuels is absorbed by the oceans [6,7], and there is now concern that this will decrease the pH of the oceans, by as much as 0.4–0.5 pH units by 2100 [8,9].

In estuaries, total alkalinity may behave conservatively, i.e. the observed concentration change is due only to dilution by mixing of marine and freshwaters, or it may behave non-conservatively in response to the effects of processes such as calcite dissolution or deposition [10], rapid, high river flow events [11], or respiration and primary production. In the anoxic bottom waters and/or sediments of an estuary, alkalinity increases in response to microbially mediated processes such as denitrification, and sulfate, iron and manganese reduction that consume H_3O^+ [12].

Because of the transient nature of dispersion and mixing processes in estuaries, which are highly dependent on river flows and tidal fluxes, high frequency or spatially intense sampling and analysis is desirable in order that these processes be properly studied and understood. Ideally rapid, on-line or *in situ* analytical techniques should be employed either onboard or from a sampling vessel to enable underway collection of chemical information.

Total alkalinity in marine and estuarine systems has historically been determined by potentiometric acid–base titration [13], and this approach has subsequently been adapted for shipboard use [14]. However shipboard measurements of total alkalinity are technically demanding, and involve painstaking measurements of combined titrant-acid and sea water volumes, as well as careful standardisation and storage of acids [15]. Thus, the development of simpler, more robust methods for the determination of total alkalinity in a variety of aquatic systems, that do not require the constant supervision of an experienced analyst, and which can be operated autonomously are highly desirable. While automated lab-

* Corresponding author. Tel.: +61 3 99054558; fax: +61 3 99054196.
E-mail address: ian.mckelvie@sci.monash.edu.au (I.D. McKelvie).
[1] Current address: Nanotechnology Victoria Ltd., PO Box 229, Dingley 3127, Victoria, Australia.

0039-9140/$ – see front matter © 2008 Elsevier B.V. All rights reserved.
doi:10.1016/j.talanta.2008.03.020

oratory titrators suitable for measurement of total alkalinity are widely available, there are few reports of methods that are suitable for continuous deployment, e.g. in underway mode at sea. A flow injection system with potentiometric detection has been described for total alkalinity monitoring in wastewaters [16] and an *in situ* flow-through analyser [7] has been reported for use in seawater. These measurements are dependent on well-behaved potentiometric systems, which can be difficult to maintain in the electrically noisy and mechanically aggressive conditions that occur onboard ship or smaller sampling craft [6].

Flow injection titrations with spectrophotometric detection have also been reported for total alkalinity determination in drinking [3] and surface waters [6], but the application of these methods to the analysis of estuarine waters is likely to be problematic because of errors associated with either salt effects on the detection chemistry or due to the schlieren (refractive index) effect that occurs when there is wide variation in salinity from one sample to another [17].

FIA coupled with gas diffusion techniques has previously been reported for the determination of *total* inorganic carbon (TIC) in water samples. In this approach, sample is acidified and the gaseous carbon dioxide that is evolved diffuses through a gas permeable membrane into an acceptor stream, a process that is monitored by following changes in electrical conductivity [18] or the absorbance of a pH indicator [19].

This paper describes a FIA gas diffusion system for the determination of total alkalinity in estuarine and fresh waters that is based on a similar approach to that described above for total inorganic carbon analysis, except that a pH 4.5 buffer is employed to adjust the sample pH rather than a strong acid. At this pH, which corresponds to the endpoint used in the titrimetric procedure for total alkalinity determination, the amount of carbon dioxide produced is proportional to the total alkalinity of the water sample. Diffused carbon dioxide was detected in the acceptor stream by measuring the change in absorbance of a bromothymol blue indicator at 640 nm. In addition to carbonate species, the total alkalinity value strictly includes the titratable hydroxyl, borate and silicate species, but these are generally present in concentrations that are small compared with the carbonate/hydrogen carbonate alkalinity at 6 the pH of seawater (pH ca. 8.2) [4]. The validation data shown later confirms that the exclusion of non-carbonate species in the determination of TA is not problematic for surface fresh, estuarine and marine waters, but it is recognized that substantial errors are likely to occur using the proposed method for waters at pH $\leq$ 9.

The proposed method for TA was implemented using a portable FIA instrument that was previously described for the rapid, underway determination of filterable reactive phosphorus in estuarine waters. This instrument operates in multiple reagent-injection or reagent multi-commutation mode, i.e. by insertion of multiple adjacent sample and reagent zones, rather than the conventional injection of a single zone of sample into a continuously flowing stream of carrier or reagent. Reagent is held in a series of reservoirs pressurized with helium gas, and is injected for carefully controlled periods using miniature solenoid valves [20]. Use of multi-commutation promotes better sample and reagent mixing, potentially improves sensitivity, reduces reagent consumption, simplifies FIA manifold design and provides greater potential for miniaturization [21]. The compact flow injection system used in this instance is a hybrid of both conventional sample injection and multi-commutation systems. This confers advantages of improved mechanical reliability (use of a rotary injection valve is avoided), simplicity (only two peristaltic pump channels are used), and reduced reagent consumption, making it suitable for rapid on-line monitoring of total alkalinity in estuarine environments from small sampling craft and larger marine vessels for extended periods. Furthermore, because this flow injection system exploits the gas diffusion technique, it is tolerant to sample matrices with widely varying salinities.

2. Experimental

2.1. Reagents

All solutions were prepared using analytical grade materials (minimum purity 99%) and ultra pure water (UPW) obtained from a Modulab® Analytical water purification system (Continental Water Systems Corporation, Seven Hills NSW 2147, Australia). Total alkalinity working standards in the range 40–160 mg $CaCO_3$ L^{-1} were prepared daily by dilution of a 10 g $CaCO_3$ L^{-1} sodium hydrogen carbonate stock solution (1.6797 g/100 mL) that was stored at 4 °C in the dark.

The indicator stream, an 8×10^{-5} M bromothymol blue solution (pK_{In} = 7.1) [22], was prepared in 1 mM phosphate buffer solution at pH 6.5. A potassium hydrogen phthalate buffer solution at pH 4.5 [23] was used for reagent-injection.

The standard reference material (SRM) for total alkalinity was supplied by Analytical Products Group, Inc. (Belpre, OH 45714, USA), with a certified value of 43.0 $\pm$ 1.9 mg $CaCO_3$ L^{-1}.

2.2. Sample collection

Samples used for the laboratory validation of the total alkalinity method included five commercial still spring water samples (Pump, Golden Circle, Farmland, Summit and Cool Ridge), purchased from a local supermarket, a variety of tap waters, and a sample from a freshwater pond (Monash University). Marine water samples were collected from Werribee and Queenscliff in Port Phillip Bay, south-eastern Australia. All water samples were filtered on-site (0.2 μm Acrodisc® syringe filter, Pall Life Sciences, Ann Arbor, MI 48103, USA), and stored at 4 °C in prewashed polypropylene bottles.

The underway analysis of total alkalinity was performed from a 5 m powerboat, with the portable FIA system housed in a waterproof container amidships. Sample was pumped continuously using a 12 V dc portable peristaltic pump (7518-00, Masterflex, Cole-Parmer Instrument Co, Vernon Hills, IL 60061, USA), through a 3 mm i.d. × 6 m PVC feed tube which was attached to a finned metal "fish" used to weight the sample line and maintain it below the water surface at depths of ca. 1 or 0.2 m, depending on the cruise speed (2.5 or 5 knots respectively). The sample was coarse filtered through a 25 μm mesh nylon screen (Swiss Screens (Aust) Pty. Ltd., Huntingwood, NSW 2148, Australia) mounted in a membrane filter assembly (Swinnex® 47, Millipore Corp., Billerica, MA 01821, USA) before passing through a tangential flow filtration (TFF) unit (Vivaflow 50, Gelman, Pall Life Sciences) at a flow rate of ca. 200 mL min^{-1} (Fig. 1). This high flow rate was used to ensure minimal sample transit time from the sampling intake to the entrance port of the TFF (ca. 13 s), and to promote turbulent flow through the tangential flow filter. Depending on the suspended solids concentration of samples, filtrate flow rate varied between 4 and 20 mL min^{-1} as a filter cake gradually accumulated on the membrane surface. A T-piece was used as a differential flow splitter (FS), to regulate the pressure of filtrate feed to the analyser. Sample was drawn into the analyser using the peristaltic pump on the instrument at 2.4 mL min^{-1}, and the excess flow from the flow splitter was collected in HDPE bottles for validation analysis.

During the cruise, twenty-five samples were manually collected in prewashed polypropylene bottles from the filtrate waste line from the flow splitter, and these were returned to the laboratory stored on dry ice for comparative analysis, which was performed

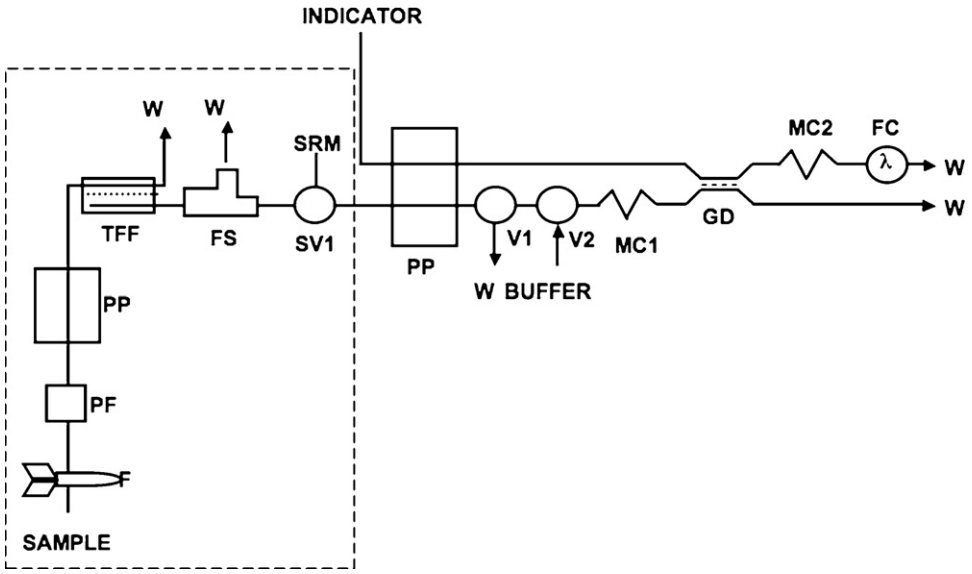

Fig. 1. Manifold diagram for total alkalinity analysis. Indicator (2.4 mL min^{-1}); sample (2.4 mL min^{-1}); PP, peristaltic pump; V1, valve 1 (miniature solenoid valve) feeds sample into the gas diffusion unit; V2, valve 2 pH 4.5 buffer reagent-injection; MC1 and MC2, 20 cm knotted mixing coils; GD, gas diffusion unit; FC, flow cell and flow through detector; W, waste.
Components enclosed by a broken line are only used for in the underway analysis mode of operation. Sample (200 mL min^{-1}); F, "Fish" for weighing down sample collection line; PF, pre-filter; PP, peristaltic pump; TFF, 0.2 μm tangential flow filter; FS, differential flow splitter; SV1, switch valve 1 for intermittent introduction of a standard reference material.

within 24 h. The salinity, electrical conductivity, temperature, time and global positioning system (GPS) data corresponding to each automated measurement of total alkalinity were logged by the portable analyser software.

2.3. Instrumentation

The FIA system used in the development of this total alkalinity method was constructed in-house, based on the design used for dissolved reactive P determination [20] and more recently for ammonia [24].

Indicator and sample from the sampling unit were pumped continuously through the manifold (Fig. 1). Immediately prior to an injection sequence, valve V1 was switched to divert sample to waste, and buffer was injected into the stationary sample stream using a computer controlled miniature solenoid valve, V2 (LFVA series, The Lee Company, Westbrook, CT 06498-1591, USA). Following reagent-injection, valve V1 was switched to resume sample flow through the manifold. This sequence of sample and buffer switching is essential to avoid pressure pulses that would otherwise occur, causing distortion of the gas diffusion membrane, shortening its operational life. The sample-reagent zone, containing gaseous carbon dioxide generated by injection of pH 4.5 buffer was then passed over unstretched PTFE plumbing tape (0.1 mm thickness), that was supported on either side by polymethylmethacrylate blocks, each with a machined linear channel, 75 mm long, 2 mm wide, and 0.3 mm deep. Carbon dioxide that diffused through the membrane into the indicator stream caused a colour change of the bromothymol blue that was monitored using a low dispersion, multi-reflection cell with an effective optical path length of ca. 20 mm [25]. Transmitted light from a super-bright red LED (P/N HLMP-C116, Hewlett-Packard, λ_{max} = 654 nm, spectral bandwidth 30.4 nm, 2000 mcd, 15° viewing angle) was detected using a CCD detector (S2000 Series, 400 μm fibre, Ocean Optics spectrometer, Dunedin, FL 34698, USA). Peak response at 640 nm was measured in mV. System control and data acquisition were achieved using a LabVIEW™ program (National Instruments, Austin, TX 78759-3504, USA) written in-house.

A manual switch valve, SV1 (Model 5031, Rheodyne, Rohnert Park, CA 94928 USA) was used to periodically introduce a standard reference material as part of the field analysis quality assurance program.

3. Results and discussion

3.1. Selection of injection and detection conditions

The multi-commutation approach was used for total alkalinity analysis because it permits electronic control of sample or reagent dispersion [21]. Previous experience with this particular multi-commutation flow injection system for the determination of filterable reactive phosphorus showed that optimal mixing could be achieved by the use of two injected slugs of reagent. On this basis, use of two injections of pH 4.5 buffer of varying volumes interspersed with a sample slug of the same volume was investigated to determine the optimum injection volume for analysis. Peak responses obtained for different injection volumes are shown in Table 1, and show that as injected reagent volume is increased, the peak response also increases, as a result of the production of larger amounts of carbon dioxide.

Changes in the absorbance of the indicator acceptor stream in response to carbon dioxide diffusion were detected using a red LED with maximum emission intensity at 654 nm with a spectral bandwidth of ca. 30 nm as the light source. While the absorbance maximum of the bromothymol blue indicator occurs at 620 nm, there is appreciable overlap between the emission spectrum of the LED and the absorbance spectrum of the indicator solution. Comparison of the emission and absorption spectra suggest that the compromise wavelength of detection is approximately 640 nm, and in all subsequent measurements the Ocean Optics CCD detector was set to measure absorbance at this wavelength.

All calibration data sets showed some concentration dependent deviations from linearity, but fitting of the curves to quadratic equations resulted in correlation coefficients of >0.999 for all three reagent-injection volumes used. Limits of detection were calculated as the concentration equivalent to $3\sigma_{n-1}$ of the blank value

Table 1
Calibration data for reagent-injection FIA determination of total alkalinity, using two buffer injections for standards over the range 0–160 mg $CaCO_3$ L^{-1}

Volume of buffer injected (μL)	Sample volume (μL)	Peak response at 160 mg $CaCO_3$ L^{-1} standard (mV)	%R.S.D. (n = 3)	Calibration equation (correlation coefficient)	LoD (mg CaO_3 L^{-1})
6	6	594	2	PkHt = $-0.0167[CaCO_3]^2 + 6.25[CaCO_3] + 13.7$ (r = 0.999)	1.0
12	12	771	2	PkHt = $-0.0136[CaCO_3]^2 + 6.91[CaCO_3] + 12.2$ (r = 0.999)	0.5
18	18	894	1	PkHt = $-0.0118[CaCO_3]^2 + 7.38[CaCO_3] + 12.0$ (r = 0.999)	0.5

Table 2
Total alkalinity concentrations (mg $CaCO_3$ L^{-1}) for various water samples and a standard reference material, obtained using the total alkalinity reagent-injection gas diffusion method

Sample	Salinity, S (Practical Salinity Scale 1978)	This method-6μL injections			This method-12μL injections			This method-18μL injections			Reference method	
		Concentration (mg L^{-1})	%R.S.D. (n = 3)	%Difference from reference method	Concentration (mg L^{-1})	%R.S.D. (n = 3)	%Difference from Reference Method	Concentration (mg L^{-1})	%R.S.D. (n = 3)	%Difference from reference method	Concentration (mg L^{-1})	%R.S.D. (n = 3)
Pump	0	0.530	8	−74	1.92	5	−5	1.93	5	−4	2.02	3
Golden Circle	0	84.7	1	1	84.6	1	1	85.6	0.3	2	83.7	0.4
Farmland	0	187	1	−2	189	1	−1	192	2	1	190	0.3
Summit	0	188	2	−1	196	1	3	191	1	1	189	0
Cool Ridge	0	144	2	0.4	151	3	6	142	1	−1	143	0
Fitt. kit. tap	0	12.3	5	3	11.9	5	−0.1	11.6	4	−3	11.9	2
Kitchen tap	0	12.6	3	3	12.4	4	1	11.8	3	−4	12.3	2
Pond	0	106	6	−4	111	1	1	110	0.3	−0.3	110	0.5
Werribee 1	36	82.1	1	−37	130	3	−0.5	130	1	−0.6	131	0.4
Werribee 2	36	91.9	4	−28	137	2	7	131	1	3	128	0.4
Queenscliff	36	80.9	4	−30	112	2	−2	112	0.5	−2	115	0.5
SRM	–	45.8	1	7	44.9	1	4	43.8	1	2	43.0	4 (n = 16)

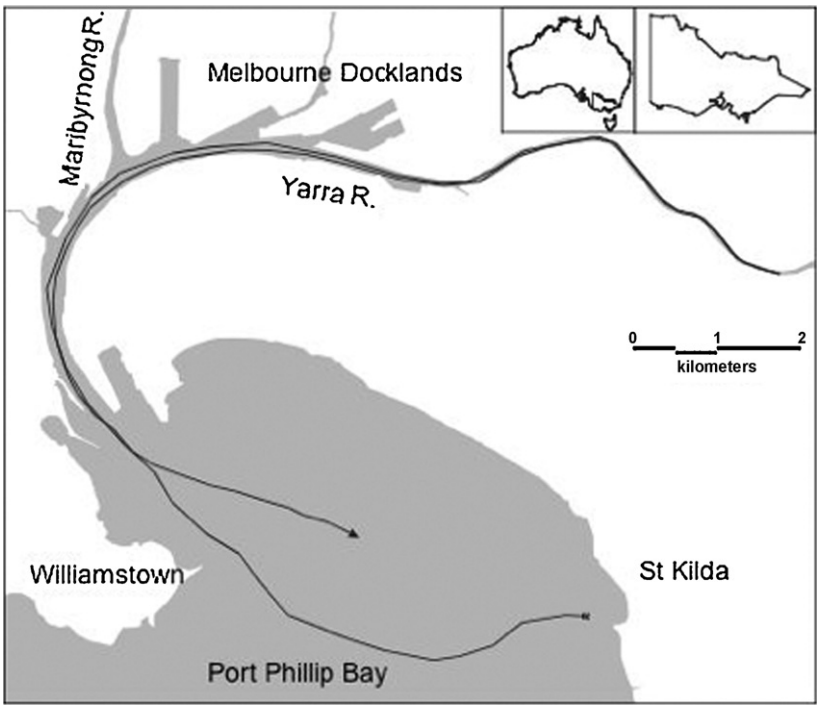

Fig. 2. Cruise path undertaken on Port Phillip Bay and the Yarra River, southeast Australia, for the underway analysis of total alkalinity.

for the three reagent injection volumes tested, and these were all $\leq$1 mg $CaCO_3$ L^{-1}, suggesting that the method was suitable for determining total alkalinity in both fresh and marine waters. The measurement rate was calculated to be 71 injections h^{-1}.

3.2. Laboratory validation

The total alkalinity of a number water samples with chemical matrices of varying salinity was determined in the laboratory using the proposed reagent-injection flow injection method. All samples were analysed using double injections of the three reagent-injection volumes (6, 12 and 18 μL volumes), over a calibration range appropriate to the sample concentration. These results were compared with those obtained using a standard potentiometric titration method, in which the sample was titrated to an endpoint at pH 4.5 [26], being the point at which all carbonate and bicarbonate are nominally converted to $H_2CO_3^*$.[2] A standard reference material was also analysed (Table 2).

For reagent-injection volumes of 6 μL, there were minor concentration differences between the reagent-injection FIA and potentiometric titration methods for freshwater samples. These differences ranged from −2 and +7%, with the exception of the Pump sample (−74%), which had a concentration that was very close to the detection limit, which may account in part for the large error observed.

In contrast to these results, large errors (−28 to −37%) were observed for the marine samples. This large, systematic bias is most likely due to the effect of the natural buffering capacity of seawater [27]. In samples such as these, the use of 6 μL buffer injections did not result in the adjustment of the pH of the seawater to 4.5, and thus the carbon dioxide generated and detected via the gas diffusion procedure would not correlate with the total alkalinity concentration.

However, when an injection volume of 12 μL was employed, the conversion efficiency of carbonate species to carbon dioxide improved, as indicated by much closer agreement between the two methods (−5 and +7% difference), for samples spanning freshwater to marine matrices. Further improvement was observed when injection volumes of 18 μL were used, with the largest differences between the developed method and the reference method being −4 and +3%. Use of larger volumes of injected reagent did not result in markedly greater sensitivity, and were disadvantageous because of the requirement for longer mixing coils with a resultant reduction in sample throughput. Thus, for the analysis of total alkalinity in fresh and marine waters, an injection volume of 18 μL (with a double injection) was found to give the best results, and this reagent-injection condition was used in all subsequent work.

A very strong agreement was observed between the gas diffusion reagent-injection flow analysis method, using 18 μL injection volumes, and the titrimetric laboratory method [26] as shown by the regression equation:

$$[CaCO_3]_{\text{Reagent-injection}} = 1.007[CaCO_3]_{\text{Lab}} - 0.359 \quad (r = 0.9997, n = 12) \tag{1}$$

A paired *t*-test was performed on the data and the results indicated that there was no significant difference between this proposed method and the laboratory reference method (paired $t = 2.07$, $P = 0.990$, d.f. = 22).

3.3. Field application and validation

Underway analysis of total alkalinity in estuarine and marine waters was undertaken over the course of 5 h, in Port Phillip Bay and the Yarra River, southeastern Australia. The cruise path (Fig. 2) was tracked throughout the day by logging GPS data along with time-stamped total alkalinity concentration values from the FIA system. During this field deployment, three by five-standard, trip-

[2] $H_2CO_3^* = \sum(H_2CO_3 + CO_2(aq))$ [4].

Table 3
Total alkalinity (as mg $CaCO_3$ L^{-1}) calibration data obtained at various times during underway field deployment

Calibration	Calibration equation	%R.S.D. at 160 mg L^{-1} (n = 3)	Limit of detection (mg L^{-1} as $CaCO_3$)
1 (1046 h)	PkHt = $-0.00167[CaCO_3]^2 + 2.79[CaCO_3] + 7.15$ (r = 0.999)	1	2.0
2 (1441 h)	PkHt = $-0.00511[CaCO_3]^2 + 3.33[CaCO_3] + 9.79$ (r = 0.999)	1	1.3
3 (1644 h)	PkHt = $-0.00343[CaCO_3]^2 + 2.56[CaCO_3] + 10.4$ (r = 0.999)	1	1.0

licate point calibrations were performed, using standards of 0, 40, 80, 120 and 160 mg $CaCO_3$ L^{-1}.

The calibration data are summarized in Table 3, and these equations show that the sensitivity decreased slightly during the course of the day, while the intercept (reagent blank) increased from 7.15 to 10.4 arbitrary detector units. While calibrations 1 and 2 were quite similar, calibration 3 had a markedly reduced peak response. These changes in sensitivity may have occurred for a number of reasons. The indicator solution was housed in a 1 L plastic collapsible bag (Platypus™, Cascade Designs, Inc., Seattle, WA, USA), which was used with the intention of excluding atmospheric gases from the remaining solution, and thus avoiding any changes to the pH of the indicator solution. As the indicator solution was consumed, the bag progressively collapsed, maintaining a zero headspace volume, thus ensuring that there was no contact between the buffered indicator and atmospheric carbon dioxide. However in the process of collapsing the reagent bag, there may have been a slight reduction in flow rate because of resistance to the pump, but this would be likely to result in increased rather than decreased sensitivity [28]. Ambient temperature, dropped from 21.8 to 12.0 °C during the course of the cruise, but it is unlikely that this would have had a pronounced effect on sensitivity because the sample and reagent streams were passed through a heat exchanger at ca. 35 °C in an attempt to minimize such effects. The most tenable explanation however, is that there was some diffusion of atmospheric carbon dioxide through the polymer reagent bags with time, causing decreased sensitivity. Indicator solutions left overnight in the laboratory in sealed reagent bags were observed to change colour, and such a change would also be consistent with the increasing blank signal and decreased sensitivity shown by the data in Table 3.

Subsequent to this study, use of glass containers with a CO_2 trap for the indicator reagent has been shown to avoid this problem of atmospheric CO_2 interference. Despite slow reaction of the indicator with atmospheric CO_2, the reproducibility remained constant at ca. 1% R.S.D. for the 160 mg $CaCO_3$ L^{-1} standard throughout the field trials, and the detection limit was always less than 2 mg $CaCO_3$ L^{-1} (based on three standard deviations of the mean substituted into the corresponding calibration equation) for each of the calibrations.

A standard reference material solution was switched into the portable system periodically, as a check of the accuracy of the reagent-injection FIA method. The concentration of the standard reference material was calculated using the most proximate calibration data, and each calculated concentration obtained in the field was plotted on a Shewart plot [29] (Fig. 3). The data in this figure indicates that the measurement precision for total alkalinity of the portable instrument under field deployment conditions was excellent (mean = 42.2 mg $CaCO_3$ L^{-1}, σ_{n-1} = 1.6, n = 14), with more than 80% of the values obtained for the standard reference material samples falling within $\pm 1\sigma_{n-1}$ of the certified value, and no values occurring outside the $\pm 2\sigma_{n-1}$ action limit.

Sample analysis was undertaken continuously for most of the 5-h cruise, at an approximate measurement rate of 71 injections h^{-1}. For a cruise speed of 2.5 knots (4.6 km h^{-1}), a spatial resolution of one sample every 65 m was achieved at this measurement rate, while at 5 knots (9.3 km h^{-1}), this corresponded to a spatial resolution of a measurement every 130 m.

Twenty-five samples were collected by hand and analysed using a potentiometric titration method for comparative analysis, within 24 h of collection. The total alkalinity concentrations of the samples determined using the reagent-injection FI method were calculated using the calibration obtained in the corresponding time period. These samples were collected whilst underway, and the concentrations measured therein will be averaged over space and time. When a fresh filter was used, filtrate flow was 20 mL min^{-1}, and the total sample collection time for one sample was approximately 4 min. However, as the filter became fouled with fine particulate matter, the filtrate flow rate progressively slowed to 4 mL min^{-1}, and collection time for manually collected samples was as much as 20 min. This factor should be taken into consideration when comparing the results from the reagent-injection flow injection and reference methods that are shown in Fig. 4 (comparative samples have been plotted over the average time span for collection).

In the time period between approximately 12:18 and 12:56 pm, two large vessels passed the sampling craft, and the bow wave and wake of these ships was sufficient to disturb the salinity stratification of the estuary, which is clearly demonstrated by the pronounced fluctuation in salinity that accompanied this event. This disturbance was tracked effectively by results from the portable FIA system for both salinity and total alkalinity. How-

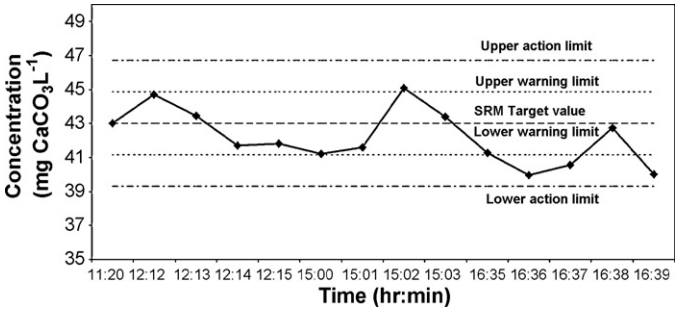

Fig. 3. Shewart plot for the results of standard reference material analysis performed during underway field application of the hybrid reagent-injection flow analysis system.

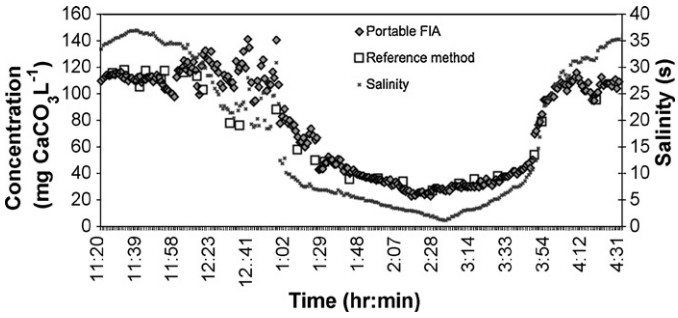

Fig. 4. Comparison between total alkalinity analysis between the underway reagent-injection FIA method and the reference method. Salinity data collected underway are also reported with respect to the Practical Salinity Scale 1978 [34].

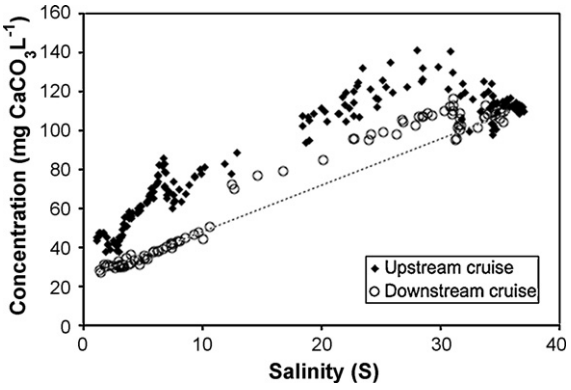

Fig. 5. Plot of total alkalinity concentration versus salinity, for data collected from both upstream and downstream cruises. The dotted line indicates the expected plot for conservative (dilution-only) behaviour.

ever this change in alkalinity was not detected using comparative samples, with two outliers being observed at 12:31 and 12:36 pm. Despite this caveat, the results in Fig. 4 show excellent agreement between the proposed reagent-injection method for total alkalinity, and the reference titration method as indicated by the regression equation obtained after excluding the two outliers:

$$[CaCO_3]_{\text{Reagent-injection}} = 1.01[CaCO_3]_{\text{Lab}} + 1.27$$
$$(r = 0.970, n = 23) \quad (2)$$

3.4. Observed physico-chemical behaviour of alkalinity in the Yarra River estuary

A plot of total alkalinity versus salinity using this underway data (Fig. 5) may be used to determine whether total alkalinity behaves conservatively in the Yarra River estuary, i.e. that any observed changes in total alkalinity concentration are due only to dilution.

Conservative behaviour would be shown by a strong linear relationship between salinity and total alkalinity [30]. If a constituent behaves non-conservatively, or there is some perturbation to the system, the data points will lie above or below the line, indicating addition or removal of the constituent from the water, respectively [31]. Significant deviations from conservative behaviour may result through interactions involving removal of the dissolved constituent by precipitation, through uptake by particulate phases already present, or through addition by dissolution of, or exchanges with, the solid phases [32].

The data plotted in Fig. 5 show that the total alkalinity data corresponding to the upstream cruise appear to be much less conservative, i.e. greater positive deviation from the theoretical conservative mixing line, than those obtained during the return leg downstream. The probable explanation for this observation relates to the speed at which the sampling vessel was traveling for both legs of the cruise. While cruising upstream, the vessel traveled at ca. 2.5 knots, and under these conditions, the sampling probe was located approximately one meter below the surface, whereas for the for the return leg, the cruise speed was ca. 5 knots, and the sampling probe traversed the top 0.2 m of the water column. Since a pronounced halocline has been reported at a depth of ca. 1–1.5 m in this portion of the estuary [33], the upstream and downstream cruise data sets represent different unmixed bodies of water. Thus the less-conservative behaviour exhibited by total alkalinity measured during the upstream cruise data is most likely due to the additive effects of anaerobic processes such as denitrification and sulfate reduction that occur below the halocline. In contrast, samples collected for total alkalinity determination during the downstream leg, which was conducted at higher cruise speed, originated from the aerobic near-surface waters of the estuary, and under these circumstances conservative conditions might be expected to prevail.

The ability to collect large amounts of data rapidly, in this case for total alkalinity, by the use of portable flow injection equipment clearly demonstrated the importance and versatility of this approach. Reliable data can be obtained rapidly and successfully, enabling the elucidation of biogeochemical processes such as non-conservative addition.

4. Conclusions

A method for the determination of total alkalinity was developed using a reagent-injection FIA technique, and was applied to estuarine samples with a wide range of salinities. This gas diffusion method offers a fast, simple and viable alternative to the titrimetric methods that are currently used for alkalinity determinations. This method was used successfully for underway analysis in the Yarra River estuary and Port Phillip Bay, southeast Australia, and the data obtained has provided the basis for a better understanding of the biogeochemical behaviour of total alkalinity in estuarine systems.

Acknowledgements

SMG gratefully acknowledges the support of an Australian Postgraduate Award. The authors thank Dr. Simon Roberts for his assistance in the field.

References

[1] APHA-AWWA-WEF, Standard Methods for the Examination of Water and Wastewater, Centennial edition, Washington, 2005.
[2] A.G. Dickson, Deep Sea Res. Part A. Oceanogr. Res. Pap. 28 (1981) 609.
[3] F. Canete, A. Rios, M.D. Luque de Castro, M. Valcarcel, Analyst 112 (1987).
[4] W. Stumm, J.J. Morgan, Aquatic Chemistry, John Wiley and Sons, Inc., NY, 1996.
[5] C.T. Driscoll, K.M. Driscoll, M.J. Mitchell, D.J. Raynal, Environ. Pollut. 123 (2003) 327.
[6] M.P. Roche, F.J. Millero, Mar. Chem. 60 (1998) 85.
[7] A. Watanabe, H. Kayanne, K. Nozaki, K. Kato, A. Negishi, S. Kudo, H. Kimoto, M. Tsuda, A.G. Dickson, Mar. Chem. 85 (2004) 75.
[8] Ocean Acidification due to Increasing Atmospheric Carbon Dioxide Contents, The Royal Society, London, 2005, p. 68.
[9] R.A. Feely, C.L. Sabine, K. Lee, W. Berelson, J. Kleypas, V.J. Fabry, F.J. Millero, Science 305 (2004) 362.
[10] K.K. Yates, R.B. Halley, Estuaries Coasts 29 (2006) 24.
[11] R.J.M. Howland, A.D. Tappin, R.J. Uncles, D.H. Plummer, N.J. Bloomer, Sci. Total Environ. 251–252 (2000) 125.
[12] P.A. Raymond, J.E. Bauer, J.J. Cole, Limnol. Oceanogr. 45 (2000) 1707.
[13] D. Dyrssen, Acta Chem. Scand. 19 (1965) 1265.
[14] A.L. Bradshaw, P.G. Brewer, Mar. Chem. 24 (1988) 155.
[15] J.A. Breland, R.H. Byrne, Anal. Chem. 64 (1992) 2308.
[16] F.V. Almeida, J.R. Guimaraes, W.F. Jardim, J. Environ. Monitor. 3 (2001) 317.
[17] I.D. McKelvie, D. Peat, P.J. Worsfold, Anal. Proc. 32 (1995) 437.
[18] T. Aoki, Y. Fujimaru, Y. Oka, K. Fujie, Anal. Chim. Acta 284 (1993) 167.
[19] V. Kuban, P.K. Dasgupta, Talanta 40 (1993) 831.
[20] A.J. Lyddy-Meaney, P. Ellis, P.J. Worsfold, E.C.V. Butler, I.D. McKelvie, Talanta 58 (2002) 1043.
[21] M. Catala Icardo, J.V. Garcia Mateo, J. Martinez Calatayud, TRAC Trends Anal. Chem. 21 (2002) 366.
[22] P.W. Atkins, J.A. Beran, General Chemistry, Scientific American Books, New York, 1992.
[23] R.C. Weast, M.J. Astle (Eds.), CRC Handbook of Chemistry and Physics, CRC Press Inc., Florida, 1981.
[24] S.M. Gray, G. Hanrahan, I.D. McKelvie, A. Tappin, F. Tse, P.J. Worsfold, Environ. Chem. 3 (2006) 3.
[25] P.S. Ellis, A.J. Lyddy-Meaney, P.J. Worsfold, I.D. McKelvie, Anal. Chim. Acta 499 (2003) 81.
[26] APHA-AWWA-WEF, in: L.S. Clesceri, A.E. Greenberg, A.D. Eaton (Eds.), Standard Methods for the Examination of Water and Wastewater, American Public Health Association, Baltimore, 1998, p. 2.
[27] G.A. Cole, Textbook of Limnology, The C.V Mosby Company, St. Louis, 1983.

[28] S. Satienperakul, T.J. Cardwell, R.W. Cattrall, I.D. McKelvie, D.M. Taylor, S.D. Kolev, Talanta 62 (2004) 631.
[29] J.C. Miller, J.N. Miller, Statistics for Analytical Chemistry, Ellis Horwood Limited, Chichester, 1993.
[30] M.J. Kennish (Ed.), Practical Handbook of Marine Science, CRC Press, Boca Raton, 2001.
[31] P.C. Head (Ed.), Practical Estuarine Chemistry: A Handbook, Cambridge University Press, Cambridge, 1985.
[32] J.D. Burton, P.S. Liss (Eds.), Estuarine Chemistry, Academic Press, London, 1976.
[33] R. Beckett, A.K. Easton, B.T. Hart, I.D. McKelvie, Aust. J. Mar. Freshwater Res. 33 (1982) 401.
[34] E.L. Lewis, IEEE J. Oceanic Eng. OE-5 (1980) 3.

Talanta 77 (2008) 624–627

Contents lists available at ScienceDirect

Talanta

journal homepage: www.elsevier.com/locate/talanta

Effects of soil pH and organic matter on distribution of thorium fractions in soil contaminated by rare-earth industries

Pengran Guo[a,b], Taicheng Duan[a], Xuejie Song[a,b], Jingwei Xu[a,c], Hangting Chen[a,*]

[a] National Analytical Research Center of Electrochemistry & Spectroscopy, Changchun Institute of Applied Chemistry, Chinese Academy of Science, Changchun 130022, China
[b] Graduate School of Chinese Academy of Sciences, Beijing 100039, China
[c] State Key Laboratory of Electroanalytical Chemistry, Changchun Institute of Applied Chemistry, Chinese Academy of Science, Changchun 130022, China

ARTICLE INFO

Article history:
Received 18 March 2008
Received in revised form 3 June 2008
Accepted 4 June 2008
Available online 11 June 2008

Keywords:
Thorium
Soil pH
Soil organic matter
Availability

ABSTRACT

The labilities of thorium fractions including mobility and bioavailability vary significantly with soil properties. The effects of soil pH and soil organic matter on the distribution and transfer of thorium fractions defined by a sequential extraction procedure were investigated. Decrease of soil pH could enhance the phytoavailability and the potential availability of thorium in soil. Increase of organic matter reduced the phytoavailability of thorium, but enhanced the potential availability of it. The reasons why soil pH and soil organic matter affect thorium fractions were discussed, and the behavior of the effects of soil properties on thorium fractions was elucidated. Fourier-transform infrared (FTIR) spectra were employed to reveal the positive relationship between the amounts adsorbed in humic material and/or amorphous oxides and the content of soil organic matter.

1. Introduction

The behaviors of heavy metals and radionuclides in soil are significantly related to soil properties. Soil factors such as pH, ferromanganese oxides and organic matter are likely to be more appropriate predictors for metal mobility [1]. The phytoavailability of heavy metals and radionuclides that is commonly used to estimate the phytotoxicity of elements is affected by soil characteristics [2–4]. The adsorption of radionuclides on soil is affected by soil properties, especially by soil pH and soil organic matter. The transfer of metals between the easily available and less-available phases is significantly influenced by the competition of other cations (especially H^+) on the organic matter surface [5,6]. The bioavailability of heavy metals is higher at lower pH value in the root–soil interface [7]. At a low temperature, the formation of thorium complexes is affected by pH value in a natural system, and these strong complexes enhance the potential transport of thorium [8]. Many reports indicated that exogenous organic matter resulted in the decrease of the availability of heavy metals and radionuclides [9–11], however, non-dissolved organic matter could retard radionuclide transport [12], and dissolved organic matter resulted in the increase of the mobility of heavy metals only in high pH soil systems [13]. As the major fraction of soil organic matter, humic acids with big adsorptive surface [14] have the inequable effects on thorium adsorption on different minerals. The sorption and retention of thorium on hematite were obviously affected [15,16], however less obviously on bentonite [17]. In a word, the study of effect of soil properties on thorium fractions in soil is scarce.

The rare earth mineral existing in Baotou area, Inner Mongolia, China is concomitant with natural radiothorium in the form of ThO_2. In the passed 30 years, the intensive development of the rare-earth industries in Baotou area without the effective control of pollution resulted in an accumulation of thorium in soil [18]. The strong acidic and alkaline wastewater and scoria, which contained thorium, were transferred to soil during the rare-earth mining and processing. Thorium accumulated in soil is the potential cause of phytotoxicity or poisoning for the food chain [19]. To explore potential pollution behavior it is obviously necessary to understand the distribution of the different fractions of thorium, the transfer and the mobility of thorium fractions in soil. The object of this study is to investigate the effects of soil pH and soil organic matter on the distribution and mobility of thorium fractions in soil contaminated by the rare-earth industry in Baotou area of Inner Mongolia, and to explain the reasons of these effects in detail so as to predict the transform of thorium fractions in natural environment. A sequential extraction procedure optimized based on the previous literatures [20,21] was applied to quantify the fractions of thorium in soil samples.

* Corresponding author. Tel.: +86 431 5262348; fax: +86 431 5262383.

0039-9140/$ – see front matter © 2008 Elsevier B.V. All rights reserved.
doi:10.1016/j.talanta.2008.06.002

Table 1
The physicochemical properties of soil samples

Sample number	Series A	Series B
pH value	7.5	7.6
Hygroscopic water (%)	1.18	3.08
Soil organic matter ($g\,kg^{-1}$)	4.80	22.6
CEC ($cmol\,kg^{-1}$ soil)	5.84	20.8
Particle size (<10 m%)	26	35
Content of Fe ($g\,kg^{-1}$)	30	32
Content of Mn ($g\,kg^{-1}$)	0.6	0.4
Content of Th ($mg\,kg^{-1}$)[a]	24.8 ± 1.9	23.9 ± 1.5

[a] Data are shown as mean ± standard deviation ($n = 3$).

2. Materials and methods

2.1. Soil sampling

The soil samples were collected from the different sites of the rare earth industrial areas in Baotou, Inner Mongolia, China. The samples collected from five sites adjacent to temporary deposited location of scoria were marked as series A, and those from six sites in cornfield near rare earth separating workshop as series B. At each sampling site, three replicate samples were collected from a depth of 0–20 cm below soil surface. All samples of series A were mixed and homogenized, air-dried, ground and sieved through 160 mesh (size <97 μm), then stored in polyethylene bags at 4 °C, so did series B.

2.2. Determinations of soil properties and thorium content

A PB-10 type pH meter (Sartorius Corp., Germany) was employed for pH determination by suspending 25 g of soil sample in 50 ml of ultra pure water (18.2 MΩ, prepared by Millipore, Simplicity 185) and shaking it for 5 min. The contents of soil organic matter were estimated by $K_2Cr_2O_7$ oxidation at 180 °C in paraffin bath [22]. The content of soil hygroscopic water was measured by drying the sample at 105 ± 2 °C to a constant weight and then the weight loss was calculated. Soil cation exchange capacity (CEC) was evaluated by CH_3COONa-Atomic absorption method [22]. The sample properties of series A and series B are shown in Table 1.

The determination of ^{232}Th was accomplished by ICP-MS (X series II, Thermo Fisher Corp., USA). The operating conditions were: r.f. power, 1.35 kW; Ar gas flow rates of $13.0\,l\,min^{-1}$ for cooling, $0.86\,l\,min^{-1}$ for nebulizer and $0.70\,l\,min^{-1}$ for auxiliary gas; solution uptake rate, $30\,r\,min^{-1}$, sampling depth, 150 steps; Ni skimmer cone orifice, 1.0 mm. The feasibility of ICP-MS method was testified by standard reference materials and standard addition [23]. The determinations of Fe and Mn were accomplished by AAS (AA 800, PerkinElmer, USA) and testified by standard addition technique. The operating conditions were: analytical wavelength of 248.3 nm for Fe and 279.5 nm for Mn; hollow cathode lamps; gas flow rate of $2.0\,l\,min^{-1}$ for C_2H_2 and $19\,l\,min^{-1}$ for air; slit, 0.2 mm.

All chemicals were at least analytical reagents, and the standard solutions of Th, Fe and Mn were provided by Beijing Research Institute of Chemical Engineering and Metallurgy, China. All wares were soaked in 33% of nitric acid for at least 24 h, and then rinsed with ultra pure water.

2.3. Sample preparation and treatment

Aliquot soils of serials A were mixed with ultra pure water at a ratio of 1:2 (w/v), then the pH values of the solutions were adjusted with 0.1 M HCl and 0.1 M NaOH to desired pH values. After water was vaporized at room temperature, these samples were kept in their original humidity by adding ultra pure water according to weight loss and incubated for 1.5 months room temperature under air condition, then air-dried, ground and sieved. After incubation, the final pH values of the soil samples were 1.0 (as SPH1.0), 2.7 (SPH2.7), 5.2 (SPH5.2), 7.5 (SPH7.5), 10.0 (SPH10.0) and 12.0 (SPH12.0), respectively. All the samples were prepared in triplicate.

The content of soil organic matter has very close relation with microbial biomass that will decrease with the decomposition of soil organic matter, and addition of 30% H_2O_2 could result in decomposition of soil organic matter and decrease of microbial biomass. 2.4 ml and 1.2 ml of 30% H_2O_2 solutions were respectively added to 5.0 g of series B (original soil marked as SOM3 and contained soil organic matter $22.6\,g\,kg^{-1}$) to lower the content of soil organic matter to $4.5\,g\,kg^{-1}$ (SOM1) and $13.6\,g\,kg^{-1}$ (SOM2). Hydrosols of aliquot soil of series B were made firstly, then 114 mg of and 228 mg of humic acid (Jingke Research Institute of Fine Chemical and Technology, Tianjin, China) were respectively added to the above hydrosols to increase the content of soil organic matter to $31.6\,g\,kg^{-1}$ (SOM4) and $40.7\,g\,kg^{-1}$ (SOM5). These samples were kept in their original humidity and incubated for 1.5 months at room temperature under air condition, then air-dried, ground and sieved. All the samples were prepared in triplicate.

2.4. Sequential extraction procedure

Because the amounts of incubated samples were not enough for single extraction and the attention of this work was focused on the trends of fraction variations rather than the amounts of fractions, the sequential extraction procedure [24] was employed to estimate thorium fractions in soil samples. Extractions were performed by adding 2 g of soil samples and the quantified extractant into 100 ml polypropylene centrifuge tubes followed by mechanical shaking. The fractions and extractants were specified as follows—Exchangeable (F1): 20 ml of 1 M magnesium chloride (pH 7.0), shaking for 2 h; carbonates (F2): 30 ml of 1 M sodium acetate (pH 5.0), shaking for 7 h; adsorbed in humic material and/or amorphous oxides (F3): 20 ml of 0.1 M sodium pyrophosphate (pH 9.8), shaking for 2 h; coprecipitated with amorphous ferromanganese oxyhydroxides (F4): 20 ml of Tamm's acid oxalate, shaking for 5 h; crystalline ferromanganese oxyhydroxides (F5): 20 ml of Coffin's reagent, shaking for 5 h; residual phase (F6). Following each fraction extraction, the mixture was centrifuged, and the supernatant was reserved for analysis. Before the next extraction, the residue was washed with 10 ml of ultra pure water. The final residue was decomposed with aqua regia and HF by microwave digestion (step1, $5\,kg\,cm^{-2}$ for 60 s; step2, $10\,kg\,cm^{-2}$ for 100 s; step3, $15\,kg\,cm^{-2}$ for 200 s; step4, $20\,kg\,cm^{-2}$ for 300 s). For each incubated sample, three replicates were extracted, respectively, and then nine extraction operations were performed for each incubation.

F1–F4 are referred as non-residual parts of thorium. F1 and F2 are labile or phytoavailable. F3 and F4 are potentially phytoavailable. F5 and F6 are residual parts and hardly transferred to environment during a short time-scale under natural conditions [20].

2.5. FTIR analysis

Fourier-transform infrared (FTIR) spectra were used for the identification of the main compounds and functional groups of SOM series [25]. To limit moisture interference, both the samples and KBr were separately dried at 105 °C before making the potassium bromide pellets, which were prepared by pressing a mixture of 2 mg of a sample with 400 mg of KBr. FTIR spectra were obtained by exposing samples to a frequency range from $4000\,cm^{-1}$ to $370\,cm^{-1}$ at a resolution of $4\,cm^{-1}$ (Bruker Vertex 70, Germany).

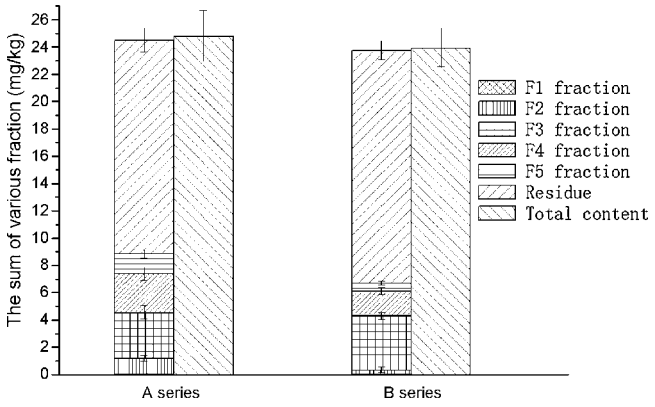

Fig. 1. The distribution of thorium fractions and the comparison between thorium fractions of sequential extraction with total content of thorium in soil samples of series A and B. Error bars represent ±standard deviation of triplicates samples ($n = 3$).

Humic acids and fulvic acids in SOM samples were extracted and concentrated by 0.1 M NaOH–0.1 M $Na_2P_2O_7$ solution (1:5, w/v) with shaking for 24 h at room temperature. The supernatants were separated and vaporized at 70 °C and dried at 83 °C, then readied for FTIR analysis.

3. Results and discussion

3.1. Results of sequential extraction

By comparison of the sum of all fractions (M_S) in the sequential extraction with the total content (M_T) of thorium, the recoveries (M_S/M_T) were 101% and 99.2% for series A and series B samples, respectively. The distribution of thorium fractions and the comparison between the fractions and M_T are represented in Fig. 1. The agreement between M_S and M_T suggests the reliability of the sequential extraction.

3.2. Effects of pH variation on thorium fractions

The amounts of F1 and the non-residual fractions were unobviously decreased by increasing soil pH from 1.0 to 12.0, while the inverse trend for residue fraction (F6). The variation tendencies of F2, F4 and F5 were similar, in contrast to that of F3 (Fig. 2). A higher amount of exchangeable fraction was obtained at lower soil pH, the reason should be that resistant minerals were decomposed under stronger acidic conditions, and the presence of acid radical ions in soil enhanced the solubility of ThO_2 by forming thorium-sulfate, fluoride and phosphate complexes below pH 7 [8].

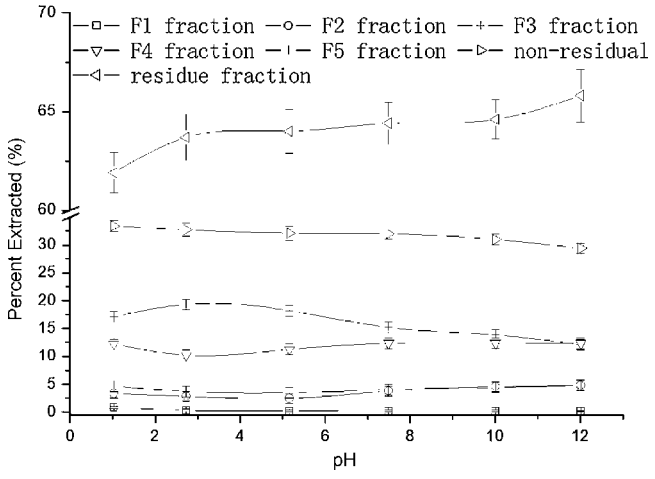

Fig. 2. The variations of thorium fractions with soil pH in SPH series samples. Error bars represent ±standard deviation of nine extraction operations ($n = 9$).

The percentages of F2, F4 and F5 fractions were increased with the increase of soil pH. Murphy et al. [26] indicated that the amounts of $Th(OH)_3CO_3^-$ and $Th(CO_3)_5^{6-}$ in solution phase would be increased above pH 6 due to hydrolysis in the presence of natural organic matter. Under strong alkaline conditions, a few amount of thorium adsorbed by soil organic matter was released and then bound to carbonates. The two aspects resulted in the tendency of F2. Sorption and coprecipitation are the predominant means by which most of metals are retained in ferromanganese oxide and hydroxide. $Th(OH)_n^{4-n}$ increased with the increase of soil pH, which enhanced the sorption and coprecipitation of thorium with Fe/Mn oxide and hydroxide, and then the percents of F4 and F5 increased gradually.

There was an increase of F3 from pH 1.0 to approximate 3.5, which was due to two reasons: the first was that humic acids were insoluble and precipitated below pH 2 [27], which caused an enwrapment of thorium in the precipitate and the decrease of extraction amount; the second was the competition of H^+ with Th^{4+} in the process of ion-exchange adsorption under very strong acidic conditions. The amount of F3 was obviously decreased from pH 3.5 to 12.0. It was the reasons that humic acids were soluble above approximately pH 3.5 [28], thus thorium associated with humic acids would be partially released to aqueous solution (F1) or coprecipitated with Fe/Mn hydroxides (F4 and F5), and such a process could be enhanced with the increase of soil pH. Besides, in a pH range from 2 to 5, some thorium hydroxides, such as $Th(OH)_2^{2+}$, $Th(OH)^{3+}$ [8,29] had the stronger affinity to the adsorption sites of organic matter than free thorium ions that were existed at pH < 3 because of lower solvation energies for surface binding [30], and they had much stronger static affinity to electronegative humic acids than $Th(OH)_3^+$,$Th(OH)_4$ that were existed at pH > 4.5, so F3 was relatively higher in this pH range.

3.3. Dependence of thorium fractions on organic matter variation

The amounts of F1 and the phytoavailable fraction (F1 + F2) decreased with the increase of soil organic matter from 4.5 g kg^{-1} to 40.7 g kg^{-1}, and an inversing trend was found for those of F3 and the non-residual fractions. No significant changes for F4 and F5 were observed, and F2 was slightly decreased with increasing organic matter (Fig. 3).

Most of thorium adsorbed on soil organic matter that was decomposed by H_2O_2 could be released and transferred into other labile fractions and a little amount of the thorium into the residual fractions. Although H_2O_2 might solubilize some oxides of Fe, Mn, Al [31] and carbonates, the amounts of F2, F4 and F5 were hardly changed upon the addition of H_2O_2 (Fig. 3) because of abundant oxides and carbonates but few H_2O_2. The adsorptions of humic acids for actinide ions took place due to the affinity of adsorption sites and complexing reactivities of organic functional groups. The addition of humic acid with negative charges could increase the adsorption of thorium ions onto the amorphous oxides due to static electronic affinity, and forming ternary surface complexes through carboxyl and hydroxyl [28], which resulted in the increase of F3. Humic acids enhanced the complexation adsorption of free thorium ions with humic materials and reduced the amount of F1. Being weak acids, humic acids could dissolve a part of carbonate and resistant minerals, which reduced the amount of F2 and the residual fractions of thorium. Though the addition of humic acids decreased the phytoavailability of thorium, however, the potential availability of thorium was enhanced by the formation of relative stable com-

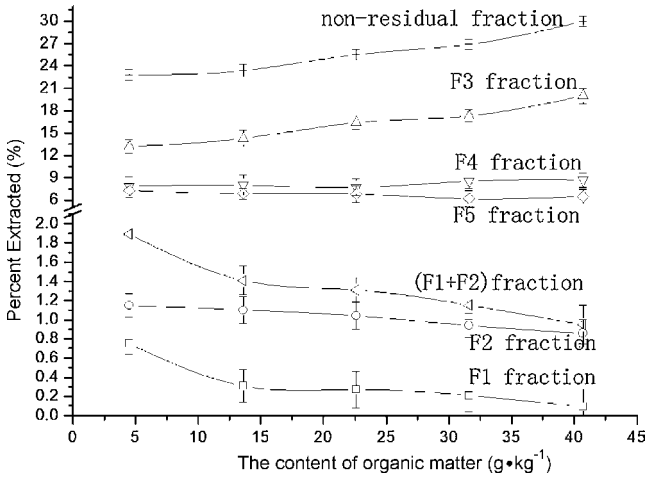

Fig. 3. The variations of thorium fractions with soil organic matter in SOM series samples. Error bars represent ±standard deviation of nine extraction operations ($n = 9$).

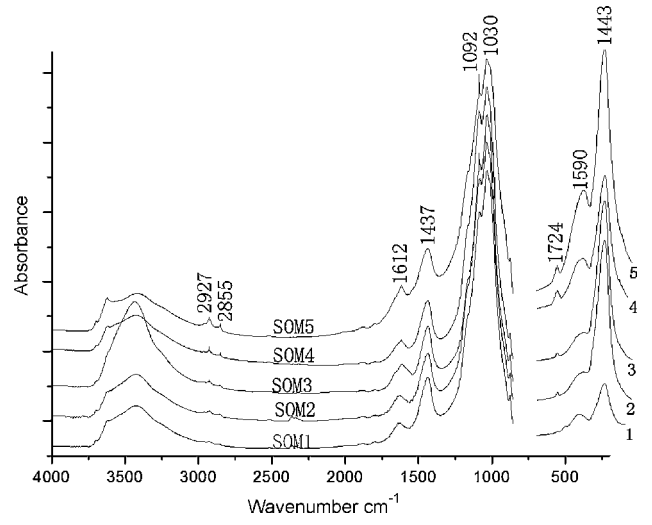

Fig. 4. FTIR spectra of SOM series samples and the corresponding extractants from SOM series by 0.1 M NaOH–0.1 M $Na_2P_2O_7$ solution. (1) Extraction from SOM1; (2) extraction from SOM2; (3) extraction from SOM3; (4) extraction from SOM4; (5) extraction from SOM5.

plexes with original thorium ions and thorium ions released from minerals, which caused the potential harm to environment.

3.4. FTIR analysis of characterization of soil organic matter

Fig. 4 shows the results of FTIR analysis. Soil samples contained silicates (1030 cm^{-1}) and carbonates (1443 cm^{-1} and 879 cm^{-1}) and organic matter.

The same absorbance peak frequencies for the samples containing different amounts of organic matter were observed in FTIR spectra, but some peaks differed slightly in intensity, such as those of aliphatic structures and lipids (2927 cm^{-1} and 2855 cm^{-1}), C=O of carboxyl groups (1724 cm^{-1}), C=O and C=C of aromatic rings (1612–1590 cm^{-1}), C–H of aliphatic aldehyde structures (1442–1432 cm^{-1}), C–O of carbohydrates and carbohydrate-like substances structures (1157–1092 cm^{-1}). The increase of peaks intensity at 2927 cm^{-1}, 2855 cm^{-1}, 1724 cm^{-1} and so on suggested the increase of adsorption sites and functional groups with the increase of soil organic matter content, which enhanced the amount of F3. The adsorption of thorium onto soil organic matter was principally duo to the affinity of adsorption sites and the complexation of thorium with the ligands of the functional groups of soil organic matter.

4. Conclusion

The significant variations of thorium fractions with soil pH and soil organic matter were observed although some variations were slight because of the small extracted amounts. In soil contaminated by rare-earth mining and processing activities, the amounts of F1 and non-residual fraction decreased with the increase of soil pH, and an inversed trend was for those of F2, F4 and F5. The amount of F3 decreased with soil pH except for pH from 1.0 to about 3.5. Acid catalyzed dissolution, inorganic complexation, hydrolysis, coprecipitation are responsible for these variations. Soil organic matter affected thorium fractions through its adsorption affinity and complexation ligands favored by FTIR spectra analysis, as well as acidity. The amounts of F1 and the phytoavailable fraction decreased with the increase of soil organic matter from 4.5 g kg^{-1} to 40.7 g kg^{-1}, while F3 and the non-residual fraction acted contrarily by the formation of stable thorium-organic complexes. The investigations of this work would be useful for pollution control of thorium in soil.

Acknowledgements

This work was financially supported by the National Natural Science Foundation of China (No. 20677057 and No. 20605021). The samples were collected with the help of Center of Physical Testing and Chemical Analysis, Baotou Research Institute of Rare Earths.

References

[1] S.M. Ross, in: S.M. Ross (Ed.), Toxic Metals in Soil Plant System, Chichester, England, 1994, pp. 275–301.
[2] J.S. Rieuwerts, I. Thornton, M.E. Farago, M.R. Ashmore, Chem. Spec. Bioavailab. 10 (1998) 83.
[3] A. Martínez-Aguirre, R. Periañez, J. Environ. Radioact. 45 (1999) 67.
[4] Y. Ge, P. Murray, W.H. Hendershot, Environ. Pollut. 107 (2000) 137.
[5] H.A. Elliot, M.R. Liberati, C.P. Huang, J. Environ. Qual. 15 (1986) 214.
[6] N.T. Basta, M.A. Tabatabai, Soil Sci. 153 (1992) 195.
[7] D.C. Su, J.W.C. Wong, H. Jagadeesam, Chemosphere 56 (2004) 957.
[8] D. Langmuir, J.S. Herman, Geochim. Cosmochim. Acta 44 (1980) 1753.
[9] L.M. Shuman, J. Environ. Qual. 28 (1999) 1442.
[10] M. Halim, P. Conte, A. Piccolo, Chemosphere 52 (2003) 265.
[11] M.A. Wasserman, F. Barttoly, A.P. Portilho, E.R.R. Rochedo, A.G. Vianna, D.V. Pérez, C.C. Conti, J. Environ. Radioact. 99 (2008) 554.
[12] G.R. Chopin, Radiochim. Acta 58/59 (1992) 113.
[13] C.A. Impellitteri, Y.F. Lu, J.K. Saxe, H.E. Allen, W.J.G.M. Peijnenburg, Environ. Int. 28 (2002) 401.
[14] M.P. Sauvant, D. Pepin, J. Guillot, Ecotox. Environ. Safe. 44 (1999) 47.
[15] P. Reiller, V. Moulin, F. Casanova, C. Dautel, Radiochim. Acta 91 (2003) 513.
[16] P. Reiller, F. Casanova, V. Moulin, Environ. Sci. Technol. 39 (2005) 1641.
[17] D. Xu, X.K. Wang, C.L. Chen, X. Zhou, X.L. Tan, Radiochim. Acta 94 (2006) 429.
[18] L.N. Bai, L.C. Zhang, L.X. Wang, Chinese Rare Earths 22 (2001) 76.
[19] S.D. Cunningham, W.R. Berti, J.W. Huang, Trends Biotechnol. 13 (1995) 393.
[20] A. Martínez-Aguirre, M. Garcia-León, M. Ivanovich, Sci. Total Environ. 173/174 (1995) 203.
[21] R. Periañez, A. Martínez-Aguirre, J. Environ. Radioact. 37 (1997) 29.
[22] R.H. Shi, Assay on Agro-Chemical Properties of Soil, 2nd ed., Agriculture Press, Beijing, 1986 (in Chinese).
[23] P.R. Guo, T. Xu, X.J. Song, T.C. Duan, Y.M. Zhang, H.T. Chen, Chinese J. Anal. Chem. 9 (2006) 1239.
[24] P.R. Guo, T.C. Duan, X.J. Song, H.T. Chen, Talanta 71 (2006) 778.
[25] S. Amir, M. Hafidi, G. Merlina, J.C. Revel, Chemosphere 59 (2005) 801.
[26] R.J. Murphy, J.J. Lenhart, B.D. Honeyman, Colloid Surf. A 157 (1999) 47.
[27] S.J. You, S. Thakali, H.E. Allen, Environ. Int. 32 (2006) 101.
[28] V.L. Chen, X.K. Wang, Appl. Geochem. 22 (2007) 436.
[29] C. Moulin, B. Amekraz, S. Hubert, V. Moulin, Anal. Chim. Acta 441 (2001) 269.
[30] Y. Yin, C.A. Impellitteri, S.J. You, H.E. Allen, Sci. Total Environ. 287 (2002) 107.
[31] X.Q. Shan, B. Chen, Anal. Chem. 65 (1993) 802.

Talanta 77 (2008) 522–526

Contents lists available at ScienceDirect

Talanta

journal homepage: www.elsevier.com/locate/talanta

Exploiting sequential injection analysis technique to automate on-line sample treatment and quantitative determination of morphine in human urine

Abubakr M. Idris*, Ahmed O. Alnajjar

Department of Chemistry, King Faisal University, Hofuf 31982, Saudi Arabia

ARTICLE INFO

Article history:
Received 30 October 2007
Received in revised form 19 March 2008
Accepted 4 April 2008
Available online 20 April 2008

Keywords:
Morphine
Sequential injection analysis
Forensic analysis
Clinical analysis

ABSTRACT

A simple uni-stream sequential injection analysis (SIA) manifold was developed to automate a method for the assay of morphine in human sample. The proposed SIA method includes on-line sample treatment, coupling reaction and spectrophotometric measurement. A rapid algorithm controlled the adopted procedure was critically programmed. For sample treatment, solid-phase extraction (SPE) was carried out into a homemade microcolumn, installed in the SIA manifold. Sufficient sample clean-up, extraction and preconcentration were obtained by SPE. A coupling reaction of morphine with diazonium salt of aniline hydrochloride was adapted to SIA. The product of the reaction, an azo-morphine derivative, was spectrophotometrically detected at 390 nm. Parameters that influenced the efficiency of the proposed method, including solution volumes, diazonium concentration, flow rate and residence time, were optimized. The proposed method was linear in a range of 0.10–2.5 $\mu g\,ml^{-1}$. The limits of detection and quantification were 0.023 and 0.076 $\mu g\,ml^{-1}$, respectively. The detectability of the method was enhanced by the preconcentration and the use of an extended pathlength (50 mm) of a flow cell. The method was validated by an HPLC method. Comparable results with respect to accuracy (recovery 96.3–97.1), repeatability (R.S.D. < 2.4%) and intermediate precision (R.S.D. < 3.1) were gained. The full-automation and miniaturization of the utilized technique offer rapidity, safety in handling urine sample and reagents as well as reduction of reagent and sample volumes. The method is suitable for the application in forensic cases as an initial test and clinical analysis to prevent overdose-induced toxicity.

1. Introduction

Morphine is an analgesic drug used for the treatment of moderate to severe pain, especially for patients undergoing surgical procedures. It is recommended by the World Health Organization for the relief of moderate cancer-related pain [1]. Toxic effects of morphine usage include many serious symptoms. A dose of 120 mg morphine can be fatal. It has been reported that around 90% of orally administrated morphine is excreted in urine within 24 h. Around 10% of the excreted morphine remains un-metabolized [2]. Therefore, to prevent overdose-induced toxicity, the determination of morphine concentration in urine is required for clinical medicine.

Morphine is the primary constituent of opium. It is the most important drug of the opiates group. Commercial opium is usually standardized to contain 10% morphine [3]. In some cases, 6-monoacetylmorphine, the definitive metabolite of heroin, could not be detected in biological fluids for its short half-life of approximately 30 min. In such cases, a detectable amount of morphine and codeine as well as the ratio of morphine-to-codeine of higher than 2 are important criterion to judge the recent use of heroin [4,5]. Therefore, the determination of morphine concentration in urine is also required for forensic cases to prevent the drug of abuse.

In forensic cases, the analytical strategy generally employed for drugs of abuse testing in human urine is a two-stage process, initial and confirmation tests. Initial tests may be immunoassays or chromatographic. The positive result of an initial test is usually confirmed by chromatography–mass spectrometry (MS) [6]. Immunological assay methods are very sensitive and simple. However, they could be impaired by specific (cross-reaction of antiserums) and non-specific (pH and ion strength) interferences. Thin layer chromatography, as another alternative technique for the initial test of morphine, is also simple and inexpensive. Nevertheless, it suffers from a lack of sensitivity and specificity [7]. Recently, other non-separation techniques were also utilized for morphine assay in urine as initial tests including colorimetry [8], flow injection analysis [9] and amperometry [10]. A review manuscript that reported analytical methodologies for morphine assay and its metabolites is available elsewhere [11].

Morphine presents in the urine of patients and addicts in a trace level; thus, a sensitive assay method is desirable. In this

* Corresponding author. Fax: +966 3 5886437.
E-mail address: abubakridris@hotmail.com (A.M. Idris).

0039-9140/$ – see front matter © 2008 Elsevier B.V. All rights reserved.
doi:10.1016/j.talanta.2008.04.016

challenge, many approaches could be applied to improve sensitivity. Detectors with high efficiency such as fluorescence and MS could be used. However, MS is an expensive technique. Fluorescence always requires critical derivatization reactions. The use of extended pathlength in a spectrophotometric detection, which is a simple and inexpensive technique, can improve sensitivity. However, this improvement may not reach the required limit of detection. Solid-phase extraction (SPE), as another approach, can also enhance sensitivity by preconcentration. SPE is also necessary in the analyses of complex samples such as biological fluids to reduce the influence of interferences.

In both forensic and clinical analyses, rapidity and safety in sample handling are of vital interest. The advantages of the sequential injection analysis (SIA) technique, including full-automation, miniaturization and versatility, can meet these requirements. The full-automation offers rapidity and safety in solution handling; and enhances accuracy and precision. The miniaturization also accelerates analysis and drastically reduces consumption of solutions and, consequently, provides better safety to the environment. The versatility empowers analysis with potential manipulations in reagents and sample, i.e. SIA could be used for widely different chemistries simply by changing the flow program. The versatility also allows conducting different on-line analytical processes by installing suitable devices in a SIA manifold. Possible on-line processes include sample treatment (SPE, liquid/liquid extraction, dilution, etc.), developing reactions (chromogenic, fluorescence, chemiluminescence, etc.) and detection (spectrophotometric, potentiometric, etc.). Critical articles that reported the principles, developments and applications of SIA are available in the literature [12–17]. It is noteworthy mentioning that Barnett's research groups utilized the SIA [18,19] and the pulsed flow [20] techniques for adopting methods, with chemiluminescence detection, for the assay of morphine in process samples. The utilized techniques offered high sampling frequency, 120 samples h^{-1}.

In spite of the outstanding advantages of SIA, few on-line SIA methods including sample treatment and developing reactions for drugs assay in biological fluids were proposed [21–24]. The current work proposes constructing a simple and inexpensive SIA manifold to conduct a fully automated method for the assay of morphine in human urine. The proposed procedure includes on-line SPE, coupling reaction and spectrophotometric measurement. The sensitivity of the proposed method was enhanced by applying two approaches, preconcentration and the use of an extended pathlength of a flow cell.

2. Experimental

2.1. Chemicals and reagents

All chemicals and reagents that used in this study were of analytical grade quality; water was double distilled deionized. Codeine, morphine and 6-monoacetylmorphine were supplied from Lipomed Inc. (Cambridge, MA, USA). Aniline hydrochloride, sodium dihydrogen phosphate, phosphoric acid, hydrochloric acid, sodium nitrite, sodium hydroxide and methanol were supplied from Sigma–Aldrich (Taufkirchen, Germany).

2.2. Instrumentation

The SIA system used in this study is a FIAlab 3500 (Medina, WA, USA). It is composed of a syringe pump (SP), a multi-position valve (MPV), a holding coil (HC), a reaction coil (RC) and a personal computer (Fig. 1). The syringe has a volume of 5.0 ml. The MPV is chemically inert and has eight ports with a maximum pressure of 250 psi (gas)/600 psi (liquid) and a minimal dead volume. 0.03 in. i.d. Teflon tubings and a T-connector, which are supplied from Upchurch Scientific, Inc. (Oak Harbor, WA, USA), were used to connect different units of the SIA manifold and to make both the HC (600-cm long) and the RC (200-cm long). The SIA manifold was controlled by FIAlab for Windows version 5.0.

A C_{18} cartridge (5-cm length, 4.6-mm i.d.), which was supplied from Supelco (Bellefone, PA, USA), was packed in our laboratory with modified silica 45 μm particles.

2.3. Preparation of solutions and samples

To prepare diazonium solution, 0.065 g aniline hydrochloride was dissolved in 1 ml of 1 mmol l^{-1} hydrochloric acid. Then, 0.105 g sodium nitrite was added to the solution. The mixture was stirred for 5 min at 0 °C. The obtained solution is stable for 3 days at 0 °C. Phosphate/phosphoric acid buffer solution adjusted at pH 9.5 was prepared for conditioning the cartridge.

Human urine samples were collected from drug-free volunteers. The samples were adjusted at pH 9.5 by sodium hydroxide. Then, the samples were filtered through a membrane filter (0.45-μm pore size) [25]. The filtrate was spiked with different volumes of morphine to obtain different concentrations ranging from 0.05 to 5.0 μg ml^{-1}.

2.4. SIA procedure

A uni-stream SIA manifold was constructed to perform on-line sample treatment, developing reaction and spectrophotometric measurement. As shown in Fig. 1, water was linked with both the SP and port-1 in the MPV. The buffer solution was linked with port-2. 85 and 100% (v/v) methanol were attached to ports-3 and -4, respectively. Diazonium solution was attached to port-5. A standard solution/sample was attached to port-6. The length of the tubings which connected port-1 with -6 with their respective solutions was 10 cm. The C_{18} cartridge was installed between port-8 and the T-connector. The other side of the T-connector was linked to port-7. The HC was placed between the SP and the MPV while the RC was placed between the T-connector and the Z. The length of tubing which connected port-7 with the RC through the T-connector was 4 cm. The length of tubing which connected port-8 with the RC was 3 cm.

A rapid protocol that performed the proposed SIA procedure was programmed. It is briefly described as follows:

(i) Following the practice of SIA, each solution was first loaded into the HC by aspiration using the SP and then dispensed into the required channel.
(ii) To propel solutions, the syringe was filled with 1000 μl of water. Next, tubes were loaded for the first run with 100 μl of their respective solutions.
(iii) For conditioning the cartridge, 200 μl of each of 100% (v/v) methanol, water and buffer solution were sequentially injected into the cartridge at a flow rate of 20 μl s^{-1}.
(iv) At a flow rate of 10 μl s^{-1}, 200 μl of standard/sample was introduced into the cartridge. Thereafter, standard/sample was flushed with 300 μl of water at a flow rate of 20 μl s^{-1}.
(v) For the elution step, 20 μl of 85% (v/v) methanol was injected at a flow rate of 20 μl s^{-1}.
(vi) At a flow rate of 50 μl s^{-1}, 30 μl of diazonium was injected into the RC directly, i.e. without passing through the cartridge. To allow mixing reagent/eluate, six short reverse strokes were performed with a volume of 10 μl at a flow rate of 50 μl/s.
(vii) For the maximum color development, the flow was stopped for 180 s at 0 °C.

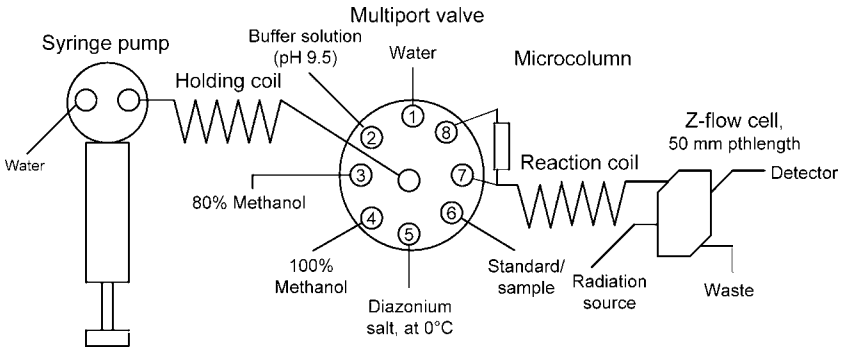

Fig. 1. Schematic diagram of a SIA manifold constructed for on-line solid-phase extraction, coupling reaction and spectrophotometric measurement for the assay of morphine in urine sample.

(viii) At a flow rate of 30 μl s^{-1} and detection at 390 nm, the resultant dye was propelled through the Z. The peak height (PA) of the absorbance was recorded.

3. Results and discussion

3.1. Coupling reaction of morphine with diazonium

The product of the reaction of morphine with diazonium was purified by TLC using 1:1 tetrahydrofuran and dichloromethane as a solvent. The purified product was subjected to FTIR, NMR and MS measurements. The results obtained were reported in our previous manuscript [26]. The proposed reaction scheme is depicted in Fig. 2.

3.2. Method optimization

3.2.1. Optimization of SIA-SPE procedure

Many conventional SPE procedures for morphine in human urine were published. Wilson et al. [25] surveyed the extraction techniques of drugs of abuse in urine. In the current study, a SPE procedure [7,25,27,28] which obtained acceptable recovery was adapted to SIA. Experimental conditions controlling SIA-SPE procedure, including volumes of sample and solvents as well as flow rate, were optimized. The optimization criterion is to obtain acceptable recovery, high sampling frequency and low consumption of solvents and sample. Although high flow rate fastened SIA-SPE process, reverse back pressure took place in the cartridge at a flow rate higher than 20 μl s^{-1}. At flow rate of 15 μl s^{-1}, 200 μl of each of 100% (v/v) methanol, water and buffer solution were found to be sufficient for conditioning the cartridge. For the sample clean-up, 300 μl of water at a flow rate of 15 μl s^{-1} was found to be sufficient for removing interferents. The optimization in these steps was verified by obtaining smooth SIA-baseline resulting from the analysis of blank sample, i.e. drug-free human urine. The elution step was successfully achieved by injecting 20 μl of 85% methanol. This low volume gained a preconcentration factor of 10. The preconcentration factor was calculated as a ratio of the absorbance of morphine in urine with SPE to that without SPE. The preconcentration factor could be more improved by minimizing the desorption volume and maximizing the introduction volume of sample.

3.2.2. Optimization of coupling reaction and spectrophotometric measurement

Experimental conditions controlling the coupling reaction and the spectrophotometric measurement, namely diazonium concentration, residence time and flow rate, were optimized. The criterion judging the optimization is to get the maximum peak height of the absorbance of the az-morphine derivative.

Different diazonium concentrations in a range of 0.01–1.0 mol l^{-1} were examined using 2.0 μg ml^{-1} morphine. It was found that higher diazonium concentration produced yellow color, which caused spectrophotometric interference with the detectable species. Low diazonium concentration may not be enough to couple with relatively high morphine concentration.

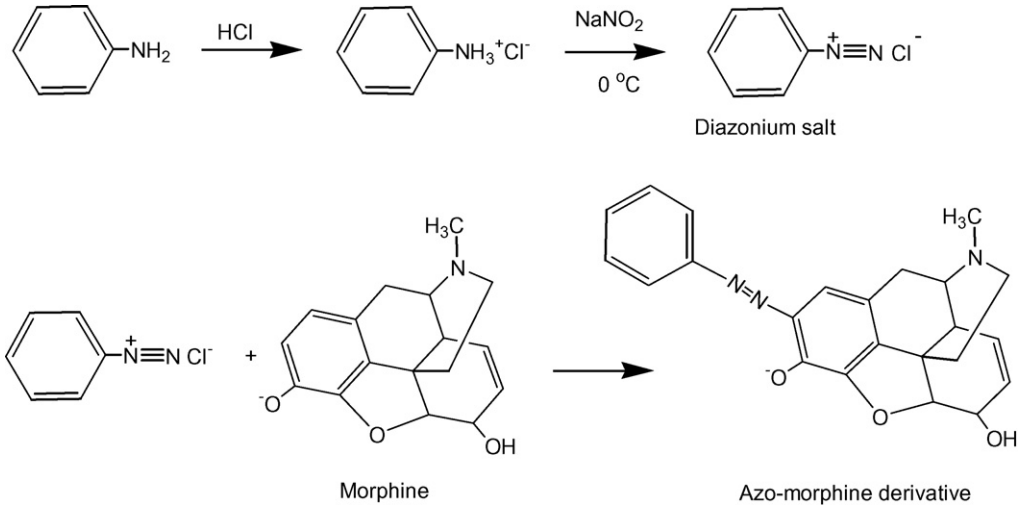

Fig. 2. Proposed coupling reaction scheme of morphine with a diazonium salt.

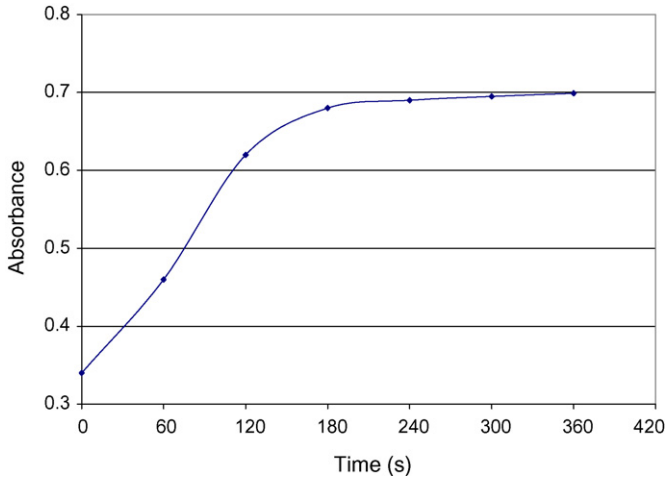

Fig. 3. Absorbance development of the product of a coupling reaction of morphine with a diazonium salt throughout residence time in the reaction coil of a sequential injection manifold at 0 °C.

0.05 mol l^{-1} diazonium was found to be suitable, and thus it was set for further experiments.

A preliminary investigation revealed that the reaction of morphine with diazonium was found to be time dependant. Therefore, different residence times in the RC ranging from 0 to 300 s at 0 °C were examined. The obtained results are depicted in Fig. 3. The figure shows that up to 180 s, the peak height of the absorbance significantly increases as residence time increases. Therefore, 180 s was set as the optimum.

For the optimization of flow rate, based upon our experience in SIA with spectrophotometric detection [29–33], flow rates ranging from 10 to 60 μl s^{-1} were examined. At a high flow rate, the absorbance peak was distorted and repeatable peaks were not obtained. 30 μl s^{-1} was found to be a suitable flow rate.

3.3. Analytical appraisals and application

For the purpose of calibration, urine samples spiked with different concentrations of morphine ranging from 0.05 to 3.5 μg ml^{-1} were subjected to the proposed SIA method. Relatively, wide dynamic range was obtained (0.1–2.5 μg ml^{-1}) with good linearity (correlation coefficient was 0.9993). The weighed regression of the calibration equation was "$A = 0.369C + 0.0076$", where A is the absorbance of the azo-morphine derivative and C is the concentration of morphine in μg ml^{-1}.

To examine the limits of detection (LOD) and limits of quantitation (LOQ), three blank urine samples were subjected to the proposed SIA method. LOD was calculated as 3.3 (s/S) while LOQ was calculated as 10 (s/S); where s is the standard deviation for seven replicates of the absorbance measurement of a blank urine sample, S is the slope of the weighed regression of the calibration equation. LOD and LOQ obtained were 0.023 and 0.076 μg ml^{-1}, respectively. These limits reach the level of morphine possibly found in the urine of addicts and patients [34,35].

The proposed SIA method was applied to five urine samples collected from drug-free volunteers after spiking with morphine in different concentrations. The same samples were also subjected to a previous HPLC method [36]. The recovery values of both methods were calculated. The SIA method gained acceptable recovery (96.3%). The obtained results are introduced in Table 1. To examine the repeatability and the intermediate-precision, each sample was subjected to both methods 5 times a day and 7 times over a week, respectively. The obtained results are introduced in Table 1. Acceptable repeatability and intermediate-precision of the SIA method were obtained (R.S.D. < 3.2%).

Table 1
Some analytical characteristics of the proposed SIA method and an HPLC method for the assay of morphine in human urine

Analytical characteristic	SIA	HPLC
Recovery (%)	96.3	97.1
Repeatability[a]	2.3	2.4
Intermediate precision[b]	3.1	2.8
Sampling frequency (sample h^{-1})	11	3

[a] Expressed as R.S.D. values ($n = 7$ in a day).
[b] Expressed as R.S.D. ($n = 5$ over a week).

Sample frequency of both the SIA and the HPLC methods were also recorded. The SIA method analyzed 11 samples h^{-1} while the HPLC method analyzed 3 samples h^{-1}. As the HPLC method applied manual SPE while the proposed method applied automated and miniaturized SPE, the SIA method is more rapid than the HPLC method.

In general, the SIA method showed comparable results with the HPLC method regarding accuracy and precision. However, the SIA method enjoys other advantages regarding rapidity, safety in solution handling, reagents/sample consumption and eventually simplicity and cost-effectiveness in instrumentation.

To examine the selectivity of the proposed SIA method, three urine samples were spiked with morphine and codeine in different concentrations. The obtained results revealed that codeine did not interfere with morphine. For clinical purpose, interference of codeine with morphine is a critical issue because some patients are treated with a combination of morphine and codeine. For forensic cases, positive result of morphine assay is an indicator of heroin [4,5].

4. Conclusion

This work reports the construction of a simple and inexpensive SIA manifold and its application to automated on-line method for the assay of morphine in human urine. The proposed procedure involved on-line sample treatment, developing reaction and spectrophotometric measurement. Efficient sample clean-up and extraction as well as significant preconcentration were obtained by SIA-SPE. The proposed SIA method enjoys rapidity, safety in solution handling, simplicity and cost-effectiveness in instrumentation as well as reduction in reagent and sample volumes.

Acknowledgments

Authors would like to thank the financial support from King Abdulaziz City for Science and Technology, Saudi Arabia, award # MT-1-2. Authors also thank the Department of Chemistry, College of Science, King Faisal University for allowing them to conduct this research.

References

[1] J. Stjernsward, Cancer Surv. 7 (1988) 195.
[2] R.C. Baselt, Disposition of Toxic Drugs and Chemicals in Man, Second ed., Biomedical Publications, Davis, CA, USA, 1982.
[3] B.A. Goldberger, in: Y.H. Caplan (Ed.), Opiates Abused Drugs Monograph Series, Abbott Laboratories, Irving, 1994.
[4] S. Foster, S.E. Leslie, Encyclopedia Ind. Chem. Anal. 16 (1972) 258.
[5] E. Cone, P. Welch, J. Mitchell, D. Buddha, J. Anal. Toxicol. 15 (1991) 1.
[6] F. Moriya, K. Chan, Y. Hashimoto, Legal Med. 1 (1999) 140.
[7] A. Alnajjar, B. McCord, J. Pharm. Biomed. Anal. 33 (2003) 463.
[8] H. Hsu, L. Chen, K. Ho, Anal. Chim. Acta 504 (2004) 141.
[9] P. Norouzi, M.R. Ganjali, A.A. Moosavi-movahedi, B. Larijani, Talanta 73 (2007) 54.

[10] K. Hoa, C. Chena, H. Hsua, L. Chenb, S. Shiesh, X. Lin, Biosens. Bioelectron. 20 (2004) 3.
[11] M.E. Bosch, A.R. Sīanchez, F.S. Rojas, C.B. Ojeda, J. Pharm. Biomed. Anal. 43 (2007) 799.
[12] J. Ruzicka, G.D. Marshal, Anal. Chim. Acta 237 (1990) 329.
[13] F. Mas, A. Cladera, J.M. Estela, V. Cerd, Analyst 123 (1998) 1541.
[14] Z.L. Fang, Anal. Chim. Acta 400 (1999) 233.
[15] C.E. Lenehan, N.W. Barnett, S.W. Lewis, Analyst 127 (2002) 997.
[16] E. Economou, TrAC 24 (2005) 416.
[17] E.H. Hansen, M. Miro, TrAC 26 (2007) 18.
[18] N.W. Barnett, S.W. Lewis, D.J. Tucker, Fresen. J. Anal. Chem. 355 (1996) 591.
[19] N.W. Barnett, C.E. Lenehana, S.W. Lewis, D.J. Tucker, K.M. Essery, Analyst 123 (1998) 601.
[20] S.W. Lewis, P.S. Francis, K.F. Lim, G.E. Jenkins, X.D. Wang, Analyst 125 (2000) 1869.
[21] M.T. Vidal, A. Chisvert, A. Salvador, Talanta 59 (2003) 591.
[22] J. Huclova, D. Satinsky, H. Sklenarova, R. Karlicek, Anal. Bioanal. Chem. 376 (2003) 448.
[23] G. Theodoridis, C.K. Zacharis, P.D. Tzanavaras, D.G. Themelis, A. Economou, J. Chromatogr. A 1030 (2004) 69.
[24] A. Balaguer, A. Chisvert, A. Salvador, J. Pharm. Biomed. Anal. 40 (2006) 922.
[25] J.F. Wilson, B.L. Smith, P.A. Toseland, I.D. Watson, J. Williams, A.H. Thomson, N.E. Capps, G. Sweeney, L.N. Sandle, Forensic Sci. Int. 119 (2001) 23.
[26] A.O. Alnajjar, M.E. El-Zaria, Eur. J. Med. Chem. 43 (2007) 357.
[27] A. Alnajjar, J.A. Butcher, B. McCord, Electrophoresis 25 (2004) 1592.
[28] M.J. Telepchak, T.F. August, G. Chaney, Forensic and Clinical Applications of Solid Phase Extraction, Humana Press, New Jersey, 2004.
[29] S.M. Sultan, A.M. Idris, K.E. Ibrahim, J. Flow Inject. Anal. 21 (2004) 19.
[30] S.M. Sultan, A.M. Idris, K.E. Ibrahim, J. Flow Inject. Anal. 22 (2005) 118.
[31] A.M. Idris, S.M. Sultan, K.E. Ibrahim, F.N. Assubaei, J. Flow Inject. Anal. 22 (2005) 123.
[32] A.M. Idris, F.N. Assubaie, S.M. Sultan, Microchem. J. 83 (2006) 7.
[33] A.M. Idris, F.N. Assubaie, S.M. Sultan, J. Autom. Methods Manag. Chem. 2007 (2007) 1 (article ID 32470).
[34] F. Mofwa, K. Chain, Y. Hashimoto, Legal Med. 1 (1999) 1404.
[35] M.E. Bosch, A.R. Sanchez, F.S. Rojas, C.B. Ojeda, J. Pharm. Biomed. Anal. 43 (2007) 799.
[36] A.S. Low, R.B. Taylor, J. Chromatogr. B 663 (1995) 225.

Talanta 77 (2008) 581–586

Contents lists available at ScienceDirect

Talanta

journal homepage: www.elsevier.com/locate/talanta

Autocalibration technique based on SIA and integrated multisensor chip

Andrey Ipatov*, Natalia Abramova, Andrey Bratov

Institute of Microelectronics of Barcelona, CNM CSIC, Campus UAB, Bellaterra, E-08193 Cerdanyola del Valles, Barcelona, Spain

ARTICLE INFO

Article history:
Received 31 October 2007
Received in revised form 21 March 2008
Accepted 4 April 2008
Available online 16 April 2008

Keywords:
ISFET sensor array
Sequential injection analysis
Multicomponent analysis

ABSTRACT

An analytical system based on a multisensor ISFET array monolithically integrated in one chip, sequential injection analysis (SIA) and Partial Least Squares (PLS) method for data processing is presented. Along with these the system carried a custom made flow cell with inner volume of 10 μl for the sensor array and a 400 μl of mixing cell for automatic preparation of liquid samples. The system was tested analyzing mineral water samples with very similar ion contents (sodium, potassium, chloride). SIA technique was applied for automatic preparation of calibration solutions by mixing four stock solutions. Ion concentrations of calibration solutions were calculated using the PLS model. Results obtained on each step of the measuring cycle were used as a feedback to update the model and recalculate ion concentrations. The precision of the developed system was typical for potentiometric method with standard deviation of determined ion concentrations of about 3–5%. Proposed approach may be applied for automatic analysis of complex samples that require a large number of multicomponent calibration solutions.

1. Introduction

Sequential injection analysis is a well-established tool for automation of chemical analysis of liquids which includes steps of a calibration model development, based on solutions with known concentrations of components, and application of this model for determination of unknowing concentrations in a sample. Autocalibration techniques are often used for the development of autonomic systems for monitoring natural waters, waste waters, air pollution, etc. [1,2]. Main advantages of these systems are that they require minimum manual operations and allow the compensation of the detector drift.

Analysis of real samples is not an easy task. One of the difficulties is the large number of chemical variables (e.g. ions) that may be found in a sample in a wide range of their concentrations. Another problem is the possible presence of interfering ions which may affect sensors response. To reduce the interfering ions influence it is proposed [3–6] to use chemometric approaches treating the signals obtained from a set of several detectors.

A large number of components in real samples imply the requirement of a large number of calibration solutions. In case of a full factorial design of an experimental plan [7] the required number of calibration solutions that cover all possible ion combinations in the selected concentration range is equal to C^n, where "C" is the number of concentration levels and "n" is the number of components. Thus, for 3 components and 3 levels of concentration 27 calibration solutions would be required. Alegret with co-workers [8–10] used from 30 up to 60 solutions to construct an adequate model based on an artificial neural network. One of the possible ways to reduce the number of calibration solutions is to optimize the experiment design. To develop an experimental plan fractional factorial designs are often used instead of full factorials [11]. Fractional designs "sacrifice" interaction effects, still permitting the main effects to be computed correctly. Thus, developed experimental plans require much less runs (calibration solution) and are more reasonable from the point of view of labor employed. The general mechanism of generating fractional factorial designs for example at 3 levels ($3^{**}(k-p)$ designs) (for 3 component) starts with a full factorial design at 2 levels, and then uses the interactions of the full design to construct "new" factors (or blocks) by making their factor levels identical to those for the respective interaction terms (i.e., by making the new factors aliases of the respective interactions). For example, the following $3^{**}(3-1)$ factorial design for three levels of concentration of sodium, potassium and chloride gives 9 mixed solution instead the 27. These 9 solutions constructed from the full design for potassium, sodium and chloride levels are computed as:

$$C(\mathrm{Cl}) = 3 - \mathrm{mod}_3(C(\mathrm{Na}) + C(\mathrm{K})) \quad (1)$$

Here, $\mathrm{mod}_3(x)$ stands for the so-called modulo-3 operator, which will first find a number y that is less than or equal to x, and that is evenly divisible by 3, and then compute the difference (remainder) between number y and x. For example, $\mathrm{mod}_3(0)$ is equal to

* Corresponding author. Tel.: +34 935947700; fax: +34 935801496.
E-mail address: andrey.ipatov@cnm.es (A. Ipatov).

0039-9140/$ – see front matter © 2008 Elsevier B.V. All rights reserved.
doi:10.1016/j.talanta.2008.04.013

0, $\mathrm{mod}_3(1)$ is equal to 1, $\mathrm{mod}_3(3)$ is equal to 0, $\mathrm{mod}_3(5)$ is equal to 2 (3 is the largest number that is less than or equal to 5, and that is evenly divisible by 3; finally, $5-3=2$), and so on. If we apply this function to the sum of sodium concentration and potassium concentration, we will obtain the third factor for chloride concentration and finally fractional design gives us 9 mixed solutions for 3 components and 3 levels of concentration. There are some other approaches for fractional design (Plackett–Burman designs, Box–Behnken designs, Latin square, etc.) which permit to carry out calibration using an incomplete (reduced) set of standard solutions without significant loss of accuracy of analysis [12].

In this work we propose an automatic system for mixing and preparation of the required number of calibration solutions directly during the measurement cycle using the initial data from the sensor array as a feedback. This is a cyclic optimization process that permits to reduce the concentration range of the calibration solution components during analysis.

2. Experimental

2.1. Apparatus and devices

All the sensors in this work are monolithically integrated in one chip (20.71 mm × 8.00 mm) combining NMOS and thin film technology and using BESOI (Bond and Etch back Silicon On Insulator) wafers. These wafers are formed by three layers, a lower thick silicon substrate, an intermediate silicon oxide layer, and an upper thin silicon layer used to form semiconductor devices. The developed technology permits to isolate electrically sensors one from another in order to guarantee their independent functioning. The array consists of six Ion Selective Field Effect Transistors (ISFETs) with polymeric membranes sensitive to different ions developed earlier [13].

The encapsulation process performed with a photocured polymer layer [14] is facilitated due to the on-chip electrical isolation of all the devices of the multisensor. For this reason it is required only to cover the contact pads of the chip with bonded wires and conducting lines of the PCB substrate. The final step of the multisensor fabrication is the deposition of different photocurable polymer membranes sensitive to K^+, Na^+, and Cl^- ions over ISFET gates. Preparation and deposition of these membranes are reported elsewhere [13,14].

Encapsulated multisensor chip with deposited ion-selective membranes is presented in Fig. 1. A special computer controlled set-up for a multisensor implementation was designed. It consists on a six-channel ISFET-meter working in a constant drain current/constant drain voltage mode. ISFET sensors were biased through the double junction Ag/AgCl reference electrode immersed into the test solution.

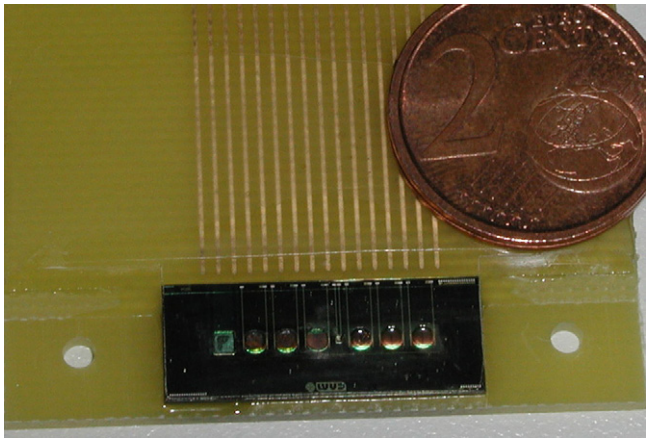

Fig. 1. A multisensor chip with sensitive membranes.

A flow cell to incorporate the sensor array chip was developed and made from polymethylmethacrylat (PMMA) plate with the help the micromilling technique (Stepfour GmbH, Salzburg, Austria). Different milled parts of the PMMA were glued together using methacrylic acid. Dimensions of the inner channel were: length: 14.3 mm, height −0.5 mm, width −1.3 mm (Fig. 2). Standard tubes for flow injection analysis with a 0.75 mm inner diameter were connected to the inlet and outlet of the cell and glued with epoxy resin. Experiments were carried out using a double junction reference electrode (ORION) positioned at the output of the flow cell. For tight contact between the flow cell and the multisensor chip PDMS gaskets were made. Gaskets were formed in a special mould and polymerized during 48 h.

For automatic solution preparation a mixing cell with inner volume of 400 μl was fabricated using PMMA as a material.

The designed automatic system is shown schematically in Fig. 3. To mix solutions and deliver them to the flow cell a syringe pump (1) is used, while a multiposition valve (3) permits to select among various solutions (6–9) with different concentration ranges (10^{-3} to 10^{-4} mol/l). The high precision syringe pump with the minimal volume of 1.0 ± 0.1 μl delivers solutions from the mixing vessel (5) with the total volume of 400 μl to the hold coil (2) and then to the sensor array (4).

2.2. Reagents and solutions

The multisensor chip ISFET sensors with photocurable membranes sensitive to K^+, Na^+, and Cl^- ions were tested and characterised for their sensitivity, selectivity, stability and lifetime. It is important to emphasize that all determined parameters were the same as for conventional ISFETs reported earlier [13,14]. Along with mentioned ions, pH was measured by one of the ISFETs with a silicon nitride gate.

Three different brands of bottled mineral water were analysed (Font Vella, Solan de Cabras, Lanjaron). All of them are of low mineralization and Lanjaron has a very low chloride and bicarbonate content. The test cycle for each water sample consisted in the following steps. Firstly, the measurements were performed in four calibration solutions. These four solutions were prepared from corresponding salts and contained all the mentioned ions in concentrations covering the range between high and low values of corresponding components reported for the commercial bottled waters [15]. Results obtained in these solutions were used to create a preliminary PLS model establishing the correspondence between the sensor array output signals and ions concentration. After this a real water sample was analysed. Using the preliminary PLS model concentrations for each ion component in the measured sample were calculated. A new calibration solution was prepared with concentrations of ions close to those determined in the real sample. Ion concentrations and sensors signal values were used to update the calibration model. After each new calibration solution result of the real sample determination was checked with requisition of the precision. If the standard deviation between consecutive measurements was high, the cycle of calibration solution preparation and the sample measurement was repeated. Fig. 4 illustrates the steps of the analysis process.

2.3. Programming and data processing

Output signals of all the sensors, the valve and the pumps operation were controlled by a computer with a 16 bits data acquisition

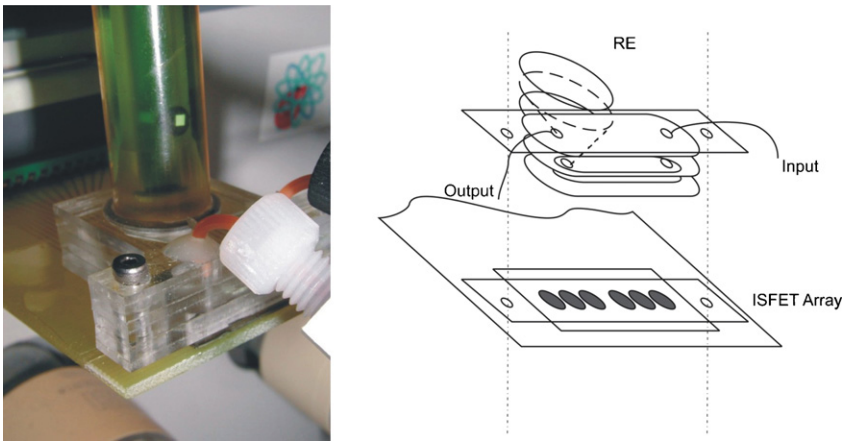

Fig. 2. A flow cell with reference electrode.

board with the help of a specially developed software. Multisensor response signals measured in each of the sample were processed by PLS method forming the matrix of *X*-variables. The data set was used to construct the PLS regression model. All this data treatment was performed using the software package Tanagra [16]. The solution components concentrations (which correlate with volumes of the stock solutions used to prepare a calibration solution) were used as *Y*-variables within the PLS model. Taking into consideration that potentiometric sensors response depends on ion concentration logarithmically the concentration values were transformed into $p_{\mathrm{Ion}} = -\log(C_{\mathrm{Ion}})$, with C_{Ion} expressed in moles per dm^3.

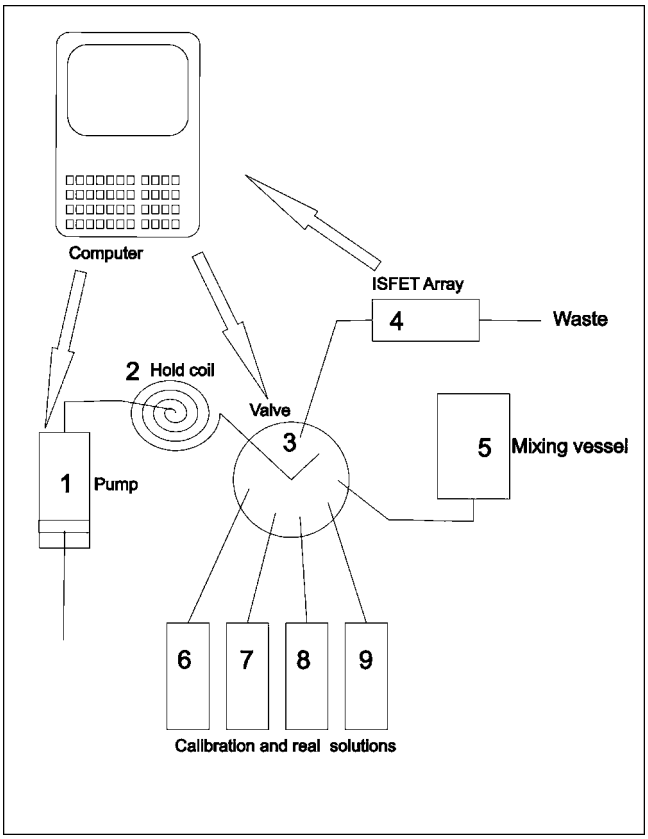

Fig. 3. Schematic presentation of the experimental system for the SIA multicomponent analysis. (1) Syringe pump, (2) hold coil, (3) multiposition valve, (4) sensor array with reference electrode, (5) mixing vessel, (6–9) individual solutions for mixing at different proportions.

3. Results and discussion

3.1. Choice of optimum parameters of the sequential injection analysis

Optimization of sequential injection parameters was performed after studying the response time of the sensor array. For all ISFET sensors the output signal achieved 95–98% of its equilibrium value during the first 50–60 s. Since all the measurements were carried out in a stop–flow mode, after dispensing the sample to the detector cell the cycle was stopped for 60 s and then mean signal values from ISFETs sensors were registered. During analysis it was necessary to prepare a mixture containing stock solutions in different proportions. We carried out series of experiments to guarantee complete mixing of the components and homogeneity of the calibration solution and repeatability of its parameters. Firstly, small volumes (few microlitres) of stock solution were added to the mixing chamber and at the last step the required amount of distilled water was flushed. To prevent the mixing of small volumes of a stock solution with the carrying background solution bubbles of air were injected to separate the sample. After aspirating the required volumes of different stock solutions into the sample hold coil they were dispensed to the mixing cell. The injected air bubbles separating the samples also helped to achieve better mixing of the final solution. To optimize the volume of thus prepared calibration solution different volumes (250, 133, 80, 67 μl) were choused. For 250 and 133 μl sample volumes sensors signals showed better repeatability. Differences in sensors response in consecutively prepared samples with the same concentration did not exceed 0.5 mV which means that the mixing was complete. For the stop flow mode the flow rate has no high influence on the system functioning and in our case it was fixed at 50 μl/s.

Development of a flow through system requires optimization of the sample volume. For very small volumes the effect of the sample dilution during travelling to the detector may cause distortions. For large samples volume the consumption of chemicals and the time of analysis significantly increases. Another reason for decreasing of the sample volume is to prolong the sensors lifetime, because in case of ISFET sensors with polymeric membranes intensive flow provokes washout of active components from sensor membranes.

To optimize the volume of real samples experiments were performed with a sample volume changing in the range from 20 up to 250 μl. For all sensors small sample volumes (less than 20 μl) caused reproducibility deterioration. For 25 μl of the sample volume sensors signal peak values reached only 60–70% of their equilibrium value in the same solution and were not reproducible.

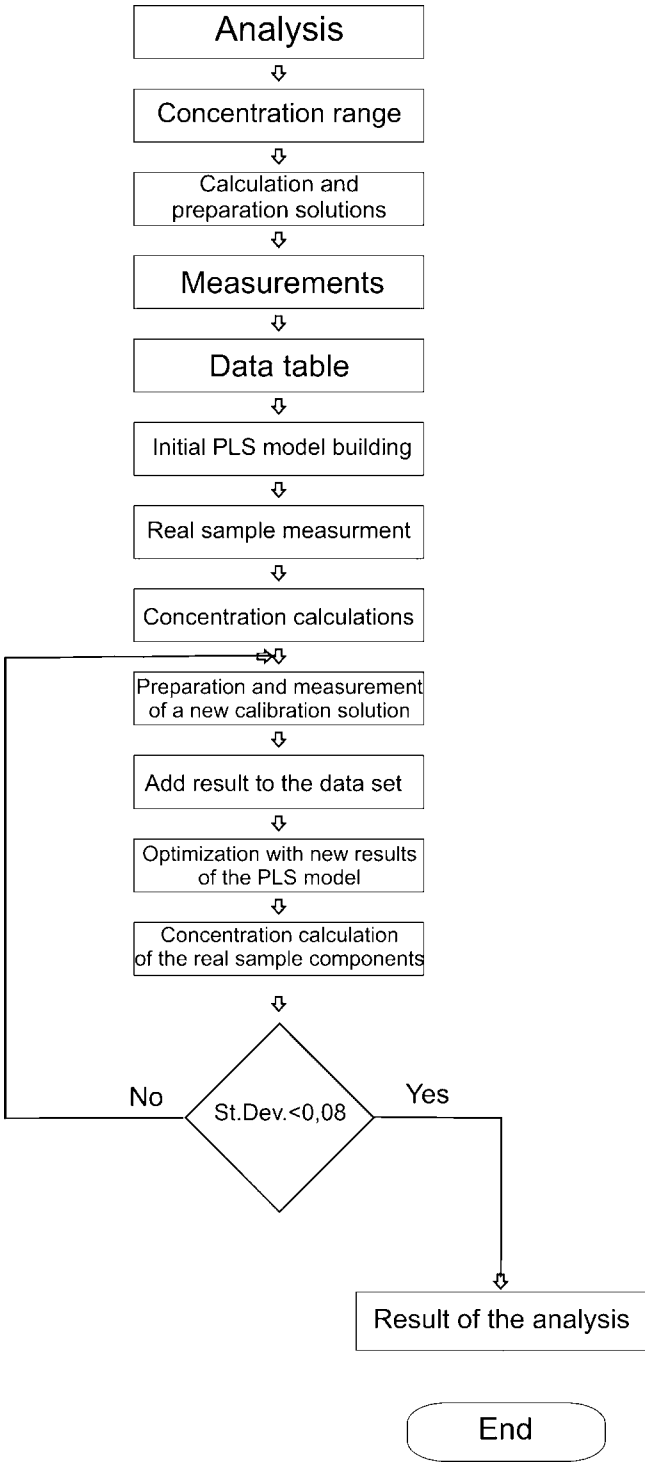

Fig. 4. The algorithm of the automatic operation for analysis of the mineral waters.

Increase of the sample volume up to 100 μl resulted in reproducible sensors signals equal to 94–95% of their equilibrium values.

For calibration solutions and real samples as optimal parameters for our system the flow rate of 50 μl/s and the sample volume of 133 μl were fixed.

Multisensor chip was calibrated in individual solution with optimal flow parameters in the range of 10^{-5} to 10^{-1} mol/l. The average slope of sensors response for K^+, Na^+, Cl^- ISFETs was 54–56 mV per decade and for pH ISFET—55.2 mV/pH in a 2–8 pH range.

Table 1
Concentration of the components in mineral water samples and calibration solutions

Sample	Na^+ contents (mol/l)	K^+ contents (mol/l)	Cl^- contents (mol/l)
Minimal value	2.19×10^{-4}	2.29×10^{-5}	5.62×10^{-5}
Maximum value	5.75×10^{-4}	3.31×10^{-5}	3.09×10^{-4}
Calib sol 1	1.00×10^{-4}	1.00×10^{-5}	5.00×10^{-5}
Calib sol 2	1.00×10^{-3}	1.00×10^{-4}	8.00×10^{-4}
Calib sol 3	2.00×10^{-4}	5.00×10^{-5}	1.00×10^{-4}
Calib sol 4	5.00×10^{-4}	2.00×10^{-5}	3.00×10^{-4}

3.2. Mineral water components (sodium, potassium, chloride and pH value) determination

The ion concentration range in mineral waters which were chosen for testing the autocalibration technique was in the 10^{-4} to 10^{-3} mol/l range. For analysis of commercial mineral waters ion contents the initial stock solutions were prepared with the following concentrations: 10^{-2} mol/l NaCl, 10^{-3} mol/l KCl, 5×10^{-3} mol/l $NaHCO_3$. The sodium ion contents in mineral waters is typically higher then the potassium ion concentration. To prepare the calibration solution the following procedure was developed. Firstly, the required volume of the KCl solution was calculated. Secondly, the volume of the NaCl solution was determined to give the required amount of chloride ions in the calibration solution. Finally, the total sodium ion concentration was fixed by adding the sodium hydrocarbonate stock solution. Initial calculations usually give partial volume values, thus all volumes were rounded to their integer values and final ion concentrations in thus prepared calibration solution were recalculated.

In Table 1 are listed the maximum and minimum ion concentrations in tested mineral waters (as declared by water manufacture) as well as ion contents of the initial calibration solutions required to build the preliminary PLS model. This model characterizes a relatively wide concentration range and gives initial estimation of ion concentrations in real samples. It should be noted that pH ISFET has high selectivity in front of other ions present in the sample. Hence, sample pH values were determined directly. Others ISFETs have no ideal selectivity, so changes in concentration of one of the components may affect the response of several other sensors. PLS model accounts for these possible interactions and diminishes the effect. Thus, only the sodium, potassium and chloride sensors output signals were used for PLS modelling as *X*-variables. As commented earlier, the respective ion concentrations were chosen as *Y*-variables.

The autocalibration and analysis process was carried out taking the following steps.

1. To cover the possible concentration range of all the components (Table 1) four calibration solutions were prepared and analysed. From the obtained data set, presenting sensors signals and concentrations of the components, the preliminary PLS model was built. According to the model each ion component concentration (Y_i) is presented by a regression equation using which the ion concentration may be calculated basing on the sensor output signal readings (X_i).

$$Y_{1(\mathrm{Naconc})} = A_1 X_{(\mathrm{Na\,pot})} + A_2 X_{(\mathrm{K\,pot})} + A_3 X_{(\mathrm{Cl\,pot})} + A^0_{\mathrm{Na}} \quad (2)$$

$$Y_{2(\mathrm{Kconc})} = A_4 X_{(\mathrm{Na\ pot})} + A_5 X_{(\mathrm{K\ pot})} + A_6 X_{(\mathrm{Cl\ pot})} + A^0_{\mathrm{K}} \quad (3)$$

$$Y_{3(\mathrm{Clconc})} = A_7 X_{(\mathrm{Na\ pot})} + A_8 X_{(\mathrm{K\ pot})} + A_9 X_{(\mathrm{Cl\ pot})} + A^0_{\mathrm{Cl}} \quad (4)$$

In equations above $Y_{(X\mathrm{conc})}$ are respective values of the sodium, potassium and chloride concentrations; A_1–A_9 are regression

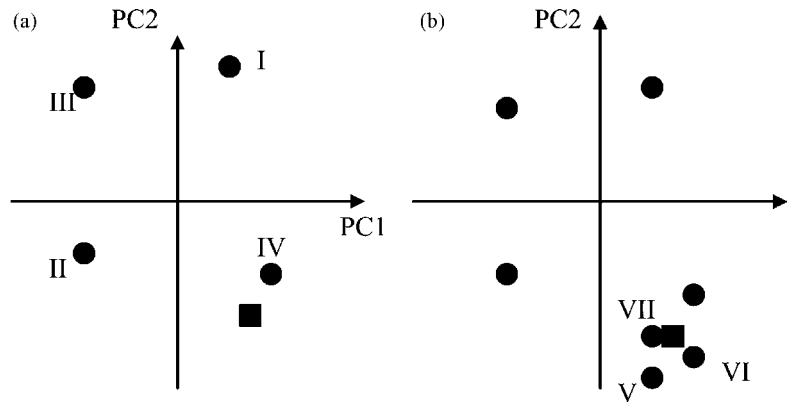

Fig. 5. Preliminary (a) and final (b) PLS models. (■) Real sample, (●) calibration solutions. (I–IV) Four calibration solutions for preliminary PLS model. (V–VII) Calibration solutions for refining PLS model.

coefficients of the PLS model and A^0 is the regression coefficient for the intercept.

2. Measurement of the unknown sample was performed and ion concentrations were calculated using the preliminary PLS model.
3. New calibration solution was prepared with components concentrations equal to those determined in the sample and the measurement cycle was performed.
4. New data were added to the PLS model and regression coefficients were recalculated giving a new set, A'_n.

Ion concentrations in the measured sample were recalculated using the optimized PLS model. The standard deviation of the results obtained in two consecutive cycles was determined. If the standard deviation value was higher than 0.08 the process of the calibration solution preparation and the PLS model optimization was repeated.

Fig. 5(a) shows an example of the principle component analysis (PCA) plot presenting sensors responses in the initial four calibration solutions and in the real sample (preliminary PLS model). In this case we cannot determine the component concentration in the sample because the point falls out of the calibration area. Nevertheless, from this first measurement we determine what the level of the concentration in the sample is. With this data the next calibration solution is automatically prepared with ion components within the range estimated in the real sample. After few cycles of the measurements we have the final PLS model with higher precision that can determine the real sample concentration with a lower error (Fig. 5(b)).

Table 2 presents the evolution of the real sample analysis results during the experiment. Each new calibration solution prepared using the feedback gives a more precise PLS model. From Table 2 it follows that most of ion concentrations are found with better accuracy using PLS model which was modified during analysis. The four components can be determined simultaneously using a sensor array of four ISFET sensors with an average precision of 2–4% for Na^+, K^+, pH (by direct measurement) and 3–8% for Cl^- ions. In case of the "Lanjaron" water the error of the chloride concentration determination is higher than in other water samples. This is due to the fact that the actual chloride ion concentration in this water is close to the limit of detection of the chloride sensor.

Proposed approach of the analysis permits to reduce the number of calibration solutions from 27 to 7. We have also estimated the time required for the analysis for different experimental plans. In case of the full factorial experimental plan it takes 45–50 min, for the fractional factorial design it takes more than 17 min, while the developed system finishes the analysis in 10–15 min. This effect will be much more important in case of a larger number of sample components and their levels of concentration because the required number of calibration solution grows geometrically. At the same, reduction of the number of calibration solutions has negligible effect on the precision of component determination which stays within a 3–5% range that is typical for potentiometric measurements.

Table 2
Determination of the mineral water components with modified PLS model

Sample	Preliminary model (4 sol) (mol/l)	Model 2 (5 sol) (mol/l)	Model 3 (6 sol) (mol/l)	Model 4 (7 sol) (mol/l)	Mineral water ion concentration (mol/l)
Sodium					
Solan de cabras	2.38×10^{-4}	2.10×10^{-4}	2.12×10^{-4}	2.12×10^{-4}	2.19×10^{-4}
Lanjaron	2.31×10^{-4}	2.44×10^{-4}	2.50×10^{-4}	2.56×10^{-4}	2.63×10^{-4}
Font Vella	5.02×10^{-4}	5.45×10^{-4}	5.58×10^{-4}	5.66×10^{-4}	5.75×10^{-4}
Potassium					
Solan de cabras	2.02×10^{-5}	2.43×10^{-5}	2.31×10^{-5}	2.24×10^{-5}	2.29×10^{-5}
Lanjaron	2.80×10^{-5}	2.32×10^{-5}	2.38×10^{-5}	2.49×10^{-5}	2.57×10^{-5}
Font Vella	2.75×10^{-5}	3.06×10^{-5}	3.42×10^{-5}	3.38×10^{-5}	3.31×10^{-5}
Chloride					
Solan de cabras	2.56×10^{-4}	2.43×10^{-4}	2.36×10^{-4}	2.34×10^{-4}	2.29×10^{-4}
Lanjaron	5.02×10^{-5}	5.15×10^{-5}	5.25×10^{-5}	5.32×10^{-5}	5.62×10^{-5}
Font Vella	3.43×10^{-4}	3.31×10^{-4}	3.30×10^{-4}	3.17×10^{-4}	3.09×10^{-4}
pH (pH units) with direct potentiometry					
Solan de cabras				7.45	7.40
Lanjaron				6.71	6.77
Font Vella				7.57	7.62

4. Conclusions

An autocalibration technique based on sequential injection analysis with a miniaturised integrated multisensor chip has been used to analyse different brands of mineral water. The device comprises an array of ISFETs with different gate membranes sensitive to pH, K^+, Na^+ and Cl^- ions. Multivariate approach using PLS model has been applied to determined different components in the water samples. Using the initially obtained data as a feedback the multivariate regression applied to the whole data set permits to determine with sufficient precision concentrations of different ions in water samples. The obtained results show that the use of such array with chemometric technique can be a promising method for automatic, simple, fast, reproducible, selective and sensitive detection of ions in liquid samples.

On the other hand, it must be emphasized that in many cases the sequential injection analysis gives a unique possibility to optimize the process of the analysis and to reduce the time of analysis and amount of reagents used.

Acknowledgments

This work was supported by the Spanish R&D Project (MEC Project AGL2005-07700-C06-05 (BIMBA)). Andrey Ipatov and Natalia Abramova acknowledge the support by a Ramon y Cajal program, Spain.

References

[1] W. Tsujita, A. Yoshino, H. Ishida, T. Moriizumi, Sensors and Actuators B 110 (2005) 304.
[2] F. Hahn, Biosystems Engineering 92 (2005) 275.
[3] K.-S. Park, H. Lee, C.-H. Jun, K.-H. Park, J.-W. Jung, S.-B. Kim, Chemometrics and Intelligent Laboratory Systems 51 (2000) 163.
[4] C. di Natale, A. Macagnano, F. Davide, A. D'Amico, A. Legin, Y. Vlasov, A. Rudnitskaya, B. Selezenev, Sensors and Actuators B: Chemical 44 (1997) 423.
[5] A. Rudnitskaya, A. Ehlert, A. Legin, Y. Vlasov, S. Buttgenbach, Talanta 55 (2001) 425.
[6] F. Sales, A. Rius, M.P. Callao, F.X. Rius, Quimica Analitica 19 (2000) 233.
[7] W.S. Connor, S. Young, in: R.A. McLean, V.L. Anderson (Eds.), Applied Factorial and Fractional Designs, Marcel Dekker, New York, 1984.
[8] J. Gallardo, S. Alegret, M. del Valle, Talanta 66 (2005) 1303.
[9] M. Cortina, A. Gutés, S. Alegret, M. del Valle, Talanta 66 (2005) 1197.
[10] A. Gutés, F. Céspedes, S. Alegret, M. del Valle, Talanta 66 (2005) 1187.
[11] K.H. Esbensen, Multivariate Data Analysis In Practice. An Introduction to Multivariate Data Analysis and Experimental Design, 5th edn., Camo ASA/Camo Process AS, 2001, p. 430.
[12] http://www.statsoft.com/.
[13] A. Bratov, N. Abramova, J. Muñoz, C. Dominguez, S. Alegret, J. Bartroli, Analytical Chemistry 67 (1995) 3589.
[14] L. Moreno, A. Merlos, N. Abramova, C. Jimenez, A. Bratov, Sensors and Actuators B 116 (2006) 130.
[15] http://www.mineralwaters.org/.
[16] http://eric.univ-lyon2.fr/~ricco/tanagra/en/tanagra.html.

Talanta 77 (2008) 827–832

Contents lists available at ScienceDirect

Talanta

journal homepage: www.elsevier.com/locate/talanta

Fractionation analysis of iodine in bovine milk by preconcentration neutron activation analysis

K. Isaac-Olive [a], R. Acharya [a,b], A. Chatt [a,*]

[a] SLOWPOKE-2 Facility, Trace Analysis Research Centre, Department of Chemistry, Dalhousie University, Halifax, NS B3H 4J3, Canada
[b] Radiochemistry Division, Bhabha Atomic Research Centre, Trombay, Mumbai 400085, India

ARTICLE INFO

Article history:
Received 25 June 2008
Received in revised form 18 July 2008
Accepted 18 July 2008
Available online 29 July 2008

Keywords:
Milk components
Iodine distribution
Fractionation analysis
Speciation analysis
NAA
Protein-bound iodine
Lipid-bound iodine
Inorganic iodine

ABSTRACT

Iodine is an essential trace element for human beings. The main source of iodine is generally food items such as fish and milk. Either the lack or the excess of iodine can cause health problems. There exists an increasing interest in the determination of total iodine as well as various species of iodine in milk. We have developed an epithermal neutron activation analysis method with a Compton suppression (ENAA–CS) counting system for the determination of ng mL^{-1} levels of iodine. We have also employed chemical separation methods prior to ENAA–CS to measure the fraction-specific concentrations of iodine in bovine milk. We have measured the following iodine concentrations in homogenized milk (3.25%milk fat): 0.48 ± 0.02 μg mL^{-1} of total iodine, 0.020 ± 0.003 μg mL^{-1} of lipid-bound iodine, 0.039 ± 0.002, 0.019 ± 0.002 and 0.021 ± 0.004 μg mL^{-1} of protein-bound iodine depending on the protein separation method and 0.45 ± 0.02 μg mL^{-1} of inorganic species.

1. Introduction

The World Health Organization (WHO) has estimated that about 740 million people around the world suffer from the iodine deficiency disorders (IDDs) due to the lack of this essential trace element in their diets [1]. The WHO recommended an average daily dietary intake (ADDI) of 100–300 μg iodine for adults. The recommended intakes in many countries fall within this range, *e.g.* 140 μg d^{-1} for U.K., 150 μg d^{-1} for Nordic Countries, Australia, EU and USA, and 160 μg d^{-1} for Canada [1–4]. It has been reported; however, that about 34 countries have sufficient or even excessive iodine consumption [5]. Canada is among this group of countries where the ADDI significantly exceeds the recommended intakes for iodine [1–3]. So far no side effect has been reported for an iodine intake higher than 300 μg d^{-1} [1]. The Joint Expert Committee on Food Additives (JECFA) of the Food and Agriculture Organization (FAO) and the WHO recommended a Provisional Maximum Tolerable Daily Intake (PMTDI) for iodine as 17 μg kg^{-1} of body weight. In Canada, it has been estimated that the ADDI for iodine is about six times the recommended nutrient intake (RNI) value of 160 μg d^{-1} [6] making the Canadian daily intake close to the PMTDI value for a 60 kg person.

The reasons for the increased iodine intake in Canada and other countries are not very clear. It could be related to the iodine concentration in milk. Milk provides 16–30% of the dietary iodine intake [2,7], and in countries such as U.K. with high milk consumption it could be the major contributor to bodily iodine intake. The major cause of high iodine levels in milk could be due to the use of organic iodine compounds for the prevention and treatments of foot rot disease in dairy cattle [2,8]. Significant amounts of iodine may also be introduced in milk through the disinfection of teats by iodine containing agents [2,9]. Iodine solutions are often used to sterilize the mechanical systems employed to extract milk from cows; any residual iodine may be passed on to milk. There is an increasing interest in the determination of iodine levels in milk which is the focus of the present work.

There are a variety of techniques capable of determining total iodine in milk at low levels (<1 μg g^{-1}). Catalytic reactions have been extensively used since the 1940s and they are still being employed [6]. Electrochemical techniques, chromatographic techniques such as HPLC and GC, atomic absorption spectroscopy, and ICP-MS [8,10–16] have also been used to some extent. All of these methods require either a digestion and/or a derivatization step prior to determination. The situation is different in the case of instrumental neutron activation analysis (INAA) of iodine [17–25]

* Corresponding author. Tel.: +1 902 494 2474; fax: +1 902 494 2474.
E-mail address: a.chatt@dal.ca (A. Chatt).

0039-9140/$ – see front matter © 2008 Published by Elsevier B.V.
doi:10.1016/j.talanta.2008.07.033

where no sample dissolution is needed. Epithermal INAA (EINAA) coupled to a Compton suppression (EINAA–CS) counting system can be conveniently used to lower the detection limits for iodine [21]. Chemical separation methods either preceded or followed by NAA can be employed to further improve the detection limits [20,22–25].

The total concentration of an element provides incomplete information about the biological status of that element in a system [26]. The bioavailability and toxicity of an element depends strongly on its chemical species. Despite the large number of papers on the total determination of iodine in milk not much work has been published on its speciation of iodine, perhaps due to the lack of sensitive methods. Moreover those papers where some iodine species have been determined so far, deal mostly with inorganic species. For instance, ICP-MS coupled to ion chromatography (IC) was employed to determine inorganic species such as iodide and iodate [27]. NAA has been couple to IC and to polymer inclusion sorbent for the same purpose [28,29]. Some others published papers are only related to the detection of organic species. For example, ICP-MS was coupled to size exclusion chromatography (SEC) for determining iodide, T3 and other small organic molecules containing iodine [8]. It has also been used to identify iodine associated with whey proteins in milk [26].

Recently, ICP-MS was employed for the determination of iodine species in different human milk and infant formulas [16]. In this case, iodine bound to casein, whey and fat was reported quantitatively. The method employed for the separation of the milk phases was ultracentrifugation. It is very simple and fast and does not need chemical reagents to carry it out. The sample size required is small which could be very advantageous but at the same time makes difficult further fractionation analysis, such as fat fractionation. This procedure also does not separate the inorganic species from the whey proteins, since caseins precipitate but whey proteins remain in the clear fraction. Therefore, the iodine associated to inorganic species and whey proteins is quantified as one fraction. ICP-MS is undoubtedly a very sensitive technique and many elements can be quantified with it. However, the determination of iodine using this technique required special care during the digestion step, since the volatilization of iodine is always a threat.

The main objectives of the work reported in this paper were to develop methods for the separation of the main milk fractions in bovine milk and the further iodine determination on these separated fractions (total inorganic iodine, as well as, iodine associated with total proteins: casein + whey and lipids). The iodine quantification was carried out using EINAA–CS, a sensitive technique in the iodine determination that does not require chemical digestion, preventing any iodine loss. The iodine mass balance based on the summation of separated milk phases have been assessed in human milk and infant formulas [15]; in this case, however, it is carried out in bovine milk.

2. Experimental

2.1. Iodine comparator standards

An iodine comparator standard stock solution of 2 μg iodine mL^{-1} was prepared by dissolving ultrapure ammonium iodide (SPEX) in 5% (v/v) ultrapure ammonia solution. The final solution was placed in a pre-cleaned, dark polyethylene bottle and stored away form light in a refrigerator. Under these conditions, the solution was found to be stable for several months. The working standard solutions of iodide in the range of 0.1–1.0 μg were prepared by transferring appropriate portions of the stock solution using a calibrated Eppendorf pipette into pre-cleaned 1.2-mL polyethylene irradiation vials and diluting to half of the vial with distilled deionized water (DDW).

2.2. Reference materials (RMs)

Several reference materials and standard reference materials (SRMs) obtained from the U.S. National Institute of Standards and Technology (NIST) were analyzed to evaluate the accuracy of the EINAA–CS method developed. The materials used were: SRM-1549 non-fat milk powder, RM-8435 whole milk powder, SRM-1566a oyster tissue, RM-8415 whole egg powder and RM-8414 wheat gluten.

2.3. Irradiation and counting

Samples and standards were irradiated at the inner, outer and the cadmium-shielded outer sites of the Dalhousie University SLOWPOKE-2 Reactor (DUSR) facility at a maximum neutron flux of 2.5×10^{11} cm^{-2} s^{-1}. The details of the stability, homogeneity and reproducibility of the DUSR facility has previously been described [30–32]. The samples were irradiated for 10 or 25 min, allowed to decay time for 3 or 5 min and counted for 10 or 25 min. The gamma-ray spectrometry system consisted of an EG&G Ortec HPGe p-type coaxial detector with a resolution (FWHM) of 1.72 keV at the 1332.5 keV photopeak of ^{60}Co and a relative efficiency of 25% with respect to a standard NaI(Tl) detector in conjunction with an Ortec pulse height analyzer. The guard detector used in the Compton suppression gamma-ray spectrometry system consisted of a 10″ × 10″ NaI(Tl) annulus with five photomultiplier tubes (PMTs) supplied by Harshaw and a 3″ × 3″ NaI(Tl) plug with one PMT supplied by Teledyne. The peak-to-Compton ratio of this system was 582:1 at the 662-keV photopeak of ^{137}Cs.

2.4. Milk samples

Commercially available homogenized milk (milk fat = 3.25%) in paper containers was purchased from the local supermarkets in Halifax, NS, and kept in a refrigerator at 4 °C until use. When needed, a few mL of the milk sample was taken from the container in a pre-cleaned Pyrex beaker and allowed to reach room temperature before processing.

2.5. Determination of total iodine

Approximately 0.75 mL of the milk from the beaker was placed in a 1.2-mL pre-cleaned polyethylene irradiation vial and heat-sealed. The sample was irradiated for 25 min in the Cd-shielded site, allowed to decay for 5 min, and counted for 25 min using the Compton suppression system for the determination of total iodine in milk.

2.6. Separation scheme for iodine fractions in milk

Fig. 1 shows the scheme applied for the separation of the different milk fractions. Lipid-bound iodine fraction was separated first using a solvent extraction method. The aqueous layer was treated to separate the protein-bound iodine fraction using $(NH_4)_2SO_4$ precipitation leaving the inorganic fraction in the supernatant. To remove any organic compound that might have been present in this inorganic-aqueous phase the solution was passed through a C_{18} solid phase extraction column (SPE, Supelclean envi-18, 12 mL column). The eluate solution contains the purified milk inorganic fraction. Dialysis was also studied as a protein separation method where lipids and inorganic species migrate out of the dialysis membrane. Dialysis was applied directly from the initial milk sample.

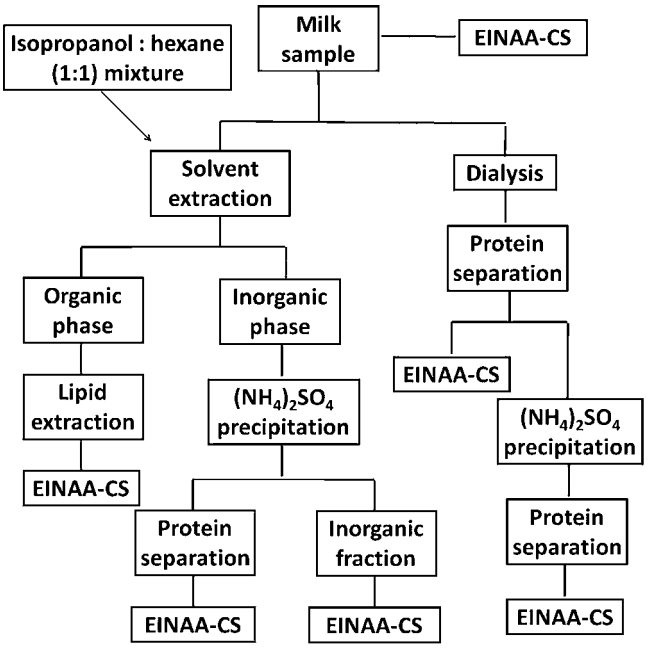

Fig. 1. Separation scheme for the determination of iodine bound to milk fractions.

A combination of dialysis and $(NH_4)_2SO_4$ precipitation was also studied. All separate fractions were irradiated in half volume vial geometry in the conditions described above.

3. Separation of lipid-bound iodine fraction

The method reported here seems to be (up to the knowledge of the authors) a new system for milk lipid extraction. To achieve this separation a modification of Hara's method [33] made in our laboratory by Indrasenna [34] was carried out. About 25 mL of milk were placed in a separatory funnel to which 2 mL of concentrated ammonia solution were added. The first extraction step was done using 25 mL of a hexane:isopropanol (1:1) mixture. After separating the organic phase, the second step was carried out using 15 mL of the extracting mixture and the third step using 10 mL of hexane. The three organic phases were combined and washed twice with 10 mL of DDW. The organic solvent was evaporated under air in fumehood until reach constant weight. Protein determination was assessed in the separated lipid fractions by Bradford method [35] where casein was used as standard protein. The non-organic layer was saved for the separations of protein-bound iodine and inorganic fractions.

4. Separation of protein-bound iodine species

4.1. $(NH_4)_2SO_4$ precipitation

It was necessary to find the concentration of ammonium sulfate required to precipitate all proteins in the sample. To carry out this step, a saturated ammonium sulfate solution at 4 °C (3.93 mol L^{-1}) was prepared. Skimmed Farmers' milk was then placed in micro-centrifuge tubes for centrifugation and the required amount of ammonium sulfate solution was added to obtain the desired final concentration of the salt from 0 to 3 mol L^{-1}. The sample was centrifuged at 15,000 rpm at 4 °C for 90 min and then the mass of protein in solution was determined. This value was compared with the initial amount of protein in the milk in order to calculate the amount of precipitated protein. Proteins were in all cases assessed by Bradford method.

4.2. Dialysis

A dialysis procedure was applied to small portions (50 mL) of 3.25% farmers milk. This was intended to purify proteins by removing inorganic compounds and lipid from the samples. Milk samples were placed into dialysis tubing (Spectra/Por membrane MWCO 3500 Dialysis 34 mm diameter), which was then sealed. Six samples were suspended in a 2-L beaker filled with DDW. Every 8 h, 400 mL of DDW was replaced, and one sample was removed from the beaker. The removed water and the samples were stored at 6 °C. Dialysis was stopped after 48 h, one tube remained at that time. In each dialyzed sample, and dialysate (stored every 8 h) proteins (by Bradford method) and iodine (by NAA) were determined.

4.3. $(NH_4)_2SO_4$ precipitation + dialysis

Then 10 mL of each dialyzed sample were taken to which approximately 30 mL of 3.93 mol L^{-1} $(NH_4)_2SO_4$ solution were added to precipitate proteins. These samples were centrifuged at 15,000 rpm at 4 °C for 90 min. Iodine was determined in both the precipitated proteins and the supernatant, while protein was only determined in the supernatant.

5. Results and discussion

5.1. Irradiation conditions and counting systems

In order to select the most suitable reactor site and the counting system available in our facility, milk samples were irradiated for 10 min, allowed to decay for 3 min and counted for 10 min. The detection limits were calculated using Currie's method [36]. The results are presented in Table 1.

The Compton suppression counting system always gave a better detection limit than the corresponding conventional system. The dead times were comparable. The combination of EINAA and CS gave a better suppression of the interfering activities from ^{24}Na and ^{38}Cl because of the reduced activities of these two nuclides under epithermal neutron irradiations, increased activity of ^{128}I due to its higher cross section for epithermal neutrons, and a reduced Compton background in the gamma-ray spectrum. An additional effect of EINAA–CS was the reduction of the dead time as shown in Table 1. As a result, a more defined photopeak was obtained at the 443-keV of ^{128}I, which in turn produced reliable results. Therefore, the EINAA–CS system was selected for the determination of iodine in milk.

5.2. Precision and accuracy

In order to evaluate the precision and accuracy of the EINAA–CS method developed, a number of RMs and SRMs were ana-

Table 1
Sensitivities and detection limits for iodine in milk under different experimental conditions ti-td-tc = 10-3-10 min

Reactor site	Counting mode	Sensitivity (count μg^{-1})	Detection limit ($\mu g\,mL^{-1}$)	Dead-time (%)
Inner	Conventional	4965 ± 189	0.23	>10
Inner	CS	4796 ± 68	0.15	>10
Outer	Conventional	1494 ± 44	0.24	6–10
Outer	CS	1368 ± 23	0.12	6–10
Cd-shielded	Conventional	587 ± 14	0.29	<2
Cd-shielded	CS	560 ± 6	0.17	<2
Cd-shielded[a]	CS	1094 ± 12	0.05	<2

[a] ti-td-tc = 25-5-25 min, (n = 5).

Table 2
Iodine content ($\mu g\,g^{-1}$) of NIST reference materials by EINAA–CS ti-td-tc = 25-5-25 min, ($n = 5$)

Name	This work	Certified value
Non-fat milk powder NIST SRM-1549	3.15 ± 0.15	3.38 ± 0.03
Whole milk powder NIST RM-8435	2.35 ± 0.08	2.3 ± 0.4
Oyster tissue NIST SRM-1566A	4.44 ± 0.08	4.46 ± 0.40
Whole egg powder NIST RM-8415	1.92 ± 0.19	1.97 ± 0.45
Wheat gluten NIST RM-8414	0.064 ± 0.009	0.06 ± 0.01

lyzed. The irradiation, decay and counting times were 25, 5 and 25 min, respectively. The sensitivity under these conditions was 1094 counts μg^{-1} iodine. Our values along with the certified values are given in Table 2.

The average of five samples for each of the materials, except that for wheat gluten, is given in Table 2. The concentration of iodine in wheat gluten was below the detection limit under the experimental conditions used for the other RMs and SRMs. A pseudo-cyclic EINAA–CS method involving 15 portions of the sample was developed for measuring such low iodine levels. The excellent agreement between the iodine concentrations measured in this work and the certified values shows the accuracy of the EINAA–CS method developed.

5.3. Separation of lipid-bound iodine fraction

After three extractions using the proposed solvent system isopropanol–hexane (1:1) the lipid mass in milk did not increased and it was comparable to the milk fat reported in the container by the producer, indicating the suitability of the solvent system used. It is advisable to perform lipid extraction previous to protein precipitation (if this is the method to be used for protein separation) otherwise lipids precipitate with proteins. No proteins were detected in the organic phase of the solvent extraction process, where lipids are present, meaning that the solvent organic system is specific to the extraction of lipids.

5.4. Separation of protein-bound iodine fraction

Fig. 2 shows the results of protein precipitation using different concentrations of $(NH_4)_2SO_4$. A concentration of 3.0 mol L^{-1}, was enough for the precipitation of all the protein present in solution. This concentration was used for protein precipitation in subsequent

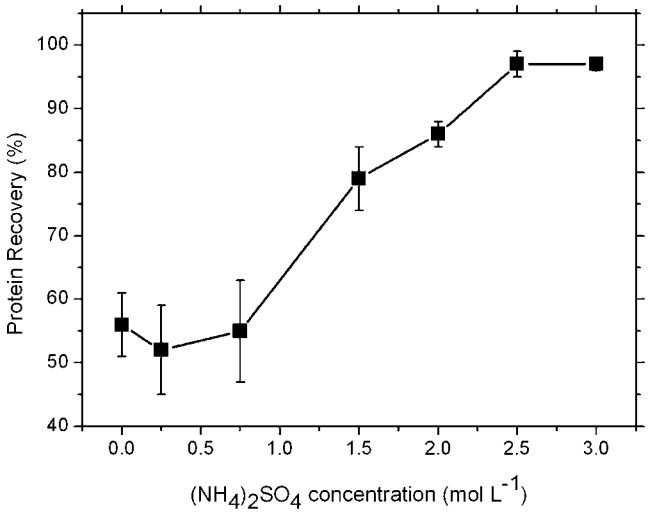

Fig. 2. Protein precipitation using ammonium sulfate.

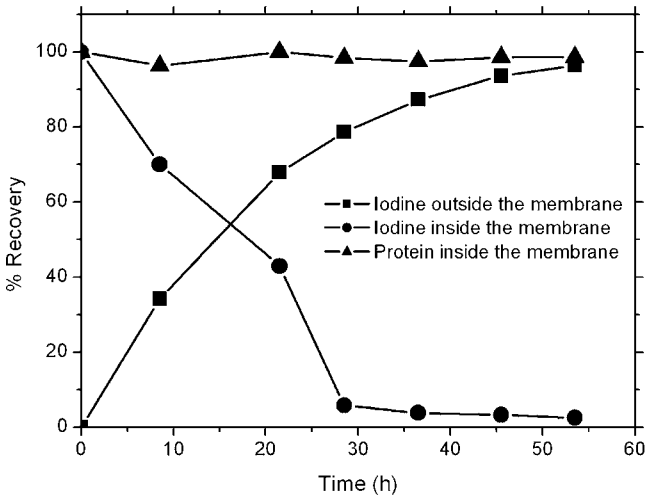

Fig. 3. Protein separation by dialysis.

experiments. The dialysis results are presented in Fig. 3. Thirty hours were enough to remove all inorganic iodine and any lipid-bound iodine from the sample leaving inside the membrane only the iodine bound to proteins. No protein was lost during the process, as it is shown in the figure.

5.5. Iodine content of various fractions

The concentration of iodine in each fraction was determined by EINAA–CS and the results are shown in Table 3. There are no significant differences ($p > 0.05$) in the results obtained in the protein-bound iodine using dialysis and the $(NH_4)_2SO_4$ precipitation after dialysis. However, there are slight differences between these two methods and the protein precipitation alone ($p < 0.05$). A possible explanation for this fact could be that iodine is occluded in the precipitated protein after the lipid separation. On the other hand, after the dialysis of the sample there is no iodine occluded because it is passed through the dialysis membrane. Mass balance calculation of iodine in milk is also shown in Table 3. In general any of the studied methods or protein separation can be used. The advantage of protein precipitation is that it is a rapid method unlike dialysis and dialysis plus protein

Table 3
Iodine mass (μg) in total milk and separated fractions from 10 mL of milk ti-td-tc = 25-5-25 min (EINAA–CS)

Milk phase	Iodine mass (μg)	%R.S.D.	% from total
Total milk	4.8 ± 0.2	4.1	
Lipid-bound iodine	0.20 ± 0.03	15	4.2
Protein-bound iodine			
1. $(NH_4)_2SO_4$ precipitation	0.39 ± 0.02	5.1	8.1
2. Dialysis	0.19 ± 0.02	10.5	4.0
3. Dialysis + $(NH_4)_2SO_4$	0.21 ± 0.04	19	4.4
Inorganic fraction	4.5 ± 0.2	4.4	94
Mass balance	**Summation**	**Total**	**%Recovery**
Lipids + protein(1) + inorganic	0.20 + 0.39 + 4.5	5.09	106
Lipids + protein(2) + inorganic	0.20 + 0.19 + 4.5	4.89	102
Lipids + protein(3) + inorganic	0.20 + 0.21 + 4.5	4.91	102
			Detection limit ($\mu g\,L^{-1}$)
Lipid-bound iodine		2	
Protein-bound iodine		4	
Inorganic fraction		4	

Table 4
Iodine associated to different milk phases in bovine milk and infant formulas reported in the literature

	Iodine species	Iodine concentration	Main species	Method	Detection limit	Reference
1	Total iodine	Range: 17–490 $\mu g\,L^{-1}$; R.S.D.: 1.9%	Iodide: 89%	IC–ICP-MS	1 $\mu g\,L^{-1}$	27
2	Total iodine Iodide	$68.6 \pm 2.9\ \mu g\,L^{-1}$ $62.6 \pm 2.9\ \mu g\,L^{-1}$	Iodide: 91%	IC–NAA	10 ng in 10 mL	28
3	Total iodine Iodide + iodate Iodide	$5.55 \pm 0.16\ \mu g\,g^{-1}$ $5.63 \pm 0.27\ \mu g\,g^{-1}$ $1.47 \pm 0.06\ \mu g\,g^{-1}$	Iodide + iodate: ~100%	PIS–NAA	No reported	29
4	Total iodine Whey fraction Iodide/whey fraction	$167 \pm 14.6\ \mu g\,g^{-1}$ $148.7 \pm 13.6\ \mu g\,g^{-1}$ 145	Iodide: 86%	SEC–ICP-MS	1 $\mu g\,L^{-1}$	8
5	Total iodine Whey fraction Fat Casein	$41.5 \pm 4.0\ \mu g,\ 100\ g^{-1}$ $40.2 \pm 3.4\ \mu g,\ 100\ g^{-1}$ $4.1 \pm 1.1\ \mu g,\ 100\ g^{-1}$ $2.3 \pm 1.1\ \mu g,\ 100\ g^{-1}$	Whey fraction: 96%	Ultra-centrifugation–ICP-MS	0.27 $\mu g\,L^{-1}$	16

1 and 2, bovine milk; 3, milk powder; 4, bovine milk: (France-I); 5, infant formula: (Nidina-1). IC: ion chromatography; PIS: polymer inclusion sorbent; SEC: size exclusion chromatography.

precipitation which need longer time, but are perhaps more reliable.

The results obtained in this study are in good agreement with already published works, as it is shown in Tables 3 and 4. The inorganic fraction from the analyzed milk presents the highest iodine content (94%). This result is expected since iodide has been reported as the major iodine species in milk and is present in this fraction. Any other inorganic iodine species such as iodate is also included in this fraction. Fernandez-Sanchez et al. [8,16] reported as the fraction with highest iodine content the whey fraction, but in the separation method applied by them the whey fraction also contains the inorganic species. They also proved [8] that the main species in that separated whey fraction is in fact iodide. The reported iodide concentrations in milks in Table 4 are 89%, 91% and 86% which are in the range of the inorganic fraction obtained in this work.

When the iodide is present in the whey fraction, then the reported concentrations are 89% and 96%, meaning that the other compounds present in this fraction, such as iodate, whey proteins, etc., have low iodine content because these values are not significantly higher than the isolated iodide. In this work, about 4% of the iodine was bound to lipids and 4–8% bound to proteins (depending of the separation method employed). Fernández-Sánchez et al. [16] reported an iodine bound to lipid and iodine bound to casein content of 10% and 5%, respectively. The iodine bound to protein values is similar to previous reported works (see Table 4). In the case of the iodine bound to lipids the value obtained in this work is lower than the reported iodine content in fat from Table 4, but still comparable. It is assumed that there were no losses in the lipid extraction since the extracted lipid concentration was not significantly different from the fat value reported by the producer (3.25% M.F).

It seems that, up to the moment, the determination of iodine species and/or fractions in milks have been carried out mainly using either ICP or NAA. In general the detection limit of both techniques in these determinations is similar, although NAA can always improve this parameter extending both the irradiation and counting time. In this work the detection limits obtained (Table 3) agree with those reported in Table 4. Similar situation is seen with precision values which are comparable among the reported methods (ICP-MS and NAA) in Table 4. In this work however, the precision in the iodine determination in comparison to ICP-MS was improved for the case of lipids and proteins, despite their low iodine content, because of the use of EINAA–CS.

6. Conclusions

Results from this work have shown that the isopropanol–hexane (1:1) solvent system is suitable for the lipid extraction from milk. The total protein separation (casein + whey proteins) can be achieved by $(NH_4)_2SO_4$ precipitation, dialysis, or a combination of both. Dialysis requires around 30 h for completing the removal of lipids and other inorganic species; hence this method for protein separation is time-consuming. Lipid should be separated from milk before protein, otherwise coprecipitate with them. Iodine determination was performed with high precision and accuracy using EINAA–CS without any sample digestion and the detection limit for the species was very low. The main iodine fraction in milk is inorganic, which represents 94% of the total iodine, proteins and lipids account for around 4% each. Results from this study are in good agreement with previous reported works.

Acknowledgments

The authors would like to acknowledge the assistance of Dr. J. Holzbecher of the DUSR facility for irradiations. The financial assistance from the NSERC Canada in the form of a research grant, the Dalhousie University Faculty of Graduate Studies for a scholarship (K.I.-O.), and the High Institute of Nuclear Science and Technologies of the Ministry of Science of the Government of Cuba for a study leave (K.I.-O.) are also acknowledged.

References

[1] Assessment of iodine deficiency disorders and monitoring their elimination. A guide for programme managers, second edition, WHO, 2001. On line document www.who.int.
[2] Iodine in Salt: A Statement by WHO, Press Release WHO/90, 1994. On line document www.who.int.
[3] MAFF UK-Iodine in Milk (sheet 198), MAFF food surveillance Sheets 2000, Food Standard Agency, On line document www.foodstandards.gov.uk.
[4] Diet & Nutrition, Iodine Tables, On line document www.internethealthlibrary.com.
[5] M.B. Zimmermann, J. Trace Elem. Med. Biol. 22 (2008) 81.
[6] P. Fischer, M.R. L'Abbe, A. Giroux, J. Assoc. Off. Anal. Chem. 69 (1986) 687–689.
[7] M. Abdulla, Inorganic Chemical Elements in Prepared Meals in Sweden, Department of Clinical Chemistry, University of Lund, S-221 85, Lund, Sweden, 1986.
[8] L. Fernandez-Sanchez, J. Szpunar, J. Anal. At. Spectrom. 14 (1999) 1697.
[9] R. Early, The Technology of Dairy Products, second edition, Blackie Academic, London/New York, 1998.
[10] A.R. Curtis, P. Hamming, J. Assoc. Off. Anal. Chem. 65 (1982) 20.
[11] D. Sertl, W. Malone, J. Assoc. Off. Anal. Chem. 76 (1993) 711.
[12] St. Grys, J. Chromatogr. 100 (1974) 43.
[13] P. Bermejo-Barrera, M. Aboal-Somoza, A. Bermejo-Barrera, J. Anal. At. Spectrom. 14 (1999) 1009.

[14] P. Bermejo-Barrera, M. Aboal-Somoza, A. Bermejo-Barrera, M.L. Cervera, M. De la Guardia, J. Anal. At. Spectrom. 16 (2001) 382.
[15] Y. Gelinas, G.V. Iyengar, R. Barnes, Fresenius J. Anal. Chem. 362 (1998) 483.
[16] L.M. Fernández-Sánchez, P. Bermejo-Barrera, J.M. Fraga-Bermudez, J. Szpunar, R. Lobinski, J. Trace Elem. Med. Biol. 21 (2007) 10.
[17] R.R. Rao, J. Holzbecher, A. Chatt, Fresenius J. Anal. Chem. 352 (1995) 53.
[18] T.A. Nichols, J.S. Morris, V.L. Spate, C.J. Tharp, C.K. Baskett, T.L. Horsman, M.M. Mason, T.P. Cheng, J. Radioanal. Nucl. Chem. 236 (1998) 65.
[19] J. Kucera, Z. Randa, L. Soukal, J. Radioanal. Nucl. Chem. 249 (2001) 61.
[20] R.R. Rao, W.H. Zhang, J. Holzbecher, A. Chatt, Trans. Am. Nucl. Soc. 81 (1999) 21.
[21] W.H. Zhang, A. Chatt, Trans. Am. Nucl. Soc. 78 (1998) 95.
[22] R.R. Rao, A. Chatt, Anal. Chem. 63 (1991) 1298.
[23] R.R. Rao, A. Chatt, Analyst 118 (1993) 1247.
[24] R.R. Rao, A. Chatt, Trans. Am. Nucl. Soc. 64 (1991) 12.
[25] R.R. Rao, A. Chatt, Trans. Am. Nucl. Soc. 71 (1994) 27.
[26] F.A. Rivero-Martino, M.L. Fernandez-Sanchez, A. Sanz-Medel, J. Anal. At. Spectrom. 17 (2002) 1271.
[27] M. Leiterer, D. Trukenbrodt, K. Franke, Eur. Food Res. Technol. 213 (2001) 150.
[28] X. Hou, H. Dahlgaard, U. Jacobsen, S.P. Nielsen, J. Radioanal. Nucl. Chem. 244 (2000) 87.
[29] P.R. Bhagat, A.K. Pandey, R. Acharya, A.G.C. Nair, N.S. Rajurkar, A.V.R. Reddy, Talanta 71 (2007) 1226.
[30] D.E. Ryan, D.C. Stuart, A. Chattopadhyay, Anal. Chim. Acta 100 (1978) 87.
[31] D.C. Stuart, D.E. Ryan, Can. J. Chem. 59 (1981) 1470.
[32] J. Holzbecher, A. Chatt, D.E. Ryan, Can. J. Spectrosc. 30 (1985) 67.
[33] A. Hara, N.S. Radin, Anal. Biochem. 90 (1978) 420.
[34] W.M. Indrasenna, Dalhousie University, Personal Communication.
[35] C.V. Span, R.L. Lunbland, N.C. Price, Biotechnol. Appl. Biochem. 29 (1999) 99.
[36] L.A. Currie, Anal. Chem. 40 (1968) 586.

Talanta 77 (2008) 659–662

Contents lists available at ScienceDirect

Talanta

journal homepage: www.elsevier.com/locate/talanta

Entrapment of invertase in an interpenetrated polymer network of alginic acid and poly (1-vinylimidazole)

Müjgan Kartal[a], Senem Kıralp Kayahan[a], Ayhan Bozkurt[b], Levent Toppare[a,*]

[a] Department of Chemistry, Middle East Technical University, 06531 Ankara, Turkey
[b] Department of Chemistry, Fatih University, 34900 Büyükçekmece, Istanbul, Turkey

ARTICLE INFO

Article history:
Received 19 January 2008
Received in revised form 21 June 2008
Accepted 3 July 2008
Available online 16 July 2008

Keywords:
Alginic acid
Poly (1-vinylimidazole)
Invertase
Enzyme immobilization
Proton conductivity

ABSTRACT

In this work, we have investigated the synthesis and characterization of a proton conductor based on alginic acid and poly (1-vinylimidazole). The polymer network was obtained by mixing alginic acid and poly (1-vinylimidazole) at various stoichiometric ratios. The polymer electrolytes were characterized by elemental analysis and FT-IR spectroscopy. Invertase was entrapped in the polymer networks during complex formation. Additionally, the maximum reaction rate and Michaelis–Menten constant were investigated for the immobilized invertase. The temperature and pH optimization, operational stability and shelf life of the polymer network were examined.

1. Introduction

Polymer electrolyte membrane fuel cells (PEFCs) are one of the attractive energy conversion systems used in many industrial applications including electric vehicles, mobile telephones, and on-site power generations [1,2]. Since their development in the 1960s, perfluorinated ionomers such as Nafion® have emerged as standard materials for low-temperature fuel cell applications due to their high proton conductivity and their excellent chemical and thermal stability. Without doubt, the most extensive limitations arise from the fact that these materials are proton-conducting only when hydrated, which results in a maximum operating temperature of ~100 °C [3]. To get rid off these limitations several attempts have been made such as doping of the polymers bearing basic units such as amide, imine, either with strong acids, i.e. H_3PO_4 or H_2SO_4 [4]. Although they have already been illustrated to have high protonic conductivity in the anhydrous state, dissociation of acidic units may be a problem at higher operation temperatures [5]. Recently, neutral (or basic) proton conducting polymer electrolytes have already been announced as they are likely to be more stable in the presence of electrode materials. From this point of view imidazole or benzimidazole have been reported to be promising under anhydrous and intermediate temperature (100–200 °C) conditions [4,6,7]. Their nitrogen sides act as proton acceptors thus forming protonic charge carriers. Their protonated and unprotonated nitrogen sides act as donors and acceptors in proton exchange reactions which in return give rise to proton transport via diffusion [8].

Alginic acid, one of the elements of marine algae, is a natural polysaccharide containing linear chains of 1,4′-linked β-D-mannuronic acid and α-L-guluronic acid (Fig. 1). Alginic acid is a biodegradable, biocompatible, non-toxic, and low cost polymer, which shows many interesting properties, such as wound healing, ion-exchange ability, and absorption of metal ions. Besides these uses alginic acid can be used as an electrical or optical material [9,10].

Enzymes are sensitive substances. Their catalytic properties change when exposed to high temperatures or to certain reagents. Immobilized enzyme has many operational advantages over free enzyme such as, multiple or repetitive use of a single batch of enzymes, enhanced stability, continuous operational mode, rapid termination of reaction, easy separation of biocatalyst from product, and reduced cost of operation.

Invertase catalyzes the hydrolysis of sucrose to glucose and fructose, which is known as the invert sugar. Sucrose crystallizes more readily than invert sugar, so the latter is widely used in the production of noncrystallizing creams, in making jam and artificial honey [11]. Although, invertase has little potential for commercial use in its immobilized form, it is one of the most studied of

* Corresponding author. Tel.: +90 312 2103251; fax: +90 312 2101280.
E-mail address: toppare@metu.edu.tr (L. Toppare).

0039-9140/$ – see front matter © 2008 Elsevier B.V. All rights reserved.
doi:10.1016/j.talanta.2008.07.017

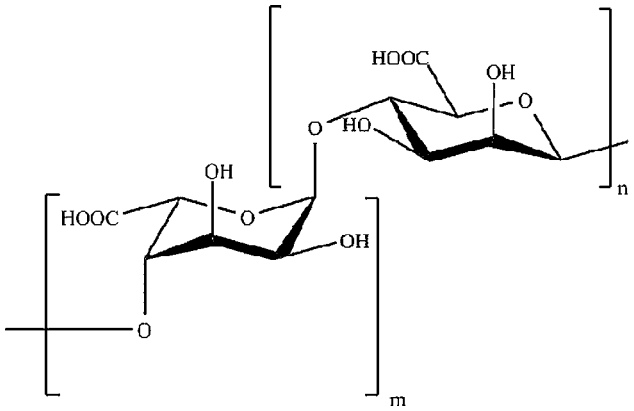

Fig. 1. Structure of alginic acid.

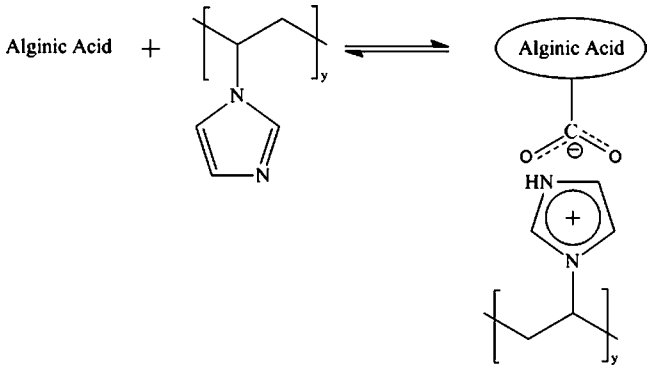

Fig. 2. Complexation of AA and PVI.

all enzymes since it is a model enzyme for experimental purposes [12].

Immobilization of enzymes into complexed polymer electrolyte networks is rather new and easy where the process is carried out during ionic complexation.

In this article, the aim was to prepare a bioreactor by immobilizing invertase into a polymer network obtained by mixing alginic acid (AA) and poly (1-vinylimidazole) (PVI). We report the synthesis and some characteristics of AA/PVI/invertase polymer electrolyte.

2. Experimental

2.1. Materials

Invertase (β-fructofuranoxidase) (E.C. no. 3.2.1.26) (from bakers yeast, 53 U/mg solid) was purchased from Sigma. PVI was synthesized by solution polymerization [13]. AA and sucrose were obtained from Sigma.

2.2. Instrumentation

2.2.1. UV–vis spectrophotometer

A Shimadzu UV–1601 model spectrophotometer was employed in the determination of activities of immobilized enzyme. For the spectrophotometric activity determination, the Nelson method was used. For acetate buffer, acetic acid and sodium acetate were used.

2.2.2. Fourier transform infrared spectrophotometer (FT-IR)

The FT-IR spectra of conducting polymer blends were obtained as dispersed in KBr pellets, using a Nicolet–510 FTIR and Mattson 1000 FTIR Spectrometer.

2.3. Synthesis of AA/PVI network and entrapment of invertase

First we determined the maximum degree of complexation and the swelling behavior of the gels. To obtain the most suitable AA/PVI matrix, 0.10 g of AA were mixed with different amounts of PVI. Since AA is a dibasic acid, the maximum protonation was expected with $x = 2$ (where x is the number of moles of 1-VIm per moles of –COOH units in AA). To check maximum protonation, four samples were prepared with x from 1 to 4. The elemental analysis and FT-IR results showed that the maximum protonation was obtained with $x = 1$. Therefore, in this study the AA/PVI matrix was obtained with $x = 1$ (Fig. 2).

Additionally, the maximum water absorbing capacity was checked. The maximum capacity of intake was 1.6 ml in 2.0 ml of AA (0.10 g/ml) and PVI (0.0556 g/ml).

The enzyme solution was prepared in pH 5.1 acetate buffer with an enzyme concentration of 4.0 mg/ml. Finally, AA/PVI matrix–enzyme solutions were stirred to obtain enzyme entrapped polymer network (EEPN). When 1 ml AA was mixed with 1 ml PVI/enzyme, the network absorbs 1.6 ml liquid (80% yield). As a result, 3.2 mg (170 U) enzyme were incorporated into the matrix. EEPN was used in activity determinations.

2.4. Determination of invertase activity

Nelson's method was used for activity determination [14]. Different concentrations of sucrose solutions prepared in acetate buffer (pH 5.1) were kept in a water bath at 25 °C for 5 min. Different incubation times (2, 4, and 6 min) were applied to allow enzyme to react with substrate in a total volume of 2.0 ml. After incubation time, 1 ml of this solution was drawn and added into 1 ml Nelson reagent. Then, test tubes were kept in boiling water for 20 min to stop the reaction, and they were cooled to room temperature. Finally, 1.0 ml of an arsenomolybdate solution and 7.0 ml of distilled water were added. Absorbances were determined at 540 nm.

2.5. Determination of kinetic parameters

For determination of the maximum reaction rate (V_{max}) and the Michaelis–Menten constant (K_m), the activity assay was applied for different substrate (sucrose) concentrations. Sucrose solutions (5, 8, 10, 20, 30 and 50 mM) were prepared in acetate buffer (pH 5.1) and kept in a water bath at 25 °C for 5 min, and then the EEPN was added to the test tubes and shaken for incubation times of 2, 4, and 6 min.

2.6. Determination of optimum temperature and pH

Optimum temperature and pH were determined by changing incubation temperature between 10 and 80 °C while keeping the substrate concentration constant ($10K_m$). In addition to temperature optimization, pH optimization is also important for a bioreactor. pH optimizations were carried out by changing the pH range between 2 and 11 at constant temperature (25 °C) and constant substrate concentration ($10K_m$).

2.7. Operational stabilities and shelf life

The operational stability of the enzyme bioreactor was determined at optimum activity conditions using the same electrodes in 40 activity assays per day. The shelf life of the electrodes was investigated by performing activity measurements within 25 days.

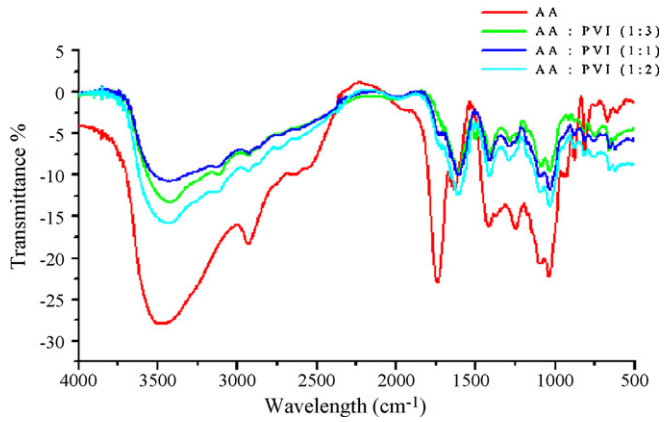

Fig. 3. FT-IR results of AA and AA/PVI networks at different *x*.

3. Results and discussion

3.1. FTIR results

A strong absorption appears at 1742 cm^{-1} that belongs to C=O stretching. 1247 cm^{-1} and 1419 cm^{-1} represent the C–O–H stretching of carboxylic acid groups of the AA (Fig. 3). After obtaining polymer network by mixing AA and PVI in different ratios, a new peak was observed at 1604 cm^{-1}, and the intensity of the carbonyl stretching at 1742 cm^{-1} decreased due to the protonation of PVI with AA. These occur by the transfer of the acidic proton of carboxylic acid to the 'free' nitrogen side of PVI to form imidazolium ion. A broad peak centered at 3433 cm^{-1} was observed due to stretching vibration of the isolated non-hydrogen bonded NH group and a broad peak approximately located between 3050 and 3300 cm^{-1} was assigned to the stretching vibration of NH groups involved in hydrogen bonding of the protonated heterocycle [15]. The percent protonation was evaluated for the peaks that are located at around 1742 and 1604 cm^{-1}.

Before immobilization of enzyme, the degree of protonation was evaluated. Presence of two acidic protons on AA rise the expectations of highest protonation with $x = 2$ (molar ratio of the monomer repeat units). The percent protonation of the complex electrolyte AA: PVI was 96% for 1:1, 83% for 1:2, 89% for 1:3 and 87% for 1:4. The values for 1:2, 1:3 and 1:4 ratios are close to each other whereas the highest protonation was 1:1 ratio. The reason can be attributed to the structure of AA. AA is a linear copolymer with homopolymeric blocks of (1,4)-linked β-D-mannuronate (M) and its C-5 epimer α-L-guluronate (G) residues, respectively, covalently linked together in different sequences or blocks. The monomers can appear in homopolymeric blocks of consecutive G-residues (G-blocks), consecutive M-residues (M-blocks), alternating M and G-residues (MG-blocks) or randomly organized blocks. For that reason the highest protonation occurs with $x = 1$ instead of 2. Hence, we can conclude that all carbonyl groups are not involved in the complexation reactions.

3.2. Elemental analysis

Table 1 shows the feed and the final compositions of the complex polymer electrolytes. Stable gels were collected form the solution and dried under vacuum for elemental analysis. While the PVI content in the feed was varied from 50 to 80%, the PVI composition of the polymer electrolyte was changed from 48 to 69%. As the composition of the complex materials are known, they are successfully used for invertase immobilization.

Table 1
Results of elemental analysis

Sample (AA:PVI)	% VIm in the feed (mol)	% VIm in the complex (mol)
1:1	50	48
1:2	66	55
1:3	75	67
1:4	80	69

Table 2
Kinetic parameters for free and immobilized invertase

	K_m (mM)	V_{max} (μmol/min ml)
Free invertase	24.3	84.3
AA/PVI/invertase	80	3.33

3.3. Kinetic parameters

In this matrix, 170 U (3.2 mg) invertase were incorporated. Kinetic parameters K_m and V_{max} were found using Lineweaver–Burk plots at constant temperature and pH while varying the substrate concentration [16]. The maximum rate for an enzymatic reaction is given by V_{max}. The Michaelis–Menten constant (K_m) of an enzyme is a measure of the affinity of the enzyme to its substrate. The value of apparent K_m for a particular enzyme is defined as the substrate concentration at which half of the enzyme molecules are complexed with substrate. The results (Table 2) show that there is an increase in K_m values compared to that of the free enzyme [17]. The high K_m value indicates lower enzyme–substrate affinity. In other words, the observed increase in K_m value is due to the tendency of enzyme to leave substrate within a short time without giving a product. In this network, enzyme and substrate interaction and complex formation became more difficult, hence K_m value increases as V_{max} decreases.

3.4. Temperature influence on enzyme-entrapped polymer

The temperature optimization is very important in enzyme immobilization and bioreactor construction. The effect of temperature on the enzyme activity is shown in Fig. 4. At 50 °C, the free invertase completely lost its activity [13], however, the EEPN for $x = 1$ showed a maximum at 40 °C, and also EEPN did not lose its enzymatic activity at 50 °C. Additionally, this matrix shows adequate activity in a low temperature range (10–40 °C). EEPN provides a suitable immobilization medium for invertase and can be used as a bioreactor for a wide temperature range.

3.5. pH influence on enzyme-entrapped polymer

The variation of invertase activity for a pH range from 2 to 11 was investigated for the AA/PVI matrix. In pH optimization experiments, the temperature of medium and concentration of the substrate

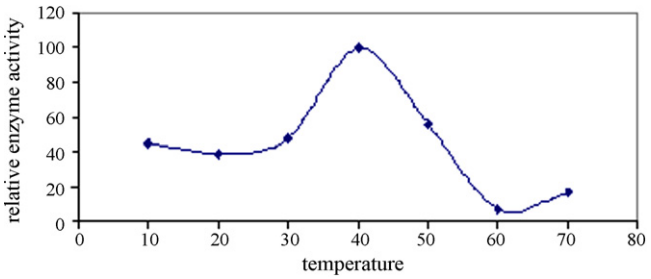

Fig. 4. Temperature influence on enzyme bioreactor.

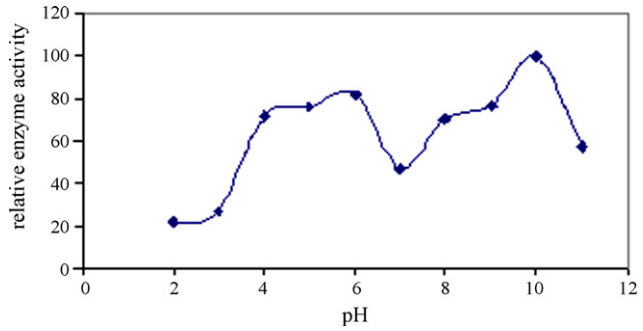

Fig. 5. pH influence on enzyme bioreactor.

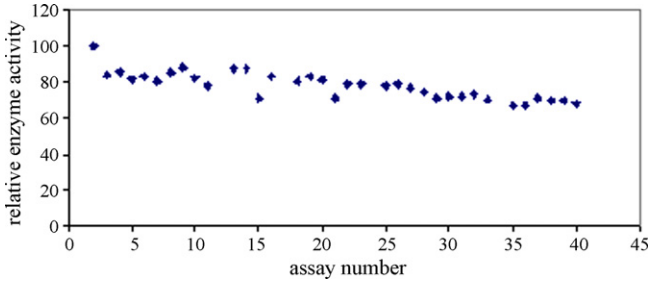

Fig. 6. Operational stability of enzyme bioreactor.

($10K_m$) were kept constant. The results are presented in Fig. 5. The maximum activity of free invertase was observed at pH 5 [11]. The immobilized invertase in the AA/PVI matrix showed a maximum activity at pH 10. There is a continuous increase in the enzyme activity from pH 2 to 6. In AA/PVI matrix, there is a protonated medium, for that matter the pH value in EEPN is different than that of bulk.

At pH 7, there was a drastic decrease. Probably, the pH of microenvironment of enzyme is lower than 7 and close to the isoelectric point. The isoelectric point is the pH at which a molecule or surface carries no net electrical charge. The solubility and hence the activity of the enzyme are often at a minimum when the pH is close to the isoelectric point.

3.6. Operational stability and shelf life of the enzyme bioreactor

The operational stability was obtained by running 40 measurements in the same day at a constant temperature, pH and substrate concentration (Fig. 6). An activity loss of 20% was observed after the third use. At the end of 40 measurements, total activity loss of 30% was observed. As a consequence, immobilized enzyme provides multiple uses whereas the free enzyme can only be used once unless it is recovered from the reaction mixture without any denaturation. The activity of EEPN was measured for every 5 days within consecutive 25 days to determine shelf life of immobilized enzyme. This enzyme lost 50% of its activity in the first 3 days, and completely

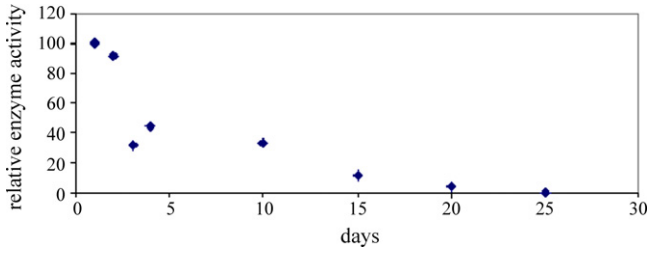

Fig. 7. Shelf life of the bioreactor.

lost its activity within the next 25 days (Fig. 7). The enzymatic activity decreases during the storage period. The soluble free invertase loses its activity completely within 8 days [18]. Thus, it can be concluded that a bioreactor constructed with this matrix on an enzyme shows good stability for a short time.

4. Conclusion

In this work, the immobilization of invertase was successfully achieved in an AA/PVI polymer matrix. The proton exchange reactions between polymers PVI and AA was studied by FT-IR spectroscopy and demonstrated that maximum protonation occur when $x = 1$. The composition of the materials was studied by elemental analysis and found that PVI composition depends on the feed composition and was changed from 48 to 69%. The AA/PVI matrix has very high temperature resistance and the invertase-entrapped matrix possesses reasonable values for pH optimization, operational stability, and shelf life. Entrapped invertase exhibits high stability over a broad pH range when compared the free invertase enzyme. This is due to the protection of invertase by the polymer electrolyte matrix.

References

[1] K.D. Kreuer, Chem. Phys. Chem. 3 (2002) 771.
[2] K.D. Kreuer, in: B.V.R. Chowdari, K. Lal, S.A. Agnihotry (Eds.), Solid State Ionics: Science and Technology, World Scientific, Singapore, 1998.
[3] M.F.H. Schuster, W.H. Meyer, Annu. Rev. Mater. Res. 33 (2003) 233.
[4] J.-C. Lassegues, Proton Conductors Solids Membranes, and Gels–Materials and Gels–Materials and Devices, Cambridge University Press, Cambridge, 1992 (Chapter 20).
[5] A. Bozkurt, W.H. Meyer, J. Polym. Sci. B: Polym. Phys. 39 (2001) 1987.
[6] A. Bozkurt, W.H. Meyer, J. Gutmann, G. Wegner, Solid State Ionics 164 (2003) 169.
[7] M. Yamada, I. Honma, J. Phys. Chem. B 108 (2004) 5522.
[8] K.D. Kreuer, Chem. Mater. 8 (1996) 610.
[9] K. Iwata, T. Sawadaishi, S. Nishimura, S. Tokura, N. Nishi, Int. J. Biol. Macromol. 18 (1996) 149.
[10] H. Ertesvag, S. Valla, Polym. Degrad. Stab. 59 (1998) 85.
[11] J.S. Melo, S.F. D'Souza, J. Biochem. Biophys. Methods 42 (2000) 133.
[12] A. Tanioka, Y. Yokoyama, K. Miyasaka, J. Colloidal Interf. Sci. 200 (1998) 185.
[13] X. Li, S.H. Goh, Y.H. Lai, A.T.S. Wee, Polymer 42 (2001) 5463.
[14] N. Nelson, J. Biol. Chem. 153 (1944) 375.
[15] F. Sevil, A. Bozkurt, J. Phys. Chem. Solids 65 (2004) 1659.
[16] T. Palmer, Understanding Enzymes, Prentice Hall, London, 1995.
[17] S. Alkan, L. Toppare, Y. Yagci, Y. Hepuzer, J. Biomater. Sci. Polym. Ed. 10 (1999) 1223.
[18] D. Bagal, M. Karve, Anal. Chim. Acta 555 (2006) 316.

Talanta 77 (2008) 737–743

Contents lists available at ScienceDirect

Talanta

journal homepage: www.elsevier.com/locate/talanta

Construction of novel simple phosphate screen-printed and carbon paste ion-selective electrodes

Elmorsy Khaled[a,*], H.N.A. Hassan[a], A. Girgis[b], R. Metelka[c]

[a] Microanalysis Laboratory, National Research Centre, Dokki, Cairo, Egypt
[b] Department of Pesticide Chemistry, National Research Centre, Dokki, Cairo, Egypt
[c] Department of Analytical Chemistry, Faculty of Chemical Technology, University of Pardubice, nam. Cs legii 565, CZ-532 10 Pardubice, Czech Republic

ARTICLE INFO

Article history:
Received 8 July 2008
Accepted 9 July 2008
Available online 17 July 2008

Keywords:
Phosphate ion-selective electrodes
Screen-printed electrodes
Carbon paste electrodes
PVC membrane electrodes
Bisthiourea ionophores

ABSTRACT

The construction and performance characteristics of different phosphate ion-selective electrodes are described. Three types of electrodes are demonstrated, namely screen-printed, carbon paste and the conventional PVC membrane electrodes. The cited electrodes are based on bisthiourea ionophores and show a considerable selectivity towards hydrogenphosphate with Nernstian slopes depending on the type of the electrode and the ionophore used. Matrix compositions of each electrode are optimised on the basis of effects of type and concentration of the ionophore as well as influence of the selected plasticizers. The screen-printed electrodes work satisfactorily in the concentration range 10^{-5} to 10^{-2} mol L^{-1} with anionic Nernstian compliance (32.8 mV/decade activity) and detection limit 4.0×10^{-6} mol L^{-1}. The screen-printed electrodes show fast response time of about 2.2 s and exhibit adequate shelf-life (4 months). The fabricated electrodes can be also successfully used in the potentiometric titration of HPO_4^{2-} with Ba^{2+}.

1. Introduction

Fast determination of low level of phosphate ion by a simple method was of critical importance in water, food, feed and environmental analyses. Among chemical sensors, ion-selective electrodes (ISEs) were mainly used for routine analysis because they had number of advantages, such as simplicity, low cost, short measurement time, adequate precision and accuracy as well as ability to measure the activity of various species in colored or turbid samples and therefore, ISEs would be more suitable for monitoring phosphate in different samples [1]. Construction of phosphate ion-selective electrode was one of the most challenging targets, due to the strongly hydrophilic character of the phosphate ion (positioned at the end of the well-known Hofmeister series). Recently, a series of new anion-selective electrodes had been described which displayed selectivity deviating from the Hofmeister sequence as a result of unique interactions between the carriers and the anions [2–4]. Organic tin compounds had traditionally been used as phosphate selective ionophores [5], together with cobalt phthalocyanine [6], uranyl salophenes [7], vanadyl salen [8], cyclic polyamine [9], bis(guanidinium) [10], immobilized macrocyclic ionophore [11], ferrocene-bearing macrocyclic amide [12], macrocyclic dithioxamide [13] or modified calixarines [14,15]. For design and fabrication of new anion receptors applied in ISEs, the thiourea group had drawn much interest as a functional group for neutral receptors to recognize acetate, halide, sulfate as well as phosphate and had been already used as ionophores for construction of PVC electrodes of such anions [16–19].

Drawbacks in the use of PVC electrodes were arisen from the time consuming and inconsistent manual fabrication typically employed as well as short lifetime of these electrodes. The constant developments of ISEs led to sensors which not only had better performance but also of simpler and more reliable construction. Carbon paste electrodes (CPEs) had been employed as useful materials for the fabrication of simple sensors since their emergence in the mid-1970s [20]. In comparison to PVC electrodes, the CPEs possessed advantages of much lower Ohmic resistance, very fast and stable response with easy renewal of the electrode surface as well as long functional lifetime [21]. Although a considerable attention had been given to the preparation of CPEs, their applications in analytical chemistry was mainly based on selective preconcentration followed by the voltammetric determination of the target species [22] and just a few of these CPEs had been used as ion-selective electrode by incorporation of different ionophores for the potentiometric determination of selected species [23,24]. However, designs and shapes of such electrodes were not suitable for every purpose as in the case of measurements in flowing streams or field monitoring with portable analyzers

* Corresponding author. Tel.: +20 1 0378 1777; fax: +20 2 3337 0931.
E-mail address: elmorsykhaled@yahoo.com (E. Khaled).

0039-9140/$ – see front matter © 2008 Elsevier B.V. All rights reserved.
doi:10.1016/j.talanta.2008.07.018

where the respective detection units required electrodes of special constructions.

Over the past few years, an interest had been increased in the application of simple, rapid, inexpensive and disposable sensors in different fields such as clinical, environmental or industrial analyses [25–27]. Screen-printing seemed to be one of the most promising technology allowing sensors to be placed large-scale on the market in the near future. Screen-printed electrodes (SPEs) were ideally used for the potentiometric determination of various species using different commercial printing inks [28–31]. The commercial ink formulations were usually unknown in many respects, because they were secret of the producers and some of the ink components could interfere in the electrochemical measurements.

The present work aims to introduce the disposal SPEs as a potentiometric phosphate sensor using home made printing carbon ink as well as compare the performance of such electrodes with those of the CPEs and conventional PVC membrane electrodes. The work is also devoted for the synthesis of new bisthiourea ionophores as electrode modifiers which show a remarkable selectivity towards hydrogenphosphate ion.

2. Experimental

2.1. Reagents

All reagents were of the analytical grade and double distilled water was used throughout the experiments. *o*-Nitrophenyloctylether (*o*-NPOE, Sigma) was used for preparation of the sensors. Other plasticizers, namely dibutylphthalate (DBP), dioctylphthalate (DOP), dioctylsebacate (DOS) and tricresylphosphate (TCP) were purchased from BDH, Sigma, AVOCADO and Fluka, respectively. Tridodecylmethylammonium chloride (TDDMACl) was purchased from Fluka. Polyvinylchloride (PVC, relative high molecular weight, Aldrich) and graphite powder (synthetic 1–2 μm, Aldrich) were used for the fabrication of different electrodes.

2.2. Apparatus

All the potential measurements were carried out using Metrohm 692-pH meter with silver–silver chloride double-junction reference electrode (Metrohm 6.0726.100) and combined pH glass electrode (Metrohm 6.0202.100). The electrode response times and the electrical resistances of the SPEs were measured using 46-Range Digital Multimeter (Radioshack) with PC interface. Melting points were recorded on an Electrothermal 9100 melting point apparatus. Elemental analysis was carried out using Elementar, Vario EL and IR spectra in KBr tablets were recorded on a JASCO FT/IR 300E spectrophotometer. ^{1}H NMR spectra were recorded on a Varian MERCURY 300 MHz spectrometer.

Table 1
Optimal matrix compositions of the different hydrogenphosphate sensors

Sensor	Matrix composition
SPE	6 mg **2d** + 1.8 g *o*-NPOE + 5 g PVC 8% + 3 g carbon powder
CPE	12.5 mg **2d** + 500 mg carbon powder + 200 μL *o*-NPOE
PVC	1.8 mg **2d** + 240 mg *o*-NPOE + 120 mg PVC + 6 mL THF

2.3. Synthesis of host compounds

The starting compound (2,2′-[1,2-ethanediylbis(thio)]bisbenzenamine) **1** was prepared according to the previously reported procedure [32]. A mixture of **1** (5 mmol) and the corresponding isocyanate or isothiocyanate (10 mmol) in dry tetrahydrofuran (THF, 25 mL) was stirred at room temperature for the appropriate time. The separated solid was collected and crystallized from a suitable solvent affording the corresponding **2** (Fig. 1). In case of **2e**, the reaction mixture was evaporated till dryness under reduced pressure and the remaining residue was triturated with diethylether (5 mL). The separated solid was collected and treated as above.

2.4. Sensors construction

Matrixes compositions for the different phosphate sensors were given in Table 1.

2.4.1. Screen-printed electrodes

An array of 12 electrodes was printed on a PVC film through a process involving several stages. A screen consisting of a heavy

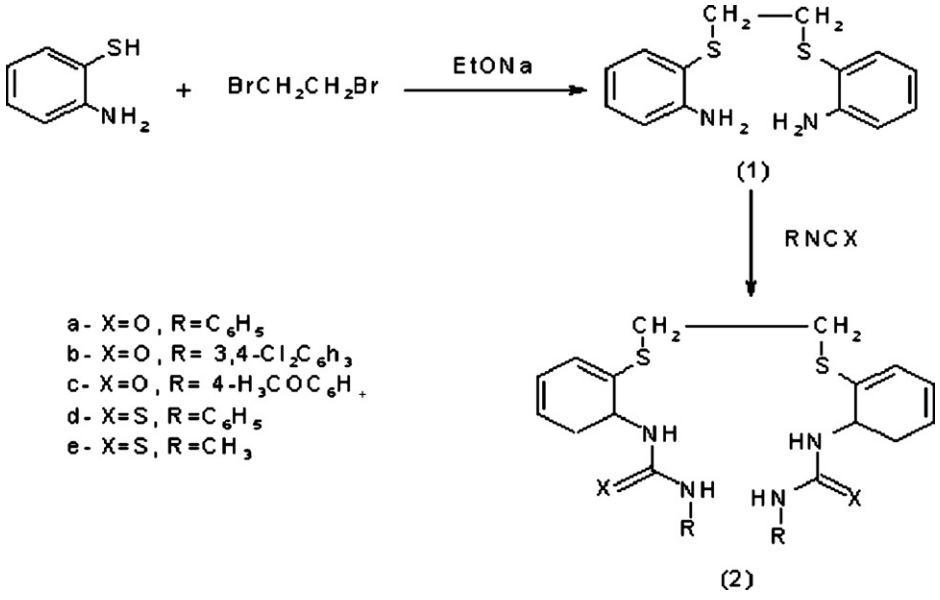

Fig. 1. Synthesis scheme of bisurea and bisthiourea ionophores.

duty polyester fabric (mesh count 36) was pre-tensioned to ca. 30 cm × 40 cm wooden frame and the photographic emulsion (Sericol S22) was spread on the fabric screen then the emulsion-coated screen was dried at 50 °C for 15 min. The required final electrode shape consisted of (3 × 4 electrodes each 5 mm × 35 mm) was printed twice on a polyester sheet and this photographic positive sheet was used to produce the electrode template. The photographic positive containing the electrode shape was taped to the emulsion-coated screen and exposed to UV light for 13–15 min afterwards. The UV light fixed the emulsion to the screen and caused permanent blockage of mesh pores outside the photographic positive while emulsion covered by the positive image remained "soft" and washed out with water. This left the screen containing the electrode image.

The home made printing ink was prepared as described in details elsewhere [33] by thoroughly mixing 6 mg of the bisthiourea ionophore **2d** with 1.8 g *o*-NPOE, 5 g PVC solution (8% in cyclohexanone–acetone mixture 1:1) and 3 g carbon powder. The working electrodes were printed on the PVC substrate and cured at 60 °C for 2 h to evaporate the residual solvent. A layer of an insulator was then placed onto the printed electrodes, leaving a defined rectangular shaped (5 mm × 5 mm) working area and a similar area on the other side for the electrical contact. Fabricated SPEs were used directly in measurements after two calibrations which served as a preconditioning process.

2.4.2. Carbon paste electrodes

The sensing electrode was prepared by mixing 12.5 mg ionophore **2d** with 500 mg graphite powder and 200 μL *o*-NPOE and the resulting paste was used to fill the electrode body [22]. The electrode was soaked in 10^{-3} mol L^{-1} hydrogenphosphate solution titrated to pH 7.2 for 24 h before measurement. A new electrode surface was obtained by screwing the piston to eject a part of the paste followed by the polishing of the surface with a wet filter paper.

2.4.3. PVC membrane electrode

The electrode matrix cocktail was prepared by dissolving 1.8 mg of the bisthiourea ionophore **2d**, 240 mg *o*-NPOE and 120 mg PVC powder in 6 mL THF. After complete mixing, the cocktail was poured into a 5 cm Petri dish and a master membrane with 0.11 mm thickness was obtained after evaporation of the solvent. A disk of the PVC membrane was mounted on the softened end of the PVC tubing filled with 10^{-3} mol L^{-1} hydrogenphosphate solution titrated to pH 7.2 and soaked in the same solution for 24 h before use.

2.5. Potentiometric measurements

The fabricated sensors were calibrated by transferring 25 mL aliquots of 10^{-6} to 10^{-2} mol L^{-1} hydrogenphosphate solutions titrated to pH 7.2 into the measuring cell followed by immersing the phosphate sensors in conjugation with the reference electrode in these solutions. Calibration graphs were obtained by plotting the observed potential versus the logarithm of the hydrogenphosphate ion activity which was derived from the Debye–Huckel limiting low according to the method of Carey and Riggan [9] and the electrode performances were evaluated according to IUPAC recommendation [34].

2.6. Response time

The electrode response time was evaluated by measuring the average time required for the electrode to reach a steady potential reading when the concentration of the hydrogenphosphate ion was suddenly increased from 10^{-6} to 10^{-5}, 10^{-5} to 10^{-4}, 10^{-4} to 10^{-3} and 10^{-3} to 10^{-2} mol L^{-1} by fast injection of microliter amounts of the concentrated hydrogenphosphate solutions.

3. Results and discussions

3.1. Bisthiourea and bisurea derivates as ionophores

Thiourea moiety had effective binding sites to recognize anions such as acetate, halide, sulfate and phosphate through hydrogen bonding interaction [16–19]. Ionophores based on these functional groups were now commercially available within chemical catalogs [18] with relative high prices making their application in the present comparative study of the efficiency of different sensors not economical; therefore the present work was also devoted for finding a simple method for the synthesis of new bisthiourea ionophores which were expected to have a remarkable selectivity towards anion of interest.

Reaction of **1** with a variety of arylisocyanates (namely, phenyl-, 3,4-dichlorophenyl- and 4-methoxyphenylisocyanate) in dry THF at room temperature afforded almost exclusively the corresponding bisurea derivatives **2a–c** in good yield. The structures of **2a–c** were established through spectroscopic (IR, ^{1}H NMR) and elemental analyses data (Table 2). The IR spectra of **2a–c** exhibit bands at ν = 3336–3284, 1662–1643 cm^{-1} assignable for the imino and carbonyl urea functional groups respectively. In addition, ^{1}H

Table 2
Characterization of the different bisurea and bisthiourea ionophores

Ionophore	Reaction time (h)	Yield (%)	m.p. (°C)	Chemical formula	Elemental analysis	IR	^{1}H NMR (DMSO-d_6)
2a	10	86	238–240	$C_{28}H_{26}N_4O_2S_2$ (514.64)	Calculated C, 65.34, H, 5.09, N, 10.89. Found C, 65.21, H, 5.01, N, 10.77	ν 3299 (NH), 1650 (C=O), 1598, 1579 cm^{-1} (C=C)	δ 2.96 (s, 4H, $2SCH_2$), 6.95–8.08 (m, 18H, arom. H), 8.28 (s, 2H, 2NH), 9.43 (s, 2H, 2NH)
2b	3	92	248–250	$C_{28}H_{22}Cl_4N_4O_2S_2$ (652.44)	Calculated C, 51.54, H, 3.40, N, 8.59. Found C, 51.75, H, 3.49, N, 8.55	ν 3336, 3284 (NH), 1662 (C=O), 1577, 1536 cm^{-1} (C=C)	δ 2.98 (s, 4H, $2SCH_2$), 6.98–8.10 (m, 14H, arom. H), 8.37 (s, 2H, 2NH), 9.74 (s, 2H, 2NH)
2c	5	87	236–238	$C_{30}H_{30}N_4O_4S_2$ (574.69)	Calculated C, 62.69, H, 5.26, N, 9.75. Found C, 62.88, H, 5.37, N, 9.81	ν 3293 (NH), 1643 (C=O), 1581, 1552 cm^{-1} (C=C)	δ 2.95 (s, 4H, $2SCH_2$), 3.73 (s, 6H, $2OCH_3$), 6.86–8.11 (m, 16H, arom. H), 8.21 (s, 2H, 2NH), 9.27 (s, 2H, 2NH)
2d	48	73	176–177	$C_{28}H_{26}N_4S_4$ (546.78)	Calculated C, 61.50, H, 4.79, N, 10.25. Found C, 61.29, H, 4.60, N, 10.43	ν 3237 (NH), 1533, 1498, 1473 cm^{-1} (C=C, C=S)	δ 3.14 (s, 4H, $2SCH_2$), 7.21–7.62 (m, 18H, arom. H), 9.32 (s, 2H, 2NH), 10.00 (s, 2H, 2NH)
2e	168	85	148–150	$C_{18}H_{22}N_4S_4$ (422.65)	Calculated C, 51.15, H, 5.25, N, 13.26. Found C, 51.06, H, 5.19, N, 13.23	ν 3162 (NH), 1540, 1509, 1467 cm^{-1} (C=C, C=S)	δ 2.98 (s, 6H, $2NCH_3$), 3.11 (s, 4H, $2SCH_2$), 7.21–7.54 (m, 8H, arom. H), 7.74 (br. s, 2H, 2NH), 9.01 (s, 2H, 2NH)

Table 3
Electrochemical performance of phosphate sensors modified with different bisurea and bisthiourea ionophores

Sensor	Ionophore	Slope (mV/decade)	DL (mol L^{-1})	log $K^{pot}_{PO_4^{2-},j}$ [a]								
				SO_4^{2-}	Cl^-	Br^-	I^-	F^-	NO_3^-	SCN^-	CH_3COO^-	HCO_3^-
PVC	Blank	8.7 ± 1.4	10^{-4}									
	2a	18.3 ± 2.9	10^{-4}	−1.7	−0.2	−1.3	−1.4	−1.7	−0.1	+1.8	+1.2	+0.3
	2b	17.7 ± 1.0	10^{-5}	−1.9	−0.2	−1.5	−1.7	−1.4	−0.1	+1.6	+1.0	−0.1
	2c	19.7 ± 0.8	10^{-5}	−1.6	−0.2	−1.6	−1.5	−1.2	−0.3	+1.4	+0.2	−0.6
	2d	28.0 ± 1.0	10^{-5}	−2.1	−0.3	−2.1	−3.5	−2.5	−0.5	+1.3	+0.7	+0.8
	2e	25.6 ± 2.0	10^{-5}	−1.5	−0.5	−2.0	−2.9	−2.3	−0.4	+1.3	+0.3	−0.5
CPE	Blank	9.0 ± 2.9	10^{-3}									
	2a	31.5 ± 0.9	10^{-4}	−1.5	−1.6	−1.6	−0.6	−0.9	−1.7	+0.7	+0.7	+0.1
	2b	29.6 ± 3.8	10^{-4}	−1.6	−1.4	−1.1	−0.2	−0.7	−0.9	+0.3	+0.5	+0.4
	2c	22.5 ± 0.9	10^{-4}	−2.1	−1.7	−0.7	−1.2	−0.5	−1.6	+0.6	+0.5	−0.1
	2d	29.0 ± 1.1	10^{-5}	−1.5	−1.9	−1.7	−1.8	−1.6	−0.4	+0.5	+0.5	+0.7
	2e	26.4 ± 0.5	10^{-5}	−1.0	−1.9	−1.9	−2.0	−1.8	−0.1	+0.6	−0.2	−0.5
SPE	Blank	7.5 ± 0.9	10^{-4}									
	2a	34.0 ± 1.7	10^{-4}	−1.1	−1.6	−0.3	−1.0	−1.3	−0.3	+2.6	+0.7	+2.2
	2b	24.9 ± 1.3	10^{-4}	−0.9	−1.5	−0.4	−2.0	−1.0	−0.4	+2.4	+1.2	+1.8
	2c	22.8 ± 3.7	10^{-4}	−0.7	−1.3	−0.1	−3.0	−0.8	−0.3	+2.0	+1.1	+1.4
	2d	30.7 ± 0.5	10^{-5}	−1.8	−2.3	−0.7	−3.6	−1.5	−0.7	+1.7	+0.5	+1.0
	2e	24.9 ± 0.2	10^{-5}	−1.6	−2.2	−0.6	−3.3	−1.4	−0.6	+1.9	+0.6	+1.2

[a] Selectivity coefficients were measured by the matched potential method at pH 7.2. Lower and upper concentration of phosphate ion: 10^{-4} to 10^{-2} mol L^{-1}, respectively.

NMR spectra revealed two D_2O-exchangeable singlet signals at δ = 8.21–8.37, 9.27–9.74 regions, each integrated to 2NH residues, confirming the formation of bisurea derivatives.

Similarly, reaction of **1** with either aryl or alkylisothiocyanates (namely, phenyl- and methylisothiocyanate) under the previously described reaction conditions gave the corresponding bisthiourea derivatives **2d** and **2e**. Their structures were also determined from spectroscopic (IR, ^{1}H NMR) and elemental analyses data.

3.2. Optimal electrode matrixes compositions

Parallel studies were carried out on all investigated electrodes (namely SPEs, CPEs and PVC membrane) using the five synthesized ionophores (**2a–e**). Besides the critical role of the nature of the ionophore in the electrode matrix, the amount of the ionophore, the nature of the plasticizer used and the additives significantly influenced the sensitivity and selectivity of the fabricated electrodes.

3.2.1. Effect of ionophore type

In preliminary experiments, the synthesized ionophores (**2a–e**) were incorporated in different electrodes matrixes (2, 10 and 8 mg for PVC, CPEs and SPEs, respectively) and both the sensitivity and selectivity of the fabricated electrodes were tested towards different anions. For PVC membrane electrodes, the internal filling solution was 10^{-3} mol L^{-1} of the corresponding anion and the electrode was conditioned in the same solution overnight. The obtained results (Table 3) showed that the fabricated sensors had a remarkable selectivity towards the hydrogenphosphate anion, with Nernstian slopes, while those without ionophores (dummy electrodes) showed insignificant Nernstian responses (7.5–9 mV/decade activity). As it can be seen, the sensors exhibited selective response toward HPO_4^{2-} and followed selectivity pattern in the order of $HPO_4^{2-} > SCN^- > HCO_3^- > CH_3COO^- > NO_3^- > Br^- > F^- > SO_4^{2-} > Cl^- > I^-$. Although the prepared electrodes showed a considerable selectivity towards acetate, thiocyanate and bicarbonate, calibration graphs of these ions (Fig. 2) were non-linear with Nernstian slopes ranging from 30.5 to 42.0 mV/decade activity. Generally, the selectivity of the anion-selective electrodes based on urea and thiourea moieties are determined by the shape and the distance between hydrogen bond forming sites [35,36] and the remarkable higher selectivity towards hydrogenphosphate over other expected anions may result from the different distance between the hydrogen bond donors with absence of the fixed xylene ring [17,18]. Further study of such mechanism is still under investigation.

Sensors containing the different synthesized ionophores showed calibration graphs for hydrogenphosphate with anionic slope values depended on the type of the ionophore within the electrode matrixes which demonstrated the role of the ionophore in the electrode response. Generally, the bisthiourea ionophores had the ability to form a stronger hydrogen bond than bisurea ionophores [17,18]; the potentiometric responses of the sensors prepared using **2d** and **2e** as ionophores were better than those modified with **2a–c** ionophores. Also, the replacement of the methyl group in **2e** by the phenyl substituent in **2d** led to much stronger complex stabilities with hydrogenphosphate which could be understood by considering the electron withdrawing effect of the phenyl groups

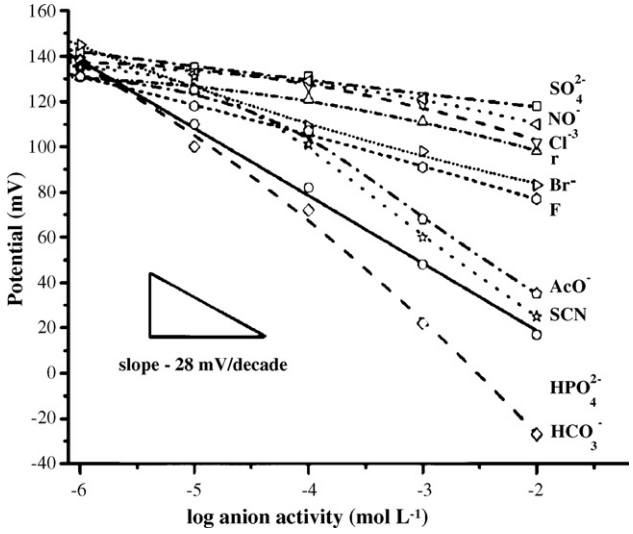

Fig. 2. Potentiometric responses for different anions using PVC membrane electrode containing ionophore **2d** plasticized with *o*-NPOE. The sample solutions were adjusted to pH 7.2 with NaOH.

and to stronger hydrogen binding capability [18]. Thus, the all-subsequent potentiometric measurements were performed with the bisthiourea ionophore **2d**.

3.2.2. Effect of ionophore concentration

Constructing the ion-selective electrodes, the amount of the ionophore in the electrode matrix should be sufficient to obtain reasonable complexation at the electrode surface that is responsible for the membrane potential. If such ionophore is present in excess, the over-saturation occurs in the membrane network will hinder the complexation process and lead to unsatisfactory measurements. Thus, the influence of the bisthiourea **2d** concentration in the PVC, CPEs and SPEs matrixes was investigated.

For PVC membrane electrodes, the **2d** content was changed from 0.72 to 7.2 mg in the membrane matrix and the potentiometric performances of the fabricated electrodes were evaluated. Incorporation of 1.8 mg of the aforementioned ionophore was found to be the best as it gave a Nernstain slope (28.0 ± 1.0 mV/decade activity) in the working concentration range of 10^{-5} to 10^{-2} mol L^{-1} hydrogenphosphate. With CPEs, **2d** concentration was changed from 0.5 to 25 mg and 12.5 mg was selected (slope was 28.7 ± 1.9 mV/decade activity). When preparing the screen-printed electrodes, addition of 6 mg of the ionophore **2d** to the printing ink was sufficient to obtain anionic slope of 30.6 ± 1.4 mV/decade activity.

3.2.3. Effect of plasticizer

It is well known that the sensitivity and selectivity obtained for a given ionophore based ion-selective electrode is greatly influenced by the polarity of the electrode matrix, which is defined by the dielectrical constant of the electrode plasticizer [37,38]. It should be noted that the nature of the plasticizer affects not only the polarity of the electrode phase but also the mobility of ionophore molecules and the state of the formed complexes.

The influence of the plasticizer on the performance of different phosphate sensors modified with bisthiourea ionophore **2d** was studied using five plasticizers having different dielectrical constants, namely, o-NPOE, DOS, DOP, DBP and TCP (ε values were 24, 3.88, 5.2, 4.7 and 17.6, respectively). Generally, PVC membrane electrodes plasticized with *o*-NPOE had significantly better responses for hydrogenphosphate (slope was 27.5 ± 1.6 mV/decade activity) while other plasticizers gave potentiometric responses with sub-Nernstian slopes (17.7 ± 2.1, 17.0 ± 1.5, 18.1 ± 0.9 and 24.6 ± 0.8 mV/decade activity for DOP, DBP, DOS and TCP, respectively).

Similar results were also obtained using SPEs and CPEs as the electrodes plasticized with o-NPOE gave superior results than others indicated by the highest slope values (32.8 ± 0.5 and 29.0 ± 1.1 for SPEs and CPEs, respectively). This may be attributed to the high affinity of ionophore and ability of *o*-NPOE to extract phosphate anion from aqueous phase to the organic electrode phase and agreed with the previously published phosphate sensors [10,12,13,15–18] in which *o*-NPOE was selected as the electrode plasticizer.

3.2.4. Effect of ionic sites

It is well established in literature that lipophilic ionic additives promote the interfacial ion-exchange kinetics and decrease the membrane resistance by providing mobile ionic sites in the membrane matrix [39,40]. The response of ISE containing various kinds of ionic sites distinguished whether the ionophores act as an electrically charged or neutral carrier. ISEs modified with electrically neutral carriers functional only if sites with a charge opposite to that of the analyte are present in the electrode matrix while those with charged carriers, on the other hand, do not need the addition of such ionic sites.

Table 4
Performance characteristics* of hydrogenphosphate sensors fabricated with different techniques

Sensor	PVC	CPE	SPE
Regression equation[a]			
Intercept (mV)	−2.7 ± 2.9	27.7 ± 4.6	199.4 ± 1.5
Slope (mV/decade)	−28.0 ± 2.0	−29.0 ± 1.1	−32.8 ± 0.5
Correlation coefficient	0.9980	0.9979	0.9997
Detection limit (mol L^{-1})	1.0×10^{-5}	4.4×10^{-6}	4.0×10^{-6}
Response time (s)	4	3	2.2
Shelftime (weeks)	2–3	4	16

* Average of five calibration graphs.
[a] $A = a + bC$, where A is the potential readings and C is the logarithm of phosphate ion activity.

TDDMACl as ionic site was added to PVC membrane electrodes in the ratio 0–30% mol with respect to the ionophore **2d** and the potentiometric performances of the prepared membranes were tested towards hydrogenphosphate. It was found that the fabricated electrodes responded to the phosphate target anion with and without the TDDMACl. This phenomenon can be explained by the charged carrier mechanism; due to the high basicity of bisthiourea, it is expected that, after conditioning, the **2d** ionophore in the membrane matrix becomes protonated so it acts as a charged carrier and therefore the ionic sites serve only to reduce the electrical resistance of the membrane rather than acting as anion-exchanger. This explanation agreed with the fact that many of the membrane electrodes based on different neutral ionophores can act without addition of ionic sites and showed good selectivity and sensitivity towards the target anion [9,11,35].

3.3. Performance of sensors

3.3.1. Calibration graphs

The potentiometric response characteristics of the different phosphate sensors containing **2d** ionophore (5 electrodes each at the optimal electrode matrixes compositions) were evaluated by plotting the potential readings against the logarithmic hydrogenphosphate activity. The prepared sensors displayed Nernstian anionic responses depended on the type of the electrode. Results presented in Table 4 showed that the SPEs gave the highest sensitivity and reproducibility compared with other tested electrodes (slope values 32.8 ± 0.5, 29.0 ± 1.1 and 28.0 ± 2.0 mV/decade activity, for SPEs, CPEs and PVC, respectively) as well as the lowest detection limit (4.0×10^{-6} mol L^{-1}).

3.3.2. Response time

For analytical applications, the response time of a new fabricated sensor is of critical importance. The average response times of the different phosphate sensors were illustrated in Fig. 3. SPEs and CPEs showed very fast responses (2.2 and 3 s for concentration $\geq 10^{-3}$ mol L^{-1} comparing to 5 and 7 s for lower concentrations) which were shorter than the previously published phosphate sensors [11,12,14,18]. PVC electrode showed slower response times (6 and 10 s, respectively) which may be attributed to the presence of the internal reference solution.

3.3.3. Effect of pH

Whereas the selection of an appropriate buffer for usual ISE measurements is rarely a major problem, the choice of the buffer when using ionophores with hydrogen bond donor groups requires special attention. In view of the relatively high stabilities of the ionophore complexes with acetate and other oxoanionic

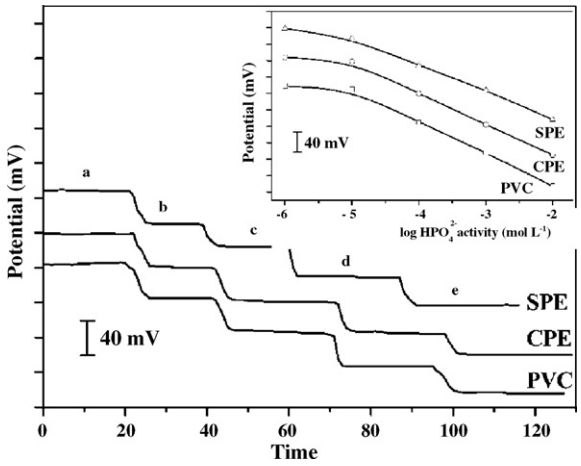

Fig. 3. Dynamic response of different phosphate sensors: (a) 1×10^{-6}, (b) 1×10^{-5}, (c) 1×10^{-4}, (d) 1×10^{-3} and (e) 1×10^{-2} mol L^{-1} HPO_4^{2-}.

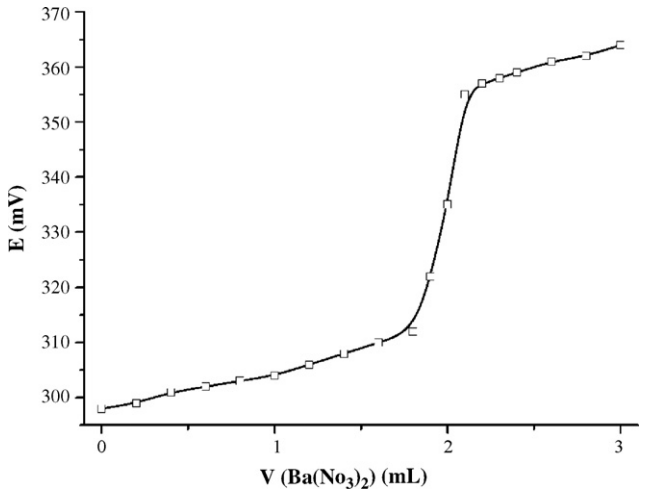

Fig. 4. Potentiometric titration curve of 20 mL phosphate ion solution (1×10^{-3} mol L^{-1}) with Ba $(NO_3)_2$ solution (1×10^{-2} mol L^{-1}) using hydrogenphosphate screen-printed electrode modified with ionophore **2d**.

groups of many commonly used buffers, the interferences of such buffers had to be expected. The highly hydrophilic buffers (HEPES (2-[4-(2-hydroxyethyl)-1-piperazinyl]ethansulfonic acid), ACES (2-[(carbamoylmethyl)amino] ethanesulfonic acid) and MES (2-[*N*-morpholino]ethanesulfonic acid monohydrate) were tested at pH 7.2. Considering that, all three buffers were present in zwitterionic and anionic forms at this pH and could compete with phosphate ion, the potentiometric measurements were performed without addition of buffer and the pH of the solution was adjusted to the optimum pH value by titration with NaOH.

The influence of the pH on the response of different phosphate sensors was investigated in the pH range 6–10. The fabricated electrodes showed stable Nernstian responses in the working pH range 6–8 with shifting the detection limit to higher values at lower pHs, the pH of 7.2 was selected for potentiometric measurements which agreed with many previously reported hydrogenphosphate sensors [9–11,15,18].

3.3.4. Durability of sensors

Day to day calibration was performed using the different phosphate sensors to evaluate their useful lifetime. During a period of 2–3 weeks, the PVC electrodes showed Nernstian slopes which did not change significantly (within ± 2 mV/decade), while the detection limit was shifted from 10^{-5} to 10^{-4} mol L^{-1} at the end of this period. This short lifetime may be related to the leaching of the sensing material to both the internal and the sample solutions. CPEs showed a relatively longer working lifetime of 4 weeks after preparation while storing the electrode in distilled water when not used [21,41,42]. This improvement of the electrode lifetime may be attributed to the diminishing of the ionophore leaching from the electrode matrix due to an insufficient lipophilicity of the bisthiourea ionophores as well as the new technique applied for the electrode fabrication without internal reference solution. A new electrode surface for measurement could be achieved daily by squeezing out a small amount of the paste and polishing the electrode on a smooth filter paper till a shiny surface was obtained.

After fabrication of SPEs, they were kept in a storage box at 4 °C and directly used for potentiometric measurements after two calibrations which served as a preconditioning process. The SPEs showed shelf-time of 4 months after printing without significant change in slopes of the calibration graphs and successive calibration measurements by the same strip could be done for at least 10 times.

3.3.5. Application

The proposed electrodes were successfully used as an indicator electrode in the potentiometric titration of hydrogenphosphate with the Ba^{2+} at pH 7.2 (Fig. 4). As seen, the titration curve was of sigmoid shape showing 1:1 stoichiometry of barium–hydrogenphosphate complex. The SPEs showed better titration curves compared with the corresponding CPE and PVC electrodes with respect to the total potential change, potential jump at the end point as well as the titration time.

4. Conclusion

The present work has successfully demonstrated the fabrication of novel phosphate ion-selective electrodes based on screen-printed, carbon paste and PVC membrane electrodes utilizing newly synthesized bisthiourea compounds as ionophores. The chemically modified screen-printed electrodes are produced more easily and rapidly with saving large amounts of reagents especially expensive ionophores; 6 mg ionophore is sufficient for printing more than 80 electrodes. Screen-printing technology also offers the highest reproducibility in the sensor fabrication. The different hydrogenphosphate sensors presented in this study showed fast dynamic response times and longer lifetimes when compared with all previously published phosphate sensors [9–15,18].

A comprehensive study will focus on ways to increase more association strengths by using bisthioureas with various R, X groups and to improve the complexation selectivity by increasing the number of hydrogen bonding sites. Other ionophores with different length of chain between the two sulfur atoms as well as cyclic structures were also synthesized and their performance for the potentiometric measurements is still under investigation. Fabrication of a two-electrode potentiometric strip containing both the working and the reference electrodes with the application of such electrode in the field determination of phosphate ion in combination with the FIA system will be also involved. These results may be the base for further research (optimization of qualitative and quantitative composition of printing ink) leading to improvement of the analytical parameters of prepared sensors and expanding of the spectrum of analyzed ions and commercialization of such electrodes for various potentiometric purposes.

Acknowledgements

Authors acknowledge the support from the bilateral project between the Czech Republic and the Egypt (project No. 27). R.M. thanks for the financial support from the Ministry of Education, Youth and Sports (project No. MSM0021627502 and LC06035).

References

[1] R.A. Durst, in: R.A. Durst (Ed.), Ion-Selective Electrodes, Special Publication 314, National Bureau of Standards, Washington, DC, 1969 (Chapter 11).
[2] D. Midgley, Ion Sel. Electrode Rev. 8 (1986) 3.
[3] E. Bakker, P. Buhlmann, E. Pretsch, Electroanalysis 11 (1999) 915.
[4] M.M.G. Antonisse, D.N. Reinhoudt, Electroanalysis 11 (1999) 1035.
[5] D. Liu, W.C. Chen, R.H. Yang, G.L. Shen, R.Q. Yu, Anal. Chim. Acta 338 (1997) 209.
[6] J. Liu, Y. Masuda, E. Sekido, S. Wakida, K. Hiiro, Anal. Chim. Acta 224 (1989) 145.
[7] M.M.G. Antonisse, B.H.M. Snellink-Ruël, J.F.J. Engbersen, D.N. Reinhoudt, Sens. Actuators, B 47 (1998) 9.
[8] M.R. Ganjali, F. Mizani, M. Emami, M.S. Niasari, M. Shamsipur, M. Yousefi, M. Javanbakht, Electroanalysis 15 (2003) 139.
[9] C.M. Carey, W.B. Riggan, Anal. Chem. 66 (1994) 3587.
[10] M. Fibbioli, M. Berger, F.P. Schmidtchen, E. Pretsch, Anal. Chem. 72 (2000) 156.
[11] T. Goff, J. Braven, L. Ebdon, D. Scholefield, Anal. Chim. Acta 510 (2004) 175.
[12] W. Liu, X. Li, M. Song, Y. Wu, Sens. Actuators, B 126 (2007) 609.
[13] A.K. Jain, V.K. Gupta, J.R. Raisoni, Talanta 69 (2006) 1007.
[14] V.K. Gupta, R. Ludwing, S. Agarwal, Anal. Chim. Acta 538 (2005) 213.
[15] F. Kivlehan, W.J. Mace, H.A. Moynihan, D.W.M. Arrigan, Anal. Chim. Acta 585 (2007) 154.
[16] S. Amemiya, P. Buehlmann, Y. Umezawa, R.C. Jagessar, D.H. Burns, Anal. Chem. 71 (1999) 1049.
[17] K.P. Xiao, P. Buehlmann, S. Nishizawa, S. Amemiya, Y. Umezawa, Anal. Chem. 69 (1997) 1038.
[18] S. Nishizawa, P. Buhlmann, K.P. Xiao, Y. Umezawa, Anal. Chim. Acta 358 (1998) 35.
[19] S. Uchida, Y. Komatsu, H. Satoh, S. Yajima, K. Kimura, Y. Tobe, S. Sasaki, M. Mizuno, Y. Watanabe, K. Hirose, Bunseki Kagaku 53 (2004) 943.
[20] S. Mesaric, E.A.M.F. Dahmen, Anal. Chim. Acta 64 (1973) 431.
[21] K. Vytras, J. Kalous, J. Jezkova, Egypt. J. Anal. Chem. 6 (1997) 107.
[22] K. Kalcher, I. Švancara, R. Metelka, K. Vytras, A. Walcarius, in: Craig A. Grimes, Elizabeth C. Dickey, Michael V. Pishko (Eds.), Encyclopedia of Sensors, vol. 4, American Scientific Publishers, Stevenson Ranch, pp. 283–430, ISBN: 1-58883-060-8 (vol. 4), 2006.
[23] K.I. Ozoemena, R.I. Stefan, J.F. van-Staden, H.Y. Aboul-Enein, Talanta 62 (2004) 681.
[24] B.N. Barsoum, W.M. Watson, I.M. Mahdi, E. Khaled, J. Electroanal. Chem. 567 (2004) 277.
[25] J.P. Hart, S.A. Wring, Trends Anal. Chem. 16 (1997) 89.
[26] V.B. Nascimento, L. Angnes, Quim. Nova 21 (1998) 614.
[27] O. Dominguez Renedo, M.A. Alonso-Lomillo, M.J. Arcos Martinez, Talanta 73 (2007) 202.
[28] S. Walsh, D. Diamond, J. McLaughlin, E. McAdams, D. Woolfson, D. Jones, M. Bonner, Electroanalysis 9 (1997) 1318.
[29] R. Koncki, S. Glab, J. Dziwulska, I. Palchetti, M. Mascini, Anal. Chim. Acta 385 (1999) 451.
[30] L. Tymecki, E. Zwierkowska, S. Glab, R. Koncki, Sens. Actuators, B 96 (2003) 482.
[31] P.G. Veltsistas, M.I. Prodromidis, E. Efstathiou, Anal. Chim. Acta 502 (2004) 15.
[32] R.D. Cannon, B. Chiswell, L.M. Venanzi, J. Chem. Soc. A (1967) 1277.
[33] E. Khaled, G. G. Mohamed, T. Awad, Sens. Actuators, B (2008), in press.
[34] R.P. Buck, E. Lindner, Pure Appl. Chem. 66 (1994) 2527.
[35] J.H. Shim, I.S. Jeong, M.H. Lee, H.P. Hong, J.H. On, K.S. Kim, H.S. Kim, B.H. Kim, G.S. Cha, H. Nam, Talanta 63 (2004) 61.
[36] A.N. Leung, D.A. Degenhardt, P. Buhlmann, Tetrahedron 64 (2008) 2530.
[37] E. Bakker, P. Buhlmann, E. Pretsch, Chem. Rev. 97 (1997) 3083.
[38] W.E. Morf, The Principles of Ion-Selective Electrodes and Membrane Transport, Elsevier, New York, 1981.
[39] U. Schaller, E. Bakker, U.E. Spichiger, E. Pretsch, Anal. Chem. 66 (1994) 391.
[40] U. Schaller, E. Bakker, E. Pretsch, Anal. Chem. 67 (1995) 3123.
[41] E. Khaled, H.N.A. Hassan, M.S. Kamel, B.N. Barsoum, Curr. Pharm. Anal. 3 (2007) 262.
[42] E. Khaled, M.S. Kamel, H.N.A. Hassan, Anal. Chem. An Indain. J. 7 (2008) 466.

Talanta 77 (2008) 587–592

Contents lists available at ScienceDirect

Talanta

journal homepage: www.elsevier.com/locate/talanta

Novel approach to calibration by the complementary dilution method with the use of a monosegmented sequential injection system

Joanna Kozak*, Marzena Wójtowicz, Alicja Wróbel, Paweł Kościelniak

Department of Analytical Chemistry, Faculty of Chemistry, Jagiellonian University, Ingardena 3, 30-060 Krakow, Poland

ARTICLE INFO

Article history:
Received 15 November 2007
Received in revised form 14 March 2008
Accepted 17 March 2008
Available online 25 March 2008

Keywords:
Calibration
Monosegmented flow analysis
Sequential injection analysis

ABSTRACT

Novel approach to calibration by the complementary dilution method (CDM) is presented. The CDM integrates in a single procedure the set of standards and the standard addition calibration methods. The approach is implemented with the use of the fully automated monosegmented sequential injection system coupled to FAAS as a detector. It relies on generation of a series of standard solutions consistent with the CDM calibration method in subsequent monosegments using a single stock standard solution, sample and diluent in appropriate proportions. Two versions of the method, basic and extended have been verified. They have been tested on the example of magnesium determination in a synthetic sample with errors of repeatability (R.S.D.) and accuracy (R.E.) less than 3.2%. Subsequently, they have been applied to magnesium and calcium determinations in water. The results obtained are comparable with the appropriate certified values as well as with the results received by traditional calibration methods performed separately in batch system. Using the system, a complete sample analysis takes 8 or 21 min with sample or standard consumption less than 1 or 2 mL in basic and extended versions, respectively.

1. Introduction

Calibration is an indispensable step of most analytical methods. Its correct performance is important especially on account of result accuracy. Several calibration methods have been developed in analytical chemistry, but only two of them became common among analysts: the set of standards method (SSM) and the standard addition method (SAM). As they allow an analytical result to be calculated differently, interpolatively (SSM) or extrapolatively (SAM), they are characterized by different abilities and limitations.

Flow analysis offers a variety of possibilities of rationalization or automation of both the SSM and the SAM methods. Underneath, some of the approaches representing a basis of many others, have been quoted: merging zones approach [1] in which segments of standard and sample can be superimposed and merged in a controlled way in a flow injection (FI) system; zone sampling method [2] where a small portion of a dispersed standard zone can be injected into another carrier stream; reversed FI system [3] where standard is injected into sample carrier; gradient techniques [4–7] using a concentration–time profile generated by a single standard injection; peak width measurement method [8]; continuous dilution methods exploiting mixing chamber inserted into a FI system [9], or peristaltic pumps to create linear flow gradients [10]; sequential injection method [11] where several discrete standard volumes are introduced simultaneously into a carrier stream; network [12] or variable tube dimensions [13] methods when dispersion of a single standard solution is changed by directing it to loops of different lengths; automatic dilution method [14] where additional dilution loop is used for a standard dilution; SIA approaches exploiting an additional loop to generate concentration gradient of the introduced standard [15], or exploiting a sample as a carrier [16] or systems using a concept of monosegmented continuous flow analysis (MSFA) [17,18].

The MSFA relies on forming in a reaction coil a zone consisted of a sample and a reagent [19]. In order to reduce dispersion with carrier solution, the zone is located between two air bubbles forming a monosegment. The influence of an axial dispersion caused by a thin film of solution linking a monosegment with its liquid carrier on an analyte concentration in the monosegment is very limited, hence it is usually omitted during results calculation. The concept has been exploited for rationalization of the SAM using an automated manifold with a solenoid valve incorporated [17]. In the developed procedure, different quantities of a single standard solution were added to the sample by controlling the time interval in which the solenoid valve was switched on. Since absorbance versus time analytical curves were obtained it was necessary to calibrate the system prior the use in order to determine the quantities of standard solution added to the sample in each injection. Pinto

* Corresponding author. Tel.: +48 126632232; fax: +48 126340515.
E-mail address: janiszew@chemia.uj.edu.pl (J. Kozak).

0039-9140/$ – see front matter © 2008 Elsevier B.V. All rights reserved.
doi:10.1016/j.talanta.2008.03.024

Silva and Masini [18] exploited SIA and MSFA approaches to perform in-line SAM method. In the system, standard solutions were generated from a single stock standard solution, in monosegments of the same total volume by introducing into each monosegment the same volume of sample, increasing volumes of standard and decreasing volumes of diluent. As a syringe pump was exploited for solutions aspiration into the system, the concentration of standard added was calculated directly using the volume of standard introduced into a monosegment and the total volume of monosegment.

In the approaches presented above analytical results are always obtained using exclusively one of the calibration methods. Recently, an idea of integrated calibration method (ICM) arose [20]. The concept of this approach relies on unification of the SSM and SAM methods in a single calibration procedure. As a consequence, an analytical result is able to be estimated at least twice in two ways—interpolatively and extrapolatively. One of the versions of the ICM method is the complementary dilution method (CDM) [21]. The specificity of the CDM is typified by special preparation procedure of the calibration solutions. Namely, three solutions, each containing two or three constituents (diluent, standard or sample solutions) in appropriate volumes p or q (where $p > q$) are generated in two series. The prerequisite is that if in one of the series a constituent is diluted to degree P (where $P = p/(p+q)$) in the other series it is diluted to degree Q (where $Q = q/(p+q)$), which is complementary to degree P, i.e. $P + Q = 1$. Flow injection systems have been designed to perform the CDM calibration [21,22] in such a way, that the calibration solutions are prepared by strictly controlled partial superimposing and merging zones of standard and sample solutions propelled in two streams of diluent with different flow rates.

In the present work, the calibration procedure based on the CDM concept has been developed with the use of monosegmented sequential injection system. The method relies on the subsequent generation of solutions in monosegments of a defined, constant total volume, containing standard and/or sample and diluent in various volumetric proportions corresponding to the rules of the CDM method. Two procedures, basic and extended, have been developed. The system has been tested by applying it to the FAAS determination of magnesium in a synthetic sample and subsequently exploited to the determination of magnesium and calcium in water samples.

2. Experimental

2.1. Reagents and solutions

Standard stock solutions of magnesium and calcium of concentration 1 mg L^{-1} were prepared from titrisol standards (Merck, Germany). Standard solutions of magnesium and calcium used directly for calibration purposes, were prepared by dilution of the appropriate standard stock solution with the use of nitric (Merck, Germany) and hydrochloric (Merck, Germany) acids respectively, of concentration 1% (v/v). Analytical-reagent grade chemicals and double distilled water were used throughout.

SPS-SW2 Batch 105 Reference Material for Measurements of Elements in Surface Waters (SPS Spectrapure Standards AS, Norway) was used for the method verification. Spring water used as a sample was commercially available in the Polish market.

2.2. Instrumentation

Atomic absorption spectrometer PerkinElmer 3100 (PerkinElmer, USA) was used in the experiments. Air–acetylene flame was applied and nebulizer free uptake rate was fixed to 4.3 mL min^{-1}. Magnesium and calcium hollow cathode lamps were operated at 12 and 17 mA, respectively. The wavelengths were set to 285.5 and 423.0 nm, respectively with a spectral slit width of 0.7 nm. PC AMD K5 computer with program written in our laboratory was connected to the spectrometer and served for data collection and handling.

The sequential injection system applied consisted of the following units: 10-positional selection valve (Valco, Switzerland), two-positional injection valve (Alitea Instruments, USA), peristaltic pump (Gilson, France), syringe pump (Alitea Instruments, USA), operation of which was modified in our laboratory, electronic adapter developed in our laboratory that enables remote control of all the units of sequential injection system.

Tygon tubes for carrier transport with the use of the peristaltic pump and PTFE tubing of i.d. 0.8 (tubes) or 1.6 mm (a mixing coil and a holding coil) were used. The length of the holding and the mixing coil was 1000 and 300 mm, respectively.

3. Results and discussion

3.1. Operation of the sequential injection system

The sequential injection system developed for the research is depicted in Fig. 1. The system is operated in three stages: aspiration, homogenization and washing. In the first stage (shown in Fig. 1), strictly controlled volumes of air and diluent, standard and/or sample are aspirated through the selection valve (operated in anticlockwise direction) to the holding coil with the use of the syringe pump. At the same time carrier is propelled by peristaltic pump through the two-positional valve to the spectrometer. The total volume of a monosegment was established to 450 μL, to achieve the possibility of generating several standard solutions of required concentrations by appropriate dilution of a single standard solution. Carrier flow rate was fixed to 4.6 mL min^{-1} and was a little higher than the nebulizer uptake rate. In the second stage the position of selection valve is changed into diluent position and

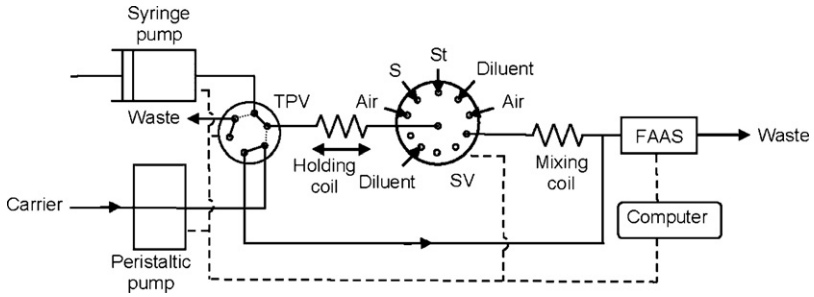

Fig. 1. Instrumental system developed for realization of CDM procedure in monosegmented sequential injection mode. St, standard; S, sample; TPV, two-positional valve; SV, selection valve.

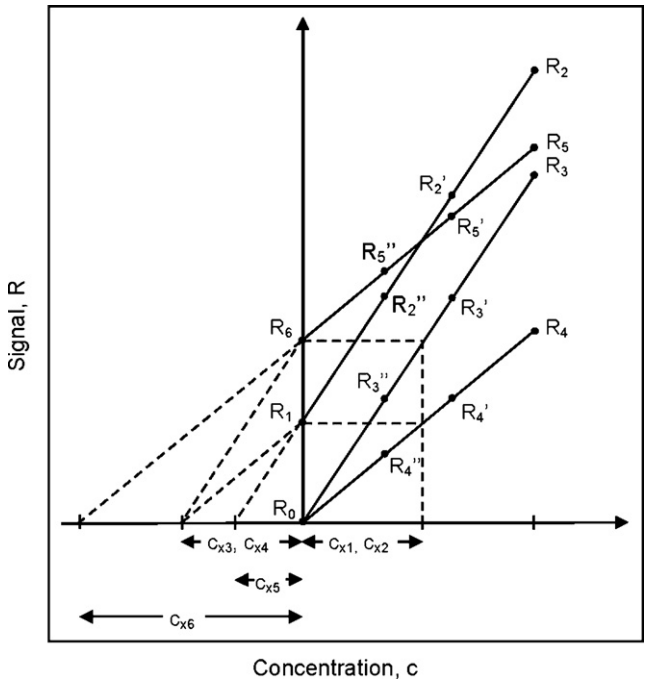

Fig. 2. Analytical curves constructed in the CDM method.

200 μL of diluent is introduced into a holding coil with the flow rate 2.5 mL min^{-1}, than the flow direction is reversed and 150 μL of the solution is removed with the same flow rate. The procedure is repeated twice. This way, solutions contained in the monosegment move quickly in reverse directions and are homogenized in recurrent way. In the last stage of system operation, after changing the position of the two-positional valve (clockwise, Fig. 1), the carrier propelled by peristaltic pump is directed to the holding coil (dashed line in the scheme of the two-positional valve, Fig. 1) and washes the whole monosegment to the detector. Simultaneously, the carrier is removed from the syringe pump. As the flame atomic absorption spectrometer was used as the detector there was no necessity of removing air segments before detection.

The performance of the system was checked in terms of its applicability for dilution. For the aim, the repeatability of signals generated in the system has been checked in the following way. Nine solutions of increasing standard concentration were subsequently generated in the system. Firstly, 50 μL of Mg standard solution of concentration 0.8 mg L^{-1} and 400 μL of diluent were subsequently aspirated into a holding coil between two air segments. The solution was homogenized, as described in the previous section, and directed to the detector. The absorbance corresponding to the plateau of the signal registered was regarded as an analytical signal. Afterwards, the procedure was repeated for higher volumes of standard (in sequence: 100, 150, 200, 250, 300, 350, 400 and 450 μL) and respectively lower volumes of diluent (in sequence: 350, 300, 250, 200, 150, 100, 50 and 0 μL) aspirated into the holding coil. The whole procedure was repeated eight times and average values of the signals registered as well as relative standard deviations were calculated. The values of R.S.D. always lower than 1.5% and linear calibration curve were obtained (R = 0.9999). The repeatability of a single measurement, when only a stock standard solution was inserted between air segments lower than 0.8% was fund.

3.2. Calibration procedure

Two versions of the procedure consistent with the rules of the CDM method have been proposed. They differ in the number of standard solutions containing two or three constituents – diluent, standard and sample – in the basic procedure a blank solution and six standard solutions are created, whereas in the extended procedure the blank and 14 standard solutions are generated. In each solution (in the form of a monosegment) a constituent is diluted in the complementary mode.

The constant volumes of p = 300 μL and q = 150 μL were selected to receive analytical curves of considerably different slopes (see Fig. 2) and to achieve the total volume of monosegment equal 450 μL. As the total volume of a monosegment was always constant, the dilution degree for standard or sample could be calculated and was always equal P or Q, respectively. In case of the solutions generated in the extended version of the procedure, the dilution degree was calculated including the diluent volume necessary to receive the complementary volume p or q. The detailed composition of monosegments containing subsequent standard solutions, the appropriate dilution degrees and the corresponding analytical signals are shown in Table 1.

On the basis of the registered signals in both procedures, four analytical curves can be constructed as shown in Fig. 2. In the basic procedure each analytical curve is based on two analytical signals, whereas in the extended procedure on four analytical signals. Hence, the latter procedure can be useful in such a case when the analytical curves are suspected to be nonlinear.

Table 1
Conditions of signals generation according to the CDM method in basic and extended versions of the proposed procedure

Dilution degree		Monosegment composition[a] (μL)			Signal for procedure	
Standard	Sample	Diluent	Standard	Sample	Basic	Extended
–	–	Continuous stream	–	–	R0	R0
–	Q	300	–	150	R1	R1
P	Q	–	300	150	R2	R2
P	–	150	300	–	R3	R3
Q	–	300	150	–	R4	R4
Q	P	–	150	300	R5	R5
–	P	150	–	300	R6	R6
P	Q	100	200	150	–	R2′
P	Q	200	100	150	–	R2″
P	–	250	200	–	–	R3′
P	–	350	100	–	–	R3″
Q	–	350	100	–	–	R4′
Q	–	400	50	–	–	R4″
Q	P	50	100	300	–	R5′
Q	P	100	50	300	–	R5″

[a] Air volume at both sides of monosegment: 100 μL.

Table 2
Determination of Mg in a synthetic sample; $n = 6$

Element	Concentration expected ($mg\,L^{-1}$)	Procedure	CDM calibration	Concentration found ($mg\,L^{-1}$)		R.S.D. (%)	R.E. (%)
Mg	0.200	Basic	Interpolative	c_{x1}	0.201	1.80	0.51
				c_{x2}	0.198	2.15	−0.90
			Extrapolative ICM	c_{x3}	0.201	2.29	0.54
				c_{x4}	0.201	3.13	0.55
			Extrapolative	c_{x5}	0.203	1.19	1.33
				c_{x6}	0.194	1.64	−3.09
				Mean	0.200	1.60	−0.17
	0.200	Extended	Interpolative	c_{x1}	0.203	1.72	1.27
				c_{x2}	0.197	2.08	−1.33
			Extrapolative ICM	c_{x3}	0.197	1.94	−1.47
				c_{x4}	0.199	2.50	−0.28
			Extrapolative	c_{x5}	0.198	1.29	−1.02
				c_{x6}	0.194	1.35	−3.15
				Mean	0.198	1.50	−1.01

In the basic procedure the analytical result is estimated in the interpolative mode from the following analytical equations:

$$c_{x1} = \frac{R_6}{R_3} \cdot c_{St} \quad (1)$$

$$c_{x2} = \frac{R_1}{R_4} \cdot c_{St} \quad (2)$$

and in the extrapolative mode characteristic for the ICM method with no necessity to determine dilution degrees P and Q [21]:

$$c_{x3} = \frac{R_6}{R_2 - R_1} \cdot c_{St} \quad (3)$$

$$c_{x4} = \frac{R_1}{R_5 - R_6} \cdot c_{St} \quad (4)$$

and finally in the traditional extrapolative mode using calculated values of dilution degrees:

$$c_{x5} = \frac{R_6}{R_5 - R_6} \cdot \frac{Q}{P} \cdot c_{St} \quad (5)$$

$$c_{x6} = \frac{R_1}{R_2 - R_1} \cdot \frac{P}{Q} \cdot c_{St} \quad (6)$$

where R_1–R_6 are signals registered for the generated standard solutions (see Table 1) and c_{St} is the analyte concentration in the stock standard solution.

In the extended version of the proposed procedure, the parameters of analytical curves are determined and than the values of appropriate standard concentrations are related to the mathematical model obtained. Next, the values of signals received in this mode serve for the analyte concentration calculation with the use of the above analytical equations.

The calculated values of concentrations, c_{x1}–c_{x6} can be compared and verified mutually. If they do not differ statistically, their average value can be considered as the analytical result [22].

3.3. Test examinations and procedure verification

The proposed procedures were tested on the example of Mg determination in a synthetic sample. Stock standard solution of

Table 3
Application of the developed method to the determination of Mg and Ca in surface water, CI: confidence interval ($\alpha = 0.05$)

Element	Concentration certified ($mg\,L^{-1}$)	Procedure	Calibration	Developed method		Traditional method
				Concentration found ± CI ($mg\,L^{-1}$)		Concentration found ± CI ($mg\,L^{-1}$)
Mg	2.00 ± 0.01	Basic	Interpolative	c_{x1}	2.13 ± 0.03	2.06 ± 0.01
				c_{x2}	2.16 ± 0.01	
			Extrapolative ICM	c_{x3}	2.11 ± 0.02	–
				c_{x4}	2.01 ± 0.01	
			Extrapolative	c_{x5}	2.09 ± 0.04	2.12 ± 0.09
				c_{x6}	2.03 ± 0.05	
				Mean	2.09 ± 0.05	
		Extended	Interpolative	c_{x1}	2.13 ± 0.04	2.06 ± 0.02
				c_{x2}	2.14 ± 0.01	
			Extrapolative ICM	c_{x3}	2.11 ± 0.03	–
				c_{x4}	2.01 ± 0.05	
			Extrapolative	c_{x5}	2.06 ± 0.04	2.10 ± 0.05
				c_{x6}	1.99 ± 0.06	
				Mean	2.07 ± 0.05	
Ca	10.00 ± 0.05	Basic	Interpolative	c_{x1}	10.27 ± 0.34	9.89 ± 0.13
				c_{x2}	9.93 ± 0.12	
			Extrapolative ICM	c_{x3}	10.90 ± 0.29	–
				c_{x4}	10.74 ± 0.32	
			Extrapolative	c_{x5}	11.08 ± 0.41	11.36 ± 0.14
				c_{x6}	10.03 ± 0.15	
				Mean	10.49 ± 0.38	
		Extended	Interpolative	c_{x1}	10.33 ± 0.37	9.75 ± 0.14
				c_{x2}	9.90 ± 0.11	
			Extrapolative	c_{x3}	10.92 ± 0.27	–
			ICM	c_{x4}	10.80 ± 0.27	
			Extrapolative	c_{x5}	10.96 ± 0.38	11.85 ± 0.25
				c_{x6}	9.91 ± 0.24	
				Mean	10.47 ± 0.39	

Table 4
Application of the developed method to the determination of Mg and Ca in spring water, CI: confidence interval ($\alpha = 0.05$)

Element	Concentration declared ($mg\,L^{-1}$)	Procedure	Calibration	Developed method		Traditional method
				Concentration found ± CI ($mg\,L^{-1}$)		Concentration found ± CI ($mg\,L^{-1}$)
Mg	4.91	Basic	Interpolative	c_{x1}	4.54 ± 0.05	4.65 ± 0.05
				c_{x2}	4.60 ± 0.05	
			Extrapolative ICM	c_{x3}	4.48 ± 0.09	–
				c_{x4}	4.41 ± 0.14	
			Extrapolative	c_{x5}	4.66 ± 0.13	4.69 ± 0.14
				c_{x6}	4.27 ± 0.09	
				Mean	4.49 ± 0.11	
		Extended	Interpolative	c_{x1}	4.55 ± 0.07	4.67 ± 0.06
				c_{x2}	4.56 ± 0.03	
			Extrapolative ICM	c_{x3}	4.48 ± 0.09	–
				c_{x4}	4.40 ± 0.13	
			Extrapolative	c_{x5}	4.49 ± 0.15	4.62 ± 0.19
				c_{x6}	4.15 ± 0.05	
				Mean	4.44 ± 0.12	
Ca	28.00	Basic	Interpolative	c_{x1}	32.60 ± 0.77	31.76 ± 0.52
				c_{x2}	32.35 ± 0.83	
			Extrapolative ICM	c_{x3}	32.52 ± 0.81	–
				c_{x4}	32.66 ± 1.19	
			Extrapolative	c_{x5}	34.81 ± 1.23	32.06 ± 0.56
				c_{x6}	30.54 ± 1.15	
				Mean	32.58 ± 1.21	
		Extended	Interpolative	c_{x1}	32.80 ± 0.83	31.50 ± 0.51
				c_{x2}	32.20 ± 0.64	
			Extrapolative ICM	c_{x3}	32.57 ± 0.77	–
				c_{x4}	32.34 ± 1.06	
			Extrapolative	c_{x5}	34.06 ± 1.23	31.80 ± 0.16
				c_{x6}	30.28 ± 1.50	
				Mean	32.38 ± 0.98	

concentration of Mg 0.400 $mg\,L^{-1}$ were used. The sample was analyzed six times and the results are presented in Table 2. It is seen that both procedures provide results with precision (R.S.D.) and accuracy (R.E.) less than 3.2%. Comparable precision of the results obtained in interpolative and extrapolative ways were obtained. It can be noticed, that in case of the results obtained with the use of the traditional extrapolative method, that exploits values if dilution degrees, in case when the widen range of extrapolation was employed (c_{x6}), the results of worsen accuracy (R.E. = −3.09 and −3.15%) than accuracy of the results of the other methods ($|R.E.| \leq 1.47\%$) were obtained.

In order to verify the proposed procedures, Mg and Ca were determined in the reference sample of surface water and in commercially available spring water. Stock standard solutions of Mg and Ca of concentration 0.400 and 4.00 $mg\,L^{-1}$, respectively, were used. Entire procedures were repeated six times. Samples were diluted before the determination. For comparison, the same samples were examined according to traditional interpolative (SSM) and extrapolative (SAM) calibration methods with using of an appropriate single analytical curve. In the traditional basic procedures analytical curves were based on two analytical signals whereas in traditional extended procedures they were based on four signals. Results of determinations in surface and spring water are presented in Tables 3 and 4, respectively.

Regarding the analysis of surface water (Table 3), the results obtained with the use of the propose procedures agree with the certified values and with the values determined with the use of the traditional calibration methods. No differences have been observed, between the results obtained using the basic or the extended procedures. It can be noticed, that despite the fact that in the sample of surface water potential interferents were contained (as Al, Fe, K, Na, Pb, Sr or V) no interference effect was detected. The results obtained for the spring water samples differ from those declared by a producer but they are in agreement with results obtained by traditional calibration methods.

In Table 5 the comparison between some parameters of interpolative and extrapolative calibration methods are presented when they are realized separately in traditional batch way as well as in

Table 5
Comparison of chosen analytical parameters when performing calibration using batchwise method or CDM method in flow injection and monosegmented sequential injection versions

	Calibration method					
	Batchwise approach		FI approach [22]		Developed approach	
	I + E[a] Basic[b]	I + E[a] Extended[b]	CDM Basic	Extended	CDM Basic	Extended
Number of standard solutions	2 + 2	4 + 4	7	15	7	15
Number of analytical curves	1 + 1	1 + 1	4	4	4	4
Number of analytical results	1 + 1	1 + 1	4 (or 6)	4 (or 6)	6	6
Time of analysis, min	10	20	3.6	12	8	21
Standard consumption (mL)	0.4	3.2	4	12	0.9	1.7
Sample consumption (mL)	4	8	4	12	0.9	1.8

[a] Interpolative and extrapolative methods performed separately.
[b] Procedures.

accordance with the complementary dilution calibration method performed in flow injection system and in the proposed monosegmented sequential injection system. The presented values were established for cases when appropriate complete calibration procedures were performed for each of a sample analyzed. It is seen, that complementary dilution calibration method provides rich analytical information in the form of at least four analytical results. As far as the performance of the CDM method in flow injection or the proposed system is concerned, the latter system is competitive in terms of low standard and sample consumption. Regarding the time of analysis, the proposed procedures last longer than FI CDM procedures and the time necessary to perform them is comparable with the time of realization of traditional batch interpolative and extrapolative methods separately. The reason is that in monosegmented sequential injection procedures calibration solutions are generated separately one after another and each of them must be homogenized before reaching the detector. However, during the comparable time the CDM procedure performed in the proposed system provides more analytical results than traditional calibration methods performed separately.

The advantage of the proposed CDM calibration procedures realized in the developed system in relation to CDM methods performed in flow injection systems is that they do not exploit merging of two streams of diluent [21,22]. Hence, they are not prone to random fluctuations of the streams flow rates. In the FI extended system [22] each subsequent calibration solution is generated from the previous one by its controlled dilution so there is a risk of accumulation of errors arising during the successive dilutions. In the developed system calibration solutions are generated independently from each other and a number of solutions of required analyte concentration can be generated. This can be exploited for both, an analytical curve nonlinearity detection and subsequently CDM calibration performance in the extended version. Differently from FIA systems, for the system developed it is easy to calculate directly dilution degrees P and Q and exploit them for results calculation in traditional extrapolative mode.

In the system, unlike in the other systems known from literature [18], solutions are introduced into a monosegments in two or three segments and homogenized afterwards, and there is no necessity of introducing them using 'sandwich' way. Although the system has been applied for realization of the CDM calibration method, it can be also used to perform interpolative or extrapolative calibration methods separately or for the dilution purposes as well.

4. Conclusions

The proposed monosegmented sequential injection system was successfully employed for rationalization of calibration stage of analysis using the complementary dilution calibration method. The approach provides reach analytical information with the use of a single stock standard solution and minimum reagent consumption. Two procedures of the realization of the CDM method in the proposed system, basic and extended, were developed and verified. The basic procedure can be exploited when linear calibration range is confirmed whereas the extended procedure in each case when there is necessary to establish linear calibration range or when calibration curve is not linear. The proposed system is versatile and can be adapted to various analyzes performed with atomic absorption detection. It is also worth to emphasize, that complete automation of the procedures constrains the risk of random errors during calibration solutions generation and allows the analytical results to be obtained in less laborious way.

References

[1] E.A.G. Zagatto, F.J. Krug, H. Bergamin F., S.S. Jorgensen, B.F. Reis, Anal. Chim. Acta 104 (1979) 279.
[2] B.F. Reis, A.O. Jacintho, J. Mortatti, F.J. Krug, E.A.G. Zagatto, H. Bergamin F., L.C.R. Passenda, Anal. Chim. Acta 123 (1981) 221.
[3] J.F. Tyson, Anal. Proc. 18 (1981) 542.
[4] S. Olsen, J. Růžička, E.H. Hansen, Anal. Chim. Acta 136 (1982) 101.
[5] M.C.U. Araújo, C. Pasquini, R.E. Bruns, E.A.G. Zagatto, Anal. Chim. Acta 171 (1985) 337.
[6] Z. Fang, J.M. Harris, J. Růžička, E.H. Hansen, Anal. Chem. 57 (1985) 1457.
[7] M. Sperling, Z. Fang, B. Welz, Anal. Chem. 63 (1991) 151.
[8] J.F. Tyson, Analyst 109 (1984) 319.
[9] J.F. Tyson, J.M.H. Appleton, Talanta 31 (1984) 9.
[10] I. López-García, P. Viñas, M. Hernández-Córdoba, Anal. Chim. Acta 327 (1996) 83.
[11] E.A. Zagatto, M.F. Giné, E.A.N. Fernandez, B.F. Reis, F.J. Krug, Anal. Chim. Acta 173 (1985) 289.
[12] J.F. Tyson, S.R. Bysouth, J. Anal. At. Spectrom. 3 (1988) 211.
[13] J.F. Tyson, C.E. Adeeyinwo, J.M.H. Appleton, S.R. Bysouth, A.B. Idris, L.L. Sarkissian, Analyst 110 (1985) 487.
[14] M. Agudo, A. Ríos, M. Valcárcel, Anal. Chim. Acta 264 (1992) 265.
[15] A. Baron, M. Guzman, J. Růžička, G.D. Christian, Analyst 117 (1992) 1839.
[16] F. Mas, A. Cladera, J.M. Estela, V. Cerdà, Analyst 123 (1998) 1541.
[17] M. Assali, I.M. Raimundo Jr., I. Facchin, J. Autom. Methods Manage. Chem. 23 (2001) 83.
[18] M.S. Pinto Silva, J.C. Masini, Anal. Chim. Acta 466 (2002) 345.
[19] C. Pasquini, W.A. Oliviera, Anal. Chem. 57 (1985) 2575.
[20] P. Kościelniak, Anal. Chim. Acta 438 (2001) 323.
[21] P. Kościelniak, J. Kozak, M. Herman, M. Wieczorek, A. Fudalik, Anal. Lett. 37 (2004) 1233.
[22] P. Kościelniak, M. Wieczorek, J. Kozak, M. Herman, Anal. Chim. Acta 600 (2007) 6.

Talanta 77 (2008) 779–785

Contents lists available at ScienceDirect

Talanta

journal homepage: www.elsevier.com/locate/talanta

On-line gradient liquid chromatography–Fourier transform infrared spectrometry determination of sugars in beverages using chemometric background correction

J. Kuligowski, G. Quintás, S. Garrigues, M. de la Guardia *

Analytical Chemistry Department, Universitat de València, Edifici Jeroni Muñoz, 50th Dr. Moliner, 46100 Burjassot, Spain

ARTICLE INFO

Article history:
Received 30 April 2008
Received in revised form 7 July 2008
Accepted 11 July 2008
Available online 31 July 2008

Keywords:
On-line liquid chromatography–Fourier transform infrared spectrometry
Background correction based on the use of a reference spectra matrix
Carbohydrate analysis

ABSTRACT

An on-line gradient reversed phase liquid chromatography–Fourier transform infrared spectrometry (LC–FTIR) method was developed for the determination of fructose, glucose, sucrose and maltose in beverages. Improved chromatographic resolution was obtained using a linear gradient from 75 to 55% (v/v) acetonitrile in water in 15 min. Changes in the background spectra were corrected employing "univariate background correction based on the use of a reference spectra matrix" (UBC-RSM) and using the ratio of absorbance (AR) at 2256 and 2253 cm^{-1} for the identification of the eluent spectra within the RSM. The method provided limits of detection in the order of 0.75 mg ml^{-1}. The precision (as relative standard deviation) ranged between 3.3 and 4.1% for glucose and fructose, respectively at a concentration level of 3.0 mg ml^{-1}. Quantitative recovery values on spiked samples confirmed the accuracy of the method. A set of samples from the Spanish market were analysed to test the suitability of the procedure.

1. Introduction

The term sugar is frequently used to describe monosaccharides as glucose and fructose and disaccharides as sucrose and maltose that are absorbed, digested and fully metabolized [1].

The current interest in the physiological role of carbohydrates, the technological developments in food processing and manufacturing, and the different existing mandates of nutrition labeling (e.g. Food and Drug Administration [2]) have created a need for carbohydrate analysis at different production stages in food industries like in alcoholic and non-alcoholic drinks, fruit juices, sweets or dairy products.

Liquid chromatography (LC) has often been employed for sugar analysis in different food matrices where the most commonly used detector is the refractive index detector (RID). However, it shows poor sensitivity, high instability with regard to fluctuations in mobile phase composition and eluent temperature, low selectivity and incompatibility with mobile phase gradients [3,4].

Evaporative light scattering detection (ELSD) is compatible with gradient elution and provides a significant increase in sensitivity as compared with RID, but it is also a low-selective detector.

UV detection is not directly applicable for sugar analysis, without a pre- or post-column derivatization of the analytes, due to the low UV-absorbance of these compounds. The short wavelength required for their detection in UV reduces the selectivity of the obtained chromatographic signal increasing the number of possible interferences, thus requiring extensive sample clean-up prior to the detection.

Mass spectrometry (MS) is an expensive detection technique which provides high selectivity and sensitivity levels, but its field of application focuses on compounds at trace levels and not in the percentage range as it is the case of the main sugars present in foods.

Alternatively, infrared (IR) spectrometry is a versatile analytical tool which can be used for both, qualitative and quantitative determinations regarded as a general detection tool for organic analytes. On-line hyphenated with separation techniques as LC or capillary electrophoresis (CE) increases both, the applicability and the accuracy of IR-based methods by a significant reduction of potential spectral interferences. On the other hand, with limits of detection in the high mg l^{-1} range, it is clear that this technique cannot meet the current demands of trace analysis. However, IR spectrometry has proven to be a simple and rapid technique for quantitative and qualitative determination of analytes in the percentage level.

On-line LC–IR methods carried out under isocratic conditions use a constant eluent reference spectrum to correct the eluent spectral contribution. The advantages of this approach are its simplicity and the good quality of the recovered spectra obtained.

Using a constant mobile phase composition, also known as isocratic conditions, the capability of on-line LC–Fourier transform

* Corresponding author. Tel.: +34 96 3544838; fax: +34 96 3544838.
E-mail address: miguel.delaguardia@uv.es (M. de la Guardia).

0039-9140/$ – see front matter © 2008 Elsevier B.V. All rights reserved.
doi:10.1016/j.talanta.2008.07.036

infrared (FTIR) spectrometry for the determination of sucrose, glucose and fructose in aqueous samples was demonstrated by Vonach et al. [5,6]. Edelmann et al. [7] reported the use of a quantum cascade laser as mid-IR source for the direct determination by on-line LC–IR of glucose and fructose in wine samples. Later, Edelmann et al. [8] used on-line LC–attenuated total reflectance (ATR) measurements for the analysis of organic acids, sugars and alcohols in red wine using multivariate curve resolution–alternating least squares (MCR–ALS) for the quantitative analysis of overlapping compounds. Moreover, a FTIR spectrometer has been on-line coupled with CE for the separation and quantification of sucrose, glucose and fructose in fruit juices [9]. The use of micro-machined flow cells in on-line CE–FTIR enables non-destructive, real time detection of analytes. However from the instrumental point of view the complexity of the required set-up for the CE–FTIR coupling is much higher than that for LC–FTIR.

On the other hand, the use of on-line gradient LC–FTIR is still challenging, because the use of a constant reference spectrum is not suitable if the relative concentration of the different IR-absorbing mobile phase components (e.g. water, acetonitrile or methanol) is modified during the chromatographic run [10]. Therefore, in recent years much attention has been paid to background correction in order to increase both, the applicability and the peak separation capabilities of on-line LC–FTIR [11–13]. Recently, Quintás et al. proposed a strategy named "*univariate background correction method based on the use of a reference spectra matrix* (*UBC-RSM*)" to perform an automated background correction in continuous liquid flow systems [14]. This approach is based on the assumption that using characteristic absorption bands of the mobile phase, it is possible to correct the background eluent spectral contribution to the overall absorption, by using a previously measured reference spectra matrix which covers a wide range of mobile phase compositions. This background correction method has already been successfully applied using acetonitrile:water (1% acetic acid) [14] and methanol:water [15] mobile phase gradients in reversed phase LC for the determination of atrazine and diuron pesticides in aqueous solutions and for the determination of the critical conditions of polyethyleneglycol, respectively.

In this study, FTIR is used as an on-line detector for the LC separation under gradient conditions of four model carbohydrates (fructose, glucose, sucrose and maltose) in beverages in order to: (i) test the suitability of the UBC-RSM approach in the presence of increasing concentrations of sugars; (ii) enable a higher sample throughput than that obtained under isocratic conditions in an equivalent LC–FTIR system and (iii) evaluate the method for the analysis of commercially available beverage samples.

2. Experimental

2.1. Apparatus and reagents

A Dionex (Sunnyvale, CA, USA) P680 high performance liquid chromatograph system, equipped with a Kromasil 100 NH_2 column (250 mm × 2 mm, 5 μm) fro, Spain) and a sample injection loop of 20 μl, was employed for chromatographic separations. Linear acetonitrile:water gradients were run from 75 to 55% acetonitrile (Merck, Darmstadt, Germany) in 15 min.

A flow cell with CaF_2 and ZnSe windows and a pathlength of 10 μm installed on a Bruker (Bremen, Germany) IFS 66/v FTIR spectrometer equipped with a liquid nitrogen refrigerated mercury–cadmium–telluride (MCT) detector, a vacuum system and a dry air purged sample compartment was employed for the FTIR spectra acquisition. The scanner for the interferometer was operated at a HeNe laser modulation frequency of 100 kHz. Spectra were recorded in the range between 4000 and 950 cm^{-1} using the spectrum of the empty sample compartment as background, with a resolution of 8 cm^{-1} and a zero filling factor of 2. Zero filling consists in adding zeros on both ends of the interferogram before the Fourier transformation so that the spectral lines have a smoother shape.

During on-line LC–FTIR gradient experiments, 25 scans per spectrum were averaged, providing a spectra acquisition frequency of 15 spectra min^{-1}.

For instrumental and measurement control and data acquisition, the OPUS program (Version 4.1) from Bruker was employed.

Background correction and data treatment were run under Matlab 7.0 from Mathworks (Natick, USA, 2004) using in-house written Matlab files available from the authors of this paper.

D(−)-Fructose, D(+)-glucose, sucrose and maltose-1-hydrate of analytical grade were purchased from Scharlab (Barcelona, Spain). Beverage samples were directly obtained from the Spanish market.

2.2. Sample preparation

A volume of homogenized sample between 50 and 500 μl was introduced in a 5 ml volumetric flask. Then 3.5 ml of acetonitrile were added and the flask was filled up to volume with water. Before the injection in the chromatographic system the solution obtained was sonicated in an ultrasound water bath for 5 min and filtered through a 0.22 μm PFTE membrane. Carbonated liquid samples were previously degassed in an ultrasound water bath for 15 min prior to their dilution.

In order to increase the applicability of the method reducing possible interferences, acetonitrile was selected for sample dilution and chromatographic separation because according to a previously published work [16] it precipitates proteins and starch present in sample matrices.

2.3. Univariate background correction based on the use of a reference spectra matrix (UBC-RSM)

A detailed description of the UBC-RSM method can be found in a previous work [14]. In brief, the eluent correction method can be divided in five steps: in Step 1 a reference spectra matrix RSM (r, c) is measured. The acquisition of the RSM is carried out in practice by measuring a LC gradient in a defined composition range. This step also include the measurement of the sample matrix SM (z, c). The eluent composition range of the SM should be within the RSM composition interval.

Step 2 involves the calculation of the absorbance ratio (AR) at two selected wavenumbers (r_1 and r_2) for each spectrum included in the SM and the RSM. The obtained AR values are characteristic for the mobile phase composition as defined in Eq. (1).

$$\mathrm{AR}_s = \frac{y^s_{r_1}}{y^s_{r_2}} \tag{1}$$

where $y^s_{r_1}$ and $y^s_{r_2}$ are the absorbance values at the wavenumbers r_1 and r_2 (cm^{-1}) measured in the spectra $s = (1, \ldots, z)$ for spectra included in the SM and $s = (1, \ldots, r)$ for the RSM.In Step 3, for each of the z spectra included in the SM, the most appropriated background spectrum ($S_{\gamma,s}$, $s = 1, \ldots, z$) included in the RSM is located.

Step 4 consists of the calculation of a correction factor (KF) which is determined for each sample spectrum. The objective of the KF is to correct slight changes in the spectral intensity of the eluent during the run. The KF is defined as the ratio of absorbance of the sample S_s at wavenumber φ ($y^{S_s}_{\varphi}$) and the previously selected background spectrum $S_{\gamma,s}$ at a defined wavenumber φ ($y^{S_{\gamma,s}}_{\varphi}$) using the following expression:

$$\mathrm{KF}_s = \frac{y^{S_s}_{\varphi}}{y^{S_{\gamma,s}}_{\varphi}} \tag{2}$$

Step 5 includes the subtraction to the eluent background spectrum from the sample spectrum using the following expression:

$$\text{Corrected}S_s = S_s - \text{KF}_s\ S_{\gamma,s} \quad (3)$$

where CorrectedS_s is the background corrected sample spectrum s; S_s is the original sample spectrum; $S_{\gamma,s}$ is the background spectrum included in the RSM and KF_s is the calculated correction factor for the sample spectrum S_s. The use of the KF is optional and a prior evaluation of its usefulness is recommended.

3. Results and discussion

3.1. FTIR spectra of sugars

Fig. 1 shows the spectra of solutions of fructose, glucose, sucrose and maltose dissolved in 70:30 acetonitrile:water. All four studied compounds show the characteristic absorption bands of carbohydrates in the spectral region between 1500 and 950 cm^{-1}. The bands at 1035, 1015 and 1260 cm^{-1} were identified to, respectively, the C–O stretch, C–C stretch and C–OH deformation modes [9,17,18]. So, it can be concluded that any of the aforementioned bands are suitable for the quantitation of sugars in beverages.

However, in order to do a correct quantification of sugars in LC–FTIR, the changes in the spectrum of the mobile phase during the elution of analytes must be carefully checked to achieve an appropriate chemometric background correction.

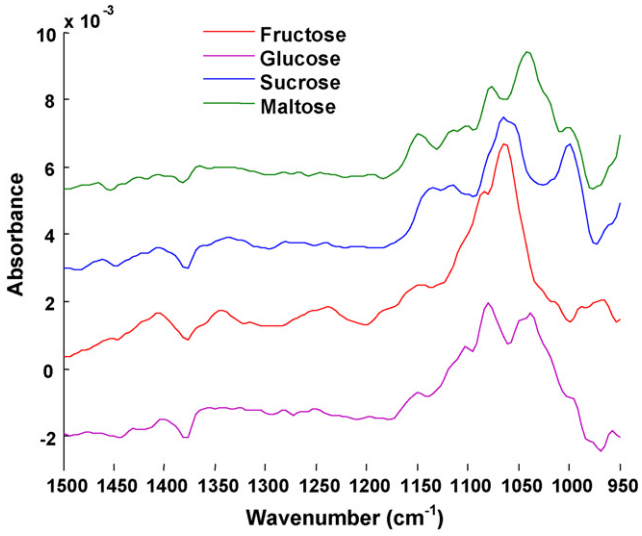

Fig. 1. FTIR spectra of sugars in acetonitrile:water (70:30, v/v). Fructose (6.1 mg ml^{-1}); glucose (6.0 mg ml^{-1}); sucrose (6.2 mg ml^{-1}) and maltose (6.0 mg ml^{-1}). Spectra are shifted along the y-axis for a better clarity.

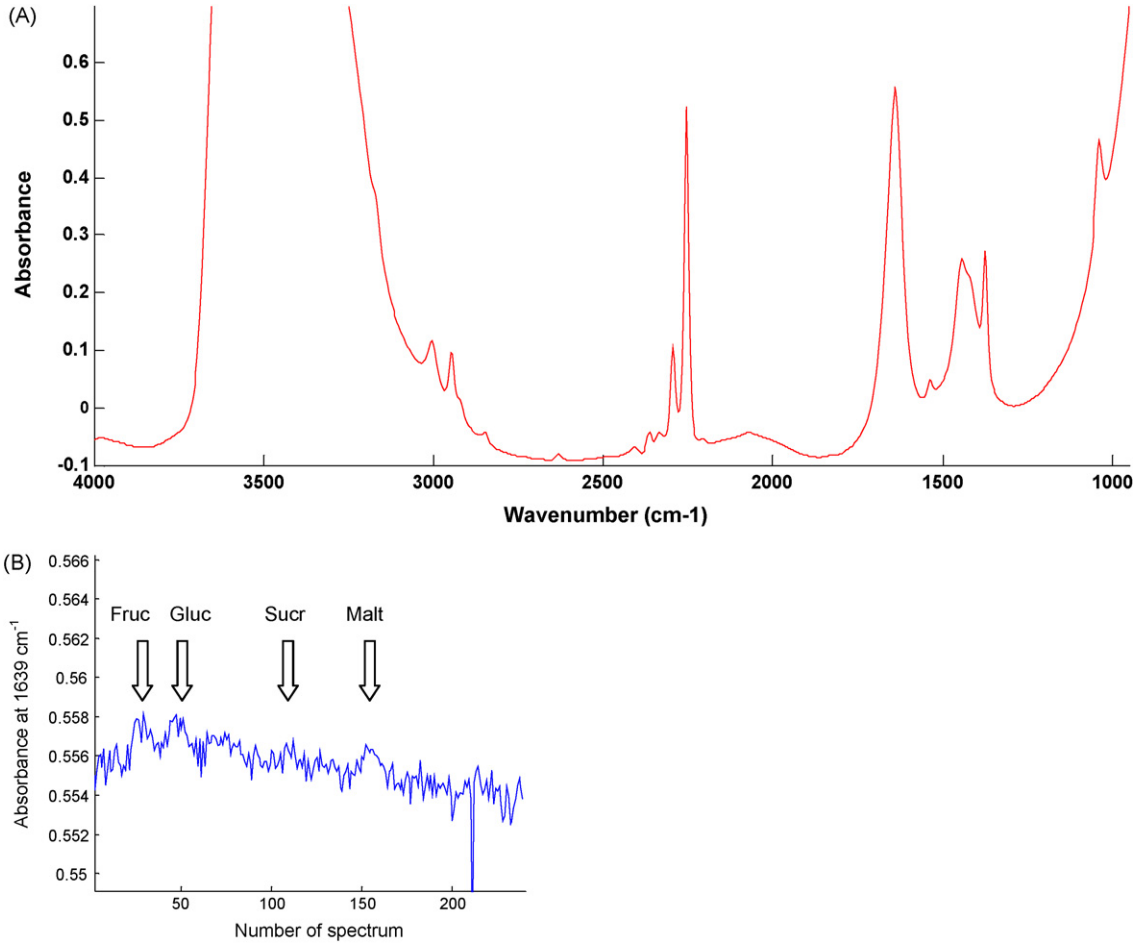

Fig. 2. FTIR spectra of an acetonitrile:water (70:30, v/v) mixture (A) and variation of the absorbance at 1639 cm^{-1} (B). In this case the arrows indicate the sugar elution time windows.

3.2. Changes in the FTIR spectra of the mobile phase components during the elution of the analytes

For a proper use of the RSM-based background correction method, the mobile phase spectra should present at least an absorption band which could be used to identify the exact composition of the eluent during the chromatographic run. Special attention must be paid on the selection of the wavenumbers r_1 and r_2 employed for the calculation of AR because spectral overlapping between the mobile phase and the eluting analytes at the wavenumbers leads to an inaccurate identification of the eluent spectra in the RSM, thus causing severe errors in both, the spectra and elution profiles [14]. Additional difficulties can be created by modification in position and bandwidth due to intermolecular interactions between analytes and the mobile phase components.

Fig. 2A shows the spectrum between 4000 and 950 cm^{-1} of an acetonitrile:water (70:30, v/v) mixture. The spectrum showed four main water absorption bands at ~3400 cm^{-1} (stretching band), 2115 cm^{-1} (combination band), 1639 cm^{-1} (deformation band) and a latter one starting near 1000 cm^{-1} (water libration bands), in good agreement with reported data [9,17,18]. When using FTIR detection in aqueous systems, the intense absorptivity of water at ~3400 cm^{-1} leaves no detectable light, reducing the signal to noise ratio and obscuring the absorption of the analytes in this spectral region. Because of that, the region above 2400 cm^{-1} was not used throughout this work.

Two main acetonitrile bands were clearly distinguishable at 2252 and 2291 cm^{-1}, the first corresponding to the CN stretching mode (ν_2) while the second one was assigned to a combination of both CH_3 bending (ν_3) and C–C stretching (ν_4) modes [19].

It is well known that IR water bands can be modified by the presence of sugars, increasing considerably the difficulty of performing an adequate IR background correction under gradient conditions. Recent studies of the interaction of water and carbohydrates by Max and Chapados [17,18], have evidenced that the water deformation band (δ_{HOH}) at 1640 cm^{-1} increases its intensity and slightly shifts towards the blue region due to the formation of sugar hydrates, being displaced even several wavenumbers. Furthermore, the spectra and abundances of the different hydrates of fructose, glucose or sucrose in aqueous solutions depend on their concentration [17,18].

To evaluate the effects of gradually increasing carbohydrate concentrations on the spectra of an acetonitrile:water mixture, 20 μl of 5 mg ml^{-1} fructose, glucose, sucrose and maltose solutions were injected in an acetonitrile:water (70:30) flow system.

It was found that, at the studied concentrations, isocratic conditions and using a spectral resolution of 8 cm^{-1}, the position of the maximum of the water deformation band at 1639 cm^{-1} is constant during the elution of the studied carbohydrates. On the contrary, a slight increase in its intensity can be observed (see Fig. 2B). Therefore, in order to assure the accuracy of the background correction process during the elution of the four analytes it is not recommended to use the band at 1639 cm^{-1} for the characterization of the mobile phase composition. In contrary no effect on the peak shape of the CN bands in the 2300–2200 cm^{-1} spectral region was observed, therefore indicating that at this concentration level the spectra of the eluent in this region is not affected by the presence of the analytes.

3.3. Selection of the UBC-RSM background parameters

One of the main features of the UBC-RSM method is its simplicity, limiting the user interaction during the background correction to the selection of the wavenumbers r_1 and r_2 used for the calculation of the AR. For an easy selection of these wavenumbers, all the

Table 1
Absorbance ratios (AR) that provided the lowest noise values in the extracted chromatograms

Noise as RMS	1st wavenumber (cm^{-1})	2nd wavenumber (cm^{-1})
Chromatogram extracted using absorbance values at 2063 cm^{-1}		
9.082×10^{-5}	2256.5	2252.6
0.00010885	2260.3	2252.6
0.00011515	2264.2	2248.7
0.00012287	2260.3	2248.7
0.00012594	2291.2	2268
Chromatogram extracted using absorbance values at 1640 cm^{-1}		
0.0029791	2256.5	2252.6
0.0037747	2291.2	2268
0.0038919	2260.3	2252.6
0.003985	2264.2	2248.7
0.0040928	2268	2244.9
Chromatogram extracted using absorbance values at 1442 cm^{-1}		
0.0004805	2256.5	2252.6
0.00053281	2260.3	2256.5
0.0005719	2248.7	2268
0.00058188	2264.2	2252.6
0.00061794	2298.9	2291.2
Chromatogram extracted using absorbance values at 1065 cm^{-1}		
0.00041775	2295	2244.9
0.00042011	2291.2	2268
0.00042661	2256.6	2252.6
0.00044693	2298.9	2268
0.00044947	2260.3	2248.7

Noise measured using the root mean square of the extracted chromatogram at 2063, 1640, 1442 and 1065 cm^{-1} in the background corrected blank gradient injection.

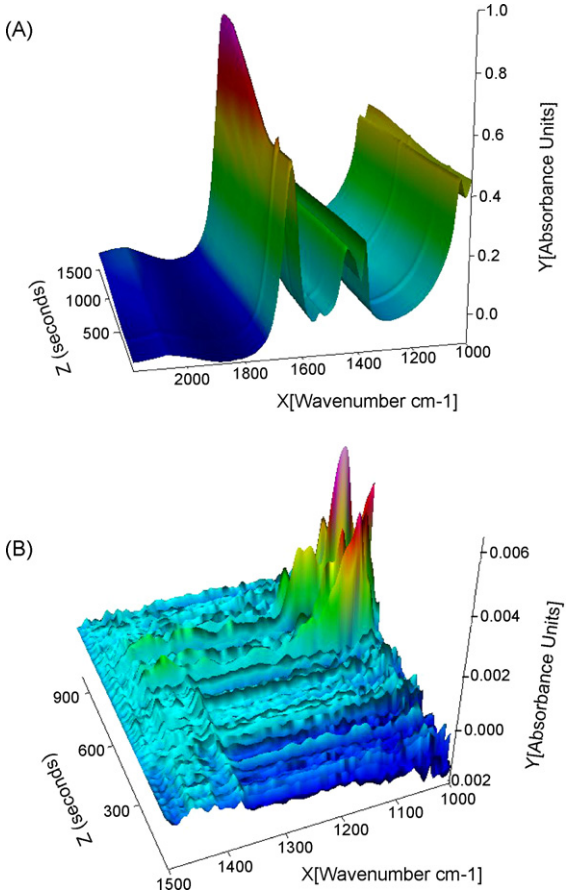

Fig. 3. On-line gradient LC–FTIR spectra obtained from the injection of a sugar standard solution containing 2.5 mg ml^{-1} of fructose, glucose, sucrose and maltose. (A) Raw spectra between 2200 and 1000 cm^{-1}. (B) Spectra in the wavenumber range between 1500 and 1000 cm^{-1} corrected using the UBC-RSM method.

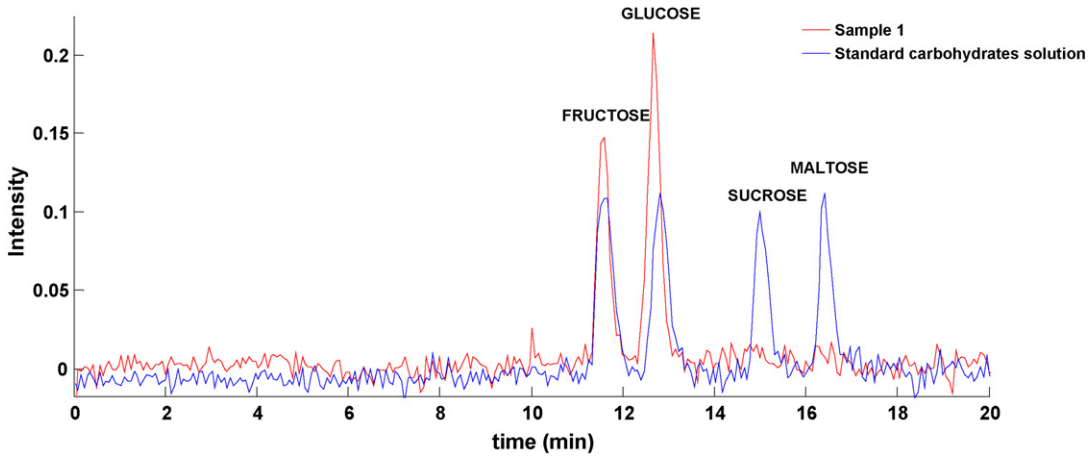

Fig. 4. LC–FTIR chromatograms extracted from the injection of a standard solution containing 5.5 mg ml^{-1} of fructose, glucose, sucrose and maltose (red) and from the injection of sample 1 (blue). Chromatograms were obtained from the measurement of the area between 1108 and 1069 cm^{-1}, corrected using a baseline established at 1203 cm^{-1}. (For interpretation of the references to color in this figure legend, the reader is referred to the web version of the article.)

possible ARs within a previously selected range were assayed for an appropriate background selection from the spectra included in the RSM. The employed output function was the noise (measured as RMS) in the extracted chromatograms at four characteristic eluent wavenumbers. So, low chromatographic noise values indicated adequate background correction. In an earlier work [14], for acetonitrile:water (with 1% acetic acid) gradients in the range between (40:60, v/v) and (99:1, v/v), the selection of the AR was made in the spectral region between 2310 and 2180 cm^{-1}. As a result, the quotient between absorbance values at 2256.3 and 2248.6 cm^{-1} was selected.

In spite of the high similarity between the aforementioned mobile phase and that employed in this work, slight changes in the mobile phase composition might shift the position of eluent bands. To ensure that the AR used throughout this work was appropriate, the AR selection process described in the aforementioned work [14] was carried out using the absorbance values at 2063, 1640, 1442 and 1065 cm^{-1} for the evaluation of the chromatographic noise.

Table 1 summarizes the five pairs of wavenumbers which provided the lowest noise in the extracted chromatograms using a RSM composed by 986 spectra covering acetonitrile concentrations between 75 and 55% (v/v) acetonitrile and a blank gradient injection formed by 317 spectra of mobile phase solutions in the same concentration range.

The noise level in the extracted chromatograms at 2063, 1640, 1442 cm^{-1} reached the minimum value using the absorbance at 2256.5 and 2252.6 cm^{-1} for the calculation of the AR, obtaining RMS values between 9×10^{-5} and 2.9×10^{-3} for 2063 and 1640 cm^{-1}, respectively. On the other hand, the minimum noise in the extracted chromatogram at 1065 cm^{-1} was achieved using the AR calculated

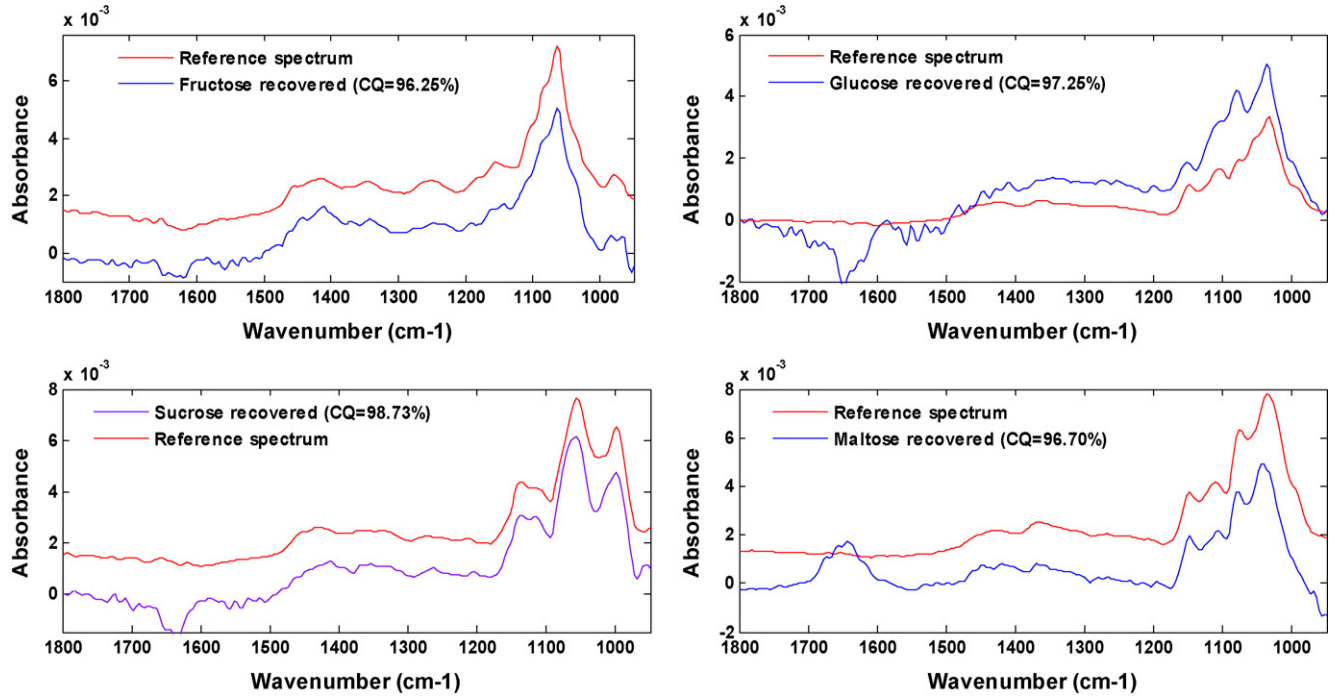

Fig. 5. Recovered spectra of fructose, glucose, sucrose and maltose at their respective peak apex extracted from the sugar standard solution LC run shown in Fig. 4, compared to reference spectra.

from absorbance values at 2295 and 2249.5 cm^{-1}. The difference between the obtained noise using this pair of wavenumbers and that obtained using the absorbance ratio between 2256.5 and 2252.6 cm^{-1} is only 2.1% and cannot be considered as statistically significant. Based on the foregoing data, the quotient between the absorbance values at 2256.5 and 2252.6 cm^{-1} was selected for the background correction of further measurements.

3.4. On-line LC–FTIR separation of carbohydrates

Fig. 3 shows the original (A) and background corrected (B) spectra acquired during the elution of a standard carbohydrate solution of fructose, glucose, sucrose and maltose at a concentration of 3 mg ml^{-1} for each one. Visual inspection of the 3D graphs reveals that changes in the background signal due to the mobile phase gradient have been corrected in a great extent by the UBC-RSM subtraction procedure.

As an example, LC–FTIR chromatograms extracted from the injection of a standard solution containing 5.5 mg ml^{-1} of fructose, glucose, sucrose and maltose and from the injection of sample 1 are shown in Fig. 4. The depicted chromatograms were obtained from the measurement of the area values of the spectra between 1108 and 1069 cm^{-1}, corrected using a baseline established at 1203 cm^{-1}. It can be seen, that the resolution is very good and the specific spectra of the analytes can clearly be distinguished (see Fig. 5). The retention times, established from four injections of standard mixtures of the considered compounds were 11.8 ± 0.2, 12.7 ± 0.2, 15.0 ± 0.2 and 16.5 ± 0.2 min for fructose, glucose, sucrose and maltose, respectively.

As it can be seen in the chromatograms of Fig. 4, the lack of sloping baselines and the random distribution of the chromatographic noise support the suitability of the selected background correction conditions for obtaining the chromatograms of sugars during gradient elution.

3.5. Identification of the analytes

To quantify the accuracy of the background correction, a numerical correlation was made through the determination of a "Correlation coefficient (QC)" defined for two spectra (S_1 and S_2) as the ratio from the covariance ($Cov(S_1,S_2)$) and the product of the two standard deviations σ_{S_1} and σ_{S_2}. Hence, a QC = 100% indicates identical spectra. Using the spectral region between 1250 and 1060 cm^{-1}, the obtained QC for the spectra shown in Fig. 5 ranged between 96.25 and 98.73%. On the other hand, QCs were also calculated for the corrected spectra obtained from sample injections obtaining also an excellent agreement between extracted and reference spectra (data not shown), which confirmed the identity of carbohydrates, thus increasing the reliability of the results.

3.6. Analytical characteristics of the method

Calibration of analytes was made in the previously described experimental conditions. Fructose chromatograms were obtained from the measurement of the spectra area between 1108 and 1069 cm^{-1}, corrected using a baseline at 1203 cm^{-1}. Glucose, sucrose and maltose chromatograms were calculated from area measurements between 1177 and 1025 cm^{-1}, corrected using a baseline at 1177 cm^{-1}. Table 2 shows the obtained analytical parameters using peak height values from the extracted chromatograms.

The linear regression coefficients obtained indicate a good adjustment of data to each calibration curve. Limits of detection in the 0.4–0.6 mg ml^{-1} range were estimated for each analyte as the concentration at which the chromatographic signal to noise ratio was higher than 3. Precision of six-independent injections of

Table 2
Analytical figures of merit of the on-line LC–FTIR determination of sugars

	Calibration curve[a] [$y = a + bC$ (mg ml^{-1})]	R^2	Noise[b]	LOD[c] (mg ml^{-1})	LOD[d] (g/100 ml)	LOD[c] (mg ml^{-1})	Repeatability[e] (%)	Linear range (mg ml^{-1})	Linear range (mg/100 ml[a])
	$(a \pm s_a)$ (CI)[f] $(b \pm s_b)$								
Fructose	(0.0008 ± 0.0006) (0.0014) (0.0264 ± 0.0002)	0.9995	0.4	0.0037	0.4	0.4	4.1	0.5–6.0	0.5–6.0
Glucose	(0.000 ± 0.006) (0.014) (0.0933 ± 0.0018)	0.9965	0.6	0.0175	0.6	0.6	3.3	0.5–5.2	0.5–5.2
Sucrose	(0.006 ± 0.006) (0.014) (0.0921 ± 0.0011)	0.9962	0.5	0.0175	0.5	0.5	3.7	0.5–4.9	0.5–4.9
Maltose	(0.013 ± 0.007) (0.016) (0.0895 ± 0.0009)	0.9980	0.4	0.0175	0.4	0.4	3.8	0.5–5.2	0.5–5.2

[a] Calibration curve from 10 standard solutions. a and b are the intercept and the slope of the calibration lines.
[b] Chromatographic noise measured as the root mean square (RMS) of the chromatographic signal extracted from a background correct blank gradient injection.
[c] Limit of detection established as the concentration at which the signal to noise ratio is higher than 3.
[d] Limit of detection in beverage samples for a sample volume of 500 μl.
[e] Relative standard deviation for six-independent measurements carried out at a concentration level of 3.0 mg ml^{-1}.
[f] Confidence interval calculated as $IC = s_a t_{p,n-2}$ ($p = 95\%$).

Table 3
On-line LC–FTIR determination of sugars in commercial samples

Sample	Presentation	Found concentration (g/100 ml)					Label content (g/100 ml)
		Fructose	Glucose	Sucrose	Maltose	Total	
1	Soft drink	5.14	7.84	<LOD	<LOD	13.0	12.9
2	Soft drink	6.39	4.75	<LOD	<LOD	11.1	11.6
3	Soft drink (sugar free)	<LOD	<LOD	<LOD	<LOD	0.00	0.00
4	Soft drink	3.50	4.18	1.33	<LOD	9.0	8.9
5	Soft drink	0.16	0.87	6.26	<LOD	7.3	7.9
6	Energy drink	0.33	3.08	6.43	<LOD	9.8	10.7
7	Fruit juice	3.77	3.69	2.61	<LOD	10.1	12.4

Table 4
Recovery study of fructose, glucose, sucrose and maltose in spiked commercial samples

Sample	Presentation	g/100 ml added				g/100 ml found[a] (% recovery)			
		Fructose	Glucose	Sucrose	Maltose	Fructose	Glucose	Sucrose	Maltose
1	Soft drink	2.54	1.90	2.98	1.84	7.69 ± 0.08 (100.4)	9.84 ± 0.09 (105.1)	2.92 ± 0.014 (98.1)	1.84 ± 0.05 (100.2)
2	Soft drink	2.06	2.36	3.33	3.34	8.36 ± 0.04 (95.6)	7.19 ± 0.09 (103.5)	3.34 ± 0.02 (100.2)	3.39 ± 0.09 (101.3)
4	Soft drink	1.00	0.93	0.97	1.19	4.48 ± 0.06 (98.0)	5.11 ± 0.04 (99.8)	2.39 ± 0.02 (104.0)	1.28 ± 0.05 (99.1)
5	Soft drink	0.97	0.90	1.30	1.10	1.13 ± 0.08 (100.0)	1.76 ± 0.09 (98.9)	7.54 ± 0.06 (98.7)	1.02 ± 0.08 (92.5)
6	Energy drink	1.43	0.97	1.07	1.17	1.78 ± 0.09 (101.4)	4.06 ± 0.04 (101.9)	7.45 ± 0.03 (95.8)	1.15 ± 0.07 (98.4)
7	Fruit juice	2.20	2.18	1.74	1.57	5.92 ± 0.02 (97.7)	5.90 ± 0.08 (101.4)	4.32 ± 0.08 (98.1)	1.65 ± 0.07 (104.9)

[a] Recoveries from two-independent replicates.

a standard calibration solution containing 3.0 mg ml^{-1} of each analyte provided relative standard deviations ranging between 3.3 and 4.1% for glucose and fructose, respectively. This obtained sensitivity and precision results together with the good correlation factors obtained for the recovered analyte spectra suggested that they were appropriate for the quantitative determination and identification of sugars in beverages.

3.7. Determination of sugars in beverages

The applicability of the proposed method was evidenced by the analysis of a set of 7 commercially available samples purchased from the Spanish market. Sample treatment was reduced to an adequate dilution and filtration of samples before their injection in the chromatographic system. Table 3 lists the different obtained sugar contents from duplicate analysis of diluted samples. Additionally, a recovery study was carried out in six of the analysed samples. The employed spiked concentration ranges were: 0.97–2.54 (g/100 ml), 0.90–2.36 (g/100 ml), 0.97–3.133 (g/100 ml) and 1.10–3.34 (g/100 ml) for fructose, glucose, sucrose and maltose, respectively. Mean recovery values ranged between 105.1 and 92.5% (see Table 4).

4. Conclusions

A simple on-line gradient LC method in combination with FTIR detection and chemometrics has been developed for the determination of four characteristic carbohydrates in beverages. Fructose, glucose, sucrose and maltose could be separated, identified and quantified in commercial samples with limits of detection between 0.4 and 0.6 mg ml^{-1}. The use of the univariate method for the selection of the background from a reference spectra matrix permitted an accurate chemometric eluent correction yielding distinguishable spectra of good quality for the studied analytes with correlation factors between 96.25 and 98.73%. The main advantages provided by the proposed on-line LC–FTIR approach include instrumental simplicity and low cost (due to the possibility of using commercial flow cells).

Acknowledgements

Authors acknowledge the financial support of Ministerio de Educación y Ciencia (Project CTQ205-05604, FEDER) and Direcció General d'Investigació I Transferència Tecnològica de la Generalitat Valenciana (Project ACOMP/2007/131). J.K. acknowledges the "V Segles" grant provided by the University of Valencia to carry out this study. G.Q. is grateful for a post-doctoral grant ("*Ayudas para estancias de doctores en centros de investigación de excelencia de la Comunidad Valenciana*") from the *Conselleria de Industria, Generalitat Valenciana* (Spain).

References

[1] M.L. Wheeler, F.X. Pi-Sunyer, J. Am. Diet Assoc. 108 (2008) S34.
[2] FDA Nutrition Labeling Manual, U.S. Food and Drug Administration, Center for Food Safety and Applied Nutrition, 1998.
[3] A. Cáceres, S. Cárdenas, M. Gallego, A. Rodríguez, M. Valcárcel, Chromatographia 52 (2000) 314.
[4] W.L. Qian, Z. Khan, D.G. Watson, J. Fearnley, J. Food Comp. Anal. 21 (1) (2008) 78.
[5] R. Vonach, B. Lendl, R. Kellner, J. Chromatogr. A 824 (1998) 159.
[6] R. Vonach, B. Lendl, R. Kellner, Anal. Chem. 69 (1997) 4286.
[7] A. Edelmann, C. Ruzicka, J. Frank, B. Lendl, W. Schrenk, E. Gornik, G. Strasser, J. Chromatogr. A 934 (2001) 123.
[8] A. Edelmann, K. Diewok, J. Rodriguez-Baena, B. Lendl, Anal. Bioanal. Chem. 376 (2003) 92.
[9] M. Kölhed, B. Karlberg, Analyst 130 (2005) 772.
[10] G.W. Somsen, C. Gooijer, U.A.Th. Brinkman, J. Chromatogr. A 856 (1999) 213.
[11] K. István, R. Rajkó, G. Keresztury, J. Chromatogr. A 1104 (1-2) (2006) 154.
[12] R.J. Dijkstra, H.F.M. Boelens, J.A. Westerhuis, F. Ariese, U.A.Th. Brinkman, C. Gooijer, Anal. Chim. Acta 519 (2004) 129.
[13] H.F.M. Boelens, R.J. Dijkstra, P.H.C. Eilers, F. Fitzpatrick, J.A. Westerhuis, J. Chromatogr. A 1057 (2004) 21.
[14] G. Quintás, B. Lendl, S. Garrigues, M. de la Guardia, J. Chromatogr. A 1190 (2008) 102.
[15] J. Kuligowski, G. Quintás, S. Garrigues, M. de la Guardia, Anal. Chim. Acta 624 (2) (2008) 278.
[16] J.T. Gotsick, R.F. Benson, J. Liq. Chromatogr. 14 (1991) 1887.
[17] J.J. Max, C. Chapados, J. Phys. Chem. A 111 (2007) 2679.
[18] J.J. Max, C. Chapados, J. Phys. Chem. A 105 (2001) 10681.
[19] T. Takamuku, M. Tabata, A. Yamaguchi, J. Nishimoto, M. Kumamoto, H. Wakita, T. Yamaguchi, J. Phys. Chem. B 102 (1998) 8880.

Talanta 77 (2008) 744–750

Contents lists available at ScienceDirect

Talanta

journal homepage: www.elsevier.com/locate/talanta

Silicate electrochemical measurements in seawater: Chemical and analytical aspects towards a reagentless sensor

Marielle Lacombe [a], Véronique Garçon [a,*], Danièle Thouron [a], Nadine Le Bris [b], Maurice Comtat [c]

[a] *Laboratoire d'Etudes en Géophysique et Océanographie Spatiales, Centre National de la Recherche Scientifique, UMR 5566, 18 Avenue Edouard Belin, 31401 Toulouse Cedex 9,France*
[b] *Ifremer, Département Etude des Ecosystèmes Profonds, BP70, 29280 Plouzané, France*
[c] *Laboratoire de Génie Chimique, UMR 5503, Université Paul Sabatier, 118 route de Narbonne, 31062 Toulouse Cedex, France*

ARTICLE INFO

Article history:
Received 4 December 2007
Received in revised form 27 June 2008
Accepted 11 July 2008
Available online 23 July 2008

Keywords:
Molybdenum
Silicate
Reagentless
Amperometry
Cyclic voltammetry

ABSTRACT

From the study of molybdenum oxidation in aqueous solutions we developed a semi-autonomous method to detect silicate in aqueous samples. Molybdenum oxidation was used to form molybdate in acidic media. The silicomolybdic complex formed with silicate is detectable by amperometry or cyclic voltammetry. The new electrochemical method is in good agreement with the method conventionally used for environmental water silicate analysis. In the second stage, a completely reagentless method was developed using molybdate and proton produced during molybdenum oxidation. Reproducibility tests show a precision of 2.6% for a concentration of 100 μmol L^{-1}. This new method will be very suitable for the development of new autonomous silicate sensors easy to handle and without reagents. In this paper we present the analytical and chemical aspects necessary for a complete documentation of the method before the development of a new reagentless sensor.

1. Introduction

The common analytical technique to measure silicate in natural waters is the spectrophotochemical method. It involves the addition to the sample of an acidic molybdate solution to convert the silicate to a Keggin anion, $SiMo_{12}O_{40}^{4-}$ and subsequent chemical reduction to a mixed oxidation state, a molybdenum complex which is intensely blue with a maximum of absorption at 810 nm [1]. This method is now frequently carried out in automated continuous flow systems [2], and *in situ* analyzers have been developed to measure nutrients autonomously in the ocean [3–6]. Selectivity between silicate and phosphate remains a significant problem because of their very similar chemical behaviour [7], and a systematic salt effect is present in automated nutrient determination in seawater [8]. Simultaneous determination of phosphate and silicate is possible by first-derivative spectrophotometry [9].

Silicate determination was also performed by ion exclusion chromatography with UV detection in leaching process waters [10] and in fresh water using flow injection with luminol chemiluminescence detection [11]. Recently a sorption-chromatographic method for determining phosphate and silicate ions in waters as molybdic heteropoly acids was developed [12]. Silicate was also measured in seawater by inductively coupled plasma atomic emission spectrometry [13], by ion exclusion chromatography with conductivity detection [14], by ion exclusion chromatography in combination with inductively coupled plasma-mass spectrometer [15].

Some electrochemical methods have been reported to measure silicate and phosphate using heteropolymolybdates [16–18]. The orthophosphate amperometric detection was investigated by flow injection analysis by Harden and Nonidez [19] and by batch injection analysis by Quintana et al. [20]. The amperometric detection was also used for phosphate determination with a bienzyme electrode [21]. Carpenter et al. [22] presented fundamental studies with ultra microelectrodes, for the determination of silicate and phosphate in water. Hodgson and Pletcher extended this study and discussed the ways to enhance selectivity between silicate and phosphate [23]. The response of the silicomolybdic complex was investigated by Lee and Gerwirth on silver and gold electrodes [24]. Finally, a differential pulse polarographic method was used to detect the trace of phosphate in environmental samples [25].

Some *in situ* voltammetric probes have already been developed for chemical monitoring and speciation [26,27]. Electrochemistry allows to measure several species simultaneously with very good spatial and time resolutions, at low cost and very low concentrations, without reagents and therefore is a very promising method

* Corresponding author. Tel.: +33 5 61 33 29 57; fax: +33 5 61 25 32 05.
E-mail address: Veronique.Garcon@legos.obs-mip.fr (V. Garçon).

0039-9140/$ – see front matter © 2008 Published by Elsevier B.V.
doi:10.1016/j.talanta.2008.07.023

for the development of a small, precise and autonomous *in situ* sensor.

First steps towards the development of a reagentless method for silicate determination in seawater samples were presented in a previous paper [28]. This previous paper was the description of the seawater application of the method during the Drake ANT XXIII/3 oceanographic cruise by oxidizing molybdenum in a measurement cell and adding sulphuric acid. The comparison of the results of this method with those of the classical spectrophotometric ones showed a very good agreement between both methods. The aim of the work here is to describe in detail the chemical and electrochemical bases of this new method and to discuss its advantages and potential as compared to other methods. These aspects are necessary for the development of a new sensor. Experiments described here present a new step towards an autonomous sensor. We first present the method used to measure silicate and to describe the electrochemical behaviour of the silicomolybdic complex, then the study of the molybdenum oxidation and the development of the semi-autonomous method. Finally a complete reagentless method for silicate detection is presented and we conclude by the discussion on this new method.

2. Experimental

2.1. Apparatus

Cyclic and linear sweep voltammetry and chrono-amperometry were carried out with a potentiostat μ-Autolab III (Metrohm). The rotating disk electrode (RDE) was controlled by an RDE controller (Metrohm). Voltammograms at a stationary or rotating disk electrode were recorded in a three electrode cell with a carbon counter electrode. Working electrodes were in gold, platinum, or glassy carbon with an area of 0.07 cm^2 (Metrohm). All potentials are given versus an Ag/AgCl (KCl 3 mol L^{-1}) reference electrode. The glassy carbon disk was polished with lapping film sheet (3 M aluminium oxide, 1 micron) before each measurement.Amperometry was made with a glassy carbon disk working electrode held at a constant potential of 200 mV.

The reference colorimetric analysis of silicate was performed according to Le Corre and Tréguer's method [29]. Laboratory colorimetric measurements were made with an Auto-Analyzer Technicon II (AAII, Bran Luebbe). On board colorimetric measurements were made with an Auto-Analyzer (Skalar).

pH measurements were made with a 744 pH meter Metrohm calibrated with Bioblock buffered solutions.

2.2. Reagents and solutions

All solutions were prepared in Milli-Q water (Millipore Milli-Q water system) with reagent grade salts. Artificial seawater for standards calibration, silicate and phosphate samples was prepared at a salinity of 34.7 g L^{-1}, with 32.13 g of sodium chloride (NaCl), 7.13 g of magnesium-sulphate heptahydrate ($MgSO_4$, $7H_2O$) and 0.17 g of sodium carbonate ($NaCO_3$), per liter of water.

Silicate standard solutions were prepared with sodium silicofluoride (Na_2SiF_6, Merck) and potassium dihydrogen phosphate (KH_2PO_4, Merck) [30].

Solutions used for silicate and phosphate voltammetric measurements are sodium molybdate 10 mmol L^{-1} (Na_2MoO_4, $2H_2O$) and sulphuric acid (H_2SO_4, 2.5 mol.L^{-1}) to adjust the pH at 1.5.

Reagents used for silicate spectrophotometric determinations are: an acidified ammonium heptamolybdate solution (10 g of ammonium heptamolybdate, 40 mL of sulphuric acid, H_2SO_4 2,5 mol L^{-1} in 1000 mL of Milli-Q water); an oxalic acid solution (7 g of oxalic acid and 50 mL H_2SO_4 in 1000 mL of Milli-Q water and 1 mL of Aerosol 22(Sigma)); an ascorbic acid solution (17.8 g of L-ascorbic acid and 25 mL of acetone in 1000 mL of Milli-Q water and 1 mL of Aerosol 22).

Spectrophotometric baseline measurements were made with artificial seawater. Standard solutions used on board were tested back in the laboratory with commercial standards (OSIL, 1000 μmol L^{-1}) and no difference was observed.

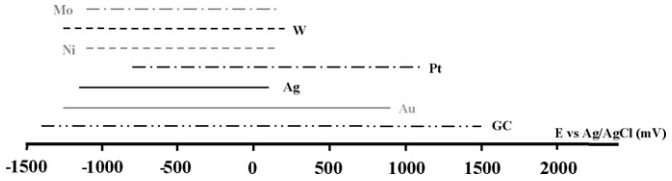

Fig. 1. Electroactivity domains of molybdenum, tungsten, nickel, platinum, silver gold and glassy carbon electrodes in seawater (pH 8.1).

2.3. Procedure

Electrochemical measurements with addition of reagents were made in 100 mL of artificial seawater with sodium molybdate at 10 mmol L^{-1} and the pH adjusted to 1.5. Measurements were made after at least 6 min at 25 °C. For amperometric measurements a rotating disk electrode (1000 rpm) was used.

For the semi-autonomous method, molybdate was produced by molybdenum anodic oxidation. The molybdenum electrode (Good Fellow Metals, purity: 99.9%) has an area of 1.2 cm^2. The oxidation was performed at a constant electrolysis current (50 mA) during 420 s, in a 5 mL cell. pH was adjusted to 1.5 by addition of sulphuric acid H_2SO_4 5 mol L^{-1} [28].

For the reagentless method, a 6 mL cell divided in two by a porous polyethylene membrane was used. Molybdenum, reference and sensing electrodes were placed in the anodic compartment while the counter electrode was in the cathodic compartment. Molybdate was produced by molybdenum anodic oxidation performed at a constant electrolysis current (50 mA) during 360 s [28].

2.4. Seawater collection

The collection of seawater samples was made during the ANT XXIII/3 cruise aboard the R/V Polarstern during the austral summer 2006 from January 14th to February 8th between Punta Arenas (Chile) and the Antarctic Peninsula [28].

3. Results and discussion

3.1. Electrode material

As electronic exchanges are extremely dependent on the nature of the electrode material, we first evaluated the electroactivity domains of various materials in seawater. So we made voltammograms in seawater (at 34.7 g L^{-1} and pH 8.2) on gold, silver, platinum, glassy carbon, tungsten, and molybdenum. Theses domains, represented on Fig. 1, are limited by the reduction of water (Eq. (1)), its oxidation (Eq. (2)) or the oxidation of the metal for silver (Eq. (3)) and molybdenum (Eqs. (4)–(6)) for a current density (j) of 0.7×10^{-3} A cm^{-2}.

$$2H_2O + 2e^- \rightarrow H_2 + 2OH^- \quad (1)$$

$$2H_2O \rightarrow O_2 + 4H^+ + 4e^- \quad (2)$$

$$Ag + Cl^- \rightarrow AgCl + 1e^- \quad (3)$$

$$Mo + 2H_2O \rightarrow MoO_2 + 4H^+ + 4e^- \quad (4)$$

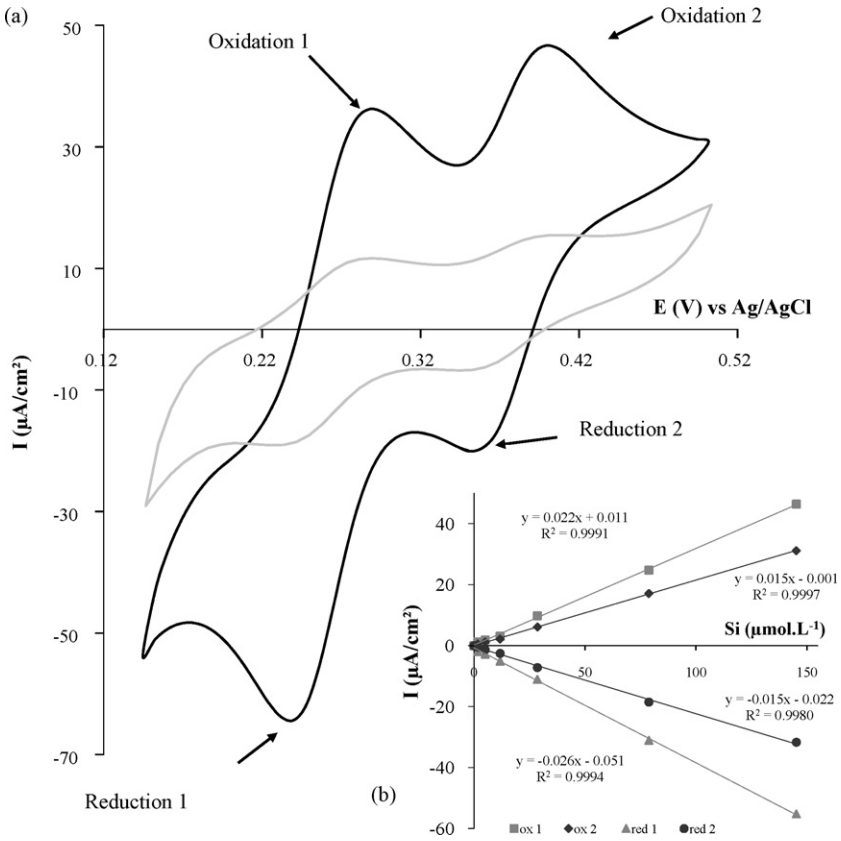

Fig. 2. (a) Voltammograms with $Si(OH)_4$ = 10 μmol L^{-1} (grey line) and 120 μmol L^{-1} (black line); sodium molybdate = 10 mmol L^{-1}, pH 1.5, scan rate = 200 mV/s with vitreous carbon working electrode and Ag/AgCl reference electrode. (b) Calibrations for concentrations from 0.3 to 145 μmol L^{-1}, obtained by the two oxidation and two reduction peaks.

$$Mo + 3H_2O \rightarrow MoO_3 + 6H^+ + 6e^- \quad (5)$$

$$Mo + 4H_2O \rightarrow {MoO_4}^{2-} + 8H^+ + 6e^- \quad (6)$$

3.2. Molybdosilicate complex

Silicate is non-electroactive species thus the voltammetric determination of this ion involves the treatment of the sample with an acidic molybdate solution to form a Keggin anion, $Si(Mo_{12}O_{40})^{4-}$ (Eq. (7)).

$$Si(OH)_4 + 12{MoO_4}^{2-} + 24H^+ \rightarrow H_4Si(Mo_{12}O_{40}) + 12H_2O \quad (7)$$

This complex shows two reduction waves on glassy carbon (Fig. 2), platinum and gold. The voltammograms for the solution containing the molybdosilicate complex show the two well formed reduction peaks at about 350 mV and 240 mV and the two well formed oxidation peaks at 400 mV and 290 mV (versus Ag/AgCl). A linear correlation of the four peak intensities versus silicate concentration is observed between 0.3 and 145 μmol L^{-1} [28]. Silver is unusable because of its reaction with chloride in seawater. Moreover it has been reported that the Keggion anion passivates the Ag surface towards solution redox events [24]. For commodity reasons all our experiments were made on glassy carbon electrode but they could have been made on platinum or gold materials. We chose to use a glassy carbon electrode to be able to compare results with the previous studies [28]. Moreover measurements on other materials need more investigations on the protocols of preparation of the surface electrodes in order to obtain reliable and repeatable results.

The response of molybdate on glassy carbon electrode is shown in Fig. 3 by consecutive linear sweep voltammograms at 50 mV/s. The first peak at about −200 mV appears to be due to the oxygen reduction. The molybdate reduction is characterized by the second peak at −410 mV. It increases with the number of scans if the electrode is not polished, while after polishing the voltammogram recovers its first appearance. This gradual increase of the peak intensity could be due to a molybdate polymerization at the electrode surface, doubling the number of electrons involved during the reduction [31].

At ambient temperature the complex is totally formed in less than 6 min. The very slow scan rate voltammogram (5 mV/s) with glassy carbon rotating disk electrode (1000 rpm) in Fig. 4 presents

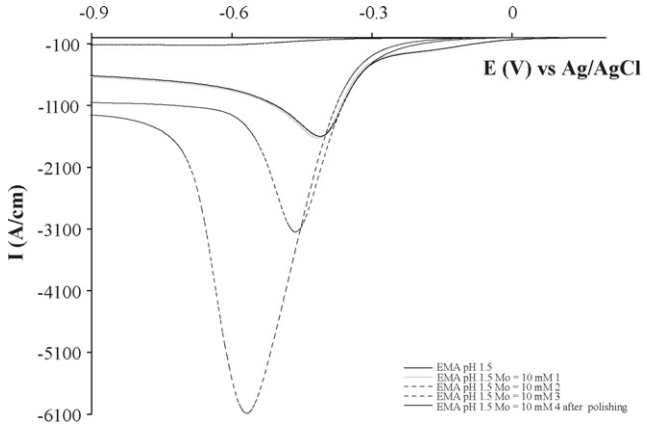

Fig. 3. Linear sweep voltammograms on glassy carbon electrode at 50 mV/s and pH 1.5: first, second and third consecutive voltammograms in seawater + sodium molybdate at 10 mmol L^{-1} and voltammogram in seawater + sodium molybdate at 10 mmol L^{-1} after polishing of the electrode.

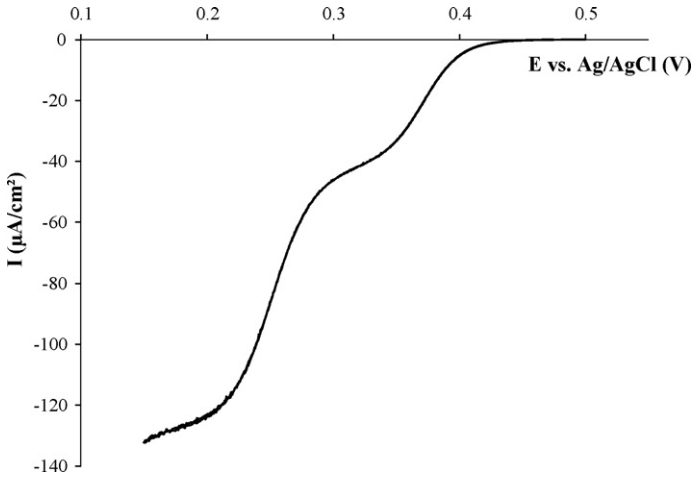

Fig. 4. Steady state voltammogram (5 mV/s) with glassy carbon rotating disk electrode (1000 rpm) in artificial seawater, 100 µmol L^{-1} of $Si(OH)_4$, sodium molybdate = 10 mmol L^{-1}, pH 1.5.

two reduction waves with half-wave potentials at 335 mV for the first reduction and 246 mV for the second reduction.

This stationary state voltammogram shows that the first reaction involves two electrons and the second reaction involves three electrons, in agreement with previous studies [22]. Thus, the first reduction is the reduction of molybdenum (VI) in molybdenum (IV) and the second reaction is the reduction of molybdenum (IV) in molybdenum (I). Moreover the forward scan is similar to the backward scan indicating the absence of absorption and of chemical reaction of the complex during the time of the experiment.

Intensity potential curves obey the law described by Eq. (8) indicating the irreversibility of the electron transfer [32]:

$$E = \frac{RT}{\alpha nF} \ln \frac{I_0}{I_{\lim}} + \frac{RT}{\alpha nF} \ln \frac{I_{\lim} - I}{I} \quad (8)$$

where R is the gas constant (8.314 J mol^{-1} K^{-1}), T is the absolute temperature (Kelvin), F is the Faraday constant, α is the transfer coefficient, I_0 is the exchange current, and $I_{\lim}$ is the limiting current.

We can deduce from Eq. (8) the two cathodic transfer coefficients (α) to characterize the reaction rate. From the linearization of the curves a α_{1c} coefficient equal of 0.5 is determined for reduction 1 and α_{2c} = 0.8 for reduction 2. Typical values of α are between 0.3 and 0.7 [32]. The high value of the transfer coefficient of α_{2c} means that during the second reduction the electrons are transferred faster than normally.

3.3. Temperature effect on the complexation rate

As we developed this new method in order to build a new *in situ* sensor it is extremely important to know the impacts of temperature on the analytical response. In the different applications of the future sensor and particularly in the environmental applications temperature can vary from 0 °C to more than 25 °C. In the field of oceanography temperature measurement is a key parameter. The complexation process is expected to be strongly dependent on temperature. Its influence on the kinetics of molybdosilicate complexation (from 1.4 to 24.8 °C) was quantified by measuring the intensity current of the first reduction peak as a function of time (Fig. 5a). The rate constant is calculated by Eq. (9):

$$\ln\left(\frac{I_\infty}{I_\infty - I}\right) = kt \quad (9)$$

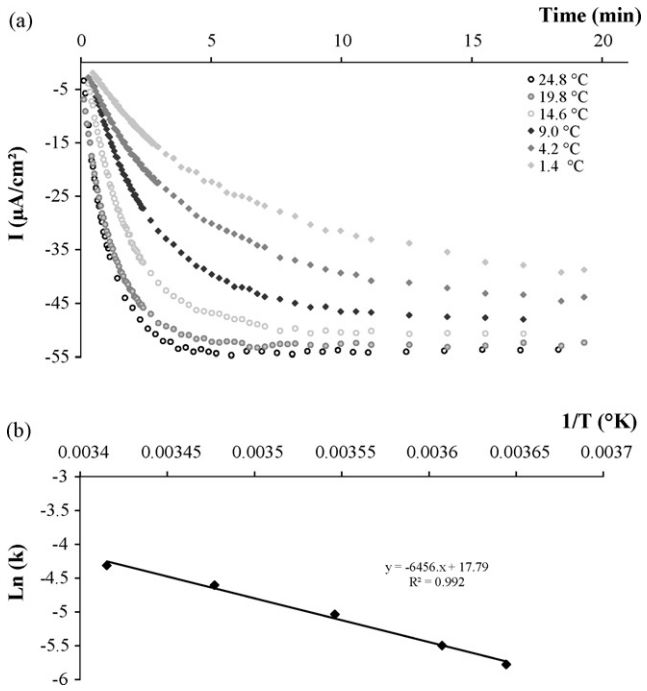

Fig. 5. (a) Kinetics of molybdosilicate complexation at different temperatures (1.4, 4.2, 9.0, 14.6, 19.8 and 24.8 °C) by measuring the intensity current of the first reduction peak as a function of time, $Si(OH)_4$ = 170 µmol L^{-1}, sodium molybdate = 10 mmol L^{-1}, pH 1.5; (b) Ln (k) = f(1/T (K)) corresponding plot to calculate the activation energy E_A.

where t is the time (s), I_∞ is the current at $t \to \infty$ (A), I is the current (A) and k is the rate constant (s^{-1}).

We thus determined the rate constant k as a function of temperature (Fig. 5b). According to the Arrhenius equation, an activation energy of about 54 kJ mol^{-1} was defined for the complexation reaction at pH 1.5 from the slope of the plot represented in Fig. 5b. This value will be useful to estimate the temperature sensitivity for a future silicate sensor.

3.4. Amperometric response

The working electrode held at a potential of 200 mV to avoid its deterioration presents a linear response with silicate concentration (molybdate concentration of 10 mmol L^{-1} at pH 1.5). This response is presented in Fig. 6 with the working glassy carbon disk electrode rotating at 1000 rpm.

Previous studies have dealt with phosphate interferences and have suggested a method based on the differences of kinetics for the complexes formation [23,28]. The molybdophosphate has a very fast response while molybdosilicate takes longer to be formed.

This method presents the advantage to be very fast and easy to handle. A simple sensor could be adapted from this simple method.

3.5. Molybdenum oxidation

As the aim of this study was to develop an autonomous method we investigated the different ways to produce the silicomolybdic complex without reagent. We have first studied the molybdenum oxidation in different aqueous solutions (H_2SO_4 0.5 mol L^{-1}, NaOH 0.5 mol L^{-1}, H_2SO_4 0.5 mol L^{-1} + NaCl 30 g L^{-1} and artificial seawater). The intensity potential curves are shown in Fig. 7a. The anodic branches of the Tafel plots (Fig. 7b) can be described by Eq. (10) [32]:

$$\ln j = \ln j_0 + \alpha nFR^{-1}T^{-1}\eta \quad (10)$$

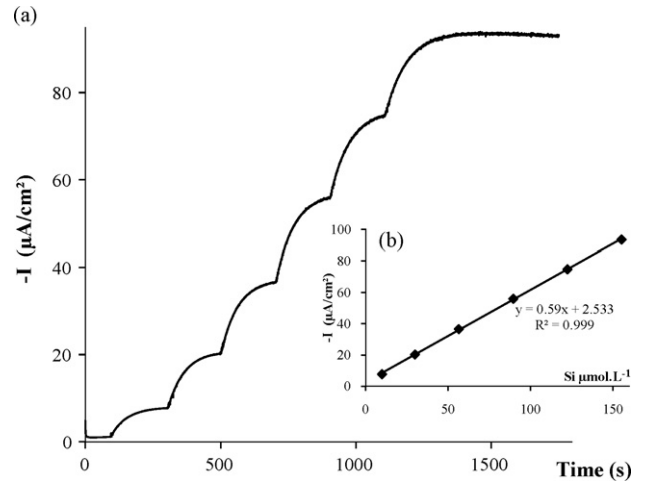

Fig. 6. (a) Chrono-amperometric measurements at a glassy carbon rotating disk electrode (at 200 mV) for different silicate concentrations (10, 30, 56, 90, 122 and 155 µmol L^{-1}), sodium molybdate = 10 mmol L^{-1}, pH 1.5 and (b) corresponding calibration plot.

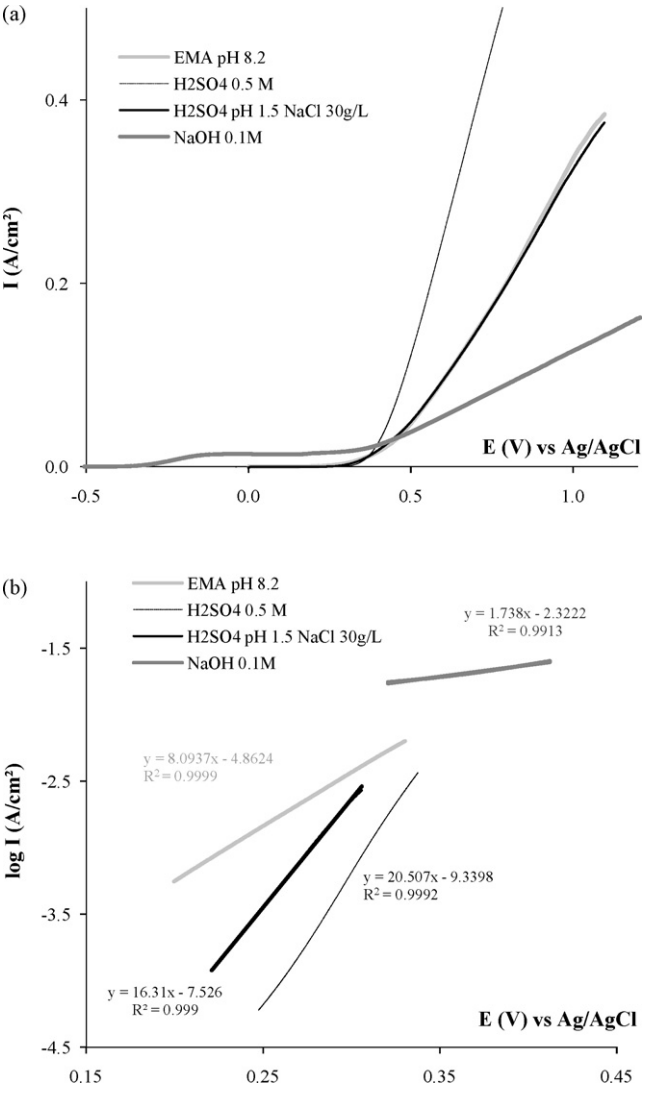

Fig. 7. (a) Linear sweep voltammograms (1 mV/s) for molybdenum oxidation in artificial seawater at pH 8.2, sulphuric acid 0.5 mol L^{-1}, sodium chloride 30 g L^{-1} in sulphuric acid at pH 1.5 and sodium hydroxide 0.5 mol L^{-1}; (b) corresponding Tafel plots.

where j is the current density (A cm^{-2}), j_0 is the exchange current density (A cm^{-2}), α is the anodic transfer coefficient, η is the overpotential (V), F is the Faraday constant (C mol^{-1}), n is the number of electrons and R is the molar gas constant (J mol^{-1} K^{-1}).

The electrochemical oxidation of the molybdenum wire has been studied in alkaline and acidic media by Hull [33]. In both media the mechanism of the anodic dissolution proceeds through the formation of Mo(III) at low overvoltages and Mo(V) at higher values.

Impedance measurements of the anodic behaviour of Mo in alkaline media have been performed by Armstrong et al. [34] and showed that each new type of film had a valence state between III and VI. Bojinov et al. [35,36] then investigated the transpassivity of molybdenum in H_2SO_4 solution. The polarization curves of molybdenum in H_2SO_4 0.5 mol L^{-1} can be divided in three regions: the first Tafel region where the logarithm of the current varies linearly with potential E; the transition region where a pronounced curvature is observed in the log i-E curves and the second Tafel region (above 0 V) where the current increases slowly with the potential [35]. The Tafel plot slope is 20.5 and the exchange current density is $10^{-9.3}$ A cm^{-2}. It is assumed that, at open circuit, the Mo is almost completely covered with Mo(III) species (either a chemisorbed layer or a thin oxide-hydroxide film) which is oxidized to Mo(IV). At small positive overpotentials there is a continuous increase in the formal coverage of Mo(IV). At potentials of −0.2 V and above, further oxidation of Mo(IV) to Mo(V) begins. At potentials close to −0.1 V, the coverage of Mo(V) reaches a maximum to form Mo (VI) in solution [35–37]. Molybdate in aqueous acidic solution is in equilibrium with hepta-molybdate and octa-molybdate according to Eqs. (11) and (12). It was found that the dominant species was MoO_4^{2-} in the pH range 7–12 and the protonated species were $Mo_7O_{24}^{6-}$ and $Mo_8O_{26}^{4-}$ in the pH range 3–5 and below pH 2, respectively [31,38,39].

$$7MoO_4^{2-} + 8H^+ \leftrightarrow Mo_7O_{24}^{6-} + 4H_2O \quad (11)$$

$$8MoO_4^{2-} + 12H^+ \leftrightarrow Mo_8O_{26}^{6-} + 6H_2O \quad (12)$$

In alkaline media the anodic waves correspond to the formation of molybdenum (III), (IV) and (VI), oxide or hydroxide species. The Tafel plot slope is 1.7 and the exchange current density is $10^{-2.3}$ A cm^{-2}. In artificial seawater we determined the Tafel plot slope at 8.1 and the exchange current density at $10^{-4.9}$ A cm^{-2}. It is of the same order of magnitude than those obtained for molybdenum oxidation in several media [38,40]. Using Eq. (10) we determine the factor $\alpha \cdot n$, equal to 0.63. Molybdenum oxidation in acidic media and sodium chloride 30 g L^{-1} is very similar to molybdenum oxidation in artificial seawater.

3.6. Semi-autonomous silicate method

A semi-autonomous method for silicate detection has been developed based on the electrochemical anodic oxidation of molybdenum, the complexation of the oxidation product with silicate and the detection of the complex by cyclic voltammetry. Molybdate is produced in a small electrochemical cell with the addition of sulphuric acid to pH 1.5. The quantity of molybdate formed is then controlled by a constant current intensity of 50 mA imposed to the molybdenum electrode. The theoretical charge necessary to form molybdate in large excess is given by the Faraday law (Eq. (13)). Different oxidation times were used measuring the kinetics of the reaction and the molybdenum oxidation of 420 s corresponding to a concentration of 7.3 mM presented a higher limiting current (2.5 µA).

$$Q = nFVC = It \quad (13)$$

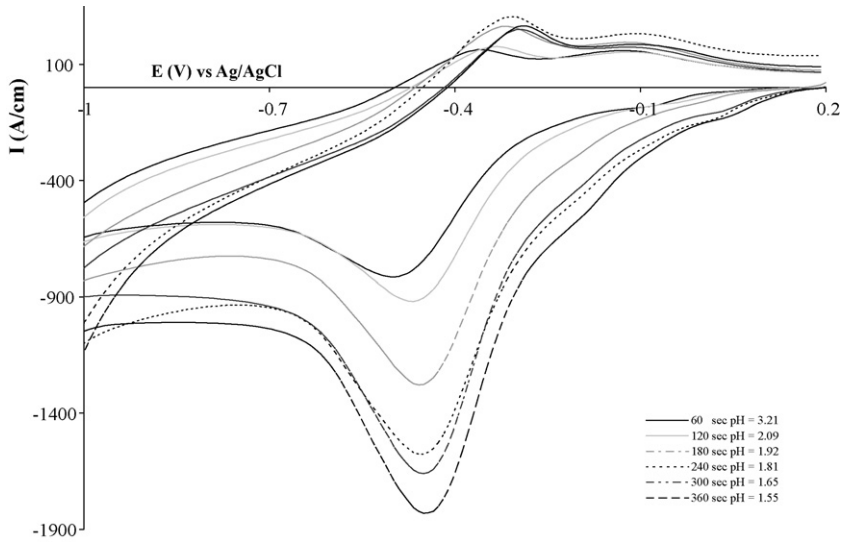

Fig. 8. Monitoring of pH and molybdenum oxidation versus time during the reagentless method: voltammograms obtained in the reaction cell (near the anode) at 200 mV/s on glassy carbon electrode at several time intervals of Mo oxidation.

where Q is the electricity quantity (Coulombs), V is the volume (cm^3), C is the molybdate concentration ($mol\,cm^{-3}$), I is the intensity (A) and t is the time (s).

This method was tested and compared with the classical colorimetric one on real marine samples during the ANT XXIII/3 cruise across Drake Passage (January–February 2006). The detection limit is 1 $\mu mol\,L^{-1}$ and the deviation between both methods is less than 3% for concentrations higher than 10 $\mu mol\,L^{-1}$ [28]. Typical vertical profile (depth versus silicate concentration) obtained in Drake Passage, demonstrates that our electrochemical method is in good agreement with the spectrophotometric flux injection analysis conventionally used for seawater silicate analysis [28].

3.7. Reagentless method

The semi-autonomous method was required to acidify the solution to a pH of about 1.5. The molybdenum oxidation liberates protons in the reaction cell (Eq. (6)) and provides an alternative solution to the addition of acid [28]. To prevent the subsequent reduction of the proton formed at the cathode, the anode was separated from the cathode by a polyethylene diaphragm. The pH obtained in the anode cell (1.5) after 360 s of oxidation was close to the theoretical pH (1.1) calculated using Eqs. (6) and (13) while in the cathode cell it was of about 10.6. The molybdosilicate complexation after 360 s of molybdenum oxidation is completely formed within 15 min at 19 °C. Reproducibility tests show a precision of 2.6% for a concentration of 100 $\mu mol\,L^{-1}$ [28]. Fig. 8 shows the evolution of the molybdate peaks in the reaction cell as a function of the molybdenum oxidation time and pH. In the negative currents, the first peak is due to the oxygen reduction (at about −100 mV) while the second (−500 mV) is the molybdate reduction, consistently with previous studies [31]. The increase of the peak intensity is clearly only due to the increase of the molybdate concentration.

4. Conclusions

The electrochemical study of molybdenum oxidation and complexation by silicate ions in several aqueous solutions enabled us to build a semi-autonomous method for silicate detection using voltammetry. This new method that was only required to acidify the sample to pH 1.5 was tested on seawater samples during the Drake ANTIII/3 cruise and compared with the classical spectrophotometric flux analysis. This electrochemical method is in good agreement with the method conventionally used for environmental water silicate analysis. In this article, we have also presented an upgraded method which is completely reagentless. This latter method using molybdate and protons produced during molybdenum oxidation should be very useful for developing a new reagentless sensor suitable for measurements in several environments where the use of reagent such as sulphuric acid is dangerous or impossible. This new method needs about 12 min to be completed but the time can be easily shortened to about 7 min by the reduction of the volume of the measurement cell or the increase of the intensity of the molybdenum. The limit of detection is less than 1 $\mu mol\,L^{-1}$ with the oxidation of molybdenum, thus this value is high compared to the colorimetric method (about 0.04 $\mu mol\,L^{-1}$) [41]. But this detection limit is about 0.3 $\mu mol\,L^{-1}$ without oxidation thus this limit can be reduced with a better optimization of the oxidation step [28]. As the detection is fast and easy we can consider a sensor with several measurement cells in parallel with various detection electrodes to reduce the time of analysis in the laboratory or to increase the time resolution of the *in situ* measurement. One of the main advantages of this method compared to the classical spectrophotometric measurements is of course the absence of reagent reducing the weight, the size and increasing the autonomy of the future sensor. The power required is also reduced by using an electrochemical detection without reagent (and thus without pumps). Comparing with the *in situ* spectrophotometric analyzers that already exist [3–6] the size of the future sensor will be considerably reduced (less than 3 kg). This sensor will be easily adaptable on different platforms (particularly moorings, gliders or floats in the oceanographic field) and the low cost of the analysis will allow the multiplication of the sensors to increase the spatial resolution of silicate data. Electrochemistry will provide a small sensor suitable for long term *in situ* deployments (on oceanic biogeochemical observatories or in process imposing no human intervention, for instance).

Acknowledgments

We are grateful to Hélène Durliat from the Laboratoire de Génie Chimique (UMR 5503, University Paul Sabatier) for her very useful

contribution. We thank the officers, scientists and crew of Drake ANT XXIII/3 cruise aboard R/V FS Polarstern for their invaluable assistance in the collection of data set and particularly Christine Provost the cruise Principal Investigator. M. L. was supported by a PhD grant from CNRS and IFREMER.

References

[1] A. Aminot, R. Kérouel, Hydrologie des systèmes marins. paramètres et analyses, Ifremer, Plouzané, 2004, p. 336.
[2] V.W. Truesdale, C.J. Smith, Analyst 101 (1976) 19.
[3] R. Vuillemin, D. Thouron, G. Gallou, L. Pares, B. Brient, A. Dubreule, V. Garçon, Sea Technol. 40 (1999) 75.
[4] D. Thouron, R. Vuillemin, X. Philippon, A. Lourenco, C. Provost, A. Cruzado, V. Garçon, Anal. Chem. 75 (2003) 2601.
[5] T. Gamo, H. Sakai, E. Nakayama, K. Ishida, H. Kimoto, Anal. Sci. 10 (1994) 843.
[6] K.S. Johnson, C.L. Beehler, C.M. Sakamoto-Arnold, Anal. Chim. Acta 179 (1986) 245.
[7] C. Neal, M. Neal, H. Wickham, Sci. Total Environ. 251–252 (2000) 511.
[8] B.M. Stewart, P.A.W. Elliott, Water Res. 30 (1996) 869.
[9] A. Youssef El-Sayed, Y.Z. Hussein, M.A. Mohammed, Analyst 126 (2001) 1810.
[10] M. Ikedo, M. Mori, K. Kazumasa, W. Hu, K. Tanaka, Anal. Sci. 22 (2006) 117.
[11] M. Yaqoob, A. Nabi, P.J. Worsfold, Anal. Chim. Acta 519 (2004) 137.
[12] A.V. Medvetskii, T.I. Tikhomirova, A.D. Smolenkov, E.N. Shapovalova, O.A. Shpigun, J. Anal. Chem. 62 (2007) 213.
[13] K. Abe, Y. Watanabe, J. Oceanogr. 48 (1992) 283.
[14] H. Li, F. Chen, J. Chromatogr. A 874 (2000) 143.
[15] A. Hioki, J. Lam, J. McLaren, Anal. Chem. 69 (1997) 21.
[16] W. Er-Kang, W. Meng-Xia, Anal. Chim. Acta 144 (1982) 147.
[17] A.G. Fogg, N.K. Bsebsu, B.J. Birch, Talanta 28 (1981) 473.
[18] K. Matsunaga, I. Kudo, M. Yanada, K. Hasebe, Anal. Chim. Acta 185 (1986) 355.
[19] S.M. Harden, W.K. Nonidez, Anal. Chem. 56 (1984) 2218.
[20] J.C. Quintana, L. Idrissi, G. Palleschi, P. Albertano, A. Amine, M. El Rhazi, D. Moscone, Talanta 63 (2004) 567.
[21] S. Cosnier, C. Gondran, J. Watelet, W. De Giovani, R. Furriel, F. Leone, Anal. Chem. 70 (1998) 3952.
[22] N.G. Carpenter, A.W.E. Hodgson, D. Pletcher, Electroanalysis 9 (1997) 1311.
[23] A.W.E. Hodgson, D. Pletcher, Electroanalysis 10 (1998) 321.
[24] L. Lee, A.A. Gewirth, J. Electroanal. Chem. 522 (2002) 11.
[25] P. Sharma, K. Gehlot, S. Songara, Rev. Anal. Chem. 25 (2006) 140.
[26] G.W. Luther, T.F. Rozan, M. Taillefert, D.B. Nuzzio, C. Di Meo, T.M. Shank, R.A. Lutz, S.C. Cary, Nature 410 (2001) 813.
[27] M. Tercier-Waeber, F. Confalonieri, G. Riccardi, A. Sina, S. Noel, J. Buffle, F. Graziottin, Mar. Chem. 97 (2005) 216.
[28] M. Lacombe, V. Garçon, M. Comtat, L. Oriol, J. Sudre, D. Thouron, N. LeBris, C. Provost, Mar. Chem. 106 (2007) 489.
[29] P. Le Corre, P. Tréguer, Contribution à l'étude de la matière organique dissoute et des sels nutritifs dans l'eau de mer. Caractéristiques physiques du Golfe de Gascogne et des upwellings côtiers de l'Afrique du Nord Ouest, Université de Bretagne Occidentale, Brest, 1976, p. 490.
[30] L. I. Gordon, J C. Jennings, A A. Ross, J M. Krest, WOCE Method Manual, Office Report, 1993, pp. 68–91.
[31] C.V. Krishnan, M. Garnett, B. Hsiao, B. Chu, Int. J. Electrochem. Sci. 2 (2007) 29.
[32] A.J. Bard, L.R. Faulkner, Electrochemical Methods: Fundamentals and Applications, second ed, Wiley J. and Sons, New York, 2001, p. 833.
[33] M.N. Hull, J. Electroanal. Chem. 38 (1972) 143.
[34] R. Armstrong, M. Bell, A.A. Metcalfe, J. Electroanal. Chem. 84 (1977) 61.
[35] M. Bojinov, I. Betova, R. Raicheff, J. Electroanal. Chem. 381 (1995) 123.
[36] M. Bojinov, I. Betova, R. Raicheff, Electrochim. Acta 41 (1996) 1173.
[37] M. Itagaki, T. Suzuki, K. Watanabe, Electrochim. Acta 42 (1997) 1081.
[38] K. Wang, L. Ying-Sing, P. He, Electrochim. Acta 43 (1998) 2459.
[39] J.J. Cruywagen, J.B.B. Heyns, Inorg. Chem. 26 (1987) 2569.
[40] L. De Rosa, C.R. Tomachuk, J. Springer, D.B. Mitton, S. Saiello, F. Bellucci, Mater. Corros. 55 (2004) 602.
[41] A. Aminot, R. Kérouel, Dosage automatique des nutriments dans les eaux marines, Ifremer, Plouzané, 2007, p. 188.

Talanta 77 (2008) 546–550

Contents lists available at ScienceDirect

Talanta

journal homepage: www.elsevier.com/locate/talanta

Determining Cr(III) and Cr(VI) in urine using a flow injection on-line sorption separation system coupled with electrothermal atomic absorption spectrometry and a UV/nano-Au/TiO_2 photocatalysis reduction device

Cheng-Fa Lee[a], Bai-Hsiun Chen[b], Yeou-Lih Huang[a,c,d,*]

[a] Graduate Institute of Medicine, Kaohsiung Medical University, Kaohsiung, Taiwan
[b] Faculty of Medicine, Kaohsiung Medical University, Kaohsiung, Taiwan
[c] Center of Excellence for Environmental Medicine, Kaohsiung Medical University, Kaohsiung, Taiwan
[d] Faculty of Biomedical Laboratory Science, Kaohsiung Medical University, No. 100, Shih-Chuan 1st Road, Kaohsiung, Taiwan

ARTICLE INFO

Article history:
Received 7 October 2007
Received in revised form 11 March 2008
Accepted 17 March 2008
Available online 25 March 2008

Keywords:
Cr(III)
Cr(VI)
Flow injection
ETAAS
Nano-Au/TiO_2
Photocatalysis

ABSTRACT

In this study, an on-line nano-Au/TiO_2 photocatalysis reduction device coupled with flow injection electrothermal atomic absorption spectrometry was developed for chromium speciation in urine samples. The nano-Au/TiO_2 photocatalysis reduction device comprised a UV lamp and a Tygon tube coated with nanocrystalline Au/TiO_2 films. The process of chromium speciation in urine was based on the adsorption of Cr(III) and Cr(VI) on this photocatalysis reduction device. The absorbed Cr(VI) was photoreduced to Cr(III), and Cr(III) was eluted using 1 M formic acid. Suitable conditions for adsorption, photoreduction, elution, and subsequent ETAAS determination of the levels of Cr(III) and Cr(VI) were established. The detection limits for Cr(III) and Cr(VI) using this analytical method were 0.08 and 0.13 ng mL^{-1}, respectively. This intra- and inter-assay precisions (relative standard deviation) for the analyses of 1 μg L^{-1} Cr(III) and 3.0 μg L^{-1} Cr(VI) were less than 10%. When urine samples were spiked at levels of 1 μg L^{-1} Cr(III) and 2 μg L^{-1} Cr(VI), the analyzed recoveries were 98.3–96.0%, respectively ($n = 3$). We applied this method to the determination of Cr(III) and Cr(VI) in urine samples of human volunteers before and after supplementing their diet with chromium picolinate.

1. Introduction

Trivalent chromium(III) is an essential trace element for maintaining glucose, cholesterol, and fatty acid metabolism [1]; its toxicity is relatively low. Hexavalent chromium(VI), however, is a carcinogenic and mutagenic agent that can inflict many health problems, including allergic contact dermatitis and other immunomodulatory diseases [1]. Therefore, living organisms usually reduce Cr(VI) in vivo to Cr(III) to decrease its toxicity [2]. In recent years, large quantities of chromium compounds have been used in industrial processes, leading to serious occupational problems and hazards to human health [3]. Owing to the different toxicities of Cr(III) and Cr(VI), the distinction of chromium species is an essential aspect of understanding their diverse biological effects. Therefore, for speciation analysis in biomedicinal studies, the determination of redox Cr(VI)/Cr(III) species is a very important process.

Chromium species are excreted mainly by the kidneys and can be detected in the urine. Although much research has been undertaken on the speciation of chromium in environmental samples, only a few methods have been reported for the speciation of chromium in urine samples [4–7]. A supported liquid membrane approach has been described based on the adsorption of urinary Cr(VI) on a membrane and subsequent determination of its concentration using adsorptive stripping voltammetry [4]. Spectrophotometric methods have been reported [5,6] based on the reaction of Cr species with 1,5-diphenylcarbazide to determine the levels of Cr(VI) in urine samples. In addition, Cr(III) can be separated and determined using gas chromatography [7]. These analytical methods can be used to determine concentration of only a single chromium species, Cr(III) or Cr(VI), in urine.

To obtain the levels of both Cr(III) and Cr(VI) in a urine sample in a single test, it is necessary to use powerful, sensitive, and highly selective techniques. The most widely used approaches toward the separation of trace elements involve chromatography [8], liquid–liquid extraction [9], and solid phase extraction [10]. Chromatography and spectrometry can usually be coupled on-line for various analytical purposes. For metal speciation using electrothermal atomic absorption spectroscopy (ETAAS), a highly sensitive discrete atomization technique, might be limited to off-line coupling methods because the discontinuous nature of ETAAS

* Corresponding author. Tel.: +886 7 312 1101x2251; fax: +886 7 311 3449.
E-mail address: yelihu@kmu.edu.tw (Y.-L. Huang).

0039-9140/$ – see front matter © 2008 Elsevier B.V. All rights reserved.
doi:10.1016/j.talanta.2008.03.018

makes it troublesome when used in combination with continuous flow systems [11]; i.e., it is not easy for the continuous monitoring of chromatographic eluents. Difficulties encountered in the direct coupling of flow injection on-line to ETAAS are due to the discrete non-flow-through nature of ETAAS and the limited sample volume capacity of the graphite tube [12].

Titanium dioxide is an ideal model adsorbent for studies of the relationship between the surface charge and the degree of adsorption [13]. TiO_2 is widely studied because of its high chemical stability and insolubility in acidic and alkaline solutions; these features, together with its point of zero charge being located in the middle of the pH scale, make it possible to study adsorption events on both positively and negatively charged TiO_2 surfaces over a broad range of pH and ionic strength [13]. In addition, TiO_2 displays strong adsorption behavior toward heavy metal ions over a wide range of values of pH. In recent years, nanocrystalline TiO_2 has become a promising material for adsorbing, preconcentrating, and separating heavy metal ions, such as arsenic [14,15], chromium [16,17], and selenium [18], which are readily adsorbed from solution onto the particles' surfaces at various values of pH.

Titanium dioxide receives most of its attention because of its photocatalytic activity, high stability under irradiation with light, and environmental friendly characteristics [19]. TiO_2 photocatalysis is a technique that is employed for the photodegradation of inorganic and organic compounds. TiO_2 photocatalytic redox processes for the oxidation or reduction of pollutants upon irradiation with light is a particularly clean analytical method. It proceeds without the need for additional reagents, and the structurally simple products of the process are usually nontoxic. For the photoreduction of heavy metals, TiO_2 is usually utilized in one of two forms: particles suspended in aqueous solution or as thin films immobilized on substrates [20]. The use of TiO_2 thin films immobilized on substrates can alleviate the problems associated with slurry-based photocatalytic systems [20].

The aim of this study was to develop an analytical method for the determination and speciation of Cr(III) and Cr(VI) ions in urine samples. Our analytical method was based on the use of a UV/nano Au/TiO_2 photocatalysis reaction device on-line coupled with an ETAAS system. We studied the effects of several conditions on the adsorption and UV photocatalysis, including the pH, flow rate, and concentration of formic acid.

2. Experimental

2.1. Reagents

The ultrapure water (>18 MΩ) used throughout this study was prepared using a deionized water system (Milli-Q, Millipore). Stock solutions (1000 mg L^{-1}) of Cr(III) and Cr(VI) were purchased from Merck, as were formic acid (Suprapur grade), sodium hydroxide (Suprapur grade), and trisodium citrate (ACS grade). Hydrochloric acid (Actual analysis grade) and ammonium hydroxide (Ultrapure grade) were purchased from J.T. Baker. Sodium borohydride (≧95%) was purchased from Riedel–de Haën. Tetrachloroauric acid trihydrate (ACS grade) was purchased from Sigma. P25 TiO_2 nanoparticles were purchased from Degussa.

2.2. Preparation of immobilized nanocrystalline TiO_2

Nano-Au/TiO_2 films can be prepared by coating support substrates with a TiO_2 solution using sol–gel methods [21,22]. The Au nanoparticle colloid was prepared by placing deionized H_2O (18.5 mL), 1.0×10^{-2} M aqueous $HAuCl_4$ trihydrate solution (0.5 mL), and 0.01 M aqueous sodium citrate solution (0.5 mL) in a clean Erlenmeyer flask, stirring for 5 min, and then adding 0.1 M aqueous $NaBH_4$ solution (0.5 mL). The solution color changed from yellow to orange [23]. This colloid was injected into Tygon tubing for 1 h, at which point 15% P25 TiO_2 colloid (pH 5.5) mixture was injected into the tubing for 1 h. Finally, the Tygon tubing was inoculated for 48 h at 50 °C.

2.3. Apparatus

Fig. 1 presents a schematic illustration of the on-line nano-Au/TiO_2 photoreduction device/FI-ETAAS system for the separation and determination of Cr(III) and Cr(VI) in urine. The nano-Au/TiO_2 photocatalysis device comprised a UV lamp and a Tygon tube internally coated with a film of nanocrystalline Au and TiO_2. The photocatalysis device was connected to seven-and six-port injection valves (Omnifit Smart Actuator, Cambridge, UK). A ten-port valve was connected to the six-port valve through PTFE tubing. A microdialysis pump (CMA, CMA/100) was connected to the seven-port valve through PTFE tubing to control the pH of the samples. The volume of formic acid was controlled using a sample loop (0.5 mm i.d., 10 cm length) on a ten-port valve (Omnifit Smart Actuator, Cambridge, UK). An atomic absorption spectrometer (PerkinElmer, model 5100 PC) was equipped with a transversally heated graphite atomizer, a chromium hollow cathode lamp, and an AS-70 furnace autosampler. The signals for chromium were corrected through Zeeman-effect background correction. The graphite furnace temperature/time program for the determination of Cr(III) and Cr(VI) ions in the eluate is summarized in Table 1. A personal computer running Microsoft Excel 2003 software was used for statistical data collection. Statistical analyses of the results were performed using pair-*T*-tests with JMP Statistic Discovery software (v. 4, SAS Institute, USA). Statistical significance was assigned at $p < 0.05$.

2.4. Procedure

Each urine sample (100 mL) was first adjusted to pH 3 using concentrated HCl solution. The urine sample was then diluted with an aqueous solution having a pH of 3 (also prepared using concentration HCl). Finally, the pH of the diluted urine sample was rechecked using a pH meter. A portion (2 mL) of the diluted sample was injected into the on-line system. The Cr(VI) ions in the solution were first adsorbed onto the surface of the nanocrystalline Au/TiO_2 films and the outflow sample collected in store tubing. The adsorbed Cr(VI) ions were transformed into Cr(III) species through

Table 1
Temperature program for the determination of Cr in 1 M formic acid

Step	Temperature (°C)	Ramp time (s)	Hold time (s)	Argon flow rate (mL min^{-1})	Read
Preheating	110	5	10	250	
Drying	130	10	30	250	
Pyrolysis	700	10	20	250	
Atomization	2500	0	5	0	On
Cleaning	2600	1	3	250	

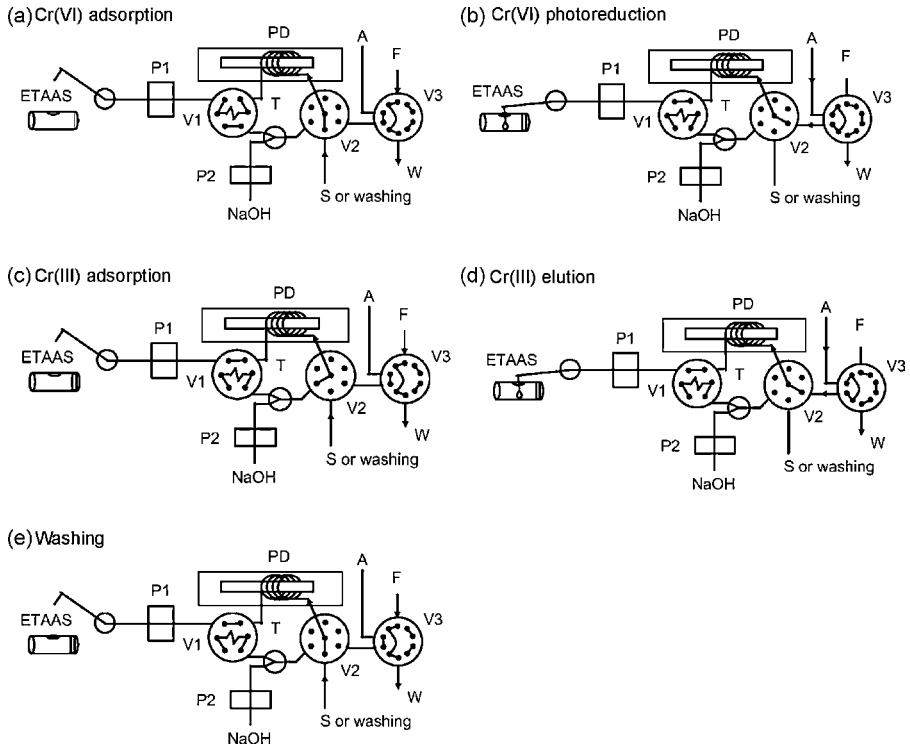

Fig. 1. Schematic illustration of the UV/nano-Au/TiO_2-FI-ETAAS on-line system. ETAAS, electrothermal atomic absorption spectrometer; P1, peristaltic pump; V1, six-port valve; P2, microdialysis pump; T, micro-tee; PD, nano-Au/TiO_2 photocatalysis reduction device; V2, seven-port valve; S, sample; A, air; F, formic acid; V3, ten-port valve; W, waste. (a) Cr(VI) adsorption; (b) Cr(VI) photoreduction; (c) Cr(III) adsorption; (d) Cr(III) elution; (e) washing.

photoreduction with 1 M formic acid (pH 1.75) under UV irradiation. The Cr(III) ions obtained were introduced directly into the graphite tube. The pH of the outflow was adjusted to greater than 9 through on-line mixing with a NaOH solution (0.03 mL min^{-1}). The alkaline sample was again injected into the tube containing the nanocrystalline Au/TiO_2 film. The Cr(III) ions in the outflow were adsorbed onto the surface of the TiO_2 film. The HCOOH solution was then used to elute the adsorbed Cr(III) ions from the surface of a TiO_2 film. The eluate was once again introduced into the graphite tube using the same procedure as that employed for Cr(VI) detection.

2.5. Urine sample collection

Five healthy, adult volunteers participated in this study. Two sets of 24 h worth of urine samples were collected from each volunteer on day 1 (non-supplemented diet) and on last day of study (after supplementing their diet with 1000 mg of chromium picolinate for 1 week [24]). The pH of urine samples was adjusted to 3 using HCl and then the samples were stored at −40 °C prior to analysis.

3. Results and discussion

3.1. Adsorption of Cr(III) and Cr(VI)

Yang and Lee [25] reported the characteristic forms of chromium in aqueous solution. The Cr(III) and Cr(VI) ions exist in different forms at different values of pH. At values of pH less than 4.5, Cr(VI) exists in the form of the $HCrO_4^-$ ion, which gradually transforms to the CrO_4^{2-} ion upon increasing the pH. Under strongly acidic conditions (pH <3), Cr(III) exists mainly as free ions; upon increasing the pH, Cr(III) is gradually transformed into $Cr(OH)^{2+}$, $Cr(OH)_2^+$, $Cr(OH)_3$, $Cr_2(OH)_2^{4+}$, and $Cr_3(OH)_4^{5+}$ ions [26].

Fig. 2 displays the effect of the pH on the adsorption of Cr(III) and Cr(VI) individually on the tubing-immobilized nanocrystalline TiO_2. Sample solutions were adjusted to values of pH in the range 1–12 using 1 M HCl or 1 M ammonia solutions. The percentage adsorption was calculated based on the difference between the amounts of Cr in the original sample and in the solution exiting the photoreduction device. Fig. 2 indicates that the pH is an important factor controlling the adsorption of Cr(III) and Cr(VI) species. The adsorption efficiency of Cr(VI) decreased upon increasing the pH; its maximum adsorption occurred at pH 3.0. The degree of adsorption of Cr(III) at pH 3 was minimal. Thus, to separate Cr(III) from Cr(VI), we selected a pH of 3.0 for our subsequent studies.

We found that the properties of the tubing coated with the nano-Au/TiO_2 film also affected the adsorption of Cr(VI). A smaller

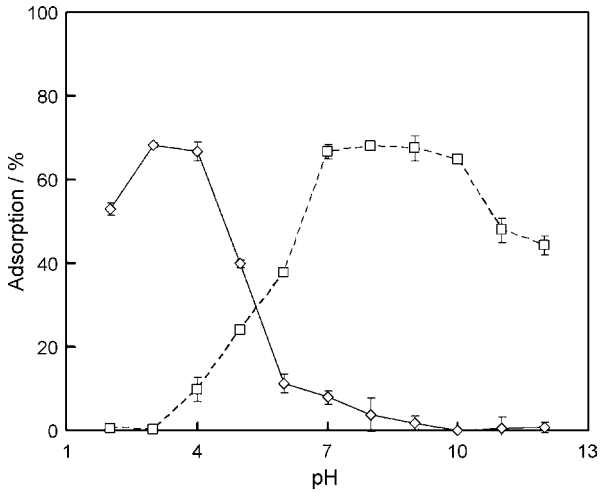

Fig. 2. Effect of pH on the adsorption of Cr(III) (□) and Cr(VI) (◊) on a TiO_2 film. Initial concentration of chromium: 50 ng mL^{-1}; flow rate of adsorption: 0.5 mL min^{-1}.

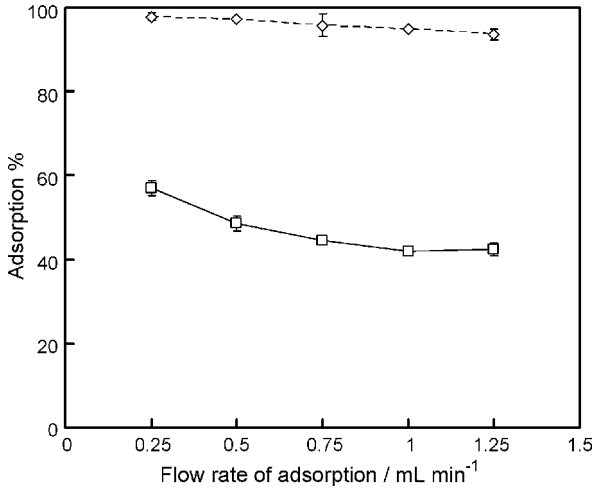

Fig. 3. Effect of flow rate on the adsorption of Cr(III) (□) and Cr(VI) (◊) on a nano-Au/TiO_2 photoreduction device. Initial concentration of chromium: 10 ng mL^{-1}; for Cr(III), pH 10; for Cr(VI), pH 3.

inner diameter improved the adsorption efficiency of Cr(VI) at the same flow rate. We monitored a series of tubes (50–300 cm long) to investigate the effect of the tubing length on the adsorption of Cr(VI). The adsorption efficiency of Cr(VI) increased upon increasing the length to 300 cm, at which point the Cr(VI) ions were almost completely adsorbed onto the nano-Au/TiO_2 film. The adsorption flow rate was also a factor affecting the efficiency of Cr(III) and Cr(VI) adsorption. Fig. 3 indicates that near-quantitative retention (>95%) occurred for Cr(VI) ions when this flow rate was less than 0.5 mL min^{-1}. Thus, we selected this flow rate for our subsequent investigations. The retention efficiency of 98.5 ± 2.5% for Cr(VI) on the inner surface of the tubing was observed.

3.2. Photoreduction efficiency

Ku et al. [27] and Lee et al. [28] previously reported that the pH of Cr(VI) solutions plays a role in the photocatalytic reduction of chromium in aqueous solution. The rate of reduction increases upon decreasing the solution pH. Our experimental results indicate that the rate of reduction at pH 3 increased upon increasing

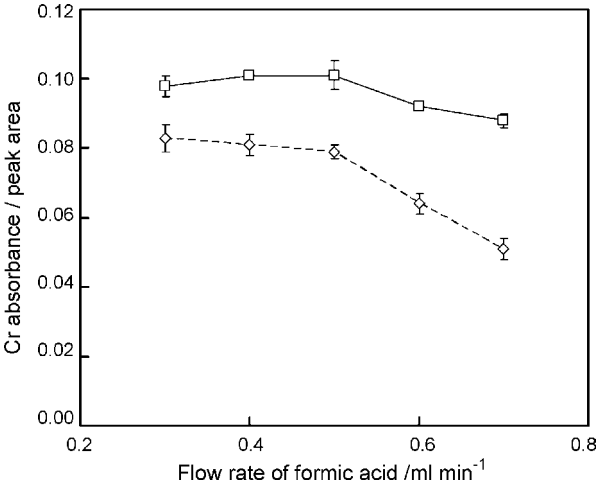

Fig. 4. Effect of formic acid flow rate on the elution of Cr(III) (□) and photoreduction of Cr(VI) (◊) on a nano-Au/TiO_2 photoreduction device. Initial concentration of chromium: 2 ng mL^{-1}.

Table 2
Analytical performance of the nano-Au/TiO_2 photocatalysis reduction device/FI-ETAAS system

	Cr(III)	Cr(VI)
Calibration curve		
Linear range (μg L^{-1})	0.25–2.00	0.50–6.00
Slope	0.1079	0.0341
Correlation coefficient (r^2)	0.9974	0.9979
Detection limit (μg L^{-1}) (n = 7)	0.08	0.13
Precision		
Intra-assay (R.S.D., %)	4.0	6.2
Inter-assay (R.S.D., %)	4.0	5.2
Recovery (n = 3, %)	98.3	96.0
Enrichment factor	7.1	4.6

the concentration of formic acid up to 1 M. The pH of the formic acid solution also plays an important role in the photoreduction of Cr(VI). When we decreased the pH from 3.0 to 1.75, the rate of reduction of Cr(VI) in the presence of 1 M formic acid increased. The flow rate of formic acid was also a factor affecting the efficiency of Cr(III) elution and Cr(VI) photoreduction. The photoreduction efficiency of 99.3 ± 2.0% for Cr(VI) retained on the inner surface of the tubing was found. Fig. 4 indicates that the signals of Cr(III) increased in intensity when we decreased the flow rate of formic acid to 0.5 mL min^{-1}. The effect of the flow rate of formic acid on Cr(VI) photoreduction was similar to that for Cr(III) elution.

3.3. Optimization of pyrolysis and atomization temperature

The influence of the pyrolysis temperature and matrix modifier on the ETAAS signals of 10 μg L^{-1} Cr(III) in 1.0 M aqueous formic acid solution was studied to remove the matrix and retain the Cr in the graphite tube of the atomiser. We varied the atomization temperature from 1900 to 2500 °C. The signals for chromium had good absorbance intensity when the atomization temperature was 2500 °C without using any chemical modifier. The signals for Cr had the maximum absorbance and minimum background signals when the ashing temperature was 700 °C. When the pyrolysis time was greater than 15 s, the signal for Cr was most intense, but it did not change much until the pyrolysis time reached 25 s. Table 1 lists the optimized temperature program.

3.4. Analytical performance

The responses of the on-line system were linear over the ranges from 0.25 to 2.00 μg L^{-1} Cr(III) and 0.50 to 6.00 μg L^{-1} Cr(VI), with correlation coefficients of the calibration curves for Cr(III) and Cr(VI) both being greater than 0.995. According to the definition provided by IUPAC, the detection limits for the on-line separation of the Cr(III) and Cr(VI) species were 0.08 and 0.13 μg L^{-1}, respectively. The intra- (n = 7) and inter-assay (n = 5) precisions for Cr(III) and Cr(VI) determination of 1 μg L^{-1} Cr(III) and 3 μg L^{-1} Cr(VI) standard solutions with this analytical method were both less than 10%. In urine samples analyzed at spiked levels of 1 μg L^{-1} Cr(III) and 2 μg L^{-1} Cr(VI), the recoveries were 98.3–96.0%, respectively. The enrichment factor, calculated as the ratio of slopes of the calibration curves obtained with and without preconcentration, is 7.1 for Cr(III) and 4.6 for Cr(VI), respectively. Thus, this on-line analytical method provides valid data with regard to their accuracy and repeatability, suggesting that it should be suitable for the determination of Cr(III) and Cr(VI) in samples of human urine. Table 2 summarizes the results of analytical merit.

Table 3
Urinary Cr(III) and Cr(VI) levels at baseline and after 1 week of dietary supplementation with chromium picolinate

Urine sample	Baseline		Chromium picolinate supplementation	
	Cr(III) ($\mu g\,L^{-1}$)	Cr(VI) ($\mu g\,L^{-1}$)	Cr(III) ($\mu g\,L^{-1}$)	Cr(VI) ($\mu g\,L^{-1}$)
M1	0.39 ± 0.06	0.94 ± 0.23	1.75 ± 0.13	2.51 ± 0.14
M2	0.57 ± 0.12	0.39 ± 0.19	1.76 ± 0.18	1.64 ± 0.14
M3	0.15 ± 0.03	0.52 ± 0.14	1.17 ± 0.13	1.35 ± 0.20
M4	0.53 ± 0.05	0.50 ± 0.14	1.21 ± 0.10	2.19 ± 0.15
M5	0.37 ± 0.03	0.81 ± 0.10	0.43 ± 0.04	1.59 ± 0.04

Note: Significant difference ($p < 0.05$) in the levels of both Cr(III) and Cr(VI) was observed for all the five volunteers before and after supplementing with chromium picolinate.

3.5. Determination of Cr(III) and Cr(VI) in urine samples

Chromium picolinate is a widely used nutritional supplement for patients with diabetes mellitus and has demonstrated beneficial effects [24]. We used our analytical method to detect the concentrations of Cr(III) and Cr(VI) in urine samples collected from volunteers before and after they had supplemented their diets with chromium picolinate for 7 days. As indicated in Table 3, the levels of urinary Cr(III) and Cr(VI) were significantly higher in the urine samples obtained after the volunteers had consumed the chromium picolinate supplement.

4. Conclusions

In this study, we developed a nano-Au/TiO_2 photocatalysis reduction device on-line coupled with an ETAAS system using a flow injection device. The determination of Cr(III) and Cr(VI) ions in this system was based on nano-Au/TiO_2 photocatalytic reduction. We applied this developed method successfully to the determination of Cr(III) and Cr(VI) species in urine samples; the precision and accuracy of the method were both satisfactory. We then used this method to quantify the levels of Cr(III) and Cr(VI) in the urine samples of volunteers who had consumer supplemental chromium picolinate for 7 days.

Acknowledgment

We thank the National Science Council of the Republic of China for financial support (grant NSC 95-2113-M-037-020-MY3).

References

[1] D.G. Barceloux, Clin. Toxicol. 37 (1999) 173.
[2] J.M. LaVelle, Environ. Health Perspect. 92 (1991) 127.
[3] F.H. Chang, S.L. Wang, Y.L. Huang, M.H. Tsai, S.T. Yu, L.W. Chang, J. Expo. Sci. Environ. Epidemiol. 16 (2005) 138.
[4] L. Soko, E. Cukrowska, L. Chimuka, Anal. Chim. Acta 474 (2002) 59.
[5] B.D. Paul, A. Jacobs, J. Anal. Toxicol. 29 (2005) 658.
[6] B.D. Paul, K.K. Martin, J. Maguilo Jr., M.L. Smith, J. Anal. Toxicol. 24 (2000) 233.
[7] T.R. Ryan, C.R. Hastings, J. Chromatogr. 130 (1977) 346.
[8] W.C. Tseng, M.H. Yang, T.P. Chen, Y.L. Huang, Analyst 127 (2002) 560.
[9] M.D.L. de Castro, L. Gámiz-Gracia, Anal. Chim. Acta 351 (1999) 23.
[10] C. Yu, Q. Cai, Z.X. Guo, Z. Yang, S.B. Khoo, J. Anal. At. Spectrom. 19 (2004) 410.
[11] Y. Li, Y. Jiang, X.P. Yan, Anal. Chem. 78 (2006) 6115.
[12] W.C. Tseng, Y.C. Sun, M.H. Yang, T.P. Chen, T.H. Lin, Y.L. Huang, J. Anal. At. Spectrom. 18 (2003) 38.
[13] H. Tel, Y. Altas, M.S. Taner, J. Hazard. Mater. B 112 (2004) 225.
[14] R.K. Dutta, A.K. Ray, V.K. Sharma, F.J. Millero, J. Colloid Interface Sci. 278 (2004) 270.
[15] T. Balaji, H. Matsunaga, Anal. Sci. 18 (2002) 1345.
[16] E. Vassileva, K. Hadjiivanov, T. Stoychev, C. Daiev, Analyst 125 (2000) 693.
[17] P. Liang, T. Shi, H. Lu, Z. Jiang, B. Hu, Spectrochim. Acta B 58 (2003) 1709.
[18] S. Li, N. Deng, Anal. Bioanal. Chem. 374 (2002) 1341.
[19] S. Turprakay, W. Liengcharernsit, J. Hazard. Mater. B 124 (2005) 53.
[20] J. Cen, X. Li, M. He, S. Zheng, M. Feng, Chemosphere 62 (2006) 810.
[21] N.J. Peill, M.R. Hoffmann, Environ. Sci. Technol. 29 (1995) 2974.
[22] A. Mills, S.K. Lee, A. Lepre, J. Photochem. Photobiol. A: Chem. 155 (2003) 199.
[23] S.O. Obare, R.E. Hollowell, C.J. Murphy, Langmuir 18 (2002) 10407.
[24] C.L. Broadhurst, P. Domenico, Diab. Technol. Ther. 8 (2006) 677.
[25] J.K. Yang, S.M. Lee, Chemophere 63 (2006) 1677.
[26] J.C. Yu, X.J. Wu, Z.L. Chen, Anal. Chim. Acta 436 (2001) 59.
[27] Y. Ku, I.L. Jung, Water Res. 35 (2001) 135.
[28] S.M. Lee, T.W. Lee, B.J. Choi, J.K. Yang, J. Environ. Sci. Health A 38 (2003) 2219.

Talanta 77 (2008) 833–838

Contents lists available at ScienceDirect

Talanta

journal homepage: www.elsevier.com/locate/talanta

Covalent immobilization of single-walled carbon nanotubes and single-stranded deoxyribonucleic acid nanocomposites on glassy carbon electrode: Preparation, characterization, and applications

Yongxin Li[a,b,*], Po Wang[a], Feng Li[b], Xue Huang[a], Lun Wang[a], Xiangqin Lin[c]

[a] College of Chemistry and Materials Science, Anhui Normal University, Wuhu 241000, China
[b] Department of Chemistry, Kansas State University, 111 Willard Hall, Manhattan, KS 66506, USA
[c] Department of Chemistry, University of Science and Technology of China, Hefei, Anhui 230026, China

ARTICLE INFO

Article history:
Received 29 April 2008
Received in revised form 17 July 2008
Accepted 19 July 2008
Available online 29 July 2008

Keywords:
Single-walled carbon nanotubes
Single-stranded deoxyribonucleic acid
Covalent immobilization
Glassy carbon electrode

ABSTRACT

Single-stranded deoxyribonucleic acid (ssDNA)-wrapped single-walled carbon nanotubes (SWNTs) were modified on the surface of glassy carbon electrode (GCE) by covalent modification technique. Field emission scanning electron microscope (FE-SEM), X-ray photoelectron spectrum (XPS), electrochemical impedance spectroscopy (EIS), and cyclic voltammetric (CV) were used to characterize the properties of this modified electrode. The results showed that SWNTs–ssDNA composites were successfully immobilized onto the surface of GCE. Moreover, this modified electrode exhibited high stability, largely active areas, and efficiently electrocatalytic activities. It had been used for the analysis of various biomolecules, such as dopamine (DA), uric acid (UA), and ascorbic acid (AA), and the results were satisfactory.

1. Introduction

Carbon nanotubes (CNTs) represent an important group of nanomaterials with unique properties such as high electrochemically accessible area, good electronic conductance and strong mechanical property, which make them extensively applicable in electrochemistry as biosensors [1–4]. Traditionally, some common methods, such as solution-casting [5,6], layer-by-layer technique [7,8], and sol–gel technique [9] were developed for the immobilization of CNTs onto the surface of electrodes. But it must be pointed out that some problems, such as instability and irreproducibility, were often appeared when using above methods. Recently, covalent modification [10] and screen-printed [11,12] techniques were used for immobilization of CNTs to improve the stability of modified electrode.

Deoxyribonucleic acid (DNA), which is a well-known natural biocompatible macromolecule, has now gained more attention in the various biotechnology fields, such as biosensor, bioimplant, and so forth [13,14]. DNA's unique properties have inspired many people to combine this macromolecule with single-wall carbon nanotubes (SWNTs) to explore its applications, such as covalent conjugation of DNA to oxidized SWNTs for self-assembled molecular-scale electronic systems [15], noncovalent binding of DNA to side walls of SWNTs for dispersion and separation of SWNTs [16], and DNA/SWNTs-templated for the programmed assembly of materials [17]. Zheng et al. have found that DNA single strands with specific base sequences have a very strong tendency to wrap around SWNTs, and thus can help to disperse SWNTs in aqueous solutions under sonication [16,18]. This finding has encouraged researchers to further find new properties and applications for these DNA-wrapped carbon nanotubes [19,20]. Our previous studies [21,22] showed that DNA also was a conductive molecule. It could be covalently immobilized on the surface of carbon materials, and be used as biosensors for real applications.

In this work, we fabricated the nanocomposites of ssDNA and SWNTs, and then immobilized this composite onto the surface of glassy carbon electrode (GCE) by use of electrochemical deposition (Scheme 1). In comparision with previously modified methods [5,6,23], the obvious advantage of this proposed method was that the modified electrode was very stable, and it could remain undamaged even after being dipped into an aqueous solution for more than 14 days. Meanwhile, the ssDNA/SWNTs nanocomposites greatly enhanced the active areas of GCE, and strongly exhibited electrocatalytic activities towards some biomolecules, such as dopamine

* Corresponding author at: College of Chemistry and Materials Science, Anhui Normal University, Wuhu 241000, China. Tel.: +1 785 317 6521; fax: +1 785 532 6666.
E-mail addresses: yongli@mail.ahnu.edu.cn, liyongxin@hotmail.com (Y. Li).

0039-9140/$ – see front matter © 2008 Elsevier B.V. All rights reserved.
doi:10.1016/j.talanta.2008.07.034

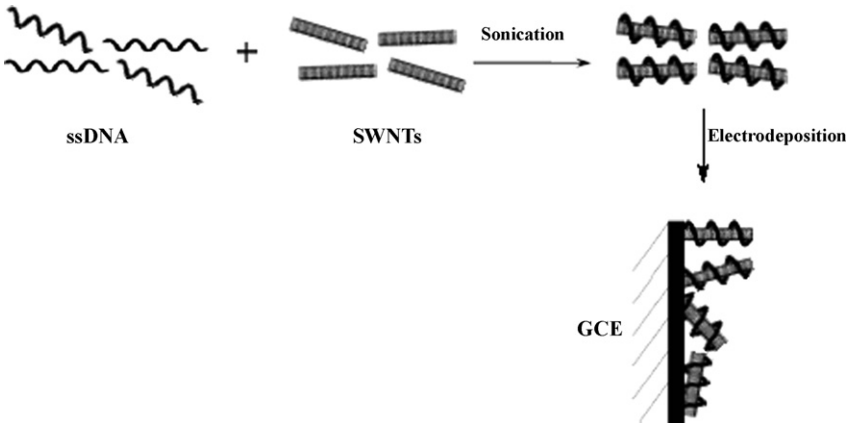

Scheme 1. The fabrication process of ssDNA–SWNTs modified GCE. First, ssDNA was mixed with SWNTs to form ssDNA–SWNTs hybrid, and then, the ssDNA–SWNTs hybrids were covalently deposited onto a glassy carbon electrode to form a uniform film.

(DA), uric acid (UA), and ascorbic acid (AA). So, this proposed modified electrode could be used to detect these target analytes sensitively.

2. Experimental

2.1. Chemicals

Single-stranded DNA with sequence $d(GT)_{15}$ was purchased from Integrated DNA Technologies, Inc. (Coralville, IA). Single-walled carbon nanotubes used in this work were purchased from Nanoport Co. Ltd. (Shenzhen, China). Dopamine hydrochloride (DA) was obtained from Sigma (USA). Ascorbic acid (AA) and uric acid (UA) were obtained from Shanghai Chemical Co. Ltd. (Shanghai, China). Potassium ferricyanide (A.R., $K_3Fe(CN)_6$) was obtained from Alfa Products. All other reagents used were of analytical grade. Phosphate-buffered saline (PBS; 0.1 mol L^{-1}) solutions of different pH were prepared by mixing four stock solutions of 0.1 mol L^{-1} H_3PO_4, KH_2PO_4, K_2HPO_4 and K_3PO_4.

All aqueous solutions were prepared in doubly distilled, deionized water. High purity nitrogen was used for deaeration.

2.2. Apparatus

Electrochemical experiments such as cyclic voltammetry (CV), electrochemical impedance spectroscopy (EIS), and differential pulse voltammetry (DPV) were performed on CHI 660A workstation (ChenHua Instruments Co., Shanghai, China) with a conventional three-electrode system, which consisted of a saturated calomel electrode (SCE), a Pt foil auxiliary electrode, and a testing electrode. All potentials were reported *vs* SCE unless stated otherwise. Solutions in the electrochemical cell were deaerated by N_2 bubbling before experiments and kept under a N_2 atmosphere during experiments.

Field emission scanning electron microscope (FE-SEM) images were obtained on a S-4800 field emission scanning electron microanalyser (Hitachi, Japan)

X-ray photoelectron spectroscopy (XPS) was performed on ESCALAB MKII spectrometer (VG Co., UK).

2.3. Preparation of ssDNA-wrapped SWNTs

Before use, samples of the SWNT undergo to various chemical–physical purification procedures [24]. In brief, the samples were purified by refluxing in HNO_3–H_2SO_4 (v/v, 1:1) mixture for 2 h at 55 °C and then for 3 h at 80 °C, washed with redistilled water and dried under vacuum.

Dispersion of SWNTs by ssDNA was carried out by use of the method described by Zheng et al. [16,18]. 1 mg of SWNTs was suspended in 1 mL aqueous ssDNA solution (1.0 mg mL^{-1} in 0.1 mol L^{-1} NaCl), and the mixture was sonicated at a power of about 4 W using a cup-horn sonicator (JinTan Instrument Co. Ltd., China). The sample was kept in an ice-water bath for 60 min during sonication. The oligonucleotide with a sequence of $d(GT)_{15}$ has a very high tendency to wrap around carbon nanotubes [16,18], and, therefore, can help them dissociate from bundled ropes under the action of sonication.

2.4. Electrochemical deposition of ssDNA-wrapped SWNTs

The deposition of ssDNA-wrapped SWNTs onto GCE was carried out according to previous report [21,22]. A freshly cleaned GCE was immersed in above obtained ssDNA/SWNTs solution, and performed by applying +1.8 V for 15 min, and the obtained electrode was described as ssDNA/SWNTs/GCE.

For the sake of comparison, a ssDNA/GCE and a SWNTs-modified GCE (solution-casting method [5,6], and denoted as SWNTs/GCE) were also prepared under the same condition.

3. Results and discussion

3.1. Characterizations of ssDNA-wrapped SWNTs modified GCE

Fig. 1a and b shows the typical FE-SEM images of SWNTs and ssDNA/SWNTs modified on the surface of GCE. It can be seen that both SWNTs and SWNTs/DNA could be dispersed uniformly on the surface of GCE. In comparison with SWNTs and SWNTs/DNA composites, it can be found that the diameter of SWNTs in Fig. 1b is much larger than that in Fig. 1a, which means that ssDNA is wrapped on the surface of SWNTs, and the diameter becomes much larger. Meanwhile, the existence of SWNTs in Fig. 1b means that some of the wrapped SWNTs may be covalently modified onto the surface of GCE, and form a kind of uniform nanocomposites. More evidences will be given in the following sections.

Impedance spectroscopy is an effective method for probing the features of a surface-modified electrode using the redox probe $Fe(CN)_6^{4-/3-}$ [25]. Fig. 2 illustrates the results of impedance spectroscopy on bare GCE (a), ssDNA/GCE (b) and ssDNA/SWNTs/GCE (c) in the presence of equivalent 10 mM $Fe(CN)_6^{4-/3-}$ + 0.1 M KCl, which are measured at the formal potential of $Fe(CN)_6^{4-/3-}$. It

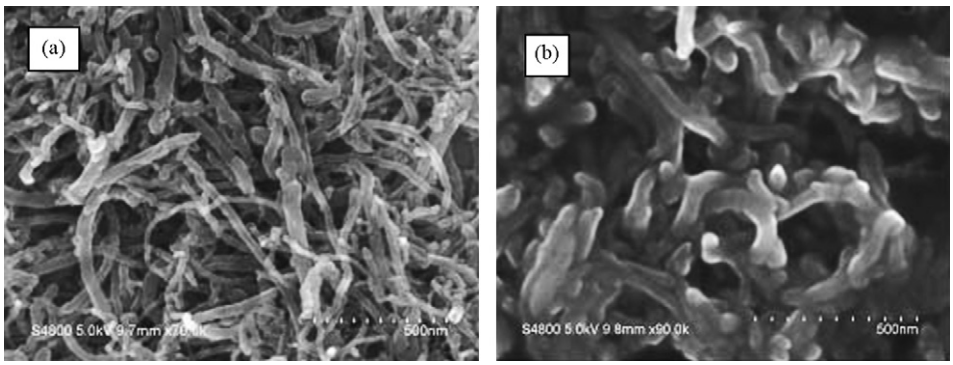

Fig. 1. FE-SEM images of SWNTs (a) and SWNTs/ssDNA (b) modified onto the surface of GCE.

can be seen at the bare GCE, a semicircle of about 230 Ω diameter with an almost straight tail line is present, implying very low electron transfer resistance to the redox-probe dissolved in the electrolyte solution. The diameter of the high frequency semicircle was significantly enlarged by the surface deposition of the DNA layer (b), an R_{ct} value of ~7850 Ω can be estimated, which indicates an increased resistance to the anion redox reaction at the ssDNA/GCE. However, the diameter of the high frequency semicircle was obviously reduced by the modification of composite of SWNTs and ssDNA on the surface of GCE (c), a charge transfer resistance value of ~2300 Ω can be estimated, which indicates a decreased resistance to the anion redox reaction at the ssDNA/SWNTs/GCE. This may be attributed to the well conductivity of SWNTs. The impedance change of the modification process indicated that the composite of SWNTs and ssDNA had been modified to the GCE surface. Meanwhile, from the cyclic voltammetry (CV) curves of $K_3Fe(CN)_6$ shown in Fig. 3 at bare GCE (a), ssDNA/GCE (b), and ssDNA/SWNTs/GCE (c), it can be observed that the peak current increased largely and the peak potential difference (ΔE_p) decreased at ssDNA/SWNTs/GCE. This result also proved that ssDNA and SWNTs had been immobilized onto the surface of GCE. For comparison, we also prepared ssDNA-wrapped SWNTs modified GCE using solution-casting method [5], and got its impedance spectroscopy (Fig. 2, curve d) and CV of $K_3Fe(CN)_6$ (Fig. 3, curve d). It could be found that the R_{ct} was smaller and peak current is larger than that obtained from ssDNA/SWNTs/GCE prepared by covalent modification method, which is agreed with the SEM image result (Fig. 1a).

XPS is a powerful tool to examine the elemental distribution on the electrode surfaces. To verify that ssDNA have been immobilized on the surface of GCE, an XPS experiment was performed, and the result is shown in Fig. 4. In Fig. 4a, the C, N, O, and P peaks were observed, showing the evidence that the DNA has been immobilized on the surface. Furthermore, Fig. 4b shows the deconvolution spectra of the C 1s spectrum, which indicate the presence of C–C (284.60 eV), C–O (286.00 eV), C═O (287.05 eV), and COOH (288.60 eV) surface functional groups. These oxygen containing groups are attributed to the anodic oxidation processes [26,27]. In addition, the high-resolution O 1s peak at 532.25 eV (Fig. 4c) indicates that a large amount of the surface oxygen was present in the form of C–O bonds most likely of a phenolic or hydroquinone type [28]. Although the phenolic-like groups are also present in the bases of the DNA, the strong O 1s peak suggests that the DNA molecules could be linked to the carbon surface by the C–O–C bonds.

On the other hand, it was possible that ssDNA could just be absorbed onto the surface of GCE at high positive potential, and no covalent bond was formed. But it was found that, after immersing the modified electrode into pH 14 NaOH solution for 10 min, the CV curves of $K_3Fe(CN)_6$ at the ssDNA/SWNTs/GCE had almost no change. This indicated that the DNA molecules deposited at +1.8 V were covalently bonded to the GCE surface, since any non-specifically adsorbed DNA molecules should be removed by NaOH, whereas only covalently bonded molecules should still remain immobilized [29]. And it also excluded a possibility of forming phosphate ester or carbonic ester which can be easily hydrolyzed in alkaline solution. In addition, the specific potential of +1.8 V was

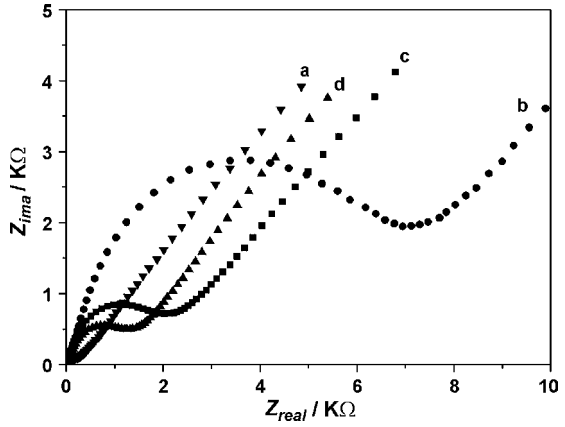

Fig. 2. Complex plane impedance plots in 10 mM $K_3[Fe(CN)_6]$:$K_4[Fe(CN)_6]$ (1:1) mixture containing 0.1 M KCl at bare GCE(a), ssDNA/GCE (b), ssDNA/SWNTs/GCE using covalent modification technique (c), and ssDNA/SWNTs/GCE using solution-casting technique (d), respectively.

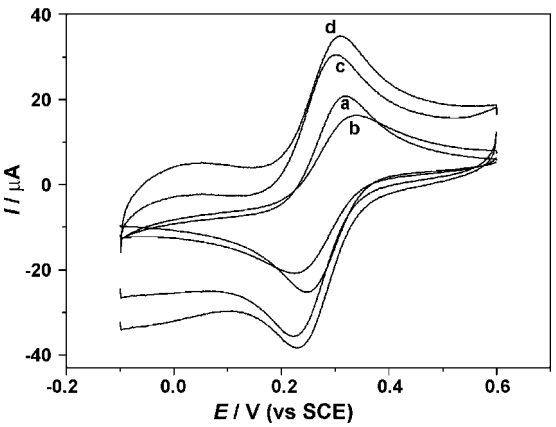

Fig. 3. Cyclic voltammograms of 5 mmol L^{-1} $K_3[Fe(CN)_6]$ + 0.1 mol L^{-1} KCl at bare GCE (a), ssDNA/GCE (b), ssDNA/SWNTs/GCE using covalent modification technique (c), and ssDNA/SWNTs/GCE using solution-casting technique (d), respectively. Scan rate: 50 mV s^{-1}.

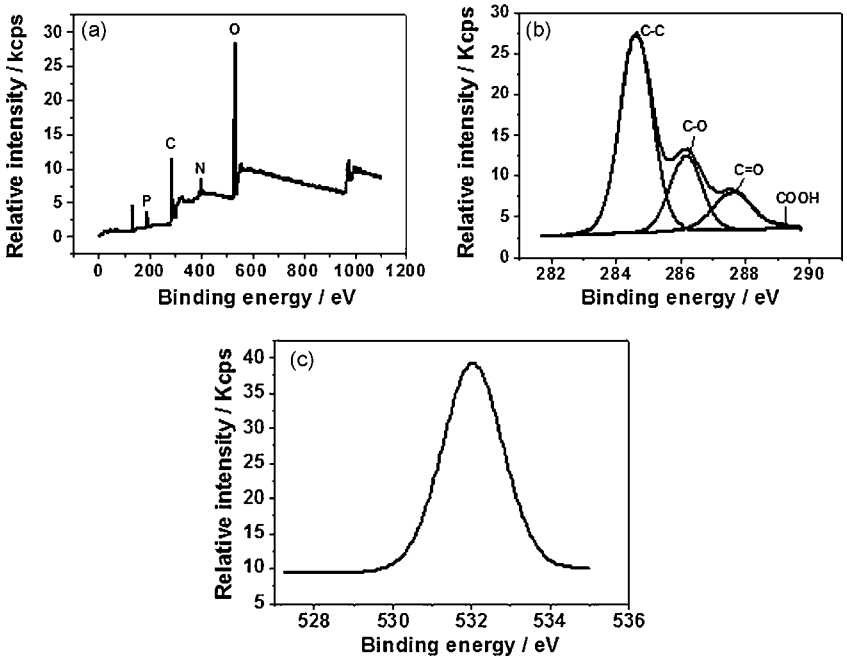

Fig. 4. XPS spectra of ssDNA/SWNTs/GCE prepared at 1.8 V (a), the deconvolution spectra of the C1s obtained at 1.8 V (b), and the high-resolution peak of O 1s obtained at 1.8 V (c).

characteristic for the surface oxidation of carbon electrodes to generate aromatic free radicals [30]. It is most probable that joining of the carbon electrode to the 3-OH of DNA through this linkage minimizes steric hindrances [31]. This covalent bonding ensured the conductive and stable immobilization of the DNA molecules on the surface.

3.2. The electrochemical applications of ssDNA/SWNTs/GCE

3.2.1. Electrochemical oxidation of DA, AA, and UA using ssDNA/SWNTs/GCE

To explore the potential applications of the ssDNA/SWNTs modified electrode in electrochemical detection, we chose dopamine (DA), ascorbic acid (AA), and uric acid (UA) to test its selectivity and sensitivity. Actually, these three molecules generally coexist in the extra cellular fluid of the central nervous system and serum, and their oxidation potentials are similar at most solid electrodes, which lead to the overlapped signals appeared when people try to detect these three compounds simultaneously.

Fig. 5 gives the results of voltammetric detection of DA, AA and UA by use of our proposed ssDNA/SWNTs/GCE in 0.1 mol L^{-1} PBS (pH 7.0). Peaks for AA, DA and UA can be clearly identified at 0.10, 0.28, and 0.41 V, respectively, with peak separation of 0.13 and 0.18 V (Fig. 5A, curve b), and these peak potential differences are large enough to detect these three compounds simultaneously. On the other hand, for bare GCE, it can be seen that the peaks are completely overlapped, and the peak current is much smaller (Fig. 5A, curve a).

We also try to analyse the mixed compounds containing DA, AA and UA using differential pulse voltammetry (DPV). Results showed that, for the determination of AA, the sensitivity is low due to the large background current of modified electrode though its CV oxidation peak can be separate completely from the oxidation peaks of DA and UA (Fig. 5A). So we just selected DA and UA to analyse the potential applications of this proposed method. The changes of peak current *vs* the concentration of DA can be distinguished, while the concentration of UA is kept constant, as shown in Fig. 5B. Similarly and obviously, as shown in Fig. 5C, keeping the concentrations of DA constant, the oxidation peak current of UA was positively proportional to its concentration. From above discussion, it can be obtained that the electrochemical response, for DA and UA oxidation at ssDNA/SWNTs/GCE, alone exists when they coexist in pH 7.0 PBS. Therefore, it is possible to simultaneously determine DA and UA in the same sample by use of the ssDNA–SWNTs modified GCE.

DPV curves obtained in PBS (pH 7.0) solution containing DA and UA, as shown in Fig. 5B and C, keeping the concentration of another compound constant. The catalytic peak current was linearly related to DA and UA concentration in the range 2.0×10^{-6} to 4.0×10^{-5} and 6.0×10^{-6} to 7.0×10^{-5} mol L^{-1}, with correlation coefficients of

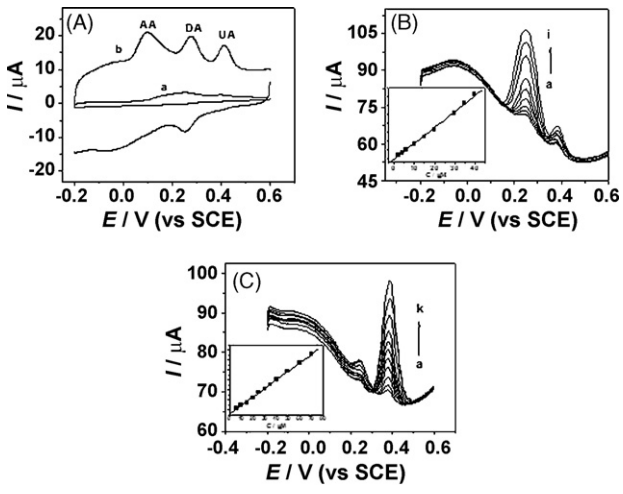

Fig. 5. (A) Cyclic voltammograms of bare GCE (a) and ssDNA/SWNTs/GCE (b) in PBS (pH 7.0) containing 0.05 mmol L^{-1} AA, 0.01 mmol L^{-1} DA, and 0.01 mmol L^{-1} UA. (B) DPVs of DA at ssDNA/SWNTs/GCE in the presence of 0.01 mmol L^{-1} UA in PBS (pH 7.0). DA concentrations (from a to k): 2, 4, 6, 10, 15, 20, 30, 35, and 40 μmol L^{-1}. Inset is the linear relationship between peak current and the concentration of DA. (C) DPVs of UA at ssDNA/SWNTs/GCE in the presence of 0.01 mmol L^{-1} DA in PBS (pH 7.0). UA concentrations (from a to k): 6, 10, 15, 20, 25, 30, 35, 40, 50, 60, and 70 μmol L^{-1}. Inset is the linear relationship between peak current and the concentration of UA.

Table 1
Determination results of DA in dopamine hydrochloride injections ($n = 5$)

Samples	Labeled (mg mL^{-1})	Found (mg mL^{-1})	R.S.D. (%)	Added (mg mL^{-1})	Found (mg mL^{-1})	Recovery (%)
1	10	10.08	2.2	2	12.04	98
2	10	9.81	3.1	2	11.75.	97
3	10	10.11	1.8	2	12.20	104

Table 2
Determination of UA in human urine samples ($n = 5$)

Urine samples	Detected (μmol L^{-1})	Added (μmol L^{-1})	Found (μmol L^{-1})	Recovery (%)
1	4.52	5.0	9.39	97.4
2	3.98	5.0	8.91	98.6
3	4.33	5.0	9.46	102.6
4	4.27	5.0	9.42	103.1

0.9985 and 0.9992, respectively. The corresponding detection limit (3δ) was 8.6×10^{-7} and 4.3×10^{-6} mol L^{-1}, respectively.

Under the optimum conditions, using the DPV mode, the relative standard deviation (R.S.D.) for nine successive determinations of 10 μM DA and 10 μM UA were 2.23% and 2.87%, respectively, indicating the excellent reproducibility of the present system.

The potential interfering effects from coexisting species were also studied. As demonstrated in the text, such an intrinsic property of the modified electrode could substantially differentiate AA, DA and UA. Therefore, the interference from AA can be neglected. Other influences from common coexisting substances were also investigated. It was found that no significant interference for the detection of 10 μM UA or DA was observed for these compounds: NaCl (600), CaCl2 (300), citric acid (800), glucose (200), urea (100), tryptophan (100), tyrosine (50) and cysteine (50), where the data in the brackets were the concentration ratios.

3.2.2. Effect of pH

In most case, the solution pH is an important influence factor to the electrochemical reaction. For UA determination, the pH effect on DPV signals at the ssDNA/SWNTs/GCE was examined. As shown in Fig. 6, it was observed that the peak potentials shifted towards positive direction with the decrease of pH. The relationship of E_{pa} and pH could be described by the following equation: E_{pa} (V) = 0.7324 − 0.0486 pH (r = 0.9952), which showed that the uptake of electrons is accompanied by a $2e^-/2H^+$ reaction. For the change of pH from 4.0 to 9.0, it can be seen that the peak current change slightly. So, pH 7.0 PBS was chosen as supporting electrolyte since it is close to the pH value of physiological condition.

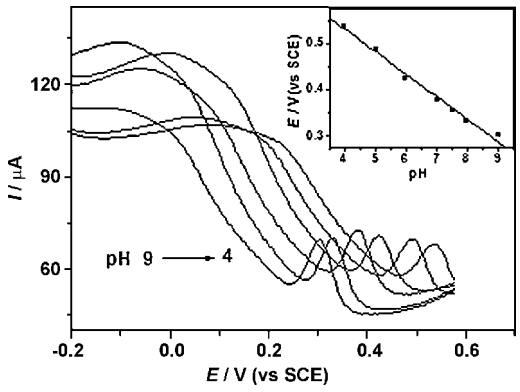

Fig. 6. DPVs of ssDNA/SWNTs/GCE in a 0.01 mmol L^{-1} UA in 0.1 mol L^{-1} PBS at different pH (4.0–9.0). Inset: the dependence of formal potential on pH at a scan rate of 0.05 V s^{-1}.

The effect of solution pH on the response of DA was also investigated in the range 4.0–9.0 (data not shown). The DPV peak potential of DA oxidation also shifted towards negative direction at a slope of 53.9 mV per pH unit, which is close to the anticipated Nernstian theoretical value of 59 mV. The linear regression equation was obtained as: E_{pa} (V) = 0.4791 − 0.0539 pH with the correlation coefficient 0.9978. Also, the peak current changes slightly with the change of pH. So, in order to mimic the physiological environment, pH 7.0 was still chosen in the following experiments.

3.2.3. Samples analysis

In order to check the possibility of this proposed method, we selected commercial dopamine hydrochloride injection solution and human urine samples for sample analysis, and the results are listed in Tables 1 and 2. It can be seen that the results are reasonable, and this method can be used for the detection of real samples.

3.3. Stability of ssDNA/SWNTs/GCE

The stability of the ssDNA/SWNTs/GCE was also examined by CV. The modified electrode was stored in pH 7.0 PBS all the time and CVs were performed after a period of storage time. The decrease of the peak current for DA was less than 2.0% after 8 h, and only 10% after two weeks, which demonstrated that ssDNA–SWNTs modified electrode was stable in buffer solution. Compared with other cast modification of CNTs [5,6,23], the stability is improve obviously by use of this covalently modified method.

4. Conclusions

In summary, the thoroughly dispersed SWNTs have been obtained by wrapping with ssDNA. For the first time, it is demonstrated that SWNTs-ssDNA composites can be covalently modified on the surface of GCE. The resulting nanocomposites show excellent properties. For example, the huge surface areas of the carbon nanotubes greatly increased the density of the functional groups accessible for sensitive detection of the target analyte. The stability of modified electrode was improved greatly. We believed this novel method can be applied extensively in chemistry and biochemistry in the future.

Acknowledgements

We thank Prof. Takashi Ito (Department of Chemistry, Kansas State University) for his suggestions. This work was supported financially by the Natural Science Foundation of Educational Department of Anhui Province (No. 2006kj039a), the National Natural Science Foundation of China (No. 20575001), and a Project for the Author of Excellent Teacher of Anhui Province.

References

[1] P.M. Ajayan, Chem. Rev. 99 (1999) 1787.
[2] G. Jin, F. Huang, W. Li, S. Yu, S. Zhang, J. Kong, Talanta 74 (2008) 815.
[3] A. Salimi, L. Miranzadeh, R. Hallaj, Talanta 75 (2008) 147.
[4] J. Xu, H. Zhang, G. Chen, Talanta 73 (2007) 932.
[5] Y. Liu, J. Lei, H. Ju, Talanta 74 (2008) 965.
[6] J. Wang, M. Li, Z. Shi, N. Li, Z. Gu, Anal. Chem. 74 (2002) 1993.
[7] C. Xiang, Y. Zou, L.X. Sun, F. Xu, Talanta 74 (2007) 206.
[8] G.A. Rivas, S.A. Miscoria, J. Desbrieres, G.D. Barrera, Talanta 71 (2007) 270.
[9] X. Kang, Z. Mai, X. Zou, P. Cai, J. Mo, Talanta 74 (2008) 879.
[10] Y. Li, P. Wang, L. Wang, X. Lin, Biosens. Boelectron. 22 (2007) 3120.
[11] P. Fanjul-Bolado, P. Queipo, P.J. Lamas-Ardisana, A. Costa-García, Talanta 74 (2007) 427.
[12] J.W. Shie, U. Yogeswaran, S.M. Chen, Talanta 74 (2008) 1659.
[13] J. Wang, M. Chicharro, G. Rivas, X. Cai, N. Dontha, P.A.M. Farias, H. Shiraishi, Anal. Chem. 68 (1996) 2251.
[14] C.S. Yun, G.A. Khitrov, D.E. Vergona, N.O. Reich, G.F. Strouse, J. Am. Chem. Soc. 124 (2002) 7644.
[15] H. Yanagi, H. Mukai, K. Ikuta, T. Shibutani, T. Kamikado, S. Yokoyama, S. Mashiko, Nanotechnology 13 (2002) 601.
[16] M. Zheng, A. Jagota, M.S. Strano, A.P. Santos, P. Barone, S.G. Chou, B.A. Diner, M.S. Dresselhaus, R.S. McLean, G.B. Onoa, G.G. Samsonidze, E.D. Semke, M. Usrey, D.J. Walls, Science 302 (2003) 1545.
[17] X. Han, Y. Li, Z. Deng, Adv. Mater. 19 (2007) 1518.
[18] M. Zheng, A. Jagota, E.D. Semke, B.A. Diner, R.S. Mclean, S.R. Lustig, R.E. Richardson, N.G. Tassi, Nat. Mater. 2 (2003) 338.
[19] C. Hu, Y. Zhang, G. Bao, Y. Zhang, M. Liu, Z.L. Wang, J. Phys. Chem. B 109 (2005) 20072.
[20] Y. Ma, S.R. Ali, A.S. Dodoo, H. He, J. Phys. Chem. B 110 (2006) 16359.
[21] X. Lin, X. Jiang, L. Lu, Biosens. Bioelectron. 20 (2005) 1709.
[22] L. Lu, S. Wang, X. Lin, Anal. Chim. Acta 519 (2004) 161.
[23] Y. Li, X. Lin, C. Jiang, Electroanalysis 18 (2006) 2085.
[24] F. Xiao, F. Zhao, J. Li, R. Yan, J. Yu, B. Zeng, Anal. Chim. Acta 596 (2007) 79.
[25] C. Saby, B. Ortiz, G.Y. Champagne, D. Belanger, Langmuir 13 (1997) 6805.
[26] P.L. Runnels, J.D. Joseph, M.J. Logman, R.M. Wightman, Anal. Chem. 71 (1999) 2782.
[27] T.E. Edmonds, Anal. Chim. Acta 175 (1985) 1.
[28] G.N. Kamau, W.S. Willis, J.F. Rusling, Anal. Chem. 57 (1985) 545.
[29] C.M.Y. Hellas, L.C. Hing, F.S. Sen, Y. Mengsu, Thin Solid Films 413 (2002) 218.
[30] L.J. Kepley, A.J. Bard, Anal. Chem. 60 (1988) 1459.
[31] H. Maeda, Y. Yamauchi, M. Hosoe, T.X. Li, E. Yamaguchi, M. Kasamatsu, H. Ohmori, Chem. Pharm. Bull. 42 (1994) 1870.

Talanta 77 (2008) 473–478

Contents lists available at ScienceDirect

Talanta

journal homepage: www.elsevier.com/locate/talanta

Flow sandwich immunoassay for specific anti-OVA IgG antibody by use of surface plasmon resonance sensor

Yan Li, Jujie Ren, Hizuru Nakajima, Byung Kyu Kim, Nobuaki Soh, Koji Nakano, Toshihiko Imato*

Department of Applied Chemistry, Graduate School of Engineering, Kyushu University, 744 Motooka, Nishi-Ku, Fukuoka 819-0395, Japan

ARTICLE INFO

Article history:
Received 30 September 2007
Accepted 10 March 2008
Available online 18 March 2008

Keywords:
Surface plasmon resonance sensor
Flow immunoassay
Allergy diagnosis
Ovalbumin

ABSTRACT

A simple and sensitive method for the determination of a specific IgG antibody against ovalbumin (anti-OVA IgG antibody) for diagnosis of egg allergy by use of a surface plasmon resonance (SPR) immunosensor in a flow system is described. An OVA conjugate was immobilized on a sensor chip via a self-assembled monolayer of 11-mercaptoundecanoic acid through an amino coupling method. The determination of the anti-OVA IgG antibody was based on a kind of sandwich immunoassay using an anti-IgG secondary antibody in order to enhance the sensitivity of the SPR immunosensor. The sensitivity and detection limit of the present method for the anti-OVA IgG antibody were 7 mdeg/ppm and 300 ppb, respectively. The present method showed an enhanced sensitivity and detection limit for the determination of the anti-OVA antibody, compared with a direct immunoassay, by which the sensitivity and detection limit were 3 mdeg/ppm and 1 ppm, respectively. By assuming a Langmuir type of adsorption isotherm, the affinity constants of an anti-OVA IgG antibody immunocomplex with the anti-IgG secondary antibody and of the anti-OVA antibody to the OVA conjugate immobilized on the sensor chip were calculated to be $2.1 \times 10^6\ M^{-1}$ and $2.0 \times 10^6\ M^{-1}$, respectively. The present flow immunoassay for the anti-OVA IgG antibody by an SPR sensor has potential applications in both research and diagnosis of egg allergy.

1. Introduction

There have been reports that up to 2% of the adult population and up to 8% of children are suffering from allergies [1]. In highly sensitized individuals, even the intake of minute amounts of allergens can provoke digestive disorder (emesis, diarrhoea), respiratory symptoms (rhinitis, asthma), circulatory symptoms (oedema, hypotension) and skin reactions (urticaria, atoptic dermatitis/eczema). For some allergic individuals, contact with a specific food can provoke life-threatening reaction (anaphylactic shock) [2]. Egg allergy is one of the most frequent causes of an adverse reaction of foods for children. The prevalence of egg allergy is about 35% in food allergic children and child with atopic dermatitis. Several allergens have been identified in egg, and the major allergens in egg white are ovonucoid Gal D 1 (28 kDa), ovalbumin Gal d 2 (44 kDa) and lysozyme Gal d 4 (14 kDa) [3–6].

According to the classification scheme of allergy symptom by Gell et al., an allergic reaction to food in body is either type I reaction or type III reaction. Type I reaction is often referred to an immediate hypersensitivity reaction. Thus, allergic symptoms are mediated by an allergen-specific immunoglobulin (IgE). When allergens in human body crosslink with a mast cell, the mast cell will release histamine, which is one kind of chemical mediator. The released histamine will affect normal movement of organs so that allergic symptoms come out [7–11]. While, in type III reaction, it is a specific immunoglobulin (IgG) antibody that leads to allergic symptoms. The IgG antibody has several subclasses. In human body, the specific IgG antibodies related to foods circulating in the bloodstream is 60–70% of whole IgG antibodies. In a previous research of food allergy in type III reaction by Aalberse et al., it was concluded that an atopic symptom for foods was associated with high levels of the specific IgG antibody, which is in a range from sub-ppm to several ppm [12–14].

Surface plasmon resonance (SPR) is an optical phenomenon, in which surface plasmon waves are excited at the interface between a metal and a dielectric medium under specific conditions of total internal reflection of p-polarized light. SPR is extremely sensitive to small changes in mass on the surface of the metal due to a binding reaction with a receptor on the metal with a target molecule. Therefore, the surface of the metal is appropriately immobilized with a receptor molecule such as an antibody, a sensor based on SPR so called an SPR sensor would be sensitive and

* Corresponding author. Tel.: +81 92 802 2889; fax: +81 92 802 2889.
E-mail address: imato@cstf.kyushu-u.ac.jp (T. Imato).

0039-9140/$ – see front matter © 2008 Elsevier B.V. All rights reserved.
doi:10.1016/j.talanta.2008.03.007

selective. Compared with other analytical techniques, an SPR sensor has advantages with respect to labeling free and real-time analysis with easier operation [15–19]. In our previous papers, we proposed a flow immunoassay method for histamine and an IgE antibody as a rapid and simple diagnosis of allergy by using an SPR sensor [20,21]. In this paper, we wish to report on a methodology for the determination of the specific IgG antibody for ovalbumin by a surface plasmon resonance immunosensor, which provides an accurate and reliable allergy diagnosis by conjunction with our previously proposed flow immunoassay for histamine and the IgE antibody.

2. Experimental

2.1. Chemicals and equipments

Ovalbumin and 11-mercaptoundecanoic acid (11-MUA) were purchased from Sigma Co. 1-Ethyl-3-(3-dimethylaminopropyl)-carbodiimide (EDC) and *N*-hydroxy succinimide (NHS) were purchased from Dojindo Laboratories Co. (Japan). A mouse anti-OVA IgG antibody (abbreviated as anti-OVA antibody hereafter) and a goat anti-mouse IgG antibody (abbreviated as anti-IgG antibody hereafter) were purchased from Funakoshi Co. (Japan). All other reagents were of analytical grade and were used without further purification. Deionized water (resistance higher than 18 MΩ cm) was used for preparing all solutions. Phosphate buffered saline (PBS, pH 7.2) containing 1 wt.% Tween 20 was used as a carrier solution. An SPR sensor system used in this work was constructed from an SPR sensor with a flow cell (SPR 20, Denki Kagaku Keiki Co., Japan), a sample injector (Rheodyne, 7125) and a syringe pump (Carvo 3000X). The SPR sensor was controlled by a personal computer (Macintosh G4, USA) and SPR signals were stored on the hard drive. The sensor chip was purchased from Eliotech Co. (Japan). The sensor chip is composed of a gold thin film (thickness 45 nm) deposited on a cover glass (18 mm × 18 mm × 0.15 mm *t*) with the assistance of a thin chromium film (thickness 3 nm) between them for improving the adhesion of the gold thin film to the cover glass. The sensor chip was attached to the flow cell using a 0.5-mm thick silicon sheet with a groove of 3 mm × 14 mm. The resulting flow cell was set on a prism of the SPR sensor by coating matching oil (refractive index of 1.516, from Margil, USA) on the prism.

2.2. Immobilization of an OVA conjugate on a sensor chip

The surface of the sensor chip was cleaned by soaking in a Piranha solution (mixture of H_2SO_4 and H_2O_2 at a volume ratio 3:1) for 15 min. After washing with pure water, the sensor chip was washed with ethanol at three times. As shown in step (a) in Fig. 1, the sensor chip was then immersed in a 50 mM 11-MUA solution for 24 h to form a self-assembled monolayer of 11-MUA as an anchor membrane on the Au film [22]. As shown in step (b) in Fig. 1, the carboxylic groups of the 11-MUA layer on the sensor chip were activated by immersing the sensor chip in a mixed EDC/NHS solution (0.2 M/0.1 M) for 50 min. The sensor chip with activated carboxylic groups was set up with the flow cell on the SPR sensor system. As shown in step (c) in Fig. 1, a 100-μL aliquot

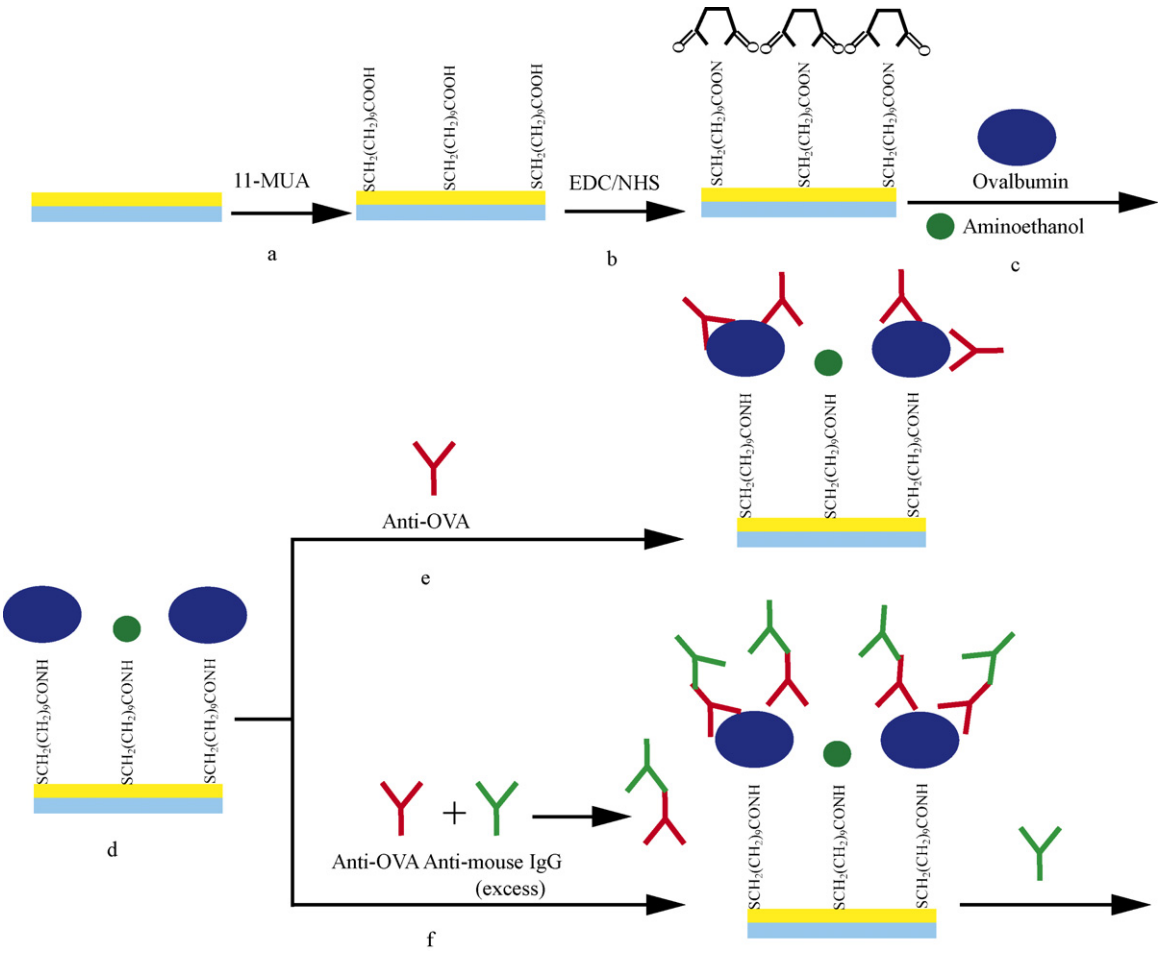

Fig. 1. Schematic diagram of immobilization of OVA on a sensor chip and determination of anti-OVA antibody by direct and sandwich immunoassays.

of a 1000 ppm OVA solution was introduced into the activated sensor chip for immobilization of OVA on the sensor chip. Non-reacted carboxylic groups on the sensor chip were deactivated by introducing a 1 M 2-aminoethanol solution on the sensor chip by the step (d) in Fig. 1, which reduces nonspecific adsorption of primary and secondary antibodies introduced in the following procedure. As a result, a sensor chip, on a surface of which was immobilized with the OVA conjugate, was obtained.

2.3. Direct immunoassay for anti-OVA IgG antibody

As shown in step (e) and step (f) in Fig. 1, a sensor chip immobilized with the OVA conjugate was used for the determination of anti-OVA antibody in two assay modes. One is a direct assay mode, where an anti-OVA antibody was directly reacted to the OVA conjugate immobilized on the sensor chip. A 100-μL aliquot of an anti-OVA antibody solution of different concentrations from 7 ppm to 35 ppm in the increment was 7 ppm was introduced into the sensor chip. The PBS buffer solution was flowed at a flow rate of 0.02 mL/min throughout the experiments. Each sample of the anti-OVA antibody solution was analyzed with a different new sensor chip freshly immobilized with the OVA conjugate without regeneration.

2.4. Sandwich immunoassay of anti-OVA antibody by use of anti-IgG antibody

To enhance the sensitivity for the determination of the anti-OVA antibody, a sandwich immunoassay was utilized for increasing a mass change on the sensor surface, where an anti-OVA antibody solution was mixed and incubated with an excess amount of an anti-IgG antibody to form an immunocomplex with large molecular weight. In this work, an anti-OVA antibody solution at the concentration from 1 ppm to 10 ppm containing 10 ppm anti-IgG antibody was used. A sample solution incubated was introduced into the sensor chip immobilized with the OVA conjugate prepared under the same conditions described above. The flow rate of the carrier solution was the same as 0.02 mL/min for the direct immunoassay. Each sample of the anti-OVA antibody was analyzed by using a new sensor chip freshly immobilized with the OVA conjugate without regeneration.

2.5. Evaluation of the affinity constants of the anti-OVA antibody and an immunocomplex of anti-IgG antibody–anti-OVA antibody to the OVA conjugate immobilized on the sensor chip

The affinity constant of the anti-OVA antibody to the OVA conjugate immobilized on the sensor chip can be evaluated by assuming a Langmuir-type adsorption, as follows. When a solution of the anti-OVA antibody is introduced on the sensor chip, where the OVA conjugate was immobilized, an immunoreaction of the anti-OVA antibody and the OVA conjugate that occurs on the sensor chip and its equation is expressed as follows (step (e) in Fig. 1):

$$\underline{\text{OVA}} + \text{anti-OVA Ab} \rightarrow \underline{\text{OVA–anti-OVA Ab}}, \quad (1)$$

where $\underline{\text{OVA}}$ and $\underline{\text{OVA–anti-OVA Ab}}$ denote the molecules of OVA immobilized on the sensor chip and of an immunocomplex of the anti-OVA antibody bound to the OVA conjugate on the surface of the sensor chip, respectively. Anti-OVA Ab without an underline denotes the anti-OVA antibody in the sample solution.

The affinity constant, K_1, of the immunoreaction Eq. (1) can be expressed by

$$K_1 = \frac{[\underline{\text{OVA–anti-OVA Ab}}]}{([\underline{\text{OVA}}][\text{anti-OVA Ab}])}, \quad (2)$$

where the parentheses without any underline denotes the concentration of the chemical species in the solution, expressed in mol/dm^3, and that with an underline denotes the surface concentration of the chemical species immobilized on the sensor chip, expressed in nmol/mm^2. If a Langmuir-type adsorption is assumed to hold for binding of the anti-OVA antibody to the OVA conjugate on the sensor chip, and the total surface concentration of the OVA conjugate on the sensor chip is assumed to be constant as $[\underline{\text{OVA}}]^{\text{T}}$, the following equation can be derived taking into account of a mass balance of OVA species on the sensor chip:

$$\frac{[\underline{\text{OVA–anti-OVA Ab}}]}{[\underline{\text{OVA}}]^{T}} = \frac{[\text{anti-OVA Ab}]}{(1 + K_1[\text{anti-OVA Ab}])}. \quad (3)$$

In this case, since the change in the SPR sensor signal (angle shift), $\Delta\theta_1$, is proportional to the surface concentration of the anti-OVA antibody bound to the OVA conjugate on the sensor chip, $\Delta\theta_1$ can be rewritten in following form:

$$\frac{\Delta\theta_1}{\Delta\theta_{1,\max}} = \frac{[\text{anti-OVA Ab}]}{(1 + K_1[\text{anti-OVA Ab}])}, \quad (4)$$

where $\Delta\theta_{1,\max}$ denotes the maximum of the angle shift of the SPR sensor, where all of the OVA conjugates immobilized on the sensor chip are completely bound with the anti-OVA antibody.

The following equation can be derived from Eq. (4):

$$\frac{1}{\Delta\theta_1} = \frac{1}{\Delta\theta_{1,\max}} + \frac{1}{([\text{anti-OVA Ab}]K_1\Delta\theta_{1,\max})}. \quad (5)$$

When $1/\Delta\theta_1$ is plotted against 1/[anti-OVA Ab], a linear relationship can be obtained and $\Delta\theta_{1,\max}$ and K_1 can be evaluated from the values of a slope and an intercept of the straight line. In the case of the immunocomplex of the anti-OVA antibody with the anti-IgG antibody in a solution, the affinity constant of the immunocomplex to the OVA conjugate immobilized on the sensor chip (step (f) in Fig. 1) can be evaluated with the same manner as for the case of the affinity constant of the anti-OVA antibody [23–28].

3. Results and discussion

3.1. Direct immunoassay for anti-OVA antibody

A typical sensorgram obtained by a direct immunoassay for the anti-OVA antibody at the concentration of 7 ppm is shown in Fig. 2.

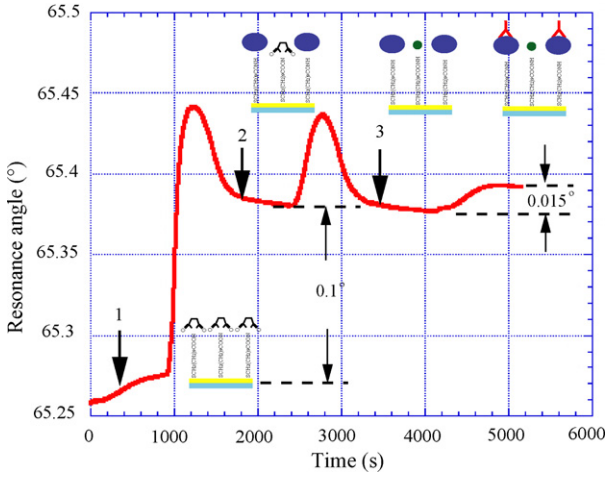

Fig. 2. A typical SPR sensorgram obtained by direct immunoassay for analysis of 7 ppm anti-OVA antibody. (1) Introduction of 1000 ppm OVA solution; (2) introduction of 1 M aminoethanol solution; (3) sample of 7 ppm anti-OVA antibody. Carrier solution: PBS, flow rate: 0.020 ml/min, sample volume: 100 μL.

For preparation of the sensor chip immobilized with the OVA conjugate, a 100-μL aliquot of a 1000 ppm OVA solution was injected into the carrier stream at a time indicated by arrow 1 in Fig. 2. A resonant angle increased abruptly due to immobilization of OVA on the sensor chip, which induces the refractive index in the vicinity of sensor chip higher by reaction of OVA as well as passing the OVA solution through the sensor chip. After a zone of the OVA solution passed through the sensor chip, the resonant angle decreased after peak-shaped signal, which was due to a decrease in bulk refractive index in the vicinity of the sensor chip by replacing the OVA solution with the carrier solution. The resonant angle reached at a constant value of 65.38° finally, and an angle shift from the initial resonant angle was about 0.1°, which induces that OVA molecules were successfully immobilized on the surface of the sensor chip. According to a specification of the BIACORE's SPR sensor, an angle shift of 0.1° corresponds to the increase in the surface concentration by 1 ng/mm^2, the surface concentration of OVA molecules on the sensor chip was estimated to be 2.2×10^{-5} nmol/mm^2 [29,30]. In order to deactivate the residues of imidazol groups, which were used for immobilization of OVA molecules on the sensor chip, a 100-μL aliquot of 1 M aminoethanol solution was introduced onto the sensor chip at a time indicated by arrow 2. The second peak in Fig. 2 means the bulk response of the SPR sensor for an introduction of the aminoethanol solution, whose refractive index is larger than that of the carrier solution. After the aminoethanol solution passed through the sensor chip, the resonance angle returned to nearly the same initial value, which means no significant change in the refractive index at surface of the sensor chip after deactivation of the imidazol groups. Finally, a 100-μL aliquot of a 7 ppm anti-OVA antibody solution was introduced onto the sensor chip at a time indicated by arrow 3 in Fig. 2. The resonance angle increased gradually with time and reached a constant resonance angle of 65.395°. This increment in the resonance angle is due to binding of the anti-OVA antibody to OVA molecules immobilized on the sensor chip. About 0.015° of angle shift was obtained from difference in the resonance angles before and after the injection of the anti-OVA antibody solution. The surface concentration of the anti-OVA antibody on the sensor chip was estimated to be about 0.15 ng/mm^2 from the increase in the angle shift. By taking into consideration of the surface concentrations of OVA immobilized on the sensor chip and the anti-OVA antibody bound to the OVA conjugate on the sensor chip, the mole ratio for the anti-OVA antibody to the OVA conjugate on the sensor chip was calculated to be 1:30. Namely, 1 mole of the anti-OVA antibody binds to 1 mole of 30 moles of the OVA conjugate immobilized on the sensor chip. The sensorgrams for the anti-OVA antibody at different concentrations up to 34 ppm were obtained by the same procedure. A calibration curve based on the angle shift for the direct immunoassay of the anti-OVA antibody in the concentration range from 7 ppm to 34 ppm is shown in Fig. 4 (2). As shown in Fig. 4 (2), a good linear relationship was obtained between the angle shift and concentration of anti-OVA antibody. The sensitivity for the direct immunoassay of the anti-OVA antibody calculated from the slope of the straight line was 0.0033 °/ppm. The detection limit of the direct immunoassay defined as three times of the noise level (about 0.002°) was about 1 ppm.

3.2. Sandwich immunoassay for anti-OVA antibody

A typical sensorgram obtained by a sandwich immunoassay for the anti-OVA antibody is shown in Fig. 3. In this case, the sample was a 5 ppm anti-OVA antibody solution containing 10 ppm anti-IgG antibody. As shown in Fig. 3, a resonance angle of the baseline was about 65.28°. The preparation of the sensor chip immobilized with the OVA conjugate was same as that for the direct immunoassay. After an introduction of a 100-μL aliquot of a 1000 ppm OVA solution, the angle shift for immobilization of OVA was about 0.12°, which was almost the same as for the direct immunoassay. Sensor chips with the almost same surface conditions were used for both experiment modes. The deactivation step of the residues of imidazol groups on the sensor chip was same as for the direct immunoassay by injecting the 1 M aminoethanaol at a time indicated by arrow 2 in Fig. 3. After introduction of an incubation solution containing 5 ppm anti-OVA antibody and 10 ppm anti-IgG antibody, an angle shift of 0.038° due to binding an immunocomplex of anti-OVA antibody–anti-IgG antibody formed in the incubation solution to the OVA conjugate on the sensor chip was obtained. Similar sensorgrams were obtained for incubation solutions containing the anti-OVA antibody at the different concentrations from 1 ppm to 10 ppm and the anti-IgG antibody at the same concentration as 10 ppm. The angle shift for each incubation solution was plotted against the concentration of the anti-OVA antibody, as shown in Fig. 4 (1). The sensitivity to the anti-OVA antibody

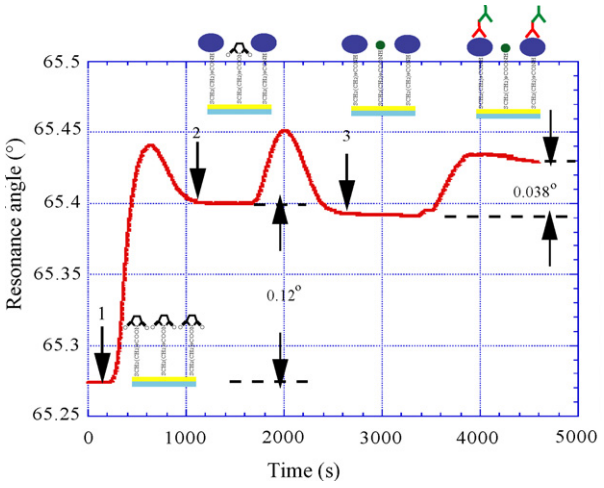

Fig. 3. A typical SPR sensorgram obtained by sandwich immunoassay for analysis of 5 ppm anti-OVA antibody incubated with 10 ppm anti-mouse IgG antibody. (1) Introduction of 1000 ppm OVA solution; (2) introduction of 1 M aminoethanol; (3) sample of 5 ppm anti-OVA + 10 ppm anti-mouse IgG antibodies. Carrier solution: PBS, flow rate: 0.020 ml/min, sample volume: 100 μL.

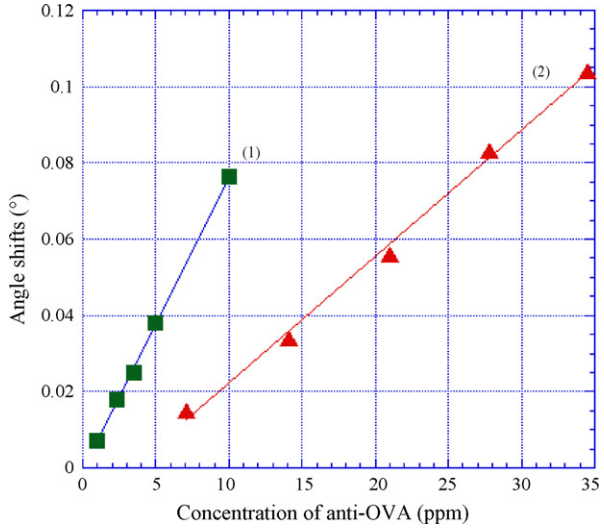

Fig. 4. Comparison of two calibration curves obtained in two experimental modes. Calibration curve obtained by introduction of mixture of 10 ppm anti-mouse IgG antibody and anti-OVA antibody. Calibration curve obtained by direct analysis of anti-OVA antibody.

by the sandwich immunoassay was calculated to be 0.007°/ppm from the straight line in Fig. 4 (1). By comparing the two calibration lines in Fig. 4, the sensitivity for the sandwich immunoassay was improved to be two times, compared with the direct immunoassay. Since the noise level of the present SPR sensor was about 0.002°, the detection limit for the sandwich immunoassay for the anti-OVA antibody was about 300 ppb. This enhanced sensitivity as well as detection limit can be explained by the fact that the large change in dielectric constant in the vicinity of the sensor chip was generated by binding of the immunocomplex of the anti-OVA antibody–anti-IgG antibody to the OVA conjugate immobilized on the sensor chip. Since the level of a specific IgG antibody in serum for human showing allergy symptom was reported in a range from sub-ppm to several ppm [12–14], the present sandwich immunoassay enhanced by the secondary antibody may be satisfied with the demand for the detection limit for a specific IgG level for allergens.

3.3. Comparison of affinity constants for anti-OVA antibody and immunocomplex of anti-IgG antibody–anti-OVA antibody to the OVA conjugate immobilized on the sensor chip

As described in Section 2.5, the affinity constant of the anti-OVA antibody to OVA immobilized on the sensor chip and that of the immunocomplex of the anti-OVA antibody–anti-IgG antibody to the OVA conjugate immobilized on the sensor chip were evaluated from the calibration data shown in Fig. 4 by using Eq. (5). As shown in Fig. 5, a linear relationship between the inverse of the angle shift and inverse of the concentration of the anti-OVA antibody for both immunoassays was obtained, which indicates that a Langmuir-type adsorption isotherm held. By use of Eq. (5), the affinity constant for the anti-OVA antibody with OVA immobilized on the sensor chip was calculated to be $2.1 \times 10^6\ M^{-1}$, and the $\Delta\theta_{1,max}$ was calculated to be 0.16° from the straight line 1 in Fig. 5. In sandwich immunoassay, the sensitivity was enhanced by the secondary anti-IgG antibody where the immunocomplex of the anti-IgG–anti-OVA binds to the OVA conjugate immobilized on the sensor chip. The affinity constant of the immunocomplex to the OVA conjugate immobilized on the sensor chip was calculated to be $2.0 \times 10^6\ M^{-1}$, and the $\Delta\theta_{1,max}$ was calculated to be 0.51° from the straight line 2 in Fig. 5. The use of the secondary antibody in the operation has two effects, one is the enhancement of the dielectric constant in the vicinity of the sensor chip due to the large molecular weight of the immunocomplex, the other is that steric hindrance may affect the affinity for the immunocomplex with the OVA conjugate immobilized on the sensor chip. Judging from the minor difference of affinity constants obtained by the direct immunoassay and the sandwich immunoassay, the anti-OVA antibody and the immunocomplex of anti-IgG antibody–anti-OVA antibody showed almost the same affinity to the OVA conjugate immobilized on the sensor chip, and thus a steric hindrance of the immunocomplex can be omitted.

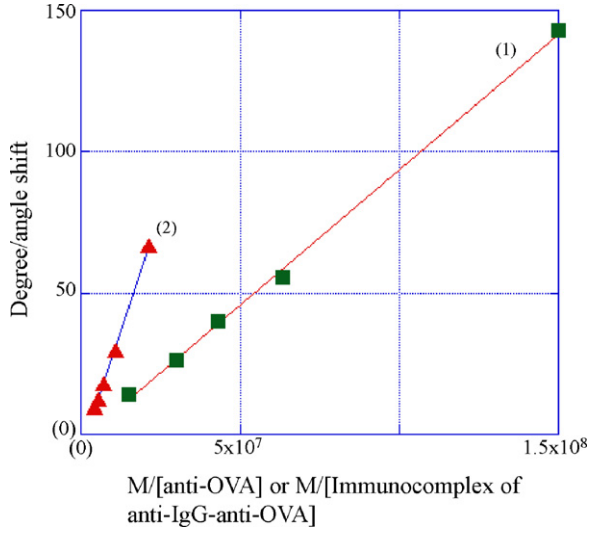

Fig. 5. Relationship between degree/angle shift and M/[anti-OVA] or M/[immunocomplex of anti-IgG-anti-OVA].

4. Conclusion

A flow sandwich immunoassay based on the SPR sensor for the anti-OVA antibody was proposed for a rapid and simple diagnosis for allergy as well as allergy researches. In the present immunoassay, the anti-OVA antibody was bound to the second antibody, anti-IgG antibody in an incubation solution, and the resulted immunocomplex was bound to the OVA conjugate immobilized on the sensor chip. The sensitivity was improved to twice as that in a direct immunoassay, where the anti-OVA antibody is directly bound to the OVA conjugate immobilized on the sensor chip. The detection limit for the sandwich immunoassay was enhanced to be 300 ppb, corresponded to that of the direct immunoassay of 1 ppm. The detection limit obtained in present immunoassay was satisfied with demand for diagnosis for specific IgG antibody level for an OVA allergy. The affinity constant of the anti-OVA IgG antibody to the OVA conjugate immobilized on the sensor chip and $\Delta\theta_{1,max}$ were calculated to be $2.1 \times 10^6\ M^{-1}$ and 0.158°, respectively. The affinity constant of the immunocomplex of the anti-IgG antibody–anti-OVA antibody to the OVA conjugate immobilized on the sensor chip was calculated to be $2.0 \times 10^6\ M^{-1}$, which is nearly same as the affinity constant of the anti-OVA antibody to the OVA conjugate immobilized on the sensor chip. While the value of $\Delta\theta_{1,max}$ was calculated to be 0.51°, which is about three times larger than that obtained in the direct immunoassay. The sensitivity for the sandwich immunoassay was found to be two times higher than that obtained by the direct immunoassay, which is due to the fact that mass of the immunocomplex of the anti-IgG antibody–anti-OVA antibody is much larger than that of the anti-OVA antibody. The present immunosensor method for the specific anti-OVA IgG antibody provides for more accurate and reliable diagnosis of allergy when the immunoassay for histamine and an IgE antibody, which developed by our previous work [20,21], is conjugated with on one sensor chip simultaneously. Simultaneous determination of histamine, an IgE antibody and a specific IgG antibody for allergens is now underway along with our development of an SPR sensor with multidetection points.

References

[1] N. Matsubashi, H. Asagawa, Meneki Kesei Gaku, Kodansha Press, Tokyo, 1979, 25 pp. (in Japanese).
[2] H. Saito, T. Okamura, Allergy, Natsumesha Press, Tokyo, 2000, 20 pp. (in Japanese).
[3] http://en.wikipedia.org/wiki/Allergy.
[4] J.H. Seo, J.W. Lee, J.H. Kim, E.B. Byun, S.Y. Lee, H.J. Kang, M.W. Byun, Radiat. Chem. 76 (2007) 1855.
[5] J.A. Huntington, P.E. Stein, J. Chromatogr. B 756 (2001) 189.
[6] J.W. Lee, J.H. Seo, J.H. Kim, S.Y. Lee, K.S. Kim, M.W. Byun, Radiat. Phys. Chem. 72 (2005) 645.
[7] Y. Mine, P. Rupa, Biochem. Biophys. Res. Commun. 311 (2003) 223.
[8] P. Demoly, B. Lebel, B. Arnoux, Allergy 58 (2003) 553.
[9] D.G. Ebo, M.M. Hagendorens, C.H. Bridts, A.J. Schuerwegh, L.S. De Clerck, W.J. Stevens, Clin. Exp. Allergy 34 (2004) 332.
[10] F. Wegner, R. Hockamp, A. Rutschke, B. Becker, D. Renhardt, Klin. Wochenschr. 61 (1983) 43.
[11] A.D. Crockand, M. Ennis, Clin. Exp. Allergy 31 (2001) 975.
[12] J.O. Warner, M.A. Kaliner, C.D. Crisci, S.D. Giacco, A.J. Frew, G.H. Liu, J. Maspero, H.B. Moon, T. Nakagawa, P.C. Potter, L.J. Rosenwasser, A.B. Singh, E. Valovirta, P.V. Cauwenberge, Int. Arch. Allergy Immunol. 139 (2006) 166.

[13] R.C. Aalberse, J. Schuurman, R.V. Ree, S. Stapel, Res. Immunol. 149 (1998) 263.
[14] D.B.K. Golden, D.A. Meyers, A.K. Sobotka, M.M. Valentine, L.M. Lichtenstein, J. Allergy Clin. Immunol. 69 (1982) 489.
[15] M. Siltanen, M. Kajosaari, E.M. Savilhtl, M. Pohjavuori, E. Savilahtl, J. Allergy. Clin. Immunol. 110 (2002) 658.
[16] R. Rieben, K. Blaser, J. Immunol. Method 119 (1989) 1.
[17] R.J. Green, R.A. Frazier, K.M. Shakesheff, M.C. Davies, C.J. Roberts, S.B. Tendler, Biomaterials 21 (2000) 1835.
[18] J. Homola, S.S. Yee, G. Gauglitz, Sens. Actuator 54 (1999) 3.
[19] X.D. Hoa, A.G. Kirk, M. Tabrizian, Biosens. Bioelectron. 23 (2007) 151.
[20] Y. Li, M. Kobayashi, K. Furui, N. Soh, K. Nakano, T. Imato, Anal. Chim. Acta 576 (2006) 77.
[21] Y. Li, J.J. Ren, H. Nakajima, N. Soh, K. Nakano, T. Imato, Anal. Sci. 23 (2007) 31.
[22] W.M. Mullett, E.P.C. Lai, J.M. Yeung, Methods 22 (2000) 77.
[23] B. Oh, Y. Kim, W. Lee, Y. Bae, W. Lee, J. Choi, Biosens. Bioelectron. 18 (2003) 605.
[24] K.V. Gobi, N. Miura, Sens. Actuator 103 (2004) 265.
[25] K.V. Gobi, M. Sasaki, Y. Shoyama, N. Miura, Sens. Actuator 89 (2003) 137.
[26] D.R. Shankaran, K.V. Gobi, T. Sakai, K. Matsumoto, K. Toko, N. Miura, Sens. Actuator 100 (2004) 450.
[27] Y. Sato, K. Sato, K. Hosokawa, M. Maeda, Anal. Biochem. 355 (2006) 125.
[28] G. Sakai, S. Nakata, T. Uda, N. Miura, N. Yamazoe, Electrochim. Acta 44 (1999) 3849.
[29] P. Sriamarao, P. Steffner, K.R. Gehlsen, J. Biol. Chem. 268 (1993) 22036.
[30] E. Laplantine, L. Vallar, K. Mann, N. Kieffer, M. Aumailley, J. Cell Sci. 113 (2000) 1167.

Talanta 77 (2008) 500–506

Contents lists available at ScienceDirect

Talanta

journal homepage: www.elsevier.com/locate/talanta

Sunflower leaves tissue-based bioelectrode with amperometric flow-injection system for glycolic acid determination in urine

S. Liawrungrath[a,*], P. Purachat[b], W. Oungpipat[c], C. Dongduen[d]

[a] Department of Chemistry, Faculty of Science, Chiang Mai University, Chiang Mai 50200, Thailand
[b] Department of Chemistry, Faculty of Science, Thepsatri Rajabhat University, Lopburi 10500, Thailand
[c] Division of Analytical Chemistry, Department of Chemical Technology, Rajamangala University of Technology, Bangkok Technical Campus, Bangkok, Thailand
[d] Chemical Research Institute, Rajamangala University of Technology, Patoomthani, Thailand

ARTICLE INFO

Article history:
Received 1 November 2007
Received in revised form 11 June 2008
Accepted 13 June 2008
Available online 1 July 2008

Keywords:
Plant tissue-based
Biosensors
Glycolic acid
Flow injection
Amperometry

ABSTRACT

A novel plant tissue-based bioelectrode obtained by incorporating sunflower (*Helianthus annuus* L.) leaves tissue as a source of glycolate oxidase and peroxidase into a ferrocene-mediated carbon paste electrode for the determination of glycolic acid was developed. It was coupled with the flow-injection (FI) system and used as the basis to develop a novel FI amperometric procedure for glycolic acid determination. The flow-injection amperometric measurements were performed by injecting aliquot of glycolic acid solution into the flowing stream of 0.05 mol L^{-1} of phosphate buffer solution having pH 8.0 with a flow rate of 0.3 mL min^{-1}. The bioelectrode consisted of 20% (w/w) of sunflower leaves tissue and 5% (w/w) of ferrocene at 0.00 V (*vs* Ag/AgCl). The bioelectrode exhibited a linear response from 1.0×10^{-6} up to 2.0×10^{-3} mol L^{-1} glycolic acid with a detection limit (S/N = 3) and a quantitation limit (S/N = 10) of 1×10^{-6} and 3.3×10^{-6} mol L^{-1}, respectively. The sampling rate of 12 h^{-1} and a relative standard deviation of 1.67% (n = 15) were achieved. The bioelectrode response decreased to 70% of the original value within 90 continuous injections. The proposed bioelectrode was satisfactorily applied to glycolic acid determination in human urine samples after appropriate sample pretreatment. Results obtained by the FI method were compared favorably with those obtained by HPLC. It offers advantages, which included rapidity, high activity, limited stability, ease of preparation and low cost.

1. Introduction

Glycolic acid (hydroxyacetic acid) is most commonly used in numerous areas of technology for example in adhesives, metal cleaning, dairy cleaning, water-well cleaning, electroplating, biodegradable polymers, dyeing, masonry, textiles, detergents and cosmetic products [1–4]. Moreover, the concentration of glycolic acid in biological fluids has been used as an index for differential diagnosis of hyperoxaluria syndromes [5]. Recently, the determinations of glycolic acid concentration for such applications have received considerable attention. All these have prompted attempts to develop a reliable, rapid and economical method for its assay.

Numerous methodologies for the determination of glycolic acid have been developed such as colorimetric [6,7], isotope dilution [8], chromatographic [9–24], capillary electrophoresis [25] enzymatic [26,27] and gas chromatographic–mass spectrometric (GC–MS) methods [28]. These methods have inherent problems. The spectrophotometric methods are non-specific. The isotope dilution methods are used in combination with colorimetric method, which are unreliable. Gas chromatographic (GC), GC–MS and liquid chromatographic (LC) methods require isolation and derivatization steps as well as involve the use of expensive apparatus. Enzymatic methods appear to be the most widely used but suffer from instability and high cost of the commercially purified enzyme glycolate oxidase.

Plant tissues have received considerable interest in recent years as alternative biocatalysts for replacing isolated enzymes to construct biosensors [29]. Various plant tissue-based bioelectrodes have been reported for analyzing a wide range of organic and inorganic species in several sample matrices for example: In a previous paper, Oungpipat and Alexander [30] describe an amperometric plant tissue-based electrode for monitoring glycolic acid by using spinach leaves (*Spinacia oleracea*) as a source of glycolate oxidase and peroxidase.

An asparagus-based bioelectrode was fabricated by incorporating asparagus (*Asparagus officinalis*) tissue into a ferrocene-mediated carbon paste electrode for determining fluoride. It is

* Corresponding author.
E-mail address: scislwrn@chiangmai.ac.th (S. Liawrungrath).

0039-9140/$ – see front matter © 2008 Elsevier B.V. All rights reserved.
doi:10.1016/j.talanta.2008.06.031

based on the amperometric determination of the inhibitory effect of fluoride on the asparagus peroxidase activity. Measurements were made in non-de-aerated 0.05 M NaH_2PO_4–NaOH buffer (pH 5.0) containing 0.1 mM H_2O_2 at −0.05 V (*vs* Ag/AgCl). The bioelectrode consisted of 7.0% (m/m) of asparagus tissue and 6.0% (m/m) of ferrocene. The bioelectrode shows a linear response up to 14.0 mg L^{-1} fluoride with a detection limit (S/N = 3) of 0.5 mg L^{-1}. A response time (t_{90}) of 60 s and a coefficient of variation of 2.1% (n = 15) were obtained [31].

Flow-injection (FI) amperometric procedure was developed for dopamine determination in pharmaceuticals based on polyphenol oxidase biosensor obtained from soursop pulp. [32]. An enzymatically modified carbon paste electrode was fabricated. It was made from 25% (m/m) of polyphenol oxidase obtained from soursop (*Annona muricata* L.) tissue, 30% (m/m) of 7,7,8,8-tetracyanoquinodimehane (TC NQ) which was used as flow-through detector. The biosensor exhibited good stability and reproducibility.

An amperometric biosensor for hydrogen peroxide determination was reported. The plant tissue-based bioelectrode was developed using homogenized artichoke (*Cynara scolymus* L.) tissue incorporating with a dissolved oxygen probe and applied to determination of hydrogen peroxide in milk samples. The bioelectrode was developed, in which Artichoke tissue was immobilized with gelatin by means of glutaraldehyde and fixed on a pretreated teflon membrane [33].

Recently, a biosensor for direct sulfite determination in food samples was developed. *Malva vulgaris* tissue containing sulfite oxidase enzyme was used as biomaterial. The plant tissue homogenate was crosslinked with gelatin by means of glutaraldehyde and fixed on a pretreated Teflon membrane. In the presence of dissolved oxygen, sulfite was enzymatrically converted to sulfite which was monitored amperometrically. A linear calibration graph over the range 0.2–1.8 mM at 35 °C and pH 7.5 was established [34].

A plant tissue-based biosensor coupled with flow-injection system was described for epinephrine determination in pharmaceuticals. Fibers of palm tree fruits (*Livistona chenesis*) contain polyphenol oxidase enzymes which catalyse the oxidation of epinephrine to epinephrinequinone as a primary product which was then electrochemically reduced (at −0.01 V *vs* Ag/AgCl) on the biosensor surface. The resulting current was used for determining epinephrine. Linear calibration curve over the range of 5.0×10^{-5} mol L^{-1} and the correlation coefficient was 0.998. The RSD was 3.1% [35].

More recently, a novel unmediated hydrogen peroxide biosensor based on the incorporation of fibrous tissue of coconut fruit in carbon paste matrix has been reported [36]. Cyclic voltammetry and amperometry were employed to characterize the main electrochemical parameters and the performance of the new biosensor under different preparation and operation conditions. The developed biosensors have been satisfactorily applied to determination of hydrogen peroxide in four pharmaceutical products namely: antiseptic solution, contact lenses cleaning solution, hair coloring cream and antiseptic dental rinse solution. However, no previously published articles have mentioned on the development of sunflower leaves tissue-based bioelectrode for glycolic acid determination by flow-injection amperometry.

This paper describe a flow-injection determination of glycolic acid with a new amperometric plant tissue-based electrode by using sunflower leaves (*Helianthus annuus* L.) as a source of glycolate oxidase and peroxidase [37]. It offers interesting advantages, including rapidity, high activity, limited stability, ease of preparation and low cost. The methods for bioelectrode fabrication and characterization are also reported.

2. Experimental

2.1. Apparatus

Amperometric measurement were performed with an AUTOLAB® model PGSTAT 20 voltammetric analyzer (Eco Chemie, Utrecht, Netherlands), equipped with *CC-5* flow-through thin-layer electrochemical cell (Bioanalytical Systems Inc.; BAS, Indiana, USA) and a monitor. All experiments were carried out in a laboratory-made flow-injection system coupled with the easily available equipment in the laboratory. PTFE tubings were used as flow lines. The detection system comprises of a Ag/AgCl reference electrode, a stainless steel auxiliary electrode, a sunflower leaves tissue-based and ferrocene-mediated working electrode in serial configuration. The design of the amperometric cell is a thin-layer cell. The cell gaskets/spacer is made from Perspex plastic with the same design as the commercial one (cell gaskets/spacer, MF-1048). The size of the electrode body is said to be 27 mm × 27 mm × 10 mm. The dimensions of the flow channel are the same design as those of dual-series cross flow. A dual carbon paste working electrode used was build in-house from Perspex plastic (PEEK) but is similar in design to those commercially available from BAS. A single-channel EYELA peristaltic pump (EYELA, Model MP-3A, Tokyo, Rikakikai, Co.,Ltd. Japan) supplied with Tygon pump tubing was used for the propulsion of reagent and/or carrier solution into the FI system. A single-channel FI manifold with amperometric detection, using sunflower leaves tissues-based bioelectrode was fabricated. The manifold was assembled with PTFE tubing (0.8 mm id). The six-port injection valve was purchased from PYE UNICAM (Cambridge, England).

2.2. Materials, chemical and reagent solutions

2.2.1. Materials

Sunflower (*Helianthus annuus* L.) was grown in chamber environment for the experiment. Sunflower seeds were purchased from a local supermarket. Sunflower leaves were used immediately after harvesting, washing with water and removal of the residual water on the leaves by leaving them on the tissues paper for a few minutes.

2.2.2. Chemicals

All chemicals were of analytical grade and were used as received without further purification. De-ionized distilled water prepared by passing distilled water through a Mili-Q system (Millipore) was used throughout. Glycolic acid, mineral oil and graphite powder were obtained from Fluka. Ferrocene and chloroform were purchased from Aldrich and Merck, respectively. Sodium dihydrogen phosphate dihydrate was purchased from Carlo Erba. Chemicals for interference studied were purchased from Fluka, Ajax and Merck.

2.2.3. Standard and reagent solutions

Stock standard glycolic acid solution (0.10 mol L^{-1}) was prepared by dissolving about 0.76 g glycolic acid (accurately weighed) in water in a 100 mL volumetric flask diluting to the mark, mixing well, and storing in a polyethylene bottle. Stock solutions in concentration lower than 0.10 mol L^{-1} were obtained by appropriate dilution of this stock solution.

Stock standard H_2O_2 solution (0.10 mol L^{-1}) was prepared by dissolving 1.066 g of 31.9% (w/w) H_2O_2 (previously standardized with standard $KMnO_4$ solution) [38] in water and diluting to 100 mL with water in a 100 mL volumetric flask. The solution was transferred into a reagent bottle and stored at 4 °C until use.

A 0.05 mol L^{-1} sodium dihydrogen phosphate solution (pH 8.0) was prepared by dissolving about 7.8 g NaH_2PO_4 (accurately

weighed) in 900 mL water. The solution pH was adjusted to pH 8.0 with 0.05 mol L^{-1} NaOH (previously standardized) and diluted to 1000 mL with water.

A 0.05 mol L^{-1} sodium dihydrogen phosphate solution (pH 5.0) was prepared by dissolving about 7.8 g NaH_2PO_4 (accurately weighed) in 900 mL water. The solution pH was adjusted to pH 5.6 with 0.05 mol L^{-1} NaOH and diluted to 1000 mL with water [39].

Total ionic strength adjustment buffer (TISAB) solution was prepared by mixing 57.7 mL of glacial acetic, 58.4 g of NaCl, 5.0 g of cyclohexanediamine tetraacetic acid (CDTA) and 500 mL water in a 1000 mL beaker. The mixture was cooled to room temperature and adjusted to pH 5.4 with 6.0 mol L^{-1} NaOH, diluted to 1000 mL with water and stored in a polyethylene bottle.

2.2.4. Urine samples

Urine samples were collected from six volunteers and kept at 4 °C until use. A 10 mL of 10-fold-diluted human urine sample was mixed with 300 mg of activated charcoal. After removal of the charcoal by centrifugation, the supernatant was then used for glycolic acid assay.

2.3. Electrode construction

The plant tissue-modified carbon paste was prepared as follows. A 10.5% (w/w) ferrocene-modified graphite powder was first prepared by mixing 0.895 g of graphite powder with 0.105 g of ferrocene dissolved in 10 mL of chloroform. After evaporation of the solution, about 0.600 g (accurately weighed) of this ferrocene-modified graphite powder was mixed with 0.400 g of mineral oil (paraffin oil purchased from Sigma) to yield ferrocene-modified carbon paste. This paste (0.800 g) was then thoroughly mixed with 0.200 g of ground tissue of fresh and green sunflower leaves. Sunflower leaves were collected from the sunflower plants growing in the chamber environment for this purpose and used immediately after washing and air-drying. The fresh sunflower leaves were grinding by mean of a small mortar made of glass for about 1 min to obtain a paste looking like tooth-paste. The approximate particle size of the sunflower leaves powders after grinding was not measured. The resulting mixture containing 5% ferrocene and 20% of ground plant tissue was ultimately packed into the dual-series electrode body (27 mm × 27 mm × 10 mm size) made from Perspex plastic with two circular cavities, each 2 mm in diameter and 2 mm deep. The working electrode designed was similar to the commercial one known as a dual-series cross flow type consisting of two electrodes. Each electrode provided a surface area of 3.14 mm^2 to obtain the total surface area of the two electrodes of 2 x 3.14 mm^2. The surface of each carbon paste electrode was smoothed by sweeping motion or slice on the polishing pad made of a piece of paper. The electrode connection to the carbon paste was established via a copper wire. When not in use, the bioelectrode was stored in a refrigerator at 4 °C.

In some experiments, plant tissue-modified plain carbon paste was utilized. This was prepared by the same procedure as mentioned above except that a plain carbon paste (60% graphite powder and 40% mineral oil) was substituted for ferrocene-modified carbon paste to investigate the cyclic voltammogram of glycolic acid for comparison with that obtained by using the ferrocene-modified carbon paste electrode. It was found that no cyclic voltammogram of glycolic acid was observed with the plain carbon paste electrode. Thus, the present work was based on utilization of the ferrocene-modified carbon paste electrode.

2.4. Procedure

2.4.1. Recommended procedure

Amperometric flow-injection measurements were performed by successive injections of aliquots of stock glycolic acid solution into flow system. The electrode was conditioned in a solution of sodium dihydrogen phosphate (pH 8.0) pumped through the flow system with a constant flow rate of 0.3 mL min^{-1} (except as otherwise state) at 0.0 V (*vs* Ag/AgCl) until a stable baseline was established. The sample was then injected into the flow analysis system via an injection valve equipped with a fixed sample loop of 150 μL (optimal injection volume obtained by using univariate method). The resulting peak was recorded. The peak height (ΔI) was used for subsequent interpretation of the data. All experiments were performed at room temperature.

2.4.2. Procedure for investigation of suitable experimental conditions

The optimal experimental conditions were investigated using univariate method. The effect of applied potential on the bioelectrode consisting 20.0% (w/w) of sunflower leaves tissue and 5.0% (w/w) ferrocene mediator was examined in the potential from −0.15 to +0.15 V (*vs* Ag/AgCl). This was carried out by injecting 50 μL of the standard glycolic acid (5×10^{-3} M) into the carrier 0.05 M NaH_2PO_4–NaOH buffer (pH 7.5) flowing at a constant flow rate of 0.4 mL min^{-1}. These fixed values were selected by trial and error except the variable to be studied (i.e., operating potential as the first variable to be studied).

The pH dependence of the bioelectrode response was monitored by injecting 50 μL of the standard glycolic acid (5×10^{-3} mol L^{-1}) into the carrier stream of 0.05 mol L^{-1} NaH_2PO_4–NaOH buffer of varying pH ranging between 5.0 and 10.0 flowing at a constant flow rate of 0.4 mL min^{-1}. The potential was set at 0.00 V (*vs* Ag/AgCl).

Similarly, the effect of working buffer on the bioelectrode response was investigated using injection of 50 μL standard glycolic acid (5×10^{-3} mol L^{-1}) in 0.05 mol L^{-1} concentration of five different buffer systems with the same pH and flow rate (pH, 8.0; flow rate, 0.4 mL min^{-1}), namely NaH_2PO_4–NaOH, Na_2HPO_4–NaH_2PO_4, boric acid–Na_2HPO_4, tartaric acid–NaOH and Tris–HCl. The potential was set at 0.00 V (*vs* Ag/AgCl). The composition of the bioelectrode used in the study was the same as above.

The effect of sunflower leaves tissue composition was studied at 0.0%, 10.0%, 15.0%, 17.5%, 20.0%, 22.5%, 25.0% and 30.0% (w/w) of sunflower leaves tissue with ferrocene loading held constant at 5.0% (w/w). Likewise, the effect of ferrocene loading on bioelectrode response was also studied at eight different loadings of 0.0%, 2.0%, 4.0%, 5.0%, 6.0%, 7.0%, 9.0% and 11.0% (w/w) at 20.0% of tissue composition. These studies were carried out by injecting 50 μL of the standard glycolic acid (5×10^{-3} mol L^{-1}) into the carrier 0.05 mol L^{-1} NaH_2PO_4–NaOH buffer (pH 8.0) flowing at a constant flow rate of 0.4 mL min^{-1} at 0.00 V (*vs* Ag/AgCl).

The effect of flow rate of 0.05 mol L^{-1} NaH_2PO_4–NaOH buffer (pH 8.0) was studied by varying it from 0.2 to 1.8 mL min^{-1}. A 50 μL of the standard glycolic acid (5×10^{-3} mol L^{-1}) was injected into the carrier buffer at 0.00 V (*vs* Ag/AgCl). The fabricated bioelectrode consisted of 20.0% (w/w) of sunflower leaves tissue and 5.0% (w/w) ferrocene mediator was used in this study. Similarly, the effect of sample volume on bioelectrode response was studied at 50, 100, 150, 200, 250 and 300 μL of the standard glycolic acid (5×10^{-3} mol L^{-1}) at carrier buffer flow rate of 0.3 mL min^{-1}.

Calibration graphs for the bioelectrode response were measured over the concentration range 1×10^{-4} to 4×10^{-3} mol L^{-1} of standard glycolic acid (150 μL) under optimized experimental conditions.

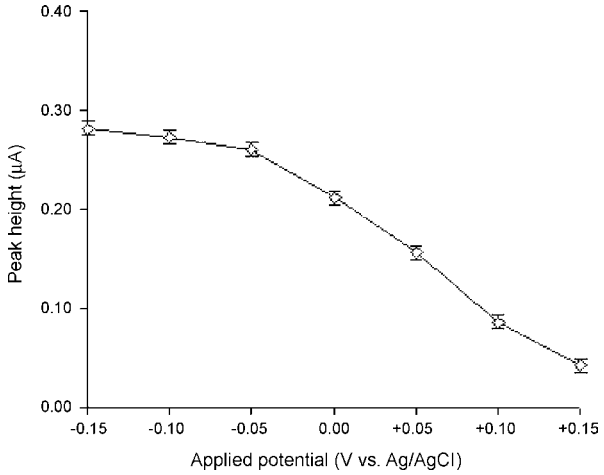

Fig. 1. Effect of operating potential (50 μL of 5×10^{-3} M glycolic acid; 20.0% (w/w) sunflower leaves tissue and 5.0% (w/w) ferrocene; 0.05 M NaH_2PO_4–NaOH buffer (pH 7.5); flow rate, 0.4 mL min^{-1}).

3. Results and discussion

The effect of applied potential on bioelectrode response to 5×10^{-3} mol L^{-1} glycolic acid is shown in Fig. 1. It was found that the reduction current decrease slightly from −0.281 to 0.043 μA on changing the potential from −0.15 to +0.15 V (*vs* Ag/AgCl). At −0.15 V the cathodic current kept increasing even without injecting glycolic acid and the noise increased dramatically. This behavior was ascribed to the reduction of dissolved oxygen at this potential. The potential of 0.0 V was selected for the remainder of the experiments as the best compromise between the resulting signal and the noise level. Moreover, this low potential is expected to minimize possible interference.

The pH dependence of the bioelectrode was studied at 5×10^{-3} mol L^{-1} glycolic acid over the pH range from 4.0 to 10.0. The resulting peak-shaped pH profile illustrated in Fig. 2 reveals that the bioelectrode showed a maximum sensitivity of response at pH 8.0. An optimum pH value of 8.3 has been reported for the spinach glycolate oxidase [40] and pH 7.5 has been reported in previous work [30]. This indicated that the pH profile of the bioelectrode is governed by the enzymatic activity. Regarding to the results obtained, the phosphate buffer solution pH 8.0 was selected for subsequent studies.

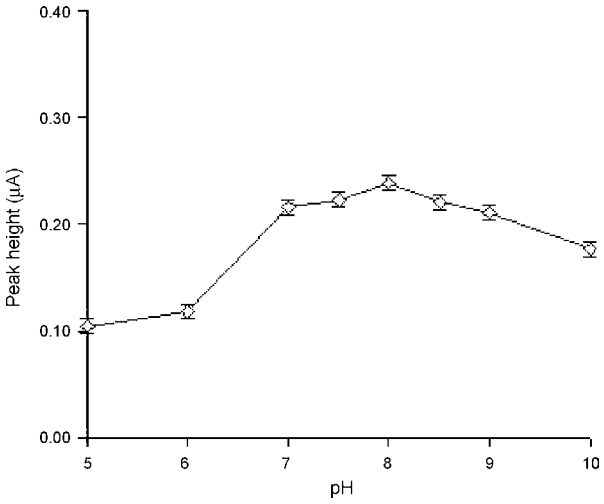

Fig. 2. Influence of pH on the bioelectrode response (20.0% (w/w) sunflower leaves tissue and 5% (w/w) ferrocene; 50 μL of 5×10^{-3} M glycolic acid; 0.05 M NaH_2PO_4–NaOH buffer; flow rate, 0.4 mL min^{-1}; applied potential, 0.0 V (*vs* Ag/AgCl)).

The effect of five buffer types (NaH_2PO_4–NaOH, Na_2HPO_4–NaH_2PO_4, boric acid–Na_2HPO_4, tartaric acid–NaOH and Tris–HCl) on the response of bioelectrode was investigated. It can be seen that the NaH_2PO_4–NaOH buffer was the most efficient working buffer giving the highest response (0.240 ± 0.007 μA) among the five types of buffers studied 0.222 ± 0.016, 0.14 ± 0.013, 0.140 ± 0.012 and 0.053 ± 0.005 μA for tartaric acid–NaOH, boric acid–Na_2HPO_4, Na_2HPO_4–NaH_2PO_4 and Tris–HCl, respectively. Hence, it was employed for the further study.

Tissue loading showed a profound effect upon the response of bioelectrode to glycolic acid. As would be expected, increasing the tissue composition of the bioelectrode from 10% to 20% resulted in an increase in the bioelectrode response, reflecting the increase in the biocatalytic activity. On the other hand, the noise level also gradually increased with the increase in tissue composition. Increasing the tissue composition beyond 20.0% caused lower response. This behavior could be attributed to the increased resistance of the carbon paste [41] and likewise as previous work [30]. The tissue loading of 20% was selected for the next experiments.

The influences of mediator loading on bioelectrode response were investigated. It can be seen that signals increase substantially with increase in mediator loading from 2.0% to 5.0%. Further increase in mediator loading above 5.0% resulted in a decrease in the bioelectrode response. Such a decrease in response of the bioelectrode when a larger amount of mediator is used is typical behavior of a mediator-based sensor [42]. Again this behavior is ascribed to the lowering of the electrical conductivity due to the reduction in graphite loading [29,43]. Based on these results, the bioelectrode with a composition of 20.0% tissue and 5.0% ferrocene was employed.

The flow rate dependence of the bioelectrode was pursued by varying the flow rate from 0.2 to 1.8 mL min^{-1}. It was found that the maximum response is obtained at the lowest flow rate tested, 0.2 mL min^{-1}, then slightly decreased when the flow rate of buffer solution was 0.3 mL min^{-1} and an exponential decay in response is observed when increasing the flow rate up to 1.8 mL min^{-1}. The explanation for this is that at lower flow rate there is more time for enzymatic reaction and a larger response would be expected. On the other hand, diffusion layer thickness increases so that analyte transport to the surface can become the limiting factor. In order to study effect of flow rate on sensitivity (μA/mM) of the peak current obtained from glycolic acid by FIA, the same solution containing glycolic acid was analyzed by batch method with amperometric detection. With the batch method, it is essential to stir the reaction mixture to avoid local concentration. Therefore, the stirring rate dependence of the bioelectrode was pursued by varying the stirring rate from 50 to 300 rpm. It was evident that the maximum sensitivity was obtained at the lowest stirring rate tested (50 rpm). On further increment of the stirring rate, the sensitivity decreased successively and reached the minimum value at the stirring rate of 300 rpm as follows: 0.345, 0.321, 0.264, 0.233, 0.164 and 0.153 μA/mM glycolic acid at stirring rate 50, 75, 100, 150, 200 and 300 rpm, respectively. However, the maximum response time was obtained at the stirring rate of 50 rpm for the batch method. In addition, the maximum response time (t_{90}, it is the time taken to reach 90% of the response) is obtained at flow rate of 0.2 mL min^{-1}. The rapid decrease in bioelectrode response with flow rate is due to a reduced response time at the bioelectrode giving more time for the bi-enzyme system reaction [29]. Diffusion within electrode surface also plays an important role in the mass transfer because less substrate reaches the electrode surface at shorter response time [44]. The flow rate of buffer stream was therefore set at

0.3 mL min^{-1} for compromise between bioelectrode response and sample throughput.

The dependence of the bioelectrode response on the sample volume was examined. It was found that the electrode response increased rapidly when the sample volume was increased from 50 to 150 μL and reached the maximum electrode response at 150 μL above which the electrodes response began slightly decreasing and reached the minimum value when the sample volume increased up to 300 μL. The explanation for decreases in the electrode response with a sample volume of greater than 150 μL is probably owing to dilution effect. In addition, the peak width increase with injected volume. Based on the result, the sample volume of 150 μL was employed as the highest electrode response.

4. Bioelectrode characterization

4.1. Calibration curve

Fig. 3 displays typical current recording for FIA response under the optimized experimental conditions for determining glycolic acid over the concentration range 1×10^{-4} to 4×10^{-3} mol L^{-1}. It was found that the bioelectrode exhibits linearity of calibration up to 2×10^{-3} mol L^{-1} with curvature at higher concentration. The slope of the initial linear range is 1.92×10^{2} μA mol^{-1} with a correlation coefficient of 0.9901. The value 0.9901 suggests a non-linear relationship. Therefore, it would be interesting to cheek whether a higher polynomial makes considerably better fit. It was shown that with the higher polynomial the regression equation was $Y = 180.62X + 0.017$ with a correlation coefficient of 0.9956 which is better fit.

4.2. Detection limit

A detection limit (S/N = 3) of 1×10^{-6} mol L^{-1} was obtained for the proposed bioelectrode compared with 1×10^{-6} mol L^{-1} [30] and 1×10^{-3} mol L^{-1} [45] reported previously for a glycolic acid biosensors by Oungpipat and Alexander [30] and Dick et al. [45], respectively. Hence, the present method exhibited the lower detection limit than that previously obtained by Dick et al. (1.0×10^{-3} mol L^{-1}) and the same detection limit as that previously reported by Ouangpipat and Alexander (1.0×10^{-6} mol L^{-1}). Beside the different tissue, comparison between the previous paper [30] and the present one are as follows. The previous paper describes a batch-wise or static method whereas the present paper describes a flow-based method so that the amperometric cell designs are different. The former method employs a conventional amperometric cell whereas the latter method utilized a flow-through cell. Both methods are based on plant tissue biosensor as plant tissue-based bioelectrodes with amperometric detection. However, the electrode body designs are different; the former electrode body is made from glass tube with a geometric area of 3.14 mm^2 and the surface was smoothed with a piece of weighing paper; the latter electrode body was a dual-series one with the size of 27 cm × 27 cm × 10 cm. It is made from Perspect plastic with two circular cavities. Each cavity is 2 mm in diameter and 2 mm deep. The design of cell gaskets/spacer is similar to that of the commercial one (cell gasket/spacer, MF-1048). The dimensions of the flow channels are dual series with crossflow. The carbon paste mixture used to pack in the electrode body was consisting of 32% ferrocene and 12% tissue for the former carbon paste electrode and that containing 5% ferrocene and 20% ground plant tissue was the latter carbon paste electrode.

4.3. Reproducibility

This is one of the important parameters to evaluate during fabrication of a sensor. For the present bioelectrode, it was found that replicate measurements of 1×10^{-3} mol L^{-1} glycolic acid for the same bioelectrode yielded 1.67% ($n = 15$) relative standard deviation from the mean. Five independently made bioelectrodes that were prepared from the same batch of carbon paste on the same day showed acceptable bioelectrode reproducibility with a relative standard deviation of 4.52%.

4.4. Sample throughput

The half peak-widths were found to be 90 s. These allow injection rates of 12 samples h^{-1} ($t_{base} = 5$ min) to be achieved. The high sample throughput reflects the inherent advantage of the FIA technique over the batch measurements.

4.5. Stability (life time)

An important parameter when considering the merit of the bioelectrode in the flow system is the electrode stability. To investigate the present electrode stability, aliquots of a standard solution of glycolic acid (1×10^{-3} mol L^{-1}) were injected continuously into the FIA system under the optimized condition. It can be seen that the response of bioelectrode remains almost constant initially, up to 70 injections (of standard and/or urine samples), because the enzyme is in excess. After 90 and 110 injections, the bioelectrode response decreased to 70% and 50% of the original value, respectively. The loss of bioelectrode response is, therefore, ascribed to the leaching of ferrocene from the electrode and loss of the enzyme activity [46,47]. The proposed bioelectrode was stable over 24 h during successive inflections and having breaks between measurements (e.g., 1–12 h or up to overnight) the electrode response remained constant. This indicated that during the breaks the leaching of the ferrocene from the electrode did not occur.

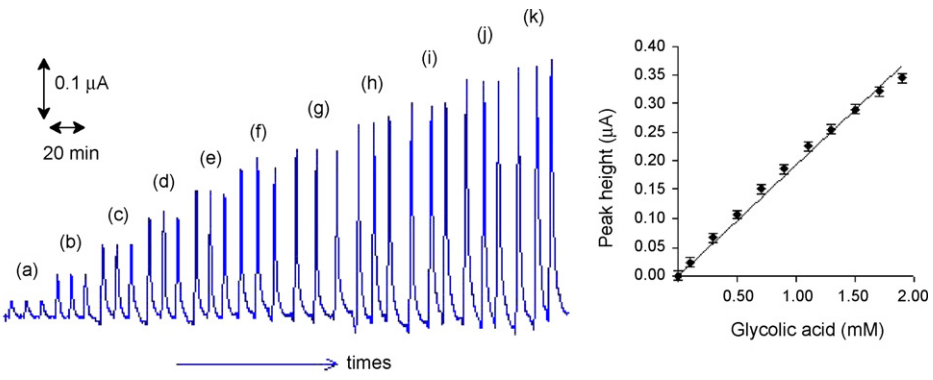

Fig. 3. Typical response and calibration graph of glycolic acid; (a) 0.1×10^{-3} M (b) 0.3×10^{-3} M, (c) 0.5×10^{-3} M, (d) 0.7×10^{-3} M, (e) 0.9×10^{-3} M, (f) 1.1×10^{-3} M, (g) 1.3×10^{-3} M, (h) 1.5×10^{-3} M, (i) 1.7×10^{-3} M, (j) 1.9×10^{-3} M and (k) 2.1×10^{-3} M.

Table 1
Possible interference tested with the glycolic acid bioelectrode

Substance (X)	Concentration (10^{-3} M)	Current ratios[a]
Ascorbic acid	0.005	0.99
	0.1	0.29
Uric acid	2.0	1.04
	5.0	1.52
Lactic acid	2.0	1.05
	5.0	1.67
Oxalic acid	5.0	0.84
Tartaric acid	5.0	0.84
Salicylic acid	5.0	0.88
Glucose	5.0	0.90
Fructose	5.0	0.93
Succinic acid	5.0	0.95
Malonic acid	5.0	0.99
Maleic acid	5.0	1.05
Formic acid	5.0	1.09
Citric acid	5.0	1.14
Acetic acid	5.0	1.16
Glutamic acid	5.0	1.27

Glycolic acid compared with 5×10^{-4} mol L^{-1} glycolic acid alone. Note that a current ratio of 1 has the meaning of no interference.

[a] Current ratios for mixture of concentration of substance (X) and 5×10^{-4} mol L^{-1}.

4.6. Selectivity

Fifteen possible interfering compounds (ascorbic acid, urine acid, lactic acid, oxalic acid, tartaric acid, salicyclic acid, glucose, fructose, succinic acid, maleic acid, formic acid, citric acid, acetic acid and glutamic acid) were used to evaluate the selectivity of the proposed bioelectrode. The current obtained for each interference substance at 5×10^{-3} mol L^{-1} (unless otherwise stated) in the presence of glycolic acid at a concentration of 5×10^{-4} mol L^{-1} was used as an indicator for bioelectrode selectivity in comparison with the glycolic acid reading alone. It was shown that ascorbic acid at higher concentration (1.0×10^{-4} mol L^{-1}) has a strong inhibition effect on glycolic acid determination whereas uric and lactic acids show a slight increase of the electrode response to glycolic acid. These results are listed in Table 1, showing that the bioelectrode is quite selective for glycolic acid. Of these interferences studied, only ascorbic acid (1×10^{-4} mol L^{-1}), uric acid 5×10^{-3} mol L^{-1} and lactic acid 5×10^{-3} mol L^{-1} interfered to a significant extent judging from the current ratio by comparison with a current ratio of 1 that has the meaning that no interference greater or smaller than 1 should be regarded as suffering from interference. As for most amperometry sensors, electroactive species such as ascorbic acid can easily oxidize directly on the electrode surface at low potential, thus changing the enzyme-mediated current, resulting in inhibition effect on glycolic acid determination. This effect became strong as well as increases in ascorbic acid concentration. These effects clearly occur in the present work. However, in the presence of lower concentrations of ascorbic acid (5×10^{-6} mol L^{-1}), lactic acid (2×10^{-4} mol L^{-1}) and uric acid (2×10^{-4} mol L^{-1}), it was found that no interference effects on the glycolic acid determination were observed. The small bioelectrode response to uric acid and lactic acid implies some cross-reactivity of enzyme glycolate oxidase towards uric acid and lactic acid. These results are consistent with those reported in previous work [48–51] regarding the ability of glycolate oxidase to oxidize uric acid and lactic acid.

4.7. Recovery study

The recovery of the method was determined by using method of standard addition, in which various known concentrations of standard glycolic acid were added into the urine samples. In order to evaluate the performance and the reliability of the bioelectrode the recoveries of glycolic acid in the spiked urine samples were determined after 0.0005 and 0.001 mol L^{-1} were added to a 10-fold dilution of charcoal pretreated urine samples. Other compounds may interfere by reacting with hydrogen peroxide, ferrocene or by direct electrochemical activity at the operating voltage. The pretreatment step of urine sample with charcoal is essential and recommended in order to eliminate any ascorbic acid and other electroactive compounds contained in the sample. The samples were mixed with 300 mg of activated charcoal and the charcoal was removed by centrifugation. A 10-fold dilution of the supernatant was then used for the glycolic acid assay [26]. Typical recoveries of glycolic acid spiked in the range 0.5×10^{-3} to 1.0×10^{-3} mol L^{-1} to urine samples were 94.0–100.2%. The bioelectrode shows satisfactory results with an average recovery of 98.33%. It is well possible that the charcoal treatment has more or less influence on glycolic acid concentration, because any adsorption losses are reflected in a decreased glycolic acid concentration. Therefore, comparative recovery determination of glycolic acid has been carried out by spiking the 10-fold dilution of the untreated urine samples with 0.0005 and 0.001 mol L^{-1} of standard glycolic acid before treatment with charcoal. It was found that the relative average recoveries of the spiked glycolic acid were over the range of 94.3–98.8% indicating that the charcoal treatment of the spiked urine samples exhibited slight effect on glycolic acid concentration.

Table 2
Determination of glycolic acid in 10-fold dilution of pretreated urine sample by the present method and HPLC method [20]

Samples no.	Glycolic acid concentration ($\times 10^{-3}$ mol L^{-1})		%Relative difference (C)[a]
	Present method (a)	HPLC method (b)	
1	0.49	0.49	0.0
2	0.72	0.71	1.4
3	0.72	0.71	1.4

$C = (a - b)\backslash a \times 100$.

[a] Mean of triplicate determinations.

4.8. Analysis of glycolic acid in urine samples and validation of the method

A 10-fold dilution of pretreated urine samples was analyzed by the present method under optimal experimental conditions. Comparative determinations of glycolic acid in the same pretreated urine samples by HPLC method [20] have been also carried out to investigate the accuracy of the proposed method (validation). Results obtained by both methods (Table 2) were compared favorably and verified by the Student's t-test at the 95% confidence level. A satisfactory agreement between the results was found with mean relative differences in the range 0.0–1.0%. This indicated that the proposed FI method was very accurate.

5. Conclusion

This work has presented the feasibility of utilizing the available bi-enzyme system in sunflower leaves for fabrication of a novel plant tissues-based biosensor coupled with the sample flow-injection system for the determination of glycolic acid. The simple design and low cost of the bioelectrode construction are further distinctive features of the proposed electrode. It is typical of amperometric sensors based on mixed tissue carbon paste electrode to provide high sensitivity and rapid response. Moreover, the use of a low operating potential together with the specific enzymatic

reaction resulted in minimal interference effects. Pretreatment of sample containing ascorbic acid with activated charcoal is required to achieve bioelectrode accuracy.

Acknowledgments

The authors are grateful to Center for Innovation in Chemistry: Postgraduate Education and Research Program in Chemistry (PERCH-CIC), for financial support. These sincere thanks are also expressed to Department of Chemistry, Faculty of Science, Chiang Mai University, Department of Chemistry, Faculty of Science and technology, Thepsatri Rajabhat University, Lopburi and Chemical Research Institute, Rajamangala University of Technology Patoomthani for partial support.

References

[1] Kirk-Othmer, Encyclopedia of Chemical Technology, vol. 13, Wiley, New York, 1981, p. 92.
[2] D. Scholz, G.J. Brooks, D.F. Parish, F. Burmeister, Int. J. Cosmet. Sci. 16 (1994) 265.
[3] US Food and Drug Administration, Office of Cosmetics Facts Sheet, May 3, 1995.
[4] W.P. Smith, Int. J. Cosmet. Sci. 18 (1996) 75.
[5] H.E. Williams, Kidney Int. 13 (1978) 410.
[6] J.P. Viccaro, E.L. Ambye, Microchem. J. 17 (1972) 710.
[7] A. Niederwieser, A. Matasovic, E.P. Leeumann, Clin. Chim. Acta 89 (1978) 13.
[8] T.D.R. Hockaday, E.W. Frederick, J.E. Clayton, L.H. Smith, J. Lab. Clin. Med. 65 (1965) 677.
[9] N.E. Skelly, Anal. Chem. 54 (1982) 712.
[10] R. Pecina, G. Bonn, E. Burtscher, O. Bubleter, J. Chromatrogr. 287 (1984) 245.
[11] T. Okada, Anal. Chem. 60 (1988) 1666.
[12] M. Gennaro, M. Sbuttoni, E. Mentasti, C. Sarzanini, V. Porta, Ann. Chim. 78 (1988) 137.
[13] D.B. Gomis, M.J. Gutierrez, M.D. Gutierrez, Alvarez, M.J. Alonso, Chromatographia 25 (1988) 1054.
[14] M. Petrarulo, S. Pellegrino, O. Bianco, M. Marangella, F. Linari, E. Mentasti, J. Chromatogr. 465 (1989) 87.
[15] M. Petrarulo, O. Bianco, D. Cosseddu, M. Marangella, S. Pellegrino, F. Linnari, J. Chromatogr. 532 (1990) 130.
[16] T.R. Wandzilak, L.E. Hagen, H. Gughes, R.A.L. Sutton, L.H. Smith, H.E. Williams, Kideny Int. 39 (1991) 765.
[17] S. Scalia, R. Callegari, S. Villani, J. Chrommatogr. A 795 (1998) 219.
[18] M.I. Daneshvar, J.B. Brooks, J. Chromatrogr. 433 (1988) 248.
[19] Y. Mardens, A. Kumps, C. Planchon, C. Wurth, J. Chromatogr. 577 (1992) 3441.
[20] A. Cherchi, L. Spanedda, C. Tuberoso, P. Cabras, J. Chromatogr. A 669 (1994) 59.
[21] D. Lagoutte, G. Lombard, S. Nisseron, M.P. Papet, Y. Saint-Jalm, J. Chromatrogr. A 684 (1994) 251.
[22] K. Fischer, H.P. Bipp, D. Bieniek, A. Kettrup, J. Chromatrogr. A 706 (1995) 361.
[23] H.H. Yao, W.H. Porter, Clin. Chem. 42 (1996) 292.
[24] S. Peldszus, P.M. Huck, S.A. Andrews, J. Chromatogr. A 723 (1996) 27.
[25] S.P.D. Lalljie, J. Vindevogel, P. Sandra, J. Chromatogr. A 652 (1993) 563.
[26] G.P. Kasidas, G.A. Rose, Clin. Chim. Acta 96 (1979) 25.
[27] R. Bais, J.M. Nairn, N. Potenzny, A.M. Fore, R.A.J. Conyers, A. Bar, Clin. Chem. 3 (1991) 255.
[28] N. LK, P. Lafontaine, J. Harnois-J, J. Chromatogr. A 873 (2000) 29.
[29] J. Wang, Electroanalysis 3 (1991) 255.
[30] W. Oungpipat, P.W. Alexander, Anal. Chim. Acta 295 (1994) 37.
[31] S. Liawruangrath, W. Oungpipat, S. Watanesk, B. Liawruangrath, C. Dongduen, P. Purachat, Anal. Chim. Acta 448 (2001) 37.
[32] V.S. Bezerra, J.L. de Lima Filho, M.C.B.S.M. Montenegro, A.N. Araujo, J. Pharm. Biomed. Anal. 33 (2003) 1025.
[33] G. Ozturk, F.N. Ertas, E. Akyilmaz, E. Dinckaya, H. Tural, Artif. Cell Blood Sub. 32 (2004) 637.
[34] M.K. Sezginturk, E. Dinckaya, Talanta 65 (2005) 998.
[35] F.S. Felix, M. Yamashita, L. Angnes, Biosens. Bioelectron. 21 (2006) 2283.
[36] J.V.B. Kozan, R.P. Silva, S.H.P. Serrano, A.W.O. Lima, L. Angnes, Anal. Chim. Acta 591 (2007) 200.
[37] N.E. Tolbert, A. Oeser, R.K. Yamazaki, R.H. Hageman, T. Kisaki, Plant Physiol. 44 (1969) 135.
[38] A.I. Vogel, Textbook of Quantitative Inorganic Analysis, Longman, London, 1989.
[39] D.D. Perin, B. Dempsey, Buffers for pH and Method Ion Control, Chapman and Hall, London, 1974.
[40] I. Zelitch, S. Ochoa, J. Biol. Chem. 201 (1953) 700.
[41] L. Zhihong, Q. Wenjian, W. Meng, Anal. Lett. 25 (1992) 1175.
[42] P.D. Hale, L.I. Boguslavsky, H.I. Karan, H.L. Lan, H.S. Lee, Y. Okamoto, T.A. Skotheim, Anal. Chim. Acta 248 (1991) 155.
[43] H. Gunasingham, C.H. Tan, Analyst 115 (1990) 35.
[44] M. Khayyami, G. Johansson, K. Kriz, B. Xie, P.-O. Larsson, B. Danielsson, Talanta 43 (1966) 957.
[45] J.M. Dick, W.J. Aston, G. Davis, A.P.F. Turner, Anal. Chim. Acta 182 (1986) 103.
[46] R.A. Kamin, G.S. Winson, Anal. Chem. 52 (1980) 1198.
[47] B.A. Gregg, A. Heller, Anal. Chem. 62 (1990) 258.
[48] W. Oungpipat, P.W. Alexander, P. Southwell-keely, Anal. Chim. Acta 309 (1995) 35.
[49] I. Zelith, S. Ochoa, J. Biol. Chem. 201 (1953) 707.
[50] I. Zelith, J. Biol. Chem. 201 (1953) 719.
[51] N.A. Frigerio, H.A. Harbury, J. Biol. Chem. 231 (1985) 135.

Talanta 77 (2008) 679–683

Contents lists available at ScienceDirect

Talanta

journal homepage: www.elsevier.com/locate/talanta

Determination of seven polyphenols in water by high performance liquid chromatography combined with preconcentration

Qian Liu, Wensheng Cai, Xueguang Shao*

Research Center for Analytical Sciences, College of Chemistry, Nankai University, Weijin Road No. 94, Tianjin 300071, PR China

ARTICLE INFO

Article history:
Received 9 April 2008
Received in revised form 29 June 2008
Accepted 4 July 2008
Available online 15 July 2008

Keywords:
Polyphenols
Adsorption
Desorption
XAD-4 resin
High performance liquid chromatography

ABSTRACT

A method for determination of seven polyphenols (chlorogenic acid, esculetin, caffeic acid, scopoletin, rutin, quercetin hydrate, kaempferol) by reversed-phase high performance liquid chromatography (RP-HPLC) combined with preconcentration was developed. The preconcentration was accomplished by adsorption–desorption method with a styrene-divinylbenzene resin (XAD-4), and the analytes were desorbed by methanol. The parameters of adsorption and desorption, such as the amounts of resin, adsorption time, pH of the adsorption solution, and the volume of methanol for desorption were optimized. RP-HPLC with photodiode array detector (PAD) was employed for the qualitative and quantitative analysis. Methanol and acetic–water (1:99, v/v) solution were used as the mobile phase, and a gradient program was established for separation. Calibration curves of the seven analytes were obtained in the range of 0.8–3 mg L^{-1}, with correlation coefficients (R) higher than 0.9990. With standard samples, the recoveries for the preconcentration step under optimal conditions were 93–99%, and the relative standard deviations were 0.2–2.0% (n = 5). Polyphenols in simulated tobacco-polluted water were analyzed with the optimized conditions. Chlorogenic acid and rutin were found and determined, whose concentrations were 32.8 and 19.2 μg L^{-1}, respectively. The spiked recoveries of the polyphenols were 83–95% except quercetin hydrate (63%), the relative standard deviations were less than 3.5% (n = 5).

1. Introduction

Polyphenols are widely distributed in plants, such as fruits, vegetables, tea, olive oil, tobacco and so on. As a large group of bioactive chemicals, they have diverse biological functions. Polyphenols are essential to plant life, which can provide defense against microbial attacks and make food unpalatable to predators. As antioxidants, they can be used in the treatment of disease and cancer as well. Moreover, polyphenols have many industrial applications, for example, they are used as natural colorants and preservatives for foods, and applied in the production of paints, paper, and cosmetics [1–3].

Cigarettes are the most littered item in the world and it is estimated that several trillion cigarette butts are littered worldwide every year. The vast amounts of cigarette butts are flicked on our sidewalks, beaches, nature trails, gardens, and other public places every day [4]. Polyphenols (chlorogenic acid, rutin, scopoletin, esculetin, caffeic acid, quercetin and kaempferol) and other organic residues in the cigarette butts which are difficult to decompose are released into the environment. Thus, the monitoring of environmental water and recovery of the valuable compounds have both environmental and economic benefits.

There is an increasing demand for highly sensitive and selective analytical method for the determination of polyphenols. In most of previous studies, polyphenols have been analyzed by thin-layer chromatography (TLC) [5,6], gas chromatography (GC) [7–9], high performance liquid chromatography (HPLC) [10–14], capillary electrophoretic, capillary electrochromatographic techniques [15–19] and other methods [20]. GC has great separation capacity, and offers high sensitivity and selectivity when combined with mass spectrometry. However, preparation of samples for GC is very troublesome, including the removal of lipids from the extract, liberation of phenolics from ester and glycosidic bonds, and derivatisation for low volatile polyphenols [21]. Electrophoretic separation techniques have the characteristic features of high separation efficiency as well as short analysis time and low consumption of solvents and samples. At the same time, their drawbacks are generally lower sensitivity and worse reproducibility compared to HPLC [21,22]. Reverse phase (RP) HPLC has become a dominating analytical tool for the separation and determination of polyphenols with different detection systems such as diode array detector (DAD), mass or tandem mass spectrometry [23–25]. Sakakibara et al. [26] determined all polyphenols in foodstuffs simultaneously with HPLC-DAD and constructed a library comprising respective

* Corresponding author. Tel.: +86 22 23503430; fax: +86 22 23502458.
E-mail address: xshao@nankai.edu.cn (X. Shao).

0039-9140/$ – see front matter © 2008 Elsevier B.V. All rights reserved.
doi:10.1016/j.talanta.2008.07.011

calibration curves for 100 standard chemicals. Abad-Garcia et al. [27] analyzed polyphenolic compounds in fruit juices by RP-HPLC with DAD. Nevertheless, due to the disadvantages in detection limit and sensitivity, HPLC methods are helpless for low content samples, especially in complex matrix, such as crude plant extracts and environmental samples.

Thus, the purification and preconcentration of the polyphenols from complex matrix are crucial prior to the instrumental analysis. Polyphenols can usually be purified by adsorption–desorption processes by using high efficient sorbents, of which C18 and highly crosslinked styrene-divinylbenzene (S-DVB) copolymers are very popular [28–33]. Scordino et al. [28–30] recovered hesperidin, anthocyanins and hydroxycinnamates from aqueous solutions employing commercial S-DVB and acrylic resins. The results indicated that S-DVB copolymers with large specific surface area were most effective, and the loaded anthocyanins could be totally removed by methanol or ethanol. Agalias et al. [31] recovered the polyphenols from olive oil mill waste water, and the results demonstrated that both XAD-4 and XAD-16 were capable of successfully adsorbing hydroxytyrosol. However, in most of the works for determining polyphenols, solid phase extraction (SPE) was used for purification, but concentration was not achieved or the concentration was accomplished by a following treatment like rotary evaporation and nitrogen blowing, which may lead to loss of polyphenols [34–39]. A few researches were reported on the concentration of the tobacco-polyphenols by SPE.

In the present work, a method for determination of the seven low content polyphenols by HPLC combined with a preconcentration step was developed. The adsorption of low content polyphenols was investigated to increase the sensitivity of HPLC analysis. Since environmental water analysis is the aim for the method, the commonly used resin (XAD-4) was selected in view of industrial application and practicability. The central works were searching the optimal conditions for the adsorption–desorption processes and assessing the feasibility for determination of the low content polyphenols in environmental water. Results show that the enrichment is very effective and the recoveries are considerable for both standard solution and environmental water sample.

2. Experimental

2.1. Materials and reagents

Methanol (Concord Technology Co., Ltd. Tianjin, China) was of HPLC grade. Acetic acid and hydrochloric acid, provided by Beifang Chemicals (Tianjin, China), were of analytical reagent grade. Purified water, provided by Wahaha Company (Hangzhou, China), was used throughout.

Chlorogenic acid, esculetin, caffeic acid, scopoletin, quercetin hydrate were purchased from ACROS Company (America), rutin hydrate and kaempferol were purchased from DR.E Company (Augsburg, Germany) and Tokyo Kasei Kogyo Co., Ltd (Japan), respectively. Each stock solution of polyphenol standards was made up at 1.0×10^3 mg L^{-1} in methanol. All stock standard solutions were stored at 4 °C in darkness. The working solutions were prepared weekly by mixing each stock solution and diluting with methanol, and the aqueous solutions for adsorption were prepared by mixing each diluted stock solution and diluting with purified water.

The Amberlite XAD-4 resin was a macroporous S-DVB copolymer, which was purchased from Rohm & Haas (Chauny, France). The characteristics of the resin are as follows: average particle size, 640 μm; average pore size, 100 Å; surface area, 750 m^2 g^{-1}; porosity, 0.5 mL mL^{-1}; specific gravity, 1.01–1.03; moisture content, 54–60%; maximum temperature, 150 °C; pH range, 0–14.

2.2. Samples

To evaluate the feasibility of the developed method, local river water was collected. The pH of the river water was around 7 and there were some laurel-green suspended solids which were filtered before use. The water was analyzed by HPLC, no polyphenol was found and only a small quanlity of organic compound was detected. A blank run for the preconcentration of the river water was also done by using the adsorption–desorption method, polyphenol was still not found. Thus, a little of cigarette was added to the river water artificially to simulate the tobacco-polluted water as the test sample in this work. 0.0500 g cigarette was put to 200 mL river water for static extraction for 15 min at room temperature. The extract was filtered, 5.00 mL filtrate was diluted to 50 times (250 mL) with river water and adjusted to pH 2.5 with dilute hydrochloric acid prior to the adsorption.

2.3. HPLC analyses

The chromatographic system consists of a Waters 1525 binary pump and a waters 2996 photodiode array detector (Milford, MA, USA). C_{18} column (SunFire™ 5 μm, 4.6 mm × 150 mm, waters, USA) was used for separation. Data acquisition and analyse were carried out using the Empower software (Waters Technologies, America). The photodiode array detector was operated between 210 and 400 nm. The solvent system was composed of methanol (eluent A) and the mixture of acetic acid–water solution (1:99, v/v) (eluent B). The gradient elution program was used, i.e., initial condition was A:B = 3:7 for 6.5 min, followed by linear gradient to A:B = 8:2 at 14 min, and maintained this proportion until the end of run. The flow rate was 1 mL min^{-1} and the injection volume was 10 μL. Each of the polyphenols is monitored and quantified at the wavelength of its maximal absorbance, i.e., chlorogenic acid, 327.5 nm; esculetin, 345.4 nm; caffeic acid, 323.9 nm; scopoletin, 345.4 nm; rutin, 356.2 nm; quercetin hydrate, 370.3 nm; and kaempferol, 365.5 nm. Both the retention time and the UV spectra were used to identify the polyphenols in the simulated environmental samples.

2.4. Adsorption and desorption method

Activation of the resin was performed by overnight soaking in 96% ethanol with two bed volumes (BV) of 96% ethanol, followed by rinsing with five BV of purified water. Batch adsorption experiments were carried out in 500 mL glass-stoppered flask. 250 ml aqueous solution of low content polyphenols was introduced into the flask. The solution pH was adjusted to the desired level (between 2.5 and 5.0) with dilute hydrochloric acid. Then, the predetermined amounts of XAD-4 resin were introduced into the flask. Each suspension was stirred using magnetic stirring bar at 400 rpm for certain hours at room temperature (20 ± 1 °C) in darkness. The main parameters, such as the amounts of resin, contact time and pH, were optimized as discussed in the following section.

When the adsorption was complete, the adsorbed XAD-4 resin was separated and dried by fast filtration. Then, it was filled into a glass column (7 cm × 4 cm i.d.). The analytes were desorbed with certain amounts of methanol (≤5 mL) at a flow rate of approximately 1 mL min^{-1}, and the column was dried by air pressure to collect the analytes to the greatest extent. The effluents were collected, diluted to 5 mL with methanol. The obtained solution was filtered through 0.45 μm polytetrafluoroethylene (PTFE) filters and analyzed by HPLC system immediately.

Because the initial concentrations of the polyphenol standards were below the lowermost point of the calibration curve, the adsorption and desorption efficiency were evaluated by the total

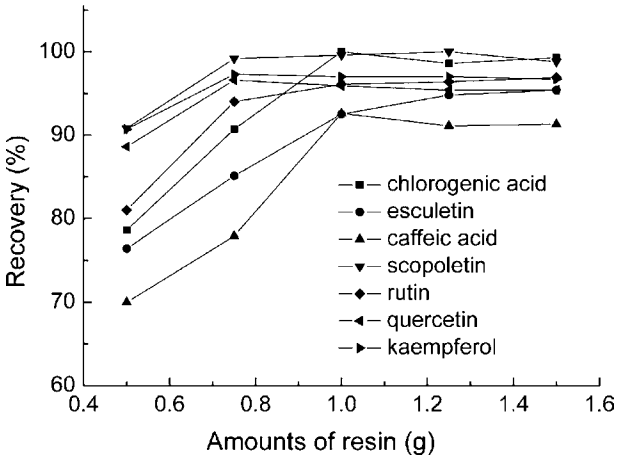

Fig. 1. Effect of resin dosage on the adsorption of polyphenols (V, 250 mL; C_0, 0.024 mg L^{-1}; T, 293 K; contact time, 2 h; pH, 2.5; volume of methanol, 5 mL).

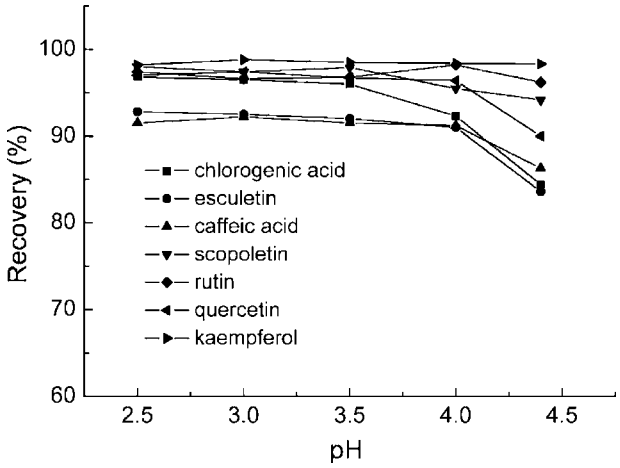

Fig. 3. Effect of pH on the adsorption of polyphenols (V, 250 mL; C_0, 0.024 mg L^{-1}; T, 293 K; amounts of resin, 1 g; contact time, 2 h; volume of methanol, 5 mL).

recovery. The recoveries were defined as the ratios between the measured and initial quantity of the polyphenols.

3. Results and discussion

3.1. Optimization of the adsorption and desorption conditions

With the purpose to increase the recovery of the analytical method, the amounts of resin, the pH and contact time for adsorption, and the volume of methanol for desorption, were optimized by using 250 mL mixed solution containing 0.024 mg L^{-1} of each polyphenol.

At first, different amounts of XAD-4 resin (0.50, 0.75, 1.00, 1.25, 1.50 g) were used for adsorption of the polyphenol standard solutions to study the effect of the sorbent dosage. 2 h contact time and pH 2.5 were employed. The recoveries are shown in Fig. 1. The points are connected just for expressing the trends clearly, instead of representing a mathematical function. It is clear that 1.0 g resin is sufficient for the adsorption.

Secondly, the variation of the recoveries with contact time was investigated varying from 0.5 to 4 h by using 1.0 g sorbent dosage and pH 2.5. Fig. 2 shows the result, from which it can be found that the recoveries increase with the contact time at the beginning stage, but after 2 h they reach a platform. This result indicates that the adsorption equilibrium can be established within 2 h. Therefore, 2 h was used for the adsorption contact time.

The pH of the adsorption solution is also a key parameter that affects the adsorption behavior of the sorbent. Considering the stability of the polyphenols [40,41], the pH range from 2.5 to 5 was investigated. 5 is the pH value without any adjustment. Fig. 3 shows the effect of pH on the recoveries, which clearly indicates that the increase of the acidity of the solution improves the efficiency of the adsorption. This result is consistent with that reported by Kammerer et al. [42], saying that protonation of phenolic compounds in highly acidic conditions significantly enhances their affinity to nonpolar resins. So, pH 2.5 is chosen for the adsorption.

On the other hand, for the desorption step, methanol was used as suggested in literatures [42,43], and effect of the methanol volume used in the desorption was investigated. Fig. 4 shows the variation of the recoveries with the methanol volume. It is clear that 5 mL is an adequate quantity to elute the adsorbed polyphenols.

With the optimized conditions above, the recoveries for the standard samples are 93–99%, and the relative standard deviations are 0.2–2.0% (n = 5). Moreover, the parameters were used to investigate the effect of the sample volumes on the recoveries. 25, 50, 100, 250 mL sample solutions containing the same mass of the polyphenols were used. Results show that the recoveries are influenced slightly by the sample volume when it is below 250 mL.

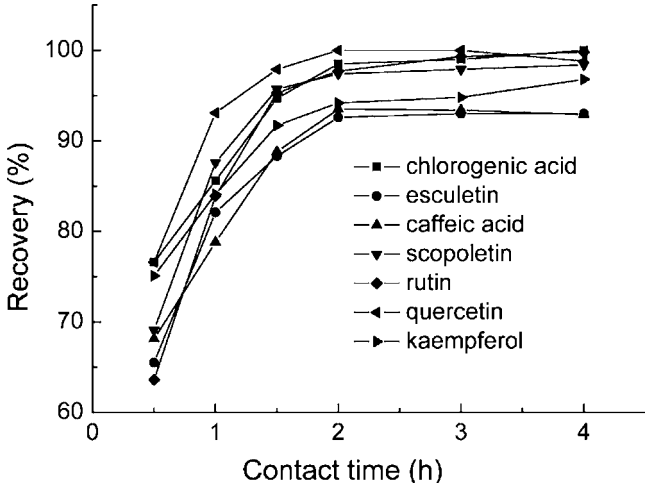

Fig. 2. Effect of contact time on the adsorption of polyphenols (V, 250 mL; C_0, 0.024 mg L^{-1}; T, 293 K; amounts of resin, 1 g; pH, 2.5; volume of methanol, 5 mL).

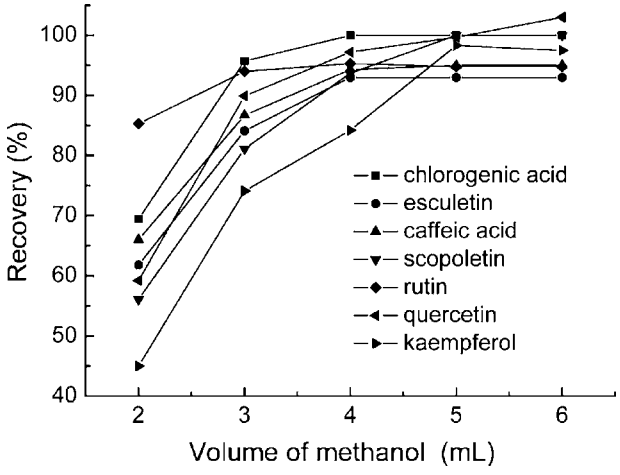

Fig. 4. Effect of the volume of methanol on the desorption of polyphenols (V, 250 mL; C_0, 0.024 mg L^{-1}; T, 293 K; amounts of resin, 1 g; contact time, 2 h; pH, 2.5).

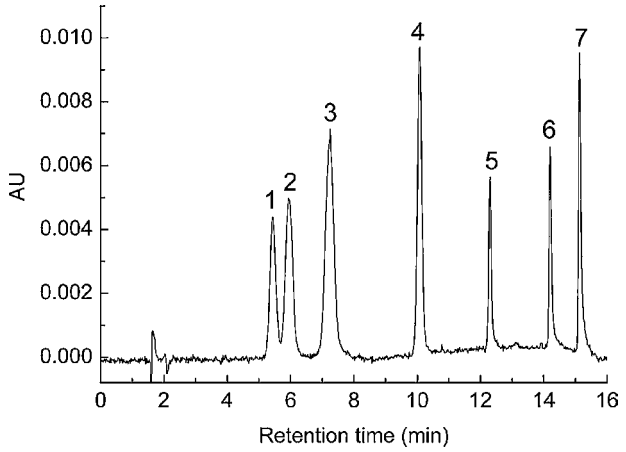

Fig. 5. Typical chromatogram at 327.5 nm obtained for polyphenol standards. Identified compounds of peaks 1–7 are chlorogenic acid, esculetin, caffeic acid, scopoletin, rutin, quercetin hydrate, kaempferol, respectively.

3.2. Separation and qualitative analysis

Because the acidic condition is required to get a satisfactory separation and peak shapes due to the nature of the polyphenols, acetic acid was chosen to regulate the pH of the mobile phase. But considering the stability of the C_{18} column, the pH of acetic acid–water was fixed at 2.5, in which the percentage of acetic acid is 1%. Methanol was used as an organic elution agent and the influence of its content on the retention of the analytes was investigated. It was found that the retention time of the polyphenols decreases with the increase of the methanol content, and gradient elution must be used for a better resolution. With the influence of the methanol content on the retention and trials, the gradient elution described in Section 2.3 was used, with which the seven polyphenols can be separated successfully and the run time was 16 min. Fig. 5 shows a typical chromatogram at 327.5 nm.

To identify the polyphenols, both the retention time and the UV spectra were used. Retention time with the standard deviation ($n = 5$) and maximal absorption wavelength for the identification of the polyphenols are listed in Table 1.

3.3. Quantitative analysis

Quantitative determination was performed by external calibration. For establishing the calibration curves, different working solutions were prepared by dilution of the mixed stock solutions with methanol. With the aim for determination of low content polyphenols, a relatively low concentration and a narrow concentration range from 0.8 to 3 mg L^{-1} were investigated. Each polyphenol was monitored at its maximal absorption wavelength, and the calibration curve of each compound was established with five samples with different concentration. The limits of detection were estimated by decreasing the concentration of the analytes down to the smallest detectable peaks (S/N = 3). The regression equation, correlation coefficient and limit of detection are listed in Table 2. In order to investigate the reproducibility of the method, five measurements of the sample with the highest concentration were repeated. The relative standard deviations (R.S.D.s) of the peak area are found between 0.8% and 6.0% ($n = 5$), which are also listed in Table 2.

Table 1
Retention time and maximal absorption wavelength for the identification of the polyphenols

Peak no.	Polyphenol	$t_R \pm$ S.D. (min)	λ_{max} (nm)
1	Chlorogenic acid	5.43 ± 0.13	327.5
2	Esculetin	5.60 ± 0.30	345.4
3	Caffeic acid	7.24 ± 0.22	323.9
4	Scopoletin	10.10 ± 0.11	345.4
5	Rutin	12.30 ± 0.07	356.2
6	Quercetin hydrate	14.20 ± 0.04	370.3
7	Kaempferol	15.20 ± 0.04	365.5

Table 2
Calibration curves of the polyphenols and the related parameters

Polyphenols	Regression equation[a]	R	LOD (mg L^{-1})	R.S.D. (%, $n = 5$)
Chlorogenic acid	$y = -1.04 \times 10^5 + 2.44 \times 10^5 x$	0.9997	0.2	6.0
Esculetin	$y = -8.89 \times 10^4 + 3.97 \times 10^5 x$	0.9998	0.3	1.2
Caffeic acid	$y = -1.51 \times 10^5 + 4.81 \times 10^5 x$	0.9996	0.3	5.6
Scopoletin	$y = -4.74 \times 10^4 + 4.37 \times 10^5 x$	0.9999	0.1	0.8
Rutin	$y = -1.54 \times 10^4 + 1.66 \times 10^5 x$	0.9999	0.2	3.3
Quercetin hydrate	$y = -7.60 \times 10^4 + 2.30 \times 10^5 x$	0.9997	0.3	1.0
Kaempferol	$y = -8.66 \times 10^4 + 3.48 \times 10^5 x$	0.9995	0.3	3.5

[a] y is the peak area and x the concentration in mg L^{-1}.

3.4. Analysis of polyphenols in the simulated environmental samples

To investigate the applicability of the method, environmental water sample was analyzed. At first, local river water was collected and analyzed, but no polyphenol was found. Therefore, the simulated tobacco-polluted environmental sample was prepared by putting a little of cigarette power into a large volume of the river water. The contents of the simulated sample stated in Section 2.2 were under the limits of detection, so 250 mL of the sample was concentrated by using the same conditions, i.e., resin dosage, 1 g; contact time, 2 h; pH, 2.5; volume of methanol for desorption, 5 mL. The chromatogram of the simulated environmental sample after preconcentration using XAD-4 was given in Fig. 6. Identified compounds of peaks 1 and 2 are chlorogenic acid and rutin, respectively. With the calibration curves listed in Table 2, the concentrations of the two compounds were found to be 32.8 and 19.2 μg L^{-1}, respectively.

Furthermore, polyphenol standard solutions were added to the simulated sample prior to the preconcentration for estimation of the recoveries of this method, and the precision of the method was also evaluated through a five-replicated determination. Table 3

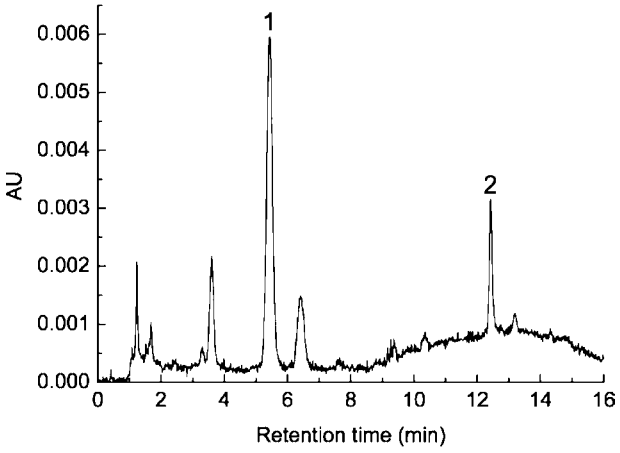

Fig. 6. Chromatogram of the simulated tobacco-polluted water sample after preconcentration using XAD-4. Peak 1 and 2 are identified as chlorogenic acid and rutin, respectively.

Table 3
Analytical results for the polyphenols in the simulated samples

Component	Determined[a] (μg)	Spiked (μg)	Found (μg)	Recovery[b] (%)	R.S.D. (%, $n = 5$)
Chlorogenic acid	8.2	4	11.8	90	2.8
Esculetin	0	6	5.0	83	3.5
Caffeic acid	0	6	5.6	93	2.3
Scopoletin	0	6	5.7	95	0.8
Rutin	4.8	2	6.7	95	3.2
Quercetin hydrate	0	6	3.8	63	3.2
Kaempferol	0	6	5.0	83	1.1

[a] Because 250 mL simulated tobacco-polluted water was used, the corresponding concentrations of chlorogenic acid and rutin are 32.8 and 19.2 $\mu g\,L^{-1}$, respectively.
[b] The recovery is calculated by the quantities (Q) determined, spiked and found, i.e. $(Q_{found} - Q_{determined})/Q_{spiked}$.

summarized the results. It can be found that the recoveries of the polyphenols were between 83% and 95% except for quercetin hydrate (63%), and the R.S.D.s were from 0.8% to 3.5%. With the similar conditions, low recoveries for quercetin were also obtained in the works of de Villiers et al. [39] and Michalkiewicz et al. [44] The relatively low recovery for quercetin may be caused by the poor solubility, or the strong interaction with the complex matrix because it has more phenol hydroxyl than the others, especially compared with kaempferol and rutin.

4. Conclusions

A method for determination of seven polyphenols by RP-HPLC combined with a preconcentration step was developed. The adsorption–desorption method for low content polyphenols by XAD-4 was investigated. The appropriate pH for adsorption was 2.5, it needs 2 h to reach the adsorption equilibrium, and methanol can be used for desorption. Methanol and acetic–water (1:99, v/v) solution were used as the mobile phase, and a gradient program was established for separation. With the optimal experimental conditions, environmental water was analyzed, and the results show that the method has a good reproducibility and acceptable recoveries for the studied analytes. It may provide a good way for determination of low concentration polyphenols in environmental water.

Acknowledgements

This study is supported by National Natural Science Foundation of China (Nos. 20575031 and 20775036).

References

[1] T.P. Kondratyuk, J.M. Pezzuto, Pharm. Biol. 42 (2004) 46–63.
[2] X.Z. Han, T. Shen, H.X. Lou, Int. J. Mol. Sci. 8 (2007) 950–988.
[3] H.Y. Wang, M.M. Zhao, B. Yang, Y.M. Jiang, G.H. Rao, Food Chem. 107 (2008) 1399–1406.
[4] http://www.cigarettelitter.org/.
[5] T. Karting, I. Gobel, J. Chromatogr. A 740 (1996) 99–107.
[6] M. Bagul, H. Srinivasa, H. Padh, M. Rajani, J. Sep. Sci. 28 (2005) 581–584.
[7] T.Y. Chu, C.H. Chang, Y.C. Liao, Y.C. Chen, Talanta 54 (2001) 1163–1171.
[8] L. Minuti, R.M. Pellegrino, I. Tesei, J. Chromatogr. A 1114 (2006) 263–268.
[9] A. Zafra, M.J.B. Juarez, R. Blanc, A. Navalon, J. Gonzalez, J.L. Vilchez, Talanta 70 (2006) 213–218.
[10] H. Wang, L. Kong, H. Zou, J. Ni, Y. Zhang, Chromatographia 50 (1999) 439–445.
[11] Y.G. Zuo, H. Chen, Y.W. Deng, Talanta 57 (2002) 307–316.
[12] A.M. Danila, A. Kotani, H. Hakamata, F. Kusu, J. Agric. Food Chem. 55 (2007) 1139–1143.
[13] S. Mas, G. Fonrodona, R. Tauler, J. Barbosa, Talanta 71 (2007) 1455–1463.
[14] V.E. Fernand, D.T. Dinh, S.J. Washington, S.O. Fakayode, J.N. Losso, R.O. van Ravenswaay, I.M. Warner, Talanta 74 (2008) 896–902.
[15] D.L.D. Lima, A.C. Duarte, V.I. Esteves, Talanta 72 (2007) 1404–1409.
[16] P. Jac, M. Polasek, M. Pospisilova, J. Pharm. Biomed. Anal. 40 (2006) 805–814.
[17] A. Cifuentes, Electrophoresis 27 (2006) 283–303.
[18] J. Xu, H. Zhang, G. Chen, Talanta 73 (2007) 932–937.
[19] X.K. Wang, Y.Z. He, L.L. Qian, Talanta 74 (2007) 1–6.
[20] S. Li, X. Li, J. Xu, X. Wei, Talanta 75 (2008) 32–37.
[21] A. Carrasco-Pancorbo, L. Cerretani, A. Bendini, A. Segura-Carretero, T. Gallina-Toschi, A. Fernandez-Gutierrez, J. Sep. Sci. 28 (2005) 837–858.
[22] C.D. Stalikas, J. Sep. Sci. 30 (2007) 3268–3295.
[23] J.L. Wu, L.P. Yee, Z.H. Jiang, Z.W. Cai, Talanta 73 (2007) 656–661.
[24] J. Zhang, D. Tao, J. Duan, Z. Liang, W. Zhang, L. Zhang, Y. Huo, Y. Zhang, Anal. Bioanal. Chem. 386 (2006) 586–593.
[25] X. Yang, Y. Xia, X. Liao, Y. Zuo, Y. Liao, H. Liu, Talanta 70 (2006) 75–87.
[26] H. Sakakibara, Y. Honda, S. Nakagawa, H. Ashida, K. Kanazawa, J. Agric. Food Chem. 51 (2003) 571–581.
[27] B. Abad-Garcia, L.A. Berrueta, D.M. Lopez-Marquez, I. Crespo-Ferrer, B. Gallo, F. Vicente, J. Chromatogr. A 1154 (2007) 87–96.
[28] M. Scordino, A. Di Mauro, A. Passerini, E. Maccarone, J. Agric. Food Chem. 51 (2003) 6998–7004.
[29] M. Scordino, A. Di Mauro, A. Passerini, E. Maccarone, J. Agric. Food Chem. 52 (2004) 1965–1972.
[30] M. Scordino, A. Di Mauro, A. Passerini, E. Maccarone, J. Agric. Food Chem. 53 (2005) 651–658.
[31] A. Agalias, P. Magiatis, A.L. Skaltsounis, E. Mikros, A. Tsarbopoulos, E. Gikas, I. Spanos, T. Manios, J. Agric. Food Chem. 55 (2007) 2671–2676.
[32] S. Yamamoto, M. Hakoda, T. Oda, M. Hosono, J. Chromatogr. A 1162 (2007) 50–55.
[33] H. Niu, Y. Cai, Y. Shi, F. Wei, J. Liu, S. Mou, G. Jiang, Anal. Chim. Acta 594 (2007) 81–92.
[34] X. Gu, J. Cai, J. Yang, Q. Su, J. Sep. Sci. 28 (2005) 184–188.
[35] X. Gu, J. Cai, X. Zhu, Q. Su, J. Sep. Sci. 28 (2005) 2477–2481.
[36] K. Ishii, T. Furuta, Y. Kasuya, J. Chromatogr. B 759 (2001) 161–168.
[37] K. Ishii, T. Furuta, Y. Kasuya, J. Chromatogr. B 794 (2003) 49–56.
[38] A.H. Liu, H. Guo, M. Ye, Y.H. Lin, J.H. Sun, M. Xu, D.A. Guo, J. Chromatogr. A 1161 (2007) 170–182.
[39] A. de Villiers, F. Lynen, A. Crouch, P. Sandra, Chromatographia 59 (2004) 403–409.
[40] E.M. Silva, D.R. Pompeu, Y. Larondelle, H. Rogez, Sep. Purif. Technol. 53 (2007) 274–280.
[41] M. Friedman, H.S. Jurgens, J. Agric. Food Chem. 48 (2000) 2101–2110.
[42] D.R. Kammerer, Z.S. Saleh, R. Carle, R.A. Stanley, Eur. Food Res. Technol. 224 (2007) 605–613.
[43] A. Schieber, P. Hilt, P. Streker, H.U. Endreβ, C. Rentschler, R. Carle, Innov. Food Sci. Emerg. Technol. 4 (2003) 99–107.
[44] A. Michalkiewicz, M. Biesaga, K. Pyrzynska, J. Chromatogr. A 1187 (2008) 18–24.

Talanta 77 (2008) 915–923

Contents lists available at ScienceDirect

Talanta

journal homepage: www.elsevier.com/locate/talanta

Test films for test-determinations on the base of reagents, immobilized in gelatinous gel

Lidia P. Loginova*, Olga Yu. Konovalova

Department of Chemical Metrology, V.N. Karazin Kharkov National University, Svoboda Sq. 4, 61077 Kharkov, Ukraine

ARTICLE INFO

Article history:
Received 25 January 2008
Received in revised form 21 July 2008
Accepted 26 July 2008
Available online 3 August 2008

Keywords:
Test film
Gelatinous gel
Reductant
Primary aromatic amine

ABSTRACT

Gelatinous solidified layers of the photographic film were used for the immobilization of analytical reagents for detection and determination of reductants and primary aromatic amines. It was shown, that the films with immobilized iron(III)-Dipy or iron(III)-Phen complexes as test films for reductants and films with immobilized aldehydes (vanillin, *p*-dimethylaminobenzaldehyde) as the test films for primary aromatic amines can be used. The improving of reagents immobilization in the presence of sodium dodecylsulfate micelles was obtained. Metrological characteristics of visual detection and photometric determination using test films were evaluated on the basis of statistical approach and investigation of detection probability distribution in the concentration range of unreliable reaction. The suggested test films for the determination of ascorbic acid, analgin (dipyrone), novocaine and streptocide in drugs were examined successfully.

1. Introduction

Different test tools such as indicator strips, indicator tubes, powders, etc., are used for the identification of individual substances, for fast screening numerous analyzed samples or for in-real-site control of the composition and quality of the consumption products [1]. One of the ways of the new test tools creation is the search of new materials for immobilization of analytical reagents. Of special interest are the transparent materials, which allow registering analytical effect by UV–visible photometry. For instance, polymethacrylate matrixes were successfully used for obtaining the transparent test films for determination of ascorbic acid, iron(II, III), fluoride-ions [2–4]. Another example of a transparent material for immobilization of reagents is gelatinous gel. Gelatinous solidified layers of the commercial photographic films have been used earlier for the synthesis of low water soluble metal complexes and studying their spectral properties [5–7], for photometric investigation of the mechanism of the gelatine staining with fluorone derivative dyes [8], for study of the medium effects of acid–base indicators [9]. Test films for detection and determination of drug nitroxoline [10] and determination of heavy metals ions total concentration [9] on the basis of a gelatinous layer have been obtained in our previous works. It was shown recently, that in gelatinous gel of the films it is possible to immobilize the reagents for diazotization and azocoupling reactions; on this base the sensitive elements for determination of nitrites are offered [11]. Gelatinous layer of the photographic film as medium for photometric studies has following advantages: transparency, isotropic of the physico-mechanical properties, mechanical stability and colour uniformity of the samples obtained on the basis of the films. Creation of the new test tools with using of the gelatinous gel of the photographic films as medium for immobilization of reagents is of interest.

Many practically important organic substances which are constituents of drugs, food-additives, food-stuffs have the reductant and antioxidant properties. The best-known substance of such type is ascorbic acid. The commercial test strips for detection and semi-quantitative determination of ascorbic acid are produced [12,13]. Indicator powders [14–19], test films [2–4], special cuvettes with integrated sensor layer made of dye Prussian blue [20–22] for the test-determination of ascorbic acid are suggested also. Application of the same test tools for determination of other reductants, for example, medicine analgin [15], and for the control total amount of reductants [18] or antioxidants [19] is described.

The group of primary aromatic amines (PAA) includes widespread substances: aniline, its derivatives and many drugs such as a local anesthetic drugs and sulfanamides. For the test-determination of PAA the indicator powders [23,24], indicator tubes [25–27], papers [28,24], test strips [27,29] have been suggested.

Present work is devoted to further study of the immobilization possibilities of analytical reagents into gelatinous solidified layer

* Corresponding author. Tel.: +380 57 7075367.
E-mail address: loginova@univer.kharkov.ua (L.P. Loginova).

0039-9140/$ – see front matter © 2008 Elsevier B.V. All rights reserved.
doi:10.1016/j.talanta.2008.07.051

and to creation of new test tool for identification and determination of reductants and primary aromatic amines.

2. Experimental

2.1. Reagents

The analytes (detected and determined substances) are shown in Fig. 1, they were pharmaceutical substances.

2.1.1. Analytical reagents

2,2′-Dipyridyl (Dipy), 1,10-phenantroline (Phen) from Reanal (Hungary); vanillin, *p*-dimethylaminobenzaldehyde (*p*-DMAB), terephthalic aldehyde, salicylaldehyde, furfurol were of analytical grade; bromphenolic blue (BPB) was of analytical grade.

2.1.2. Auxiliary reagents

$NH_4Fe(SO_4)_2{\cdot}12H_2O$ was of analytical grade; sodium dodecyl sulfate (SDS, 97% m/m) from AppliChem (Germany) was used without further purification; aqueous ethanol (96% v/v). Hydrochloric acid, perchloric acid, acetic acid, sodium acetate trihydrate were of analytical grade and were used for regulation of the solution acidity.

2.2. Preparation of the solutions

Stock solutions of analgin and sodium ascorbate (ascorbic acid) were prepared by dissolving a weighted amount of substances in 0.1 M $HClO_4$ solution just before investigation to prevent decomposition of the target component. Working solutions were obtained by suitable dilution of the stock solutions by 0.1 M $HClO_4$.

Stock solutions of novocaine, streptocide and streptocide soluble were prepared by dissolving a weighted amount of amines in water or in 2 M HCl solution. Working solutions were obtained by suitable dilution of the stock solutions by water or by 2 M HCl solution.

Iron(III) solution was prepared by dissolving a weighted amount of $NH_4Fe(SO_4)_2{\cdot}12H_2O$ in water, the undissolved residue was filtered out. Concentration of iron(III) was determined by titration with disodium dihydrogen ethylenediaminetetraacetate at pH 2.5 in presence of sulfosalicylic acid as indicator [30].

Aldehydes solutions (0.3 M vanillin, 0.1 M *p*-DMAB, 0.5 M furfurol, 0.2 M salicylaldehyde, 0.05 M terephthalic aldehyde) were prepared by dissolving a weighted amount of aldehydes in ethanol and diluting to the mark with water (the ratio of ethanol: water volumes was equal 2:3).

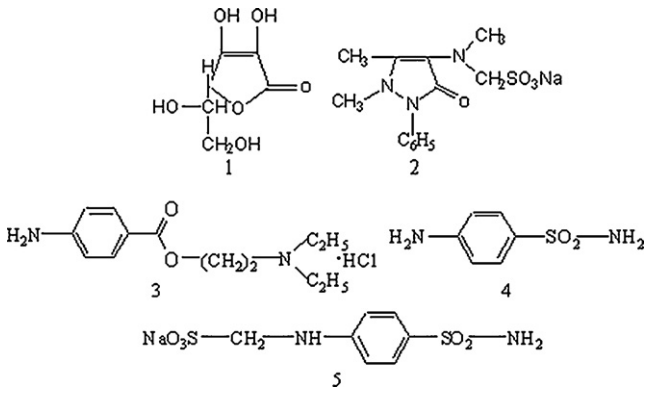

Fig. 1. Structure of the substances–analytes: (1) ascorbic acid (γ-lactone-2,3-dehydro-L-gulonic acid); (2) analgin (dipyrone; sodium 2,3-dimethyl-1-phenyl-4-methylaminopyrazolone-5-*N*-methanesulfonate hydrate); (3) novocaine (4-aminobenzoic acid 2-(diethylamino)ethyl ester hydrochloride); (4) streptocide (4-aminobenzenesulfonamide); (5) streptocide soluble (sodium *p*-sulfamidebenzeneaminomethylenesulfonate).

To prepare all solutions for investigations with reductants the double distilled water was used. To prepare all solutions for investigations with PAA the distilled water was used.

2.3. Preparation of the initial films

Gelatinous solidified layers of the commercial photographic films "Micrat-300" were used to obtain test films after removing of silver compounds [31]. In order to remove of silver compounds an initial film was spoiled (by exposing it to light for 4 days) and was immersed in a solution contained 88 g/l sodium citrate and 6 g/l potassium hexacyanoferrate(III) for 10 min. The obtained film was washed and immersed in aqueous solution of 1.6 mol/l sodium thiosulfate for 10 min, then was washed in the running distilled water for 20 min and was dried on air. Colourless resulting films were used for immobilization of analytical reagents and obtaining of test films.

2.4. Equipment

Absorption spectra were registered with a photometer KFK-3 (Zagorsk, Russia). Absorbance of the solutions and of the coloured films was measured against the blank solution or blank film containing all reagents except analyte respectively.

Hydrophobicity parameters $\log P_{o/w}$ were calculated using the HyperChem 6.01 program packet (2000 Hypercube, Inc.).

3. Results and discussion

3.1. Test films for detection and determination of reductants

3.1.1. The choice of analytical reagents for test-determination of reductants

The different analytical reagents are used by developing of test tools for determination of reductants, namely ascorbic acid and analgin, as described in works [2,3,15–22]. There are copper(II) complexes with tetrabenzo[*b*,*f*,*j*,*n*][1,5,9,13]tetraazacyclohexadecine [15], iron(III) complexes with Dipy [2] or Phen [19], Bindshendler's Green [16], phosphomolybdic acids and compounds of copper(II) [17], ionic associates of Methylene Blue and Toluidine Blue with triiodide ions [18], 2,6-dichlorphenolindophenol [3] and Prussian blue [20–22].

We chose the iron(III) complexes with Dipy and Phen as reagents for immobilization in gelatinous solidified layer. These complexes are widely used as redox-indicators (e.g., ferroin) and their analytical property are appropriate for application in test tools. The reaction of reductant and iron(III) complexes with Dipy and Phen in aqueous solutions at pH < 3 produces contrast colour change from light blue to red colour [32]. Colour change is caused by reduction/oxidation of the central atom of complexes. This one-electronic process is not complicated by secondary reaction, is reversible and run with high rate.

The film containing iron(III) complexes with Dipy (Fe-Dipy-film) after contact with the solutions of analgin or ascorbic acid became brightly pink; the film containing iron(III) complexes with Phen (Fe-Phen-film) became reddish-orange. The colour brightness intensified after drying of the films. The absorption spectra of reduced forms of complexes are shown in Fig. 2. Absorbance maximum of film-immobilized reduced complexes was observed at the wavelength similar to one in the alcohol–aqueous or aqueous solution: for the complex iron(II)-Dipy in film λ_{max} 525 nm, in aqueous solution λ_{max} 522 nm [30,32]; for the complex iron(II)-Phen in film λ_{max} 515 nm, in aqueous solution λ_{max} 508 nm [32] or 512 nm [30].

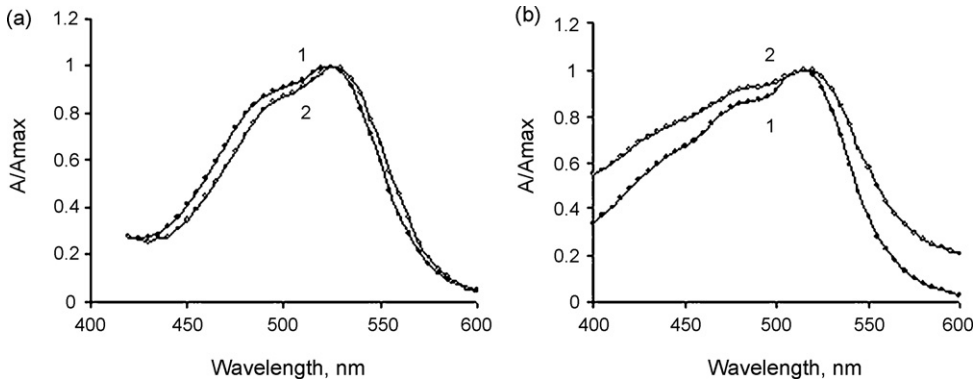

Fig. 2. Absorption spectra of the solutions (1) and the films (2), containing $Fe(Dipy)_3(ClO_4)_2$ (a), $Fe(Phen)_3(ClO_4)_2$ (b).

3.1.2. The optimization of test films obtaining

3.1.2.1. The immobilization of analytical reagents in gelatinous solidified layer. Conditions for reagents immobilization into gelatinous layer of the initial film were chosen according to intensity of the final analytical effect—a film colour after contact with analyte solution. For preparation iron(III) complexes Dipy and Phen was dissolved in 10 ml of ethanol in a 25 ml standard flask and $HClO_4$ or HCl solution was added up to pH 4. Then iron(III) solution aliquot was added into flask and all were diluted up to 25 ml with water. The obtained solution was placed into Petri dish and pieces of the films (2 cm × 3 cm) were immersed into solution for 20 min at periodical stirring. The films were dried on air up to removal of solvent drops and kept in glass bottles with covers. The films with immobilized iron(III) complexes looked almost colourless or slightly yellow just as the solution containing iron(III) complexes at working pH value. Fe-Dipy-films were stable during some months and Fe-Phen-films were stable during 1 month.

The optimal properties of test films were achieved by immobilization of complexes from solutions with following concentrations of reagents: 0.2 M Dipy and 0.004 M iron(III); 0.025 M Phen and 0.002 M iron(III).

The complexes were immobilized into film from acidic solutions. It is observed, that perchloric acid $HClO_4$ was better acidic reagent than HCl. The films obtained in presence of HCl were less coloured after contact with analgin solution and the coloured form was washed out by solution. Obviously, $HClO_4$ promoted the immobilization of complexes $Fe(Dipy)_3^{3+}$ and $Fe(Phen)_3^{3+}$ owing to formation of ionic associates of these cationic complexes with ClO_4^- anions [33]. Formation of ionic associates with Cl^- anions is not typical.

3.1.2.2. The influence of SDS on immobilization of reagents in gelatinous solidified layer. It is known, that anionic surfactants more strongly associate with gelatine, than cationic [34]. Macromolecules of gelatine associate with SDS monomers in aqueous solutions that are accompanied by conformation changes of the macromolecules and their hydrophobization [34,35]. Gelatine macromolecules, adsorbed on the polystyrene surface, form associates with SDS micelles or monomers by electrostatic and hydrophobic interactions too [36]. Hydrophobization of gelatine in the presence of SDS can be used for modification of the properties of the gelatinous gel medium and increasing the ability of gelatinous layer to solubilize the moderately hydrophobic reagents. In this view SDS at concentration above and below the critical micellar concentration (*cmc*) was added into solutions at immobilization of reagents into films.

The test films with immobilized iron(III)-Phen complexes obtained in the presence of 0.01 mol/l SDS were coloured more strongly after contact with reductant solutions than films obtained in the absence of SDS. However, SDS did not effect practically on the property of films containing iron(III) Dipy complexes. The different influence of SDS is attributable to different hydrophobicity of the immobilized ionic associates. Phen is more hydrophobic ligand then Dipy (the values $\log P_{o/w}$ are equal 1.78 and 1.28 respectively). Ionic associates formed by cation $Fe(Phen)_3^{3+}$ are more hydrophobic and less soluble in water than ionic associates formed by $Fe(Dipy)_3^{3+}$, hence, they are sorbed and retained in gelatinous layer better while gelatine is hydrophobized by SDS. On the other hand, SDS anion can also participate in formation of the ionic associates with cations $Fe(Dipy)_3^{3+}$ or $Fe(Phen)_3^{3+}$.

3.1.3. Conditions of the test-determinations using the test films

In order to obtain the best colour effect, the Fe-Dipy-film and Fe-Phen-film were immersed into solution of reductant for 15 s, and were dried on air during 15–20 min. The maximum signal was obtained when analyzed solution contained 0.1 M $HClO_4$ (pH 1). In weak-acidic solutions (pH 4–6, acetate buffer) the partial wash-out of the coloured products from film was observed. The absorbance of the films was found to depend linearly on the ascorbic acid or analgin concentration in analyzed solution (Table 1). Thus, Fe-Dipy-film and Fe-Phen-film can be used for visual identification and for visual and spectrophotometric quantitative determination of reductants in solution. Test films are suitable for determination of trace amount of reductants on the solid surfaces also and, hence, can be recommended for the control of cleanness of the industrial equipment at pharmaceutical factories. In last case it is enough to moisten the surface by $HClO_4$, to put test films on wetted surface for 15 s and to observe the colour change of film after 20 min visually or with spectrophotometer.

3.2. Test films for detection and determination of PAA

3.2.1. The choice of analytical reagents for test-determination of PAA

The test tools for detection and determination of novocaine, streptocide, streptocide soluble and other PAA are described in several articles [23,25–29]. Colour change of such test tools is caused by chemical reaction resulting in formation of azodyes, Shiff's bases and other PAA derivatives. It is known the use of following analytical reagents for PAA testing: 1-naphthol and sodium nitrite [23], *p*-dimethylaminocinnamic aldehyde [25], *N*,*N*-diethyl-*p*-phenylenediamine [26], 7-chlor-4,6-dinitrobenzofuroxan and 4-chlor-5,7-dinitrobenzofurazan [27,29], 1-naphthylamine and sodium nitrite [28].

The formation of Shiff's bases by interaction PAA with aldehydes has some advantages as analytical reaction for test tools. In contrast

Table 1
Estimated calibration parameters of the spectrophotometric determination of analgin and ascorbic acid with test films containing immobilized iron(III) complexes with Dipy or Phen

Test film	Analyte	Number of observation	Concentration range of linear calibration (mM)	Parameters of calibration equation $A = a + bc$, 95% confidence level		Correlation coefficient (R)
				a	b	
Fe-Dipy-film	Analgin	5	0.04–2.9	0.024 ± 0.008	0.081 ± 0.006	0.995
Fe-Dipy-film	Ascorbic acid	4	0.09–2.4	0.026 ± 0.012	0.072 ± 0.009	0.994
Fe-Phen-film	Analgin	5	0.09–7.3	0.06 ± 0.03	0.051 ± 0.009	0.97

to reaction with 1-naphthylamine and 1-naphthol the formation of Shiff's bases is realized as one-stage procedure without use of toxic reagents. It was chosen by us for creation of test tools for PAA.

The preliminary investigation has shown that vanillin and *p*-DMAB were the best for obtaining test films, than others investigated aldehydes: salicylaldehyde, terephthalic aldehyde, furfurol. The films with immobilized aldehydes sometimes had yellow hue; it is possible owing to interaction of aldehydes with N-terminal amino acid residues of gelatine [37]. This colour hue disappeared in the presence of 2 M HCl, which must be added into analyzed solution when testing PAA.

The film containing vanillin (vanillin-film) after contact with the solutions of PAA became citric-yellow; the film containing *p*-DMAB (*p*-DMAB-film) became bright yellow. The absorption spectra of analytical reactions products are shown in Fig. 3. Absorbance maximum was observed at the wavelength λ_{max} 455 nm for the reaction product of *p*-DMAB with novocaine in film as well as in alcohol–aqueous solution; 405 nm for the product of vanillin with PAA in film and 395 nm in alcohol–aqueous solution. Streptocide soluble does not include the primary aromatic amine group, but this group forms by hydrolysis of streptocide soluble in the presence of 2 M HCl and the obtained product interacts with vanillin. Corresponding Shiff's base has absorbance maximum at the wavelength 400 nm in film and 390 nm in alcohol–aqueous solution (Fig. 3).

3.2.2. The optimization of test films obtaining

3.2.2.1. The immobilization of analytical reagents in gelatinous solidified layer. The aldehydes were immobilized into initial colourless film from 0.3 M vanillin neutral solution or from 0.1 M *p*-DMAB weak-acidic solution (pH 4.8–5.0), because *p*-DMAB was badly sorbed by film at higher pH.

For immobilization of aldehyde into film several pieces of the film (2 cm × 3 cm) were immersed into alcohol–aqueous solution of corresponding aldehyde for 20 min and were dried on air. The optimal properties of test films were achieved by immobilization of aldehydes from solutions with ethanol:water ratio 2:3 by volume. The less amount of ethanol could not provide the sufficient solubility of aldehydes, particularly *p*-DMAB and the greater amount of ethanol caused the distortion of obtained films.

3.2.2.2. The influence of SDS on immobilization of reagents in gelatinous solidified layer. Positive effect of SDS was observed for test films for PAA also. The test films with immobilized aldehydes obtained in the presence of SDS gave more strongly colour after contact with PAA solutions that films obtained in the absence of SDS. However, reproduced results were obtained at SDS concentration above *cmc* only. This agrees with data of other authors about Shiff's base formation in solutions. It has been demonstrated in work [25], the analytical effect of reaction of PAA with *p*-dimethylaminocinnamic aldehyde was increased only in micellar solutions of SDS, not in solutions below *cmc*. The optimal concentrations of SDS in present work were equal 0.1–0.2 M, the films obtained at greater concentrations of SDS had irregular surface of gelatinous layer and nonuniform colour after drying.

Improvement of test films properties obtained in the presence of SDS is caused by hydrophobization of gelatine with SDS and corresponding increase the ability of gelatinous layer to solubilize the moderately hydrophobic aldehydes (the values $\log P_{o/w}$ are equal 1–2) and rather hydrophobic Shiff's bases (the values $\log P_{o/w}$ are equal 2–4.5) also.

Vanillin-films and *p*-DMAB-films were stable during 1 year.

3.2.2.3. Peculiarities of the colour reaction p-DMAB with PAA in a gelatinous layer and influence of dye BPB. The reactions of aldehydes with PAA are usually performed in acidic medium [38] or in non-aqueous solvents because of Shiff's bases undergo a hydrolysis up to initial reagents in weak-acidic solutions [38]. The colour reaction of vanillin-film with PAA occurred in solutions containing 2 M

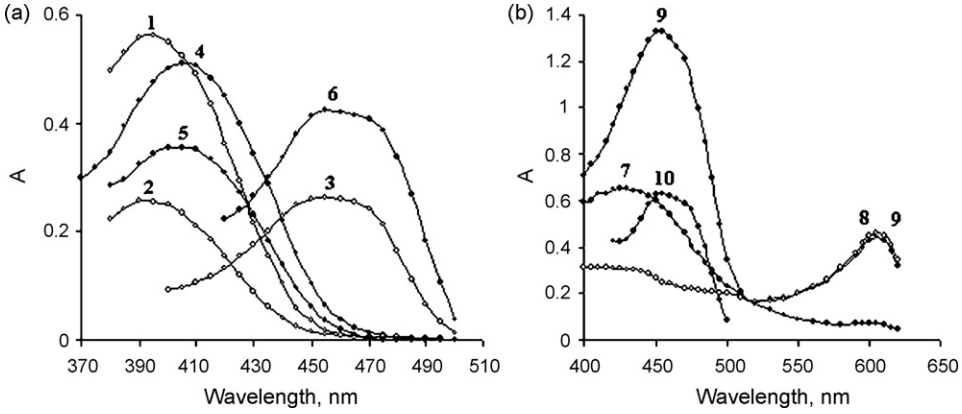

Fig. 3. Absorption spectra of the reaction products of aldehydes with PAA without BPB (a) and in the presence of BPB (b). (1) Vanillin + novocaine in solution; (2) vanillin + streptocide soluble in solution; (3) *p*-DMAB + novocaine in solution; (4) vanillin-film + novocaine; (5) vanillin-film + streptocide soluble; (6) *p*-DMAB-film + novocaine; (7) *p*-DMAB-BPB-film; (8) *p*-DMAB-BPB-film in solution at pH 6; (9) *p*-DMAB-BPB-film + novocaine at pH 6, observation after 30 min; (10) *p*-DMAB-film + novocaine at pH 6, observation after 5–10 min.

HCl only. In contrast to vanillin-film the colour reaction of *p*-DMAB-film with PAA occurred in less acidic solutions with pH from 2 to 6 also. However, in last case the colour of *p*-DMAB-film was unstable, passed through a maximum and disappeared through 10 min.

In order to stabilize colour effect, the test films with immobilized *p*-DMAB were worked up by 5×10^{-4} M dye BPB solution at pH 1 ($HClO_4$) during 10 min. It is known, that mixture of BPB and *p*-DMAB has been used earlier as solid-phase reagent in a gas analyzer for automatic determination of aniline in air [39]. In our work mixture-contained film (*p*-DMAB-BPB-film) had yellow colour which changed to blue in aqueous solution at pH 6, and changed to green in a novocaine solution at the same pH value. Apparently, the rate of colour change is limited by rate of the penetration of an external solution into the gelatinous layer containing immobilized reagents.

Obtained *p*-DMAB-BPB-films were stable during some months.

It was found, that the ionization constant of BPB in gelatinous gel was shifted into acidic region ($pK_a = 2.22 \pm 0.17$) [9] in comparison with $pK_a = 4.10$ in aqueous solution [40]. Thus, initial *p*-DMAB-BPB-film contains the yellow acid (monoanionic) form of dye. Monoanion of BPB is dissociated completely at pH 6 and blue colour of BPB dianion with yellow colour of Shiff's base give green colour. Really, in an absorption spectrum of *p*-DMAB-BPB-film after contact with PAA solution two absorbance maxima are registered: λ_{max} 455 nm (Shiff's base) and λ_{max} 605 nm (dianion of BPB), Fig. 3. Apparently, BPB dianion stabilizes the cationic quinoid structure formed by *p*-DMAB with novocaine in acidic medium in the same way as large anions stabilize the product of interaction of *p*-dimethylaminocinnamic aldehyde with aniline [25,41]. Dependences shown in Fig. 4 confirm this assumption. If *p*-DMAB-film contacted with novocaine solution at pH 6, absorption maximum at 455 nm disappeared with time because of hydrolysis of Shiff's base (curve 1 in Fig. 4). In the case of *p*-DMAB-BPB-film absorbance at 455 nm is stabilized at the instant the film-immobilized dye BPB transforms into blue dianion completely and absorbance at 605 nm become stable (curve 2 in Fig. 4). Unfortunately, complicated character of colour reaction in this case results in colour irregularity of the *p*-DMAB-BPB-film; however, contrast of colour change is suitable for visual observation, but not for spectrophotometric measurement.

3.2.3. Conditions of the test-determinations using the test films

In order to obtain the best colour effect, the vanillin-film and *p*-DMAB-film were immersed into solution of PAA containing 1×10^{-3} M SDS and 2 M HCl for 10 s and were dried on air. The

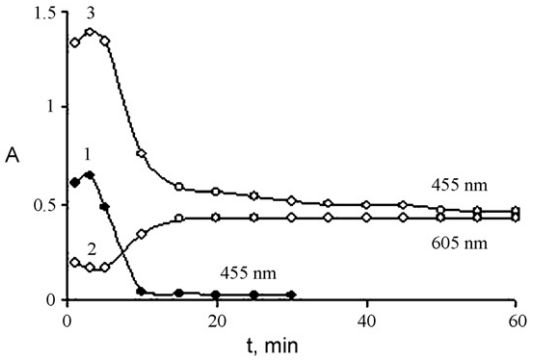

Fig. 4. Time dependence of the absorbance of the *p*-DMAB-film (1) and the *p*-DMAB-BPB-film (2, 3) after film contact with solution of novocaine at pH 6. (1) Film absorbance at 455 nm measured against blank film; (2) film absorbance at 605 nm measured against blank film; (3) film absorbance at 455 nm measured against *p*-DMAB-BPB-film treated in solution at pH 6.

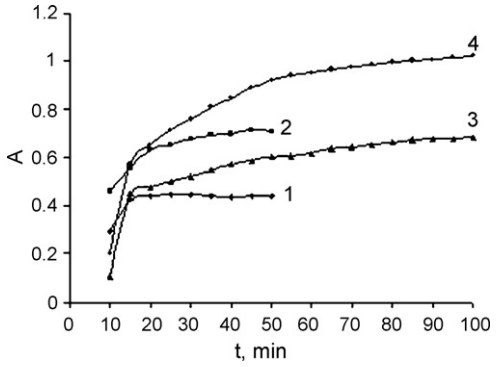

Fig. 5. Time dependence of the absorbance of the test films, containing vanillin (1, 2) and *p*-DMAB (3, 4), after contact with solution of novocaine. Reagents were immobilized in films without (1, 3) or with 0.1 M SDS (2, 4).

vanillin-film colour was observed after 30 min, the *p*-DMAB-film colour was observed after 60 min visually or with spectrophotometer (Fig. 5). The *p*-DMAB-BPB-film was immersed into solution of PAA at pH 6 for 1 min, was dried on air and the *p*-DMAB-BPB-film colour was observed after 20 min visually.

The absorbance of the films was found to depend linearly on the amines concentration in analyzed solution (Table 2). Thus, vanillin-film and *p*-DMAB-film can be used for visual identification and for visual and spectrophotometric quantitative determination of PAA in solution and trace amount of PAA on the solid surfaces. In last case it is enough to moisten the surface by solution, containing 2 M HCl and 1×10^{-3} M SDS, to put test films on wetted surface for 1 min and to observe the colour change of film after 30 min for vanillin-film and after 60 min for *p*-DMAB-film visually or with spectrophotometer.

3.3. Metrological characteristics of the test-determinations using the test films

The most important metrological characteristics of the analytical methods are detection limit (L_D) and quantification limit (L_Q) [42]. Detection limit L_D is minimum concentration at which the analyte can be detected with specified confidence level, as a rule 0.95 [42]. Evaluation of the L_D value of test tools with visual indication is based on investigations of the range of unreliable reaction (RUR) where the detection probability of analyte changes from 0 to 1. Komar has achieved early, that robustness of test-systems is related to half-width of RUR: the narrower is half-width of RUR, the better is the reaction in analytical sense [43,44]. To compare test-systems quality, whose RUR belong to different concentration level, it is suitable to use the value of relative width of RUR (r). The relative width of RUR is defined as a difference between upper and lower concentration limits of RUR divided into the lower concentration limit [45].

To determine the detection limit, frequencies of the detection in RUR are found experimentally in dependence on concentration and frequency distribution is fitted by using of knowledge function of probability distribution. The calculation [46] and graphical [47] methods can be used for this purpose.

Algorithm of the L_D determination described in [46] was used in present work. First of all, RUR was found as the concentration range where results of analyte detection obtained by 15–20 independent observers could be positive as well as negative. In obtained concentration range 7–12 regularly spaced points were chosen, difference between adjacent selected concentrations was greater than triple standard deviation of concentration, which related to solution preparation.

Table 2
Estimated calibration parameters of the spectrophotometric determination of amines with test films containing immobilized aldehydes

Test film	Analyte	Number of observation	Concentration range of linear calibration (mM)	Parameters of calibration equation $A = a + bc$, 95% confidence level		Correlation coefficient (R)
				a	b	
Vanillin-film	Novocaine	6	0.3–10	−0.00 ± 0.03	0.115 ± 0.006	0.995
	Streptocide	6	0.27–8.6	0.013 ± 0.015	0.114 ± 0.004	0.998
	Streptocide soluble	6	0.36–12	0.064 ± 0.015	0.113 ± 0.003	0.999
p-DMAB-film	Novocaine	8	0.18–23	0.03 ± 0.02	0.101 ± 0.002	0.998
p-DMAB-BPB-film	Novocaine	3	0.3–2.7	0.14 ± 0.12	0.11 ± 0.07	0.97

Detection was repeated 3–4 times for each concentration using single test film samples. The results of each test were visually observed by 15–20 observers. Detection frequency $P(c_k)$ of each concentration c_k was calculated as the ratio of the positive observations number to the total number of the observations for each test. The mean value $\overline{P(c_k)}$ and standard deviation of the detection frequency s_k were calculated from results of replicate tests for each concentration value of analyte by Eqs. (1) and (2):

$$\overline{P(c_k)} = \frac{\sum_{i=1}^{I} P(c_k)_i}{I}, \quad (1)$$

$$s_k = \sqrt{\frac{1}{I-1}\sum_{i=1}^{I}\{P(c_k)_i - \overline{P(c_k)}\}^2}, \quad (2)$$

where I is the number of repeated tests; $P(c_k)$ is the experimental value of frequency (probability) of detection of concentration c_k.

The experimental dependence of the detection frequency on analyte concentration was fitted by using known probability distribution functions: normal distribution, lognormal distribution, Weibull function and exponential function [48]. The parameters of functions of the probability distribution were estimated as regression coefficients. The χ^2-criterion and criterion of Kolmogorov–Smirnov (λ) [49] served as a criterion for estimation of the fitting quality of the experimental data by using different distribution function. The χ^2-criterion values are calculated by Eq. (3):

$$\chi^2_{exp} = \sum_{k=1}^{J} \frac{\{\hat{P}(c_k) - P(c_k)\}^2}{s_k^2}, \quad (3)$$

where J is the number of investigated concentration values in RUR; $\hat{P}(c_k)$ is the value of probability of concentration c_k detection, calculated by using corresponding fitting function; s_k is the standard deviation of the $P(c_k)$, calculated by Eq. (2).

The values of Kolmogorov–Smirnov criterion (λ) are determined as the estimate of maximal deviation of experimental value $P(c_k)$ from calculated value $\hat{P}(c_k)$ in according to Eq. (4):

$$\lambda_{exp} = \max_{1\le k\le J} |P(c_k) - \hat{P}(c_k)| \sqrt{J}. \quad (4)$$

The hypothesis about agreement of the experimental distribution to the given function of probability distribution was accepted, if the values χ^2_{exp} and λ_{exp} did not exceed theoretical values of χ^2-criterion and Kolmogorov–Smirnov criterion at the significance level 0.05 [49]. When these conditions were observed for several functions of probability distribution, the function with lower range values of the criteria χ^2 and λ was chosen. The value of the L_D was calculated using selected distribution function by probability level 0.95.

The Weibull distribution function fitted of experimental distribution of the detection frequencies of analytes more adequately then other distribution functions in most cases; the close results were obtained by using of normal distribution function. As an example, the results of the experimental data treatment for *p*-DMAB-film by novocaine detection are presented in Table 3. As it is shown in Table 3, the Weibull distribution function provided lowest values of the criteria χ^2 and λ and the corresponding value of the L_D is equal 0.16 mM (printed bold).

Visual quantitative determinations are based on comparison of the colour, obtained after contact of the test tool with the analyzed solution, with the colour scale. To construct the colour scale, the film samples were immersed into solutions with known concentration of analyte. The concentration of analyte was increased in geometric progression from a solution to a solution with a factor of 2 or 3 [50]. The minimum concentration that can be determined with this method with relative standard deviation 0.33 was accepted as the quantification limit L_Q. Hence, $L_Q = 3s_c$, where s_c is the standard deviation of the concentration determination [50]. The value of the standard deviation s_c was estimated experimentally according to the technique described in [46].

Metrological characteristics of detection and determination with using test films are presented in Tables 4 and 5. Lower r-values and, therefore, the greater robustness of the test results were observed using the Fe-Dipy-film for detection of reductants and using the vanillin-film for detection of PAA.

3.4. Application of the test films for determination of active ingredient in drugs

3.4.1. Procedure of reductants determination in drugs

Transfer an accurately weighed amount of powder of tablets or aliquot of liquid drug containing 0.05–0.25 mmol reductant into a 100 ml standard flask and dilute to the mark with 0.1 M $HClO_4$ solution. Immerse the test films into obtained solutions for 15 s, dry the films on air and measure the absorbance

Table 3
The theoretical and estimated values of statistical criteria obtained for fitting of experimental dependence of detection frequencies on novocaine concentration in the RUR by different functions of probability distribution and corresponding detection limit estimations for *p*-DMAB-film

Fitting function of probability distribution	χ^2-criterion	Kolmogorov–Smirnov criterion (λ)	Detection limit L_D (mM)
Normal distribution	16.5	0.3	0.2
Lognormal distribution	60.1	0.5	0.3
Weibull function	**11.4**	**0.2**	**0.16**
Exponential function	57.6	0.7	0.3
Theoretical values of criteria with 7 degrees of freedom and 0.05 significance level [49]	14.01	0.48	–

Table 4
Metrological characteristics of the detection and the visual determination of analgin and ascorbic acid using test films containing immobilized reagents

Metrological characteristics	Test film/analyte		
	Fe-Dipy-film/analgin	Fe-Dipy-film/ascorbic acid	Fe-Phen-film/analgin
Concentration range of unreliable reaction (mM)	0.002–0.026	0.002–0.051	0.002–0.056
Relative width of range of unreliable reaction	12	24.5	27
Detection limit L_D (mM)	0.023	0.046	0.051
Standard deviation of concentration s_c (mM)	0.012	0.030	0.029
Quantification limit L_Q (mM)	0.036	0.090	0.087

Table 5
Metrological characteristics of the detection and the visual determination of amines using test films containing immobilized reagents

Metrological characteristics	Test film/analyte				
	Vanillin-film/novocaine	Vanillin-film/streptocide	Vanillin-film/streptocide soluble	*p*-DMAB-film/novocaine	*p*-DMAB-BPB-film/novocaine
Concentration range of unreliable reaction (mM)	0.06–0.24	0.05–0.17	0.04–0.27	0.01–0.17	0.05–0.17
Relative width of range of unreliable reaction	3	2.4	5.8	16	2.4
Detection limit L_D (mM)	0.22	0.16	0.24	0.16	0.15
Standard deviation of concentration s_c (mM)	0.11	0.09	0.11	0.06	0.11
Quantification limit L_Q (mM)	0.33	0.27	0.33	0.18	0.33

of the films after 20 min at 525 nm against a reference test films.

3.4.2. Procedure of PAA determination in drugs

Transfer an accurately weighed amount of powder of tablets or aliquot of liquid drug containing 0.2–0.8 mmol PAA into a 100 ml standard flask, add 10 ml of 0.01 M SDS solution and dilute to the mark with 2 M HCl solution. Immerse the test films into obtained solutions for 10 s, dry the films on air and measure the absorbance of the films after 30 min at 405 nm against a reference test films.

Transfer aliquot of liquid drug containing 0.03–0.27 mmol PAA into a 100 ml standard flask, add acetic buffer solution up to pH 6 and dilute to the mark with water. Immerse the *p*-DMAB-BPB-film into obtained solutions for 1 min, dry the films on air and observe the colour of the films after 20 min.

3.4.3. Accuracy of determination of reductants and PAA with test films

The test films were used for determination of active ingredients in drugs from Ukrainian pharmaceutical factories. Reductants were determined with Fe-Dipy-film in the tablets "Analgin-Darnitsa, 0.5 g", "Askorutin", "Ascorbic acid with sugar" and in the solution for injection "Analgin, 50%". PAA were determined with photometric measurement with vanillin-film in the tablets "Streptocidum, 0.3 g" and in the solution for injection "Novocaine, 0.5%". Novocaine in the solution for injection was determined also visually with *p*-DMAB-BPB-film. The calibration curves were obtained with the test films in standard solutions of corresponding substance and were used in all determinations except for determination of ascorbic acid in tablets "Ascorbic acid with sugar". In last case known addition method was used to minimize matrix effects. Four equal aliquots of sample solution obtained from tablets were transferred into four 10 ml standard flasks and 0, 1, 2, 3 ml of standard 4.0×10^{-3} M sodium ascorbate solution were added into flasks respectively and diluted to the mark with 0.1 M $HClO_4$ solution. The amount of ascorbic acid was estimated from dependence of the film's absorbance from the added volume of standard solution.

The results of determination of reductants and PAA in drugs with test films were compared with results obtained by the pharmacopoeia procedures (iodometric titration of analgin and ascorbic acid, bromatometric titration of streptocide and two-phase acid–base titration of novocaine [51,52]) (Table 6). In all cases the results of determination with test films are in satisfactory agreement with results obtained by the pharmacopoeia procedures. It

Table 6
Spectrophotometric and visual determination of active ingredients in drugs using the test films (95% confidence level, number of observation is equal 3)

Active ingredient	Drug	Amount determined using pharmacopoeia method	Ref.	Amount determined using test film
Analgin	"Analgin-Darnitsa, 0.5 g", tablets	(469 ± 7) mg per 1 tablet	[51]	(460 ± 30) mg per 1 tablet (after filtering of sample solution) (464 ± 14) mg per 1 tablet (without filtering of sample solution)
	50%-solution of analgin for injections, bottles	(523 ± 10) mg ml^{-1} ***		(530 ± 30) mg ml^{-1} ***
Ascorbic acid	"Ascorutin", 0.05 g ascorbic acid and 0.05 g rutin, tablets	(52.2 ± 0.8) mg per 1 tablet	[51,52]	(53 ± 3) mg per 1 tablet
	"Ascorbic acid with sugar", on 0.025 g, tablets	(25.5 ± 0.8) mg per 1 tablet		(27.8 ± 1.6) mg per 1 tablet*
Novocaine	Solution for injection "Novocaine, 0.5%"	(4.74 ± 0.12) mg ml^{-1} (4.99 ± 0.14) mg ml^{-1}	[51] [51]	(4.7 ± 0.3) mg ml^{-1} (6.1 ± 1.4) mg ml^{-1} **
Streptocide	"Streptocidum, 0.3 g", tablets	(308 ± 4) mg per 1 tablet	[51]	(310 ± 12) mg per 1 tablet

* Known addition method.
** Visual test-determination by colour scale.
*** Number of observation is equal 4.

Table 7
Results of spiked probes analysis using the test films (95% confidence level, number of observation is equal 3)

Active ingredient	Drug	Active ingredient content in aliquot of sample solution	Recovery of added active ingredient	
		Found (mg)	Added, mass (mg)	Founded addition mass (mg)
Analgin	"Analgin-Darnitsa, 0.5 g", tablets	1.71 ± 0.10 (after filtering of sample solution)	1.76	1.9 ± 0.3
		1.71 ± 0.04 (without filtering)	1.75	1.65 ± 0.10
	50%-solution of analgin for injections, bottles	1.90 ± 0.11***	1.76	1.77 ± 0.19***
Ascorbic acid	"Ascorutin", 0.05 g ascorbic acid and 0.05 g rutin, tablets	0.93 ± 0.05	0.89	0.92 ± 0.09
	"Ascorbic acid with sugar", on 0.025 g, tablets	1.17 ± 0.08*	1.06	1.02 ± 0.05*
Novocaine	Solution for injection "Novocaine, 0.5%"	23.3 ± 1.7	13.5	12.3 ± 1.2
		2.8 ± 0.7**	3.8	4.3 ± 1.2**
Streptocide	"Streptocidum, 0.3 g", tablets	14.2 ± 0.7	8.53	7.7 ± 0.9***

* Known addition method.
** Visual test-determination by color scale.
*** Number of observation is equal 4.

should be remarked that test films could be used for spectrophotometric determination without filtering or without centrifuging the solutions obtained from tablets.

The accuracy of suggested procedures of determination of reductants and PAA in drugs was tested by method of spiked probe also. In this purpose the sample solutions of drugs were prepared and analyzed as described in Sections 3.4.1 and 3.4.2. The preparation of sample solutions of drugs was repeated adding into a standard flask known volume of standard solution of analyte and obtained solution with known additive was analyzed. As shown in Table 7, the founded amounts of reductants as well as PAA are in good agreement with added amounts. It is evidence of accuracy of determination with test films.

4. Conclusions

Gelatinous solidified layers of the photographic film are applicable to immobilization of analytical reagents, which are used for detection and determination of reductants and primary aromatic amines. The films with immobilized iron(III)-Dipy or iron(III)-Phen complexes and films with immobilized aldehydes can be used as test films for reductants and PAA respectively. These immobilized reagents provide the contrast colour change and are not washed out from films at contacting of test films with analyzed solutions. The characteristics of the test films were improved when the reagents immobilization was provided from micellar solutions of SDS. The sorption of SDS results in hydrophobization and increasing the ability of gelatinous layer to solubilize the moderately hydrophobic reagents.

The films with immobilized iron(III)-Dipy and iron(III)-Phen complexes can be used for identification and visual and spectrophotometric determination of reductants, as was shown by successful examination of films for the determination of analgin and ascorbic acid in drugs. However, the films with immobilized iron(III)-Dipy complexes have somewhat better characteristics than films with iron(III)-Phen complexes. The films with immobilized vanillin can be used for identification and visual and spectrophotometric determination of substances containing a primary aromatic amino groups and substances giving PAA by hydrolysis, as was achieved for streptocide soluble. The yellow films containing *p*-DMAB and indicator BPB after contact with the solutions of PAA became green; these films are suitable for reliable visual determinations of PAA. The test films can be used for photometric determination in turbid medium and for analysis of tablets without filtering or without centrifuging the pharmaceutical excipients.

Metrological characteristics of test films (the range of unreliable reaction, detection limit and quantification limits of visual and spectrophotometric determinations) were determined on bases of statistical approach and investigation of detection probability distribution in the unreliable reaction range of concentration.

Acknowledgments

This work was partly supported by Ministry of Education and Sciences of Ukraine (Research projects No. 0107U000659, No. 0106U003109). The authors wish to acknowledge A.S. Vlasenko for helping with translation of the paper.

References

[1] Yu.A. Zolotov, V.M. Ivanov, V.G.Amelin, Khimicheskie test-metodi analiza (The chemical test-methods of analysis), Editorial URSS, Moscow, 2002, 304 p.
[2] N.A. Gavrilenko, G.M. Mokrousov, O.V. Dzhiganskaya, J. Anal. Chem. 59 (9) (2004) 871.
[3] N.A. Gavrilenko, O.V. Mokhova, G.M. Mokrousov, A.V. Sukhanov, Proc. International Congress on Analytical Sciences (ICAS-2006). V. 2, Moscow (Russia), 2006, p. P620.
[4] N.A. Gavrilenko, O.V. Mokhova, N.V. Saranchina, G.M. Mokrousov, Proc. International Congress on Analytical Sciences (ICAS-2006). V. 2, Moscow (Russia), 2006, p. P641.
[5] O.V. Mikhailov, V.K. Polovnyak, Zavodsk. Laboratoriya 55 (12) (1989) 34.
[6] O.V. Mikhailov, Russ. J. Coord. Chem. 26 (10) (2000) 702.
[7] O.V. Mikhailov, Rossiiskiy Khim. Zhurn. (3) (2000) 70.
[8] H. Birkedal-Hansen, Histochemie 36 (1973) 73.
[9] E.A. Reshetnyak, N.A. Nikitina, N.O. Mchedlov-Petrossyan, Kharkov University Bulletin, No 669 (13) (2005) 67.
[10] L.P. Loginova, O.Yu. Nesterenko, I.V. Kudris, Kharkov University Bulletin, No 669 (13) (2005) 93.
[11] S.V. Sheremet'ev, V.V. Kuznetsov, J. Anal. Chem. 62 (4) (2007) 319.
[12] Merckoquant. Simply rapid, Merck, Darmstadt, 2006, 20 p.
[13] Schnellteste, MACHEREY-NAGEL, Dűren, 2004, 137 p.
[14] O.A. Zaporozhets, E.A. Krushinskaya, J. Anal. Chem. 57 (No 4) (2002) 286.
[15] O.A. Zaporozhets, E.A. Krushinskaya, N.A. Lipkovskaya, V.V. Sukhan, J. Anal. Chem. 56 (6) (2001) 524.
[16] E.I. Morosanova, D.Yu. Marchenko, Yu.A. Zolotov, J. Anal. Chem. 55 (1) (2000) 76.
[17] E.I. Morosanova, E.A. Reznikova, A.A. Velikorodnyi, J. Anal. Chem. 56 (2) (2001) 173.
[18] D.Yu. Marchenko, E.I. Morosanova, N.M. Kuz'min, Yu.A. Zolotov, Zhurn. Analyt. Khimii. 52 (12) (1997) 1287.
[19] O.A. Zaporozhets, O.A. Krushynska, N.A. Lipkovska, V.N. Barvinchenko, J. Agric. Food Chem. 52 (2004) 21.
[20] R. Koncki, O.S. Wolfbeis, Sens. Actuators B: Chem. 51 (1–3) (1998) 355.
[21] R. Koncki, T. Lenarczuk, S. Gtab, Anal. Chim. Acta 379 (1–2) (1999) 69.
[22] T. Lenarczuk, S. Gtab, R. Koncki, J. Pharm. Biomed. Anal. 26 (1) (2001) 163.
[23] A.A. Velikorodnyi, E.I. Morosanova, J. Anal. Chem. 55 (10) (2000) 994.
[24] R.K. Chernova, N.N. Gusakova', S.U. Doronin, I.V. Myznikova, K.G. Petrovich, A.K. Sudarushkina, E.M. Adamova, Proc. International congress on Analytical Sciences (ICAS-2006). V. 2, Moscow (Russia), 2006, pp. 559–560.

[25] S.Yu. Doronin, R.K. Chernova, N.N. Gusakova, J. Anal. Chem. 60 (5) (2005) 412.
[26] D.Yu. Marchenko, I.A. Morozkin, E.I. Morosanova, N.M. Kuz'min, Yu.A. Zolotov, Zhurn. Analyt. Khimii. 52 (12) (1997) 1292.
[27] M.I. Evgen'ev, S.Yu. Garmonov, I.I. Evgen'eva, S.M. Goryunova, N.G. Nikolaeva, F.S. Levinson, Zhurn. Analyt. Khimii. 53 (2) (1998) 175.
[28] V.G. Amelin, I.S. Kolodkin, J. Anal. Chem. 56 (2) (2001) 182.
[29] M.I. Evgen'ev, S.Yu. Garmonov, I.I. Evgen'eva, J. Anal. Chem. 57 (2) (2002) 159.
[30] F. Umland, A. Janssen, D. Thierig, G. Wünsch, Theorie und praktische Anwendung von Komplexbildnern, Akademische Verlagsgesellschaft, Frankf./M, 1971, 759 p.
[31] L.P. Loginova, O.Yu. Nesterenko, Kharkov University Bulletin, No 731(14) (2006) 112.
[32] K. Burger, Organic Reagents in Metal Analysis, Pergamon Press, Oxford, 1973, 267 p.
[33] A.T. Pilipenko, M.M. Tananaiko, Geteroligandnie i geterometalicheskie kompleksi i ih primenenie v analiticheskoi khimii (Heteroligand and heterometallic complexes and their application in analytical chemistry), Khimiya, Moscow, 1983, 224 p.
[34] V.N. Izmailova, S.R. Derkach, K.V. Zotova, R.G. Danilova, Kolloidniy Zhurn. 55 (3) (1993) 54.
[35] R. Wustneck, N.P. Wustneck, H. Hermel, L. Zastrow, Kolloidniy Zhurn. 49 (2) (1987) 244.
[36] S.F. Turner, S.M. Clarke, A.R. Rennie, et al., Progr. Colloid Polym. Sci. 112 (1999) 206.
[37] A. Courts, Biochem. J. 58 (1) (1954) 70.
[38] N.S. Zefirov, et al., Khimicheskaya enciklopediya (The chemical encyclopedia), vol. 5, Bolshaya Rossiyskaya enciklopediya, Moscow, 1998, 783 p.
[39] I.I. Stencel, Zavodsk. Laboratoriya 51 (2) (1985) 1.
[40] E. Bishop, Indicators, Pergamon Press, Oxford, 1972, 543 p.
[41] S.Yu. Doronin, R.K. Chernova, N.N. Gusakova, J. Anal. Chem. 59 (4) (2004) 335.
[42] Lloyd A. Currie, Pure Appl. Chem. 67 (10) (1995) 1699.
[43] N.P. Komar, Osnovi kachestvennogo khimicheskogo analiza (The Bases of qualitative chemical analysis), vol. 1, Izdatelstvo Kharkovskogo universiteta, Kharkov, 1955, 442 p.
[44] N.P. Komar, Trudi nauchno-issledovatelskogo instituta khimii Kharkovskogo gosudarstvennogo universiteta im. A.M. Gorkogo, 8 (1951) 143.
[45] E.A. Reshetnyak, N.A. Nikitina, L.P. Loginova, V.M. Ostrovskaya, J. Anal. Chem. 60 (10) (2005) 982.
[46] E.A. Reshetnyak, N.A. Nikitina, Yu.V. Kholin, N.V. Svetlova, V.M. Ostrovskaya, Kharkov University Bulletin, No 596 (10) (2003) 90.
[47] M.S. Kravchenko, M.S. Fumarova, A.A. Bugaevski, Intern. J. Environ. Anal. Chem. 33 (1988) 257.
[48] W.J. Dixon, F.J. Massey, Introduction to Statistical Analysis, third ed., McGraw-Hill, New York, 1969, 638 p.
[49] H. Müller, P. Neumann, R. Storm, Tafeln der mathematischen Statistik, Fachbuchverlag, Leipzig, 1973, 275 p.
[50] V.M. Ostrovskaya, J. Anal. Chem. 54 (11) (1999) 994.
[51] M.D. Mashkovskiy, et al., Gosudarstvennaya pharmakopea SSSR (The USSR state pharmacopoeia), MEDGIZ, Moscow, 1961, 912 p.
[52] European Pharmacopoeia, 6th Ed., COE-EDQM, 2007, 4392 p.

Talanta 77 (2008) 701–709

Contents lists available at ScienceDirect

Talanta

journal homepage: www.elsevier.com/locate/talanta

Determination of sugar cane herbicides in soil and soil treated with sugar cane vinasse by solid-phase extraction and HPLC-UV

Carolina Lourencetti[a], Mary Rosa Rodrigues de Marchi[b], Maria Lúcia Ribeiro[a,*]

[a] Organic Chemistry Department, Chemistry Institute, São Paulo State University - Unesp, P.O. Box 355, Araraquara, SP 14801-970, Brazil
[b] Analytical Chemistry Department, Chemistry Institute, São Paulo State University - Unesp, P.O. Box 355, Araraquara, SP 14801-970, Brazil

ARTICLE INFO

Article history:
Received 24 March 2008
Received in revised form 2 July 2008
Accepted 4 July 2008
Available online 16 July 2008

Keywords:
Herbicides
Soil
Vinasse
Solid-phase extraction
HPLC-UV

ABSTRACT

This work reports on the development and validation of a small-scale and efficient SPE-HPLC-UV method for the simultaneous determination of the most used herbicides (diuron, hexazinone, and tebuthiuron) applied to soil and soil treated with sugar cane vinasse (soil-vinasse) in areas where sugar cane crops are grown in the state of São Paulo, Brazil. The analytical procedure was optimized for solvent extraction and HPLC-UV conditions. Extraction and clean-up were combined in a single step employing solid-phase extraction, avoiding sophisticated techniques, organic–solvent–water mixtures and consequently a longer concentration step. Recovery studies with soil and soil-vinasse samples spiked at two herbicides levels (around 0.25 and 2.0 mg kg^{-1}) and sample stability (sample frozen for 20 days before analysis) were applied as parameters to control the efficiency of the method. Good accuracy and precision were achieved with average recoveries ranging from 78% to 120% and relative standard deviations less than 10% throughout the whole recovery test. The method's limit of detection ranged between 0.025 and 0.050 mg kg^{-1} for diuron, hexazinone, and tebuthiuron in soil and soil-vinasse. The feasibility of this method was applied to determine the herbicide half-lives ($t_{1/2}$) in soil and soil-vinasse in a laboratory study. Sugar cane vinasse added to soil increased the degradation of diuron and tebuthiuron ($p < 0.05$), reducing the $t_{1/2}$ from 80 to 7 days and 128 to 73 days, respectively. This method is presented as an alternative which could be applied to assess herbicide behavior in soil in order to prevent water contamination and to contribute to establish pesticide limits in soil.

1. Introduction

Brazil is one of the world leaders in the production of sugar cane, sugar, and fuel alcohol (ethanol) [1], which has been considered as a renewable alternative for conventional fossil fuels [2]. The sugar cane monoculture requires a large amount of pesticides, and the herbicides represent approximately 56% of the total dollar value of the pesticide business in Brazil [3], and these are the most widely employed class of pesticide applied as a pre- and post-emergent weed control agent to improve sugar cane crop yields.

It has been claimed that only 1–3% of the agricultural pesticide application reaches the site of action [4]. In the soil, the fate of the pesticide is controlled by the chemical, biological and physical dynamics of this matrix. These processes can be grouped into those that affect persistence, including chemical and microbial degradation, and those that affect mobility, involving adsorption, plant uptake, volatilization, wind erosion, run-off and leaching [5]. The degree to which each process will contribute to the overall loss of the pesticide is in turn dependent on the physicochemical properties of each pesticide (e.g., water solubility, adsorptive affinity), characteristics of the soil (e.g., pH, organic content, biomass and redox status), environmental conditions (e.g., temperature and moisture), and management practices (e.g., application rate and formulation type) [6].

The determination of pesticide behavior in soil has been presented as an alternative to prevent superficial and groundwater contamination since it is the first step to detect and alert to possible cases of water contamination [7].

The development and application of methodologies to determine pesticides in soil are challenging tasks as a result of some of the aspects encountered, such as the pesticide concentration in the soil, which can be high or extremely low; a great variety of pesticides can cover a wide range of polarities; a strong binding of the analytes to the soil; and there is also a lack of analytical standards for the degradation products formed [5]. Other factors that can affect the efficacy of a method are factors which involve the soil itself, such as: (1) the amount of organic matter present in soil, and (2) the compounds present in the soil which could

* Corresponding author. Tel.: +55 16 33016664; fax: +55 16 33016692.
E-mail address: mlucia@iq.unesp.br (M.L. Ribeiro).

0039-9140/$ – see front matter © 2008 Elsevier B.V. All rights reserved.
doi:10.1016/j.talanta.2008.07.013

interfere in the extraction or quantification steps. Nowadays, many organic products have been applied to soil in order to improve soil conditions, such as municipal solid waste compost [8], sludge compost [9], and sugar cane vinasse [10,11], but the influence of these additives to the behavior of pesticides in soil is still not totally known.

Andreu and Picó [5] reviewed the most relevant analytical methods to determine pesticides and their transformation products in soil, regarding a discussion about the steps involved in method development, such as matrix preparation, extraction, clean-up, fractionation and determination. In this review, Soxhlet is appointed as one of the most frequently used techniques since it has been adopted in many standardized analytical methodologies to determine pesticides in soil. However, this technique uses drastic conditions that have often broken the structural integrity of thermolabile pesticides, and requires much time and solvent consumption. Sonication and shaking are other traditional techniques for organic analytes, but these also consume large quantities of solvent, and are labor intensive. Modern technologies, including the use of new sources of energy, have been described. However these new extraction procedures, based on instrumental techniques, such as microwave-assisted extraction (MAE), supercritical fluid extraction (SFE), pressurized fluid extraction (PLE), and subcritical water extraction (SWE), have been tested to facilitate sample pre-treatment [5,12], they require special equipments. Small-scale methods have brought about a combination of extraction and clean-up steps into one step, using a chromatographic column prepacked with sorbents, using [13] or not using sonication [14].

The extraction methods described in literature to determine herbicides applied to sugar cane crops have been carried out by shaking [15–18], accelerated solvent (ASE) [19], sonication [20], pressurized fluid (PFE) and Soxhlet [21]. However, the simultaneous determination of the most utilized herbicides in current use for this culture in the state of São Paulo, Brazil, which are diuron [(3-(3,4-dichlorophenyl)-1,1-dimethylurea)], CAS number 330-54-1, hexaninone [(3-cyclohexyl-6-(dimethylamino)-1-methyl-1,3,5-triazine-2,4(1H,3H)-dione], CAS number 51235-04-2, both presented as a mixture in commercial products, and tebuthiuron (*N*-[5-(1,1-dimethylethyl)-1,3,4-thiadiazol-2-yl]-*N*,*N*′-dimethylurea), CAS number 34014-18-1, is very rare and no analytical method has been reported so far.

This study takes into account the development and validation of a new analytical method employing solid-phase extraction and HPLC-UV to determine diuron, hexazinone and tebuthiuron in soil and soil treated with sugar cane vinasse (soil-vinasse), and also the application of this method in a laboratory study to determine the half-lives of these three herbicides in soil and soil-vinasse.

2. Experimental

2.1. Reagents

Pesticide standards of hexazinone (99.9%) and tebuthiuron (99.9%) (Riedel de Haën) were obtained from Sigma–Aldrich Laborchemikalien GmbH (United Kingdom) and diuron (97.5%) from Ehrenstorfer GmbH (Augsburg, Alemanha). Stock solutions (200 mg l^{-1} for hexazinone and tebuthiuron and 255 mg l^{-1} for diuron) and different working standard mixtures of pesticides were prepared in methanol and were stored at −18 °C. Acetone (Mallinckrodt Ultiam AR®, Paris, Kentucky), methanol and acetronitrile (J.T. Baker, USA) were pesticide-residue analysis grade. HPLC-grade water was obtained from a Millipore water purification system (Milford, MA, USA). Solid-phase extraction (SPE) cartridges AccuBOND II ODS-C18 (500 mg, 6 ml capacity) were purchased from Agilent Technologies (United Kingdom).

2.2. Apparatus

A high-performance liquid chromatograph (Waters, Milford, MA, USA), equipped with two solvent delivery pumps (Model 501), manual injector with a 20 μl loop (Model UK), UV–vis absorbance detector (Model 485) and a reporting integrator (Model 746) was used to determine the diuron, hexazinone and tebuthiuron. A stainless steel analytical column Gemini C18 (150 mm × 4.6 mm i.d., 5 μm; Phenomenex) was employed. The mobile phase consisted of a mixture of methanol and water (45:55, v/v) and was delivered in isocratic mode at a flow rate of 1.0 ml min^{-1}. Before using, the mobile phase was passed through a 0.45 μm membrane filter from Millipore (Bedford, MA, USA) and degassed in an ultrasonic bath. Simultaneous pesticide detection was performed at 247 nm and all measurements were carried out at room temperature.

2.3. Procedure

2.3.1. Sample collection and treatment

One composite non-agricultural soil sample (total of 10 kg) was taken at different points, from 0 to 20 cm depth, in a regular area located in Araraquara City, São Paulo State, Brazil. The texture of the soil was 19.2% sand, 58.1% clay and 22.7% silt. Two laboratory samples (3 kg) were reduced by quarting and air-dried at room temperature.

Five liters of soil sample were treated with sugar cane vinasse (750 ml) (150 m^3 ha^{-1}). This dose corresponds to the regular application dose in sugar cane crops in the Araraquara region. The soil-vinasse sample was thoroughly mixed to assure complete homogeneity and was air dried at room temperature for 3 days. Soil and soil-vinasse samples were reduced to approximately 1 kg by quarting and sieving through a 0.84 mm sieve.

Soil and soil-vinasse, containing approximately 20 g dm^{-3} of organic carbon, 3% of humidity and pH 5.0, were used to develop and validate the method and for the degradation study of diuron, hexaninone and tebuthiuron.

2.3.2. Spiked samples and extraction

Spiked soil and soil-vinasse samples were prepared by adding 1.0 ml of a standard mixture of herbicides to 40 g of sample, resulting in two spiked sample levels: one at 0.25, and the other at 2.0 mg kg^{-1} for hexazinone and tebuthiuron and 0.26 and 2.57 mg kg^{-1} for diuron. In both cases, field application rates were used at the lowest and highest recommended doses. The spiked samples were kept at room temperature for 24 h for total solvent evaporation and after this, the extractions were carried out.

The solid-phase cartridge packed with a reverse phase (C18) was previously conditioned by rinsing with 10 ml of methanol (5 ml min^{-1}) under vacuum before transferring 4 g of soil sample (dry weight) to the top of the cartridge (Fig. 1). During the conditioning, the cartridges were not allowed to be dried before sample addition, as recommended [22].

At the beginning of the experiments, two elution solvent systems were compared as extraction solvents: 20 ml of methanol and 20 ml of acetone at 2 ml min^{-1}. For the method validation, methanol was used as the extraction solvent to determine diuron, hexazinone and tebuthiuron in soil and soil-vinasse samples. The eluent was concentrated to a small volume (approximately 0.5 ml) with a rotary vacuum evaporator at 40 °C. The concentrated extract was adjusted with methanol to 2.0 ml and stored at −18 °C until analysis. The 20 μl aliquots were injected into the HPLC-UV system (λ = 247 nm) for analyses. After the method validation, evaluation of the analytes stability in frozen samples was carried out analyzing the spiked samples, the soil and the soil-vinasse, stored for a period of 20 days under refrigeration (−18 °C).

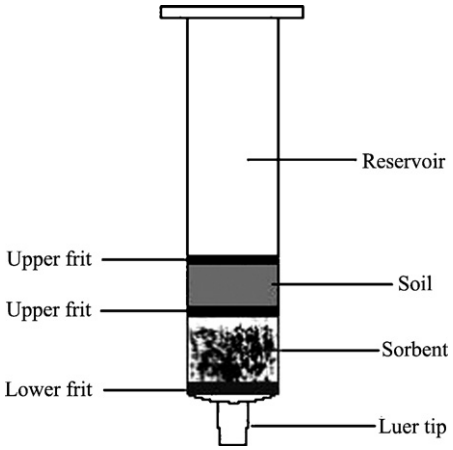

Fig. 1. SPE column packed with soil [24,modified].

2.3.3. Quality control and method validation

For each herbicide determined by HPLC-UV, the range of herbicide concentrations (0.25–12.7 mg l^{-1}) was appropriated to the recommended dose usually applied to sugar canes crops for this kind of soil (approximately 0.774–1.714 mg kg^{-1} for diuron, 0.251–0.364 mg kg^{-1} for hexazinone and 0.735–1.103 mg kg^{-1} for tebuthiuron). Quantitative measurements were obtained using external standard calibration curves. Three injections were performed for each calibration point.

Two different fortification levels were considered for the method validation step, one low at approximately 0.25 mg kg^{-1} and one high at approximately 2.0 mg kg^{-1}. Also, soil and soil-vinasse spiked samples were processed to asses the influence of aging and freezing on the extraction efficiency, which were performed by accuracy and precision determination.

The accuracy and precision of the extraction procedure were carried out by extracting replicate spiked sample ($n = 5$). These two parameters were expressed in terms of the percentage recovery and the percentage relative standard deviation (R.S.D.), respectively. The specificity of the assay was established analyzing the soil and soil-vinasse samples without standard addition. The chromatograms were visually inspected for interfering chromatographic peaks from the sample matrix substances.

The limits of quantification (LOQ) and detection (LOD) of this method were calculated according to the Thier and Zeumer criteria [23]. The LOQ was determined as the lowest concentration of the compounds that gives a response that could be quantified with an R.S.D. of less than 20% and a recovery of at least 70%. The LOD (Eq. (1)) was estimated from recovery experiments by the equations:

$$\mathrm{LOD} = \frac{2t_{f,95}\hat{\sigma}_{\mathrm{com}}}{S} \quad (1)$$

The standard deviation ($\hat{\sigma}_{\mathrm{com}}$) (Eq. (2)) is computed from the standard deviation of the blank signal ($\hat{\sigma}_B$) (Eq. (3)) and from the standard deviation $\hat{\sigma}_A$ (Eq. (4)), estimated during the experiment with the lowest fortification level.

$$\hat{\sigma}_{\mathrm{com}} = \sqrt{\frac{(m-1)\hat{\sigma}_A + (n-1)\hat{\sigma}_B}{m+n-2}} \quad (2)$$

$$\hat{\sigma}_B = \sqrt{\frac{\sum_{i=1}^{n}(B_i - \bar{B})^2}{n-1}} \quad (3)$$

where m is the number of analytical values (A_i) and n is the number of the blanks values (B_i). The degree of freedom (f) = $m + n - 2$.

$$\hat{\sigma}_A = \sqrt{\frac{\sum_{i=1}^{n}(A_i - \bar{A})^2}{m-1}} \quad (4)$$

where $\bar{B}$ and $\bar{A}$ are the mean blank and mean analytical value, respectively.

The sensitivity of the analytical method (S), which means the change in signal value per change of concentration, can be estimated from the mean analytical value and from the lowest fortification level (q) (Eq. (5)).

$$S = \frac{\bar{A}}{q} \quad (5)$$

2.3.4. Degradation study

The study of herbicide degradation in soil to determine the half-life was conducted under laboratory conditions according to specifications given by the Organization for Economical Co-operation and Development, 2002 [24]. An aliquot of 0.4 ml of a methanolic solution was applied to both the soil and the soil-vinasse at doses of 1.61 mg kg^{-1} for diuron, 0.374 mg kg^{-1} for hexazinone and 1.03 mg kg^{-1} for tebuthiuron. These doses correspond to the highest agricultural dose for sugar cane crops cultivated in the kind of soil used in this study. Soils samples (50 g) placed into aluminum boxes (210 cm^3 of capacity) were previously incubated for 5 days in a totally darkened incubator. Temperature (30 °C) and humidity of soil (at 60–75% of its maximum water holding capacity) were kept constant during the entire period of this experiment.

All soils were thoroughly stirred to complete homogeneity after the addition of the water and the herbicides. The aluminum boxes were lightly closed to allow air exchange. The soil moisture was controlled by weighing the boxes containing the soils periodically and by replacing any losses by adding deionized water.

The method described above was employed to quantify the herbicide residue contents at intervals of 0, 3, 5, 7, 14, 21, 28 and 50 days for the diuron, hexazinone and tebuthiuron treatment. For this, at each fixed time, three replicates of each treatment were frozen during 2 days in order to minimize the action of soil micro-organisms and to avoid differences in the samples after taking them out of the incubator. Before doing the analyses, the samples were kept in ambient temperature until defrosted.

3. Results and discussion

3.1. Optimization of chromatographic separation

Both the mobile phases, methanol:water and acetonitrile:water, are the most used mixtures applied in analytical methods reported for diuron, hexazinone and tebuthiuron determination in different matrices [15,25–27]. However acetonitrile:water (30:70, v/v) resulted in a faster chromatographic elution when compared with methanol:water (45:55, v/v), this mixture was avoided with regard to the elevated cost and elevated toxicity of acetonitrile. This first chromatographic optimization was obtained employing $\lambda = 254$ nm, the most common value used for the simultaneous determination of hexazinone and tebuthiuron [16,18,20,27].

To optimize the sensitivity of the HPLC-UV, absorbance spectrums were produced for diuron, hexazinone and tebuthiuron and the following wavelength values were obtained as maximum values for these compounds, 251, 147 and 255 nm, respectively. The value 247 nm resulted in the best sensitivity for simultaneous detection. Isocratic elution (Fig. 2A) was applied instead of the gradient elution

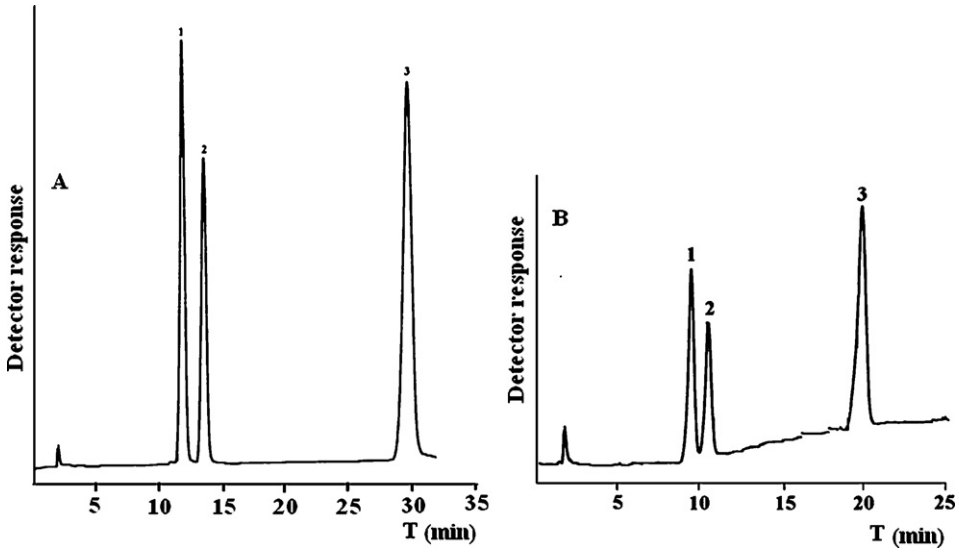

Fig. 2. HPLC-UV chromatograms (λ = 247nm) of standard mixture (10.0 mg l^{-1}) using isocratic (A) and gradient (B) mode elutions.

mode (Fig. 2B) as it resulted in a better chromatographic resolution and avoided time stabilization required for the gradient elution mode.

3.2. Method development and validation

Under the chromatographic conditions described, calibration curves were constructed using external standard method calibration. Good linearity (range: 0.25–12.7 mg l^{-1}) and good correlation coefficients ($r^2 > 0.999$) were achieved for all herbicides. The retention time and detector response precision were determined over intra- and inter-day periods injecting standards solutions at the beginning and between sample injections. Satisfactory results were obtained and these are presented in Table 1.

Environmental extracts contain high proportions of co-extracted materials which may deteriorate the HPLC system and affect the analysis results. Therefore, these co-extracted substances should be avoided during extraction and clean-up steps and removed prior to quantification by HPLC. The influence of vinasse constituents, a dark brown effluent with high organic matter and salt contents, on the chromatographic analysis for diuron, hexazinone and tebuthiuron had not been described in literature before now. Taking this into account, this method was also validated for soil treated with sugar cane vinasse, trying to simulate similar conditions present in the environment. Considering this aspect, preliminary experiments were conducted in order to select the solvent to extract these herbicides from soil. By substituting organic–solvent–water mixtures, methanol and acetone were tested as extraction solvents. These experiments were carried out employing the procedure described and the extraction efficiency of both solvents was evaluated realizing a recovery study at the level of the most highly spiked soil sample. A second fraction of solvent (10 ml) was used to evaluate the remaining residues in soil after the first extraction. No compounds of interest were detected in the extract of the second extraction, thus a volume of 20 ml was enough to extract all herbicides at the highest spiked level studied. However the extraction efficiency of both solvents was satisfactory, with an average recovery from 92% to 107% and a R.S.D. lower than 7%, methanol was select as the extraction solvent to carry out the validation method, since the chromatogram obtained using methanol was cleaner than the one obtained using acetone (Fig. 3). These results show that it is possible to avoid organic–solvent–water mixtures and consequently, a long concentration step can be eliminated.

Fig. 4 shows the chromatographic data obtained for herbicides extracted from spiked soil-vinasse compared with soil-vinasse (sample control) and the standard solution. Sugar cane vinasse constituents did not interfere in the analyses. Average recovery (78–104%) and R.S.D. (5–7%) were considered satisfactory for the recovery experiments with spiked sample at 2.0 mg kg^{-1} for hexaninone and tebuthiuron and at 2.57 mg kg^{-1} for diuron. Vinasse addition to soil only affected the potassium content, which increased almost 30-fold. Neither the pH, nor the organic matter content suffered modification (Table 2).

A procedural chemical and sample control were checked to assure the absence of interfering compounds. The chromatographic data confirmed the selectivity of the proposed method for diuron, hexaninone and tebuthiuron, and presented no interference from the matrix during the analysis. The clean-up step, coupled with the extraction step, resulted in the elimination of possible substances that could interfere during the identification and quantification of the target analytes.

Due to the lack of certified natural-matrix materials containing relevant pesticides in soil [5], as in this case of the mixture of

Table 1
Retention time (t_R), calibration data, repeatability and inter-days precision of the herbicides analyzed by HPLC-UV

Herbicides	t_R (min)	Calibration data		Repeatability[a] (R.S.D., %)		Inter-days precision[a] (R.S.D., %)	
		Equation	r^2	t_R	Peak area	t_R	Peak area
Hexazinone	11.8	$y = 158{,}550x - 12{,}468$	0.9996	0.8	1.9	1.0	2.2
Tebuthiuron	13.5	$y = 128{,}826x - 10{,}975$	0.9996	1.3	1.3	1.6	1.6
Diuron	30.6	$y = 218{,}321x - 24{,}522$	0.9996	0.7	1.6	0.8	1.8

[a] Relative standard deviation of retention time and peak area ($n = 15$); x: concentration (mg l^{-1}); y: detector response (HPLC-UV).

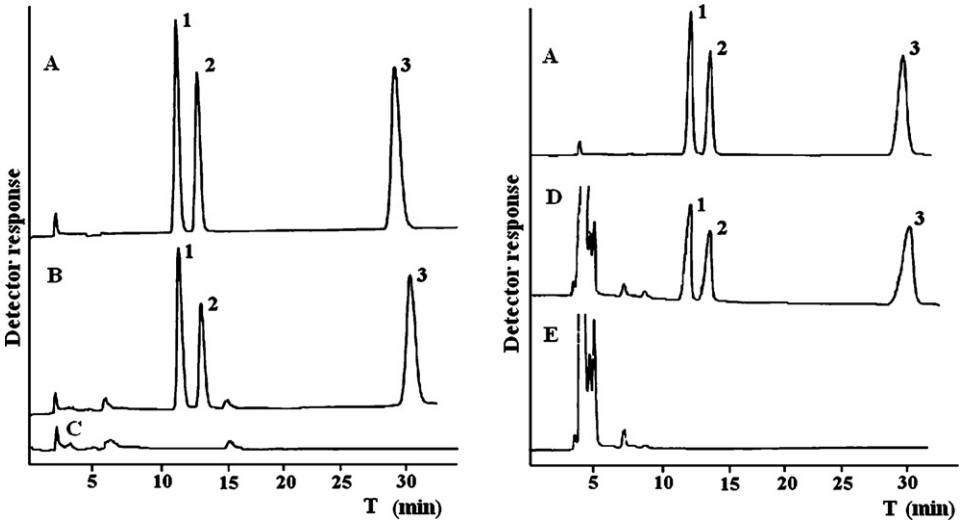

Fig. 3. HPLC-UV chromatograms (λ = 247 nm) of: (A) standard mixture (5.0 mg l^{-1}) [hexazinone (1), tebuthiuron (2) and diuron (3)]; spiked soil sample at 2.0 mg kg^{-1} (hexazinone and tebuthiuron) and 2.57 mg kg^{-1} (diuron) extracted with methanol (B) and acetone (D); control soil sample, methanol (C) and acetone (E) as extraction solvent.

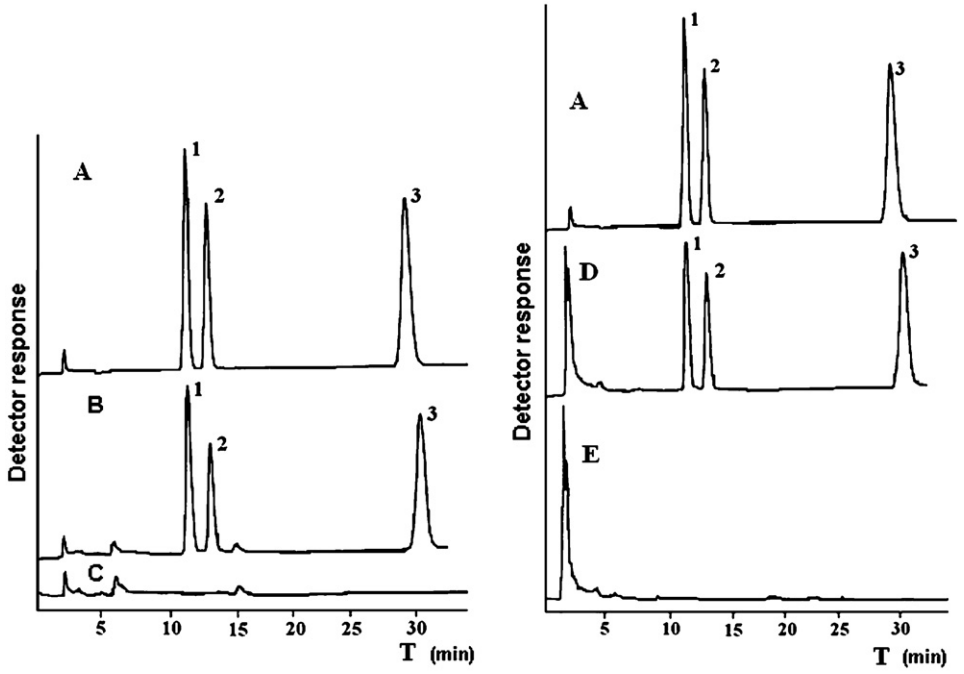

Fig. 4. HPLC-UV chromatograms (λ = 247nm) of: (A) standard mixture (5.0 mg l^{-1}) [hexazinone (1), tebuthiuron (2) and diuron (3)]; (B) spiked soil and (D) soil-vinasse sample at 2.0 mg kg^{-1} (hexazinone and tebuthiuron) and 2.57 mg kg^{-1} (diuron); (C) control soil sample; (E) control soil-vinasse sample. Methanol as extraction solvent for all chromatograms.

herbicides studied in this work, the method was validated using spiked samples of soil and soil-vinasse at two levels, and thus, the lowest and highest recommended dose for sugar cane crops were contemplated.

Detection limits obtained for diuron, hexazinone and tebuthiuron in soil and soil-vinasse are summarized in Table 3. The LOQ was determined as the lowest concentration of the compound that gives a response that could be quantified with an R.S.D. of less than

Table 2
Soil and soil-vinasse properties

	P (mg dm^{-3})	O.M. (g dm^{-3})	O.C. (%)	pH	K[a]	Ca[a]	Mg[a]	P.A.[a]	T.E.B.[a]	C.E.C.[a]	B.S. (%)
Soil	2	20	1.2	4.9	0.4	9	2	32	11	43	26
Soil-vinasse	3	20	1.2	5.0	11.7	8	4	31	24	55	44

P: Phosphorus, O.M.: organic matter, O.C.: organic carbon, K: potassium, Ca: calcium, Mg: magnesium, P.A.: potential acidity, T.E.B.: total exchangeable bases, CEC: cation exchange capacity and B.S.: base saturation.

[a] Presented as mmol dm^{-3}.

Table 3
Method detection limits for diuron, hexazinone and tebuthiuron in soil and soil-vinasse

Herbicides	Method detection limits (mg kg^{-1})		
	Hexazinone	Tebuthiuron	Diuron
Soil	0.025	0.040	0.042
Soil-vinasse	0.030	0.050	0.035

20% and a recovery of at least 70%. So the LOQ value for diuron, hexazinone and for tebuthiuron was 0.26, 0.25 and 0.25 mg kg^{-1}, respectively. These values are in agreement with the advised values established for some soil-pesticide levels in the state of São Paulo [28].

The accuracy and precision were considered adequate to recover diuron, hexazinone and tebuthiuron in soil and soil-vinasse samples at both lowly and highly spiked levels, with recoveries ranging from 81% to 119% and an R.S.D. lower than 10% (Table 4). In this recovery experiment, spiked samples were extracted 24 h after the herbicides were added to soil.

The elapsed time between sample collection and laboratory sample processing is an important aspect in the analysis of the pesticide residues, and it also should be considered during method validation [29]. Soil samples can be frozen until they are required for analysis, but is necessary to define the time that samples will remain stable and that analytes concentrations will not be affected. In a previous study, spiked samples with hexazinone and tebuthiuron at 1.25 mg kg^{-1} were frozen for 3, 10 and 20 days before analysis. Good preliminary results were obtained and a second experiment was performed to evaluate the influence of storing soil and soil-vinasse samples, which contained the three target herbicides at two levels (the low and the high level applied in this study) and were frozen for 20 days at the aforementioned herbicide concentrations. Similar to the recovery experiments employed on non-frozen spiked samples, good results were also obtained (Table 4) for the frozen ones. This experiment showed that it is possible to keep soil and soil-vinasse samples at the spiked sample levels studied frozen for 20 days without any modification of the herbicide concentrations.

As can be seen in Table 4, a greater recovery was obtained for all herbicides at the low spiked level, except for hexazinone and tebuthiuron in frozen soil. This fact can be justified by the possible formation of herbicides bound to residues in soil. This factor was pointed out by Andreu and Picó [5] as one of the challenging aspects related to the development of analytical methods to determine pesticides in soil.

A comparison of the proposed method with other analytical methods previously presented in literature for the determination of diuron, hexazinone and tebuthiuron in soil is shown in Table 5.

From our knowledge, the presented method is the first study for the simultaneous determination of these three widely employed herbicides applied to soil used for sugar cane crops. Most of the compared methods involve laborious extraction and clean-up procedures or they require special apparatus when considering the pressurized fluid extraction (PFE) technique. On the other hand, some described methods did not show important analytical parameters, such as limit of detection and quantification, which are necessary for the validation of an analytical method [30–32]. The proposed method shows good precision and accuracy, as do the other cited methods.

3.3. Degradation study

Herbicides are a widely applied class of pesticides employed in agriculture and they are causing concern regarding the potential contamination of ground and surface waters, which has been systematically reported in literature [27,33–38]. Knowledge regarding the fate of pesticides and monitoring studies have been focused on assessing the exposure of these to humans and the environment [4,39]. Pesticide dissipation in soil is an important parameter to estimate the persistence of pesticides in the environment. Racke et al. [6] emphasized that the contribution made by each of the loss mechanisms, such as microbial degradation, chemical hydrolysis, photolysis, volatility, leaching and surface runoff, to the overall dissipation is generally assessed by conducting laboratory and/or field studies.

Taking into account that diuron, hexazinone and tebuthiuron have been detected in groundwater samples from different countries [40–43], and the fact that the assessment of their behavior in soil is an important contribution to understand the pathway to avoiding water contamination, the degradation of herbicides in soil and the influence of vinasse addition to soil was evaluated in this study employing the analytical method presented above.

The soil degradation experiment carried out with soil and soil-vinasse under laboratory conditions indicated that the behavior of diuron, hexazinone and tebuthiuron varied between themselves and for different kinds of treatment (Fig. 5).

However the degradation of diuron gave a more representive result when compared with that of hexazinone and tebuthiuron (Fig. 5), its principal product of biodegradation, 3,4-dichloroaniline, exhibits a higher toxicity, and it is also persistent in soil, water and groundwater [44]. Giazomazzi and Cochet [44] alerted to the fact that biodegradation and toxicological studies must not be only focused on the disappearance of a polluting agent that could not be mineralized and transformed into another compound, but also on the intermediate degradation products in order to define the real environmental impact of a pollutant, since the intermediate compounds may be more toxic than the initial compound itself.

Table 4
Recoveries and R.S.D.s of the three studied herbicides from soil and soil-vinasse samples, no frozen and frozen (20 days)

Herbicides	Soil treatment	No frozen samples				Frozen samples (20 days)			
		Low level		High level		Low level		High level	
		Recovery (%)	R.S.D. (%)	Recovery (%)	R.S.D. (%)	Recovery (%)	R.S.D. (%)	Recovery (%)	R.S.D. (%)
Diuron	Soil	111 (101–119)	6	86 (81–90)	4	104 (98–112)	5	91 (87–92)	2
	Soil-vinasse	115 (105–119)	5	86 (84–87)	1	116 (11–120)	3	86 (78–91)	6
Hexazinone	Soil	110 (108–114)	4	102 (98–106)	4	97 (93–101)	4	101 (95–106)	4
	Soil-vinasse	109 (105–114)	3	98 (95–99)	2	105 (102–110)	3	98 (90–104)	5
Tebuthiuron	Soil	111 (103–119)	6	93 (85–99)	6	100 (93–105)	5	100 (98–101)	1
	Soil-vinasse	113 (106–119)	5	93 (91–95)	2	107 (100–112)	5	96 (87–102)	7

Low level: 0.25 mg kg^{-1} for hexazinone and tebuthiuron, and 0.26 mg kg^{-1} for diuron; high level: 2.0 mg kg^{-1} for hexazinone and tebuthiuron, and 2.57 mg kg^{-1} for diuron. Recovery (n = 5) expressed as: mean (max–min). R.S.D.: Relative standard deviation.

Table 5
Comparison of literature methods and the present method for diuron, hexazinone and tebuthiuron determination in soil sample

Pesticides	Sample (g)	Analytical procedure			Recovery (R.S.D., %)	LOD, LOQ (mg kg^{-1})	Reference
		Extraction	Clean-up	Analytical technique			
Diuron, hexazinone, tebuthiuron	4	SPE[a] (C18; 20 ml MeOH)	–	HPLC-UV (EF: C18, 5 μm; MF: MeOH:H_2O 45:55; λ = 247 nm)	76–120, 1–10	0.025–0.05, 0.25–0.26	Proposed method
Tebuthiuron	25	Sonication (20 ml MeOH:H_2O (55:45, v/v))	LLE[b] (40 ml diethyl ether)	HPLC-UV (EF: C18, 10 μm; MF: MeOH:H_2O (45:55); λ = 254 nm)	77–86 (4–5)	s	[20]
Hexazinone, tebuthiuron	20	Shaking (75 ml MeOH:H_2O (80:20) 1 h; 25 ml, 15 min	GPC[c]	HPLC-UV (EF: fenil, 4 μm; MF: MeOH:H_2O (50:50); λ_{teb} = 254 nm, λ_{hex} = 249 nm)	98–102 (2)	0.005, s	[17]
Hexazinone and degradation products	50	Shaking (3 × 68 ml MeOH:H_2O (4:1))	2 ml lead acetate	HPLC-UV (EF: C18; MF: ACN:H_2O (≠ conditions); λ_{teb} = 254 nm)	s	s	[18]
Hexazinone, tebuthiuron[e]	5	PFE[d] (acetone; 1500 psi, 100 °C) Soxhlet (250 ml acetone, 18 h)	SPE[a] (C18, MeOH) Na_2SO_4 (10 g)	GC–MS	SPE: 86–107 (4–7) Soxhlet: 88–96 (3–8)	s	[21]
Diuron[f]	100	Shaking (200 ml acetone:H_2O (80:20), 1 h); LLE[b] (2 × 20 ml ethyl acetate, 15 g NaCl)	TLC[g] (silica gel)	GC-ECD/GC–MS	84–97 (s)	s	[21]
Diuron and degradation products	200	Sonication (vol. MeOH = 2 times the weight soil) 40 °C, 24 h	–	HPLC-UV (EF: C18; MF: ACN:H_2O (35:65); λ_{teb} = 252 nm)	s	s	[22]
Diuron, metolachlor	5	Shaking (8 ml acetone, 10 min)	–	HPLC-DAD (EF: RP-amida C16, 5 μm; MF: ACN:H_2O (50:50); 30 °C)	70–96 (2–8)	s	[23]

R.S.D.: Relative standard deviation; s, not described.
[a] Solid-phase extraction.
[b] Liquid–liquid extraction.
[c] Gel permeation chromatography (60 g Bio-Beads® SX-3; chloroform-hexane, 50:50).
[d] Pressurized fluid extraction.
[e] Pesticide multi-residue: hexazinone, tebuthiuron, alachlor, bromacil, and metribuzin.
[f] Pesticide multi-residue: diuron, chlorotoluron, simazine, propizamide, and diflufenican.
[g] Thin layer chromatography.

Table 6
First-order equations and half-lives (days) obtained after fitting data of incubation study to a first order kinetic

	Soil			Soil-vinasse		
	Equation	$t_{1/2}$ (R.S.D.)[a]	r^2	Equation	$t_{1/2}$ (R.S.D.)[a]	r^2
Hexazinone	$\ln(C/C_i) = 0.0559 - 0.0083t$	84 (16)	0.9497	$\ln(C/C_i) = 0.0717 - 0.0131t$	53 (5)	0.9548
Tebuthiuron*	$\ln(C/C_i) = -0.2713 - 0.0054t$	128 (15)	0.8755	$\ln(C/C_i) = -0.2713 - 0.0054t$	73 (7)	0.9557
Diuron*	$\ln(C/C_i) = -0.3369 - 0.0086t$	80 (3)	0.9456	$\ln(C/C_i) = -0.1207 - 0.0996t$	7 (0.4)	0.9753

[a] Relative standard deviation ($n = 3$).
* $p < 0.05$.

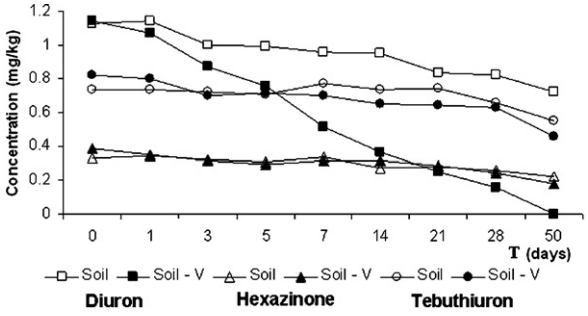

Fig. 5. Dissipation rate of diuron, hexazinone and tebuthiuron in soil and soil treated with sugar cane vinasse ($n = 3$).

The degradation of diuron, hexazinone and tebuthiuron in the studied soil of Araraquara, with and without the addition of vinasse at 30 °C, tented to follow the first-order kinetics (Eq. (6)) as is evident from the correlation coefficients (r) listed in Table 6.

$$\ln[C] = \ln[C_i] + (-k)t \quad (6)$$

where C is the herbicide concentration in soil at time t, C_i the initial herbicide concentration in soil, k the dissipation rate constant, and t is the time since treatment with herbicides.

The half-life values ($t_{1/2}$) (Table 6), when 50% of the initial amount of residues is left in the soil, were obtained from the regression between $\ln(C/C_i)$, according to Eq. (7):

$$t_{1/2} = \frac{\ln 2}{k} \quad (7)$$

The addition of sugar cane vinasse to soil affected the diuron and tebuthiuron degradation at a significant level of $p < 0.05$ (t-student) as a consequence of a possible increase of microbial activity, as reported by Prata et al. [45]. Under the conditions of this study, diuron gave the greatest factor of degradation (11.4), followed by tebuthiuron (1.8) and then hexazinone (1.6).

A recent study determining tebuthiuron leaching and its half-life in sugar cane fields in Brazil did not detect measurable residues of tebuthiuron in soil below a depth of 40 cm after 180 days from its application [46]. However laboratory studies do not elucidate the overall behavior of a compound in an ecosystem, due to the multiples forces of dissipation and transport that are simultaneously at work in field conditions, laboratory investigations are often aimed to study isolated processes or isolated component of an ecosystem, presenting results not highly variable when compared with field studies [6], as is the case in the assessment of the effect of vinasse on the degradation of herbicides.

4. Conclusion

The developed method was demonstrated to be efficient for the simultaneous determination of diuron, hexazinone and tebuthiuron in soil and soil-vinasse, showing itself to be easy to operate and permitting the treatment of a reduced sample. It is an alternative to the use of sophisticated analytical methods that determine these herbicides in soil, thus avoiding organic–solvent–water mixtures and a long concentration step. It also increases the possibilities of automation, economizing sample manipulation and analysis time. The method's quantification limits were similar to those established as the advised values for some pesticides in Brazilian soil (São Paulo State). Finally, the method was efficient to determine the half-life of herbicides in soil and soil treated with sugar cane vinasse. It was fast, efficient and robust as is required for the monitoring of pesticides widely distributed in soil, which is especially true for the monoculture of sugar cane.

Acknowledgment

C.L. wishes to thank CNPq (Conselho Nacional de Desenvolvimento Científico e Tecnológico) for the fellowship.

References

[1] C. Bolling, N.R. Suarez, Sugar Sweetener Situation Outlook SSS-232 (2001) 14.
[2] J. Goldemberg, S.T. Coelho, P.M. Nastari, O. Lucon, Biomass Bioener. 26 (2004) 301.
[3] R.S. Oliveira Jr., W.C. Koshinen, F.A. Ferreira, Weed Res. 41 (2001) 97.
[4] R. Hüskes, K. Levsen, Chemosphere 35 (1997) 3013.
[5] V. Andreu, Y. Picó, Trends Anal. Chem. 23 (2004) 83.
[6] K.D. Racke, M.W. Skidmore, D.J. Hamilton, J.B. Unsworth, J. Miyamoto, S.Z. Cohen, Pure Appl. Chem. 69 (1997) 1349.
[7] A. Farran, A. Chentouf, J. Chromatogr. A 869 (2000) 481.
[8] M.S. Cravo, T. Murakota, M.F. Giné, Rev. Bras. Ci. Solo 22 (1998) 547.
[9] M.D. Webber, H.R. Rogers, C.D. Watts, A.B.A. Boxall, R.D. Davis, R. Scoffin, Sci. Total Environ. 185 (1996) 27.
[10] E. Gloeden, R.C.A. Cunha, M.J.B. Fraccaroli, R.W. Cleart, Water Sci. Technol. 24 (1991) 147.
[11] E. Madejón, R. López, J.M. Murillo, F. Cabrera, Agric. Ecosys. Environ. 84 (2001) 55.
[12] P. Richter, B. Sepúlveda, R. Oliva, K. Calderón, R.J. Seguel, J. Chromatogr. A 994 (2003) 169.
[13] C. Sanchez-Brunete, E. Miguel, J.L. Tadeo, J. Chromatogr. A 976 (2002) 319.
[14] L. Polese, E.V. Minelli, E.F.G. Jardim, M.L. Ribeiro, Fresenius J. Anal. Chem. 354 (1996) 474.
[15] D.C. Bouchard, T.L. Lavy, J. Chromatogr. 270 (1983) 396.
[16] S.G. Whisenant, W.P. Clary, J. Environ. Qual. 16 (1987) 397.
[17] J. Lyndon, B.F. Engelke, C. Helling, J. Chromatogr. 536 (1991) 223.
[18] J.B. Fischer, J.L. Michael, J. Chromatogr. A 704 (1995) 131.
[19] Y. Zhu, Q.X. Li, Chemosphere 49 (2002) 669.
[20] A.E. Smith Jr., L.M. Shuman, N. Lokey, J. Agric. Food Chem. 32 (1984) 416.
[21] Y. Zhu, K. Yanagihara, F. Guo, X.Q. Li, J. Agric. Food Chem. 48 (2000) 4097.
[22] J.S. Fritz, Soil-phase extraction, in: G. Laurent, S. Shapiro (Eds.), Encyclopedia of Analytical Science, second ed., Elsevier, Amsterdam, 2005, p. 604.
[23] H.P. Thier, H. Zeumer, Manual of Pesticide Residue Analysis, Deutsche Forschungsgemeinschaft, Pesticide Commission, Verlag Chemie, Weinheim, New York, 1987, p. 433.
[24] Organization for Economical Co-operation and development, Aerobic and anaerobic transformation in soil (OECD Guideline for Testing of Chemicals, 307), 2002, 17 pp.
[25] V.L. Ferracini, S.C.N. Queiroz, M.A.F. Gomes, G.L. Santos, Quim. Nova 28 (2005) 380.
[26] P.S. Bonato, V.L. Lanchote, S.A.C. Dreossi, J. High Resolut. Chromatogr. Chromatogr. Commun. 22 (1999) 239.
[27] S.H.G. Brondi, F.M. Lanças, J. Liq. Chromatogr. Relat. Technol. 27 (2004) 171.
[28] http://www.cetesb.sp.gov.br/Solo/relatorios/tabela_valores_2005.pdf (Last revision: November 2005).
[29] M.P. Maskarinec, R.L. Moody, Storage and preservation of environmental samples, in: L.H. Keith (Ed.), Principles of Environmental Sampling, American Chemical Society, United States of America, 1988, pp. 145–155.

[30] N.M. Brito, O.P. Amarante Jr., L. Polese, T.C.R. Santos, M.L. Ribeiro, Pesticidas: Rev. Ecotoxicol. Meio Ambiente 12 (2002) 155.
[31] E. Francotte, A. Davatz, P. Richert, J. Chromatogr. B 686 (1996) 77.
[32] R. Causon, J. Chromatogr. B 689 (1997) 175.
[33] S.N. Hamlin, K. Belitz, S. Kraja, B. Dawson, Ground-water quality in the Santa Ana Watershed, California: overview and data summary, Water Resources Investigations Report, United States Geological Survey, United States, 2002, I–xi, pp. 1–137.
[34] R.L. Bengtson, H.M. Selim, R. Ricaud, Trans. ASAE 41 (1998) 1331.
[35] B.P. Wood, F. Gumbs, J.V. Headley, Commun. Soil Sci. Plant Anal. 33 (2002) 3501.
[36] M.C.P.Y. Pessoa, M.A.F. Gomes, M.C. Neves, A.L. Cerdeira, M.D. Souza, Pesticidas: Rev. Ecotoxicol. Meio Ambiente 13 (2003) 111.
[37] H.F. Filizola, V.L. Ferracini, L.M.A. Sans, M.A.F. Gomes, C.J.A. Ferreira, Pesq. Agropec. Bras. 37 (2002) 659.
[38] M.B. Matallo, L.C. Luchini, M.A.F. Gomes, C.A. Spadotto, A.L. Cerdeira, G.C. Marin, Pesticidas: Rev. Ecotoxicol. Meio Ambiente 13 (2003) 83.
[39] T.A. Albanis, D.G. Hela, T.M. Sakellarides, I.K. Konstantinou, J. Chromatogr. A 823 (1998) 59.
[40] D.A. Williamson, Water Pollut. Res. J. Canada 23 (1988) 434.
[41] J.L. Domagalski, N.M. Dubrovsky, J. Hydrol. 130 (1992) 299.
[42] W. Abke, H. Korpien, B. Post, Vom Wasser 81 (1993) 257.
[43] M.A.F. Gomes, C.A. Spadotto, V.L. Lanchote, Pesticidas: Rev. Ecotoxicol. Meio Ambiente 11 (2001) 65.
[44] S. Giacomazzi, N. Cochet, Chemosphere 56 (2004) 1021.
[45] F. Prata, A. Lavorenti, J.B. Regitano, V.L. Tornisielo, Rev. Bras. Ci. Solo 24 (2000) 217.
[46] A.L. Cerdeira, M.D. Desouza, S.C.N. Queiroz, V.L. Ferracini, D. Bolonhezi, M.A.F. Gomes, M.A. Rosa, O. Balderrama, P. Rampazzo, R.H.C. Queiroz, C.F. Neto, M.B. Matallo, J. Environ. Sci. Health Part B 42 (2007) 635.

Talanta 77 (2008) 561–565

Contents lists available at ScienceDirect

Talanta

journal homepage: www.elsevier.com/locate/talanta

Photo-induced chemiluminescence determination of the pesticide Buminafos by a Multicommutation flow-analysis assembly

D. López Malo, J. Martínez Calatayud *

Department of Analytical Chemistry, University of Valencia, Valencia, Spain

ARTICLE INFO

Article history:
Received 26 March 2008
Accepted 4 April 2008
Available online 22 April 2008

Keywords:
Buminafos
Pesticides
Photo-induced chemiluminescence
Multicommutation

ABSTRACT

The preliminary experiments in this paper deal with the photo-induced chemiluminescent behaviour of Buminafos family, after the experimental screening tests and several of them resulted positive, the herbicide Buminafos was selected to develop a new analytical method.

The determination of Buminafos was performed with the aid of a Multicommutation (a solenoid valve set) assembly. The method involves the on-line photo-degradation of the analyte (stopped flow, 5 s) with the selected suitable medium (0.05% hydrogen peroxide) and its subsequent chemiluminescent oxidation by the potassium permanganate. Sample solution alternated segments with the photo-degradation medium; and, after the irradiation, aliquots of the resulting mixture were alternated with the oxidant system. Both streams merged 2 cm before the flow-cell of the luminometer.

The chemical optimization study was performed separately for photo-degradation and for oxidation by including different media and oxidants; it also included the study on the influence of sensitizers and tensoactive agents. Linear interval was from 0.01 to 1.0 mg l^{-1} with a limit of detection of 0.005 mg l^{-1}. Sample throughput and the reproducibility were 48 h^{-1} and 3%, respectively. After testing the analytical figures of merit foreign compounds were studied as possible interferents of the method. The proposed method was applied to the determination of the pesticide in spiked water and soil samples.

1. Introduction

Buminafos ($C_{18}H_{38}NO_3P$) presents a couple of commercial names [1] as Pestanal, Trakephon or Aminophon. Its molecular structure is depicted in Fig. 1 and it is dibutyl 1-butylaminocyclohexylphosphonate according to IUPAC or dibutyl [1-(butylamino)cyclohexyl]phosphonate according to CAS.

It is a widely used pesticide; however, the bibliographic information available is almost inexistent. It is classified into the group of grow plant regulators and it is applied to cultures of potato, clover and lucerne; and it can be applied with little harm to bees [2]. It is a low-toxic pesticide for haulm destruction, desiccation, defoliation and weed control. The analytical literature on Buminafos is also null; as far as authors know, only one reference can be found dealing with the pesticide dispersion on soil in which the Buminafos was extracted with methanol and evaluated with the aid of a gas chromatograph provided with an electron capture detector; relative amounts of the pesticide in soil samples were compared after different time intervals up to 12 days [3]. Other article deals with the residue and leaching behaviour of Buminafos in soil [4]. An article deals with the Buminafos behaviour on different types of soil to check its biological degradation [5].

In the present work, we used the photo-induced chemiluminescence of Buminafos to determine it in a continuous-flow system. Some preliminary experiments were performed to test the photo-induced chemiluminescent behaviour of several members of this family of pesticides, after the experimental screening tests the herbicide Buminafos was selected for further analytical work. The determination was performed with the aid of a Multicommutation assembly and the developed method involves the on-line photo-degradation of the analyte and its subsequent chemiluminescent oxidation by the potassium permanganate. The proposed method was applied to the determination of the pesticide in spiked water and soil samples.

2. Experimental

2.1. Reagents and apparatus

All reagents used were analytically pure unless stated otherwise and prepared in purified water; reverse osmosis and deionised (18 MΩ cm) with a Sybron/Barnstead Nanopure II water

* Corresponding author.
E-mail address: jose.martinez@uv.es (J.M. Calatayud).

0039-9140/$ – see front matter © 2008 Elsevier B.V. All rights reserved.
doi:10.1016/j.talanta.2008.04.030

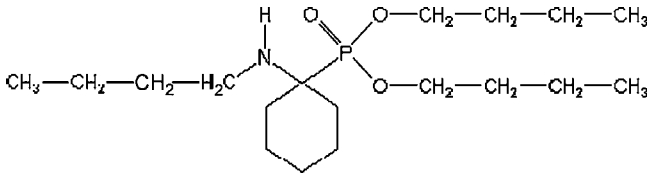

Fig. 1. Molecular structure of Buminafos.

purification system provided with a fibber filter of 0.2 μm pore-size.

The Buminafos was from Dr. Ehrenstorfer GmbH (99.0%, Germany). For the preliminary studies were also used the pesticides Malathion, Methidathion and Tiomethon from the same manufacturer. Other used reagents were alkalis, salts and mineral acids; oxidants as $KMnO_4$, $Ce(NH_4)_2(NO_3)_6$, $K_3(Fe(CN)_6$ and H_2O_2 (all from Panreac, Spain), organized media and sensitizers as: formic acid, acetonitrile, sodium dodecylsulphate (SDS), hexadecyl pyridinium chloride, β-cyclodextrine, 2-propanol (Fluka, Switzerland), benzalkonium chloride (Guinama, Valencia, Spain), *N*-cetyl-*N*,*N*,*N*-trimethyl ammonium bromide (Merck, Darmstadt, Germany), quinine sulphate (Sigma–Aldrich Química S.A., Spain), Triton X-100, *N*,*N*-dimethylformamide (Scharlau, Spain), ethanol (Prolabo, Spain). As photo-degradation media were used: $Fe(NO_3)_3{\cdot}7H_2O$ (Probus) and $FeSO_4{\cdot}9H_2O$ (Merck).

2.2. Apparatus

The pH control on different solutions was performed with the aid of a pHmeter Crison pH 2001 (Alella, Barcelona, Spain) and the spectrophotometer Agilent 8453 (Las Rozas, Madrid, Spain) was used to test the stability of the Buminafos solutions.

2.2.1. Flow assembly and procedure

The flow manifold is depicted in Fig. 2, consisted of a PTFE coil of 0.8 mm i.d.; a Gilson (Worthington, OH, USA) Minipuls 2 peristaltic pump provided with tygon pump tubing from Omnifit; and, three solenoid valves Model 161T031 (Nresearch, Northboro, MA, USA). The photoreactor consisted of a 150 cm length and 0.8 mm i.d. PTFE tubing helically coiled around a 15 W low-pressure mercury lamp (Sylvania) for germicidal use. The flow-cell was a flat-spiral quartz tube of 1 mm i.d. and 3 cm total diameter backed by a mirror for maximum light collection. The photo-detector work-package was a P30CWAD5F-29 Type 9125 photomultiplier tube (PMT) supplied by Electron Tubes operating at 1280 V; it was located in a laboratory-made light-tight box. The output was fed to a computer equipped with a counter-timer, also supplied by Electron Tubes.

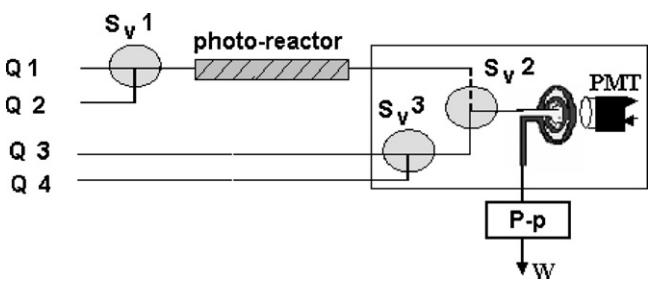

Fig. 2. Continuous-flow manifold of Multicommutation for the determination of Buminafos. Channels: Q1, photo-degradation medium, 0.05% hydrogen peroxide; Q2, aqueous solution of Buminafos; Q3, Carrier (water); Q4, Oxidant solution ($KMnO_4$ in H_2SO_4 medium). Flow-rate: 10 ml min^{-1}. P-p, peristaltic pump; W, waste; PMT, photomultiplier tube; Sv: solenoid valves. The lamp of the photo-reactor was a 15 W low-pressure mercury lamp (Sylvania) for germicidal use.

Table 1
Solenoid valves working program

Vl: 0, 50 × (0.4, 0.2), 0.5 V2: 0, 30, 150, 30 × (0.6, 0.2), 0.5 V3: 165, 39 T_{cycle}: 235 s
⋮
V1: 0, 50 × (0.4, 0.18), 0.5 V2: 0, 28.5, 5, 30 × (0.6, 0.2), 0.5 V3: 32, 26 T_{cycle}: 75 s

Up, preliminary program. Bottom, Optimized program with the simplex method.

The manifold depicted in the figure includes a set of three solenoid valves; each one acting as an independent commutator ON/OFF and the complete cycle can be described in terms of $N \times (t_1, t_2)$; where t_1 is the time interval in ON position, t_2 corresponds to the OFF mode; and N is the number of the repeated ON/OFF sequence. Preliminary program set is depicted in Table 1. The system configuration was the same during the whole experimental work; only the ratio t_1/t_2 and N were varied. The pump was placed after the detector, being sample and reagent solutions aspirated to the flow-cell at flow-rate 10 ml min^{-1}.

The insertion profile in the finally proposed flow manifold was as follows; valve Sv1 segmented the analyte solution with hydrogen peroxide as the suitable photo-degradation medium, leading theses segments to the photo-reactor. During each micro insertion, Sv1 was ON during 0.4 s (aspiration of Buminafos) and, deactivated during 0.18 s (valve OFF, aspiration of the hydrogen peroxide). During the required interval (N 28.5 s) for the process, valve Sv2 was ON allowing the peristaltic pump to aspirate Buminafos and medium. Next 5 s period, the UV-photo-degradation stopped flow interval, all valves were in mode OFF. Then valve Sv3 was activated to allow the stream of the oxidant solution, which was divided in micro segments in Sv2 and alternated with micro insertions of the resulting photo-fragments of Buminafos 30 (0.6, 0.2). This generated the chemiluminescent emission and, when base-line was reached again by circulating pure water, a new cycle stared; total time 75 s.

2.3. Procedures

2.3.1. Preparation of samples

Water from irrigation ditches located in Xirivella (Valencia), tap water (laboratory) and bottled water (commercial trade mark) were spiked with a known amount of Buminafos into the dynamic range of application (up to 2 mg l^{-1}) to obtain a solution in the vicinity of 1.0 mg ml^{-1} in Buminafos. The content of the pesticide in the resulting solutions was determined and compared with the added amount to determine evidences of constants or proportional systematic errors.

A sample from an agricultural soil was collected (argillaceous type from Lliria, Valencia, Spain) and it was treated according to official rules [6] in which the Buminafos solution was sprayed at low pressure to 25 g of soil. The pesticide solution to be added to the sample soil contained 10 mg l^{-1} of Buminafos (25 ml). This sample was treated with 100 ml of pure water with the aid of magnetic stirring during 5 min, then it was filtered and the Buminafos content determined.

2.3.2. Preparation of standards and test of stability

An stock solution of Buminafos (20 mg l^{-1}) was prepared by weighing the exact required amount of pesticide; then it was solved in pure water with the help of an ultrasonic bath and magnetic stir-

ring. The resulting solution of Buminafos was protected from room light and kept at 4 °C into the refrigerator. UV–vis spectra were periodically recorded, from 200 to 500 nm up to 5 days; it resulted in a very short stability. The working standard solutions were freshly prepared by diluting the stock solution in the appropriate volume of water.

2.3.3. Optimization of chemical and hydrodynamic parameters

The optimization of chemical and manifold variables was performed by a sequential methodology. First we optimized by the univariate methodology the physico-chemical parameters, namely: oxidation system, medium for the photo-degradation, influence of both concentrations, presence of sensitizers and organized medium and temperature. Then with the selected values were optimized the hydrodynamic variables (Multicommutation parameters) by using the multivariate method known as the Modified Simplex Method (MSM).

The initial simplex was selected according to Yabro and Derming [7,8] which recently was improved in this laboratory [9] with the target Multicommutation variables and the emission value corresponding to each combination of such variables provided by the simplex inputs. The program was written to optimize the height of the output and in the second series; the interval for each variable was restricted to the zone that gave the former best results. Then the higher vertices were chosen for a new comparative study to choose the output resulting in the best compromise sensitivity (peak height)-sample throughput (peak–base width)-reproducibility (R.S.D., %). Finally the robustness study can be considered as the last process of optimization.

3. Results and discussion

3.1. Preliminary studies

The application of molecular topology methods allowed predicting the photo-induced chemiluminescent behaviour of some pesticides from the Buminafos family [10,11] (Buminafos, Malathion, Methidathion and Tiomethon) and after the empirical screening tests, all of them resulted positive being the herbicide Buminafos selected as a test substance for further analytical work.

The suitable oxidant was established by testing some strong oxidant systems, namely: 4×10^{-4} mol l^{-1} potassium permanganate or 6×10^{-3} mol l^{-1} Ce(IV) (both of them in 1.5 mol l^{-1} H_2SO_4); 6×10^{-3} mol l^{-1} $Fe(CN)_6^{3-}$ and 4×10^{-2} mol l^{-1} *N*-bromosuccinimide (both in 1.5 mol l^{-1} NaOH). The best outputs were obtained with potassium permanganate (see Fig. 3).

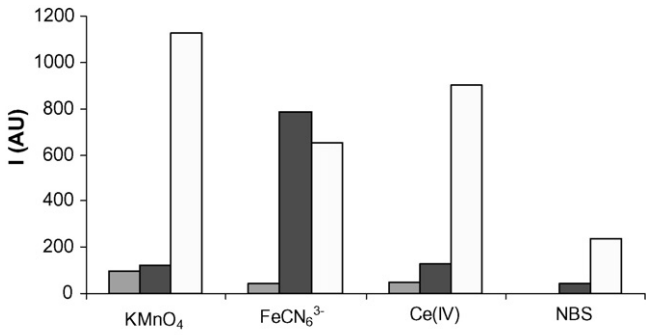

Fig. 3. Selection of the suitable oxidant system for Buminafos determination. The grey box is for the blank solution; other two are for sample solution (black, lamp OFF).

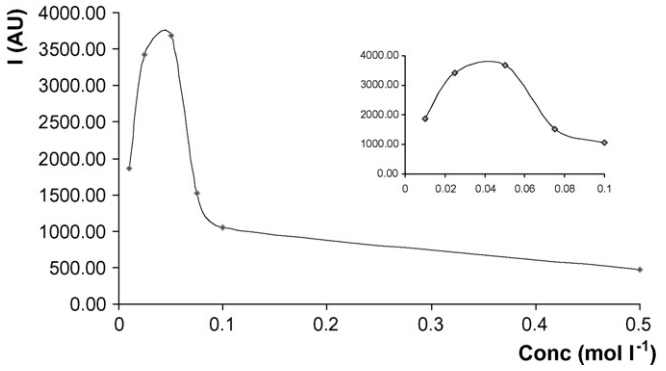

Fig. 4. Influence of the hydrogen peroxide concentration.

3.2. Optimization of chemical parameters

3.2.1. Photo-degradation

The sample solution (pesticide aqueous solution, 5 mg l^{-1}) was mixed with the different photo-degradation medium solution: H_2O, 10^{-3} mol l^{-1} NaOH, 0.05% H_2O_2, 6×10^{-5} mol l^{-1} Fe(III) or 6×10^{-5} mol l^{-1} Fe(II). Tests were performed with lamp ON and lamp OFF and results compared with the blank solution (containing no pesticide). The obtained results demonstrated the hydrogen peroxide was the suitable medium. Then were tested different concentrations of hydrogen peroxide over the range 0.01–0.5%; emitted light intensity was growing with the hydrogen peroxide concentration with a maximum clearly in the neighbour of 0.05%; then the emitted light decreased up to 0.1% in which a very small output was kept constant (see Fig. 4).

3.2.2. Influence of the medium of oxidant concentration and oxidant concentration

The influence of potassium permanganate concentration was tested up to 0.05 mol l^{-1} and with 1.0 mg l^{-1} of Buminafos. As observed in formerly published articles [12,13] this parameter resulted to be critical with a relatively short maximum interval around to 5×10^{-3} mol l^{-1}. This concentration of potassium permanganate was tested with different acids ($HClO_4$, $H_4P_2O_7$, HNO_3, H_2SO_4 and NaOH) 0.5 mol l^{-1} all of them were tested with lamp ON and OFF. The best acidic media were H_2SO_4 and $HClO_4$ and to decide the most suitable we performed a pre-calibration graph in both acidic media being the Buminafos content from 1 to 10 mg l^{-1}. Calibration in sulphuric medium resulted in higher slope and then, sulphuric acid was selected for further work. The influence of sulphuric acid concentration (tested from 0.5 to 2.5 mol l^{-1}) was not a critical parameter; however, it resulted in a clearly defined maximum output at 1.5 mol l^{-1}. To implement these experiments we tested the sample solution in different pH (range 2–10); the chemiluminescence outputs were increasing with the pH value up to 6 and then clearly diminished. Pure water was selected for the pesticide solution (see Fig. 5).

3.2.3. Effect of temperature on the emission intensity

The effect of temperature of photo-induced chemiluminescent processes is very complex. The temperature can influence the reaction kinetics of both processes (UV-degradation and chemiluminescence oxidative process) favouring their quantitativeness and it can also favour radiationless de-excitation of excited states and decrease the emission intensity; as a result of the first one it would lead to an increased emission intensity and as consequence of the second it can decrease the emission intensity as a result. In addition, raising the temperature can result in unwanted side effects

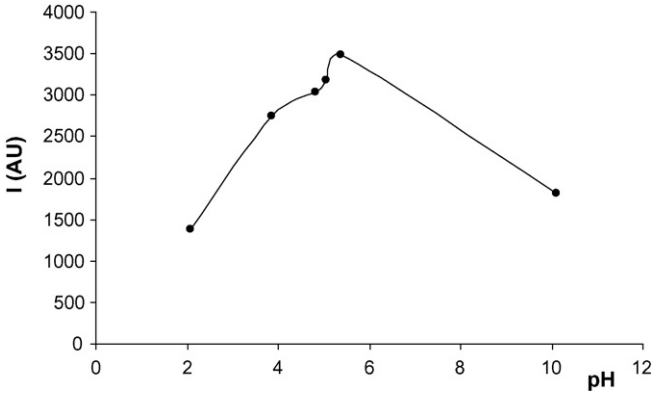

Fig. 5. Influence of the pH in the analyte solution.

such as the formation of gas bubbles which can alter flow-rates with a negative influence on the reproducibility [14,15].

The influence of temperature was tested with the aid of three independent experiments; influence on the oxidation reaction; influence on the photo-degradation; and, influence on the whole process. The temperature influence was studied by immersing the vessels containing the corresponding solutions in a J.P. Selecta Tectron 2000 water bath at 20, 40, 60 or 80 °C. Temperature changes on the oxidation reaction were no influencing the emission outputs up to 60, then it abruptly increased; however its influence on the whole process resulted in growing curve up to 60 °C and then (up to 80 °C) it was constant. The study of its influence on the photo-degradation resulted in increasing outputs in the tested range (from 20 to 80 °C). Selected temperature for further work was only on the photo-degradation at 80 °C.

3.2.4. Influence of the photo-degradation time

The influence of the photo-degradation time was studied over the range 5–150 s, using an aqueous solution containing 5.0 mg l^{-1} of Buminafos. The photo-degradation time usually results as a highly influential variable as the chemiluminescence can originate from both photo-degradation intermediates and end-products; also, photo-degradation reactions can differ markedly in kinetic terms [16]. The higher outputs were observed for minor tested time intervals. 5 s was the selected value for next work. For details see Fig. 6.

3.2.5. Effect of sensitizers and surfactants

The chemiluminescence emission can be enhanced by using a sensitizer or an organized medium. In the present work the influence of many substances was studied by preparing mixtures of

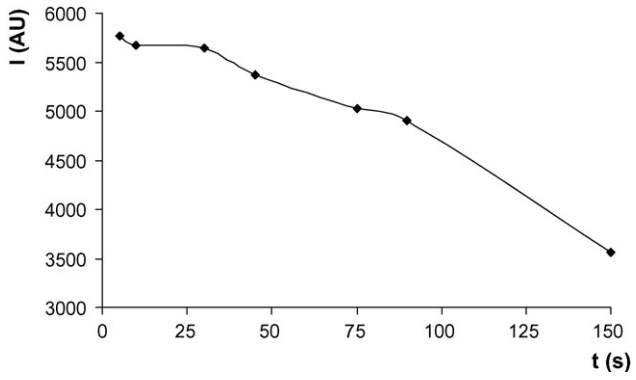

Fig. 6. Influence of the photo-degradation time.

the analyte and the tested substance at the suitable selected concentration; the observed analytical signal was compared with the obtained with pure aqueous herbicide solution [14,17,18]. Tested sensitizers were: ethanol (20%), dimethylformamide (5%), formic acid (0.5%), 2-propanol (20%), acetonitrile (20%), quinine sulphate (10^{-4} mol l^{-1}) and hexadecylpyridinium chloride (0.2%), benzalkonium chloride (0.6%); and, studied organized media were: *N*-cetyl-*N*,*N*,*N*-trimethylammonium chloride (0.2%) sodium dodecylsulphate (1.2%), Triton X-100 (0.72%) and β-cyclodextrine (1.2%). No interesting results were observed as the difference of both outputs (with and without presence of the sensitizer or organized medium) was nearby null.

3.2.6. Optimization of hydrodynamic parameters and irradiation interval

A multiparametric strategy, the Modified Simplex Method [7,8], was selected for the optimization of hydrodynamic parameters. The parameters studied were flow-rate and for valve 1 and 2 the number of segments and their interval (ON–OFF) and the total number of segments on each valve and cycle; and the total flow-rate. Chemical parameters were kept constant, 2.0 mg l^{-1} Buminafos and 0.05% of hydrogen peroxide and 5×10^{-3} mol l^{-1} potassium permanganate in 1.5 mol l^{-1} sulphuric acid. Two consecutive series of experiments were performed by fitting the limits for the second simplex (n 9) according the obtained results in the first series (n 12). Then the two vertices selected as optimum, when the system did not merit further research, were tested again (n 20) to obtain the best compromise sensitivity (output height)-reproducibility (R.S.D. in %) and sample throughput (see Table 1).

Then, more experiments were applied to the most critical parameters (chemical parameters) by univariate method around the selected values (±10%); robustness of the method.

3.2.7. Analytical figures of merit

The continuous-flow allows Buminafos to be determined, being the linear observed range from 0.01 to 1 mg l^{-1}. The analytical signal and the Buminafos concentration in the linear range were related by: $I = 2261.1X + 624.25$ (r^2 0.9999).

A measure of repeatability and reproducibility is also the R.S.D. (%) for the peaks, which was determined by using 11 consecutive insertions (intra-day reproducibility or repeatability) of the same solution containing 0.05 mg l^{-1} of Buminafos; the calculated R.S.D. (%) was 3.0 (n 11). The same experiment was repeated on 4 different days with freshly prepared solutions (inter-day reproducibility), the mean R.S.D. obtained being 5.0%. The limit of detection, which was taken to be the lowest pesticide concentration that yielded a signal equal to the blank signal plus three times its standard deviation, was 0.005 mg l^{-1}. The sample throughput was of 48 samples h^{-1}. To obtain a peak required sample, medium for photo-degradation and oxidant volumes (in ml) to be 0.92, 0.42 and 0.28 ml, respectively.

The influence of different foreign compounds (anions and cations) was studied to check the possible interference with the Buminafos determination. Mixtures of Buminafos and tested interference were prepared containing 1.0 mg l^{-1} of Buminafos and different amounts of the interference, up to 500 mg l^{-1}. Outputs were compared with the obtained with pure Buminafos solutions; no interference was considered when the relative error (vs. Buminafos solution) was less than 5%. Results are depicted in Table 2; some metallic cations (Fe(II), Fe(III), Mn(II), Cu(II) and Cr(III)) and two anions like acetate and nitrite interfered the determination. Therefore, for application to water and soil samples, this kind of interference should be easily removed by passage through appropriate adsorbents. Duolite C20 (Probus, cationic) which was prepared by packing Omnifit 5 cm × 4 mm i.d. methacrylate chromatographic columns with the resin. Prior to use, the column was

Table 2
Study of the influence of foreign compounds on the determination of Buminafos

Tested interferent (parent compound)	Concentration ($mg\,l^{-1}$)	Relative error (%)
Fe^{3+} ($Fe(NO_3)_3$)	1	56
Fe^{2+} ($FeSO_4$)	1	60
$H_2PO_4^-$ (NaH_2PO_4)	100	4.1
NH_4^+ (NH_4Cl)	100	2
Mn^{2+} ($MnCl_2{\cdot}4H_2O$)	1	26
K^+ (KCl)	100	5
Na^+ (NaCl)	500	6
CH_3COO^- (CH_3COOK)	1	-
CN^- (NaCN)	1	3
Zn^{2+} ($ZnCl_2$)	500	3
Mg^{2+} ($MgCl_2{\cdot}6H_2O$	500	6
Cl^- (KCl)	2044	5
Pb^{2+} ($Pb(NO_3)_2$)	10	5
Ni^{2+} ($Ni(NO_3)_2$)	100	2
Co^{2+} ($Co(NO_3)_2$)	500	3
CO_3^{2-} (K_2CO_3)	500	3
Cr^{3+} ($Cr(NO_3)_3$)	1	6
CrO_4^{2-} (K_2CrO_4)	100	4
Cu^{2+} ($Cu(NO_3)_2$)	1	52
SO_4^{2-} (Na_2SO_4)	500	5
NO_2^- ($NaNO_2$)	1	0
NO_3^- (KNO_3)	500	1
Ca^{2+} ($CaCl_2$)	500	5
HCO_3^- ($NaHCO_3$)	500	5
HPO_4^{2-} (Na_2PO_4)	500	4
Urea	500	3
Cd^{2+} ($Cd(NO_3)_2$)	500	2

conditioned by passage of a $0.1\,mol\,l^{-1}$ HCl solution. Cyanide was passed through a Duolite A-102 D (Probus, anionic) which was conditioned by passage of $0.1\,mol\,l^{-1}$ NaOH. Their performance was checked with Fe(II), Fe(III), Mn(II), Cu(II) and Cr(III)) (cationic mini-column) and acetate, NO_2^- and CN^- (anionic mini-column) at $500\,mg\,l^{-1}$ each. The results were (recovery) 102% for either cations or anions.

Several water samples were collected from different places and were spiked with a known amount of the pesticide ($1.0\,mg\,l^{-1}$). Collecting place and obtained recoveries (five replicates) were as follows: irrigation channel (Xirivella, Valencia, Spain) 101.0, R.S.D. 5.0%; tap water (Burjassot, Valencia, Spain), 97.0, R.S.D. 2%; and, bottled mineral water (trade mark Agua de Bejis, Castellón, Spain), 106.0, R.S.D. 1.0%. A soil sample (Lliria, Valencia, Spain) was collected and treated as reported in Section 2; results were of 97%, R.S.D. 3%.

4. Conclusions

The photo-induced chemiluminescent determination of Buminafos (an plant grow regulator pesticide) is presented. The method is performed with the aid of a continuous-flow procedure into the methodology known as Multicommutation.

As far as the authors know this is the first published article dealing with the analytical determination of this pesticide.

The method presents competitive sensitivity and reproducibility and the selectivity is improved with the aid of separation mini-columns.

The method is applied to different kind of water samples and a soil sample.

References

[1] http://www.alanwood.net/pesticides/buminafos.html.
[2] http://www.aces.edu/pubs/docs/A/ANR-1088.
[3] H. Reifenstein, W. Czyrnia, H. Beitz, Nachrichtenblatt fur den Pflanzenschutz-dienst in der DDR 10 (1973) 204.
[4] R. Binner, H. Schmidt, H. Beitz, Nachrichtenblatt fur den Pflanzenschutz in der DDR 43 (1989) 101.
[5] A. Kolbe, A. Bernasch, H.R. Schutte, Nachrichtenblatt fur den Pflanzenschutz in der DDR 43 (1989) 98.
[6] http://www.mapya.es/agricultura/pags/fitos/registro/productos/pdf/17489.pdf.
[7] L.A. Yabro, S.N. Derming, Anal. Chim. Acta 73 (1974) 1043.
[8] S.L. Morgan, S.N. Derming, Anal. Chem. 46 (1974) 1170.
[9] A.N. Araujo, unpublished work.
[10] M. Catalá Icardo, L. Lahuerta Zamora, G.M. Antón-Fos, J. Martínez Calatayud, M.J. Duart, TrAC 24 (2005) 782.
[11] I. Sahuquillo Ricart, J.R. Albert-García, G.M. Antón-Fos, M.J. Duart, J.V. García Mateo, L. Lahuerta Zamora, J. Martínez Calatayud, Talanta 72 (2007) 378.
[12] C.M.P.G. Amorim, J.R. Albert-García, M.C.B.S. Montenegro, A.N. Araújo, J. Martínez Calatayud, J. Pharm. Biomed. Anal. 43 (2007) 421.
[13] T. Gamazo Climent, J.R. Albert-García, J. Martínez Calatayud, Anal. Lett. 29 (2007) 629.
[14] A. Chivulescu, M. Catalá Icardo, J. Martínez Calatayud, Anal. Chim. Acta 519 (2004) 113.
[15] J. Martínez Calatayud, Flow Injection Analysis of Pharmaceuticals, Taylor and Francis, Cambridge, 1996.
[16] Z. Pawlicová, J.R. Albert-García, I. Sahuquillo, J.V. García Mateo, M. Catalá Icardo, J. Martínez Calatayud, Anal. Sci. 22 (2006) 29.
[17] E. Polo Martí, M. Catalá Icardo, L. Lahuerta Zamora, G.M. Antón Fos, J. Martínez Calatayud, Anal. Chim. Acta 527 (2004) 177.
[18] M. Catalá Icardo, J.V. García Mateo, J. Martínez Calatayud, TrAC 21 (2002) 366.

Talanta 77 (2008) 635–641

Contents lists available at ScienceDirect

Talanta

journal homepage: www.elsevier.com/locate/talanta

Determination of nitrous acid in air using wet effluent diffusion denuder–FIA technique

Pavel Mikuška*, Kamil Motyka, Zbyněk Večeřa

Institute of Analytical Chemistry, Academy of Sciences of the Czech Republic, v.v.i., Veveří 97, CZ-60200 Brno, Czech Republic

ARTICLE INFO

Article history:
Received 31 March 2008
Received in revised form 18 June 2008
Accepted 3 July 2008
Available online 12 July 2008

Keywords:
Nitrous acid
Wet effluent diffusion denuder
Flow-injection analysis
Monitoring

ABSTRACT

A sensitive and fast method for the determination of nitrous acid (HONO) in air is described. The method combines a continuous collection of nitrous acid into a thin film of absorption liquid in a cylindrical wet effluent diffusion denuder (CWEDD) and on-line analysis of collected nitrous acid at the denuder concentrate employing a flow-injection analysis (FIA) where nitrous acid is oxidized into peroxynitrous acid and a chemiluminescent light emitted during the reaction of peroxynitrite with luminol is detected. Various absorption solutions (carbonate, bicarbonate, phosphate) as well as deionized water were compared from point of view of collection efficiency of nitrous acid at the CWEDD and selectivity and sensitivity of nitrous acid determination in air.

All tested liquids provide quantitative collection of HONO in the CWEDD at the air flow rate of 1 L min^{-1}. The detection limit of nitrous acid of 15 ppt (v/v) is the same for all tested liquids. Small positive interference of nitrogen dioxide and peroxyacetylnitrate has been found. The lowest interference of NO_2 was found for 1×10^{-4} M $NaHCO_3$ (pH 6.4; 0.18%) while for deionized water interference of NO_2 (0.28%) was slightly higher. The lowest interference of peroxyacetylnitrate was found for deionized water (1.46%). No enhanced formation of HONO inside the cylindrical wet effluent diffusion denuder was observed for simultaneous bringing of nitrogen dioxide together with phenol, *p*-cresol, guaiacol, catechol, *o*-nitrophenol as well as with *n*-octane, *n*-nonane, *n*-decane, isoprene, α-pinene, β-pinene, camphene, 3-carene, α-phellandrene, *S*-limonene, benzene, toluene or *o*-xylene in comparison with formation of HONO only in the presence NO_2.

Deionized water was chosen as the optimum absorption liquid for the sampling of atmospheric nitrous acid at the CWEDD as well as for FIA chemiluminescent detection. The time resolution is 70 s and the response time is 164 s. The calibration curve is linear over 4 orders of magnitude (0.045–450 ppb HONO). The CWEDD–FIA technique has been applied to the measurement of nitrous acid in urban air.

1. Introduction

Nitrous acid (HONO) plays an important role in atmospheric chemistry due to its photolysis at sunrise to form hydroxyl radicals [1,2]. In the morning, when OH production rate from other sources is low, HONO is thus a major source of OH radicals in the troposphere. Consequently, nitrous acid is regarded as one of the main initiators of photochemical smog production mechanism in the urban atmosphere. Nitrous acid as a significant indoor pollutant [3,4] can produce carcinogenic nitrosoamines [5,6] via the reaction with amines. In addition, it takes part in an acidification of the environment [7] and the production of tropospheric ozone [8].

In spite of the importance, the formation mechanisms of nitrous acid, especially in daytime, are still not completely understood. Nitrous acid is emitted as a primary pollutant from various combustion processes, mainly traffic [3,4,9–11]. Secondary formation of nitrous acid involves a gas phase reaction of NO and OH radical [12,13] or a heterogeneous conversion of NO_2 either on the aerosol [14–16] or the ground [17–20] surfaces. Recently, photochemical sources of HONO have been identified [21], including a photolysis of nitrate and nitric acid deposited on the ground and vegetation surfaces [22,23], reduction of NO_2 on photosensitized organic surfaces like humic acids [24] and photolysis of *o*-nitrophenol and its methylated analogues [25]. In addition, reaction of excited NO_2^* with water vapour yielding OH and HONO has been newly reported [26].

The increasing interest paid to nitrous acid has led to the development of various methods for its determination in air [27]. Fast and sensitive measurement of HONO provides tunable diode laser

* Corresponding author. Tel.: +420 532290167; fax: +420 541212113.
E-mail address: mikuska@iach.cz (P. Mikuška).

0039-9140/$ – see front matter © 2008 Elsevier B.V. All rights reserved.
doi:10.1016/j.talanta.2008.07.008

absorption spectroscopy [28], nevertheless, its sensitivity is not sufficient for detection of trace concentration of HONO. Other spectroscopic methods such as long-path differential optical absorption spectroscopy [29,30] and photo-fragmentation/laser-induced fluorescence [31,32] allow specific and sensitive detection of HONO in air but complex and expensive instrumentation limits widespread use of these methods for routine applications. Solid sorbent-coated diffusion denuders on the other hand offer a cheap field application, however, discontinuous sampling of HONO on carbonate sorbent [19,33–37] provides information only about integrated HONO concentration during sampling period. Wet chemical methods collect continuously HONO in glass coils [20,30,38–43] or wet diffusion denuders [44–53] into various absorption liquids and collected HONO is on-line detected in the coil concentrate by ion chromatography [38], HPLC – spectrophotometry after derivatization with sulfanilamide and *N*-(1-naphthyl)ethylenediamine [39,40] or with 2,4-dinitrophenylhydrazine [41]. Alternatively, an azo dye is detected using a long path absorption detection (LOPAP) [20,30,42]. Finally, nitrite could be determined by a chemiluminescent NO_x analyzer after its reduction to NO [43]. HONO in the denuder concentrate is on-line detected by spectrophotometry [44,45], fluorimetry [46] or ion chromatography [47–53]. Nevertheless, despite of on-line detection, these methods offer mostly relatively low time resolution resulting from their low sensitivity. Consequently, a pre-concentration of nitrite in the coil or the denuder concentrate is required, which together with separation step at HPLC or IC limit application of chromatographic methods for monitoring fast variations in ambient HONO concentration. Moreover, sampling of HONO in the coil suffers from interferences of particulate nitrites due to aerosol particle collection in the coil absorption liquid.

The proposed method allows fast and sensitive determination of atmospheric HONO by coupling the continuous sampling of HONO in the cylindrical wet effluent diffusion denuder (CWEDD) with on-line chemiluminescent (CL) FIA detection of nitrite in the denuder concentrate. Due to high sensitivity of the CL detection, no pre-concentration of nitrite is required providing thus HONO determination in air with high time resolution.

2. Experimental

The cylindrical wet effluent diffusion denuder and the flow-injection analysis system are two main parts of the measuring apparatus. A detailed illustration of individual parts is given in Fig. 1.

2.1. Wet effluent diffusion denuder

The cylindrical wet effluent diffusion denuder consisting of a glass denuder tube (50 cm length × 1.1 cm i.d.) and untreated inlet and outlet glass tubes, assembled together with two polycarbonate fittings [45], is used for the collection of HONO from ambient air. The tubes are sealed by Viton O-rings to avoid leakage. The inlet tube (length 11 cm, i.d. 1.1 cm) adjusts the laminar flow of sampled air through the denuder. The absorption liquid (AL) is pumped ($400\,\mu L\,min^{-1}$) by a peristaltic pump (PP_1) into a vertically oriented denuder tube through a porous PTFE O-ring located between the outlet tube and the wetted part of the CWEDD. The liquid is distributed by the PTFE O-ring over top of the inner wall of the denuder tube and flows continuously down under the influence of gravity. A specially treated inner surface of the denuder tube ensures even wettability of inner denuder wall over several months [45]. Analyzed air ($1\,L\,min^{-1}$) is sucked counter-currently through the denuder by means of a membrane pump (MP). The denuder concentrate, i.e., the absorption liquid with collected HONO, is aspirated at the bottom of the denuder tube through the second porous PTFE O-ring using the peristaltic pump (PP_2) at the flow rate of $600\,\mu L\,min^{-1}$ into a glass–PTFE debubbler (DB) with an inner volume of 200 μL. Depending on the position of the electrically actuated four-way solenoid (S), the effluent passes directly into the FIA system to be analyzed or is wasted when the calibration of the FIA system is performed. The denuder tube is thermoelectrically thermostated to a constant temperature of 20 ± 0.2 °C by means of Peltier devices. The whole denuder is closed in an aluminium box to protect the glass tubes from breaking and sunlight.

2.2. FIA system

A detailed design of the FIA system has been described elsewhere [54], therefore only a brief description is given here (Fig. 1). Instead of high-pressure syringe pumps that are recommended in a previous paper [54] peristaltic pumps (PP; Ismatec, type ISM 852 and ISM 597A, Switzerland) are used for transportation of the sample, the reagent solutions as well as carrier stream. Ismatec pumps in combination with flow RC regulation (resistor-capacity couple) that act as effective pulse dampers provide stable, pulse-free flow that is necessary for the sensitive detection of nitrous acid. 50 μL of sample (CWEDD "concentrate" or standard solution) is injected by means of a pneumatic six-way injection valve (V; type C6WP, Rheodyne, USA) into the carrier stream (deionized water; CA; flow rate of $100\,\mu L\,min^{-1}$) which is merged at a tee (T) with hydrogen peroxide reagent (HP; 4 mM H_2O_2, 0.3 M sulfuric acid, 1 mM EDTA; the flow rate of $30\,\mu L\,min^{-1}$). Nitrous acid is oxidized into peroxynitrous acid when it moves through a reaction coil (RC; PTFE, 0.5 mm i.d. × 30 cm length). Peroxynitrous acid reacts with a chemiluminescent reagent (CL; 2 mM luminol, 0.6 M KOH, 3 mM EDTA; the flow rate of $130\,\mu L\,min^{-1}$) in front of photomultiplier tube (PMT) and the chemiluminescent light emitted as a result of luminol oxidation by peroxynitrite is detected and evaluated using a computer (PC).

2.3. Reagents

All reagents with the exception of luminol (pure, Serva, Heidelberg, Germany) were of analytical reagent grade (Aldrich or Lachema Brno). Deionized water was used for the preparation of the solutions.

A gaseous nitrous acid was continuously generated ($0.052\,\mu g\,min^{-1}$) at a flow generation system [55] based on the reaction of sodium nitrite solution (5×10^{-5} M) with diluted sulfuric acid (0.05 M) at temperature 20 ± 0.5 °C. The reagent solutions were continuously pumped into a reaction vessel at the flow rates of $205\,\mu L\,min^{-1}$ and after the reaction they were sucked out. Pure air ($1.1\,L\,min^{-1}$) was passed through the reagent mixture in the HONO generator to carry formed HONO away.

Gaseous standard of nitrogen dioxide was prepared by diluting of nitrogen dioxide from a gravimetrically calibrated gas permeation device (an emission rate of $0.278\,\mu g\,NO_2\,min^{-1}$) with nitrogen. The sources of ammonia ($0.34\,\mu g\,NH_3\,min^{-1}$), nitric acid ($0.038\,\mu g\,HNO_3\,min^{-1}$) and sulfur dioxide ($8.67\,\mu g\,SO_2\,min^{-1}$) were based on the diffusion of ammonia, HNO_3 or SO_2 from the solution through the wall of microporous membrane tube (Gore-Tex TA 001, 1 mm i.d., 0.4 mm wall, 2 μm mean pore size, length 5 cm) immersed into 1×10^{-4} M $(NH_4)_2SO_4$ alkalized by KOH (for NH_3), mixture of concentrated H_2SO_4 and concentrated HNO_3 in ratio 3:1 (for HNO_3) or 5×10^{-5} M $NaHSO_3$ acidified by H_2SO_4 (for SO_2) in a 250-ml flask into clean air stream ($25\,mL\,min^{-1}$) passing through the microporous tube. Peroxyacetylnitrate was generated from a capillary diffusion system containing PAN dissolved in a *n*-tridecane solvent ($0.031\,\mu g\,min^{-1}$) [56]. Vapours of volatile organic compounds (*n*-octane ($4.66\,\mu g\,min^{-1}$),

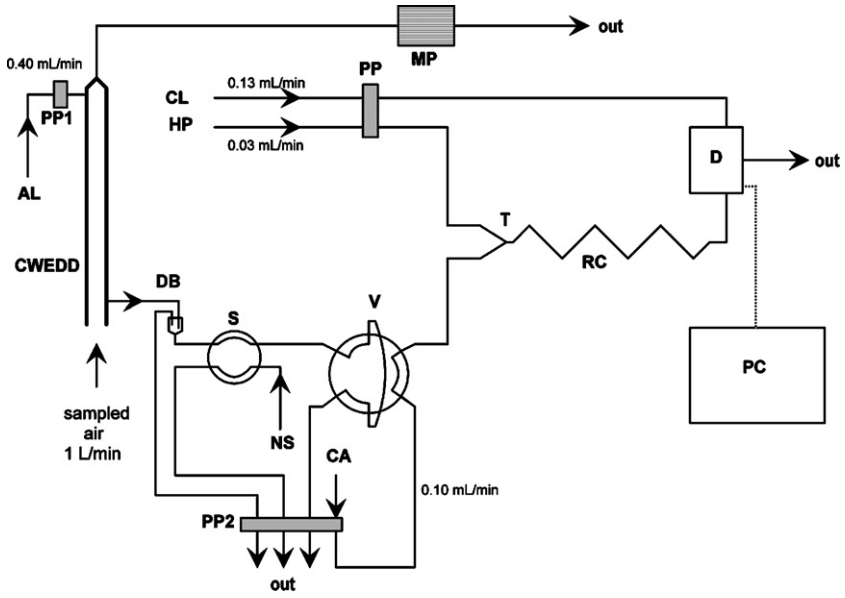

Fig. 1. Scheme of measuring apparatus. CWEDD, cylindrical wet effluent diffusion denuder; PC, computer; DB, glass–Teflon debubbler; PP, PP_1, PP_2, peristaltic pumps; MP, membrane pump; S, four-way solenoid; V, six-way injection valve; D, detector; RC, reaction coil; T, tee-piece; CA, deionized water; AL, absorption liquid; HP, hydrogen peroxide reagent; CL, chemiluminescent reagent; NS, nitrite standard solution.

n-nonane (6.30 μg min^{-1}), *n*-decane (1.73 μg min^{-1}), isoprene (2.78 μg min^{-1}), α-pinene (7.81 μg min^{-1}), β-pinene (6.68 μg min^{-1}), camphene (4.46 μg min^{-1}), 3-carene (7.79 μg min^{-1}), α-fellandrene (3.34 μg min^{-1}), *S*-limonene (11.13 μg min^{-1}), benzene (4.15 μg min^{-1}), toluene (3.39 μg min^{-1}) and *o*-xylene (4.76 μg min^{-1})) were produced at a diffusion-based system by forcing a dry nitrogen stream through a thermostated glass vessel containing miniature glass test-tubes (length 32 mm, i.d. 4 mm, o.d. 6 mm) filled with the individual compound of interest. Gaseous *p*-cresol (0.38 μg min^{-1}), phenol (1.8 μg min^{-1}), guaiacol (0.41 μg min^{-1}), catechol (1.5 μg min^{-1}) and *o*-nitrophenol (0.98 μg min^{-1}) were produced at a thermostated glass tube filled with the compound of interest. Nitrogen stream, transported vapours of studied compounds to the denuder, was passed continuously (at the flow rate of 0.5 ml min^{-1}) through the glass tube maintained at temperature 2 or 30 °C (catechol), respectively.

The production of sulfur dioxide was determined by thiosulfate-iodide method after collection of SO_2 in the impinger with I_2 solution. The nitric acid source was calibrated by sampling of HNO_3 in the dilute KOH solution with subsequent titration of unreacted KOH. The ammonia source was calibrated by sampling of NH_3 in $NaHSO_4$ solution and collected NH_3 after derivatization with *o*-phthaldialdehyde was determined fluorimetrically. Peroxyacetylnitrate was sampled at the dilute KOH solution and formed nitrite after neutralization was detected with the FIA system [54]. The production of volatile compounds (monoterpenes, isoprene, *n*-alkanes, BTX) was measured gravimetrically by means of an analytical microbalance (Sartorius M5P model) from the weight loss of the diffusion tube with a compound of interest. The production of *p*-cresol, phenol, guaiacol, catechol and *o*-nitrophenol was measured by LC-MS detection after their collection in methanol.

3. Results and discussion

A combination of the CWEDD and the chemiluminescent FIA method has been chosen for the semi-continuous measurement of HONO in air. The CWEDD applied recently for the sampling of various water soluble gaseous pollutants like SO_2, HNO_3, HONO, HCl, NH_3 and HCHO allows selective sampling of nitrous acid without interference of particulate nitrite. The FIA system developed originally for the nitrite determination in water [54] has not been so far used for the determination of HONO in air. The whole system (CWEDD–FIA) is necessary to optimise to obtain both the maximal collection efficiency of HONO in the CWEDD and the highest sensitivity of the CL detection of HONO in the denuder concentrate as well as the fast response to quick changes in concentration of HONO in air and to minimize the effect of potentially interfering gaseous compounds.

To collect HONO in wet diffusion denuders, deionized water is mostly employed [44–46,49,50], however, a few other liquids like $NaHCO_3$ [38,52], Na_2CO_3 [38,43,47,48], phosphate buffer [39–41] or the high acidic sulfanilamid [42] were used recently for the collection of HONO in wet denuders or coil samplers. To find the best absorption liquid for our system, we compared in detail all these liquids (with exception of sulfanilamid) with respect to the collection efficiency of HONO, the sensitivity and the selectivity of HONO detection in the CWEDD. To our knowledge, such detailed comparison was not performed before.

3.1. FIA system

The original FIA system [54] provides fast and selective detection of nitrite in water with a detection limit of 1×10^{-9} M. The sensitivity of the presented FIA setup (Fig. 1) is a little bit cut-down due to used peristaltic pumps. In spite of this, the sensitivity is still sufficient (1.5×10^{-9} M) to allow the direct detection of nitrous acid in aqueous concentrate leaving the CWEDD without a need of pre-concentration of nitrous acid in the denuder concentrate as it is required, for example, at ion chromatography. Aqueous solutions of Na_2CO_3 (1×10^{-2}, 1×10^{-3}, 1×10^{-4}, 1×10^{-5} M), $NaHCO_3$ (1×10^{-2}, 1×10^{-3}, 1×10^{-4}, 1×10^{-5} M) and sodium phosphate solutions (1×10^{-4} M, pH 6–8) tested as alternative absorption liquids of HONO in the CWEDD were studied if they influence the nitrite detection at the FIA system. We found out that these solutions, with exception of 1×10^{-2} M Na_2CO_3, have no effect on the sensitivity of nitrite detection at the FIA system and the detection limit of nitrite with these liquids is the same as for deionized

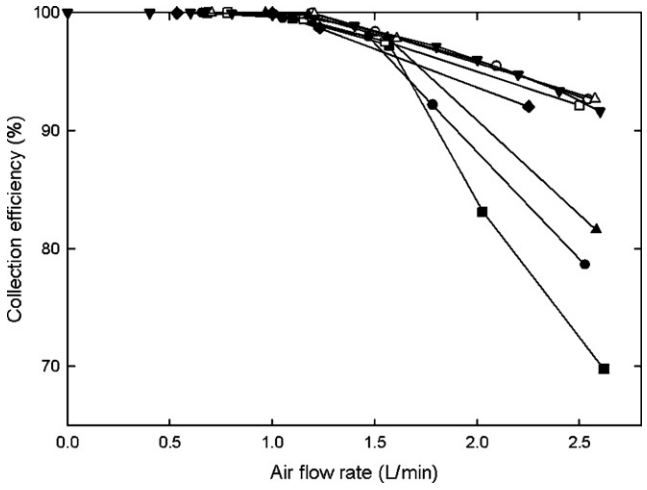

Fig. 2. The dependence of collection efficiencies of HONO on the air flow rate for various absorption liquids. (■) 1×10^{-5} M Na_2CO_3; (□) 1×10^{-2} M Na_2CO_3; (●) 1×10^{-5} M $NaHCO_3$; (○) 1×10^{-2} M $NaHCO_3$; (▲) 1×10^{-4} M NaH_2PO_4 (pH 6); (△) 1×10^{-4} M NaH_2PO_4 (pH 8); (♦) deionized water; (▼) theoretical curve. Flow rate of all absorption liquids is 400 μL min^{-1}. Nitrous acid concentration 5.3 ppb (v/v).

water. 1×10^{-2} M sodium carbonate reduces the sensitivity by 10% in comparison with that for deionized water.

The analysis time of the FIA system (time from sample injection to peak maximum) depends on the carrier flow rate (Fig. 1). At the carrier flow rate of 100 μL min^{-1}, the analysis time of the FIA system is 70 s. Using higher carrier flow rate of 200 μL min^{-1}, the analysis time decreases to 30 s, which allows analysis up to 120 samples per hour. However, simultaneously with higher carrier flow rate, the sensitivity of nitrite determination goes slightly down too. Nevertheless, a sampling period of two minutes has been applied during most field measurements.

3.2. Performance of the CWEDD

The efficiency of HONO collection in the CWEDD was investigated by sampling gaseous standard of HONO. In contrast to highly soluble gases for which, under a constant temperature, the flow rate of air streaming through the diffusion denuder is the only factor affecting their collection efficiency in water [57-60], the collection efficiency of nitrous acid in aqueous solutions also depends on the effective Henry's law constant [52] that takes into account dissociation and/or acido-basic reactions of nitrous acid within the absorbing process [52]. That is reason why we measured the collection efficiency (CE) of HONO in the CWEDD as a function of air flow rate (at the range 0.5–2.5 L min^{-1}) for selected absorption liquids in wide concentration and pH range (Fig. 2). For lucidity, the results are shown only for deionized water and for the absorption solutions with the lowest and the highest concentration of sodium carbonate or sodium bicarbonate and for sodium phosphate with the lowest and the highest pH value. The collection efficiencies of other tested absorption solutions lie among the CEs of solutions with these boundary concentrations or pH levels. For the comparison, the curve describing the theoretical CE of HONO calculated according to Gormley–Kennedy equation [59] is also demonstrated (D_{HONO} = 0.1749 cm^2/s). It is evident that for the air flow rates equal or smaller than 1.0 L min^{-1}, the collection efficiency of HONO in the CWEDD does not depend on the composition of the absorption solution and for all studied absorption liquids (deionized water, 1×10^{-2}, 1×10^{-3}, 1×10^{-4} and 1×10^{-5} M Na_2CO_3, 1×10^{-2}, 1×10^{-3}, 1×10^{-4} and 1×10^{-5} M $NaHCO_3$, 1×10^{-4} M sodium phosphate solution at pH 6, 7 and 8) the collection efficiency of HONO is 100%. For the air flow rates higher than 1.0 L min^{-1}, the CE of HONO decreases with increasing air flow rate depending significantly on the composition of absorption liquid. In general, the collection efficiency of HONO increases with increasing pH of absorption solution, i.e., with increasing concentration of carbonate or bicarbonate or with increasing pH in the case of phosphate. In further work, to attain the quantitative collection of nitrous acid, the flow rate of air through the CWEDD of 1 L min^{-1} is chosen for the sampling of HONO in the CWEDD.

In heavily polluted areas, the collection efficiency of HONO in the CWEDD may be affected due to change in the pH of absorption solution resulting from the collection of acid gases like HNO_3 and SO_2, for example, that are co-present with HONO at the sampled air. To verify this possibility, we measured the collection efficiencies of HONO also in the presence of sulfur dioxide and nitric acid. The difference between collection efficiencies of HONO in the presence SO_2 (the concentration range 1.3–6.6 ppm (v/v)) and in the absence of SO_2 does not exceed 2% for all absorption liquids (up to the air flow rate of 2 L min^{-1}) and the effect of SO_2 on the efficiency of HONO collection in the CWEDD can thus be neglected. The collection efficiency of HONO in the co-presence of HNO_3 (14.8 ppb (v/v)) was investigated only for deionized water. In spite of decrease in pH of deionized water down to 5.8, the collection efficiency of HONO in the presence of HNO_3 did not change and at the air flow rate of 1 L min^{-1} HONO was quantitatively collected.

3.3. Interference

HONO determination via chemical instruments was reported to suffer from several interferences caused by, e.g. $NO_2 + SO_2$ or PAN [61–63]. Recent studies observed for example HONO formation on aqueous or humid surfaces in the reaction of NO_2 with semi-volatile hydrocarbons emitted from a diesel engine [11] or biomass burning [62].

The effect of various compounds concurrently presented in air on the determination of HONO was investigated (the air flow rate of 1 L min^{-1}). The effect of ammonia (484 ppb (v/v)), nitric acid (14.8 ppb (v/v)) and especially, the effect of nitrogen dioxide (76 ppb (v/v)), PAN (6.3 ppb (v/v)) and a mixture of nitrogen dioxide and sulfur dioxide (3.3 ppm (v/v)) for all absorption liquids were tested.

Ammonia does not interfere even at very high concentration that many times exceeds common ambient concentrations. Nitrate obtained after nitric acid collection in the CWEDD also has no effect on nitrous acid chemiluminescent detection via used detection system [54].

The presence of NO_2, PAN and the mixture of NO_2/SO_2 influence the HONO determination more significantly (Fig. 3) because their collection in the denuder absorption liquids results in positive interference due to formation of nitrous acid. For deionized water, interference (a ratio of signals for equivalent concentrations of HONO and interfering compound) of NO_2 of 0.28% was found. For other liquids, the positive interference of NO_2 ranged from 0.57% for 1×10^{-5} M to 5.66% for 0.01 M carbonate solution, from 0.36% for 1×10^{-5} M to 1.17% for 0.01 M bicarbonate solution and from 0.62% for phosphate solution at pH 6 to 0.79% for solution at pH 8. In the presence of SO_2 at ppm levels a higher interference of NO_2 was observed: 2.54–9.10% for carbonate solutions, 1.27–3.46% for bicarbonate solutions, 0.75–2.58% for phosphate solutions and 1.54% for deionized water. These results confirm a formation of secondary nitrite in the denuder concentrate as a result of decay of a relatively stable intermediate $[NO_2–SO_3]^{2-}$ formed in aqueous phase during the reaction of NO_2 with water in the presence of SO_2 [61]. However, low concentration of SO_2 (41 ppb (v/v)) did not increase the interference of NO_2, therefore the effect of SO_2 at current concentrations on NO_2 interference during the HONO determination can

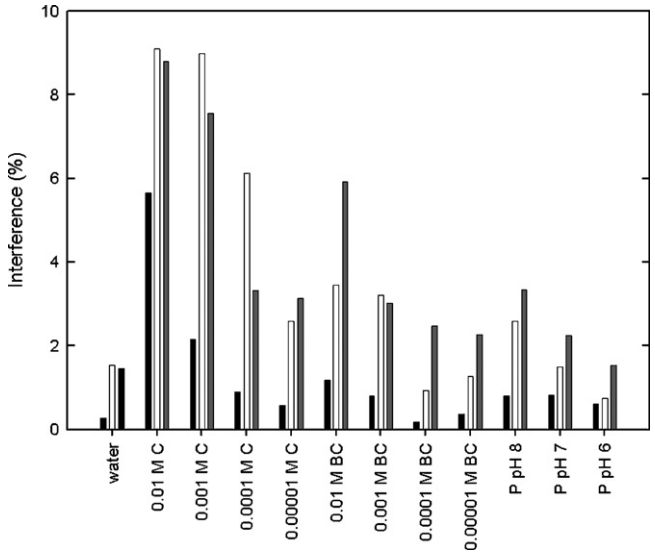

Fig. 3. Interferences of NO_2, PAN and the mixture of NO_2 and SO_2 at nitrous acid determination for all tested absorption liquids. C, carbonate; BC, bicarbonate; P, phosphate; black filled bar, NO_2 interference; white filled bar, interference of NO_2 and SO_2 mixture; grey filled bar, PAN interference.

thus be neglected. Interference of PAN for deionized water is 1.46% while for other tested liquids it ranges from 3.14% for 1×10^{-5} M to 8.80% for 0.01 M carbonate solution, from 2.28% for 1×10^{-5} M to 5.92% for 0.01 M bicarbonate solution and from 1.54% for phosphate solution at pH 6 to 3.34% for solution at pH 8.

From obtained results it is evident that interferences of NO_2, PAN and the mixture of NO_2/SO_2 are dependent on the pH of absorption liquid. With increasing pH of absorption solution (i.e., with increase in pH of phosphate or with increase in concentration of carbonate or bicarbonate) increases efficiency of collection of interfering pollutants like NO_2 or PAN at these solutions resulting in increasing interferences of these gases at the HONO determination. The lowest interference of NO_2 was observed for the 1×10^{-4} M $NaHCO_3$ (pH 6.4; 0.18%) whereas the interference for deionized water was only slightly increased (0.28%) against those for 1×10^{-4} M $NaHCO_3$ and the values of NO_2 interference for other absorption liquids are mostly higher in comparison with those for deionized water. The lowest interference of PAN was found for the deionized water (1.46%) while for other absorption liquids the interference of PAN at the nitrous acid determination increases. In field application, to obtain correct level of the interference of nitrogen dioxide on HONO detection, the concentration of nitrogen dioxide is measured in parallel [64,65] and the concentration of nitrous acid in ambient air is PC retroactively corrected for the presence of NO_2.

Interference of NO_2 in the presented method is comparable with interferences reported for other techniques ranging from 0.01 to 0.4% [39,42–45,50–52]. The interference of PAN found in the proposed method for deionized water (1.46%) is also comparable with the PAN values for other scrubbing solutions (0.015–1.9% [39,42,43,46,50]).

Finally, we studied in detail interference of various organic compounds known as important constituents of biomass burning or diesel exhaust. Moreover, we also tested effect of other organic compounds present in ambient air like monoterpenes and isoprene on the detection of HONO. In addition, we investigated effect of *o*-nitrophenol that was mentioned recently as a potential interfering compound during the HONO detection. Effect of volatile (monoterpenes, isoprene, BTX, *n*-alkanes) and semivolatile (phenol, *p*-cresol, guaiacol, catechol, *o*-nitrophenol) organic compounds on the determination of HONO was examined only for deionized water used as the absorption liquid. We brought these compounds simultaneously with NO_2 to the denuder, however, no production of HONO was observed for *n*-octane (1 ppm (v/v)), *n*-nonane (1.2 ppm (v/v)), *n*-decane (298 ppb (v/v)), isoprene (1 ppm (v/v)), α-pinene (1.4 ppm (v/v)), β-pinene (1.2 ppm (v/v)), camphene (800 ppb (v/v)), 3-carene (1.4 ppm (v/v)), α-phellandrene (600 ppb (v/v)), S-limonene (2 ppm (v/v)), benzene (1.3 ppm (v/v)), toluene (900 ppb (v/v)), *o*-xylene (1.1 ppm (v/v), phenol (7–28 ppb (v/v)), *p*-cresol (11–59 ppb (v/v)), guaiacol (6–16 ppb (v/v)), catechol (9–18 ppb (v/v)) and *o*-nitrophenol (7–14 ppb (v/v)). These results did not prove thus the findings of recent studies where biomass burning (e.g., catechol, guaiacol) or diesel exhaust components (phenol) were reported to enhance the uptake of NO_2 in water solutions resulting in production of HONO [11,62]. The different results may be explained by much smaller residence time (2.85 s) of air in the used denuder system in comparison with residence time (125 s) of sample in denuder system applied in the recent studies [11,62]. Moreover, contrary to the recent study [62], where studied organic compounds were dissolved directly in liquid phase flowing through the denuder, in our study organic compounds were present in gas phase. These facts result in non-measurable conversion of NO_2 to HONO in the co-presence of these compounds inside the applied cylindrical wet effluent diffusion denuder.

3.4. Analytical parameters

High sensitivity of employed CL–FIA technique enables the direct determination of collected HONO at the CWEDD concentrate without need of nitrite pre-concentration. The calibration curve is linear at the measured range of HONO concentrations 0.045–450 ppb (v/v). The detection limit (a signal-to-noise ratio of 3) of nitrous acid at the CWEDD–FIA system is 15 ppt (v/v) regardless if deionized water or sodium carbonate, sodium bicarbonate or sodium phosphate solutions are used as the absorption liquid. The detection limit of the present method is higher than those reported by other methods employing glass coils [39,41,42] or wet diffusion denuders [44,46,47,49–51]. In our opinion, the sensitivity of the presented method at described configuration is fully sufficient to measure nitrous acid concentration in ambient air.

As a compromise of results obtained for all studied liquids concerning the sensitivity and the selectivity of HONO detection and from the practical point of view when the constitution absorption liquid as simple as possible is preferred, for other measurements deionized water is chosen as the optimum liquid for the collection of nitrous acid at the CWEDD.

Small inner volume of used CWEDD (47.5 cm^3) enables short residence time of 2.85 s of analyzed air in the CWEDD (at the air flow rate of 1 L min^{-1}) as well as short residence time of absorption liquid of 74 s (at the liquid flow rate of 400 μL min^{-1}). The response time of the whole system (i.e., time between enter of HONO into the CWEDD and obtaining a 95% of steady state signal in the detector) then depends on the analysis time of the FIA method and on the denuder concentrate flow rate (Fig. 1). The FIA analysis time depends on the carrier flow rate. Consequently, at the carrier flow rate of 100 μL min^{-1} the response time is 164 or 122 s for the carrier flow rate of 200 μL min^{-1}, respectively. It is obvious that with increasing carrier flow rate the response time of the system decreases; however, simultaneously sensitivity of nitrite determination goes down too. In further experiments, the carrier flow rate of 100 μL min^{-1} at the FIA is employed because the response time of 2.7 min is quite satisfactory for most field applications where high sensitivity rather than high response time is mostly preferred. Time resolution (i.e., time between maxima of two following peaks in the detector) is other important parameter to characterize the system performance. The shortest accessible

time resolution of the presented method is 30 s (at the carrier flow rate of 200 μL min^{-1}), or alternatively, 70 s (at the carrier flow rate of 100 μL min^{-1}) compared with 10–20 min time interval at IC and other chromatographic methods [39–41,47–53].

The reproducibility of the method was determined by long-term sampling of HONO standard (1.2 ppb (v/v)). The relative standard deviation (n = 50) is ± 4.1%.

During the field application, the evaporation of water within the CWEDD can induce losses of absorption liquid between 3 and 10 μL min^{-1}, respectively, when the relative humidity of sampled air varies between 45% and 85%. Under the above mentioned flow rate conditions (at temperature of 20 °C), the change in liquid volume due to evaporation losses causes a +2.5% error in the total flow rate of absorption liquid and hence the calculated gas-phase HONO concentration. In practice, the error in water loss because of evaporation is reduced as a result of a drop in temperature (5–7 °C) inside the cylindrical wet effluent diffusion denuder.

3.5. Real air analysis

The developed CWEDD–FIA method has been applied to the measurement of HONO in ambient air in Brno city during summer of 2006. The sampling site was located at the balcony at the first floor of the Institute of Analytical Chemistry, about 5 m above ground level and at a distance of about 20 m from a main road with relatively heavy traffic. The denuder was installed on the balcony and the analyzed air was sampled into the denuder through a short PTFE tube of 4 cm long that is shielded from light with black self-shrinkable tubing to avoid heterogeneous and photochemical formation of HONO inside the sampling tube. In parallel, nitrogen dioxide has been also measured with the monitor based on the chemiluminescent reaction of NO_2 with a luminol reagent dispersed in an aerosol stream [64,65]. Time resolution of NO_2 detection was 1 s. The reliability of the CWEDD–FIA setup was controlled once per day using the standard solutions of sodium nitrite (1×10^{-7} and 2×10^{-7} M) corresponding to nitrous acid concentration of 0.98 and 1.96 ppb (v/v).

A several day overview of nitrous acid concentration as well as nitrogen dioxide concentration in ambient air in Brno is shown in Fig. 4. During the depicted measurement period the weather was sunny with global radiation intensity between 980 and 1050 W/m^2 at noon. HONO was measured with time resolution of 3 min. Gaps in the data are caused by the calibration of the FIA system. The data show a diurnal pattern with high concentration of nitrous acid during night with maxima up to 1.1 ppb (v/v) around midnight (21:10–1:57), which is in agreement with a common conception of HONO behaviour in troposphere [1,2]. Comparison of temporal profiles for HONO and NO_2 concentrations reveals that over night there is a time shift between HONO maximum and corresponding NO_2 maximum. Maxima in HONO concentration in night on 9/10, 10/11 and 11/12 September were about 80 min delayed against corresponding NO_2 maxima while in night during 12/13 and 13/14 September the delay was about 270 min and during night on 14/15 September the concentrations both HONO and NO_2 were nearly constant without any sharp maxima. The observed temporal shift between HONO and NO_2 concentrations confirms the heterogeneous production of nitrous acid during night period. Except of night maxima we recorded high concentrations of nitrous acid occurring periodically in the morning mostly around 8 p.m. (alternatively, at midday on 9 September). Despite HONO photolysis by sunlight the daytime concentrations of HONO were often higher than night concentrations. Contrary to night shifts, peaks in daytime concentration of HNO and NO_2 were time coincident. Because the sampling site was close to the street with a heavy traffic, we assume that the morning maxima are caused by direct emission of nitrous acid from cars during morning rush transport periods. Over the rest of day HONO concentration remained mostly low in the range from 200 to 400 ppt (v/v) as a result of HONO photolysis. Our observations of high daytime concentrations of nitrous acid are in agreement with recent studies [44–46,48,49,52,53] when unexpectedly high HONO concentrations have been observed during the day too.

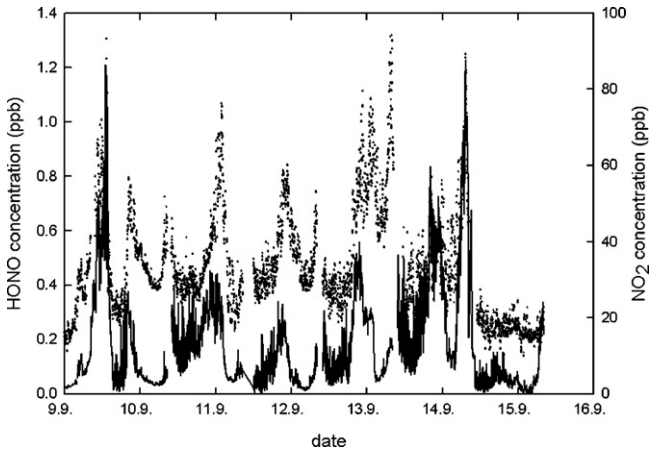

Fig. 4. Diurnal patterns of nitrous acid and nitrogen dioxide concentration (Brno, September 9–15, 2006). (●) HONO; (—) NO_2.

4. Conclusion

The proposed method combines unique advantages both the diffusion denuder and the CL detection of nitrous acid. The CWEDD enables sampling of gaseous HONO while aerosol particles pass through the denuder without collection. The detection limit (a signal-to-noise ratio of 3) of nitrous acid at the CWEDD–FIA system is 15 ppt (v/v). High sensitivity of employed CL–FIA technique enables the direct determination of collected HONO at the CWEDD concentrate without need of nitrite pre-concentration. The calibration curve is linear at the range of 0.045–450 ppb (v/v) HONO.

Deionized water was chosen as the optimum absorption medium for the sampling of nitrous acid in the CWEDD from point of view both the collection efficiency of HONO and the selectivity and the sensitivity of HONO detection.

High selectivity, high sensitivity, short response time of the system and high time resolution offer employment of the method for the routine widespread application as an alternative to current wet denuder methods. Ambient measurements showed the capability of the system for the continuous long-term monitoring of atmospheric nitrous acid in the frame of pollution control of ambient air. Moreover, due to high time resolution, the proposed method is suitable for the recording of very fast processes such as various kinetic studies or gradient measurements.

Acknowledgements

This work was supported by an Institutional research plan of the Institute of Analytical Chemistry of the Academy of Sciences of the Czech Republic No. AV0 Z40310501 and by the grant No. SP/1b7/189/07 from Ministry of the Environment of the Czech Republic.

References

[1] B.J. Finlayson-Pitts, J.N. Pitts Jr., Chemistry of the Upper and Lower Atmosphere. Theory, Experiments, and Applications, Academic Press, San Diego, CA, 2000.

[2] B. Alicke, A. Geyer, A. Hofzumahaus, F. Holland, S. Konrad, H.-W. Pätz, J. Schäfer, J. Stutz, A. Volz-Thomas, U. Platt, J. Geophys. Res. 108 (2003) 8247.
[3] Z. Večeřa, P.K. Dasgupta, Int. J. Environ. Anal. Chem. 56 (1994) 311.
[4] C.W. Spicer, D.V. Kenny, I.H. Billick, G.F. Ward, J. Air Waste Manag. Assoc. 43 (1993) 1479.
[5] P.L. Hanst, J.W. Spence, M. Miller, Environ. Sci. Technol. 11 (1977) 403.
[6] D. Grosjean, J. Air Waste Manag. Assoc. 41 (1991) 306.
[7] G.P. Cobb, R.S. Braman, Chemosphere 31 (1995) 2945.
[8] K.C. Clemitshaw, Environ. Chem. 3 (2006) 31.
[9] R. Kurtenbach, K.H. Becker, J.A.G. Gomes, J. Kleffmann, J.C. Lörzer, M. Spittler, P. Wiesen, R. Ackermann, A. Geyer, U. Platt, Atmos. Environ. 35 (2001) 3385.
[10] T.W. Kirchstetter, R.A. Harley, D. Littlejohn, Environ. Sci. Technol. 30 (1996) 2843.
[11] L. Gutzwiller, F. Arens, U. Baltensperger, H.W. Gäggeler, M. Ammann, Environ. Sci. Technol. 36 (2002) 677.
[12] J.G. Calvert, G. Yarwood, A.M. Dunker, Res. Chem. Intermediat. 20 (1994) 463.
[13] G. Lammel, J.N. Cape, Chem. Soc. Rev. 25 (1996) 361.
[14] J. Notholt, J. Hjorth, F. Raes, Atmos. Environ. 26A (1992) 211.
[15] M. Ammann, M. Kalberer, T.D. Jost, L. Tobler, E. Rössler, D. Piquet, H.W. Gäggeler, U. Baltensperger, Nature 395 (1998) 157.
[16] A.R. Reisinger, Atmos. Environ. 34 (2000) 3865.
[17] C. George, R.S. Strekowski, J. Kleffmann, K. Stemmler, M. Ammann, Faraday Discuss. 130 (2005) 195.
[18] J. Stutz, B. Alicke, A. Neftel, J. Geophys. Res. 107 (2002) 8192.
[19] R.M. Harrison, A.-M.N. Kitto, Atmos. Environ. 28 (1994) 1089.
[20] J. Kleffmann, R. Kurtenbach, J. Lörzer, P. Wiesen, N. Kalthoff, B. Vogel, H. Vogel, Atmos. Environ. 37 (2003) 2949.
[21] J. Kleffmann, ChemPhysChem 8 (2007) 1137.
[22] X.L. Zhou, K. Civerolo, H.P. Dai, G. Huang, J. Schwab, K. Demerjian, J. Geophys. Res. 107 (2002) 4590.
[23] K.A. Ramazan, D. Syomin, B.J. Finlayson-Pitts, Phys. Chem. Chem. Phys. 6 (2004) 3836.
[24] K. Stemmler, M. Ammann, C. Donders, J. Kleffmann, C. George, Nature 440 (2006) 195.
[25] I. Bejan, Y. Abd El Aal, I. Barnes, T. Benter, B. Bohn, P. Wiesen, J. Kleffmann, Phys. Chem. Chem. Phys. 8 (2006) 2028.
[26] S. Li, J. Matthews, A. Sinha, Science 309 (2008) 1657.
[27] K.C. Clemitshaw, Crit. Rev. Environ. Sci. Technol. 34 (2004) 1.
[28] Y.Q. Li, J.J. Schwab, K.L. Demerjian, Geophys. Res. Lett. 35 (2008) L04803.
[29] D. Perner, U. Platt, Geophys. Res. Lett. 6 (1979) 917.
[30] J. Kleffmann, J.C. Lörzer, P. Wiesen, C. Kern, S. Trick, R. Volkamer, M. Rodenas, K. Wirtz, Atmos. Environ. 40 (2006) 3640.
[31] M.O. Rodgers, D.D. Davis, Environ. Sci. Technol. 23 (1989) 1106.
[32] W. Liao, A. Hecobian, J. Mastromarino, D. Tan, Atmos. Environ. 40 (2006) 17.
[33] A. Febo, C. Perrino, I. Allegrini, Atmos. Environ. 30 (1996) 3599.
[34] C. Perrino, F. DeSantis, A. Febo, Atmos. Environ. 24A (1990) 617.
[35] M. Ferm, A. Sjödin, Atmos. Environ. 19 (1985) 979.
[36] A. Febo, C. Perrino, M. Cortiello, Atmos. Environ. 27A (1993) 1721.
[37] P. Koutrakis, C. Sioutas, S.T. Ferguson, J.M. Wolfson, J.D. Mulik, R.M. Burton, Environ. Sci. Technol. 27 (1993) 2497.
[38] S.S. Park, S.B. Hong, Y.G. Jung, J.H. Lee, Atmos. Environ. 38 (2004) 293.
[39] G. Huang, X. Zhou, G. Deng, H. Qiao, K. Civerolo, Atmos. Environ. 36 (2002) 2225.
[40] Y. He, X. Zhou, J. Hou, H. Gao, S.B. Bertman, Geophys. Res. Lett. 33 (2006) L02813.
[41] X. Zhou, H. Qiao, G. Deng, K. Civerolo, Environ. Sci. Technol. 33 (1999) 3672.
[42] J. Heland, J. Kleffmann, R. Kurtenbach, P. Wiesen, Environ. Sci. Technol. 35 (2001) 3207.
[43] Y. Kanda, M. Taira, Anal. Chem. 62 (1990) 2084.
[44] Z. Večeřa, P.K. Dasgupta, Environ. Sci. Technol. 25 (1991) 255.
[45] Z. Večeřa, P.K. Dasgupta, Anal. Chem. 63 (1991) 2210.
[46] N. Takenaka, H. Terada, Y. Oro, M. Hiroi, H. Yoshikawa, K. Okitsu, H. Bandow, Analyst 129 (2004) 1130.
[47] M.T. Oms, P.A.C. Jongejan, A.C. Veltkamp, G.P. Wyers, J. Slanina, Int. J. Environ. Anal. Chem. 62 (1996) 207.
[48] Z. Genfa, S. Slanina, C.B. Boring, P.A.C. Jongejan, P.K. Dasgupta, Atmos. Environ. 37 (2003) 1351.
[49] K. Acker, G. Spindler, E. Brüggemann, Atmos. Environ. 38 (2004) 6497.
[50] A. Neftel, A. Blatter, R. Hesterberg, T. Staffelbach, Atmos. Environ. 30 (1996) 3017.
[51] P.K. Simon, P.K. Dasgupta, Environ. Sci. Technol. 29 (1995) 1534.
[52] C. Zellweger, M. Ammann, P. Hofer, U. Baltensperger, Atmos. Environ. 33 (1999) 1131.
[53] M. Takeuchi, J.Z. Li, K.J. Morris, P.K. Dasgupta, Anal. Chem. 76 (2004) 1204.
[54] P. Mikuška, Z. Večeřa, Z. Zdráhal, Anal. Chim. Acta 316 (1995) 261.
[55] M. Taira, Y. Kanda, Anal. Chem. 62 (1990) 630.
[56] J.S. Gaffney, R. Fajer, G.I. Senum, Atmos. Environ. 18 (1984) 215.
[57] Z. Ali, C.L.P. Thomas, J.F. Alder, Analyst 114 (1989) 759.
[58] Z. Zdráhal, P. Mikuška, Z. Večeřa, Chem. Listy 88 (1994) 353.
[59] P.K. Gormley, M. Kennedy, Proc. R. Ir. Acad. 52 (1949) 163.
[60] W. Winiwarter, Atmos. Environ. 23 (1989) 1997.
[61] G. Spindler, J. Hesper, E. Brüggemann, R. Dubois, Th. Müller, H. Herrmann, Atmos. Environ. 37 (2003) 2643.
[62] M. Ammann, E. Rössler, R. Strekowski, C. George, Phys. Chem. Chem. Phys. 7 (2005) 2513.
[63] J. Kleffmann, P. Wiesen, Atmos. Chem. Phys. Discuss. 8 (2008) 3497.
[64] P. Mikuška, Z. Večeřa, Anal. Chem. 64 (1992) 2187.
[65] P. Mikuška, Z. Večeřa, Anal. Chim. Acta 410 (2000) 159.

Talanta 77 (2008) 593–605

Contents lists available at ScienceDirect

Talanta

journal homepage: www.elsevier.com/locate/talanta

Review

Critical review on analytical methods for biodiesel characterization

Marcos Roberto Monteiro[a,*], Alessandra Regina Pepe Ambrozin[a], Luciano Morais Lião[b], Antonio Gilberto Ferreira[c]

[a] *Laboratório de Combustíveis, Centro de Caracterização e Desenvolvimento de Materiais, Departamento de Engenharia de Materiais, Universidade Federal de São Carlos, 13560-971 São Carlos - SP, Brazil*
[b] *Instituto de Química, Universidade Federal de Goiás, Campus Samambaia, 74001-970 Goiânia - GO, Brazil*
[c] *Departamento de Química, Universidade Federal de São Carlos, 13560-905 São Carlos - SP, Brazil*

ARTICLE INFO

Article history:
Received 11 March 2008
Received in revised form 30 June 2008
Accepted 1 July 2008
Available online 9 July 2008

Keywords:
Biodiesel
Fatty mono-alkyl esters
Analytical methods
Spectroscopy
Chromatography

ABSTRACT

Biodiesel is an alternative fuel composed of mono-alkyl esters and obtained mainly from the base-catalyzed transesterification reaction of oils or fats. Its use (pure or blended) does not demand any modification in the diesel engine and in the existing fuel distribution and storage infrastructure. Moreover, biodiesel has a high energetic yield, fixes the solar energy and contains insignificant amounts of sulphur. Therefore, biodiesel is currently the best substitute for fossil diesel fuel.

Besides mono-alkyl esters, glycerol (main co-product), alcohol, catalyst, free fatty acids, tri-, di- and monoglycerides compose the final mixture of biodiesel production process. These and other kinds of contaminants can lead to severe operational and environmental problems. Therefore, the quality control of biodiesel is greatly significant to the success of its commercialization and market acceptance. Some important issues on the biodiesel quality control involve the monitoring of transesterification reaction, the quantification of mono-alkyl esters and free- and bonded glycerol as well as determination of residual catalysts and alcohol. Moreover, the determination of blend levels is another key aspect of biodiesel analyses. Chromatography and spectroscopy are the analytical methods most used for the biodiesel characterization, but procedures based on physical properties are also available.

Previously, a review on analytical methods used to evaluate biodiesel quality was written by Knothe. Due to the importance of this field, we made an update of Knothes' review. Therefore, in this paper, we will describe new developments in biodiesel analyses and some references showed in Knothes' paper. Specially, we will describe analytical methods used for quantification of glycerol, mono-, di-, triglycerides, methanol, water, Na, K, P, and steroids in biodiesel or along the transesterification reaction. Also, the determination of biodiesel content in blends and some physicochemical parameters are discussed. At the end, we will assess the available techniques and point out some improvements on analytical methods for biodiesel characterization.

Contents

* Corresponding author. Tel.: +55 16 3351 8844; fax: +55 16 3351 8850.
E-mail address: monteiro@ccdm.ufscar.br (M.R. Monteiro).

0039-9140/$ – see front matter © 2008 Published by Elsevier B.V.
doi:10.1016/j.talanta.2008.07.001

1. Introduction

The petroleum market instability, limited availability of crude oil, and mainly the serious impact of the use of petroleum-based fuels on the environment have currently stimulated the spread of alternative fuels [1]. Many researches have been held on biodiesel, an alternative fuel for diesel engines that has recently obtained increasing attention worldwide [2]. This fuel is the best substitute for diesel due to its physical properties, which are close to those of fossil diesel. Therefore, its use (neat or blended) does not demand any modification in the diesel engine and in the existing fuel distribution and storage infrastructure [3]. Besides that, biodiesel has a high energetic yield, fixes the solar energy and contains insignificant amounts of sulphur [4]. Nevertheless, cold-flow properties, NO_x emissions, and oxidative stability are issues that have to be overcome. At the moment, the main problem of biodiesel commercialization is its price, which is higher than for fossil diesel [5,6]. Actually, the average price per gallon of diesel in the USA in June 2006 was US $2.98, while the cost of pure biodiesel was US $3.76 [7]. Moreover, it is worth to mention that the economical utilization of glycerine, the main co-product of biodiesel, is also an important aspect for the feasible commercialization of this alternative fuel [8].

According to the Brazilian Biodiesel Programme, biodiesel is defined as "a fuel obtained from mixtures, in different proportions, of fossil diesel and alkyl esters of vegetable oils or animal fats". Thus, biodiesel, under the chemical point of view, is composed mainly by fatty acids mono-alkyl esters. Transesterification is a widespread process used for obtaining biodiesel and involves the catalyzed reaction of triglycerides (major compounds of oils and fats) and short-chain alcohols such as methanol and ethanol. Most transesterification industrial processes employ alkaline catalysis (KOH, NaOH, and $NaOCH_3$) and methanol. The utilization of potassium hydroxide is more suitable since, at the end of reaction, the mixture can be neutralized with phosphoric acid to afford potassium phosphate, which is a fertilizer. In Brazil, the use of ethanol is more advantageous due to its large-scale production. Furthermore, the whole biodiesel manufacture process is independent of petroleum because ethanol is obtained from biomass [8]. The designation of pure biodiesel is B100 (100% fatty acid alkyl esters). However, this fuel could be also used in blends with fossil diesel and the BXX abbreviation will indicate the volume (in percent) of B100 in the mixture. Consequently, B2 is constituted by 2% of B100, and 98% of diesel [4]. In Brazil, B2 will be mandatory in 2008 and B5 in 2013 [9].

As stated before, the transesterification reaction affords fatty esters. However, the final mixture is also composed of glycerol (main co-product), alcohol, catalyst, tri-, di- and monoglycerides [4], as well as free fatty acids. These and other contaminants of biodiesel can lead to severe operational and environmental problems. Therefore, standards that limit the amount of contaminants in biodiesel fuel are necessary. Additionally, the establishment of standards is also required to the description of the product quality [10]. Knothe [11] states that the successful introduction and commercialization of biodiesel has been accompanied by the development of standards to ensure high product quality and user confidence. In fact, EN 14214 and ASTM D 6751 biodiesel standards [12,13] were already established in Europe and USA, respectively. These standards are usually employed as references to establish other standards and their analysis. Therefore, ASTM D 6751 and EN 14214 specifications as well as their analysis methods for biodiesel are illustrated in Table 1. In Brazil, Resolution number 7 (from 19/3/2008) of the National Agency of Petroleum, Natural Gas and Biofuels (ANP) supplies the specification of the pure biodiesel (B100) and the methodologies for its characterization. In fact, the Brazilian analyses are performed in accordance with the standards of the American Society for Testing and Materials (ASTM) and Brazilian Association of Technical Standards (ABNT) [14].

Therefore, the quality control of biodiesel is greatly important to the successful commercialization of this fuel and its blends [6]. In this point, it is worth to note that the type (chain length, degree of unsaturation and presence of other chemical functions) and concentration of fatty esters as well as the structure of the ester moiety derived from the alcohol have an outstanding effect on biodiesel properties, which will also influence its storage and oxidation [4,11]. Besides, biodiesel composition is completely dependent on the source used to produce it [1]. Also, since some contaminants come up from the transesterification reaction, it is important to monitor the status of biodiesel production to recognize and correct problems at an early stage [15]. Fernando et al. [16] describe complete reaction to mono-alkyl esters, the removal of free glycerine, catalysts, alcohol, and free fatty acids in biodiesel as critical issues of the quality control. Moreover, the determination of blend levels is another key point of biodiesel analyses since its use has been increasing considerably [15].

The parameters, which are used to define the quality of biodiesel, can be divided in two groups [10]. One of them is also used for mineral diesel, and the second describes the composition and purity of fatty esters. The former includes, for example, density, viscosity, flash point, sulphur %, Conradson carbon residue, sulphate ash %, cetane number, and acid number. The latter comprises, for example, methanol, free glycerol, total glycerol, phosphorus contents, water and esters content as well as others properties described in Table 1.

Chromatography and spectroscopy are the most used analytical methods on biodiesel analyses, but procedures based on physical properties are also available [6]. Moreover, it is worth to mention that most chromatographic analyses, mainly GC, have been applied to methyl and not to ethyl esters [15].

Previously, a review on analytical methods used for biodiesel analysis was published [15]. It showed the main techniques developed until 2006. Due to the importance of evaluating biodiesel quality, we made an update of biodiesel references described by Knothe [15]. Therefore, in our review, we will describe new techniques as well as methods developed before 2006. Particularly, analytical methods used for quantification of glycerol, mono-, di-, triglycerides, methanol, water, Na, K, P, and steroids in biodiesel or along the transesterification reaction will be described. Also, the determination of biodiesel content in blends and some physicochemical parameters are discussed. At the end, we will assess the available techniques and discuss some improves on analytical methods for biodiesel characterization.

Table 1
Biodiesel specifications according to ASTM D6751, and EN 14214 standards

Property	ASTM D 6751		EN 14214	
	Test method	Limits	Test method	Limits
Ester content	–	–	EN 14103	96.5% (mol mol^{-1}) min
Linolenic acid content	–	–	EN 14103	12.0% (mol mol^{-1}) max
Content of FAME[a] with ≥4 double bonds	–	–	–	1.0% (mol mol^{-1}) max
MAG[b] content	–	–	EN 14105	0.80% (mol mol^{-1}) max
DAG[c] content	–	–	EN 14105	0.20% (mol mol^{-1}l) max
TAG[d] content	–	–	EN 14105	0.20% (mol mol^{-1}) max
Free glycerine	ASTM D 6584	0.020% (w/w) max	EN 14105	0.020% (mol mol^{-1}) max
Total glycerine	ASTM D 6584	0.240% (w/w) max	EN 14105	0.25% (mol mol^{-1}) max
Water and sediment or water content	ASTM D 2709	0.050% (v/v) max	EN ISO 12937	500 mg kg^{-1} max
Methanol content	–	–	EN 14110	0.20% (mol mol^{-1}) max
(Na + K) content	UOP 391	5.0 mg kg^{-1} max	EN 14108	5.0 mg kg^{-1} max
(Ca + Mg) content	–	–	prEN 14538	5.0 mg kg^{-1} max
P content	ASTM D 4951	0.001% (w/w) max	EN 14107	10.0 mg kg^{-1} max
Oxidative stability (110 °C)	–	–	EN 14112	6 h min
Density (15 °C)	–	–	EN ISO 3675	860–900 kg m^{-3}
Kinematic viscosity or viscosity (40 °C)	ASTM D 445	1.9–6.0 mm^2 s^{-1}	EN ISO 3104	3.5–5.0 mm^2 s^{-1}
Flash point	ASTM D 93	130 °C min	EN ISO 3679	120 °C min
Cloud point	ASTM D 2500	Not specified	–	–
Sulphur content	ASTM D 5453	0.05% (w/w) max	EN ISO 20864	10.0 mg kg^{-1} max
Carbon residue	ASTM D 4530	0.050% (w/w) max	EN ISO 10370	0.30% (mol mol^{-1}) max
Cetane number	ASTM D 613	47 min	EN ISO 5165	51 min
Sulphated ash	ASTM D 874	0.020% (w/w) max	ISO 3987	0.02% (mol mol^{-1}) max
Total contamination	–	–	EN 12662	24 mg kg^{-1} max
Copper strip corrosion (3 h, 50 °C)	ASTM D 130	No. 3 max	EN ISO 2160	1 (degree of corrosion)
Acid number or acid value	ASTM D 664	0.50 mg KOH g^{-1} max	EN 14104	0.50 mg KOH g^{-1} max
Iodine value	–	–	EN 14111	120 g I_2·100 g^{-1} max
Distillation temperature (90% recovered)	ASTM D 1160	360 °C max	–	–

[a] FAME = fatty acid methyl esters.
[b] MAG = monoacylglycerols.
[c] DAG = diacylglycerols.
[d] TAG = triacylglycerols.

2. General considerations on biodiesel analysis techniques

Several factors such as composition of feedstock (oil or fat), production process (reaction and purification steps), storage and handling can influence biodiesel fuel quality. The evaluation of biodiesel quality is achieved through the determination of chemical composition and physical properties of the fuel. In fact, some contaminants and other minor components are the major issues in the quality of biodiesel. As stated before, glycerol, mono-, di-, triglycerides, alcohol, catalysts and free fatty acid are compounds that could be present in biodiesel. Moreover, the biodiesel composition could be modified along the storage and handling. For example, biodiesel can absorb water or undergoes oxidation. Therefore, these parameters and their analytical methods are addressed in standards as well as alternative methodologies have been investigated. Additionally, the monitoring of transesterification reaction and the blend level determination are significant aspects on biodiesel analysis.

The most important parameters of biodiesel (fatty mono-alkyl esters, fatty acids, glycerol and their acyl derivatives) are commonly analyzed by gas chromatography (GC) and high-performance liquid chromatography (HPLC). In fact, GC has been the most used technique due to its high accuracy for the quantification of minor components. However, baseline drift, overlapping signals, and aging of standards and samples can destructively affect the GC accuracy. Moreover, GC analyses frequently require sample derivatization, mainly to afford trimethylsilyl derivatives of the hydroxyl groups. Although this procedure improves chromatographic separation, it also increases the analysis time. Flame ionization detection (FID) is the most widespread detector used in GC, but the utilization of mass spectrometer has increased. The latter eliminates any ambiguities about the identification of the eluting materials, but their quantification could be affected.

HPLC analysis is less employed in biodiesel characterization, but the analysis time is shorter than GC one and sample derivatization is not needed. Moreover, this technique can be applied to biodiesel from different feedstock and it is more appropriate for blend analysis than GC. Several detectors for HPLC biodiesel analysis are described, among them evaporative light scattering detection (ELSD) is quite suitable.

Spectroscopic analyses are most employed for monitoring the transesterification reaction and for the determination of blend level. Nuclear magnetic resonance (NMR) spectroscopy and several techniques based on infrared spectroscopy (IR) are commonly applied to these analyses. NMR is an excellent technique, but the instrumentation and maintenance costs are relatively high.

In the next sections, we will show some analytical methods described for the determination of several compounds in biodiesel.

3. Monitoring of the transesterification reaction

As stated before, the transesterification monitoring is an important issue to biodiesel quality control since some contaminants arise from this reaction. Then, such monitoring allows recognizing and correcting problems at an early stage.

The first method for monitoring the transesterification reaction of vegetable oils was developed by Freedman et al. [17]. For such, they employed thin layer chromatography (TLC) with FID. Besides fatty esters, this method allows to analyze tri- di-, and monoglycerides. Moreover, the analysis time is quite short; 30 samples could be analyzed in 2–3 h. However, this method shows lower accuracy, sensitivity to humidity, material discrepancies as well as fairly high cost of the instrument. Subsequently, other TLC on silica gel methodology was developed [18]. In this method, the area of triacylglycerol spot of mixture is compared to a standard. However, the analysis is only qualitative and does not allow the exact deter-

mination of the degree of conversion. Actually, TLC is quite used for qualitative analyses, especially, for the evaluation of the oil conversion, since it is fast and effective [4].

Afterward, Freedman et al. [19] developed the first GC methodology to monitor fatty acids, tri-, di-, and monoglycerides in the transesterification reaction of soybean oil. In this method, before performing the analyses, mono- and diglycerides have to be silylated with *N*,*O*-bis(trimethylsilyl)trifluoroacetamide (BSTFA). Such procedure affords the trimethylsilyl derivatives, allowing a better separation and tailing reduction. In this first GC work, authors used a short fused silica capillary column (1.8 m; 100% dimethylpolysiloxane), and tridecanoin as internal standard. The complete separation of acylglycerols and fatty esters was obtained in a run time of 12 min. After that, other papers [20–22] described a GC–FID method with a packed column to evaluate the conversion of rapeseed oil to fatty ethyl or methyl esters. The evaluation was performed through the peak areas of esters during the reaction. The advantages of this method were the requirement of already available compounds and the use of cheap columns.

The first HPLC method for monitoring transesterification was developed by Trathnigg and Mittelbach [23]. They describe a HPLC methodology with density detection (DD), which allows the determination of the overall content of tri-, di-, and monoglycerides in biodiesel samples from methanolysis mixtures as well as the methyl esters detection. The analyses were performed through coupling a cyano-modified silica with two-gel permeation chromatography (GPC)-columns, and using an isocratic eluent (chloroform/ethanol 0.6%). According to the authors, this method is simple and reliable. Subsequently, Holcapek et al. [24] employed reversed-phase (RP)-HPLC with several detection methods (UV, at 205 nm; ELSD; and APCI–MS, atmospheric pressure chemical ionization–mass spectrometry) to monitor the transesterification of rapeseed oil to methyl esters as well as to quantify the residual content of triacylglycerols. These detection methods are suitable for the analysis of complex mixtures due to their compatibility with gradient elution, which is necessary to good resolution of methyl esters, mono-, di-, and triacylglycerols. The main disadvantage of the UV detection is a weak absorbance of acylglycerols at wavelengths higher than 220 nm, besides the non-quantification of saturates. However, the sensitivity of APCI–MS and ELSD decreases strongly with the increasing of double bonds in acylglycerols. In conclusion, APCI–MS was considered the most suitable method for biodiesel analysis.

Only in 1995, Gelbard et al. [25] described the first work on the utilization of nuclear magnetic resonance, particularly ^{1}H NMR, for monitoring the yield of transesterification reaction. The peaks of methylene group adjacent to ester moiety in triacylglycerols (α-CH_2, 2.3 ppm, *t*) and the methoxy group in the esters (OCH_3, 3.7 ppm, *s*) were used to follow the reaction progress. The conversion was calculated from the areas of those peaks, using an equation: $C = 100 \times (2A_{OCH_3}/3A_{\alpha\text{-}CH_2})$. The authors state that this method is faster and simpler than chromatographic ones. However, instrumentation and maintenance costs are relatively high and must be evaluated. Another work with NMR spectroscopy describes the use of ^{13}C NMR for monitoring the rapeseed oil transesterification [26]. The signal at 14.5 ppm of the terminal methyl groups, which are not affected by reaction, was chosen as internal standard, and the glyceridic carbons at 62–71 ppm along with methoxy carbon of fatty esters at 51 ppm were selected to determine the conversion rate. After that, a ^{1}H NMR methodology to monitor the soybean oil ethanolysis as well as to quantify the content of fatty ethyl esters in mixtures of biodiesel and oil was developed [27]. The region of 4.05–4.40 ppm (ester ethoxy and glycerol methylene hydrogens) was chosen for the quantification of the reaction. The authors [27] state that the method is quicker and simpler than GC and HPLC. Moreover, a small amount of sample is required and it could be analyzed without a prepurification process. After that, Morgenstern et al. [28] developed a ^{1}H NMR method to monitor the transesterification reaction of soybean oil. Through NMR analysis, they were able to establish the average degree of fatty acid unsaturation and methyl esters in biodiesel.

Other alternative for monitoring the transesterification of oils/fats is IR spectroscopy. The first reported work in this area is from Knothe [29,30], which developed a fiber-optic near infrared (NIR) method to monitor the transesterification reaction of soybean oil, which was based on the differences in the NIR spectra at 6005 and 4425–4430 cm^{-1}, where fatty esters display peaks and triglycerides exhibit shoulders. Thus, these peaks were chosen for monitoring the reaction. In fact, the former peak was used for quantification since it is more suitable. Besides the transesterification monitoring, the biodiesel quality can be assessed through this methodology by the correlation with other analytical data, as pointed by Knothe [30], which correlated the NIR results with ^{1}H NMR spectroscopy. This kind of procedure is a way of cross-checking the results. In addition, NIR method can also be used for the quantification of methanol in biodiesel, which can be an alternative to flash point evolution of biodiesel. Finally, the NIR method could be used to monitor the reaction of several oils as well as ensure the quality control of biodiesel when employed with other analytical techniques. Another work reports a FT-IR method and a multivariate approach (PLS, partial least squares regression), which uses the ester peak at 1700–1800 cm^{-1} to monitor the ethanolysis of degummed soybean oil [31]. Such method was considered fast and accurate to predict reaction yields. Later, Siatis et al. [32] developed a FT-IR method to monitor the ultrasonically assisted extraction transesterification of seed and seed cakes from cotton, sunflower, sesame, and *Cynara cardulus* seeds. The method affords the simultaneous determination of fatty acid methyl ester and triglycerides. They used PLS algorithm and 1300–1060 cm^{-1} spectral region to determine the percentage of fatty ester in the mixture of reaction. The most characteristic peak at 1200 cm^{-1} is that related to O—CH_3 vibrations in the methyl fatty esters. Subsequently, Ghesti et al. [33] described a FT-Raman spectroscopic method to monitor and quantify the transesterification of soybean oil. The differences between the vegetable oil Raman spectrum and the fatty ethyl esters spectrum were observed in bands at 2932 cm^{-1} (ν_{CH_2}), 861 cm^{-1} ($\nu_{R-C=O}$ and ν_{C-C}), 372 cm^{-1} (δ_{CO-O-C}), as well by the displacement of the C=O band from 1748 to 1739 cm^{-1}. They employed uni- and multivariate analysis methods to build analytical curves and to check the method. Using an internal normalization standard ($\nu_{=CH-}$ band), the best results were achieved by Raman/PLS calibration models. Afterward, the same authors [34] correlated this method with a new NMR technique developed for monitoring the ethanolysis of soybean oil but that could be extended to the transesterification of other vegetable oils. Also, a FT-IR method to assess the extent of transesterification reaction of oils was recently described [35]. The author states that methyl peak areas intensities and positions could be employed to monitor the reaction. Finally, mid-IR with a multivariate approach was used to monitor on line the transesterification of soybean oil with ethanol [36]. For such, a cylindrical reflectance cell of PbSe and the range of 3707–814 cm^{-1} were employed. The monitoring was carried out for 12 min. The yield of the reaction was also achieved through ^{1}H NMR analysis of samples collected from the reactor. The proposed method could be used in the process control and for reaction optimization since it is fast and shows low-cost.

Also, GPC (or SEC-size exclusion chromatography) is used for monitoring the transesterification. Dubé et al. [37] suggested two

distinct methods for monitoring the biodiesel production from waste canola frying oil: GPC with refractive index detector (RID), and attenuated total reflectance (ATR)–FT-IR spectroscopy. The decreasing of the peak at 1378 cm^{-1} (terminal methyl and OCH_2 in acylglycerols) in the ATR–FT-IR spectrum was used for monitoring the biodiesel synthesis. The results of the analyses of 100 biodiesel samples by both methods showed very small differences. Thus, the authors consider that the methodologies could be equivalent. However, the GPC–RID methodology allows only the quantification of monoglycerides and fatty methyl esters, while the ATR–FT-IR just consents the quantification of the sum of mono-, di- and triglycerides. Finally, Arzamendi et al. [38] described a method based on SEC to determine simultaneously the total amount of tri-, di-, monoglycerides, fatty acid methyl esters, free glycerol and methanol in samples from the transesterification reaction of sunflower oil. Two Styragel® HR0.5 and HR2 columns with RID and viscometer detectors as well as THF solvent were employed for the analyses. According to the authors, the method is simple, robust, relatively fast, it may be conducted at room temperature and it gives accurate and reproducible results.

Other techniques were also proposed. Xie and Li [39] demonstrated a method for monitoring the progress and the end-point of the transesterification of soybean oil and to determine the yield of the reaction, without the necessity of sample derivatization. Such method is based on hydroxyl content or refractive index measurements of transesterified mixture since the compounds of such blend (glycerin, mono-, di-, triglycerides, and fatty methyl esters) have significantly differences in those properties. The hydroxyl content were measured according to AOCS Official Method Cd 13–60, which consists in an acetylating reaction with acetic anhydride in pyridine followed by a titration with potassium hydroxide. The refractive measurements were performed after washing the transesterified mixture three times with NaCl solution. Authors believe that this methodology is advantageous and useful for control process, while it is simple, rapid, and inexpensive. Also, the use of an acoustic wave solid-state viscometer (ViSmart™) to monitor the transesterification reaction is described [7]. The progress of the reaction is evidently indicated for the decreasing viscosity of the mixture. The viscometer was able to detect the end-point of the reaction in pilot-scale and could therefore be used in the future to monitor the batch production process of biodiesel. The main advantage of the use of this kind of viscometer is that it does not require an extra step of measuring the density like others.

4. Determination of fatty mono-alkyl esters in blends or pure biodiesel

Pure biodiesel is mostly composed of fatty mono-alkyl esters, usually by ethyl or methyl esters. Best engine performance requires 98.8% of esters minimum content [40].

In the literature, there are many reports about esters determination in blends, and pure biodiesel. Frequently, spectroscopy and chromatography have been used for assessing biodiesel quality and for monitoring transesterification reaction, as previously discussed. For analyzing fatty methyl ester content in pure biodiesel, there is the EN 14103 standard method, which employs GC–FID. However, for determining the blend level of biodiesel in diesel, chromatography seems to be less suitable due to the complexity of diesel composition [41]. Currently, the most widely used technique is medium FT-IR spectroscopy, which is also the base of the European standard reference method [42].

The first work for the quantification of methyl esters, as well as mono-, di- and triglycerides in pure biodiesel, describes the use of GC–MS with a (5%-phenyl)-methylpolysiloxane capillary column [43]. For such, the analyses were carried out with selected ion monitoring (SIM) mode and the sample was submitted to a silylation reaction. The authors stated that the method also allows distinguishing between un- and distillated products. After that, the same authors described the quantification of fatty methyl esters in biodiesel/diesel blends using GC–FID [44]. The process consists in the separation of biodiesel from diesel on silica cartridge with hexane/diethyl ether, and thus in the GC analysis. Additionally, a relationship was established between saponification value (SV) and percent of biodiesel in blends, which could also be useful for such determinations. In a subsequent work of these authors [45], they described a GC–FID for the determination of biodiesel levels in biodiesel/diesel blends, which differs from the former on the sample pre-treatment. This new methodology consists on a preliminary acetylation of the sample followed by a separation process using a silica cartridge and hexane as solvent. The authors state that the results are very encouraging in terms of precision and accuracy. Additionally, capillary GC–FID was also employed for the identification of fatty acid methyl ester composition of biodiesel samples from six edible vegetable oils (rapeseed, peanut, corn, cotton-seed, sesame and soybean oil) as well as for the determination of the fatty acid composition of those oils [46]. A similar work with GC–FID, employing HP-1 wide-bore column, was also described [47]. According to the authors, this method is simple, rapid, and accurate. Subsequently, Li et al. [48] developed a simple and rapid GC–FID method for the quantification of fatty acid methyl esters and glycerides in biodiesel without the need of sample derivatization. This could be achieving due to the use of a non-polar and high temperature-resistance capillary column. After that, another GC–FID method for qualitative and quantitative analysis of fatty acid methyl esters in biodiesel, which employs a polar capillary column (J&W INNOVAX), was developed [40]. They stated that the method has high accuracy and precision, and it does not require special preliminary sample preparation. However, this method requires the use of several internal standards (lauric, myristic, palmitic, stearic, oleic, linoleic, and linolenic esters). An accurate GC–FID method is also described for evaluating fatty methyl esters in biodiesel [49]. According to the authors, recovery and standard deviations were satisfactory. Finally, Schober et al. [50] developed a GC–FID method for quantifying the methyl esters in biodiesel, which is based on EN 14103. The latter does not include heptadecanoic acid ester that is found in animal fats. Thus, the authors showed that the amount of esters is increased in 2–7 wt.% by the use of their methodology. Moreover, such method allows the determination of short-chain fatty acid esters (C_8–C_{12}), which occur in some biodiesel samples from coconut and palm oil. In these cases, the ester content of such biodiesel differed by >40 wt.%. The authors suggest the use of fresh standard solutions, since the stability of the methyl heptadecanoate (internal standard) influences the values of ester content.

Another method described for evaluating the methyl ester content of biodiesel samples is based on viscosity measurements [51]. There is a correlation between the content of esters and the viscosity: the higher the viscosity, the lower the esters content. According to these authors, since the method is quick and simple, it is especially suitable for process control purposes, such as, transesterification monitoring.

After that, Fillieres et al. [52] employed a high-performance size exclusion chromatography (HPSEC or SEC) for the quantification of ethyl esters, mono-, di-, and triglycerides, and glycerol in biodiesel from rapeseed oil. Their purpose was to evaluate the influence of different parameters on the transesterification reaction. After that, another GPC–RID method for quantifying methyl esters, tri-, di-, and monoglycerides, glycerol in biodiesel samples from palm oil was developed [53]. Such methodology employs two

Phenogel columns and tetrahydrofuran as solvent. Moreover, the sample preparation is simple, involving only dilution and neutralization with HCl.

A HPLC method was described for quantifying fatty ethyl, isopropyl, 2-butyl, and isobutyl esters as well as fatty acids, tri-, di-, and monoglycerides in biodiesel samples from fats, oils, and recycled greases [54]. The process involves the use of an ELSD detector and a gradient elution profile (hexane and *tert*-butyl ether, both with 0.4% acetic acid). This method is based on a previous methodology described in the literature, but it showed a reduction of 25% in analysis time. Succeeding the first HPLC work, Holcapek and Jandera [55] developed a HPLC–APCI–MS method for the identification of fatty methyl esters, mono-, di-, and triacylglycerols in different kinds of biodiesel from rapeseed, sunflower, soybean, palm, macadamia, almond, poppy seed, and hazelnut oils. The authors emphasize that the method can be used with any kind of biodiesel. Subsequently, HPLC method for quantifying soy biodiesel (1–30%, v/v) in diesel was developed [42]. This analytical methodology could also be used for the determination of the same amount of triglycerides in diesel. The methodology employs silica column with isocratic elution (hexane 90% and methyl *t*-butyl ether 10%) and UV or ELSD detectors. The authors state that ELSD detector is preferred over UV because its response is directly related to the mass of solute injected. On the other hand, UV detector's response is proportional to the number of double bonds. However, there is no statistical difference between the analyses of both detectors. Therefore, Foglia et al. [42] concluded that HPLC is a fast technique that can analyze blends of biodiesel produced from various feedstocks in petrodiesel. Subsequently, Kaminski et al. [56] described a procedure that enables the simultaneous determination of aromatic hydrocarbons, total content of polycyclic aromatic hydrocarbons, and fatty acid methyl esters in diesel, which contain up to 30% of these esters. A normal-phase separation (LiChrospher NH_2 5 μm column), using *n*-heptane as mobile phase, was employed. Besides that, two HPLC detectors connected in series were used. The first one was UV–DAD (ultraviolet diode array detector) followed by RID. The UV detection at 260 nm is preferred as it provides higher accuracy and precision than RID. According to the authors, this method with detectors in series is advantageous since it provides correct and precise determination of the backflush point, confirmation of the fatty acid methyl esters, and detection of the presence of resins, which occur because of long-term storage. Additionally, HPLC and GC could also be used together for the quantification of ethanol, fatty ethyl esters, mono-, di-, and triglycerides in ethanol biodiesel from waste cooking oil [57]. A new RP–HPLC–UV method was recently developed in order to determine fatty acid methyl esters, free fatty acids, mono-, di-, and triacylglycerols in biodiesel [58]. Detection was mostly affected by flow rate and gradient end time. Such method allowed the identification of all components in less than 30 min. Also, a high speed LC–MS system, which employs electrospray ionization (ESI) and a patented cone-wash feature, was described as a efficiency way to identify fatty methyl esters and other compounds in biodiesel [59]. The main advantage of this technique is the reduction of the analysis time.

Supercritical fluid chromatography (SFC) was also used to determine fatty acid methyl esters, fatty acids and glycerol in biodiesel samples [60]. This is a preliminary study that allowed the analysis of these compounds in less than 5 min. The experiments were carried out in a SFC–MS–UV–ELSD system, using a C-18 column and isocratic elution.

Recently, several works have reported the use of IR spectroscopy to assess the biodiesel quality control. For example, Baptista et al. [61] described a PLS-NIR methodology, which allowed to determine esters content and some specific acid methyl esters (myristic, palmitic, stearic, oleic, and linolenic) in biodiesel. Determination of esters content showed errors lower than those obtained through reference method. After that, Soares et al. [62] developed a PLS–ATR–FT-IR method to quantify raw oil, from 1 to 40% (v/v), in different biodiesel samples. Such calibration model could preview with 95% of significance the samples analyzed.

A recent work [63] suggested the evaluation of biodiesel quality through determination of oil content by an optical fiber sensor. Such method showed errors of 0.4 and 2.6% for pure biodiesel and soybean oil, respectively. This fiber sensor, which is a compact and cheap device, has high sensitivity and allows the ease assessment of biodiesel quality.

The blend level of biodiesel in diesel could be determined through the use of both NIR and ^{1}H NMR techniques [41]. Soybean biodiesel was employed in this study. Two spectral regions (6.005 and 4.800–4.600 cm^{-1}) were chosen to the NIR analyses. Moreover, in ^{1}H NMR procedure were used the peaks of the methyl ester moiety (3.6–3.7 ppm), the clusters of peaks (0.8–3.0 ppm) from the methylene and terminal methyl protons of the hydrocarbon moieties in biodiesel and diesel, and the olefinic hydrogen (5.3–5.4 ppm) in biodiesel for determining blend levels. Both methods were in good agreement, and the NIR methodology is easy and rapid.

Additionally, Birova et al. [64] described two methods to evaluate the fatty methyl esters content in biodiesel/diesel fuel blends. One of them is based on the ester number (difference between the saponification and the acid values) and the other one uses the IR spectroscopy, specially the measurement of carbonyl band intensity. According to the authors, both methods are suitable to the desirable determination. Oliveira et al. [65] also developed an analytical method for the identification of methyl esters in biodiesel blends by ATR–FT-IR and NIR spectroscopies combined to PLS and ANN (artificial neural network) analysis. Through these methodologies were analyzed blends of one type of biodiesel and diesel (Group I) besides mixtures of three kinds of biodiesel and diesel (Group II). The biodiesel was obtained from different vegetable oils: soybean, soybean fried, babassu, and dende. According to the results, PLS model based on NIR was more precise and accurate than the one based on ATR–FT-IR for the analysis of Group I samples. However, NIR and ATR–FT-IR ANN models for Group I presented similar precisions and accuracies. For Group II, both PLS methods (NIR and ATR–FT-IR) had similar accuracies while the precision of PLS NIR was better. However, ANN models for Group II presented almost equivalent precisions and accuracies. The authors mentioned that these methods are faster than the chromatographic ones and sample integrity is preserved. Consequently, they could be used to determine different methyl esters contents in biodiesel blends. A similar work was described by Pimentel et al. [66]. However, in such work, PLS multivariable calibration models based on mid-FT-IR and NIR spectroscopy were developed in order to determine the level of biodiesel and/or raw vegetable oils in blends with fossil diesel. Additionally, PCA (principal component analysis) methods were employed to fast identification of diesel samples contaminated with raw vegetable oils. Soybean, castor and used frying oils as well as their biodiesel were employed in the preparation of diesel blends. Subsequently, Oliveira et al. [67] showed that NIR and Raman spectroscopy combined with chemometric methods are quite useful to identify residual oils in biodiesel/diesel blends. PLS, principal component regression (PCR), and ANN calibration models were applied to NIR and FT-Raman spectroscopic data aiming to determine adulterations of B2 and B5 blends with vegetable oils. Among the designed models, FT-Raman ANN showed the best accuracy (0.03%, w/w). Also, Aliske et al. [68] developed a FT-IR method to the determination of biodiesel and diesel mixtures. The method covers the full ranges of mixture (0–100%) and it employs the

carbonyl peak present only in biodiesel spectrum for the quantification. This methodology stands for a simple way to perform quality control and monitoring of biodiesel–diesel blends. It is worth to notice that the method was developed using ethyl biodiesel from soybean oil and diesel blends. Recently, Guarieiro et al. [69] also described a FT-IR method to determine biodiesel content in diesel blends through area measurement of the peak at 1754 cm^{-1}. The method is fast, low-cost and it allows the determination of biodiesel content upper than 0.1%.

One spectrophotometric technique was also established for the determination of biodiesel content in blends [70]. The spectrophotometric features in the wavelength range of 190–1100 nm of diesel/biodiesel blends were investigated. Biodiesel from six different feedstocks and five distinct diesel samples were used for such study. The authors concluded that UV spectroscopy is a reliable and reasonable method for blend level detection of any biodiesel and different diesel samples. After that, Sastry et al. [71] also described the use of spectroscopic and conventional methods for the determination of biodiesel in biodiesel/diesel blends. The authors state that such methods are simple, fast and reliable.

A practical procedure using hydrometry was also developed for the determination of biodiesel content in blends [72]. In this work, several procedures and instruments for determining biodiesel blends were evaluated at different temperatures. Specific gravity (hydrometer), density (balance/volumetric flask), electromagnetic absorbance (spectrophotometer) and viscosity (zahn viscometer) of different blends were measured. In fact, diesel, B5, B10, B20 and B100 from distinct feedstocks (canola, sunflower, soybean and corn) were evaluated. According to the authors, the best method is hydrometry due to its simplicity, accuracy and low instrument cost.

Recently, Corgozinho et al. [73] showed that synchronous fluorescence spectroscopy (SFS) and chemometrics are useful to identify and quantify residual oils in biodiesel/diesel blends. Specially, PLS, PCA and Linear Discriminant Analysis (LDA) applied to spectrofluorimetry data allowed both discrimination and quantification of vegetable oil in diesel and B2 blends. According to the authors, the method is simple, fast, accurate and reliable to detect adulteration of diesel and B2 blends with vegetable oils.

Also, a radiocarbon-based method was developed to quantify biodiesel in diesel blends with accuracy of ±1% [74]. Such method does not require any knowledge about biodiesel type or diesel components as well as a calibration curve. However, cost and turn-around-time of analysis are critical disadvantages of this method.

5. Determination of free and total glycerol

Glycerol is the major by-product in the manufacturing of biodiesel. Its removal is desirable since it can cause damage to the engine and hazardous emissions. As a consequence, quality control of this compound is essential [75]. According to ANP legislation, 0.02% of free glycerol is the maximum quantity permitted [2]. Moreover, European and US standards specify the tolerate limits of free and total glycerol (sum of glycerol, mono-, di- and triacylglycerols) (Table 1). Such compounds can contaminate biodiesel samples due to incomplete transesterification and insufficient purification. In fact, during the biodiesel production, washing steps can easily remove free glycerol, while a low content of glycerides can only be achieved by the use of suitable catalysts and reaction conditions or by further distillation of the product [10]. Also, some distilled biodiesel samples may contain free glycerol distilled as a head product of this unit operation [76]. Finally, Knothe [30] and Mittelbach [10] propose that the amount of glycerol and glycerides is a major factor in determining fuel quality.

Since the limits of bonded and free glycerol are very low, there is a need for precise and reliable analytical methods for both determinations [10]. In the literature, there are several procedures for the determination of free and total glycerol in biodiesel and its blends, such as HPLC and GC methods. Usually capillary GC is used for it [75]. According to Mittelbach [10], only GC meets all requirements for the determination of low contents of mono-, di- and triglycerides in biodiesel. However, the purity of standard substances must be checked by HPLC since such feature can lead to inaccurate analyses.

The first method, described for determining the total glycerol in biodiesel, is based on enzymatic procedure [77]. The process involves solid-phase extraction, saponification reaction, followed by enzymatic analysis of the sample. This method, which was developed for the rapeseed biodiesel, does not distinguish among mono-, di-, and triglycerides. Moreover, it is relatively complex and it shows fairly low reproducibility. Afterward, the Sigma–Aldrich Fine Chemicals developed a kit (BQP-02) for enzymatic determination of free and total glycerin in biodiesel. The method is based first on the enzymatic reaction of free and bonded glycerol and then on the spectrometric measurement of obtained colored product.

Subsequently, Bondioli et al. [78] described a GC–FID method for the determination of free glycerol in biodiesel. Sample derivatization was not necessary and a glass column (2 m × 4 mm i.d.), loaded with Chromosorb 101, was employed. The method is only reliable for rapeseed oil, sunflower-oil, and soybean biodiesel and it is suitable if the quantity of free glycerol present in the sample is higher than 0.02%. Most of the reports on GC utilization for biodiesel analysis describe the use of FID [15]. However, there is a GC–MS method for the quantification of mono-, di-, and triglycerides in methyl biodiesel fuels [79], which employs a (5% phenyl)-methylpolysiloxane column (10 m × 0.25 mm i.d.) and MS in SIM mode. The analysis is performed after silylation with BSTFA. According to the authors, the method gives excellent quantification data. Mittelbach [80] also described a GC method with FID or MS detection for the determination of free glycerol in methyl biodiesel, using a DB-5 column (60 m × 0.25 mm). The methodology is quite similar to that described by Plank and Lorbeer [79], involving sample derivatization with BSTFA, and analysis by GC–MS in SIM mode. The author states that such method is more sensitive and quicker than the others that had been described. Subsequently, Mittelbach et al. [81] improved the GC–FID, GC–MS method [80], which allowed the simultaneous determination of free glycerol and methanol in biodiesel. After that, an important GC–FID procedure was developed [75], which later became the EN 14105 and ASTM 6584 methods. Such analytical method allows the simultaneous determination of glycerol, mono-, di-, and triglycerides in vegetable oil methyl esters predominantly consisting of C_{18} methyl esters, such as biodiesel from rapeseed, sunflower, soybean and used frying oil. The method was mainly developed to the methyl rapeseed biodiesel. However, it could not be applied to methyl esters obtained by transesterification of lauric oils without modifications. The determination of all classes of compounds was achieved by the silylation of the free hydroxyl groups, employing *N*-methyl-*N*-trimethylsilyltrifluoroacetamide (MSTFA), followed by capillary GC analysis in a DB-5 column (10 m × 0.32 mm). Moreover, the use of 1,2,4-butanetriol and tricaprin as internal standards allowed for reliable quantitative analysis within a run time of 30 min. Therefore, this method is suited for the quality control of biodiesel. However, Bondioli and Della Bella [76] state that the use of an alternative method sometimes is necessary for the efficient control of biodiesel since the presence of trace of volatile products in some samples may cause interference in the Plank's method. Ruppel and Hall [82] also evaluated the ASTM D 6584 method and consider that the method is simple, sensitive and reliable, and it requires only a small amount of

sample preparation. Subsequently, the ASTM D 6584 method was improved through the use of capillary flow technology [83] and high temperature GC columns [84–86]. An alternative methodology for the chemical derivatization of glycerides, which employed fluorinated acid anhydrides and affords perfluoro alkyl esters, was described [87]. Such procedure can reduce both the analysis time and cost. After derivatization, the authors used GC–MS technique and FT-IR spectroscopy to measure the amount of mono- and diglycerides in biodiesel.

The first HPLC procedure for the analysis of glycerol was described in the work of Lozano et al. [88]. They employed a HPLC method with pulsed amperometric detection (PAD) to measure free glycerol in methyl or ethyl biofuels. This method also allows the detection of residual alcohol in the biodiesel sample. According to the authors, the method is simple, rapid and accurate. In fact, the sensitivity seems to be the major advantage of this method. In a subsequent work, Sala and Bondioli [89] evaluated two distinct methodologies for determining glycerol. One of the methods employed a titration with periodate and the other one was based on HPLC technique. From the results, the authors concluded that the periodate method showed very good precision and accuracy, which were improved by the use of a potentiometric titration, and HPLC analysis is less time-consuming and it supplies more information about the sample. Also, an HPLC–RID methodology for the determination of free glycerol in biodiesel is described [90]. Before the analysis, the sample has to be extracted with water. This method is reliable and faster than GC ones, giving the same analytical results. Finally, Foglia et al. [91] described a comparison between high temperature gas chromatography (HTGC) and HPLC for the determination of bound glycerol in soybean and rapeseed biodiesel. HTGC–MS and HPLC–ELSD showed similar results. However, in the point of view of operation, HPLC is better than HTGC because it does not require sample derivatization, it has shorter analysis time (as proposed before) and it is directly applicable to most biodiesel fuels. Besides that, HPLC shows versatility in analyzing biodiesel from different feedstocks and several alkyl esters (methyl, ethyl, isopropyl).

The combination of HPLC and GC is also reported to the free or total glycerol analysis in biodiesel. This practice reduces the complexity of the GC chromatograms and it allows more reliable peaks assignments. Lechner et al. [92] developed a LC–GC method for determining mono-, di-, and triacylglycerols in methyl biodiesel samples, which has 52 min of run time. Before the analyses, samples are submitted to acetylation and then analyzed through HPLC–DAD, and GC–FID, employing a DB-5 column (10 m × 0.32 mm i.d.).

In a recent work, Catharino et al. [93] developed a MS method, which employs direct infusion ESI and it allows the determination of residual glycerol, mono-, di-, and triglycerides, besides fingerprinting typification of biodiesel, alcohol identification, and monitoring of degradation and adulteration. Typification and biodiesel degradation were performed in the negative ion mode (ESI−), while other parameters were determined using positive ionization (ESI+). This technique seems to be very useful since it allows both typification and fast screening of some important parameters related to biodiesel quality.

A spectrophotometric method based on measurements of 3,5-diacetyl-1,4-dihydrolutidine at 410 nm was also developed for the glycerol determination [76]. This compound is obtained from Hantzsch reaction of glycerol, which consists in two successive reactions: periodate oxidation of free glycerol affords formaldehyde and then the reaction of this compound and acetylacetone in the presence of ammonium acetate gives the desirable product. The 3,5-diacetyl-1,4-dihydrolutidine has a very high absorption at 410 nm, increasing the potential to get a very low detection limit for glycerol. According to the authors, this methodology is simple, quick, economical and sufficiently reliable. They also demonstrated the feasibility of this procedure applied to a diesel fuel/biodiesel blends (5 and 20%). However, more tests are necessary to evaluate the robustness and the suitability of the procedure to this kind of matrix.

Finally, Gonçalves Filho and Micke [2] developed a capillary electrophoresis method (EC–DAD) for the quantification of free glycerol in biodiesel. Before the analysis, the reaction between glycerol and periodate (HIO_4) is carried out, in less than 2 min, to afford iodate (HIO_3). Commercial biodiesel from chicken fat, soybean, and castor oil were analyzed by this methodology. All samples had a value less than the specified by ANP. According to the authors, this methodology for the extraction and analysis of free glycerol in biodiesel is fast, simple, and reliable.

6. Determination of other compounds and parameters

6.1. Water content

The water content in biodiesel is an important factor in the quality control. Water can promote microbial growth, lead to tank corrosion, participate in the formation of emulsions, and cause hydrolysis or hydrolytic oxidation. Therefore, the content of water is limited to 0.05% (w/w) according to EN 14214 and ASTM D 6751 standards (Table 1). Moreover, such standards establish the use of centrifugation or Karl–Fischer titration for determining water content in biodiesel. A procedure based on the latter method was recently described [94]. Besides that, Felizardo et al. [95,96] developed a NIR method together with PLS and PCR analyses to determine water and methanol content in biodiesel. The authors emphasize that the use of a pre-processing method, such as OCS (orthogonal signal correction), is especially important in the development of PLS and PCR models employed for water and methanol determination. They also consider that the use of NIR spectroscopy, in combination with multivariate calibration, is a promising technique to assess the biodiesel quality. Finally, Todd et al. [97] describe a novel direct sampling mass spectrometry membrane to measure the water content in biodiesel. This method could be used for monitoring the synthesis process of biodiesel.

6.2. Methanol content

The residual methanol in biodiesel can cause corrosion of metals, mainly of aluminium, and decrease the biodiesel flash point. Besides, it is responsible for cetane number and lubricity decreasing of fuel. ASTM D 6751 limits indirectly the methanol content through the flash point minimum value. However, the EN 14214 standard, beside the flash point, establishes 0.2% (w/w) as the maximum content of methanol (Table 1). Previously, we described analytical methods [38,81,95,96] that allow, beside the determination of other compounds, the quantification of methanol in biodiesel. Moreover, Fang and Zeng [98] developed a UV spectroscopy procedure for the determination of methanol in biodiesel samples. According to the authors, this method was reasonable and it had good reproducibility and accuracy. Subsequently, Li et al. [99] described a GC–FID method for the determination of small amounts of methanol in biodiesel. Such methodology employs two columns (a pre-column and a polar PEG-20M one) with pressure backflush system and it was used for the analysis of 8 different biodiesel samples. Additionally, the authors discuss several parameters that affect fatty acid methyl esters, free fatty acids, mono-, di-, triglycerides, and methanol determinations in biodiesel. After that, Araujo et al. [100] developed a fast and reliable flow methodology, which employs a microporous hydrophilic membrane to extract methanol from biodiesel, and it

determines methanol content by UV measurements (at 240 nm), after derivatization with alcohol oxidase (AOD), soluble peroxidase, and 2,2′-azinobis(3-ethylbenzothiazoline-6-sulphonic acid) (ABTS). Such methodology showed good precision, with a relative standard deviation <5.0% ($n = 10$) and detection capacity of 0.211% (w/w). The results obtained with this method showed good correlation with those furnished by GC. However, the flow method seems to be more environmental friendly and cost-effective than the GC reference one. Other method to determine methanol content in biodiesel was recently proposed by Paraschivescu et al. [101]. It involves a headspace solid-phase microextraction, using a carboxen-polydimethylsiloxane SPME fiber, and a subsequent GC–FID analysis, employing a HP-5 capillary column. Such method showed good reproducibility and recovery, allowing analysis of methanol in concentrations lower than those imposed by the standard specifications.

6.3. Steroids content

Sterols are natural non-glyceridic compounds that occur in vegetable oils, and can arise in biodiesel due to their solubility in such fuel. Consequently, their amount may influence biodiesel quality. The GC–FID and on-line LC–GC methods are described to determine the sterols and their esters in biodiesel. The LC–GC is more recommended because of additional information, short analysis time, and reproducibility [15]. In fact, Plank and Lorbeer [102–104] have some works concerning sterols analysis in biodiesel. In their first work [102], they describe a GC–FID method for determining free and esterified sterols in methyl biodiesel from rapeseed oil. Before the analysis, free sterols were silylated with BSTFA, which hold 1% of trimethylchlorosilane (Me_3SiCl), and thus they were analyzed in a (5% phenyl)methylpolysiloxane column. Brassicasterol, β-sitosterol, campesterol, cholesterol, stigmasterol, and 5-avenasterol as well their esters were identified in rapeseed biodiesel. After that, Plank and Lorbeer [103] developed a similar GC–FID for determining free sterols in rapeseed methyl esters as well as an online LC–GC method to determine free sterols and sterol esters in the same samples. The former analyses were carried out after saponification. The results showed the total sterol content (0.70–0.81 wt.%) consisted of cholesterol, brassicasterol, campesterol, stigmasterol, β-sitosterol, and 5-avenasterol. Moreover, by online LC–GC, 0.24–0.34 wt.% of free sterols and 0.55–0.71 wt.% of sterol esters were found. Subsequently, the same authors [104] improved the LC–GC method for the analysis of free and esterified sterols in five different kinds of biodiesel from rapeseed, soybean, sunflower, high-oleic sunflower, and used frying oil. The analyses were carried out without saponification, but the free sterols were silylated with MSTFA.

6.4. Metals and metalloids content

Metals and metalloids are also important issues in biodiesel quality control, since high contents can cause environmental problems or damage the engines. ASTM D 6751 and EN 14214 standards of biodiesel limit to 5.0 mg kg^{-1} the amount of Na and K. Indirectly, these contents are also restricted through the sulphated ash value. On the other hand, the quantity of phosphorous is limited to 10.0 mg kg^{-1}, Ca and Mg to 5.0 mg kg^{-1}, and S to 10.0 mg kg^{-1}, according to EN 14214 (Table 1). Also, there are some works described in the literature, which employ mainly atomic absorption methodologies for the determination of metals and metalloids in biodiesel. In fact, there is a recent review [105] on the atomic spectrometric methods to determine metals and metalloids in fuels like biodiesel.

In the first work described, the determination of Ca, Cl, K, Mg, Na, and P in biodiesel was carried out through inductively couple plasma optical emission spectrometry (ICP-OES) [106]. This technique is absolutely suitable to control the production of biodiesel and the quality of final product since it has excellent analytical properties such as multi-element capability, higher power of detection, high precision and short analysis time. The monitoring of Ca, K, Mg, and Na amount is necessary due to their ability to form undesirable compounds in the engines. In addition, the evaluation of Na and K is also important since some production processes employ KOH or NaOH as catalysts. Additionally, environmental issues justify the control of Cl content. The authors of this first work also determined that oxygen addition to the outer, intermediate or nebulizer gas or argon addition to nebulizer gas reduce the background emission of the spectral lines of Na and K. The most significant improvement of background ratio is acquired when oxygen or argon is added to nebulizer gas. In fact, the addition of an argon–oxygen mixture to the nebulizer gas improves significantly the detection of Na and K. The sensitivity of these elements searches out the μg kg^{-1} range. Finally, the authors state that the method demonstrates linear calibration range and short analysis time with high sample throughput. Besides that, chemical and spectral interferences are less encountered than in AAS (atomic absorption spectrometry). Another work that employs ICP-OES for simultaneous determination of Ca, P, Mg, K and Na was described by dos Santos et al. [107]. In contrast to other methods, this procedure uses a less toxic solvent (ethanol) for dilution of the biodiesel sample. Woods and Fryer [108] also used ICP to determine several inorganic species in biodiesel samples. However, MS detection and an octopole reaction system were used, allowing measurements at levels below those obtained by ICP-OES. Besides that, the simultaneous analysis of a wide variety of elements is a valuable feature of ICP–MS. Nowka [109] developed a flame atomic absorption spectrometry (FAAS) method for the determination of Na and K in biodiesel. In this method, air was used as oxidant aiming at avoiding the baseline shift of K. Moreover, interferences of the particle emissions from the matrix were minimized by the use of a suitable technique. Finally, the method was compared with other techniques and the results correlated well. Furthermore, a photometry method for the determination of phosphorous in biodiesel samples was developed [110]. This method is based on phosphomolybdenum blue photometry and it involves carbonization and sample transformation in ash before the analysis. A similar methodology was described previously, but this new one has shorter analytical time and the sample size is only 1/5 of the previous one. The methodology was employed for analyzing 6 biodiesel samples from distinct feedstocks (rapeseed, peanut, corn, cottonseed, sesame and soybean oil). The phosphorus content of these six samples was less than 5 mg kg^{-1}. The review of Korn et al. [105] shows the use of flame emission spectrometry (FAES) for the determination of Na and K in biodiesel. Recently, de Jesus et al. [111] have also developed a FAAS method to determine Na and K in biodiesel that employs a water-in-oil microemulsion as sample preparation. Such method showed detection limits of 0.1 and 0.06 μg g^{-1} for Na and K, which are two times better than those obtained according to EN 14108 and EN 14109 norms. Moreover, microemulsions procedure has several advantages: high stability and easy handle of sample and standard microemulsions; and, no need of using organometallic standards and carcinogenic solvents.

Finally, Castilho and Stradiotto [112] developed a potentiometric method to determine K ions in biodiesel, using a nickel hexacyanoferrate-modified electrode. Such method allowed the determination of K content in the concentration range of 4.0×10^{-5} to 1.0×10^{-2} mol L^{-1}, showing a detection limit of 1.9×10^{-5} mol L^{-1}. The obtained results were similar to those

acquired by flame photometry (good reproducibility and low standard deviations).

6.5. Biodiesel oxidation

The presence of light, high temperature, metal, the material of the container, and other extraneous materials can affect the quality of biodiesel. Biodiesel oxidation leads to a variety of species including shorter-chain fatty acids and aldehydes as well as higher-molecular-weight species through oxidative polymerization. Besides that, the fatty acid profile of some feedstocks for biodiesel production can also affect the oxidative stability of this fuel. Therefore, this parameter is one of the major issues affecting the use of biodiesel [15,113]. In fact, Bouaid et al. [114] propose that the resistance to oxidative degradation during storage is an essential issue for the successful development and viability of alternative fuels such as biodiesel.

The Rancimat and AOCS Oil Stability Index methods are used for determining the oxidative stability of biodiesel. Knothe [15] proposes that, with the inclusion of specification for this measurement in EN 14214, the iodine value will be not necessary anymore.

One example of biodiesel oxidation study is described in the paper of Bouaid et al. [114]. They investigated the oxidation stability of three biodiesel during the storage. Distinct types of biodiesel obtained from sunflower, *Brassica carinata*, and used frying oils were stored in white and amber glass containers at room temperature for a period of 30-months. After regular intervals, some physicochemical parameters such as acid value, peroxide value, viscosity, iodine value and insoluble impurities were measured. Results showed that the iodine value decreased with increasing storage time, but the other parameters increased through the storage. Therefore, all kinds of biodiesel were very stable because the increase of the three parameters was not fast. However, there is deterioration of the biodiesel after 12 months of storage and the specification limits of the parameters studied was exceeded after this period. Besides that, samples exposed to daylight degrade faster than the other fuels. Another conclusion is that the oxidative stability is more strongly influenced by the presence of small amounts of more highly unsaturated fatty acid compounds than by increasing quantities thereof. The results obtained suggested that it is necessary to limit access to oxygen and exposure to light and moisture in order to obtain a highly stable biodiesel.

6.6. Biodiesel thermal stability

In the last few years, thermal analyses (thermogravimetry, TG; differential scanning calorimetry, DSC; differential thermal analysis, DTA) have become very important for supplying data that can be useful, for example, for the establishment of thermal stability [14]. Such techniques have also been employed for biodiesel characterization. Dantas et al. [8] described the characterization of methyl and ethyl corn biodiesel. They employed TG to verify the influence of the heating rate on the biodiesel thermogravimetric profile. Moreover, physicochemical analysis was used to demonstrate that both biodiesels meet the specifications of the ANP standards, as well as GC–FID, ^{1}H NMR, and FT-IR were utilized to monitor the transesterification reaction. After that, the physicochemical and thermoanalytical (TG and DSC) characterization of the biodiesel obtained from castor oil was described [14]. The volatilization temperatures of this biodiesel are very close to those of fossil diesel. The TG curve of castor biodiesel presented two stages of thermal decomposition at 150–334 °C and 334–513 °C with mass losses of 97 and 3%, which were related to volatilization and/or decomposition of methyl esters. On the other hand, the calorimetric curve of castor biodiesel showed four exothermic transitions attributed to the decomposition of esters at 259, 317, 431, and 516 °C. Additionally, there was established the calorific capacity of castor biodiesel (1.855–2.179 J/g K) in the 55–125 °C range of temperature. Regarding physicochemical analysis, castor biodiesel shows higher flash point and viscosity than diesel. The high flash point ensures more security in the handling and storage and the high viscosity can be corrected through the use of blends. Recently, thermal behavior of babassu biodiesel was investigated [115]. TG and DTA curves were obtained in air and nitrogen. Babassu biodiesel was stable up to 52 °C in air and 60 °C in nitrogen. DTA curves obtained in air showed a high number of decomposition steps.

7. Physicochemical parameters and biodiesel chemical composition

Several physical properties are limited by ASTM D 6751 and EN 14214 standards in order to ensure the biodiesel fuel quality (Table 1). Recently, two papers [10,15] have discussed intensely such parameters. Adding to the contribution of these papers, we intend to describe only the works that correlate physical parameters with biodiesel chemical composition. Flash point, kinematic viscosity, ash content, carbon residue, and acid number are the main properties that could be associated with biodiesel composition. In fact, flash point strictly corresponds to the amount of methanol and the viscosity correlates with the content of unreacted triglycerides, or with existing undesirable materials such as crude vegetable oil in biodiesel [10,116]. Therefore, the viscosity depends on the fatty acid composition of the oil/fat from which biodiesel is made, as well as on the extent of oxidation and polymerization of biodiesel [3]. Moreover, kinematic viscosity is useful for monitoring the fuel quality of biodiesel during storage, and the ash content of biodiesel indicates the residual Na or K from the catalyst. According to Mittelbach [10], the carbon residue is the most important indicator for the quality of biodiesel since it corresponds strictly to the content of glycerides, free fatty acids, soaps, remaining catalysts, and other impurities. However, Mahajan et al. [117] state that one of the most important features of biodiesel is the acid number, which represents almost exclusively the fatty acid content.

In the literature, there is a work that describes a method to predict the biodiesel viscosity from the knowledge of its fatty acid composition [118]. The method is reliable for fatty acid methyl and ethyl esters and it was checked in methyl biodiesel from canola, coconut, palm, peanut, and soy oil. It was identified that the viscosity, which is the most significant property to affect the biodiesel as a fuel, reduces with the increase in unsaturation and it is also affected by small amounts of glycerides. Moreover, the viscosities of saturated ethyl esters (C_8–C_{18}) were slightly higher than those for the correspond methyl esters. Finally, the method was employed to predict the viscosities of 15 biodiesel samples. A 100% difference in viscosity range was observed; the rapeseed methyl biodiesel had the highest predicted viscosity (4.72 mPA s) and coconut biodiesel had the lowest (2.25 mPA s). Subsequently, Tat and Van Gerpen [3] described kinematic viscosity data of biodiesel and its blends (B20, B50, and B75) with No. 1 and 2 diesel fuels from −20 to 100 °C. The measurements were carried out according to ASTM D 445-88. The results showed that viscosity quickly increases as the temperature decreases, and that biodiesel and its blends demonstrate temperature-dependent behavior similar to diesel, despite the fact that viscosity of biodiesel is higher. Moreover, the viscosity difference among the blends with No. 2 diesel was less than those of No. 1 diesel/biodiesel blends, since the former diesel has viscosity closer to biodiesel. Finally, the authors established a blending equation that allows the estimation of the kinematic viscosity as a function of the biodiesel fraction. Recently, Froehner et al. [119] established a method that relates density and ethyl esters content in biodiesel.

This method is quick and simple, allowing the determination of ester content by a single density measurement.

Also, several parameters were used for the characterization of biodiesel from 100% canola oil, green seed canola oil as well as processed and unprocessed waste vegetable cooking oils [120]. According to standard procedures, the densities, viscosities, iodine values, acid numbers, cloud points, pour points, heats of combustion, lubricity properties, and thermal properties of the four biodiesel were evaluated. Besides that, the fatty esters and lipid compositions were determined by GC–FID and HPLC–ELSD methods, respectively. GC analyses were carried out with a DB-FFAP column and HPLC analyses employed a gel permeation liquid chromatography column with tetrahydrofuran as mobile phase. The authors concluded that all the four types of oils could be employed to produce biodiesel. However, 100% canola oil, and green seed canola oil are more suitable since they afford a biodiesel that has similar physicochemical properties to diesel. However, green seed canola oil afforded a biodiesel with a low lubricity number. So, it is not appropriate to be used as an additive until further modifications. Therefore, the biodiesel from canola oil is the best as a fuel or additive. Later, a similar work was described [11], in which the relationship between biodiesel fuel properties and its fatty acid alkyl esters composition was investigated. It was established that structural features such as chain length, degree of unsaturation, and branch of the chain, influence the physical and fuel properties of biodiesel, mainly cetane number, heat of combustion, melting point, oxidative stability, viscosity, and lubricity. Usually, cetane number, heat of combustion, melting point, and viscosity increase with the increasing chain length and they decrease with the increasing unsaturation.

Subsequently, Imahara et al. [121] developed a model to predict the cloud point of biodiesel, which is related only to the amount of saturated methyl esters. They stated that the model permits to estimate cloud point of biodiesel made from several oil/fats feedstocks, thus being a useful tool to determine optimized fatty acid methyl ester composition.

Finally, Fernando et al. [16] studied the relationship between the amount of unconverted triglycerides (or a low content of monoalkyl esters) in biodiesel and some biodiesel specifications (flash point, water and sediment, kinematic viscosity, sulphur content, sulphated ash, copper strip corrosion, cetane number, cloud point, carbon residue, acid number, free and total glycerin, phosphorous content, and distillation temperature). According to standard test methods, they evaluated B100 and mixtures of biodiesel and soybean oil (95, 90, 85, 80, and 75%). The results showed that the increase of oil content affects mainly the total glycerin, which failures in acquires its specification. Besides that, there was increase of viscosity, carbon residue, and flash point as well as decrease of cetane number. In spite of the increasing of unconverted triglycerides has affected biodiesel properties, flash point, water and sediment, sulphur content, sulphated ash, copper strip corrosion, cloud point, acid number, free glycerin, phosphorous content, and distillation temperature agreed to the ASTM D 6751 specifications.

8. Final considerations

The biodiesel quality control is ensured to the limitation of some contaminants and minor components as well as to the monitoring of transesterification reaction and oxidation process. Several analytical methodologies were described for such control (Table 2). The transesterification monitoring is carried out mainly by spectroscopy methods, such as NMR or IR. The same techniques are employed in blends determinations, which are performed mainly by IR techniques. In contrast, chromatography methods, mainly GC ones, are commonly used for the quantification of fatty methyl

Table 2
Analytical methods described for biodiesel analyses

Compounds	Methods	References
1, 3, 4, 5	TLC–FID	[17]
1, 2, 3	TLC	[18]
3, 4, 5, 11	GC–FID	[19]
1, 2	GC–FID	[20–22]
1, 3, 4, 5	HPLC–DD	[23]
1, 3, 4, 5	HPLC–UV, –ELSD, –MS	[24]
1, 3, 4, 5	GPC	[37]
1, 3, 4, 5, 6, 7	SEC–RID, –viscometer	[38]
1, 3	^{1}H NMR	[25]
2, 3	^{1}H NMR	[27]
1	^{1}H NMR	[28]
2	^{1}H NMR	[34]
1, 3, 4, 5	^{13}C NMR	[26]
1, 2, 3, 7	NIR	[29,30]
1, 3, 4, 5	ATR–FT-IR	[37]
2	FT-IR	[31,36]
1, 3	FT-IR	[32]
1	FT-IR	[35]
2	FT-Raman	[33,34]
1, 3, 4, 5, 6	Titration (hydroxyl content)	[39]
1, 3, 4, 5, 6	Refractive index measurements	[39]
–	Viscometry	[7]
1, 3, 4, 5	GC–MS	[43]
1	GC–FID	[44]
1	GC–FID	[45]
1	GC–FID	[46]
1	GC–FID	[47]
1, 3, 4, 5	GC–FID	[48]
1	GC–FID	[40]
1	GC–FID	[49]
1	GC–FID	[50]
1	Viscometry	[51]
2, 3, 4, 5, 6	GPC (HPSEC)	[52]
1, 3, 4, 5, 6	GPC–RID	[53]
2, 3, 4, 5, 8, 9, 10, 11	HPLC–ELSD	[54]
1, 3, 4, 5	HPLC–MS	[55]
1, 3	HPLC–ELSD, –UV	[42]
1	HPLC–UV –RID	[56]
2, 3, 4, 5, 12	HPLC and GC	[57]
1, 3, 4, 5, 11	RP–HPLC–UV	[58]
1	LC–MS	[59]
1, 6, 11	SFC	[60]
1	NIR	[61]
22	ATR–FT-IR	[62]
22	Fiber sensor	[63]
1	NIR, ^{1}H NMR	[41]
1	FT-IR	[64]
1	ATR–FT-IR and NIR	[65]
1	FT-IR and NIR	[66]
22	NIR and Raman	[67]
2	FT-IR	[68]
1	FT-IR	[69]
1	UV–Vis	[70]
1	Spectroscopy	[71]
1	Hydrometry	[72]
22	SFS	[73]
1	^{14}C-based method	[74]
13	Enzymatic	[77]
6, 13	Enzymatic, spectrometric	–[a]
6	GC–FID	[78]
3, 4, 5	GC–MS	[79]
6	GC–FID, –MS	[80]
3, 4, 5, 6	GC–FID	[75]
6, 7	GC–FID, –MS	[81]
6, 13	GC–FID	[83,84–86]
3, 4, 5	HTGC–MS, HPLC–ELSD	[91]
4, 5	GC–MS, FT–IR	[87]
6	HPLC–PAD	[88]
6	HPLC, titration	[89]
6	HPLC–RID	[90]
3, 4, 5	LC–GC (HPLC–DAD, GC–FID)	[92]
3, 4, 5, 6, 7, 12	ESI–MS	[93]
6	UV	[76]
6	EC–DAD	[2]

Table 2 (*Continued*)

Compounds	Methods	References
14	Karl–Fischer titration	[94]
7, 14	NIR	[95,96]
14	MS	[97]
7	UV	[98]
7	GC–FID	[99]
7	UV	[100]
7	GC–FID	[101]
15	GC–FID	[102]
16	GC–FID	[103]
16, 17	LC–GC	[103,104]
18, 19, 20, 21	ICP-OES	[106,107]
–	ICP-OES	[108]
19, 20	FAAS	[109]
21	Spectrophotometry	[110]
19, 20	FAAS	[111]
20	Potentiometry	[112]
19, 20	FAES	[105]
2	Density	[119]

[a] BQP-02 kit from Sigma–Aldrich. 1 = Fatty acid methyl esters; 2 = Fatty acid ethyl esters; 3 = Triglycerides; 4 = Diglycerides; 5 = Monoglycerides; 6 = Glycerol; 7 = Methanol; 8 = Fatty isopropyl ester; 9 = Fatty 2-butyl ester; 10 = Fatty isobutyl ester; 11 = Fatty acids; 12 = Ethanol; 13 = Total glycerol; 14 = Water; 15 = Total sterols; 16 = Free sterol; 17 = Sterol esters; 18 = Ca, Cl, Mg; 19 = Na; 20 = K; 21 = P; 22 = Raw oil.

esters, glycerol and their acyl esters. The amount of water, methanol and sterols are also established by spectroscopy or chromatography methodologies, and metals and metalloids mainly through atomic spectrometry.

In general, classes of compounds are analyzed, not individual species. Such data are enough to meet the requirements of biodiesel standards. However, most chromatography and spectroscopic methods were developed for methyl esters analysis, and thus they should be modified to the characterization of higher esters, such as ethyl esters, which will be increasingly used in the future. Probably, this will be an important challenge for the biodiesel analysis field. On the other hand, methods that correlate some easily measured properties with biodiesel quality can be especially useful. Some of them were recently developed and they were described in the last section of this paper. Therefore, the development of alternative and practical analytical methods, which can be used in field analysis along the production process, handling and storage, will be important issues in the progress of biodiesel analysis.

Acknowledgements

The authors are grateful to Centro de Caracterização e Desenvolvimento de Materiais (CCDM,UFSCar/UNESP), Fundação de Amparo à Pesquisa do Estado de São Paulo (FAPESP), Conselho Nacional de Desenvolvimento Científico e Tecnológico (CNPq), and Financiadora de Estudos e Projetos (FINEP) for the financial support.

References

[1] E. Stauffer, D. Byron, J. Forensic Sci. 52 (2007) 371.
[2] L.C. Gonçalves Filho, G.A. Micke, J. Chromatogr. A 1154 (2007) 477.
[3] M.E. Tan, J.H. Van Gerpen, J. Am. Oil Chem. Soc. 76 (1999) 1511.
[4] A.C. Pinto, L.L.N. Guarieiro, M.J.C. Rezende, N.M. Ribeiro, E.A. Torres, W.A. Lopes, P.A.P. Pereira, J.B. de Andrade, J. Braz. Chem. Soc. 16 (2005) 1313.
[5] J.M. Encinar, J.F. González, A.R. Reinares, Fuel Process. Technol. 88 (2007) 513.
[6] G. Knothe, Trans. ASAE 44 (2001) 193.
[7] N. Ellis, F. Guan, T. Chen, C. Poon, Chem. Eng. J. 138 (2008) 200.
[8] M.B. Dantas, A.A.F. Almeida, M.M. Conceição, V.J. Fernandes Jr., I.M.G. Santos, F.C. Silva, L.E.B. Soledade, A.G. Souza, J. Therm. Anal. Calorim. 87 (2007) 847.
[9] J.R.O. Lima, R.D. da Silva, C.C.M. da Silva, L.S.S. dos Santos, J.R. dos Santos Jr., E.M. Moura, C.V.R. de Moura, Quim. Nova 30 (2007) 600.
[10] M. Mittelbach, Bioresour. Technol. 56 (1996) 7.
[11] G. Knothe, Fuel Process. Technol. 86 (2005) 1059.
[12] European Committee for Standardization, EN 14214.
[13] American Society of Testing Materials, ASTM D 6751.
[14] M.M. Conceição, R.A. Candeia, F.C. Silva, A.F. Bezerra, V.J. Fernandes Jr., A.G. Souza, Renew. Sustain. Energy Rev. 11 (2007) 964.
[15] G. Knothe, J. Am. Oil Chem. Soc. 83 (2006) 823.
[16] S. Fernando, P. Karra, R. Hernandez, S.K. Jha, Energy 32 (2007) 844.
[17] B. Freedman, E.H. Pryde, W.F. Kwolek, J. Am. Oil Chem. Soc. 61 (1984) 1215.
[18] J. Cvengros, Z. Cvengrosova, C. Hoka, Petrol. Coal 44 (2002) 67.
[19] B. Freedman, W.F. Kwolek, E.H. Pryde, J. Am. Oil Chem. Soc. 63 (1986) 1370.
[20] J. Cvengros, Z. Cvengrosova, J. Am. Oil Chem. Soc. 71 (1994) 1349.
[21] Z. Cvengrosova, J. Cvengros, M. Hronec, Petrol. Coal 39 (1997) 36.
[22] Z. Cvengrosova, J. Cvengros, M. Hronec, Petrol. Coal 40 (1998) 97.
[23] B. Trathnigg, M. Mittelbach, J. Liquid Chromatogr. 13 (1990) 95.
[24] M. Holcapek, P. Jandera, J. Fischer, B. Prokes, J. Chromatogr. A 858 (1999) 13.
[25] G. Gelbard, O. Bres, R.M. Vargas, F. Vielfaure, U.F. Schuchardt, J. Am. Oil Chem. Soc. 72 (1995) 1239.
[26] T. Dimmig, W. Radig, C. Knoll, T. Dittmar, Chemische Technik (Chem. Tech.) 51 (1999) 326.
[27] P.R. Costa Neto, M.S.B. Caro, L.M. Mazzuco, M.G. Nascimento, J. Am. Oil Chem. Soc. 81 (2004) 1111.
[28] M. Morgenstern, J. Cline, S. Meyer, S. Cataldo, Energy Fuels 20 (2006) 1350.
[29] G. Knothe, J. Am. Oil Chem. Soc. 76 (1999) 795.
[30] G. Knothe, J. Am. Oil Chem. Soc. 77 (2000) 489.
[31] G.F. Zagonel, P. Peralta-Zamora, L.P. Ramos, Talanta 63 (2004) 1021.
[32] N.G. Siatis, A.C. Kimbaris, C.S. Pappas, P.A. Tarantilis, M.G. Polissiou, J. Am. Oil Chem. Soc. 83 (2006) 53.
[33] G.F. Ghesti, J.L. de Macedo, V.S. Braga, A.T.C.P. de Souza, V.C.I. Parente, E.S. Figueredo, I.S. Resck, J.A. Dias, S.C.L. Dias, J. Am. Oil Chem. Soc. 83 (2006) 597.
[34] G.F. Ghesti, J.L. de Macedo, I.S. Resck, J.A. Dias, S.C.L. Dias, Energy Fuels 21 (2007) 2475.
[35] J.R. Barone, 233rd ACS National Meeting, paper AGRO-153, Chicago, March 25–29, 2007.
[36] M.G. Trevisan, C.M. Garcia, U. Schuchardt, R.J. Poppi, Talanta 74 (2008) 971.
[37] M.A. Dubé, S. Zheng, D.D. McLean, K. Morris, J. Am. Oil Chem. Soc. 81 (2004) 599.
[38] G. Arzamendi, E. Arguinarena, I. Campo, L.M. Gandiá, Chem. Eng. J. 122 (2006) 31.
[39] W. Xie, H. Li, J. Am. Oil Chem. Soc. 83 (2006) 869.
[40] R. Wawrzyniak, W. Wasiak, M. Frackowiak, Chem. Pap. 59 (2005) 449.
[41] G. Knothe, J. Am. Oil Chem. Soc. 78 (2001) 1025.
[42] T.A. Foglia, K.C. Jones, J.G. Phillips, Chromatographia 62 (2005) 115.
[43] C. Mariani, P. Bondioli, S. Venturini, E. Fedeli, Riv. Ital. Sostanze Grasse 68 (1991) 549.
[44] P. Bondioli, A. Lanzani, E. Fedeli, M. Sala, S. Veronese, Riv. Ital. Sostanze Grasse 71 (1994) 287.
[45] P. Bondioli, L. Della Bella, Riv. Ital. Sostanze Grasse 80 (2003) 173.
[46] M. Wu, G. Wu, Y. Han, P. Zhang, Zhongguo Youzhi 28 (2003) 65.
[47] D. Guo, M. Sheng, S. Luo, Zhongguo Youzhi 29 (2004) 44.
[48] C. Li, Z. Tang, H. Yang, Fenxi Ceshi Xuebao 24 (2005) 66.
[49] X. Liu, C. Liu, S. Wu, F. Zeng, Q. Hu, Huaxue Yanjiu Yu Yingwong 18 (2006) 591.
[50] S. Schober, I. Seidl, M. Mittelbach, Eur. J. Lipid Sci. Technol. 108 (2006) 309.
[51] P. de Filippis, C. Giavarini, M. Scarsella, M. Sorrentino, J. Am. Oil Chem. Soc. 72 (1995) 1399.
[52] R. Fillieres, B.B. Mlayah, M. Delmas, J. Am. Oil Chem. Soc. 72 (1995) 427.
[53] D. Darnoko, M. Cheryan, E.G. Perkins, J. Liquid Chromatogr. Relat. Technol. 23 (2000) 2327.
[54] T.A. Foglia, K.C. Jones, J. Liquid Chromatogr. Relat. Technol. 20 (1997) 1829.
[55] M. Holcapek, P. Jandera, Adv. Mass Spectrom. 15 (2001) 583.
[56] M. Kaminski, E. Gilgenast, A. Przyjazny, G. Romanik, J. Chromatogr. A 1122 (2006) 153.
[57] H. Gecol, E. Ergican, S.R. Hiibel, 61st Northwest Regional Meeting of the ACS, paper RE06-195, Reno, June 25–28, 2006.
[58] G. di Nicola, M. Pacetti, F. Polonara, G. Santori, R. Stryjek, J. Chromatogr. A 1190 (2008) 120.
[59] J. Huang, R. Chen, D. Cavagnino, E. Long, LC–GC N. Am. Suppl. (2007) 54.
[60] J. Cole, J. Lefler, R. Chen, LC–GC N. Am. Suppl. (2008) 40.
[61] P. Baptista, P. Felizardo, J.C. Menezes, M.J.N. Correia, Anal. Chim. Acta 607 (2008) 153.
[62] I.P. Soares, T.F. Rezende, R.C. Silva, E.V.R. Castro, I.C.P. Fortes, Energy Fuels 22 (2008) 2079.
[63] R. Falate, K. Nike, P.R. da Costa Neto, E. Cação Jr., M. Muller, H.J. Kalinowski, J.L. Fabris, Quim. Nova 30 (2007) 1677.
[64] A. Birova, E. Svajdlenka, J. Cvengros, V. Dostalikova, Eur. J. Lipid Sci. Technol. 104 (2002) 271.
[65] J.S. Oliveira, R. Montalvão, L. Daher, P.A.Z. Suarez, J.C. Rubim, Talanta 69 (2006) 1278.
[66] M.F. Pimentel, G.M.G.S. Ribeiro, R.S. da Cruz, L. Stragevitch, J.G.A. Pacheco Filho, L.S.G. Teixeira, Microchem. J. 82 (2006) 201.
[67] F.C.C. Oliveira, C.R.R. Brandão, H.F. Ramalho, L.A.F. da Costa, P.A.Z. Suarez, J.C. Rubim, Anal. Chim. Acta 587 (2007) 194.
[68] M.A. Aliske, G.F. Zagonel, B.J. Costa, W. Veiga, C.K. Saul, Fuel 86 (2007) 1461.
[69] L.L.N. Guarieiro, A.C. Pinto, P.F. de Aguiar, N.M. Ribeiro, Quim. Nova 31 (2008) 421.

[70] A. Zawadzki, D. Shrestha, B. He, Trans. ASABE 50 (2007) 1349.
[71] G.S.R. Sastry, A.S.R.K. Murthy, P.R. Prasad, Energy Source Part A 28 (2006) 1337.
[72] J. Duban, R. Turner, 2006 ASAE Annual International Meeting, paper 06-6239, Portland, July 9–12, 2006.
[73] C.N.C. Corgozinho, V.M.D. Pasa, P.J.S. Barbeira, Talanta 76 (2008) 479.
[74] C.M. Reddy, J.A. Demello, C.A. Carmichael, E.E. Peacock, L. Xu, J.S. Arey, Environ. Sci. Technol. 42 (2008) 2476.
[75] C. Plank, E. Lorbeer, J. Chromatogr. A 697 (1995) 461.
[76] P. Bondioli, L. Della Bella, Eur. J. Lipid Sci. Technol. 107 (2005) 153.
[77] J. Bailer, K. de Hueber, Fresenius' J. Anal. Chem. 340 (1991) 186.
[78] P. Bondioli, C. Mariani, A. Lanzani, E. Fedeli, S. Veronese, Riv. Ital. Sostanze Grasse 69 (1992) 7.
[79] C. Plank, E. Lorbeer, J. High Res. Chromatogr. 15 (1992) 609.
[80] M. Mittelbach, Chromatographia 37 (1993) 623.
[81] M. Mittelbach, G. Roth, A. Bergmann, Chromatographia 42 (1996) 431.
[82] T. Ruppel, G. Hall, LC–GC N. Am. Suppl. (2007) 53.
[83] J.D. McCurry, C. Wang, LC–GC N. Am. Suppl. (2007) 48.
[84] K. Kelly, S. Countryman, N. Nguyen, LC–GC N. Am. Suppl. (2007) 60.
[85] N. Nguyen, K. Kelly, S. Countryman, LC–GC N. Am. Suppl. (2008) 36.
[86] B. Burger, G. Stidsen, LC–GC N. Am. Suppl. (2008) 38.
[87] N.S. Chong, S. Ramamoorthy, C. Ashford, A. Buerstetta, K. Donthula, B.G. Ooi, 233rd ACS National Meeting, paper CELL-080, Chicago, March 25–29, 2007.
[88] P. Lozano, N. Chirat, J. Graille, D. Pioch, Fresenius' J. Anal. Chem. 354 (1996) 319.
[89] M. Sala, P. Bondioli, Riv. Ital. Sostanze Grasse 75 (1998) 305.
[90] M. Hajek, F. Skopal, J. Machek, Eur. J. Lipid Sci. Technol. 108 (2006) 666.
[91] T.A. Foglia, K.C. Jones, A. Nunez, J.G. Phillips, M. Mittelbach, Chromatographia 60 (2004) 305.
[92] M. Lechner, C. Plank, E. Lorbeer, J. High Res. Chromatogr. 20 (1997) 581.
[93] R.R. Catharino, H.M.S. Milagre, S.A. Saraiva, C.M. Garcia, U. Schuchardt, M.N. Eberlin, R. Augusti, R.C.L. Pereira, M.J.R. Guimarães, G.F. de Sá, J.M.R. Caixeiro, V. de Souza, Energy Fuels 21 (2007) 3698.
[94] B. Faas, R. Schlink, LaborPraxis 31 (2007) 34.
[95] P. Felizardo, P. Baptista, J.C. Menezes, M.J.N. Correia, Anal. Chim. Acta 595 (2007) 107.
[96] P. Felizardo, P. Baptista, M.S. Uva, J.C. Menezes, M.J.N. Correia, J. Near Infrared Spectrosc. 15 (2007) 97.
[97] M.S. Todd, T. Peters, D.J. LeCaptain, 233rd ACS National Meeting, paper CHED-299, Chicago, March 25–29, 2007.
[98] F. Fang, H. Zeng, Jingxi Huagong Zhongjianti 35 (2005) 66.
[99] C. Li, H. Yang, L. Wang, S. Tian, Sepu 24 (2006) 524.
[100] A.R.T.S. Araujo, M.L.M.F.S. Saraiva, J.L.F.C. Lima, M.G.A. Korn, Anal. Chim. Acta 613 (2008) 177.
[101] M.C. Paraschivescu, E.G. Alley, W.T. French, R. Hernandez, K. Armbrust, Bioresour. Technol. 99 (2008) 5901.
[102] C. Plank, E. Lorbeer, J. High Res. Chromatogr. 16 (1993) 483.
[103] C. Plank, E. Lorbeer, Fett Wiss. Technol. 96 (1994) 379.
[104] C. Plank, E. Lorbeer, J. Chromatogr. A 683 (1994) 95.
[105] M.G.A. Korn, D.S.S. dos Santos, B. Welz, M.G.R. Vale, A.P. Teixeira, D.C. Lima, S.L.C. Ferreira, Talanta 73 (2007) 1.
[106] M. Edlund, H. Visser, P. Heitland, J. Anal. At. Spectrom. 17 (2002) 232.
[107] E.J. dos Santos, A.B. Hermann, E.S. Chaves, W.W.D. Vechiatto, A.C. Schoemberger, V.L.A. Frescura, A.J. Curtius, J. Anal. At. Spectrom. 22 (2007) 1300.
[108] G.D. Woods, F.I. Fryer, Anal. Bioanal. Chem. 389 (2007) 753.
[109] R. Nowka, GIT Labor-Fachzeitschrift 47 (2003) 518.
[110] M.X. Wu, G.Y. Wu, J. Wang, H. Xuan, Jiangsu Gongye Xueyuan Xuebao 16 (2004) 23.
[111] A. de Jesus, M.M. Silva, M.G.R. Vale, Talanta 74 (2008) 1378.
[112] M.S. Castilho, N.R. Stradiotto, Talanta 74 (2008) 1630.
[113] G. Knothe, Eur. J. Lipid Sci. Technol. 108 (2006) 493.
[114] A. Bouaid, M. Martinez, J. Aracil, Fuel 86 (2007) 2596.
[115] N.A. Santos, M.L.A. Tavares, R. Rosenhaim, F.C. Silva, V.J. Fernandes Jr., I.M.G. Santos, A.G. Souza, J. Therm. Anal. Cal. 87 (2007) 649.
[116] P. Bondioli, C. Mariani, E. Fedeli, A.M. Gomez, S. Veronese, Riv. Ital. Sostanze Grasse 69 (1992) 467.
[117] S. Mahajan, S.K. Konar, D.G.B. Boocock, J. Am. Oil Chem. Soc. 83 (2006) 567.
[118] C.A.W. Allen, K.C. Watts, R.G. Ackman, M.J. Pegg, Fuel 78 (1999) 1319.
[119] S. Froehner, J. Leithold, L.F. Lima Jr., Quim. Nova 30 (2007) 2016.
[120] S.L. Dmytryshyn, A.K. Dalai, S.T. Chaudari, H.K. Mishra, M.J. Reaney, Bioresour. Technol. 92 (2004) 55.
[121] H. Imahara, E. Minami, S. Saka, Fuel 85 (2006) 1666.

Talanta 77 (2008) 527–532

Contents lists available at ScienceDirect

Talanta

journal homepage: www.elsevier.com/locate/talanta

Spectrophotometric flow system using vanadomolybdophosphate detection chemistry and a liquid waveguide capillary cell for the determination of phosphate with improved sensitivity in surface and ground water samples

M. Sofia A.C. Neves [a], M. Renata S. Souto [b], Ildikó V. Tóth [a], Sérgio M.A. Victal [a], M. Cláudia Drumond [a], António O.S.S. Rangel [a,*]

[a] Escola Superior de Biotecnologia, Universidade Católica Portuguesa, Rua Dr. António Bernardino de Almeida, 4200-072 Porto, Portugal
[b] Universidade Fernando Pessoa, Faculdade de Ciências da Saúde, Rua Carlos da Maia 296, 4200-150 Porto, Portugal

ARTICLE INFO

Article history:
Received 24 July 2007
Received in revised form 12 March 2008
Accepted 17 March 2008
Available online 25 March 2008

Keywords:
Phosphate determination
Flow injection
Liquid waveguide capillary cell
Long pathlength spectrophotometry
Silicate interference

ABSTRACT

A flow injection procedure based on the vanadomolybdate method for the determination of dissolved reactive phosphorus in water samples is described. The system includes a liquid waveguide long pathlength cell connected to a charge coupled device (CCD) spectrophotometer. Calibration was linear up to 500 $\mu g\,P\,L^{-1}$, with a detection limit of 17 $\mu g\,P\,L^{-1}$ and a quantification limit of 56 $\mu g\,P\,L^{-1}$. An injection throughput of 60 determinations h^{-1} and repeatability (R.S.D.) of 2.2% were achieved. Potential interference from silicate was effectively masked by addition of a tartaric acid stream. The accuracy of the proposed methodology was assessed through analysis of a certified reference material and recovery tests on water samples. The developed procedure allows the determination of phosphorus in water samples at trace levels with high sensitivity, reduced reagent consumption and low waste production.

1. Introduction

Phosphorus is an essential element for the growth of plants and animals. It is the limiting nutrient in fresh water ecosystems, and an increase in its concentration usually leads to an increase in the aquatic vegetation. This process may result in eutrophic conditions and depletion of oxygen in water, due to the heavy oxygen demand of microorganisms as they decompose organic material. The disturbance of the normal functioning of the ecosystem will eventually cause degradation in water quality. European Union directive sets the limit of 100 $\mu g\,L^{-1}$ $P\text{-}PO_4^{3-}$ as an indicator level for probable problematic algae growth [1].

In water samples, phosphorus can be found in the form of different inorganic and organic species and can be present in either the dissolved, colloidal or particulate form. The dominant and most stable inorganic species is dissolved in reactive phosphorus [2–4]. Reference procedures are usually based on phosphorus determination in this form, on aliquots of previously filtered samples. Most of them are based on the colorimetric assay of phosphomolybdate or vanadophosphomolybdate heteropoly acids. Orthophosphate reacts with molybdate in acidic medium to yield 12-molybdophosphoric heteropolyacid; subsequently, detection is undertaken either on the molybdophosphate reduction product (molybdenum blue method) or on the yellow vanadomolybdate complex [2,5,6]. The molybdenum blue method became broadly used due to its higher sensitivity and lower susceptibility to interferences [4,7,8], than the vanadophosphomolybdate method. Nevertheless, the low concentration levels imposed by legislation are difficult to achieve. Therefore, the development of new methodologies capable of monitoring trace phosphate levels in environmental samples with adequate precision, has gained importance [9].

Flow injection analysis (FIA) is a widespread and well established approach to determine phosphorus. In fact, the first publication on FIA is dedicated to phosphate determination [10] and discusses both the yellow vanadomolybdate and the molybdenum blue method. Compared to the blue molybdenum method, the yellow vanadomolybdate analytical procedure can present some advantages that make it more suitable for flow systems: (i) the use of a single reagent mixture with extended stability makes the method suitable for field portable applications and for unattended operation in water monitoring [11,12] and (ii) the formation of a fine precipitate, accompanying the development of the blue colour, does not occur. However, maybe because of its limited sensitiv-

* Corresponding author. Tel.: +351 225580064; fax: +351 225090351.
E-mail address: aorangel@esb.ucp.pt (A.O.S.S. Rangel).

0039-9140/$ – see front matter © 2008 Elsevier B.V. All rights reserved.
doi:10.1016/j.talanta.2008.03.014

ity, the yellow vanadomolybdate method has been rarely used in flow systems. This limitation might be overcome by resorting to instrumental advances in spectrophotometry. Recently, with the development of the liquid waveguide capillary cell (LWCC), the increase of the flow cell pathlength can be easily achieved without deteriorating other analytical characteristics of the method. The long pathlength spectrophotometric measurements can increase the method sensitivity by up to two orders of magnitude [4,13,14].

The objective of this work was to develop a flow system based on the vanadomolybdate method, capable of quantifying phosphate at trace concentrations in waters, using a LWCC coupled to a charge coupled device (CCD-array) detector. Different flow strategies were employed and the effect of silicate (the most commonly referred interfering compound) on the analytical measurements was assessed.

2. Experimental

2.1. Reagents and solutions

All chemicals presented an analytical reagent grade. Solutions and reagents were prepared with deionised water (with specific conductance lower than 0.1 $\mu S\,cm^{-1}$) and subsequent dissolution was done in appropriate solvents. Due to the low phosphorus level analysed in the LWCC flow system, all solutions were prepared with ultra-pure water (Barnstead-Easypure-LF) in volumetric material that was previously rinsed with this type of water.

Phosphorus stock solution (100 $mg\,L^{-1}$) was prepared dissolving potassium dihydrogen phosphate (KH_2PO_4) previously dried overnight at 105 °C. Silicate stock solution (100 $mg\,L^{-1}$) was prepared by dissolving sodium metasilicate pentahydrate ($Na_2SiO_3{\cdot}5H_2O$). Working phosphorus and silicate standard solutions were prepared daily by suitable dilution of the stock solutions.

A 10 mM tartaric acid solution was prepared dissolving 0.37 g of L(+) tartaric acid ($C_4H_6O_6$) in 0.25 L of water.

The vanadomolybdate reagent was a solution of 25 $g\,L^{-1}$ ammonium heptamolybdate tetrahydrate [$(NH_4)_6Mo_7O_{24}{\cdot}4H_2O$] and 1.9 $g\,L^{-1}$ ammonium monovanadate (NH_4VO_3), in either 2 M or 3.25 M HCl.

All groundwater samples were filtered through a 0.45 μm Whatman cellulose acetate membrane. Mineral water samples had no previous treatment. Two surface waters certified reference materials were used: SPS-SW2 (Spectrapure, Oslo, Norway) and QC RW1 (VKI, Denmark).

2.2. Flow manifolds and instrumentation

The preliminary flow injection system used in this work is shown in Fig. 1(a). The initial conditions were based on the American Public Health Association (APHA) recommended batch procedure [5].

A peristaltic pump (Gilson, Minipuls 3) and Tygon PVC tubes were used to propel water (carrier, C), and reagent (R) solution into the system at flow rates of 3.2 and 0.8 mL min^{-1}, respectively.

The tubing (0.8 mm i.d.) connecting the different parts of the flow systems was made of poly(tetrafluoroethylene) with Gilson end fitting and connectors.

Sample and standard injections in the flow injection set-up were made using a Rheodyne type 5020 six-port rotary injection valve. Carrier and reagent streams then merged in a laboratory made acrylic Y-shaped connector used as confluence point and the resulting solution further mixed while passing a reaction coil (170 cm).

Another flow configuration (Fig. 1(b)) was used to reduce the effect of the silicate interference, with a stream of tartaric acid

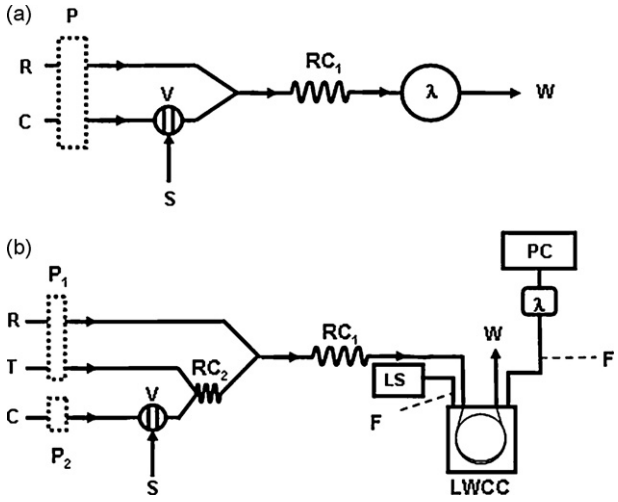

Fig. 1. Flow injection manifolds: (a) set-up used in preliminary studies and (b) manifold used for the determination of phosphorus in waters with long pathlength liquid core waveguide technology. R, vanadomolybdate reagent; C, carrier (deionised water); T, tartaric acid solution; P_i, peristaltic pump; S, sample or standard solution; V, injection valve; RC_1, reaction coil (170 cm); RC_2, reaction coil (50 cm); λ, detector (conventional or CCD array spectrometer); PC, computer; F, optical fibre; LS, light source; LWCC, liquid waveguide capillary cell; W, waste.

merging the carrier stream after the injection port. A reactor coil of 50 cm was used to enhance mixture between these solutions. Carrier (ultra-pure water), tartaric acid and reagent flow rates were reset to 2.7, 0.7 and 0.8 mL min^{-1}, respectively with the aid of a second peristaltic pump.

Different detection systems were used. For the manifold presented in Fig. 1(a), a Thermo Spectronic Helios Gamma UV–vis Spectrophotometer equipped with a Hellma model 178.712-QS flow cell (10 mm light path, inner optical volume 30 μL), connected to a Kipp & Zonen BD112 recorder was used. Subsequently this detector was replaced by an OceanOptics (Dunedin, FL, USA) USB2000-FLG Spectrometer (slit: 200 μm, grating: 600 lines blazed at 500 nm; bandwidth 380–1020 nm) connected via a 400 μm fibre optical cable (model P400-2-UV–vis) to the flow cell, placed in an Ocean Optics CUV cell support (Fig. 1(a)). A Mikropack (Ostfildern, Deutschland) Deuterium–halogen light source, model DH-2000-BAL was used with a 400 μm illumination optical fibre (model P400-2-UV–vis). Registration of the analytical signal was made using the OOIBase32 Spectrometer Operating Software. Dual-wavelength spectrophotometry was used to reduce the refractive index effect and the blank absorbance of the vanadomolybdate reagent. The analytical wavelength was 380 nm and the reference wavelength 600 nm; the absorbance signal at 600 nm was subtracted from the one at 380 nm for schlieren effect [15] correction. The collected absorbance data was treated and analysed in a lab-developed Microsoft Excel based software.

Afterwards, the conventional flow cell was replaced by a World Precision Instruments (Sarasota, FL, USA) liquid waveguide capillary cell, with a pathlength of 100 cm, model 2100. The absorbance change was monitored at 446 nm. During the optimisation process, it was observed that the LWCC gave the best day-to-day performance when sequentially flushed with 1 M NaOH, 1 M HCl and ultra-pure water (in counter current) at the end of each day.

2.3. Reference procedure

To assess the quality of the results obtained with the different analytical systems, results were compared with those given by the American Public Health Association recommended reference

method 4500-PC Vanadomolybdophosphoric Acid Colorimetric Method [5]. The methodology is based on the fact that dissolved reactive phosphorus reacts with ammonium molybdate under acid conditions to form a heteropoly acid–molybdophosphoric acid. In the presence of vanadium, yellow vanadomolybdophosphoric acid [$(NH_4)_3PO_4NH_4VO_3{\cdot}16MoO_3$] is then obtained being the intensity of the yellow colour proportional to phosphorus concentration. The determination range of phosphorus by this procedure is 1–20 mg L^{-1} with a minimum detectable concentration of 200 μg L^{-1} (in 1 cm spectrophotometer cells). A wavelength of 470 nm is usually used.

3. Results and discussion

3.1. Flow injection manifold with a conventional flow cell

The influence of several chemical and physical parameters – total flow rates, flow ratios, sample injection volume, reaction coil lengths, configuration and reagent concentrations – were then tested in order to maximise sensitivity and sample throughput, reduce reagent consumption and waste formation and minimise silicate interference. In this optimisation studies, the iterative univariate method was applied. Initial experimental conditions were set to: 1:1 flow ratio between reagent and sample streams, total flow rate of 1.5 mL min^{-1}, 280 cm reaction coil, 570 μL injection volume and vanadomolybdate reagent composition consisting of 25 g L^{-1} $(NH_4)_6Mo_7O_{24}{\cdot}4H_2O$, 1.25 g L^{-1} NH_4VO_3 and 4 M HCl.

Maintaining the total flow rate at 1.5 mL min^{-1}, different flow ratios between reagent and sample streams were assayed: 1:1, 1:2, 1:3, 1:4. A 22-fold increase in sensitivity (from 0.0015 to 0.033 L g^{-1}) was noticed with the decrease in the reagent to sample proportion. To maintain this lower sample dispersion but assure adequate reagent concentration and also enhance reaction sensitivity, vanadomolybdate reagent concentration was doubled—50 g L^{-1} $(NH_4)_6Mo_7O_{24}{\cdot}4H_2O$ and 2.5 g L^{-1} NH_4VO_3 in 4 M HCl. Sensitivity increased to 0.044 L g^{-1}. A 1:5 flow ratio was then tested. A slight increase in sensitivity occurred (0.046 L g^{-1}) but repeatability decreased. Therefore, a 1:4 ratio was adopted throughout the rest of the work.

Under these conditions, total flow rate was re-evaluated – from 1.5 to 4.5 mL min^{-1}, with 0.5 mL min^{-1} increments – in order to further increase the determination rate. No significant change in sensitivity was noticed. A flow rate of 4.0 mL min^{-1} was chosen, as a compromise between determination rate, saving of reagent and waste formation.

The effect of sample volume was studied within the range of 73–930 μL. As expected, up to 570 μL, sensitivity increased with increasing sample volume (from 0.0067 to 0.045 L g^{-1}). This volume was set for the subsequent studies.

The effect of the reaction coil length was tested with 50, 100, 170 and 280 cm reactors. Although higher sensitivity was achieved with the 100 cm reactor, the 170 cm was chosen for the following experiments since it presented better repeatability due to a more efficient sample and reagent mixture. Regarding reactor configuration (knotted *versus* coiled) no difference was detected. Therefore, the initial coiled design was used.

Optimisation experiments continued with the study of the influence of the composition of the vanadomolybdate reagent components. Ammonium molybdate concentrations of 20, 30, 40 and 50 g L^{-1} were tested. Sensitivity (0.041, 0.042 and 0.042 L g^{-1}) was approximately the same for the three highest concentrations. A concentration of 40 g L^{-1} was chosen to guarantee an excess of reagent for high phosphate concentrations.

Four different concentrations of ammonium vanadate (0.6, 1.2, 1.9 and 2.5 g L^{-1}) were tested. Maximum sensitivity was achieved with the 1.9 g L^{-1} solution; this concentration was used throughout the experimental work. The decrease in sensitivity that was noticed with the 2.5 g L^{-1} solution, can be attributed to an increase of baseline absorbance.

Table 1
The results obtained in the study of Si interference with a bench-top spectrophotometer

[P] (mg L^{-1})	[Si] (mg L^{-1})	$[P]_{apparent}$ (mg L^{-1})[a]	RD (%)
5.00	5.00	5.09 ± 0.06	+1.8
5.00	8.00	5.36 ± 0.02	+7.2
5.00	10.00	5.41 ± 0.03	+8.2

[a] The results expressed as a mean of 3 determinations ± standard deviation.

The acid concentration was the last parameter to be studied. It is well known that the vanadomolybdate mixture is only soluble at high acid concentrations [16]. The acid concentration also affects the blank absorbance signal. In this study, hydrochloric acid concentrations were varied between 1 and 4 M. No significant decrease in sensitivity was noticed with increased acid concentrations. A 2 M acidity was preferred, as lower acid concentrations can lead to precipitation in the tubing, and because silicate interference decreases if acidity increases. The silicate interference during phosphate analysis occurs because silicate also reacts with the vanadomolybdate reagent to form a molybdosilicate heteropoly acid. However, the vanadomolybdophosphate and molybdosilicate heteropoly acids complexes have different rates of formation—silicate reacts more slowly than phosphate and this reaction is impaired when pH is decreased [2,16–18]. Several 5.0 mg L^{-1} phosphorus solutions containing different silica concentrations – 5, 8 and 10 mg L^{-1} – were prepared, and their analytical signals evaluated. As expected, silicate interference increases with its concentration. However, results displayed in Table 1 show that even for the highest silica concentration (i.e. lower phosphorus/silica ratio) relative deviations lower then 8% were obtained.

3.1.1. Analytical characteristics of the method

The linear calibration graph (over the range 0.5–10 mg P L^{-1}) corresponds to the following equation: absorbance = 4.61×10^{-2} ($\pm 2.4 \times 10^{-3}$) [P (mg L^{-1})] − 1.10×10^{-3} ($\pm 2.40 \times 10^{-3}$) with a correlation coefficient (R^2) of 0.9997 ($\pm 4 \times 10^{-4}$). This equation represents an average of the values obtained for seven independent calibration curves and between parentheses are the respective standard deviations. The limit of detection (LOD) was calculated as $3s_d/S$, and the quantification limit (LOQ) as $10s_d/S$, where s_d is the standard deviation estimated from the regression line established through 5 standard solutions each injected in triplicate, and S is the slope of the calibration graph [19]. The values obtained were 50 μg L^{-1} for the LOD and 150 μg L^{-1} for LOQ. A determination rate of 60 samples per hour was achieved. Repeatability, assessed from five consecutive injections of three samples with different phosphorus concentration, presented relative standard deviation (R.S.D.) values lower than 1.87%.

The accuracy of the proposed procedure was tested through the analysis of the dissolved reactive phosphorus content of four samples (ground waters), by the developed and reference methodologies. As samples presented analyte concentrations below the quantification limit of the reference APHA method, they were spiked with different phosphorus concentrations, prior to analysis. Relative deviations lower than 15% ($n = 3$) were obtained in all cases.

The applicability of the developed system was then tested with a surface water certified reference material, SPS-SW2, having certified phosphorus level of 0.500 ± 0.003 mg L^{-1}. The result obtained by the FIA methodology, for five consecutive assays of this sample, was 0.47 ± 0.02 mg P L^{-1}.

Table 2
Features of the developed FIA system and of the reference procedure (APHA)

Parameter	APHA procedure	Flow method
Concentration range	1 to 18 mg L^{-1}	At least, up to 50 mg L^{-1}
Minimum detectable concentration	0.200 mg L^{-1}	0.050 mg L^{-1}
Assay time	At least 10 min	1 min
Reagents consumption per assay		
Ammonium molybdate	250 mg	32 mg
Ammonium vanadate	12.5 mg	1.5 mg
Hydrochloric acid concentrated	3.3 mL	2.1 μL
Estimated amount of waste produced per assay	50 mL	4 mL

Table 3
Apparent phosphorus concentration for standard phosphorus solutions containing silicate

[P] (mg L^{-1})	[Si] (mg L^{-1})	$[P]_{apparent}$ (mg L^{-1})[a]	RD (%)
0.50	5.00	1.10 ± 0	120
5.00	2.00	5.18 ± 0.03	3.4
5.00	5.00	5.43 ± 0.03	8.4
5.00	10.00	5.82 ± 0.02	16

[a] Apparent phosphate concentrations are the mean of three determinations ± standard deviation.

Taking into account the accuracy of results obtained and the figures of merit of the methodology reported it can be concluded that this system presents advantages over the reference procedure in terms of detection limit, dynamic working range, determination rate, reagent consumption and produced waste (Table 2). However, the detection limit of the method makes it still not adequate for the determination of phosphate in non-contaminated natural water samples.

Subsequently, the conventional detector system was replaced by a CCD array spectrophotometer to improve the analytical features and portability of the overall apparatus. Because sensitivity was slightly higher at 380 nm than at the recommended (>400 nm), this wavelength was used. A reference wavelength of 600 nm was used for background and sample matrix correction.

In these conditions, linear calibration curves were obtained over the range 0.5–10 mg P L^{-1}. The following equation represents an average of six independent analytical curves (and the values between parentheses are the respective standard deviations): absorbance = 8.31×10^{-2} ($\pm 2.9 \times 10^{-3}$) [P (mg L^{-1})] − 1.63×10^{-3} ($\pm 8.15 \times 10^{-3}$); $R^2 = 0.9999$ ($\pm 2 \times 10^{-4}$). With the increase in sensitivity, a concomitant a decrease in the limit of detection (30 μg L^{-1}) was obtained.

The repeatability of the method was assessed by the determination of the relative standard deviation (R.S.D.) values (expressed as percentage) of 10 consecutive injections of three samples with 0.57, 1.9 and 3.5 mg P L^{-1}. Values of 3.80, 1.28 and 1.59%, respectively, were obtained.

Table 4
Determination of dissolved reactive phosphorus (mg P L^{-1}) in ground waters by a FIA system with a CCD spectrometer connected to a conventional flow cell and by the reference method and corresponding relative deviations (RD)

Sample	FIA (mg P L^{-1})[a]	Reference method (mg P L^{-1})[b]	RD (%)
1	4.60 ± 0.02	4.19 ± 0.01	9.80
2	1.00 ± 0.05	0.99 ± 0.01	0.80
3	2.01 ± 0.05	2.04 ± 0.01	−1.75
4	3.78 ± 0.02	4.03 ± 0.02	−6.25
5	1.21 ± 0.03	1.05 ± 0.01	14.6
6	2.22 ± 0.02	2.09 ± 0.03	6.30
7	4.09 ± 0.06	4.08 ± 0.01	0.23

[a] The results are expressed as the mean of five determinations ± standard deviation.
[b] The results are expressed as the mean of three determinations ± standard deviation.

Table 5
Apparent (blank corrected) phosphorus concentration in phosphorus standards containing silicate

[P] (μg L^{-1})	[Si] (μg L^{-1})	[Tartaric acid] (mM)	$[P]_{apparent}$ (μg L^{-1})[a]
100	50	–	107 ± 3
100	100	–	110 ± 2
100	200	–	113 ± 2
100	50	2	102 ± 4
100	100	2	103 ± 3
100	200	2	105 ± 2

[a] The results are expressed as the mean of three determinations ± standard deviation.

Due to the change in the monitoring wavelength and increase of sensitivity, the interference of silicate was re-assessed (Table 3).

The results confirm that silicate interference is more significant when the shorter wavelength is used, being this difference greater for the solutions having lower phosphorus to silica ratio.

Four groundwater samples were analysed for dissolved reactive phosphorus content by the developed and reference methods. Again, samples presented analyte concentrations below the quantification limit of the reference method and therefore were spiked with different phosphorus concentrations. Paired results and relative deviations, are presented in Table 4.

With these results, the following linear correlation was obtained: $C_{FIA} = 0.998\ (\pm 0.163)\ C_{REF} + 0.067\ (\pm 0.480)$ with a correlation coefficient of 0.9784. Confidence limits for the slope and intercept, at 95% significance level for 6 degrees of freedom (values shown above between parentheses after the respective values), point out that no evidence for systematic differences between procedures exists.

The surface water certified reference material, SPS-SW2, was also analysed. A concentration of 0.49 ± 0.05 mg P L^{-1} (five determinations) was found.

3.2. Flow injection systems with long pathlength absorbance spectrophotometry

Although the detection limit was 30 μg L^{-1}, the quantification limit (185 μg L^{-1}) was still too high. With the objective of decreas-

Table 6
Recovery tests for determination of phosphorus in surface and ground waters using the modified FIA-LWCC method

Sample type	Added concentration (μg L^{-1})	Found concentration (μg L^{-1})[a]	Recovery (%)
Ground	0	96.3 ± 1.8	–
	50	136 ± 2	78.7 ± 3.4
	100	186 ± 2	90.1 ± 2.2
	200	274 ± 2	88.7 ± 0.7
Surface	0	44.7 ± 1.7	–
	50	93.3 ± 0.7	97.2 ± 1.5
	100	124 ± 1	79.5 ± 1.1
	200	214 ± 2	84.7 ± 1.2
Surface	0	226 ± 3	–
	50	278 ± 2	104 ± 4
	100	326 ± 4	101 ± 4
	200	413 ± 3	93.5 ± 1.4
Surface	0	88.0 ± 2.1	–
	50	143 ± 1	110 ± 1
	100	182 ± 2	94.0 ± 1.7
	200	261 ± 4	86.5 ± 1.8

[a] The results are expressed as the mean of three determinations ± standard deviation.

Table 7
Comparison of some analytical characteristics of the developed flow systems for phosphate determination

Parameter	Conventional flow cell		LWCC-CCD detector	
	Conventional spectrophotometer	CCD detector	Without tartaric acid addition	With in-line tartaric acid addition
Monitoring wavelength (nm)	470	380	446	446
Linear calibration range	0.5–10 mg P L^{-1}	0.5–10 mg P L^{-1}.	20–500 μg P L^{-1}	20–500 μg P L^{-1}
Sensitivity (L mg^{-1})	4.61×10^{-2} ($\pm 2.4 \times 10^{-3}$)	8.31×10^{-2} ($\pm 2.9 \times 10^{-3}$)	8.80×10^{-1} ($\pm 1.1 \times 10^{-3}$)	1.36 ($\pm 3.4 \times 10^{-2}$)
Detection limit (μg P L^{-1})	50	30	8	17
Quantification limit (μg P L^{-1})	150	185	28	56
Repeatability (R.S.D.)[a]	<1.9%	<3.8%	<4.0%	<2.2%

[a] Assessed from at least five consecutive injections.

ing the limit of determination and increasing the sensitivity of the method, the next approach was to replace the conventional flow-cell by an increased optical pathlength cell. A LWCC was incorporated and the sample volume was changed to 1500 μL. However, the increase of the pathlength led to a concomitant increase in the blank absorption signal. In practice, this resulted in the impossibility of using the same light source and this lower (380 nm) monitoring wavelength, due to the insufficient light intensity at the detector. Therefore, the data acquisition was carried out at a higher wavelength (446 nm).

Linear calibration curves were performed over the range 20–500 μg P L^{-1}. The following equation represents an average of three independent analytical curves and the values between parentheses are the respective standard deviations: absorbance = 8.80×10^{-1} ($\pm 1.1 \times 10^{-3}$) [P (mg L^{-1})] + 2.10×10^{-3} ($\pm 2.86 \times 10^{-3}$); R^2 = 0.9998 ($\pm 2 \times 10^{-4}$). If all analytical experimental conditions were maintained, an 100-fold increase in the slope of the calibration curve would be expected (due to change in the optical path from 1 to 100 cm). However, as mentioned earlier, the analytical wavelength had to be altered from 380 to 446 nm. In these conditions, a 10-fold increase in the method sensitivity and improvement in detection and quantification limits were noticed. Detection and quantification limits of 8 and 28 μg P L^{-1} were obtained making the determination of phosphorus in natural waters possible according to the limits imposed by European Directives.

Repeatability, assessed by 15 consecutive injections of a sample containing 100 μg P L^{-1}, was 4.0%.

To ascertain method accuracy, a surface water certified reference material, QC RW1 (0.0987 ± 1.15 mg P L^{-1}) was analysed. The mean phosphorus concentration for the 15 determinations performed was 0.0981 ± 0.0043 mg P L^{-1}.

3.2.1. Interference studies

A recent study [17] pointed out that silicate interference could be reduced using tartaric acid as masking agent, provided that it was added prior to molybdophosphate or molybdosilicate formation. Therefore, two sets of 100 μg L^{-1} phosphorus standard solutions containing either 50, 100 or 200 μg L^{-1} of silica (i.e. phosphorus and silica ratios between 2 and 0.5) were prepared. One of these groups also contained tartaric acid at a 2 mM concentration. The results obtained are given in Table 5.

These assays demonstrated that an increase in silicate concentration leads to an increased interference. However, within both sets of solutions, smaller differences were found for the solutions containing tartaric acid. In fact, the change between apparent phosphorus concentration for the 200 μg L^{-1} of silica solutions and the equivalent blank solutions was significantly reduced in the set of standards containing the masking agent (from 12.8 to 4.6%).

From the data in Table 6, it can be concluded that tartaric acid should be added in-line so that its concentration could be maintained at the same level for both standards and samples. Therefore, the system was reconfigured to accommodate the in-line addition of tartaric acid stream (Fig. 1(b)).

Silicate interference was then assessed using a 100 μg L^{-1} of phosphorus solution with 2 mg L^{-1} of silica. This silica level was chosen because, levels as high as 2 mg L^{-1} of silicate can be found in water and because the improvement of the sensitivity of phosphate analysis made possible to quantify the silicate interference signals relative to the low phosphate concentrations typical of most surface water samples [17].

Using this new system configuration, experiments using vanadomolybdate hydrochloric acid concentrations of 2 or 3.25 M and a tartaric acid stream with concentrations between 7 and 20 mM (1.5–4.5 mM at the confluence point, respectively) were conducted. The best conditions for minimizing the interference of silicate corresponded to using a 10 mM tartaric acid solution (2 mM at the confluence point) and a 3.25 M hydrochloric acid concentration. The apparent phosphorus concentration in these experimental conditions was 108 ± 4 μg L^{-1}. These concentrations were used throughout the work.

3.2.2. Analytical characteristics of the proposed method

Linear calibration curves over the range 20–500 μg P L^{-1} were traced. The following regression equation represents an average of the values obtained for five independent calibration curves: absorbance = 1.36 ($\pm 3.4 \times 10^{-2}$) [P (mg L^{-1})] – 1.68×10^{-2} ($\pm 4.99 \times 10^{-3}$); R^2 = 0.9990 ($\pm 5 \times 10^{-4}$), between parentheses are the respective standard deviations. Improved limits of detection and quantification of 17 and 56 μg L^{-1} were obtained, respectively. Repeatability, assessed through 10 consecutive injections of two water samples, was better then 2.2%.

To test the applicability of the developed system, recovery tests were made using several water samples (surface and ground waters). Caution was taken so that the added volumes of phosphorus standard solution did not affect the overall characteristics of the sample matrixes. The results obtained were in the 80–110% range and are shown in Table 6.

A surface water certified reference material, QC RW1 (98.7 ± 1.15 μg L^{-1}), was also analysed. Mean concentration phosphorus of 98.7 ± 2.8 μg L^{-1} (corresponding to 11 consecutive injections) was found.

The results show that the developed method presents high sensitivity for the determination of phosphorus at low levels as demanded by European Union regulatory directives, and that silicate interference was quenched up to a range of 2 mg L^{-1}.

4. Conclusions

This paper describes a flow methodology based on the vanadomolybdate reaction applicable to the determination of trace levels of phosphate in natural waters (European Union regulatory directives set the limit of 100 μg L^{-1} P-PO_4^{3-}). This is a significant breakthrough as this colorimetric reagent is more stable than those

based on the alternative molybdenum blue detection chemistry. Additionally, problems associated with tube clogging and baseline instability are avoided. This was achieved by replacing a conventional flow cell by liquid waveguide capillary cell, increasing the sensitivity and setting the LOD to 17 $\mu g\,L^{-1}$. Some of the figures of merit of the flow systems studied are summarized in Table 7.

When compared to some previous works, using the same reaction [7,16,20], the proposed system presents some significantly better analytical features. The potential interference of silicate was successfully masked by the in-line addition of tartaric acid.

Acknowledgements

The authors thank Fundação para a Ciência e a Tecnologia (FCT) for financial support through Project PTDC/AMB/64441/2006. Ildikó Tóth thanks FCT and FSE (III Quadro Comunitário) for the grant SFRH/BPD/5631/2001.

References

[1] P. Crouzet, J. Leonard, S. Nixon, Y.S. Rees, W. Parr, L. Laffon, J. Bøgestrand, P. Kristensen, C. Lallana, G. Izzo, T. Bokin, J. Bak, T.J. Lack, N. Thyssen, Nutrients in European Ecosystems—Environmental Assessment Report No. 4, European Environment Agency, Office for Official Publications of the European Communities, Copenhagen, 1999.
[2] J.M. Estela, V. Cerdà, Talanta 66 (2005) 307.
[3] O. Tue-Ngeun, P. Ellis, I.D. McKelvie, P. Worsfold, J. Jakmunee, K. Grudpan, Talanta 66 (2005) 453.
[4] S. Motomizu, Z.H. Li, Talanta 66 (2005) 332.
[5] American Public Health Association (APHA), Standard Methods for the Exam of Water and Wastewater, 20th ed., APHA Press, Washington, DC, 1998.
[6] P.J. Worsfold, L.J. Gimbert, U. Mankasingh, O.N. Omaka, G. Hanrahan, P.C.F.C. Gardolinski, P.M. Haygarth, B.L. Turner, M.J. Keith-Roach, I.D. McKelvie, Talanta 66 (2005) 273.
[7] A. Muñoz, F. Mas-Torres, J.M. Estela, V. Cerdà, Anal. Chim. Acta 350 (1997) 21.
[8] J.-Z. Zhang, C.J. Fischer, P.B. Ortner, Talanta 49 (1999) 293.
[9] P.J. Worsfold, Microchim. Acta 154 (2006) 45.
[10] J. Ruzicka, E.H. Hansen, Anal. Chim. Acta 78 (1975) 145.
[11] M. Bowden, D. Diamond, Sens. Actuators B: Chem. 90 (2003) 170.
[12] M. Bowden, M. Sequiera, J.S. Krog, P. Gravesen, D. Diamond, J. Environ. Monit. 4 (2002) 767.
[13] Q. Li, K.J. Morris, P.K. Dasgupta, I.M. Raimundo Jr., H. Temkin, Anal. Chim. Acta 479 (2003) 151.
[14] A.R. Roerdink, J.H. Aldstadt III, Anal. Chim. Acta 539 (2005) 181.
[15] A.C.B. Dias, E.P. Borges, E.A.G. Zagatto, P.J. Worsfold, Talanta 68 (2006) 1076.
[16] F. Mas-Torres, A. Muñoz, J.M. Estela, V. Cerdà, Analyst 122 (1997) 1033.
[17] L.J. Gimbert, P.M. Haygarth, P.J. Worsfold, Talanta 71 (2007) 1624.
[18] A.K. Pettersson, B. Karlberg, Anal. Chim. Acta 378 (1990) 183.
[19] J.C. Miller, J.N. Miller, Statistics for Analytical Chemistry, 3rd ed., Ellis Horwood, Chichester, UK, 1993.
[20] F. Mas-Torres, A. Muñoz, J.M. Estela, V. Cerdà, Int. J. Environ. Anal. Chem. 77 (2000) 185.

Talanta 77 (2008) 786–792

Contents lists available at ScienceDirect

Talanta

journal homepage: www.elsevier.com/locate/talanta

A portable sensor for the rapid detection of naphthalene acetic acid in fruits and vegetables using stabilized in air lipid films with incorporated auxin-binding protein 1 receptor

Dimitrios P. Nikolelis[a,*], Tzanetos-Ioannis Chaloulakos[b], Georgia-Paraskevi Nikoleli[a], Nikos Psaroudakis[c]

[a] Laboratory of Environmental Chemistry, Department of Chemistry, University of Athens, Panepistimiopolis-Kouponia, 15771 Athens, Greece
[b] Hellenic Food Authority, Ministry of Development, 124 Kifissias Avenue, 11523 Athens, Greece
[c] Laboratory of Inorganic Chemistry, Department of Chemistry, University of Athens, Panepistimiopolis-Kouponia, 15771 Athens, Greece

ARTICLE INFO

Article history:
Received 2 May 2008
Received in revised form 5 July 2008
Accepted 11 July 2008
Available online 25 July 2008

Keywords:
Stabilized lipid films
Optical portable biosensor
Naphthalene acetic acid
Auxin-binding protein 1

ABSTRACT

The present technique describes the development of a simple sensitive spot optical test and the construction of a portable biosensor for the rapid one-shot detection of naphthalene acetic acid (NAA) using stabilized lipid films supported on a methacrylate polymer on a glass fiber filter with incorporated auxin-binding protein 1 receptor. The lipid films without the receptor provided fluorescence under a UV lamp. The use of the receptor in these films quenched this fluorescence and the colour became similar to that of the filters without the lipid films. A drop of aqueous solution of naphthalene acetic acid provided a "switching on" of the fluorescence which allows the rapid detection of this stimulant at the levels of 10^{-9} M concentrations. It was also possible to have quantitative data based on a calibration graph. The effect of potent interferences included a wide range of compounds. The results showed no interferences from these compounds in concentration levels usually found in real samples. The method was applied for the determination of NAA in fruits and vegetables and the reproducibility of the method was checked in about 50 samples. A quantitative method for the detection of NAA in crops that can be complimentary to HPLC methods is provided in the present paper. These lipid films can be used as portable biosensors for the rapid one-shot detection of NAA in fruits and vegetables by non-skilled personnel in the field.

1. Introduction

1-Naphthaleneacetic acid, commonly abbreviated NAA, is an organic compound with the formula $C_{10}H_7CH_2CO_2H$. This colourless solid is soluble in organic solvents. It features a carboxylmethyl group linked to the "1-position" of naphthalene. NAA is a plant hormone in the auxin family and is an ingredient in many commercial plant rooting horticultural products; it is a rooting agent and used for the vegetative propagation of plants from stem and leaf cutting. The toxicity believed to be low up to date and its degradation behaviour is still not clear; however EPA regulations decided a Reregistration Eligibility Decision and Amendment in December 2007 to establish new tolerance limits for this pesticide in fruits [1]. To produce an appropriate biological effect, this compound must be applied at concentrations of 20–100 mg/mL in the spraying solution [2]. Recent reports have reported the toxicological data on NAA to be ORAL (LD50): acute 1 g/kg (rat), 0.743 g/kg (mouse) and 1 g/kg (mammal). However, the same reports provide the information that NAA is extremely hazardous in skin contact; the amount of tissue damage depends on length of contact and eye contact can result in corneal damage or blindness [3]. It is therefore important to develop simple and effective methods to monitor the level of NAA in foods, fruits and vegetables.

Since phytohormones are typically present and active in minor concentrations in plant tissue, the determination of phytohormone concentration in plants is extremely difficult. Note that endogenous auxin found in plants is usually around 1–100 ng g^{-1} fresh weight [4]. Apart from occurring at low concentrations, many phytohormones exist in different side groups and with many endogenous organic compounds that may interfere with the final assay. There are many analytical techniques for the analysis of NAA, including capillary micelle electrokinetic chromatography (CMEK) [5], room-temperature phosphorescence (RTP) [2,6,7], gas chromatography [8], high-performance liquid chromatography [4], etc. An evaluation of these analytical techniques has been previously reported [2].

* Corresponding author. Tel.: +30 2107274754; fax: +30 2107274269.
E-mail address: Nikolelis@chem.uoa.gr (D.P. Nikolelis).

0039-9140/$ – see front matter © 2008 Elsevier B.V. All rights reserved.
doi:10.1016/j.talanta.2008.07.030

The electrochemical interactions of NAA with lipid films were previously reported in the literature [9,10]; however, these lipid films were formed by the hairbrush technique and the lipid solution was prepared in an *n*-decade solvent. It is now well known that these lipid films are highly unstable and the results are not very reproducible and as such cannot be used for the construction of a stable biosensor device for commercialisation.

Significant progress has recently been achieved in the design, analytical applications and stabilization of biosensors based on lipid films [11–13]. This significant progress in the stabilization of biosensors based on lipid films, now allows their analytical uses for the detection of dopamine and ephedrine using dry spot tests [12,13].

The first candidate auxin receptor was identified in the early 1970s in membrane fractions of *zea coleoptiles* [14]. Following decades of research on auxin molecular biology, several elements of the auxin signalling pathway have been elucidated [15]. These include two apparent types of receptors that perceive the auxin signal and factors influenced by these receptors, resulting in induced gene expression and also possibly cell wall modifications important for cell expansion. These two types of receptors include ABP1 (auxin-binding protein 1), a membrane-bound protein thought to initiate cell wall expansion [14,16] and more recently TIR1 (Transport Inhibitor Response 1) and related auxin signalling F-box (AFB) proteins, soluble proteins that initiate the induction of gene expression [17–19]. Undoubtedly, ABP1 is an essential protein and is likely to be an auxin receptor [14]. Detailed auxin-binding data have been reported previously for ABP1 [14,20,21]. However, we know a great deal more about the TIR1 signalling pathway than we do about the signalling pathway of ABP1, even though ABP1 has been studied for longer. For auxin-mediated transcriptional control, the substrate-specifying F-box protein is TIR1, and the complex is known as the SCF^{TIR1} complex. Key components of the SCF^{TIR1} complex are a cullin, a RING finger protein (RBX1), ASK1 (equivalent to SKP1 in yeast) and the F-box protein TIR1. If we compare the SCF^{TIR1} binding data with data from *Zea* ABP1 there are similarities and differences [21]. The affinity of ABP1 for 1-NAA is reported variously as being between 50 and 200 nM, whereas its affinity for IAA is much lower (5–10 μM). Therefore, the selectivity of the two binding sites differs, TIR1 favouring the natural ligand indole-3-acetic acid (IAA). The affinity each site shows for their favoured ligand is similar. Tryptophan and benzoic acid are not bound by either SCF^{TIR1} or ABP1. Both proteins bind the strong auxin 2,4-D relatively weakly. One additional difference between the binding characteristics of ABP1 and SCF^{TIR1} is their pH-dependences. The binding of 1-NAA to ABP1 is acutely pH-dependent, with an optimum between pH 5.0 and 5.5 and only a few percent of the optimum binding activity persists at pH 7.0 [22]. The binding experiments with IAA reported for SCF^{TIR1} were done at pH 7.2 [17] and 7.5 [18]. The pH-dependence for not been shown but, in each case, the pH at which high-affinity binding is found is appropriate for the compartments in which they are reported to act: the nucleus (pH 7.2–7.5 for TIR1) and at the cell surface (pH 5.0–6.0 for ABP1). Therefore, the binding affinities and selectivities of the SCF^{TIR1} complex and of ABP1 are consistent with the properties anticipated for different auxin receptors acting in different compartments.

The present paper describes the development of a simple spot test for the rapid one-shot detection of naphthalene acetic acid. Stabilized lipid films supported on a polymer with incorporated ABP1 were used as detectors. Microporous filters composed of glass fibers were used as supports for the stabilization of these sensors. The lipid film was formed on the filter by polymerisation using UV irradiation prior its use. Methacrylic acid was the functional monomer, ethylene glycol dimethacrylate was the crosslinker and 2,2′-azobis-(2-methylpropionitrile) was the initiator. The polymerisation is completed within 4 h and ABP1 was incorporated within the lipid mixture prior to polymerisation. The results described below show that the natural receptor retains its activity. The novelty of the present paper is that for first time in literature is reported the preparation of air stabilized lipid film detectors with an incorporated ion channel protein that can detect nM (or 10 fmol of toxicant/spot test) concentrations of a toxicant and can be used as a portable biosensor for in field applications. The films without ABP1 provided fluorescence under a UV lamp. The use of the protein in these films quenched this fluorescence and the colour became similar to that of the filters without the stabilized lipid films (purple). NAA was injected in microliter volumes on the filters and the fluorescence develops within 5 min and a "switching on" of the fluorescence is obtained. Quantitative data based on a calibration graph were also obtained herein. The effect of potent interferences included a wide range of compounds, usually found in fruits and vegetables. The method was applied for the determination of NAA in fruits and vegetables and the reproducibility of the method was checked in about 50 samples. The present method now provides a technique for the rapid detection of naphthalene acetic acid at the levels of 10^{-9} M concentrations without interferences from the other constituents and can be used as complimentary rapid technique to HPLC methods. Most importantly, it can be used as a portable sensor for the in field and market for the rapid detection of NAA in fruits and vegetables by even non-skilled personnel.

2. Experimental

2.1. Materials and apparatus

Dipalmitoyl phosphatidylcholine (C16:0) (DPPC) and dipalmitoyl phosphatidic acid (DPPA) were supplied by Sigma, St. Louis, MO, USA and were used as lipids for the formation of the films supported on a polymer. The functional monomer, methacrylic acid, and the cross linker, ethylene glycol dimethacrylate, were both supplied by Aldrich (Aldrich-Chemie, Steinheim, Germany). The initiator, 2,2′-azobis-(2-methylpropionitrile) (AIBN), was supplied by Merck KgaA (Darmstadt, Germany). All other chemicals were of analytical-reagent grade. Water was purified by passage through a Milli-Q cartridge filtering system (Milli-Q, Millipore, El Paso, TX, USA) and had minimum resistivity of 18 MΩ cm. All other chemicals were of analytical-reagent grade. The filters and (nominal) pore sizes used were glass microfiber (0.7 and 1.0 μm, Whatmam Scientific Ltd., Kent, UK).

The procedure for the collection, isolation, and purification of the receptor has been described in detail [10,23]. We have used the ABP1 receptor, because the receptor is selective for 1-NAA as previously reported [10,14–16,23,24]. The solution containing the purified receptor was lyophilised in 100 μL aliquots and stored dry at 4 °C until needed. Each aliquot was reconstituted in 100 μL of distilled water. Volumes of 10 μL were used for the preparation of the stabilized lipid films with incorporated receptor.

A UV deuterium lamp (Black-Ray, Ultra-Violet Products Inc., San Gabriel, CA) was used for the fluorescence experiments.

The fluorescence was measured with a PerkinElmer Model 612 double beam fluorescence spectrophotometer using excitation beam 279 nm. The emission beam for the determination of both compounds was 389 nm.

A PerkinElmer differential scanning calorimeter (Model DSC-4) was used for the DSC experiments; the thermograms were processed by means of the Thermal Analysis Data Station (TADS) of the DSC-7.

2.2. Procedures

The formation of stabilized lipid film was previously described [11,25,26]. The lipid film is formed on a microporous filter glass fiber disk (diameter of ca. 0.9 cm) by polymerisation prior to its use. Stabilized lipid films were prepared by polymerisation with a procedure similar to that as previously described, however, the polymerisation took place by using UV irradiation instead of the thermal polymerisation [25]; 0.15 mL of a mixture containing 5 mg of DPPC were mixed with 0.070 mL of methacrylic acid, 0.8 mL of ethylene glycol dimethacrylate, 8 mg of 2,2′-azobis-(2-methylpropionitrile) and 1.0 mL of acetonitrile. The mixture was sparged with nitrogen for about 1 min and sonicated for 30 min. This mixture could be stored in the refrigerator. For the preparation of the stabilized lipid films, 0.15 mL of this mixture was spread on the microfilter. The filter with the mixture was then irradiated using the UV deuterium lamp. Raman spectrometry was used to monitor the kinetics of the process of polymerisation [25].

Auxin was incorporated in these BLMs during polymerisation by spreading 10 μL of the receptor suspension with the polymerisation mixture (i.e., for the preparation of the stabilized lipid films, 0.15 mL of the polymerisation mixture and 10 μL of receptor suspension were spread on the microfilter).

The stock solution of naphthalene acetic acid was prepared in methanol. The dilute aqueous solutions of naphthalene acetic acid were prepared daily just before use in a 0.1 M KCl electrolyte solution that contained HEPES as a buffer (pH 5.5) and 4 μM ATP. The solutions (ca. 10 μL) were placed on the microfilter disk with the lipid film, using a microsyringe. The fluorescence spectrum was measured by cutting the microfiber disk in half and placing it at 45° angle to the incident radiation, vertical to the bottom of the cell of the fluorometer. The fluorescence developed within 5 min after the sample injection on the filters. All experiments were done at 25 ± 1 °C.

2.3. Analysis of vegetable and fruit samples

Chopped vegetables and fruits (25 g) were blended with the aid of a mixer and 2.5 g of the homogenate sample were spiked with known amounts of standard NAA solution and also homogenized. Special care was exercised so that the final samples contained all parts of the product. The samples were mixed with 5 mL of HEPES buffer (100 mM, pH 5.5) and sonicated for 15 min. The sonication stage is important because it allows the extraction of NAA into the aqueous phase and the use of an organic solvent is not necessary. The mixture was then centrifuged at 3000 rpm for 5 min, and the supernatant was collected. The procedure was repeated twice and the collected samples were diluted to a final volume of 25.0 mL with 100 mM HEPES buffer in order to adjust the pH to 5.5. The concentration of NAA in the sample to be analysed was about 10 nM and therefore the homogenate sample that spiked with known amounts of standard NAA solution should contain 0.05 μg of NAA. Blank samples were prepared following the previous procedure without NAA spiking.

3. Results and discussion

The preparation of stabilized in the air lipid films for repetitive uses has been reported in literature [11,26]; however, these works did not incorporate any protein or receptor during the polymerisation process, because the polymerisation was made by heating at 60–80 °C. This process may deactivate an enzyme or a natural receptor that is incorporated in the lipid mixture, and for this reason the enzyme (i.e., acetylcholinesterase) was incorporated after polymerisation.

Raman spectroscopy has also provided information on the mechanism of polymerisation and how the lipid film is attached to the polymer [25]. The lipid is attached to the polymer through electrostatic bonding [25]. The peak at 1690 cm^{-1} (that corresponds to the C=O stretching of the methycrylate) was decreased with time, showing that the C=O bond is altered to $C–O^-$, therefore there is a formation of electrostatic bonding between the $C–O^-$ and $–NHR_3^+$ of phosphatidylcholine. There was also a shift of wavenumber of the peak at 1176 to 1195 cm^{-1}, that showed a strong electrostatic interaction between those two groups. These forces retain the lipid for multiple uses after storage in air and at the same time allow response similar to freely suspended BLMs [25,26]. The enzyme in our recent work [25] was incorporated during the preparation of these polymerised lipid films and the results have shown that no denaturation of the enzyme has occurred. These results have shown that it is now possible to incorporate a natural protein in these stabilized lipid films before polymerisation and presently extend the work in using a natural receptor instead of an enzyme.

Stabilized lipid films supported on a polymer were used as detectors for the development of a simple optical test for the rapid detection of naphthalene acetic acid. Fig. 1(I) shows the UV spectra of the filters with the polymer containing the lipid film, with incorporated auxin receptor, having a drop of aqueous solution of naphthalene acetic acid. As it can be seen in the figure, the absorption maximum appears at 279 nm. Therefore, an excitation beam of 279 nm was used for the present measurements. Fig. 1(II-A) shows the fluorescence emission spectrum of the filters with the polymer,

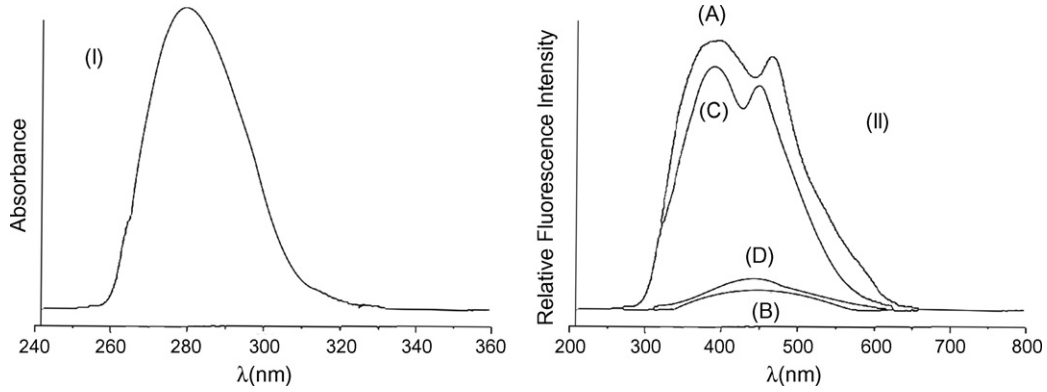

Fig. 1. (I) UV spectra of the filters that contain the lipid film supported on the polymer with incorporated auxin receptor. A drop of naphthalene acetic acid has deposited on the filters. (II) Fluorescence emission spectrum of (A) methacrylate polymer containing the lipid film; (B) filter papers; (C) methacrylate polymer containing the lipid film, with incorporated auxin receptor having a drop of naphthalene acetic acid; (D) polymer containing the lipid film with incorporated auxin receptor.

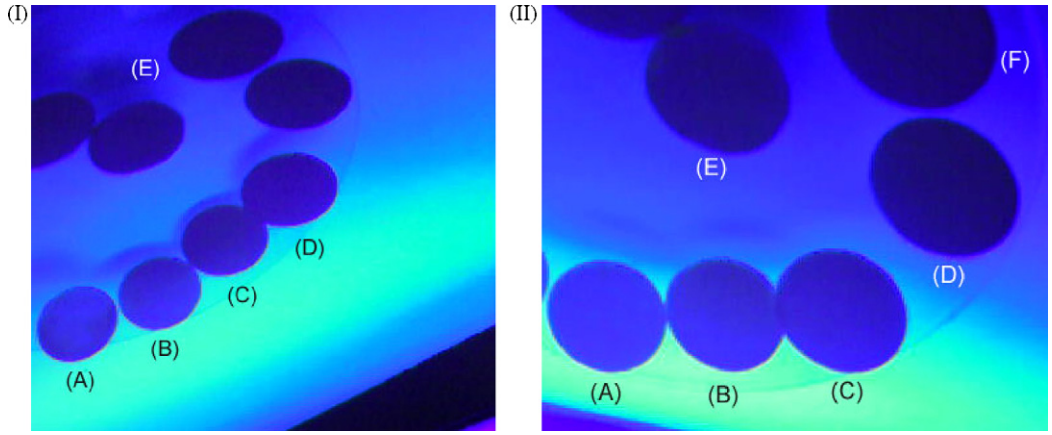

Fig. 2. Photographs that show (I) the "switching on" of fluorescence due to NAA with concentration (A) 1×10^{-7} M, (B) 3×10^{-8} M, (C) 1×10^{-8} M, (D) 3×10^{-9} M, and (E) Blank; (II) the "switching on" of fluorescence due to NAA using real sample of apples spiked with NAA concentration (A) 1×10^{-7} M, (B) 3×10^{-8} M, (C) 1×10^{-8} M, (D) 3×10^{-9} M, (E) 1×10^{-9} M, and (F) Blank.

containing the lipid film. It can be seen that two main peaks appear in this spectrum (at 397 and 471 nm). When the auxin receptor is incorporated in the lipid film structure the fluorescence emission is quenched (Fig. 1(II-D)). Fig. 1(II-C) shows the fluorescence emission spectrum of the methacrylate polymer containing the lipid film with incorporated auxin receptor having a drop of naphthalene acetic acid. As it can be seen in this figure, two main peaks appear in this spectrum (at 389 and 448 nm). The slight alteration of the wavelength is probably due to the introduction of a protein that alters the fluidity of the lipid film to more fluid [27,28]. Fig. 1(II-B) shows the emission spectrum of the filters; it can be noticed that the filters do not provide any fluorescence.

A comparison was made between the spectra in Fig. 1(II). This comparison has shown that these spectra consist of several overlapping bands. In order to ensure that these spectra are due to the same emitters, they were analysed in energy symmetric Lorentzian components [12]. The fluorescence spectra of Fig. 1 were expressed as linear combinations of six Lorentzian components using the equation:

$$I = I_0 + \sum_{i=1}^{6} \frac{2A_i}{\pi} \frac{w_i}{4(\tilde{\nu} - \tilde{\nu}_i)^2 + w_i^2}$$

where I is the fluorescence intensity, I_0 the offset (background correction), $\tilde{\nu}$ the wavenumber and A_i, $\tilde{\nu}_i$ and w_i are, respectively, the area, the band maximum and the half-band width of the ith Lorentzian component. The results of the analysis have shown that these spectra are due to the same emitters.

The present lipid films were found to show fluorescence emission using a UV lamp. The polymerisation could be seen optically under a mercury lamp with naked eye. The filters scatter the light (because the colour is the same as that of the mercury lamp), whereas the polymer with incorporated lipids has a different colour (bluish) [12]. The fluorescence emission phenomenon generation was previously described to be due to the formation of an electrostatic bond between the amino groups of the lipid film with the carbonyl group of methacrylic acid during the polymerisation stage [13]. This provides no mobility of the polyacrylate in the x-axis and therefore the fluorescence emission is obtained.

The colour of the polymer with the lipid film containing the auxin receptor is again purple under a UV lamp similar to that of the glass fiber filters (Fig. 2(I)). When a drop of an aqueous solution of naphthalene acetic acid (Fig. 2(I)) or sample of extracts from fruits and vegetables, containing naphthalene acetic acid (Fig. 2(II)), is deposited on the filter with the polymerised lipid film, the fluorescence is again "switched on" and the colour becomes again blue in the spot where the drop of the solution was deposited. A simplified schematic diagram of the portable instrument with sensor is provided in Fig. 3 (alternatively a Spectrotline CM UV viewing cabinet Cat. No. Z169447-1EA or Spectroline CX UV viewing cabinet Cat. No. Z169528-1EA, Sigma, Aldrich can be used).

In order to study the present system, the pH effect was investigated. The pH effect on the signal magnitude of BLMs formed from egg PC was examined in the pH range of 4.0–8.0. These results (Fig. 4) have shown that the fluorescence intensity depend on the pH value between pH values 4 to 8 with maximum activity at pH 5.5 which is in agreement with previous observations [9,10].

When the auxin receptor molecules are incorporated in the structure of polymerised lipid films, the polymer with the lipid film becomes more flexible due to the incorporation of the auxin recep-

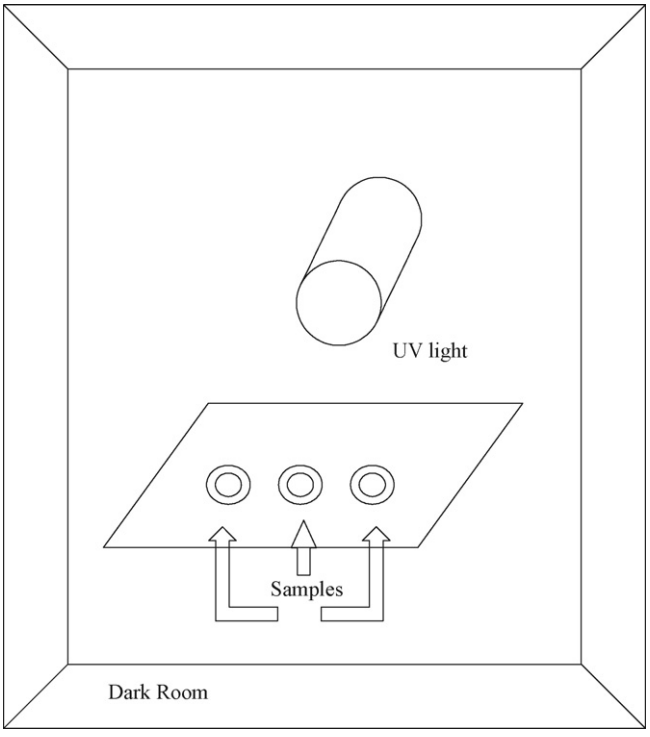

Fig. 3. Simplified schematic diagram of the portable instrument with sensor.

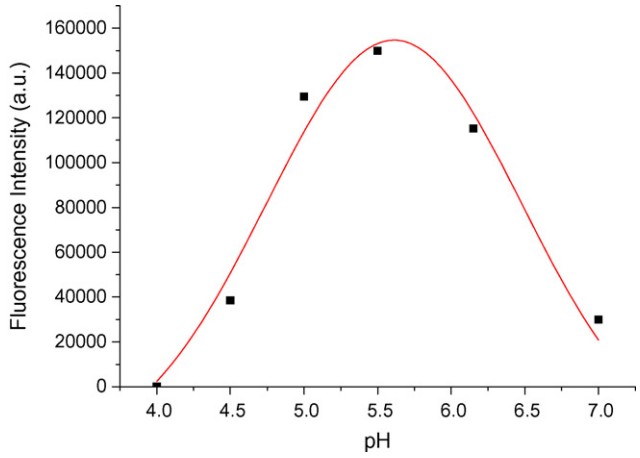

Fig. 4. Effect of pH in the response of ABP1. A concentration of 0.100 μM of 1-NAA was used.

tor in the structure of the polymer [27,28]. The incorporation of an auxin receptor (i.e., protein, see Ref. [28]) alters the phase structure of the lipid to more fluid. This has as a result that the fluorescence emission is quenched. The incorporation of a receptor alters the phase structure of the lipid to more fluid. The mechanism of signal generation was presently studied using DSC experiments. The phase transition temperature (T_m) of solid DPPC was found to be $62 \pm 1.0\,^{\circ}C$ ($N = 5$, Fig. 5A). Note that the T_m of DPPC liposomes is 42 °C. However, presently DPPC in lipid films is polymerised and therefore exists in the solid state. Therefore, a small piece of microporous filter glass fiber disk was cut with the polymerised stabilized lipid film in a size to fit inside the cell of the DSC. To test whether the phase transition of the lipid films were modulated by the glass substrate, a polymerisation step has taken place on a glass substrate and a small amount of pulverized polymerised lipid film was placed inside the DSC cell. The results obtained were similar to that of the solid DPPC (i.e., T_m ca. 62). When the receptor was incorporated within the lipid film, the phase transition temperature was decreased to $56 \pm 1.0\,^{\circ}C$ ($N = 5$, Fig. 5B). These results show that the fluidity of the lipid film is increased and therefore the fluorescence is expected to be decreased. In the presence of NAA, the phase transition of the lipid film is increased to $61 \pm 1\,^{\circ}C$

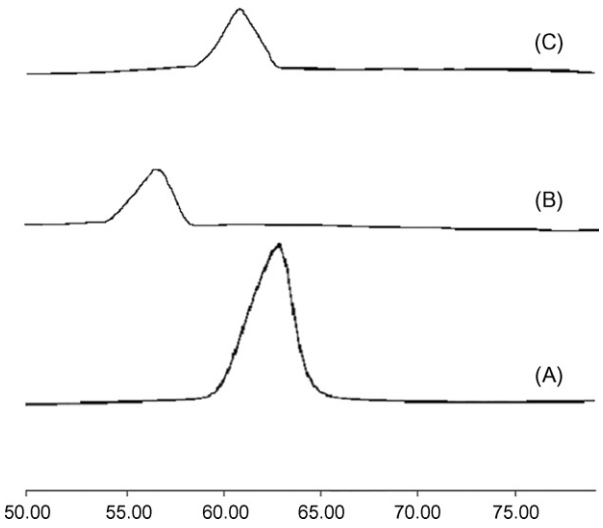

Fig. 5. DSC thermographs of DPPC (A), DPPC with incorporated ABP1 (B) and DPPC with incorporated ABP1 having a drop of NAA 1×10^{-3} M.

($N = 5$, depending on NAA concentration, presently a concentration of 1×10^{-3} M of NAA was used) (Fig. 5C) which shows that the lipid film again becomes more rigid and as a result the fluorescence is again "switched on". Further exploration of signal generation is under investigation using Raman spectroscopy.

Detailed auxin-binding data have previously reported for ABP1 [14,20,21]. The affinity of ABP1 of ABP1 for 1-NAA is between 50 and 200 nM, whereas the affinity for IAA is much lower (5–10 μM). Tryptophan and benzoic acid are not bound by ABP1. ABP1 binds the strong auxin 2,4-D relatively weakly. Interference studies were done electrochemically with the present sensor and included other synthetic auxins present in crops. The interference of the biologically inactive 2-NAA and IAA was investigated and these compounds have shown no significant binding even at concentration levels of 10^{-4} M. Investigation of interference studies of other bioactive auxins which may be present in harvested samples has shown that 2,4-D provide a signal similar to that of 1-NAA, however at concentration levels higher than 10^{-5} M. The fluorescence for 2,4-D appeared within (155 ± 6.2) s by these interactions. This difference in the delay time appearance of fluorescence between 1-NAA and 2,4-D can be correlated to their chemical structure. The appearance of the signals from the different auxins follows the order 2,4-D and 1-NAA. This sequence is in order to their relative hydrophilicities. A rapid adsorption, followed by a complex formation between the receptor and auxins take place. The adsorption of molecules in solution to a membrane surface is rapid and also driven by the relative hydrophilicity. The sequence of appearance of the signal of these catecholamines is in order to their lipophilicity factor [4]. It is well known that 2,4-D is more hydrophilic than 1-NAA. This is well known and studied through the sequence of separation of these two compounds with reverse phase HPLC [4]. This trend is followed in terms of the sequence of the auxins that produce fluorescence. These experiments also included investigation of interferences of most commonly found compounds in real samples of fruits and vegetables. The effect of potent interferences included also a wide range of compounds, usually found in fruits and vegetables (i.e., ascorbic acid, glucose, leucine, glycine, tartrate, citrate, bicarbonate, and caffeine). The results showed no interferences from these compounds in concentrations usually found in real samples (i.e., the relative error in all the cases was less than 5%; the tested amount of interferent was up to 1 mM). Note that stabilized lipid films without ABP1 were tested with injections of 1-NAA and no fluorescence was obtained (i.e., blank experiments). These results and the results obtained using the above blank experiments show that the present technique can be applied in fruit and vegetable samples without interferences from the matrix.

Similar results were obtained using real samples of fruits and vegetable extracts spiked with naphthalene acetic acid, with different concentrations (Fig. 2(II)). The samples were prepared as previously was described [26,29–31]. None of the analysed samples contained detectable 1-NAA (i.e., no fluorescence was obtained when the fruit sample was injected in the polymerised lipid film with incorporated ABP1) and, therefore, they were spiked in the laboratory with 1-NAA at different concentrations in order to perform recovery studies. Recovery studies were made in order to validate the technique and examine the matrix effects. Various kinds of fruits and vegetables were used for our experiments (Table 1).

NAA is a weak acid (K_a is ca. 1×10^{-4}) and has a water solubility 0.042 g/100 mL, whereas its sodium salt has a water solubility of 340 g/100 mL [1]. This allows a simple and fast sample preparation of extraction of NAA into an aqueous phase without necessary to use organic solvents [7,26,29–31]. Therefore, the sample preparation as previously described was used to prepare the real samples of fruits and vegetables [7,26,29–31]. The chopped vegetables and fruits were blended and spiked with known amounts of standard

Table 1
Results of analysis of fruit samples with the present biosensor

Sample ID	Naphthalene acetic acid found	% Recovery
Cherries	n. d.	95–103
Nectarines	n. d.	96–106
Oranges	n. d.	97–104
Apples	n. d.	95–103
Pears	n. d.	97–102
Grapefruits	n. d.	98–102
Peaches	n. d.	97–104
Tangerines	n. d.	96–103
Apple Juice	n. d.	97–102
Orange Juice	n. d.	97–103
Cherry Syrup	n. d.	95–104
Tomatoes	n. d.	97–103
Carrots	n. d.	96–104
Spinach	n. d.	98–103
Beans	n. d.	95–105
Green peppers	n. d.	95–103
Red peppers	n. d.	96–104
Onions	n. d.	96–103
Potatoes	n. d.	97–106
Lemons	n. d.	96–104
White cabbage	n. d.	96–103
Lettuce	n. d.	95–104
Parsley	n. d.	98–103
Dill	n. d.	97–105
Red beets	n. d.	96–102
Celery	n. d.	96–105
Strawberries	n .d.	95–104
Melon	n. d.	96–103
Watermelon	n. d.	97–103
Bananas	n. d.	96–104
Cherry juice	n. d.	95–103
Peach juice	n. d.	98–102
Strawberry juice	n. d.	96–104
Pineapple juice	n. d.	97–103
Grapefruit juice	n. d.	98–102

NAA solution. The concentration of NAA in the sample to be analysed was about 10 nM and therefore the homogenate sample that spiked with known amounts of standard NAA solution should contain ca. 0.05 μg of NAA. At these low concentrations, NAA is water soluble and can be extracted in the aqueous phase. The pH also of these solutions was adjusted to 5.5 with a HEPES buffer. In the case of some acidic samples (i.e., oranges), the buffer capacity was such to adjust the pH value at pH 5.5. 1-NAA is mainly allowed to be only used in the first 11 samples of crops [32]. 1-NAA, its salts, ester, and acetamide are plant growth regulators currently registered for use on various orchard and fruit crops including apple, cherry, olive, orange, pear, tangelo, and tangerine. As plant growth regulators, they may be used on the above-listed crops to prevent preharvest drop of fruits trees, and delay flower induction. However, a wide variety of crops were tested. None of these samples was found to contain NAA. The recovery in all cases was ca. 100%. This gives the possibility of validating the sensor now and comparing with Official Methods of Analysis, prior to its commercialisation. The advantage of the present detection is that this "switching on" or "switching off" of the fluorescence can be seen with naked eye and offers a simple detection route with detection limits down to 10^{-9} M concentration levels.

The above results only provide a semi-quantitative method for the rapid detection of NAA that can be used as a portable simple screening optical device/sensor. However, in order to obtain more quantitative data, the fluorescence intensity was quantitatively measured using a PerkinElmer Model 612 double beam fluorescence spectrophotometer using excitation beam 279 nm and emission at 389 nm (because this peak has the largest intensity). Fig. 6 shows the calibration graph for NAA. The concentration range that can be determined is between 0–100 nM.

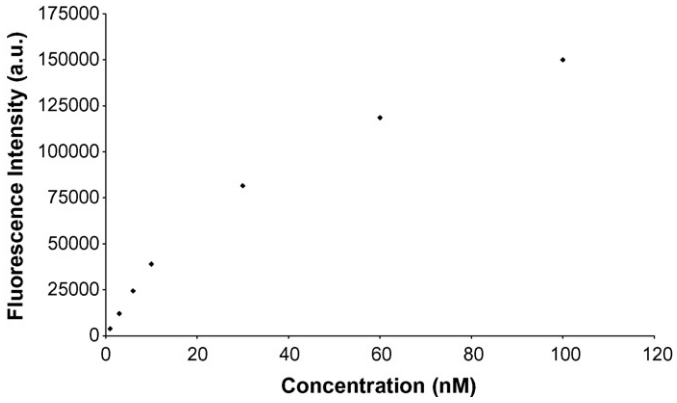

Fig. 6. Calibration graph for NAA.

The present paper describes the preparation of a sensor, based on a lipid film supported on a polymer with incorporated auxin receptor stable in air. This sensor can be used as a simple optical test for the rapid screening of naphthalene acetic acid and potentially could be commercialised. The sensor revealed detection limits of 10^{-9} M. The lowest detection limit for naphthalene acetic acid that was reported up to date in literature was 0.25 ng/spot [4]. Our present system based on lipid film technology offers lower detection limits to those previously described. However, the most important aspect of our present efforts is to provide a portable sensor that can be used for in field and market applications. Our present biosensor can be portable and be used by non-specialized personnel. Therefore, it can be used even as a rapid detector of naphthalene acetic acid for in house applications.

Acknowledgements

This work was carried out in the framework of the "Receptronics" EC project (NMP4-CT-2005-017114) with the financial contribution of the European Commission (Contract no. 70/3/8307). The authors express their acknowledgements for the financial help of the Greek Ministry of Development, General Secretariat of Research and Technology (Contract 70/3/8268) and of Special Account for Research Grants of the National & Kapodistrian University of Athens (Contract 70/4/5730). The authors express their acknowledgements to Prof. E. Melissari (Chemistry Department, University of Athens) for the preparation and donation of the auxin receptor.

References

[1] http://www.epa.gov/oppsrrd1/reregistration/naphthalene acetic acid/, December 7, 2007.
[2] M.T. Fernandez-Arguelles, B. Canabate, A. Segura, J.M. Costa, R. Pereiro, A. Sanz-Medel, A. Fernandez, Talanta 66 (2005) 696.
[3] http://www.sciencelab.com, Material Safety Data Sheet, 1-NAA MSDS.
[4] Z. Ma, L. Ge, A.S.Y. Lee, J.W.H. Yong, S.N. Tan, E.S. Ong, Anal. Chim. Acta 610 (2) (2008) 274.
[5] M. Yuan, M. Zhang, W. Kangjing, Chromatography 15 (1997) 482.
[6] R. Zhu, C. Liu, S. Zhang, Anal. Chem. 21 (1993) 177.
[7] R. Zhu, X. Wang, P.L. Wang, Luminescence 20 (2005) 389.
[8] Y. Li, H. Yang, C. Peng, X. Zhang, Chromatography 18 (2000) 371.
[9] M. Thompson, U.J. Krull, Anal. Chim. Acta 147 (1983) 1.
[10] M. Thompson, U.J. Krull, M.A. Venis, Biochem. Biophys. Res. Commun. 110 (1) (1983) 300.
[11] D.P. Nikolelis, M. Mitrokotsa, Biosen. Bioelectron. 17 (2002) 565.
[12] D.P. Nikolelis, D.A. Drivelos, M.G. Simantiraki, S. Koinis, Anal. Chem. 76 (2004) 2174.
[13] D.P. Nikolelis, N. Psaroudakis, N. Ferderigos, Anal. Chem. 77 (10) (2005) 3217.
[14] R.M. Napier, K.M. David, C. Perrot-Rechenmann, Plant Mol. Biol. 49 (2002) 339.

[15] K.B. Kelley, D.E. Riechers, Pesticide Biochem. Physiol. 89 (1) (2007) 1.
[16] H. Macdonald, Physiol. Plant. 100 (1997) 423.
[17] N. Dharmasiri, S. Dharmasiri, M. Estelle, Nature 435 (2005) 441.
[18] S. Kepinski, O. Leyser, Nature 435 (2005) 446.
[19] N. Dharmasiri, S. Dharmasiri, D. Weijers, E. Lechner, M. Yamada, L. Hobbie, J. Ehrismann, G. Jürgens, M. Estelle, Dev. Cell 9 (2005) 109.
[20] M.A. Venis, R.M. Napier, Crit. Rev. Plant Sci. 14 (1995) 27.
[21] G.O. Badescu, R.M. Napier, Trends Plant Sci. 11 (5) (2006) 217.
[22] R.M. Napier, J. Exp. Bot. 46 (1995) 1787.
[23] M.A. Venis, Nature 266 (1977) 268.
[24] M. Shishova, V. Yemelyanov, E. Rudashevskaya, S. Lindberg, J. Plant Physiol. 164 (2007) 1323.
[25] D.P. Nikolelis, G. Raftopoulou, G.-P. Nikoleli, M. Simantiraki, Electroanalysis 18 (24) (2006) 2467.
[26] D.P. Nikolelis, M.G. Simantiraki, C.G. Siontorou, K. Toth, Anal. Chim. Acta 537 (2005) 169.
[27] J.-M. Boggs, Biochem. Cell Biol. 906 (1987) 353–404.
[28] P. Yeagle, The Structure of Biological Membranes, CRC Press, Boca Raton, FL, 1992, p. 107.
[29] M.P. Xavier, B. Vallejo, M.D. Marazuela, M.C. Moreno-Bondi, F. Baldini, A. Falai, Biosens. Bioelectron. 14 (2000) 895.
[30] J. Lui, M. Tan, C. Liang, K.B. Ying, Anal. Chim. Acta 329 (1996) 297.
[31] G.S. Nunes, P. Skladal, H. Yamanaka, D. Barcelo, Anal. Chim. Acta 362 (1998) 59.
[32] EPA-HQ-OPP-2006-0507-0001, FR Document Number E7-23306, v. 72, pp. 68582–68584.

Talanta 77 (2008) 484–489

Contents lists available at ScienceDirect

Talanta

journal homepage: www.elsevier.com/locate/talanta

Enzymatic oxidation in aqueous and micellar media based on horseradish peroxidase–hydrogen peroxide system using a SIA manifold

Marieta L.C. Passos, M. Lúcia M.F.S. Saraiva*, José L.F.C. Lima

REQUIMTE, Serviço de Química-Física, Faculdade de Farmácia, Universidade do Porto, Rua Aníbal Cunha, 164, 4099-030 Porto, Portugal

ARTICLE INFO

Article history:
Received 31 October 2007
Received in revised form 14 March 2008
Accepted 17 March 2008
Available online 25 March 2008

Keywords:
Micellar medium
Peroxidase
Sequential injection analysis
Spectrophotometry
Phenothiazines

ABSTRACT

Aqueous and micellar catalysis of horseradish peroxidase was studied in a sequential injection system through selecting the oxidation by hydrogen peroxide of two phenothiazines: the water-soluble chlorpromazine and perphenazine, a low water soluble, micellised in a Tween 80 medium. The coloured free-radical intermediate formed was monitored spectrophotometrically at 527 nm. The system enables the determination of chlorpromazine in water and perphenazine in micellar medium up to 1.25×10^{-4} mol L^{-1}, with quantification limits of 2×10^{-5} and 1.25×10^{-5} mol L^{-1}, respectively. R.S.D. values were in both cases less than 1.6%.

The SIA system optimized consumed 125 μL of sample, 1.5 μg of peroxidase and 5×10^{-8} mol of hydrogen peroxide per determination, which guarantees economy in the use of sample and reagents with reduced residue production, in good agreement with the current recommendations of green chemistry.

The developed system was applied to the determination of chlorpromazine and perphenazine in pharmaceutical preparations. Results revealed different reaction rates for aqueous and micellar media, which yielded determination frequencies of 17 and 31 determinations per hour, respectively.

The potential effect of several compounds commonly used as excipients on analytical signals was studied and no interfering effect was noticeable. Statistical comparison of the results obtained with the proposed methodology and with the reference methods showed good agreement and indicate no significant difference at the 95% confidence level.

1. Introduction

Biocatalysis has traditionally been applied in water solutions as it was believed that enzymes could not work in other media. However, this idea changed and enzymatic action is now being studied in different solvents and, depending on the way enzyme activity is affected, used for diverse purposes. Horseradish peroxidase (EC 1.11.1.7; donor-H_2O_2 oxidoreductase) the most popular member of the heme peroxidases, catalyses a variety of oxidative transformations of organic and inorganic substrates by hydrogen peroxide or alkylperoxides [1,2]. It is a very versatile enzyme having activity over a broad pH and temperature range, characteristics that have encouraged the study of its activity and promoted its application in solvents other than water [3–5].

In the present study, it was intended to apply the catalytic action of HRP in the oxidation of phenotiazines by hydrogen peroxide in aqueous and micellar media.

Phenotiazines exhibit certain interesting analytical properties, resulting from their characteristic structure, i.e. the presence of the chemically active sulphur and nitrogen atoms and substituents in positions 2 and 10 [6]. One of these properties is the susceptibility to oxidation by chemical [6,7], electrochemical [8,9], enzymatic [10,11] and photochemical [12] agents, with the formation of cation radicals whose colour depends on the types of substituents in positions 2 and 10 [6].

For oxidation in aqueous medium, chlorpromazine was used while in micellar medium, perphenazine was chosen (Fig. 1).

While chlorpromazine is soluble in water, perphenazine is practically insoluble in water and generally requires use of ethanol [13] or other organic solvents, as methanol used in the HPLC reference method [14] for its determination. Aqueous surfactant media can provide an aqueous phase for hydrolytic enzymes and an organic phase for hydrophobic substrates, permitting the catalytic action and avoiding the use of organic solvents, a current demand related to environmental control.

The association of enzymatic analysis with automatic methods is clearly justified by the possibility of precisely controlling the reaction time, sequence of operations and reagents volumes. Sequential injection analysis (SIA) [15] has been successfully applied as its

* Corresponding author. Tel.: +351 222078939; fax: +351 222004427.
E-mail address: lsaraiva@ff.up.pt (M.L.M.F.S. Saraiva).

0039-9140/$ – see front matter © 2008 Elsevier B.V. All rights reserved.
doi:10.1016/j.talanta.2008.03.022

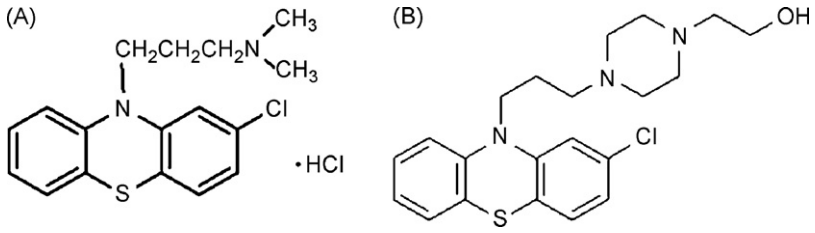

Fig. 1. (A) Chlorpromazine and (B) perphenazine structure.

characteristics fulfil these requirements: its computer-controlled nature guarantees reproducibility in fluid handling. Moreover, the multiposition valve, the core of the system, allows the clustering of all solution and device types, such as mixing chambers, dialysis units, in each of its inlets. Along with the bi-directional nature of the fluids and the stopped-flow periods, it encompasses a variety of on-line sample manipulations and reduced consumption of reagents along with less waste disposals.

Organised medium such as micellar medium in SIA flow systems has been explored to provide microenvironments with different purposes such as stabilization of the water insoluble metal ion–ligand complex [16], alteration of spectral properties, with enhancement of emission properties [17–21] and avoiding quenching mechanisms [22]. On-line emulsification of oil samples for direct analysis by atomic spectroscopy [23] has also illustrated the advantages of using the SIA technique when using surfactants. Additionally, several SIA applications with enzymes can be found but none regarding non-conventional solvents. HRP has been used in various SIA systems in solution [24,25] or immobilised [26–28], but to our knowledge this is the first application in water and micellar medium. Therefore, by taking advantage of the SIA characteristics, the objective of this work was to evaluate the performance of the peroxidase–hydrogen peroxide system in aqueous and micellar systems and at the same time verify its applicability to the determination of hydro and liposoluble phenotiazines in pharmaceutical preparations.

2. Experimental

2.1. Reagents and solutions

All solutions were prepared with analytical reagent grade, high purity water (milli Q) with a specific conductivity of <0.1 μS/cm. All chemicals were of analytical reagent grade.

Two acetic/acetate buffer solutions were prepared by mixing a 2 mol L^{-1} acetic acid solution with required volumes of sodium acetate solution with the same concentration to obtain pH values of 3.5 and 6. The solution obtained with a pH value of 6, was used to prepare a stock solution of 300 μg mL^{-1} peroxidase (EC 1.11.1.7; from Horseradish type VI-A), since this pH value was in the optimum range of the optimum pH for to stock this enzyme. The buffer solution with a pH value of 3.5 was used to prepare the other reagent solutions.

A 5×10^{-4} mol L^{-1} hydrogen peroxide solution in acetic/acetate buffer solution was prepared from the 3×10^{-2} mol L^{-1} stock solution obtained from the commercial solution (Panreac) with the same buffer solution.

A 15 μg mL^{-1} peroxidase solution was prepared by dilution of a required volume of the stock solution with the buffer solution (pH 3.5).

Chlorpromazine hydrochloride working standard solutions were prepared by appropriately diluting with water the 5×10^{-3} mol L^{-1} stock solution of chlorpromazine hydrochloride (Sigma), prepared in water from the solid.

In the same way, perphenazine working standard solutions were prepared by diluting with water the 5×10^{-3} mol L^{-1} stock solution of perphenazine (Sigma), prepared in a 9.2×10^{-2} mol L^{-1} polyoxyethylen–sorbitan–monooleat (Tween 80) solution. This surfactant solution was prepared by diluting a required amount of the commercial solution (Aldrich) in water. Sodium laurate (Fluka) and lauryl sulphate sodium (Sigma) solids were also used to prepare the corresponding solutions of perphenazine.

The chlorpromazine hydrochloride solutions, of commercially available pharmaceutical preparations were prepared by dissolving the required amounts of powdered tablets or by diluting the required volume of the liquid formulation in water.

The perphenazine solutions, of commercial available pharmaceutical preparations were prepared by dissolving the required amount of powdered tablets in a Tween 80 solution with the same concentration as the one used to prepare the working solutions of the same concentration.

All sample solutions were analysed by the developed SIA procedure without any pre-treatment.

2.2. Apparatus

The SIA flow system (Fig. 2) operated at room temperature, consisted of a Gilson Minipuls 3 (VilliersleBel, France) peristaltic pump, equipped with a 0.90 mm i.d. Gilson PVC pumping tube and a 10-port selection valve (Valco, Vici C25-3180EMH, Houston, USA).

All connections, including the holding and reaction coils were made with 0.8 mm i.d. PTFE tubing. The holding coil was 2 m and the reaction coil 1 m in length, and both were serpentine-shaped in configuration.

In this type of system the aspiration and propulsion volumes of the diverse solutions are controlled within a time based, according to the flow rate used. In order to guarantee reproducibility in

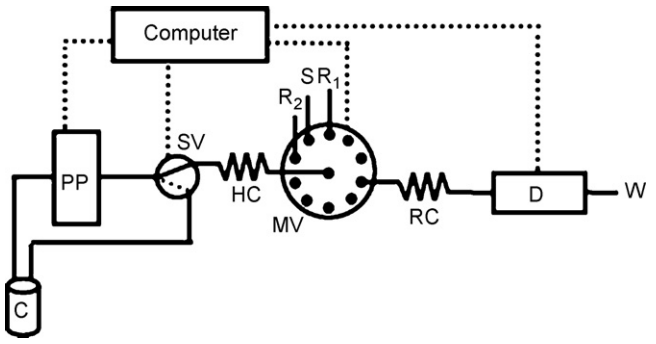

Fig. 2. SIA manifold for the determination of phenothiazines in aqueous and micellar media. C, carrier (H_2O); PP, peristaltic pump; SV, solenoid valve; HC, holding coil (2 m/0.8 mm); R_1, peroxidase 15 μg mL^{-1}; S, sample; R_2, H_2O_2 5×10^{-4} mol L^{-1}; MV, multiposition selection valve; RC, reaction coil (1 m/0.8 mm); D, spectrophotometric detector (527 nm); W, waste.

Table 1
SIA analytical cycle used in the determination of phenothiazines in aqueous and micellar media

Position	Volume (μL)		Time (s)		Flow rate (mL min^{-1})	Direction
	Aqueous medium	Micellar medium	Aqueous medium	Micellar medium		
1	100		2.05		2.92	Aspiration
2	125		2.56		2.92	Aspiration
3	100		2.05		2.92	Aspiration
4	1057.5	2585	45	110	1.41	Propulsion
4	0	–	60	–	0	Stopped flow
4	2115	–	90	–	1.41	Propulsion

the aspirated and propelled volumes, especially when dealing with reduced volumes, the starting position of the peristaltic pump at the beginning of each cycle was controlled. To this end, it was used a NResearch 161 T031 solenoid valve (W. Caldwell, NJ, USA), a magnet and a reed relay fixed, on the rotative and fixed components of the pump head, respectively. When an approximation between the magnet and the reed relay was reached, the reed relay was activated, permitting electrical flow. The signal detected by the computer set the beginning for each step of the analytical cycle from a fixed position of the peristaltic pump. The solenoid valve, placed between the pump and the holding coil was activated, enabling the solutions to flow through the holding coil. At the end of the cycle, the peristaltic pump returned to the initial position. During this time, the carrier solution flowed in closed circuit by inactivation of the solenoid valve.

This system was controlled by a homemade programme written in QuickBasic language and implemented in a microcomputer equipped with an interface card (Advantech Corp., PCL 711B, San Jose, CA).

A Jenway 6100 spectrophotometer, with an 80-μL Hellma flow cell (178.710 QS, Mullheim/Baden, Germany) was also used as a detection system. Analytical signals were recorded on a Kipp & Zonen BD 111 (Delft, The Netherlands) strip chart recorder or acquired via computer.

2.3. Sequential injection procedure

The intermediate product formed [6] in the enzymatic oxidation of chlorpromazine and perphenazine by hydrogen peroxide in aqueous and micellar media was monitored spectrophotometrically at 527 nm. The developed analytical cycle (Table 1) began with the aspiration of 100 μL of peroxidase solution to the holding coil, followed by 125 μL of sample and the hydrogen peroxide solution. This aspirated sequence was sent by flow reversal, through the reaction coil to the spectrophotometric detector. Thereafter, and depending on the medium used, the analytical cycle ended (micellar) or involved, additionally, a stopped-flow period of 1 min at the detector, before sending the product zone to waste (aqueous).

The increase of signal, due to the formation of free-radical intermediate is proportional to phenothiazines concentration in the sample.

2.4. Reference methods

For a comparative evaluation of the results obtained, samples analysed by the developed methodology were also analysed by reference methodologies, of the British Pharmacopoeia 2005 (BP) [29] or of the American Pharmacopoeia (USP) [14]. The samples preparation procedure differed for each of the drugs and each of the pharmaceutical preparations. Although, the references methods for chlorpromazine formulations [29] were different, all of them were based in the measurement of the absorbance of a solution at a maximum at 254 nm. The content of chlorpromazine hydrochloride was calculated taking in 915 as the value of A (1%, 1 cm) at the maximum at 254 nm.

For perphenazine determinations it was used a reference method referred by the USP for perphenazine and amitriptyline hydrochloride tablets, since the pharmaceutical formulations commercially available have the both drugs. This method was based in HPLC, using a mobile phase prepared with water, acetonitrile, methanol and methanesulfonic acid.

3. Results and discussion

Under peroxidase action, phenotiazines form a cation radical intermediate that gives rise, by a non-enzymatic second order reaction, to a colourless sulfoxide (see Eqs. (1) and (2)) [13,30–32].

$$2\mathrm{PHT} + \mathrm{H_2O_2} \overset{\mathrm{HRP}}{\longleftrightarrow} 2\mathrm{PHT}^{\bullet +} + 2\mathrm{H_2O} \quad (1)$$

$$2\mathrm{PHT}^{\bullet +} \overset{\mathrm{breakdown}}{\longrightarrow} \mathrm{Products\ (PHT\ and\ PHT\ sulfoxide)} \quad (2)$$

The coloured cation radicals formed from chlorpromazine and perphenazine are monitored at 527 nm.

This reaction was studied in a sequential injection system and the optimum conditions were set for the aqueous and micellar oxidation of chlorpromazine and perphenazine, respectively. Thereafter, the designed and optimized SIA system was applied in the determination of these phenotiazines in pharmaceutical formulations.

3.1. Choosing the micellar medium

In choosing the surfactant, it was considered that cationic surfactants are generally inhibitors of the enzyme [3]. Therefore, a non-ionic surfactant (Tween 80) and anionic surfactants (sodium laurate and lauryl sulphate sodium) were tested. Horseradish peroxidase action was affected in the presence of high surfactant concentration which could be associated either with the drug localization in the micelles in a way not accessible to the enzyme or to the inactivation of the enzyme [33]. Therefore, for each one of the surfactants, the lowest concentration of surfactant was used that was sufficient to dissolve the necessary amount of perphenazine when preparing the 5×10^{-3} mol L^{-1} stock solution. For all surfactants, this was obtained with concentrations above the critical micelle concentration. Thereafter, to evaluate the performance of the determination with different perphenazine micellar solutions, 125 μL aliquots were aspirated between peroxidase and hydrogen peroxide aliquots (100 μL) to the holding coil of the SIA system and then propelled to the detector through a l m coil, at a flow rate of 2.92 mL min^{-1}. It was verified that sodium laurate caused a decreased precision, as particles of a precipitate appeared occasionally, while with the lauryl sulphate sodium a decrease in the upper limit of the analytical concentration range to 7×10^{-5} mol L^{-1} was shown. The chosen surfactant was Tween 80, since with this it was possible to improve the sensitivity of about 220% and the upper limit of the linear concentration range

to 1.25×10^{-4} mol L^{-1}, when compared with the lauryl sulphate sodium medium. This may result because as the non-ionic surfactants are considered "soft" surfactants, they do not interact electrostatically with enzymes and therefore do not cause cooperative denaturation [34].

The importance of using micellar medium was also evident in the increment of sensitivity obtained in the determination of chlorpromazine when aqueous medium was replaced by micellar medium.

3.2. SIA system optimisation

Preliminary studies involved the establishment of the physical characteristics of the manifold, being defined a 2 m serpentine holding coil, sufficient to prevent the stack of zones aspirated from entering the pump conduit, and a 1 m serpentine-shaped coil, placed between the valve and the detector. The flow rate used for the aspiration of solutions to the system was 2.9 mL min^{-1} as with higher values the precision of the results was adversely affected. A lower flow rate (1.4 mL min^{-1}) was used to propel the solutions towards the detector, enabling the time required for production of the coloured cation radical to be extended. Regarding the aspiration order of the solutions to the holding coil, the aspiration of the sample plug between the peroxidase and H_2O_2 solutions was set. In this way, when flowing towards the detector, the peroxidase zone superimposed the mixing zones of sample and hydrogen peroxide to exert its catalytic action. This option was confirmed as a 36% decrease in sensitivity was obtained when the inverse option was tested.

Low pH is essential for the stability of the cation radical formed and for its detection by spectrophotometry [10,35–38] as in alkaline media values, the rate of decay of the coloured radicals appears to be faster. The pH dependence of the peroxidase catalysed oxidation of chlorpromazine and perphenazine was however examined in the pH range 3.5–6. This interval was chosen as a pH of 3.5 was reported as optimum for the stability of several cation radicals [11] and 6 is in the optimum pH interval referred for peroxidase activity [39]. Consequently, both the hydrogen peroxide solution and the enzyme were prepared in an acetic/acetate buffer solution of different pH values. There was a threefold increase in sensitivity, observed between the pH interval limits, showing the versatility of peroxidase in catalysing at different pH values. Afterwards, and in face of the results obtained, it was also assayed the replacement of the water, used as carrier and solvent of the standard solutions, by the buffer solution. Comparing the results obtained, no significant differences in analytical signals were observed and consequently the replacement was not made.

The solvent of the reagent and sample solutions was then defined as water and surfactant in the case of perphenazine. Thereafter, it was necessary to evaluate the volumes of solutions to be introduced into the system.

The volume of peroxidase solution was tested between 50 and 125 μL. While for volumes below 100 μL the amount of peroxidase (1.5 μg) became insufficient and the reaction rate decreased, with higher volumes the analytical signals obtained were similar. A similar range of volumes was tested for H_2O_2 solution. The phenotiazines' response increased 40% until 100 μL; volumes lower than 100 μL gave rise to smaller linear concentration ranges. For the highest concentration of the linear range (1.25×10^{-4} mol L^{-1}), the analytical signal decreased by 13% and 30% when volumes of 75 and 50 μL, respectively were used.

Using 100 μL of peroxidase solution and 100 μL of hydrogen peroxide, the optimum sample volume in the range of 75–150 μL was evaluated. Between 75 and 125 μL there was a 49% increase in attained sensitivity. For sample volumes greater than 125 mL, the proportion of reagents/sample became lower, which would make it necessary to use greater volumes of peroxidase and H_2O_2.

Therefore, having established these volumes, the concentrations were evaluated. As this was a two-substrate reaction and as the objective was to determine just one, it was important to ensure that co-substrate concentration was not limiting, nor the enzyme amount.

Several calibration curves were made for peroxidase concentration between 3 and 120 μg mL^{-1}. Results confirmed that a 15 μg mL^{-1} solution was sufficient to guarantee progression of the reaction. In fact, with lower concentrations there was a decrease in reaction rate and no enhancement was seen when the concentration was raised. The dependence of the reaction on H_2O_2 concentration was also studied between 1×10^{-4} and 3×10^{-3} mol L^{-1}. A slight increase in sensitivity (30%) of the measurements occurred but a pronounced increase (350%) in the dynamic concentration range until 5×10^{-4} mol L^{-1} was obtained, highlighting a severe shortage of co-substrate present in the reaction. This concentration was then used for further studies.

As this is a fixed-time methodology, the absorbance monitored for each sample with the same concentration, independently of the medium used, should correspond to the same concentration. However, in the event of different reaction kinetics between the enzyme and substrate in the presence of different media, this may result in an underestimation of the respective substance [40]. Therefore, to confirm this possibility, the flow was halted in the detector and the absorbance measured during stop periods between 60 and 300 s. Standards and pharmaceutical samples of chlorpromazine and perphenazine with the same concentration were analysed. A similar behaviour between samples and standards dissolved in Tween 80 was observed while for chlorpromazine the kinetics of the enzymatic reaction were different and, only after 60 s of stop period, the absorbance value was the same. It seemed that with surfactant, there was an increase in reaction rate. However, a stopped-flow period of 60 s was adopted for aqueous samples. The defined conditions allowed a sampling rate of approximately 17 and 31 determinations per hour, for aqueous and micellar media, respectively.

3.3. Interferences

Considering that the developed methodology can be applied in the determination of phenothiazines, as the active components

Table 2
Interfering effect of excipients on the developed methodology

Excipient	Tolerance weight ratio	
	Aqueous medium	Micellar medium
Lactose	100[a]	50
Titanium dioxide	50	–
Ethanol	10	–
Magnesium stearate	100[a]	100[a]
Sacarose	100[a]	50
NaCl	5	–
Sodium sulphite	5[b]	–
Ascorbic acid	5[b]	–
PVP	–	50
Amide	–	100[a]
Amitryptiline hydrochloride	–	50

[a] The highest value tested.
[b] The lowest value tested. With this value the interference was noted.

Table 3
Figures of merit of SIA system

	Aqueous medium	Micellar medium
Regression equation	$AU = (1.97 \pm 0.16) \times 10^3\ Conc + (1.9 \pm 1.3) \times 10^{-2}$	$AU = (2.72 \pm 0.14) \times 10^3\ Conc - (0.15 \pm 1.12) \times 10^{-2}$
R^2	0.9981	0.9993
Detection limit (mol L^{-1})	6.00×10^{-6}	3.76×10^{-6}
Quantification limit (mol L^{-1})	2.00×10^{-5}	1.25×10^{-5}
Upper limit (mol L^{-1})	1.25×10^{-4}	1.25×10^{-4}
R.S.D.% (sample concentration, mol L^{-1})	1.6 (5.03×10^{-5})	1.5 (5.47×10^{-5})
R.S.D.% (sample concentration, mol L^{-1})	1.0 (1.09×10^{-4})	0.6 (1.03×10^{-4})
Determination frequency (determ. h^{-1})	17	31

Table 4
Results obtained by the proposed flow methodology and the comparison reference methodologies for the determination of chlorpromazine and perphenazine in pharmaceutical formulations

Medium	Drug	Pharmaceutical preparation	Amount declared (mg/formulation)	Amount found (mg/formulation) ± S.D.		Relative error (%)
				Reference methodology	Developed methodology	
Aqueous	Chlorpromazine-HCl	Largactil 25 (tablets)	27.86	28.54 ± 0.12	27.87 ± 0.43	−2.4
		Largactil 100 (tablets)	111.44	111.18 ± 0.10	106.52 ± 0.93	−4.2
		Largactil I.V. (injection)	55.72 mg/2 mL	55.66 ± 0.55	54.53 ± 1.13	−2.0
		Largactil I.M. (injection)	27.85 mg/5 mL	30.26 ± 0.28	29.12 ± 0.82	−3.8
		Largactil (oral solution)	44.57 mg/mL	46.23 ± 1.87	46.22 ± 0.91	0.0
Micellar	Perphenazine	Mutabom D (tablets)	2	2.08 ± 0.03	2.01 ± 0.01	−3.4
		Mutabom F (tablets)	4	4.04 ± 0.04	4.12 ± 0.01	+2.0
		Mutabom M (tablets)	2	1.96 ± 0.05	2.05 ± 0.01	+4.6

in pharmaceutical formulations, it was important to assess the potential interfering effect of several compounds commonly used as excipients in the analysed formulations. Standard solutions, in aqueous media, with a fixed amount of chlorpromazine and increasing concentrations of lactose, titanium dioxide, ethanol, magnesium stearate, sacarose, NaCl, sodium sulphite and ascorbic acid were analysed in the flow system. Perphenazine standard solution, in micellar medium, with a fixed amount of drug and increasing concentrations of lactose, magnesium stearate, sacarose, PVP, amide and amitryptiline hydrochloride were also analysed. A species was considered as non-interfering when the analytical signal variation was lower than 3% when compared to the analytical signal obtained in the absence of the referred species.

In aqueous medium, it was observed (Table 2) that up to a 100 ratio of interferent/drug (highest value tested) for lactose, magnesium stearate and sacarose, no interfering effect was noticeable. Regarding titanium dioxide and ethanol, no interference was observed for a ratio under 50 and 10, respectively. Finally, NaCl, sodium sulphite and ascorbic acid were shown to interfere with the analytical signal at a ratio of 5. However these did not affect the determination of chlorpromazine in the pharmaceutical preparations since these excipients are present at very low concentrations, so that the present procedure could be applied directly.

No interfering effect was observed in micellar medium, when an interferent/drug ratio of 100 for magnesium stearate and amide was studied. For lactose, sacarose, PVP and amitryptiline hydrochloride, no interference was noted for a ratio lower than 50.

3.4. Analysis of pharmaceutical formulations

After system optimisation, the linear working range, detection and quantification limits, sampling rate and repeatability (Table 3) were evaluated for chlorpromazine hydrochloride in aqueous medium, and for perphenazine in micellar medium.

Detection and quantification limits were calculated as the concentrations corresponding to the intercept value plus 3 and 10 times $S_{y/x}$, respectively [41].

Sample throughput was calculated by adding the time necessary to perform each step of the protocol sequence, including aspiration of solutions to the holding coil, propulsion to the detector and stopped flow in the detector (for aqueous medium). Repeatability was estimated by calculating the relative standard deviation (R.S.D.%) from 10 consecutive sample injections of different concentrations.

The developed analytical methodology was then applied to commercially available pharmaceutical formulations containing chlorpromazine hydrochloride and perphenazine.

To evaluate the accuracy of the proposed system all samples were analysed according to the proposed method and their reference batch methods [14,29]. Relative deviations of <4.2% for aqueous medium and <4.6% for micellar medium were found (Table 4).

Furthermore, linear relationships, described by the equation $C_{SIA} = (0.951 \pm 0.042)\ C_{REF} + (1.1 \pm 2.6)$ for the aqueous medium and $C_{SIA} = (1.03 \pm 0.89)\ C_{REF} - (0.0 \pm 2.6)$ for the micellar medium, were established. C_{SIA} and C_{REF} correspond to the sequential injection and reference procedure results respectively, with 95% confidence limits for the intercept and slope. From these figures it is evident that the estimated intercept and slope values do not differ significantly from 0 and 1, respectively [41].

The agreement between both methods was also evaluated, using the *t*-test, carried out as a bilateral coupled test [41]. The tabulated *t*-values of 2.78 and 12.71 when compared with the calculated *t*-values of −1.88 and 0.64 show the absence of statistical differences for those results obtained by the methodologies (using the aqueous and micellar medium, respectively) at the 95% confidence level.

4. Conclusions

Enzymatic oxidation in aqueous and micellar media was successfully applied in a sequential injection system. The peroxidase–hydrogen peroxide system promoted the oxidation of the two phenothiazines in both media in a near mode. After optimisation of the SIA manifold it was obtained similar working ranges and precisions in the determination of the two compounds. However it was observed for perphenazine determination in the

micellar medium a better sensitivity and a superior determination frequency.

The advantages of performing this evaluation by SIA were evident by the ease in manipulating the solutions and changing the studied parameters simply by computer control. Moreover, the working mode of these systems guarantee economy in the spent reagents and effluents produced.

The applicability of the developed system to the determination of both phenotiazines was demonstrated. The system is simple and versatile requiring only a change of samples to perform the determination of any of the phenotiazines. The obtained results were in good agreement (95% confidence level) with those furnished by the British Pharmacopoeia and United States Pharmacopoeia.

The use of the surfactant led to the solubilisation of the low water-soluble phenothiazine and avoided the use of organic solvents, which carry a greater toxic and pollutant effect. Moreover, the reagents used involved only the enzyme and hydrogen peroxide as an oxidant with benign reaction products.

Acknowledgements

Marieta Passos thanks the Fundação para a Ciência e Tecnologia and FSE (III Quadro Comunitário) for the Ph.D. grant (SFRH/BD/22752/2005).

References

[1] A. Bodtke, W.D. Pfeifer, N. Ahrensb, P. Langerc, Tetrahedron 61 (2005) 1092.
[2] B. Tang, Y. Tang, L. Ma, Anal. Bioanal. Chem. 378 (2004) 523.
[3] S. Roy, A. Dasgupta, P.K. Das, Langmuir 22 (2006) 4567.
[4] S. Mahiuddin, A. Renoncourt, P. Bauduin, D. Touraud, W. Kunz, Langmuir 21 (2005) 5259.
[5] L.V. Bindhu, T.E. Abraham, Biochem. Eng. J. 15 (2003) 47.
[6] A. Kojlo, J. Karpinska, L. Kuzmicka, W. Misiuk, H. Puzanowska-Tarasiewicz, M. Tarasiewicz, J. Trace Microprobe T. 19 (2001) 45.
[7] J. Karpińska, B. Starczewska, H. Puzanowska-Tarasiewicz, Anal. Sci. 12 (1996) 161.
[8] Y. Ni, L. Wang, S. Kokot, Anal. Chim. Acta 439 (2001) 159.
[9] J. Wang, G. Rivas, X.H. Cai, H. Shiraishi, P.A.M. Farias, N. Dontha, D.B. Luo, Anal. Chim. Acta 332 (1996) 139.
[10] L.H. Piette, G. Bulow, J. Yamazaki, Biochim. Biophys. Acta 88 (1964) 120.
[11] X. Yang, A.P. Kulkarni, Teratogen. Carcinogen. Mutagen. 17 (1997) 139.
[12] C.C. Nascentes, S. Cardenas, M. Gallego, M. Valcarcel, Anal. Chim. Acta 462 (2002) 275.
[13] J. Kulys, K. Krikstopaitis, A. Ziemys, J. Biol. Inorg. Chem. 5 (2000) 333.
[14] The United States Pharmacopeial Convention, Inc., USP 28/NF 23 The United States Pharmacopoeia, Official Monographs, 28th edn., The United States Pharmacopeial Convention, Inc., Rockville, 2005, p. 1522.
[15] J. Ruzicka, G.D. Marshal, Anal. Chim. Acta 237 (1990) 329.
[16] W. Thanasarakhan, S. Liawruangrath, S. Wangkarn, B. Liawruangrath, Talanta 71 (2007) 1849.
[17] S.M.Z. Al-Kindy, F.O. Suliman, S.B. Salama, Microchem. J. 74 (2003) 173.
[18] P.C.A.G. Pinto, M.L.M.F.S. Saraiva, J.L.M. Santos, J.L.F.C. Lima, Anal. Chim. Acta 539 (2005) 173.
[19] G. de Armas, M. Miro, J.M. Estela, V. Cerda, Anal. Chim. Acta 471 (2002) 173.
[20] G. de Armas, J.R. Torres, A. Cladera, J.M. Estela, V. Cerda, Quim. Anal. 20 (2002) 211.
[21] G. de Armas, A. Cladera, E. Becerra, J.M. Estela, V. Cerda, Talanta 52 (2000) 77.
[22] S.M.Z. Al-Kindy, F.E.O. Suliman, A.A. Al-Wishahi, H.A.J. Al-Lawati, M. Aoudia, J. Lumin. 127 (2007) 291.
[23] J.L. Burguera, M. Burguera, R.E. Anton, J.L. Salager, M.A. Arandia, C. Rondon, P. Carrero, Y.P. de Pena, R. Brunetto, M. Gallignani, Talanta 68 (2005) 179.
[24] G.D. Liu, S.L. Riechers, C. Timchalk, Y.H. Lin, Electrochem. Commun. 7 (2005) 1463.
[25] J.I. Rhee, Biotechnol. Bioprocess. Eng. 12 (2007) 289.
[26] R.I. Stefan, R.G. Bokretsion, J.F. van Staden, H.Y. Aboul-Enein, Biosens. Bioelectron. 19 (2003) 261.
[27] R.Q. Zhang, K. Hirakawa, D. Seto, K. Nakano, T. Masadome, K. Nagata, K. Sakamoto, T. Imato, Talanta 68 (2005) 231.
[28] E.M. Alhadeff, A.M. Salgado, O. Cos, N. Pereira, B. Valdman, F. Valero, Appl. Biochem. Biotechnol. 137 (2007) 17.
[29] Stationary Office, British Parmacopoeia 2005, Stationary Office, London, 2005, p. 2324.
[30] C. Petit, K. Murakami, A. Erdem, E. Kilinc, G.O. Borondo, J. Liegeois, J. Kauffmann, Electroanalysis 10 (1998) 1241.
[31] S.S. Razola, B. Blankert, G. Quarin, J. Kauffmann, Anal. Lett. 36 (2003) 1819.
[32] M.A. Eghbal, S. Tafazoli, P. Pennefather, P.J. O'Brien, Chem. Biol. Interact. 151 (2004) 43.
[33] L.E. Almeida, H. Imasato, M. Tabak, Biochim. Biophys. Acta 1760 (2006) 216.
[34] M. Jurgas-Grudzinska, L. Gebicka, Biocatal. Biotransfor. 23 (2005) 293.
[35] A. Vazquez, J. Tudela, R. Varon, F. Garcia-Canovas, Anal. Biochem. 202 (1992) 245.
[36] M. Perez-Gilabert, A. Sanchez-Ferrer, F. Garcia-Carmona, Biochem. Pharmacol. 47 (1994) 2227.
[37] M. Perez-Gilabert, A. Sanchez-Ferrer, F. Garcia-Carmona, Biochim. Biophys. Acta 1214 (1994) 203.
[38] H.Y. Cheng, P.H. Sackett, R.L. McCreery, J. Med. Chem. 21 (1978) 948.
[39] Sigma-Aldrich Co., Sigma Aldrich Chemie GmbH Peroxidase from Horseradish, Product information, 2007.
[40] H. Bisswanger, Practical Enzymology, Wiley-VCH, Weinheim, 2004, p. 35.
[41] J.C. Miller, J.N. Miller, Estadística para Química Analítica, 2nd edn., Addison-Wesley Ibroamerican, SA, Wilmington, 1993.

Talanta 77 (2008) 852–857

Contents lists available at ScienceDirect

Talanta

journal homepage: www.elsevier.com/locate/talanta

Flow-through photochemically induced fluorescence optosensor for the determination of linuron

Gisela N. Piccirilli[a], Graciela M. Escandar[a,*], Florentina Cañada Cañada[b], Isabel Durán Merás[b], Arsenio Muñoz de la Peña[b,*]

[a] Departamento de Química Analítica, Facultad de Ciencias Bioquímicas y Farmacéuticas, Universidad Nacional de Rosario, Instituto de Química Rosario (CONICET), Suipacha 531, Rosario S2002LRK, Argentina
[b] Departamento de Química Analítica, Facultad de Ciencias, Universidad de Extremadura, 06071 Badajoz, Spain

ARTICLE INFO

Article history:
Received 8 April 2008
Received in revised form 15 July 2008
Accepted 22 July 2008
Available online 5 August 2008

Keywords:
Pesticides
Linuron
Photochemically induced fluorescence
Flow-through sensor
Environmental waters

ABSTRACT

This manuscript presents the development of a new photochemically induced fluorescence flow-injection system, combined with solid-surface adsorption, for the determination of the benzoylurea pesticide linuron. The determination is carried out by measuring the fluorescence intensity of a photoproduct, formed by on-line irradiation with ultraviolet light, and retention on a solid matrix filling the flow-cell. The procedure is developed in the presence of two surfactants: sodium dodecyl sulphate and hexadecyltrimethylammonium chloride, which are critical for the detection of the fluorescence emission in the solid surface. The possible interactions between the linuron photoproduct, the micellar medium employed and the solid support (C_{18} silica gel) are discussed. Parameters related to the analytical signal and to the FIA manifold are optimized. Finally, the feasibility of the developed method was tested by the determination of linuron in both environmental and drinking water samples. Determinations at $\mu g\,L^{-1}$ level were accomplished after a solid-phase pre-concentration procedure.

1. Introduction

Phenylureas constitute a large and important family of herbicides widely used in agriculture for both selective and non-selective weed control [1]. Because of their persistence in the environment, they represent a risk of contamination for natural and drinking waters [2].

Phenylurea herbicides have been determined by different methods including capillary electrophoresis [3], gas chromatography [4–6] and liquid chromatography (LC) [7–9]. On the other hand, it was previously demonstrated that UV irradiation of non-fluorescent phenylureas yielded fluorescent photoproducts and, taking advantage of this property, several methods for determination of phenylureas using photoinduced fluorescence (PIF) were proposed. This is due the advantages of PIF over ordinary chemical reactions, such as quicker reaction times, lower dilution factors and less chemicals involved. A method based on PIF for the determination of linuron, diuron, isoproturon and neburon was developed by the Aaron group in collaboration with the Muñoz de la Peña group [10]. This method was then improved by using organized media such as micellar systems and cyclodextrins to enhance the fluorimetric emission [11,12]. It was also corroborated that coupling LC with on-line PIF detection was a very suitable approach for the analysis of these compounds in river water samples [13,14]. More recently, the determination of phenylurea herbicides [15] and other compounds of pharmaceutical, agricultural and environmental interest [16–18] have been performed by measuring on-line PIF in a flow-injection analysis (FIA) system.

Several authors have demonstrated that both sensitivity and selectivity of techniques employing FIA coupled to luminescence detection can be improved using solid-matrix fluorescence (SMF) employing an active solid support placed inside the flow-cell [19–21]. A review of the fundamental principles of flow-through optosensors describing practical considerations and applications has been published by Molina Díaz et al. [22]. The potentiality of the combination of PIF and SMF methodologies was proposed for the determination of vitamins B2 and B6 [23]. Similarly, a photochemically induced fluorescence-based optosensor was recently proposed for the determination of the pesticide imidacloprid in peppers and environmental waters [24], taking advantages of on-line PIF and FIA–SMF.

In the present paper, we report the development of a new optosensor for linuron (Fig. 1), based on PIF detection in an FIA system, combined with solid-surface immobilization in the flow-cell.

* Corresponding authors.
E-mail address: arsenio@unex.es (A. Muñoz de la Peña).

0039-9140/$ – see front matter © 2008 Elsevier B.V. All rights reserved.
doi:10.1016/j.talanta.2008.07.052

The interest is focused in this phenylurea derivative since a possible carcinogenic effect has been reported in humans [25]. Further, it is an emerging pollutant considered by the United State Environmental Protection Agency (US EPA) as a drinking water contaminant candidate [26,27].

The nature of the interaction between the linuron photoproduct, the surfactants employed for detecting the signals and the used solid-surface (silica gel C_{18}-bonded phase), as well as the optimum conditions to carried out the determinations are analysed and discussed. The improvement in sensitivity when PIF is coupled to an FIA–SMF system in comparing with those determinations in homogeneous solution, is demonstrated. Finally, the application of the developed method in natural waters is evaluated.

2. Experimental

2.1. Reagents and solutions

All reagents were of high-purity and used as received. Linuron (3-(3,4-dichlorophenyl)-1-methyl-1-methoxyurea) was purchased from Riedel-de Haën (Seelze, Germany). Methanol was purchased from Merck (Darmstadt, Germany) and 2-propanol was obtained from Panreac (Barcelona, Spain). Hexadecyltrimethylammonium chloride (HTAC) was purchased from Fluka (Buchs, Switzerland) and sodium dodecyl sulfate (SDS) was obtained from Merck (Darmstadt, Germany). Silica gel 100 C_{18}-bonded phase of 0.040–0.063 mm particle size (Fluka, Seelze, Germany) was used without any preliminary treatment. C_{18} solid-phase extraction disks were purchased from Varian (Lake Forest, CA, USA). Water was obtained from a Milli-Q System (Waters Millipore, Milford, MA, USA).

Stock solutions of linuron (in the range c.a. 700–1050 $\mu g\,mL^{-1}$) were prepared in 2-propanol. Working solutions were prepared by dilution with the appropriate surfactant.

2.2. Instrumentation

A Gilson Minipuls-3 (Villiers-Le-Ber, France) peristaltic pump with rate selector was used to generate the flow stream. A six-port medium pressure injection valve, equipped with exchangeable fixed volume loops, was used to introduce the sample. A photoreactor (Softron, Gynkotek HPLC, Germany), consisted of a polytetrafluoroethylene (PTFE) tube network (2 m × 0.5 mm i.d.) knitted around a 4 W mercury lamp, was used for the photoirradiation. A Hellma (Müllheim, Germany) 176.052-QS flow-through

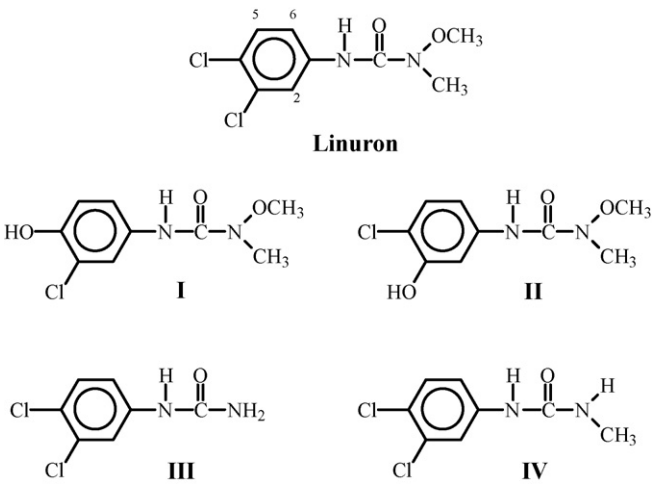

Fig. 1. Structures of linuron and its photoproducts.

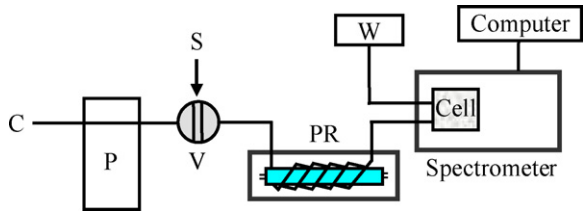

Fig. 2. The manifold for FIA on-line PIF. C, carrier; P, peristaltic pump; V, injection valve; S, sample solution; PR, photoreactor, Cell, filled with C_{18}; W, waste.

cell, with a light-path length of 1.5 mm and 25 μL inner volume, was packed with C_{18} bonded phase silica gel and placed in the sample compartment of the fluorescence spectrometer. The entire light-path of the cell was filled with a methanol suspension of the C_{18} silica gel with the aid of a syringe. While the inlet of the flow-through cell was kept free, its outlet was blocked with some glass wool to prevent displacement of solid support particles by the carrier. PTFE tubing (0.50 mm i.d.) and fittings were used to connect the flow-through cell, the rotatory valves and the carrier solution reservoir.

Fluorescence signals were measured using a Varian Cary-Eclipse spectrofluorimeter (Varian, Mulgrave, Australia) which was controlled by a microprocessor fitted with the Cary Eclipse software package. Instrumental variables were optimized to obtain the maximum sensitivity for the detection of the linuron photoproduct. The finally selected values were: excitation and emission slit widths of 10 and 20 nm, respectively, and excitation and emission wavelengths of 324 and 418 nm, respectively.

2.3. Optosensing manifold and general procedure

A schematic FIA-PIF–SMF system is shown in Fig. 2. A volume of sample solution was inserted into the carrier stream, composed by methanol 40%, v:v, and pumped through the flow system. The photolysis reaction on-line was performed by irradiating with UV light (254 nm) the injected linuron solution in the photoreactor. No cooling device was necessary, since no significant heat was generated during irradiation. When the linuron photoproduct reached the solid support filling the flow-cell, it was transiently retained and its PIF was measured at the maximum peak height. The photoproduct was eluted by the carrier itself, avoiding the use of an additional eluting solution. Every sample was inserted in the system at least in triplicate, and all PIF intensity measurements, at λ_{ex} = 324 nm and λ_{em} = 418 nm, were corrected for the background signal using the appropriate blank.

2.4. FIA-PIF–SMF calibration curves

Convenient dilutions of the linuron standard solutions with either SDS or HTAC were performed in order to obtain concentrations in the range 0–6 $\mu g\,mL^{-1}$. Thus, small volumes of linuron were transferred into a 10.00 mL flask, and diluted with the corresponding surfactant solution in order to obtain its optimal concentration. It is necessary to point out that the maximum percentage of 2-propanol in the most concentrated final solution is negligible (0.5%, v/v). FIA-PIF and SMF measurements were then performed using the procedure described above. Each calibration curve was obtained using seven linuron concentration levels by triplicate.

2.5. Water sample procedure

FIA-PIF–SMF methodology was applied for the quantification of linuron in water samples. All investigated water samples were pre-

pared by spiking them with linuron, obtaining concentration levels between 0.7 and 4.9 $\mu g\,mL^{-1}$, and solid surfactant was added in order to achieve their optimum concentrations. Tap, underground and mineral water samples underwent no treatment, were used as received. Guadiana river and Paraná river samples were collected near Badajoz (España) and Rosario (Argentina) cities, respectively, and after spiking them with linuron, they were filtered through a filter paper to remove suspended solid materials.

In order to improve the sensitivity of water analysis, an SPE technique was applied to several river waters. Thus, linuron was spiked in 200 mL of river water samples, and concentration levels between 5 and 50 $\mu g\,L^{-1}$ were obtained. These solutions were filtered through a filter paper, and the compound was then extracted on a C_{18} silica gel disk, previously conditioned with 8 mL of acetonitrile and 8 mL of water. The retained compound was washed with 10 mL of water and 5 mL of acetonitrile:water (1:4). Finally, linuron was eluted with 2 mL of acetonitrile and the solvent was evaporated under a nitrogen stream at room temperature. The residue was re-dissolved with 2.00 mL of the surfactant at its corresponding optimal concentration and the procedure described above was performed.

3. Results and discussion

3.1. Preliminary studies

Although linuron is a naturally non-fluorescent compound, fluorescence signals develop upon UV irradiation, indicating the formation of one or more emissive photoproducts [28]. The four main photoproducts when a water solution of linuron is irradiated during 1 h at 254 nm were identified as: 3-(3-chloro-4-hydroxyphenyl)-1-methoxy-1-methylurea (I), 3-(4-chloro-3-hydroxyphenyl)-1-methoxy-1-methylurea (II), 3,4-dichlorophenylurea (III) and 3-(3,4-dichlorophenyl)-1-methylurea (IV) (Fig. 1), with compound IV being the main reaction product [28]. On the other hand, it was verified that upon UV irradiation, a 2-propanol:water 90:10 (v/v) linuron solution shows two distinct fluorescent photoproducts. It has not been determined whether these two products coincide with those produced in the former more drastic conditions. They show emission maxima at 345 nm (λ_{ex} = 283 nm) and 405 nm (λ_{ex} = 325 nm) [10], and according to the excitation and emission wavelengths selected for our experiments (see above) this latter photoproduct is the compound detected in our studies.

The selection of the solid support was restricted to those supports potentially able to retain compounds of non-ionic nature such as the linuron photoproduct. Preliminary experiments showed that no significant signals were observed in nylon powder, silica gel and silica gel C_{18}-bonded phase. However, the addition of certain surfactants such as SDS and HTAC to the samples produced higher fluorescence signals when C_{18} silica gel was used as solid support. Thus, these systems were selected for subsequent studies.

According to the non-ionic nature of the linuron photoproduct, a negligible protonation effect is expected with changes in the pH. The pH values of the sample solutions were approximately neutral and therefore the pH was not adjusted. In fact, exploratory experiments demonstrated that the change of the pH in the range 3–10 does not produce any significant modifications in the read signal.

3.2. FIA parameters

Different methanol–water ratios (0, 10, 20, 30, 35, 40, 45, 50 and 60% methanol) were checked as carrier solutions and it was concluded that 40% (v/v) methanol produced the highest photoproduct PIF signal and a faster recovery of the baseline. The retention of the photoproduct in the solid support is transient, and the same carrier acts as an effective eluting solution. Higher methanol percentages produce detrimental effects in the signals, possibly due to a high methanol amount favouring the photoproduct desorption process.

In a FIA-PIF system, for each sample volume there is an optimum irradiation time which is related to the flow rate and to the length of the photoreactor. For the three sample volumes assayed (68, 104 and 150 μL), three photoreactor lengths (120, 200 and 300 cm) and flow rates in the range 0.6–1.1 mL min^{-1} were probed. It was corroborated that 200 cm photoreactor length and a flow rate of 0.9 mL min^{-1} produced better signals. Besides, the PIF signal obtained by using 150 μL as injection volume was similar to that using 104 μL. Therefore, taking into account that smaller volumes lead to better sampling frequencies, the value of 104 μL was selected. In conclusion, the final conditions for subsequent determinations were: 104 μL loop, using a 200 cm photoreactor length and a flow rate of 0.9 mL min^{-1}.

The stability of the optosensor is also an important variable in flow-through sensor analysis. It was established that it is possible to perform at least thirty and twenty uninterrupted determinations with the same C_{18} solid-phase, when SDS and HTAC are employed as surfactants, respectively. It is important to indicate that the cell is filled with few milligrams of C_{18} silicagel support (about 20 mg) and its replacement is easy and quick.

3.3. Effects of SDS and HTAC

In general, the use of micellar media significantly enhance the PIF signals of pesticides relative to an aqueous solution [2,4,13]. This may be attributed to the decrease of vibrational motions and increase of the rigidity of photoproduct molecules when they become included in the organized media [4].

However, in our case the surfactant could play a different function, due to the fact that interactions with the solid support (C_{18}) may occur. Lavine et al. have studied the interactions of two surfactants (SDS and hexadecyltrimethylammonium bromide, HTAB) with silica gel C_{18}-bonded phase, concluding that the use of the surfactant solutions above the corresponding critical micellar concentration (cmc) produces adsorption of surfactant into or onto the bonded phase, modifying its retention properties [29]. Two different forms of surfactant monomer association with the bonded phase have been proposed. The authors suggest that both the hydrophobic alkyl tail and the α-carbon of SDS are associated with the bonded-phase, with the polar head group projected away from it. Thus, the hydrophobic adsorption of SDS monomers to C_{18} leads to the formation of an anionic hydrophilic surface layer, which would favour some type of selective hydrogen bonding interaction between certain compounds with this layer. On the other hand, the head group of HTAB is oriented closer to the silica surface due to hydrophobic interactions between the *N*-methyl groups and the bonded phase. Incorporation of HTAB as described yields a significantly denser phase and would ensure that much of the hydrophobic character of the modified bulk phase would be retained.

Due to the deleterious effect of bromide in the fluorescence signals, in our experiments HTAB was replaced by HTAC. It is also important to point out that the adsorbed amount of surfactant remains constant for surfactant concentrations higher than the corresponding cmc [30]. The cmc for SDS and HTAC are 8.1 and 1.3×10^{-3} M, respectively [31]. Therefore, the surfactant concentrations were optimized ranging from 9×10^{-3} M to 0.024 M for SDS and from 2×10^{-3} M to 5×10^{-2} M for HTAC. The optimum concentration which generated the maximum PIF signal when SDS is used was 0.012 M, while the optimum value for HTAC was 0.020 M. Con-

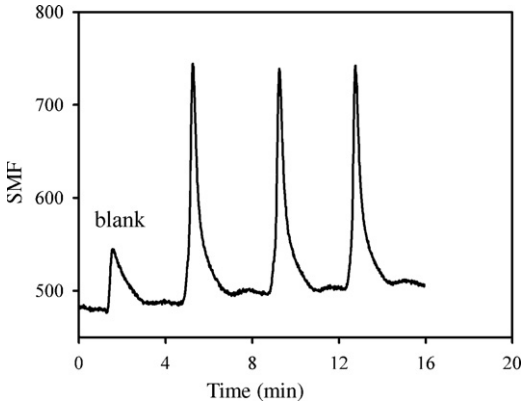

Fig. 3. Flow injection response for successive 104 μL of 3.50 μg mL^{-1} linuron injections in the presence of 0.020 M HTAC after on-line UV irradiation and using methanol 40% (v/v) as carrier; λ_{ex} = 324 nm, λ_{em} = 418 nm. The blank signal corresponds to a 0.020 M HTAC solution.

sequently, these surfactant concentration values were selected for the corresponding experiments.

Fig. 3 shows typical shapes of PIF signals vs. time obtained when a linuron-HTAC solution is subjected to flow analysis under the experimental conditions discussed above. As can be appreciated in this figure, the blank (an HTAC solution) produces a signal which is related to surface modifications produced by this surfactant over the silica gel C_{18}-bonded phase, as discussed above. This blank signal is subtracted from each signal subsequently obtained in the presence of linuron. In this figure, it can also be observed that after the first injection with blank solution, the baseline slightly changes. This variation can be attributed to the fact that the support is modified by the surfactant. Further, the slight changes observed after linuron injections, could be attributed to some non-monitored linuron photoproduct which is not eluted by the carrier. However, this small baseline modification did not produce significant problems in the repeatability of the obtained results.

3.4. Analytical figures of merit

Table 1 shows the figures of merit obtained in the present work using SDS and HTAC as surfactants and those previously reported for linuron by using PIF methods. The linear relationship between the amount of retained photoproduct and the fluorescence intensity was corroborated applying the *F* test recommended by IUPAC [32]. The statistical values in Table 1 suggests that the use of HTAC in the FIA-PIF–SMF system produces better figures of merit than SDS. This table also suggests that the use of a solid support in the FIA system does improve the results. In comparing the limit of detection of the presently proposed method employing HTAC (LOD = 0.13 μg mL^{-1}) with those carried out using PIF in organized medium solutions, such as surfactants (LOD = 0.41 μg mL^{-1}) or cyclodextrins (LOD = 0.58 μg mL^{-1}), and with micellar-enhanced PIF combined with FIA (LOD = 0.33 μg mL^{-1}), we may assert that the results here obtained are very satisfactory. On the other hand, although the sensitivity of the proposed method is similar to that obtained using HPLC with PIF detection, the sampling frequency here attained (about 17 samples h^{-1}) is larger than that employing chromatographic techniques.

3.5. Interference study

The methods here presented for the determination of linuron might be susceptible to interference from compounds concomitantly retained in the solid support. These interferences can either increase the resulting signal (if they emit near the photoproduct emission), or produce a less intense signal by quenching or by competition with the binding sites. Therefore, a systematic study for detecting interferences was undertaken, testing SDS and HTAC as surfactants. Foreign agrochemicals and inorganic ions which are likely to be present in water samples were analysed (Table 2). The interferents were assayed at concentrations five times higher than linuron, with the exception of certain compounds with very low water solubility. In these cases, the highest interferent concentration tested was around the corresponding solubility value (see Table 2).

Table 1
Comparison of the analytical performance of reported PIF methods for linuron determination

Method	Linear range (μg mL^{-1})	LOD (μg mL^{-1})	LOQ (μg mL^{-1})	Analytical sensitivity (μg mL^{-1})	R.S.D (%)[a]	References
MEPIF[b]	0.87–6.23	0.41[c]		0.17	4.0 (2.49)	[11]
CDEPIF[d]	2.5–8.7	0.66[c] 0.58[e]	1.93	0.27	4.8 (3.73)	[12]
FIA-MEPIF[f]	0.5–12.5	0.33	0.41		11	[15]
HPLC-PIF[g]	0.6–3.6	0.19[c,h] 0.22[c,i]		0.08[h] 0.09[i]	2.5 (1.4)[h] 2.4 (1.4)[i]	[13]
HPLC-PIF[g]	0.4–2.8[i] 0.5–2.4[i]	0.26[c,i] 0.13[c,i]		0.10[i] 0.04[i]	1.6 (2.0)[i] 1.2 (1.7)[i]	[14]
FIA-PIF–SPF (SDS)[j]	0.64–6.00	0.22[e]	0.64	0.09	1.6 (3.1)	This work
FIA-PIF–SPF (HTAC)[k]	0.39–6.00	0.13[e]	0.39	0.06	0.8 (3.5)	This work

[a] Relative standard deviation for the concentrations (μg mL^{-1}) given in parentheses.
[b] Micellar (SDS)-enhanced photochemically induced fluorescence.
[c] LOD calculated by Clayton's method ($\alpha = \beta = 0.05$) [36].
[d] Cyclodextrin (β-CD)-enhanced photochemically induced fluorescence.
[e] LOD according to IUPAC [37].
[f] Micellar (SDS)-enhanced photochemically induced fluorescence combined with flow injection analysis.
[g] High-performance liquid chromatography with photochemically induced fluorescence detection.
[h] Results obtained from the chromatographic peak height.
[i] Results obtained from the chromatographic peak area.
[j] Flow injection analysis combined with photochemically induced fluorescence and solid-phase-spectroscopy, in the presence of SDS.
[k] Flow injection analysis combined with photochemically induced fluorescence and solid-phase-spectroscopy, in the presence of HTAC.

Table 2
Interference study

Foreign species	Water solubility ($\mu g\,mL^{-1}$)[a]	Tolerated foreign species/linuron ($\mu g\,mL^{-1}/\mu g\,mL^{-1}$) ratio[b]	
		SDS system	HTAC system
Fungicides			
Thiram	30	5	5
Carbendazim	2	0.3	[c]
2,3-Dichloro-1,4-naphthoquinone	8	[c]	[c]
Imazalil	0.44	[c]	[c]
Dichlorophene	30	0.5	1
Thiabendazole	50	0.01	0.8
Fuberidazole	71	[d]	[d]
Insecticides			
Dimethoate	25000	5	5
Carbaryl	40	0.25	1
Cypermethrin	0.01	[c]	[c]
Herbicides			
2,4-Dichlorophenoxy acetic acid	900	5	5
4-Chloro-2-methylphenoxy acetic acid	825	5	5
Neburon	5	0.1	0.8
Isoproturon	65	0.1	0.05
Plant growth regulator			
1-Naphthylacetic acid	420	3	3
Inorganic ions[e]			
Sulfate		200	100
Chloride		100	100
Phosphate		20	50
Nitrate		0.5	0.5
Fe^{3+}		1	3
Al^{3+}		5	50
Cu^{2+}		200	50
Co^{2+}		10	15
Ni^{2+}		10	25

[a] Refs. [33,38–42].
[b] $C_{linuron} = 3.50\,\mu g\,mL^{-1}$; unless otherwise indicated, the maximum tested tolerance levels for organic and inorganic compounds were 5 and 200, respectively.
[c] These species were probed at concentrations around their water solubilities and no interference was detected.
[d] Tolerance lower than 0.01.
[e] Other ions are indirectly evaluated in the recovery studies carried out in real water samples (see Table 3).

In the SDS system, the systematic study was performed adding known amounts of each tested species to a solution containing $3.5\,\mu g\,mL^{-1}$ of linuron. Then, each solution was injected in the FIA system and processed by the usual procedure. When interference effects occurred, the concentration of the foreign species was progressively reduced until the effect was not significant. Tolerance was defined as the relative amount of interfering species that produced an error not exceeding ±4.8% in the determination of linuron. This value represents three times the relative standard deviation (R.S.D) corresponding to the evaluated experimental condition (R.S.D = 1.6, see Table 1). When HTAC was used as surfactant, a similar procedure was developed, but in this case the tolerance was defined as the relative amount of interfering species that produced an error not exceeding ±2.4% (3 × R.S.D) in the determination of linuron. A rapid inspection of Table 2 indicates that the phase formed by C_{18}-HTAC seems to be less susceptible to suffer interference by the assayed species than C_{18}-SDS.

Most of the evaluated inorganic ions do not produce serious changes in the measured fluorescence intensity of linuron. The highest interference in both systems is produced by iron (III). Aluminum (III) interferes in the SDS system when it is present at concentrations five times higher than linuron, probably due to the interaction between the metal ion and the anionic surfactant. Nitrate ion produces a decrease of the signal intensity, probably due to an inner filter effect, since this anion absorbs electromagnetic radiation at a wavelength near that corresponding to the excitation of linuron photoproduct.

In both C_{18}-HTAC and C_{18}-SDS systems, the highest interferences are produced by fuberidazole, thiabendazole, neburon and isoproturon. These compounds produce an increase of the resulting fluorescence signal, due to the fact that they also fluoresce with emission wavelengths near that of the linuron photoproduct. The remaining species do not produce severe interference in the determination of the studied analyte at the evaluated tolerance levels.

On the basis of all these interference studies, we can conclude that the tolerance of the proposed methods is, in several cases, not optimal. In these cases, the direct univariate determination might be replaced by a more complex analysis (e.g. multivariate calibration). This type of analysis will be included in future investigations.

3.6. Application of the method

With the purpose of evaluating the application of the present method and the potential interference from background matrices, waters from different origins were analysed. Since HTAC showed better results, this surfactant was selected to carry out the experiments.

The water solubility of linuron ($64\,\mu g\,mL^{-1}$) [33] suggests that it may filter readily through soils, reaching natural waters. In regions of intensive agriculture, linuron concentrations up to 1.1 and $2.8\,\mu g\,mL^{-1}$ have been detected in surface waters and ground waters, respectively [34]. These levels can be directly investigated with the proposed method without a pre-concentration step. Thus, in a first phase, a recovery study was performed by spiking each water sample with an appropriate amount of linuron in triplicate

Table 3
Recovery study of linuron for spiked water samples[a]

	Taken ($\mu g\,mL^{-1}$)	Found ($\mu g\,mL^{-1}$)	Recovery ± R.S.D. (%)[b]
Tap water[c]	0.73	0.74	101 ± 2
	2.10	1.99	95 ± 3
	4.90	5.00	102 ± 4
Tap water[d]	0.73	0.75	103 ± 2
	2.10	2.08	99 ± 1
	4.90	5.00	102 ± 2
Underground water[e]	0.73	0.75	103 ± 6
	2.10	1.99	95 ± 3
	4.90	4.87	99 ± 2
Mineral water[f]	0.73	0.70	96 ± 1
	2.10	1.98	94 ± 2
	4.90	4.91	100 ± 1
River water[g]	0.73	0.76	104 ± 1
	2.10	1.92	91 ± 2
	4.90	4.90	100 ± 1
	0.0050[h]	0.0048	96 ± 4
River water[i]	0.73	0.70	96 ± 1
	2.10	2.16	103 ± 2
	4.90	4.67	95 ± 3
	0.010[h]	0.010	100 ± 6
	0.050[h]	0.054	107 ± 6

[a] Using HTAC as surfactant.
[b] Mean of three determinations.
[c] From Buenos Aires City (Buenos Aires, Argentina).
[d] From Rosario City (Santa Fe, Argentina).
[e] From Funes City surroundings (Santa Fe, Argentina).
[f] From Villavicencio hills (Mendoza, Argentina). This water contains $NaHCO_3$ ($350\,\mu g\,mL^{-1}$), $Ca(HCO_3)_2$ and $Mg(HCO_3)_2$ ($259\,\mu g\,mL^{-1}$), Na_2SO_4, $CaSO_4$ and $MgSO_4$ ($234\,\mu g\,mL^{-1}$), NaCl, $CaCl_2$ and $MgCl_2$ ($47\,\mu g\,mL^{-1}$), CaF_2 ($1.4\,\mu g\,mL^{-1}$) and oligoelements ($1.5\,\mu g\,mL^{-1}$).
[g] From the Paraná River (Santa Fe, Argentina).
[h] A pre-concentration step was performed (see text).
[i] From the Guadiana River (Extremadura, España).

at three different concentration levels. The results are shown in Table 3, and suggest that interference from the background (inorganic ions and organic compounds possibly present in the studied samples) is absent in the investigated waters.

Additionally, taking into account that residue concentrations reported for ground waters are at the part-per-billion levels ($0.1–30\,\mu g\,L^{-1}$) [35], the sensitivity of the present method was improved using a pre-concentration step by employing C_{18} membrane-SPE. The technique was applied to the two river water samples, and the results are shown in Table 3.

4. Conclusions

A novel and simple FIA-PIF–SMF method for linuron determination was developed and successfully applied to the quantitation of this toxic herbicide in tap, underground, mineral and river water samples. The method is rapid and shows good sensitivity in comparison with other PIF methods. The results suggest that the use of the surfactant HTAC leads to a more sensitive and selective method. Although the use of an active solid support placed inside the flow-cell produced an improvement on the sensitivity, allowing linuron determination in water at concentrations usually found in regions of intensive agriculture, the attained limits of quantification are not proper for trace linuron residues. In these cases, it was found that the determination could be carried out by applying a simple pre-concentration step, without interferences from matrix compounds and also without chemical treatment.

Acknowledgments

The authors gratefully acknowledge the Ministerio de Educación y Ciencia of Spain, Project CTQ2008-06657/BQU, Agencia Española de Cooperación Internacional (AECI), Project A/6576/06, Universidad Nacional de Rosario. Agencia Nacional de Promoción Científica y Tecnológica (Project PAE 22204) and Consejo Nacional de Investigaciones Científicas y Técnicas, for financially supporting this work.

References

[1] P. Schneider, M.H. Goodrow, S.J. Gee, B.D. Hammock, J. Agric. Food Chem. 42 (1994) 413.
[2] J. Tekel', J. Kovacicova, J. Chromatogr. 643 (1993) 291.
[3] M.B. Barroso, L.N. Konda, G. Morovjan, J. High Res. Chromatogr. 22 (1999) 171.
[4] M.L. Escuderos-Morenas, M.J. Santos-Delgado, S. Rubio-Barroso, L.M. Polo-Dıez, J. Chromatogr. A 1011 (2003) 143.
[5] H. Berrada, G. Font, J.C. Moltó, Chromatographia 54 (2001) 253.
[6] H. Berrada, J.C. Moltó, G. Font, Chromatographia 54 (2001) 360.
[7] T. Yarita, K. Sugino, T. Ihara, A. Nomura, Anal. Commun. 35 (1998) 91.
[8] J. Chen, J. Pawliszyn, Anal. Chem. 67 (1995) 2530.
[9] H.H. Lin, Y.H. Sung, S.D. Huang, J. Chromatogr. A 1012 (2003) 57.
[10] M. Maafi, K. Taha-Bouamri, A. Bautista, J.J. Aaron, M.C. Mahedero, A. Muñoz de la Peña, F. Salinas, Biomed. Chromatogr. 13 (1999) 189.
[11] A. Bautista, J.J. Aaron, M.C. Mahedero, A. Muñoz de la Peña, Analusis 27 (1999) 857.
[12] M.C. Mahedero, A. Muñoz de la Peña, A. Bautista, J.J. Aaron, J. Incl. Phenom. Macrocyclic Chem. 42 (2002) 61.
[13] A. Muñoz de la Peña, M.C. Mahedero, A. Bautista Sánchez, J. Chromatogr. A 950 (2002) 287.
[14] A. Muñoz de la Peña, M.C. Mahedero, A. Bautista Sánchez, Talanta 60 (2003) 279.
[15] S. Irace-Guigand, E. Leverend, M.D.G. Seye, J.J. Aaron, Luminescence 20 (2005) 138.
[16] J.L. Vilchez, M.C. Valencia, A. Navalón, B. Molinero-Morales, L.F. Capitán-Vallvey, Anal. Chim. Acta 439 (2001) 299.
[17] A.M. García-Campaña, J.J. Aaron, J.M. Bosque-Sendra, Talanta 55 (2001) 531.
[18] C. Huang, Q. He, H. Chen, J. Pharm. Biomed. Anal. 30 (2002) 59.
[19] K. Yoshimura, S. Matsukoka, T. Tabuchi, H. Waki, Analyst 117 (1992) 189.
[20] J.F. Fernández-Sánchez, A. Segura-Carretero, C. Cruces-Blanco, A. Fernández-Gutierrez, Anal. Chim. Acta 462 (2002) 217.
[21] G.N. Piccirilli, G.M. Escandar, Anal. Chim. Acta 601 (2007) 196.
[22] A. Molina Díaz, A. Ruiz Medina, M.L. Fernández de Córdova, J. Pharm. Biom. Anal. 28 (2002) 399.
[23] E.J. Llorent-Martínez, J.F. García-Reyes, P. Ortega-Barrales, A. Molina-Díaz, Anal. Chim. Acta 555 (2006) 128.
[24] J. López Flores, A. Molina Díaz, M.L. Fernández de Córdova, Talanta 72 (2007) 991.
[25] N.N. Ragsdale, R.E. Menzer, Carcinogenicity and Pesticides: Principles, Issues, and Relationships, American Chemical Society, Washington, DC, 1989.
[26] US Environmental Protection Agency, Fed. Regist. 63 (40) (1998), 10273.
[27] W.R. Chena, C. Wub, M.S. Elovitzc, K.G. Lindenb, I.H. Suffeta, Water Res. 42 (2008) 137.
[28] V. Faure, P. Boule, Pestic. Sci. 51 (1997) 413.
[29] B.K. Lavine, W.T. Cooper III, Y. He, S. Hendayana, J.H. Han, J. Tetreault, J. Colloid Interface Sci. 165 (1994) 497.
[30] M. Cuenca-Benito, S. Sagrado, R.M. Villanueva-Camañas, M.J. Medina-Hernández, J. Chromatogr. A 814 (1998) 121.
[31] E. Pramauro, E. Pelizzetti, in: S.G. Weber (Ed.), Wilson & Wilson's Comprehensive Analytical Chemistry, XXXI, Elsevier, Amsterdam, The Netherlands, 1996, p. 12.
[32] K. Danzer, L.A. Currie, Pure Appl. Chem. 70 (1998) 993.
[33] L.M.L. Nollet (Ed.), Handbook of Water Analysis, Marcel Dekker, New York, 1999.
[34] P.Y. Caux, R.A. Kent, G.T. Fan, C. Grande, Environ. Toxicol. Water Qual. 13 (1998) 1.
[35] A. Cappiello, G. Famiglini, F. Bruner, Anal. Chem. 66 (1994) 1416.
[36] C.A. Clayton, J.W. Hines, P.D. Elkins, Anal. Chem. 59 (1987) 2506.
[37] L.A. Currie, Anal. Chim. Acta 391 (1999) 105.
[38] http://extoxnet.orst.edu/.
[39] www.ars.usda.gov/.
[40] T.R. Roberts, D.H. Hutson (Eds.), Metabolic Pathways of Agrochemicals: Insecticides and Fungicides (Part Two), Royal Society of Chemistry, UK, 1999.
[41] http://www.chemblink.com/.
[42] http://www.sciencelab.com/.

Talanta 77 (2008) 479–483

Contents lists available at ScienceDirect

Talanta

journal homepage: www.elsevier.com/locate/talanta

Sequential injection analysis as a tool for implementation of enzymatic assays in ionic liquids

Paula C.A.G. Pinto*, M. Lúcia M.F.S. Saraiva, José L.F.C. Lima

REQUIMTE, Serviço de Química-Física, Faculdade de Farmácia, Universidade do Porto, Rua Aníbal Cunha 164, 4099-030 Porto, Portugal

ARTICLE INFO

Article history:
Received 1 October 2007
Received in revised form 13 March 2008
Accepted 17 March 2008
Available online 25 March 2008

Keywords:
SIA
Horseradish peroxidase
Ionic liquids
[Bmim][BF4]
Methanol

ABSTRACT

An approach based on the use of water/1-butyl-3-methylimidazolium tetrafluoroborate ([bmim][BF4]) mixtures in a sequential injection analysis (SIA) system is presented. The rapid and robust procedure developed was used to evaluate horseradish peroxidase activity in [bmim][BF4] and is intended to be a generic tool for enzymatic assays in ionic liquids.

The horseradish peroxidase activity tests were based on the implementation of the 4-aminoantipyrine (4AAP)/phenol test in the SIA system, using 1-naphtol as substrate. Small volumes (12 μL) of sample, reagents and enzyme were sequentially aspirated to the holding coil before being sent to the spectrophotometric detector (λ = 510 nm), where a coloured product proportional to the enzyme activity was measured.

The results were compared to those obtained when the assay was performed in water/methanol mixtures under the same conditions, to evaluate [bmim][BF4] as an alternative to conventional organic solvents. Comparative evaluation of the enzyme behaviour revealed that the enzyme activity increased significantly when the assay was performed in water/[bmim][BF4] mixtures.

The SIA methodology exhibited good repeatability over the full concentration range (R.S.D. < 3.3%, $n = 15$) studied, produced approximately 1.7 mL of effluent and consumed approximately 36 μL of solutions prepared in water/[bmim][BF4] mixtures for each analytical cycle.

1. Introduction

The implementation of procedures involving enzymatic reactions in flow systems has grown with the evolution of enzyme catalysis and use of new reaction media, leading to a large number of enzymatic procedures with a wide range of analytical purposes [1]. Among flow techniques, sequential injection analysis (SIA) has been used for a large variety of analytical determinations including enzymatic reactions, proving itself to be a robust and accurate solution handling approach [2,3]. Its unique mode of operation, based on the forward and reversed flow of well defined zones of sample and reagent solutions through a multiposition valve makes it a very economic tool since it permits the aspiration of precise volumes and an effective utilisation of solutions, in the process drastically reducing the consumption of sample and reagents [4]. Furthermore, the effective computer control of the most relevant analytical parameters at run-time ensures great operational flexibility, which allows the assessment of distinct analytical strategies without physical reconfiguration of the flow set-up and facilitates system optimisation [5]. This is particularly important in procedures that demand precise control of the reaction conditions such as enzymatic reactions, since it guarantees standardised conditions with all assays. These features greatly increase the analytical potential of SIA manifolds, making it a first choice technique and explain why SIA has been increasingly used for the mechanisation of enzymatic procedures that either involve expensive enzymes or small sample amounts, mostly in the biological area. The new developments in the enzymatic catalysis field that transcended from totally aqueous procedures not so many years ago, to techniques based on organic solvents [6] and more recently to other non-aqueous media [7], reinforced the idea that the benefit of most enzymatic processes passes trough its implementation in flow systems. Within this perspective, SIA, due to its particular advantages, can once again become a powerful tool in this area.

The use of water as solvent in enzymatic reactions for years limited the field of application of enzymes in biocatalysis and the productivity of some processes, particularly those involving hydrophobic substrates [6]. As a consequence, the applicability of catalysis in non-aqueous solvents has been tested and discussed and as a result, new reaction media have been suggested [8]. The possibility of working with hydrophobic substances, the decrease in microbial contamination and reduction of side reactions are the

* Corresponding author. Tel.: +351 222078939; fax: +351 222004427.
E-mail address: ppinto@ff.up.pt (P.C.A.G. Pinto).

0039-9140/$ – see front matter © 2008 Elsevier B.V. All rights reserved.
doi:10.1016/j.talanta.2008.03.017

main advantages related with the development of procedures in non-aqueous media [6]. Organic solvents helped to reduce some problems such as the insolubility of hydrophobic compounds and propagation of radicals in aqueous solutions and were shown to be good solvents for enzymes catalysis, in some cases offering benefits related with enzyme stability and selectivity [9,10]. However, organic solvents exhibit known disadvantages such as human and environmental toxicity and high volatility that make their application in routine procedures difficult. These drawbacks can be substantially reduced through implementation of these procedures in closed flow systems but some cases of enzyme inactivation in organic polar solvents have been related, limiting the applicability of these solvents and requiring specific activity studies [11].

As a consequence, researchers have in the last decade embarked upon exploring a new group of compounds, room temperature ionic liquids (ILs), in an attempt to establish their applicability in biocatalysis [12]. Due to their particular characteristics, ILs have emerged as "green" substitutes for conventional organic solvents in enzymatic reactions, sometimes with remarkable results, offering new possibilities for the application of solvent engineering to biocatalytic reactions [13]. Their specific properties such as nonflammability, nonvolatility and good chemical and thermal stability made them a safe alternative to conventional organic solvents [14]. However, the study of enzyme activity in ILs, apart from enzyme availability and reagents toxicity, must consider the high cost of these solvents that hinder their routine utilisation. Moreover, although IL are known as green solvents, the assays must still be performed in order to produce minimum wastes, since its long-term toxicity is not as yet known [15].

Considering the characteristics of enzymatic assays in ILs, its implementation in a SIA manifold, although having never been tried, seems very promising and challenging, since it combines the advantageous features of enzyme catalysis in IL with the versatility and low consumption of SIA. Thus, the present paper describes the implementation of an enzymatic assay, performed in a water miscible IL in a SIA system. The assay was based on implementation of the 4-aminoantipyrine (4AAP)—phenol test [16] using horseradish peroxidase as catalyst, 1-naphtol as substrate and 1-butyl-3-methylimidazolium tetrafluoroborate ([bmim][BF4]) as solvent. This is a very well known reaction catalysed by an enzyme that is very abundant in nature and involved in many biological reactions. Besides this, the peroxidase mediated coupling of phenols is one of the most studied redox processes in biochemistry and highlights the importance of the use of non-aqueous reaction media to aid solubilisation of hydrophobic substances, increasing the field of the studies [17].

The developed work also involved a comparative study of the enzyme activity in methanol, to evaluate ILs as an alternative to conventional organic solvents. The presented approach was intended to provide a fast, robust and economic generic means of evaluating enzyme activity in IL which could additionally represent a basis for the future mechanisation of analytical procedures.

2. Experimental

2.1. Reagents

All solutions were prepared using chemicals of analytical reagent grade and high purity water (milli-Q) with a specific conductance <0.1 $\mu S\,cm^{-1}$.

The carrier solution of the flow system comprised a Briton and Welford universal buffer solution with pH adjusted between 6 and 12.

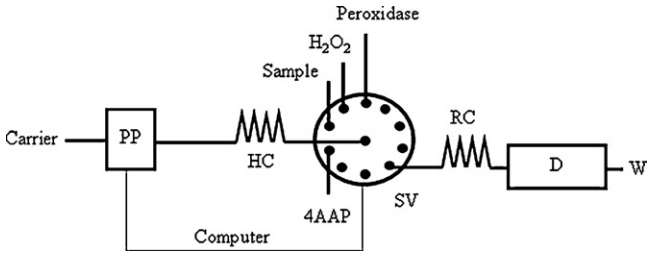

Fig. 1. SIA system. PP, peristaltic pump; SV, selection valve; HC, holding coil (4 m); RC, reaction coil (1 m); D, spectrophotometric detector; W, waste.

Daily, a horseradish peroxidase solution (Sigma, Type VI-A) of 0.1 $mg\,mL^{-1}$ was prepared in water from a 1 $mg\,mL^{-1}$ stock solution. The stock solution was stored in the refrigerator and remained stable for about 3 days.

A stock solution of 1-naphtol 0.15 $mol\,L^{-1}$ was prepared by dissolving the appropriate amount of powder in a water/[bmim][BF4] mixture (1:2), which guaranteed the full solubilisation of the compound. Standard solutions of 1-naphtol were prepared from the stock solution by suitable dilutions in water/[bmim][BF4] mixtures of 1:0.5, 1:1 and 1:1.5, all of which were stable for several weeks. For the comparative studies of enzyme activity, stock and standard solutions of 1-naphtol were prepared as described but by replacing [bmim][BF4] with methanol.

4AAP 0.025 $mol\,L^{-1}$ and hydrogen peroxide 0.0175 $mol\,L^{-1}$ were prepared daily in water/[bmim][BF4] mixtures of 1:0.5, 1:1 and 1:1.5.

2.2. Apparatus

Spectrophotometric measurements were made in a 6300 Jenway spectrophotometer, set at 510 nm and equipped with a 30 μL flow cell (Helma 178.711QS, Müllheim, Balden, Germany).

The SIA system (Fig. 1) consisted of a Gilson Minipuls 3 peristaltic pump, equipped with PVC pumping tube (1.2 mm i.d.) and a 10-port multiposition Vici Valco selection valve. Manifold components were connected by means of 0.8 mm i.d. PTFE tubing which was also used for the holding and reaction coil (4 and 1 m, respectively).

Analytical system control, including the operation of the peristaltic pump and selection valve, was achieved by means of an Advantech PCL 711B interface card and a Pentium-I-based microcomputer. Software was developed in Microsoft Quick-Basic and permitted the control of flow rate, flow direction, valve position, sample and reagent volume as well as data acquisition and processing. During optimisation, the analytical signals were also recorded on a Kipp & Zonen BD 111 strip chart recorder.

In the evaluation studies on the influence of temperature on horseradish peroxidase, the reaction coil was thermostatized between 30 and 45 ± 0.5 °C in a Falc FA90 temperature controller.

2.3. Sequential injection procedure

The analytical cycle established for the implementation of the 4AAP-phenol test in the SIA system is summarised in Table 1. Initially, small volumes (12 μL) of horseradish peroxidase, H_2O_2, 1-naphtol and 4AAP were sequentially aspirated to the holding coil. Then, the flow was reversed and the reaction zone propelled by the carrier solution through the reaction coil, directly to the detector where the product of the reaction was measured. For the comparative assays involving the use of water/methanol mixtures, the procedure was exactly the same in order to conduct a comparison under the same conditions.

Table 1
Analytical cycle for the evaluation of horseradish peroxidase activity

Step	Position	Time (s)	Flow rate (mL min^{-1})	Volume (μL)	Description
1	1	1	0.67	12	Aspiration of peroxidase
2	2	1	0.67	12	Aspiration of H_2O_2
3	3	1	0.67	12	Aspiration of 1-naphtol
4	4	1	0.67	12	Aspiration of 4AAP
5	7	50	2	–	Propulsion to the detector

3. Results and discussion

This approach based on insertion of water/[bmim][BF4] mixtures in a SIA system to evaluate horseradish peroxidase activity was developed in four steps that involved the implementation of the 4AAP-phenol test in the flow system, evaluation of enzyme activity in [bmim][BF4], study of the influence of media conditions (pH, temperature, concentration of IL) on the activity and comparison of these results with those obtained when the reaction took place in water/methanol.

3.1. Implementation of the 4AAP-phenol test on a SIA system

The 4AAP-phenol test was used as a means to evaluate horseradish peroxidase activity since it is a very well known chemical reaction that fits the purpose of the developed work which does not involve, at this time, an innovative analytical application. The reaction is based on the oxidation of phenol by H_2O_2 in the presence of horseradish peroxidase and subsequent reaction of the formed radical with 4AAP to form a coloured product, with maximum absorption at 510 nm. The enzymatic reaction was performed in [bmim][BF4], a water miscible IL that has been successfully tested in some enzymatic reactions.

The main problem related with the insertion of IL, namely [bmim][BF4], in a SIA system is its high viscosity that complicates the reproducible aspiration of small IL volumes and its dispersion on an aqueous carrier solution. However, [bmim][BF4] is a water miscible IL, so it is possible to work with mixtures that exhibit less viscosity and can be reproducibly aspirated to the flow system. Nevertheless, while optimising the procedure it proved very difficult, even with water/IL mixtures, to get an effective mixture of the aspirated aliquots in the SIA system. It is important to highlight that, due to the specific characteristics of SIA manifolds, the interdispersion of the aspirated zones in this kind of system is only partial but is essential for development of the chemical reaction. In the studied situation, when the aspirated volumes were between 50 and 150 μL, double peaks were recorded, revealing mixing problems due to different viscosities of the aspirated zones and carrier solution. To solve this problem, the aspirated volumes were reduced to a minimum in order to get a homogeneous reaction zone and measurable analytical signal. The final analytical cycle involved the aspiration of 12 μL of each solution since this volume guaranteed repeatable results and high analytical signals in a single peak shape.

The concentrations of 4AAP and H_2O_2 were established as 0.025 and 0.0175 mol L^{-1}, respectively. These were maximum concentrations above which no variation in analytical signal was apparent, so that the future analysed changes were undoubtedly related with the change of enzyme activity and not due to the lack of reagents.

The aspiration flow rate was 0.67 mL min^{-1} since it permitted the reproducible aspiration (R.S.D. < 3%) of the chosen small volumes. Due to the high sensitivity of the 4AAP-phenol reaction, the propulsion flow rate was set at 2 mL min^{-1} in order to decrease the residence time and dispersion of the reaction zone. Flow rates between 0.8 and 1.5 led to an increase in residence time of the reaction zone which could reach 75 s, resulting in a decrease in analytical signals due to the enhanced dispersion.

Among several coils (0.5–1.5 m), a 1 m long figure-eight-shaped reaction coil was chosen to perform the assays since it permitted efficient mixing of the aspirated zones without excessively increasing the dispersion of formed product.

The developed analytical procedure exhibited very interesting characteristics, performing around 60 determinations per hour and producing around 1.7 mL of effluent per analytical cycle. Repeated analysis of samples (n = 15) of different concentrations did not show R.S.D. (%) greater than 3.3, which is very acceptable considering the small aspirated volumes.

3.2. Evaluation of horseradish peroxidase activity in [bmim][BF4]

Under the described set of conditions it was possible to produce 1-naphtol calibration curves up to 0.015 mol L^{-1}, showing that the enzymatic catalytic action is proportional to the amount of 1-naphtol. The evaluation studies of enzyme activity were based on the sensitivity of the determinations.

Once established the initial assay conditions, the effect of pH, temperature and concentration of [bmim][BF4] on horseradish peroxidase activity were studied.

The composition of the buffer carrier solution was changed in order to attain solutions with pH values between 6 and 12 and then study the effect of this parameter on the enzyme activity. These studies were performed at room temperature using a water/[bmim][BF4] mixture (1:0.5) as reaction media. It was observed that enzyme activity increased with pH up to 11.2, above which the analytical signals decreased, being inexistent at pH 12 (Fig. 2). These observations confirmed the results of Sgalla et al. [10] and showed that under these conditions, the maximum activity peak is achieved in conditions distinct from that obtained in aqueous media [18]. This difference could be related with the inhibition of horseradish peroxidase by the F^- anion of [bmim][BF4], which binds to the heme iron of peroxidase under acidic pH conditions [10]. Thus, the enzyme activity in ILs is strongly pH dependent and increases under alkaline conditions.

The effect of temperature on enzyme activity was studied by immersing the reaction coil of the SIA system in a thermostatically controlled water bath. Assays were performed with a carrier solution of pH 11.2 and as before, with a water/[bmim][BF4] mixture (1:0.5) as reaction media. Analytical signals increased very slightly with the temperature of the water bath up to 40 °C and higher temperatures led to a significant decrease in analytical signals, revealing the onset of the process of enzyme denaturation. With the aim of evaluating the influence of concentration of [bmim][BF4] on horseradish peroxidase activity, a study involving

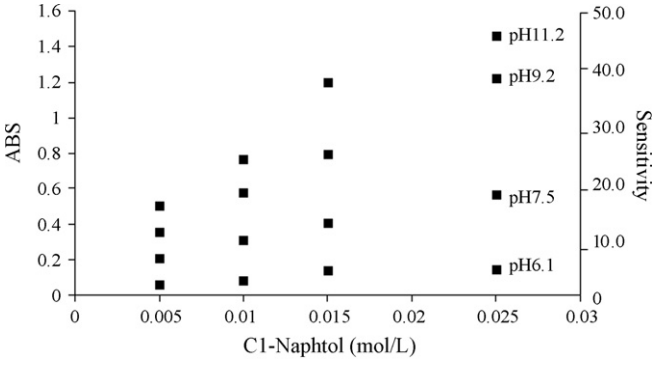

Fig. 2. Influence of the pH of the carrier solution on horseradish peroxidase activity in [bmim][BF4].

the use of water/[bmim][BF4] mixtures using different proportions (1:0.5, 1:1, 1:1.5) was performed. As previously described in Section 2, these mixtures were used as solvent for the preparation of 1-naphtol, 4AAP and H_2O_2 solutions which were then introduced in the SIA system. It was verified that the sensitivity of the determination as well as enzyme activity, increased with the increase in [bmim][BF4] concentration until proportions with water of 1:1.5. These observations confirm the excellent activity of horseradish peroxidase in this IL but also its enhancement in the presence of increasing concentrations of [bmim][BF4]. The implementation of the assay in a SIA system hindered efforts to test more concentrated mixtures due to the increased viscosity of the resulting solutions. However as expected, it was verified that the enzyme activity was totally lost if prepared exclusively in [bmim][BF4], showing that the presence of water is essential for enzyme activity. This issue has already been discussed regarding other enzymes activity in organic media [19] and very recently in IL [20] and it is accepted that a few water molecules, presumably bound to charged groups on the surface of the enzyme, are required for catalytic function. It is also important to consider the problem of enzyme solubility which also hinders the exclusive use of organic solvents or IL [13]. If it was technically possible to continue increasing the amount of [bmim][BF4] in the solvent mixture, in the SIA system, the enzyme activity would increase until the amount of water was so small that deactivation of the enzyme occurred.

3.3. Evaluation of horseradish peroxidase activity in methanol

The study of horseradish peroxidase activity in methanolic media was intended to provide information on performing a comparative evaluation of enzyme behaviour in [bmim][BF4] and methanol, with a view to suggesting the utilisation of ILs as an alternative to conventional organic solvents. On this basis, using the same manifold and the same conditions used in the test involving [bmim][BF4], an evaluation of horseradish peroxidase activity in methanol was performed. This evaluation comprised the implementation of the 4AAP-phenol test in the SIA system, using water/methanol mixtures as reaction media, the assessment of pH influence, temperature and methanol concentration on enzyme activity and a comparison of the results obtained with those obtained in the presence of [bmim][BF4].

The 4AAP-phenol test was again implemented in the SIA system, maintaining all of the established conditions except the solvent for the preparation of the solutions, which in this case was methanol. At this point it was important to evaluate whether the optimum enzyme activity would be achieved under the same conditions described in the studies with IL and if the studied parameters would have the same influence on enzyme activity.

To begin, the evaluation of horseradish activity was performed at room temperature and pH 11.2, and using a 1:0.5 water/methanol mixture, which comprised the initial set of conditions for the assays with [bmim][BF4]. These conditions were chosen in order to conduct the studies in the same direction and perform comparisons step by step. This assay showed that the enzyme activity was maintained but decreased significantly when compared under the same conditions, with the activity exhibited in the presence of [bmim][BF4] (Fig. 3).

The study of pH influence on the sensitivity of the determination was performed as before by changing the pH of the carrier solution between 6 and 12. It was concluded that the optimum situation in terms of the enzyme activity was achieved at pH 7.5. Effectively, there was an enhancement of horseradish peroxidase activity until this value and beyond which a significant decrease occurred, showing that, in the absence of inactivation phenomena by ILs in acid solutions, the enzyme exhibits maximum activity at

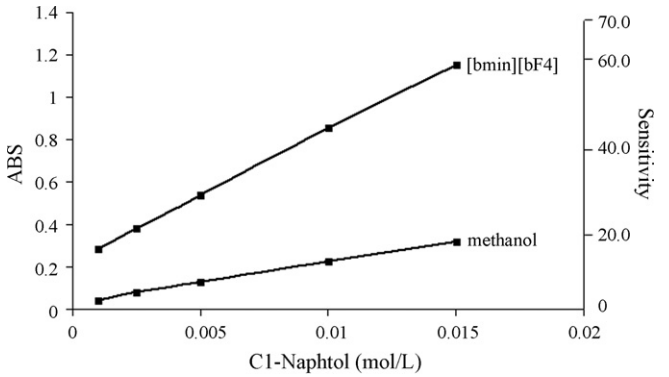

Fig. 3. Comparison of horseradish peroxidase activity in [bmim][BF4] and methanol. Assays performed at room temperature, with carrier solution pH 11.2 and water/[bmim][BF4] and water/methanol mixtures 1:0.5.

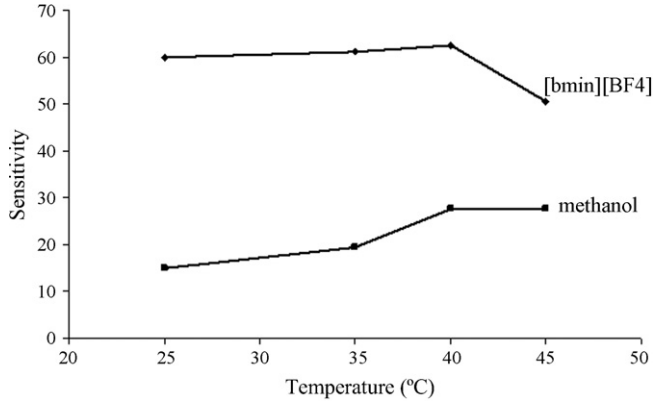

Fig. 4. Influence of the temperature on horseradish peroxidase activity in [bmim][BF4] and methanol. Assays performed with carrier solution pH 11.2 and water/[bmim][BF4] and water/methanol mixtures 1:0.5.

pH values similar to those described as the optimum in water [18]. These results are in good agreement with several studies involving peroxidase catalyzed reactions performed in methanol at pH between 7 and 7.5 [21,22].

The influence of temperature on the activity of horseradish peroxidase in methanol was evaluated using a carrier solution of pH 11.2 (Fig. 4). A significant enhancement in enzyme activity up to 40 °C was observed, showing that in this media, temperature performs an important role on enzyme activity, probably due to an increase in stability of the enzyme–substrate complex. Above 40 °C, it was only possible to evaluate the enzyme activity at 45 °C but already with some problems related with the volatility of the solvent which resulted in the formation of air bubbles inside the flow system. Nevertheless, the obtained results showed that the enzyme maintained its activity at this temperature, meaning that under these conditions there is no denaturation of the proteic structure of horseradish peroxidase and confirming the theory of enhanced thermal stability of enzymes in organic media [23].

Solutions of water/methanol 1:0.5, 1:1 and 1:1.5 were prepared and as previously described, tested in the SIA system, in order to evaluate the influence of methanol concentration on horseradish peroxidase activity. As in the case of [bmim][BF4], an increase in enzyme activity up to proportions of 1:1.5 was observed, showing that a predominantly aqueous media does not provide the best conditions for horseradish peroxidase performance. The results are similar and probably related to the high solubility of 1-naphtol in both [bmim][BF4] and methanol that results in a preferential partition of the hydrophobic compound into the non-aqueous phase.

As a result, when the non-aqueous phase increases, there is also an increase of substrate in the interface between the organic and aqueous phase, enhancing its contact with the enzyme and consequently, the sensitivity of the determination.

4. Conclusions

This approach based on the insertion of water/[bmim][BF4] mixtures in a SIA system is intended to be a generic tool for the implementation of enzymatic assays in ILs and has allowed us to confirm once again that SIA is an accurate fluids handle technique that minimizes consumption of reagents and production of effluents, thus being an excellent choice for enzymatic assays in general.

Furthermore, it is important to highlight that the presented approach resulted in a fully automatic procedure and represents an evolution relative to the classic methods traditionally used in this kind of study that are subject to constant operator intervention and all the drawbacks and errors associated with this. On this basis, the developed methodology reduced the operator exposure to 1-naphtol and solvents and produced a very small amount of effluent when compared to conventional batch procedures, resulting in increased environmental and human safety. Moreover, the consumption of reagents was dramatically reduced due to the possibility of strictly aspirating the required small solution volumes on a reproducible basis. This fact is of utmost importance considering the high prices of the commercial ILs and makes the assays less expensive and more promising due to the possibility of exploiting all potentialities of this kind of solvent with reduced amounts of solutions.

Moreover, the implementation of the 4AAP-phenol test in the SIA using water/[bmim][BF4] as reaction media, led to a fast, versatile and robust methodology that could also be applied in routine determination of phenols.

Regarding horseradish peroxidase activity, the assays showed that the enzyme has maximum activity at pH 11.2 and 40 °C and maintained its activity in water/[bmim][BF4] mixtures up to 1:1.5. Furthermore, the comparative evaluation of enzyme behaviour under these conditions showed that there is an enhancement in enzyme activity of about 5 times when the assay was performed in water/[bmim][BF4], confirming the thesis that in this media enzymes exhibit improved stability, selectivity and activity and that this solvent can be advantageously used as an alternative to conventional organic solvents [14]. This is probably explained by the polarity of ILs that results in strong charge–charge interactions with the enzyme that may be responsible for its activation. However, it is obvious that this complex issue is related to other parameters, most of them unexplained, that affect enzyme–solvent interactions. Globally, it is accepted that IL generate a stabilizing microenvironment that enhances enzyme activity. Nevertheless, the enormous variety of IL and its tuning nature open up many possibilities in terms of research and do not allow general conclusions and considerations to be taken.

With this work it was possible to yet again confirm the potential and importance of SIA for the mechanisation of biocatalytic procedures by opening a new perspective on the implementation of enzymatic assays in IL, so that in the near future, this kind of strategy could become an important analytical tool for enzymatic procedures that demand increased sensitivity.

References

[1] E.H. Hansen, Anal. Chim. Acta 216 (1989) 257.
[2] P.C.A.G. Pinto, M.L.M.F.S. Saraiva, S. Reis, J.L.F.C. Lima, Anal. Chim. Acta 531 (2005) 25.
[3] S.K. Hartwell, B. Srisawang, P. Kongtawelert, J. Jakmunee, K. Grudpan, Talanta 66 (2005) 521.
[4] J. Ruzicka, G. Marshall, Anal. Chim. Acta 237 (1990) 329.
[5] C.E. Lenehan, N.W. Barnett, S.W. Lewis, Analyst 127 (2002) 997.
[6] A.M. Klibanov, Trends Biochem. Sci. 14 (1989) 141.
[7] S. Cantone, U. Hanelfe, A. Basso, Green Chem. 9 (2007) 954.
[8] E.P. Hudson, R.K. Eppler, D.S. Clark, Curr. Opin. Biotechnol. 16 (2005) 637.
[9] A.M. Klibanov, Nature 409 (2001) 241.
[10] S. Sgalla, G. Fabrizi, S. Cacchi, A. Macone, A. Bonamore, A. Boffi, J. Mol. Catal. B 44 (2006) 144.
[11] S. Park, R.J. Kazlauskas, Curr. Opin. Biotechnol. 14 (2003) 432.
[12] C.M. Gordon, Appl. Catal. A: Gen. 222 (2001) 101.
[13] Z. Yang, W. Pan, Enzyme Microb. Technol. 37 (2005) 19.
[14] S. Imabayashi, K. Ishii, M. Watanabe, Electrochem. Commun. 8 (2006) 45.
[15] B. Jastorff, R. Stormann, J. Ranke, K. Molter, F. Stock, B. Oberheitmann, W. Hoffmann, J. Hoffmann, M. Nuchter, B. Ondruschka, J. Filser, Green Chem. 5 (2003) 136.
[16] P. Trinder, Ann. Clin. Biochem. 6 (1969) 24.
[17] N. Caza, J.K. Bewtra, N. Biswas, K.E. Taylor, Water Res. 33 (1999) 3012.
[18] D. Schomberg, M. Salzmann, D. Stephan, Enzyme Handbook 7 (1993) 1–6.
[19] A. Zaks, A.M. Klibanov, J. Biol. Chem. 263 (1988) 8017.
[20] S. Wang, T. Chen, Z. Zhang, D. Pang, Electrochem. Commun. 9 (2007) 1337.
[21] L. Dai, A.M. Klibanov, Biotechnol. Bioeng. 70 (2000) 353.
[22] F. Pezzotti, M. Therisod, Tetrahedron: Asymmetry 18 (2007) 701.
[23] A.M.P. Koskinen, A.M. Klibanov, Enzym. Reactions Organic Media (1996) 83.

Talanta 77 (2008) 765–773

Contents lists available at ScienceDirect

Talanta

journal homepage: www.elsevier.com/locate/talanta

Optimization of Polyurethane Foams for Enhanced Stir Bar Sorptive Extraction of Triazinic Herbicides in Water Matrices

Fátima C.M. Portugal[a], Moisés L. Pinto[a,b], J.M.F. Nogueira[a,b,*]

[a] University of Lisbon, Faculty of Sciences, Chemistry and Biochemistry Department, Campo Grande Ed. C8, 1749-016 Lisbon, Portugal
[b] University of Lisbon, Faculty of Sciences, Center of Chemistry and Biochemistry, Campo Grande Ed. C8, 1749-016 Lisbon, Portugal

ARTICLE INFO

Article history:
Received 8 April 2008
Received in revised form 27 June 2008
Accepted 11 July 2008
Available online 23 July 2008

Keywords:
Triazines
Herbicides
Stir bar sorptive extraction
Novel polymeric phases
Polyurethane foams
High performance liquid chromatography
Water matrices

ABSTRACT

In this work, polyurethane foams (PU) were developed, characterized and applied as new generation polymeric phases for stir bar sorptive extraction (SBSE) using seven triazinic herbicides (simazine, atrazine, prometon, ametryn, propazine, prometryn and terbutryn) as model compounds in water matrices. Assays performed for PU synthesis and characterization demonstrated that seven formulations presented remarkable stability and excellent mechanical and chemical resistance, for which the P_6 formulation showed the best results. By performing systematic assays on 25 mL of water samples spiked at the 10 μg/L level, it was established that the best experimental conditions using stir bars coated with P_6 were an equilibrium time of 6 h (1250 rpm), 5% of methanol as organic modifier, followed by liquid desorption with methanol as back extraction solvent under ultrasonic treatment (20 min) and high performance liquid chromatography with diode array detection (SBSE(PU)-LD-HPLC-DAD). This methodology provided good recoveries (20.4–62.0%) and remarkable reproducibility (R.S.D. <7.0%). Furthermore, excellent linear dynamic ranges between 0.9 and 16.7 μg/L ($r^2 > 0.9949$) and detection limits (0.1–0.5 μg/L) at trace level were also achieved. The application of the proposed analytical approach to analyze triazinic herbicides in ground and superficial water matrices, showed remarkable performance and by using the standard addition methodology the matrix effects are negligible. By comparing the best PU formulation (P_6, 71 μL) with commercial stir bars coated with PDMS (126 μL), recoveries normalized to the polymeric volume up to five times higher (atrazine) were attained. The ability of PU foams to extract the more polar compounds rather than PDMS makes this polymer a very valuable contribution for SBSE.

1. Introduction

Stir bar sorptive extraction (SBSE) is an emerging sample preparation technique, proposed in the last decade, for the enrichment of organic compounds from aqueous matrices prior to chromatographic analysis [1–5]. So far, several research studies applied successfully this "environmental friendly" methodology in different scientific fields, namely, in the study of the aroma wine compounds [6], pharmaceutical drugs [7–10], as well as to monitor many classes of anthropogenic substances in environmental matrices, such as pesticides, polyaromatic hydrocarbons and polybrominated diphenyl ethers [11–14]. This analytical approach has, however, been based in the use of polydimethylsiloxane (PDMS), which is an extracting phase with higher affinity for the less polar compounds, but presents limitations concerning the extraction of the more polar ones ($\log K_{O/W} < 3$), leading to low affinity and poor sensitivity, in particular during trace analysis. The attempt to develop new polymeric phases for SBSE with higher affinity for the more polar compounds is therefore, of great importance. To overcome this limitation, several authors have proposed new strategies, such as the dual-phase stir bar [15], involving PDMS combined with adsorbents, such as activated carbons, to enhance the recovery of the more polar analytes. Nevertheless, these enrichment approaches have presented a limited range of applicability and proved to be much more acceptable for headspace analysis of particular matrices or classes of compounds [16,17]. Furthermore, other authors have already proposed new polymeric phases, but for very specific analytes without embracing the robustness and the wide range of applicability demonstrated by the PDMS alone [18–20]. Despite all these efforts, there is still the need for a polymeric material that allows better sensibility to recover the broad group of polar organic compounds, enlarging further the SBSE applicability. Since most of the polar compounds are thermolabile or non-volatile, liquid desorption (LD) and high performance liquid chromatography (HPLC) analysis are preferable, avoiding the

* Corresponding author at: DQB/FCUL, Campo Grande Ed. C8, 1749-016 Lisbon, Portugal. Tel.: +351 217500899; fax: +351 217500088.
E-mail address: nogueira@fc.ul.pt (J.M.F. Nogueira).

0039-9140/$ – see front matter © 2008 Elsevier B.V. All rights reserved.
doi:10.1016/j.talanta.2008.07.026

undesirable derivatization step required when thermal desorption and gas chromatography are used. In recent years, solid adsorbent materials have been gaining great importance in applications related with the environmental protection [21]. Polyurethane (PU) foams are polymers with a wide variety of applications [22–24], which have been described to have a high capacity to retain organic vapors in their open cell structure [21,25,26]. These polymers are produced by the reaction of polyisocyanate with polyols and water in the presence of a specific catalyst [22,27]. Through this reactional synthesis, a very versatile material is obtained, whose degree of rigidity depends on the desired application [22], making of this type of material a very attractive polymeric phase for SBSE, as it has been demonstrated recently by our group [28].

Among the class of compounds for which SBSE(PDMS) has showed weak affinity, are some triazinic herbicides, in particular atrazine and simazine [29,30], widely used in agriculture and frequently detected in surface and ground waters [31]. Due to their high toxicity, endocrine disrupting effect, persistence, water solubility, low $\log K_{O/W}$ and widespread application [32,33], state-of-the art analytical methodologies proposed for the determination of triazines in water samples involve an enrichment step, i.e. liquid–liquid extraction, solid phase extraction and solid phase microextraction prior to analysis by chromatographic or hyphenated techniques [14,29–33,34]. However, to our knowledge, SBSE has never been proposed exclusively for this particular class of herbicides, which can represent a great analytical alternative to analyze triazines in water matrices. In the present contribution, we describe in detail the synthesis, optimization, characterization and application of PU foams as new and valuable generation polymeric phases for SBSE. Among the tested formulations, one showed remarkable stability and excellent mechanical and chemical resistance. This formulation was tested in the SBSE of seven triazinic herbicides (simazine, atrazine, prometon, ametryn, propazine, prometryn and terbutryn) in water matrices, chosen according to their $\log K_{O/W}$ ($2.40 < \log K_{O/W} < 3.77$), in order to include examples of compounds to which PDMS has a reasonable affinity (e.g. prometryn and terbutryn) and simultaneously others to which it has low affinity (e.g. simazine and atrazine). The performance of the proposed methodology was evaluated in terms of limits of detection and quantification, linearity and precision for which systematic studies were carried out in order to foresee the best experimental parameters that could affect the overall efficiency. The application of the optimized methodology to analyze triazines in water matrices and the comparison between SBSE(PU) and SBSE(PDMS) performance were also addressed.

2. Experimental

2.1. Chemicals, materials and samples

A certified standard mixture of seven triazinic herbicides (simazine, atrazine, prometon, ametryn, propazine, prometryn and terbutryn) with 100 mg/L each was supplied from Sigma–Aldrich. The chemical structures of the triazines under study are depicted in Fig. 1. HPLC-grade methanol (MeOH) and acetonitrile (ACN) were obtained from Sigma–Aldrich. Ammonium acetate (99%, Lot: 2259A) and acetic acid (99.8%, Lot: 90740) were supplied from Riedel-de Haën. Sodium chloride (NaCl, 99.9%) was supplied by AnalaR (BDH Chemicals, Poole, England). Ultra-pure water was obtained from Milli-Q water purification systems (Millipore, Bedford, MA, USA). For the synthesis of the polymeric phases, a tin catalyst was used, silicone oil (Dow Corning, Midland, MI) was the foam stabilizer, methylene bisphenyl diisocyanate (MDI, Lupanat, BASF, Lemförde, Germany) was used as the isocyanate monomer and ultra-pure water as the expander. The polyols were ethylenediamine tetrakis (ethoxylate-block-propoxylate) tetrol (EDA-PO-EO), glycerol propoxylate (PPG), trimethylolpropane ethoxylate (TMPE) and glycerol (99.8%), all supplied from Sigma–Aldrich. Conventional teflon bars (15 mm × 4.5 mm) and commercial stir bars coated with 126 μL of PDMS (Twister; Gerstel, Müllheim a/d Ruhr, Germany) were used for the SBSE assays. A stock standard solution of the analytes (5 mg/L) was prepared by dilution of 75 μL of the standard mixture to 1.5 mL MeOH. The working and calibration solutions were prepared by dilution of the stock solution with MeOH at the desired concentration and stored refrigerated at −20 °C. The 0.1% ammonium acetate buffer (pH 6) used as mobile phase was prepared by dissolution of 7.71 g of ammonium acetate (Riedel-de Haën) in 1 L of ultra-pure water and addition of 0.32 mL of acetic acid (Riedel-de Haën). Superficial and ground water samples were collected in a dam (Castelo de Bode, Portugal) and in a well near of an orchard area (Tomar, Portugal), respectively.

2.2. PU synthesis, preparation and characterization

The polyurethane (PU) foams were prepared combining one or more poyols from the available ones with MDI, water, silicone oil and a catalyst, in different amounts, yielding different formulations. For simplicity, we only present the seven best formulations, which provided the best recovery yields for simazine (Table 1). The water and isocyanate quantities varied accordingly in order to maintain the NCO index (i.e. the number of NCO groups per OH group in the reaction mixture) [26] in 105% for each formulation, thus allowing an excess of isocyanate, assuring that the reaction is complete. The specific quantities of polyols, ultra-pure water, foam stabilizer and catalyst were added to a polyethylene flask and mixed vigorously for 1 min using a mechanical stirrer (Heidolph Elektro KG, Kelheim, Germany), followed by the addition of the isocyanate and stirring for about 15 s. The resulting mixture was left undisturbed for 1 min, allowing the formation and growth of the foam, and then kept in an oven at 60 ± 1 °C for 24 h. The resulting polymer was cut into homogeneous and symetrical polymeric cilinders (13 mm in length and 0.2 mm film thickness) that were pre-conditioned by a clean-up step before use, consisting in an ultrasonic treatment (Branson 3510) with ACN and MeOH for 20 min (2×), after which they were dried in an oven. The PU cilinders were weighed (Mettler Toledo AG135, Switzerland) and used to coat the conventional teflon bars used for the SBSE assays.

For determination of the density of the PUs, an automatic picnometer (Micromeritics AccuPyc 1330) was used. For the calibration of the picnometer, a steel sphere with known volume was applied. The various PUs were weighted and introduced in the picnometer. Since the picnometer determines the volume of the sample, by introducing the weight we can therefore, determine the density. The procedure for determination of the density included ten purges and ten assays, at a pressure of 10 psi. In Table 1, we present the density of the studied formulations as well as the volume corresponding to a bar with the dimensions (13 mm × 0.2 mm) previously described for the PUs. For the morphological characterization of the synthesized PU foams, scanning electron microscopy (SEM) micrographs were obtained using a JEOL JSM-5200LV, operated at 15 kV, with a metalizer JEOL JFC-1200. For the characterization of the chemical bonds involved, Fourier transform infrared spectroscopy (FTIR) was performed in a Nicolet 6700 FT-IR spectrometer (Thermo Electron Corporation), at a resolution of 4 cm^{-1}, with the collection of 256 scans [27], using the attenuated total reflectance (ATR) technique with a multibounce ZnSe crystal (Smart Multibounce HATR Combo Kit Nexus 0028-299).

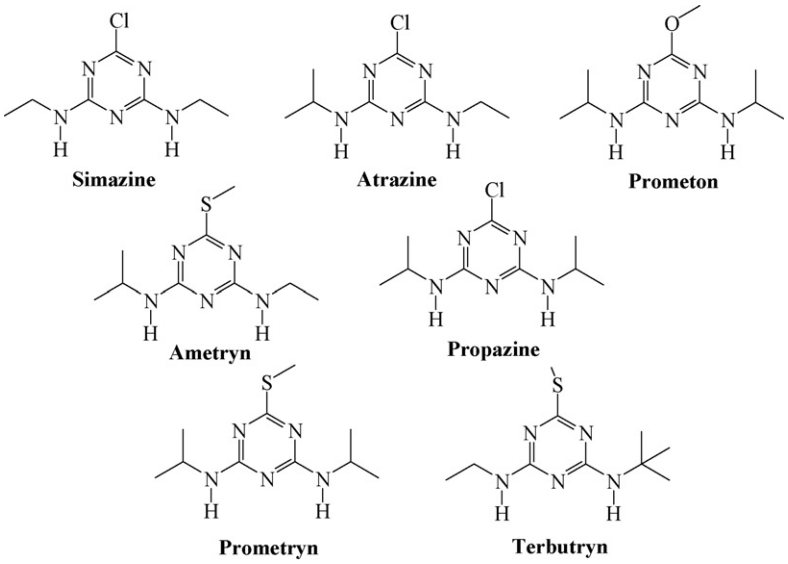

Fig. 1. Chemical structures of the seven triazinic herbicides used in the present study.

2.3. SBSE-LD assays

In a typical assay, 25 mL of ultra-pure water spiked at a concentration level of 10 μg/L were introduced in a glass vial (Macherey-Nagel, Düren, Germany), where a teflon stir bar coated with PU was immersed and closed with a seal using a hand crimper. The assays were performed in a fifteen-agitation point plate (Variomag Multipoint, Germany) at room temperature (25 °C). For the optimization procedure, parameters such as extraction time (0.5, 1, 2, 4, 6 and 16 h), agitation speed (750, 1000 and 1250 rpm), ionic strength (5, 10 and 15% of NaCl) and organic modification (5, 10 and 15% of MeOH) were studied in triplicate. For LD assays, the stir bars were removed with clean tweezers, squeezed to remove residues of water, placed in a sealed 10 mL glass vial filled with 5 mL of organic solvent, ensuring their total immersion, and subjected to ultrasonic treatment for 20 min at constant temperature (25 °C). In order to optimize the LD conditions, triplicate assays were performed to test back extraction solvents (MeOH, ACN and an equimolar mixture of both) and time (20, 40 and 60 min). The occurrence of carry-over was tested by performing a consecutive second back extraction of 20 min with ultrasonic treatment. After the LD, the stir bars were removed and the stripping solvent was evaporated to dryness (Minivap 6MV EA, Sigma–Aldrich) under a gentle stream of purified nitrogen (>99.5%). The dried residues were redissolved in 100 μL MeOH and transferred to a 2 mL glass vial (VWR International), which was sealed using a hand crimper and placed in the automatic sampler tray for HPLC-DAD analysis. To ensure that the losses occurred during the evaporation to dryness were minimum, triplicate assays were performed by spiking 5 mL MeOH at three concentration levels (5, 10 and 20 μg/L), evaporating them to dryness under a gentle stream of nitrogen and redissolving in 100 μL of MeOH. The signal obtained for the standards used to spike the MeOH and for the samples obtained after redissolution were compared. Blank assays were also performed using the same procedure as described above, with ultra-pure water samples without spiking. For data comparison, the optimized methodology was performed with commercial stir bars coated with 126 μL of PDMS. The optimized methodology was applied in triplicate to real matrices, previously filtered and spiked at the desired concentration and blank assays were performed for each sample using the same procedure as described before. The standard addition methodology (SAM) was used, consisting in the addition to the matrix of known amounts of the compounds under study prior to analysis using the proposed methodology. The data obtained was used to define a calibration plot. Therefore, 25 mL of real samples with concentrations between 0.8 and 16.7 μg/L of triazinic herbicides and blank assays (*zero-point*) were analyzed in triplicate using the optimized SBSE(PU)-LD-HPLC-DAD methodology.

2.4. HPLC-DAD analysis

HPLC analysis were carried out on an Agilent 1100 Series LC chromatographic system (Agilent Technologies, Waldbronn, Germany) equipped with the following devices: vacuum degasser, quaternary pump, autosampler, thermostated column compartment and a diode array detector (DAD). Data acquisition was performed with the software LC3D ChemStation (version Ver.A.08.03 [847]; Agilent Technologies). A Tracer Excel 120 octadecilsilica-

Table 1
Formulations of the seven PU foams developed, average density, volume and recovery yields obtained for simazine under standard conditions

	P_1	P_2	P_3	P_4	P_5	P_6	P_7
Formulation	10.00 g PPG 3.40 g MDI	10.00 g PPG 0.50 g glycerol 5.70 g MDI	10.00 g PPG 0.50 g glycerol 4.60 g MDI	5.00 g PPG 5.00 g EDA-PO-EO 3.66 g MDI	10.00 g EDA-PO-EO 3.93 g MDI	5.00 g PPG 5.00 g TMPE 4.90 g MDI	7.00 g PPG 0.50 g glycerol 1.00 g EDA-PO-EO 1.50 g TMPE 6.15 g MDI
Average density (g/mL)	1.1788	1.2151	1.1729	1.0756	1.1691	1.2014	1.2015
Average volume (μL)	63	100	140	99	88	71	89
Recovery for simazine (%)	17.3 ± 4.3	19.5 ± 5.5	20.2 ± 8.3	16.6 ± 5.4	16.6 ± 3.7	23.2 ± 2.7	18.7 ± 5.2

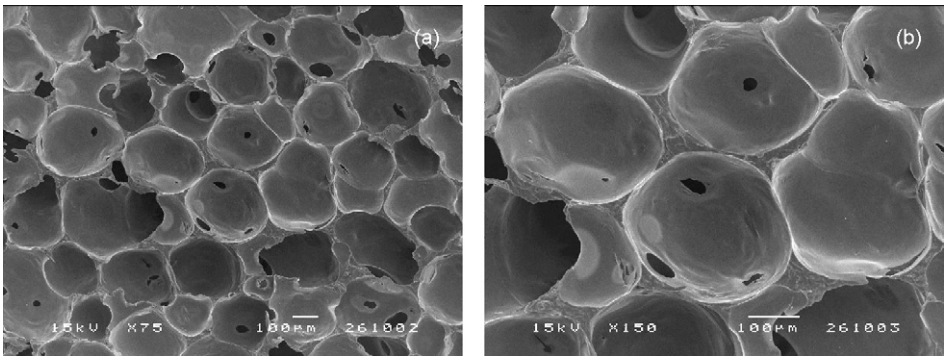

Fig. 2. SEM micrographs of P_6 formulation with different enhancements; 75× (a) and 150× (b).

A, 150 mm × 4.0 mm column, with 5 μm particle size from Teknokroma (Spain) was used. The injection volume was 20 μL with a draw speed of 200 μL/min. The analysis were performed at 25 °C in isocratic conditions with a flow of 1 mL/min, using a mobile phase consisting of a mixture of 42% of ACN and 58% of 0.1% ammonium acetate buffer (pH 6). UV spectra of the analytes were recorded from 220 to 300 nm using a fixed wavelength at 226 nm. For identification purposes, the samples were spiked with pure standards. The identification was based on the retention parameters and UV–vis spectra information obtained from pure standards, while for quantification purposes calibration plots using the external standard methodology were performed. For recovery calculations, peak areas obtained for each assay were compared with those obtained from the standard controls used for spiking the samples. The quantification on real matrices was performed by the SAM.

3. Results and discussion

3.1. Synthesis and characterization of the PUs

In this work, we intended to optimize new PU foams and test their ability as polymeric phases for SBSE. Thus, we synthesized and tested seven formulations in the extraction of simazine, the most polar triazine ($\log K_{O/W} = 2.40$) of the model compounds selected. Table 1 summarizes the different tested PU formulations (P_1–P_7), their average volumes and densities, as well as the simazine recovery yields achieved under standard experimental conditions (SBSE: 90 min (750 rpm); LD: 5 mL MeOH, 20 min with ultrasonic treatment). The highest average recovery observed was obtained for P_6 (23.2 ± 2.7%), whose formulation includes the polyols PPG and TMPE, with an average density of 1.2014 g/mL. This polymer also showed the best mechanical and chemical resistance, which are important features for the SBSE analytical process, as well as for regeneration purposes, which makes P_6 the best formulation for further assays. The volumes of the tested formulations ranged between 63 μL (P_1) and 140 μL (P_3), thus showing that the volumes of the polymeric formulations present the same order of magnitude of those available in the commercial stir bars coated with PDMS (24–126 μL). The average density of the several formulations studied, as well as the corresponding volumes of the polymeric bars, allowed us to conclude that the recovery yields for simazine should not be related with the polymer's volume, since the best average recovery yield was achieved for P_6, which presents the second lowest volume (71 μL). This variation should be related to the specific morphology of each polymer and possibly with the different affinities of the analytes with the functional groups present on the specific formulation. This question is under study and will be addressed soon. Fig. 2 shows SEM micrographs, where it can be observed, in a qualitative way, some surface characteristics such as the cell shape, size, and homogeneity for P_6 formulation. In both micrographs (Fig. 2a and b), it can be observed that P_6 is a very homogeneous material, with both open and closed cells, with spherical shape and slightly wrinkled, and an average cell size of 319 ± 8 μm.

Subsequently, to better understand the nature of the chemical bonds formed on P_6, FTIR analysis was performed using the ATR technique, as depicted in Fig. 3. ATR is a technique that allows the investigation of the surface-near area of the substances, by direct contact with a crystal, through which the infrared beam

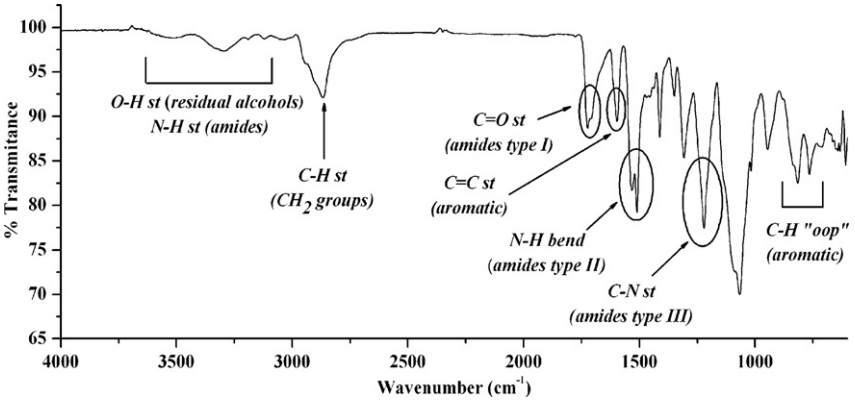

Fig. 3. FTIR spectra of P_6 formulation obtained with ATR, at a resolution of 4 cm^{-1} and 264 scans.

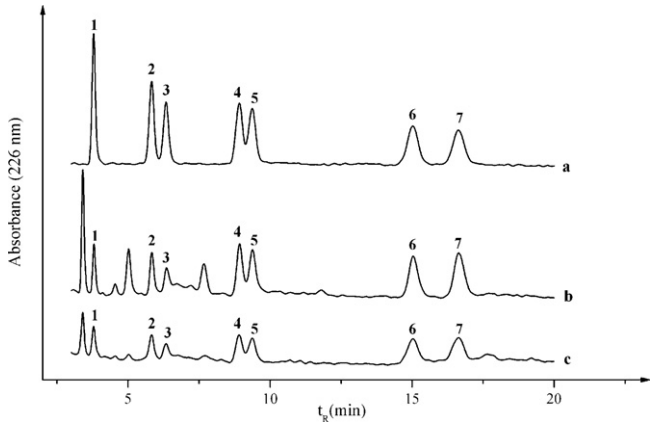

Fig. 4. Chromatograms obtained for the mixture of triazinic herbicides by HPLC-DAD (a) and after analysis by SBSE(P_6)-LD-HPLC-DAD in ground (b) and superficial (c) waters (10 μg/L), under optimized experimental conditions; (1-simazine, 2-atrazine, 3-prometon, 4-ametryn, 5-propazine, 6-prometryn and 7-terbutryn).

passes, penetrating into the PU sample and being totally reflected [27,35]. According to Zhang et al. [36], the bands at 1533 and 1510 cm^{-1} (N—H bend) and 1220 cm^{-1} (C—N stretching), indicate the occurrence of amides type II and III, respectively, confirming the formation of PU foams. Comparing the obtained spectra with MDI spectral data in the Spectral Database for Organic Compounds (SDBS) [37], we can observe in the latter the disappearance of the single band at 2282 cm^{-1}, related to the N=C=O group in MDI, while the single band at 1641 cm^{-1} (related to the C=O stretching in N=C=O group of MDI), moved to 1721 and 1723 cm^{-1}, which is related to the formation of amide bonds in PU foams. These bands are broad, consisting on overlapping peaks, due to the existence of various carbonyl groups in the polymeric matrix, since the polyols and the MDI used were constituted by monomer mixtures. In the spectra, it can also be observed bands at 2870 cm^{-1}, corresponding to C—H stretching of CH_2 groups, and at 1596 cm^{-1} from C=C stretching in aromatic rings of MDI. Therefore, from the FTIR-ATR data of P_6 formulation we can confirm the occurrence of polar sites constituted by chemical groups that commonly occur in PU foams.

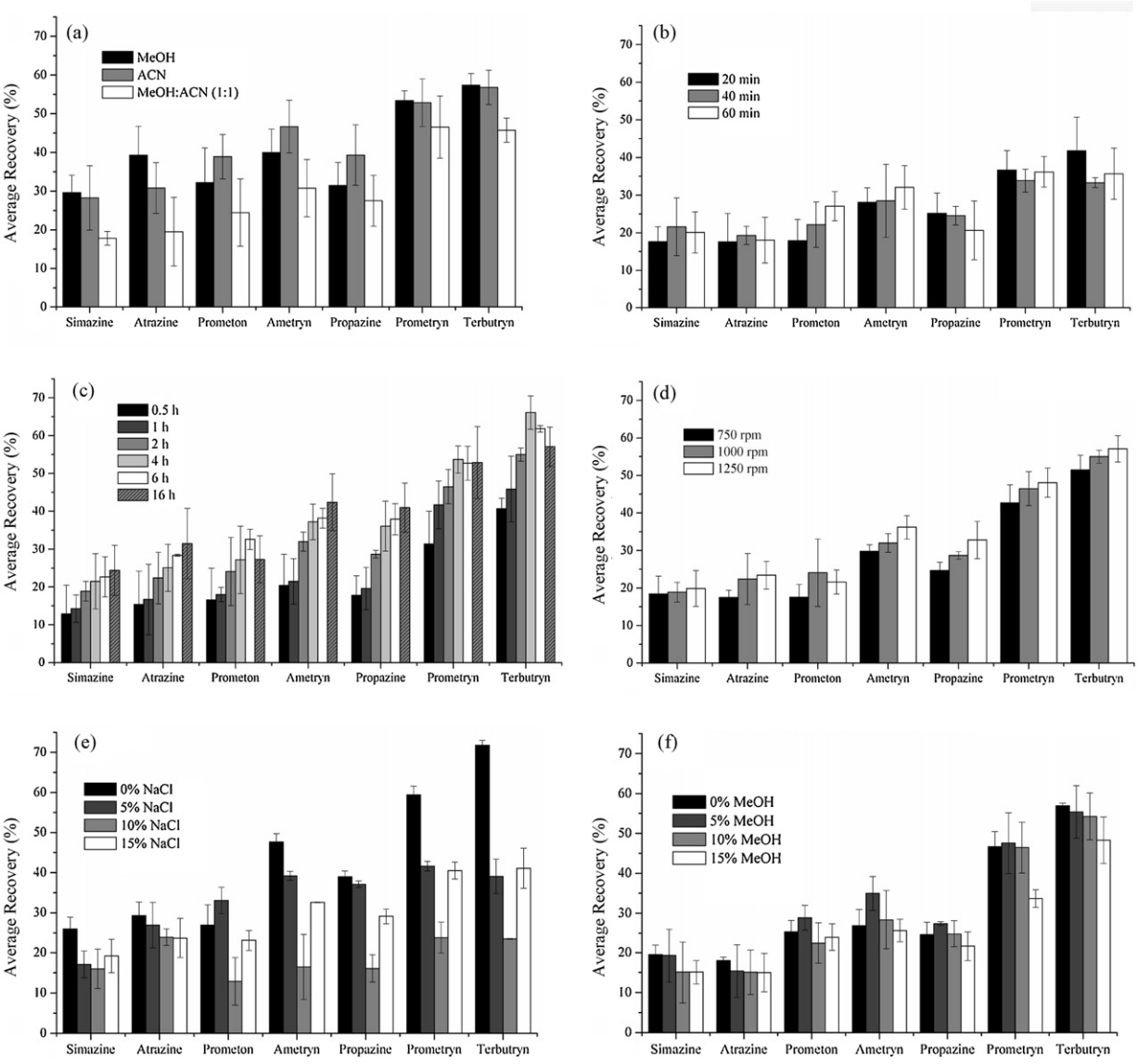

Fig. 5. Effect of back-extraction solvent (a) and time (b), extraction time (c), agitation speed (d), ionic strength (e) and matrix polarity (f) during the optimization evaluation by SBSE(P_6)-LD.

Table 2
Estimated log $K_{O/W}$, LODs, LOQs, linear dynamic range, correlation coefficients, precision (R.S.D.) and average recoveries obtained for the seven triazinic herbicides by SBSE(P_6)-LD-HPLC-DAD, under optimized experimental conditions

Triazinic herbicide	log $K_{O/W}$[a]	LOD (μg/L)[b]	LOQ (μg/L)[c]	Linear range (μg/L)	r^2	R.S.D.[d] (%, n = 6)	Average recovery[d] (%)
Simazine	2.40	0.5	1.5	2.5–16.1	0.9993	4.3	20.4 ± 6.1
Atrazine	2.82	0.5	1.7	1.7–16.3	0.9979	4.3	30.2 ± 3.6
Prometon	3.57	0.1	0.5	1.7–16.3	0.9949	5.6	29.7 ± 4.8
Ametryn	3.32	0.2	0.5	0.9–16.4	0.9993	4.4	36.0 ± 7.7
Propazine	3.24	0.3	0.9	0.9–16.2	0.9995	5.4	34.7 ± 5.7
Prometryn	3.73	0.3	1.0	1.7–16.2	0.9956	6.7	62.0 ± 1.8
Terbutryn	3.77	0.5	1.7	2.6–16.7	0.9988	4.6	58.0 ± 4.8

[a] According to Ref. [38].
[b] S/N = 3.
[c] S/N = 10.
[d] Assays at 10 μg/L level.

3.2. SBSE(P_6)-LD-HPLC-DAD assays

3.2.1. HPLC-DAD operating conditions

Before evaluating the performance of the SBSE methodology using the P_6 formulation, the instrumental conditions were assessed, including the HPLC retention parameters and the DAD response (220–300 nm) for the detection of the triazinic compounds under study. According to the UV–vis spectral data, 226 nm was the wavelength that provided the maximum response for the seven herbicides. Subsequently, the mobile phase was also optimized in order to achieve the best separation under isocratic conditions, using 42% of ACN and 58% of 0.1% ammonium acetate buffer aqueous solution (pH 6), allowing reasonable resolution in a suitable analytical time (<20 min), as depicted in Fig. 4(a). The instrumental calibration was performed with working standard solutions having concentrations ranging from 0.1 to 4.0 mg/L, where excellent linear response was observed for the seven triazinic herbicides under study, with correlation coefficients higher than 0.9979. The instrumental precision was evaluated by six repeatability injections of a standard solution (2.5 μg/L), resulting in relative standard deviations (R.S.D.) ranging from 0.9% (prometon) to 3.6% (atrazine). The instrumental sensitivity was also checked through the limits of detection (LOD) and quantification (LOQ) obtained by injecting six times the most diluted standard and calculated with signal-to-noise ratio (S/N) of 3/1 and 10/1 for each herbicide, respectively. LODs and LOQs ranged from 15.9 to 52.5 μg/L and 53.0 to 175.0 μg/L, respectively, and no carry-over was noticed.

3.2.2. Optimization of the SBSE(P_6)-LD efficiency

According to literature [1,5], several experimental parameters are known to affect the SBSE-LD efficiency, such as extraction time, agitation speed, matrix characteristics (polarity and ionic strength), and back extraction conditions. These parameters were optimized by performing systematic assays using the P_6 formulation. Starting with the LD studies, the solvent type and desorption time are important parameters concerning the back extraction of the compounds from the polymeric phase. The solvent must have enough capacity to ensure the best recovery of the triazinic herbicides from the PUs, which can be accelerated by ultrasonic treatment. During these assays, we tested MeOH, ACN and an equimolar mixture of both solvents. Fig. 5(a) shows that the equimolar mixture of MeOH and ACN decreases the recovery yields, while the differences observed with MeOH and ACN alone can be considered negligible. Since four triazinic herbicides (simazine, atrazine, prometryn and terbutryn) present maximum yields with MeOH, we chose this solvent for the back extraction process. After assessing the desorption solvent, the time of desorption was tested, by comparing 20, 40 and 60 min under ultrasonic treatment with 5 mL of MeOH. As shown in Fig. 5(b), the best time is not the same for all compounds, but since the differences between the tested times can be considered negligible and, 20 min was the best for three of them, this was the desorption time used for the further studies. The occurrence of carry-over was also assessed, by performing consecutive second back extraction assays after desorption with 5 mL of MeOH for 20 min, under ultrasonic treatment, and no evidence for this phenomenon was observed. It must be emphasized that the PU foams developed in the present study, in particular the P_6 formulation, are regenerable, which makes them suitable phases for dozens of SBSE analysis, by just making a clean-up step between runs, using the procedure described in Section 2. After LD, takes place an evaporation step to eliminate the solvent to dryness, under a gentle stream of purified nitrogen followed by redissolution of the dried residues in MeOH. Since this step can lead to some losses of analytes, we also evaluated the performance of this procedure by spiking 5 mL of MeOH at three concentration levels (5, 10 and 20 μg/L), where insignificant losses were observed. After establishing the best LD conditions, we proceeded to the optimization of the SBSE(P_6) by performing assays during 0.5, 1, 2, 4, 6 and 16 h at room temperature. Fig. 5(c) shows the extraction profile obtained for all the seven herbicides under study. For prometryn and terbutryn the optimum extraction time was achieved at 4 h, whereas for prometon was 6 h, and 16 h for the remaining herbicides. Since 16 h is an excessive period for any analytical process, and taking into consideration that there are negligible variations among the recoveries observed, we selected 6 h for the subsequent experiments. The agitation speed influences the SBSE efficiency as well, since it controls the mass transfer of the analytes from the aqueous media towards the polymeric phase during the equilibrium process and thus, we tested three stirring speeds (750, 1000 and 1250 rpm) using a period of 6 h. Although the differences were negligible (Fig. 5d), in general it can be observed that the higher the agitation speed, the higher are the recovery yields achieved, with the exception of prometon. Consequently, 1250 rpm was chosen as the agitation speed for the subsequent assays. The characteristics of the aqueous matrix play a very important role in the SBSE efficiency. For compounds that have lower log $K_{O/W}$, the ionic strength is very important, usually controlled by the addition of NaCl to the matrix. This procedure can promote the "salting out" effect, by increasing the recovery yields of the more hydrophilic compounds. Fig. 5(e) shows the effect of the NaCl content (5, 10 and 15%), where all the compounds present higher recoveries in the absence of salt. This phenomenon can be explained through the occupation of the superficial area of the polymeric phase with the salt ions, which diminishes the superficial area available to interact with the herbicides. A substantial loss of efficiency can also occur by the adsorption of the analytes onto the glass of the sampling flask "wall-effect", which can play a very negative role leading to analyte loss and decreasing the recovery yields [30]. In order to reduce possible adsorption effects, several

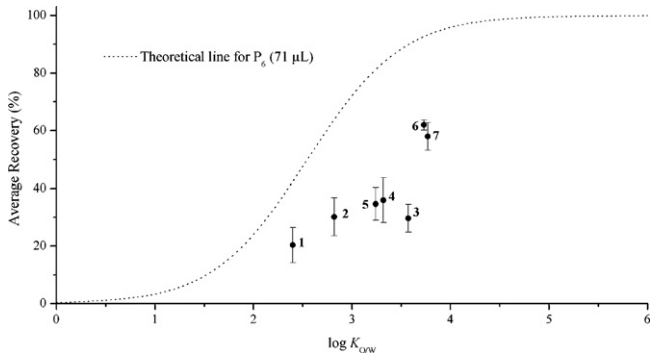

Fig. 6. Theoretical line and experimental recovery data against log $K_{O/W}$ for the seven triazinic herbicides by SBSE(P_6)-LD-HPLC-DAD, under optimized experimental conditions; (1-simazine, 2-atrazine, 3-prometon, 4-ametryn, 5-propazine, 6-prometryn and 7-terbutryn).

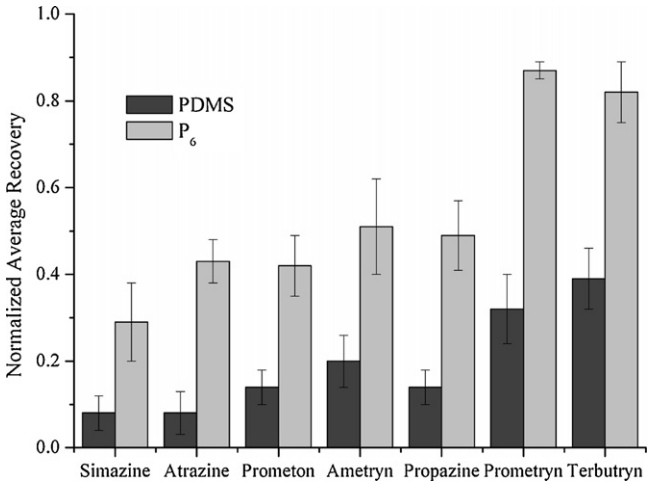

Fig. 7. Comparison of the average recovery normalized to the polymeric volume involved, obtained for the seven herbicides at 10 μg/L, using SBSE(PDMS, 126 μL) and SBSE(P_6, 71 μL) followed by LD-HPLC-DAD, under optimized experimental conditions.

assays were performed through the addition of MeOH (5, 10 and 15%). Although the results exhibit only slight variations (Fig. 5f), maximum recovery yields were obtained for matrices with 5% MeOH, with the exception of simazine, atrazine and terbutryn, for which better efficiency was obtained in the absence of this organic modifier. In general, this phenomenon can promote a higher solubility of the more hydrophobic compounds in the aqueous medium, becoming less polar and therefore, reducing their affinity towards the polymeric phase, hence diminishing the recovery yields [8]. In short, the absence of NaCl and the addition of 5% MeOH seem to be the best matrix characteristics to increase the overall SBSE(P_6) efficiency for the herbicides under study. The pH of the matrix was also tested by performing assays with pH values of 3, 7 and 10, where negligible differences were observed and therefore, did not show any influence during the assays performed, demonstrating not to be a critical parameter during the recovery studies of the seven triazines by SBSE(P_6)-LD.

3.3. Validation of the SBSE(P_6)-LD-HPLC-DAD methodology

After establishing the best experimental conditions to implement the SBSE(P_6)-LD-HPLC-DAD methodology, we proceeded to the corresponding analytical validation. In a first approach, assays performed in water samples spiked at 10 μg/L level, under optimized experimental conditions (SBSE(P_6): 6 h (1250 rpm), 5% MeOH as organic modifier; LD: MeOH (20 min)), showed that the proposed methodology presents good performance, with average recovery yields between 20.4 ± 6.1% (simazine) and 62.0 ± 1.8% (prometryn). According to SBSE theory [1], the distribution coefficients of the analytes between the aqueous matrix and PDMS are correlated with the corresponding octanol–water partitioning coefficients ($K_{PDMS/W} \approx K_{O/W}$). Thus, if we apply to the PU phase the same principles, i.e. $K_{PU/W} \approx K_{O/W}$, we can establish the corresponding equilibrium theoretical line (% recovery *vs* log $K_{O/W}$). Considering 25 mL of water sample (V_W) and a stir bar coated with 71 μL of P_6 (V_{PU}), a phase ratio ($\beta = V_W/V_{PU}$) value of 352 is established (while the commercial stir bars coated with 126 μL of PDMS have a β value of 198). On the other hand, the log $K_{O/W}$ for each triazinic herbicide can be estimated according to a fragment constant estimation methodology (Table 2) [38]. Fig. 6 depicts the equilibrium theoretical line and the experimental recovery data obtained using the optimized methodology for the seven triazines plotted against their correspondent log $K_{O/W}$, with their precision values being also denoted by means of error bars for each compound. By comparing these data, it can be observed that the average recovery yields for each compound do not fit the theoretical line, which means that $K_{PU/W}$ is slightly lower than $K_{O/W}$. Nevertheless, it must be emphasized that the values of log $K_{O/W}$ estimated do not take into consideration the specific interactions between the analytes and the polymeric phase during the sorption equilibrium process. Therefore, if this affinity is weak, $K_{PU/W}$ is only roughly similar to $K_{O/W}$. Moreover, the polymeric phase used at this stage is not PDMS, which means that, although we are applying the same theoretical principles as those proposed for SBSE [1], PUs may not obey them entirely, which can also explain the deviations observed. Even so, calibration can still be performed, according to literature [1]. The linear dynamic range of the global methodology (SBSE(P_6)-LD-HPLC-DAD) was evaluated using nine calibration standards on 25 mL of spiked water samples having the seven triazinic herbicides with concentrations ranging from 0.9 to 16.7 μg/L. The data obtained (Table 2) showed excellent linearity ($r^2 > 0.9949$). The precision was evaluated through repeatability assays calculated as R.S.D. on six replicates, which gave rise to values between 4.3% (simazine and atrazine) and 6.7% (prometryn). The sensitivity of the optimized methodology was defined by the LODs and LOQs, measured at a S/N ratio of 3/1 and 10/1, respectively. The values achieved ranged from 0.1 to 0.5 μg/L for the LODs and from 0.5 to 1.7 μg/L for the LOQs. Table 2 summarizes the estimated log $K_{O/W}$, LODs, LOQs, linear dynamic range, precision (R.S.D.) and average recoveries obtained for all herbicides in water samples by SBSE(P_6)-LD-HPLC-DAD, under optimized experimental conditions. In order to prove that the PU phase proposed exhibits better ability to recover the triazinic compounds, SBSE assays were performed with the P_6 formulation (71 μL) and the commercial stir bars coated with PDMS (126 μL), under the optimized experimental conditions. Fig. 7 shows the average recoveries obtained by SBSE(P_6) and SBSE(PDMS) in both polymers normalized to the polymeric volume involved, where better efficiencies are definitely obtained with the former for all herbicides under study. For atrazine in particular, the average yields normalized to the polymeric volume are up to 5 times higher in comparison with PDMS, while for the remaining are between 2 and 4 times higher. These results allowed us to conclude that these PUs, a new generation of polymeric phases for SBSE, definitely proved to have much more affinity for this particular type of polar compounds, for which PDMS did not show enough performance. The fact that P_6 is a more reticulated polymer than PDMS, with more possibilities for analytes sorption and polar sites as demonstrated before, is a possible explanation for the better yields achieved for this particular class of compounds. Moreover,

Table 3
Contamination (C_0) and regression parameters obtained for the seven herbicides using the SAM on real matrices by SBSE(P_6)-LD-HPLC-DAD, under optimized experimental conditions

Triazinic herbicide	Superficial water			Ground water		
	Slope	r^2	C_0 (μg/L)	Slope	r^2	C_0 (μg/L)
Simazine	6.0728	0.9957		6.1843	0.9944	
Atrazine	6.4601	0.9991		7.6484	0.9992	
Prometon	6.0174	0.9891		6.8140	0.9995	
Ametryn	7.5663	0.9948	<LOD	8.9667	0.9947	<LOD
Propazine	8.8084	0.9899		6.5973	0.9978	
Prometryn	13.2751	0.9937		11.8200	0.9914	
Terbutryn	13.3474	0.9965		11.5069	0.9964	

the volume of polymeric phase used (71 μL) is much lower than the maximum amount of PDMS available in the commercial stir bars (126 μL), which shows that even with less polymeric phase we can achieve much higher sensibility for the herbicides under study.

3.4. Application to water matrices

Although the present methodology (SBSE(P_6)-LD-HPLC-DAD) demonstrates excellent performance to analyze the seven triazinic compounds in water matrices at trace level, there is lack of sensitivity in particular to be in compliance with international regulatory directives on water quality. The European Union directive on drinking water quality (98/83/CE) establishes 0.10 μg/L as the maximum concentration level for individual pesticides and 0.50 μg/L for the sum of them, while in surface water these limits are about an order of magnitude higher, i.e. 1–3 μg/L [32]. On the other hand, the United States Environmental Protection Agency considers the toxicity of the pesticides, thus establishing different limits for each one [32]. Throughout the present work we have decided to test the analytical ability of the proposed methodology in real matrices, including surface and ground water samples. The SAM is always the preferred approach for quantification, in particular when sample matrices are too complex, accounting the occurrence of potential interferences and thus minimizing possible errors [39]. Table 3 summarizes the data obtained from the SAM assays performed by the present methodology for surface and ground waters spiked with the seven triazines. From the data achieved, the regression parameters showed convenient correlation coefficients ($r^2 > 0.9891$) as well as slopes presenting the same order of magnitude in both matrices, meaning that matrix effects are almost negligible by using the present methodology. Additionally, the particular water matrices studied showed the absence of contamination ($C_0 <$ LOD) of the seven herbicides studied. For surface waters, and according to literature [32], the obtained limits of detection can be considered acceptable, since the sum of them is lower than 3 μg/L, but they are not in compliance with the directive 98/83/CE for drinking water matrices. Therefore, altough the present methodology has proven to be a suitable analytical tool to analyze triazinic herbicides at trace level, the performance can be further improved by using HPLC coupled to mass spectrometry or tandem systems (HPLC-MS or HPLC-MS/MS), to achieve much better analytical selectivity and sensitivity, and lower the limits of detection. Fig. 4(b and c) exemplify chromatograms obtained after the application of the proposed methodology, showing a remarkable selectivity and enough sensitivity to analyze triazinic herbicides in ground and superficial water matrices.

4. Conclusions

In this work, polyurethane foams were developed and characterized as new generation polymeric phases for SBSE and successfully applied to analyze triazinic herbicides in water samples. By performing systematic assays with stir bars coated with 71 μL of the P_6 formulation, using an amount of 5% of methanol as organic modifier, an equilibrium time of 6 h (1250 rpm) and methanol as back extraction solvent under ultrasonic treatment (20 min), very good analytical data to analyze triazinic herbicides in water matrices was obtained. Under optimized conditions, a remarkable precision, linearity and limits of detection at trace level were achieved. The application of the present method to analyze triazinic herbicides in ground and superficial water matrices, allowed convenient performance and negligible matrix effects using the standard addition methodology. This work can be used as a starting point to develop a new method to monitor these herbicides. By comparing the best polyurethane formulation (P_6, 71 μL) with the commercial stir bars coated with PDMS (126 μL), recoveries normalized to the polymeric volume up to five times higher (atrazine) were attained. The ability of polyurethane foams to extract the more polar compounds rather than PDMS, makes this polymer a very attractive new generation phase for SBSE. Furthermore, these polymeric phases are very resistant and regenerable materials, suitable for several dozens of analysis.

Acknowledgements

Fátima C.M. Portugal acknowledges Fundação para a Ciência e a Tecnologia (FCT) for a Ph.D. grant (BD/24598/2005) and Dr. Pedro Vaz by the helpful discussions on FTIR-ATR analysis. Moisés L. Pinto acknowledges FCT for a post-doctoral grant (BPD/26559/2006).

References

[1] E. Baltussen, P. Sandra, F. David, C. Cramers, J. Microcol. Sep. 11 (1999) 737.
[2] E. Baltussen, C. Cramers, P. Sandra, Anal. Bioanal. Chem. 373 (2002) 373.
[3] M. Kawaguchi, R. Ito, K. Saito, H. Nakazawa, J. Pharm. Biomed. Anal. 40 (2006) 500.
[4] Y. Picó, M. Fernández, M.J. Ruiz, G. Font, J. Biochem, Biophys. Methods 70 (2007) 117.
[5] F. David, P. Sandra, J. Chromatogr. A 1152 (2007) 54.
[6] R.F. Alves, A.M.D. Nascimento, J.M.F. Nogueira, Anal. Chim. Acta 546 (2005) 11.
[7] B. Tienpont, F. David, T. Benijts, P. Sandra, J. Pharm. Biomed. Anal. 32 (2003) 569.
[8] C. Almeida, J.M.F. Nogueira, J. Pharm. Biochem. Anal. 41 (2006) 1303.
[9] C. Fernandes, P. Jiayu, P. Sandra, F.M. Lanças, Chromatographia 64 (2006) 517.
[10] A. Stopforth, C.J. Grobbelaar, A.M. Crouch, P. Sandra, J. Sep. Sci. 30 (2007) 257.
[11] P. Serôdio, M.S. Cabral, J.M.F. Nogueira, J. Chromatogr. A 1141 (2007) 259.
[12] P. Rosário, J.M.F. Nogueira, Electrophoresis 27 (2006) 4694.
[13] E. Bonet-Domingo, S. Grau-González, Y. Martín-Biosca, M.J. Medina-Hernández, S. Sagrado, Anal. Bioanal. Chem. 387 (2007) 2537.
[14] W. Liu, Y. Hu, J. Zhao, Y. Xu, Y. Guan, J. Chromatogr. A 1095 (2005) 1.
[15] C. Bicchi, C. Cordero, E. Liberto, P. Rubiolo, B. Sgorbini, F. David, P. Sandra, J. Chromatogr. A 1094 (2005) 9.
[16] C. Bicchi, C. Cordero, E. Liberto, B. Sgorbini, F. David, P. Sandra, P. Rubiolo, J. Chromatogr. A 1164 (2007) 33.
[17] C. Bicchi, C. Cordero, E. Liberto, B. Sgorbini, P. Rubiolo, J. Chromatogr. A 1184 (2008) 220.
[18] Y. Hu, Y. Zheng, F. Zhu, G. Li, J. Chromatogr. A 1148 (2007) 16.
[19] X. Zhu, J. Cai, J. Yang, Q. Su, Y. Gao, J. Chromatogr. A 1131 (2006) 37.
[20] J.-P. Lambert, W.M. Mullett, E. Kwong, D. Lubda, J. Chromatogr. A 1075 (2005) 43.

[21] M.L. Pinto, J. Pires, A.P. Carvalho, M.B. de Carvalho, J.C. Bordado, Microporous Mesoporous Mater. 89 (2006) 260.
[22] D.W. Hatchett, G. Kodippili, J.M. Kinyanjui, F. Benincasa, L. Sapochak, Polym. Degrad. Stab. 87 (2005) 555.
[23] A.L. Silva, J.C. Bordado, Catal. Rev. 46 (2004) 31.
[24] D.R. Harbron, C.J. Page, R.K. Scarrow, J. Cell. Plastics 37 (2001) 43.
[25] M.L. Pinto, J. Pires, A.P. Carvalho, M.B. de Carvalho, J.C. Bordado, J. Phys. Chem. B 108 (2004) 13813.
[26] M.L. Pinto, J. Pires, A.P. Carvalho, J.C. Bordado, M.B. de Carvalho, J. Appl. Polym. Sci. 92 (2004) 2045.
[27] H. Oka, Y. Tokunaga, J. Cell. Plastics 42 (2007) 307.
[28] N.R. Neng, M.L. Pinto, J. Pires, P.M. Marcos, J.M.F. Nogueira, J. Chromatogr. A 1171 (2007) 8.
[29] V.M. León, B. Álvarez, M.A. Cobollo, S. Muñoz, I. Valor, J. Chromatogr. A 999 (2003) 91.
[30] P. Serôdio, J.M.F. Nogueira, Anal. Chim. Acta 517 (2004) 21.
[31] L. Balduini, M. Matoga, E. Cavalli, E. Seilles, D. Riethmuller, M. Thomassin, Y.C. Guillaume, J. Chromatogr. B 794 (2003) 389.
[32] S.-D. Huang, H.-I. Huang, Y.-H. Sung, Talanta 64 (2004) 887.
[33] H. Katsumata, S. Kaneco, T. Suzuki, K. Ohta, Anal. Chim. Acta 577 (2006) 214.
[34] O. González-Barreiro, C. Rioboo, C. Herrero, A. Cid, Environ. Pollut. 144 (2006) 266.
[35] K. Sahre, U. Schulze, T. Hoffmann, M.A. Elrehim, K.-J. Eichhorn, D. Pospiech, D. Fischer, B. Voit, J. Appl. Polym. Sci. 101 (2006) 1374.
[36] C. Zhang, Z. Ren, Z. Yin, H. Qian, D. Ma, Polym. Bull. 60 (2008) 97.
[37] SDBSweb: http://riodb01.ibase.aist.go.jp/sdbs/ (Nacional Institute of Advanced Industrial Science and Technology, SDBS Nr. 2289, date of access: november 6th 2007).
[38] W.M. Meylan, SRC KOWWIN Software SRC-LOGKOW Version 1. 66, Syracuse Research Corporation, USA, 2000.
[39] M. Ribani, C. Bottoli, C.H. Collins, I. Jardim, L. Melo, Quim. Nova 27 (2004) 771.

Talanta 77 (2008) 733–736

Contents lists available at ScienceDirect

Talanta

journal homepage: www.elsevier.com/locate/talanta

Micelle-mediated cloud point extraction and spectrophotometric determination of rhodamine B using Triton X-100

N. Pourreza*, S. Rastegarzadeh, A. Larki

Department of Chemistry, College of Science, Shahid Chamran University, Ahvaz, Iran

ARTICLE INFO

Article history:
Received 2 July 2008
Accepted 9 July 2008
Available online 25 July 2008

Keywords:
Rhodamine B
Triton X-100
Cloud point extraction
Spectrophotometry

ABSTRACT

A new micelle-mediated cloud point extraction method is described for sensitive and selective determination of trace amounts of rhodamine B by spectrophotometry. The method is based on the cloud point extraction of rhodamine B from aqueous solution using Triton X-100 in acidic media. The extracted surfactant rich phase is diluted with water and its absorbance is measured at 563 nm by a spectophotometer. The effects of different operating parameters such as concentration of surfactant and salt, temperature and pH on the cloud point extraction of rhodamine B were studied in details and a set of optimum conditions were obtained. Under optimum conditions a linear calibration graph in the range of 5–550 ng mL^{-1} of rhodamine B in the initial solution with $r = 0.9991$ ($n = 15$) was obtained. Detection limit based on three times the standard deviation of the blank ($3S_b$) was 1.3 ng mL^{-1} ($n = 10$) and the relative standard deviation (R.S.D.) for 50 and 350 ng mL^{-1} of rhodamine B was 2.40 and 0.87% ($n = 10$), respectively. The method was applied for the determination of rhodamine B in soft pastel, hand washing liquid soap, matches tip and textile dyes mixture samples.

1. Introduction

Rhodamine B with the chemical structure shown in Fig. 1, belongs to the class of xanthene dyes, which is highly water-soluble. It is among the oldest and most commonly used synthetic dyes. Initially, it was used as a colorant in textiles and foodstuffs, and is also a well-known water tracer fluorescent. Rhodamine B is harmful if swallowed by human beings and animals, and causes irritation to the skin, eyes and respiratory tract. The carcinogenicity, reproductive and developmental toxicity, neurotoxicity and chronic toxicity towards humans and animals have been experimentally proven [1]. Thus, due to the hazardous nature and harmful effects of rhodamine B, it was considered worthwhile to make efforts to develop a simple method for the determination of rhodamine B in different samples. Only few methods are available for the determination of rhodamine B [2–6]. These methods are based on electrokinetic capillary chromatography [5] and high-pressure liquid chromatography (HPLC) [2–4].

In the last decade, there has been an increasing interest on the use of aqueous micellar solution in the field of separation science. Micellar-mediated cloud point technique is often used as a preconcentration method prior to instrumental analysis, e.g. HPLC. This technique can be also used to recover various organic pollutants and metal cations [7,8], the latter after complexation with hydrophilic reagents [9].

At certain temperature, aqueous solution of a non-ionic surfactant separates into two phases. The first one is a surfactant-rich phase containing a high concentration of surfactant, which has small volume compared to the solution and the second one is the aqueous phase containing a low concentration of surfactant. This temperature is known as cloud point temperature (CPT) of the surfactant [10]. The solute molecule present in aqueous solution of non-ionic surfactant is distributed between the two phases above the cloud point temperature [11]. This phenomenon is known as cloud point extraction (CPE).

In the present paper, a simple and sensitive cloud point extraction procedure has been developed for the spectrophotometric determination of rhodamine B using Triton X-100 as non-ionic surfactant. The effect of temperature, concentrations of surfactant and salt on the extraction of dye has been studied.

2. Experimental

2.1. Instrumentation

A GBC Cintra 101, UV–Visible spectrophotometer was used for recording absorption spectra and absorbance measurements using 1 cm glass cells. A Metrohm digital pH-meter model 632 with a

* Corresponding author. Tel.: +98 611 3331042; fax: +98 611 3337009.
E-mail address: npourreza@yahoo.com (N. Pourreza).

0039-9140/$ – see front matter © 2008 Elsevier B.V. All rights reserved.
doi:10.1016/j.talanta.2008.07.031

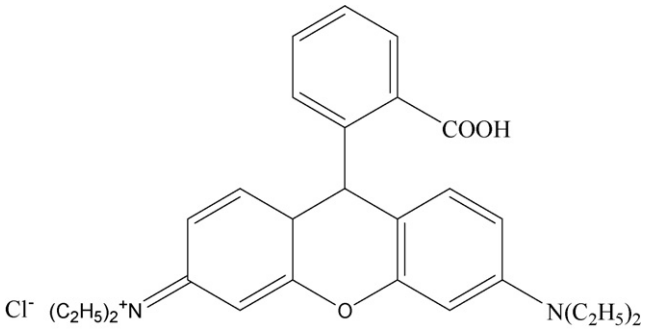

Fig. 1. Chemical structure of rhodamine B.

combined glass electrode was used for pH adjustments. A Colora thermostat bath maintained at the desired temperature was used for the cloud point temperature experiments.

2.2. Reagents

All chemicals used were of analytical grade and double distilled water was used throughout.

A solution of Triton X-100 (0.5 mol L^{-1}) was prepared by dissolving 64.88 g of Triton X-100 (Aldrich) in water and diluting to 200 mL in a volumetric flask.

A stock solution of 500 μg mL^{-1} of rhodamine B was prepared by dissolving 0.05 g of the rhodamine B (Merck) in water and diluting to 100 mL in a volumetric flask. More diluted solutions were prepared daily using this stock solution.

A solution of hydrochloric acid (0.1 mol L^{-1}) was prepared by diluting 8.3 mL of HCl (Merck, d = 1.19 and 37%) in water and diluting to 1000 mL in a volumetric flask.

A 1.0 mol $L^{-1}$of sodium chloride was prepared by dissolving 5.85 g of NaCl (Merck) in water and diluting to 100 mL in a volumetric flask.

2.3. General procedure

In a 50 mL volumetric flask were added: an aliquot of the rhodamine B solution, 3.5 mL of 0.5 mol L^{-1} of Triton X-100, 5 mL of 1.0 mol L^{-1} of NaCl and 5 mL of 0.1 mol L^{-1} HCl. This solution was then diluted to the mark with water and transferred to a 50 mL tube and placed in a thermostat bath at 78 °C for 30 min. After the separation of two phases, the turbid solution was placed in an ice bath for the surfactant rich phase to become viscose. Then the dilute phase was removed by decantation. The surfactant rich phase was diluted with water in a 5 mL volumetric flask. The absorbance of the solution was measured at 563 nm. A blank solution was also run using water instead of rhodamine B.

2.4. Preparation of samples

Appropriate amounts of soft pastel (Mongyu, Korea), hand washing liquid soap (Top Company, Iran), matches tips (Tabriz Company, Iran) or textile dyes mixture (Textile Company, Iran) samples were dissolved in water, filtered if necessary and diluted to 50 mL in a volumetric flask. An aliquot of the above solutions was treated under the general procedure for cloud point extraction and subsequent determination of rhodamin B.

3. Results and discussion

The rhodamine dyes exist in solution as ionized specie, neutral form, lactone and/or molecular aggregates, depending on pH, solvent, temperature and concentration. Each form of rhodamine is characterized by typical absorption spectra, which is further influenced by specific medium effect, i.e. ionic strength and presence of additives [12]. The absorption spectrum of rhodamine B in acidic media shows that maximum absorbance occurs at 563 nm and the presence of surfactant does not have significant effect on its λ_{max}. Therefore, all the absorbance measurements were performed at this wavelength. As the extent of cloud point extraction is influenced by the presence of additives, the surfactant concentration and the pH of the medium, these parameters were optimized in order to achieve the highest sensitivity.

3.1. Effect of hydrochloric acid concentration

The absorption band of rhodamine B at 563 nm was observed in acidic media, an increase in the pH of the solution caused a decrease in intensity of this absorption band. At higher pH values, the cationic form is converted to the neutral one and its absorbance at 563 nm is decreased. Thus, the effect of different acids such as nitric, sulfuric and hydrochloric acid in the same concentration was investigated. The results indicated that there is not much difference between them. Therefore, hydrochloric acid was chosen as convenient and the effect of its concentration was studied. Maximum absorbance was observed when acid concentration was in the range of 0.008–0.014 mol L^{-1}. Thus, an acid concentration of 0.010 mol L^{-1} in the final solution was chosen as the optimum for subsequent experiments.

3.2. Effect of Triton X-100 concentration

For successful cloud point extraction of dye, it is desirable to use minimum amount of surfactant for maximum extraction of dye. Therefore, the effect of the surfactant concentration was investigated in order to ensure maximum extraction efficiency. Quantitative extraction was observed when the Triton X-100 concentration was above 0.030 mol L^{-1}. The surfactant concentration of 0.035 mol L^{-1} was chosen as optimum.

3.3. Effect of electrolytes

It has been reported that the presence of electrolytes decreases the cloud point temperature (salting-out effect), resulting in a more efficient extraction. The lower cloud point is attributed to electrolytes promoting dehydration of the poly(oxyethylene) chains. The salting-out phenomenon is directly related to the desorption of ions from the hydrophilic parts of the micelles, increasing inter-attraction between micelles and consequently leading to the precipitation of surfactant molecules [13].

In order to study the effect of the addition of electrolytes and additives on micellar solutions of rhodamine B, NaCl, KCl and $CaCl_2$ solutions were tested. The results indicated that the presence of NaCl, KCl and $CaCl_2$ provoked the clouding phenomena and decreased the cloud point temperature. In addition, the presence of electrolytes increased the phase separation and enhanced the concentration of the solubilized dyes in coacervate phase. The extraction efficiency of the dye increased similarly in the presence of NaCl, KCl and $CaCl_2$. The results of this study are shown in Fig. 2. As can be observed the results were more consistent in the presence of NaCl. Therefore, it was chosen as the electrolyte for this study. An increase in the concentration of NaCl up to 0.06 mol L^{-1} increased the absorbance and above this value, no significant change was observed. Thus, a concentration of 0.10 mol L^{-1} was chosen for further work.

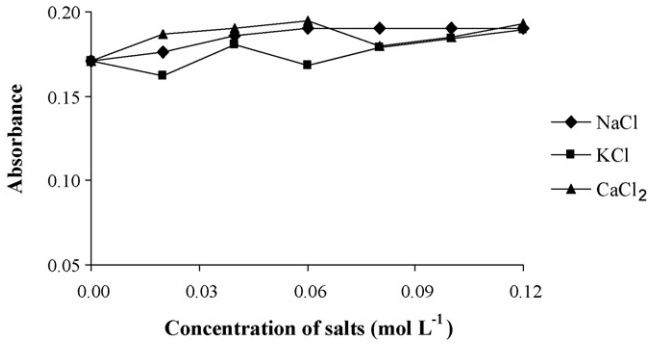

Fig. 2. The effect of different concentrations of NaCl, KCl and $CaCl_2$ on the absorbance of 100 ng mL^{-1} of rhodamine B after cloud point extraction.

3.4. Effects of equilibration temperature and incubation time

Two important parameters in cloud point extraction are incubation time and equilibration temperature. The effect of the equilibration temperature (50–90 °C) on the cloud point extraction was also investigated. Although the solution turns cloudy at room temperature, it was found that better phase separation and thus maximum extraction efficiency is obtained above 78 °C. So, an equilibration temperature of 78 °C was used. The incubation time was also studied. Maximum extraction efficiency was observed at 78 °C after 30 min. Accordingly, an incubation time of 30 min was chosen for use in the next experiments.

3.5. Analytical performance

A linear calibration graph in the range of 5–550 ng mL^{-1} of rhodamine B in the initial solution was obtained by applying the optimized conditions. The equation for the line was $A = 1.7 \times 10^{-3}C + 0.0141$ with regression coefficient (r) of 0.9991 ($n = 15$) where A is the absorbance and C is the concentration of rhodamine B in ng mL^{-1}. Detection limit based on three times the standard deviation of the blank ($3S_b$) was 1.3 ng mL^{-1} ($n = 10$) and the relative standard deviation (R.S.D.) for 50 and 350 ng mL^{-1} of rhodamine B was 2.40 and 0.87% ($n = 10$). The preconcentration factor defined as the ratio of the slopes of calibration curve before and after preconcentration was 8.5.

3.6. Interference studies

The influence of some ions and dyes on the determination of rhodamine B was studied. Various amounts of other species were added to a solution containing 200 ng mL^{-1} of rhodamine B and the recommended procedure was applied. An error of less than or equal to ±5% in the absorbance reading was considered tolerable. The results presented in Table 1 show the good selectivity of the procedure. Two similar dyes, amaranth and allura red were also tolerable up to 15 and 8 ratios, respectively.

Table 1
The effect of species ions on the determination of 200 ng mL^{-1} of rhodamine B

Foreign ions	Tolerance ratio (w/w)
Ni^{2+}, Cu^{2+}, Cd^{2+}, Ca^{2+}, Mg^{2+}, and Zn^{2+}	1000
Pb^{2+}, Co^{2+}, Cr^{3+}, NH_4^+, Br^-, Mn^{2+}, K^+, F^-, NO_3^-, Hg^{2+}, HPO_4^{2-}, CO_3^{2-}, HCO_3^-, I^-, SO_4^{2-}, and Fe^{3+}	500
Allura red	8
Amaranth	15

Table 2
Determination of rhodamine B in different samples

Sample	Rhodamine B added (ng mL^{-1})	Rhodamine B found [a] (ng mL^{-1})	Recovery (%)
Soft pastel 1[b]	–	31.0 ± 0.5	–
	50.0	78.0 ± 1.5	96.0
	100.0	135.0 ± 1.6	103.0
Soft pastel 2[c]	–	16.5 ± 0.4	–
	20.0	37.0 ± 1.5	101.5
	40.0	56.5 ± 1.5	100.0
Textile dyes mixture[d]	–	23.5 ± 0.4	–
	25.0	50.0 ± 1.5	103.0
	50.0	76.0 ± 1.5	103.5
Hand washing liquid soap[e]	–	6.5 ± 0.2	–
	10.0	16.0 ± 0.5	97.0
	20.0	27.0 ± 0.9	102.0
Matches tips[f]	–	11.0 ± 0.5	–
	10.0	21.0 ± 0.6	100.0
	20.0	30.0 ± 0.9	97.0

[a] $x \pm ts/\sqrt{n}$ at 95% confidence ($n = 3$).
[b] Amount of rhodamine B was 97.0 μg g^{-1}.
[c] Amount of rhodamine B was 51.0 μg g^{-1}.
[d] Amount of rhodamine B was 112.5 mg g^{-1}.
[e] Amount of Rhodamine B in hand washing liquid soap was 5.3 μg g^{-1}.
[f] Amount of Rhodamine B in matches tips was 770.8 μg g^{-1}.

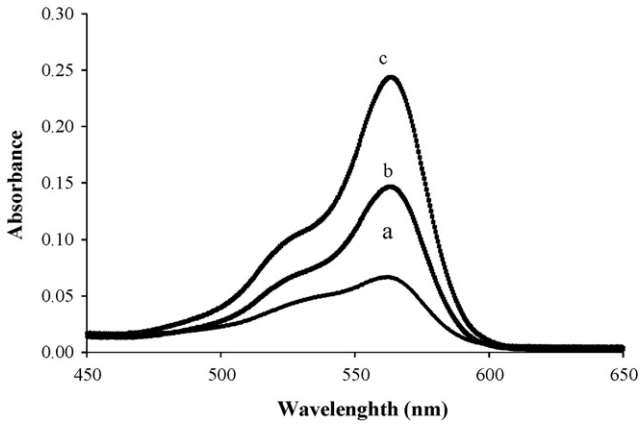

Fig. 3. The absorption spectrum of (a) soft pastel (b) rhodamine B and (c) rhodamine B and soft pastel.

4. Application to real samples

In order to test the reliability of the proposed methodology for the assay of rhodamine B, it was applied to the determination of its concentrations in soft pastel, hand washing liquid soap, matches tip and textile dyes mixture samples. Since an official or standard method does not exist for the determination of rhodamine B [6], the developed methodology was validated by recovery studies. The results shown in Table 2 confirm the validity of the proposed method. As also shown in Fig. 3, the UV–vis spectrum of the component present in soft pastel (a) corresponded very well with the standard spectrum of rhodamine B (b).

5. Conclusion

Up to our knowledge, only few methods are available for determination of rhodamine B [2–6] and this method offers a simple way for the determination of rhodamine B in different samples.

The detection limit of the method is lower than some of the previously reported methods [3–5] and does not require sophisticated instruments. The proposed cloud point extraction is an easy, safe and inexpensive methodology for the separation and determination of trace amounts of rhodamine B in aqueous solutions using non-ionic surfactant Triton X-100. The analytical results obtained lead to the conclusion that the method developed can be successfully adopted for the separation and determination of rhodamine B with high sensitivity and selectivity.

Acknowledgement

The authors wish to thank Shahid Chamran University Research Council for financial support of this project (Grant No. 259-1386).

References

[1] R. Jain, M. Mathur, S. Sikarwar, A. Mittal, J. Environ. Manage. 85 (2007) 956.
[2] J.W. Hofstraat, M. Steendijk, G. Vriezekolk, W. Schreurs, G.J.A.A. Broer, N. Wijnstok, Water Res. 25 (1991) 883.
[3] C. Franke, H. Westerholm, R. Niessner, Water Res. 31 (1997) 2633.
[4] L. Gagliardi, D. De Orsi, G. Cavazzutti, G. Multari, D. Tonelli, Chromatographia 43 (1996) 76.
[5] C. Desiderio, C. Marra, S. Fanali, Electrophoresis 19 (1998) 1478.
[6] C.C. Wang, A.N. Masi, L. Fernandez, Talanta 75 (2008) 135.
[7] S. Akita, H. Takeuchi, Sep. Sci. Technol. 30 (1995) 833.
[8] D. Bai, J. Li, S.B. Chen, B.H. Chen, Environ. Sci. Technol. 35 (2001) 3936.
[9] S. Akita, M. Rovira, A.M. Sastre, H. Takeuchi, Sep. Sci. Technol. 33 (1998) 2159.
[10] W.L. Hinze, E. Pramauro, Crit. Rev. Anal. Chem. 24 (1993) 133.
[11] Z. Wang, F. Zhao, D. Li, Colloid Surf. A 216 (2003) 207.
[12] S. Miljani, Z. Cimerman, L. Frkanec, M. Zini, Anal. Chim. Acta 468 (2002) 13.
[13] L.M. Coelho, M.A.Z. Arruda, Spectrochim. Acta: Part B 60 (2005) 743.

Talanta 77 (2008) 463–467

Contents lists available at ScienceDirect

Talanta

journal homepage: www.elsevier.com/locate/talanta

Towards the development of a fully integrated polymeric microfluidic platform for environmental analysis

Sonia Ramírez-García[a,*], Mireia Baeza[b], Martina O'Toole[a], Yanzhe Wu[c], James Lalor[d], Gordon G. Wallace[c], Dermot Diamond[a]

[a] Adaptive Sensors Group, National Centre for Sensor Research, School of Chemical Sciences, Dublin City University, Ireland
[b] Grup de Sensors i Biosensors, Departament de Química, Facultat the Ciencies, Edifici C-Nord, Universitat Autònoma de Barcelona, Spain
[c] ARC Centre of Excellence for Electromaterials Science, Intelligent Polymer Research Institute, University of Wollongong, Australia
[d] National Centre for Plasma Science and Technology, School of Physical Sciences, Dublin City University, Ireland

ARTICLE INFO

Article history:
Received 31 October 2007
Received in revised form 19 March 2008
Accepted 4 April 2008
Available online 12 April 2008

Keywords:
Biomimetic pump
Low-power microanalytical platform
Polypyrrole actuators
LED detector
Nitrite determination

ABSTRACT

In this paper we report the development and assessment of a biomimetic pump based on soft polymeric actuators, i.e. polyurethane tubes (950 μm internal diameter) with polypyrrole, which expands and contracts during redox cycling and provides the driving force for liquid movement. This pump can be integrated in the microfluidic channels, functioning in a similar manner similar to blood vessels. In principle, these biomimetic pumps and low power detectors could be integrated into a fully functional and totally integrated microanalytical platform. It was also low power (of the order of 100 mJ/μL to obtain a flow rate of 0.08 μL/s), operating using voltages of up to ±1 V, and requiring currents of less than 100 mA. The flow rates achieved are comparable to miniaturised commercial pumps, with the benefit of considerably reduced power consumption (a conventional miniaturised peristaltic pump consumes ca. 3.6 J/μL to obtain the same flow rates as the pump integrated in this system).

The microchip was constructed using polydimethylsiloxane (PDMS) and designed to provide the appropriate mixing of reagents in order to obtain optimum response from the sensors. The chip incorporated an optical detection system constructed using miniaturised light emitting diodes (LED) for both the light source and the detector. This low-cost and low-power detector was surprisingly sensitive due to its integrating mode of operation, and exhibited very low limits of detection. In the present system, conventional LEDs were employed as proof of concept. However, surface mount LEDs will be employed which will allow for a much more compact and compatible format for use in microfluidic manifolds than conventional LEDs.

The low-power biomimetic pump, and the low power detector system were assessed as components that could be integrated into a futuristic integrated microanalytical platform.

1. Introduction

The emergence of the lab-on-a-chip concept, which envisages microanalytical instruments capable of performing complex sample processing and analysis procedures, is one of the most exciting developments in analytical chemistry in recent years [1]. The development of these sensing platforms involves miniaturisation strategies and has stimulated advances in nanotechnology. The output of this research is a range of techniques for generating microfluidic channels and structures with staggeringly small dimensions using a wide range of materials [2,3].

Spatial and temporal monitoring of environmental quality using autonomously deployed sensor networks is an attractive vision [4–6] but its realisation is severely inhibited by the lack of low-cost, low-maintenance, reliable chemical sensors and biosensors [7,8]. Microfluidic systems offer a route forward in that the sensing device can be housed within a protective environment and only occasionally exposed to the sample, which is drawn into the fluidic manifold through a filter interface from the external environment. Between measurements, the instrument can perform automated calibration routines to detect and compensate for baseline drift and changes in sensitivity. However, a key issue with microfluidic analytical instruments is how to control the fluid movement, as high power demand pumps and valves are still employed in many systems [9]. Consequently, there is significant interest in alternative, low-power approaches to moving liquids through microfluidic manifolds. One

* Corresponding author.
E-mail address: sonia.ramirez@dcu.ie (S. Ramírez-García).

0039-9140/$ – see front matter © 2008 Published by Elsevier B.V.
doi:10.1016/j.talanta.2008.04.002

strategy, which we report in this paper, is to employ electroactive soft actuators, which can be regarded as biomimetic, in that as soft actuators, they mimic to some extent the behaviour of muscle. In this particular case, we coated thin-walled polyurethane tubes with polypyrrole, which expands and contracts during redox cycling.

The present paper reports the efforts made towards development of essential components (pump and detector) of a futuristic integrated microanalytical instrument. The work is still in a proof of concept phase, and future efforts will focus on the total integration of these components in a fully functioning microfluidic chip. However, the results obtained were very encouraging.

The pump was based on polypyrrole (ppy) actuators [10]. Ppy based actuators for pumping applications have been previously reported [10,11]. Ppy is a type of conducting polymer. Ppy can be synthesised electrochemically by oxidising the monomer. If the electrosynthesis is performed in the presence of large anions, the anions become trapped in the structure of the polymer. When the backbone of the polymer is then reduced, there is an excess of negative charges that are compensated by diffusion of hydrated cations to the polymeric matrix. This leads to swelling of the polymer that can be utilised to produce mechanical work. The oxidation and reduction of the ppy can be achieved by applying 1 V between the working electrode (ppy) and a reference electrode. Since very low currents flow through this system, the power consumption of this type of pumps can be as low as 8.7 mW [10]. In this project, the swelling of the polypyrrole was used to deform thin-walled polyurethane tubes. This effect could be used to generate liquid movement in microfluidic channels. Moreover, stand-alone polypyrrole tubes were also constructed [12]. This will allow further miniaturisation of the pumps and their integration inside the actual channels of the microchip.

The chip was constructed using polydimethylsiloxane (PDMS). This is a soft polymer that allows easy integration of different components in the chip. The design of the chip is shown in Fig. 1A. The detector was based on Light Emitting Diodes (LEDs). These detectors have shown outstanding properties, from low-power consumption and long lifetime to extremely low detection limits [13]. Moreover, the availability of LEDs of a broad range of sizes and wavelengths, make them a very attractive type of detectors for their implementation in microanalytical platforms for a broad range of analytes.

2. Experimental

The electrosynthesis of polypyrrole (ppy) was performed in propylene carbonate (Sigma–Aldrich, HPLC grade) containing 1% of Milli-Q water. Pyrrole was purchased from Sigma–Aldrich and vacuum distilled previous to electropolymerisation or chemical deposition. The solution used for electrosynthesis contained 0.06 M pyrrole and 0.05 M support electrolyte, tetrabutylammonium hexafluorophosphate ($TBAPF_6$) (Sigma–Aldrich, electrochemical grade) unless otherwise stated. Polypyrrole was electrosynthesised following a previously reported procedure [10,12].

A pump was constructed using electromechanical actuators based on Nafion-ppy, and two other methods for micropump construction were also attempted with promising results. The pump produced consisted of two Nafion-ppy actuators in a tweezers configuration deforming a polydimethylsiloxane (PDMS) chamber. The actuators were constructed using Nafion-117 films obtained by casting 150 mL of a 50 vol.% mixture of dimethylformamide (DMF), purchased from Sigma and used as received, and a 5% Nafion-117 solution of saturated alcohols, also obtained from Sigma, in a 9 cm diameter circular-flat bottom mould. The polypyrrole was then deposited by chemical oxidation of pyrrole on the Nafion film using a procedure reported previously [14]. A Nafion-117 film was pre-treated by first roughening it using sandpaper and it was then sonicated for 15 min in Milli-Q water. The Nafion-117 film was then boiled in HCl 1 M for 30 min and in Milli-Q water for another 30 min to swell it. The polypyrrole was synthesised in situ by chemical oxidation and polymerisation. The Nafion-117 film was dipped in a 0.2 M pyrrole solution containing 0.005 M naphthalene-1,5-disulfonic acid disodium salt (NDSA) and a solution of 0.2 M $FeCl_3$ was then slowly added while constantly stirring the solution. Once all the $FeCl_3$ solution was added, the mixture was allowed to react overnight. The actuator was then washed in Milli-Q water and stored in 2 M LiCl for 3 days before use. To construct the pump, two actuators were placed on each side of a PDMS chamber (1.5 cm long, 6–7 mm i.d. and 100 μm thick walls) and the chamber was deformed by the actuators, producing fluid displacement. The direction of the flow was controlled using conical inlet and outlet channels, following the nozzle-diffuser principle [15,16].

A second approach for pump construction that was attempted involved the by deposition of ppy onto polyurethane tubes (NOVEON, inner diameter 950 μm and outer diameter 1050 μm) sputter-coated with platinum [10]. The ppy coated polyurethane tubes were then wrapped in polyvinylidene fluoride membranes (PVDF membrane, 110 μm, 0.45 μm pore size, Millipore) also sputter-coated with platinum and ppy electrodeposited on one of their sides. Ppy was grown galvanostatically (0.1 mA/cm^2 for 12 h at −20 °C), producing films of ∼30 μm thickness.

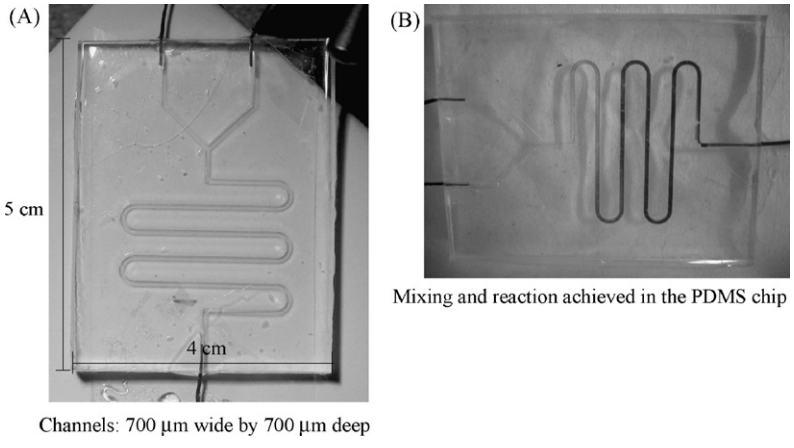

Fig. 1. (A) Picture of the PDMS microchip with dimensions. (B) Photograph of the PDMS chip demonstrating effective mixing. The Griess-Ilosvay reagent is pump through the upper channel and the nitrites solution is pumped through the lower channel. The flow rate was 30.4 μL/min for both solutions.

Finally, the third approach to pump construction involved the electrosynthesis of polypyrrole onto a 500 μm platinum wire with 125 μm platinum wire wrapped around it (to facilitate electrical connexion) at −20 °C during 6 h [12]. Ppy was also grown galvanostatically at 0.15 mA/cm^2.

Polydimethylsiloxane (PDMS) was purchased from Dow Corning and used as received. The chips were made using a polymethylmetacrylate (PMMA) mould constructed using milling technology. The Light Emitting Diode (LED) detector was constructed as previously described [13]. The optical device was fabricated using two identical (5 mm) LEDs (λ_{max} at 530 nm) (Knightbright, France). All solutions were prepared using deionised water from a Milli-Q system (Millipore, Billerica, MA, USA). The standard nitrite solutions were prepared daily from a concentrated stock solution of 1 g/L of nitrite sodium salt (Sigma–Aldrich, 99.5%) previous to analysis. The chromogenic reagent (Griess-Ilosvay) was prepared by dissolving 2.5 g of sulfanilamide (Sigma–Aldrich, 99%), 0.250 g of *N*-(1-naphtyl)ethylenediamine dihydrochloride (NED) (Sigma Aldrich, 98%) and 40 g of phosphoric acid (Sigma Aldrich, 99%) in 250 mL of Milli-Q water [17]. The solution was stored at 4 °C.

3. Results and discussion

The final aim of this project was to produce a fully integrated microanalytical system. To achieve this, a miniaturised pump and a miniaturised detector were developed. The first pump studied was constructed using Nafion-polypyrrole actuators. The dimensions of this pump were of the order of centimetres (the PDMS pump chamber had 5 mm internal diameter and 2 cm length, and the actuators were 4–5 mm wide and 0.8–1.2 cm long). Fig. 2 shows an image of the prototype of this miniaturised pump. This pump was capable of producing flow in mainly one direction with very small backflow. This was achieved by using conical inlets and outlets. The difference in diameter between the smallest and the largest cross-section of the conical channels was more than two orders of magnitude. This valveless strategy for flow control is based on the nozzle-diffuser principle, previously reported [15,16]. The actuators were stimulated by applying 3 V between the two ppy layers coated on both sides of the Nafion film. A capacitor was thus formed. The voltage applied between the two ppy electrodes promoted migration of the hydrated cations trapped in the Nafion (which is an ionic polymer) towards the cathode. During migration, the cations also dragged water molecules with them [18]. This produced a differential swelling of the Nafion film on one of the sides of the polymer, causing a bending motion to the actuator. Therefore, it was possible to control the flow rate by simply changing the length of the potential steps used to actuate the Nafion-ppy actuators [11]. The average current going through

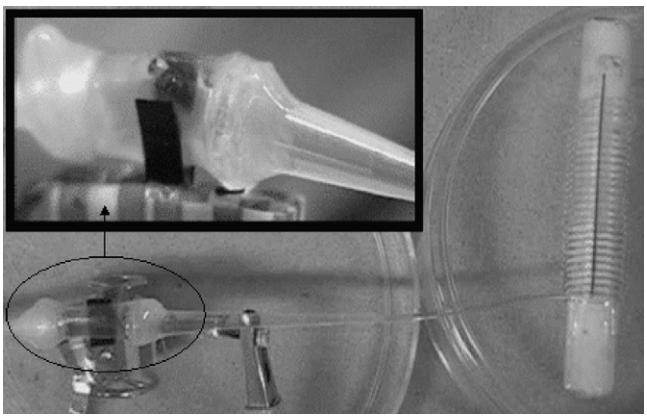

Fig. 2. Image of the first miniaturised pump developed in this work. The pump was constructed using Nafion-ppy actuators and the pump chamber was constructed using a 100 μm thick PDMS film. The inlet and outlet were conical polyethylene peaces.

the system was of the order of milliamps. Consequently, it was found that the power consumption of this pump was significantly lower than that of other miniaturised pumps reported to date, particularly at low flow rates. For example, at 0.4 μL/s, the power consumption of this pump was 188 mJ/μL, while that of a miniature peristaltic pump (BVT Technologies, model 2PP10.S [19]) was 750 mJ/μL and that of a piezoelectric pump (Deak Technologies, models DTI-200-12 P and DTI-200-12A [20]) was 375 mJ/μL. However, as it can be seen in Fig. 2, further miniaturisation was required if the pump was to be integrated inside the actual channels of the chip.

The next step in the miniaturisation of the pump was its integration onto the actual microfluidic tubes. A first prototype was constructed by coating a polyurethane tube with ppy as detailed in the experimental section. This prototype was tested in a closed system, i.e. no overall flow movement was achieved; instead the liquid was moved back and forth in response to ppy swelling/contraction around the polyurethane tube on actuation of the ppy coating. Actuation was achieved by applying 1 V between the ppy deposited onto the polyurethane tube and the ppy deposited onto the PVDF membrane using a potentiostat. The inner Pt layer was used as both reference and counter electrode and the ppy layer was used as working electrode. Flow in one direction avoiding the use of valves using the nozzle-diffuser principle was no longer feasible due to the dramatic decrease of the dimensions of the pump chamber, which with this latter design had 950 mm internal diameter. The nozzle-diffuser principle operates based on a large difference of diameter between the two cross-sections of the conical channels. Once the 'larger' diameter is dramatically reduced, the 'lower'

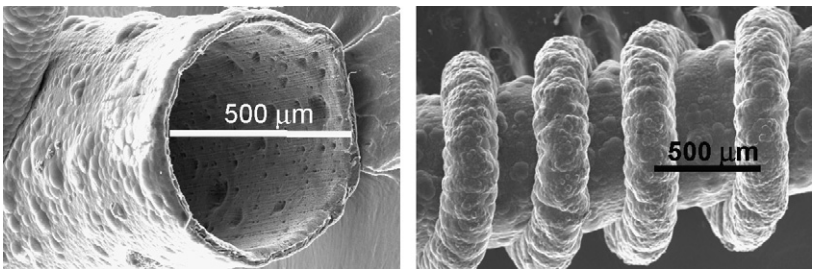

Fig. 3. Scanning electron microscopy (SEM) images of a ppy tube obtained by electrodeposition of ppy onto a 500 μm diameter platinum wire, in a propylene solution containing pyrrole monomer, $TBAPF_6$ and 1% water, at −20 °C during 6 h.

diameter becomes practically impossible to achieve with current microfabrication technologies. Therefore, peristaltic motion can only be achieved by placing several miniaturised pumps at different locations in the channel or by attaining a swelling gradient throughout the length of the tube. The first approach involves using electrical circuitry capable of applying 1 V to the different pumps in a pre-programmed sequence. The construction and assembly of the different pump segments is currently undergoing. The second approach can be achieved by making the electrical connection of the actuator to the power source on one end of the tube. The reproducibility of this latter actuation method is currently being optimised and therefore it has not been yet applied to the construction of the pumping device.

The third type of pumps currently being developed in our laboratory consists of stand-alone ppy tubes. This approach broadens the range of internal diameters that can be achieved, since it is now determined by the diameter of the platinum wire used to electrodeposit the ppy tube. Fig. 3 shows Scanning Electron Microscopy (SEM) images of a ppy tube obtained by galvanostatic electrodeposition of ppy onto a 500 μm diameter platinum wire, in a propylene carbonate solution containing pyrrole monomer, $TBAPF_6$ and 1% water, at −20 °C, using a current density of 0.15 mA/cm^2 during 6 h. Different electrodeposition conditions are currently being studied to optimise the properties of these ppy tubes. However, preliminary results are very encouraging.

Future efforts will focus on the full integration of these pumps inside a PDMS chip. The first prototype of PDMS chip developed in this work was shown in Fig. 1A. The chip was designed to produce effective mixing at low flow rates. Fig. 1B shows a photograph demonstrating the effectiveness of the mixing in the chip. The Griess-Ilosvay reagent was pumped through the upper channel and the nitrite solution was pumped through the lower channel using a commercial peristaltic pump. This figure shows that mixing was effectively achieved at flow rates as low as 30.4 μL/min. As it can be observed, mixing and chemical reaction were achieved very soon after the two channels joined. Therefore, mixing can be expected using the same flow rate but reducing the diameter and maintaining the same length of the channels in the chip. Furthermore, the ppy based biomimetic pumps will provide lower flow rates, thus ensuring mixing and chemical reaction even with channels of smaller diameter. Future design of the PDMS chip will involve a reduction of the diameter of the channels and therefore a reduction of the overall size of the chip.

The detector used in this work was based on LEDs of λ_{max} at 530 nm (Fig. 4). This type of detectors have been characterised and validated off line in previous works [13]. In this paper we report a LED based detector coupled to a PDMS chip (Fig. 1B). In this case, the mixing and chemical reaction between the Griess-Ilosvay reagent and nitrite takes place in the actual chip. Fig. 5 illustrates a typical

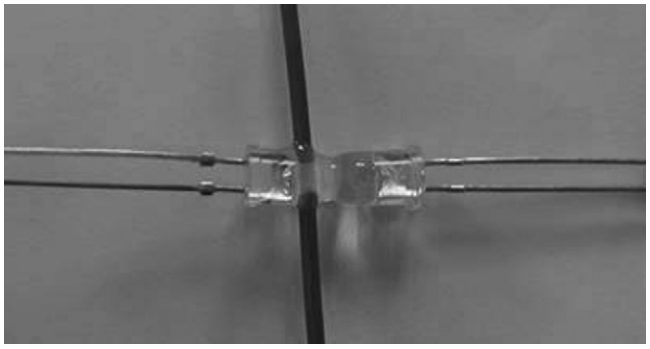

Fig. 4. Photograph of the LED detector used in this project.

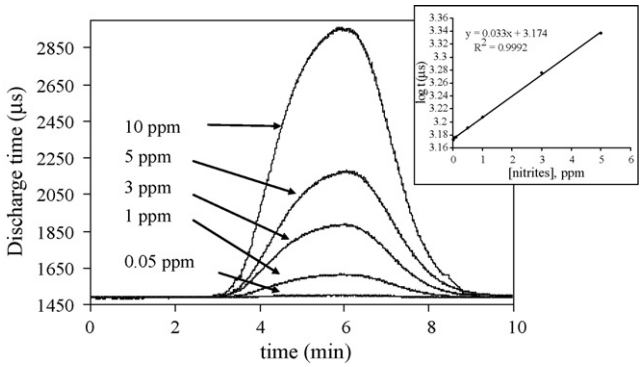

Fig. 5. Typical responses obtained with the LED based sensor when the Griess-Ilosvay reagent and the analyte are mixed in the PDMS microchip for different concentrations of nitrites. The flow rate was 30.4 μL/min.

response obtained with the detector attached to the PDMS chip, and the inset in Fig. 5 shows a typical calibration curve. Slopes of 0.033 ± 0.001 μs/ppm and regression coefficients with four nines were typically obtained. The response of the detector coupled to the PDMS chip was comparable to that reported previously with the detector used with pre-mixed solutions. This proves the effectiveness of the chip as mixer and reactor for this application. Moreover, good reproducibility for different injections was obtained. The relative standard deviation for these injections was less than 1% (0.2%).

An important drawback of the current platform design and integration is the formation of bubbles due to sudden changes of channel diameter. These changes arise from the different tubing used to attach the detector to the PDMS chip. Future work will involve the use of surface mounted LED for the construction of the detector. These LEDs can have dimensions of the order of few millimeters. This will allow their integration in the actual PDMS chip, thus eliminating the need for tubing of different diameters.

In conclusion this paper reports preliminary work on the miniaturisation of the different parts of a microanalytical platform, from pumps to detectors, with the ultimate aim of their integration into a functioning microfluidic chip. Both the miniaturised pump and the chip were made of soft materials. Moreover, the miniaturised biomimetic pump and the LED based detector both have low-power consumption. The resulting microanalytical platform will be suitable for field deployment, since it will be low power, corrosion resistance since it will be mostly constructed using polymeric materials, and also resistant to ingress due to the flexibility of its components.

Encouraging results were obtained both with the pump and with the detector. This work describes an important step towards the realization of a functioning microfluidic analytical device with integrated low-power pumping and detection. This approach can open the way to much more reliable, low-cost and low-power approaches to controlling fluidic movement within microfluidic manifolds. Work is continuing to further optimize and integrate the various elements of the microdimensioned analytical platform.

Acknowledgements

The authors acknowledge funding from Science Foundation Ireland under the ‘Adaptive Information Cluster’ award no. SFI 03/IN.3/1361 and the Australian Research Council (GGW).

References

[1] P.S. Dittrich, K. Tachikawa, A. Manz, Anal. Chem. 78 (2006) 3887.

[2] D. Janasek, J. Franzke, A. Manz, Nature 442 (2006) 374.
[3] M.M. Baeza, N. Ibanez-Garcia, J. Baucells, J. Bartroli, J. Alonso, Analyst 131 (2006) 110.
[4] D. Culler, D. Estrin, M. Srivastava, Computer 37 (2004) 41.
[5] K.S. Johnson, J.A. Needoba, S.C. Riser, W.J. Showers, Chem. Rev. 107 (2007) 623.
[6] J.K. Hart, K. Martinez, Earth-Sci. Rev. 78 (2006) 177.
[7] D. Diamond, Anal. Chem. 76 (2004) 278A.
[8] R. Byrne, D. Diamond, Nat. Mater. 5 (2006) 421.
[9] D. Diamond, K.T. Lau, S. Brady, J. Cleary, Talanta 75 (2008) 606–612.
[10] Y. Wu, G.M. Spinks, P.c. Innis, W.M. Megill, G.G. Wallace, Smart Mat. Struct. 14 (2005) 1511.
[11] S. Ramirez-Garcia, D. Diamond, Sens. Actuators A 135 (2007) 229.
[12] J. Ding, L. Liu, G.M. Spinks, D. Zhou, G.G. Wallace, J. Gillespie, Synth. Met. 138 (2003) 391.
[13] M. O' Toole, K.T. Lau, D. Diamond, Talanta 66 (2005) 1340.
[14] A. Malinauskas, Polymer 42 (2001) 3957.
[15] E. Stemme, G. Stemme, Swedish Patent Applic. N. 9 300 604-7.
[16] E. Stemme, G. Stemme, Sens. Actuators A 39 (1993) 159.
[17] APHA-AWWA-WEF Standard methods for the examination of water and wastewater, 20th ed, American Public Health Association, American Water Works Association, Water Environment Federation, Washington DC, 1999.
[18] M. Shahinpoor, Electrochim. Acta 48 (2003) 2343.
[19] http://www.bvt.cz/, 2006.
[20] http://news.thomasnet.com/fullstory/454483/954, 2004.

Talanta 77 (2008) 774–778

Contents lists available at ScienceDirect

Talanta

journal homepage: www.elsevier.com/locate/talanta

Solid-phase microextraction—Gas chromatography to determine volatile organic sulfur compounds in the air at sewage treatment plants

Maria Rosa Ras, Rosa Maria Marcé*, Francesc Borrull

Departament de Química Analítica i Química Orgànica, Universitat Rovira i Virgili, Campus Sescelades, Marcel·lí Domingo, s/n, 43007 Tarragona, Spain

ARTICLE INFO

Article history:
Received 28 April 2008
Received in revised form 1 July 2008
Accepted 11 July 2008
Available online 23 July 2008

Keywords:
Air monitoring
Carboxen–polydimethylsiloxane
Sewage treatment plant
Solid-phase microextraction
Volatile organic sulfur compounds

ABSTRACT

Solid-phase microextraction (SPME) was applied to the determination of 7 volatile organic sulfur compounds (VOSCs), which were analysed by gas chromatography–mass spectrometry. The compounds studied were ethyl mercaptan (CH_3CH_2SH), dimethyl sulfide ($(CH_3)_2S$), carbon disulfide (CS_2), propyl mercaptan (C_3H_8S), butyl mercaptan ($C_4H_{10}S$), dimethyl disulfide ($(CH_3)_2S_2$) and 1-pentanethiol ($C_5H_{12}S$). Temperature and time conditions of SPME extraction were optimised and the method was validated, with good linearity in a calibration range between 0.1 and 1000 $\mu g\,m^{-3}$. Method detection limits ranged between 0.01 and 0.08 $\mu g\,m^{-3}$ and method quantification limits were between 0.10 and 0.25 $\mu g\,m^{-3}$, allowing real samples taken from several different areas of a sewage treatment plant to be analysed. Repeatability of the method between samples went from 5.6% for pentanethiol up to 14.2% for carbon disulfide, and concentrations of total target compounds were found between 18 and 529 $\mu g\,m^{-3}$, depending on the sampling site.

1. Introduction

In the past two decades there has been increasing interest in detecting volatile sulfur compounds (VSCs) in the atmosphere. This is mainly due to their effects on the environment, to their toxicity even at very low levels, and to the frequent unpleasant smells associated with them [1]. Volatile sulfur compounds are released into the atmosphere from several natural and anthropogenic sources. Natural sulfur compounds such as hydrogen sulfide, dimethyl sulfide and dimethyl disulfide are released from oceans, marshes, soils, vegetation, and geothermal and volcanic activity [2]. Anthropogenic VSCs are commonly discharged during industrial processes that involve the handling or degradation of organic material. These processes include biogas production, sewage treatment, landfilling, pulp milling, and slaughtering [3,4]. VSCs have also been identified as the predominant odorants from bioindustry emissions [5] because of their very low odour threshold and extremely negative hedonic value. They therefore contribute to odour pollution even when very small amounts are emitted, which is bothersome to the population, especially workers and local residents [2,5,6]. Moreover, exposure to high levels of VSCs can lead to unconsciousness and even death [3].

VSCs, which includes volatile organic sulfur compounds (VOSCs) and the inorganic species SH_2 and SO_2, are generally determined in air by means of gas chromatography (GC), and detected using mass spectrometry (MS), a specific sulfur detector, like the sulfur chemiluminescence detector (SCD) or a pulsed flame photometric detector (PFPD). Since these compounds are present in the air at very low concentrations, the analytical methods employed to detect them must also include an enrichment step [7]. Volatile organic sulfur compounds have been determined in the atmosphere using solid adsorbents or cryogenic trapping to concentrate the sulfur compounds and gas chromatography has been used to separate them [6,8–12]. In these methods, air is pumped through a solid sorbent, and analytes are thermally desorbed and transferred to a cool trap-a process which requires expensive equipment and is quite time consuming.

As an alternative to solid sorbent enrichment methods, solid-phase microextraction (SPME) has been used, being a solvent-free enrichment method that combines sampling and preconcentration of analytes in a single step [13,14], without the need for expensive devices. Numerous studies have used SPME to determine volatile organic compounds in many different matrices, applying SPME to the headspace of both liquid and solid samples [15–18]. SPME has also been applied to the analysis of air samples [15,19] by extraction from air collected in containers or sampling bags [14,20–22], field extraction [23–25], or extraction from the headspace of previously enriched solid sorbents [26,27], to determine VOCs in general, and to determine VOSCs in particular [2,4,7,28–30]. For example, Li and

* Corresponding author. Tel.: +34 977 55 81 70; fax: +34 977 55 84 46.
E-mail address: rosamaria.marce@urv.cat (R.M. Marcé).

0039-9140/$ – see front matter © 2008 Elsevier B.V. All rights reserved.
doi:10.1016/j.talanta.2008.07.027

Shooter [2] detected carbonyl sulfide, hydrogen sulfide, sulfur dioxide, carbon disulfide, methyl mercaptan, dimethyl sulfide, dimethyl disulfide and butyl mercaptan in air samples from a sewage treatment plant and geothermal areas in Rotorua City (New Zealand) by air sampling in Tedlar bags and analysis using SPME-GC/PFPD, and Nielsen and Jonsson [4] quantified nine VOSCs in samples collected in Tedlar bags from Swedish biogas production and sewage treatment plants and analysed them using SPME-GC/MS.

There are several difficulties associated with detecting VOSCs, including their broad range of concentrations, their highly reactive nature, and the complexity of matrices. Special precautions therefore need to be taken in all steps of their analysis. In the SPME extraction process, fibre selection is an important step and several studies comparing different SPME fibres have observed that the most effective coating for extracting VOSCs is carboxen–polydimethylsiloxane (Car–PDMS) fibre coating. This coating does, however, present some limitations, such as competitive adsorption which leads to inaccurate quantification [4,21,28,29]. Calibration problems have also been studied through determining the effects of temperature and relative humidity on sampling extraction [14,31,32], or by comparing equilibrium and non-equilibrium extraction approaches [33]. Another characteristic of using SPME for air-samples is the need for standard gas mixtures; several methods of generating them through dynamic or static dilution [19,34,35] have been described.

This study aims to develop a method for determining a group of seven VOSCs, ethyl mercaptan, dimethyl sulfide, carbon disulfide, propyl mercaptan, butyl mercaptan, dimethyl disulfide and 1-pentanethiol through field collection of samples in glass bulbs, subsequent extraction using Car–PDMS SPME fibre, and analysis by gas chromatography–mass spectrometry. This method is applied to analyse real samples taken from several points during the sewage treatment process.

2. Experimental

2.1. Chemicals and reagents

Ethyl mercaptan, dimethyl sulfide, carbon disulfide, propyl mercaptan, butyl mercaptan, dimethyl disulfide and 1-pentanethiol were supplied by Aldrich (St. Louis, USA), and standard solutions were prepared in methanol for gas chromatography (Merck KGaA, Darmstadt, Germany). Helium with a purity of 99.999% was used as the carrier gas, and 99.999% pure nitrogen gas was used to clean the glass sampling bulbs.

2.2. Instruments and materials

Glass sampling bulbs with a volume of 0.5 l (Supelco, Bellefonte, USA) were used for the static generation of standard gas and field sampling. Carboxen–polydimethylsiloxane (Car–PDMS) fibre (Supelco, Bellefonte, USA) was used for SPME extraction. An air sampling pump (SKC, Eighty Four, USA) was used for field sampling of air into the glass bulbs.

VOSCs were determined in a 6890N gas chromatograph coupled to a 5973 *inert* mass spectrometer (Agilent Technologies, Palo Alto, USA). The analytes were desorbed into a split/splitless injector equipped with a Merlin microseal (Supelco, Bellefonte, USA), and separated into a TRACSIL Meta.X5 capillary column (60 m, 0.32 mm and 1.0 μm) (TEKNOKROMA, Barcelona, Spain).

2.3. Standard generation

The glass sampling bulbs had been previously cleaned with gentle flow nitrogen gas at a flow rate of 200 ml min^{-1} for 2 h.

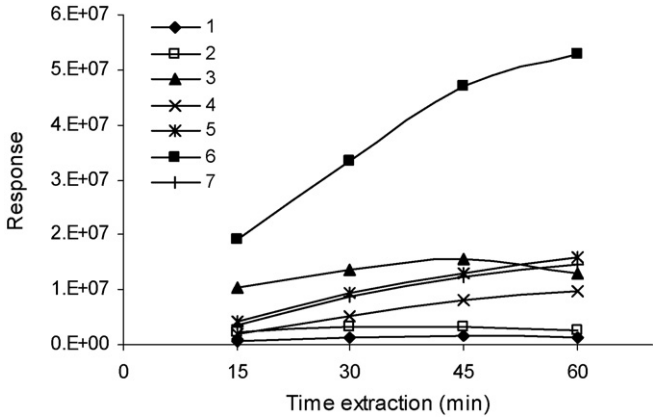

Fig. 1. Variation of response with time extraction in SPME, for seven target compounds, numbered as in Table 1.

Mixed standard solutions of the target compounds in methanol ranging between 0.01 and 100 mg l^{-1} were prepared at the time of calibration from a concentrated mixed solution of 2000 mg l^{-1} in methanol, which was kept at 4 °C. Standard gas was generated by injecting 5 μl of standard solution with a syringe through the septum into a clean glass bulb. The bulb was then kept at a temperature of 100 °C for 20 s and then cooled to room temperature for 10 min [14].

2.4. Analytical procedure

The Car–PDMS fibre, previously conditioned and kept in the split/splitless injector of the GC in order to prevent contamination, was placed in the bulb by inserting the needle through the septum. The fibre was then exposed to analytes for 45 min at room temperature. The fibre was then retracted into the needle and the needle withdrawn. The needle was immediately put into the injector of GC to desorb the analytes and focus them onto the chromatographic column.

The temperature of the injector was 200 °C and the splitless injection mode was run for 2 min with a subsequent purge flow of 10 ml min^{-1}. The fibre was kept in the injector until the end of the analysis or until the next extraction to prevent contamination. Column flow was 2 ml min^{-1} and the oven temperature was initially maintained at 36 °C for 6 min, then raised to 220 °C at a rate of 30 °C min^{-1} and maintained for 10 min. The mass spectrometer acquired data in SIM mode. The compounds were quantified using a target ion and confirmed using qualifier ions and retention time.

2.5. Field sampling

Clean glass bulbs were transported to the field sampling site in a refrigerated box. At the sampling site the air sampling pump was connected to one of the ends of a glass bulb and air was pumped through it at a flow rate of 100 ml min^{-1} for 10 min in order to allow the nitrogen gas to be completely displaced by the sampled air. The stopcocks were then immediately closed and the bulb was returned to the refrigerated box. Samples were subsequently transported to the laboratory, where the sample bulbs were removed from the refrigerated box and equilibrated for 10 min at room temperature. All samples were extracted and analysed within 3 h.

Samples were taken from a sewage management plant at several sampling points located at the sites of different plant processes: the gravitational thickening of sludge, biological settlement tank, thickening of surplus bio-sludge by flotation and the primary or acid digestion tank. The differences between samples taken in con-

Table 1
Target compounds in chromatographic elution order, their quantifier and qualifier ions, and retention times (t_R)

No.	Compound	Quantifier ion		Qualifier ion[a]		t_R (min)	LOD[b] (ng)
1	Ethyl mercaptan	62 (*100*)	47 (*58*)	45 (*20*)	–	3.8	0.001
2	Dimethyl sulfide	62 (*100*)	47 (*83*)	45 (*50*)	–	4.1	0.001
3	Carbon disulfide	76 (*100*)	44 (*11*)	–	–	4.5	0.001
4	Propyl mercaptan	76 (*100*)	61 (*11*)	47 (*68*)	43 (*57*)	6.6	0.004
5	Butyl mercaptan	90 (*70*)	56 (*100*)	61 (*20*)	47 (*31*)	9.9	0.003
6	Dimethyl disulfide	94 (*100*)	79 (*50*)	61 (*12*)	64 (*10*)	10.8	0.001
7	1-Pentanethiol	104 (*68*)	55 (*100*)	70 (*79*)	61 (*30*)	12.4	0.002

Repeatability and instrumental detection limits for the direct injection of gas standard.
[a] The values in italics next to the qualifier ions are the percent abundances of each ion.
[b] Instrumental detection limits, taken as the concentration corresponding to three times the noise of the quantifier ion, in the direct injection analysis in SIM mode acquisition.

fined spaces and samples taken in open spaces have therefore been considered, as in open spaces the dispersion of emission gases into the atmosphere will obviously greatly influence the levels of compounds in the air samples.

3. Results and discussion

3.1. Mixed gas standards

The reproducibility and stability of the mixed gas standards was tested in order to evaluate adsorption processes through direct injection analysis, directly injecting with a gas-tight syringe 20 μl of a 4 mg l^{-1} standard gas, generated by adding 200 μl of a mixed solution of 10,000 mg l^{-1}, into a clean bulb, as described in Section 2. Standard gas was analysed in triplicate, immediately after it was generated and then 1, 2 and 3 h later. Repeatability of the triplicate analysis, expressed as relative standard deviation (R.S.D.%) ranged between 0.8% and 2.3%. We also found good stability of the standard gas in the studied periods, which assured us of the stability of the real samples during the process of their collection in the field, transportation to the laboratory and their analysis within a maximum period of 3 h.

3.2. Gas chromatography–mass spectrometry analysis

We compared the responses of the analysis of 1 μl of a standard solution of 0.05 mg l^{-1} in selected ion monitoring (SIM) and in full-scan acquisition modes. SIM mode was chosen as the acquisition method despite the loss of information about other organic compounds present in the samples, because although we found only a slight increase in responses in SIM mode, we observed much lower deviations in responses in SIM than in full-scan, in addition to the lower detection limits achieved with SIM mode. Table 1 shows the instrumental detection limits obtained from the direct injection analysis in SIM acquisition mode.

3.3. SPME optimisation

SPME fibres of carboxen and polydimethylsiloxane (Car–PDMS) with a 75 μm coating thickness were selected for the extraction of compounds because according to the literature this is the most suitable fibre for the extraction of VOSCs [2–4], showing higher sensitivity and reproducibility compared to other fibres such as PDMS, or divinylbenzene (DVB)/PDMS [28,29,31].

The optimum SPME desorption temperature was studied in order to achieve a total desorption of analytes from the fibre during the injection time in splitless mode and to prevent the thermal decomposition of the analytes. Desorption temperatures of 180, 200 and 250 °C were tested by means of analysing standard gas mixtures of 10 μg m^{-3}, generated by injecting 5 μl of a 1 mg l^{-1} standard solution into a 0.5 l clean glass bulb. Triplicate analysis at each temperature showed that the increase in response with temperature was not, in general, statistically significant. However, of the three analyses we found lower deviations, expressed as a percentage of relative standard deviation (R.S.D.%), at the desorption temperature of 200 °C (from 1% to 7%), than at 180 °C (from 3% to 16%) or 250 °C (from 2% to 18%). A temperature of 200 °C was therefore fixed as the optimum value.

Extraction time was optimised and, using the desorption conditions described above, periods of 15, 30, 45 and 60 min were tested by analysing 10 μg m^{-3} gas standard mixtures, each one in triplicate. In this case, an increase in response could be seen from 15 to 45 min, when analytes reached equilibrium conditions between both the gas and fibre phases. With longer extraction times, we found differing increased responses for most compounds, and as can be seen in Fig. 1, the response of carbon disulfide even decreased slightly. Ambient temperature conditions for SPME extraction in the range of 22 ± 1 °C were used in order to make the method easier to employ.

3.4. Method validation

For the calibration, we analysed standard gas mixtures of several concentrations ranging between 0.1 and 2500 μg m^{-3}, generated by the injection of 5 μl of standard solutions ranging from 0.01 and 250 mg l^{-1} into 0.5 l glass bulbs. All compounds showed good linear correlation up to 1000 μg m^{-3}, while at higher concentrations, a loss of linearity was observed in the responses of all compounds. Although pentanethiol maintained linearity up to 2500 μg m^{-3} (r^2 = 0.992), linearity intervals were fixed at up to 1000 μg m^{-3} for all compounds, as they are usually found below this concentration in real samples. Thus, 7 standard levels between 0.1 and 1000 μg m^{-3} were used for external calibration, with determination coefficients above 0.994, as can be seen in Table 2. The lowest calibration levels, which ranged from 0.10 to 0.25 μg m^{-3}, were taken as the method quantification limits (MQL). The method detection limit (MDL) for each compound was defined as the concentration corresponding to three times the noise of the quantifier ion in the SPME analysis. Values were between 0.01 μg m^{-3} for carbon disulfide and 0.08 μg m^{-3} for ethyl mercaptan. The MQLs and MDLs of the seven target compounds are shown in Table 2.

SPME recoveries were determined through the analysis of a 50 mg m^{-3} standard gas mixture and comparison with direct injection calibration. Recoveries were found to be similar to the values presented in the literature and ranged between 4% and 25%.

Repeatability was obtained through the triplicate SPME analysis of a 10 μg m^{-3} standard gas mixture. For all compounds repeatability, expressed as relative standard deviation (R.S.D.%), was good, ranging between 1.8% and 5.2%. Reproducibility, defined as the

Table 2
Method's validation parameters for the SPME-GC/MS determination of VOSCs in air samples

No.	Compound	MDL[a] ($\mu g\,m^{-3}$)	MQL[b] ($\mu g\,m^{-3}$)	r^2	SPME repeat.[c] (R.S.D.%, $n=3$)	SPME reprod.[d] (R.S.D.%, $n=3$)	Method's repeat.[e] (R.S.D.%, $n=3$)
1	Ethyl mercaptan	0.026	0.25	0.997	2.1	4.3	7.7
2	Dimethyl sulfide	0.017	0.15	0.994	1.8	5.1	6.4
3	Carbon disulfide	0.003	0.10	0.995	5.2	6.7	14.2
4	Propyl mercaptan	0.041	0.25	0.999	2.3	5.9	12.0
5	Butyl mercaptan	0.014	0.25	1.000	3.8	4.5	11.6
6	Dimethyl disulfide	0.,015	0.25	0.998	2.8	7.3	13.3
7	1-Pentanethiol	0.017	0.25	0.999	2.1	5.2	5.6

[a] Method's detection limits, taken as the concentration corresponding to three times the noise of the quantifier ion.
[b] Method's quantification limits, taken as the lowest calibration level.
[c] Repeatability of the SPME analysis of a 10 $\mu g\,m^{-3}$ standard gas mixture.
[d] Reproducibility interday of the SPME analysis of a 10 $\mu g\,m^{-3}$ standard gas mixture.
[e] Repeatability among real samples, determined by sampling three bulbs in parallel, that underwent identical sampling, transport and analytical processes.

Table 3
Average levels of volatile organic sulfur compounds in $\mu g\,m^{-3}$ found at the sampled sections of a sewage management plant ($n=2$)

No.	Compound	Gravitational thickening of sludge	Biological settlement tank	Thickening of sludge by flotation	Primary digestion tank
1	Ethyl mercaptan	n.d.[a]	n.d.	21.7	20.0
2	Dimethyl sulfide	5.9	23.9	380.1	1.7
3	Carbon disulfide	2.5	2.5	8.2	9.8
4	Propyl mercaptan	3.4	4.0	50.3	66.3
5	Butyl mercaptan	3.9	4.1	33.2	7.9
6	Dimethyl disulfide	n.d.	n.d.	31.6	0.5
7	1-Pentanethiol	3.0	n.d.[a]	3.8	22.1

[a] n.d.: compound not detected (value < MDL); n.q.: compound no quantified (value < MQL).

R.S.D.% of a triplicate SPME interday analysis, was also checked through the analysis of a 10 $\mu g\,m^{-3}$ standard gas mixture and obtained good results with R.S.D.% less than 7.4%. Repeatability of the method, defined as the repeatability between real samples, was determined by sampling three bulbs in parallel that underwent identical sampling, transport and analytical processes. Values, expressed as R.S.D.%, ranged between 5.6% and 14.2%. Repeatability, reproducibility and method repeatability values can be seen in Table 2.

3.5. Sample analysis

Samples were taken from different sections of the sewage treatment process at a wastewater treatment plant. The sections sampled were the gravitational thickening of sludge area, which receives the primary sludge collected from the primary settlement tank; the biological settlement tank located next to the biological treatment tank, which receives the bio-sewage; the thickening of surplus bio-sludge by flotation area, which receives the sludge from

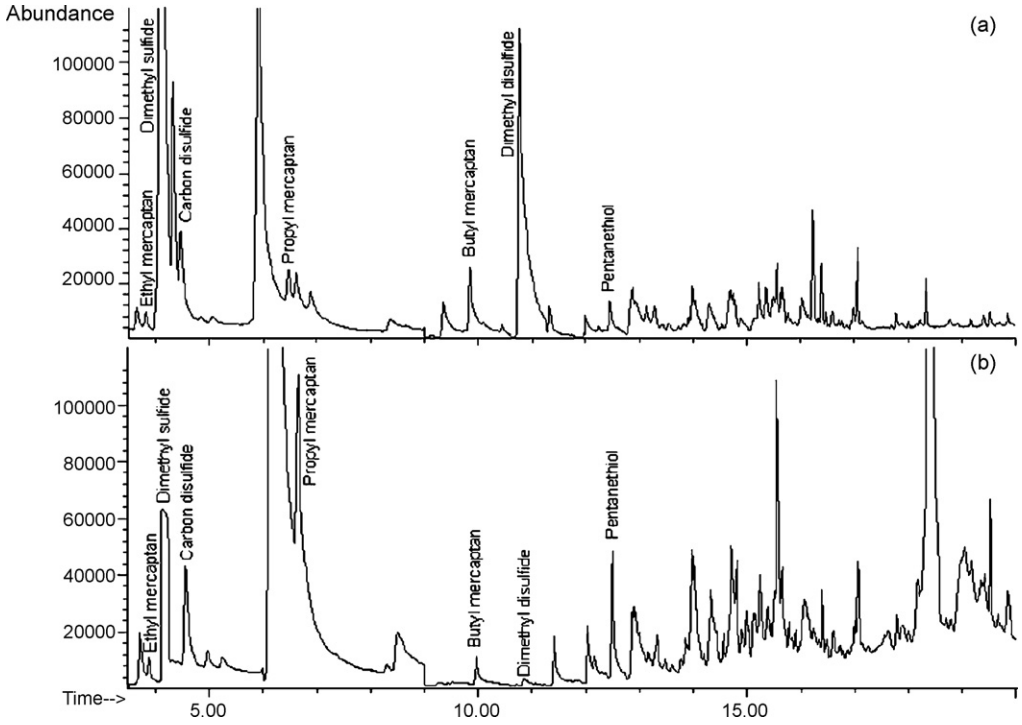

Fig. 2. Chromatogram of two samples taken in (a) thickening of surplus bio-sludge by flotation and (b) primary digestion tank, from a sewage management plant.

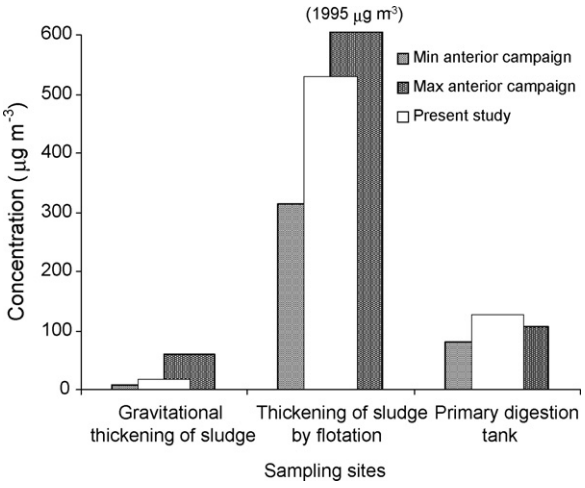

Fig. 3. Comparison of levels found in present work with minimum and maximum levels found at the same sampling points in anterior campaign.

the biological settlement tank; and the primary or acid digestion tank, which receives the sludge from the gravitational thickening and thickening by flotation areas. The design characteristics of each sampling site were different, and while samples from the gravitational thickening of sludge area and biological settlement tank were taken in the open air, samples from the thickening of sludge by flotation area and primary digestion tank were taken in confined spaces. Samples were taken from the four sites on two different days. The average concentrations for individual compounds found at each site, which showed relative standard deviations (R.S.D.%) between 10% and 17%, are shown in Table 3.

The most abundant compound found was dimethyl sulfide, which was detected at all four sampling sites and appeared at a high concentration of 380.1 $\mu g\,m^{-3}$ in the thickening of sludge by flotation area. This compound was also measured at high concentrations (about 2000 $\mu g\,m^{-3}$) by Nielsen and Jonsson [4] in an outdoor air sample taken during the loading of digested sludge at a sewage treatment plant. The next highest concentrations found were those of propyl mercaptan, butyl mercaptan and dimethyl disulfide, although the levels recorded varied greatly depending on the sampling site.

As can be seen in Table 3, the total VOSCs found at the open-air sites – the gravitational thickening of sludge area and biological settlement tank – were less than 50 $\mu g\,m^{-3}$, while the total VOSCs found in the confined sites were over 100 $\mu g\,m^{-3}$. Previous studies have shown that the design of the sewage treatment plant sections from which samples are collected determine VOSC concentrations [12]. Li and Shooter [2] also found higher levels of VOSCs in sampling sites at a sewage treatment plant with little ventilation than in other, open-air sampling sites. Furthermore, concentrations of individual compounds were generally higher at confined sites, and we found similarities among the concentrations at open sites, and among those at confined sites, such as in the case of ethyl mercaptan, carbon disulfide and propyl mercaptan. On the other hand, levels of dimethyl sulfide varied greatly at all the sampling sites. Fig. 2a and b shows the chromatograms of samples taken at both confined sample sites.

If we compare these results with those obtained in a previous study carried out in winter 2006 [12], in which target compounds were determined by active sampling, thermal desorption and gas chromatography–mass spectrometry, we can see that in general, the total VOSC concentrations found in both studies are consistent. Fig. 3 compares the results of this study with regard to the gravitational thickening of sludge area, thickening of sludge by flotation area and primary digestion tank, with the range of concentrations found in a previous study of the same sampling points.

4. Conclusions

We have developed an analytical method for determining seven volatile organic sulfur compounds in air by means of Car–PDMS SPME fibre extraction of grab samples, and analysis by gas chromatography and mass spectrometry. The method showed good detection and quantification limits in SIM acquisition mode as well as good precision values. Linear intervals allowed us to determine compounds in real samples. Finally, the SPME method was found to be suitable for the quantification of complex samples, offering an alternative method using easy and simple instrumentation to detect VOSCs.

Acknowledgements

The authors would like to thank the *Dirección General de Investigación* for financial support (CTM2005 01774), the *Agència de Gestió d'Ajuts Universitaris i de Recerca* of the *Generalitat de Catalunya* for M.R. Ras' predoctoral grant (2005FI 00018), and the Reus Sewage Management Plant for allowing us to take samples.

References

[1] W. Wardencki, J. Chromatogr. A 793 (1998) 1.
[2] K.-C. Li, D. Shooter, Int. J. Environ. Anal. Chem. 84 (2004) 749.
[3] F. Lestremau, F.A.T. Andersson, V. Desauziers, J.L. Fanlo, Anal. Chem. 75 (2003) 2626.
[4] A.T. Nielsen, S. Jonsson, J. Chromatogr. A 963 (2002) 57.
[5] E. Smet, H. Van Langenhove, Biodegradation 9 (1998) 273.
[6] C. Vassilakos, A. Papadopoulos, M. Lahaniati, T. Maggos, J. Bartzis, P. Papagianakopoulos, Fresen. Environ. Bull. 11 (2002) 516.
[7] A.T. Nielsen, S. Jonsson, Analyst 127 (2002) 045.
[8] A. Muezzinoglu, Chemosphere 51 (2003) 245.
[9] K.-H. Kim, Y.J. Choi, E.C. Jeon, Y. Sunwoo, Atmos. Environ. 39 (2005) 1103.
[10] K.-H. Kim, H. Swan, Z.-H. Shon, G. Lee, J. Kim, C.-H. Kang, Chemosphere 54 (2004) 515.
[11] I. Devai, R.D. DeLaune, Water Environ. Res. 71 (1999) 203.
[12] M.R. Ras, F. Borrull, R.M. Marcé, Talanta 74 (2008) 562.
[13] Y. Chen, J. Pawliszyn, Anal. Chem. 75 (2003) 2004.
[14] M. Chai, J. Pawliszyn, Environ. Sci. Technol. 29 (1995) 693.
[15] K. Demeestere, J. Dewulf, B. De Witte, H. Van Langenhove, J. Chromatogr. A 1153 (2007) 130.
[16] P. Pastore, G. Favaro, D. Badocco, I. Lavagnini, Chemosphere 95 (2005) 741.
[17] K. Ridgway, S.P.D. Lalljie, R.M. Smith, J. Chromatogr. A 1153 (2007) 36.
[18] F.M. Musteata, J. Pawliszyn, Trends Anal. Chem. 26 (2007) 36.
[19] J. Namiesnik, B. Zygmunt, A. Jastrzebska, J. Chromatogr. A 885 (2000) 405.
[20] J. Lee, S.M. Hwang, D.W. Lee, G.S. Heo, B. Kor, Chem. Soc. 23 (2002) 488.
[21] V. Larroque, V. Desauziers, P. Mocho, J. Environ. Monitor. 8 (2006) 106.
[22] G. Mangani, A. Berloni, M. Maione, J. Chromatogr. A 988 (2003) 167.
[23] M. Jia, J.A. Koziel, J. Pawliszyn, Field. Anal. Chem. Technol. 4 (2–3) (2000) 73.
[24] K. Li, A. Santilli, M. Goldthorp, S. Whiticar, P. Lambert, M. Fingas, J. Hazard. Mater. 83 (2001) 83.
[25] S. Tumbiolo, J.F. Gal, P.C. Maria, O. Zerbinati, Ann. Chim. 95 (2005) 757.
[26] A. Saba, A. Cuzzola, A. Raffaelli, S. Pucci, P. Salvadori, Rapid Commun. Mass Spectro. 15 (2001) 2404.
[27] C. Domeño, F. Martínez, L. Campo, Anal. Chim. Acta 524 (2004) 51.
[28] K.K. Kleeberg, Y. Liu, M. Jans, M. Schlegelmilch, J. Streese, R. Stegmann, Waste Manage. 25 (2005) 872.
[29] F. Lestremau, V. Desauziers, J.C. Roux, J.L. Fanlo, J. Chromatogr. A 999 (2003) 71.
[30] E. Davoli, M.L. Gangai, L. Morselli, D. Tonelli, Chemosphere 51 (2003) 357.
[31] C. Haberhauer-Troyer, E. Rosenberg, M. Grasserbauer, J. Chromatogr. A 848 (1999) 305.
[32] J. Namiesnik, D. Gorlo, W. Zygmunt, B. Zygmunt, Analysis 26 (1998) 170.
[33] V. Larroque, V. Desauziers, P. Mocho, Anal. Bioanal. Chem. 386 (2006) 1457.
[34] J.A. Koziel, P.A. Martos, J. Pawliszyn, J. Chromatogr. A 1025 (2004) 3.
[35] G. Xiong, J. Pawliszyn, Anal. Chem. 74 (2002) 2446.

Talanta 77 (2008) 909–914

Contents lists available at ScienceDirect

Talanta

journal homepage: www.elsevier.com/locate/talanta

An amperometric sensor based on hemin adsorbed on silica gel modified with titanium oxide for electrocatalytic reduction and quantification of artemisinin

José Rui M. Reys[a], Phabyanno R. Lima[b], Alessandra G. Cioletti[a], Adriana Santos Ribeiro[a], Fabiane Caxico de Abreu[a], Marília O.F. Goulart[a,*], Lauro T. Kubota[b,*]

[a] Instituto de Química e Biotecnologia, Universidade Federal de Alagoas, 57072-970 Maceió, AL, Brazil
[b] Institute of Chemistry, UNICAMP, P.O. Box 6154, 13084-971 Campinas, SP, Brazil

ARTICLE INFO

Article history:
Received 14 May 2008
Received in revised form 18 July 2008
Accepted 21 July 2008
Available online 31 July 2008

Keywords:
Artemisinin
Hemin
Silica gel
Titanium oxide
Amperometric sensor

ABSTRACT

The present work describes the development of an amperometric sensor based on hemin immobilized on a titanium oxide modified silica toward detection of artemisinin (ARN) in neutral medium at an applied potential of −0.5 V vs. Ag/AgCl. The sensor presented its best performance in 0.1 mol L^{-1} phosphate buffer solution, at pH 7.0. After optimizing the operational conditions, the sensor provided a linear response range for ARN reduction from 50 nmol L^{-1} to 1000 nmol L^{-1} with a sensitivity, detection and quantification limits of 24.66 A L mol^{-1}, 15 nmol L^{-1} and 52 nmol L^{-1}, respectively. The proposed sensor showed a stable response for at least 80 successive determinations. The repeatability of the measurements with the sensor and the preparation of a series of electrodes, evaluated in terms of relative standard deviation, were 4.1% and 5.0%, respectively, for $n = 10$. The developed sensor was applied for the determination of ARN in the crude extracts of *A. vulgaris* L and the average recovery for these samples is 101.4 (± 3.1)%.

1. Introduction

Malaria remains in the world as the most widespread and devastating infectious disease. It is a mosquito borne parasitic disease caused by four protozoan *Plasmodium* species that infect exclusively man, *P. falciparum*, *P. vivax*, *P. malariae* and *P. ovale*. After the initial stage in hepatocytes where parasites differentiate and undergo multiplication originating merozoites, red blood cells are invaded. The destruction of a massive number of host infected erythrocytes to release new parasites leads to the characteristic paroxysm, chill and fever, associated to the malaria clinical infection [1,2]. Nowadays approximately 40% of the world's population mostly, those living in the world's poorest countries, is at risk of malaria. The disease was once more widespread but it was successfully eliminated from many countries with temperate climates during the mid 20th century. However malaria is still found throughout the tropical and sub-tropical regions of the world and annually causes more than 300 million acute illnesses and at least one million of deaths [3]. Cerebral malaria, the most serious life-threatening complication caused by *P. falciparum* species, is usually fatal, if not immediately treated [4].

A range of antimalarials are effective against malaria [5–12]. The majority of drugs are blood antimalarial agents that eliminate the erythrocytic stages of the plasmodia life cycle. Lately with the increasing rise and spread of drug-resistant strains of plasmodia, the number of effective antimalarial drugs are becoming limited [8–10,12–14].

Artemisinin (quinghaosu, ARN) (Fig. 1), a sesquiterpene lactone endoperoxide isolated from Chinese herb Qinghao, and semisynthetic derivatives, including artesunate, artemether and dihydroartemisinin, are short-acting antimalarial agents that kill parasites more rapidly than conventional antimalarials, and are active against both the sexual and asexual stages of the *P. falciparum* cycle [13]. WHO recommends that all countries experiencing resistance to conventional monotherapies, such as chloroquine, amodiaquine or sulfadoxine–pyrimethamine, should use combination therapies, preferably those containing artemisinin derivatives (ACTs – artemisinin-based combination therapies) for *falciparum* malaria [15].

The antimalarial activity of this drug involves a rapid mechanism that allows its use for the treatment of multidrug-resistant cases. Studies of the structure-activity relationships have shown that this antimalarial activity appears to involve the endoperoxide moiety of artemisinin which interacts with intraparasitic heme to generate unstable free radical intermediates [8–10,14,15]. There are currently no effective alternatives to artemisinins for the treatment of *P. falciparum* malaria either on the market or towards the

* Corresponding authors. Tel.: +55 19 3521 3127; fax: +55 19 3521 3023.
E-mail addresses: mofg@qui.ufal.br (M.O.F. Goulart), kubota@iqm.unicamp.br (L.T. Kubota).

0039-9140/$ – see front matter © 2008 Elsevier B.V. All rights reserved.
doi:10.1016/j.talanta.2008.07.043

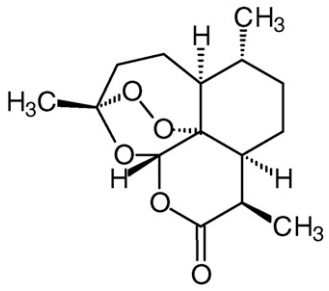

Fig. 1. Molecular structure of artemisinin (ARN).

end of the development pipeline. Many patents claim new synthetical antimalarials, with an attempt to identify the next generation of antimalarials [16].

Studies focusing ARN determination in several matrices, have attracted considerable attention nowadays [17], both for quality assurance and consumer safety. In this sense, several methods for its detection and quantification have been reported [17], including, high performance liquid chromatography [18,19] and electrochemical methods [20–23]. However, most of them experienced difficulties with sample preparation, necessity of molecules derivatization or lack of sufficient sensitivity, which limit their practical utility.

Electrochemical techniques have proved to be a sensitive and selective approach for the detection of numerous compounds. Unfortunately, ARN needs a large overpotential to be reduced at ordinary electrodes, being unsuitable for these methods [23,24]. Thus, the use of chemically modified electrodes containing efficient redox mediators immobilized on conventional electrode surfaces can be used to decrease the overpotential for ARN reduction. In this context, the surface modification of conventional electrodes is an important development in electroanalysis. A variety of efficient catalysts has been developed to induce the reduction or oxidation of some organic compounds [25–27], since these catalysts promote a faster electron transfer between the electrode surface and electroactive species in solution. The versatility of the silica gel surface in immobilizing many species, while retaining its general properties such as rigidity, porosity, particle size, high specific surface area, and chemical stability, makes it very attractive to immobilize electron mediators for catalytic and electroanalytical purposes [28]. Silica gel chemically modified with titanium(IV) oxide presents a surface with amphoteric properties [29].

In a previous report, it was demonstrated that the porphyrin Fe(III) moiety in hemoglobin and synthetic porphyrin Fe(III) displays interaction with artemisinin [30–35].

Inspired by the success of the above outlined molecular recognition research, in the present article, attempts to develop a sensor for ARN with amperometric detection are described.

2. Experimental

2.1. Chemical and solutions

All chemicals were of analytical grade. Graphite powder (99.9%) and mineral oil were purchased from Aldrich, Milwaukee, USA and used to prepare carbon paste. Hemin (iron(III) protoporphyrin IX chloride (Fe(III)P), was acquired from ACROS, New Jersey, USA and Artemisinin (ARN), McIlvaine (Na_2HPO_4 and citric acid), PIPES [piperazine-*N*-*N*-bis[2-ethanesulfonic acid]], HEPES[*N*-(2-hydroxyethyl)piperazine-*N*-(2-ethanesulfonic acid)], [tris(hydroxymethyl) aminomethane], hydrogen peroxide solution (H_2O_2), ferric chloride ($FeCl_3$) and EDTA iron(III) sodium salt were acquired from Sigma, St. Louis, USA. Disodium, monosodium phosphate (Na_2HPO_4 and NaH_2PO_4) and sodium cyanide (NaCN) were acquired from Synth, São Paulo, Brazil. Silica gel was supplied by Fluka, Buchs, Switzerland, with an average pore diameter of 6 nm and particle size of 0.04–0.063 mm and was used without further treatment. The solutions were prepared by using Milli-Q-purified water and the pH values of the buffer solutions were determined with a Corning pH/Ion Analyser model 350. Stock working solution was prepared by dissolving 1.41 g ARN in 500 ml ethanol. The resulting solution (1.0×10^{-2} mol L^{-1}) was stocked in a refrigerator at 4 °C. All ARN solutions in this study were prepared by diluting the stock working solution with buffer solution containing 20% ethanol.

2.2. Construction of the sensors

An electrode with geometrical area of 0.2 cm^2 (5 mm diameter) was used for modified electrode construction. The preparation of titanium oxide modified-silica was performed modifying the silica gel surface with titanium oxide according to the procedure described by Kubota and coworkers [36]. The first step is based on the grafting of $TiCl_4$ on the silica surface, and the second is based on the hydrolysis of remaining chloride, represented by the following equations [36]:

$$n(\equiv\mathrm{SiOH}) + \mathrm{TiCl_4} \rightarrow (\equiv\mathrm{SiO})_n\mathrm{TiCl}_{4-n} + n\mathrm{HCl} \quad (1)$$

$$(\equiv\mathrm{SiO})n\mathrm{TiCl}_{4-n} + (4-n)\mathrm{H_2O} \rightarrow (\equiv\mathrm{SiO})_n\mathrm{Ti(OH)}_{4-n} + (4-n)\mathrm{HCl} \quad (2)$$

where $(\equiv\mathrm{SiO})_n\mathrm{Ti(OH)}_{4-n}$ is denominated as ST. The quantity of ST grafted on surface of the material was 0.33 mmol g^{-1} determinated by X-ray fluorescence and the surface area was determined by BET method (294 m^2 g^{-1}) [37].

The immobilization of hemin on modified silica was carried out by preparing a solution of 1.0 mmol L^{-1} hemin in DMSO. After this step, 600 μL of this solution were added to 75 mg of ST under stirring. After 12 h, the resulting solid was filtered and washed for several times with DMSO, and then it was dried at 323 K for 30 min. The immobilization occurs through the carboxylic group of the hemin and titanium oxide grafted onto silica surface in a similar way to those described by Kennedy and Cabral [38]. The quantity of the immobilized mediator was determined by a PerkinElmer-2400 elemental analyzer (48 μmol g^{-1}).

This material is denoted as "hemin immobilized on titanium oxide-modified silica" (STH). The modified electrode was prepared by mixing 20 mg of graphite, 20 mg of STH, and 30 μL of mineral oil, until a homogeneous paste is achieved. About 10 mg of this paste was transferred to the cavity of a home-made Teflon holder with an internal diameter of 5 mm and 1 mm deep using pyrolytic graphite in the bottom for the electric contact. The modified carbon paste electrode obtained in this work is denoted as CPE/STH. All the responses obtained with the proposed sensor are given as the observed current for a known geometric area of the work electrode (sensor), determined as ($A = \pi r^2$).

2.3. Electrochemical measurements

The voltammetric and amperometric measurements were carried out with a potentiostat PGSTAT-30 Model from Autolab Echo Chemie (Utrecht, The Netherlands) connected to a PC (Software GPES 4.9). An electrochemical cell with three electrodes was used with an Ag/AgCl (saturated KCl) electrode as reference, a Pt wire as auxiliary and unmodified or modified carbon pastes as working electrodes, for all measurements. The measurements were carried

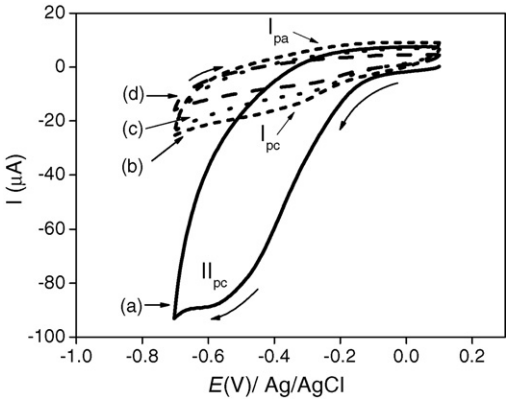

Fig. 2. Cyclic voltammograms for a CPE/STH, in the presence (a) and absence (b) of 0.4 mmol L^{-1} ARN; unmodified carbon paste electrode in the presence (c) and absence (d) of 0.4 mmol L^{-1} ARN, in 0.1 mol L^{-1} phosphate buffer solution at pH 7.0. Scan rate: 100 mV s^{-1}. $E_{initial}$ = 0.1 V and E_{λ} = −0.7 V.

out, using 5.00 mL of buffer solutions. Oxygen was removed by bubbling nitrogen through the solution for at least 10 min. For the experiments performed at constant potential, the current response was recorded as a function of time, following the addition of ARN. The sensor response was measured as the difference between total and residual currents.

2.4. Procedure for sample preparation

For amperometric analysis, 1 g of dried leaves of *A. vulgaris* L. were ground into powder, in a porcelain mortar. The resulting powder was then extracted with ethanol (100 mL, 3×). After this step, an aliquot of 25 μL of the solution was added to the cell containing 5.00 mL of the supporting electrolyte to be measured.

3. Results and discussion

3.1. Electrocatalytic reduction of ARN by CPE/STH

In order to verify the catalytic activity of hemin in the presence of ARN, several assays were carried out. Fig. 2 shows cyclic voltammograms for a CPE/STH in phosphate buffer solution (pH 7.0), using a cathodic scan, with $E_{initial}$ = 0.1 V and E_{λ} = −0.7 V, in the presence (a) and absence of ARN (b). For comparative purposes, cyclic voltammograms obtained with an unmodified carbon paste electrode in the presence (c) and absence of ARN (d) are also presented. In these voltammograms (Fig. 2c and d), there is no evidence of peaks, indicating that the direct reduction of ARN is out of these limits (E_{pc} < −0.7 V vs. Ag/AgCl). In Fig. 1b, the redox system I_{pc}/I_{pa}, relative to the Fe(III)/Fe(II) redox couple is observed at potentials of E_{pIa} = −0.2 V and E_{pIc} = −0.3 V vs. Ag/AgCl (see arrows, Fig. 2). After adding ARN to the solution (Fig. 2a), the reduction peak is significantly increased (II_{pc}) and is shifted towards more negative values (−500 mV), whilst the oxidation peak current is diminished, indicating that there is an interaction between ARN and protoporphyrin leading to an electrocatalysis. This implies that ARN can be reduced at a significant less negative potential on the hemin-modified electrode than on unmodified electrode (about −1 V) as reported by Yang et al. [22]. Furthermore, the reduction of ARN on the CPE/STH takes place in a similar way to that observed for ARN in the presence of hemin in solution phase. According to the works reported by Chen et al. [39] and Zhou et al. [40], the catalytic reduction mechanism of ARN, in the presence of hemin, can be expressed by the following equations:

$$\text{Hemin}(Fe^{3+}) + 1e- \leftrightarrow \text{Hemin}(Fe^{2+}) \quad (3)$$

$$2\text{Hemin}(Fe^{2+}) + \text{ARN}_{ox} + 2H^{+} + 2e^{-} \rightarrow 2\text{Hemin}(Fe^{3+}) + \text{ARN}_{red} + H_2O \quad (4)$$

The complete elucidation of the mechanism of catalysis is out of the scope of the present paper.

These results indicate that the electrocatalytic activity of the modified electrode can be applied for ARN determination at significantly less negative potentials.

3.2. Influence of the graphite power and CPE/STH

The influence of the ratio of STH and graphite powder used in the modified electrode preparation on the peak current was investigated in the proportions of 2:3, 1:1, 3:2 and 4:2 (w/w), in phosphate buffer solution (pH 7.0) containing 0.15 μmol L^{-1} of ARN, with a reduction potential of −0.50 V vs. Ag/AgCl. The results indicated that the best analytical signal was obtained using a 1:1 ratio (4.30 μA) and therefore, this was chosen for further experiments. For ratios greater than 1:1, good homogenization of the carbon paste was not obtained, and for lower ratios, the current was smaller.

3.3. Influences of the solution pH, buffer nature and concentration

In order to optimize the electrocatalytic response of the CPE/STH after adding ARN (0.15 μmol L^{-1}), the effect of pH on the catalytic reduction was also investigated in 0.1 mol L^{-1} phosphate buffer solution (Fig. 3a). Thus, the current (ΔI) was investigated in the pH range from 6.0 to 8.0. At pH 7.0, the current reached a maximum. Thus, the optimum pH for the further studies was set to 7.0 as shown in Fig. 3a.

The influence of the buffer solution on the sensor response was also tested in four different buffer solutions (HEPES, PIPES, McIlvaine, TRIS and phosphate) with concentrations of 0.1 mol L^{-1}. In phosphate buffer solutions, modified electrodes presented optimised responses (Fig. 3b). In this sense, the phosphate buffer solution was chosen.

Table 1 shows the results obtained for the measurements carried out in different concentrations of phosphate (0.025 mol L^{-1}, 0.05 mol L^{-1}, 0.10 mol L^{-1}, 0.2 mol L^{-1} and 0.25 mol L^{-1}). Phosphate buffer concentrations from 0.10 mol L^{-1} to 0.20 mol L^{-1} presented almost a constant current. In [PBS] values less than 0.1 mol L^{-1}, it is noticeable that the electron transfer rate is apparently diminished, a fact that can be attributed to the lack of charge transport to keep the electroneutrality of the electrode. In this sense, the concentration of 0.1 mol L^{-1} was chosen for further experiments.

Table 1
Influence of the phosphate buffer concentration on the current (ΔI) obtained by amperometry with the sensor

[Buffer] (mol L^{-1})	$-\Delta I$ (μA)
0.025	2.98 (±0.04)[a]
0.05	4.01 (±0.02)
0.1	4.30 (±0.01)
0.2	4.07 (±0.05)
0.25	3.89 (±0.04)

[a] Measurements carried out in phosphate buffer (pH 7.0), containing 0.15 μmol L^{-1} ARN applying −0.5 V vs. Ag/AgCl. Standard deviation for three replicates.

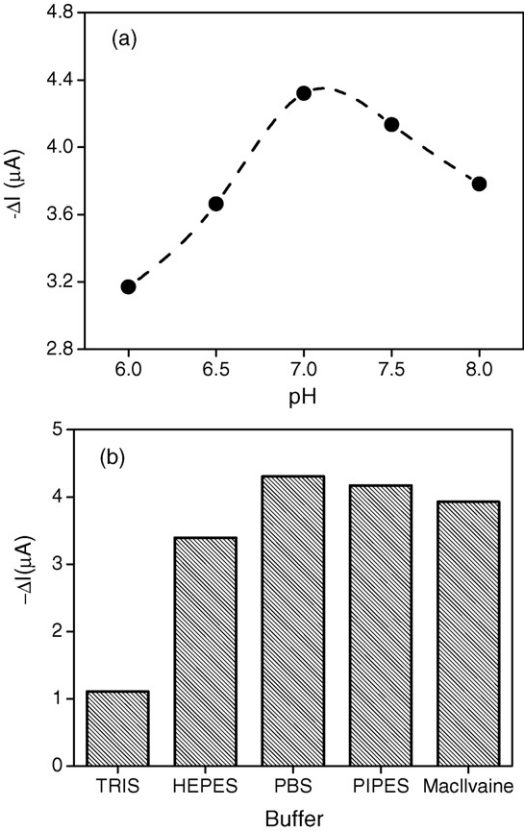

Fig. 3. (a) Response profile for the CPE/STH in 0.1 mol L^{-1} phosphate buffer solutions with different pH values and (b) effect of the buffer nature solution on the current. Applied potential of −500 mV vs. Ag/AgCl, containing 0.15 μmol L^{-1} of ARN at pH 7.0.

3.4. Analytical characterization

For amperometric measurements, the applied potential has an important influence over the sensor response, because the applied potential contributes to the sensitivity of the system. Thus, the characteristics of the CPE/STH were verified by amperometric experiments and an initial study was performed in order to determine the best potential to be applied to the electrode. In this sense, the applied potential was chosen based on the measurements of the catalytic current intensities in the optimized conditions and the highest current was verified at an applied potential of −0.5 V vs. Ag/AgCl (Fig. 4).

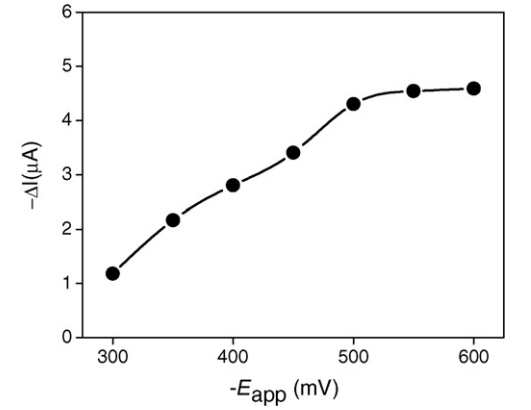

Fig. 4. Influence of the applied potential on the CPE/STH response containing 0.15 μmol L^{-1} of ARN in 0.1 mol L^{-1} phosphate buffer solution at pH 7.0.

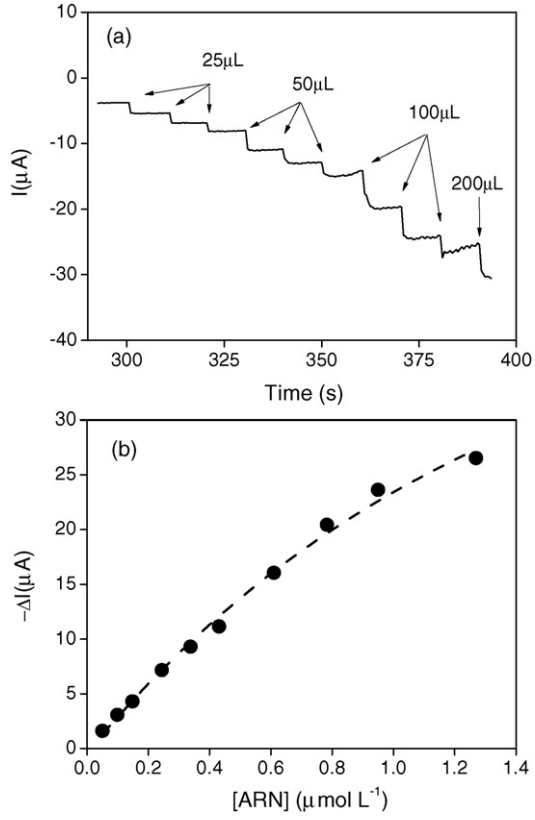

Fig. 5. (a) Amperometric response obtained with the CPE/STH sensor for eletroreduction of ARN after successive injections of a 10 μmol L^{-1} ARN solution in to the cell and (b) typical calibration graph. Applied potential of −500 mV vs. Ag/AgCl, in 0.1 mol L^{-1} phosphate buffer solution at pH 7.0.

In order to obtain an analytical calibration curve for the developed sensor, amperograms for ARN were carried out at different concentrations in 0.1 mol L^{-1} phosphate buffer at pH 7.0, after optimizing the experimental parameters (Fig. 5a). The proposed sensor showed a linear response range from 50 nmol L^{-1} to 1000 nmol L^{-1} (Fig. 5b), which can be expressed according to the following equation:

$$\Delta I\ (\mu A) = 0.70(\pm 0.20) + 24.66(\pm 0.36)[ARN]\,(\mu mol\,L^{-1}) \quad (5)$$

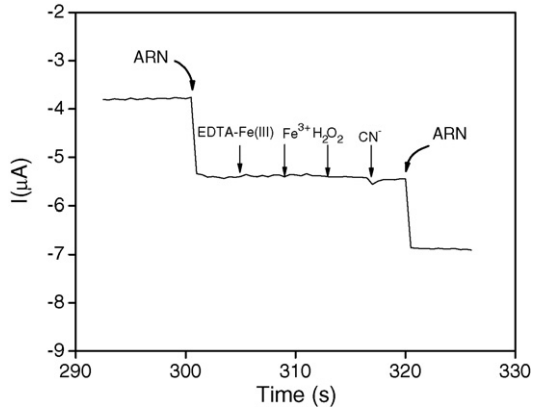

Fig. 6. Current-time recordings to successive additions of: (a, c) 0.05 μmol L^{-1} ARN, (b) 0.05 μmol L^{-1} EDTA-Fe(III), 0.05 μmol L^{-1} Fe^{3+}, 0.05 μmol L^{-1} H_2O_2 and 0.05 μmol L^{-1} CN^- at CPE/STH. Applied potential of −500 mV vs. Ag/AgCl, in 0.1 mol L^{-1} phosphate buffer at pH 7.0.

Table 2
Addition and recovery of ARN in three crude extract samples ($n = 3$) obtained with the CPE/STH

Samples	ARN added (μmol L^{-1})	ARN expected (μmol L^{-1})	ARN found (μmol L^{-1})	ARN found (mg g^{-1} dried plant)	Recovery (%)
A	0.0	–	0.100(±0.020)	1.7 (±0.5)	
	0.05	0.150	0.150 (±0.020)		100 (±1)
B	0.0	–	0.130 (±0.030)	2.2 (±0.4)	
	0.05	0.180	0.190 (±0.050)		105 (±3)
C	0.0	–	0.090 (±0.010)	1.5 (±0.2)	
	0.05	0.140	0.139 (±0.030)		99 (±4)

with a correlation coefficient of 0.999 (for $n = 9$). Such good sensitivity of 24.66 A L mol^{-1} can be attributed to the efficiency of the electron transfer between the hemin and ARN due to the catalytic effect and a consequence of a highly dispersed hemin on the ST. A detection limit of 15 nmol L^{-1} was determined using a 3σ/slope ratio and quantification limit was 52 nmol L^{-1} using 10σ/slope, where (is the standard deviation of the mean value for 10 amperograms of the blank, determined according to the IUPAC recommendations [41].

The sensor response time was very short, reaching 95% of its maximum response in 0.5 s as observed in Fig. 5a, which also shows the high stability of the signal as a function of time. This response time is excellent considering that it is a carbon paste electrode. In part, this behaviour may stem from the design and procedure used to construct the electrode ensured that it was well-packed, so that it becomes difficult for the solution to diffuse through the paste.

3.5. Effects of interferences

The study of interferences on the electrode response is useful so as to ensure correct sample preparation via the minimisation of their effects. In this sense, four possible interfering substrates were used to evaluate the selectivity of the CPE/STH for ARN. This was performed by investigating the amperometric response, in the presence of the possible interferences such as EDTA-Fe(III), Fe^{3+}, H_2O_2 and CN^-. Amperograms were recorded after adding 0.05 μmol L^{-1} ARN, using CPE/STH as working electrode. The reduction current rises sharply (Fig. 6). Further additions of 0.05 μmol L^{-1} EDTA-Fe(III), 0.05 μmol L^{-1} Fe^{3+} and 0.05 μmol L^{-1} H_2O_2 into the electrolyte, provoked no response at CPE/STH. A sequential addition of 0.05 μmol L^{-1} ARN returned the stable response (Fig. 6). These results indicate that the above mentionned analytes do not interfere in the steady state current of ARN at these concentration levels. It seems that CN^- can bind to the central metal Fe(III) of hemin, and thus, interferes in the determination of ARN.

3.6. Stability of CPE/STH

The stability of the CPE/STH was determined with successive ARN additions equivalent to 0.15 μmol L^{-1} in the electrochemical cell, recording the current (ΔI) associated with the analyte reduction by amperometric measurements in 0.1 mol L^{-1} phosphate buffer solution (pH 7.0). After 80 measurements, no significant change in the response was observed for the modified electrode. When the modified electrode was stored in air at room temperature no significant change in the response was observed, for at least 1 month. The modified electrode presented a good repeatability for ARN determination. The relative standard deviation (R.S.D.) for 10 determinations of 0.15 μmol L^{-1} ARN was 4.1%. Additionally, a series of 10 sensors prepared in the same manner and tested in phosphate buffer (pH 7.0) containing 0.15 μmol L^{-1} ARN gave responses with a relative standard deviation lower than 5.0%. These experiments indicate that hemin adsorbed onto ST matrix has good stability and repeatability, probably associated with the ability of the matrix to fix hemin by a strong adsorption.

3.7. Application to samples

The modified electrode was applied for ARN determination in three samples of the crude extract of *A. vulgaris* L. in triplicate (Table 2). The samples presented values of 1.7 (±0.5) mg g^{-1}, 2.2 mg g^{-1} and 1.5 (±0.2) mg g^{-1} of ARN in dried plant, respectively. The concentration of ARN was determined using the standard addition method. The results suggest that the method is very effective for ARN determination in low levels.

For an additional check on the accuracy of the developed method and the matrix interferences, analytical recovery experiments were performed by adding known amounts of ARN in three samples of the crude extract of *A. vulgaris* L. The percentage of recovery was calculated by comparing the concentration obtained from the samples with actual and added concentrations according to the equation:

$$\text{Recovery (\%)} = \frac{\text{concentration found}}{\text{concentration expected}} \times 100 \quad (6)$$

The recovery values for the samples are listed in Table 2. It can be clearly observed that the matrices did not influence the sensor response.

4. Conclusions

This work has demonstrated that ST has great potential to be used as a support for immobilizing hemin to develop new modified electrodes as well as to investigate the behaviour of the ARN electroreduction. This system is a feasible alternative for the analytical determination of ARN in crude extract of *A. vulgaris* L. The modified electrode exhibited high electrocatalytic activity and shifted the ARN reduction overpotential to much less negative values when compared to its reduction on the CPE/ST. Under optimized conditions, amperometry measurements in phosphate buffer (pH 7.0) solutions yielded low detection limit and high sensitivity for ARN. The modified electrode showed good repeatability (R.S.D. = 4.1%) and stability for ARN sensing. These results suggest that the CPE/STH system can be used as an efficient catalyst for ARN reduction in aqueous solutions, and, therefore, be used as a simple, non-time-consuming method and, therefore, suitable for routine work and for in field experiments and to analysis of pharmaceutical products.

Acknowledgements

The authors thank financial support from the FAPESP, FAPEAL, CNPq, CNPq/PADCT, CAPES, PROCAD/NF, BNB, RENORBIO and Instituto do Milênio-Inovação em Fármacos/CNPq. PRL and JRMR are indebted to FAPESP and FAPEAL for fellowships, respectively.

References

[1] M.O.F. Goulart, A.E.G. Santana, G. Fontes, E.M.M. Rocha, in: J.A. Squella, S. Bollo (Eds.), Biological Significance Compounds, Transworld Research Network, Kerala, 2006, pp. 1–32.
[2] J. Martin, Malaria Nurs. Stand. 15 (2001) 47.
[3] URL: http://rbm.who.int/cmc_upload/0/000/015/372/RBMInfosheet_1.htm. Accessed 2008, March 26.
[4] H.W. Murray, J. Pépin, T.B. Nutman, S.L. Hoffman, A.F. Mahmoud, Br. Med. J. 320 (2000) 490.
[5] G.A. Biagini, P.M. O'Neill, A. Nzila, S.A. Ward, P.G. Bray, Trends Parasitol. 19 (2003) 479.
[6] C.W. Wright, J. Ethnopharmacol. 100 (2005) 67.
[7] C. Wongsrichanalai, A.L. Pickard, W.H. Wernsdorfer, S.R. Meshnick, Lancet Infect. Dis. 2 (2002) 209.
[8] D.A. Fidock, P.J. Rosenthal, S.L. Croft, R. Brun, S. Nwaka, Nat. Rev. 3 (2004) 509.
[9] U. Eckstein-Ludwig, R.J. Webb, I.D. van Goethem, Nature 424 (2003) 957.
[10] R.L. Krauth-Siegel, R.H. Schirmer, H. Bauer, Angew. Chem. Int. Ed. 44 (2005) 690.
[11] D.L. Klayman, Science 228 (1985) 1049.
[12] V.F. Andrade-Neto, M.O.F. Goulart, J.F. da Silva Filho, M.J. da Silva, M.C.F.R. Pinto, A.V. Pinto, M.G. Zalis, L.H. Carvalho, A.U. Krettli, Bioorg. Med. Chem. Lett. 14 (2004) 1145.
[13] Facts on ACTs (artemisinin-based combination therapies): January 2006 update [online]. WHO, Geneva, 2006. Available from URL: http://www.rbm.who.int/cmc_upload/0/000/015/364/RBMInfosheet_9.htm. Accessed 2008, February 17.
[14] F.T. Aweeka, P.I. German, Clin. Pharmacokinet. 47 (2008) 91.
[15] J. Golenser, J.H. Waknine, M. Krugliak, N.H. Hunt, G.E. Grau, Int. J. Parasitol. 36 (2006) 1427.
[16] A. Mital, Curr. Med. Chem. 14 (2007) 759–773.
[17] P. Christen, J.-L. Veuthey, Curr. Med. Chem. 8 (2001) 1827.
[18] C.Z. Liu, H.Y. Zhou, Y. Zhao, Anal. Chim. Acta 581 (2007) 298.
[19] G.P. Qian, Y.W. Yang, Q.L. Ren, J. Liq. Chromat. Rel. Technol. 28 (2005) 705.
[20] C. Debnath, E. Haslinger, A. Ortner, Nat. Prod. Commun. 1 (2006) 487.
[21] C. Debnath, E. Haslinger, W. Likussar, J. Pharm. Biomed. Anal. 41 (2006) 638.
[22] P.-H. Yang, Z.-J. Zhou, J.-Y. Cai, Colloids Surf. A: Physicochem. Eng. Aspects 257–258 (2005) 467–472.
[23] M.A. La-Scalea, H.S.R.C. Silva, E.I. Ferreira, Braz. J. Pharm. Sci. 43 (2007) 372–383.
[24] R.L. Donkers, M.S. Workentin, J. Phys. Chem. B 102 (1998) 406110.
[25] P.R. Lima, W.J.R. Santos, R. de, C.S. Luz, F.S. Damos, A.B. Oliveira, M.O.F. Goulart, L.T. Kubota, J. Electroanal. Chem. 612 (2008) 87.
[26] P.R. Lima, W.J.R. Santos, A.B. Oliveira, M.O.F. Goulart, L.T. Kubota, J. Pharm. Biomed. Anal. 47 (2008) 758.
[27] C.O. Costa, P.R.B. Miranda, B. Hazra, M.D. Sarma, R.C.S. Luz, L.T. Kubota, M.O.F. Goulart, Talanta 68 (2006) 1378.
[28] L.T. Kubota, B.G. Milagres, F. Gouvêa, G. Oliveira Neto, Anal Lett 29 (1996) 893.
[29] L.T. Kubota, Y.J. Gushikem, J. Electroanal. Chem. 362 (1993) 219.
[30] A.F.G. Slater, W.J. Swiggard, B.R. Orton, Proc. Natl. Acad. Sci. U.S.A. 88 (1991) 325.
[31] R. Anne, M.J. Bernard, J. Am. Chem. Soc. 119 (1997) 5968.
[32] L. Messori, F. Piccioli, B. Eitler, M.C. Bergonzi, F.F. Vincieri, Bioorg. Med. Chem. Lett. 13 (2003) 4055.
[33] S.R. Meshnick, A. Thomas, A. Ranz, C.-M. Xu, H.-Z. Pan, Mol. Biochem. Parasitol. 49 (1991) 181.
[34] P.L. Olliaro, R.K. Haynes, B. Meunier, Y. Yuthavong, Trends Parasitol. 17 (2001) 122.
[35] W.M. Wu, Y.L. Wu, J. Chem. Soc.-Perkin Trans. 1 (2000) 4279.
[36] L.T. Kubota, Y. Gushikem, S. Castro, J.C. Moreira, Colloids Surf. 57 (1991) 11.
[37] F. Rouquerol, J. Rouquerol, K. Sing, Adsorption by Powers and Porous Solids: Principles, Methodology and Applications, Academic Press, San Diego, 1999, pp. 41–50.
[38] J.F. Kennedy, J.M.S. Cabral, Transition Met. Chem. 11 (1986) 11.
[39] Y. Chen, J.-M. Zheng, S.-M. Zhu, H.-Y. Chen, Electrochim. Acta 44 (1999) 2345.
[40] Z.-J. Zhou, P.-H. Yang, D.-X. Feng, Y.-T. Zhu, M.-Y. Zhang, Chin. J. Anal. Lab. 23 (2004) 28.
[41] Analytical Methods Committee, Analyst 112 (1987) 199.

Talanta 77 (2008) 507–513

Contents lists available at ScienceDirect

Talanta

journal homepage: www.elsevier.com/locate/talanta

Application of monofluorophosphate/alkaline phosphatase system in flow injection analysis

Beata Rozum, Robert Koncki*

University of Warsaw, Department of Chemistry, Pasteura 1, 02-093 Warsaw, Poland

ARTICLE INFO

Article history:
Received 19 October 2007
Received in revised form 17 March 2008
Accepted 4 April 2008
Available online 12 April 2008

Keywords:
Bioanalysis
Flow injection analysis
Potentiometry
Alkaline phosphatase
Enzyme assay
Inhibitors
Cofactor

ABSTRACT

Monofluorophosphate was found to be a specific substrate for alkaline phosphatase (EC 3.1.3.1) forming novel biosensing schemes with potentiometric detection. Several utilities of this substrate/enzyme system in analytical chemistry will be demonstrated. The system is useful for direct detection of enzymes and substrates as well as for indirect determination of enzyme inhibitors and cofactors using common potentiometric instrumentation. The analytical values of reported biosensing schemes are significantly improved by their implementation into flow injection analysis. This paper presents recent developments in this area and suggests important prospects for further investigations and applications.

1. Introduction

Alkaline phosphatase (ALP, EC 3.1.3.1) is a nonspecific esterase catalyzing the hydrolysis of various monoesters of phosphoric acid like monophosphates of sugars, alcohols, phenols, nucleotides and many other organic compounds. According to the name, ALP is a biocatalysts exhibiting the highest activity in weakly alkaline solutions (pH range 8–10). Generally, in the course of the enzymatic reaction P–O bonds are cleaved leading to the release of an alcohol and phosphoric acid:

$$ROPO_3^{2-} + H_2O \rightarrow ROH + HPO_4^{2-}$$

At least three areas of modern analytical chemistry where ALP detection is applied can be indicated. One area is clinical chemistry. ALP is one of the enzymes which activity is the most commonly determined in routine clinical analysis nowadays. Its blood serum activity provides useful medical information in case of many disorders, mainly liver and skeletal diseases [1]. Significant increase in ALP activity occurs with all forms of cholestasis, including obstructive jaundice. High enzyme activity is also observed during skeletal disorders like Paget's disease, osteomalacia, bone's fractures and rickets. Moreover, the determination of ALP serum activity is especially important for oncological patients, because its elevated level is an indication for sarcoma and malignant tumors. Secondly, ALP is frequently used as an enzymatic label in different immunoassays. The popularity of this marker is due to its relatively small molecular size, high turnover rate, high stability, simplicity of isolation and low cost. Moreover, in this case the low substrate selectivity of ALP is advantageous, because a variety of substrates implicate a variety of available detection methods. Therefore, a large number of ALP conjugated immunoreagents is commercially available and different assays have been developed with the use of ALP-labeled compounds [2–12]. Owing to the same reasons, several genoassays applying ALP as enzyme marker have been developed recently [13–16]. Finally, the application of ALP enables indirect determinations of its cofactor [17–23] and inhibitors [24–29]. In contrast to non-selective substrate biorecognition this kind of biodetection is quite specific.

The recommended clinical method for ALP activity determination employs chromogenic *p*-nitrophenylphosphate [30,31]. The other spectrophotometric methods utilize substrates such as phenylphosphate or phenolophthalein phosphate [32]. ALP activity can be also assayed with conventional spectrophotometric methods via the determination of released phosphates in the enzymatic reaction that reduce phosphomolybdate to molybdenum blue [33]. Diverse substrates have been found suitable for optical methods with phosphorescence [33], fluorescence [34,35] and chemilumi-

* Corresponding author. Fax: +48 22 8225 996.
E-mail address: rkoncki@chem.uw.edu.pl (R. Koncki).

0039-9140/$ – see front matter © 2008 Elsevier B.V. All rights reserved.
doi:10.1016/j.talanta.2008.04.005

nescence [11,28,29] detection. The second large group consists of amperometric methods developed for ALP determination. Among the substrates used phosphates of phenol [2,12,36,37], naphthol [3,4], ferrocene [5,6], indol [8] and quinone [9] derivatives are the most common. These esters after biocatalytic hydrolysis form electroactive products easily detected electrochemically. Potentiometric methods for ALP determination are not common. An original method utilizes unusual ion-selective electrode sensitive to hordenine released from hordenine phosphate (substrate) in the course of the enzymatic reaction [38]. Unfortunately, to apply this method the mentioned substrate has to be synthesized according to a rather laborious, multi-step protocol.

In this paper monofluorophosphate (MFP), an alternative substrate for potentiometric determination of ALP enabling two different detection methods is presented. Advantages of MFP/ALP system and its applications for various kinds of potentiometric biodetections are discussed in detail. Special emphasis is put on flow injection analysis (FIA) employing this substrate/enzyme system. Finally, some directions for future investigations will be indicated.

2. Coupling of MFP/ALP system with potentiometric detection

The Achilles heel of methods developed for ALP detection is the substrate. Unfortunately, the majority of compounds mentioned in Section 1 are expensive (when commercially available), and rather unstable (hygroscopic and easily hydrolysable). Exemplary prices for the most common ALP substrates are listed in Table 1. MFP recommended in this contribution has none of these drawbacks. From the analytical point of view it is important that MFP is commercially available in crystalline, non-hygroscopic, stable form. It should be emphasized, that in comparison with other ALP substrates MFP is an extremely cheap reagent (Table 1).

MFP is commonly known as a caries-preservative additive in dentifrices. Its decomposition is significantly accelerated by "MFPase" present in saliva and dental plaque and recognized as ALP [39,40]. Enzymatic degradation of MFP by ALP finds application in FIA systems dedicated for toothpaste analysis based on spectrophotometric detection of released phosphate ions [41,42]. ALP-catalyzed decomposition of this compound has also been investigated as experimentally safe model of enzymatic degradation of sarin, a highly toxic organofluorophosphorus MFP analogue [43].

From chemical point of view MFP can be considered as the simplest derivative of phosphoric acid containing a P–F bond. This means that in contrast to organic phosphoesters this compound should be classified as mixed anhydride. MFP undergoes the hydrolysis very slowly. However, in the presence of ALP the reaction is significantly accelerated. Fig. 1 illustrates this enzymatic process. Potentiometric detection of fluoride ions using fluoride ion selective electrode (FISE) imposes itself. Such detector with crystalline ion-selective membrane made of lanthanum fluoride is known to be robust, highly sensitive and selective as well as to have excellent dynamics. Its operational conditions and analytical characteristics are well-defined. Utilities of FIA based on this FISE coupled with MFP/ALP system, recently developed in our group [44,45], will be discussed in the next paragraphs of this paper. Obviously, other kinds of potentiometric as well as optic fluoride sensors should be also suitable for such applications.

Table 1
Conventional substrates applied for ALP assays (prices from Sigma–Aldrich catalogue 2007)

Substrate	Detection method	Price (€ mol^{-1})
L-Ascorbic acid phosphate	Voltamperometry	~3×10^3
p-Nitrophenyl phosphate	Spectrophotometry (Vis) Voltamperometry	~20×10^3
1-Naphtyl phosphate	Spectrophotometry (UV) Voltamperometry	~50×10^3
3-Indoxyl phosphate	Voltamperometry	~80×10^3
D-Lucyferin phosphate	Chemiluminescence	~15×10^6
Fluorescein diphosphate	Fluorescence	~40×10^6
Monofluorophosphate (MFP)	Potentiometry	~15

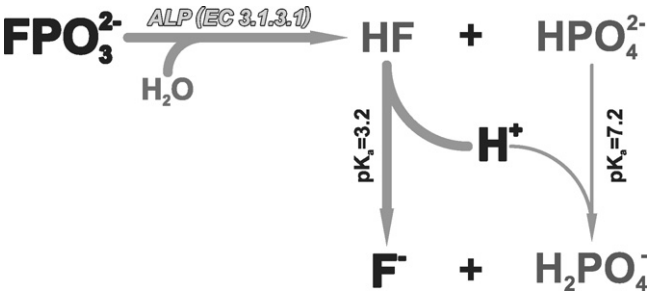

Fig. 1. Scheme of MFP hydrolysis catalyzed by ALP.

Beside the assays with FISE, there is one more possibility of potentiometric ALP activity detection. The hydrolysis of anhydrides is accompanied with strong environment acidification. Products of hydrolysis catalyzed by ALP have protolytic properties that can cause a change in the pH of the reaction environment (Fig. 1). Potentially this change can be followed using any kind of pH-sensor (potentiometric, as well as optical). It has been already proved [46] in assay performed under stationary measurements conditions, that MFP is a specific substrate enabling this kind of detection. While comparing with other organic ALP substrates, in the course of MFP hydrolysis, an additional proton responsible for changes in the pH of the reaction environment is generated (compare stoichiometry of reaction given in Section 1 with this shown in Fig. 1). The products formed during the hydrolysis of MFP are dihydrophosphate ions $H_2PO_4^-$ (more acidic than HPO_4^-), that cause extraordinary environment acidification. The specificity of MFP among other ALP substrates should be stressed—only for this compound significant pH changes are observed [46]. This way, the second specific opportunity of potentiometric detection for MFP/ALP system has been developed. Finally, it should be noticed that this sensing scheme could be also suitable for the development of pH-ALP-biosensors [46,47]. The potentialities of such biosensor in FIA will be discussed in the next section.

3. FIA based on MFP/ALP system

The proposed MFP/ALP system could be easily adapted for analytical chemistry needs in several ways. Enzyme can be applied in soluble as well as in immobilized forms as bioreactor or biosensor. Two kinds of electrodes may be applied as separate detectors or as internal sensors integrated with enzyme. Finally, these bioanalytical systems could be designed for direct detection of MFP and ALP as well as for indirect detection of ALP cofactor and inhibitors. Some of these applications performed in FIA format are presented below.

3.1. MFP detection

The detection of MFP is mainly wanted in the control of commercial products for oral hygiene. Toothpastes with MFP contain also the excess of free fluorides, so the application of FISE-based systems is difficult if these species are not separated before detection.

Probably due to this reason, the ALP-based FIA system developed by Tzanavaras and Themelis [41,42] is based on optical detection of phosphates formed in the course of enzymatic conversion of MFP. For such kind of samples pH-enzyme-based detection seems to be more promising as it is free from mentioned interferences. pH-sensors are insensitive to fluoride ions until they did not change photolytic equilibria. Only recently a polymeric membrane pH-electrode modified with covalently bound monomolecular layer of ALP has been developed [46,47]. This MFP-biosensor incorporated into simple single-channel FIA setup enables selective detection of this substrate in the millimolar concentration range [47]. The main drawback of this biosensor, common for all kind of pH-based enzyme electrodes, is its cross-sensitivity to pH and buffer capacity of samples. However, in case of toothpaste analysis this drawback could be easily overcome because MFP detection can be performed in saline extracts from pastes having low and well-defined buffer capacity.

3.2. ALP activity detection

In principles, enzyme activity measurements have a kinetic character. According to Michaelis-Menten theory the amount of fluoride ions generated in any time in the course of MFP hydrolysis is directly proportional to ALP activity. This way, the measurement of fluoride ions released from MFP using FISE provides a direct potentiometric method for ALP detection. The utility of LaF_3-crystalline membrane FISE has been presented in the analytical literature [48,49]. The reported results obtained with serum standards were promising, although the measurements were not performed under optimal conditions. For example, the choice of pH for such assays was a compromise between optimal pH for the enzyme and sensor. Moreover, the analytical procedures, including the conditioning of FISE in substrate solution between consecutive sample analyses, were rather long.

Beside obvious advantages accruing from the implementation of this analytical procedure into the FIA format, such as its automation and minimization of operations with potentially infectious samples, many others should be pointed out too. Firstly, the FIA system ensures stable conditions for FISE operation like constant flow rate and ionic composition of analyzed solutions. Due to extremely low cost, MFP can be permanently present at FISE as a component of the carrier stream. Commercially available MFP reagents contain about 1% of free fluoride ions, what is of considerable importance for the proposed detection scheme. On one hand this fluoride ions content limits the possibility to obtain a useful signal, since the total conversion of MFP into hydrolysis products can cause a change in free fluoride concentration of only two orders of magnitude. Thus the observed maximal change in FISE potential can be 120 mV. On the other hand, free fluoride ions continuously present in the system stabilize the electrode potential and ensure its short return time to baseline. These characteristics are especially important when FISE is applied as a detector in FIA. Moreover, in contrast to batch measurements, conditions of enzyme reaction and detector operation can be optimized independently, as in FIA manifold shown in Fig. 2A, where these processes are separated. In this three-channel FIA system, samples are injected into carrier solution containing MFP in weakly alkaline buffer. Enzymatic reaction takes place in the reaction coil at pH of 9 optimal for enzyme. The stream is acidified before it reaches the detector by merging with an acid stream to obtain pH of 5, which is optimal for FISE operation. Finally, enzyme reactions conditions, crucial for the accuracy of the assay, like time and transport parameters, are strictly defined by flow rate and reaction coil length. Typical FIAgram showing the detection of ALP activity is in Fig. 2A. Peaks are recorded in relatively short time with excellent reproducibility caused by highly reproducible FIA conditions.

The FIA system presented was calibrated with control sera having defined physiological and pathological ALP activity levels as well as with intermediate activities and applied for real human serum samples analysis [45]. The correlation between results obtained for samples with physiological and a little exceeded ALP activities was satisfactory. However, for pathological samples with very high enzyme activity results were lowered. The reason for these errors is assumed to be the non-linear characteristic of FISE response (logarithmic, accordingly to Nernst equation) as well as the depletion of MFP in the reaction segment. The system was optimized for standards with activities from 30 to 400 U L^{-1}. However, strongly pathological samples (from oncological patients) can exhibit higher activities (even to 2000 U L^{-1}). Therefore, without modification of the FIA manifold, it is possible only to recognize the pathology of sample, but quantitative ALP determination is rather inaccurate. To increase the precision of assay (to perform determinations within the linear range of FISE response), samples with extremely high ALP activity were diluted similarly as samples are pretreated when routine clinical methods are applied. As expected, the accuracy of such determinations was significantly improved.

Moreover, it was found that after proper sample pretreatment selective determination of dominant isoenzymatic ALP forms is also possible. Sometimes the activity of ALP in serum can be unequivocally assigned to a particular pathological complex, while the enzyme sources are different organs of human body. Dominant isoforms are so-called bone and liver ALP, both coded by this same gene. The only difference is the glycosyl part of biomolecule formed after translation stage and therefore discrimination between their activities is troublesome. Nevertheless, the mentioned differences in structure result in diversified resistance for thermal denaturation. Skeletal fraction is more heat-sensitive. Thanks to this, if a serum sample is thermally pretreated before analysis the result of determination concerns only the activity of more heat-resistant liver fraction. The activity of bone fraction is calculated as a difference in ALP activity for incubated serum sample and sample analyzed without incubation (in that case the sum of both isoforms—total ALP activity is determined). Details on the reported FIA system and results while applied to clinical analysis have been published only recently [45].

The assays of ALP activity are also possible using MFP as substrate and pH-electrode as a detector. As shown previously [46], changes of electrode potential are proportional to enzyme activity within the range of near two orders of magnitude and the detection limit is lower than physiological ALP activity in blood serum. However, such analytical characteristics of this biosensing scheme are possible under strictly defined conditions (sample with constant and low buffer capacity). The signal generated in discussed sensing scheme can be considered as the effect of acidimetric titration of sample with a titrant generated in the course of the enzymatic process. The rate of titrant generation is proportional to ALP activity. Thus, the method is not applicable for serum analysis, since these samples are known to have high and variable buffer capacity. Due to mentioned reasons, pH-based sensing found applications in analytical systems where the detection step is performed under well-defined conditions without contact with sample. Examples of such approach will be demonstrated in sections below.

3.3. ALP inhibitor detection

Methods developed for ALP detection can be easily adapted for the detection of enzyme inhibitors. These determination methods stand a chance to be relatively sensitive due to enzymatic

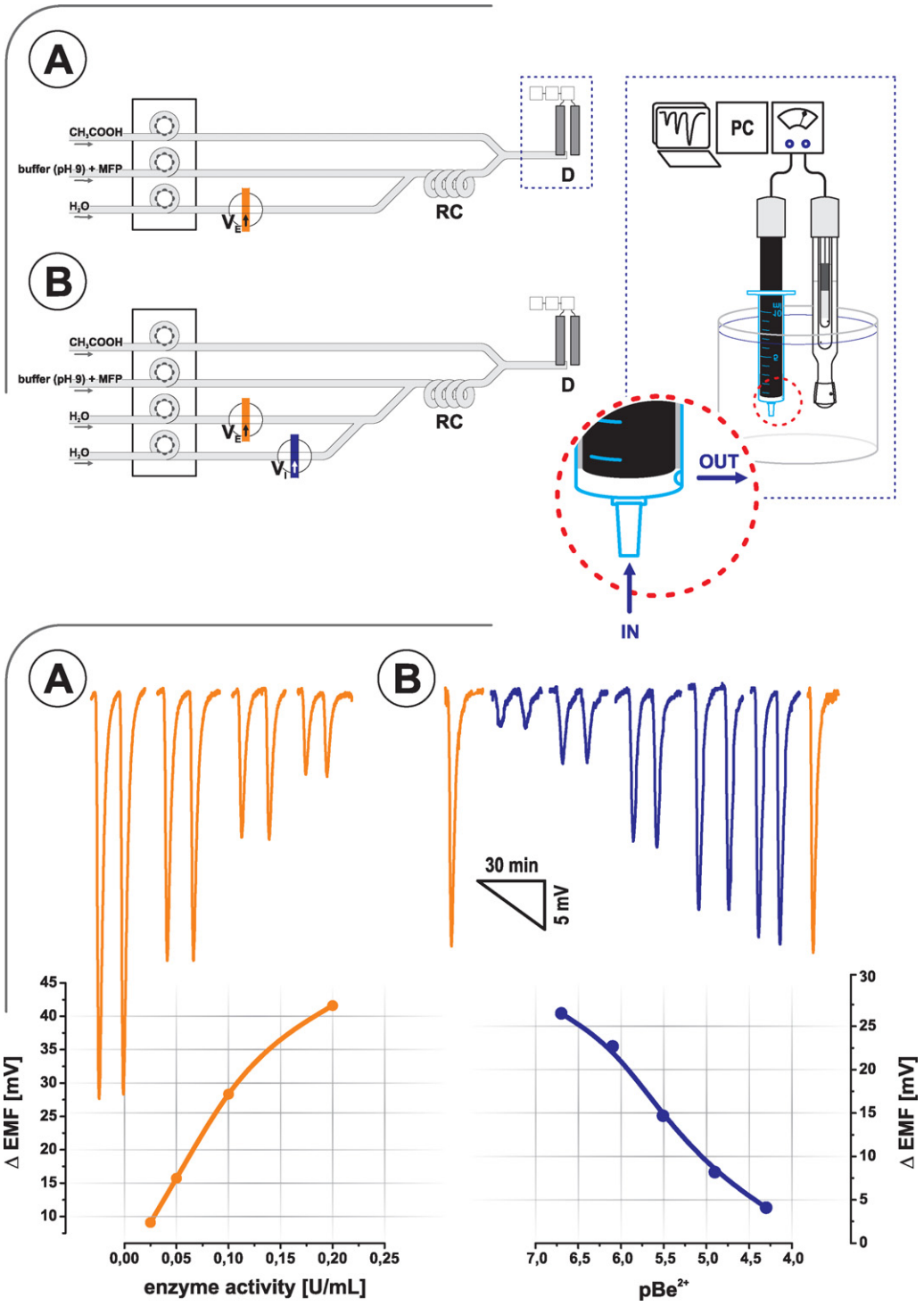

Fig. 2. FIA manifold for potentiometric detection of ALP activity (A) and ALP inhibitors (B) with fluoride ion selective electrode as detector. Typical FIAgrams and corresponding calibration graphs (insets) are given below.

amplification of signal and selective depending on the nature of enzyme-inhibitor interactions as well as on conditions in which inhibition process is performed. It is known from the analytical literature that ALP (even if very stable) is sensitive for inhibitive action of compounds such as some pesticides [24–26] and selected heavy metal ions [26–29]. Therefore, these substances can be considered as target analytes detected using the MFP/ALP biosensing system. It is worth to pay attention for economical aspect of such analyses. Besides cheap substrate, second utilized substance is ALP that is one of the cheapest biocatalysts, available in the form of stable enzymatic preparates with high specific activity. On the other hand, in case of inhibitive detections the lowest detection limits are reached when low enzyme activities are utilized.

In the course of preliminary investigations the inhibition processes were performed outside the FIA system (off-line) whereas measurements of residue ALP activity were performed in FIA sys-

tem with LaF_3-based FISE detector [44]. Manifold the same as described in section about direct detection of enzyme activity was utilized (Fig. 2A). As mentioned, inhibition process was performed outside the FIA system expecting that in fixed conditions inhibition rate is dependent mainly on: kind of inhibitor, its concentration and inhibition time. Effects from several cations were investigated and results obtained allow to distinguish (i) metal ions inhibiting ALP strongly and fast like beryllium, (ii) metal ions exhibiting strong but slow inhibition of ALP like copper and mercury, and (iii) finally a large group of ions that do not have any inhibitive effect on the enzyme. It was also found that nitric acid solutions, in which some metal ion standards were prepared, slowly deactivate ALP as well.

For further investigations the FIA manifold was modified to enable inhibition on-line. In the extended manifold the enzyme and the inhibitor solutions were introduced to the system using two independent injection valves working synchronously (Fig. 2B). The distances between valves as well as the lengths of lines were matched to ensure that after solution mixing, the segment of enzyme with inhibitor was surrounded by the excess of inhibitor. The system in that form utilizes the main advantages of flow techniques, enables to eliminate pre-analytical manual inhibition step and to shorten the time of analytical procedure as processes of inhibition and enzymatic reaction are performed on-line. Additionally, modified flow system gives possibility to define strict conditions under which the process is performed (inhibition time and transport conditions). Nevertheless, the most important and expected advantage of this system was the elimination of effects from weaker and slower inhibitors (time discrimination method). The manifold was configured to perform inhibition process in FIA system in much shorter time (few minutes only) and in the presence of buffer and substrate. As was expected under such conditions only potent inhibitors can cause a change of the analytical signal. As shown in Fig. 2B, the developed system enables selective and relatively fast (6–8 samples per hour) determination of beryllium ions at ppb concentration levels. This very low detection limit, uncommon for potentiometric detection under non-stationary measurement conditions, is worth emphasizing. Similarly strong inhibition was observed only for vanadate, tungstate and arsenate. Due to the applied kinetic discrimination approach, no effects from heavy metal cations, carbamates, phosphoorganic compounds and sample acidity were observed. Details on the indirect determination of inhibitors using MFP/ALP/FISE system under flow conditions are given elsewhere [44].

In case of inhibitive detection, the MFP/ALP sensing scheme with pH detection seems to be effective because the analyte (inhibitor) recognition step could be separated from the detection step. Thus, the signal could be measured after the inhibition, in the absence of sample, under conditions optimal for pH-based biosensing of residual ALP activity. The enzyme could be applied in free or immobilized form as well as a part of a biosensor. The biosensor mentioned in Section 3.1 was tested according to a two-step procedure in a simple single channel FIA system [47]. Samples of inhibitor (beryllium was applied as a model ALP inhibitor) and substrate were injected by turn. Conditions of inhibition were defined by the flow rate and volume of injected samples. Differences in peak heights for MFP before and after inhibition were treated as inhibitor-dependent signal. Surprisingly, inhibitive effects from beryllium and vanadate were not observed. This result can be explained in terms of the high durability of the enzyme layer formed by covalent immobilization. This means that the proposed inhibitive biosensing should be realized using biosensors with weakly immobilized ALP. In our opinion, for such applications biosensors with physically immobilized enzyme could be effective. Especially promising seem to be disposable biosensors similar to those for urease-inhibitor detection fabricated by means of screen-printing technology [50,51]. Due to the extremely low cost and high reproducibility these pH-based biosensors can be applied as single-use devices, until effective methods for their regeneration have been developed. On the other hand such strip bioelectrochemical cells are easily implemented into FIA manifold [50]. For the present, the development of FIA systems based on such biosensors dedicated to ALP-based inhibitive detection requires further investigations.

3.4. ALP cofactor detection

This kind of analysis is concerned only for complex enzymes which consist of two parts, the protein part called apoenzyme and the non-protein element, i.e. the coenzyme. ALP with zinc ions playing the cofactor role, became a versatile enzyme for such assays. The concept of cofactor recognition using apoALP was developed nearly 40 years ago [17]. Unfortunately, to obtain the apoenzyme is the most strenuous, time-consuming and laborious step, which is realized for instance by the dialysis of enzyme in appropriate chelator solution for several hours. Despite this drawback, detailed studies on the use of soluble apoenzyme for cofactor determination are continued [18–20]. Satoh [21–23] developed another approach based on the use of immobilized ALP. In this case processes of apoALP generation and regeneration after cofactor recognition were significantly faster enabling reversible and reproducible operation. Two biodevices have been developed, a flow-through apoenzyme thermistor [21] and an amperometric bi-enzyme biosensor containing ALP and ascorbate oxidase [22,23]. As ALP substrates *p*-nitrophenyl phosphate and ascorbate phosphate have been applied. The MFP/ALP system forms several opportunities for the development of apoenzyme-based sensing scheme with potentiometric detection performed in FIA format. To the best of our knowledge, up to now FISE has not been utilized in such assays. However, mentioned above pH-based MFP biosensor has been successfully applied.

Generally, coenzyme determination is put into practice by carrying out the following steps of analytical procedure. At the beginning the fully active enzyme needs to be converted into an apoenzyme, what means that the cofactor needs to be removed from the active site of an enzyme. This first step of analytical procedure is reached by the incubation of the biosensor with an appropriate chelator solution. If the cofactor is absent, resulted apoenzyme activity is negligibly low, or not observed at all. In a second step the cofactor (present in the sample) is added, thus the enzyme is reactivated and the catalytic activity reappears. The recovered enzyme activity is proportional to the cofactor concentration. All listed stages are divided by washing steps. This analytical procedure even if complicated and laborious seems to be easy to perform under FIA conditions. The general scheme of such multistep procedure is illustrated in Fig. 3.

The developed biosensor working under FIA conditions can be easily applied for ALP inhibitors detection, due to the advantages of the utilized enzyme immobilization method. ALP is strongly, covalently immobilized in the form of extremely thin (monomolecular) layer, that is easily penetrated (no transport limitations through protective membranes or matrix material used for immobilization do appear). Therefore the apoenzyme generation should be relatively fast and repeatable. The performing of each single step of analytical procedure is very easy in FIA system. All reagents (chelator, cofactor/analyte and substrate) were injected into very simple single channel FIA system through the same valve. The most effective chelator, that converts immobilized ALP into its apoform, was found to be cysteine. The separation of molecular recogni-

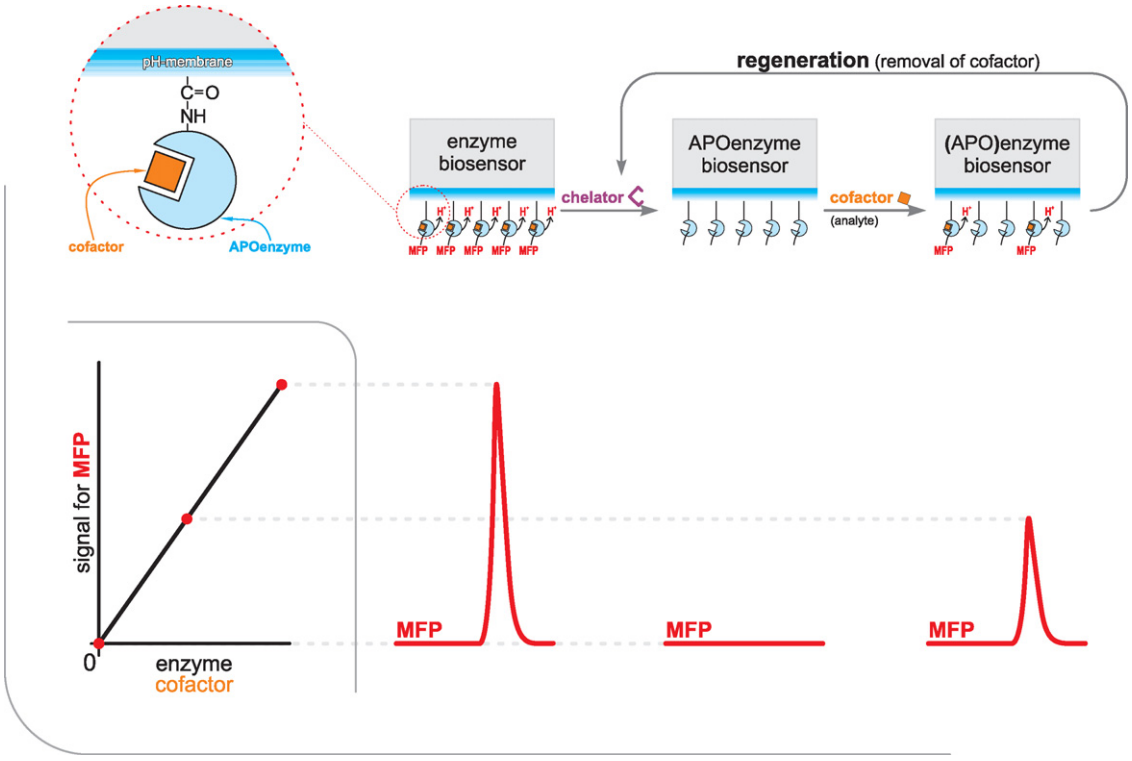

Fig. 3. Biosensing scheme for cofactor biodetection using pH-based apoenzyme electrode in FIA system. Detailed description is given in the text.

tion step (Zn^{2+} binding by immobilized apoALP) from the step of recovered activity detection (signal for MFP) allows eliminating the main disadvantage of pH-based biosensors. Results of preliminary investigations proved that with the developed biosystem, selective detection of zinc ions is possible without influence of the sample composition. Even a non-optimized FIA system enables selective potentiometric determination of zinc ions in the micromolar concentration range. Details on this bioanalytical system have been published only recently [47].

4. Conclusions and prospects

The main goal of this paper was to show that MFP as a specific ALP substrate enables various potentiometric biodetection schemes using this enzyme. The MFP advantages are worth to emphasize once again. This compound is chemically stable, non-hygroscopic and commercially available in crystalline form. In contrast to other organic monophosphates, applied as substrates for ALP, MFP is extremely cheap. Products of MFP hydrolysis allow measurements using both pH and fluoride ion-selective electrodes as detectors. The pros and cons of the two different biodetection systems MFP/ALP/FISE and MFP/ALP/pH are demonstrated. Both systems can be successfully performed under FIA conditions exploiting the advantages of this technique. As it was demonstrated, adequate designing of FIA system allows determination of all players involved in MFP/ALP system, i.e. detection of substrate, enzyme, inhibitor and cofactor. All presented FIA systems are based on common potentiometric instrumentation and simple sensors.

It should be stressed that the detection schemes presented can be further developed by respective rearrangements of reported FIA systems. For example, simple introduction of stop-flow steps into reported FIA procedures should cause a significant increase in sensitivity and an improvement of detection limits. Moreover, these detection schemes could be coupled with advanced FIA systems designed to automate some pre-detection steps of analytical procedure, for example the separation of isoforms of detected enzyme, in similar way as it was only recently shown by Hartwell et al. [52].

Other prospects for further studies are connected with several MFP-based biosensing schemes not investigated till now. It is worth to notice that all presented systems could be developed using optical sensors for fluoride and pH, which are simple to implement into FIA manifolds also. Moreover, alternative potentiometric fluoride sensors like polymeric membrane electrodes only recently developed and applied for enzyme based FIA by Gorski et al. [53] could be applied for such applications. Similarly promising seems to be pH-based biosensors for inhibitive detection as well as apoenzyme-based biosensing systems with FISE as separate or internal detector. Another field of investigation important in clinical analysis is the detection of acid phosphatase activity, since it was found that MFP is decomposed by this enzyme in the same way as in case of ALP [49].

Finally, it is worth to pay attention to one additional emerging bioanalytical aspect. As it was mentioned in Section 1, ALP is one of the most commonly used labels in bioanalytical methods based on bioaffinity (immunoassays [2–12,54] and genosensors [13–16]). Such molecular recognition is especially attractive due to high specificity and very wide spectrum of available analytes important in clinical and environmental analysis. The main problem is to follow the proceeding of such processes. ALP activity detection schemes shown in this review could be useful for these biomolecular recognition assays. The use of proposed substrate and detectors could significantly reduce costs and simplify such bioanalysis, whereas performing measurements in FIA format would additionally automate such multistep procedures. The prospect of future investigation on applications of MFP/ALP system coupled with FIA seems to be the most promising.

References

[1] M.L. Bishop, E.P. Fody, L. Schoeff, Clinical Chemistry. Principles, Procedures, Correlations, Williams & Wilkins, New York, 2005.
[2] O. Niwa, Y. Xu, H.B. Halsall, W.R. Heineman, Anal. Chem. 65 (1993) 1559.
[3] M. Del Carlo, I. Lionti, M. Taccini, A. Cagnini, M. Mascini, Anal. Chim. Acta 342 (1997) 189.
[4] M. Masson, O.V. Runarsson, F. Johannson, M. Aizawa, Talanta 64 (2004) 174.
[5] A.L. La Salle, B. Limoges, C. Degrand, P. Brossier, Anal. Chem. 67 (1995) 1245.
[6] B. Limoges, C. Degrand, Anal. Chem. 68 (1996) 4141.
[7] R.E. Gyurcsanyi, A. Bereczki, G. Nagy, M.R. Neuman, E. Lindner, Analyst 127 (2002) 235.
[8] W.O. Ho, D. Athey, C.J. McNeil, Biosens. Bioelectron. 10 (1995) 683.
[9] M.S. Wilson, R.D. Rauh, Biosens. Bioelectron. 20 (2004) 276.
[10] E. Ishikawa, Clin. Biochem. 20 (1987) 375.
[11] I. Bronstein, C.J. Voyta, G.H. Thorpe, L.J. Kricka, G. Armstrong, Clin. Chem. 35 (1989) 1441.
[12] R.K. Wehmeyer, H.B. Halsall, W.R. Heinemann, C.P. Volle, I.W. Chen, Anal. Chem. 58 (1986) 135.
[13] D. Hernandez-Santos, M. Diaz-Gonzalez, M.B. Gonzalez-Garcia, A. Costa-Garcia, Anal. Chem. 76 (2004) 6887.
[14] G. Carpini, F. Lucarelli, G. Marrazza, M. Mascini, Biosens. Bioelectron. 20 (2004) 167.
[15] F. Farabullini, F. Lucarelli, I. Palchetti, G. Marrazza, M. Mascini, Biosens. Bioelectron. 22 (2007) 1544.
[16] R. Miranda-Castro, P. De Los Santos-Alvarez, M.J. Lobo-Castanon, A.J. Miranda-Ordieres, P. Tunon-Blanco, Anal. Chem. 79 (2007) 4050.
[17] A. Townsend, A. Vaughan, Talanta 17 (1970) 289.
[18] A.M. Zhavoronkova, S.V. Muginova, T.N. Shekhovtsova, J. Anal. Chem. 58 (2003) 594.
[19] S.V. Muginova, A.M. Zhavoronkova, T.N. Shekhovtsova, J. Anal. Chem. 60 (2005) 218.
[20] T.N. Shekhovtsova, S.V. Muginova, Anal. Bioanal. Chem. 381 (2005) 1328.
[21] I. Satoh, Biosens. Bioelectron. 6 (1991) 375.
[22] I. Satoh, Sens. Actuators B 13 (1993) 162.
[23] I. Satoh, Y. Iijima, Sens. Actuators B 23–24 (1995) 103.
[24] Y. Su, A. Cagnini, M. Mascini, Chem. Anal. 40 (1995) 579.
[25] F. Mazzei, F. Botre, S. Montilla, R. Pilloton, E. Podesta, C. Botre, J. Electroanal. Chem. 574 (2004) 95.
[26] F. Garcıa-Sanchez, A. Navas-Dıaz, M.C. Ramos-Peinado, C. Belledone, Anal. Chim. Acta 484 (2003) 45.
[27] I.A. Veselova, T.N. Shekhovtsova, Anal. Chim. Acta 413 (2000) 95.
[28] S.D. Kamtekar, R. Pande, M.S. Ayyagari, K.A. Marx, D.L. Kaplan, J. Kumar, S.K. Tripathy, Mater. Sci. Eng. C 3 (1995) 79.
[29] S.D. Kamtekar, R. Pande, M.S. Ayyagari, K.A. Marx, D.L. Kaplan, J. Kumar, S.K. Tripathy, Anal. Chem. 68 (1996) 216.
[30] N.W. Tietz, A.D. Rinker, L.M. Shaw, J. Clin. Chem. Clin. Biochem. 21 (1983) 731.
[31] N.W. Tietz, D.F. Shuey, Clin. Chem. 32 (1986) 470.
[32] J.H. Wilkinson, A.V. Vodden, Clin. Chem. 12 (1966) 701.
[33] F. Watanabe, M. Takano, F. Tanaka, N. Amino, C. Hayashi, K. Miyai, Clin. Chim. Acta 91 (1979) 273.
[34] R.A. Evangelista, A. Pollak, E.F. Templeton, Anal. Biochem. 197 (1991) 213.
[35] X. Zhu, Ch. Jiang, Clin. Chim. Acta 377 (2007) 150.
[36] S. Ito, S. Yamazaki, K. Kano, T. Kieda, Anal. Chim. Acta 424 (2000) 57.
[37] M.P. Kreuzer, C.K. O'Sullivan, G.G. Guilbault, Anal. Chim. Acta 393 (1999) 95.
[38] T. Katsu, K. Yamanaka, S. Hiramaki, T. Tanaka, T. Nagamatsu, Electroanalysis 8 (1996) 1101.
[39] J.R. Harley, N.M. Tarbaux, K.H.W. Lau, D.J. Baylink, Calif. Tissue Int. 40 (1987) 35.
[40] J. Klimek, M. Jung, S. Jung, Arch. Oral. Biol. 42 (1997) 181.
[41] P.D. Tzanavaras, D.G. Themelis, Analyst 126 (2001) 1608.
[42] P.D. Tzanavaras, D.G. Themelis, Anal. Chim. Acta 467 (2002) 83.
[43] N. Yoza, S. Nakashima, T. Nakazato, Chem. Lett. 26 (1997) 53.
[44] R. Koncki, K. Rudnicka, L. Tymecki, Anal. Chim. Acta 577 (2006) 134.
[45] D. Ogonczyk, R. Koncki, Anal. Chim. Acta 600 (2007) 194.
[46] R. Koncki, B. Rozum, S. Glab, Talanta 68 (2006) 1020.
[47] B. Rozum, R. Koncki, L. Tymecki, Sens. Actuators B 127 (2007) 632.
[48] W.P. Venetz, C. Mangan, I.W. Sidiqqi, Anal. Biochem. 191 (1990) 127.
[49] R. Koncki, D. Ogonczyk, S. Glab, Anal. Chim. Acta 538 (2005) 257.
[50] L. Tymecki, E. Zwierkowska, R. Koncki, Anal. Chim. Acta 538 (2005) 251.
[51] D. Ogonczyk, L. Tymecki, I. Wyzkiewicz, R. Koncki, S. Glab, Sens. Actuators B 106 (2005) 450.
[52] S.K. Hartwell, D. Somprayoon, P. Kongtawelert, S. Ongchai, O. Arppornchayanon, L. Ganranoo, S. Lapanantnoppakhun, K. Grudpan, Anal. Chim. Acta 600 (2007) 188.
[53] L. Gorski, D. Klimaszewska, M. Pietrzak, E. Malinowska, Anal. Bioanal. Chem. 389 (2007) 533.
[54] M. Diaz-Gonzalez, M.B. Gonzalez-Garcia, A. Costa-Garcia, Electroanalysis 21 (2005) 1901.

Talanta 77 (2008) 468–472

Contents lists available at ScienceDirect

Talanta

journal homepage: www.elsevier.com/locate/talanta

Flow-injection assay of the pathogenic bacteria using lectin-based quartz crystal microbalance biosensor

Gulnara Safina[a,b], Margret van Lier[a], Bengt Danielsson[a,*]

[a] Pure and Applied Biochemistry, Chemical Center, Lund University, Getingevagen, 60, Box 124, 221 00 Lund, Sweden
[b] FGU "Federal Center of Toxicology, Radiology and Safety", Nauchnyi gorodok, 2, 420075 Kazan, Russia

ARTICLE INFO

Article history:
Available online 30 March 2008

Keywords:
Quartz crystal microbalance
Flow-injection analysis
Immobilized lectins
Pathogenic bacteria
Campylobacter jejuni
Helicobacter pylori

ABSTRACT

A novel flow-injection assay of the pathogenic enterobacteria using novel lectin-based quartz crystal microbalance (QCM) biosensor has been proposed. The biosensing part of the analytical device contained the lectins – Concanavalin A, lectins from *Ulex europeus*, *Maackia amurensis*, *Lens culinaris*, wheat germ agglutinin – immobilized on the gold surface of quartz crystal electrode which served as a transducer. The immobilization of lectins was carried out using amine coupling on the surface of the crystal modified with 11-mercaproundecanoic acid. The biosensor makes it possible to identify the presence of different bacterial using the lectins immobilized on the surface of QCM crystal which bind specifically to the certain oligosaccharides present on the cell wall of the bacteria injected. The working conditions of the biosensor – pH of buffer solutions, concentration of the immobilized lectins, dilution of the bacterial cells, regeneration solution and flow rate – were optimized. The use of solution of glycine (pH 2.5) makes it possible to remove the formed complex from the crystal surface to make it reusable and ready for the next experiment. The proposed biosensor is able to detect 10^3 cells. The flow-injection assay of the bacterial cells takes about 30 min.

1. Introduction

The rapid and precise recognition of pathogenic enterobacteria, such as *Campylobacter jejuni*, *Helicobacter pylori*, as the most commonly reported bacterial cause of foodborne infection agents and gastrointestinal infections [1,2] has stimulated the great interests in clinical medicine and food quality control. *C. jejuni* produces an inflammatory, sometimes bloody, diarrhea, periodontitis [3] or dysentery syndrome, mostly including cramps, fever and pain. Infection with *H. pylori* is associated with a number of pathologies, including chronic gastritis, peptic ulcer disease, duodenitis, gastric adenocarcinoma [4]. However, in many cases it is difficult to discover any symptoms of disease [1]. That is why the development of the modern rapid sensitive techniques for the identification of these microorganisms is actual. There are great varieties of serotypes of these bacteria, so another important requirement for the novel methods for their indicating is high selectivity that makes it possible to distinguish different bacterial strains.

Lectins are plant or animal proteins or glycoproteins of nonimmune origin with binding specificity for carbohydrates [5–8]. Interaction between lectins and surface structure of bacteria results in specific cell agglutination [9] can be used for species identification [10]. Wong et al. described the specific interaction of *C. jejuni* using lectins as markers for strain differentiation [11,12]. Series of investigations are devoted to the *H. pylori* isolates identification using lectin typing system in a microtiter plate assay [13–15]. Described approaches are qualitative and based on the visual effect of the agglutination taking place due to the interaction between microorganisms and lectins. However, even several hundreds cells of these bacteria can be dangerous, so the development of modern sensitive techniques which can be easily automated is greatly important. One of those techniques which becomes more popular in biological measurements is quartz crystal microbalance (QCM) based on the changes in the resonant frequency of a quartz crystal which are related to the mass accumulated on it [16]. The main advantages of the application of QCM in assay odd biosamples are its ability to measure changes of very small masses and to monitor mass deposition in real time without using any labeling (enzyme, radioactive, etc.). The possibility to perform the QCM assay in flow-injection mode makes the method more attractive for rapid identification of the biological analytes. Combining bacteria and lectin recognition events with an appropriate QCM transducer can yield sensor devices highly suitable for the rapid, direct on-line screening and detection of the microorganisms in food, water and clinical and biodefense areas. Shen et al. presented the highly sensitive QCM biosensor exploited the lectin-bacterial O-antigen recognition for detection of *Escherichia coli* [17]. The working principle of biosen-

* Corresponding author. Tel.: +46 46 22 28257; fax: +46 46 22 24611.
E-mail address: Bengt.Danielsson@tbiokem.lu.se (B. Danielsson).

0039-9140/$ – see front matter.
doi:10.1016/j.talanta.2008.03.033

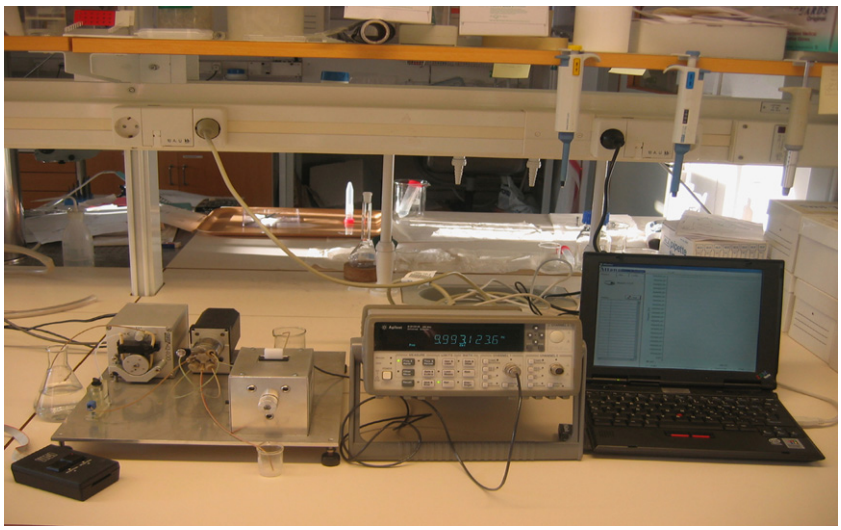

Fig. 1. Flow-through QCM system integrated with PC.

sor is based on the resonant frequency changing due to the binding of the bacterial lipopolysaccharides to the lectin attached to the surface of quartz crystal modifies with mannose SAM.

However, literature searching showed that there is no lectin-based QCM biosensor for the identification of the *C. jejuni* and *H. pylori*. In this work at first time we present fast, sensitive and selective flow-injection assay of these enterobacteria using novel quartz crystal microbalance lectin-based biosensor.

2. Experimental

2.1. Reagents

11-Mercaptoundecanoic acid, *N*-hydroxisuccinimide (NHS), 1-ethyl-3-[3-dimethylaminopropyl]carbodiimide hydrochloride (EDC), analytical grade were purchased from Sigma (Sweden). 1 M Ethanolamine–HCl (pH 8.5), 10 mM glycine (pH 2.5) was supplied from BIAcore (Sweden). 10 mM phosphate buffered saline (PBS) pH 7.4 was prepared from the chemicals of analytical grade (Merck, Germany).

2.2. Lectins

The following freeze-dried native lectins: Concanavalin A (ConA), *Ulex europeus* (UEA), *Maackia amurensis* (MAL), *Lens culinaris* (LCA), *Triticum vulgaris* (WGA) were purchased from Sigma (Sweden) and Vector Laboratories (Burlingame, CA). Lectins were dissolved in 10 mM PBS, containing 1 mM Ca^{2+}, 1 mM Mn^{2+}, at concentrations 0.1 mg/ml.

2.3. Bacterial strains

Strains of *C. jejuni*, *H. pylori* and *E. coli* were kindly provided by Prof. Anthony P. Moran (Department of Microbiology, National University of Ireland) and Prof. Torkel Wadström (Department of Infectious Diseases and Medical Microbiology, Lund University, Sweden).

Harvested bacterial biomass was prepared as described by Hynes et al. [15]. Briefly, bacteria were harvested in 10 ml of 0.1 M phosphate-buffered saline (PBS), pH 7.2, and washed once in PBS. Stored samples were washed once in PBS, resuspended in 5 ml of PBS (pH 4), and incubated for 30 min at room temperature to induce gentle lysis of the cells. The suspensions were heated at 100 °C for 5 min then centrifuged (5000 × *g*, 15 min). The resultant pellet of cell debris was resuspended in PBS to an optical density of 0.9 at A_{550} or McFarland standard 4 before lectin typing. Also, representative strains were tested in lectin agglutination assays as untreated whole-cell samples suspended in PBS (A_{550} = 0.9).

2.4. Quartz crystal microbalance (QCM)

To carry out the measurements, Attana 100 flow-injection device (Attana, Sweden) was used. The Attana 100 system contains of the main following parts: peristaltic pump, injection valve, sensor unit, sensor chip (Fig. 1). The changes in frequency of the QCM were monitored using an impedance analyzer (Aglient 53131A, Universal Counter) controlled by PC.

A nonpolished gold quartz crystal (with oscillation frequency 10 MHz) (International Crystal Manufacturing Co. Inc.) was used.

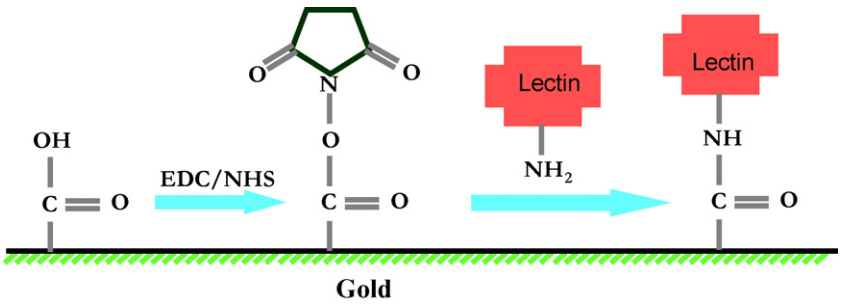

Fig. 2. Amine coupling procedure for immobilization of lectins onto the thiolizad golden surface.

2.5. Biosensor preparation

In order to make a biosensing part of the sensor immobilization of the lectin onto the working surface of quartz crystal coated with gold has been carried out. The immobilization was performed using amine coupling procedure.

Briefly, the biosensor preparation includes several steps:

(1) Cleaning of the working surface of the crystal;
(2) Thiolization of the gold surface with 11-mercaptoundecaoic acid carried out off-line;
(3) Modification of the surface with EDC/NHS;
(4) Immobilization of lectins;
(5) Blocking of the excess of reactive groups with ethanolamine–HCl.

Schematically the principle of amine coupling procedure is shown in Fig. 2.

Firstly, the crystal was treated in the boiling mixture of 35% of ammonia, 33% of hydrogen peroxide and deionized (Milli-Q) water (Millipore, 18.2 MΩ cm) in ratio 1:1:5 for 10 min to obtain the clean working surface.

Then the crystal was rinsed 3 times with double distilled water and ethanol and immediately immersed to the alcohol solution of 11-mercaptoundecanoic acid (1 mM). The crystal was kept in dark place at room temperature for at least 24 h to obtain the thiol SAM on the gold surface. Afterwards the crystal was sonicated in ethanol to remove unattached thiols, rinsed 3 times with ethanol and water, dried on the stream of nitrogen and mounted in the QCM device.

As it is shown in Fig. 3 the oscillation frequency of the quartz crystal after thiolization is decreased comparing with the frequency of the same crystal non-modified with 11-mercatoundecanoic acid which can be a confirmation of the thiolization process taken place.

All the following steps of biosensor preparation were performed on-line mode. The mixture aqueous solutions of 0.4 M EDC and 0.1 M NHS in ratio 1:1 was injected to activate the obtained carboxylic groups onto the surface of crystal. The flow rate 15 μl/min was applied. After that the lectin dissolved in 0.01 M PBS (pH 7.4, 1 mM Ca^{2+}, Mn^{2+}), which was also a running buffer, was injected at flow rate 15 μl/min. The presence of metal ions is essential for the binding activity of lectins [18]. The sensogram presenting the immobilization of lectin on the crystal surface is shown in Fig. 4.

As it can be observed from the sensogram, the injection of lectin leads to the decreasing of the frequency of the crystal that means the binding of protein to the surface modified with EDC/NHS. The lectin solution was injected until the frequency stopped to change. After that the excess of reactive sites on the surface of crystal was blocked by injection of 1 M ethanolamine–HCl (pH 8.5).

The prepared biosensors were stored in buffer solution at 4 °C.

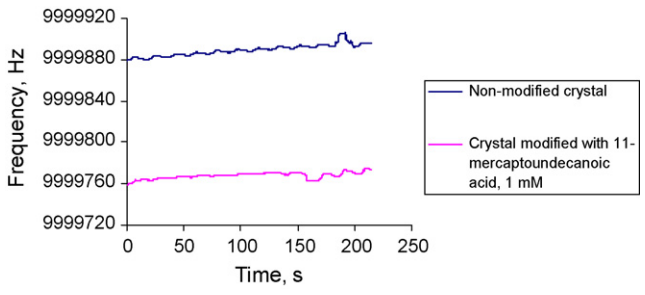

Fig. 3. Frequency of oscillation of the quartz crystal coated with gold before and after thiolization.

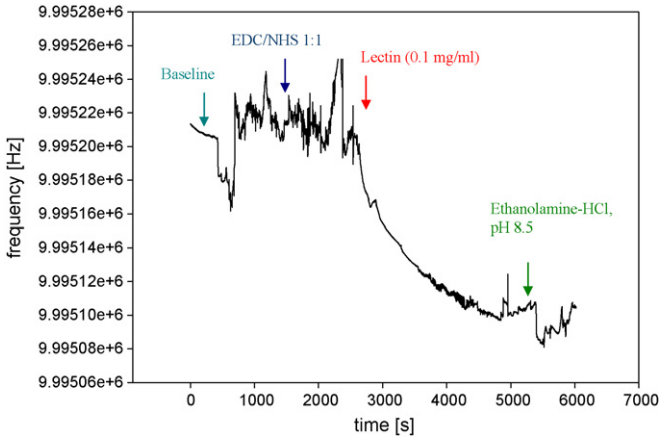

Fig. 4. Immobilization of the lectin on the surface of QCM crystal using amine coupling procedure.

3. Results and discussion

In this work the biointeractions between the immobilized lectins and the cells of various bacteria have been investigated. Lectins have been used to identify and distinguish microorganisms based on different sugar components on their cell wall. The following microorganisms–7 species of *C. jejuni*, 3 species of *H. pylori*, type of *E. coli*, and lectins–*Concanavalin A* (ConA), *Lens culinaris* (LCA), *Maackia amurensis* (MAL), *Triticum vulgaris* (wheat germ agglutinin, WGA), *Ulex europeus* (UEA)–were exploited. The lectins were selected by their specific glycan binding properties, i.e., ConA and LCA are specific to α-mannose and α-glucose, MAL and WGA-β-*N*-acetylglucosamine and sialic acid, UEA is able to bind fucose specifically.

In order to perform the experiment 50 μl of the sample suspension in dilution 1:50 (which is corresponded to 2×10^4 bacterial cells) was injected and the decreasing of the oscillation frequency of the crystal was observed. It takes place due to the increasing of the mass of the crystal because of the formation of the [lectin–sugar] complex on the surface of lectin-based biosensor.

The investigations of dependence of the analytical signal of the biosensor from the flow rate showed that the optimal flow rate is 40 μl/min (Fig. 5). If the higher flow rate is applied the time for formation of complex [lectin–oligosaccharide] is not enough, lower flow prevents the rapidity if the assay.

The biosensor makes it possible to identify the bacteria presence using the lectins immobilized on the surface of QCM crystal, which bind specifically to the certain lipopolysaccharides presenting on

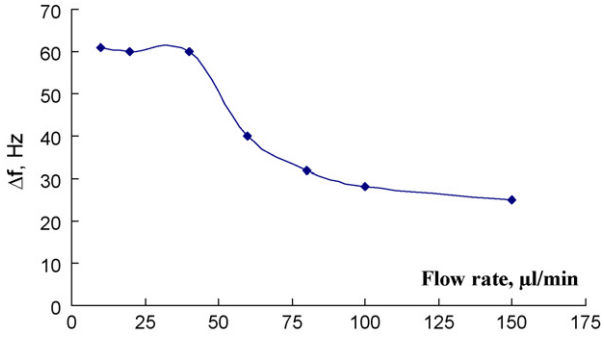

Fig. 5. Dependence of the response of the biosensor from flow rate (ligand–ConA, analyte–HS:3).

Table 1
Lectin glycan binding specificity

Lectin	Name	Source	MW	Affinity
Con A	Concanavalin A	*Canavalia ensiformis*	102,000	Branched α-mannosidic structures; high-mannose type, hybrid type and biantennary complex type *N*-Glycans (mannose binding lectin)
LCA	Lentil lectin	*Lens culinaris*	48,000	Fucosylated core region of bi- and triantennary complex type *N*-Glycans (mannose binding lectin)
WGA	Wheat germ agglutinin	*Triticum vulgaris*	34,000	GlcNAcβ1-4GlcNAcβ1-4GlcNAc, Neu5Ac (sialic acid)
MAL	Maackia amurensis lectin	*Maackia amurensis*	140,000	Neu5Ac/Gcα2-3Galβ1-4GlcNAcβ1-R (sialic acid binding lectin)
UEA	Ulex europaeus agglutinin	*Ulex europaeus*	170,000	Fucα1-2Gal-R (fucose binding lectin)

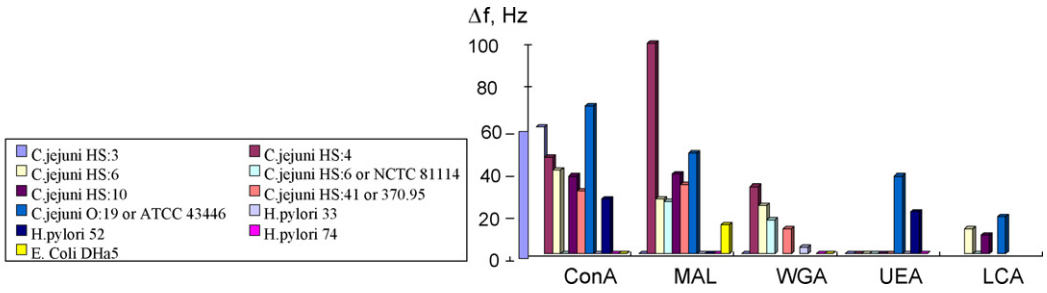

Fig. 6. The affinity interaction between the lectins immobilized on the surface of QCM chip as ligands and different bacteria as analytes.

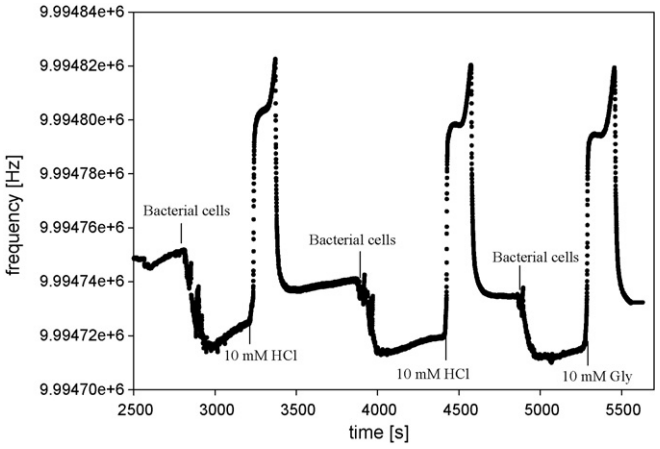

Fig. 7. Response of flow-injection lectin-based QCM biosensor. Injection of bacterial cells with following regeneration of the working surface of chip with 10 mM HCl, 10 mM Gly pH 2.5 (measurements are triplicated). (Flow rate is 40 μl/min; dilution of the bacterial sample–1:50; injected volume–50 μl.)

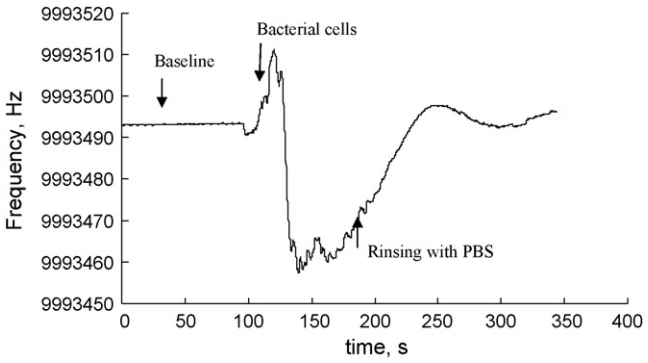

Fig. 8. Non-specific binding of bacterial cells (*C. jejuni*, O:19) with UEA (quick dissociation without using the regeneration solution).

the cell wall of the bacteria injected. Some properties of lectins used presented in Table 1.

Lectin typing system makes possible to identify/distinguish not only the different kinds of microorganisms but even shows the great diversity between the isolates. Different microbial cells of all strains of *C. jejuni* and *H. pylori* investigated showed different binding to

Table 2
The analytical responses of interaction between lectins and bacteria obtained using quartz crystal microbalance technique (10 mM PBS pH 7.4, 1 mM Ca^{2+}, 1 mM Mn^{2+})

Immobilized lectin	Microorganism									
	C. jejuni (1:50)							*H. pylori* (1:50)		
	HS:3	HS:4	HS:6	HS:6 or NCTC 81114	HS:10	HS:41 or 370.95	O:19 or ATCC 43446	33	52	74
Frequency shift (Δ*f*), Hz										
Con A	60	46	40	*	37	30	70	0	26	0
LCA	–	–	12	0	9	–	17.5	–	–	–
MAL	*	100	26	25	38	33	48	0	0	0
WGA	0	32	23	16	–	12	–	3	–	*
UEA	0	*	*	*	*	*	37	*	20	0

'–' Sample has not been tested.
* Non-specific binding.

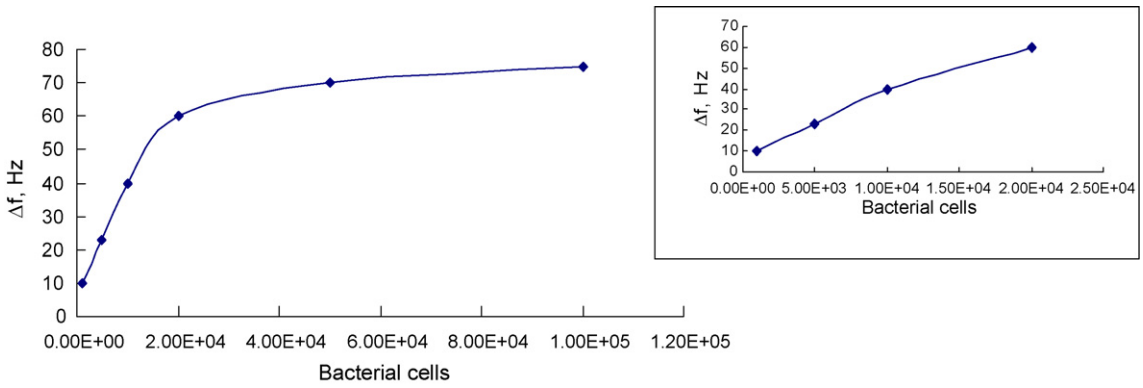

Fig. 9. Calibration curve for the detection of *C. jejuni* HS:3 using the ConA-based QCM biosensor. (The linear range is shown on the graph on the right side.)

the tested lectins (Fig. 6). Among the 5 lectins ConA demonstrated the broad range of specificity to the bacterial cells analyzed. Strong binding (affinity) on Concanavalin A to almost all the strains of *C. jejuni* can be observed from the big changes of the resonant frequency of biosensor. Lectin from *Ulex europeus* (UEA), vice versa, showed very limited specificity. As our investigations established it is enable to bind only 1 strain of *H. pylori* and *C. jejuni* (Table 2). The following injection of regeneration solution makes it possible to remove the formed complex from the crystal surface to make it reusable and ready for the next experiment (Fig. 7). The regeneration solution should satisfy to main requirements: it should be strong enough to remove all the attached analyte and it should not damage the immobilized ligand. The choice of the regeneration solution is based on the affinity between lectins and sugars on the bacterial surface and strength of the biocomplex. We tested different regeneration solutions:

(1) 10 mM glycine (Gly), pH 2.5
(2) 10 mM HCl
(3) 150 mM NaCl

The experiments have shown that Gly (pH 2.5) was the optimal regeneration solution to remove the bacterial cells from the QCM chip surface completely without destroying the lectins.

Sometimes the injection of the bacterial cells tested entailed the fast decreasing of the oscillation of the crystal with following spontaneous increasing without using any regeneration solution. That probably means the non-specific weak binding the cells with the immobilized lectins with further quick dissociation of the complex (Fig. 8).

The proposed lectin-based quartz crystal microbalance sensor makes it possible to carry out not only the qualitative detection/identification of the pathogenic bacteria in the sample analyzed but to perform the quantitative assay. Fig. 9 shows that ConA-based QCM biosensor is enable to determine the *C. jejuni* strain HS:3 in the range 10^3–10^5 cells. The linear interval is 10^3–2×10^4 bacterial cells. The duration of the assay is 30 min including the regeneration step.

4. Conclusion

A flow-injection assay for the detection and identification of the pathogenic bacteria strains using lectin-based QCM biosensor has been proposed. The affinity between the immobilized lectins and bacterial cells injected has been studied. Importantly, the present lectin typing system makes it possible to identify even the different isolates. The developed lectin-based biosensor is able to carry out not only exposure of the pathogens but also perform the rapid and sensitive quantitative assay. Simple procedure of the regeneration of the biosensor surface with 10 mM glycine (pH 2.5) makes it possible to use the same sensor several times without losing the lectins activity.

The proposed lectin-based QCM biosensor is able to carry out the direct sensitive and rapid label-free assay identification of the pathogenic bacteria *H. pylori*, *C. jejuni*, that can be proposed as a promising alternative to the traditional bacteriological analysis for clinical diagnostics of the infectious diseases and food quality control.

Acknowledgements

Authors are very grateful to Prof. Anthony P. Moran (Department of Microbiology, National University of Ireland) and Prof. Torkel Wadström (Department of Infectious Diseases and Medical Microbiology, Lund University, Sweden) for the bacterial strains kindly provided.

Gulnara Safina is a recipient of scholarship from Swedish Institute, "Guest Scholarships Programme".

References

[1] Samuel Baron (Ed.), Medical Microbiology, 1996.
[2] K.J. Ryan, C.G. Ray (Eds.), Sherris Medical Microbiology, 2004, pp. 378–380.
[3] T. Humphrey, et al., Int. J. Food Microbiol. 117 (2007) 3.
[4] R.H. Hunt, Scand. J. Gastroenterol. 31 (1996) 3–9.
[5] H.-J. Gabius, Int. J. Biochem. 26 (1994) 469–477.
[6] K. Drickamer, M.E. Taylar, Annu. Rev. Cell Biol. 9 (1993) 237–264.
[7] N. Sharon, H. Lis, Science 246 (1989) 227–234.
[8] H.J. Gabius, W.R. Springer, S.H. Barondes, Cell 42 (1985) 449–456.
[9] T.G. Pistole, Annu. Rev. Microbiol. 35 (1981) 85–112.
[10] R.L. Schaefer, K.F. Keller, R.J. Doyle, J. Clin. Microbiol. 10 (1979) 669–672.
[11] K.H. Wong, S.K. Skelton, J. Feeley, Clin. Microbiol. 22 (1985) 134–135.
[12] K.H. Wong, S.K. Skelton, J. Feeley, Clin. Microbiol. 23 (1986) 407–410.
[13] S.O. Hynes, S. Hirmo, T. Wadström, A.P. Moran, J. Clin. Microbiol. 1999 (1994).
[14] M.M. Khin, J.S. Hua, H.C. Ng, T. Wadström, B. Ho, World J. Gastroenterol. 6 (2000) 202.
[15] S. Hynes, et al., J. Clin. Microbiol. 40 (2002) 227.
[16] G. Sauerbrey, Z. Phys. 155 (1959) 206.
[17] Zh. Shen, et al., Anal. Chem. 79 (2007) 2312.
[18] B. Agrawal, I. Goldstein, Biochim. Biophys. Acta 147 (1967) 262.

Talanta 77 (2008) 490–493

Contents lists available at ScienceDirect

Talanta

journal homepage: www.elsevier.com/locate/talanta

Hydroxyapatite as a novel reversible *in situ* adsorption matrix for enzyme thermistor-based FIA

Salah Salman[a], Srimathi Soundararajan[a,*], Gulnara Safina[a,b], Ikuo Satoh[c], Bengt Danielsson[a,*]

[a] *Pure and Applied Biochemistry, Chemical Centre, Lund University, PO Box 124, Lund S-22100, Sweden*
[b] *FGU Federal Center of Toxicology, Radiology and Safety, 420075 Nauchnyi, Gorodok-2, Kazan, Russia*
[c] *Kanagawa Institute of Technology, 1030 Shimo-Ogino, Atsugi, Kanagawa 243-0292, Japan*

ARTICLE INFO

Article history:
Received 15 November 2007
Received in revised form 19 March 2008
Accepted 4 April 2008
Available online 12 April 2008

Keywords:
Hydroxapatite
Enzyme thermistor
Flow-injection analysis
Glucose biosensor
Immobilization

ABSTRACT

The application of the easily available and inexpensive chromatographic matrix hydroxyapatite for reusable and reversible immobilization of enzymes for enzyme thermistor-based flow injection analysis of glucose and urea was tested. The immobilization was achieved by simple affinity adsorption of glucose oxidase and urease by a suitable pH-induced alteration of the protein charge. A linear detection range of 0.05–8.0 mM was observed for glucose estimation depending on the sensitivity and sample loop parameters with a detection limit of 0.05 mM. A broad detection range of 0.5–50 mM was observed for urea using the flow injection calorimetric biosensor. Some real samples like commercial soft drink, syrups, honey and serum samples were analyzed. The novelty of the described work is the rapid set up of glucose analysis using hydroxyapatite as a reusable immobilization support in a flow injection thermal biosensor without any need for covalent immobilization or chemical cross-linking. The property of hydroxyapatite to adsorb and desorb proteins as a function of the buffer pH and ionic strength makes *in situ* enzyme reloading or exchange possible. The standard curves were obtained within few hours with a high degree of reproducibility and the enzyme remained fully active even after 3 months.

1. Introduction

Hydroxyapatite (HA) has been used in adsorption chromatography for many years. There are customized methods to exploit its unique characteristics. The elution of proteins adsorbed on hydroxyapatite, a microcrystalline precipitate of calcium phosphate $Ca_5(PO_4)_3OH$ is usually achieved by ascending gradient of phosphate [1–4,7,9]. Hydroxyapatite chromatography has been used for the purification and separation of acidic, neutral and basic antibodies [5,7–9]. Protein samples are normally loaded in low ionic strength buffer at higher loading concentrations of protein [2,3]. Basic proteins bind to hydroxyapatite strongly at lower pH due to increased positive charge on the protein. The lower the binding pH the higher will be the ionic strength of the eluting buffer required to desorb the proteins. It has been reported that high concentrations of sodium chloride frequently encountered in ion exchange chromatography do not interfere with the protein absorption onto hydroxyapatite [2–4,6]. The application of hydroxyapatite for enzyme immobilization has already been reported for dextransucrase, glucosyl transferase, levansucrase and urease [10–13]. In this paper we combine hydroxyapatite with the established bioanalytical calorimetric technique [15–18] to present a unique enzyme biosensor with the advantage and novelty of flow injection analysis.

Bioanalytical calorimetry exploits the exothermic nature of biological reactions to follow biological processes by measuring the heat released. The changes in the enthalpy associated with enzymatic reactions is the basis of enzyme thermistor (ET) developed and successfully employed in a variety of practical applications such as clinical diagnosis, process control, environmental and fermentation monitoring [15–21,23]. A large number of enzymatic reactions have been studied by this device among which glucose detection was studied extensively using glucose oxidase mostly covalently immobilized on controlled pore glass and packed in columns [18–20,23]. This calorimetric sensor is a good alternative to most of the electrochemical glucose sensors. Commonly used electrochemical sensors have the disadvantages such as enzyme leakage, denaturation of the enzyme on the electrode surface which affects the life time of enzyme modified electrodes and mediator leakage besides the interference from electroactive impurities [24–26]. Drawbacks of the enzyme thermistor include relatively higher instrumental complexity, limited commercial availability to date and use of rather expensive enzyme immobilization procedures (which on the other hand result in outstanding operational

* Corresponding authors. Tel.: +46 46 22 28 257; fax: +46 46 22 28 266.
E-mail addresses: srimathi_matoria@yahoo.com (S. Soundararajan), bengt.danielsson@tbiokem.lth.se (B. Danielsson).

0039-9140/$ – see front matter © 2008 Elsevier B.V. All rights reserved.
doi:10.1016/j.talanta.2008.04.003

stability). Therefore, the construction of a good glucose sensor still needs improvement not only at the device level but also by improving or innovating enzyme capturing. Most of the enzyme immobilization for biosensor applications involves covalent coupling to solid supports and thus requiring replacement of the entire biological recognition setup when the signal deteriorates. In the present work we have exploited the flow injection assisted analysis in ET (ET-FIA) for the first time to carry out on-site immobilization and sample analysis. We have chosen the well-known chromatographic material ceramic hydroxyapatite as a reusable, *in situ* adsorption support for enzyme immobilization and subsequent analyte determination using the enzyme thermistor.

In this paper, we explore the use ceramic hydroxyapatite (CHT) also known as macro-prep ceramic hydroxyapatite as a renewable matrix for repeated immobilization of enzymes for calorimetric estimation of glucose and urea. Enzymes of clinical importance such as glucose oxidase/catalase couple (GOD/CAT) and urease were the candidate enzymes for the application. We emphasize the suitability of this method for glucose estimation and a brief account of how this method could be adopted for urease is also given. The immobilization methodology, sensitivity, detection range, stability and reproducibility are investigated.

2. Materials and methods

2.1. Materials

Glucose oxidase (1.1.3.4) 324–396 units/mg from *Aspergillus niger* from Biozyme, UK, catalase (E.C.1.11.1.6) 19,000 units/mg from Beef liver and jack bean urease (E.C.3.5.1.5) 63,000 μM units from Sigma were used as obtained from the manufacturer. Ceramic hydroxyapatite type I (80 μm in diameter, surface area 50 $m^2\ g^{-1}$) was obtained from Bio-Rad laboratories. Glucose and urea (Sigma) were used as standards. All other reagents were of analytical grade from Merck, Germany. All the solutions were prepared in ultra pure water (18.2 MΩ). Human blood sample was taken from a healthy volunteer. Honey, soft drink and sodium saccharine were purchased from a local store. HemoCue Glucose 201^+ analyzer was purchased from HemoCue AB, Sweden.

2.2. Enzyme thermistor

Briefly, the enzyme thermistor employs enzymes as specific biological recognition elements. The biocatalyst is brought in close proximity to a transducer, thermistor in this case, which can measure the biological reaction and convert it into a physical signal. The device combines the selectivity of the biosensor with flow injection analysis (FIA) for continuous monitoring of analytes. A detailed account of the design, construction of the enzyme thermistor and the principle behind the calorimetric determination can be found elsewhere [15,16,18,20].

2.3. Enzymatic reaction

The principle behind the calorimetric estimation of glucose is based on heat generated in the following enzymatic reactions [18,20,23]. Glucose oxidase catalyses the oxidation of glucose according to the reaction:

$$C_6H_{12}O_6 + H_2O + O_2 \rightarrow H_2O_2 + C_6H_{12}O_7(\text{gluconicacid}) + \Delta H_1$$

The hydrogen peroxide is eliminated by the following reaction catalysed by catalase:

$$2H_2O_2 \rightarrow 2H_2O + O_2 + \Delta H_2$$

where ΔH_1 and ΔH_2 are the enthalpy changes during the enzymatic reactions with glucose oxidase and catalase, respectively. Reduction of H_2O_2 by catalase provides additional heat that increases the sensitivity of the assay. Also this eliminates the presence of hydrogen peroxide which could otherwise affect the stability of the immobilized enzyme [16,18,20]. The other enzyme tested namely urease catalyses the hydrolysis of urea according to the following reaction [22]:

$$(NH_2)_2CO + 3H_2O \rightarrow HCO_3^- + 2NH_4^+ + OH^- + \Delta H$$

2.4. Immobilization procedure

Ceramic hydroxyapatite (CHT) was thoroughly washed with 5 mM phosphate buffer containing 0.3 mM $CaCl_2$ at pH 6.5. Glucose oxidase and catalase were non-covalently adsorbed/immobilized on ceramic hydroxyapatite by ion exchange according to the following procedure: 4 mg of GOD (1500 U) and 2 μl of catalase (13,000 U) were dissolved in 2 ml 5 mM phosphate buffer (pH 6.5) and 1 ml of this suspension was mixed with 130 mg of CHT. The suspension was gently mixed for 3 h at 4 °C. The protein concentration in the solution was measured before and after immobilization by Lowry method to determine the immobilization yield [14]. The enzyme thermistor column was packed with this suspension and thoroughly washed with the running buffer to remove the unbound enzyme and equilibrated in the same buffer. Immobilization of urease was carried out by shaking 130 mg of pre-washed CHT with the enzyme at a concentration of 1 mg/ml in 5 mM phosphate buffer at pH 7.4 supplemented with 0.3 mM $CaCl_2$. Both GOD/CAT and urease were also immobilized *in situ* by recirculating the enzyme solutions for 2 h with the help of the flow injection set up in ET.

2.5. Glucose and urea estimation

Glucose and urea standard solutions (0.005–60 mM) were prepared in 5 mM phosphate buffer at pH 6.5 and 7.4, respectively. All the measurements were carried out by injection of samples at a flow rate of 100 μl/min. Sample loop sizes of 50 μl and 500 μl were tested. The thermal response to the enzyme reaction was measured by integration of ET with a PC. The linear change in the thermal signal to varying substrate concentration was used to construct standard curves. Average thermal response for three consecutive injections was used in standard curve construction. For estimation of glucose in real samples, all the samples (commercial soft drink, honey and serum) were diluted in the working buffer and filtered before analyzing. The soft drink was diluted and degassed prior to analysis. For glucose estimation in blood, the plasma required was prepared from whole blood by centrifugation at 15,000 rpm for 10 min.

3. Results and discussion

3.1. Use of hydroxyapatite as a renewable immobilization matrix for FIA

In the present work hydroxyapatite as the cheap, quick and reusable support for the thermistor-based enzymatic determination of glucose is examined. Urease was also tested to demonstrate that the method could also be used for other enzyme systems just by changing the binding pH. Enzyme attachment to the hydroxyapatite support was facilitated by the chosen immobilization pH and the protein charge. Depending on pH, HA has both positive and negative overall surface charge and hence provides multi-adsorbing sites [1,5–7,27]. By knowing the pI of the enzymes of interest it was

possible to use an optimum pH without much trade off between the immobilization yield and enzyme activity. The isoelectric point of glucose oxidase is 4.2 and that of urease is 4.9. Acidic proteins bind to HA mainly by the carboxyl groups. The carboxyl groups are repelled electrostatically from the negatively charged sites and bind specifically to the Ca^{++} sites of HA [6]. Therefore, co-immobilization of glucose oxidase and catalase was achieved at pH 6.5. The immobilization yield was 80% for GOD/CAT couple and 70% for urease. Since the adsorption is due to electrostatic interaction it was possible to desorb the proteins bound on ceramic hydroxyapatite support by simply changing the pH or increasing the ionic strength of the eluting buffer. The enzyme columns placed in a flow injection enzyme thermistor helps in easy desorption of the bound protein. The major advantage is that when the enzyme column shows reduced activity, it is possible to reload a fresh batch of GOD/CAT couple. The use of flow injection analysis makes the present work versatile since enzyme reloading can be done essentially hands free. The immobilization can be carried out in the ET system by flow injection technique without the need to do a separate immobilization involving time consuming activation, incubation and cleaning procedures as with covalent immobilization. We confirmed this by carrying out the adsorption *in situ* by circulating the GOD/CAT mixture at a flow rate of 50 μl/min for 1 h. The thermal response obtained for 5 mM standard glucose for the flow injection assisted immobilization (peak height = 43.5 mm) was comparable to that obtained for manually immobilized GOD/CAT (peak height = 44 mm). The application of this method could be exploited to the maximum for the frequently used enzymatic determinations of clinical and diagnostic importance.

3.2. Protein adsorption and recovery

We have optimized the binding conditions for GOD/CAT-CHT interaction. The quantity of protein bound on the surface was calculated by subtracting the amount of protein recovered in the combined washings after adsorption from the protein concentration present before immobilization. At pH 6.5 where immobilization was carried out we found that 85% adsorption occurred and the protein recovery was also >90% as measured by Lowry assay. In the case of urease 70% of the protein loaded was adsorbed and >90% of the loaded protein was recovered. Protein recovery was achieved by washing the enzyme column with 200 mM phosphate buffer at the same pH. The recovery of the enzymes by desorption is attractive for expensive enzymes and easy optimization of binding conditions without any wastage of the enzyme.

3.3. Determination of glucose and urea

The linear range of detection for a sample volume of 50 μl and 500 μl were found to be 0.5–8.0 mM and 0.05–1.0 mM, respectively (Fig. 1). The corresponding limits of detection (LOD) were 0.5 mM and 0.05 mM, respectively. The increase in sample volume by 10-fold though improved the LOD, 0.05 mM as opposed to 0.5 mM, resulted in reduced linear detection range. However, when a sample volume of 50 μl was used the linear detection range was extended up to 8.0 mM. The increased sensitivity when using higher sample volumes was evidenced from a higher signal response for the same concentration of the analyte (Fig. 1). Thus, it is possible to improve the sensitivity of detection in dilute solutions just by increasing the sample volume to be injected. This is also useful when glucose needs to be estimated in dilute solutions. The standard curves were highly reproducible. Each data point in the standard curve is the average of triplicate measurements. The operational characteristics of the biosensor are presented in Table 1. Comparison of our previous studies where GOD/CAT was covalently immobilized on to controlled pore glass (linear range 0.5–16 mM, LOD = 0.5 mM) [19] showed that the upper limit of detection is lowered to 8.0 mM for CHT immobilization. Estimation of glucose in real samples such as the commercially available soft drink, honey, artificial saccharine and blood serum produced excellent reliability and reproducibility. These samples were diluted, spiked with a known concentration (2.5 mM) of standard glucose and compared with the calculated glucose concentration in the pure samples. The artificial saccharine contained no glucose as specified by the manufacturer. No thermal response was observed for pure saccharine as opposed to a significant and corresponding thermal response when spiked with various concentrations of standard glucose. The excellent agreement between the glucose estimated in pure samples and the spiked samples proves the reliability of the technique (Table 1). The specificity and interference characteristics of the enzyme system GOD/CAT has been shown in many of our previous reports [16–19,23]. The linear range of detection for urea estimation using hydroxyapatite immobilized urease was 1.0–50 mM (Fig. 2). The sample volume used was 50 μl. Urease was used as another

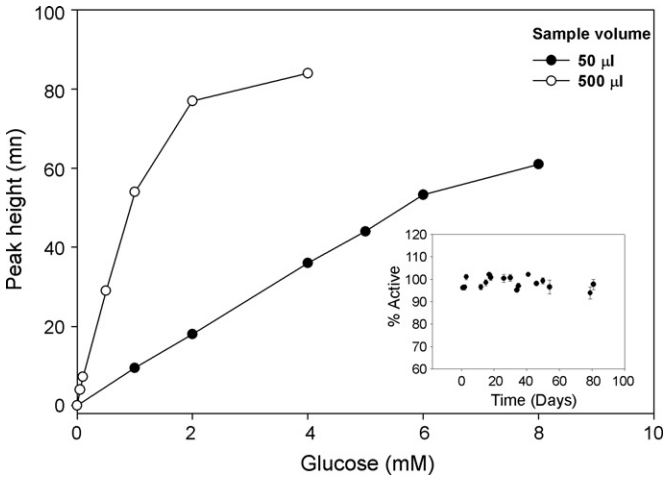

Fig. 1. Calibration curve for glucose. The sample volumes used were 50 μl and 500 μl. Inset. Stability of thermal response over time for 5 mM glucose.

Table 1
Biosensor characteristics of the CHT-ET-FIA for glucose estimation

Analyte	Sample volume (μl)	Linear range (mM)	LOD (mM)	Glucose in diluted real samples (mM, mean ± S.D.)			
				Softdrink (1:200)[a]	Honey (1:2500)[a]	Saccharine (0.5 mg/ml)[a]	Blood serum (1:100)[a]
Glucose	50	0.5–8.0	0.5	0.57 ± 0.02[b]	1.25 ± 0.03[b]	0[b]	5.44 ± 0.16[b]
	500	0.05–1.0	0.05	(3.11 ± 0.06)[c]	(3.76 ± 0.09)[c]	(2.50 ± 0.18)[c]	(5.7)[d]

[a] Dilution ratio used in the estimation. All dilutions were done in the running buffer.
[b] Glucose concentration in pure, diluted samples.
[c] Glucose concentration after spiking the diluted samples with 2.5 mM standard glucose.
[d] Value obtained using HemoCue Glucose 201+ analyzer, a commercial glucose estimation kit.

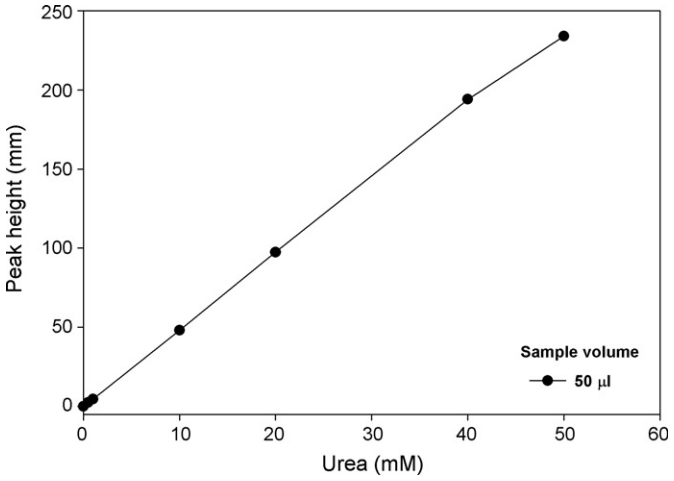

Fig. 2. Urea calibration curve. The data points are an average of triplicate measurements.

enzyme system to demonstrate the use of hydroxyapatite in the ET-FIA. Immobilization of jack bean urease on HA has already been reported to be efficient at pH 7.0–8.0 where the activity was measured by a titrimetric procedure [13]. Urease immobilization on soil constituents is of special interest because of the universal presence of plant and microbial urease in the soil and their role in the hydrolysis of urea used as a fertilizer [13]. The calorimetric FIA method proposed herein could be of use in determining the hydrolytic activity of soil urease for agricultural applications.

3.4. Storage and operational stability

The enzyme system GOD/CAT is a robust bienzyme combination and is known to be stable when immobilized [15,16]. However, the adsorption of these enzymes on hydroxyapatite is a new concept for flow injection analysis and hence we tested the column stability for a total period of 3 months. The detachable enzyme column was stored at 4 °C in between measurements. It was found that the thermal response for the injection of 5 mM standard glucose was unaltered for 80 days (Fig. 1 inset). Therefore, a good storage stability of 3 months is guaranteed. In our previous works where GOD/CAT was covalently immobilized to controlled pore glass (CPG) by glutaraldehyde cross-linking we have achieved better stability. The thermal response of CPG immobilized enzymes remained unaltered for 6 months [15,16]. However, the advantage with hydroxyapatite that it is easy to reload the enzyme and construct standard curves in 2–3 h overcomes this lowered stability. This enzyme sensor also gave reproducible activity response for multiple sample injections (>150 samples) at room temperature indicating a useful operational stability.

4. Conclusion

The novelty of the described work is the rapid glucose analysis in a flow injection mode without any need for covalent immobilization or chemical cross-linking. The immobilization can be carried out in the ET system by flow injection technique without the need to do a separate immobilization involving time consuming activation, incubation and cleaning procedures. The property of hydroxyapatite to adsorb and desorb proteins as a function of the buffer pH and ionic strength makes *in situ* enzyme reloading or exchange possible. The use of flow injection analysis makes the present work versatile since enzyme reloading can be done essentially hands free. The standard curves were obtained within 2–3 h and the system showed a high degree of reproducibility and stability for up to 3 months. Compared to covalent immobilization the proposed method may lead to higher loss of enzyme activity with time or higher risk for contamination from crude samples. The main anticipated application of the method is however, in cases such as studies of enzyme preparation or inhibition and clinical applications, where a quick and simple technique is desirable without the need for long-term use such as in. The use of hydroxyapatite in biosensors though works well with the two enzymes studied, is limited by the protein charge characteristics and pH dependence of activity and requires an enzyme to enzyme variation in methodology to avoid biocatalyst bleeding in a flow through system. But once established the method will be suitable for regular analysis just like the proven chromatographic procedures.

Acknowledgements

SS and GF acknowledge Swedish Institute for the Guest Research Scholarship. Financial assistance from SIDA and Vinnova is also acknowledged.

References

[1] T. Kawasaki, S. Takahashi, K. Ideda, Eur. J. Biochem. 152 (1985) 361.
[2] M.J. Gorbunoff, Anal. Biochem. 136 (1984) 425.
[3] M.J. Gorbunoff, Anal. Biochem. 136 (1984) 433.
[4] M.J. Gorbunoff, S. Timasheff, Anal. Biochem. 136 (1984) 440.
[5] D. Josic, K. Löster, R. Kuhl, F. Noll, J. Reusch, Biol. Chem. Hoppe Seyler 372 (1991) 149.
[6] M.J. Gorbunoff, in: M.P. Deutscher (Ed.), Methods in Enzymology, vol. 182, Academic Press Inc., San Diego, CA, USA, 1990, pp. 329–339.
[7] A. Tiselius, S. Hjertén, Ö. Levin, Arch. Biochem. Biophys. 65 (1956) 132.
[8] M.J. Mura-Galelli, J.C. Voegel, S. Behr, E.F. Bres, P. Schaaf, Proc. Natl. Acad. Sci. U.S.A. 88 (1991) 5557.
[9] J. Heimke, P. Griss, in: K. de Groot (Ed.), Bioceramics of Calcium Phosphate, vol. 4, CRC, Boca Raton, 1983, pp. 80–97.
[10] F.A. Erhardt, H.-J. Jördening, J. Biotechnol. 131 (2007) 440.
[11] M. Bronshteyn, D. Steinberg, Lett. Appl. Microbiol. 34 (2002) 205.
[12] K.H. Jang, K.B. Song, J.S. Kim, C.H. Kim, B.H. Chung, S.K. Rhee, Bioproc. Eng. 23 (2000) 89.
[13] C. Marzadori, S. Miletti, C. Gessa, S. Ciurli, Soil Biol. Biochem. 30 (1998) 1485.
[14] O.H. Lowry, N.J. Rosbrough, A.L. Farr, R.J. Randall, J. Biol. Chem. 193 (1951) 265.
[15] K. Ramanathan, B. Danielsson, Biosens. Bioelectron. 16 (2001) 417.
[16] K. Ramanathan, M. Rank, J. Svitel, A. Dzgoev, B. Danielsson, Trends Biotechnol. 17 (1999) 499.
[17] B. Xie, K. Ramanathan, B. Danielsson, Adv. Biochem. Eng. Biotechnol. 64 (1999) 1.
[18] K. Mosbach, B. Danielsson, Biochim. Biophys. Acta 364 (1974) 140.
[19] U. Harborn, B. Xie, R. Venkatesh, B. Danielsson, Clin. Chim. Acta 267 (1997) 225.
[20] B. Danielsson, K. Mosbach, Methods Enzymol. 137 (1988) 3–14.
[21] B. Danielsson, B. Mattiasson, R. Karlsson, F. Winquist, Biotechnol. Bioeng. 21 (1979) 1749.
[22] B. Xie, U. Harborn, M. Mecklenburg, B. Danielsson, Clin. Chem. 40 (1994) 2282.
[23] B. Danielsson, K. Mosbach, in: A. Turner, I. Karube, G. Wilson (Eds.), Biosensors: Fundamentals and Applications, Oxford University Press, 1986, pp. 575–595.
[24] J. Okuda, K. Sode, Biochem. Biophys. Res. Commun. 314 (2004) 793.
[25] J. Kulys, L. Tetianec, Sens. Actuators B B113 (2006) 755.
[26] A. Malinauskas, J. Kuzmarskyte, R. Meskys, A. Ramanavicius, Sens. Actuators B B100 (2004) 387.
[27] Y. Ding, J. Liu, H. Wang, G. Shen, R. Yu, Biomaterial 27 (2007) 2147.

Talanta 77 (2008) 870–875

Contents lists available at ScienceDirect

Talanta

journal homepage: www.elsevier.com/locate/talanta

An improved clean sonoreactor-based method for protein identification by mass spectrometry-based techniques

H.M. Santos[a], Cristiano Mota[a], C. Lodeiro[a], Isabel Moura[a], Issa Isaac[b], J.L. Capelo[a,*]

[a] REQUIMTE, Departamento de Química, Faculdade de Ciências e Tecnologia, Universidade Nova de Lisboa, Quinta da Torre, 2829-516 Monte de Caparica, Portugal
[b] Digilab Genomic Solutions Inc., 4355 Varsity Drive, Ann Arbor, MI 48108, USA

ARTICLE INFO

Article history:
Received 5 May 2008
Received in revised form 13 July 2008
Accepted 22 July 2008
Available online 3 August 2008

Keywords:
Desalting free
In-solution protein identification
Sonoreactor
MALDI-TOF-MS
Clean method

ABSTRACT

A new clean fast (8 min) method for in-solution protein digestion without detergent or urea for protein identification by peptide mass fingerprint and mass spectrometry-based techniques is proposed. The new method avoids the use of time consuming desalting procedures entailing the following four steps done under the effect of an ultrasonic field provided by a sonoreactor: denaturation (1 min) in a mixed solution of water:acetonitrile 1/1 (v/v); protein reduction (1 min); protein alkylation (1 min); and protein digestion (5 min). Five proteins with masses comprised between 14.4 kDa and 97 kDa and the protein split-soret cytochrome *c* from *D. desulfuricans* ATCC27774, were successfully identified with this procedure. No differences were found in the sequence coverage or in the number of peptides matched when the new clean method was compared to another one using urea. Twofold better signal-to-noise ratios were obtained in the MALDI spectra from protein samples prepared with the new method when comparing it with a method using urea. The new digestion method avoids the need to remove salt content and increases throughput (six samples at once) while reducing sample loss and contamination from sample handling.

1. Introduction

Protein identification is nowadays of primary importance in many fields of science [1,2]. The sample treatment for the in-solution identification of proteins can be considered consisting of four main steps: (i) protein denaturation; (ii) protein reduction; (iii) protein alkylation and (iv) protein digestion. Protein denaturation is done to make the proteins more accessible to the action of the enzymes. To do so, proteins are generally re-suspended in ammonium bicarbonate buffer supplemented with 8 M urea or another chaotropic agent (e.g., guanidine hydrochloride) to break intramolecular forces and thus denature proteins. To prevent protein renaturation before enzymatic attack, reduction of protein disulfide bridges and alkylation of cysteine residues, are commonly done using dithiothreitol, DTT, and iodoacetamide, IAA, respectively, although other reagents are also available for the same purposes [1]. Then, protein digestion is done by adding one enzyme to the solution, generally trypsin. The pool of peptides formed is then used to identify the protein.

A drawback of the peptide mass fingerprint, PMF, methodology lie in the chemical denaturants, such as urea or sodium dodecyl sulfate, SDS, employed to increase digestion efficiency. Thus, as a general trend, time consuming desalting/cleaning procedures are mandatory previous mass spectrometry analysis, since high contents of above mentioned reagents hinder ionization, either in electrospray or in matrix assisted laser desorption/ionization, MALDI, modes. To overcome the aforementioned drawback alternative methods have been developed to denature proteins prior to in-solution digestion, including the following: thermal denaturation [3], digestion in organic solvents [4], and the use of microwave irradiation [5].

Our research group has recently published different works highlighting the improvements obtained when the sample treatment for protein identification by PMF is accelerated using ultrasounds. The enhancement was equally obtained for sample treatments in which the proteins are separated by 1D or 2D gel-electrophoresis, named in-gel protein digestion [6,7], or for proteins in solution, named in-solution protein digestion [8,9]. However, the fast ultrasonic methods still use urea and other salts throughout the sample treatment, giving place to some drawbacks, such as mentioned above.

In the present work we report on an ultrafast in-solution protein identification procedure for PMF jointing, to the best of our knowledge for first time, ultrasonication and protein reduction, protein alkylation and protein digestion in mixed aqueous/organic solutions, avoiding the use of high salt, detergent or chaotropic agents in the sample treatment, thus simplyfing the sample han-

* Corresponding author. Tel.: +351 919 404 933; fax: +351 212 948 550.
E-mail address: jlcapelom@dq.fct.unl.pt (J.L. Capelo).

0039-9140/$ – see front matter © 2008 Elsevier B.V. All rights reserved.
doi:10.1016/j.talanta.2008.07.048

dling and lowering the amounts of protein detected by MALDI. The new method takes 8 min for the whole sample treatment including protein denaturation, protein reduction, protein alkylation and protein digestion steps. Six different proteins, including protein split-soret cytochrome *c* from *D. desulfuricans* ATCC27774, are successfully identified. In addition, for comparative purposes, parallel sample treatments with urea as denaturing agent and desalting protocols with ZipTip® were done.

2. Experimental

2.1. Apparatus

Concentrator centrifuge from UniEquip (Martinsried, Germany) model UNIVAPO 100H with a refrigerated aspirator vacuum pump model Unijet II was used for (i) sample drying and (ii) sample preconcentration. A minicentrifuge, model Spectrafugemini, from Labnet (Madrid, Spain), and a minicentrifuge-vortex, model Sky Line, from ELMI (Riga, Latvia) were used throughout the sample treatment, when necessary. A Simplicity 185 from Millipore (Milan, Italy) was used to obtain Milli-Q water throughout the experiments. A Sonoreactor, model UTR200, from Dr. Hielsher (Teltow, Switzerland) was used to accelerate chemical reactions.

2.2. Standards and reagents

The following protein standards were used: α-lactalbumin from bovine milk (>85%), BSA (>97%), and carbonic anhydrase (>93%) were from Sigma (Steinheim, Germany) and albumin from hen egg white (>95%) was from Fluka (Buchs, Switzerland). Chymotripsinogen A, catalase bovine, and aldolase from rabbit were standards for gel filtration calibration kit high molecular weight from Amersham Biosciences (Piscataway, NJ). Trypsin enzyme, sequencing grade, was purchased from Sigma. All materials were used without further purification. α-Cyano-4-hydroxycinnamic acid (α-CHCA) puriss for MALDI-MS from Fluka was used as MALDI matrix. ProteoMass Peptide MALDI-MS Calibration Kit (MSCAL2) from Sigma was used as mass calibration standard for MALDI-TOF-MS. The following reagents were used for protein digestion: acetonitrile, iodoacetamide (IAA), and DL-dithiothreitol (DTT) (99%) were from Sigma; formic acid and ammonium bicarbonate (Ambic) (>99.5%) were from Fluka; trifluoroacetic acid (TFA, 99%) was from Riedel-de-Haën (Seelze, Germany); and urea (99%) was from Pareac (Barcelona, Spain).

2.3. Sample treatments

2.3.1. Method with urea

This method was previously developed by our research group [8,9]. Protein concentrations of 1 μg/μL, prepared in 6.5 M urea for method development were used. Analyses were done by duplicate. To 20 μL of protein solution, 2 μL of a DTT solution (110 mM in Ambic 12.5 mM) was added, and then the solution was submitted to ultrasonication in the sonoreactor for 5 min. Then, 2 μL of an IAA solution (600 mM in Ambic 12.5 mM) was added. The solutions were further ultrasonicated at room temperature in the dark for 5 min. Solutions were diluted to 96 μL with Ambic 12.5 mM. Then, to 10 μL of this solution, 1 μL of the appropriate trypsin solution, in TFA 0.01%, was added to digest the protein. The protein/trypsin ratio was always 20:1 (w/w) as recommended by the manufacturer. So, 2 μg of protein were digested with 0.1 μg of trypsin. Protein digestion was accelerated with the aid of the sonoreactor during 5 min. Then, 1 μL of formic acid 50% (v/v) was added to stop the trypsin activity. Finally, desalting using the ZipTip® procedure was done, to avoid high saline concentration in the MALDI, as follows:

(a) *Activation*: aspirate and dispense, A&D, 10 μL of acetonitrile (1×), then A&D 10 μL of [50% acetonitrile + 0.1% TFA] (1×), and then A&D 10 μL of 0.1% TFA (2×).
(b) *Peptide binding*: 10 μL of sample (A&D the sample 20 cycles).
(c) *Washing*: A&D 10 μL of 0.1% TFA (3×).
(d) *Peptide elution*: 10 μL of [90% acetonitrile + 0.1% TFA] (A&D the sample 20 cycles).

2.3.2. Clean method

Bearing in mind that the sample treatment for protein identification by PMF, has the following four main steps: protein denaturation, protein reduction, protein alkylation and protein digestion, the different treatments commented below were tested, under the effects of an ultrasonic field, trying to reduce the number of steps or simplyfing the procedure by doing different steps at the same time. Solutions containing 1 μg/μL of BSA or α-lactalbumin were prepared in pure acetonitrile or in a mixture acetonitrile/water 1/1 (v/v). DTT solution (110 mM in Ambic 12.5 mM) for protein reduction and IAA solution (600 mM in Ambic 12.5 mM) for protein alkylation were used. Ambic 12.5 mM was used when necessary in the protein digestion step. No urea was used during these assays. Proteins were digested using tripsin solution in a proportion 20:1 (w/w) as recommended by the manufacturer. The following treatments were done:

(1) Protein dissolution was tried in pure acetonitrile with the aid of ultrasonication. Then, protein reduction (5 min), protein alkylation (5 min) and protein digestion (5 min) were done using the sonoreactor to speed up chemical reactions;

Proteins were dissolved in an acetonitrile:water 1:1 (v/v) and the following treatments were done:

(2) Reduction and alkylation steps were omitted. Proteins were digested during 5 min but Ambic buffer was not added. Sonoreactor was used for speed up the protein digestion process;
(3) Reduction and alkylation steps were omitted. Proteins were digested during 5 min using the sonoreactor to speed up the procedures;
(4) Protein reduction and alkylation was done in one single step with a sonication time of 5 min. Protein digestion was done in 5 min with sonication;
(5) Proteins were reduced (5 min), alkylated (5 min) and digested (5 min) using the sonoreactor to speed up the procedures.

It must be stressed that in all cases the amplitude of sonication was set in 50%. This amplitude was chosen based on our previous work with the sonoreactor device [8,9].

2.4. Protein sample from complex mixture

As a proof of the procedure, protein split-soret cytochrome *c* from *D. desulfuricans* ATCC27774 was digested according to the accelerated methods described above and identified by the PMF procedure by MALDI-TOF-MS. *D. desulfuricans* ATCC27774 cells were cultured in sulfate lactate medium. Cells were collected by centrifugation (8000 × *g* during 15 min at 4 °C), resuspended in 10 mM Tris–HCl buffer, and ruptured in a French press at 9000 psi. After centrifugation (10,000 × *g*, 45 min) and ultracentrifugation (180,000 × *g*, 60 min), the supernatant was dialyzed against 10 mM Tris–HCl buffer. The protein was isolated from the soluble extract using chromatographic columns (anionic exchange, hydroxyapatite column, and molecular exclusion chromatography). The purity

of the protein was evaluated by SDS-PAGE and UV–visible spectroscopy. All purification procedures were performed under aerobic conditions at 4 °C and pH 7.6.

2.5. Matrix formulation

Prior to MALDI-TOF-MS analysis, the sample was mixed with the matrix solution. α-CHCA matrix was used throughout this work and was prepared as follows: 10 mg of α-CHCA was dissolved in 1 mL of Milli-Q water/acetonitrile/TFA (1 mL + 1 mL + 2 μL). Then, 2 μL of the aforementioned matrix solution was mixed with 2 μL of sample and the mixture was shaken in a vortex for 30 s. Finally, 1 μL of the sample/matrix mixture was spotted on a well of a MALDI-TOF-MS sample plate and was allowed to dry.

2.6. MALDI-TOF-MS analysis

A MALDI-TOF-MS model Voyager DE-PRO Biospectrometry Workstation equipped with a nitrogen laser radiating at 337 nm from Applied Biosystems (Foster City, CA) was used to obtain the PMF. MALDI mass spectra were acquired as recommended by the manufacturer and treated with the Data Explorer software version 4 series. Measurements were done in the reflector positive ion mode, with a 20 kV accelerating voltage, 75.1% grid voltage, 0.002% guide wire, and a delay time of 80 ns. Two close external calibrations were performed with the monoisotopic peaks of the Bradykinin, Angiotensin II, P14R, and ACTH peptide fragments (m/z: 757.3997, 1046.5423, 1533.8582, and 2465.1989, respectively). Monoisotopic peaks were manually selected from each of the spectra obtained. Mass spectral analysis for each sample was based on the average of 500 laser shots. Peptide mass fingerprints were searched with the MASCOT [http://www.matrixscience.com/searchxformxselect.html] search engine with the following parameters: (i) Swiss-Prot, 2006 Database; (ii) molecular weight (MW) of protein, all; (iii) one missed cleavage; (iv) fixed modifications, carbamidomethylation (C); (v) variable modifications, oxidation (M); (vi) peptide tolerance up to 150 ppm. A match was considered successful when the protein identification score was located out of the random region and the protein analyzed scores first.

3. Results and discussion

Regarding solubilization aided by ultrasonication of proteins in pure acetonitrile, sample treatment (1), we found that sonication did not help to dissolve the protein BSA, not even partially, regardless the sonication time (0.5–5 min) or the sonication amplitude used (20–50%). It must be pointed out that acetonitrile is generally used to precipitate proteins. For α-lactalbumin, however, results obtained were comparable to those get it with the sample treatment with urea (data not shown) in terms of sequence coverage and number of peptides matched. Therefore, for some proteins, and depending on protein–acetonitrile polar interactions [10], this approach could be valuable. Our aim, however, was to find an approach or wide application, for this reason we substitute pure acetonitrile for a water:acetonitrile 1:1 (v/v) solution.

Concerning studies in water:acetonitrile 1:1 (v/v) solution, for sample treatments (2) and (3) (see Section 2.3.2), for which the reduction and alkylation steps were omitted, the spectra obtained showed few peptide peaks (data not shown) with low intensity, indicating a low protein digestion efficiency. Sonication times longer than 5 min in the enzymatic digestion step were not tested in these assays. This finding seems to suggest that cavitation caused by ultrasonication is not enough to promote protein denaturation in such a way that enzymatic digestion can be done without the previous reduction of protein disulfide bridges and alkylation of cysteine residues.

Table 1
Protein sequence coverage and number of peptides matched for sample treatment with urea, sample treatment (4), and sample treatment (5)

	α-Lactalbumin	BSA
Urea sample treatment ($n = 2$)		
Mascot score	84 ± 1	141 ± 3
Sequance coverage (%)	43 ± 3	36 ± 1
No. of identified peptides	8 ± 1	15 ± 1
Sample treatment number 4 ($n = 2$)		
Mascot score	104 ± 4[a]	123 ± 4
Sequance coverage (%)	28 ± 0[a]	24 ± 4
No. of identified peptides	9 ± 1[a]	12 ± 2
Sample treatment number 5 ($n = 2$)		
Mascot score	102 ± 8[a]	129 ± 1
Sequance coverage (%)	43 ± 0[a]	24 ± 1
No. of identified peptides	8 ± 0[a]	13 ± 3

Sample treatment (1) with urea (see sample treatment section for details); sample treatment (4): protein reduction and alkylation were done in one single step with a sonication time of 5 min. Protein digestion was done with 5 min sonication time and 50% sonication amplitude; and sample treatment (5): proteins were reduced (5 min), alkylated (5 min) and digested (5 min) using the sonoreactor with a 50% sonication amplitude. Protein concentration 1 μg/μL in water:acetonitrile 1:1 (v/v).
[a] Identified with two missed cleavages sites.

Once it was verified that protein reduction and alkylation was necessary, the next attempt was to carry out protein reduction, and protein alkylation in one single step (number (4) in Section 2.3.2), with the aim to reduce sample handling and the total time required to perform the analysis. Data presented in Table 1 and in Fig. 1 showed that protein score and sequence coverage were lower for the clean method than the ones acquired under conditions of sample treatment using urea for protein denaturation. For the clean method, unambiguous α-lactalbumin identification was only achieved when the missed cleavages was set at 2 in the MASCOT search engine, thus indicating that the procedure can partially digest the protein, but some cleavages are missed. This drawback could compromise the results for protein identification in samples of higher complexity. So far, it was decided to study the sample treatment doing reduction, alkylation and digestion steps individually, as it was done for sample treatment (5). In data shown in Table 1, it can be seen that protein identification was correctly done for BSA. Nevertheless, α-lactalbumin was identified only when the missed cleavages was set at 2, like for sample treatment (4). In addition, the sequence coverage and the number of peptides obtained were lower than the ones get it with the protocol using urea as denaturing agent.

In theory, protein denaturation, protein reduction and protein alkylation have the ultimate goal of to make the protein accessible for the enzymatic cleavage during the digestion process. Data presented in Table 1 suggest that for sample treatment with urea, (4) and (5) an incomplete protein cleavage was attained. However, as showed in spectra of Fig. 1, some cleavage was possible, suggesting that the protein was partially denatured, allowing the enzyme trypsin to break some, but not all, arginine and lysine peptide bonds.

This can be the reason why protein identification was only achieved for the mentioned sample treatments when the missed cleavage variable in the MASCOT search engine was set in 2. Amino acid residues valine and isoleucine has the potential to sterically hinder trypsin binding when an incomplete protein denaturation has been done. On the contrary, the sample treatment that uses urea as denaturing agent, as expected, provided excellent results as it can be seen in Table 1. Trying to make the protein more accessible to the enzyme, it was experimented a treatment consisted on ultrasonicate the solution containing the protein, previously to the reduction

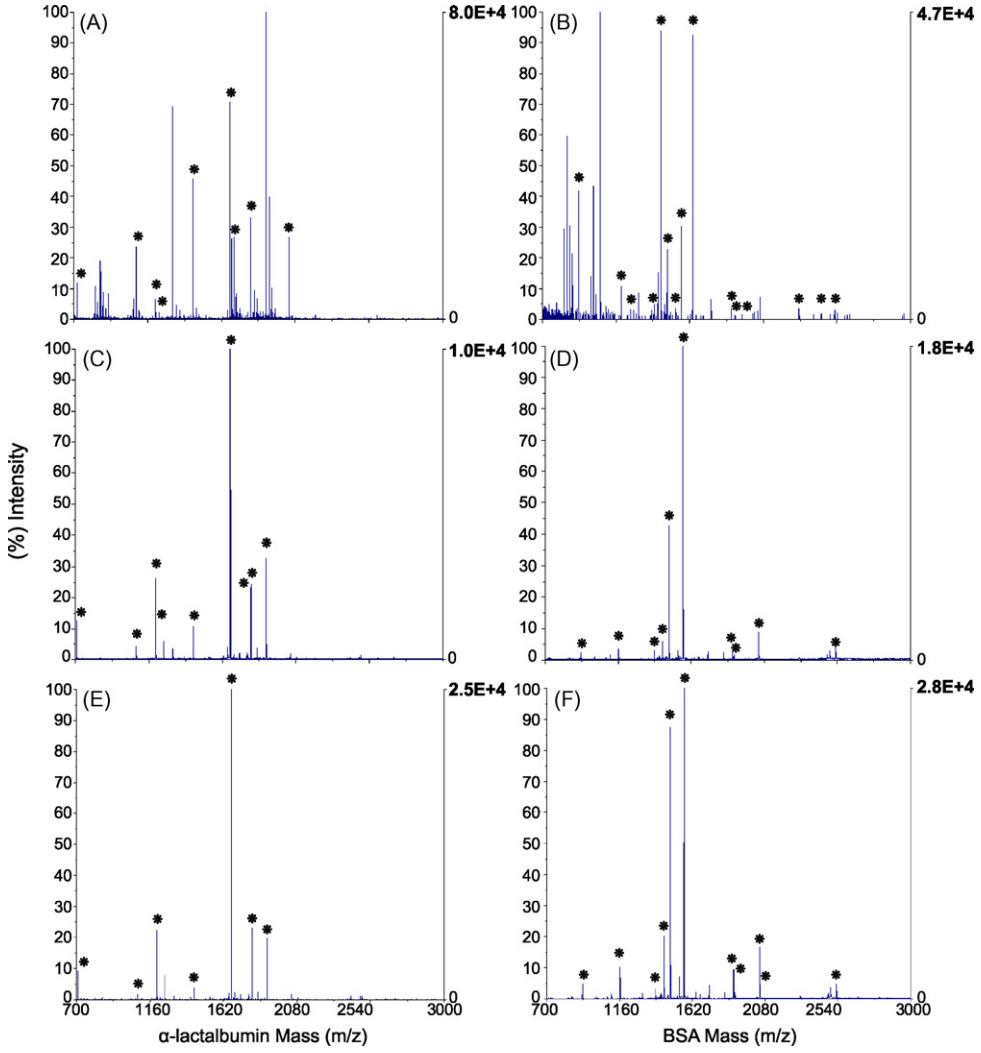

Fig. 1. (A and B) Sample treatment with urea. Proteins were dissolved in 6.5 M urea and then reduced (5 min), alkylated (5 min) and digested (5 min) using the sonoreactor with a 50% sonication amplitude. Desalting with ZipTip® was used. (C and D) Sample treatment (4); protein reduction and alkylation were done in one single step with a 5 min sonication time and 50% sonication amplitude. Protein digestion was done in 5 min with 50% sonication amplitude. (E and F) Sample treatment (5); proteins were reduced (5 min), alkylated (5 min) and digested (5 min) using the sonoreactor at 50% sonicatiom amplitude to speed up the procedures. (C and E) Protein identification was done with two missed cleavages set in the Mascot search engine.

step. The aim was to aid acetonitrile to denature the protein, making it more accessible to the subsequent steps of the sample treatment. As a general role, ultrasonication helps to enhance chemical reactions by increasing reaction rates and promoting physical processes such as mass transfer reactions [11,12], therefore it was expected a rapid protein denaturation process by the combination of the organic solvent acetonitrile and the ultrasonic field created by the sonoreactor. As a first approach, the following steps were done once the proteins were dissolved in water:acetonitrile 1:1 (v/v): (1) protein denaturation, (2) protein reduction, (3) protein alkylation and (4) protein digestion: 5 min of sonication time and 50% sonication amplitude were used at each step. For comparative purposes, the first step, protein denaturation, was also done with 20 min of agitation in the minicentrifuge-vortex. Results are showed in Table 2 and, as it can be seen, the proposed methods were comparable in terms of number of peptides matched and sequence coverage for BSA and α-lactoalbumin to the sample treatment using urea (Table 1). So far, the key for a successful clean rapid treatment using sonication and aqueous solutions containing acetonitrile lie in performing an adequate first step for protein denaturation, thus allowing a correct subsequent reduction, alkylation and degradation steps.

Regarding the possibility of simplifying sample handling, some experiments were conducted by first denaturating the protein with ultrasound, as above, and then doing the steps of reduction and alkylation, in one single step. Results showed that protein iden-

Table 2
Protein sequence coverage and number of peptides matched for sample treatments with protein denaturation using agitation (20 min in minicentrifuge-vortex) or ultrasound (5 min sonication time and 50% sonication amplitude)

	α-Lactalbumin	BSA
Denaturation with agitation ($n = 2$)		
Mascot score	98 ± 1	354 ± 13
Sequance coverage (%)	44 ± 6	64 ± 1
No. of identified peptides	7 ± 0	37 ± 1
Denaturation with ultrasound ($n = 2$)		
Mascot score	95 ± 7	252 ± 11
Sequance coverage (%)	40 ± 0	58 ± 4
No. of identified peptides	7 ± 0	37 ± 3

After denaturation, proteins were reduced (5 min), alkylated (5 min) and digested (5 min) using the sonoreactor with a 50% sonication amplitude. Protein concentration 1 μg/μL in water:acetonitrile 1:1 (v/v).

Table 3
Protein sequence coverage and number of peptides matched for sample treatments with (a) 1 min of enzymatic digestion accelerated with sonoreactor at 50% sonication amplitude and (b) 5 min of enzymatic digestion accelerated with sonoreactor at 50% sonication amplitude

	α-Lactalbumin	BSA
(a) 1 min protein digestion ($n=2$)		
Mascot score	91 ± 1	165 ± 1
Sequance coverage (%)	40 ± 0	43 ± 1
No. of identified peptides	7 ± 0	33 ± 1
(b) 5 min protein digestion ($n=2$)		
Mascot score	121 ± 1	168 ± 4
Sequance coverage (%)	52 ± 1	46 ± 2
No. of identified peptides	10 ± 1	33 ± 1

For both cases, proteins were denaturated (1 min), alkylated (1 min) and digested (1 min) using the sonoreactor with a 50% sonication amplitude. Protein concentration 1 μg/μL in water:acetonitrile 1:1 (v/v).

tification can be done, but sequence coverage and the number of peptides matched was lower than for the treatment in which reduction and alkylation are done in separated steps (data not shown).

Data obtained previously in our laboratory [9] suggest that time needed for reduction and alkylation of proteins can be reduced considerably with the aid of ultrasonication. For this reason sonication time for denaturation, reduction and alkylation was set to 1 min each one, whilst for protein digestion, two times were assayed, 5 min and 1 min. Results are showed in Table 3. As it can be seen, protein identification was achieved in all conditions. However, when the digestion time was set in 5 min, the number of peptides matched and the sequence coverage were higher for the smaller protein α-lactalbumin, so far, 5 min was chosen as optimum sonication time for protein digestion, whilst 1 min was chosen for the other steps of the sample treatment: denaturation, reduction and alkylation.

A study was conducted in order to compare the performance of the method with urea and the clean method for low protein concentrations. Thus, as shown in Table 4, when the protein concentration was reduced from 1 μg/μL to 0.1 μg/μL, the number of peptides identified was higher for the clean method, 7 vs. 6 and 34 vs. 20 for the α-lactoalbumin and BSA, respectively. This fact can be related to the desalting procedure with ZipTip® used in the urea process. It has been shown in literature that an amount of peptides comprised between 30% and 70% can be retained in the C_{18} beads, such as the ones contained in the ZipTip®, used for cleaning/pre-concentration purposes in proteomic sample treatments. In addition the amount of peptides retained seems to be higher as the peptide concentration becomes lower. The aforementioned information is consistent with our experimental results: the number of peptides identified for BSA drastically decreased, from 39 to 20, for the urea process when the protein concentration was lowered 10 times. An additional advantage of the clean procedure is that the signal to noise ratio is two times higher when comparing it with the process with urea. So far, for lower concentration of analyte, the peptide identification was done in a better way.

The optimum conditions defined, this is, 1 min sonication time at 50% sonication amplitude for protein denaturation, protein reduction and protein alkylation and 5 min sonication time at 50% sonication amplitude for protein digestion were applied to a set of different standard proteins comprising ovoalbumin, carbonic anhidrase and bovine catalase. In addition, protein split-soret cytochrome *c* from *D. desulfuricans* ATCC27774, obtained after cultivation and purification as described in Section 2.4, were used for additional proof-of-the procedure. For comparative purposes, the accelerated method with urea was also applied to the same samples. Results are given in Table 5 and spectra regarding split-soret cytochrome *c* proteins are showed in Fig. 2. As it can be seen, protein identification was always possible with both procedures, but sequence coverage and the number of peptides identified was

Table 4
Comparative study of performance for low protein concentration

	Protein							
	α-Lactalbumin				BSA			
	Sample treatment with urea		Clean sample treatment		Sample treatment with urea		Clean sample treatment	
	1[a]	0.1[a]	1[a]	0.1[a]	1[a]	0.1[a]	1[a]	0.1[a]
Mascot score	80 ± 1	75 ± 6	91 ± 1	73 ± 5	135 ± 4	172 ± 2	121 ± 1	208 ± 4
Sequence coverage (%)	40 ± 0	47 ± 5	40 ± 0	47 ± 5	39 ± 0	35 ± 1	46 ± 4	55 ± 5
No. of peptides identified	7 ± 1	6 ± 1	7 ± 0	7 ± 1	27 ± 3	20 ± 1	34 ± 1	34 ± 2

Sample treatment with urea: proteins were dissolved in 6.5 M urea and then reduced (5 min), alkylated (5 min) and digested (5 min) using the sonoreactor with a 50% sonication amplitude. Desalting with ZipTip® was used. *Clean sample treatment*: proteins were dissolved in water:acetonitrile 1:1 (v/v), and then proteins were denaturated (1 min), reduced (1 min), alkylated (1 min) and digested (5 min) using the sonoreactor with a 50% sonication amplitude.

[a] Protein concentration (μg/μL).

Table 5
Protein sequence coverage and number of peptides matched for sample treatment with urea and clean sample treatment

Protein	Sample treatment with urea ($n=2$)				Clean sample treatment ($n=2$)		
	Theor. Mr (kDa)	Mascot score	Sequence coverage (%)	No. of peptides identified	Mascot score	Sequence coverage (%)	No. of peptides identified
α-Lactalbumin	16.7	84 ± 1	43 ± 3	8 ± 1	121 ± 1	52 ± 1	10 ± 1
Carbonic anhydrase	29.1	71 ± 1	60 ± 1	13 ± 1	182 ± 2	56 ± 1	13 ± 1
Ovalbumin	43.2	71 ± 1	24 ± 2	7 ± 1	149 ± 9	41 ± 4	12 ± 0
BSA	71.2	139 ± 2	36 ± 1	15 ± 0	168 ± 4	46 ± 2	33 ± 1
Catalase bovine	60.1	216 ± 5	44 ± 1	20 ± 1	146 ± 16	52 ± 6	22 ± 3
Split-soret cytochrome *c*	27.8	157 ± 1	55 ± 0	12 ± 0	102 ± 3	75 ± 2	16 ± 1

Sample treatment with urea: proteins were dissolved in 6.5 M urea and then reduced (5 min), alkylated (5 min) and digested (5 min) using the sonoreactor with a 50% sonication amplitude. Desalting with ZipTip® was used. Protein concentration 1 μg/μL. *Clean sample treatment*: proteins were dissolved in water:acetonitrile 1:1 (v/v), and then proteins were denaturated (1 min), reduced (1 min), alkylated (1 min) and digested (5 min) using the sonoreactor with a 50% sonication amplitude. Protein concentration 1 μg/μL.

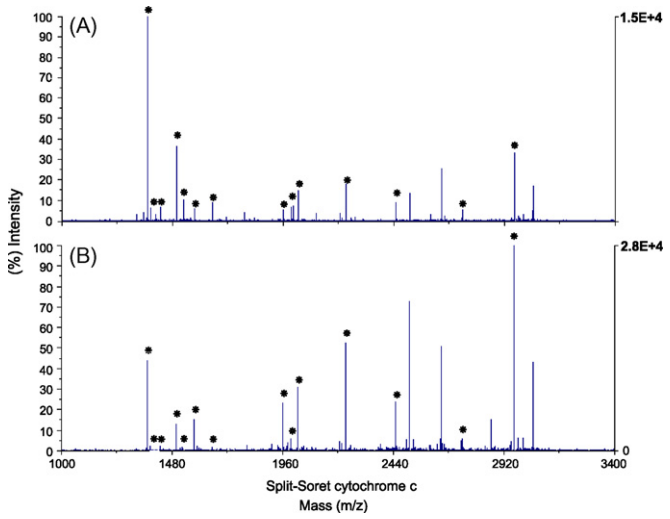

Fig. 2. (A) Sample treatment with urea. Proteins were dissolved in 6.5 M urea and then reduced (5 min), alkylated (5 min) and digested (5 min) using the sonoreactor with a 50% sonication amplitude. Desalting with ZipTip® was used. Protein concentration 1 μg/μL. (B) Clean sample treatment: proteins were dissolved in water:acetonitrile 1:1 (v/v), and then proteins were denaturated (1 min), reduced (1 min), alkylated (1 min) and digested (5 min) using the sonoreactor with a 50% sonication amplitude. Protein concentration 1 μg/μL.

higher for the clean procedure for all proteins but carbonic anhydrase.

4. Conclusions

A new, clean and ultra-fast (8 min) method for protein identification by PMF and mass spectrometry techniques is proposed. The methodology entails protein solubilization in a solution of water:acetonitrile 1/1 (v/v) and ultrasonication. The new methodology does not need desalting procedures, and reduce the total salt content to a minimum in such a way, than the spectrum signal-to-noise ratio obtained is two times lower that for sample treatments using desalting processes. The following proteins were successfully identified with the sample treatment: α-lactalbumin, BSA, ovoalbumin, carbonic anhidrase, and bovine catalase. The protein split-soret cytochrome *c* from *D. desulfuricans* ATCC27774, was also successfully identified.

Acknowledgments

H. M. Santos and C. Mota acknowledge the doctoral grants FCT (Science and Technological Foundation) from Portugal. SRFH/BD/38509/2007 and SFRH/BD/32478/2006 from FCT, respectively. Dr. J. L. Capelo acknowledges the MALDI-TOF-MS service of the Chemistry Department of the New University of Lisbon (http://www.dq.fct.unl.pt/maldi/) for their helpful assistance and valuable suggestions. The research findings here reported are protected by international laws under patent pendings PCT/IB2006/052314 and PT 103 303. FCT is also acknowledged for financial support under the project POCI/QUI/55519/2004 FCT-FEDER.

Contributions: H.M. Santos conceived the idea; J.L. Capelo and C. Lodeiro obtained financial support, conceived and designed the experimental and wrote the paper; H.M. Santos and C. Mota optimized and performed proteomic experiments; J.L. Capelo, C. Lodeiro and H.M. Santos interpreted the experimental data; Isaa Isaac contribute with financial support and comments to the final version of the manuscript. I. Moura provided the protein split-soret cytochrome *c* from *D. desulfuricans* ATCC27774 and contributed with valuable suggestions to the success of the work.

References

[1] D. Lopez-Ferrer, B. Cañas, J. Vazquez, C. Lodeiro, R. Rial-Otero, I. Moura, J.L. Capelo, Trends Anal. Chem. 25 (2006) 996–1005.
[2] M. Baker, Nat. Biotechnol. 23 (2005) 297–304.
[3] Z.Y. Park, D.H. Russell, Anal. Chem. 72 (2000) 2667–2670.
[4] W.K. Russell, Z.Y. Park, D.H. Russell, Anal. Chem. 73 (2001) 2682–2685.
[5] B.N. Pramanik, U.A. Mirza, Y.H. Ing, Y.H. Liu, P.L. Bartner, P.C. Weber, M.K. Bose, Prot. Sci. 11 (2002) 2676–2687.
[6] R. Rial-Otero, R.J. Carreira, F.M. Cordeiro, A.J. Moro, H.M. Santos, G. Vale, I. Moura, J.L. Capelo, J. Chromatogr. A 1166 (2007) 101–107.
[7] R. Rial-Otero, R.J. Carreira, F.M. Cordeiro, A.J. Moro, M.G. Rivas, L. Fernandez, I. Moura, J.L. Capelo, J. Proteome Res. 6 (2007) 909–912.
[8] H.M. Santos, R. Rial-Otero, L. Fernandes, G. Vale, M.G. Rivas, I. Moura, J.L. Capelo, J. Proteome Res. 6 (2007) 3393–3399.
[9] F.M. Cordeiro, R.J. Carreira, R. Rial-Otero, M.G. Rivas, I. Moura, J.L. Capelo, Rapid Commun. Mass Spectrom. 21 (2007) 3269–3278.
[10] K. Gekko, E. Ohmae, K. Kameyama, T. Takagi, Biochim. Biophys. Acta 1397 (1998) 195–205.
[11] H.M. Santos, J.L. Capelo, Talanta 73 (2007) 795–802.
[12] T.J. Mason, Sonochemistry, Oxford University Press, Oxford, UK, 1999.

Talanta 77 (2008) 758–764

Contents lists available at ScienceDirect

Talanta

journal homepage: www.elsevier.com/locate/talanta

Carbon nanotube networks as gas sensors for NO_2 detection

I. Sayago[a,*], H. Santos[a], M.C. Horrillo[a], M. Aleixandre[a], M.J. Fernández[a], E. Terrado[b], I. Tacchini[b], R. Aroz[c], W.K. Maser[b], A.M. Benito[b], M.T. Martínez[b], J. Gutiérrez[a], E. Muñoz[b,**]

[a] Laboratorio de Sensores IFA-CSIC, Serrano 144, 28006 Madrid, Spain
[b] Instituto de Carboquímica CSIC, Miguel Luesma Castán 4, 50018 Zaragoza, Spain
[c] Instituto de Ciencia de Materiales de Aragón, Universidad de Zaragoza-CSIC, 50018 Zaragoza, Spain

ARTICLE INFO

Article history:
Received 7 April 2008
Received in revised form 3 July 2008
Accepted 11 July 2008
Available online 23 July 2008

Keywords:
Carbon nanotubes
Gas sensor
NO_2

ABSTRACT

Networks of different carbon nanotube (CNT) materials were investigated as resistive gas sensors for NO_2 detection. Sensor films were fabricated by airbrushing dispersions of double-walled and multi-walled CNTs (DWNTs and MWNTs, respectively) on alumina substrates. Sensors were characterized by resistance measurements from 25 to 250 °C in air atmosphere in order to find the optimum detection temperature. Our results indicate that CNT networks were sensitive to NO_2 concentrations as low as 0.1 ppm. All tested sensors provided significantly lower response to interfering gases such as H_2, NH_3, toluene and octane. We demonstrate that the measured sensitivity upon exposure to NO_2 strongly depends on the employed CNT material. The highest sensitivity values were obtained at temperatures ranging between 100 and 200 °C. The best sensor performance, in terms of recovery time, was however achieved at 250 °C. Issues related to the gas detection mechanisms, as well as to CNT network thermal stability in detection experiments performed in air at high operation temperatures are also discussed.

1. Introduction

Since their discovery in 1991, carbon nanotubes (CNTs) have attracted the scientific interest due to their unique structure and promising properties that make them potentially useful for applications including nanoelectronics, multifunctional composite materials, or field emission devices [1]. CNTs are hexagonal networks of carbon atoms that can essentially be thought of as a layer of graphite rolled-up into a cylinder. Depending on the arrangement of their graphene cylinders, there are two types of nanotubes: single-walled nanotubes (SWNTs) and multi-walled nanotubes (MWNTs). SWNTs have only one single layer of graphene cylinder, while MWNTs have several concentric layers. Their high surface area (>1500 m^2/g), high aspect ratio, size, and hollow geometry also make them promising candidates for their use as components of gas and chemical sensors. As a result of their remarkable physical and structural properties, CNTs are good candidates to be utilized as components of sensors with improved real-time monitoring of combustible gas alarms, gas leak detection, and environmental pollution monitoring, etc. SWNTs and MWNTs as sensitive materials for the detection of gases such as H_2, NH_3, NO_2 or O_2 have already been successfully demonstrated [2–6].

The emission of nitrogen oxides (NO_x, NO and NO_2) results from the combustion of fossil fuels (vehicles, electricity generation, and industrial processes), contributing to both smog and acid precipitation, and affect both terrestrial and aquatic ecosystems. Nitrogen monoxide is unstable and quickly forms NO_2, which is an oxidizing gas that is present in all urban atmospheres. NO_2 is a brownish, highly reactive gas and a deadly poison by inhalation. The NO_2 gas detection has normally been carried out by chemiluminescence or non-dispersive infrared analysis [7,8]. These traditional methods employ large and expensive instruments and require sampling systems as well as complicated maintenance. Therefore, an effective method to monitor NO_2 is demanded for atmospheric environmental measurement and control. Research is being focused on the development of sensors capable of monitoring low NO_2 concentrations.

In this work, different CNT films have been tested as resistive NO_2 sensors for environmental applications. The temperature effect in the sensitivity and selectivity of these sensors has been studied. CNT films showed very good sensitivity and selectivity to NO_2. We also demonstrate that the CNT network sensitivity strongly depends on the employed CNT materials.

* Corresponding author. Tel.: +34 91 5618806.
** Corresponding author. Tel.: +34 976 733977.
E-mail addresses: sayago@ifa.cetef.csic.es (I. Sayago), edgar@icb.csic.es (E. Muñoz).

0039-9140/$ – see front matter © 2008 Elsevier B.V. All rights reserved.
doi:10.1016/j.talanta.2008.07.025

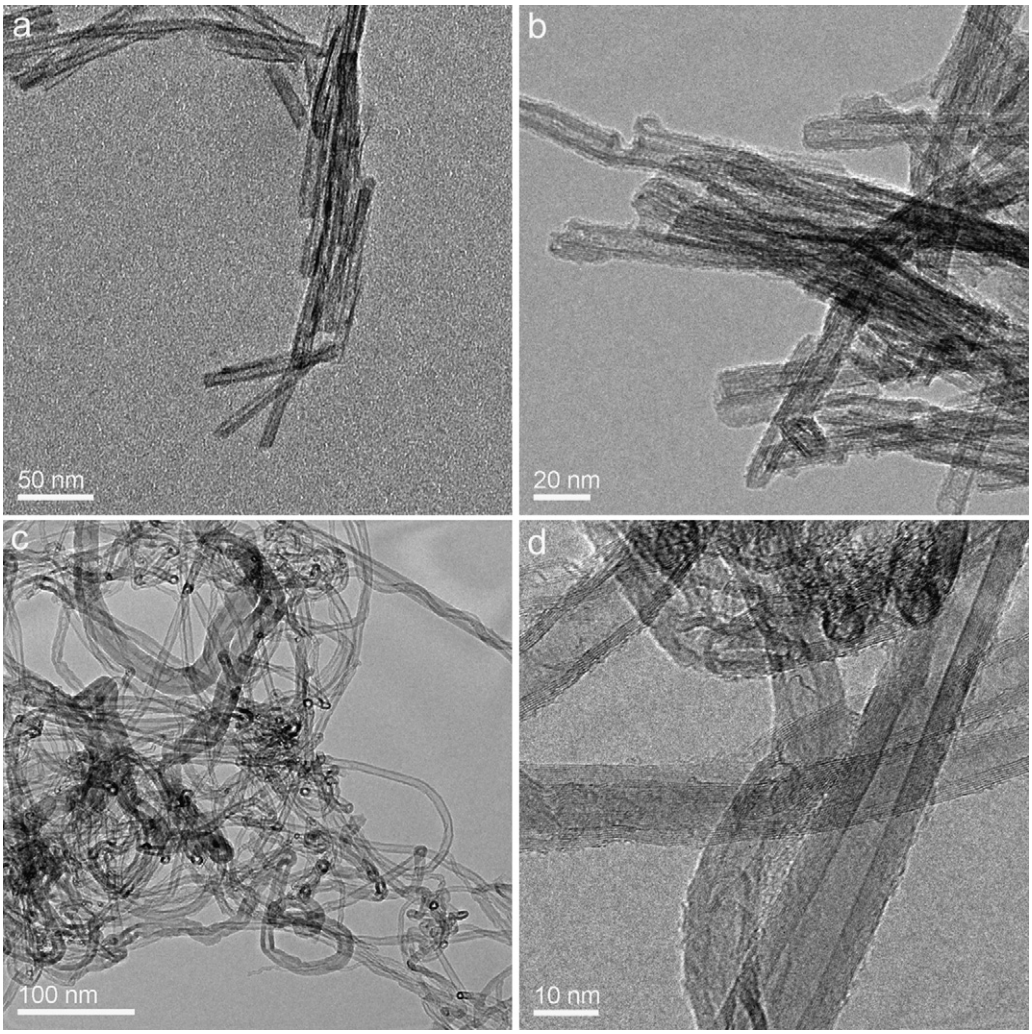

Fig. 1. TEM micrographs of the employed DWNT (a and b) and MWNT (c and d) materials.

2. Experimental

Commercial, high purity (>90%), double-walled and multi-walled CNT (DWNT and MWNT, respectively) materials produced by the chemical vapor deposition (CVD) technique were used in the fabrication of the sensor films. Short DWNTs, as well as carboxylic acid-functionalized short DWNTs (DWNT-COOH) were purchased from Nanocyl S.A. Transmission electron microscopy (TEM, JEOL JEM 2010F) characterization revealed that these materials consist of CNTs having several hundreds of nanometers in length (Fig. 1a) and ~5 nm in diameter, mainly containing two concentric graphene sheets (triple- and four-walled CNTs can also be observed in high-resolution TEM micrographs of these materials, Fig. 1b). These DWNTs commonly appear self-organized in bundles, and exhibit open end-caps and dangling bonds on the sidewalls as a result of CNT shortening and functionalization (Fig. 1b). X-ray photoelectron spectroscopy (XPS) data indicated that less than 1% of the CNT carbon atoms were modified during –COOH functionalization [9]. CNT networks were also fabricated from larger diameter (typically 10–15 nm) and longer (≥10 μm) MWNTs (Fig. 1c), purchased from Nanothinx S.A. High-resolution TEM micrographs revealed that these CNTs typically consist of 7–15 concentric layers (Fig. 1d).

Heraeus MSP 769 alumina substrates were used to prepare the resistive sensor devices (Fig. 3a). These substrates consist of 6 mm × 6 mm alumina supports containing Au electrical contacts, a heating element (Pt 25), and a temperature sensor (Pt 1000) that allow studying the sensor performance as a function of temperature. CNT materials were ultrasonically dispersed in ethanol (0.5 mg/mL). CNT sensor films were deposited by airbrushing 6 mL of the ethanol dispersions on those substrates (carrier gas: dry air, 1 bar; working distance: 20 cm). The sensors tested are listed in Table 1. The morphology of the resulting CNT networks was characterized by scanning electron microscopy (SEM, Hitachi S-3400N). Further studies on CNT structure and thermal stability of the employed CNT materials and films were performed by Raman spectroscopy (Horiba Jobin Yvon HR800 UV spectrometer, λ = 532 nm), FTIR spectroscopy (Bruker, Vertex 70 spectrometer), and thermogravimetric analyses (TGA, TA Instruments SDT Q600).

Sensors were placed in a stainless steel test cell for their characterization by dc electrical measurements. Detections were carried

Table 1
The tested CNT networks

Sensor	Sensor films
S1	DWNTs
S2	DWNTs-COOH
S3	MWNTs

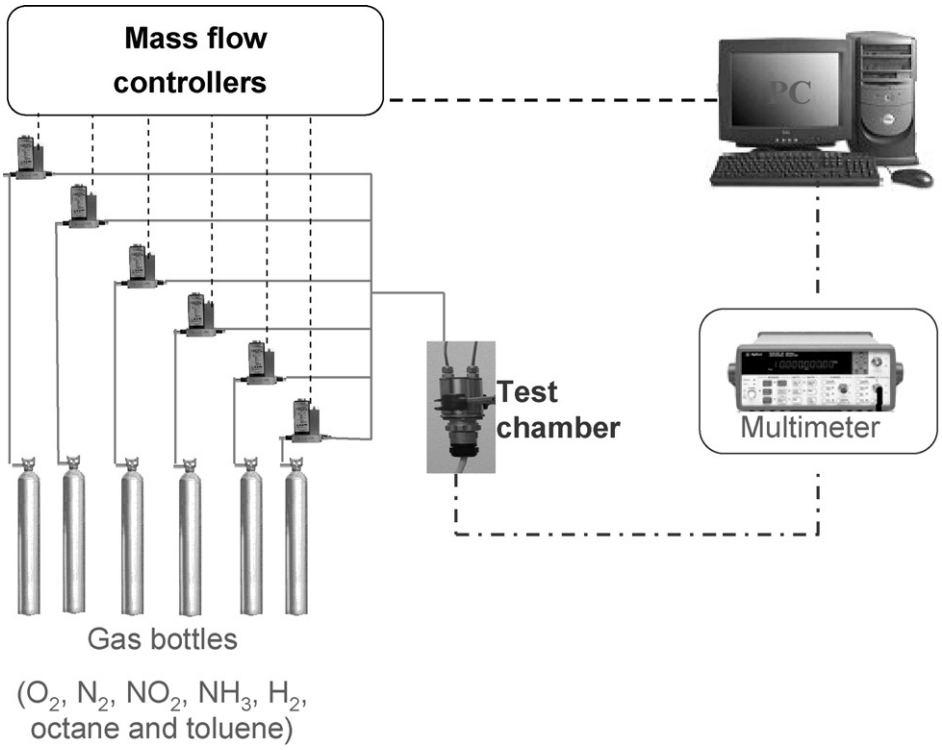

Fig. 2. Block diagram of the measuring system.

out in dry air atmospheres at fixed temperatures ranging from 25 to 250 °C, with a constant flow of 200 mL/min and exposure times of detection gases (NO_2, NH_3, H_2, octane and toluene) of 15 min. NO_2 concentrations were varied from 0.1 to 0.9 ppm. Concentrations of interfering gases were 80, 400, and 300 ppm for NH_3, toluene and octane, respectively, and 1.5% for H_2. The carrier gas (dry air, 21% O_2 and 79% N_2) was prepared by mixing high purity (99.999%) O_2 and N_2 (Praxair, Inc.). The detection gases were prepared by dilution of reference gas mixtures (0.9 ppm NO_2, 2% H_2, 113.3 ppm NH_3, 400 ppm octane and 300 ppm toluene diluted in nitrogen, certified by Praxair, Inc.). The detection gases were mixed with the carrier gas. A diagram of the employed experimental set-up is shown in Fig. 2. An automated gas line allowed us to obtain the desired detection gas concentrations by means of mass flow controllers, which change the flow of the employed reference gas mixtures by applying the following equation: $c_i f_i = f_s c_s$, where c_i is the concentration of the tested gas in the reference gas mixture (i.e. 0.9 ppm NO_2), c_s is the desired detection gas concentration (for, i.e. 0.7 ppm NO_2), f_i is the reference gas mixture flow, and f_s is the detection gas flow (200 mL/min).

The sensor resistance was measured using a digital multimeter (Keithley 2000). The measurement system was fully automated and controlled by a program developed in Testpoint™. The experimental procedure during the detection experiments was performed as follows: first, the baseline resistance was measured in dry air for all CNT sensors at the operation temperature. Secondly, a known concentration of the tested gas in dry air was introduced into the test cell during 15 min and the sensor resistance was recorded (detection process). Third, the flow of the tested gas was interrupted, and then dry air was introduced again in the test cell and the sensor recovers the starting resistance (recovery process). The experiments were carried out three times to verify the reproducibility of the sensor response.

3. Results and discussion

The airbrush spraying of CNT dispersions is a facile and inexpensive method for preparing thin CNT networks [4,10]. The measured resistance values of these CNT networks depend on the structural features of the different CNTs, as well as on the density of the employed CNT materials, that also affects the degree of CNT disentanglement achieved by sonication. MWNTs were easier to disperse than the employed DWNT materials so, for the same volume of airbrushed CNT dispersions, the use of MWNT dispersions led to the formation of more entangled, uniform and, consequently, more conducting CNT networks (Figs. 3c and 4b). Besides, the presence of long MWNTs would improve CNT entanglement and, therefore, enhance the network conductivity. On the contrary, DWNT networks mainly consisted of interconnected dense CNT aggregates (Figs. 3b and 4a), probably due to the presence of tightly packed DWNT bundles (Fig. 1a and b). The resulting CNT networks exhibited temperature dependence typical of semiconductors, i.e. the CNT network resistance values decreased when increasing temperature. DWNT networks were at least one order of magnitude less conducting (resistance values in the order of kΩ) than the MWNT films.

The sensor response and recovery times of CNT networks can be significantly improved by running successive thermal treatments prior to the gas detection experiments [10,11]. These treatments consist of heating the sensors from 25 to 250 °C (5 °C/min) in air, followed by cooling to room temperature. Table 2 shows the effect of the employed thermal treatments on the sensor sensitivity (S). Sensitivity has been calculated on a basis of $S = [100 \times (R_a - R_g)/R_g]$, where R_a and R_g stand for the sensor resistance in air and during NO_2 exposure, respectively. The sensitivity values reported here were calculated from average resistance values measured in situ and in real time during the detection experiments. We believe that these treatments may lead to the complete removal of ethanol and

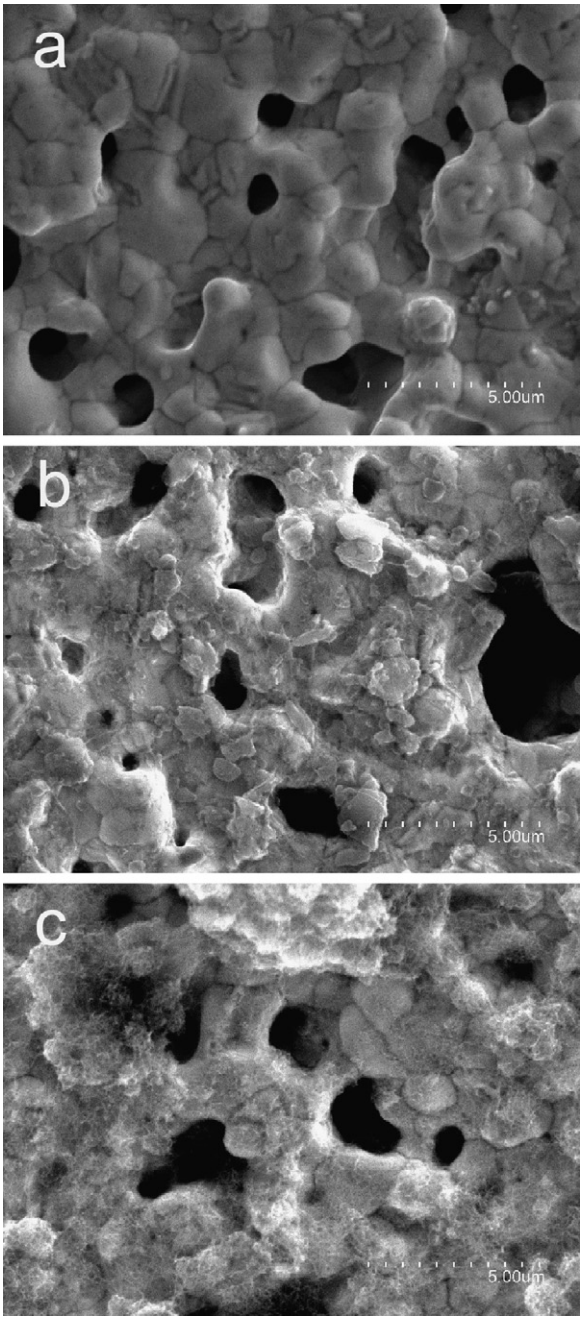

Fig. 3. SEM micrographs of (a) a sensor bare Au electrode, and of airbrushed (b) DWNT-COOH and (c) MWNT networks.

amorphous carbon traces, therefore increasing the exposed CNT surface area, and also exposing open end-caps, dangling bonds, and other CNT defects that would act as new sites for gas adsorption [2,12–14]. The removal of these impurities may also lead to an

Table 2
The effect of successive thermal treatments on the sensor sensitivity to a 0.7 ppm NO_2 in air at 200 °C

T (°C)	S_{S1} (%)	S_{S2} (%)	S_{S3} (%)
Without treatment	5.66	10.11	2.51
After first treatment	7.31	12.45	3.83
After second treatment	8.43	14.39	5.78
After third treatment	8.73	16.83	7.59

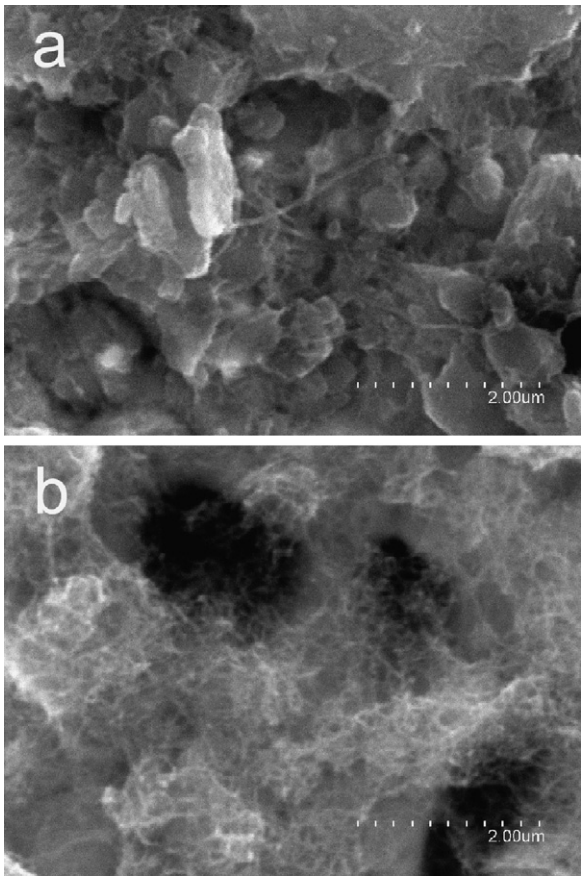

Fig. 4. SEM micrographs showing the different morphologies and entanglement of (a) a DWNT-COOH network and (b) a MWNT network.

increased network porosity and, eventually, to less CNT joints. As a result of these thermal treatments, the CNT network resistance values increase as well as its sensitivity upon gas exposure (Table 2).

While the maximum decomposition rates in air of the employed CNTs occur at temperatures (~500 °C for DWNT materials, ~600 °C for MWNTs) well above the maximum operation temperature (250 °C), the thermal stability of these CNT networks is an important issue for the potential applications of these CNT-based devices. FTIR spectra (Fig. 5) of all tested DWNT materials show a shoulder at ~1730 cm^{-1} assigned to C=O stretching modes of carboxylic acid groups introduced during DWNT shortening. This band is clearly more intense in DWNT-COOH materials. FTIR studies indicate that the starting CNT materials do not significantly further oxidize during long exposure times in air at the highest operation temperatures. Nevertheless, CNT sonication and subsequent CNT airbrushing should lead to enhanced CNT reactivity to oxygen at high temperatures as a result of an increased exposed CNT surface area. SEM and Raman spectroscopy results (Fig. 6) however reveal that the CNT films and CNT structure are not significantly affected during those long thermal treatments at the maximum operation temperatures. Two main Raman features are observed in the spectra shown in Fig. 6: the G band, at ~1590 cm^{-1}, characteristic of graphite, and the D band, located at ~1350 cm^{-1}, which is typically assigned to disordered carbon. The higher intensity ratio values of the G- and D bands (I_D/I_G) measured in the MWNT networks is the result of the higher defective structure of the employed MWNTs (~0.90 and ~0.25 for MWNT and DWNT networks, respectively). Long thermal treatments at 250 °C did not lead to shifts in the bands locations, nor in changes of the measured I_D/I_G val-

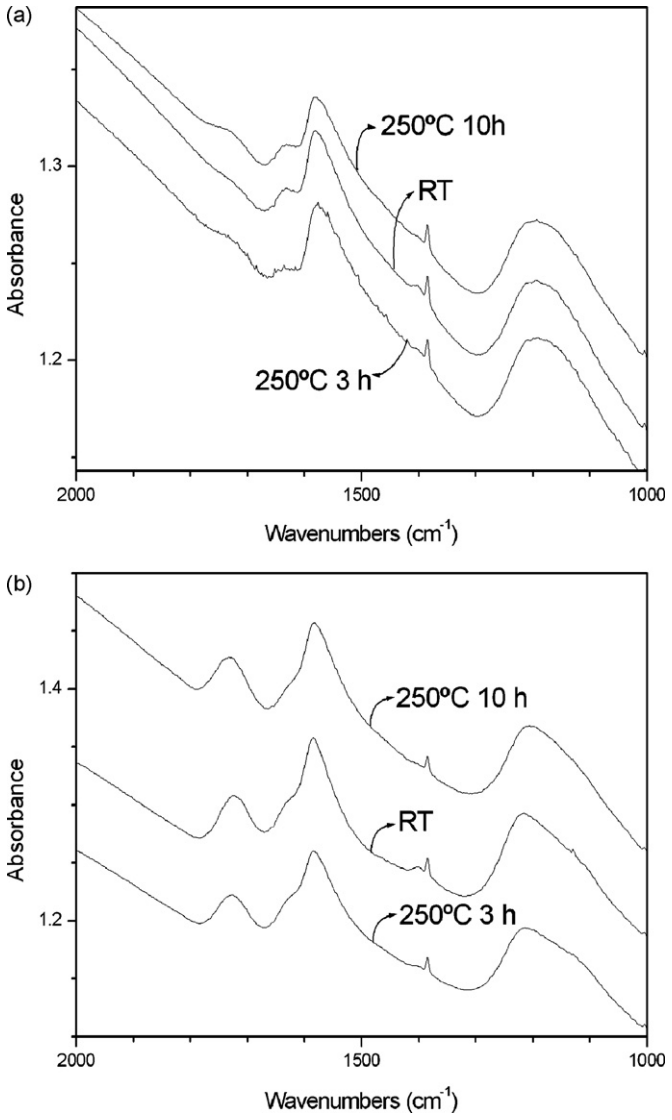

Fig. 5. FTIR spectra of (a) DWNT and (b) DWNT-COOH materials before and after thermal treatments at 250 °C.

ues. These results further account for the thermal stability of these CNT-based sensors. The operation temperatures are therefore too low to induce significant CNT damage in air atmospheres, as it was already reported for both DWNTs [15,16] and MWNTs [17–20]. On the other hand, the measured weight loss (~6 wt.% for DWNT and DWNT-COOH materials, and <2 wt.% for MWNTs) in long TGA experiments performed at the maximum sensor operation temperatures (6 h at 200 °C and 10 h at 250 °C) in air is mainly assigned to amorphous carbon removal due to its higher reactivity [17]. Some end-cap opening and propagation of oxidation at vulnerable sites (end-caps, dangling bonds, defects) might however be expected during these thermal treatments, that would lead to increased CNT porosity [21,22] and would additionally contribute to improve the sensor performance. Further end-cap opening, CNT oxidation, and defect formation should affect the temperature of maximum CNT decomposition rate in TGA experiments [19]. This, however, only occurred in thermally treated DWNT-COOH materials (this temperature decreased about 15 °C). These results further confirm that the employed CNT materials are suitable for the gas detection experiments described above.

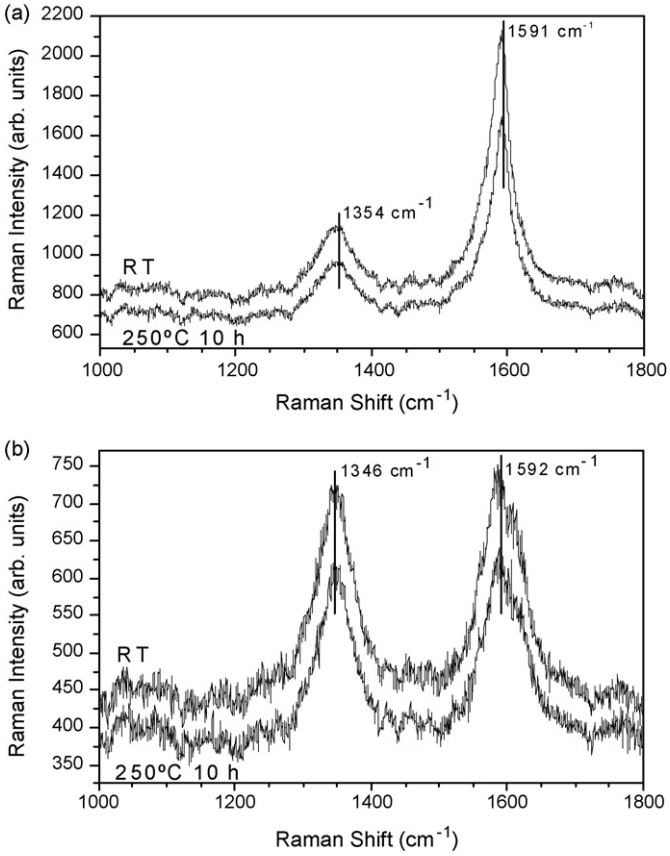

Fig. 6. Raman spectra of (a) DWNT-COOH and (b) MWNT networks at room temperature (RT) and after a 10-h-long thermal treatment at 250 °C.

Gas detection experiments were then performed between room temperature and 250 °C (Figs. 7 and 8). The responses of the tested CNT sensors to NO_2 and the interfering gases were highly reproducible. Sensor resistance decreased in the presence of NO_2, increased when exposed to NH_3 and H_2, and remained unchanged when exposed to the tested VOCs (octane and toluene). All the sensors detected NO_2 in the tested temperature range, and their response strongly depended on the operation temperature (Table 3). On the contrary, sensors showed negligible cross-sensitivity to interfering gases at all tested temperatures (Fig. 7). The highest NO_2 sensitivity values were achieved when using DWNT-COOH networks, and at temperatures ranging between 100 and 200 °C for all tested sensors. These temperature values are in the same range than those reported by other authors for NO_2 sensors based on MWNT forests grown by CVD from silicon substrates [11,23,24]. The recovery times during these NO_2 detection experiments were very long (longer than 2 h), and significantly decreased when increasing the operation temperature (Fig. 8). The best sensor performance, in terms of recovery time, was achieved at 250 °C.

The measured sensor response to NO_2 in air atmospheres can be explained as follows: CNTs behave like p-type materials due to electron withdrawing by oxygen molecules adsorbed on the CNT

Table 3
The sensor sensitivity to 0.7 ppm NO_2 in air at different temperatures

T (°C)	S_{S1} (%)	S_{S2} (%)	S_{S3} (%)
25	7.94	12.34	4.15
100	9.41	19.91	7.23
200	8.73	16.83	7.59
250	7.34	14.91	7.09

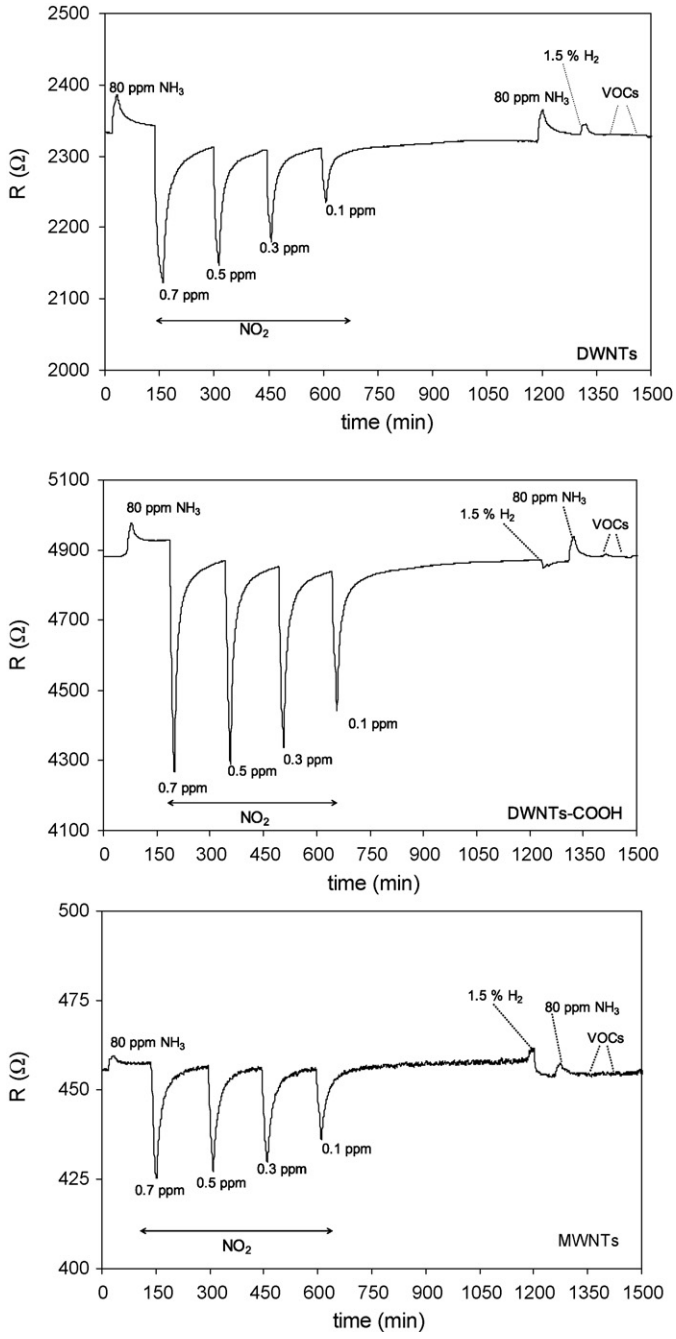

Fig. 7. Sensor response curves to different gases at 200 °C.

surface [25–27]. The observed resistance decrease when exposing the CNT networks to NO_2 can be addressed to electron transfer from the CNTs to the NO_2, that would lead to increased hole carriers in the CNTs [6]. Several mechanisms have been proposed to explain the nature of the CNT-NO_2 interaction [6,28–32]. While the measured CNT network resistance changes upon exposure to NO_2 can be explained by either proposing NO_2 physical adsorption processes [28] or NO_2 chemical adsorption processes [29–31], the observed long recovery times lead us to suggest that NO_2 chemisorption occurs during the detection experiments described above. NO_2 chemisorption may result of the interaction between NO_2 gas molecules and defects in the CNT structure [2,11,12,14]. The open end-caps and dangling bonds observed in DWNT materials (Fig. 1b) may act as adsorption sites. The introduction of defects

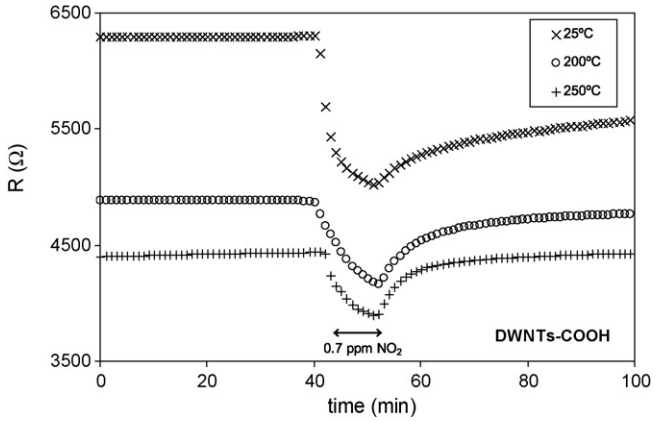

Fig. 8. S2 sensor response to 0.7 ppm NO_2 at different temperatures in air atmosphere.

during –COOH functionalization might therefore explain the higher sensitivity values measured on DWNT-COOH networks when compared to those corresponding to DWNT networks (the electron withdrawing nature of carboxylic groups in DWNT-COOH, that would lead to additional enriched hole carriers in the CNTs, might also contribute to the observed higher sensor response). On the other hand, it was expected that the employed MWNTs should be

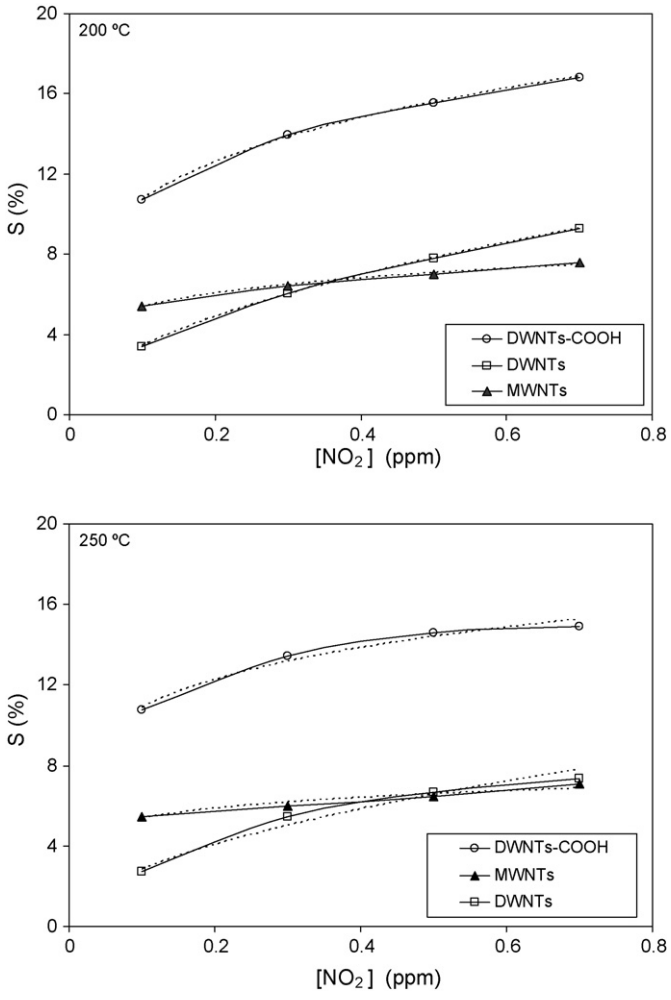

Fig. 9. Sensor calibration curves to NO_2 at 200 °C: experimental curve (solid lines) and fitting curve (dot lines).

Table 4
Parameters of sensor calibration to NO_2 according to relation $S = a[NO_2]^b$

T (°C)	a			b			R		
	S1	S2	S3	S1	S2	S3	S1	S2	S3
200	11.16	18.22	7.94	0.51	0.23	0.16	0.999	0.999	0.992
250	9.39	16.24	7.18	0.52	0.17	0.12	0.980	0.986	0.934

promising for their use as gas sensors due to their highly defective structure. On the contrary, NO_2 exposure to the employed highly conducting MWNT networks however led to smaller changes in the charge carriers, therefore resulting in lower sensor response and, consequently, in lower sensitivity values (Tables 2–4 and Fig. 7) [6,11,12,33]. Future work will focus on conveniently adjusting the MWNT network resistance during CNT airbrush deposition in order to efficiently utilize the defective structure of these MWNTs in NO_2 detection experiments.

Finally, sensor calibration curves for NO_2 detection at 200 and 250 °C in air atmosphere are shown in Fig. 9. For all tested sensors, the sensitivity depends on the gas concentration following the equation $S = a[NO_2]^b$, where a and b are coefficients calculated by curve-fitting of the response curves (Table 4). These coefficients are temperature and sensor material dependent. Very interestingly, at high operation temperatures, the CNT network sensitivity only slightly changed at high NO_2 concentrations. This observed sensitivity saturation can be explained in terms of fully occupation of NO_2 adsorption sites [13], and might therefore support the proposed dominant role of defects in the measured sensor response upon NO_2 exposure [11,13,14].

4. Conclusions

CNT networks have been efficiently employed as resistive sensors for NO_2 detection. The tested CNT networks provided good response to low NO_2 concentrations and an excellent selectivity with respect to interfering gases. Improved sensor responses were achieved after successive thermal treatments. Both the sensor response and recovery times are temperature dependent. The results described here suggest that CNT network sensitivity upon exposure to different gases can be conveniently tuned by suitably choosing the airbrushed CNT materials, and by simultaneously controlling both the CNT deposition rate and CNT transport properties, therefore offering fascinating opportunities for their use as sensor materials. Future work will focus in investigating the effect of CNT joints [13,34] and of the interaction of gas molecules with different functional groups in the CNT network sensor performance, as well as in improving the sensor recovery times.

Acknowledgments

This work has been supported by MEC (Spain, projects TEC2004-05098-C02-01/MIC and TEC2004-05098-C02-02/MIC, Programa I3 2006 8 0I 060) and the European Regional Development Fund (ERDF). The authors wish to thank Christine Würzburger of Heraeus S.A. for kindly providing the Heraeus MSP 769 substrates.

References

[1] R.H. Baughman, A.A. Zakhidov, W.A. De Heer, Science 297 (2002) 787–792.
[2] H.-Q. Nguyen, J.-S. Huh, Sens. Actuator B 117 (2006) 426–430.
[3] L. Valentini, I. Armentano, J.M. Kenny, C. Cantalini, L. Lozzi, S. Santucci, Appl. Phys. Lett. 82 (2003) 961–963.
[4] I. Sayago, E. Terrado, E. Lafuente, M.C. Horrillo, W.K. Maser, A.M. Benito, R. Navarro, E.P. Urriolabeitia, M.T. Martínez, J. Gutiérrez, Synth. Met. 148 (2005) 15–19.
[5] S. Chopra, A. Pham, J. Gaillard, A. Parker, A.M. Rao, Appl. Phys. Lett. 80 (2002) 4632–4634.
[6] J. Kong, N.R. Franklin, C. Zhou, M.G. Chapline, S. Peng, K. Cho, H. Dai, Science 287 (2000) 625–662.
[7] J. Breuer, F. Waidelich, C. Irtel Von Brenndorff, L. Sieverding, W. Rosendahl, W. Baden, M. Gass, J. Apitz, Eur. J. Pediatrics 156 (1997) 460–462.
[8] J. Meléndez, A.J. De Castro, F. López, J. Meneses, Sens. Actuator A 47 (1995) 417–421.
[9] www.nanocyl.com.
[10] I. Sayago, E. Terrado, M. Aleixandre, M.C. Horrillo, M.J. Fernández, J. Lozano, E. Lafuente, W.K. Maser, A.M. Benito, M.T. Martínez, J. Gutiérrez, E. Muñoz, Sens. Actuator B 122 (2007) 75–80.
[11] S. Santucci, S. Picozzi, F. Di Gregorio, L. Lozzi, C. Cantalini, L. Valentini, J.M. Kenny, B. Delley, J. Chem. Phys. 119 (2003) 10904.
[12] L. Valentini, L. Lozzi, C. Cantalini, I. Armentano, J.M. Kenny, L. Ottaviano, S. Santucci, Thin Solid Films 436 (2003) 95–100.
[13] J.A. Robinson, E.S. Snow, Ş.C. Bădescu, T.L. Reinecke, F.K. Perkins, Nano Lett. 6 (2006) 1747–1751.
[14] L. Valentini, F. Mercuri, I. Armentano, C. Cantalini, S. Picozzi, L. Lozzi, S. Santucci, A. Sgamellotti, J.M. Kenny, Chem. Phys. Lett. 387 (2004) 356–361.
[15] T. Sugai, H. Yoshida, T. Shimada, T. Okazaki, H. Shinohara, Nano Lett. 3 (2003) 769–773.
[16] Q. Liu, W. Ren, F. Li, H. Cong, H.-M. Cheng, J. Phys. Chem. C 111 (2007) 5006–5013.
[17] J.-F. Colomer, P. Piedigrosso, A. Fonseca, J.B. Nagy, Synth. Met. 103 (1999) 2482–2483.
[18] X. Lu, K.D. Ausman, R.D. Piner, R.S. Ruoff, J. Appl. Phys. 86 (1999) 186–189.
[19] D. Bom, R. Andrews, D. Jacques, J. Anthony, B. Chen, M.S. Meier, J.P. Selegue, Nano Lett. 2 (2002) 615–619.
[20] X.H. Chen, C.S. Chen, Q. Chen, F.Q. Cheng, G. Zhang, Z.Z. Chen, Mater. Lett. 57 (2002) 734–738.
[21] A. Fujiwara, K. Ishii, H. Suematsu, H. Kataura, S. Suzuki, Y. Achiba, Chem. Phys. Lett. 336 (2001) 205–211.
[22] A. Ansón, J. Jagiello, J.B. Parra, M.L. Sanjuán, A.M. Benito, W.K. Maser, M.T. Martínez, J. Phys. Chem. B 108 (2004) 15820–15826.
[23] L. Valentini, C. Cantalini, I. Armentano, J.M. Kenny, L. Lozzi, S. Santucci, Diamond Relat. Mater. 13 (2004) 1301–1305.
[24] W.-S. Cho, S.-I. Moon, K.-K. Paek, Y.-H. Lee, J.-H. Park, B.-K. Ju, Sens. Actuator B 119 (2006) 180–185.
[25] P.G. Collins, K. Bradley, M. Ishigami, A. Zettl, Science 287 (2000) 1801–1804.
[26] J. Kong, M.G. Chapline, H. Dai, Adv. Mater. 13 (2001) 1384–1386.
[27] M. Shim, A. Javey, N.W.S. Kam, H. Dai, J. Am. Chem. Soc. 123 (2001) 11512–11513.
[28] H. Chang, J.D. Lee, S.M. Lee, Y.H. Lee, Appl. Phys. Lett. 79 (2001) 3863–3865.
[29] W.-L. Yim, X.G. Gong, Z.-F. Liu, J. Phys. Chem. B 107 (2003) 9363–9369.
[30] M.D. Ellison, M.J. Crotty, D. Koh, R.L. Spray, K.E. Tate, J. Phys. Chem. B 108 (2004) 7938–7943.
[31] A. Ricca, C.W. Bauschlicher Jr., Chem. Phys. 323 (2006) 511–518.
[32] S. Peng, K. Cho, P. Qi, H. Dai, Chem. Phys. Lett. 387 (2004) 271–276.
[33] L. Valentini, C. Cantalini, L. Lozzi, S. Picozzi, I. Armentano, J.M. Kenny, S. Santucci, Sens. Actuator B 100 (2004) 33–40.
[34] L. Berhan, Y.B. Li, A.M. Sastry, E. Muñoz, M. Selvidge, R. Baughman, J. Appl. Phys. 95 (2004) 4335–4345.

Talanta 77 (2008) 556–560

Contents lists available at ScienceDirect

Talanta

journal homepage: www.elsevier.com/locate/talanta

MSFIA system for mercury determination by cold vapour technique with atomic fluorescence detection

A.M. Serra, J.M. Estela, V. Cerdà*

Group of Analytical Chemistry, Automation and Environment, Department of Chemistry, University of the Balearic Islands, E-07122 Palma de Mallorca, Spain

ARTICLE INFO

Article history:
Received 14 August 2007
Received in revised form 30 March 2008
Accepted 4 April 2008
Available online 22 April 2008

Keywords:
Hg determination
MSFIA
Cold vapour
Atomic fluorescence

ABSTRACT

A new multisyringe flow injection analysis system for mercury determination using cold vapour technique assembling with atomic fluorescence spectrometry is proposed.

The system consists of a multisyringe module as liquid driver, a gas–liquid separator, a gas dryer device and an atomic fluorescence detector. As reducing agent, 1% tin chloride solution is used. Standard solutions and carrier are prepared in 1% hydrochloric acid. An argon stream is employed as carrier gas for cold vapour technique.

The development of the smart analytical system is feasible due to the four internal gains of the atomic detector and the versatility of software used. According to the signal obtained, the software is able to choose the most suitable internal gain for sample analysis.

Four linear calibration curves (i.e. one for each internal gain) were obtained. The smart system developed allows to determine a wide concentration range from 120 to 0.006 $\mu g\,L^{-1}$ Hg. The detection limit ($3\sigma/S$) achieved is 0.002 $\mu g\,L^{-1}$. The relative standard deviation is inferior to 2% for each calibration curve. This system was validated by means of a solid reference material and it was applied to environmental samples successfully.

1. Introduction

Mercury hazards have been known since antiquity. In Roman times Pliny the Elder described clearly the symptoms of mercury poisoning in slaves who worked in mercury mines two millennia ago. Other more recent massive poisonings have been reported in Minamata Bay (1950) owing to consumption of fish with high mercury levels, and in Iraq (1960) for eating cereals treated with organomercurial fungicides. Among the toxic trace metals, mercury is one of the most hazardous environmental pollutants [1].

Atomic absorption spectrometry (AAS) and atomic fluorescence spectrometry (AFS) are the most widely used methods for mercury determination. A high sensitivity and selectivity are obtained when assembling both AAS and AFS with the cold vapour technique (CV).

Several flow analysis methodologies, such as flow injection analysis (FIA) [2], sequential injection analysis (SIA) [3], multicommuted flow analysis (MCFIA) [4] and, more recently, multisyringe flow analysis (MSFIA) [5] together with multipumping flow analysis (MPFA) [6] have been developed in order to automate chemical determination, increase sample throughput and reduce reagent consumption. Each flow analysis method presents its advantages and drawbacks.

Several flow methods for determination of mercury at trace levels using AAS or AFS have been developed for a great variety of samples (urine [7], fish [8,9], water [10,11], milk [12]).

In this new-approach MSFIA and CV–AFS were assembled to study the advantages of coupling this recent flow technique with a CV–AFS mercury detection system.

2. Experimental

2.1. Reagents

A Hg(II) stock solution of 1000 mg L^{-1} was prepared from $HgCl_2$ according to Standard Methods (APHA-AWWA-WPCF). A 10 mg L^{-1} Hg(II) stock solution was prepared weekly [13] in order to ensure its stability, 1 ml of 37% HCl was added to each 100 ml of total volume. Hg(II) working standard solutions were prepared daily in 1% (m/v) HCl from this stock solution.

A 1% (m/v) tin chloride solution was prepared daily in 1% (m/v) HCl dissolving the required amount of $SnCl_2{\cdot}2H_2O$ purchased from Merck (pro analysis, maximum 0.000001% Hg).

* Corresponding author.
E-mail address: victor.cerda@uib.es (V. Cerdà).

0039-9140/$ – see front matter © 2008 Elsevier B.V. All rights reserved.
doi:10.1016/j.talanta.2008.04.033

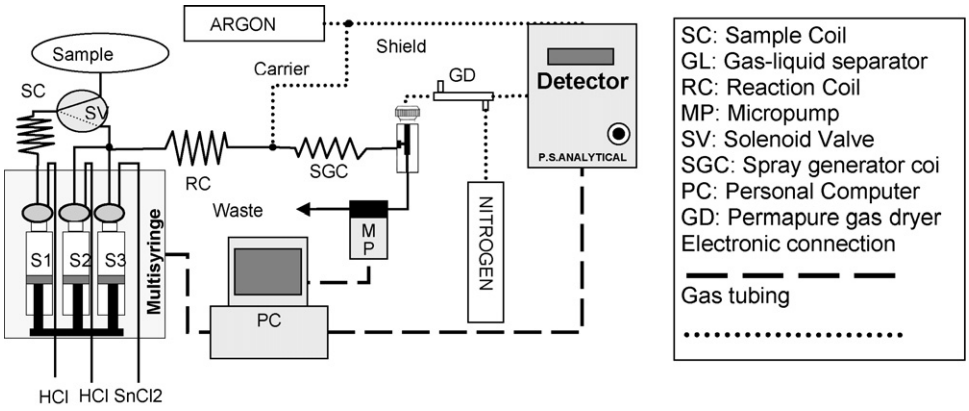

Fig. 1. MSFIA–CV–AFS system proposed for mercury determination.

A 1% (m/v) HCl solution was used as carrier. HCl minimum 37% puriss. p.a. was purchased from Riedel-de Haën (Seelze, Germany).

All solutions were made with deionised water purified by a Millipore equipment. All glassware used for preparing dissolutions was soaked in 10% (v/v) nitric acid solution and then rinsed with Millipore water.

2.2. Reagent purification

In order to obtain a lower blank signal, elimination of mercury traces from the carrier and reagents was necessary. The reducing solution was purified with a stream of nitrogen for 30 min [10] with constant stirring.

The impurity of mercury contained in the hydrochloric acid was calculated by the standard addition method. Its content was of 3.55 ± 0.28 μg Hg(II) L^{-1}.

To purify the carrier solution, a spatula tip of $SnCL_2{\cdot}2H_2O$ was added and then purged with a stream of nitrogen with constant stirring for 30 min [14]. In order to avoid these impurities in standards solutions, a 1% (m/v) HCl solution was passed through to resin column at 1 ml/min, before standards preparation. Purging after $SnCl_2$ addition cannot be used in standards solutions. Duolite® GT-73 resin from Supelco (Bellefonte, USA) was employed. Several authors have previously used this resin for mercury removal or preconcentration [15–17]. A methacrylate column 3 mm in diameter and 75 mm in length, provided with porous frit, was used to support the resin.

2.3. Apparatus

Fig. 1 shows the system set-up.

The main device is a multisyringe burette module with programmable speed (Multiburette 4S, Crison, Alella, Barcelona). In the proposed system, only three syringes were used (5, 5, and 2.5 ml). The multisyringe was equipped with an additional independent solenoid valve (Takasago Electric, Nagoya, Japan). When the valve is used a solenoid protection system (Sciware, Palma de Mallorca, Spain) is required for minimizing heat generation in order to prolong the lifetime of the solenoid valve.

The manifold for the sample and reagents treatment was built from 1.5 mm i.d. and 0.8 mm i.d. PTFE tubing. The 1.5 mm i.d. tubing was used for reagents pick up, sample coil, spray-generation coil and gas–liquid separator removal tubing. At the same time a sample and reagent mixer was built with 0.8 mm i.d. tubing. A mixing tee was used to allow gas–liquid mixing and connection with the spray-generation coil.

A gas–liquid separator from PerkinElmer model B0507959 was selected. The selection was based on a study of different kinds of liquid separators [18]. An exchangeable PTFE membrane (25 mm diameter, 1 μm, Schleicher and Schuell, Dassel, Germany) placed in the screw cap of the separator prevents liquid from being carried into the detector cell. The removal of liquid excess from the gas–liquid separators was controlled with a solenoid micro-pump (Biochem Valve Inc., Boonton, NJ, USA).

The solenoid micro-pump was computer controlled through a module (Sciware, Palma de Mallorca), constituted by an I/O digital interface card, eight digital relay output channels and an internal 12 V power source required to activate the solenoid micro-pumps. This module was connected to a PC through an RS485/RS232 interface.

A gas-dryer unit from Perma Pure (Toms River, NJ, USA) was used. The water moves through the membrane wall and evaporates into the surrounding air or gas.

A mercury atomic fluorescence spectrophotometer (P.S. Analytical model 10.023, Orpington, UK) was employed as detector. This spectrophotometer presents four internal gains and an external fine gain, which allows working on a large concentration range.

System control, data acquisition and processing were performed using the software package Autoanalysis 5.0 [19] (Sciware, Palma de Mallorca).

2.4. General procedure

An extra three-way solenoid valve is connected to a coil and syringe S1 for sample pick-up. Syringe S1 dispenses the sample with 1% (m/v) HCl solution. Syringe S2 dispenses 1% (m/v) HCl solution used as carrier. Syringe S3 is used to dispense the reducing solution. In order to attain a good reaction efficiency the flow is stopped in the reaction coil for 30 s. This stop-flow procedure provides two advantages. First dispersion ceases while chemical reaction continues, and second the consumption of solutions and waste generation are much reduced [20].

Then the mixture is impelled with the carrier to a three-way connector fitting, where the mixture is merged with an argon continuous stream. The generated spray allows an optimal separation of elemental mercury from the liquid phase. The gas–liquid mixture is separated in a gas–liquid separator. Gas phase, which contains elemental mercury, comes out of the gas–liquid separator through PTFE membrane to the mercury detector. Carrier gas humidity is removed by a Perma Pure device preventing the entrance of water vapour into the detection cell and its interference by quenching [21]. Liquid phase is removed by means of a software controlled

micropump in order to keep a constant liquid volume into the gas–liquid separator.

3. Results and discussion

MSFIA systems combine the advantages of the FIA methodologies with the versatility, robustness and reagents saving of SIA.

Tin chloride was used in our experiments as a reducing agent due to its lower cost in relation to $NaBH_4$. Also, it does not generate H_2 during the course of mercury reduction, which could produce a quenching effect on the mercury fluorescence signals [22].

In order to remove the liquid excess from the gas–liquid separator we have used a solenoid micro-pump. Micro-pumps produce constant stroke volumes at distinct pulse frequencies with high reproducibility ensuring the attainment of very stable flow rates.

A commercial AFS detector was selected for its relative inexpensive cost, extreme sensitivity (ultratrace levels) and selectivity. Argon was used as a cold vapour carrier gas. Argon is the best carrier gas for fluorescence measurements due to its small cross-section for quenching [22].

3.1. Construction of the MS–MPFIA system

The selected values of the flow system parameters in terms of sensitivity and repeatability were determined by a univariate approach. Although this method requires a great number of experiments, it allows obtaining detailed information about the behaviour of the system. On the other hand, a multivariate approach only provides knowledge of the main effects [23].

To prevent sample dilution a 2.5 ml syringe was used to dispense the reducing reagent. Multisyringes enable to simultaneously dispense sample and reagents, this characteristic allowing to obtain a good mixing of the solutions. Later, the mixture is impelled to the spray-generation coil at a high flow rate (12 ml/min), to avoid liquid phase dilution in a large argon volume, obtaining a higher sensitivity.

Since argon flow variation produces base line instabilities, different three-way fittings were tested. The best one was to inject the liquid and gas phases in the same direction, thus, a low base line variation was obtained. The selected three-way fitting can be observed in Fig. 2.

Finally, it should be noted that the separator–detector coil must be as short as possible in order to reduce the elemental mercury dispersion in the argon flow.

3.2. Mercury reduction

3.2.1. Length of the reaction coil and sample volume

In order to determine the best length of reaction coil different lengths between 1 and 6 meters were tested. For this purpose, 1 μg Hg(II) L^{-1} in 3% (m/v) HCl, 3% HCl solution and 1% (m/v) $SnCl_2 \cdot 2H_2O$ in 3% (m/v) HCl were used, being this initial condition obtained from Leal et al. [8]. A 10 cm spray coil, and 300 ml/min argon flow rate were used to obtain the signal. Results showed that the increase of the reaction coil produced a signal increase up to a length of 3 m, the height of signal remaining constant for longer lengths. This behaviour is similar to that observed by Reis et al. [10,24], Leal et al. [8] and Gallignani et al. [7] in their respective reports.

3.2.2. Hydrochloric acid and tin chloride concentrations

Concentrations of hydrochloric acid, and reducing agent were optimised. A 300 ml/min argon flow rate, 1 m spray coil and a PTFE membrane were used for mercury extraction.

The effect of hydrochloric acid on the 1 μg/L Hg^{2+} signal was tested within the 0.1–10% (m/v) range. The signal remained constant up to 4% HCl. For concentrations higher than 4% HCl the signal decreased. A concentration of 1% HCl was selected for furthers experiments.

Tin chloride concentrations were tested within the 0.03–2% (m/v) range. For higher concentrations than 0.5% tin chloride the height of signal remained constant. Finally, we decided to use a 1% tin chloride solution, for being more stable than the 0.5% tin chloride solution for a longer time.

3.3. Elemental mercury extraction

3.3.1. Different spray-generation coils

Since the base line is very sensitive to Ar flow rate variation, 0.8, 1, and 1.5 internal diameters were tested. For this purpose 1 μg Hg L^{-1} in 1% HCl (m/v), 1% (m/v) tin chloride and 1% (m/v) hydrochloric acid as carrier solution were prepared. A 300 ml/min argon flow rate and a reaction coil 3 m long were used.

The best gas liquid mixture and the lowest resistance to the spray flow were obtained by 1.5 mm i.d.

Different lengths, from 57 to 200 cm, of spray-generation coil were tested. The signal increases with the length of the spray coil up to 100 cm, the signal remaining constant for longer values. A 100 cm long and 1.5 mm i.d spray-generation coil was selected for further experiments.

3.3.2. Influence of argon flow rate

Influence of the argon flow rate on the signal was assessed under the following conditions: 1 μg L^{-1} Hg^{2+} in 1% HCl, a carrier with the same HCl concentration, a 1% $SnCl_2$ solution, a 100 cm spray coil, and a 3 m reaction coil.

The argon flow rate was evaluated within the 47–250 ml Ar/min range, the best interval resulting between 100 and 122 ml Ar/min. A worse extraction of mercury from the liquid phase is obtained with lower argon flow rates. A dilution of mercury vapour and the decrease of the residence time of the analyte in the detection cell are obtained with higher argon flow rates. In Fig. 3 below three different behaviours can been observed.

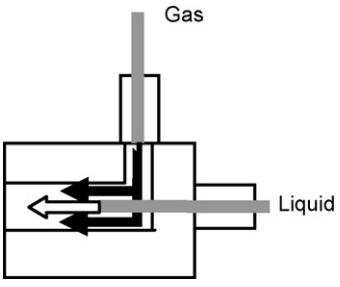

Fig. 2. Gas–liquid mixer.

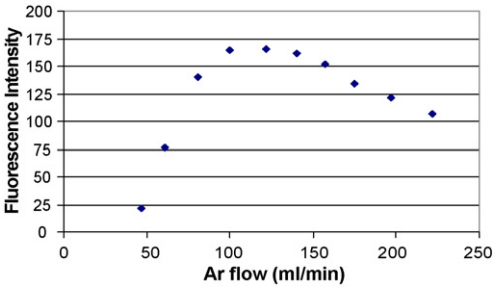

Fig. 3. Influence of argon flow rate.

Table 1
Analytical parameters

	Gain			
	$G=1$	$G=10$	$G=100$	$G=1000$
Slope	1.4349	15.2816	145.9703	1571.738
Intercept	0.9297	0.4627	1.3970	21.2833
Linear range (μg/L)	1–120	0.1–12	0.01–1.2	0.003–0.1

3.3.3. Flow rate through the spray-generation coil

The effect of the sample flow rate through the spray-generation coil on the analytical signal was evaluated. For this purpose 1 μg Hg L^{-1} of Hg^{2+} in 1% HCl, the same HCl concentration for the carrier and a 1% $SnCl_2$ solution were prepared. A 3 m reaction coil, 1 m spray coil and a flow rate of 110 ml/min were selected as instrumental conditions.

Different flow rates were tested within the 6–13 ml/min range. The best sensitivity was obtained at 12 ml/min. For lower flow rates the signal decreases because elemental mercury is extracted in a larger gas volume.

3.3.4. Different devices for moisture elimination

Different devices were tested in order remove moisture from the gas phase, since water quenches mercury fluorescence [21]. A PTFE membrane was the first tested device according to the selected gas–liquid separator. Only a 4.8% signal increase is produced with the use of this membrane compared to the system without any device for moisture elimination.

A Perma Pure LLC system was also tested and an 18.1% increase of the signal was attained compared to the system without any device for moisture elimination.

3.4. Analytical parameters

The analytical parameters were calculated under the selected experimental conditions.

The detector presents four internal gains (1, 10, 100 and 1000), and the anlyst can change this gain at the beginning of the method in order to modify the instrument sensitivity. Four different analytical curves were obtained by changing the instrumental gain. The obtained results are shown in Table 1.

Correlation coefficients between 0.9998 and 0.9993 and R.S.D. lower than 2% are showed by four calibration curves. The detection limit is 0.002 μg/L Hg, which was obtained by $G=100$. A worse detection limit, due to higher noise in the lectures, was obtained by $G=1000$.

LOD was calculated as three times the standard deviation of ten blank signals, divided by the slope of the calibration curve ($3\sigma/S$) for gains 10, 100 and 1000. Since for gain 1 calibration we had no blank signal, σ was calculated from the following equation:

$$\sigma_{yx}^2 = \frac{\sum y^2 - a\sum y - b\sum xy}{n-2}.$$

where "*a*" and "*b*" are the intercept and slope of the calibration curve, respectively, and "*n*" is the number of signals. Relative standard deviations (R.S.D.) were evaluated from ten successive lectures of 60, 6, 0.6 and 0.03 μg L^{-1} for gains 1, 10 100 and 1000, respectively.

Table 2
Results of the analysis of reference material using the proposed method

Sample	Certified value	Obtained value	*n*
DORM-2 (mg Hg/kg)	4.64 ± 0.26	4.73 ± 0.26	3

3.5. Smart system

Thanks to the conditional commands of Autoanalysis, the development of smart analytical systems [25–27] is feasible. According to the signal obtained from a sample, the Autoanalysis software is able to call different analysis procedures. This property enables to change the instrumental gain until the signal lies in the appropriate range of a calibration curve.

A large concentration range was determined with this smart system, from 120 to 0.006 μg Hg L^{-1}. The 0.006 value is the quantification limit, was calculated from ($10\sigma/S$).

3.6. Analysis of reference materials and real samples

The proposed technique was validated by the analysis of a certified solid reference material (fish muscle-DORM-2, National Research council, Canada). The reference material was digested in a high performance microwave digestion unit, model MLS 1200 mega from Milestone. Taking into account the possible presence of oxidants in the system after microwave digestion, a reducing solution was used as described by Leal et al. [8].

Three replicates were analysed, each result being calculated from four injections. As can be seen in Table 2, the obtained results are in good agreement with the certified ones.

In order to confirm that there are no significant differences between the experimental and the certified values, the *t*-test was calculated. Our $t_{exp} = 0.5995$ is lower than $t(0.05; f = n-1) = 4.3027$, thus we accepted that there is no significance difference between the obtained value and the certified one.

In order to evaluate the usefulness of the proposed method to determine Hg in some environmental samples, the recovery of spiked samples was tested. Three types of environmental samples were analysed: groundwater, rain leachates from a demolition recycling plant and the slag from an urban solid waste incinerator plant. The obtained results and recoveries are depicted in Table 3.

All environmental samples were put in storage in acidic and oxidant conditions to prevent mercury losses [28]. Previously to samples analysis, oxidant conditions must be removed with the addition of some drops of a saturated solution of ascorbic acid until elimination of the yellow colour from dichromate.

3.7. Interference study

In the present work, the influence of some contaminant ions on the determination of 1 μg L^{-1} Hg was evaluated. Our results are similar to previous works developed by others authors [11,22]. Se^{6+} and Se^{4+} show no interferences up to 1 and 100 μg L^{-1} respectively.

Table 3
Results of the analysis of environmental samples using the proposed method

Real sample	[Hg] (μg L^{-1})	Added [Hg] (μg L^{-1})	Found [Hg] (μg L^{-1})	Recovery (%)
Groundwater	0.331 ± 0.002	1	1.300 ± 0.011	97.7
Leachates	0.107 ± 0.014	1	1.084 ± 0.005	97.9
Slag[a]	0.567 ± 0.021	1	1.522 ± 0.043	97.1

[a] Recovery was determined from the microwave acidic digested slag.

Table 4
Comparison results obtained by multisyringe flow injection system (MSFIA), multicommuted flow system (MCFIA) and Flow injection system (FIA)

Parameter	FIA	MCFIA-1	MCFIA-2	MSFIA
Detection limit (ng L^{-1})	2.6	2	0.9	2
Linear range (μg L^{-1})	0–10	0–1.5	0–1.5	0–120
%R.S.D.	3.2	0.13	0.5	<2
Injection throughput (h^{-1})	102	63	43	30
Sample volume (ml/inj)	0.6	0.42	3.33	1
Reductant consumption (ml/inj)	1.5	0.83	3.75	1.25
Ar flow rate	500	240	240	110

The tolerable amounts of I^-, Br^- and S^{2-} were 1 mg L^{-1}, 10 mg L^{-1} and 1 μg L^{-1}, respectively.

3.8. Comparison between different flow techniques using CV–AFS detection: FIA, MCFIA and MSFIA

A comparison of the results obtained by the authors using the FIA–CV–AFS method [9], MCFIA–CV–AFS [10] and the proposed MSFIA–CV–AFS system has been carried out. In the MCFIA system two manifolds were compared. MCFIA-1 with reading time 30 s and sampling time 5 s and MCFIA-2 with reading time 40 s and sampling time 40 s were chosen to compare with our system.

As can be seen in Table 4, the MSFIA detection limit is of the same order as that of MCFIA and FIA systems. The smart MSFIA system allows the largest linear range. In the MSFIA system the injection throughput is lower than that of MCFIA and FIA systems due to the delay time involved during the syringe pick-up, furthermore, large sample volumes increase the sensitivity but also the analysis time [7,8].

4. Conclusions

The proposed smart MSFIA system was adapted and set up for mercury determination. The main operational parameters of the system were studied. The multisyringe module and the constructed manifold allow an efficient sample introduction. The smart MSFIA system is simple, robust and practical. It allows a wide linear range and a low detection limit without requiring any preconcentration steps. MSFIA shows a lower injection throughput against MCFIA and FIA systems, but it prevents the drawbacks involved in the use of peristaltic pumps. The proposed technique was successfully applied to mercury determination in waters, environmental samples and reference solid materials, which were previously digested in a microwave digestion unit.

Acknowledgements

The authors acknowledge the Ministerio de Educacion y Ciencia, for the financial support to projects CTQ2004-01201 and CTQ2004-03256.

References

[1] M. Leermakers, W. Baeyens, Ph. Quevauviller, M. Horvat, Trends Anal. Chem. 24 (2005) 383.
[2] J. Ruzicka, Anal. Chim. Acta 78 (1975) 145.
[3] J. Ruzicka, G.D. Marshall, Anal. Chim. Acta 273 (1990) 329.
[4] B.F. Reis, M.F. Giné, E.A.G. Zagatto, J.L.F.C. Lima, R.A. Lapa, Anal. Chim. Acta 293 (1994) 129.
[5] V. Cerdà, J.M. Estela, R. Forteza, A. Cladera, E. Becerra, P. Altamira, P. Sitjar, Talanta 50 (1999) 695.
[6] R.A.S. Lapa, José L.F.C. Lima, Boaventura F. Reis, João L.M. Santos, Elias A.G. Zagatto, Anal. Chim. Acta 466 (2002) 125.
[7] M. Gallignani, H. Bahsas, M.R. Brunetto, M. Burguera, J.L. Burguesa, Y. Petit de Peña, Anal. Chim. Acta 369 (1998) 57.
[8] L.O. Leal, O. Elsholz, R. Forteza, V. Cerdà, Anal. Chim. Acta 573–574 (2006) 399.
[9] Li-Jun Shao, Wu-Er Gan, Quina-De Su, Anal. Chim. Acta 562 (2006) 128.
[10] B.F. Reis, E. Ródenas, J. Sancenón, A. Morales, M. de la Guardia, Talanta 60 (2003) 809.
[11] H. Morita, M. Sugimoto, S. Shimomura, Anal. Sci. 6 (1990) 91.
[12] P. Cava-Montesinos, E. Ródenas-Torralba, A. Morales-Rubio, M. Luisa Cervera, M. De la Guardia, Anal. Chim. Acta 506 (2004) 145.
[13] E. Ramalhosa, S. Rio Segade, E. Pereira, C. Vale, A. Duarte, Anal. Chim. Acta 448 (2001) 135.
[14] S. Mandal, A.K. Das, Atom. Spectrosc. 3 (1982) 56.
[15] P. Pohl, B. Prusisz, Anal. Sci. 20 (2004) 1367.
[16] S. Chiarle, M. Ratto, M. Rovatti, Water Res. 34 (11) (2000) 2971.
[17] K.H. Nam, S. Gomez-Salazar, L.L. Tavlarides, Ind. Eng. Chem. Res. 42 (2003) 1955.
[18] I.D. Brindle, S. Zheng, Spectrochim. Acta B 51 (1996) 1777.
[19] E. Becerra, A. Cladera, V. Cerdà, Lab. Rob. Autom. 11 (1999) 131.
[20] J. Ruzicka, Anal. Chim. Acta 261 (1992) 3.
[21] C.G. Freeman, M.J. McEwan, R.F.C. Claridge, L.F. Phillips, Trans. Faraday Soc. 66 (1970) 2974.
[22] H. Morita, H. Tanaka, S. Shimomura, Spectrochim. Acta B 50 (1995) 69.
[23] J.C. González, I.L. Lavilla, C. Bendicho, Talanta 59 (2003) 525.
[24] B.F. Reis, E. Rodenas-Torralba, J. Sancenon-Buleo, A. Morales-Rubio, M. De la Guardia, J. Anal. At. Spectrom. 17 (2002) 537.
[25] C. Pons, R. Corteza, V. Cerdà, Anal. Chim. Acta 524 (2004) 79.
[26] C. Pons, M. Miró, E. Becerra, J.M. Estela, V. Cerdà, Talanta 62 (2004) 887.
[27] L. Ferrer, J.M. Estela, V. Cerda, Anal. Chim. Acta 573–574 (2006) 391.
[28] Water quality, sampling—International Standard, ISO 5666.

Talanta 77 (2008) 551–555

Contents lists available at ScienceDirect

Talanta

journal homepage: www.elsevier.com/locate/talanta

MultiSimplex optimization of on-line sorbent proconcentration and determination of iron by FI-AAS and microcolumn of immobilized ferron

Farid Shakerian, Shayessteh Dadfarnia*, Ali Mohammad Haji Shabani, Masoud Rohani

Department of Chemistry, Faculty of Sciences, Yazd University, 89195-741 Yazd, Iran

ARTICLE INFO

Article history:
Received 18 September 2007
Received in revised form 15 March 2008
Accepted 17 March 2008
Available online 25 March 2008

Keywords:
Iron determination
MultiSimplex optimization
Preconcentration/separation
FI-AAS

ABSTRACT

A simple flow injection on-line separation and proconcentration system for determination of iron in milk and water samples were developed. Ferron was physically immobilized on alumina particles in the pH range of 2.5–6 and was used as sorbent in microcolumn preparation. Deposition of iron was effected by processing a standard or solution of analyte at pH range of 3–6 on the microcolumn. Injection of 300 μl of HNO_3 (5 mol l^{-1}) served to elute the retained species to FAAS. Different factors affecting the performance of the system were optimized by MultiSimplex and univariable methods. MultiSimplex program based on the simplex algorithm allowed the simultaneous study of the variables affecting immobilization, sorption or elution process. The capacity of the sorbent under working condition was found to be 989.0 μg irons per gram of packing material. A sample volume of 20 and 40 ml resulted in preconcentration factors of 65 and 129, respectively. Precision (n = 6) at 125 and 50 μg l^{-1} were 2.0 and 2.9%, respectively. With 20 ml sampling volume a detection limit of 1.06 μg l^{-1} was determined. The method was applied to determination of iron in tap water, river water, rain water, spring water, infant dry formula milk, human and cow milk. The accuracy was assessed through recovery experiments, independent analysis by furnace atomic absorption, and analysis of certified reference alloy.

1. Introduction

Iron is an essential element for all forms of life, i.e. it is a cofactor in many enzymes and essential for oxygen transport and electron transfer. Although daily requirements for iron are 8–18 mg for man and woman, respectively [1], it is potentially toxic in excess concentration because of its pro-oxidant activity. Milk is the only source of nutrients for newborns and is close to ideal food due to its composition and availability. In addition to its macronutrients, i.e. protides, glucides, and lipids, milk also contains micronutrients, i.e. vitamins and elements that are absolutely essential during the first months of baby's life, since it is the only source of nutrients. This is particularly true for micronutrients that are not stored by the fetus during its growth inside the uterus [2]. Iron is in the group of essential elements that serves to protect the baby from potential deficiency during the first 4–6 months of his/her life. This clearly demonstrated the importance of the determination of traces of iron in milk. The concentration of iron in human and cow milk is relatively low ranging from 0.2 to 0.8 mg l^{-1} [3]. In addition, determination of trace amount of iron in milk is not a trivial task because of the complexity of the emulsion. On the other hand, the extremely low concentration of dissolved iron in water is one of the important aspects that characterize the quality of drinking and clinical water. Thus for determination of iron in samples such as water and milk by flame atomic absorption spectrometry a separation/preconcentration step is required to improve its detection limit and selectivity of determination. Different solid phase extraction/FAAS for determination of iron have been developed [4–8]. However, among different method used for separation and preconcentration of metal ions, on-line separation and preconcentration such as flow injection coupled with atomic absorption spectrometry have received considerable attention [9,10]. Automation of the sample pretreatment and manipulations within the manifold have increased sample throughputs and decreased the potential for sample contamination, which is critical in trace analysis. The sorbents that have most often been used for flow injection (FI) on-line preconcentration/sorbent extraction of metal ions are C_{18}-silica [11–13], functionalized silica [14–16], basic and acidic alumina powder [17–19], activated carbon [20,21], polyurethane foam [22], and microcrystalline naphthalene impregnated with stearic acid [23]. Organic ligands such as 1, 5-diphenyl carbazone [24], 2-nitrose-1-naphthol [25], DDTC [26], salens [27], oxine [28], immobilized on surfactant-coated alumina and calmagite immobilized on Amberlite XAD-2 [29] have also been used for preparation of microcolumn in FI-AAS. However, to the best of our knowledge, there have been a few reports on direct

* Corresponding author. Tel.: +98 3518212795; fax: +98 3518212793.
E-mail address: sdadfarnia@yazduni.ac.ir (S. Dadfarnia).

0039-9140/$ – see front matter © 2008 Elsevier B.V. All rights reserved.
doi:10.1016/j.talanta.2008.03.015

immobilization of ligands on alumina powder [30,31], so it was appropriate to investigate, the possibilities of direct immobilization of 8-hydroxy-7-iodoquinoline-5-sulfonic acid (ferron) on alumina powder. Ferron is a well known classical ligand, with a sulfonic group, and had been used for spectrophotometeric determination of some metal ions including iron [32,33], but its use in solid phase extraction is rare.

The MultiSimplex program described elsewhere [34,35] is designed as a true multivariate non-linear optimization tool that combines the modified simplex method [36] with the fuzzy set theory [37] by means of the membership functions or the point response measure called the aggregated value or membership. The advantage of MultiSimplex is that it allows simultaneous optimization of several response signals and considers the interaction among variables. MultiSimplex optimization is easy to follow and has been already used in some analytical application [34,38,39]. To do the MultiSimplex optimization, the variables, the range of each variable and the responses that are going to be followed are defined. Then MultiSimplex suggests a $K+1$ number of experiments; where K is the number of variables to be studied. Once the experiments are carried out, the answers of the experiments are introduced and MultiSimplex suggests one new experiment. The process is continued until the optimum conditions are reached. In order to measure the closeness to the optimum, MultiSimplex makes use of the "membership value" [36]. This value ranges from 0 to l and takes into account the results of all responses considered in the optimization. Optimized conditions are achieved when the membership value is close to 1. The optimization procedure includes a re-evaluation rule that means, for every certain number of experiments, a previous trial is repeated experimentally [34].

In this work, ferron was directly immobilized on alumina powder, and a rapid on-line system for enrichment and determination of iron by flame atomic absorption spectrometry incorporating a microcolumn of immobilized ferron was designed. Furthermore, the factors effecting the immobilization of ligand, deposition and elution steps were optimized by MultiSimplex program and univariable method. Finally, the procedure was applied to determination of iron in water and milk samples.

2. Experimental

2.1. Reagents

All chemicals were of highest purity available from Merck chemical company and were used as received and deionized water used throughout. A stock 1000 μg ml^{-1} of iron(II) or iron(III) was prepared by dissolving appropriate amount of $(NH_4)_2Fe(SO_4)_2{\cdot}6H_2O$ or $Fe(NO_3)_3{\cdot}9H_2O$ in water. Working solutions were prepared daily from the stock solutions by serial dilution.

Alumina particles (γ type, 10–50 μm, chromatographic grade, Merck, Darmstadt, Germany) was purified by shaking with 5 mol l^{-1} nitric acid and washing three times with water. Ferron (Fluka) were used without further purification.

2.2. Apparatus

A Buck Scientific atomic absorption spectrometer (Model 210 VGP, USA) was used for all absorption measurements. An iron hollow cathode lamp and air–acetylene flame was used for all measurements. The operating conditions were as follows: wavelength 248.3 nm, slit width 0.2 nm, lamp current 8.2 mA. The absorbance time response was monitored on an x–t chart recorder (L-250) and quantitative analysis was based on measurement of the peak height of transient signals. The flow injection system used were as described elsewhere [26] and consists of peristaltic pump (Ismatic, MS-REGLO/8-100 Switzerland), rotary injection valve (Rheodyne, CA, USA) and microcolumn of ferron immobilized on alumina (PTFE Tube 4 cm × 2 mm i.d.). The MultiSimplex program was downloading from www.MultiSimplex.com site.

2.3. Immobilization of ferron

Fifty milliliter of water and ~0.1 g of ferron was added to 1.0 g of alumina, and the solution was mixed with a magnetic stirrer for 10 min. The mixture was then filtered through Millipore filter, washed, air-dried, and was kept in a closed bottle before use. The microcolumn was fabricated by using PTFE (Teflon) tubing (4 cm in length, internal diameter of 2 mm) and contained immobilized ferron on alumina (~80 mg) and the end of the tube was fitted with foam to hold the sorbent. It was stable for more than 2 months.

2.4. Preparation of milk

To 10 ml of human or cow's milk, few drops of concentrated nitric acid were added, and the sample was centrifuged for few minutes. Then the supernatant solution was taken, the pH was adjusted to ~5 by ammonium hydroxide, and was diluted to 100 ml in a volumetric flask. The solution was then analyzed according to the given procedure.

For analysis of infant dry formula milk, 0.5 g of milk powder was dissolved in water the protein was separated after addition of few drops of concentration nitric acid. The pH of supernatant was adjusted to ~5 and was diluted to 250 ml. The sample was then treated according to the given procedure.

2.5. Water samples

The samples were filtered through a Millipore filter; the pH and NaCl concentration of solutions were adjusted to ~5 and 0.4 mol l^{-1}, respectively, and was treated according to the given procedure.

3. Procedure

The flow injection manifolds used were as described before (Fig. 1) and were connected directly to the nebulizer inlet tubing. The single-line system (Fig. 1a) was used to study analyte

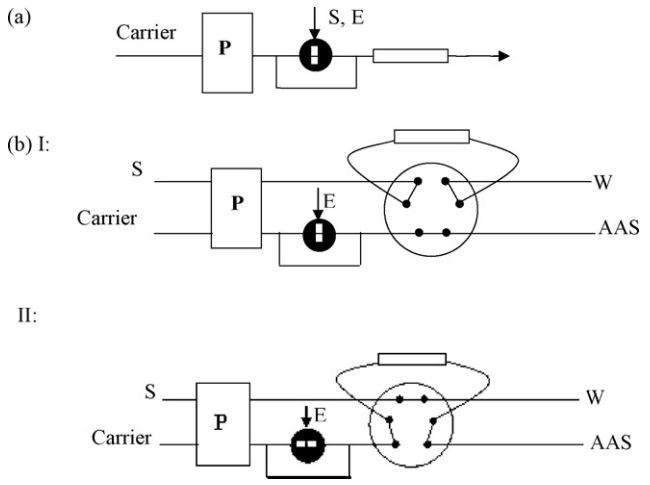

Fig. 1. Schematic diagram of the flow system used for preconcentration and determination of iron. (a) Single line FI system. (b) Two line FI system, I: sample loading; II: injection; S, sample; P, peristaltic pump; C, microcolumn and W, waste. Valve positions.

Table 1
MultiSimplex optimization of variables of group 1 (preparation of sorbent)

Variable	MultiSimplex method					Univariable method
	Lower limit	Upper limit	Reference value	Step	Optimum value	
pH of ligand solution	2.0	10.1	4.67	1.0	3.7	2.5–6.0
Amount of ligand(g) per gram of alumina	0.001	0.1	0.1	0.03	0.1	0.075–0.2

breakthrough and undertake initial method development studies. The two-line FI manifold (Fig. 2b) was used to process real samples and obtain performance data. The carrier and eluent solution were water and nitric acid (300 μl, 5 mol l^{-1}), respectively. The microcolumn was located in the sample loop of injection valve, so the sampling could be performed "off-line" and preventing matrix constituents entering the AAS. At the end of sampling, the valve was switch "on-line" and the eluent was injected with the use of second valve to effect elution.

The pH and NaCl concentration of solutions were adjusted to ~5 and 0.4 mol l^{-1}, respectively. With reference to FI manifold (Fig. 1a and b), standard solution or samples were passed through the ferron microcolumn (Fig. 1a, sample volume 300 μl, Fig. 1b, volume based sampling (e.g. 20 ml at flow rate of 3 ml min^{-1})) to effect the deposition of the analyte. The retained iron was then eluted by injection of nitric acid (300 μl 5 mol l^{-1}) and transported to flame atomic absorption spectrometer for quantization (for the system in Fig. 1b, the injection valve was switched to bring the microcolumn "on-line" prior to injection of eluent). The transient signals were monitored for quantitative analysis.

4. Results and discussion

It is known that molecules with negatively charged SO_3^- group such as sodium dodecyl sulfate strongly adsorb on the positively charged γ-alumina surface in the pH range of 1–6 [40]. Therefore, it was appreciated to investigate the possibility of immobilization of ligands such as ferron with an SO_3^- group on γ-alumina. It was found that when ferron is mixed with particle of alumina in water, the ligand adsorb on the positively charge alumina surface and the color of alumina change from white to yellow. Furthermore, the resulting sorbent was characterized by employing Fourier transform infrared spectrometry (FT-IR). The characteristic IR bands in cm^{-1} for immobilized ferron were: 1456, 1489 and 1558 (skeleton bands of aromatic rings); and in compare to free ligand, the broadness of OH streching and sharpness of C=N stretching was reduced, which further support the loading of the ferron on alumina.

The adsorption capability of sorbent for iron was examined, and was found that in the presence of sodium chloride, immobilized ferron have high affinity for retention of Fe(II) and Fe(III). This observation may be explained on the bases that ferron form negatively charged complexes with iron ions, so the presence of Na^+ neutralize its charges [41]. Next, the desorption of retained iron was studied by using different eluent such as, ethanol, methanol, dioxane, DMF, acetone, sodium acetate (4 mol l^{-1}), alcoholic solution of 1,10-phenathroline (2%), ammonium thiocyanate (5 mol l^{-1}), EDTA, hydrochloric and nitric acid (5 mol l^{-1}). Nitric and hydrochloric acid were found as most suitable eluent for this purpose, and nitric acid was selected as eluent in this study. With other examined eluent, complete recovery of analyte were not possible (with organic solvent, the recovery were ~0%, and with other eluent the recovery were between 36 and 40%). Then the factors affecting the performance of the system were optimized by MultiSimplex program and the results was compared with the results of univariable optimization method.

In order to do optimization by MultiSimplex program, the factors affecting the procedure were divided into three independent groups and the MultiSimplex program was used for optimization of the variables in each group. The groups and the variables were as follows:

Group 1; preparation of sorbent; variables were: pH and the amount of ligand per gram of alumina.
Group 2; retention of analyte; variables were: pH and NaCl concentration, flow rate and microcolumn length.
Group 3; elution of analyte; variables were: eluent concentration, flow rate and volume of eluent.

In MultiSimplex program, modified simplex method was used as appropriate algorithm with coefficients of; reflection (R) = 1, contraction = 0.5, contraction of R = 0.5, and expansion of R = 2. To reduce the possibility of local optimization of MultiSimplex, initially, the uniform design (UD) was used. The uniform design has the advantage of space filling, thus the selected experimental points are scattered uniformly in a bonded region of experimen-

Table 2
MultiSimplex optimization of variables of group 2 (retention of analyte)

Variable	MultiSimplex method					Univariable method
	Lower limit	Upper limit	Reference value	Step	Optimum value	
[NaCl] (mol l^{-1})	0.005	0.5	0.356	0.15	0.4	0.05–0.5
Flow rate (ml min^{-1})	1.0	6.0	3.2	0.7	2.8	1–3
Column length (cm)	2.0	5.0	4.6	0.7	4.0	3–5
Sample pH	3.0	10.0	3	1	5.0	3–6

Table 3
MultiSimplex optimization of variables of group 3 (elution of analyte)

Variable	MultiSimplex method					Univariable method
	Lower limit	Upper limit	Reference value	Step	Optimum value	
Eluent flow rate (ml min^{-1})	1.0	3.4	1.6	1	2.4	2–4
Eluent volume (μl)	200.0	600.0	440	100	356.7	200–600
Eluent concentration (mol l^{-1})	1.0	6.0	6	1	5.2	>5

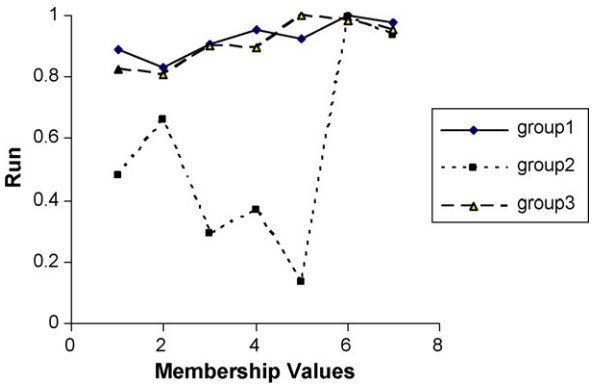

Fig. 2. Membership values of the experiment performed by MultiSimplex optimization; group 1: preparation of sorbent; group 2: retention of analyte; group 3: elution of analyte.

tal domain [42] and the sample produced is high representation of the studied experimental domain. The best response obtained by UD was selected as the reference value for MultiSimplex program. Then the upper and lower limit was defined, the program was run and the experiments were performed according to the condition suggested by MultiSimplex program and the process was continued until the optimum conditions were reached, i.e. until the membership value get close to 1 (Fig. 2). The defined parameter for variables of each group and the optimum results obtained are summarized in Tables 1–3; the results of optimization by univariable method are also given in the last column. Generally the results (Tables 1–3) show that the optimum value obtained by MultiSimplex program is within the optimum range of univariable method; thus the results of two methods support each other. Furthermore, the results of Table 1 shows that the best pH for adsorption of ferron on alumina is 3.72 (or pH range of 2.5–6) which is in agreement with the earlier report for adsorption of negatively charged surfactant on alumina [40]. From the results of Tables 2 and 3 the optimum condition selected for retention and desorption of iron were as follows; sample pH ~5.0, NaCl concentration 0.4 mol l^{-1}; flow rate during retention and elution of analyte 3 ml min^{-1}, column length 4 cm, eluent concentration 5 mol l^{-1}, eluent volume 300 μl.

Table 4
Interference study: concentrated volume 20, iron concentration 125 μg l^{-1} flow rate 3 ml min^{-1}

Foreign ion	Molar ratio (ion/iron)	Recovery (%)
Ni^{2+}	1,000	102.1 ± 0.4
Ca^{2+}	1,000	96.4 ± 0.5
Mg^{2+}	1,000	102.4 ± 0.2
Mn^{2+}	1,000	98.3 ± 0.6
Cd^{2+}	1,000	103.9 ± 0.3
Zn^{2+}	1,000	98.3 ± 0.1
Co^{2+}	250	97.4 ± 0.5
Sr^{2+}	1,000	98.9 ± 0.3
CO_3^{2-}	1,000	98.8 ± 0.3
SO_4^{2-}	100	95.1 ± 0.5
K^+	1,000	97.8 ± 0.4
Pb^{2+}	1,000	97.2 ± 0.3
Al^{3+}	250	102.5 ± 0.2
Ag^+	1,000	98.9 ± 0.6
Hg^{2+}	1,000	101.4 ± 0.3
Na^+	40,000	100 ± 0.6
Cl^-	40,000	102.3 ± 0.4
Ba^{2+}	1,000	100 ± 0.6

5. Basic analytical performance

An important aspect of method development was to demonstrate the preconcentration capability of the FI manifold. The flow system showed good linearity for processing 20 ml (10–200 μg l^{-1}) and 40 ml (5–150 μg l^{-1}) of iron solutions. The equations of calibration graphs were $H = 0.195\,C + 0.572$ and $H = 0.388\,C + 0.515$ (where H is the peak height and C is the concentration) with correlation coefficient of 0.9999 and 0.9996, respectively. A preconcentration factor (based on matching the slope of calibration graphs with and without preconcentration) of 65 and 129 with a sampling volume of 20 and 40 ml were obtained, respectively. This implies the determination capability of the method at sub μg l^{-1}. Furthermore, the calibration slopes increased proportionally with increasing preconcentration volume, which indicates the recovery of the process is independent of sample volume.

The deposition efficiency of microcolumn in preconcentration of iron in presence of various cations and anions present in real sample or forming complex with ferron were examined. A relative error of less than 5% was considered to be within the range of experimental error. The results obtained are summarized in Table 4. At the given level no interference was observed in determination of iron at trace level. These results indicated that high concentration of matrix salts have minimal effect on iron species

Table 5
Determination of iron in real sample

Sample	Iron (μg l^{-1})		Recovery (%)	GF-AAS
	Added	Found		
Tap water	0	80.9 ± 0.8	–	81.6 ± 1.2
	10	91.0 ± 0.5	101.0 ± 0.5	
Spring water	0	21.5 ± 0.6	–	21.7 ± 1.1
	10	31.4 ± 0.4	99.0 ± 0.4	
Rain water	0	35.7 ± 0.7	–	35.3 ± 0.9
	10	45.5 ± 0.3	98.0 ± 0.3	
River water	0	64.7 ± 0.6	–	64.2 ± 1.6
	10	74.5 ± 0.8	97.8 ± 0.8	
Human milk	0	962.8 ± 0.6	–	965.3 ± 0.6
	100	1061.5 ± 0.4	98.7 ± 0.4	
Cow milk	0	1275.7 ± 0.9	–	1274.6 ± 0.9
	100	1372.8 ± 0.7	97.1 ± 0.7	
Infant dry formula milk[a]	0	72.5 ± 0.4	–	72.8 ± 1.8
	10	82.8 ± 0.5	103.0 ± 0.5	

[a] μg of iron per gram of sample.

relative to matrix ion. At the 95% confidence level the relative standard deviation ($n = 6$) at 125 and 50 $\mu g\,l^{-1}$ of iron with 20 ml sampling volume were 2.9 and 2.0%, respectively. The limit of detection based on three times the standard deviation of blank signal with a sampling volume of 20 ml was found to be 1.06 $\mu g\,l^{-1}$. The capacity of the sorbent was found to be 989 μg of iron per gram of packing material. This high value suggested high performance of microcolumn even in the presence of competing ions, in other word that interfering metal ions have minimal influence on iron retention.

5.1. Application

The procedure was applied to determination of iron in tap water, spring water, rain, and river water (taken from Zayandah roud, Esphahan/Iran), human and cow milk and infant dry formula milk. Reliability was checked by recovery experiments and comparing the results with data obtained by graphite furnace atomic absorption analysis. The results of this investigation are given in Table 5. It can be seen that recovery of spiked sample is good, and at 95% confidence limit there is no difference between the results and data obtained by graphite furnace atomic absorption analysis. Furthermore, the above procedure was applied to the determination of iron in a certified oxide manganese ore (Reference Material, CRM No. 5406-90 with the percentage composition of $SiO_2 = 47.66$, $TiO_2 = 0.31$, $Al_2O_3 = 9.78$, $Mn_{tot} = 15.98$, $MnO_2 = 14.40$, $MgO = 0.74$, $CaO = 1.96$, $Na_2O = 0.70$, $K_2O = 4.99$, $P = 0.043$, $CO_2 = 1.29$, $S_{tot} = 0.22$, $Pb = 0.23$. $Zn = 0.018$, $Ba = 2.65$ and $Fe_{tot} = 2.43$). The concentration of iron in the sample was found to be 2.42 ± 0.21 which is in good agreement with the accepted value (2.43%); thus the procedure is suitable for the sample type examined.

6. Conclusions

It has been demonstrated that ferrons can be directly immobilized on alumina surface in the pH range of 2.5–6. The proposed FI system incorporating immobilized ferron permits effective on-line preconcentration of iron and final determination by FAAS. Furthermore, MultiSimplex optimization allowed reduction of the number of experiments needed for optimization, and a true optimum set of condition is attained. The proposed method offers an alternative procedure to techniques such as GFAAS for determination of iron at $\mu g\,l^{-1}$ level in different matrices. The preparation of sorbent is fairly easy and does not require any chemical reaction. Future work will be directed at the possibility of direct immobilization of ligands with different negatively charged group and to assess the suitability of the method for filed sampling of iron.

References

[1] S.B. Goldhaber, Regul. Toxiocol. Pharmacol. 38 (2003) 232.
[2] E. Coni, A. Alimonti, A. Bocca, F. La Torre, D. Pizzuti, S. Caroli, in: S. Caroli (Ed.), Elemental Speciation Bioinorganic Chemistry, Wiley, Inter Science, New York, 1996 (chapter 8).
[3] C. Casey, A. Smith, P. Zhang, Microminerals in humans and animals milks, in: R.G. Jenson (Ed.), Handbook of Milk Composition, Academic Press, San Diego, 1995 (chapter 7).
[4] E. Pehlivan, D. Kara, Microchim. Acta 158 (2007) 137.
[5] M. Ghaedi, E. Asadpour, A. Vafaie, Bull. Chem. Soc. Jpn. 79 (2006) 432.
[6] S. Tokalioglu, S. Kartal, Bull. Korean Chem. Soc. 27 (2006) 1293.
[7] Y. Bakircioglu, D. Bakircioglu, N. Tokman, Anal. Chim. Acta 547 (2005) 26.
[8] M.A.A.E. Aki, I.M. Kenawy, R.R. Lasheen, Anal. Sci. 21 (2005) 923.
[9] V. Camel, Spectrochim. Acta B 58 (2003) 1177.
[10] G.A. Zachariadis, A.N. Anthemidis, P.G. Bettas, J.A. Stratis, Talanta 57 (2002) 919.
[11] T. Prasada Rao, S. Karthikeyan, B. Vijayalekshmy, C.S.P. Lyer, Anal. Chim. Acta 369 (1998) 69.
[12] M. Sperling, X. Yin, B. Welz, Analyst 117 (1992) 629.
[13] R. Lima, K.C.L.A. Santelli, Talanta 43 (1996) 977.
[14] M. Zougagh, A. Garcia de Torres, J.M. Cano Pavon, Talanta 56 (2002) 753.
[15] D.A. Weeks, K.W. Bruland, Anal. Chim. Acta 453 (2002) 21.
[16] Q. Pu, Q. Sun, Analyst 123 (1998) 239.
[17] M. Sperling, S. Xu, B. Welz, Anal. Chem. 64 (1992) 3101.
[18] A.G. Cox, C.W. McLeod, Anal. Chim. Acta 179 (1986) 487.
[19] A.G. Cox, C.W. McLeod, Mikrochim. Acta 109 (1992) 161.
[20] J.B.B. de Silva, A.J. Curtius, M.B.O. Giacomelli, Analyst 124 (1999) 1249.
[21] S. Lin, C. Zheng, G. Yun, Talanta 42 (1995) 921.
[22] S.P. Quinaia, J.B.B. Da Silva, M.C.E. Rollemberg, A.J. Curtius, Talanta 54 (2001) 687.
[23] S. Dadfarnia, A.M. Haji Shabani, Z. Dehghani, J. Braz. Chem. Soc. 17 (2006) 548.
[24] S. Dadfarnia, A.M. Salmanzadeh, A.M. Haji Shabani, J. Anal. At. Spectrom. 17 (2002) 1434.
[25] A.M. Haji Shabani, S. Dadfarnia, K. Dehghan, Talanta 59 (2003) 719.
[26] S. Dadfarnia, A.M. Haji Shabani, M. Gohari, Talanta 64 (2004) 682.
[27] S. Dadfarnia, A.M. Haji Shabani, F. Tamaddon, M. Rezaei, Anal. Chim. Acta 539 (2005) 69.
[28] T. Assadolahi, S. Dadfarnia, A.M. Haji Shabani, J. Braz. Chem. Soc. 18 (2007) 1353.
[29] S.L.C. Ferreira, V.A. Lemos, B.C. Moreira, A.C. Spinola Costa, R.E. Santelli, Anal. Chim. Acta 403 (2000) 259.
[30] K. Brajter, E. Dabek-Zlotorzynska, Talanta 37 (1990) 613.
[31] M. Trojanowicz, K. Pyryznska, Anal. Chim. Acta 287 (1994) 247.
[32] S. Przeszlakowski, E. Habrat, Analyst 107 (1982) 1320.
[33] K. Goto, H. Tamura, M. Onodera, M. Nagayama, Talanta 21 (1974) 183.
[34] J. Bergström, T. Öberg, MultiSimplex, 98, Karlskrona, Sweden, 1998.
[35] E. Cortazar, O. Zuloaga, J. Sanz, J.C. Raposo, N. Etxebarria, L.A. Fernandez, J. Chromatogr. A 978 (2002) 165.
[36] J.A. Nelder, R. Mead, Comput. J. 5 (1965) 308.
[37] A. Otto, Chemom. Intell. Lab. Syst. 4 (1988) 101.
[38] J. Sanz, A. de Diego, J.C. Raposo, J.M. Madariaga, Anal. Chim. Acta 486 (2003) 255.
[39] N. Ferreiros, G. Iriarte, R.M. Alonso, R.M. Jimenez, Talanta 69 (2006) 747.
[40] M. Hiraide, J. Iwasawa, S. Hiramatsu, H. Kawaguchi, Anal. Sci. 11 (1995) 611.
[41] A.B.P. Lever, Inorganic Electronic Spectroscopy, Elsevier, Amesterdam, 1984.
[42] W.H. Chan, Chemom. Intell. Lab. Syst. 40 (1998) 203.

Talanta 77 (2008) 518–521

Contents lists available at ScienceDirect

Talanta

journal homepage: www.elsevier.com/locate/talanta

Single reaction interface flow system for chemiluminescent monitoring of mannitol based on its hydroxyl radical scavenger activity

Cristina I.C. Silvestre [a], João L.M. Santos [a,*], José L.F.C. Lima [a], Elias A.G. Zagatto [b]

[a] Requimte, Serviço de Química-Física, Faculdade de Farmácia, Universidade do Porto, Rua Aníbal Cunha 164, 4099-030 Porto, Portugal
[b] Centro de Energia Nuclear na Agricultura, Universidade de São Paulo, P.O. Box 96, Piracicaba 13400-970, Brazil

ARTICLE INFO

Article history:
Received 30 October 2007
Received in revised form 11 March 2008
Accepted 17 March 2008
Available online 25 March 2008

Keywords:
Single reaction interface flow analysis
Mannitol determination
Hydroxyl radical
Myoglobin
Chemiluminescence

ABSTRACT

A single reaction interface flow analysis (SIFA) system for the monitoring of mannitol in pharmaceutical formulations and human urine is presented. The developed approach takes advantage of the mannitol scavenger aptitude to inhibit the chemiluminescent reaction between luminol and myoglobin in the absence of H_2O_2. The SIFA system facilitated the fully automation of the developed methodology, allowing the in-line reproducible handling of chemical species with a very short lifetime as is the case of the hydroxyl radical generated in the abovementioned luminol/myoglobin reaction.

The proposed methodology allowed the determination of mannitol concentrations between 25 mmol L^{-1} and 1 mol L^{-1}, with good precision (R.S.D. < 4.7%, $n = 3$) and a sampling frequency of about 60 h^{-1}. The procedure was applied to the determination of mannitol in pharmaceuticals and in human urine samples without any pretreatment process. The results obtained for pharmaceutical formulations were statistically comparable to those provided by the reference method (R.D. < 4.6%); recoveries values obtained in the analysis of spiked urine samples (between 94.9 and 105.3% of the added amount) were also satisfactory.

1. Introduction

Myoglobin is a small and stable heme protein which contains a single iron protoporphyrin or heme moiety and thus classified as a metalloprotein [1]. It is mainly present in both skeletal and cardiac muscle tissue where it is responsible for oxygen storage and transportation. Several recent works refer that myoglobin in the ferric state Mb(Fe^{III}) could oxidise luminol yielding a chemiluminescence emission. This feature was applied in the determination of several species that could either inhibit or enhance the myoglobin–luminol system [2–4].

It has been also reported that some metal-containing compounds and metalloporphyrins could produce a chemiluminescence response from luminol in alkaline medium, without involving the direct oxidation of the later by myoglobin or the presence of hydrogen peroxide [5]. Seemingly, the reaction between the Fe^{III} porphyrins with NaOH generated hydroxyl radical ($OH^{\bullet}$) and Fe^{II} porphyrins, which could be subsequently oxidised to the Fe^{III} form by O_2 generating superoxide radical ($O_2^{\bullet -}$) [5]. The chemiluminescence emission was therefore a consequence of luminol oxidation induced by the free radicals generated in the redox cycle. Being a metalloporphyrin it would be expected that myoglobin would endure a similar chemical process under the same conditions.

Mannitol is a polyol (sugar alcohol) widely used in food and pharmaceutical industries as well as a therapeutical agent (osmotically active diuretic) used in situations of acute renal failure, to treat cerebral oedema, glaucoma or to reduce intracranial pressure [6]. Mannitol has been determined in different matrices including food, biological samples or pharmaceuticals mainly by chromatography [7–20] and capillary electrophoresis [21–26], using various types of detection, such as, UV, spectrophotometric, electrochemical, amperometric, conductimetric and refractometric. However, the majority of these techniques is time-consuming and requires expensive equipments and qualified operators. Two flow injection analysis (FIA) methodologies involving chemiluminescence detection upon oxidation by permanganate [27] and fluorometric detection [28], were also proposed for the determination of this polyol. However, FIA systems exhibit a low automation level and rely on the continuous addition of reagent solutions to the sample zone, which lead to a substantial consumption of reagents. Furthermore, FIA versatility is limited in terms of sample manipulation since the inserted sample volume is determined by the internal volume of the sample loop.

* Corresponding author. Tel.: +351 222078968; fax: +351 222078961.
E-mail address: joaolms@ff.up.pt (J.L.M. Santos).

0039-9140/$ – see front matter © 2008 Elsevier B.V. All rights reserved.
doi:10.1016/j.talanta.2008.03.021

Given that mannitol is a specific and strong hydroxyl radical scavenger it would have the ability, by scavenging ($OH^{\bullet}$), to inhibit the anticipated chemiluminescence response generated in the abovementioned myoglobin/luminol reaction, a capability that could be used for its determination in samples with distinct origins. It is relevant the fact that none of the methodologies proposed till now makes use of mannitol radical scavenger capability for its determination.

Chemiluminescence measurements are characterised by wide dynamic linear ranges, high speed of response and excellent sensitivity. Taking into account that a CL response is typically generated by fast reactions, its efficient monitoring requires highly reproducible and fast mixing of sample and reagents. This is even more crucial when short-lived species, as is the case of the hydroxyl radical, are involved in the reactive process. SIFA systems exhibit all the necessary features to fulfil these requisites. Therefore, in this work an automated flow methodology based on a single reaction interface flow analysis (SIFA) system [29] was implemented for monitoring mannitol levels in pharmaceutical and biological samples. The use of solenoid micro-pumps which are accountable for solutions insertion, propelling and commutation, conditioning the establishment and subsequent detection of the reaction zone, provide a great operational simplicity. These micro-pumps are ideal tools to build up compact environmentally friendly analytical systems, which are characterised by low solutions consumptions and the minimisation of hazardous waste generation. They also enhanced sample/reagent mixing ability in comparison with flow techniques that rely on laminar flow regime. Effectively, solenoid micro-pumps actuation produces a pulsed flowing stream as a consequence of the sudden pump diaphragm displacement that produces a chaotic movement of the solutions in all directions leading to the improved sample/reagent mixing, a well-known requirement of chemiluminescence measurements (fast and effective sample/reagent mixing). Nonetheless, one of the main advantages of SIFA systems is that they no longer rely on the utilisation of well-defined and compelling sample and reagent volumes, a typical characteristic of conventional flow techniques such as FIA, Sequential Injection Analysis (SIA) and Multi-Syringe Flow injection Analysis (MSFIA), but on the establishment of a single sample/reagent reaction interface, where the sample and reagent solutions have no fixed boundaries. This facilitates system configuration and control and resulted in enhanced simplicity and operational versatility while minimises the occurrence of operational errors.

2. Materials and methods

2.1. Reagents and solutions

All of the solutions were prepared with water from a Milli-Q system (conductivity $\leq 0.1\ \mu S\ cm^{-1}$) and chemicals were of analytical reagent grade quality and not subject to any purification.

A $1.0 \times 10^{-3}\ mol\ L^{-1}$ luminol solution was daily prepared dissolving 8.86 mg in 50 mL of NaOH 0.2 mol L^{-1}. Working standard solutions were prepared by suitable dilutions with NaOH 0.2 mol L^{-1}.

A $1.0 \times 10^{-5}\ mol\ L^{-1}$ myoglobin solution was daily prepared dissolving 8.48 mg in 50 mL of water. Working standard solutions were prepared by suitable dilutions with water.

Working standard solutions of mannitol were daily prepared by rigorous dilution of 1 mol L^{-1} stock solution using water.

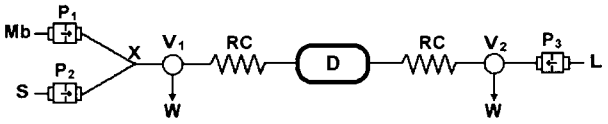

Fig. 1. Single interface flow manifold for the determination of mannitol. P_1, P_2, P_3: solenoid micro-pumps; X: confluence point; V_1, V_2: solenoid valves; RC: reaction coils (50 cm); D: chemiluminescence detector; W: waste; Mb: myoglobin ($4 \times 10^{-7}\ mol\ L^{-1}$); S: sample or standard; L: luminol ($1 \times 10^{-5}\ mol\ L^{-1}$; prepared in NaOH 0.2 mol L^{-1}).

2.2. Apparatus

The single interface flow system comprised three solenoid micro-pumps (120SP1210-4TE, Bio-Chem Valve Inc., Boonton, NJ, USA, 10 μL per stroke), two 161 T 031 (NResearch, West Caldwell, USA) two-way solenoid valves and a Camspec CL-2 chemiluminescence detector (Camspec Ltd., Cambridge, UK) equipped with a three-port 60 μL inner volume quartz flow cell. The luminometer had a wavelength response range of 320–600 nm and a flow cell working pathlenght of 5 mm. Flow lines and reaction coils were made from 0.8 mm i.d. PTFE tubing.

A Pentium-I-based computer was used for system control, and for data acquisition and treatment; software was developed in Microsoft Quick-Basic 4.5. The computer was equipped with a PC-LABCard model PCL-711B interface card from Advantech (Taipei, Taiwan). A CoolDrive (NResearch Inc., West Caldwell, USA) power drive was used to operate both the solenoid micro-pumps and solenoid valves.

Spectrophotometric measurements were carried out in a UV/Vis Spectrometer model Lambda 45 from PerkinElmer Instruments Inc. (Norwalk, CT, USA).

2.3. Single interface flow manifold

The developed flow manifold, pictured in Fig. 1, comprised three solenoid micro-pumps (P_1, P_2 and P_3), which were used to insert and propel the sample and reagent solutions. The repetitive micro-pump switching on/off created a pulsed flowing stream in which the pulse volume corresponded to the micro-pump stroke volume. Two two-way (normally closed) solenoid valves (V_1 and V_2) were used to direct the flowing streams. The detector was placed at the centre of the flow manifold. The reactions coils, identically sized, were placed on both sides of the detector.

The analytical cycle was started by establishing a baseline, which was accomplished with myoglobin/sample solutions. For establishing the baseline, V_1 was open and P_1 and P_2 were repeatedly actuated (on/off switching) propelling the solutions through the reactors as well as through the detector. After reaching V_2 these solutions were discarded. Subsequently, V_2 was opened, P_1 and P_2 were switched off and the luminol solution was inserted into the analytical path by means of P_3 and was propelled back to V_1. The mutual interdispersion of myoglobin/sample/luminol resulted in an analytical signal, which was measured when the reaction interface passed through the detector.

2.4. Reference method

Aiming at the evaluation of the accuracy of the results obtained with the developed procedure, mannitol pharmaceutical formulations were analysed according to the British Pharmacopoeia [30], by iodimetric titration.

3. Results and discussion

Preliminary experiments showed that at pH < 8 myoglobin exhibits a maximum of absorbance at 409 nm, corresponding to Mb(Fe^{III}) form (metmyoglobin), while at higher pH values the peak maximum was at 414 nm for Mb(Fe^{II}) (oxymyoglobin). It was also observed that the ferric state myoglobin reacted with luminol, in alkaline medium, producing a strong chemiluminescence (CL) emission. This CL emission was markedly reduced when mannitol, a strong and specific hydroxyl radical scavenger, was added confirming that this free radical was involved in the production of light. These results agreed with previous results obtained with other iron porphyrins [5].

3.1. Development of single interface flow methodology

In the development of the single interface flow methodology several studies were carried out in order to improve systems performance, namely in terms of analytical signal intensity, accuracy, repeatability and determination rate. These features influenced the choices made during the optimisation of the systems, which was carried out using the univariate method. Since no well-defined sample or reagent volumes were used, these parameters were not subject to evaluation which simplified the overall optimisation process.

3.1.1. Chemical parameters

Considering that the pH of the solution determined the Fe oxidation state, in order to guarantee the Mb(Fe^{III}) form myoglobin solutions were prepared directly in deionised water at pH 5.6. Effectively, when myoglobin was prepared in alkaline medium a weak CL intensity was observed. On the other hand, luminol CL emission occurred in alkaline conditions. Under these circumstances the SIFA system would have to provide good mixing conditions at the myoglobin/luminol single interface to ensure an appropriate reaction development.

The influence of myoglobin concentration in the chemiluminescence intensity was assayed for concentrations ranging from 1.0×10^{-7} to 6.0×10^{-7} mol L^{-1}. It was observed that with increasing myoglobin concentrations the intensity of the signal increased about 61.5% until myoglobin 4.0×10^{-7} mol L^{-1}, above which the chemiluminescent signal approached stabilisation. Therefore, a 4.0×10^{-7} mol L^{-1} myoglobin solution was used in the subsequent experiments.

The chemiluminescence intensity was also studied for luminol concentrations between 0.1×10^{-5} and 5×10^{-5} mol L^{-1}. The obtained results showed that with increasing luminol concentrations the intensity of the chemiluminescent response increased about 59.1% until 1.0×10^{-5} mol L^{-1}. Above this concentration value the chemiluminescent intensity remained almost unaffected. Consequently, a 1.0×10^{-5} mol L^{-1} luminol solution was chosen for the succeeding studies.

Considering that the luminol oxidation is favoured in alkaline medium, distinct NaOH solutions with increasing concentrations were evaluated. It was observed that the CL emission reached a maximum value for 0.2 mol L^{-1} NaOH.

3.1.2. Physical parameters

By comparing chemiluminescence intensities using reaction coils of different lengths (10–100 cm) in the presence of 1.0×10^{-5} mol L^{-1} luminol and 1.0×10^{-7} mol L^{-1} myoglobin, it was observed that the chemiluminescence intensity did not diverge significantly. Nevertheless, aiming at guaranteeing a good mixture and in order to not compromise the determination rate two 50-cm reaction coils were selected for the subsequent experiments. Flow rate was evaluated between 0.6 and 3.0 ml min^{-1}. Since no significant differences were verified in the chemiluminescence response, a flow rate of 2.0 ml min^{-1} was chosen. These results showed that reaction coil length and flow rate were not fundamental parameters affecting the intensity of the analytical signal obtained with the SIFA system, which could be probably explained by the fact that since sample and reagent solutions have no fixed physical limits any increase in the residence time would be compensated by the continuous surplus of solutions participating in the single reaction interface as it expands to the neighbouring intact (non-dispersed) zones.

Table 1
Results obtained in the evaluation of the interfering effect of selected compounds by using a 50 mmol L^{-1} mannitol solution

Added1species	Tolerance limit
Cl^-, NO_3^-, Ac^-, I^-, SO_4^{2-}, PO_4^{2-}	100[a]
Na^+, Ni^{2+}, Zn^{2+}, Cr^{3+}, Mg^{2+}, Ca^{2+}, Cu^{2+}	100
Sorbitol, glucose, borate, oxalate, malate, ureia	100
Uric acid, NH_4^+, BrO_3^-	10
Fe^{3+}	1

Data refer to the concentration ratio (expressed in mol L^{-1}) between the interfering specie and the analyte.
[a] Maximum tested concentration ratio.

3.2. Interferences

In order to assess the selectivity of the developed approach it was applied in the analysis of a 50 mmol L^{-1} mannitol solution containing increasing amounts of several species that are either used as excipients in pharmaceutical formulations or appeared in the composition of human urine samples. A chemical specie was considered as non-interfering if the analytical signal variation was lower than 5% regarding the one obtained in its absence. The obtained results (Table 1) showed no significant interfering effect for the majority of the tested compounds with a tolerable molar concentration ratio of about 100, except for iron(III) which interferes at concentration values similar to those of mannitol. These results confirmed that the proposed methodology can be applied in the analysis of mannitol in both pharmaceutical formulations and urine.

3.3. Application to pharmaceutical formulations and biological samples

After system optimisation and by using the analytical conditions exhibited in Table 2, a linear working range for mannitol concentrations between 25 mmol L^{-1} and 1 mol L^{-1}, was obtained (Fig. 2). The calibration curve was expressed by the equation:

$$I = -15.952C + 92.224$$

where I represents the relative chemiluminescence intensity and C is the logarithm of mannitol concentration (expressed in mol L^{-1}). The correlation coefficient was 0.9997.

In order to evaluate the applicability and the accuracy of the developed methodology in the analysis of real samples, it was

Table 2
Parameters evaluated during the optimisation of the SIFA system performance and most favourable values selected for its operation

Parameter	Evaluated range	Selected values
Reactor length (cm)	10–100	50
Flow rate (mL min^{-1})	0.6–3	2.0
Myoglobin concentration ($\times 10^{-7}$ mol L^{-1})	1.0–6.0	4.0
Luminol concentration ($\times 10^{-5}$ mol L^{-1})	0.1–5.0	1.0
Mannitol concentration (mol L^{-1})	1×10^{-3}–1	25×10^{-3}–1

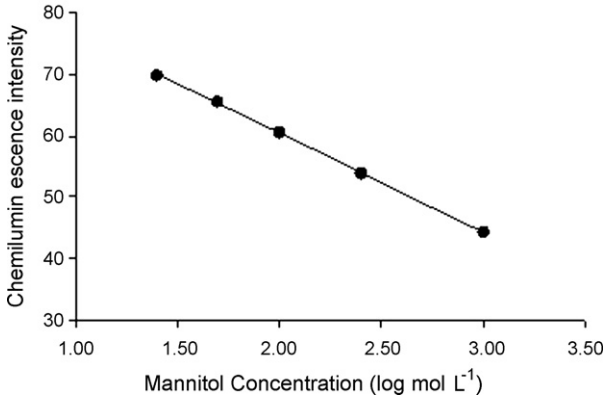

Fig. 2. Results obtained in the calibration of the system. Mannitol standards concentrations between 25 mmol L^{-1} and 1 mol L^{-1}.

Table 3
Results obtained by using the SIFA methodology (C_{SIFA}) and the reference method (C_{Ref})

Sample	C_{SIFA} (% m/V)	C_{Ref} (% m/V)	R.D. (%)[a]
Manitosteril 10%	10.2 ± 0.1	9.8 ± 0.003	3.8
Osmofundina 17.5%	17.9 ± 0.1	18.7 ± 0.034	−4.2
Manitol 20%	20.9 ± 2.4	20.0 ± 0.064	4.6

Each value corresponds to the mean ± standard deviation.
[a] Relative deviation (expressed in percentage) of the developed SIFA methodology regarding the reference procedure.

applied to the determination of mannitol in commercially available pharmaceutical formulations. The obtained results (Table 3) exhibited a good agreement between the results furnished by both methods, with relative deviations (expressed in percentage) lower than 4.6%. Furthermore, the repeatability was good, with a relative standard deviation lower than 4.7% ($n = 3$), and the determination rate was about 60 h^{-1}. For comparison purposes a paired t-test was also performed on the data obtained by the proposed method and by the reference method. A t value of 0.39 was obtained, which was lower than the tabulated t value = 4.30 ($P = 0.05$, d.f = 2) indicating no significant differences for the mean concentrations obtained by both methods. When applied in the analysis of human urine samples the developed chemiluminometric SIFA methodology showed as well a good performance, with recovery values (expressed in percentage of the added amount) ranging from 94.9 to 105.3% (Table 4), indicating that the proposed analytical approach is suitable for the monitoring of mannitol in these biological samples.

The developed flow systems exhibited good stability (no baseline drift was observed) and robustness. The utilisation of solenoid micro-pumps guaranteed a good operational simplicity, and enhanced sample/reagent mixing ability, an important feature for carrying out chemiluminescence measurements that assure as well low solutions consumptions and the minimisation of hazardous waste generation. When compared with more conventional CL flow methodologies SIFA systems revealed a simpler configuration and control while the occurrence of operational errors is minimised because they do not require the reproducible insertion of well-defined sample and reagent volumes.

Table 4
Results obtained in the determination of mannitol in spiked human urine samples (amount added: 100 mmol L^{-1}) using the SIFA methodology

Urine Sample	Original amount (mmol L^{-1})	Amount found (mmol L^{-1})	Recovery (%)
1	30.6	133.7	103.1
2	40.7	135.6	94.9
3	545.2	650.5	105.3

Each value corresponds to the average of three determinations.

4. Conclusion

The proposed single interface system allowed fast and reliable determination of mannitol in pharmaceutical formulations and in urine. For moreover, the proposed method has an innovator characteristic since, contrary to the existing methods, it uses mannitol radical scavenger property for its determination, which improves selectivity.

The developed system presented an acceptable relative standard deviation that demonstrates a good repeatability. This feature is certainly a consequence of the particular characteristic of SIFA systems that is the establishment of the reaction zone without using definite sample and reagent volumes. When compared to the reference procedure, relative deviations were inferior to 4.6%. The accuracy of the proposed methods face to the reference method was confirmed by paired t-test for pharmaceutical formulations, as well as, the obtained recoveries in urine spiked samples.

The proposed method requires no sample pretreatment, provides a wide working concentration range and is more versatile than most of the reported methods. Furthermore, single interface flow system presents a simpler optimisation than other flow techniques.

Acknowledgements

Cristina I.C. Silvestre thanks Fundação para a Ciência e Tecnologia and FSE (III Quadro Comunitário de Apoio) for the Ph.D. grant (SFRH/BD/31107/2006).

References

[1] Z.H. Song, L. Wang, S. Hou, Anal. Bioanal. Chem. 378 (2004) 529.
[2] X.D. Shao, X.F. Xie, Y.H. Liu, Z.H. Song, J. Pharm. Biomed. Anal. 41 (2006) 667.
[3] Q.L. Yue, Z.H. Song, Microchem. J. 84 (2006) 10.
[4] X.F. Xie, Z.H. Song, X.D. Shao, Int. J. Environ. Anal. Chem. 87 (2007) 149.
[5] C. Poupon- Fleuret, J.P. Steghens, J.C. Bernengo, Analyst 121 (1996) 1539.
[6] Martindale, The Complete Drug Reference, 33rd edition, Pharmaceutical Press, London, 1999, pp. 924–025.
[7] J.A. Kynaston, S.C. Fleming, M.F. Laker, A.D.J. Pearson, Clin. Chem. 39 (1993) 453.
[8] J. Prodolliet, E. Bugner, M. Feinberg, J. AOAC 78 (1995) 768.
[9] O. MartinezAugustin, J.J. Boza, J.M. Romera, A. Gil. Clin. Biochem. 28 (1995) 401.
[10] K. Miki, R. Butler, D. Moore, G. Davidson, Clin. Chem. 42 (1996) 71.
[11] J. Prodolliet, E. Bugner, M. Feinberg, J. AOAC 79 (1996) 1400.
[12] Z. Yan, X.D. Zhang, W.J. Niu, Mikrochim. Acta 127 (1997) 189.
[13] M.A. Cox, T.H. Iqbal, B.T. Cooper, K.O. Lewis, Clin. Chim. Acta 263 (1997) 197.
[14] T.R.I. Cataldi, G. Margiotta, L. Iasi, B. Di Chio, C. Xiloyannis, S.A. Bufo, Anal. Chem. 72 (2000) 3902.
[15] Y.D. Bao, T.M.J. Silva, R.L. Guerrant, A.A.M. Lima, J.W. Fox, J. Chromatogr. B 685 (1996) 105.
[16] A. Kiyoshima, K. Kudo, N. Nishida, N. Ikeda, Foren. Sci. Int. 125 (2002) 127.
[17] A. Kiyoshima, K. Kudo, Y. Hino, N. Ikeda, J. Chromatogr. B 758 (2001) 103.
[18] S.A. Wring, A. Terry, R. Causon, W.N. Jenner, J. Pharm. Biomed. Anal. 16 (1998) 1213.
[19] T.R.I. Cataldi, G. Margiotta, C.G. Zambonin, Food Chem. 62 (1998) 109.
[20] A.I. Ruiz-Matute, A. Montilla, M.D. Del Castillo, I. Martinez-Castro, M.L. Sanz, J. Sep. Sci. 30 (2007) 557.
[21] M. Pospisilova, M. Polasek, J. Prochazka, J. Chromatogr. A 772 (1997) 277.
[22] T. Soga, D.N. Heiger, Anal. Biochem. 261 (1998) 73.
[23] C. Corradini, A. Cavazza, G. Canali, I. Nicoletti, Ital. J. Food Sci. 10 (1998) 195.
[24] G. Chen, L.Y. Zhang, X.L. Wu, J.N. Ye, Anal. Chim. Acta 530 (2005) 15.
[25] M. Herrmannova, L. Krivankova, M. Bartos, K. Vytras, J. Sep. Sci. 29 (2006) 1132.
[26] M. Pospisilova, M. Polasek, J. Safra, I. Petriska, J. Chromatogr. A 1143 (2007) 258.
[27] I.B. Agater, R.A. Jewsbury, K. Williams, Anal. Commun. 33 (1996) 367.
[28] N. Kiba, Y. Inoue, M. Furusawa, Anal. Chim. Acta 244 (1991) 105.
[29] M.F.T. Ribeiro, J.L.M. Santos, J.L.F.C. Lima, A.C.B. Dias, E.A.G. Zagatto, Talanta 68 (2005) 351.
[30] British Pharmacopoeia, vol. III, The Stationery Office, London, 2005, pp. 2620–2621.

Talanta 77 (2008) 889–896

Contents lists available at ScienceDirect

Talanta

journal homepage: www.elsevier.com/locate/talanta

Investigation of ICP-MS spectral interferences in the determination of Rh, Pd and Pt in road dust: Assessment of correction algorithms via uncertainty budget analysis and interference alleviation by preliminary acid leaching

Kiril Simitchiev[a,*], Violeta Stefanova[a], Veselin Kmetov[a], George Andreev[a], Alfredo Sanchez[b], Antonio Canals[b]

[a] Department of Analytical Chemistry, University of Plovdiv, 24 Tzar Assen Street, 4000 Plovdiv, Bulgaria
[b] Department of Analytical Chemistry and Food Science, University of Alicante, P.O. Box 99, 03080 Alicante, Spain

ARTICLE INFO

Article history:
Received 26 May 2008
Received in revised form 11 July 2008
Accepted 22 July 2008
Available online 31 July 2008

Keywords:
ICP-MS
Platinum group metals
Road dust
Correction of spectral interferences
Uncertainty budget analysis
Microwave-assisted cloud point extraction

ABSTRACT

A method for classification of the potential spectral interferences in inductively coupled plasma mass spectrometry (ICP-MS) was proposed based on statistical assessment of the interfering signals. The concept was applied to investigate the variety of spectral interferences over the isotopes of Rh, Pd and Pt concerning their analysis in road dust samples. For the significant interferences the applicability of mathematical corrections using two alternative algorithms were studied by uncertainty budget analysis and the approach resulting in lower combined uncertainty of the corrected signals was selected. Further the uncertainty evaluation was used for assessment of the most appropriate Pd isotope to be measured. The adequateness of the mathematical corrections for Rh and Pd was highly relevant to the number of elements causing spectral interferences and the relative analyte/interferent concentrations. This was overcome by preliminary road dust leaching with 0.35 mol l^{-1} hydrochloric acid. Interferents present as easily soluble salts were substantially removed form the samples while the platinum group metals were not leached which allowed a relative analyte preconcentration to be obtained. For the leached samples the isotopes of Rh and Pd were still spectrally interfered from Sr, Y and Pb but at considerably lesser degree thus after mathematical correction the ICP-MS analysis of Rh, Pd and Pt was reliable and robust using the isotopes 103, 105 and 195, respectively. The method was validated via an alternative analysis based on selective separation of the platinum group metals by microwave-assisted cloud point extraction.

1. Introduction

During the last two decades it is announced that Pt, Pd and Rh content in environmental objects near motorways and city roads is much higher compared to their background levels [1,2]. The main reason for elevated values is emission of platinum group metals (PGM) from the automobile catalytic converters (auto-catalysts) introduced in 1970s to remove carbon monoxide, nitrogen oxides and hydrocarbons from the exhaust gases of the vehicles.

A disadvantage of the auto-catalysts is their physical surface abrasion resulting in PGM release in particulate form, mainly in the elemental state or as oxides [3]. The nano-crystalline PGM are attached to μm-size aluminum oxide particles from the catalyst's washcoat [4].

At the present moment PGM monitoring is needed concerning the ecological and health risks posed by their increasing concentrations [2–4]. Sensitive instrumental techniques such as electrothermal atomic absorption spectrometry (ETAAS) [5–8], inductively coupled plasma optical emission spectrometry (ICP-OES) [8–10], inductively coupled plasma mass spectrometry (ICP-MS) [10–15] and neutron activation analysis (NAA) [16,17] have been used for PGM determination in environmental and biological materials. However the analysis is usually highly sophisticated because of the very low element concentrations and complex sample matrices [18]. For these reasons a preliminary PGM separation and/or pre-concentration is commonly required. Co-precipitation [11,15], liquid–liquid extraction [7,12], solid phase extraction [5,8], ion exchange [9,16], preconcentration in knotted reactor [6,13] and cloud point extraction [14,19] have been applied for the purpose

* Corresponding author. Tel.: +359 32 261 439; fax: +359 32 261 337.
E-mail addresses: k.simitchiev@uni-plovdiv.bg, kirilsim@gmail.com (K. Simitchiev).

0039-9140/$ – see front matter © 2008 Elsevier B.V. All rights reserved.
doi:10.1016/j.talanta.2008.07.041

but an emphasis should be put on the method validation which is quite problematic, especially in the case of Pd [20].

ICP-MS is preferred for ultra-trace determination of Rh, Pd and Pt in road dust due to its inherent low detection limits and multi-elemental capabilities. Nevertheless it has been reported that spectral interferences arising from the major sample constituents complicate the PGM analysis by quadrupole spectrometers (ICP-QMS) [21,22]. Attempts have been made to determine PGM by high-resolution ICP-MS but some interferences could not be avoided even in this case [22,23]. Mathematical corrections of the spectral interferences have also been applied [12,24,25]. The advantage of the last approach is the possibility to use a conventional ICP-QMS combined with less sample manipulation in comparison to the separation methods. However when a mathematical correction is made its adequateness must be assessed in view of accuracy and resulting uncertainty of the corrected signals.

This work evaluates the contribution of spectral interferences (polyatomic, isobaric or doubly charged ions) to the Rh, Pd and Pt signals and the feasibility of mathematical corrections aiming to improve the analytical performance of ICP-QMS for PGM determination in road dust. The mathematical approaches were assessed by calculation of the combined uncertainties corresponding to the corrected signals and accuracy verification by an alternative method based on previously developed selective microwave-assisted cloud point extraction (MW-CPE) of PGM [26]. In addition a preliminary road dust leaching with diluted hydrochloric acid was also investigated as a tool for spectral interference alleviation by removal of the easily soluble interferents.

2. Experimental

2.1. Instrumentation

An inductively coupled plasma mass spectrometer Thermo Elemental VG PQ ExCell was used for spectral interference studies and PGM analysis. The instrumental conditions are summarized in Table 1 but plasma gas flows, power and interface sampling depth were daily adjusted to minimize the ratio CeO^+/Ce^+ which was kept below 1.5%.

Two microwave systems were used: (i) MSP 1000 (CEM Corp., Matthews, NC, USA) (950 W) with a pressure control system, equipped with vessels (maximum pressure of 200 psi) was used for the road dust samples digestion and (ii) MDS-81D (CEM Corp., Indian Trail, NC, USA) (600 W) was used for MW-CPE.

Table 1
Optimized instrumental parameters for ICP-MS

Plasma conditions	
RF power	1300 W
Argon plasma gas flow	14 l min^{-1}
Auxiliary gas flow	1.0 l min^{-1}
Nebulizer gas flow	0.80 l min^{-1}
Sample flow rate	1.0 ml min^{-1}
Nebulizer type	Concentric (Meinhard)
Spray chamber	Impact bead (Peltier-cooled, 4 °C)
Interface cones (sampler and skimmer)	Ni
Mass spectrometer settings	
Resolution	Normal
Acquisition mode	Peak Jump
Channels per mass	1
Dwell time	100 ms
Sweeps	1
Readings	20
Measured isotopes	
Analyte	^{103}Rh, ^{105}Pd, ^{106}Pd, ^{108}Pd, ^{110}Pd, ^{194}Pt, ^{195}Pt, ^{196}Pt
Internal standard	^{187}Re

2.2. Reagents and samples

All reagents were analytical or suprapur grade. Standard solutions of 10 mg l^{-1} Rh (Fluka Chemie GmbH, Buchs, Switzerland) and 1000 mg l^{-1} Pd and Pt (High-Purity Standards, Charleston, England) were used. Calibration standards were prepared daily in 0.1 mol l^{-1} HNO_3. Single element standards of Cu, Zn, Rb, Sr, Y, Zr, Mo, Cd, Hf and Pb were used for the interference studies. 2-mercaptobenzothiazole (2-MBT), 97% (Alfa Aesar, Karlsruhe, Germany) and Triton X-100 (Sigma, St. Louis, USA) were used without further purification. Double-distilled water was used for preparation of all solutions. Intermediate solutions of 10% Triton X-100 in water and 8% $SnCl_2$ in 6 mol l^{-1} HCl were prepared. 2-MBT was introduced as 1% solution in 0.5 mol l^{-1} ammonia. Leaching hydrochloric acid with concentration ca. 0.35 mol l^{-1} was prepared by dilution of 30% HCl (Merck, s.p.).

Investigations were carried out with two types of samples: (i) road dust collected at motorway near Alicante, Spain (*RD Alicante*) and (ii) urban dust (*RD QuaNas*) collected in a road tunnel and supplied in the frames of proficiency testing scheme (EU project No. G7RT-CT-2002-05110, acronym QuaNAS). The *RD Alicante* was subsampled with 200 μm sieve and the fine fraction was used for further analysis. The *RD QuaNas* was analyzed in the form it has been obtained.

2.3. Procedures

2.3.1. MW digestion of road dust

To 0.25 g of road dust, weighted into the MW vessel, were added 9 ml of aqua regia. Due to the exothermic reaction at room temperature, 30 min had been allowed to elapse before sample vessels were sealed and treated in the MW MSP 1000 system by a program optimised for six samples (Table 2).

The digests were transferred in volumetric flasks, Re was added as internal standard at 1 μg l^{-1} level and samples were diluted to 100 ml with water.

2.3.2. Leaching procedure

Before MW digestion, a preliminary leaching of 1 g road dust was carried out with 50 ml of 0.35 mol l^{-1} HCl at ambient temperature in an open glass beaker. The contact time was kept at 60 min and periodical shaking was applied. Later phases were separated on weighed filter disc (Filtrak, Grade: 289, d = 125 mm), precleaned with 1 mol l^{-1} HCl. The filtrate was used for direct analysis of the leached interfering elements or subjected to MW-CPE with 2-MBT. The road dust residue was dried at 80 °C for 12 h and portion of it (0.3–0.5 g) was digested as described in Section 2.3.1.

2.3.3. Microwave-assisted cloud point extraction with 2-MBT

To MW-CPE were subjected non-leached and leached road dust samples. For both digests, 10 ml aliquots were transferred in cen-

Table 2
Microwave program for road dust digestion using MSP 1000 system

	Stage				
	1	2	3	4	5
Power (W)	300	450	600	600	700
Pressure control (Psi)	50	100	120	120	160
Irradiation time (min)	10	20	10	10	5
Cooling time (min)	10	10	15	15	30

Table 3
Potential polyatomic, isobaric and doubly charged ions which overlap the PGM signals

Analyte[a]	Potential interference from ionic species		
	Polyatomic	Isobaric[a]	Doubly charged
^{103}Rh (100)	$^{63}Cu^{40}Ar^+$; $^{86}Sr^{17}O^+$; $^{86}Sr^{16}O^1H^+$; $^{87}Sr^{16}O^+$; $^{87}Rb^{16}O^+$; $^{66}Zn^{37}Cl^+$; $^{68}Zn^{35}Cl^+$		$^{206}Pb^{2+}$
^{105}Pd (22.33)	$^{65}Cu^{40}Ar^+$; $^{89}Y^{16}O^+$; $^{88}Sr^{17}O^+$; $^{88}Sr^{16}O^1H^+$; $^{87}Sr^{18}O^+$; $^{68}Zn^{37}Cl^+$; $^{70}Zn^{35}Cl^+$		
^{106}Pd (27.33)	$^{90}Zr^{16}O^+$; $^{66}Zn^{40}Ar^+$	$^{106}Cd^+$ (1.25)	
^{108}Pd (26.46)	$^{92}Zr^{16}O^+$; $^{92}Mo^{16}O^+$; $^{68}Zn^{40}Ar^+$	$^{108}Cd^+$ (0.89)	
^{110}Pd (11.72)	$^{94}Zr^{16}O^+$; $^{94}Mo^{16}O^+$; $^{70}Zn^{40}Ar^+$	$^{110}Cd^+$ (12.49)	
^{194}Pt (32.90)	$^{178}Hf^{16}O^+$; $^{177}Hf^{17}O^+$; $^{176}Hf^{18}O^+$		
^{195}Pt (33.80)	$^{179}Hf^{16}O^+$; $^{178}Hf^{17}O^+$; $^{177}Hf^{18}O^+$		
^{196}Pt (25.30)	$^{180}Hf^{16}O^+$		

[a] In brackets is presented the natural abundance as percent.

trifuge test tubes (50 ml). Then 2 ml 10% Triton X-100, 1 ml 1% 2-MBT and 0.5 ml 8% $SnCl_2$ were added in the specified order to each sample portion [26]. The solution volumes were made up to 40 ml with 1 mol l^{-1} HCl. A set of six samples was subjected to MW-CPE. After cloud point had been reached, 20 min of MW irradiation (360 W) were applied for phase separation. Further samples were cooled in a freezer and the upper aqueous phase was separated with pipette. The remained surfactant-rich phase was dissolved with 1 mol l^{-1} HCl to a total mass of 5 g and the obtained solution was directly nebulized to ICP-MS. The calibration strategy was based on the measurment of standard solutions prepared in the dissolved surfactant-rich phase obtained from the procedural blank.

2.4. Calculations

The straight-line regression parameters (slope and intercept) and the corresponding standard deviations were calculated by the "LINEST" function of MS Excel.

The combined uncertainty of the corrected signals as well as the one corresponding to the final analyte concentrations in the road dust were calculated by the method of Kragten [27] using MS Excel.

3. Results and discussion

The non-spectral matrix effects associated with the ICP-QMS measurement of the PGM in road dust solutions are usually not problematic. If such effects appear they could be successfully resolved by the methods of standard addition or internal standardization. On contrary the occurrence of spectral interferences has been claimed to make the PGM analysis very sophisticated [22,23,25]. A variety of potential polyatomic, isobaric or doubly charged ions which deteriorate the PGM determination have been reported from different authors [21–23] and the most common are summarized in Table 3. Many of these ionic species are constituted from elements (Sr, Cu, Zn, Pb, and Cd) which are typically present in the road dust at much higher levels than PGM. The rare earth Zr and Hf are also usually found in the road dust because they are components of the emitted car catalyst material [1,22]. There is also evidence that Mo can be significantly enriched in the roadway dust [28]. Hence the spectral interferences are quite probable but experimental proofs must be found for their real appearance in the studied samples [29,30] because the content of the interfering elements can vary in a broad range due to the specific road dust matrix.

3.1. Assessment of significant spectral interferences

For assessment of the interference occurrence it was defined a threshold concentration value ($C_{Threshold}$) for every interfering element above which the caused interference becomes statistically distinguishable. It is reasonable to set this limit at interferent concentration which generates a signal at the mass-to-charge ratio of the analyte corresponding to three times standard deviation of the procedural blank sample ($3s_0$).

$$C_{Threshold} = \frac{3s_0 C_I}{Sig_{AI}} \quad (1)$$

For the determination of each $C_{Threshold}$ value (Eq. (1)) a single interfering element solution with known concentration (C_I) was prepared in an acid media simulating the digestion blank. The solution was introduced into ICP-MS and the produced interfering signal (Sig_{AI}) at the specific analyte m/z was detected. The calculated threshold concentrations for all studied interfering elements are presented in Table 4.

The concentrations of the elements suspected to generate spectral interferences were determined in the investigated road dust samples (Table 5). Further, for the achieved sample digests with dilution factor of 400 (DF = 400), Threshold-ratios (T-ratios) were calculated representing how many times the interferent concentration in the working solutions exceeded the corresponding $C_{Threshold}$ (Table 6). It is evident that the larger the T-ratio, the significance of

Table 4
Threshold interferent concentrations established for acid media simulating the procedural blank[a]

Analyte	LOD[b] (ng l^{-1})	Threshold interferent concentration (μg l^{-1})									
		Cu	Zn	Rb	Sr	Y	Zr	Mo	Cd	Pb	Hf
^{103}Rh	5	410	1900	190	120	–	–	–	–	280	–
^{105}Pd	24	830	7100	–	45	1.2	–	–	–	–	–
^{106}Pd	20	–	4600	–	–	4.1	1.8	-	0.4	–	–
^{108}Pd	21	–	7200	–	–	–	6.3	13	0.6	–	–
^{110}Pd	41	–	–	–	–	–	6.1	22	0.04	–	–
^{194}Pt	27	–	–	–	–	–	–	–	–	–	1.2
^{195}Pt	25	–	–	–	–	–	–	–	–	–	2.1
^{196}Pt	32	–	–	–	–	–	–	–	–	–	1.1

[a] Aqua regia with dilution factor ca. 11.1.
[b] Limits of detection as concentration, calculated at 3s of the procedural blank signals.

Table 5
Concentrations of the interfering elements in the studied road dust samples ($n = 5$)

Interfering element ($\mu g\,g^{-1}$)		Cu	Zn	Rb	Sr	Y	Zr	Mo	Cd	Pb	Hf
RD Alicante	Conc. $\pm u_c$[a]	84 ± 7	81 ± 6	14.4 ± 1.1	630 ± 40	4.7 ± 0.3	5.0 ± 0.3	1.1 ± 0.2	0.20 ± 0.03	56 ± 4	0.13 ± 0.03
RD QuaNas	Conc. $\pm u_c$[a]	233.0[b] ± 22.0	1640.7[b] ± 174.3	24.2 ± 1.4	175 ± 8	8.2 ± 0.6	18.5 ± 1.2	32 ± 2	1.703[b] ± 0.400	778.4[b] ± 60.5	0.67 ± 0.05

[a] Combined uncertainty.
[b] Reported values from the QuaNas Proficiency Testing (mean ± standard deviation).

the spectral interference is higher. The depicted *T*-ratios are relevant to the specific study. If any of the parameters that influence the formation of interfering species as sample matrix or instrumental conditions [22,25,31] is different, the new experimental determination of the actual *T*-ratios for the currently studied sample is needed, following the suggested approach.

Statistically significant spectral effect will be produced when the interfering signal is well above the defined analyte detection limits in the signal domain. Here the studied interferences were divided into three groups: (i) insignificant (*T*-ratio < 1)—the interfering signal is below the detection limit, (ii) unappreciable (1 < *T*-ratio < 3)—where the interfering signal is detectable but not quantifiable, because it falls in the interval between the limit of detection and the limit of quantification so the magnitude of the interference can not be estimated quantitatively due to the large relative uncertainties in this range, (iii) significant (*T*-ratio > 3)—the interference with measurable effect for which is strongly recommended to be taken into consideration.

At this investigation stage the following interferences were discarded as insignificant for the both studied samples: RbO^+ species—overlapping Rh signal; all Zn and Cu-argide or Cu-chloride ions over Pd isotopes. A sample specific interference was registered for the polyatomic species of Cu and Zn over Rh—the *T*-ratios for *RD Alicante* were very low, while in *RD QuaNas* the interferences were unappreciable (1.4 < *T*-ratio < 2.2).

For platinum isotopes no significant interference from Hf was observed. The ^{195}Pt was selected for measurements as the calculated *T*-ratios of Hf were 0.2 and 0.8 for *RD Alicante* and *RD QuaNas*, respectively.

The results above illustrates that 9 of all 22 potential spectral interferences can be discarded because the corresponding *T*-ratios were below 3.

Table 6 shows that Rh was strongly interfered only from Sr in *RD Alicante* but for *RD QuaNas* the pronounced effect of Pb^{2+} must be also regarded.

The most problematic element was palladium as for every isotope there were 2 or 3 significant sources of interference. ^{105}Pd was the only isotope free from isobaric Cd interference but the highest *T*-ratios from Sr and Y were calculated. Cadmium level in the samples caused isobaric interference over all other Pd isotopes in *RD QuaNas* while the interference was apparent only over ^{110}Pd in *RD Alicante*. In *RD QuaNas* ^{106}Pd, ^{108}Pd and ^{110}Pd suffer evident oxide interference from Zr; ^{106}Pd was additionally interfered by Y; and Mo posed significant interference over ^{108}Pd and ^{110}Pd.

The proved significant and complex interferences over Rh and Pd hindered their direct determination. Hence a separation procedure or mathematical correction must be applied.

3.2. Uncertainty evaluation of algorithms for mathematical correction

The mathematical correction is frequently chosen as alternative [24,25,31] since this approach is faster and easier to accomplish in comparison to chemical separation.

In the case when an analyte isotope is interfered from several sources the effect of each interferent must be accounted in an additive scheme. Gomez et al. applied a correction for the mono-isotopic rhodium regarding the influence of Cu, Pb, Sr and Rb [25]. However this is connected with some fundamental shortcomings: (i) additional time and reagents are needed to establish the relation between each interferent and its spectral effect over the analyte signal(s), (ii) the uncertainty of the corrected analyte signal is increased because the number of variables in the model equation is enhanced, and (iii) the part of the measured signal generated from the analyte could be very small in comparison to the fraction produced from the interferents which makes the correction unreliable. The last two points make it reasonable to define some metrological requirements about the calculated signals. A feasible approach is to set maximum acceptable value for the relative combined uncertainty. In the current work to fit for the analytical purpose such limit was posed at 20% which means that the corrected signal is at least 5 times higher than its combined uncertainty.

It is common to apply the so called 'standard addition of the interfering element' in order to correct for the matrix dependant interference, spiking an interferent to the sample solution [24,25,31]. From the difference between the analyte signals measured in the interferent spiked ($Sig_{A+I,s}$) and unspiked ($Sig_{A,s}$)

Table 6
T-ratios for the interfering elements in non-leached road dust samples (DF = 400)

Analyte	Sample	*T*-ratios[a]								
		Cu	Zn	Rb	Sr	Y	Zr	Mo	Cd	Pb
^{103}Rh	*RD Alicante*	0.5	0.1	0.2	13.1	–	–	–	–	0.5
	RD QuaNas	1.4	2.2	0.3	3.6	–	–	–	–	7.0
^{105}Pd	*RD Alicante*	0.3	0.03	–	35	9.8	–	–	–	–
	RD QuaNas	0.7	0.6	–	9.7	17.1	–	–	–	–
^{106}Pd	*RD Alicante*	–	0.04	–	–	2.9	6.9	–	1.2	–
	RD QuaNas	–	0.9	–	–	5.0	25.7	–	10.6	–
^{108}Pd	*RD Alicante*	–	0.03	–	–	–	2.0	0.2	0.8	–
	RD QuaNas	–	0.6	–	–	–	7.3	6.2	7.1	–
^{110}Pd	*RD Alicante*	–	–	–	–	–	2.0	0.1	12.5	–
	RD QuaNas	–	–	–	–	–	7.6	3.6	106	–

[a] The *T*-ratio represents the ratio of the interferent concentration in the working solutions towards its threshold concentration (Table 4).

(A)

Units	Variable	Value	Std-unc	RSU, %	Sig_Rh,s	C_Sr,s	C_Sr,a	Sig_Rh+Sr,s
cps	Sig_Rh,s	3896	257	6.6%	4153	3896	3896	3896
ppb	C_Sr,s	1571	51	3.2%	1571	1622	1571	1571
ppb	C_Sr,a	2000	34	1.7%	2000	2000	2034	2000
cps	Sig_Rh+Sr,s	7385	273	3.7%	7385	7385	7385	7658
			u_c					
cps	Sig_Rh	1155	517	44.74%	1614	1066	1201	940
				diff	-459	89	-46	214
	A) eq. 2		2.67E+05	diff^2	2.11E+05	7.92E+03	2.10E+03	4.60E+04
			sum					
					Sig_Rh,s	C_Sr,s	C_Sr,a	Sig_Rh+Sr,s
	Contribution to combined uncertainty, %				79.0%	3.0%	0.8%	17.2%

(B)

Units	Variable	Value	Std-unc	RSU, %	Sig_Rh,s	F_Sr-slope	C_Sr,s
cps	Sig_Rh,s	3896	257	6.6%	4153	3896	3896
cps/ppb	F_Sr-slope	1.74	0.01	0.8%	1.74	1.75	1.74
ppb	C_Sr,s	1571	51	3.2%	1571	1571	1622
			u_c				
cps	Sig_Rh	1168	273	23.36%	1425	1146	1079
				diff	-257	22	89
	B) eq. 4		7.44E+04	diff^2	6.61E+04	4.86E+02	7.84E+03
			sum				
					Sig_Rh,s	F_Sr-slope	C_Sr,s
	Contribution to combined uncertainty, %				88.8%	0.7%	10.5%

Fig. 1. Corrected Rh signals and their combined uncertainties for *RD Alicante* regarding interference from Sr: (A) applying Eq. (2) and (B) applying Eq. (4).

sample solution, the signal originating from the amount of interferent added can be calculated (Eq. (2)).

$$\mathrm{Sig_A} = \mathrm{Sig_{A,s}} - \frac{C_{\mathrm{I,s}}(\mathrm{Sig_{A+I,s}} - \mathrm{Sig_{A,s}})}{C_{\mathrm{I,a}}} \quad (2)$$

$\mathrm{Sig_A}$ represents the corrected analyte signal, $C_{\mathrm{I,s}}$ corresponds to the initial interferent concentration in the sample solution and $C_{\mathrm{I,a}}$ is the interferent concentration corresponding to the amount of interferent added to the sample solution [31].

(A)

Units	Variable	Value	Std-unc	RSU, %	Sig_Rh,s	C_Sr,s	C_Sr,a	Sig_Rh+Sr,s	C_Pb,s	C_Pb,a	Sig_Rh+Pb,s
cps	Sig_Rh,s	3404	231	6.8%	3635	3404	3404	3404	3404	3404	3404
ppb	C_Sr,s	439	19	4.2%	439	458	439	439	439	439	439
ppb	C_Sr,a	500	9	1.8%	500	500	509	500	500	500	500
cps	Sig_Rh+Sr,s	4158	245	5.9%	4158	4158	4158	4403	4158	4158	4158
ppb	C_Pb,s	1990	80	4.0%	1990	1990	1990	1990	2070	1990	1990
ppb	C_Pb,a	2000	37	1.9%	2000	2000	2000	2000	2000	2037	2000
cps	Sig_Rh+Pb,s	4914	274	5.6%	4914	4914	4914	4914	4914	4914	5188
			u_c								
cps	Sig_Rh	1239	753	60.81%	1903	1211	1251	1024	1178	1266	966
				diff	-665	28	-12	215	60	-27	273
	A) eq. 2		5.68E+05	diff^2	4.42E+05	7.87E+02	1.37E+02	4.63E+04	3.65E+03	7.45E+02	7.43E+04
			sum								
					Sig_Rh,s	C_Sr,s	C_Sr,a	Sig_Rh+Sr,s	C_Pb,s	C_Pb,a	Sig_Rh+Pb,s
	Contribution to combined uncertainty, %				77.8%	0.1%	0.0%	8.2%	0.6%	0.1%	13.1%

(B)

Units	Variable	Value	Std-unc	RSU, %	Sig_Rh,s	F_Sr-slope	C_Sr,s	F_Pb-slope	C_Pb,s
cps	Sig_Rh,s	3404	231	6.8%	3635	3404	3404	3404	3404
cps/ppb	F_Sr-slope	1.48	0.02	1.6%	1.48	1.51	1.48	1.48	1.48
ppb	C_Sr,s	439	19	4.2%	439	439	458	439	439
cps/ppb	F_Pb-slope	0.75	0.01	1.9%	0.75	0.75	0.75	0.77	0.75
ppb	C_Pb,s	1990	80	4.0%	1990	1990	1990	1990	2070
			u_c						
cps	Sig_Rh	1257	242	19.30%	1488	1247	1229	1228	1197
				diff	-231	10	28	29	60
	B) eq. 5		5.88E+04	diff^2	5.35E+04	1.03E+02	7.60E+02	8.21E+02	3.62E+03
			sum						
					Sig_Rh,s	F_Sr-slope	C_Sr,s	F_Pb-slope	C_Pb,s
	Contribution to combined uncertainty, %				91.0%	0.2%	1.3%	1.4%	6.2%

Fig. 2. Corrected Rh signals and their combined uncertainties for *RD QuaNas* regarding combined interference from Sr and Pb: (A) applying Eq. (2) in additive scheme and (B) applying Eq. (5).

Table 7
Comparison among the spectral corrections made for Pd isotopes (DF = 400) and corresponding analyte concentrations in non-leached road dust samples

Isotope	Sample	Initial signals (cps[a])	Polyatomic interference		Isobaric interference from Cd	Conc. in road dust after spectral correction (ng g^{-1})[b]
			Regarded interferents/model equation	Corrected signals (cps)[b]	Corrected signals (cps)[b]	
^{105}Pd	*RD Alicante*	20,989 ± 1109	Sr, Y/Eq. (5)	3287 ± 1427	–	239 ± 113
	RD QuaNas	7967 ± 388	Sr, Y/Eq. (5)	106 ± 484	–	<10[c]
^{106}Pd	*RD Alicante*	4101 ± 290	Zr/Eq. (4)	2759 ± 291	Not needed	191 ± 22
	RD QuaNas	7760 ± 314	Zr, Y/Eq. (5)	417 ± 410	NA[d]	<8[c]
^{108}Pd	*RD Alicante*	2815 ± 187	–	Not needed	Not needed	182 ± 15
	RD QuaNas	3898 ± 211	Zr, Mo/Eq. (5)	172 ± 253	NA[d]	<8[c]
^{110}Pd	*RD Alicante*	2755 ± 162	–	Not needed	1286 ± 196	189 ± 34
	RD QuaNas	11,060 ± 735	Zr, Mo/Eq. (5)	7534 ± 754	NA[d]	NA[d]

[a] Signal ± instrumental standard deviation (n = 20).
[b] Signal (concentration) ± combined uncertainty.
[c] Below the corresponding detection limits.
[d] Not available due to MoO^+ formation.

A factor of interference F_I can be defined as a measure of how much the analyte signal is enhanced when the interferent concentration is raised with a single increment (Eq. (3)).

$$F_I = \frac{Sig_{A+I,s} - Sig_{A,s}}{C_{I,a}} \quad (3)$$

The evaluation of F_I can be accomplished more precisely if several sample aliquots are spiked with gradient interferent concentrations. In such way the function between the generated interfering signal and the interferent concentration can be fitted to a linear mathematical model ($Sig_{total} = F_{I\text{-slope}}C_I + Sig_A$) in which the slope ($F_{I\text{-slope}}$) represents the factor of interference. In the current study the least squares method was used for line fitting towards four experimental points and the standard deviation of the regression line slope was accepted as standard uncertainty of $F_{I\text{-slope}}$.

For a sample solution with known concentration of the interfering element, the pure analyte signal can be calculated (Eq. (4)).

$$Sig_A = Sig_{A,s} - C_{I,s}F_{I\text{-slope}} \quad (4)$$

When spectral correction, including several sources, must be made, Eq. (4) transforms in Eq. (5), where $F_{I1\text{-slope}}$, $F_{I2\text{-slope}}$, . . ., $F_{In\text{-slope}}$ are the calculated interference factors (as slopes) for the number of interferents with corresponding concentrations $C_{I1,s}$, $C_{I2,s}$,. . ., $C_{In,s}$ in the sample solution.

$$Sig_A = Sig_{A,s} - C_{I1,s}F_{I1\text{-slope}} - C_{I2,s}F_{I2\text{-slope}} - \cdots - C_{In,s}F_{In\text{-slope}} \quad (5)$$

Both approaches for estimation of the interference contribution (Eqs. (2) and (4)) seem quite similar but the combined uncertainty of the corrected analyte signal can differ substantially in dependence on the selected model equation. The last effect was studied by uncertainty budget analysis of the corrected signals.

A comparison of these alternative algorithms is presented for the corrected signals of ^{103}Rh and corresponding combined uncertainties calculated by the Kragten's method. For *RD Alicante* (Fig. 1) the strontium based interference was only regarded while for *RD QuaNas* (Fig. 2) an additive scheme was applied accounting also the effect of lead (Table 6).

Both algorithms brought to statistically identical analyte signals after correction but the corresponding combined uncertainties (u_c) were substantially higher when Eq. (2) was applied. Consequently the suggested method for correction (Eqs. (4) and (5)) was preferred as it offers the following advantages: (i) results in lower uncertainty of the corrected signals, (ii) indicates for potential outliers, and (iii) evaluates the linearity of the function: signal at analyte m/z vs interferent concentration. Additionally the sample aliquots already spiked with gradient interferent amounts can be used to determine the original interferent concentration in the working solution by the method of standard addition. The accurate determination of the interfering element concentration itself is very important as it is also included in the correction algorithm (Eqs. (4) and (5)).

The analysis of Rh was problematic because the element is mono-isotopic and strong interferences were evident due to the high T-ratios (Table 6). The uncertainty budget analysis showed that for both road dust samples no reliable calculations can be made by single interferent addition (Eq. (2)) because the corrected signals were related with very high relative uncertainties of 44.7% and 60.8%, respectively (Figs. 1 and 2(A)). It is evident that the experimentally registered signals had the greatest contribution among the variables. When Eq. (2) was applied in an additive scheme the combined uncertainty was even larger due to the greater number of measured signals (Fig. 2A).

Employing the slope based factor of interferences (Eqs. (4) and (5)) the relative signal uncertainties were on the boundary of the postulated acceptable limit of 20% even involving two interferents in the correction (Figs. 1 and 2(B)).

The most sophisticated was palladium determination. The only measurement free from spectral interferences was the one of ^{108}Pd in *RD Alicante* (Table 6). In all other cases significant interferences originating from different sources with varying T-ratios must be accounted. A comparative study aiming the selection of the most appropriate Pd isotope was carried out, based on the assessment of the combined uncertainties of the corrected signals (Eqs. (4) and (5)). The results are presented in Table 7.

The corrections for ^{105}Pd, ^{106}Pd and ^{110}Pd in *RD Alicante* reflected in signal relative uncertainty of 43.4%, 10.5% and 15.2%, respectively. Although the corresponding Pd concentrations were statistically identical to the one when interference free ^{108}Pd was used, the final concentration uncertainty was enlarged in the order: ^{106}Pd < ^{110}Pd < ^{105}Pd.

Due to the combined effects of interferents at high levels and very low Pd content in the *RD QuaNas*, the corrected signals for ^{105}Pd, ^{106}Pd and ^{108}Pd were statistically indistinguishable from zero. For this sample it was impossible to make an isobaric correction from Cd due to the elevated molybdenum content. Spread in a wide range (92–100 amu) the Mo isotopes form oxides between 108 and 116 amu thus hindering the registration of free Cd isotope upon which the isobaric correction to be made. Hence the isobaric Cd interference can not be accounted at the presence of substantial Mo amount.

Concluding the results above it can be derived that the direct analysis of Rh and Pd in road dust based on mathematical correc-

Table 8
T-ratios for the obtained MW digests of leached road dust samples (DF = 100)[a]

Analyte	Sample	*T*-ratios					
		Sr	Y	Zr	Mo	Cd	Pb
^{103}Rh	*RD Alicante*	5.2	–	–	–	–	0.8
	RD QuaNas	2.6	–	–	–	–	3.9
^{105}Pd	*RD Alicante*	14.1	4.0	–	–	–	–
	RD QuaNas	7.0	27.4	–	–	–	–
^{108}Pd	*RD Alicante*	–	–	7.3	0.7	0.5	–
	RD QuaNas	–	–	13.1	15.6	4.3	–

[a] The dilution factor is fourfold lower in respect to the non-leached samples (DF = 400) for which the corresponding *T*-ratios are presented in Table 6.

tions is very complicated. The extent of the spectral interferences can vary in a broad range, depending on the specific sample matrix i.e. relative analyte/interferent levels and the number of elements having contribution to the interference.

3.3. Spectral interference alleviation by preliminary road dust leaching

In order to develop a unified and robust method for mutual PGM analysis in diverse road dust samples it was investigated the separation of the interfering elements from the analytes. Samples were preliminary leached with diluted HCl (before MW digestion). The leaching was accomplished at ambient temperature supposing that the PGM attached to the auto-catalyst particles are chemically inert and will not react with the diluted acid under soft conditions. It is expected that some easily soluble interferents will be leached.

Preliminary experiments showed that substantial quantities of interferents were removed by using 0.35 mol l^{-1} HCl. In order to define the amount of acid needed to obtain maximum elimination of the interfering elements, 1 g of road dust was sequentially leached with aliquots of 10 ml 0.35 mol l^{-1} HCl setting 60 min as reaction time for each portion. The removed quantities of each interferent were determined at every step and their sum up ($Q_{leached}$, μg g^{-1}) was divided to the initial quantity of the interfent in the road dust ($Q_{initial}$, μg g^{-1}) to obtain the cumulative elimination (*P*%, Eq. (6)).

$$P\% = \frac{Q_{leached}}{Q_{initial}} \times 100 \quad (6)$$

After the fifth acid aliquot no further increase in the cumulative interferent elimination was observed for *RD Alicante*. Sr and Y were significantly eliminated (ca. 90%) while the lowest interferent removal corresponded to Zr, Mo and Hf (below 10%). The *P*% values for the other interferents were as follow: P_{Cd} = 84%, P_{Zn} = 61%, P_{Pb} = 59%, and P_{Cu} = 32%.

For *RD QuaNas* the cumulative elimination values were: P_{Sr} = 82%, P_Y = 60% and P_{Pb} = 86%. The removal of Zr, Mo and Hf was strongly dependant on the sample type. While these elements were hardly leached from *RD Alicante* their elimination from *RD QuaNas* was much more significant (P_{Zr} = 55%, P_{Mo} = 37% and P_{Hf} = 51%).

The effect of leaching time was also investigated and it was found that 60 min were enough for procedure completion. The leaching procedure was tested at a single step using one portion of 50 ml 0.35 mol l^{-1} HCl for 60 min and comparable results to the listed above were obtained. So for further studies the road dust samples were leached under the last conditions. The adopted leaching procedure has demonstrated its effectiveness in the current study but it should be emphasized that sample matrix could show different behavior so the suggested conditions must be verified for the sample under investigation.

After leaching, the sample mass was reduced by 69% for *RD Alicante* and 47% for *RD QuaNas*. This fact in combination with the relative analyte/interferents preconcentration in the road dust residue makes it reasonable after MW digestion to lower the sample dilution factor to ca. 100 for preliminary leached road dust, instead of DF∼400 for directly digested samples. This was beneficial for obtaining higher analyte signals especially in the case when PGM concentrations were extremely low.

The degree of interference from Sr, Y and Pb over Rh and Pd was substantially reduced after leaching even working with fourfold lower dilution factor (Table 8) because significant amounts of these elements were removed from both *RD Alicante* and *RD QuaNas*. Among palladium isotopes ^{105}Pd was selected for further measurements concerning the mutual PGM analysis and the method robustness because: (i) for spectral correction of ^{105}Pd the effect of Sr and Y must be accounted but Sr-spiked sample solutions were already prepared for determining the factor of interference over Rh and only spiked solutions with Y should be made, (ii) for ^{106}Pd, ^{108}Pd and ^{110}Pd supplementary spikes of Zr and/or Mo must be added, (iii) the leaching of Zr and Mo was less effective and depends from the sample type. A consequence from the last is the approximately 4 times increased *T*-ration of Zr for ^{108}Pd in *RD Alicante* when the dilution factor was lowered (Table 8), while the corresponding *T*-ratio in *RD QuaNas* was only twice higher because 55% of the interferent was leached.

Table 9
Comparison of the analyte concentrations obtained with mathematical spectral correction versus preconcentration by MW-CPE of leached road dust samples (DF = 100)

Isotope	Sample	Spectral correction				MW-CPE
		Regarded interferents/model equation	Initial signals (cps)[a]	Corrected signals (cps)[b]	Conc. (ng g^{-1})[b]	Conc. (ng g^{-1})[b]
^{103}Rh	*RD Alicante*	Sr/Eq. (4)	7303 ± 334	5036 ± 358	15 ± 2	16 ± 1
	RD QuaNas	Pb/Eq. (4)	5308 ± 229	4489 ± 251	17 ± 2	16 ± 1
^{105}Pd	*RD Alicante*	Sr, Y/Eq. (5)	24393 ± 965	10,642 ± 1039	184 ± 20	186 ± 11
	RD QuaNas	Sr, Y/Eq. (5)	9897 ± 518	145 ± 586	<3[c]	<1[d]
^{195}Pt	*RD Alicante*	–	5547 ± 226	Not needed	62 ± 3	59 ± 3
	RD QuaNas	–	7039 ± 356	Not needed	97 ± 5	98 ± 6

[a] Signal ± instrumental standard deviation (*n* = 20).
[b] Signal (concentration) ± combined uncertainty.
[c] Below the corresponding detection limits (0.5, 3, and 3 ng g^{-1} for Rh, Pd, and Pt, respectively).
[d] Below the corresponding detection limits (0.2, 1, and 1 ng g^{-1} for Rh, Pd, and Pt, respectively).

3.4. Method validation

The obtained results for the leached road dust samples after mathematical spectral correction were validated by alternative method of analysis (Table 9). Aliquots of the MW digests were subjected to MW-CPE with 2-MBT to separate the PGM from the sample matrix (see Section 2.3.3). Very good accordance between the results from the both approaches was observed showing the adequateness of the applied mathematical corrections. In all cases the achieved relative combined uncertainties of the corrected signals were below 10% which is twice lower than the postulated value to fit for the analytical purpose (Section 3.2).

Another critical point was to prove that PGM were not also leached from the road dust samples. For the analytes that have isotopes free form spectral interference as in the case of Pt determination in both samples as well as the quantification of ^{108}Pd in *RD Alicante* the direct analysis of non-leached samples was accomplished. The obtained results for palladium ($182 \pm 15\,ng\,g^{-1}$) and platinum ($62 \pm 4\,ng\,g^{-1}$) in *RD Alicante*, and platinum ($101 \pm 6\,ng\,g^{-1}$) in *RD QuaNas* fit very well as mean values and combined uncertainties with the data in Table 9. This demonstrates that Pd and Pt were not leached from the road dust samples. The direct analysis of the strongly interfered mono-isotope of Rh was possible only after mathematical correction resulting in $15 \pm 4\,ng\,g^{-1}$ in *RD Alicante* (Eq. (4)) and $16 \pm 4\,ng\,g^{-1}$ in *RD QuaNas* (Eq. (5)), but at the cost of enlarged relative combined uncertainty of 27% and 25%, respectively. The last does not allow to make an adequate estimation of the potential Rh loss by comparison with the data in Table 9.

The MW-CPE preconcentration with 2-MBT was applied to non-leached *RD QuaNas* with the aim to separate the PGM from interfering matrix elements and thus to lower the analysis uncertainty. The obtained concentrations were as follow: Rh: 15 ± 1; Pd < 4; and Pt: $94 \pm 5\,ng\,g^{-1}$, with the corresponding methodological detection limits of 1, 4, and $5\,ng\,g^{-1}$. The good agreement between achieved results together with their low and comparable uncertainties for leached (Table 9) and non-leached *RD QuaNas* clearly indicates that no significant amounts of the analytes were lost by preliminary acid leaching. The last was alternatively proved by subjecting also the leaching extracts to MW-CPE with 2-MBT. After preconcentration no leached PGM were detected.

4. Conclusions

The PGM analysis in road dust samples is prone to a diversity of potential spectral interferences. The *T*-ratio is suggested as a cut off for interferences of a magnitude to affect the analyte signal. Only when the interference is significant (*T*-ratio > 3), a mathematical correction will result in statistically different corrected signal compared to the initial one.

In all cases the mathematical correction increases the resulted signal uncertainty which is further strongly dependent on the used model. The uncertainty budget analysis is a useful tool for estimation of the correction algorithm as well as for the selection of the most appropriate analyte isotope for measurement.

For road dust solutions obtained after direct sample digestion the interferences over Rh and Pd are highly sample specific so the adequateness of the mathematical corrections depends on the number of elements causing spectral interference and the relative analyte/interferent ratios. The interferences can be minimized by simple preliminary leaching with $0.35\,mol\,l^{-1}$ HCl. The procedure does not remove PGM from the road dust while substantial amounts of Sr, Y and Pb are eliminated. The last makes the mutual PGM analysis reliable and robust when ^{103}Rh, ^{105}Pd and ^{195}Pt are used for ICP-MS measurements.

Furthermore, MW-CPE with 2-mercaptobenzothiazole is proved to be an efficient procedure for PGM separation from the sample matrix which can be applied as an independent and selective method of analysis.

Acknowledgements

This work has been undertaken as part of the EU sponsored COST programme (Action D32, working group D32/005/04, "Microwaves and Ultrasound Activation in Chemical Analysis"). K.S. also thanks "Vicerrectorado de Investigación, Desarrollo e Innovación" of University of Alicante for partially supporting his visit.

References

[1] K. Ravindra, L. Bencs, R. Van Grieken, Sci. Tot. Environ. 318 (2004) 1.
[2] B. Gomez, M.A. Palacios, M. Gomez, J.L. Sanchez, G. Morrison, S. Rauch, C. Mcleod, R. Ma, S. Caroli, A. Alimonti, F. Petrucci, B. Bocca, P. Schramel, M. Zischka, C. Petterson, U. Wass, Sci. Tot. Environ. 299 (2002) 1.
[3] M. Moldovan, M.A. Palacios, M.M. Gomez, G. Morrison, S. Rauch, C. Mcleod, R. Ma, S. Caroli, A. Alimonti, F. Petrucci, B. Bocca, P. Schramel, M. Zischka, C. Pettersson, U. Wass, M. Luna, J.C. Saenz, J. Santamaria, Sci. Tot. Environ. 296 (2002) 199.
[4] R. Merget, G. Rosner, Sci. Tot. Environ. 270 (2001) 165.
[5] C.B. Ojeda, F.S. Rojas, J.M.C. Pavon, A.G. de Torres, Anal. Chim. Acta 494 (2003) 97.
[6] E. Ivanova, F. Adams, Fresenius' J. Anal. Chem. 361 (1998) 445.
[7] K.S. Patel, P.C. Sharma, P. Hoffmann, Fresenius' J. Anal. Chem. 367 (2000) 738.
[8] M.L. Lee, G. Tolg, E. Beinrohr, P. Tschopel, Anal. Chim. Acta 272 (1993) 193.
[9] P. Kovacheva, R. Djingova, Anal. Chim. Acta 464 (2002) 7.
[10] R. Vlasankova, V. Otruba, J. Bendl, M. Fisera, V. Kanicky, Talanta 48 (1999) 839.
[11] M.B. Gomez, M.M. Gomez, M.A. Palacios, J. Anal. At. Spectrom. 18 (2003) 80.
[12] R. Djingova, H. Heidenreich, P. Kovacheva, B. Markert, Anal. Chim. Acta 489 (2003) 245.
[13] K. Benkhedda, B. Dimitrova, H.G. Infante, E. Ivanova, F.C. Adams, J. Anal. At. Spectrom. 18 (2003) 1019.
[14] N.N. Meeravali, S.J. Jiang, J. Anal. At. Spectrom. 23 (2008) 854.
[15] A.M.G. Figueiredo, J. Enzweiler, C.P.R. Morcelli, J.E.S. Sarkis, ICP-MS and Te Co-precipitation after nickel sulphide fire-assay collection for Pd determination in roadside soils, in: F. Zereini, F. Alt (Eds.), Palladium Emissions in the Environment—Analytical Methods, Environmental Assessment and Health Effects, Springer, New York, 2006, pp. 163–172.
[16] G. Giaveri, E. Rizzio, M. Gallorini, Anal. Chem. 73 (2001) 3488.
[17] D. Wildhagen, V. Krivan, Anal. Chim. Acta 274 (1993) 257.
[18] R.R. Barefoot, J.C. Van Loon, Talanta 49 (1999) 1.
[19] M.A.M. da Silva, V.L.A. Frescura, A.J. Curtius, Spectrochim. Acta B 56 (2001) 1941.
[20] R. Djingova, P. Kovacheva, Analytical problems and validation of methods for determination of palladium in environmental materials, in: F. Zereini, F. Alt (Eds.), Palladium Emissions in the Environment—Analytical Methods, Environmental Assessment and Health Effects, Springer, New York, 2006, pp. 145–162.
[21] L. Bencs, K. Ravindra, R. Van Grieken, Spectrochim. Acta B 58 (2003) 1723.
[22] G. Kollensperger, S. Hann, G. Stingeder, J. Anal. At. Spectrom. 15 (2000) 1553.
[23] S. Rauch, M. Motelica-Heino, G.M. Morrison, O.F.X. Donard, J. Anal. At. Spectrom. 15 (2000) 329.
[24] M. Moldovan, M.M. Gomez, M.A. Palacios, J. Anal. At. Spectrom. 14 (1999) 1163.
[25] M.B. Gomez, M.M. Gomez, M.A. Palacios, Anal. Chim. Acta 404 (2000) 285.
[26] K. Simitchiev, V. Stefanova, V. Kmetov, G. Andreev, N. Kovachev, A. Canals, J. Anal. At. Spectrom. 23 (2008) 717.
[27] J. Kragten, Analyst 119 (1994) 2161.
[28] G. Dongarra, G. Sabatino, M. Triscari, D. Varrica, J. Environ. Monit. 5 (2003) 766.
[29] I. Kolibarska, S. Velichkov, N. Daskalova, Spectrochim. Acta B 63 (2008) 603.
[30] N. Velitchkova, E.N. Pentcheva, N. Daskalova, Spectrochim. Acta B 59 (2004) 871.
[31] M. Parent, H. Vanhoe, L. Moens, R. Dams, Talanta 44 (1997) 221.

Talanta 77 (2008) 718–726

Contents lists available at ScienceDirect

Talanta

journal homepage: www.elsevier.com/locate/talanta

Nickel pyrazolyl borate complexes: Synthesis, structure and analytical application in biological and environmental samples as anion selective sensors

Ashok K. Singh*, Vaibhave Aggarwal, Udai P. Singh, Sameena Mehtab

Department of Chemistry, Indian Institute of Technology Roorkee, Roorkee 247667, India

ARTICLE INFO

Article history:
Received 1 May 2008
Received in revised form 5 July 2008
Accepted 7 July 2008
Available online 25 July 2008

Keywords:
PVC membrane
Ion selective membrane sensors
Pyrazolylborate nickel complexes

ABSTRACT

A [{hydrotris(3-phenyl-5-methyl-1-pyrazolyl)borate}(3-phenyl-5-methyl-pyrazole) nickel chloride] [$Tp^{Ph,Me}Ni(Cl)Pz^{Ph,Me}H$] (**I**) has been synthesized and explored as ionophores for the preparation of a poly (vinyl chloride) (PVC) membrane sensor for azide and thiocyanate anions. The compounds [$Tp^{Ph,Me}Ni(N_3)Pz^{Ph,Me}H$] (**II**) and [$Tp^{Ph,Me}Ni(SCN)Pz^{Ph,Me}H$] (**III**) were characterized by their crystal structures and proved to be bonded as monodentate through nitrogen atom of azide and thiocyanate anion. Potentiometric investigations also indicate high affinity of this receptor for thiocyanate and azide ions. PVC based membranes of **I** using as hexadecyltrimethylammonium bromide (HTAB) cation discriminator and *o*-nitrophenyloctyl ether (*o*-NPOE), dibutylphthalate (DBP), acetophenone (AP) and tributylphosphate (TBP) as plasticizing solvent mediators were prepared and investigated as SCN^- and N_3^- selective sensors. The best performance was shown by the membrane of thiocyanate with composition (w/w) of (**I**) (7%):PVC (31%):DBP (60%):HTAB (2%). This sensor works well over a wide concentration range 5.3×10^{-7} to 1.0×10^{-2} M with Nernstian compliance (59.2 mV decade^{-1} of activity) within pH range 2.5–9.0 with a response time of 11 s and showed good selectivity for thiocyanate ion over a number of anions. The sensor exhibits adequate life (3 months) and could be used successfully for the determination of thiocyanate content in human urine, saliva and river water samples. While the membrane of [$Tp^{Ph,Me}Ni(Cl)Pz^{Ph,Me}H$] ionophore with composition (**I**) (6%):HTAB (4%):PVC (31%):TBP (59%) showed highest sensitivity and widest linear range for azide ion. These sensors exhibit the maximum working concentration range of 8.1×10^{-6} to 1.0×10^{-2} M with Nernstian slope of 59.3 mV decade^{-1} of activity. It can be applied for the monitoring of the azide ions concentration in aqueous black tea and orange juice samples.

1. Introduction

Thiocyanate is the end product of detoxification of cyanide compounds and excreted in urine, saliva and serum. The determination of SCN^- is particularly important as its chronically elevated levels in body fluids are known to be toxic and its relation to local goiter, vertigo, or unconsciousness has been pointed out [1], it is also considered to be a biomarker in distinguishing smokers from non-smokers [2]. Another important sample where the determination of the thiocyanate anion is of interest is in water, especially wastewater. At low pH values, thiocyanate containing wastewater, when discharged into natural water, converts into cyanide ion in the presence of oxidants and thereby causes profound damage to aquatic life.

Azide is also a broad-spectrum biocide showing bactericidal, fungicidal, insecticidal, and nematocidal activity. Small quantities of this highly toxic substance are also used in the preparation of biocides, in explosives detonators, as a radical scavenger, in the formulation of getters in electric discharge tubes, and in anti-corrosion solutions [3–7]. Azide is readily protonated in the aqueous environment to yield volatile hydrazoic acid that can then pose an airborne hazard [8]. The high solubility of sodium azide implies that spills could potentially migrate into sewers, streams, lakes and groundwater systems. Azide is a potent hypotensive agent in humans [9,10]. Fatal doses occur with exposures of 700 mg (10 mg kg^{-1}), but exposure to smaller doses can cause eye and skin irritation, headache, nausea, shortness of breath, blurred vision, low blood pressure, or kidney damage. It was experimentally applied to agricultural fields in the past to study its potential as a soil fumigant against insects, microorganisms, and weeds. Therefore, the determination of thiocyanate and azide in environmental and biological samples is of important practical significance.

* Corresponding author. Tel.: +91 1332 285798.
E-mail address: akscyfcy@iitr.ernet.in (A.K. Singh).

0039-9140/$ – see front matter © 2008 Published by Elsevier B.V.
doi:10.1016/j.talanta.2008.07.029

Potentiometric detectors based on ion-selective electrodes (ISEs) offer advantages such as selectivity, sensitivity, good precision, simplicity, wide linear range, low cost and rapid determination of variety of ions in different type of samples. The key ingredients of membrane sensor is the incorporated ionophore, which defines the selectivity of the sensor *via*, selective complex formation with ion of interest. There are large efforts have been made to design thiocyanate-selective membranes for sensor applications. They were based on various ionophores *viz.*, Zn-phthalocyanine complex [11], Cu(II) bis-[*N*-(2-hydroxyethyl)salicyladiamino] complex [12], Linear polyamines [13], Ni(II)benzoN_4 macrocycle-complex [14], bis(2-pyridinethiolato) mercury(II) complexes [15], Rh(III) complex [16], Mn(II) *N*,*N*′-bis-(4-phenylazosalicylidine) complex [17], Mn-porphyrin derivative [18], crown ether [19], *etc.* While only few sensors have been reported for azide determination based on ionophores *viz.* iron(III) and cobalt(III) complexes of 2,3,7,8,12,13,17,18-octakis(benzylthio)-5,10,15,20-tetraazaporphyrin [20], cyanoaqua cobyric acid heptakis(2-phenylethyl ester) [21], substituted onium base salts [22], iron(II) and nickel(II) bathophenanthroline-azide ion-pair complexes [23] and gas electrode with Teflon membrane [24]. These reported ISEs have some limitations *viz.* narrow working concentration range, low pH range, considerable interfering effect of various anions or high response time. Therefore, there is a need for developing a better sensor for thiocyanate and azide ions. The [{hydrotris(3-phenyl-5-methyl-1-pyrazolyl)borate}(3-phenyl-5-methyl-pyrazole)nickel chloride] is used in this work to enable new insights in the field of thiocyanate and azide determination by ion-selective membrane sensors.

2. Experimental

2.1. Reagents and chemicals

All solvents used were purified by the literature methods [25]. All manipulations were carried out under air atmosphere. 3-Phenyl-5-methyl pyrazole [$Pz^{Ph,Me}H$] and potassium hydrotris(3-phenyl-5-methyl-pyrazol-1-yl)borate [$KTp^{Ph,Me}$] were synthesized by literature methods [26]. For membrane preparation, high molecular weight poly (vinyl chloride) (PVC), *o*-nitrophenyloctyl ether (*o*-NPOE), dibutylphthalate (DBP), acetophenone (AP), tributylphosphate (TBP), hexadecyltrimethylammonium bromide (HTAB), and tetrahydrofuran (THF) were used as received from Fluka. Tris-hydroxymethylaminomethane (TRIS), Glycine (Gly) and 2-morpholinoethanesulfonic acid (MES) were also purchased from Fluka.

Reagent grade sodium and potassium salts of all anions used were of highest purity available from SRL (Mumbai, India) and used without any further purification except for vacuum drying over P_2O_5. Anionic salt solutions were prepared in doubly distilled water and standardized whenever necessary.

2.2. Physical methods

Carbon, hydrogen, and nitrogen were analyzed with a Vario EL III elemental analyzer after carefully drying samples under vacuum for several hours. The UV–vis spectra were recorded on PerkinElmer Lambda 35 UV/vis spectrophotometer. IR spectra were obtained on a Thermo Nikolet Nexus FT-IR spectrometer in KBr. Room temperature magnetic susceptibility measurements were done on a Princeton applied research vibrating sample magnetometer Model 155. The X-ray data collection and processing for complex **II** and **III** were performed on Bruker Kappa Apex-CCD diffractometer by using graphite monochromated Mo-K_α radiation (λ = 0.71070 Å) at 100 K. Crystal structures were solved by direct methods. Structure solution, refinement and data output were carried out with the SHELXTL program [27,28]. All non-hydrogen atoms were refined anisotropically. Hydrogen atoms were placed in geometrically calculated positions by using a riding model. Images were created with the DIAMOND program [29]. Hydrogen bonding interactions in the crystal lattice were calculated with both SHELXTL and DIAMOND program.

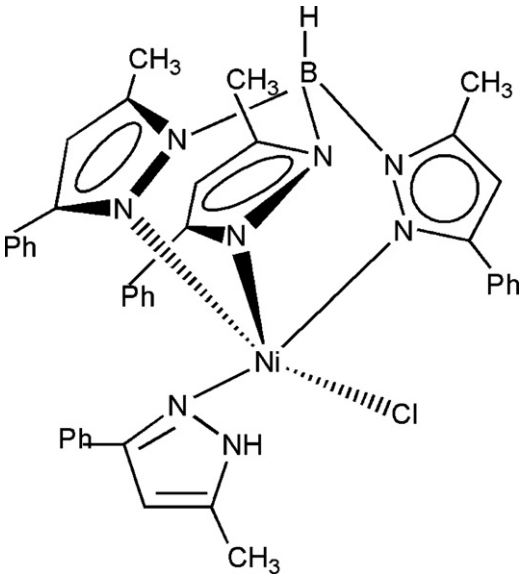

Fig. 1. Structure of [{hydrotris(3-phenyl-5-methyl-1-pyrazolyl)borate}(3-phenyl-5-methyl-pyrazole) nickel chloride] [$Tp^{Ph,Me}Ni(Cl)Pz^{Ph,Me}H$] ionophore.

2.3. Synthesis of ionophore and its azide and thiocyanate complexes

2.3.1. 2.3.1[{hydrotris(3-phenyl-5-methyl-1-pyrazolyl)borate}(3-phenyl-5-methyl-pyrazole) nickel chloride] [$Tp^{Ph,Me}Ni(Cl)Pz^{Ph,Me}H$] (***I***)

(0.47 g, 1.99 mmol) $NiCl_2{\cdot}6H_2O$, (0.32 g, 1.99 mmol) $Pz^{Ph,Me}H$ and (1.04 g, 1.99 mmol) $Tp^{Ph,Me}$ were stirred in 25 mL CH_2Cl_2 + 5 mL CH_3OH for 6 h. The mixture was filtered over celite and solvent was evaporated to dryness under vacuum. The compound in 84.8% (1.24 g, 1.69 mmol) yield was dissolved in 5 mL toluene and yellow crystals were obtained at −20 °C (Fig. 1). Anal. Calc. (%) for $C_{40}H_{38}N_8BClNi$: C, 65.26; H, 5.17; N, 15.20. Found: C, 65.10; H, 5.08; N, 15.02. IR (KBr, cm^{-1}): ν(BH) 2532. UV–vis (toluene, λ_{max}, nm, ε, $M^{-1}\,cm^{-1}$): 286 (832), 484 (272). μ_{eff} = 3.49 B.M. at 295 K.

2.3.2. Azide complex of ionophore [$Tp^{Ph,Me}Ni(N_3)Pz^{Ph,Me}H$] (***II***)

(0.22 g, 0.30 mmol) **I** and (0.02 g, 0.30 mmol) of sodium azide was allowed to react in a mixture of 5 mL methanol and 10 mL toluene for 1 h. The mixture was filtered over celite and the solvent was evaporated to dryness. The green coloured compounds in 74.8% (0.16 g, 0.21 mmol) yield were recrystallized from acetonitrile at −20 °C. Anal. Calc. (%) for $C_{40}H_{38}N_{11}BNi$: C, 64.69; H, 5.12; N, 20.75. Found: C, 64.57; H, 5.02; N, 20.28. IR (KBr, cm^{-1}): ν(BH) 2524, $\nu(N_3)$ 2075. UV–vis (acetonitrile, λ_{max}, nm, ε, $M^{-1}\,cm^{-1}$): 394 (375), 644 (194). μ_{eff} = 3.53 B.M. at 295 K.

2.3.3. Thiocyanate complex of ionophore [$Tp^{Ph,Me}Ni(NCS)Pz^{Ph,Me}H$] (***III***)

This complex was prepared in 71.7% (0.54 g, 0.71 mmol) yield as outlined above for **II**. Anal. Calc. (%) for $C_{41}H_{38}N_9SBNi$: C, 64.90;

Table 1
Crystal data and structure refinement 2.II.CH_3CN and III complexes

	2.II.CH_3CN	III
Formula	$C_{82}H_{79}N_{23}B_2Ni_2$	$C_{41}H_{38}N_9BSNi$
M	1525.68	758.37
Crystal system	Triclinic	Triclinic
Space group	$P\bar{1}$	$P\bar{1}$
a (Å)	11.3684(19)	11.707(4)
b (Å)	12.344(2)	11.806(4)
c (Å)	14.252(2)	15.481(6)
α (°)	86.878(10)	83.07(2)
β (°)	89.953(10)	80.76(2)
γ (°)	72.004(9)	64.931(19)
V (Å^3)	1899.1(5)	1909.7(12)
Z	1	2
D_{calc} (g cm^{-3})	1.334	1.319
T (K)	100	100
F (0 0 0)	798	792.0
μ (mm^{-1})	0.558	0.605
θ_{range} (°)	1.43–27.80	1.31–25.55
Reflections measured	8804	7141
Reflections used	6509	4046
Params	516	490
R^a ($I > 2\sigma$ (I))	$R1 = 0.0496$	$R1 = 0.0758$
	w$R2 = 0.1227$	w$R2 = 0.1793$
R^a (all data)	$R1 = 0.0779$	$R1 = 0.1431$
	w$R2 = 0.1510$	w$R2 = 0.2336$
S	0.940	1.338

H, 5.01; N, 16.62. Found: C, 64.77; H, 5.13; N, 16.48. IR (KBr, cm^{-1}): ν(BH) 2529, ν(NCS) 2058. UV–vis (acetonitrile, λ_{max}, nm, ε, M^{-1} cm^{-1}): 488 (136). μ_{eff} = 3.55 B.M. at 295 K.

2.4. Fabrication of normal PVC membrane and sandwich PVC membrane

The membranes were prepared as suggested by Craggs et al., [30]. It is known that the sensitivity, linearity and selectivity obtained for a given ionophore depend significantly on the membrane composition and nature of plasticizer used [31–33]. The PVC-based membranes were prepared by dissolving appropriate amounts of ionophore, cation excluder HTAB and various plasticizers (DBP, *o*-NPOE, AP or TBP) with PVC matrix in THF (5 mL).

Table 2
Selected bond lengths (Å) and angles (°) for [Tp^{Ph,Me}Ni(N_3)Pz^{Ph,Me}H] (II) and [Tp^{Ph,Me}Ni(SCN)Pz^{Ph,Me}H] (III)

[Tp^{Ph,Me}Ni(N_3)Pz^{Ph,Me}H]			
Bond lengths (Å)			
Ni(1)–N(1)	2.088(3)	Ni(1)–N(3)	2.013(3)
Ni(1)–N(5)	2.042(3)	Ni(1)–N(7)	2.113(3)
Ni(1)–N(9)	2.005(3)		
Bond angles (°)			
N(1)–Ni(1)–N(3)	90.74(10)	N(1)–Ni(1)–N(5)	90.43(10)
N(1)–Ni(1)–N(7)	174.19(10)	N(1)–Ni(1)–N(9)	86.00(11)
N(3)–Ni(1)–N(5)	95.38(11)	N(3)–Ni(1)–N(7)	90.08(10)
N(3)–Ni(1)–N(9)	116.34(12)	N(5)–Ni(1)–N(7)	83.77(10)
N(5)–Ni(1)–N(9)	148.09(12)	N(7)–Ni(1)–N(9)	98.77(11)
[Tp^{Ph,Me}Ni(SCN)Pz^{Ph,Me}H]			
Bond lengths (Å)			
Ni(1)–N(1)	2.122(8)	Ni(1)–N(3)	2.030(9)
Ni(1)–N(5)	2.032(9)	Ni(1)–N(8)	2.101(9)
Ni(1)–N(11)	2.007(13)		
Bond angles (°)			
N(1)–Ni(1)–N(3)	89.4(3)	N(1)–Ni(1)–N(5)	87.0(4)
N(1)–Ni(1)–N(8)	176.8(3)	N(1)–Ni(1)–N(11)	92.1(4)
N(3)–Ni(1)–N(5)	95.8(4)	N(3)–Ni(1)–N(8)	92.6(4)
N(3)–Ni(1)–N(11)	118.4(5)	N(5)–Ni(1)–N(8)	90.4(4)
N(5)–Ni(1)–N(11)	145.8(5)	N(8)–Ni(1)–N(11)	89.2(4)

After complete dissolution of all the components, homogenous mixture was concentrated by evaporating THF and it was then poured into polyacrylate rings placed on a smooth glass plate. The solution was then allowed to evaporate for 24 h at room temperature. Transparent membrane of about 0.3 mm thickness was obtained, which was then cut to size and glued to one end of a Pyrex glass tube of internal diameter 2.5 cm with Araldite. The ratio of membrane ingredients, time of contact and concentration of equilibrating solution were optimized so that the potential recorded was reproducible and stable within the standard deviation. The membranes, which gave reproducible result and best performance characteristics, were selected for detailed studies.

Ion-selective electrode membranes were cast from above mentioned procedure. The blank membranes (without ionophore) were also prepared having same composition. The sandwich membrane was made by pressing two individual membranes (ordinarily one without ionophore and another with the same components and an additional ionophore) together immediately after blotting them individually dry with tissue paper. The obtained sandwich membrane was visibly checked for air bubbles before mounting in electrode body with the ionophore-containing segment facing the sample solution. The combined segmented membrane was then rapidly mounted on to the electrode body and immediately measured [34].

2.5. Conditioning of membranes and potential measurements

The prepared membranes were equilibrated for 72 h in 0.1 M KSCN and NaN_3 solution. The potentials were measured for test solutions by varying the concentration in the range of 1.0×10^{-8} to 1.0×10^{-1} M. The solutions were prepared by sequential dilution of the appropriate stock solution (0.1 M). A 0.01 M thiocyanate and azide were taken as the internal solution and potential mea-

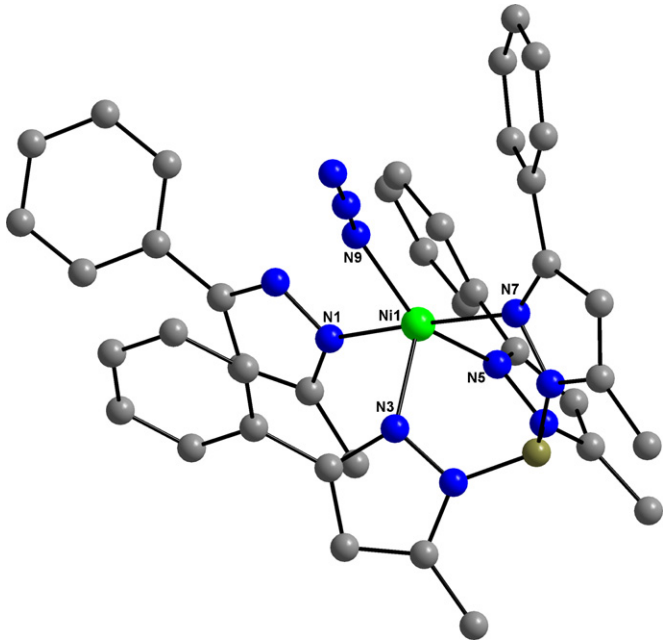

Fig. 2. Molecular structure view of complex [Tp^{Ph,Me}Ni(N_3)Pz^{Ph,Me}H] **II**. Hydrogen atoms and solvent molecule have been omitted for clarity. Color code: C, grey; N, blue; B, sea green; Ni, green. (For interpretation of the references to colors in this figure legend, the reader is referred to the web version of the article.)

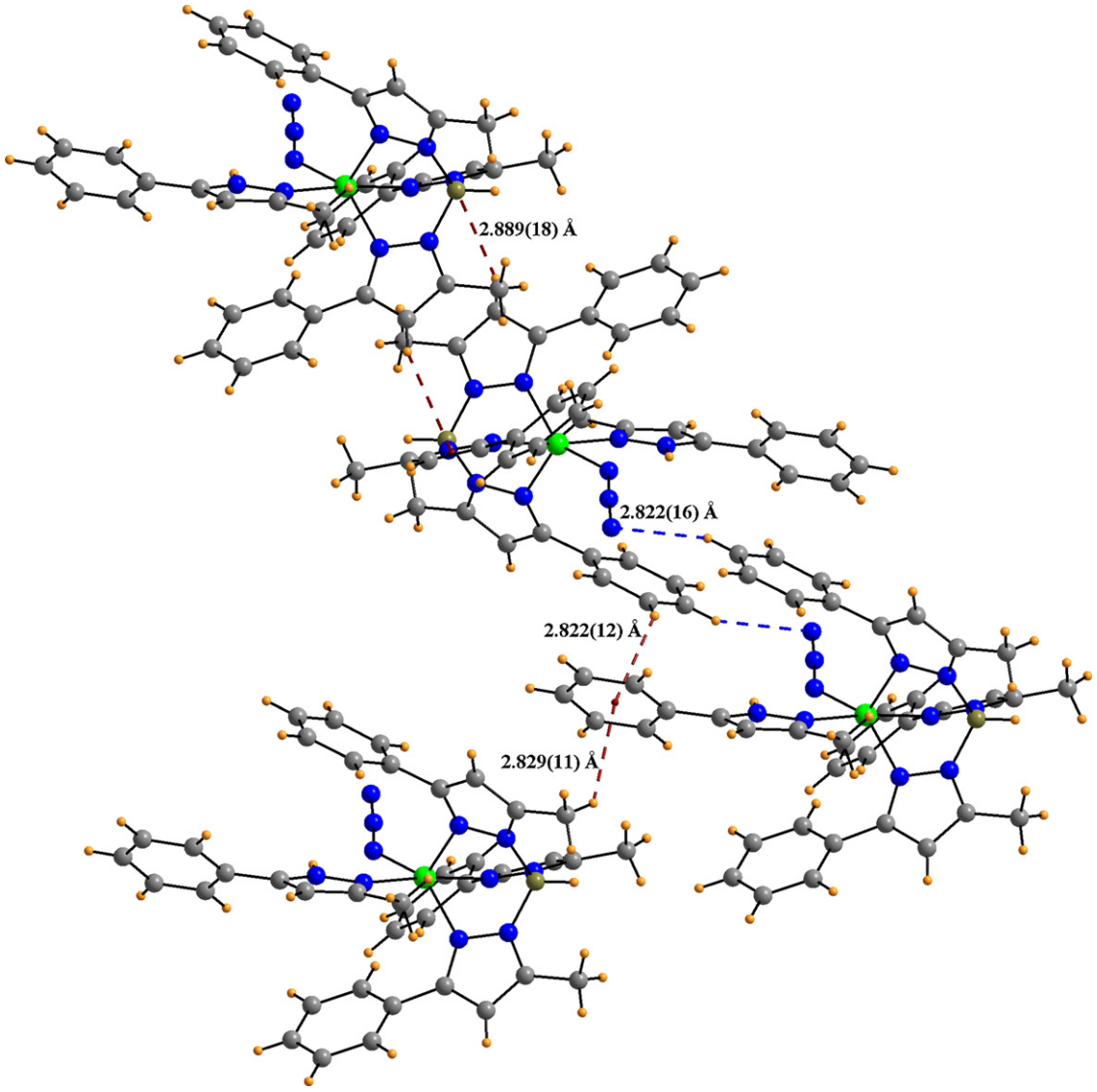

Fig. 3. Intermolecular interactions of complex [$Tp^{Ph,Me}Ni(N_3)Pz^{Ph,Me}H$] **II** showing C–H···N (blue dotted), $CH_3\cdots\pi$ (orange dotted) and C–H···π (orange dotted) interactions. Color code: C, grey; H, orange; N, blue; B, sea green; Ni, green. (For interpretation of the references to colors in this figure legend, the reader is referred to the web version of the article.)

surements were carried out at 25 ± 0.1 °C using a saturated calomel electrode (SCE) as a reference electrode with the following cell assembly:

Hg/Hg_2Cl_2KCl(satd.)|0.01 M thiocyanate or azide||PVCmembrane||

test solution|Hg/Hg_2Cl_2|KCl(satd.)

3. Result and discussions

3.1. Infrared spectral studies

In complex **II**, the presence of ν(N═N) band at 2075 cm^{-1} is in accordance with terminal coordination mode of azide. The C═N stretching frequency of thiocyanates are generally lower in the N-bonded complexes (near and below 2050 cm^{-1}), than the S-bonded complexes (near 2110 cm^{-1}) [35]. Appearance of a single strong band at 2058 cm^{-1} ν(C═N) of suggested that the thiocyanate is bonded through nitrogen atom in complex **III**.

3.2. Molecular structure of [$Tp^{Ph,Me}Ni(X)Pz^{Ph,Me}H$] (X = N_3 for **II**, SCN for **III**)

The compound **II** and **III** crystallize in triclinic with space group $P\bar{1}$. Their crystallographic data are given in Table 1 whereas their important bond lengths and bond angles are given in Table 2. The molecular structure of complex **II** is shown in Fig. 2 and different intermolecular C–H···π (2.822(12)–2.889(18) Å) and C–H···N (2.822(16) Å) interactions are present in crystal lattice (Fig. 3). The crystal structure of **II** contains a mononuclear five coordinated nickel center having three nitrogen atoms from $Tp^{Ph,Me}$, one nitrogen atom from $Pz^{Ph,Me}H$ and one nitrogen atom from terminally coordinated azide anion in end-on fashion. All the nickel–nitrogen bond distances are in the range of 2.005(3)–2.113(3) Å showing covalent character with nickel centre. The Ni–N bond distance of terminal azide (2.005(3) Å) is smaller than Ni–N bond distance present in bridged azide complexes [36]. Fig. 4 shows the molecular structure of the complex **III**. In this complex also, the nickel is five coordinated with same coordination environment as in **II**

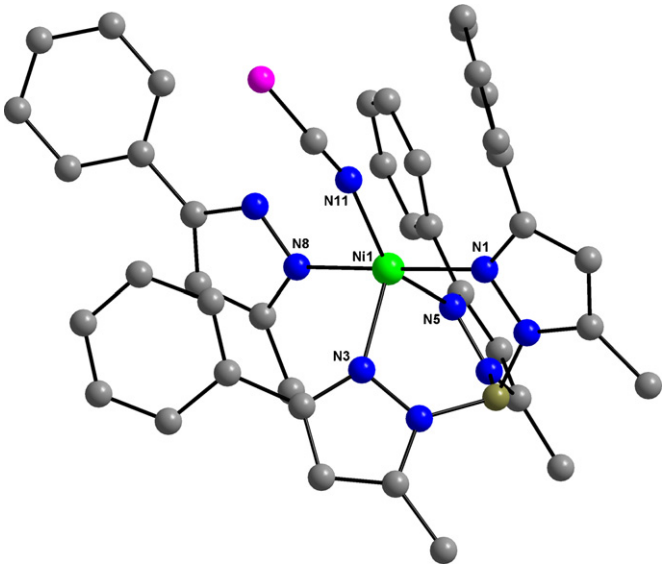

Fig. 4. Molecular structure view of complex [$Tp^{Ph,Me}$Ni(NCS)$Pz^{Ph,Me}$H] **III**. Hydrogen atoms and solvent molecule have been omitted for clarity. Color code: C, grey; N, blue; S, purple; B, sea green; Ni, green. (For interpretation of the references to colors in this figure legend, the reader is referred to the web version of the article.)

except the fifth site in this complex is occupied with nitrogen atom of thiocyanate group which is coordinated in monodentate fashion. Fig. 5 shows the presence of intermolecular C–H···π interactions (2.788(23)–3.022(31) Å) in complex **III**.

3.3. Optimization of membranes compositions

Potential of the membranes of [$Tp^{Ph,Me}$Ni(Cl)$Pz^{Ph,Me}$H] ionophore (**I**) was investigated as a function of thiocyanate and azide ion activity in the range 1.0×10^{-8} to 1.0×10^{-2} M and the results obtained are compiled in Tables 3 and 4. The electrodes with no carrier (containing PVC, plasticizer and HTAB) displayed insignificant sensitivity towards both the anions. The influence of plasticizer on the response characteristics of the thiocyanate and azide electrodes were investigated by using four plasticizers of different polarities including DBP, *o*-NPOE, AP and TBP. The sensor nos. 3 and 16 having membranes without plasticizer exhibit a narrow working concentration range of 10^{-4} to 10^{-2} M with a sub Nernstian slope. Improvement in sensors performance was observed by the addition of plasticizer. Among the several membranes tested for each of the carriers, the membranes incorporating DBP and TBP showed better potentiometric responses, *i.e.*, higher sensitivity and wider linearity of the calibration plots (sensor nos. 12 and 23). It seems that these plasticizers, have low polarity and a relatively high mobility, with respect to *o*-NPOE and AP, and provide appropriate conditions for incorporation of thiocyanate and azide ion into the

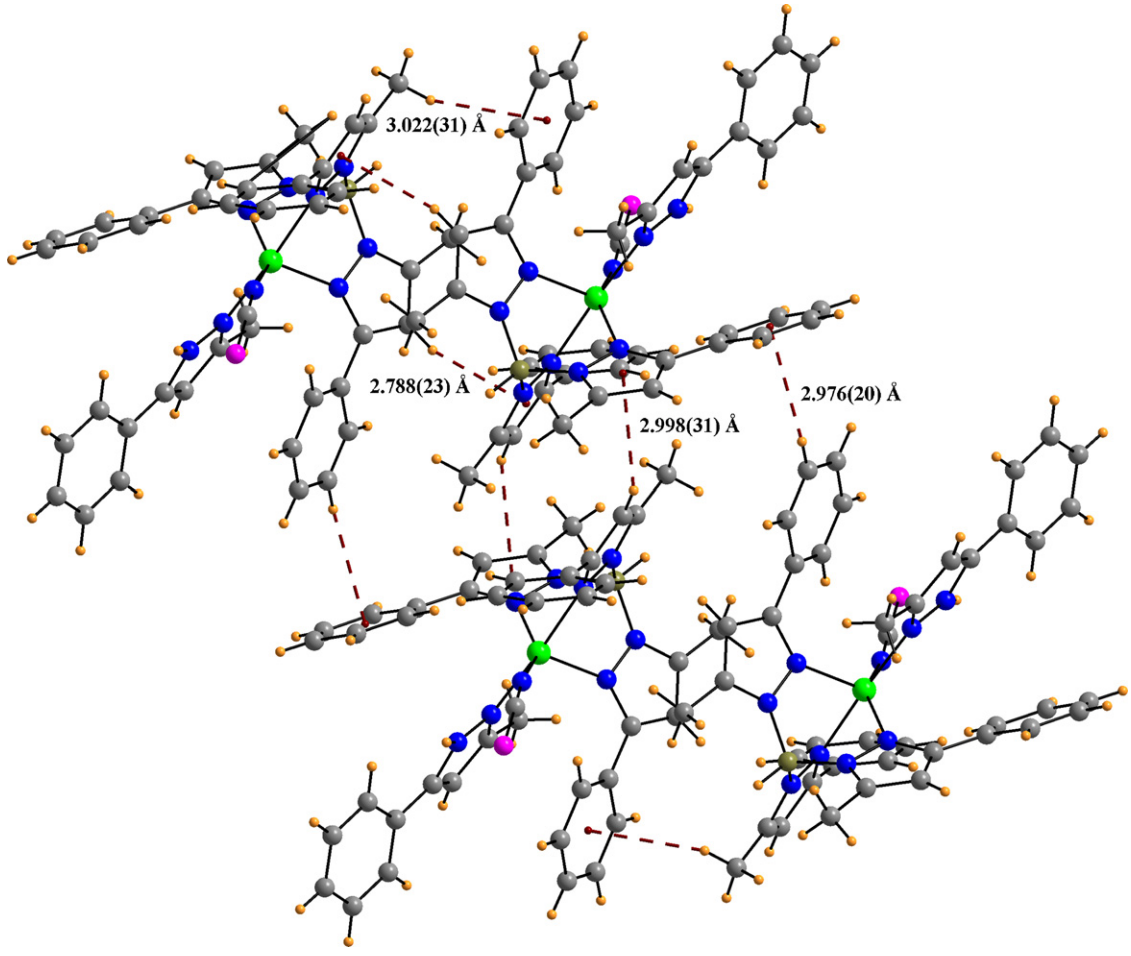

Fig. 5. Intermolecular interactions of complex [$Tp^{Ph,Me}$Ni(NCS)$Pz^{Ph,Me}$H] **III** showing C–H···π (orange dotted) interactions. Color code: C, grey; H, yellow; N, blue; S, purple; B, brown; dummy atom, orange; Ni, green. (For interpretation of the references to colors in this figure legend, the reader is referred to the web version of the article.)

Table 3
Optimized membrane compositions and their potentiometric response as in thiocyanate sensors

Sensor no.	Composition (w/w, %)				Slope (mV decade^{-1} of activity)	Linear range (M)
	Ionophore	HTAB	Plasticizer	PVC		
1	0	3	64, DBP	33	N.M.*	N.M.*
2	6	0	62, DBP	32	52.8	7.5×10^{-5} to 1.0×10^{-2}
3	6	3	0	91	47.5	6.3×10^{-4} to 1.0×10^{-2}
4	6	3	60, *o*-NPOE	31	65.3	7.8×10^{-5} to 1.0×10^{-2}
5	6	3	60, AP	31	62.0	5.6×10^{-5} to 1.0×10^{-2}
6	6	3	60, TBP	31	61.4	1.2×10^{-5} to 1.0×10^{-2}
7	6	3	60, DBP	31	60.2	7.9×10^{-7} to 1.0×10^{-2}
8	6	2	60, DBP	32	59.6	7.4×10^{-7} to 1.0×10^{-2}
9	6	1	61, DBP	32	57.8	8.4×10^{-6} to 1.0×10^{-2}
10	6	4	59, DBP	31	62.3	5.7×10^{-6} to 1.0×10^{-2}
11	5	2	61, DBP	32	58.4	3.5×10^{-6} to 1.0×10^{-2}
12	7	2	60, DBP	31	59.2	5.3×10^{-7} to 1.0×10^{-2}
13	8	2	59, DBP	31	59.8	8.2×10^{-7} to 1.0×10^{-2}

* Not measurable.

membranes prior to its coordination with the nickel atom in the complexes.

The addition of lipophilic cationic additive in anion selective membranes is necessary to introduce permselectivity [37]. The influence and concentration of the membrane additives was also investigated by incorporating HTAB into the membranes. The potentiometric sensitivity of the membranes based **I** for both anions was greatly improved in the presence of HTAB, compared to the membranes with no additive at all. Previous studies have shown that there is an optimal concentration of lipophilic ionic additives in the membranes and that gives the best electrode performance. The effect of HTAB concentration in the membrane was investigated at several additive/ionophore mole ratios. The sensors with HTAB/ionophore mole ratios of ~0.55 for both of the carriers exhibited maximum sensitivity over a wide range of thiocyanate and azide concentration.

3.4. Response of the sensor based on [$Tp^{Ph,Me}Ni(Cl)Pz^{Ph,Me}H$] (ionophore) to thiocyanate and azide ions

Among the different membrane compositions, membranes with composition (w/w, %) 7(**I**)/2(HTAB)/31(PVC)/60(DBP) (sensor no. 12) and 6(**I**)/4(HTAB)/31(PVC)/59(TBP) (sensor no. 23) showed highest sensitivity and widest linear range and these were selected as the optimum composition for further studies. Proposed thiocyanate sensor (no. 12; Table 3) exhibits the maximum working concentration range of 5.3×10^{-7} to 1.0×10^{-2} M with a slope of 59.2 mV decade^{-1} of activity and detection limit of 1.8×10^{-7} M. While azide sensor (sensor no. 23; Table 4) and working concentration range 8.1×10^{-6} to 1.0×10^{-2} M with Nernstian slope of 59.3 mV decade^{-1} of activity and detection limit of 5.2×10^{-6} M (Fig. 6).

3.5. Influence of pH on the on sensors performance

The influence of pH on the response of the potentials was examined by use of 10^{-3} and 10^{-4} M thiocyanate and azide solutions over the pH range 1.0–12.0. The responses of electrode in wide pH range have been investigated by using organic buffer solution. For this purpose, MES–NaOH buffer, for pH values of 4–6, Gly/HCl buffer for pH less then 4 and TRIS–SO_4 buffer for pH values greater than 6 were prepared and examined as background electrolyte solutions for potentiometric measurements. The results are shown in Fig. 7, which indicated that the sensors exhibit a better response and extended linearity at lower pH values. In alkaline media, the potentiometric response properties of the electrode slightly deteriorated due to hydroxide-coordinated central metal interference. The working pH range for sensor for thiocyanate was (sensor no. 12) is 2.5–9.0 and for azide (sensor no. 23) is 3.0–8.5.

3.6. Dynamic response time

The ISE dynamic response is generated by selective complexation of the primary ion by neutral carrier molecule dispersed in a PVC matrix. To measure the dynamic response time of the proposed sensor the concentration of the test solution has been successively changed from 1.0×10^{-8} to 1.0×10^{-2} M. The time needed to reach a potential with in ± 1 mV of the final equilibrium value after successive immersion of a series of thiocyanate

Table 4
Optimized membrane compositions and their potentiometric response as in azide sensors

Sensor no.	Composition (w/w, %)				Slope (mV decade^{-1} of activity)	Linear range (M)
	Ionophore	HTAB	Plasticizer	PVC		
14	0	3	64, DBP	33	N. M.*	N. M.*
15	6	0	62, DBP	32	62.4	2.4×10^{-4} to 1.0×10^{-2}
16	6	3	0	91	47.8	7.7×10^{-4} to 1.0×10^{-2}
17	6	3	60, *o*-NPOE	31	69.2	6.7×10^{-5} to 1.0×10^{-2}
18	6	3	60, AP	31	67.5	2.8×10^{-5} to 1.0×10^{-2}
19	6	3	60, TBP	31	58.0	9.4×10^{-5} to 1.0×10^{-2}
20	6	3	60, TBP	31	59.0	1.1×10^{-5} to 1.0×10^{-2}
21	6	2	60, TBP	32	57.2	5.2×10^{-5} to 1.0×10^{-2}
22	6	1	61, TBP	32	55.3	5.5×10^{-5} to 1.0×10^{-2}
23	6	4	59, TBP	31	59.3	8.1×10^{-6} to 1.0×10^{-2}
24	5	2	61, TBP	32	58.4	9.8×10^{-6} to 1.0×10^{-2}
25	7	2	60, TBP	31	58.8	8.4×10^{-5} to 1.0×10^{-2}
26	8	2	59, TBP	31	58.9	2.8×10^{-5} to 1.0×10^{-2}

* Not measurable.

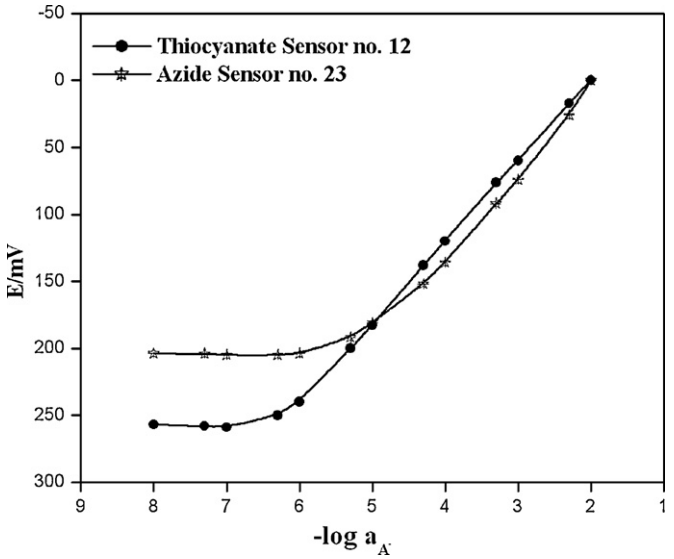

Fig. 6. Calibration plots for the proposed thiocyanate sensor no. 12 and azide sensor no. 23 in the concentration range 10^{-2} to 10^{-8} M.

and azide ion solution, each having a 10-fold difference in concentration is 11 s for thiocyanate sensor (sensor no. 12) and 15 s for azide sensor (sensor no. 23). This is most probably due to the fast exchange kinetics of complexation–decomplexation of anions with the ionophores at the test solution–membrane interface.

3.7. Lifetime of sensors

The lifetime of electrodes based on ionophores in solvent polymeric membranes depends on the distribution coefficient of the ionophore and the plasticizer between the aqueous and membrane phase. Hence, the lifetime of electrodes must depend on the components of the solution and the measured specimens with electrodes. For evaluation of the stability and lifetime of the proposed thiocyanate and azide selective sensors three electrodes were tested over a period of 3 months. During this period, the electrodes were in daily use over extended period of time (1 h per day) and the

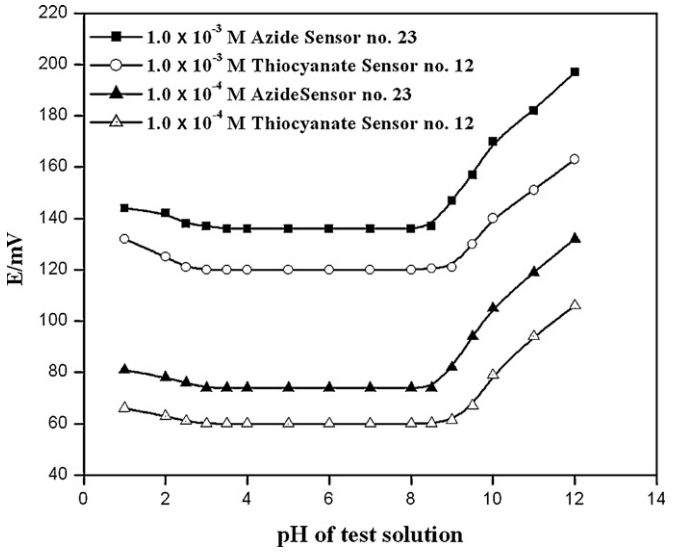

Fig. 7. Effect of pH on potential response of the thiocyanate sensor no. 12 and azide sensor no. 23 using 1.0×10^{-3} and 1.0×10^{-4} M solutions.

Table 5
Selectivity coefficients of different anions based on for thiocyanate sensor no. 12 and azide sensor no. 23

Interfering ions (B)	Selectivity coefficient ($-\log K^{Pot}_{A,B}$)	
	Sensor no. 12	Sensor no. 23
ClO_4^-	2.27	2.06
N_3^-	6.21	–
SCN^-	–	7.18
Cl^-	4.64	4.35
Br^-	4.44	4.32
CN^-	1.15	1.06
NO_2^-		
NO_3^-	3.98	3.12
	3.72	3.63
OAc^-	3.08	2.86
$H_2PO_4^-$	2.48	2.40
CO_3^{2-}	3.24	3.19
SO_4^{2-}	4.61	4.38
OH^-	3.50	3.23

slopes and detection limits of them were measured. The experimental results show that the lifetime of the present sensors were about 1 month (sensor no. 12) and 2 months (sensor no. 23), respectively. Subsequently, the electrochemical behavior of the electrode gradually deteriorated. However, it is important to emphasize that they were stored in 0.1 M anionic solutions when not in use.

3.8. Selectivity of ion sensing membranes

Selectivity is an important characteristic of a sensor that delineates the extent to which the device may be used in the estimation of analyte ion in the presence of other ions and extent of utility of any sensor in real sample measurement. In this work, the selectivity coefficients of the sensors toward different anionic species (A^{n-}) were evaluated by using both the matched potential method (MPM) [38,39].

In the MPM, the selectivity coefficient ($K^{Pot}_{A,B}$) was determined by measuring the change in potential upon increasing the primary ion (A^-) activity from an initial value of a_A to a'_A and a_B represents the activity of interfering ion added to the reference solution of primary ion of activity a_A which also brings about same potential change. It is given by expression:

$$K^{pot}_{A,B} = \frac{\Delta a_A}{a_B} = \frac{a'_A - a_A}{a_B} \quad (1)$$

In the present studies a_A and a'_A were kept at 1.0×10^{-4} and 5.0×10^{-4} M. A^- and a_B were experimentally determined. The

Table 6
Formation constant values of various ions selective membrane based on $[Tp^{Ph,Me}Ni(Cl)Pz^{Ph,Me}H]$ ionophore

Interfering ions	Formation constant ($\log \beta_{1Ln}$) ± S.D.*
N_3^-	6.4 ± 0.3
SCN^-	7.2 ± 0.2
ClO_4^-	3.9 ± 0.2
Cl^-	0.7 ± 0.8
Br^-	1.5 ± 0.5
CN^-	4.6 ± 0.4
NO_2^-	1.7 ± 0.5
NO_3^-	1.8 ± 0.3
OAc^-	2.2 ± 0.2
$H_2PO_4^-$	2.6 ± 1.2
CO_3^{2-}	2.1 ± 0.5
SO_4^{2-}	1.1 ± 0.8
OH^-	2.1 ± 0.2

* Mean value ± standard deviation (three measurements).

Table 7
Determination of thiocyanate in saliva, urine and river water samples

Thiocyanate amount ($\mu g\,mL^{-1}$) ± S.D.*	Samples				
	Saliva (smoker)	Saliva (non-smoker)	Urine (smoker)	Urine (non-smoker)	River water
Proposed thiocyanate sensor	20.2 ± 0.5	5.5 ± 0.4	7.8 ± 0.6	1.8 ± 0.2	0.95 ± 0.2
Colorimetric method	20.5 ± 0.5	5.6 ± 0.4	7.5 ± 0.6	1.6 ± 0.2	0.98 ± 0.3

* Mean value ± standard deviation (five measurements).

Table 8
Determination of azide in different aqueous samples

Samples	Calculated by proposed sensor ($\mu g\,L^{-1}$) ± S.D.*	Amount added ($mg\,L^{-1}$)	Recovery (%) ($n = 3$)	Precision (RSD) ($n = 3$)
Black tea	140 ± 2	1	91	5.4
Orange juice	155 ± 4	1	87	8.0

* Mean value ± standard deviation (three measurements).

values of selectivity coefficient so determined are compiled in Table 3. A value of selectivity coefficient equal to 1.0 indicates equal response to both primary ion and interfering ions. A value smaller than 1.0 shows that the sensor is selective to the primary ion over the interfering ions. It is seen from the Table 5, that the selectivity coefficients determined are sufficiently smaller than 1.0 indicating that the present sensors are significantly selective to thiocyanate and azide ion over all the interfering ions. Of the two sensors, selectivity of the sensor no. 12 (thiocyanate sensor) was found better than sensor no. 23 (azide sensor).

3.9. Determination of formation constant

Formation constant of the ion–ionophore complex within the membrane phase is a very important parameter that dictates the practical selectivity of the sensor. In this method, two membrane segments are fused together, with only one containing the ionophore, to give a concentration-polarized sandwich membrane. A membrane potential measurement of this transient condition reveals the ion activity ratio at both interfaces, which translates into the apparent binding constants of the ion–ionophore complex. In this method complex formation constants obtained by neglecting ion pairing. As reported, the membrane potential E_M is determined by subtracting the cell potential for a membrane without ionophore from that for the sandwich membrane. The formation constant is then calculated from the following equation:

$$\beta_{IL_n} = \left(L_T - \frac{nR_T}{Z_I}\right)^{-n} \exp\left(\frac{E_M z_I F}{RT}\right)$$

where L_T is the total concentration of ionophore in the membrane segment, RT is the concentration of lipophilic ionic site additives, n is the ion–ionophore complex stoichiometry, and R, T and F are the gas constant, the absolute temperature, and the Faraday constant. The ion carries a charge of z_I. The determined formation constants ($\log \beta_{IL_n}$ for the examined different complexes were recorded in Table 6. The elapsed time between sandwich fusion and exposure to electrolyte was typically <1 min. The potential was recorded as the mean of the last minute of a 5 min measurement period in the appropriate salt solution. The potential of such sandwich membranes remains free of diffusion-induced potential drifts for about 20 min. Standard deviations were obtained based on the measurements of sets of at least three replicate membrane disks that were made from the same parent membrane. A careful analysis of the data in Table 6 reveals that thiocyanate and azide ions have significant anion-binding characteristics.

4. Analytical applications

4.1. Thiocyanate determination

Urine and saliva samples containing different thiocyanate concentrations were collected from smoker and non-smoker patient, and same samples were assayed for multiple times. Samples were treated by MES/NaOH buffer (pH 5.5) solution, while the river water sample was used directly by adjusting pH 5.5 by dilute HCl solution. For spike recovery measurements, the urine was spiked with 10 $mg\,L^{-1}$ thiocyanate before dilution and filtration. All samples were analyzed in five replicate using the proposed electrode, and the results were compared with those obtained by a standard colorimetric method. The results given in Table 7, show that the amounts of thiocyanate ion evaluated with the help of the electrode are in good agreement with those obtained by the standard colorimetric method, thereby reflecting the utility of the proposed sensors.

4.2. Azide determination

Because of the high selectivity and the very low detection limit of the constructed N_3^- sensor, it was applied for the monitoring of the azide ions concentration in various aqueous samples (black tea and orange juice). Samples can be directly injected after minimal sample preparation. The samples must be diluted (1:10 with double distilled water) and filtered to remove particulates and treated by MES/NaOH buffer (pH 5.5) solution. Black tea was prepared by steeping a teabag in about 100 mL of hot reagent grade water for 10 min. After cooling, the infusion was diluted 10-fold with reagent grade water and filtered before injection. For spike recovery measurements, the tea was spiked with 10 $mg\,L^{-1}$ sodium azide before dilution and filtration. Orange juice was diluted 10-fold with reagent grade water and filtered before injection. For spike recovery measurements, the orange juice was spiked with 10 $mg\,L^{-1}$ sodium azide before dilution and filtration.

For each sample, precision and recovery from interferences were measured. Precision and recovery were measured by adding 1 $mg\,L^{-1}$ azide into samples; black tea and orange juice. Recovery for all samples was greater than 80%. Precision varied from 2% to 8% for all the samples. The results are shown in Table 8. Orange juice contains phosphate, sulfate, fluoride and fumarate but these compounds do not interfere with azide.

5. Conclusions

Synthesis and characterization of [{hydrotris(3-phenyl-5-methyl-1-pyrazolyl) borate}(3-phenyl-5-methyl-pyrazole) nickel

chloride] [$Tp^{Ph,Me}Ni(Cl)Pz^{Ph,Me}H$] and their analytical application in the preparation of anion selective electrodes were carried out. Crystal structure determination of [$Tp^{Ph,Me}Ni(N_3)Pz^{Ph,Me}H$] [$Tp^{Ph,Me}Ni(SCN)Pz^{Ph,Me}H$] has also been done to know the nature of binding of azide and thiocyanate with ionophore. The investigations on polymeric membranes of [$Tp^{Ph,Me}Ni(Cl)Pz^{Ph,Me}H$] ionophore have shown that they act as thiocyanate and azide selective sensors. However, the results of thiocyanate selective sensor are compared with azide anions and comparison of data revealed that thiocyanate sensor is superior to the azide sensor with regard to detection limit (1.8×10^{-7} M), response time (11 s) and selectivity. Proposed thiocyanate sensor was also applied successfully for its determination in human urine, saliva and river water while azide selective sensor used to determine azide content in aqueous black tea and orange juice samples.

6. Supporting data

The crystallographic data have been deposited with CCDC. Supplementary data are available from CCDC, 12 Union Road, Cambridge CB2 1EZ, UK on request by quoting the deposition numbers CCDC 673216 - 673217. E-mail: http://www.deposit@ccdc.cam.ac.uk or http://www.ccdc.cam.ac.uk.

Acknowledgements

Mr. Vaibhave Aggarwal and Ms. Sameena Mehtab are grateful to Council of Scientific and Industrial Research, New Delhi, India for providing financial assistance for this work.

References

[1] Z. Guien, L. Bin, F. Jing, F. Suling, Talanta 44 (1997) 1141.
[2] P.M. Maliszewski, H.E. Bass, J. Appl. Physiol. 8 (1955) 289.
[3] H.D. Fair, R.F. Walker, Energetic Materials, Plenum Press, New York, 1977.
[4] B.D. Pollock, W.J. Fisco, H.A.C. Kramer, Forsyth handling, storability, and destruction of azides, in: Energetic Materials, Plenum Press, New York, 1977.
[5] J. Akhavan, The Chemistry of Explosives, Royal Society of Chemistry, Cambridge, 1998.
[6] T. Urbanski, Chemistry and Technology of Explosives, Pergamon, Oxford, 1967.
[7] K.G. Mason, Nitrogen hydrogen azide, in: Mellor's Comprehensive Treatise on Inorganic and Theoretical Chemistry, Wiley, New York, 1967, p. 1.
[8] S. Chang, S.H. Lamm, Int. J. Toxicol. 22 (2003) 175.
[9] R.P. Smith, D.E. Wilcox, Crit. Rev. Toxicol. 24 (1994) 355.
[10] J.S. Weiss, Int. Arch. Occup. Environ. Health 68 (1996) 469.
[11] W.-J. Xu, Y.-Q. Chai, R. Yuan, S.-L. Liu, Anal. Bioanal. Chem. 385 (2006) 926.
[12] S. Erden, A. Demirel, S. Memon, M. Yilmaz, E. Canel, E. Kilic, Sens. Actuators B: Chem. 113 (2006) 290.
[13] M.J. Segui, J. Lizondo-Sabater, R. Martinez-Manez, F. Sancen'on, J. Soto, Talanta 68 (2006) 1182.
[14] A. Abbaspour, M.A. Kamyabi, A.R. Esmaeilbeig, R. Kia, Talanta 57 (2002) 859.
[15] M.K. Amini, A. Rafi, M. Ghaedi, M.H. Habibi, M.M. Zohory, Microchem. J. 75 (2003) 143.
[16] M. Shamsipur, S. Ershad, N. Samadi, A.R. Rezvani, H. Haddadzadeh, Talanta 65 (2005) 991.
[17] Z.-Q. Li, Z.-Y. Wu, R. Yuan, M. Ying, G.-L. Shen, R.-Q. Yu, Electrochim. Acta 44 (1999) 2543.
[18] J.H. Khorasani, M.K. Amini, H. Motaghi, S. Tangestaninejad, M. Moghadam, Sens. Actuators B: Chem 87 (2002) 448.
[19] M. Aravand, M.A. Zanjanchi, L. Heydari, Sens. Actuators B: Chem. 122 (2007) 301.
[20] R. Prasad, V.K. Gupta, A. Kumar, Anal. Chim. Acta 508 (2004) 61.
[21] K. Watanabe, O. Noguchi, K. Okada, T. Katsu, Jpn. J. Forensic Toxicol. 17 (1999) 180.
[22] A.M. Tsygankov, Y.I. Urusov, A.V. Kopytin, A.F. Zhukov, D.I. Zhurnal, Analitich-eskoi Khimii 42 (1987) 670.
[23] S.S.M. Hassan, F.M. Zawawy, S.A.M. Marzouk, E.M. Elnemma, Analyst 117 (1992) 1683.
[24] T. Johannes, E. Van, M.G. Constant, B. den Van, D.M. Trevor, Anal. Commun. 34 (1997) 385.
[25] D.D. Perrin, W.L. Armarego, D.R. Perrin, Purification of Laboratory Chemicals, second ed., Pergamon, New York, 1980.
[26] D.T. Puerta, S.M. Cohen, Inorg. Chim. Acta 337 (2002) 459.
[27] G.M. Sheldrick, Acta Cryst. A 46 (1990) 467.
[28] G.M. Sheldrick, SHELXTL-NT 2000, version 6.12, reference manual, University of Göttingen Göttingen, Germany.
[29] B. Klaus, DIAMOND, Version 1.2c, University of Bonn, Germany, 1999.
[30] A. Craggs, L. Keil, G.J. Moody, J.D.R. Thomas, Talanta 22 (1975) 907.
[31] G. Khayatian, S. Shariati, A. Salimi, Bull. Kor. Chem. Soc. 24 (2003) 421.
[32] T. Katsu, K. Ido, K. Takaishi, H. Yokosu, Sens Actuators B 87 (2002) 331.
[33] K.M. Park, Y.H. Lee, Y. Jin, J. Seo, I. Yoon, S.C. Lee, S.B. Park, M.S. Gong, M.L. Seo, S.S. Lee, Supramol. Chem. 16 (2004) 51.
[34] Y. Mi, E. Bakker, Anal. Chem. 71 (1999) 5279.
[35] M. Đaković, Z. Popović, G. Giester, M. Rajić-Linarić, Polyhedron 27 (2008) 465.
[36] M.A.S. Goher, A. Escuer, F.A. Mautner, N.A. Al-Salem, Polyhedron 21 (2002) 1871.
[37] U. Schaller, E. Bakker, U.E. Spichiger, E. Pretsch, Anal. Chem. 66 (1994) 391.
[38] Y. Umezawa, K. Umezawa, H. Sato, Pure Appl. Chem. 67 (1995) 507.
[39] V.P.Y. Gadzekpo, G.D. Christian, Anal. Chim. Acta 164 (1984) 279.

Talanta 77 (2008) 901–908

Contents lists available at ScienceDirect

Talanta

journal homepage: www.elsevier.com/locate/talanta

Capillary scale liquid core waveguide based fluorescence detectors for liquid chromatography and flow analysis

Guanqun Song, Ignacio Villanueva-Fierro[1], Shin-Ichi Ohira, Santosh Mishra, Howard Bailiff, Charles R. Savage, Purnendu K. Dasgupta*

Department of Chemistry and Biochemistry, The University of Texas at Arlington, Arlington, TX 76019-0065, USA

ARTICLE INFO

Article history:
Received 5 July 2008
Received in revised form 22 July 2008
Accepted 22 July 2008
Available online 5 August 2008

Keywords:
Capillary
Liquid core waveguide
Fluorescence detector
Blu-ray
Violet laser diode

ABSTRACT

A versatile, simple, liquid core waveguide (LCW)-based fluorescence detector design is described for capillary systems. A Teflon AF coated fused silica capillary serves as the LCW. The LCW is transversely excited. The light source can be a conventional or high power (HP) light emitting diode (LED) or a laser diode (LD). The source can be coupled to the LCW directly or via an optical fiber. Fiber coupling is convenient if a high power (necessarily heat sink mounted) emitter is used. The LCW is concentrically placed within a slightly larger opaque jacket tube and the LCW terminates just short of the jacket terminus, which is sealed with an optical window. The influent liquid thus exits the LCW tip, flows back around the LCW through the jacket annulus to exit via an aperture on the jacket tube. The problem of coupling the emitted light efficiently to the photodetector is thus solved by placing the tip of the annular tubular assembly directly on the detector.

For excitation wavelengths of 365 nm (LED/HPLED) and 405 nm (LD), the tris(8-hydroxyquinoline-5-sulfonic acid (sulfoxine)) chelate of aluminum ($\lambda_{em,max} \sim 500$ nm) and Coumarin 30 were respectively used as the model analyte. For source–detector combinations comprising (a) a UV LED (~1.5 mW @ 15 mA) and a photodiode, (b) a LD (~5 mW, abstracted from a "Blu-Ray" recorder) and a miniature photomultiplier tube (mPMT), and (c) a high power (210 mW @ 500 mA) surface-mount HPLED–mPMT, the S/N = 3 LODs were, respectively, 1.7 pmol Al, 3–100 fmol Coumarin 30 (depending on laser intensity and integration time), and 4 fmol Al. In the last case, the relative standard derivation (R.S.D.) at the 20 fmol level was 1.5% ($n = 10$).

1. Introduction

During the present decade, there has been a significant interest in capillary scale separation and detection techniques [1,2]. The capillary format allows for high efficiency rapid separations with low sample and reagent consumption. In favorable cases, it allows for very low pressure, even gravity-flow separations [3–5]. However, the measurement of trace amounts of analytes in ≤ 1 μL injected sample volumes demand a lot from detection techniques.

Fluorometry is among the most sensitive of analytical techniques. A focused laser beam offers an ideal way to provide small volume intense excitation. Although laser induced fluorescence (LIF) has been most often used in capillary electrophoresis (CE) and reviewed in that context [6,7], it is applicable for non-electrophoretic capillary scale applications as well. Nevertheless, commercial LIF instrumentation is still too complex and expensive to allow wide, especially pedagogic, use. Further, many laser sources are intrinsically noisy, degrading LODs from what would be predicted on the basis of illumination flux alone. More importantly, the limited number of wavelengths that laser sources can presently conveniently and affordably address require the proverbial changing of the foot to fit the shoes; a whole host of derivatization agents and methods have been developed to fit available LIF instruments. The recent availability of violet laser diode (VLD) sources in digital video disc (DVD) players and recorders, complete with focusing optics, does offer, however, inexpensive opportunities to build fluorescence detectors with such sources and optics.

The attractive performance of liquid core waveguides (LCWs) for transverse/radial excitation fluorescence detection was demonstrated a decade ago [8]. We have since reviewed the general use of LCWs for optical detection [9]. Recently Okada has reviewed LCW-based absorbance and fluorescence detection (with either axial or radial illumination) [10]. The following developments in LCW-based fluorescence detection are noteworthy: imaging the capillary

* Corresponding author. Tel.: +1 817 272 3171; fax: +1 817 272 3808.
E-mail address: dasgupta@uta.edu (P.K. Dasgupta).
[1] Permanent address: CIIDIR-IPN, Sigma S/N, Fracc. 20 de Noviembre II, Durango, Durango 34220, Mexico.

0039-9140/$ – see front matter © 2008 Elsevier B.V. All rights reserved.
doi:10.1016/j.talanta.2008.07.047

lumen on a CCD detector and being able to discriminate against the scattered light that primarily propagates along the wall [11], using a similar detector with a multicapillary separation system to perform multiplexed detection [12], imaging the whole column with either axial [13,14] or scanning transverse [15] illumination, detecting ammonia at the low nM level with a photodiode detector [16], utilizing the scheme with CCD based detectors in CE [17] and in flow injection coupled miniature CE systems [18], using multiwavelength array excitation coupled to a CCD spectrometer [19], separating and detecting DNA fragments in microfluidic systems [20] with LODs comparable to LIF detection (aided by modulation, lock-in detection and second wavelength referencing techniques) [21]. In our laboratories, we have extensively used light emitting diode (LED) excited LCW-based fluorescence detection for the determination of atmospheric H_2O_2 [22], HCHO [23] and H_2S [24], developed a flashlamp-excited gated fluorescence detection system for anthrax spores [25], a multiplexed, pulsed-LED detection system for hematin-differentiated [26] measurement system for H_2O_2 and organic peroxides [27] and methods for coating glass and silicon microchannels to render them into waveguides [28,29].

In LCW fluorescence detectors described to date, coupling the emitted light to the detector has generally been accomplished by a distally located optical fiber coupled detector; the convenience unfortunately leads to significant light loss. Preserving the lumen image [11,12] requires an involved optical arrangement where the fluid exit end remains in a liquid reservoir and the termini are imaged by a lens, filter, prism and camera objective before coupling to a CCD detector. Direct coupling to the detector window has only been achieved by allowing the liquid to leak past an exit window in an uncontained manner [20] precluding the possibility of using a subsequent serial detector. To perform affordable multidimensional detection in capillary scale analyzers, it is our objective to develop absorbance [1], conductance [30] and fluorescence detectors in a concerted manner. These detectors should be capable of being deployed singly or serially with a high performance/cost ratio.

In the present paper, we describe generic designs for inexpensive capillary scale flow through fluorescence detectors and demonstrate attractive performance in flow systems.

2. Experimental

2.1. Reagents

Sulfoxine, 8-hydroxyquinoline-5-sulfonic acid (HQS), was twice recrystallized (as the monohydrate) from large volumes of hot water. Aluminum sulfate (reagent grade), Coumarin 30 (3-(2-*N*-methylbenzimidazolyl)-7-*N*,*N*-diethylaminocoumarin), Good buffering agents [31] 3-(*N*-Morpholino)-ethane sulfonic acid (MES), 3-(*N*-Morpholino)-propane sulfonic acid (MOPS) and 2-(cyclohexylamino)-ethane sulfonic acid (CHES) were used as received (all of the above from www.sial.com). For the present experiments, the stock solutions of the Al salts were diluted serially by the carrier used in the flow analysis system. Coumarin 30 was dissolved in 50% (v/v) methanol and injected for detection in the same solvent. All other solutions were made in distilled deionized water.

2.2. Fluorescence detector cell design

Only the HPLED–mPMT detector is described here in detail; the other two designs are discussed here briefly; greater details appear in supporting information (SI).

2.2.1. Light emitting diode: photodiode design

The simplest and least expensive (total electronics cost <$20) scheme uses a modest power UV LED (NSHU550B, www.nichia.com, 5.4 mm dia. metal can) that is estimated to put out ~1.5 mW @ 365 nm at the operative drive current of 15 mA. Refer to Fig. S1 in SI and attendant description. The detector is a miniature "light-to-voltage converter", a photodiode with an integral operational amplifier (TSL250R, www.TAOsinc.com) a square-shaped (4.8 mm × 4.8 mm) clear epoxy bodied 3-pin (power, ground, signal) device that is 1.8 mm thick. A centrally placed integrally molded hemispherical lens (Ø0.90 mm) completely covers the photosensitive area (sensitivity ~100 mV/μW per cm^2 @ 500 nm). We drilled a perpendicular hole (1/32 in., Ø~0.79 mm) directly through/atop the lens terminating just atop the photosensitive surface. A second aperture (0.014 in., ~0.37 mm) is drilled parallel to the plane of the device and joins the first aperture atop the photosensitive area to form an L-shaped passage. After cleaning out the debris and polishing the bottom of the vertically drilled aperture as best as possible, a thin coat of clear epoxy was applied to the bottom to restore transparency. The LCW capillary (TSU100375, www.polymicro.com, the same LCW capillary was used in all designs) is inserted in a opaque PEEK sleeve 0.015 in. i.d., 1/32 in. o.d., F-385x , www.upchurch.com)—this is inserted through the vertical aperture. The exit capillary, 180 μm i.d., 350 μm o.d. (TSP180350) is inserted through the horizontal aperture. The assembly is covered over with epoxy adhesive intimately mixed with activated charcoal to prevent ambient light from reaching the detector. The assembly was put into an opaque Delrin fixture with provisions for illuminating the LCW capillary radially by the LED ~10 mm above where it enters the detector.

2.2.2. Laser diode: miniature photomultiplier tube design

A "Blu-Ray" DVD reader (Pioneer model BDC-2202b) was disassembled to gain access to the read/write laser sources. This particular model uses three different discrete laser diode (LD) sources at different wavelengths. The VLD is believed to have an output of 5–7 mW and is used for read functions only. Connections to the VLD leads were made directly on the board and these were then connected to external circuitry to apply power. LD's are static and surge sensitive. As shown in Fig. S3 in SI, a switch keeps the VLD disconnected both before power was applied and before power was shut off. The drive current is read by a digital panel meter via the voltage drop across a 10 Ω resistor in series that connects the VLD to ground. A 10-turn 1 kΩ potentiometer allows control of the drive current (monitored and displayed continuously) via circuitry based on a LM317 (www.nsc.com) based regulator. The fluorescence cell itself was identical to that described for the HPLED–mPMT design below, except that fluid exit connection was made here via a tee for convenience. The manner in which the LCW was illuminated was as follows. The optical lens element (Ø~1.5 mm) through which the laser beam emerges is located centrally between two horizontal highly magnetized bars (ca. 10 mm long, 2 mm wide, spaced 11 mm apart). The optics is spring loaded and can be pushed down. At its maximum elevation, the top of the lens is flush at the same level as the magnetized bars. This enables a very simple and effective means of affixing the LCW capillary to the top of the optics. The general arrangement is shown in Figs. S4 and S5. A 0.020 in. wide wedge-shaped groove is machined onto the middle of the short side of a 7.5 mm × 15 mm opaque Acetal (Delrin) sheet (~1 mm thick), intended to function as the capillary cradle. A 0.79 mm bore aperture is drilled about the center of the groove (the intended location of the optics) and a low sensitivity light to voltage converter (TSL252R, www.TAOSinc.com, for referencing the laser intensity) is cemented on the hole on the obverse side of the groove. Two thin steel pieces (~2.5 mm × 7 mm) are cemented with epoxy adhesive

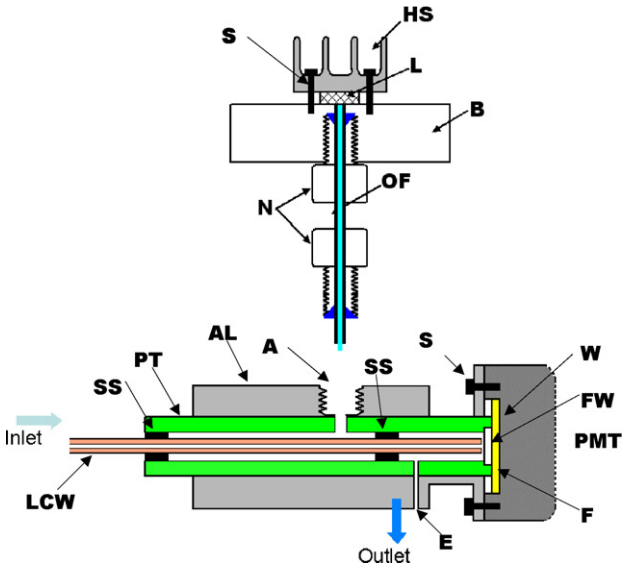

Fig. 1. Top: high power LED L is sandwiched between heat sink HS and aluminum block B by screws S. 1 mm core acrylate optical fiber OF is coupled to the LED and the fluorescence cell (bottom) with reverse-ferrule equipped (1/4)-threaded nuts N. The cell is built of an aluminum block AL provided with a (1/4)-28 threaded flat-bottomed aperture A for the fiber optic to illuminate the 100 μm bore Teflon AF coated fused silica capillary LCW held in a PEEK jacket tubing PT with the help of sealers and spacers SS. PT terminates in a 1 mm long face-polished acrylate optical fiber segment FW functioning as the window against which the LCW butts up. The front flange of the cell attaches directly to the PMT face and FW rests directly on the PMT window W. Optional thin plastic optical filter(s) F can be put on the PMT window W. Liquid enters through the LCW, leaks at the tip in the gap between it and FW and exits through aperture E. The drawing is not to scale.

on the short edges of the capillary cradle, on the same side as the groove. As the cradle, with the capillary in the groove, is lowered on to the LD optics, the capillary is held in place atop the optics by the magnetic force. It is important to use only thin pieces of steel (we used small portions scored off a razor blade). Else, the permanent magnets are so strong, once the cradle is bought near the optics, it is impossible to control the position and the cradle may be drawn with such force so as to crush the capillary. In our particular arrangement, the illumination point was ~5 cm from the mPMT tip of the capillary.

The optical output from the lens element was measured with a calibrated laser power meter (type 840011, www.sperscientific.com). This sensor is calibrated for 632.8 nm and a correction factor of 9.62× was applied for measurement at 405 nm according to manufacturer's instructions. Note that there are significant losses in the optical system and the output power at the exit of the optical element must be significantly smaller than the power generated by the VLD itself.

2.2.3. *High power light emitting diode: miniature photomultiplier tube design*

Referring to Fig. 1 (the drawing is not to scale), the light source used is a surface-mount type UV LED L (λ_{max} 365 nm, NCSU003A, Nichia Corp). This is a very high brightness excitation source (emitting typically 210 mW continuous at 500 mA, with a maximum permissible continuous current of 700 mA, [32]). It is mounted on a finned heat sink HS with heat sink compound. A pair of screws S sandwich the LED between aluminum block B and HS. A (1/4)-28 threaded male nut N holds down the 1 mm core jacketed optical fiber OF (ESKA optical grade fiber, NT02-536, www.edmundoptics.com) on the surface of the LED. The emitting chip dimension is 0.9 mm × 0.9 mm square and the fiber captures most of the emitted light. For a flat-faced LED, previous experience shows that direct interfacing of a fiber with polished termini leads to the best light coupling [33]. In the present experiments, the HPLED was operated at a current of 500 mA.

The cell holder AL is machined from aluminum, the general arrangement is schematically shown in the bottom panel of Fig. 1. A photograph and dimensional drawing is given in Fig. S6 in SI. The holder AL terminates in a flange that has screw holes for directly mounting holder AL on the face of the mPMT (H5784, www.hamamatsu.com) with a set of four M2-threaded screws S. This is a relatively low-cost miniature photosensor module [34] with its own built in high voltage supply. The mPMT has an 8 mm dia. photoactive area, contained in a 10 mm diameter window W that is recessed 1 mm inside the metallic sensor housing. One or more layers of plastic optical filters F were cut as 10 mm circles and put on the PMT window as desired. The holder AL has a central 1/16 in. diameter straight through axial hole which snugly accommodates 1/16 in. o.d. 0.75 mm i.d. PEEK tubing PT (~45 mm long). Tube PT is provided first with one inserted spacer SS (3 mm long, 457 μm i.d./635 μm o.d., PEEK, type PK018-025-BLK, www.upchurch.com). The spacer segment SS is coated thinly with epoxy adhesive on the outside and pushed inside tube PT from one end to a depth of ~15 mm and the epoxy is allowed to cure. The spacer serves to hold the inserted LCW capillary (*vide infra*) concentric. Tube PT is then provided with a terminal optical window FW at the same end, close to the spacer. We have variously used (*vide infra*) (a) a 1 mm long segment of an acrylate optical fiber (1 mm core, P/N 02-536, www.edmundoptics.com). The fiber is polished at both ends by micro-mesh sandpaper (grades 1500–12,000, www.micro-surface.com) and forcibly inserted into the end of the green PEEK tubing widened at the tip with a 0.040 in. drill bit to a depth of 1 mm, this seals tightly enough that in our experience no leakage occurs. (b) A spherical glass ball lens of 1 mm diameter (NT43-708, www.edmundoptics.com). The ball is forcibly put in at the PEEK tube tip after enlarging the tube tip i.d., in much the same way as the optical fiber segment. (c) A 125 μm thick clear polyester window (Mylar, K-Mac plastics, KS6361, Wyoming, MI). The tip perimeter of tube PT was roughened by sanding, a thin layer of epoxy adhesive was applied and a small piece of the Mylar sheet was then affixed.

With PT inserted in its place in AL, AL is fixed with screws on the top of the mPMT; PT is pushed in until it rests on the mPMT window (with any optical filters already thereon). PT is now fixed in place at its entrance point in AL with a 10–32 nut and ferrule (not shown in Fig. 1, see Fig. S6 in SI for this detail). The (1/4)-28 threaded entrance A in AL ends in a 1 mm aperture. Tubing PT is drilled through at this aperture to allow the 1 mm fiber optic to come into PT. On the opposite side of A, a 0.64 mm dia. hole is present in AL, this too is now drilled through in PT to serve as fluid exit. PT is now thoroughly washed with methanol using all entry/exit combinations to remove any debris. The capillary LCW (the length chosen ~55 mm, results in ~1 cm protruding from PT at the entrance end) is pushed in from the open end of PT until it rests on window FW. The LCW is not effectively sealed against FW. Rather, liquid entering into the LCW flows past the tip and back around the LCW in the annular space to exit at aperture E where a stainless steel exit tube (0.017 in. i.d./0.025 in. o.d., HTX-23T, www.smallparts.com) is push fit and epoxied in place. Fluorescent light originating from the excited analytes in the lumen is guided by the LCW to its tip by total internal reflection and is transmitted to the PMT via FW. A second exit sleeve SS is put in and sealed and epoxied in place where LCW enters PT. Connections to the LCW inlet to other 375 μm o.d. capillaries that constitute upstream components of the system are made with a butt-joint using a short polyvinyl chloride pump tubing segment (0.19 mm-i.d., 2.03 mm-o.d.) as a sleeve.

While the data presented comes solely from the above design, for applications where another detector is serially connected, a similar design with a smaller inner diameter for PT (0.5 mm i.d.) was used, without any spacers. The annular gap in this case is ≤60 μm. About 10 mm from the PMT end of the tube PT, a 0.015 in. diameter hole is drilled as the fluid exit aperture. After completion of the assembly, a silica capillary of desired inner diameter is inserted here and epoxied in place.

2.3. Electronics

It has been shown elsewhere [33] that short of carefully matched thermistor–resistor combinations, a stable constant voltage power supply and a low value resistor offer the best compromise to obtain a stable light output from an LED as minor variations in ambient temperature occur. Following this maxim, we used a 10 Ω, 10 W power resistor in series with the HPLED and powered it with a high current variable voltage power supply. ~8.8 V was needed to attain the desired drive current of 500 mA. For the VLD–mPMT experiments, the PMT control voltage was set at 0.9 and no further secondary signal processing was used. For the HPLED experiments, unless otherwise stated, the mPMT gain control voltage was set at 0.7, the primary mPMT output was offset and amplified 10× by a dual JFET-input operational amplifier (TL082CP, www.ti.com), the first stage providing unity gain and variable offset and the second stage providing 10× gain with a time constant of 1 s. Both stages were operated in the inverting amplifier configuration. The circuit diagram is given in SI in Fig. S7. In all cases, the detector signal was acquired at 1 Hz by a 12-bit PCM-DAS16D/12 data acquisition card (www.measurementcomputing.com) housed in a mini-notebook personal computer.

Some experiments were conducted where the light source was modulated with an N-channel MOSFET switch (IRLI530N, www.irf.com) with a function generator at ~100 Hz to address the gate of the logic-level MOSFET switch. The detector output was processed via a balanced demodulator chip (AD630, www.analogdevices.com) using the gate signal for reference. In no case were the results better than dc operation. Hence they are not reported. There are some inherent limitations of this circuitry, better lock-in detection approaches will be discussed in a future paper.

2.4. Experimental arrangement

Most experiments were conducted in the flow injection mode, using a single line system. Fluid flow was provided by a 48 K step syringe pump (V6, P/N 54022, equipped with a high pressure syringe header valve (P/N 26098) and a 1-mL capacity high pressure syringe (P/N 23994), all from www.kloehn.com. Test solutions were injected with an in-line 1 μL loop injector (070-0134H, www.vici.com). Except as stated, the carrier solution or eluent for chromatography (*vide infra*) was composed of 1 mM HQS and 1 mM MES, adjusted to pH 5.56 with NaOH and filtered through a 0.22 μm pore size nylon membrane filter and pumped at a flow rate of 4 μL/min. The injector was connected to the detector by a 5 cm long 250 μm i.d. fused silica capillary. For most experiments, the detector was simply covered with a cardboard box to provide immunity from ambient light.

3. Results and discussion

3.1. Basic detector design and performance of the simplest design

Early work on LCW-based capillary scale fluorescence detector clearly indicated the feasibility of such detectors [8]. Presently we first explored the performance of a LCW-based fluorescence detector in which a low power UV LED was used to radially illuminate the LCW capillary directly and the fluorescence was detected with a photodiode-operational amplifier integrated package, sold as a light-to-voltage converter. The response of this very simple detection system to 1 μL of 200 μM $Al(HQS)_3$ exhibited an S/N of 350. While we intended such a detector to be used primarily for pedagogic purposes and therefore made no further optimization efforts, it is worthwhile to note that an essentially identical detector with ~15× greater sensitivity (TSL257R, 1460 mV/μW per cm^2 @ 500 nm) is available at the same cost from the same manufacturer. Also it is worthwhile to note that even for HQS chelates, the Al-chelate is *not* the most fluorescent [35].

3.2. The "Blu-ray" laser based detector

This source is misnamed: at 405 nm, it is violet, rather than blue. VLD's have been available for some time; since their availability till now they continue to cost ~>US$ 2000 as scientific equipment. Lucy and coworkers were the first to use such VLDs for capillary scale fluorescence detection. They observed that at most ~30–50% of the power is coupled to a 100 μm core fiber optic (FO) when the unmodified LD is coupled to the FO [36]. While they recognized that focusing through additional optics such as a microscope objective is a superior alternative for capillary systems [37,38], they have mostly continued to use the FO coupled configuration [39–41] presumably for the simple reason that incorporating additional optics that necessarily require precise, stable positioning, is cumbersome. Availability of laser based optical drives as a consumer product removes this difficulty. Although the results described in the present work utilizes a different device which uses three different discretely packaged laser sources, based on further experience, we would recommend others to begin with a Sony Playstation 3 (PS3) reader assembly which contains three different laser sources (780, 640 and 405 nm) and a photodiode (that monitors the source output) in a single package. At 20 mW rated output for the 405 nm source, this VLD is also more powerful than the one presently used. Note that although 20 mW VLDs are being produced in quantity (~2 million /month in mid-2007) inexpensively (estimated production cost: US$ 8) [42], they are not available as discrete devices. To our knowledge, there are also no publicly accessible specification sheets. A PS3 reader assembly is however, readily available as a replacement part for <$60 (see Fig. S8 in SI) and VLD aficionados have web-accessible instructions on how to extract the VLD out of the assembly in detailed written [43] and even video [44,45] forms. However, no matter which precise source is used for the VLD, the reader assembly should not be disassembled and the LD extracted for constructing a fluorescence detector. The optics that focuses the beam down to a very small spot is integral to the read (write) assembly and makes it very convenient to simply put the capillary on the top of the lens, aided by the magnetic rails that provide a convenient means to hold the capillary down (all presently available optical drives use magnetic force to keep the disk spinning just away from the lens element without physical contact) and finally, any necessary heat sink is integrally present in an intact assembly. For the more ambitious, the rail and the stepper motor assembly provides a ready means to translate the source along the capillary and thus generate a "whole column" image (albeit the maximum translation length, <40 mm, is rather limited). In the case of the PS3 reader referred to above, any of the three laser sources (the respective pin outs, complete with magnified photos, are available in Refs. [43,45]) are available through the same optics.

In the absence of available specifications, one must necessarily be careful about the maximum current the source can be operated at to avoid irreversible damage. We had no information on the spe-

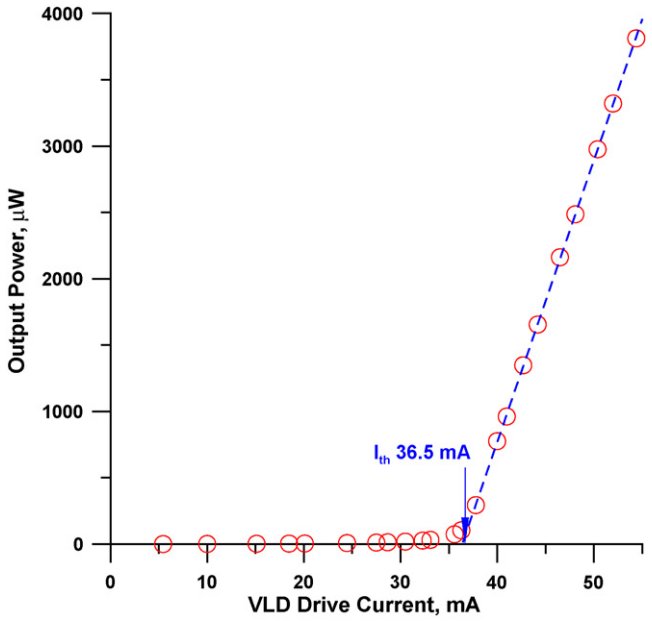

Fig. 2. Violet laser diode optical output vs. VLD drive current.

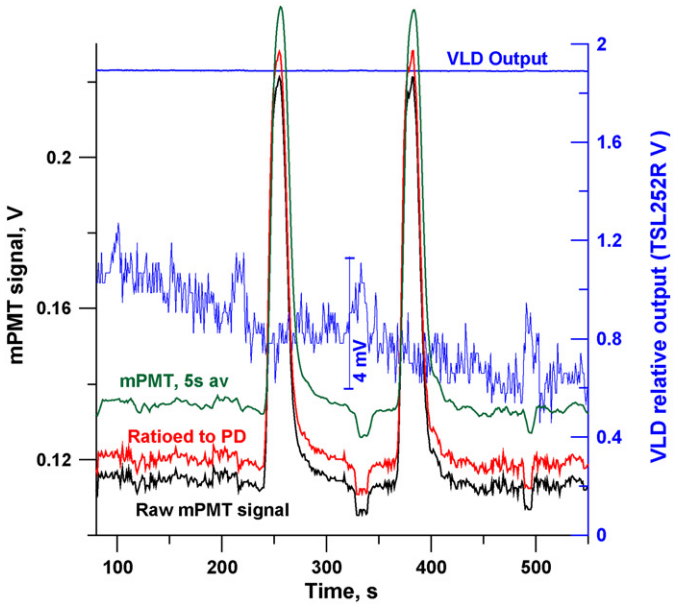

Fig. 3. Detection of 1 μL of 1 μM Coumarin 30 in 50:50 methanol:water injected in the same solvent flowing at 4 μL/min. The laser output (VLD drive current 37 mA) is shown as the top horizontal line (right ordinate); it is also shown magnified 133×. The S/N of the fluorescence signal does not significantly change upon ratioing to the laser output but does predictably improve with a moving average filter.

cific Pioneer VLD used here and to err conservatively, assumed it to be a 5 mW device, the lowest power VLDs used in Blu-ray readers. The device shows a weak diffuse output at low currents (similar to that of an LED driven at a low current). As the drive current is increased, the lasing threshold is eventually reached; past this point the light output increases dramatically. Fig. 2 shows the light output through the lens element vs. drive current. The lasing threshold is computed by extrapolation to be 36.5 mA. It has been suggested that the VLD should not be driven at currents much greater than I_{th} + 10 mA (i.e., ~47 mA in the present case) to avoid irreversible damage [43]. We operated the present VLD up to 54.4 mA for few seconds at a time with a measured power of 3.7 mW at the lens exit, which would probably be close to its maximum operating current (if it is a 5 mW device), accounting for optical losses. To be conservative and safe, we initially did most of the work at a drive current of 37 mA, just above the lasing threshold. These results are discussed as operation at this power level will permit essentially indefinite life. Subsequently, the VLD was operated at 47 mA to characterize ultimately attainable LODs from this source. A cooling fan was put on externally to prevent source drift and a smaller aperture was used with the photodiode to prevent saturation.

Although a VLD can be used to detect Al(HQS)$_3$, it is not optimally excited at this wavelength. Vos et al. indicated an LOD of 3 μM for example in a CE configuration [39], this LOD can in essence be reached by our simple LED-PD combination (Section 3.1). In addition, the excitation maximum of Al(HQS)$_3$ is listed as 395 nm [35], this is not strictly correct (*vide infra*). We chose to explore detection limits with Coumarin 30, which has a λ_{max} of 407 nm (in ethanol, for other photophysical data on Coumarin 30 see [46], we used 50:50 methanol water in flow injection experiments both as carrier and as the analyte matrix; absorption and fluorescence spectra obtained in such a matrix was nearly identical to those published for a ethanol medium [46] and are not separately given here). Coumarin dyes are also of particular interest in enzyme-linked immunosorbent assays that most commonly rely on an alkaline phosphatase enzyme utilizing 4-nitrophenylphosphate as substrate. Instead of absorbance detection of the 4-nitrophenol formed at 405 nm, the decrease in fluorescence of concurrently present Coumarin provides a much more sensitive assay [47].

In LCW-based fluorescence detection, we have generally used some form of an optical filter atop the photodetector to filter out excitation light. This unwanted background largely originates from scattering—while the optical quality of the LCW is obviously important, how tightly the excitation beam is focused also greatly governs the extent of scattering. The optics integral to present optical disk drives provide focused spot diameters of 2.11, 1.32 and 0.58 μm respectively for the 780, 640, and 405 nm lasers [48]. To our pleasant surprise, the background scattering in the present setup was small enough that even without any filter, the mPMT background signal was easily manageable (<0.2 V) (at a PMT gain of 0.9 this corresponds to within 2× of the maximum gain for this particular device) and VLD drive current of 37 mA. Without any filter, the results for 1 μL of 1 μM Coumarin 30 injection are shown in Fig. 3. The VLD output as measured by the TSL252 R photodiode on the other side of the capillary is very stable as seen in the upper horizontal line. A 133× magnified view of the VLD output is also shown. This indicates a very small but slow downward drift over time, likely due to heating and temperature equilibration. Note that the more major baseline disturbances (that are discernible both in the mPMT and the PD traces) come from injection valve actuations. Referring to the mPMT trace, switching the valve from inject to load and back to inject cause the mPMT signal to go low while the valve is in the load position. If we try to correlate the mPMT baseline signal to the TSL252R baseline signal in a region where there is no valve actuation artifacts, it is readily revealed that there is no correlation ($r < 0.02$). Predictably the S/N observed in the mPMT trace (~30, noise being defined as peak-to-peak noise, leading to an LOD of ~100 nM) is not improved by ratioing the signal to the laser output. Also predictably, running a 5 s moving average filter significantly improved the S/N, leading to an LOD <40 nM. Of course the LOD is directly dependent on the laser intensity. The above results were all obtained with a drive current of 37 mA.

As the laser output is an order of magnitude greater at a drive current of 47 mA (Fig. 2), the LODs are much better. Fig. 4 shows results for the injection of 50 and 100 nM (solution preparation and surface adsorption losses for Coumarin 30, a very hydrophobic

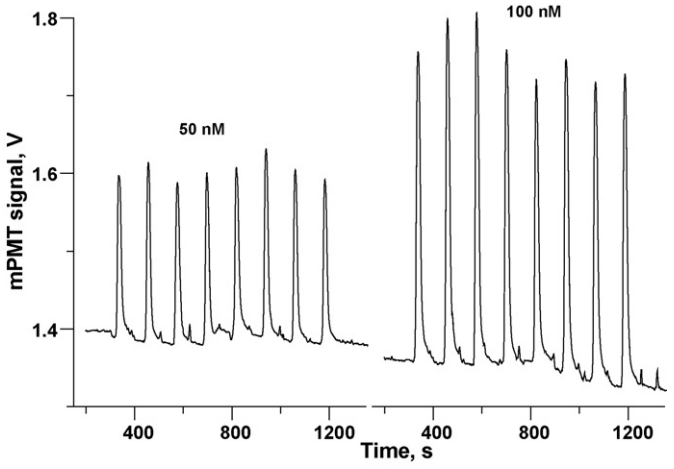

Fig. 4. Injection of 50 and 100 nM Coumarin 30 with the VLD driven at 47 mA. The data were acquired at 5 Hz and a 5-s moving average filter applied. Note that there is no secondary electronics to the mPMT output and the background signal represents the true mPMT background. No optical emission filter was used.

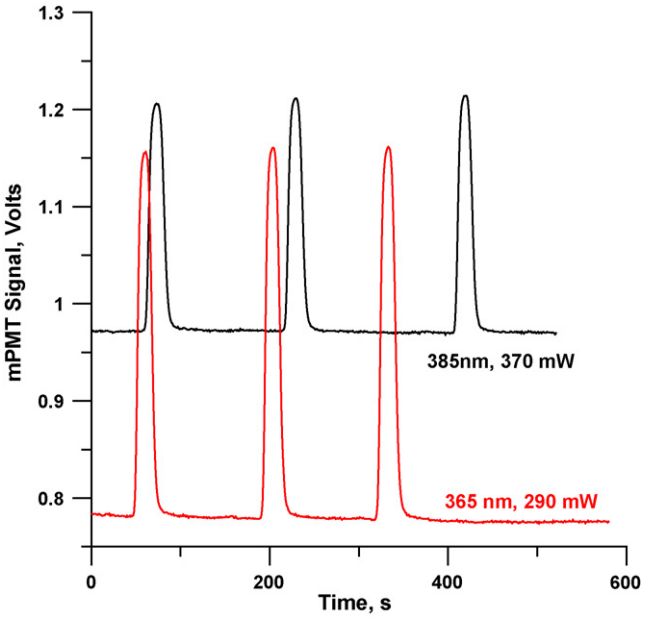

Fig. 5. Response elicited by an injection of 1 μL of 2 μM $Al(HQS)_3$, mPMT gain 0.7, secondary amplification 100×. Top trace: 385 nm emitter; bottom trace: 365 nm emitter. A double layer of Roscolux #369 green plastic filters was placed on the mPMT.

dye, preclude reproducible results at lower levels) injections. In the laser induced fluorescence literature, limit of detection has been defined in many different ways. Here, if we assume the raw data at 5 Hz and peak-to-peak noise, the S/N = 3 LOD is 7.7 nM (these and following data are based on the 50 nM injections, the LODs are more than 1.5× lower when calculated for the 100 nM injections—but this degree of change in short term noise is not unusual). Based on the p–p noise of the 5-s averaged data, the S/N = 3 LOD is 2.8 nM. Finally if noise is defined as the standard deviation of the drift corrected baseline in the 1250–1350 s region where no injections are made, the S/N = 3 LOD will correspond to 0.4 nM. If we assume that the probe volume is equivalent to a 100 μm (i.d. of LCW) long cylinder with 1 μm diameter, the probe volume is ~80 fL. For a 2.8 nM LOD, there are ~140 analyte molecules in that volume.

3.3. The HPLED based detector

3.3.1. Optimum wavelength to excite metal-sulfoxine complexes

One principal reason we are interested in capillary scale fluorescence detectors is to utilize them in metal ion chromatography. HQS forms a large number of fluorescent metal complexes, most have an excitation maximum around 390 nm with a large Stokes shift, several other derivatives of HQ with attractive fluorescence properties have been more recently synthesized as well [49–51]. The potential of HQS either in the eluent or as a postcolumn reagent in conventional scale metal ion chromatography has long been demonstrated, with or without micellar sensitization [35,52,53]. We chose to explore performance for Al-HQS detection, the fluorescent Al-chelate is often regarded as the archetypal HQS chelate [54].

The excitation maximum of $Al(HQS)_3$ at its optimum pH is reported as 395 nm [35]. Of LED sources we examined for exciting $Al(HQS)_3$, the primary candidates were two devices with center wavelengths of at 365 and 385 nm with comparable half bandwidths (10–12 nm), respectively emitting 210 and 290 mW @ 500 mA (Nichia NCSU033A and NCSU034A). The obvious expectation was that the 385 nm emitter will provide significantly better performance. To our surprise, the results were substantially the opposite (Fig. 5). We then reexamined the fluorescence characteristics of $Al(HQS)_3$; the data are shown in Fig. 6. These data show that the excitation maximum actually red shifts with increasing concentration. Near the LOD, at low concentration, excitation at 365 nm is actually superior to that at 385 nm. The 365 nm HPLED was used henceforth.

3.3.2. Cell terminal window material and light throughput

The terminal window sits directly on the PMT and conducts the light to the detector. It must also be chemically inert for the given application and withstand some modest backpressure. Aside from the optical fiber segment already mentioned in the experi-

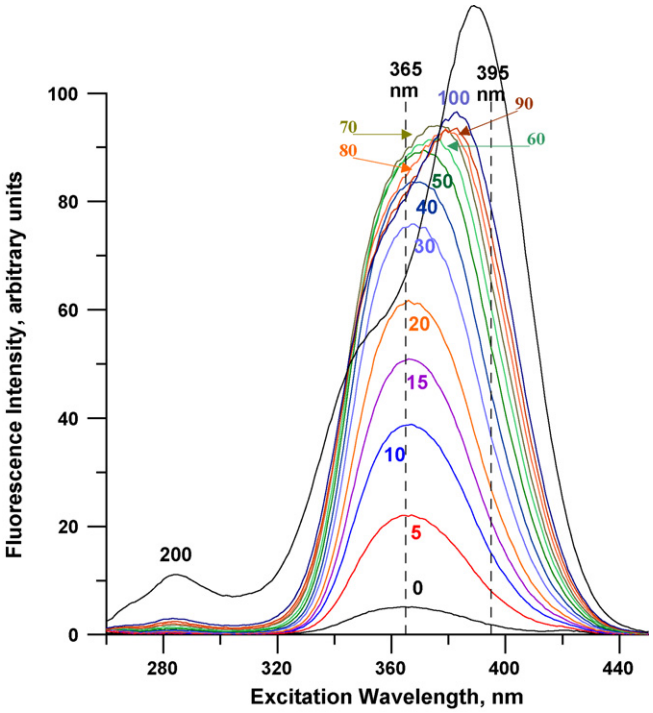

Fig. 6. Excitation spectrum of the indicated concentrations of Al^{3+} (in μM) in 1 mM HQS, pH 6. The excitation maximum red shifts with concentration.

mental section, based on initial experiments we investigated two other window types. One involved a spherical glass ball lens of 1 mm diameter (NT43-708, Edmund Industrial Optics, Barrington, NJ) that was forcibly put in at the PEEK tube tip after enlarging the tube tip i.d., in much the same way as the optical fiber segment. The other involved a 125 μm thick clear polyester window (Mylar, K-Mac plastics, KS6361, Wyoming, MI). The tip area of the PEEK tube was roughened by sanding, a thin layer of epoxy adhesive was applied and a small piece of the Mylar sheet was then affixed. Rather than measuring fluorescence emission, we simply measured the light transmission efficiency of the water-filled cell assembly. A miniature tee was put in the LCW tube entrance and an optical fiber was butted against the LCW tip. The other end of the optical fiber was connected to a LED emitting at 450 nm powered at a constant current of 10 mA. Water was pumped during the experiment through the perpendicular arm of the tee. The relative light intensities registered on the detector (adjusted to operate at a low sensitivity) were 0.376 ± 0.021, 0.340 ± 0.029 and 0.402 ± 0.012 for the polyester window, glass ball and the optical fiber , respectively. Considering that the cell tip has to be disassembled and reassembled for each test arrangement, the overall difference between the three is probably within experimental uncertainty. Nevertheless, we chose to do further experiments with the putative best, the cell with the optical fiber window.

3.3.3. Performance

Relative to coupling with a fiber optic, Melanson and Lucy [37] have shown that a pinhole and a microscope objective can provide a better focused arrangement for fluorescence excitation, leading to less scattered light and thus a better S/N. In the present case, even discounting interfacial losses, geometric considerations (HPLED emitting area vs. fiber optic cross section and far more importantly, fiber optic cross section vs. LCW bore) will dictate that maximally ~7–8% of the emitted light serves to illuminate the analyte over an estimated volume of 8 nL. Despite all this, we chose the fiber optic coupled arrangement rationalizing that the very large emitted power of the HPLED will provide enough light and counting on optical filters to filter out the scattered light; the simplicity and cost constituted a big plus. We examined three filters: Roscolux 369 (NT39-418), thin film UV filter sheet (NT39-426) and Wratten 44A (NT54-465, all from www.edmundoptics.com). The first two performed essentially equally well and the third one produced a ~2× lower S/N; the emission spectra of the LED, the emission spectra of $Al(HQS)_3$ and the transmission spectra of two sheets of the Roscolux 369 joined by a thin layer of optical grade epoxy are shown in Fig. 7. The spectra of the two other optical filters tested are provided in Fig. S10 of SI.

The performance of this detector is shown in the flow injection mode for a calibration set of samples containing 10–100 nM Al^{3+}. Data where a reference detector was used to reduce drift and then smoothed (5-s moving average filter) are shown for the low concentration data in the inset. (Fig. 8.) In this case, the smoothing actually has very little effect on the S/N. The primary noise in the baseline comes from frequent back and forth switching of the injector, as would be apparent from the trace after the last 100 nM sample, when no further injections were made. If we take the conservative approach and consider the baseline disturbances from the injector as part of noise, the S/N = 3 LOD will be 4 nM for either the raw 1 Hz data or the smoothed one. On the other hand, with noise defined as the standard deviation of the drift corrected baseline, the S/N = 3 LOD is in fact calculated to be ~0.8 nM. The signal is linear for at least two orders of magnitude (0.01–2.0 μM, linear r^2 0.9991). The relative standard deviation at the 20 nM level was 1.5% ($n = 10$).

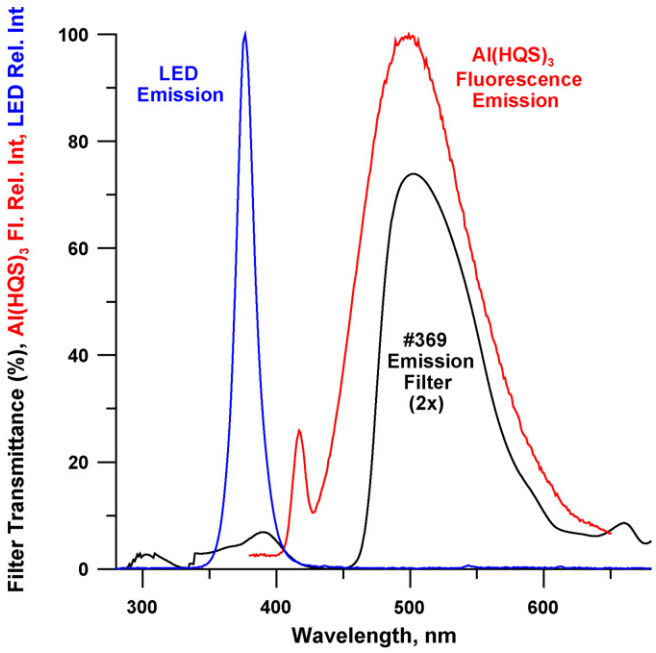

Fig. 7. Spectral characteristics of the excitation source, the fluorescence emission and two sheets of the #369 filter used for emission filtering.

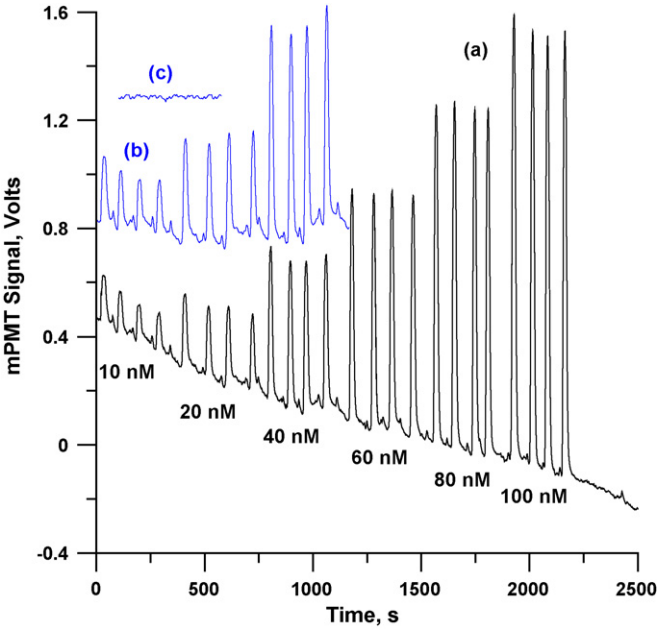

Fig. 8. (a) Typical output for Al^{3+} determination. The Al^{3+} concentration of the sample in μM is indicated. At low levels, the drift, which mostly appear to arise from thermal changes causing a difference in source output can be significant, (b) shows drift corrected magnified traces for the 10–40 nM injections and (c) shows the corresponding drift corrected baseline trace when no injections are made.

4. Conclusions

Recent advances in solid state light emitting sources, in conjunction with liquid core waveguides make possible attractive capillary scale fluorescence detectors that are both highly affordable and highly sensitive. We have provided here generic designs for LCW-based flow through detectors that can be used in series with other detectors. It is rare that a new device is made for analytical use—the

advent of short wavelength laser diodes in inexpensive commercial products is a boon to an experimentalist and can be harnessed to make very high performance very small volume detectors. Dedicated monochromatic source based fluorescence detectors do have the disadvantage that the extant source wavelength may be unsuitable for a particular application. Ref. [33] provides a discussion of many vendors and the wavelengths in which LEDs and LDs can be obtained. This is a dynamic marketplace and the corresponding websites should be visited for up to date information, however.

Acknowledgments

This research was supported by National Science Foundation through Grant CHE-0731792. IVF was supported in part by the Sabbatical Commission, the Operational Commission for Academic Activities Promotion and the Support for Development of Research program of the Instituto Politecnico Nacional, CIIDIR-IPN, Durango, Mexico.

Appendix A. Supplementary data

Supplementary data associated with this article can be found, in the online version, at doi:10.1016/j.talanta.2008.07.047.

References

[1] S.K. Mishra, P.K. Dasgupta, Anal. Chim. Acta 605 (2007) 166–174.
[2] P. Kuban, P.K. Dasgupta, J. Sep. Sci. 27 (2004) 1441–1457.
[3] P. Kuban, P.K. Dasgupta, C.A. Pohl, Anal. Chem. 79 (2007) 5462–5467.
[4] B.C. Yang, M. Takeuchi, P.K. Dasgupta, Anal. Chem. 80 (2008) 40–47.
[5] P. Kubáň, V. Kubáň, L. Klakurková, P.K. Dasgupta, J. Sep. Sci. (in press).
[6] S. Parrot, L. Bert, L. Mouly-Badina, V. Sauvinet, J. Colussi-Mas, L. Lambas-Senas, F. Robert, J.P. Bouilloux, M.F. Suaud-Chagny, L. Denoroy, B. Renaud, Cell. Mol. Neuorobiol. 23 (2003) 793–804.
[7] E. Gonzalez, J.J. Laserna, Quim. Anal. 16 (1997) 3–15.
[8] P.K. Dasgupta, G.F. Zhang, J.Z. Li, C.B. Boeing, S. Jambunathan, R. Al-Horr, Anal. Chem. 71 (1999) 1400–1407.
[9] T. Dallas, P.K. Dasgupta, Trends Anal. Chem. 23 (2004) 385–392.
[10] T. Okada, Electrophoresis 28 (2007) 3414–3419.
[11] A. Hanning, P. Lindberg, J. Westberg, J. Roeraade, Anal. Chem. 72 (2000) 3423–3430.
[12] M. Curcio, P. Stalhandske, P. Lindberg, J. Roeraade, Electrophoresis 23 (2002) 1467–1472.
[13] Z. Liu, J. Pawliszyn, Anal. Chem. 75 (2003) 4887–4894.
[14] Z. Liu, J. Pawliszyn, Anal. Biochem. 75 (2005) 94–101.
[15] J.A. Olivares, P.C. Stark, P. Jackson, Anal. Chem. 74 (2002) 2008–2013.
[16] J.Z. Li, P.K. Dasgupta, G.F. Zhang, Talanta 50 (1999) 617–623.
[17] V'. Kostal, M. Zeisbergerova, Z. Hrotekova, K. Slais, V. Kahle, Electrophoresis 27 (2006) 4658–4665.
[18] S.L. Wang, X.J. Huang, Z.L. Fang, P.K. Dasgupta, Anal. Chem. 73 (2001) 4545–4549.
[19] Q.Y. Li, K.J. Morris, P.K. Dasgupta, I.M. Raimundo Jr., H. Temkin, Anal. Chim. Acta 479 (2003) 151–165.
[20] S.L. Wang, X.F. Fan, Z.-R. Xu, Z.-L. Fang, Electrophoresis 26 (2005) 3602–3608.
[21] T. Zhang, Q. Fang, S.L. Wang, L.F. Qin, P. Wang, Z.Y. Wu, Z.-L. Fang, Talanta 68 (2005) 19–24.
[22] J. Li, P.K. Dasgupta, Anal. Chem. 72 (2000) 5338–5347.
[23] J. Li, P.K. Dasgupta, Z. Genfa, M.A. Hutterli, Field Anal. Chem. Technol. 5 (2001) 2–11.
[24] K. Toda, P.K. Dasgupta, J. Li, G.A. Tarver, G.M. Zarus, S.-I. Ohira, Anal. Sci. 17 (Suppl.) (2001) i407–i410.
[25] Q.Y. Li, P.K. Dasgupta, H. Temkin, Environ. Sci. Technol. 42 (2008) 2799–2804.
[26] Z. Genfa, P.K. Dasgupta, Anal. Chem. 64 (1992) 517–522.
[27] J. Li, P.K. Dasgupta, G.A. Tarver, Anal. Chem. 75 (2003) 1203–1210.
[28] R. Manor, A. Datta, A. Dhar, M. Holtz, J. Berg, S. Gangopadhyay, P.K. Dasgupta, H. Temkin, V. Veraraghavan, R. Vijayraghavan, T. Dallas, Proc. IEEE Sens. 1 (2002) 660–664, 64.6.
[29] A. Datta, I.-Y. Eom, A. Dhar, P. Kuban, R.M. Manor, I. Ahmad, S. Gangopadhyay, T. Dallas, M. Holtz, H. Temkin, P.K. Dasgupta, IEEE Sens. J. 3 (2003) 788–795.
[30] M. Takeuchi, Q.-Y. Li, B. Yang, P.K. Dasgupta, Talanta 76 (2008) 617–620.
[31] W.J. Ferguson, K.I. Braunschweiger, W.R. Braunschweiger, J.R. Smith, J.J. McCormick, C.C. Wasmann, N.P. Jarvis, D.H. Bell, N.E. Good, Anal. Biochem. 104 (1980) 300–310.
[32] Nichia Corporation, Specification for Nichia Chip Type UV LED Model NCSU033A(T). http://www.nichia.com/specification/led_smd/NCSU033AT-E.pdf (accessed May 25, 2008).
[33] P.K. Dasgupta, I.-Y. Eom, K.J. Morris, J. Li, Anal. Chim. Acta 500 (2003) 337–364.
[34] Hamamatsu Photonics, Metal Package PMT Photosensor Module H5784 Series. http://sales.hamamatsu.com/assets/pdf/parts_H/H5784_series.pdf (accessed May 25, 2008).
[35] K. Soroka, R.S. Vithanage, D.A. Phillips, B. Walker, P.K. Dasgupta, Anal. Chem. 59 (1987) 629–636.
[36] J.E. Melanson, C.A. Lucy, Analyst 125 (2000) 1049–1052.
[37] J.E. Melanson, C.A. Lucy, Electrophoresis 23 (2002) 1689–1694.
[38] E.P. De Jong, J.E. Melanson, C.A. Lucy, Electrophoresis 25 (2004) 3153–3162.
[39] C.J. Vos, J.E. Melanson, C.A. Lucy, Anal. Sci. 17 (2001) 225–227.
[40] J.E. Melanson, C.A. Boulet, C.A. Lucy, Anal. Chem. 73 (2001) 1809–1813.
[41] J. Jiang, C.A. Lucy, Talanta 72 (2007) 113–118.
[42] M. Hatcher, Sony ramps monthly GaN laser volume to 1.7m, April 27, 2008. Optics.org; http://optics.org/cws/article/industry/27746 (accessed May 25, 2008).
[43] L. Wright, S. Goldwasser, Dissection of a Blu-ray reader assembly, March 8, 2007. http://www.repairfaq.org/sam/Blu-ray/site1/, see also http://www.fineartradiography.com/hobbies/lasers/blu-ray/diode.html (accessed May 25, 2008).
[44] M. Taylor, Build a blue laser pointer. http://youtube.com/watch?v=R21hNxS78-I (accessed May 25, 2008).
[45] Kipkay, Blu-ray laser phaser. http://youtube.com/watch?v=xfj1n8vPWCE (accessed May 25, 2008).
[46] Prahl, S. Oregon Medical Laser Center. Optical Spectra: Coumarin 30. http://omlc.ogi.edu/spectra/PhotochemCAD/html/coumarin30.html (accessed May 25, 2008).
[47] S. Paliwal, M. Wales, T. Good, J. Grimsley, J. Wild, A. Simonian, Anal. Chim. Acta 596 (2007) 9–15.
[48] Blu-ray disc founders, August 2004. White Paper Blu-ray disc format. http://www.docstoc.com/docs/479157/Blu-ray-Disc-Format—General (accessed May 25, 2008).
[49] M.A. Palacios, Z. Wang, V.A. Montes, G.V. Zyryanov, B.J. Hausch, K. Jursikova, P. Anzenbacher, Chem. Commun. 36 (2007) 3708–3710.
[50] Y.G. Zhao, Z.H. Lin, H.P. Liao, C.Y. Duan, Q.J. Meng, Inorg. Chem. Commun. 9 (2006) 966–968.
[51] H. Zhang, L.F. Han, K.A. Zachariasse, Y.B. Jiang, Org. Lett. 19 (2005) 4217–4220.
[52] D.A. Phillips, K. Soroka, R.S. Vithanage, P.K. Dasgupta, Mikrochim. Acta I (1986) 207–220.
[53] P.K. Dasgupta, K. Soroka, R.S. Vithanage, J. Liq. Chromatogr. 10 (1987) 3287–3319.
[54] J.B. Mulon, E. Destandau, V. Alain, E. Bardez, J. Inorg. Biochem. 99 (2005) 1749–1755.

Talanta 77 (2008) 576–580

Contents lists available at ScienceDirect

Talanta

journal homepage: www.elsevier.com/locate/talanta

Amplitude modulated multiplexed flow analysis

Hideji Tanaka [a,*], Takuto Mima [b], Masaki Takeuchi [a], Hitoshi Iida [a]

[a] Institute of Health Biosciences, Tokushima University, Shomachi 1-78-1, Tokushima 770-8505, Japan
[b] Faculty of Pharmaceutical Sciences, Tokushima University, Shomachi 1-78-1, Tokushima 770-8505, Japan

ARTICLE INFO

Article history:
Received 30 September 2007
Received in revised form 11 March 2008
Accepted 17 March 2008
Available online 25 March 2008

Keywords:
Amplitude modulation
Flow analysis
Multiplex
Fast Fourier transform
Simultaneous determination

ABSTRACT

We propose a new concept, amplitude modulated multiplexed flow analysis, for the simultaneous determination of multiple analytes from a single continuous analytical signal. The flow rates (F_{S1} and F_{S2}) of two sample solutions are independently varied in response to trigonometric voltage signals each at a different anharmonic frequency. With the total flow rate F_T held constant, the solutions are merged with a reagent solution that is aspirated to the confluence point at the flow rate of $F_T - F_{S1} - F_{S2}$. Downstream, the analytical signal due to the mixed reacted solution, V_d, is monitored. V_d will show a complicated profile resulting from the trigonometrically varying flow rates of the sample solutions. The signal contains information on the multiple analytes. The signal can be demodulated to the contribution of each sample solution through fast Fourier transform (FFT). The amplitudes of the separated wave components are related to the concentration of the analytes in the sample solutions. By moving a window for FFT analysis with time, temporal profile of amplitudes can be obtained in real-time. We demonstrate the concept by applying it to the simultaneous determination of food dyes and to that of ferrous ions in two sample solutions.

1. Introduction

Amplitude modulation (AM) is a technique that transmits information signal by impressing it onto a carrier wave. The carrier is of an alternating current waveform, the frequency of which is much higher than that of the signal wave. The amplitude of thus obtained signal (modulated wave) varies depending on the information signal before the modulation. AM is commonly used for radio communication and the term "AM" is often used to refer to as radio broadcasting using medium frequency wave. In the field of analytical chemistry, AM, as well as frequency modulation (FM) is used for the extraction of signal of interest from noises and/or background noises [1]. For example, Hinoue et al. applied AM to a laser-induced photopyroelectric spectrometry for the determinations of phosphorus and ammonia water [2]. Wagatsuma reported an AM method for a radio-frequency powered glow discharge emission spectrometry [3,4].

Tanaka et al. proposed a flow ratiometry for on-line true titration [5–8]. In their method, the flow ratio of titrant and titrand was continuously increased or decreased just in the range of interest (e.g., the equivalence point) using feedback-based variable triangular wave voltage and/or fixed triangular wave voltage. They demonstrated the concept by applying it to acid–base titrations and realized a flow titrimetry with unprecedented high throughput rate (maximally 34 titrations per minute). Dasgupta and Jo applied the method to redox titrations using electrogenerated titrants [9] and to chelatometric titrations [10].

In the course of the studies on flow ratiometry using triangular wave, the senior author (HT) reached to the idea that theories on waves can be applied to flow analysis, if the information on sample (e.g., analyte concentration) to be delivered in a flow system is impressed on a carrier wave. In the present paper, we propose a new concept of flow analysis, *Amplitude Modulated Multiplexed Flow Analysis*. The concept is based on frequency analyses, which convert analytical data from time domain to frequency domain and are widely used to derive periodic signal components from complicated analytical signals or to separate analytical signals of interest from background noises. It is well known, for example, that two light sources can be modulated at different frequencies and detected by the same detector after demodulation [11]. Trigonometric wave voltage signals each having different frequencies are applied to control the flow rates of different analyte solutions. The solutions are merged with a reagent or diluent. The mixed solution, therefore, contains frequency-dependent information on each analyte. The overall signal has a periodic nature and can be separated into the contributions from each analyte solution by fast Fourier transform (FFT). The amplitudes of the fundamental and/or higher harmonic wave components obtained through FFT are closely related to the concentration of analyte in each solution. The temporal concentration profile can be obtained in real-time by moving the FFT window

* Corresponding author. Tel.: +81 88 633 7285; fax: +81 88 633 9507.
E-mail address: htanaka@ph.tokushima-u.ac.jp (H. Tanaka).

0039-9140/$ – see front matter © 2008 Elsevier B.V. All rights reserved.
doi:10.1016/j.talanta.2008.03.016

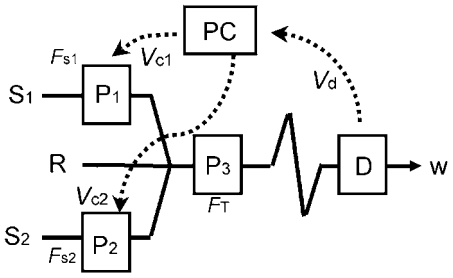

Fig. 1. Schematic diagram of the flow system. S_1 and S_2, sample solutions; R, reagent solution (or diluent, depending on the analytical method); w, waste; P_1, P_2 and P_3, peristaltic pumps; D, spectrophotometric detector; PC, notebook computer with a card type A/D–D/A converter; V_{c1} and V_{c2}, controller output voltages with cosine profiles each having different frequency; V_d, detector output voltage. F_{S1}, F_{S2} and F_T are the flow rates of S_1, S_2 and mixed solutions, respectively.

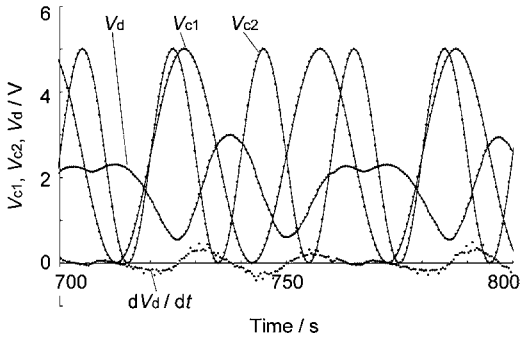

Fig. 2. Principle of amplitude modulated multiplexed flow analysis; control voltage and detector output voltage signals. V_{c1} and V_{c2}, control output voltages with the periods of 30 and 20 s, respectively; V_d, detector output voltage (fivefold values of original V_d are shown here to make the comparison among V_d, V_{c1} and V_{c2} easy). The derivative of V_d, dV_c/dt, is shown for reference. Sample solutions of S_1 and S_2 are 0.10 and 0.05 mmol dm^{-3} Fe^{2+} solutions (added as Mohr's salt), respectively. Reagent solution was 10.0 mmol dm^{-3} 1,10-phenalthoroline (pH 4.6).

over time. The validity of the proposed concept was demonstrated by applying it to the simultaneous spectrophotometric determination of food dyes and to that of ferrous ions (Fe^{2+}) in two sample solutions.

2. Experimental

2.1. Flow system

Fig. 1 shows the flow system in the present study. Three peristaltic pumps (P_1, P_2 and P_3; Rainin Dynamax RP-1) were used for delivering solutions. Pharmed tubings with 0.51-mm i.d. were used for P_1 and P_2 as pump tubes and that with 0.79-mm i.d was for P_3. The flow rates (F_{S1} and F_{S2}) of sample solutions (S_1 and S_2) delivered using P_1 and P_2, respectively, were varied in response to the controller output voltages (V_{c1} and V_{c2}, respectively) generated from a computer (PC; Toshiba DynaBook Satellite 1850 SA120C/4) through a card type A/D–D/A converter (Measurement Computing PC-CARD–DAS16/12-AO). In the present system, the flow rate per voltage was *ca.* 0.263 cm^3 min^{-1} V^{-1}. Both the solutions were merged with a reagent solution R (or diluent, depending on the analytical method) at the confluence point (polypropylene joint) while the total flow rate F_T was held constant at *ca.* 2.77 cm^3 min^{-1}. The flow rate of the reagent solution (or diluent), which was aspirated to the confluence point, was, therefore, $F_T - F_{S1} - F_{S2}$. The reason for the constancy of the total flow rate was to keep the lag time between the mixing of the three solutions (S_1, S_2 and R) and the sensing of the mixed solution by a detector D (a Japan Spectroscopic Co. (JASCO) Ubest V-550RM spectrophotometer) constant. This lag time consisted mainly of the physical transit time of the mixed solution from the confluence point to a flow cell (a JASCO SFC-333; optical path length 1 cm; inner volume 0.1 cm^3) set in the detector, and, to a lesser degree, of the response time of the detector. Output signals from the detector (1 V per absorbance unit) were quantified by the A/D–D/A converter, and the resulting digital data were acquired by the PC in the Microsoft Excel format. A program written in Visual BASIC in-house was used to generate V_{c1} and V_{c2}, acquire data, analyze them and graphically display the results automatically. In the program, we incorporated the FFT algorithm described by Nakamura [12].

2.2. Reagents

Reagents of analytical reagent grade purchased from Kanto Chemicals (Tokyo, Japan), Nacalai Tesque (Kyoto, Japan), Tokyo Chemical Industry (Tokyo, Japan) or Wako Pure Chemical Industries (Osaka, Japan) were used without further purification. Zartorius Arium 611DI grade deionized water was used throughout.

3. Principles

The principles of the proposed concept are described using actual data for the simultaneous determination of Fe^{2+} in two sample solutions (S_1 and S_2). The values of main software parameters for the determination are listed in Table 1. The results are shown in Figs. 2 and 3, where only the data during the period of 700–800 s in the total measurement time of 2000 s are shown so as to see the data easily. The concentrations of Fe^{2+} (added as $(NH_4)_2Fe(SO_4)_2{\cdot}6H_2O$) in S_1 and S_2 were 0.10 and 0.05 mmol dm^{-3}, respectively; an aqueous solution of 10.0 mmol dm^{-3} 1,10-phenanthoroline, the pH of

Table 1
Typical values of main software parameters

Main software parameters		Typical values
Sampling frequency (Hz)		2.13333 (1.5)
V_{c1}	Peak voltage, high (V)	5
	Peak voltage, low (V)	0
	Period (s)	30
V_{c2}	Peak voltage, high (V)	5
	Peak voltage, low (V)	0
	Period (s)	20
Number of data for FFT analysis		8
Interval of FFT analysis (s)		1.875 (3)

The values in the parentheses are original values imputed by an operator. These values are automatically changed to the values so that they become compatible with FFT algorithm.

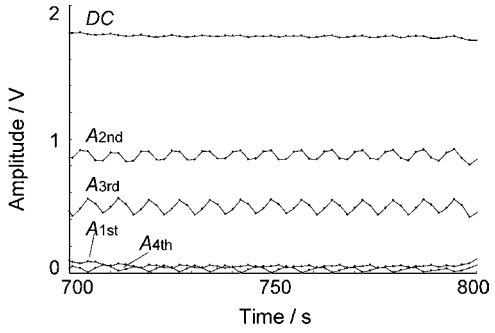

Fig. 3. Principle of amplitude modulated multiplexed flow analysis; the temporal profiles of amplitude obtained through FFT, the window of which was moved with time. DC: voltage of direct current component. A_{1st}–A_{4th}, the amplitudes of the fundamental, second harmonic, third harmonic and fourth harmonic waves components, respectively. Samples, reagent and experimental condition were the same as those in Fig. 2.

which was adjusted at 4.6 with an acetate buffer, was used as R (see Fig. 1).

3.1. Operation of the system

As shown in Fig. 2, V_{c1}, used for controlling the flow rate of S_1 (F_{S1}) is of a cosine profile with a period (=the reciprocal of frequency) of 30 s and with an amplitude expressed as peak-to-peak voltage of 5 V (0–5 V). Those for V_{c2}, used for controlling the flow rate of S_2 (F_{S2}), were 20 s and 5 V (0–5 V), respectively. Analytical signal V_d shows a complicated shape, resulting from the trigonometrically varying flow profiles of the two sample solutions. The V_d, however, has a periodic nature with the period of 60 s (=the least common multiple of the periods of V_{c1} and V_{c2} (i.e., 30 and 20 s)) so long as the concentrations of Fe^{2+} in both of the sample solutions are constant. This period is used as the length of the window for FFT, because the length should ideally be as integral multiple of the period of periodic analytical signals. In our software, the operator inputs the minimum data acquisition frequency, say, 1.5 Hz. However, the number of data in a widow for FFT analysis should be 2^n, where n is an integer, in order to do butterfly computation. When the FFT period is chosen, the program automatically chosen the next higher sampling frequency 2.13333 Hz, resulting in $n = 7$ that meets this requirement.

3.2. Fast Fourier transform

The contribution of each modulated sample solution can be obtained from V_d by FFT. Eight ($=2^3$) data in the 60 s (i.e., every 16th 8 points set) are used for FFT calculations (Eq. (1)).

$$X_k = \frac{1}{N}\sum_{n=0}^{N-1} x_n \exp\left(-j\frac{2\pi nk}{N}\right), \quad (1)$$

where N is the number of data for FFT analysis (8, in this case) and j is the imaginary number. Based on the sampling theorem, the amplitude of the fundamental wave component ($2X_1$) and those of the second–fourth harmonic waves components ($2X_2$, $2X_3$ and X_4, respectively) can be obtained together with the value of direct current component (X_0). The magnitudes of $2X_2$ and $2X_3$ are related to the concentrations of Fe^{2+} in the sample solutions (S_1 and S_2), the flow rates of which are controlled with trigonometric voltage signals V_{c1} and V_{c2} having the periods of 30 and 20 s, respectively.

Amplitudes can be measured in real-time by moving the window for FFT analysis with time. Under the values of the parameters in Table 1, FFT calculations were carried out every 1.875 s (=every fourth acquisition of the data) using a new set of 8 data. This interval (1.875 s) was automatically calculated so that the interval would not become longer than the user-imputed value (3 s). Temporal profiles of amplitudes thus obtained are plotted in a separate sheet in a Microsoft Excel file, as shown in Fig. 3. The amplitudes for the fundamental and the fourth harmonic waves components are also obtained by FFT. In this case, the frequency of the fourth harmonic wave component (6.666×10^{-2} Hz) is the Nyquist frequency (the highest frequency that can be coded at a given sampling rate in order to accurately represent the signal). Theoretically, these amplitudes should be zero because there are no control signals with a period of 60 and 15 s. The PC card used in the present study can generate maximally two analog output voltages. It should be noted, however, that four kinds of analytes could simultaneously be determined if four control signals with the periods of 60, 30, 20 and 15 s were employed to deliver four sample solutions.

4. Results and discussion

4.1. Selection of the periods of trigonometric voltage signals

In order to confirm the validity of the proposed concept, first we selected simple systems with no chemical reaction. Analytes that give relatively high absorbance at the analytical wavelength are suitable for this purpose. They should be inert to each other and absorbance additivity must apply. In preliminary experiments, metal ions (Ni^{2+}, Cu^{2+}, and Co^{2+} added as sulfate or nitrate) and dyes (methylene blue, malachite green, methyl orange, crystal violet, amaranth, erythrosine B, fast green, and indigo carmine) were examined. Two food dyes, amaranth (acid red S) and erythrosine B, were selected based on their high stability and low adsorption affinity for the conduit walls.

The effects of the periods of trigonometric voltage signals were investigated. The period of V_{c1} was set to be 1.5 times longer than that of V_{c2}. V_{c1} and V_{c2} correspond, therefore, to the second and third harmonic wave components of V_d. Three pairs of the periods of V_{c1} and V_{c2} (30 and 20 s, 45 and 30 s, 60 and 40 s) were examined for the determination of the two food dyes. The V_{c1} and V_{c2} control the flow rate of amaranth solution (0.022–0.089 mmol dm^{-3}) and erythrosine B solution (0.020 mmol dm^{-3}), respectively. The analytical wavelength was 520 nm, because both of the dyes give almost the maximum absorbance at this wavelength. We did not observe any significant difference in the qualities of data (amplitudes of their corresponding wave components, standard deviations of the amplitudes, linearity of the amplitudes for amaranth with its concentration) as a function of the choice of a particular pair of periods. Shorter periods preferred to decrease the FFT window length, and hence to increase sample throughput, because the implicit assumption is invariant concentration within a single FFT window. Consequently, the pair of 30 and 20 s was selected as the optimum periods of V_{c1} and V_{c2}, respectively. If the period is too small, however, liquid phase dispersion will make it difficult to detect a clear amplitude variation.

4.2. Selection of the number of data for FFT calculations

As described in Section 3, 2^n data were used for FFT calculations, where n is an integer, at regular intervals during the time of least common multiple of the periods of V_{c1} and V_{c2} (e.g., 60 s if the period of V_{c1} and V_{c2} are 30 and 20 s, respectively). Higher n value is desirable for increasing frequency resolution of the FFT analysis. In our program, controlling the system, acquisition of data and FFT calculations should be completed within one sampling period (0.46875 and 0.11719 s when the sampling frequencies are

Table 2
Amplitudes of harmonic wave components for amaranth and erythrosine B

Amaranth		Erythrosine B	
Concentration (mmol dm^{-3})	Amplitude (V)	Concentration (mmol dm^{-3})	Amplitude (V)
0.089	0.726 ± 0.020	0.020	0.153 ± 0.008
0.067	0.592 ± 0.015	0.020	0.157 ± 0.008
0.045	0.391 ± 0.009	0.020	0.151 ± 0.007
0.022	0.217 ± 0.005	0.020	0.155 ± 0.004

(n = 28).

2.13333 and 8.53333 Hz, respectively) for real-time analysis. In the FFT algorithm, the number of multiplication steps and addition steps are $n2^{n-1}$ and $n2^n$, respectively [13]. When 4 was adopted for n (16 data points used for FFT calculations) and the sampling frequency was 8.33333 Hz, the computing power of the presently used hardware was inadequate to complete the above-mentioned processes within one sampling period. Therefore, n was chosen to be 3. This n value seems, however, sufficient in practice because maximally four separate analytes can be simultaneously determined if four control signals at different frequencies modulate four sample solutions.

It was found that the profile of amplitude, obtained through FFT analysis, has a fine structure of oscillation with the period of one eighth of the fundamental period of V_d (7.5 (=60/8) s, for example (see Fig. 3)). This is lively because eight data points used for the FFT analysis are on the same phases of the periodic signals of V_d every one eights of the fundamental period.

4.3. Continuous measurement of various concentrations of analyte

Fig. 4 shows typical V_d trace obtained by the present method. The concentration of amaranth in S_1 was changed stepwise from 0.089, 0.067, 0.045, 0.022 and again to 0.089 mmol dm^{-3}. On the other hand, the concentration of erythrosine B in S_2 was kept constant at 0.02 mmol dm^{-3}. In this case, not a reagent but diluent water was aspirated from the third line and merged with the dyes solutions. The periods of V_{c1} and V_{c2} were 30 and 20 s, respectively. Sampling frequency was 8.53333 Hz, in this case. The derivatives of V_d were also plotted for reference. The two control signals (V_{c1} and V_{c2}) are not shown in Fig. 4 for clarity. It can be seen that V_d exhibits periodicity with a cycle time of 60 s, the least common multiple of V_{c1} and V_{c2} periods. Fig. 5 shows the results for the FFT analysis of the data shown in Fig. 4. In this case, the amplitudes of the second and third harmonic wave components correspond to the concentrations of amaranth and erythrosine B, respectively. It

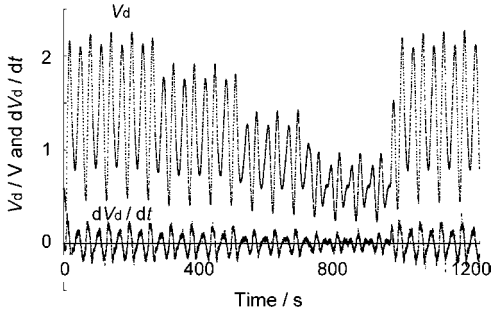

Fig. 4. Typical results of analytical signals V_d for continuous measurement. The V_d values shown here are five times of their real values, as in Fig. 2. The concentration of amaranth in S_1 was changed stepwise from 0.089 to 0.067, 0.045, 0.022 and again 0.089 mM. Each duration time was around 240 s. The concentration of erythrosine B in S_2 was kept constant at 0.02 mmol dm^{-3}. The plots of V_{c1} and V_{c2} are not shown here for clarity.

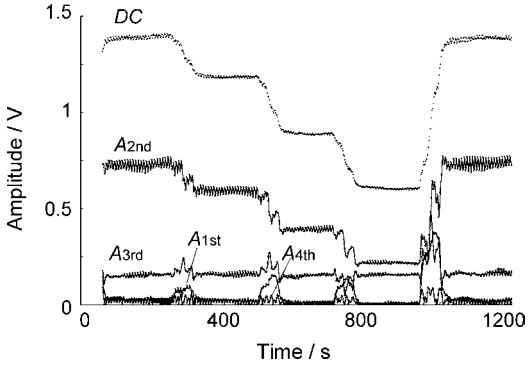

Fig. 5. The results for the FFT analysis of the data shown in Fig. 4. DC: voltage of direct current component. A_{1st}–A_{4th}, the amplitudes of the fundamental, second harmonic, third harmonic and fourth harmonic waves components, respectively. The periods of control signals for Amaranth and erythrosine B flow rates were 30 and 20 s, respectively. The amplitudes of the second and third harmonic waves components correspond to the concentrations of amaranth and erythrosine B, respectively.

shows that the amplitudes were disturbed in the region where the concentration of amaranth was changed. The FFT is based on the assumption that the signals in the window continue infinitely as periodic signals. The change of analyte concentration in these transition regions do not conform to this assumption and thus affects the results obtained from FFT. The amplitudes of the fundamental and the fourth harmonic waves components are ghost results. Except for these transition periods, the amplitude for amaranth changed stepwise and that for erythrosine B was essentially constant, as expected. The data of the amplitudes thus obtained are listed in Table 2. The amplitude for amaranth (A_A) were increased linearly with its concentration C_A: $A_A = 7.738\,C_A + 0.049$, $r^2 = 0.9944$. On the other hand, almost constant amplitudes were obtained for erythrosine B (A_{EB}: 0.154 ± 0.002 V) irrespective of the amaranth concentration (C_A); the correlation coefficient (r^2) between A_{EB} and C_A was essentially zero, meaning no correlation between them.

A similar experiment was carried out for the simultaneous determination of Fe^{2+} in two samples. In this case, the concentration of Fe^{2+} in S_1 was changed stepwise from 0.20, 0.15, 0.10, 0.05, 0.00 and again to 0.20 mmol dm^{-3}; that of Fe^{2+} in S_2 was kept constant at 0.10 mmol dm^{-3}. Aqueous solution of 1,10-phenathroline (pH 4.6) was used as a reagent solution and the analytical wavelength was 510 nm. The amplitudes of the second harmonic wave component (A_{2nd}), corresponding to the Fe^{2+} concentration in S_1, were increased linearly with the concentration of Fe^{2+} in S_1 ($A_{2nd} = 6.115\ C_{Fe^{2+}} + 0.197$, $r^2 = 0.9982$). On the other hand, those for the third harmonic wave component, corresponding to the Fe^{2+} concentration in S_2, were almost constant (0.884 ± 0.008 V).

5. Conclusion

Amplitude modulated multiplexed flow analysis is a new concept of flow analysis. Flow rates of sample solutions to be merged

with each other are amplitude modulated at different frequencies. While we use FFT for demodulation of the composite signal to determine individual concentrations, other methods can potentially be used. The method can fully be automated suitable for real-time analysis. Simultaneous determination of multiple analytes or multiple samples is possible. On the other hand, the method cannot follow rapid change in analyte concentration, because the concentrations of analytes should be unchanged during the length of FFT window. The ultimate limitation here is damping by liquid phase dispersion and mixing that limits the highest frequency that can be used.

Acknowledgements

The present study is supported by the grant-in-aid for Scientific Research (Exploratory Research, No. 19655027) from the Japan Society for the Promotion of Science (JSPS). The senior author (HT) is grateful to Prof. Satoru Goto, Faculty of Pharmaceutical Sciences, International University of Health and Welfare, Tochigi, Japan, for helpful suggestion on frequency analysis.

References

[1] D.A. Skoog, J.J. Leary, Principles of Instrumental Analysis, 4th ed., Saunders College Publishing, 1992, pp. 50–51, 213.
[2] T. Hinoue, J. Kaji, Y. Yokoyama, M. Murata, Anal. Chem. 63 (1991) 2086.
[3] K. Wagatsuma, Surf. Interface Anal. 26 (1998) 254.
[4] K. Wagatsuma, Bunseki Kagaku 52 (2003) 393.
[5] H. Tanaka, P.K. Dasgupta, J. Huang, Anal. Chem. 72 (2000) 4713.
[6] P.K. Dasgupta, H. Tanaka, K.D. Jo, Anal. Chim. Acta 435 (2001) 289.
[7] H. Tanaka, T. Baba, Talanta 67 (2005) 848.
[8] H. Tanaka, T. Baba, Anal. Sci. 21 (2005) 615.
[9] P.K. Dasgupta, K.D. Jo, Electroanalysis 14 (2002) 1383.
[10] K.D. Jo, P.K. Dasgupta, Talanta 60 (2003) 131.
[11] I.-Y. Eom, P.K. Dasgupta, Talanta 69 (2006) 906.
[12] S. Nakamura, Beginner's Digital Fourier Transform, Tokyo Denki University Press, 1989, pp. 147–152.
[13] Y. Ebara, User's Digital Signal Processing, Tokyo Denki University Press, 1991, pp. 86–87.

Talanta 77 (2008) 606–623

Contents lists available at ScienceDirect

Talanta

journal homepage: www.elsevier.com/locate/talanta

Review

Trends in DNA biosensors

F.R.R. Teles, L.P. Fonseca*

IBB-Instituto de Biotecnologia e Bioengenharia, Centro de Engenharia Biológica e Química, Instituto Superior Técnico, Av. Rovisco Pais, 1049-001 Lisboa, Portugal

ARTICLE INFO

Article history:
Received 31 December 2007
Received in revised form 4 July 2008
Accepted 11 July 2008
Available online 23 July 2008

Keywords:
DNA biosensor review
DNA chip
Lab-on-a-chip
Molecular diagnosis
Nanobiotechnology

ABSTRACT

Biosensors have witnessed an escalating interest nowadays, both in the research and commercial fields. Deoxyribonucleic acid (DNA) biosensors (genosensors) have been exploited for their inherent physicochemical stability and suitability to discriminate different organism strains. The main principle of detection among genosensors relies on specific DNA hybridization, directly on the surface of a physical transducer. This review covers the main DNA immobilization techniques reported so far, new micro- and nanotechnological platforms for biosensing and the transduction mechanisms in genosensors. Clinical applications, in particular, demand large-scale and decentralized DNA testing. New schemes for DNA diagnosis include DNA chips and microfluidics, which couples DNA detection with sample pretreatment under in vivo-like hybridization conditions. Higher sensitivity and specificity may arise from nanoengineered structures, like carbon nanotubes (CNTs) and DNA/protein conjugates. A new platform for universal DNA biosensing is also presented, and its implications for the future of molecular diagnosis are argued.

Contents

* Corresponding author. Tel.: +351 218419139 65; fax: +351 218419062.
E-mail address: luis.fonseca@ist.utl.pt (L.P. Fonseca).

0039-9140/$ – see front matter © 2008 Elsevier B.V. All rights reserved.
doi:10.1016/j.talanta.2008.07.024

1. Introduction

The enormous amount of genetic information brought by extensive genome sequencing has raised the need for simple, fast, cheap and high-throughput miniaturized and mass-producible analytical devices to attend the growing market of molecular diagnostics, thus accomplishing the basic criteria for decentralized DNA testing. Genome sequencing has allowed detecting, respectively, inherited disease-causing point mutations and human pathogens through their peculiar, specific nucleic acid sequences. Drug screening, monitoring of differential gene expression and forensic analysis have also benefited from the ongoing research in biosensor technology. Such analytical devices, known as biosensors, convert a biochemical reaction or interaction into an analytical signal that can be further amplified, processed and recorded. Among them, DNA biosensors consist of an immobilized DNA strand to detect the complimentary sequence by DNA–DNA hybridization. In a wider conception, DNA biosensors may still be conceived to detect other analytes, with the probe molecule usually in the form of an aptamer [1], but the study of these sensors is beyond the scope of this review. For their importance, large variety and widespread applications compared to other types of DNA biosensors, those based, for instance, on distinctive interactions of small analytes with single-stranded DNA (ssDNA) and double-stranded DNA (dsDNA) and in polymerase chain reaction (PCR) amplicon detection without hybridization are the subject of hybridization-based DNA biosensors justifies, by itself, a new and comprehensive overview, something that this paper intends to be. Compared to enzyme biosensors and immunosensors, there is still a scarcity of DNA biosensors available in the market and/or under research and development. Unlike enzymes or antibodies, DNA forms biological recognition layers easily synthesizable, highly stable and reusable after simple thermal melting of the DNA duplex [2]. In general, the underlying mechanism of quantitative DNA detection through DNA biosensors is the highly specific hybridization between two complimentary DNA chains which, unlike in conventional solid-state hybridization formats, occurs directly on the surface of a physical transducer. Conventional DNA microarrays also make use of sequence-specific DNA detection, but their efficiency is usually hampered by the typically large size of biological samples and by their complex treatment, which also makes it difficult to obtain real-time outputs. Moreover, their technology is still too expensive to turn them valuable in point-of-care diagnosis. In theory, DNA biosensors are able to surpass these handicaps, allowing easier, faster and cheaper results than in traditional hybridizing assays, while keeping high sensitivity and specificity of detection. A truly high performance biosensor with an immobilized DNA-probe should be able to discriminate as few as a single base-pair mismatch between different target DNA-strains. DNA multiplexed analysis of complex biological samples and related gene expression patterns have been performed with microarrays of multiple DNA biosensors, integrated with bioinformatics-processed data. In general, they are produced in the form of DNA biochips, inspired by the unending advances in planar silicon-based circuitry. The very high density of individual hybridization spots is a major highlight in microchip-based genetic analysis. However, this technology is highly costly and, unlike individual biosensors, biochip surfaces must be scanned for acquisition of full information about the genomic hybridization profile [3]. The newly developed concept of 'lab-on-a-chip' (or micro total analytical system, μTAS) integrates, in a single chip, modules for DNA extraction, purification, amplification and detection. Some advantages of these printable miniaturized devices for analyte detection include smaller sample and reagent requirements, lower cost and lower tendency for sample contamination than other detection schemes. Enhanced rapidity, high performance and high automation ability are also additional advantages. Disposability is also an advantage, especially when dealing with infectious agents. Innovative efforts have been assayed towards the development of electrical-driven microfluidic flow formats as advantageous alternatives to mechanical pumps and valves. The paper also covers some recent developments in nanotechnology, namely CNTs and DNA/protein conjugates, which are responsible for improved sensitivity and selectivity in DNA detection. Despite not being a hybridization-based platform for DNA detection – the ultimate subject of this paper – important applications of the mass-spectroscopy (MS)-based T5000 Universal Biosensor, from Ibis Biosciences, is also mentioned. This pioneering system, by using sets of broad-range primers, is able to amplify PCR products from a large number of closely related organisms without prior knowledge of their specific genomic sequences. By accurately determining the nucleotide composition (the amount of each nucleotide) of the unknown sequence through mass spectroscopy (MS), the identification of PCR products may be carried out almost instantaneously. The following text gives an overview of the DNA biosensors research and background, as well as current trends for the forthcoming future.

2. Fundamentals of hybridization DNA biosensors

Conventional methods for specific genomic sequence analysis include nucleic acid sequencing and hybridization, the later more routinely used in clinical laboratories due to its higher simplicity [4]. DNA hybridization usually occurs between a known DNA sequence (probe) and an unknown counterpart (target), but DNA–ribonucleic acid (RNA) and RNA–RNA hybridizations can also occur [5]. The duplex formation can be detected following the association of an appropriate hybridization indicator or through other changes accrued from the binding event. DNA probes may be produced by chemical methods or by molecular biology; in this case, a probe may be obtained by reverse-transcription (RT) of a previously isolated and specific messenger RNA (mRNA), or inferring its nucleotide sequence based on the amino acid sequence of the protein expressed by that DNA, despite the validity of this last strategy may be limited due to the genetic code degeneracy [6]. Conventional nucleic acid hybridization methods, like gel electrophoresis and Southern blotting, are usually lengthy and labor-intensive [7], and is also the intrinsic biomolecular recognizing event of most genosensors. However, in this case, it occurs directly on the surface of a physical-transducer [8]. In this way, the immobilized DNA-chain is a part of the biosensor itself. Both in vivo as onto a transducer surface (solid support), nucleic acid hybridization is stronger and more specific when the complimentarity degree between two DNA chains increases. The specificity and stability of the linkage reach a maximum in the case of full (100%) complimentarity. However, the molecular mechanisms of hybridization over solid supports are still greatly unknown and unpredictable, owing to the difficulty of accurately determine the concentration of the immobilized nucleic acid. Even so, it is commonly assumed that the relevant events in the solid/liquid interface are the analyte diffusion towards the surface of the sensor, bidimensional diffusion, adsorption and desorption [9]. Despite the similarity between the hybridization processes in solution and at an interface, the hybridization rate is typically dozens of times higher in the former case, assuming identical DNA sequences and conditions. This may be due to the partial unavailability of many linking groups in the immobilized chain, eventually involved in that immobilization process. The hybridization rate also decreases with the secondary structure level of one or both chains. This fact can be easily avoided with a proper selection of the probe-sequence. Moreover, the

hybridization mechanism between DNA chains with long-sized secondary structures is far more complex than that described by the traditional two-state model [10]. As in solution, the interfacial hybridization efficiency must be optimized in relation to environmental conditions (e.g.; ionic strength and temperature) and requires minimization of non-specific adsorption [11,12]. Among the most important factors affecting the hybridization efficiency is the surface coverage (Γ) of the transducing surface; above a certain density of attached DNA-probe molecules, steric effects between them become dominant, as well as repulsions between the incoming targets [13]. An ideal surface around 5×10^{12} molecules/cm^2 was estimated [14]. Repulsion of the target also depends on the ionic strength of the buffer solution and, in accordance, it was determined that, with 1 M phosphate buffer with a surface coverage up to 3×10^{12} molecules cm^{-2}, no significant electrostatic interference or steric effects between chains occur [15]. Unlike enzymes and antibodies, nucleic acids from biological recognition layers easily synthesizable in the laboratory, highly stable and readily reusable after thermal heating. Short, synthetic oligonucleotides are often preferred as sensing elements in view of the absence of complex conformational changes which decrease the hybridization speed, efficiency and selectivity. The diagnosis of infectious diseases with DNA biosensors permits to distinguish different strains of a pathogen by suitable choice of strain-specific DNA probes and to obtain an earlier diagnosis compared to immunosensors [6]. Despite the ultimate goal of autonomously determining DNA traces in clinical samples, it is still required, in general, previous PCR amplification until reaching detectable DNA levels [5]. It is convenient that hybridization does not require separation of unbound labeled probed from the matching probe–target complexes and, to achieve high detection sensitivity, amplification of the probe–target complex by PCR is usually required. Despite its ability to render, in principle, unlimited sensitivity and amplification, PCR settings are usually too complex, prone to easy contamination and require skilled manpower and bulky equipment for in-the-field applications [16]. PCR has been recently integrated in μTAS systems, a concept corresponding to the integration, in a single miniaturized device, of modules for DNA extraction, purification, amplification and detection, thus lowering contamination, reagent consumption and the time of detection. Additionally, the hybridization event occurs in a liquid instead of a solid phase, a similar condition to the in vivo microenvironment. Ongoing efforts with DNA chips, however, persecute the task of producing PCR-free DNA detection systems, despite this has not been fully achieved yet in commercially available devices [1]. The detection of the DNA duplex formation often makes use of a hybridization indicator (marker), but other changes in the system may be monitored [3]. Experimental findings showed that the interaction of cations with DNA is not affected by DNA immobilization onto a solid support [17]. In addition, the marker must not hinder significantly the formation of hydrogen bonds between the probe and the target, as well as the melting temperature (T_m) of the duplex [6]. In view of the biological hazard of the former radioactive markers, new kinds of DNA labeling have emerged. DNA immobilization is undoubtedly the key-step in genosensor development; the traditional lack of affinity and stability of DNA chains in solid surfaces has greatly benefited from recent advances in biocompatible polymer matrices production.

3. DNA-probe immobilization techniques

The use of polymeric supports in genosensors aims to overcome some traditional limitations of DNA detection in gold and glass surfaces, namely the low surface density of silanic groups – which hinders a high surface concentration of the immobilized oligonucleotide – and the high cost. Other goals include the maximization of sensitivity, surface functionality, DNA bonding density, DNA-layer stability and accessibility of interacting molecules, as well as minimization of non-specific linkages [18]. Hydrophilic surfaces are particularly amenable for nucleic acid hybridization because they facilitate exposure of hybridizing bases [19], despite being also proner to DNA detachment with increasing ionic strength [20]. Nonetheless, studies carried out with immobilized negatively charged human albumin in anionic latex showed that it is possible to link the two surfaces through a positive-potential barrier formed by the cations of the saline electrolyte [21]. However, the high hydrophobicity of silanic films and the surface tension of oligonucleotide solutions allow confining them in very small spots, thus preventing eventual mixing and cross-contamination in a microarray configuration [22]. Recently, conductive polymers have been used in biosensors for their unique advantageous electronic properties, including high electronic affinity. In general, the electrochemical response (current) with conductive cationic polymers decreases after DNA hybridization, presumably due to hindrance of the anionic exchange or to polymer reorganization [23]. On the other hand, the successful immobilization of DNA onto anionic polymers with cation exchanger-functional groups (e.g., quinine) may be attributed to the formation of a positive shield of solution cations around the DNA probe [24]. Nevertheless, the introduction of amino groups is still the main strategy to functionalize solid surfaces with biomolecules, like the covalent immobilization of oligonucleotides in bare silicon and onto polyethylenimine-coated nylon microspheres [25,26]. Several polymers may also be used simultaneously, like a polymeric gel of polyvinyl-alcohol crosslinked to polyallylamin chloride and poly(L-lysine) in polystyrene-modified surfaces [18,27]. Despite DNA attachment to solid surfaces is usually stronger via covalent linkages, adsorption may be preferred due to its slighter effect over DNA structure, which avoids its breakdown [28]. Chitosan, for example, is a natural cationic polymer which tightly binds the polyanionic DNA chains (both native and denatured), yielding a very stable immobilization [29]. However, maximization of detection sensitivity is usually achieved through one-point covalent immobilization of DNA which, by minimizing sterical hindrance, greatly favors formation of the DNA duplex. Previous works describe the use of polypyrrol in DNA biosensor build-up, by immobilization of the polymer itself or electropolymerization of the monomers directly on the surface of a transducer [30,31]. This technique exhibited high versatility since the sensor was able for reusing after simple rinsing, without altering the polymeric matrix of the immobilized polypyrrol. Bidan and coworkers used an electrocopolymerization process to immobilize an oligonucleotide [32]. A mixture of pyrrol and pyrrol covalently attached DNA was electrooxidized, resulting in irreversible immobilization of the oligonucleotides in a polypyrrolic copolymer onto an array of gold microelectrodes. The technique of self-assembled monolayers (SAMs), formed by a brief immersion of the transducer surface into a dilute solution of the polymer at room temperature, spontaneously generates an ultrathin and highly ordered layer, similar to the cell microenvironment. This monolayer strongly adsorbs to the solid surface and is thermodynamically very stable. The versatility of SAMs for several applications arises from the possibility of controlling the hydrophilicity degree and the chain length of the polymer [33]. The utilization of SAMs avoids conformational changes over the immobilized biocomponent, capable of affecting its activity. This assures higher homogeneity and reproducibility of the electrode surface. Furthermore, the molecular scale of the biolayer allows rapid diffusion of the electroactive species towards the electrode surface, in comparison with the slower kinetics observed with thin polymeric films or composites. SAMs also reduce drastically

non-Faradaic currents and electrode passivation [34]. SAMs of gold-attached aminoalcanothiols are undoubtedly the most studied and employed, taking advantage of the very high affinity in S–Au bonds. Bifunctional aminoalcanothiols allow straightforward one-point covalent immobilization of DNA through its 5′-phosphate end [35]. Nonetheless, the applicability of monolayers remains restricted owing to their poor stability and difficult synthesis.

4. New biosensor platforms

One of the major trendlines towards the research of novel diagnostic systems is the concept of DNA chips (or DNA microarrays), usually associated to microfabrication of diagnostic kits by screen-printing techniques, inspired by planar, silicon-based technologies. This aims to produce very high dense microband sensor arrays coated with different probes for simultaneous detection of multiple DNA-target sequences (with or without a label) printed on the chip by conventional photolithography [4]. DNA microarrays (DNA chips) for multiple and simultaneous target detection have been extensively used for studying genomic structure and gene expression. Despite microarrays should not be considered true biosensors – in the sense of simple, cheap and portable devices – they achieve high efficiency of analytical processing and use microfabrication techniques for highly selective immobilization of their recognition elements [36]. The ongoing progress from microarrays to biosensors will certainly be mediated by the production of disposable microchips, thus obviating the typical limitations of current microarrays. These include the difficulty of scaling-down the array and nucleotide densities, the limited resolution and the different optimal hybridization conditions between A–T and C–G linkages, which hinders the use of a single set of optimized parameters in the same chip and therefore a reliable DNA quantitative analysis, and strong sample concentration-dependence [37]. Despite the ability of DNA biochips to detect many genes in a single assay, detection at the cellular level without previous genomic sequence amplifications remains limited [38]. Bearing this task in mind, it is noteworthy the growing interest on the last few years for microfluidic analysis schemes and devices [39], essentially an adaptation of DNA chips to contain channels and chambers for flowing liquids. They integrate, in a single chip, modules for DNA extraction, purification, amplification and detection. Electroosmotic pumping is the most common technique to propagate the flow in these systems. Such flow is generated by the surface charge on the microchannel walls combined with an electric field along the microchannel. In these devices, chemical interferences arising from spatial confinement of the biorecognition and transduction elements may be avoided, thus allowing miniaturization with efficient signal transfer and highly sensitive detection. The high mass transfer rate thus achieved results from the low diffusional distance and high surface/volume ratio [40]. Gulliksen et al. detected herpes virus (HPV)-related synthetic sequences in a pioneer work with real-time nucleic acid sequence-based amplification (NASBA) for direct amplification of RNA, reaching a detection limit of 10^{-6} μM, similar to that of standard diagnostic procedures [41]. Conventional microarrays usually require relatively high volumes of reagent and solution. The diffusional rate of the reacting biomolecules is usually small, rendering long hybridization times. Wei et al., by integrating the concepts of μTAS and microarrays, was able to diminish the sample and reagent volumes to 1 μl, and the hybridization time for less than 10 min, reaching a detection limit of 19 attomole [42]. Electrokinetically driven separation schemes have been widely used to separate and detect desired analytes. They are based on the interaction of induced dipole in the bioparticles and electric fields, and are used for moving fluids through a channel network [43]. The method was implemented to detect single-nucleotide polymorphisms (SNPs) in a μTAS platform, with tight temperature control on the microarray interface, thus avoiding the need for common external temperature sensors [44]. Partial hybridization between non-complimentary chains may thus be avoided, thus enhancing the selectivity of the detection. An emergent topic in the development of new bioanalytical procedures, structures and systems is nanobiotechnology. A brand new range of electronic devices and biosensor platforms has emerged as a consequence of the inherent small size and unusual optical, magnetic, catalytic and mechanical properties of nanoparticles, unlike those of bulk materials. Moreover, with an appropriate transducing method, the selectivity of nanobiosensors may be tuned as a result of signal-dependence on nanoparticle morphology [45]. It is foreseeable, by technological and industrial reasons, the fabrication of future nanochips and nanofluidic systems as an extension of current mechanical methods for production of microsensing devices most often based on organic polymers and gels, especially PDMS frames, but the recent outburst of nanotechnology is creating a demand for a broader range of low-cost and easy fabrication methods. This may correspond essentially to shifting from top-down methods – which begin with a patterned, larger-scale layout, and reducing its dimensions to bottom-up methods, by building-up nanostructures from atoms or molecules. Such bottom-up methods are proner to cheap and easy production of small nanostructures. The sudden rise in the expected cost/benefit of miniaturizing photolitographically produced microsystems has pointed towards the assembly of micromechanical systems and functional biomimetic structures in the 5–100 nm range [46].

5. Transduction mechanisms in genosensors

5.1. Optical

5.1.1. Optical fibers

Many DNA optical biosensors use an optical fiber to propagate the signal emitted by a fluorescent label. In general, a DNA single-chain probe is placed in the end of the fiber and, after hybridization with the complimentary chain, changes in the fluorescence intensity resultant from the selective association between the DNA duplex and the label are measured. Piunno et al. used ethidium bromide as a hybridization indicator [47]. It strongly intercalates between base pairs and stacks into the major-grooves of a double-chain DNA. The hybridization event was detected by fluorescence, by measuring the total internal reflexion in the optical fiber, which is proportional to the total amount of intercalated ethidium bromide. Despite being regenerated even after prolonged storage and aggressive washings, the sensitivity was not very high compared to those of PCR and conventional nucleic acid hybridization. Another handicap is the biohazard concern of working with such a carcinogenic compound, which has triggered the search for substitutes [5]. Fergusson et al. developed a fiber-optical array biosensor for simultaneous detection of multiple oligonucleotide sequences, registering the fluorescence increase after hybridization [48]. An optical microarray-based biosensor with zeptomolar detection was developed by individually attaching the tips of a fiber-optic bundle to microspheres coated with different DNA probes, which were further identified by combinations of different fluorescent labels [49]. Biosensors based on optical fibers are suitable for miniaturization, due to the very small diameter of the fibers. By transmitting light for very long distances without signal lost, they allow remote detection of inaccessible or dangerous samples. The optical nature of the signal also avoids interference from electrical noises and, for being harmless, is appropriated for in vivo applications. These biosensors

have usually poor stability and are prone to interference from environmental light, apart the high cost of quartz optical fibers for UV light transmission.

5.1.2. SPR and evanescent waves

Until a few decades ago, the wide spreading of optical fibers motivated the consideration of photonic devices as natural substitutes for microelectronic circuits and chips, but their size and performance are constrained by the diffraction limit, resulting from interference between closely spaced light waves. However, optical transmission through minuscule structures gained a new impulse with the advent of the surface plasmon resonance (SPR) technique, by directing light waves to the interface between a metal and a dielectric. A real-time SPR system under continuous flow was applied to DNA detection, through an immobilized biotinylated probe in an avidin-coated chip, and further binding of the target-DNA [50]. Systems like these render high specificity, within 10 min, at room temperature [6]. SPR was also the basis for optimization of a DNA biosensor, in real-time, onto a gold surface previously functionalized with polypyrrol, aiming the future fabrication of DNA chips [51]. In this work, several hybridization events were detected simultaneously by an electrospotting technique, dispensing the use of thiolated reagents and several immobilization steps. Recently, Buhl and coworkers formulated a SPR biosensor chip to detect pathogenic dsDNA auto-antibodies produced by patients with systemic lupus erythematosus [52]. In accordance, an antigenic construct was formed by coupling a synthetic oligonucleotide with biotinylated human transferrin and hybridizing with the complimentary strand. The set was then linked to a human recombinant double-strand fragment and covalently immobilized in a flow-through cell; healthy and diseased sera were then compared. This format assured maximal stability for multiple serum injections and regeneration cycles, a benefic feature for clinical diagnosis and monitoring. Another well-known type of optical biosensor is the resonant mirror, an evanescent wave sensor that combines the simplicity of SPR devices with the enhanced sensitivity of wave-guiding devices [5]. These biosensors measure variations in the surface optical parameters caused by the biochemical reaction (e.g. DNA hybridization), namely the interfacial refractive index. They have found notable applications in detecting human genetic mutations and nanomolar levels of PCR products from genetically modified organisms [53,54]. The great interest of evanescent waves for biosensor applications emerges from unnecessary target-chain labeling, rapidity of the hybridization reaction (within a few minutes) and 100-fold or greater probe reutilization. A significant drawback is the somewhat low sensitivity, requiring up to 10 μg of DNA per milliliter [8].

5.1.3. Gold nanoparticles

Colorimetric biosensors have been traditionally used for DNA detection as an alternative to fluorescence tagging. Colorimetric systems are attractive for detection because they are harmless, simple and relatively inexpensive. As an example, it was proposed as a method for visual, qualitative and simultaneous detection of HIV, hepatitis C virus (HCV) and reverse-transcribed hepatitis B virus (HBV) genomes in infected blood samples with a DNA chip [55]. It was employed, in this work, a multiplex PCR for concomitant amplification and detection of all nucleic acid sequences present [56]. Detection was accomplished by color formation from an avidin-bound alkaline phosphatase reaction with a signal amplifier, and a detection limit of 1 pg of viral DNA fragments was achieved. An alternative to DNA labeling for optical detection may be performed by using functionalized gold nanoparticles (GNPs), having comparatively higher stability and lower background noise than fluorescence tagging [57]. Colorimetric biosensors were recently

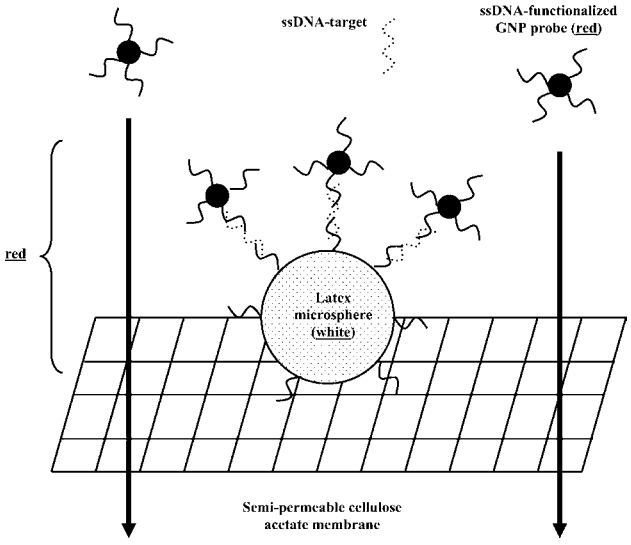

Fig. 1. Layout for DNA colorimetric detection with GNPs and latex microspheres. Free, red-colored ssDNA-functionalized GNPs freely move across the semi-permeable cellulose acetate membrane. White-colored latex microparticles, on the other hand, are too large to pass through that barrier. In the presence of an ssDNA-target, GNPs bind latex particles, generating large-size, red-colored conjugates, which become retained by the membrane.

built in conjunction with DNA/nanoparticle conjugates. An interesting scheme for drastic reduction of the background signal was developed [58] by coupling GNPs to latex microparticles. Both types of particles are linked to ssDNA-probes, which are complimentary of a given DNA-target strand. Typically, the red color of dispersed GNPs turns into blue when aggregated polymeric networks are formed upon extensive hybridization. This color variation can be measured by spectrophotometry or at naked eye, onto a solid silica-gel support. However, red and blue are not easily distinguishable at naked eye and the blue color is considerably less intense than the red of dispersed GNP probes. The use of white latex microspheres obviates such handicaps. Background signal from unbound GNP is significantly reduced by filtering the solution with the target and the probes through a size-selective cellulose acetate membrane. The unbound GNP probes pass through the membrane, while the larger latex particles are trapped (Fig. 1). An advantage of this system is that a large excess of GNP probes can be employed without interfering with signal interpretation. The method is rapid, sensitive, simple inexpensive and suitable for the utilization of other types of microspheres and nanoparticles. Metal nanoparticles, in general, are suitable for construction of high-density miniaturized DNA microarrays, taking advantage of their high signal-to-noise ratio. They are easily synthesizable and functionalized (by simple mixing at room temperature) and have a controlled, self-assembled surface structure [59]. Most GNP-based detection systems rely on the formation of aggregates of extended interconnected tridimensional networks by DNA hybridization. Most commonly, two sets of GNPs are used; each one binds a different DNA probe, and each probe binds one end of the target chain. Since each particle has multiple DNA-bound tentacles, the specificity of the target-sequence glues many particles together. Blueshifting of the emission spectrum thus occurs, and the resulting color change may then be observed at naked eye. In nanoparticle-based SPR systems, the complicated chemistry for the Au-SAM synthesis may produce structural defects in the DNA chips during mass-production, thus compromising the reproducibility and reliability of the detection. To overcome this setback, SPR was coupled to interferometry to detect picomolar amounts of synthetic and PCR-amplified DNA

sequences in a gold-deposited porous anodic alumina layer chip [60]. Gold deposition onto the chip formed a highly ordered cap-like layer on the top of the oxide nanostructures. The relative reflected intensity at the surface of the chip was strongly dependent on the effective thickness of the biomolecular layer. This format permits rapid detection of DNA in small volumes with disposable chips, which makes it amenable for miniaturization and mass-production. An interesting work [61] used a SPR imaging technique for monitoring selective deposition of GNPs modified with ssDNA and dsDNA, at high salt concentrations, in microchannel walls of a microchip formed by a surface-patterned polydimethylsiloxane (PDMS) plate bound to a gold thin film-deposited glass substrate. The detection limit thus achieved was 19 fmol and, in the form of a SPR portable device, is a promising tool for point-of-care analysis of SNPs. By avoiding the use of complex and expensive instrumentation, DNA/nanoparticle-based colorimetric biosensors seem quite promising for point-of-care diagnosis.

5.1.4. Quantum dots

One of the most important nanostructures generated by bottom-up approaches is the quantum dot, a type of nanoparticles for fluorescence tagging of probe biomolecules. They differ from conventional organic fluorophores for being much brighter (for having higher quantum yields) and photostable. In addition, their color can be directly correlated with their size, with emission of a single, well-defined wavelength after excitation (a higher size corresponding to a higher emitted wavelength); they have broad absorption spectra and narrow emission spectra with large emission shifts, which permits excitation at wavelengths far-removed from their emission peaks [62]. The fact of nearly all quantum dots of different emission peaks can be excited using a single, short-wavelength excitation source, is a powerful tool for monitoring several components in complex biological systems [63]. These properties make dots of different sizes able to be used as distinguishable labels for different targets [64]. An application of quantum dot-based DNA analysis is a surface plasmon-enhanced fluorescence microscopy detection scheme in a microarray format [65]. The resonant excitation of evanescent surface plasmons mode excites the dots chemically attached to the target molecules, giving rise to increased sensitivity for analyte monitoring. As a consequence of exciting several dot populations with a single light source, a single incidence angle for resonance surface plasmon is necessary. It has been demonstrated that quantum dots can undergo fluorescence resonance energy transfer (FRET) phenomena, basically a cascade energy transfer process from species with larger bandgaps to species with smaller ones [66]. This principle was used to build a biosensor with two target-specific probes-a fluorophore-tagged reporter and a biotinylated capture probes – and a quantum dot labeled with streptavidin molecules [67]. In the presence of DNA-target, an assembly is formed between all these structures. The result is fluorescence emission from the acceptor fluorophores by means of illumination of the quantum dot donor, thus indicating the presence of target. In this configuration, quantum dots thus serve as FRET energy donors as well as target concentrators. As the unhybridized probes do not participate in FRET and do not fluoresce, their removal is unnecessary. The detection limit of this system is 100-fold higher than that of a similar conventional FRET probe-based assay with confocal fluorescence spectroscopy, and therefore does not require target pre-amplification. Recently, Feng and colleagues reported the use of quantum dots as biomarkers to functionalize nanotubes for enhanced sensitivity of DNA detection [68]. The incorporation of the quantum dots in the nanotubes was carried out by the well-known layer-by-layer deposition approach. The key feature of this scheme is an efficient energy-transfer process that occurs from the larger bandgap quantum dots in the outer side of the nanotubes to the smaller bandgap quantum dots in the inner side, as an intrinsic energy ramp through the nanotube walls exists. The resulting sensitivity enhancement suggests a potential utility for detection of trace amounts of DNA [69].

5.1.5. Other systems

Electrochemiluminescence involves light generation near an electrode through species that undergo highly energetic electron-transfer reactions with solution reagents. It has a wide linear range of chemiluminescence and does not require the use of complex and expensive light sources and fluorescent dyes. Lee et al. [70] used the intercalator ruthenium bipyridine ($Ru(bpy)_3^{2+}$) and suitable detection of hybridization by electrochemiluminescence, with Ru complexes exhibiting excellent chemical stability and a relatively prolonged excited state. An interesting scheme to improve the detection of the hybridization signal is the utilization of DNA beacons as DNA probes [71]. A DNA beacon is a single-stranded oligonucleotide labeled with a fluorophore in one extremity and a quencher in the other; the close proximity between them, due to the stem-and-loop (hairpin) format, prevents emission of fluorescence. When the molecule becomes linearized as a consequence of hybridization with the complimentary chain, the system becomes fluorescent. It is possible, with this system, to achieve high specificity and single-base resolution in the picomolar range [72]. The major handicap of this technique, aiming the fabrication of DNA sensors and microarrays for real-time and simultaneous analysis of different targets, is the high cost and tedious preparation of hundreds of different probes, each one modified with the fluorophore and the quencher. Instead of the common methods that use an oligonucleotide probe with a covalently linked fluorophore, a new strategy employs a fluorescently labeled universal reporter strand, which binds a reporter-binding region in the hairpin [73]. This region has a base sequence common in all sequence-specific probes. By using a single sequence of fluorescently labeled universal reporter strand for all targets, a cheaper and simpler procedure is achieved. This scheme was also the basis for signal amplification with liposomes for detection and serotype-discrimination of dengue virus after amplification of the viral genome by NASBA [74]. This sandwich-system integrates a liposome-coupled reporter-probe (complimentary to a generic sequence added to RNA during the amplification step) and a membrane-immobilized biotinylated capture-probe. The number of DNA-tagged liposomes is proportional to the amount of RNA in the sample, being detected by electrochemiluminescence with a portable reflectometer within 15 min. A slight variation of this layout was the immobilization of a magnetic sphere-attached capture probe onto a permanent magnet in a detection region, built in a microfluidic format [75]. Liposomes were filled with a dye marker, thus yielding high signal amplification and sensitivity by fluorescence microscopy. Based upon the two layouts described above, a biosensor was built by integrating immobilization onto a polyethersulfone membrane with a dG-enriched universal reporter-probe and optical detection with a dye-filled liposome attached to a deoxycitosine (dC)-enriched universal probe [36]. The reporter and capture probes may be easily and quickly changed to become specific to the target-sequence. After optimization of this biosensor, previously amplified bacterial sequences were readily identified and quantified in less than 30 min. The same detection scheme was applied to the specific identification of the four dengue virus serotypes in a single, multianalyte assay, instead of four independent assays [76]. One of the most revolutionary achievements among DNA/protein conjugates is the one of single-molecule detectors; they mimetize the cellular protein machinery which reads and copies one single nucleic acid molecule at the time, with single-base resolution [8]. A common optical approach for single-molecule detectors utilizes

a SiO_2 surface-attached DNA polymerase, with real-time monitoring of the incorporation of fluorophore-labeled nucleotides into a growing DNA chain, by using a different fluorophore for each nucleotide [77]. A 'lab-on-a-chip' microsystem integrated with photolithographically patterned polymeric layers and interferometric detection was applied for real-time and label-free detection of DNA hybridization [78]. An ultrasensitive system was conceived to quantify nucleic acid traces using confocal fluorescence spectroscopy and a microfluidic reactor for molecular confinement of an ultrasmall volume of 1 fl [38]. By detecting single-molecule fluorescence, a further step for removing unbound probe molecules is avoided, with clear reduction of the overall hybridization assay cost; the detection limit was 14 zmol. Recently, a microfluidic sensor array for specific detection of ribosomal RNA-targets of several bacterial pathogens in human fluids was produced [79]. After RNA extraction, its detection was performed by immunofluorescence with labeled antibody-conjugated horseradish peroxidase (HRP); a detection limit of 2600 cultured bacterial cells was achieved within 45 min. It achieved 100% sensitivity for Gram-negative bacterial detection without previous RNA purification or amplification.

5.1.6. Commercial optical biosensors

It is noteworthy the commercial success of several optical sensing platforms in the last few years. It is unquestionable the advantage that the very high frequency of optical signals – compared, for instance, with electrical ones – may bring in terms of the enormous amount of information that can be carried by optical devices. Some well-succeeded commercial platforms include, for example, the GeneChip® high-density (high spatial resolution of individual probes) microarray from Affymetrix (Santa Clara, CA, USA), with fluorescence-based detection coupled to a confocal readout, which became the industry standard for molecular biology research. This microarray probably encloses the highest information capacity among similar chips, enabling a whole-genome approach in research studies. The GeneChip® can sequence some many thousand bases in a few days with almost very high accuracy, a clear advantage for pathogen subtyping. In addition, Affymetrix has largely benefited from its world leadership position as the first microarray ever commercialized and from resulting economical patent benefits. Moreover, this technology has exhibited improved performance and capabilities over other existing methods. Perhaps the most serious competitor for the GeneChip® is the fluorescence-detecting microbead-based BeadXpress® array system from Illumina (San Diego, CA, USA), also an industry-leading in genotyping. The high sensitivity of the BeadXpress® (owing to inherent stringency of code detection), wide multiplexing capability, assay versatility in a single platform (including a broad range of applications, e.g. nucleic acid and protein-based assays) and dual-color detection (through the industry-standard Infinium Whole-Genome Genotyping Assay) are claimed highlights [80]. BIAcore (real-time biospecific interaction analysis) SPR-based platforms have been also at the forefront of the commercial biosensor market; so far, they have been responsible for 90% of all published optical biosensor work. The BIAcore system of Pharmacia Biosensor AB (Uppsala, Sweden), is especially suitable for real-time monitoring of biological events under continuous flow [6]. A carboxymethyl dextran matrix-coated surface has been widely employed in these systems as a convenient way for applying numerous surface immobilization chemistries, for immobilized ligand stabilization and for reducing non-specific binding. It is envisaged that many of these systems may be applied to several biochemical assays, including DNA- and protein-arrays, and eventually replace the well-known enzyme immuno-assay (EIA). It seems clear that implementing sensor arrays with multiple-sample delivery, while being simple in concept, will require improved technological development fueled by strong commercial demands [81].

5.2. Piezoelectric (mass-sensitive)

A DNA sequence with a few hundred base pairs usually possesses a sufficiently high molecular weight so that the mass increase caused by hybridization of a DNA-chain with its complimentary counterpart previously immobilized on the surface of a piezoelectric quartz crystal may be specifically correlated with an increase in the fundamental resonance frequency of the crystal. This is the principle of the well-known quartz crystal microbalance (QCM). Campbell et al. used the quartz microbalance principle to detect the hybridization of DNA covalently bound to a polymer-modified piezoelectric crystal, thus achieving a near 100 Hz frequency increase compared to a control crystal to which a non-complimentary target was hybridized [82]. Similar results were obtained after DNA hybridization onto a polypyrrolic matrix [83]. Some studies reported the improvement of QCM hybridization efficiency and sensitivity by immobilizing biotin-labeled DNA multilayers in modified gold surfaces [84]. Detection of a cancer-causative mutation in the human TP 53 gene was reported with a piezoelectric transducer, by using a dextran–streptavidin surface-immobilized biotinylated probe [85]. The sensor was optimized with synthetic DNA sequences and successfully validated with PCR-amplified DNA samples, being amenable for application in routine analysis. An innovative approach was developed, with piezoelectric transduction, by designing and immobilizing a degenerate probe (chosen among a conserved genomic region) and two specific probes (chosen from less-conserved regions) for, respectively, simultaneous detection and genotyping of 16 strains of the human papilloma virus [86]. This is a straightforward method for detection, with highly specific probes, of microorganisms with high mutation rates. Besides QCM, other methods can be employed for mass detection with a piezoelectric crystal. In surface acoustic wave (SAW) devices, an electrode array in the material generates local deformations that are transmitted ahead as mechanical waves to a receiver electrode array. The interaction of these waves with a surface material changes the SAW speed and amplitude, thus enabling quantification of the deposited mass [87]. The classical SAW principle was recently applied to the fabrication of a DNA sensor in a microfluidic format [88]; the DNA-probe sequence modified with a thiol group was immobilized onto a gold surface and exhibited a sensitivity of 136 pg ml^{-1} Hz^{-1}. A similar effect can also occur in the inner transducing material with bulk acoustic waves (BAWs). Zhang's team built a BAW biosensor for on-line detection of damaged DNA, based on mass decreasing after DNA breakdown induced by UV radiation [89]. Some studies correlated resonance frequency changes with DNA concentration-dependent viscosity [90]. These biosensors can provide single-base resolution [91]. Bioanalytical applications require operation of the mass-sensing device in the liquid phase, a troublesome task owing to the typical sensitivity decrease and complex influence of multiple interfacial parameters, namely the viscosity of the surface and sample solution, the surface energy and roughness, the effect of compressional waves, the ionic strength and the dielectric constant of the electrolyte [92,93]. These effects are especially predominant when resonance frequency shifts are measured, but microcantilever platforms may circumvent this event. In a microcantilever, in addition to resonance frequency alterations, surface stress caused by the forces involved in the DNA adsorption process also occurs, and this parameter is less prone to environmental effects. When the adsorption is limited to a single surface of the cantilever, that surface becomes subjected to bending, an effect that can be amplified by making both surfaces of the cantilever chemically different [94]. A microcantilever

DNA biosensor using the micro-balancing technique was developed by incorporating a piezoelectric film, which acts both as a sensor and an actuator [95]. Unlike cantilever formats using optical detection schemes (e.g., light deflection after cantilever bending), the piezoelectric sensor does not need many external hardware and equipment, and hence is more suitable for the production of integrated analytical devices. Nevertheless, a recent report claims the development of a novel compact optical read-out scheme based on light transmission by single-mode waveguides through the cantilever structure (which also acts as a waveguide) [96]. As the cantilever deflects, less light can couple between the cantilever and the output waveguide, thus decreasing the optical output. Since a bulky external read-out detection system is not used, the production of a portable device can be envisaged. A good sensitivity was obtained, but improvements are expected by making longer and thinner cantilevers. Nanomechanical cantilevers are potentially useful for real-time monitoring, which is the basis for the description and characterization of dynamic interactions at sensor surfaces [97]. By fabricating devices with many nanocantilevers and coating each one with a different type of DNA, rapid screening of biological samples for the presence of specific genetic sequences can be performed without previous labeling. Nanocantilevers are emerging as the basic sensing-structures in array-based microsystems for sub-nanometer resolution of DNA sequences [98].

5.3. Electrochemical

In electrochemical biosensors, a single-chain of DNA is immobilized onto an electrically active surface (electrode), being measured changes in electrical parameters (e.g., current, potential, conductance, impedance and capacitance) caused by the hybridization reaction. The emergence of solid electrodes has improved enormously the applicability of electrochemical methods for nucleic acid analysis, as reviewed below.

5.3.1. Enzyme indirect detection

Enzymatic labels are commonly used to generate electrical signals for detection of DNA hybridization. The enzyme, previously bound to the DNA probe, triggers the catalysis of a redox reaction and further generates an electrochemical change due to the hybridization event. Lumley–Woodyear et al. monitored the duplex formation with a carbon fiber transducer, using a horseradish peroxidase-labeled DNA-target [99]. The resulting electrorreduction of H_2O_2 was followed by amperometry, with single base-pair resolution. An ingenious strategy was developed for detection of single-base DNA mutations by using a biotinylated nucleotide complimentary to a mutated residue in the DNA-target [100]; the subsequent binding of an avidin-bound alkalin phosphatase promotes a chemical reaction that generates a precipitate. By opposition, the non-mutated DNA-target molecule does not bind the enzyme conjugate and, therefore, does not generate the precipitate. In this study, electrochemical impedance spectroscopy (EIS) and QCM were employed for the analysis of the Tay-Sachs genetic disorder, reaching a detection limit of 10^{-14} M with no PCR pre-amplification. Efficient amplification schemes were achieved by labeling peroxidase with liposomes, with impedimetric detection, to detect PCR products with pulse techniques, as well as sequences related with human cytomegalovirus [101,102]. A dot-blot-based amperometric biosensor was produced for detection of a *Staphylococcus aureus* β-lactamase-producer oligonucleotide, using peroxidase and a graphite/epoxy electrode with a nylon membrane [103]. By using two biotinylated probes (in the 5′- and 3′-ends, respectively) instead of only one and previous PCR amplification of the bacterial DNA, a sensitivity of 10^5–10^6 bacteria was obtained, and a decrease in the overall assay time from 4–5 days to 36 h. Labeling enzymes are usually conjugated with a single DNA molecule [104]. However, a work reporting the conjugation of glucose oxidase with several oligonucleotide sequences showed significant signal amplification due to the various hybridization events and therefore an increased sensitivity [105]. Enzyme amplification schemes for DNA sensing are among the most successful for PCR-free detection in real, biological samples.

5.3.2. Label-based (indirect) detection

Electroactive hybridization indicators bind single-chain DNA and double-chain DNA with different affinities, thus resulting in unequal concentrations near the electrode surface and therefore in a variation of the electrochemical response. The ways of interaction with DNA include electrostatic attraction (to the sugar-phosphate backbone), intercalation and groove-binding (within the double-helix). Heterocyclic dyes (e.g., methylene blue and ethidium bromide), ferrocene derivatives and organometallic complexes are among the most widely used redox indicators. Pioneering studies to detect deoxyguanosine (dG)-elongated polynucleotides by cyclic voltammetry (CV), using the metallointercalators $Co(bpy)_3^{3+}$ (bpy = bipyridin) and $Co(phen)_3^{3+}$ (phen = phenanthroline), immobilized DNA onto a glassy carbon electrode (GCE) through covalent attachment with *N*-hydroxysuccinimide and a carbodiimide, and an octadecylamine/stearic acid-modified carbon paste electrode (CPE) for cystic fibrosis [106,107]. Electrochemical adsorption after positive polarization (pretreatment) of carbon paste and screen-printed electrodes was accomplished in order to increase their affinity for human immunodeficiency virus (HIV) and HBV-related DNA sequences [108,109]. Detection was performed by chronopotentiometry, using $Co(phen)_3^{3+}$ as the hybridization indicator. It was also reported the covalent immobilization of DNA onto a SAM using methylene blue and daunomycin as labels [110,111]. Jin's team reported the self-assembled immobilization of a thiolated hairpin DNA-probe sequence onto a gold electrode and specific discrimination of a complimentary target DNA from both a single-base mutation and a random oligonucleotide [112]. Detection was carried out by CV, using methylene blue as electroactive hybridization indicator. Results showed that the greatest effect on the hybridization with a hairpin DNA probe is achieved when the mutation occurs in the center of the DNA-target sequence. Ferrocene, a dsDNA electrostatic- and groove-binder, was used to electrochemically detect yeast DNA covalently attached to a SAM-functionalized gold electrode [113] and a dengue-related oligonucleotide sequence with a chitosan-coated GCE [114]. Xu et al. reported the use of ferrocene derivatives as electrochemical hybridization labels, suitable for covalent labeling of DNA [115]. This type of DNA labeling is more costly, labor-intensive and complex than non-covalent binding (due to the synthesis, labeling and product separation steps), but provides a stronger and more stable attachment to the DNA probe. However, new intercalators with higher electrochemical sensitivity are under investigation. An example is ferrocenylnaphtalene-diimide (*N*,*N*c-Bis[[4-(3-aminopropyl)-piperazinyl]propyl]-naphthalene-1,4,5,8-tetracarboxylic acid diimide), which displays higher affinity for a double-chain and negligible affinity for a single-chain DNA than classical intercalators, with sensitivities in the zmol range [116]. Traditional schemes of DNA biochips with fluorescent detection are well known, but Hashimoto et al. developed an analogue system with electrochemical detection (Fig. 2), allowing to avoid the complexity of fluorescent labeling and an expensive laser device for excitation [117,118]. In particular, screen-printed electrodes are not only prone to mass-production, but also more mechanically resistant than traditional carbon-paste electrodes; these, in addition, also suffer from poorly reproducible manufacture. With standard photolithographic components, electrochemical

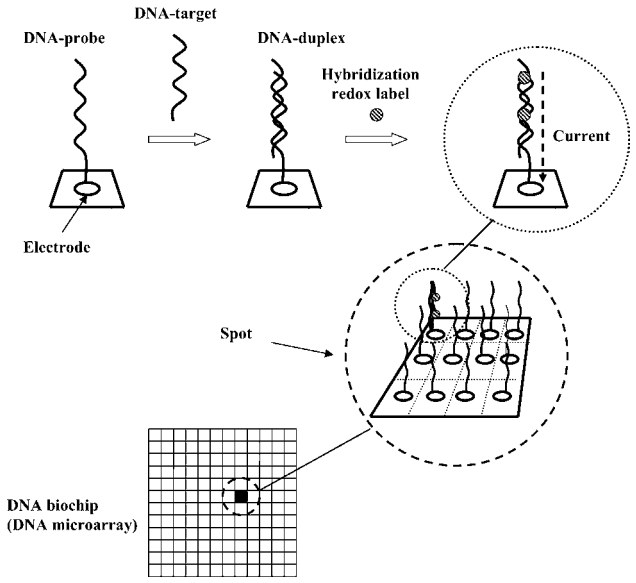

Fig. 2. DNA biochip with electrochemical detection. An unlabeled DNA-target chain hybridizes with a known electrode-bound DNA-probe chain. Further attachment of a hybridization redox label to the DNA duplex generates a current level that can be assigned to a known, specific DNA-probe sequence. The resulting current pattern in each spot corresponds to a certain level of gene expression.

detection in 20 μm gaps in a microelectrode deposited onto a silicon chip was performed with a sandwich technique, using a reporter-probe, a DNA-target and a GNP-bound capture-probe [184]. After 6–15 h of hybridization, probe-bound nanoparticles remained on the gaps, facilitating the formation of conductive silver bridges after a treatment with film-forming reagents. This system achieved single-base resolution in the femtomolar range. A disposable electrochemical printed chip for the detection of SNPs, with PCR products being analyzed directly on the chip by differential pulse voltammetry (DPV) without prior purification [119]. One notable peculiarity of high-density DNA microarrays is the need for physical addressing, by microjet deposition techniques, of picoliter volumes in discrete, highly specific spots on the chip. Fixe et al. used a pixel-addressed technique, by covalent immobilization and hybridization of DNA sequences onto a plastic-deposited thin film after the application of a very short 4.5 ns potential pulse, below 1V, which is compatible with standard, silicon-based microelectronic circuitry [120]. The enormous 10^9-fold raise in immobilization and hybridization efficiencies over an analogous system without the potential pulse may be attributed to the rapid spatial reorientation of adsorbed single-chain DNA due to the rapid change of the electrical field, which lowers sterical hindrances and accelerates both reactions. Similar works were reported earlier [121]; nevertheless, the too long 5 min pulses thus applied may trigger DNA-damaging electrochemical reactions. This highly dense hybridization spot technique may reduce both the time and cost of microarray fabrication, while increasing the data acquisition speed. Electrochemical transduction is easier to perform, simpler, faster and more suitable for miniaturization than fluorescence or MS [3]. Nowadays, chip nucleic acid immobilization still lacks optimization over sensitivity, specificity and hybridization efficiency, as well as minimization of cross-hybridizations [122]. In parallel with quantum dots, the newly discovered CNTs constitute a major class among bottom-up methods in nanobiotechnology. They exhibit a notable range of unique electronic properties and enlarged surface area for DNA immobilization, making them excellent elements for chemical sensing. Their electrical conductivity is comparable to that of copper and several orders of magnitude higher than that of polymers. In addition, they are physically robust and inert towards most chemicals [123]. Nie et al. used CNTs to modify a CPE in which an oligonucleotide was immobilized via streptavidin/biotin coupling [124]. After hybridization with a GNP-labeled DNA probe, a second hybridization between this system and additional GNPs was carried out, and total GNPs were monitored by DPV. The resulting signal was enhanced in comparison with that of a pure CPE and was about one order of magnitude higher than that with one-layer hybridization; clear distinction with one-base mismatched DNA was obtained. The high sensitivity performance of GNPs and CNTs was recently challenged by a polyaniline (PANI) nanotube array-immobilized DNA sensor; the array was built-up onto a graphite electrode, using a thin nanoporous layer as the template [125]. Some advantages of the conducting PANI biosensor include low temperature synthesis and no need for catalytic enhancement, purification or end-opening processing. In addition, the uniform orientation of the individual nanotubes on the array and the enhanced conductivity of arrayed PANI obviate the common limitations of conventional PANI. The biosensor exhibited an ultralow detection limit of DNA (1 fM) and good discrimination of one-nucleotide mismatches down to 38 fM, with obvious application for SNP analysis. Despite the undeniable advantages of CNTs, their manufacture is troublesome. A direct consequence is the high variability of shapes between different single CNTs, which renders unreproducible electrical properties, unless many average-in units are used together. Arrays of nanotubes bound to different DNA-probe molecules may be built to cheaply detect specific genes for diagnostic purposes [123].

5.3.3. Label-free (direct) detection

Variations on the intrinsic DNA electroactivity after the occurrence of hybridization are especially envisaged due to their simplicity [122]. This has obvious advantages in terms of simplicity and rapidity of the experimental procedures, and avoids signal lost caused by gradual liberation of the indicator from the immobilized DNA. Essentially, the adenine and guanine residues become oxidized in carbon electrodes and (in addition to cytosine) reduced in mercury electrodes [126]. The hybridization reaction generally causes a decrease in the redox current peak because the redox points in the DNA molecule are compromised with the hydrogen bonds that keep both chains together. In addition, the higher rigidity of a double-chain compared to that of a single-chain hinders the former to completely cover the rough microscopic surface of a solid electrode, thus decreasing the number of DNA/electrode attaching points and the overall electron transfer rate [127]. The emergence of solid electrodes has improved enormously the applicability of electrochemical methods for nucleic acid analysis. Stripping methods have the lowest detection limits among all voltammetric techniques [128]. The technique of adsorptive transfer stripping voltammetry (AdTSV) was used to detect DNA amounts below 1 pg, in sample volumes as small as 5–10 μl, without the need for a special voltammetric cell [126]. Compared to stripping voltammetry, stripping potentiometry devices exhibit smaller background noise [127]. This technique was applied to high-sensitive detection of DNA in electrochemically pretreated carbon paste and in screen-printed electrodes [11,129]. Changes in interfacial electrochemical parameters have also been used for DNA analysis, despite the molecular mechanisms underlying interfacial electrical changes as a result of affinity interactions are only fairly understood [130]. Capacitive transducers' operation relies on the decrease in capacitance caused by thickening of the electrode/solution dielectric layer as a result of displacement of water and electrolyte molecules due to the immobilization and further hybridization events. A genosensor was reported for capacitive detection of short oligonucleotides with thiolated and SAM-immobilized probes in gold electrodes

[131]. DNA detection through impedimetry is based on the fact that single-chain DNA desorption from a solid electrode corresponds to a higher dielectric loss compared to a double-chain, owing to the higher structural flexibility of the last [132]. At 100 Hz, impedance measurements on a label-free DNA gold electrode sensor increase about 25% upon hybridization, but it was reported an increase of up to 160% with an enzymatic amplification scheme [133]. The surface potential variation upon hybridization of a silicon nitride gate insulator-immobilized peptide nucleic acid (PNA) with its negatively charged DNA counterpart was used to specifically detect the hybridization event with a FET sensor [134]. The PNA, a DNA/protein hybrid, is particularly advantageous for this purpose, because it enables highly specific and selective binding at low ionic strength. PNAs are nucleic acid analogues with the sugar–phosphate backbone replaced by a peptide structure, and have received considerable attention as new recognition probes for DNA detection; they significantly improve the sensitivity and the discriminatory ability between DNA sequences differing in as few as one base-pair [3]. Other advantages include high sensitivity, low dependence on the ionic strength and high thermal stability [135]. An electrochemical detection scheme was recently developed by using a PNA probe and polythiophene which, for being a water-soluble electroactive cationic polymer, avoids the strong electrical interferences caused by the hydrophobic polymers in permanent contact with the electrodes [136]. The neutral character of the PNA probe permits its binding to polythiophene only after the hybridization reaction with the negatively charged DNA-target. Field-effect transistor (FET) biosensors operate by interaction between external charges with carriers in a nearby semiconductor [130]. FET biosensors have been used by direct immobilization of DNA strands on the gate surface of a DNA chip by chemical modification [137,138]. These silicon-based devices monitor the increase in surface charge after DNA hybridization on the sensor surface [139]. Wang et al. developed an electrochemical biosensor for detection of short Mycobacterium tuberculosis-related DNA sequences by adsorptive stripping chronopotentiometry with a redox marker [140]. The performance of this microfabricated screen-printed carbon-strip biosensor was similar to that of a carbon paste biosensor, with short detection times, in the range of 5–15 min. They also used this methodology to detect the oxidation peak current of guanine with a thick-film sensor incorporated into a battery-operated portable device, as required for in situ DNA diagnosis [141]. Low or moderate sensitivity is usually a problem in FET sensors due to significant fluctuations of the interface potential in an aqueous environment, but a recent strategy was implemented with a gold electrode-based FET DNA sensor to stabilize the sensor, by superimposing a 1 kHz high-frequency voltage to the reference electrode [142]. In addition, the stabilization time was reduced from 1 h to 5 min. An interesting innovation to increase the sensitivity and performance of genosensors are nucleic acid dendrimers, branched supermolecular structures able to be used as DNA probes. Upon hybridization of these spherical, tree-like structures with multiple target-strain molecules, the response is greatly amplified [3]. In addition, DNA dendrimers have structural homogeneity and controlled composition, making them valuable candidates for biosensing applications. Amino-terminated dendrimers were used as building blocks to form multilayer thin films and as linkers for immobilization of amino-modified DNA probes [143]. Besides the high sensitivity and selectivity thus achieved by EIS, the multilayer biosensor is very stable and regenerable. Morosity limits the utilization of impedimetry and capacitance for biosensor construction [132]. However, these biosensors may find a market where low cost, portability and analysis speed are required and moderate sensitivity is sufficient [130]. A well-succeeded diagnostic may not only require detection but also quantification of the disease-causing substance, since pathological states are usually associated with high serological levels of these compounds. Nucleic acids are usually quantified through the adenine/guanine ratio, but a method was proposed to simultaneously detect the individual levels of both nucleotides with a GCE after DNA adsorptive stripping [12]. Well-defined oxidation peaks were produced above 4 ng ml^{-1}. A label-free X-ray photoelectron microscopy detection system was recently used to detect the nitrogen content and the DNA nitrogen/sulfur ratio from alkanethiols introduced for surface immobilization to confirm the occurrence of hybridization [144]. The method was shown to be a good alternative to fluorescence radioisotope detection. The potential of photoelectrochemistry for unlabeled DNA detection was demonstrated by a 10^4-fold sensitivity enhancement over voltammetry in PCR-free biological samples [145]. Instead of electrochemical changes in nucleobases, direct electrooxidation of sugar residues in cupper electrodes may also be monitored [146]. In this case, however, the response tends to increase after hybridization, reaching detection limits in the picomolar range, since more sugar residues are accessible in an outer double-helix than in a single-chain. As an application of CNTs, multi-wall nanotubes (MWNTs) were used to improve direct detection of guanine and adenine oxidation currents in an MWNT-modified GCE [147]. The detection was highly sensitive, simple, reproducible and rapid. The surface area of MWNTs may be further enhanced by coupling end- and lateral-functionalization in CPEs, with a detection limit of 10 pg ml^{-1}, compatible with genetic testing requirements [148]. Pointing towards nanotechnology, DNA/protein conjugates have emerged has valuable tools for biosensor construction. Investigations about the interaction between DNA and DNA-binding proteins are pertinent due to the importance of DNA–protein interactions in many cellular processes (e.g., transcription) [13]. Semi-synthetic DNA–protein conjugates go far beyond the typical avidin-biotin-streptavidin affinity systems for DNA-probe labeling, and may help to solve some basic constraints of currently available biosensors. An example is a thermostable probe for DNA hybridization assays, formed by an oligonucleotide and a fungal lipase [149]. In this study, working with screen-printed carbon electrodes modified with single-wall nanotubes (SWNTs), the interaction of the SSB protein from *Escherichia coli* with ssDNA (for which the protein has high affinity) immobilized on the SWNTs was evaluated through the voltammetric oxidation peaks of the DNA-probe. There is a competition process between the SSB protein and the target DNA-chain for binding the DNA-probe; in this way, the oxidation signal of the DNA guanine and adenine residues increases after hybridization, while the oxidation signals of the tyrosine and tryptophan residues from the protein vanish, as a result of protein displacement. Thus, the electron transfer rate increases. The SWNT-amplified signal reached a detection limit of 0.15 mg ml^{-1} of target-DNA. An important topic in electrochemical biosensing with DNA/protein conjugates is the detection of individual molecules with DNA nanopores, which are usually formed by covalently immobilizing a single DNA-chain into the lumen of a *Staphylococcus aureus* α-hemolysin nanomeric pore. This strategy is based in former works, according to which nucleic acid molecules produce ionic current 'signatures' while crossing the α-hemolysin ionic channels [150]. The conjugated is able to detect, with single-base resolution, DNA target-chains that eventually bind the immobilized probe, by measuring the variation of the ionic current flowing through the nanopore [151]. This system, however, is still limited for nucleotide sequencing, since several nucleotides occupy the transmembrane pore and all contribute to the overall resistance, thus 'darkening' the effect of any individual nucleotide [152]. Moreover, high frequencies of about 10 MHz are needed to reduce the experimental noise, but they can also mislead nucleotide sequence-dependent signature currents. It is thus very likely that a future

nanopore-based sequencing device includes an enzyme to regulate the DNA translocation velocity across the nanopore from microseconds to milliseconds per nucleotide. Being an alternative to the extense DNA-probe microarrays, nanopores may constitute a next generation of DNA biosensors. A newly developed system to detect the duplex formation is based on the reduction of the ionic conductivity, after DNA hybridization, through an immobilized probe bound to a bilayer lipid membrane (BLM); this is due to alterations in the ionic permeability of the BLM as a consequence of structural changes caused by the hybridization event. An ion-channel sensor for highly specific DNA detection was built-up, making use of the electrostatic repulsion between ferrocianide (negatively charged hybridization marker) and a negatively charged DNA target-strain bound to a neutral PNA probe, on a gold electrode [153]. A similar approach is the use of negatively charged liposomes that bind the immobilized probe, thus creating a giant negatively charged surface that repels the target-DNA [154].

In general, electrochemical biosensors are relatively simple, rapid, less costly and amenable for miniaturization and mass-production [1]. Together with the compatibility with microfabrication techniques, the low power demands and the portable nature, electrochemical transduction seems to be quite appropriated for decentralized DNA diagnosis of many infectious and inherited diseases [11,12].

5.4. Magnetic particles

Labels used in bioassays are very often molecular, nanoscale-sized, in order to match the size of molecular recognition bioprobes and analyte targets. For this reason, microscale-labels, including magnetic microbeads, are usually discarded as true labels [155]. Nonetheless, when compared to smaller labels, microbeads offer two important advantages that far outweigh the disadvantages of size mismatch: the easiness of detecting a low amount of microbeds than much more abundant nanolabels (e.g., fluorophores or nanoparticles) by routine optical microscopy or magnetic detection and the possibility of applying fluidic drag forces to microbeads for, under controlled laminar flow at the capture surface, remove non-specifically bound labels, thus improving dramatically the assay performance [156]. The sensitivity, specificity and reproducibility of label-based systems is much more dependent on non-specific background signals than on the ability for label detection [157]. Very often, magnetic beads in biomolecular analysis schemes are used for target preconcentration rather than for the detection step itself, together with the additional label (e.g., metal nanoparticle or fluorophore) for detection. Sandwich models with metal nanoparticles, DNA and magnetic microbeads have been increasingly used for high-sensitivity DNA detection [158]. When magnetic nanoparticle labeled-DNA probe molecules bind their target sequences on a surface, under brief exposure to a strong magnetic field, their magnetic moments align collectively and yield a measurable signal. Meanwhile, there is no net signal from the randomly oriented DNA sequences, which permits to eliminate the common and tedious washing steps [63]. The use of magnetic micro- or nanoparticle for specific detection of low-abundant DNA analytes has drastically increased in recent years. An example recently reported was the development of a magnetically assisted DNA detection platform based on magnetic particle preconcentration [159]. Alternative schemes for detection and quantification of nucleic acids rely on the magnetic bead-based sandwich hybridization (BBSH) assay, in which the DNA-target simultaneously binds a magnetic bead-tagged DNA and the labeled DNA-probe. An application of this method was carried out with an electrochemical readout system based on interdigitated microelectrode arrays on silicon chips [160]. Another example was the sandwiching of a target-DNA between DNA probe-functionalized magnetic microparticles and DNA-modified GNPs to separate the target from the sample matrix and amplify the signal, with suitable detection with a chip-based silver metallization technique [161]. A common feature of these schemes is the so-called 'capture and release' strategy, by which a target-DNA firstly binds the DNA probe-functionalized magnetic particle and is then released (dehybridized) for final detection. This multi-step process, however, tends to lengthen the analysis time and dilute the sample. Aiming to reduce the analysis time, some modifications were introduced in the BBSH assay in a recent work of an electrical biochip for analysis of messenger RNA (mRNA) levels and gene expression [162]. The layout consisted of one biotin-labeled capture probe and two digoxigenin (DG)-labeled detection probes. After hybridization of these probes with the target, the

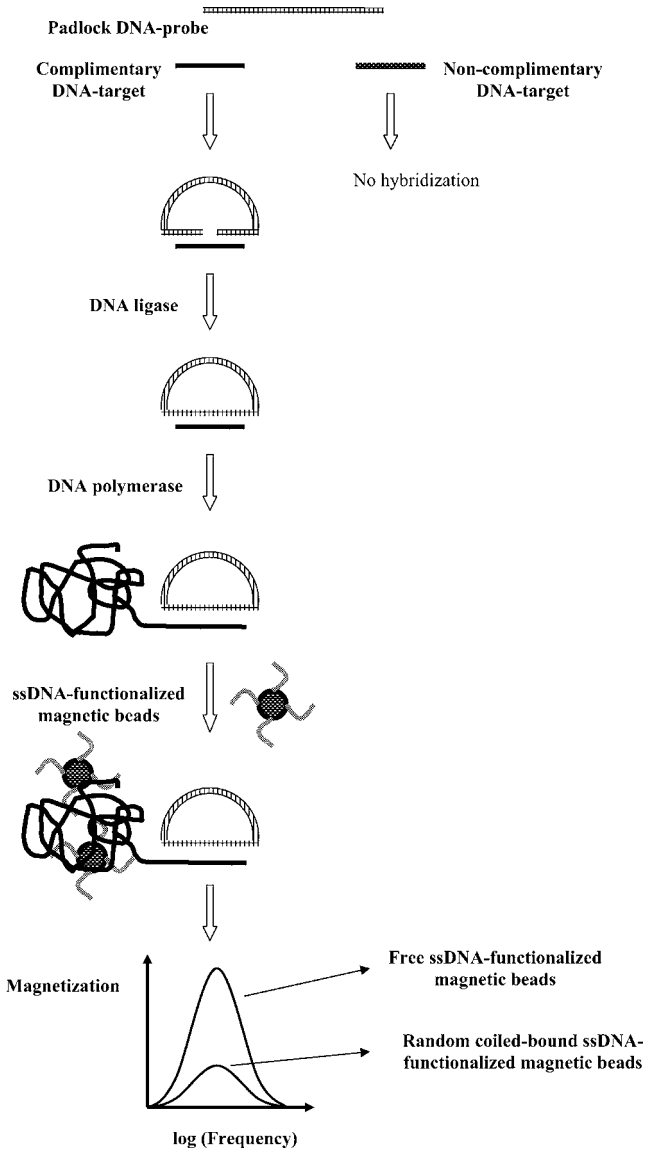

Fig. 3. Scheme of the VAM-NAD assay. The ends of the padlock DNA-probe hybridize with the complimentary DNA-target chain, forming a circularized structure. Such ends are then joined together by a DNA ligase. Afterwards, a DNA polymerase triggers the RCA process for a certain period of time. The addition of magnetic beads functionalized with ssDNA chains complimentary to a sequence in the random-coil repeating motif originates magnetic bead attachment to the macromolecular DNA structure by base-pair hybridization. This bead incorporation results in a considerable downsizing in the magnetization spectrum curve, when compared to that of unbound ssDNA-functionalized magnetic beads.

Table 1
Transduction mechanism, DNA detection assay characterization and limit of detection (LOD) for several bibliographic references on DNA biosensing

Transduction mechanism	DNA detection assay characterization	LOD [#ref.]
1. Optical		
1.1 Label-free (reagentless) detection		
SPR	Capture- and target- oligos (11–100 mer)	10 pM [189], 10 pM [60], 100 pM [190], 0.68 pM [191]
	Capture-oligo (11–25 mer) and target-DNA fragment (143–570 mer)	0.06 pg [192], 0.25 μM [193]
Fluorescence and chemiluminescence	Capture- and target-oligos (18–123 mer)	90 pM [194], 0.3 nM [72], 70 nM [195], 1.9 pM [196], 2 nM [197]
1.2 Label (dye or intercalator)-based detection		
SPR	Capture- (18 mer), target- (24–0 mer) and signaling- (18–21 mer) oligos	1.8 pM [198], 500 nM [199]
	Capture- and target- oligos (11–80 mer)	1.22 nM [200], 3.0 nM [201], 19 pM [42], 30 fM [202], 0.2 nM [203]
Fluorescence	Capture- (27 mer), target- (40 mer) and signaling- (19 mer) oligos	5 fmol [204], 0.6 fmol [205]
	Capture-oligo (15 mer) and target-DNA fragment (196 mer)	500 fmol [206]
2. Mass-change		
Resonance frequency	Capture- (20–30 mer), target- (40 mer) (or DNA fragment (104 mer)) and signaling- (20–30 mer) oligos	120 CFU/ml [207], 0.7 μM [208]
	Capture- and target- oligos (11–42 mer)	50 nM [86], −3.6 Hz/pg [209]
	Capture-oligo (26–42 mer) and target-DNA fragment (104–244 mer)	1.0 μM [210], 0.12 μM [85], 10 nM [211], 200 μg/ml [212]
SAW	Capture- and target- oligos (15–20 mer)	0.01 μM [88,213,214], 1 ng/ml [215]
3. Electrochemical		
3.1 Label-free (reagentless) detection		
Voltammetry	Capture- and target- oligos (20–38 mer)	100 pM [216], 0.01 fmol [217], 400 pM [218], 10 pM [219], 10 pg/ml [148]
	Capture-oligo (18–25 mer) and target-DNA fragment (244–300 mer)	1.8 zM [220], 30 μg/ml [221], <1000 DNA-target amplicons [222]
EIS	Capture- and target- oligos (15–30 mer)	10 fM [223], 0.5 nM [224], 5 nM [225,226], 100 pmol [227], 100 nM [228]
FET	Capture- and target- oligos (20–30 mer)	79 nM [229], 10 fM [230]
3.2 Enzyme-based detection (sandwich-assay mode)		
Streptavidin-alkaline phosphatase conjugate	Capture- and biotinylated target- oligos (13–30 mer)	8 pM [231], 6 pM [232], 1 nM [233], 30 fM [234]
	Capture- (13–35 mer), target- (23–52 mer) and signaling- (12–35 mer) oligos	340 pM [235], 0.3 fM [79], 1.2 pM [236], 50 fM [237]
Other conjugates	Capture- and biotin- or 5′-fluorescein isothiocyanate (FITC)-labeled oligos (20–50 mer)	0.1 nM [238], 0.5 fM [239], 100 pmol [103]
	Capture-oligo (20 mer) and labeled-DNA fragment (322 mer)	10 isolated genomes [240]
	Capture-oligo (20–50 mer), DNA fragment (87–362 mer) and signaling-probe (12–35 mer)	1 fmol [241], 1 fM [242], 1 fM [243]
3.3 Label (redox marker)-based detection		
Voltammetry	Capture- and target- oligos (10–35 mer)	1 nM [244], 0.3 pM [245], 0.12 pM [246], 0.54 ag/ml [247], 7 nM [248], 8.3 μM [249], 0.59 nM [250], 0.5 nM [251], 1 fM [125], 10 pM [252], 0.3 pM [253], 0.51 nM [254], 90 pM [255], 0.5 nM [256], 10 zmol [116]
	Capture-oligo (23 mer), target-DNA fragment (256 mer) and signaling-probe (23 mer)	0.78 fmol [257]
4. Magnetic particles and other oligo probe-supporting beads		
4.1 Optical	Capture- (20–30 mer), target- (20–41 mer) and signaling-probe (25–41 mer)	10 fM [258], 10 pM [75]
	Capture- and target- oligos (15–37 mer)	32 μM [61], 50 pM [259], 100 pM [49]
	Target-DNA fragment (600 mer) and signaling-probe (180 mer)	1.4 pM [260]
4.2 Electrochemical	Capture- and target- oligos (20–32 mer)	2 pM [261], 2 nM [262]
	Capture-oligo (20 mer) and target-DNA fragment (437 mer)	74.8 pM [263]
4.3 Magneto-resistive	Capture- and target-oligo (30 mer)	100 fM [264]

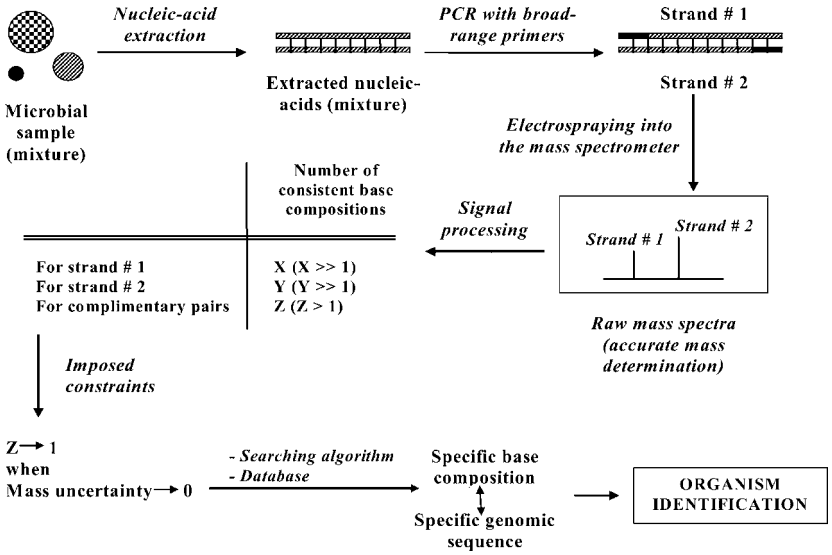

Fig. 4. Identification of microorganism species in biological mixtures by the universal MS biosensor. All nucleic acids in the sample are firstly extracted and amplified with different sets of universal, broad-range primers. The PCR products are then electrosprayed into a mass spectrometer and resulting raw mass spectra are recorded. Very accurate mass measurements of each DNA strand allow determining the number of consistent base compositions for each one, a number which is greatly reduced by imposing the condition of complimentarity between them. This number is further reduced towards unity when the uncertainties of mass measurements for both strands reach zero. Finally, an internal algorithm searches for a database that assigns a specific genomic sequence to the unique, specific base composition determined above, thus identifying the organism in the sample mixture.

sandwich-hybrid is bound to paramagnetic streptavidin-coated particles (which allow separating the sandwich-hybrid from the reaction solution by external magnets) and labeled with anti-DG alkaline phosphatase conjugates. The redox reaction catalyzed by the enzyme generates an electrical current which correlates with the level of hybridized mRNA. In contrast to former protocols in which probes were targeted to regions of the mRNA-target separated by a few hundred nucleotides, DNA-probes were, with this approach, adjacently bound to their target regions in the same mRNA molecule. The resulting enhancement of the hybridization efficiency may result from a cooperative effect of the adjacently bound probes (by modifications on the secondary structures of the mRNA molecule) [163] or from prevention of breaking or hydrolysis points that, otherwise, may occur along the structure of a mRNA strand in the case of separated probes. By using two instead of only one DG-labeled detection probe, further signal amplification was achieved, thus resulting in a substantial time reduction of the detection protocol. In addition, the expression profile exhibited by this optimized protocol is comparable with those of real-time RT-PCR assays. An alternative method proposed by Dubus et al., with optical detection, does not require the release of the hybridized target-DNA prior to its detection [164]; instead, a polymeric polythiophene derivative was attached to a magnetic microbead-grafting ssDNA followed by hybridization with the DNA-analyte, with formation of triplex-branched beads. The detection principle relies on the different conformations adopted by the polymer molecule when electrostatically bound to either ssDNA or dsDNA, giving rise to distinct fluorescence properties (chromism). The other novelty of this work was the confinement of the particle-bound target-DNA in a small volume of a microelectromagnetic trap, which allows performing the preconcentration and the detection steps simultaneously on the same support, thus decreasing the final sample volume and increasing the signal-to-noise ratio. This scheme not only avoids the hybridized DNA-releasing step, but also renders results in only 5 min, with detection limits similar to those of 'capture and release' methods. The above combination is able to extend the application of this ultrasensitive biosensor to biological samples with complex matrices and integration in lab-on-a-chip platforms.

Martins et al. developed a magnetoresistive biochip for real-time monitoring of pathogens in water [165]. With this system, DNA-target molecules may be magnetically labelled before or after the recognition process, by paramagnetic bead-driven transport and manipulation across a chip surface onto a microfluidic platform. The detection was carried out by measuring the variation of the sensor resistance with the label-borne magnetic fields. The system exhibited a fast response with high sensitivity, specificity and ease of integration and automation, thus constituting an attractive option to fluorescent labelling and allowing tight stringency control. In addition, since biomaterials usually are not magnetic, background signal subtraction is greatly simplified [166]. Such magnetic field sensors can be miniaturized to match the size of a single magnetic bead, thereby increasing the sensitivity of the detection. In another work, a magnetic splitter was used to separate, within a microchannel, two types of magnetic microspheres bound to different DNA-probes, resulting in single-base resolution of the target-DNA [167]. Recently, a non-fluorescent volume-amplified magnetic nanobead assay scheme for DNA detection was developed [16]. This method involves circularizing, 'padlock' oligonucleotide probes designed with two terminal target-complimentary segments. Upon specific hybridization with the target, the ends are joined by a ligase, creating a circular, target-catenated DNA-probe molecule, which provides highly specific and sensitive detection [168]. The DNA-target is recognized and volume-amplified to large coils by circularization of the linear padlock probes through probe hybridization and ligation, followed by rolling circle amplification (RCA) of the probes by a DNA polymerase. This generates a DNA strand consisting of a large number of tandem copies of the complement to the circularized probe, collapsing into a random-coil DNA macromolecule in solution. After nanobead binding in the RCA coils, the nanobead magnetization spectrum changes considerably, induced by the attached volume-amplified target molecules (Fig. 3). Although having been used for single-target detection, this method can be easily generalized for multi-target detection by using several nanobeads with different sizes, one for each target. The method was already applied for single-molecule DNA detection with fluorophore-tagged probes [169]. The resulting confined cluster of fluorophores

was detected and quantified with a microfluidic device mounted onto a confocal fluorescence microscope. This layout could also be applied for the simultaneous amplification of different probe and target complexes for multiplexed target analysis with fluorescence probes with different colors. The detection limit can be greatly improved by optimizing, for instance, RCA time, bead size and bead surface coverage of oligonucleotides. Since bead incorporation in the coils is diffusion-controlled, it can be accelerated by sample incubation at higher temperatures. A multiplexed technique was implemented for simultaneous and label-free detection of three short HBV-related DNA fragments in a single vessel, with detection of a chemiluminescent product of a reaction between the labeling reagent 3,4,5-trimethoxylphenylglyoxal (TMPG) and the guanine-enriched regions within the DNA-target [170]. In this work, thermosensitive poly(*N*-isopropylacrylamide), polystyrene beads and magnetic beads were employed as different labels in DNA capture-probe conjugates, which were split apart under different thermal conditions. In contrast with most of the current multiplexing detection methods, which usually require complex instrumentation (e.g., flow cytometer or imaging system) instead of a simple chemiluminescence setup, every hybridization signal for the corresponding DNA-target in this work is uniquely immobilized onto one carrier with a unique and intrinsic physico-chemical pattern. Despite not employing any extra label (e.g., organic fluorophore) unless TMPG – with potential advantages in terms of detection speed, cost and simplicity – it is possible to further enhance the detection sensitivity by increasing the amount of DNA-target strands or introducing other labels (e.g., enzymes or colloidal gold). Lee et al. [171] coupled antibody-conjugated magnetic beads and μRT-PCR on a microfluidic chip for detection of RNA viruses after thermal lysis of extracted RNA. The targeted virus in the sample was captured by the specific antibody-conjugated magnetic beads for viral pretreatment and RNA enrichment, thus avoiding the effect of interferents and inhibitors usually present when direct thermolysis of virus-containing samples is performed. After capturing the virus, magnetic beads are trapped in a magnetic field and can be then easily manipulated for further processing. This format exhibited sensitivity similar to that of a commercial RNA extraction kit and a large-scale RT-PCR apparatus. Multiplexed analysis in complex biological samples (including whole blood, serum, plasma and milk) was coupled to magnetic microbead labeling for femtomolar detection of DNA and proteins [157]. Non-specific binding of bead labels was minimized by applying fluidic force discrimination, in which a controlled laminar flow promotes chip-captured microbead labeling. The density of beads that remain bound is proportional to analyte concentration and can be determined either by optical counting or magnetoelectonic detection. Compared to a previous nanowire-based FET for multiplexed and label-free protein detection [172], this method exhibited similar sensitivity and additional ability for analysis of untreated clinical matrices onto a simple microscope slide. By combining simple optical or magnetic bead counting with microfluidics, straightforward hand-held and higher throughput analysis can be performed in a few minutes. The main advantage of using an on-chip transport system is that diffusion constraints are overcome by the attraction between a magnetic field and functionalized magnetic particles. Its combination with a magnetoresistive transducer enables the detection of minute amounts of target biomolecules in a reasonable time frame. However, biosensing applications still require improvement of field sensitivity and reduction of the sensor noise background [173].

5.5. Bibliographic revision on limit of detection of DNA biosensors

We have reviewed a large number of different systems on the literature for DNA detection, mainly concerning the transducer surface and transducing mode of optical, mass-sensitive, electrochemical and nanoparticle bead-based biosensors (Table 1). A particular focus has been given to: transducer systems; different detection methods: label-free/reagentless (direct), label- (with dye or intercalator) and enzyme-based (both indirect); characterization of the DNA detection assay; and detection limit (a measure of sensitivity). Increased attention has been given recently to direct, label-free electrochemical detection schemes and to the development of high-sensitivity DNA biosensing devices for detection of DNA targets and SNPs without the need for target amplification. The limit of detection of a given quantification method is the sample concentration or quantity that yields a signal equal to the blank signal plus a multiple of the standard deviation of the blank [174]. For practical purposes, it is usually assumed that it corresponds to signal(s)/noise(n) = 3. From the reviewed publications, it becomes clear that, despite significant differences registered for nucleic acid detection limit values among the various applications, recent published works have reported increasingly small detection limits. Nevertheless, further sensitivity enhancement is still needed in order to achieve the extremely small detection limits required for diagnostic assays with real, non-amplified biological samples – in the attomolar range [175] – which is often beyond the fundamental limits of common sensing devices.

6. A new paradigm: MS DNA sensing and the universal biosensor

A common assumption in the conception of conventional biosensors is the necessary prior knowledge of the specific genomic sequence from a given target-pathogen. Unlike nucleic acid probes or arrays, MS does not require anticipation of the analyzed products, rather measuring the masses of the nucleic acids in a sample. The commercial T5000 Biosensor System, from Ibis Biosciences, is an integrated platform for analysis of complex samples, and relies in that essential common features are encoded in all the genomes among living organisms. In practice, broad-range ('intelligent') primers are used to amplify PCR products from large groups of organisms, but more specific, division-wide primers may be used to enhance species resolution [176]. Since the exact mass of each DNA base is accurately known, a high precision measurement is able to derive a constrained list of base compositions of each DNA strand [177]. An internal detection algorithm searches a database that assigns a specific base composition to a given genomic sequence, thus identifying the corresponding organism (Fig. 4). This strategy successfully led to include the human severe acute respiratory syndrome (SARS) virus in the coronavirus family [178]. It was also tested as a rapid and inexpensive method for global surveillance of emerging influenza virus genotypes [179]. Their main advantages are high resolution speed (above one sample per minute), high degree of automation and software control, no need for specialized manpower and possibility of performing strain typing and antibiotic resistance studies. As main disadvantages, the intrinsic difficulty MS device miniaturization, the need for continuous enrichment of databases with new genomic sequences, the requirement for high-power instrumentation for unambiguous compositional assignment and the need for signal processing enhancement, in order to detect a single sequence among thousands of others, can be mentioned. It is expected, however, that future technological improvements may ally the extraordinary analytical powerfulness of universal primer-based technologies with developments in the production and ongoing miniaturization of DNA chips and flow systems.

7. Conclusions

It can be anticipated that, in a near future, the advanced level of medical diagnosis will be largely dependent on the successful development and implementation of new materials and technology envisaging the fabrication of state-of-the-art biosensors. Common drawbacks of current biosensors have already been extensively summarized in the literature. However, the still limited availability of commercialized biosensors may be due mainly to a lack in the appropriate technology for their manufacture at a competitive cost rather than a lack of fundamental knowledge [180]. In vitro diagnostic devices will likely be expensive purchase over a one-test basis, although the overall cost may be lower due to the minimal requirement for laboratory manpower. In addition, the production and commercialization of high-throughput devices, as the GeneChip® from Affimetrix, may require investments in the order of several hundred million dollars, a serious obstacle for small start-up companies. Biosensors represent a quite disruptive technology for being very different from those currently used in clinical facilities worldwide. In addition, very often they face difficulties for obtaining regulatory approvals for testing and commercialization [181]. A more technical obstacle hindering their wide acceptance by the clinical community may be the controversial usefulness of monitoring one-single analyte as a disease-biomarker. The need for point-of-care nucleic acid testing, especially in resource-limited settings, requires simpler and cheaper instrumentation. As efforts for improving the amplification and detection of nucleic acids have been a major concern, the sample preparation and the nucleic acid extraction steps remain relatively underestimated towards the development of a true point-of-care diagnostic device. In addition, many of these current systems also require off-line sample preparation and reagent handling, being therefore unable for routine home testing [182]. It seems likely that, among the vast diversity of available approaches, none will fulfill all needs for a given application, but instead the choice will depend on the particular conditions and requirements. DNA analysis has been considered lengthy since standard filter hybridization protocols last no less than 20 h [183]. Some current biosensors already yield outputs in less than 1 h, but a truly simple, rapid and low-cost biosensor for routine analysis is still missing, which is particularly limiting for clinical purposes [184]. Clinical applications still face the problem of the very low levels of nucleic acids in biological fluids, otherwise undetectable if previous PCR amplification is not performed [180]. In the case of blood infections, the amount of human genomic DNA can be 10^{14} times higher than pathogen target-DNA, an important challenge in terms of selectivity [185]. Both in solution and at an interface, nucleic acids exhibit strong salt-dependent electrostatic effects over its structure, stability and reactivity [186]. Moreover, research about the effects of interfering substances has been carried out in pure, synthetic model-DNA sequences rather than in complex real samples, while prior knowledge of the selective molecular recognition processes is needed [187]. The lack of robustness in real samples may be attributed to the usually low operational and/or long-term stability of the biological receptor and/or the physical transducer [188]. Nonetheless, DNA is a particularly suitable material for nanosystem fabrication owing to unique peculiarities, including the ability of highly specific, mutual recognition between a very short oligonucleotide and a complex, long-sized eukaryotic genome, and high physico-chemical stability. Enhanced manipulation and processing precision at the atomic, ångstrom range by very specific molecular tools such as ligases, nucleases and other DNA-processing enzymes is another remarkable feature [46]. DNA has also higher chemical stability compared with other biorrecognition elements (e.g., enzymes and antibodies) and a superior ability to distinguish different strains from the same organism, especially when isolated from different geographical locations. Nucleic acid arrays are also proner than protein counterparts for direct synthesis onto a chip surface, without the need to produce and purify the ligands [82]. Taken together, these facts hold great promise for a future outburst of DNA biosensors for clinical and other purposes.

Acknowledgment

Luis P. Fonseca thanks FCT (Fundação para a Ciência e Tecnologia), Portugal for financial support under Project SpinAquaChip PTDC/AMB/73154/2006.

References

[1] K. Kerman, M. Kobayashi, E. Tamiya, Meas. Sci. Technol. 15 (2004) R1.
[2] S.R. Mikkelsen, Electroanalysis 8 (1996) 15.
[3] J. Wang, Nucleic Acids Res. 28 (2000) 3011.
[4] M.I. Pividori, A. Merkoçi, S. Alegret, Biosens. Bioelectron. 15 (2000) 291.
[5] Z. Junhui, C. Hong, Y. Ruifu, Biotechnol. Adv. 15 (1997) 43.
[6] T. McCormack, G. Keating, A. Killard, B.M. Manning, R. O'Kennedy, in: D. Diamond (Ed.), Principles of Chemical and Biological Sensors, John Wiley & Sons, Toronto, 1998, pp. 133–194.
[7] J. Wang, Anal. Chim. Acta 469 (2002) 63.
[8] W. Vercoutere, M. Akeson, Curr. Opin. Chem. Biol. 6 (2002) 816.
[9] V. Chan, D.J. Graves, P. Fortina, S.E. McKenzie, Langmuir 13 (1997) 320.
[10] Y. Gao, L.K. Wolf, R.M. Georgiadis, Nucleic Acids Res. 34 (2006) 3370.
[11] J. Wang, P. Gründler, G.-U. Fleichsig, M. Jasinski, G. Rivas, E. Sahlin, J.L.L. Paz, Anal. Chem. 72 (2000) 3752.
[12] H.-S. Wang, H.-X. Ju, H.-Y. Chen, Anal. Chim. Acta 461 (2002) 243.
[13] K.J. Odenthal, J.J. Gooding, Analyst 132 (2007) 603.
[14] K.A. Peterlinz, R.M. Georgiadis, T.M. Herne, M.J. Tarlov, J. Am. Chem. Soc. 119 (1997) 3401.
[15] R. Levicki, T.M. Herne, M.J. Tarlov, S.K. Satija, J. Am. Chem. Soc. 120 (1998) 9787.
[16] M. Strömberg, J. Göransson, K. Gunnarsson, M. Nilsson, P. Svedlindh, M. Strømme, Nano Lett. 8 (2008) 816.
[17] A.B. Steel, T.M. Herne, M.J. Tarlov, Bioconjugate Chem. 10 (1999) 419.
[18] C. Preininger, P. Chiarelli, Talanta 55 (2001) 973.
[19] S. Chen, L. Li, C.L. Boozer, C. Jiang, Langmuir 16 (2002) 9287.
[20] T. Delair, F. Meunier, A. Elaïssari, M.-H. Charles, C. Pichot, Colloids Surf. A 153 (1999) 341.
[21] T.R. Gingeras, D.Y. Kwoh, G.R. Davis, Nucleic Acids Res. 15 (1987) 5373.
[22] Y.-H. Rogers, P.J.-B. Com, Z.-J. Huang, V. Bogdanov, S. Anderson, M.T. Boyce-Jacino, Anal. Biochem. 266 (1999) 23.
[23] J. Cha, J.I. Han, Y. Choi, D.S. Yoon, K.W. Oh, G. Lim, Biosens. Bioelectron. 18 (2003) 1241.
[24] S. Reisberg, B. Piro, V. Noël, M.C. Pham, Anal. Chem. 77 (2005) 3351.
[25] T. Strother, J. Hamers, L.M. Smith, Nucleic Acids Res. 28 (2000) 3535.
[26] J.V. Ness, S. Kalbfleisch, C.R. Petrie, M.W. Reed, J.C. Tabone, N.M.J. Vermeulen, Nucleic Acids Res. 19 (1991) 3345.
[27] E.P. Ivanova, D.K. Pham, N. Brack, P. Piagram, D.V. Nicolau, Biosens. Bioelectron. 19 (2004) 1363.
[28] G.B. Sukhorukov, M.M. Montrel, A.I. Petrov, L.I. Shabarchina, B.I. Sukhorukov, Biosens. Bioelectron. 11 (1996) 913.
[29] H. Hayatsu, Y. Tanaka, K. Negishi, Nucleic Acids Symp. Ser. 37 (1997) 139.
[30] N. Lassalle, P. Mailley, E. Vieil, T. Livache, A. Roget, J.P. Correia, L.M. Abrantes, J. Electroanal. Chem. 509 (2001) 48.
[31] A. Dupont-Filliard, A. Roget, T. Livache, M. Billon, Anal. Chim. Acta 449 (2001) 45.
[32] G. Bidan, M. Billon, K. Galasso, T. Limache, G. Mathis, A. Roget, L.M. Torres-Rodriguez, E. Vieil, Appl. Biochem. Biotechnol. 89 (2000) 183.
[33] N.K. Chaki, K. Vijayamohanan, Biosens. Bioelectron. 17 (2002) 1.
[34] R.S. Freire, C.A. Pessoa, L.T. Kubota, Quim. Nova 26 (2003) 381.
[35] Y.-D. Zhao, D.-W. Pang, S. Hu, Z.-L. Wang, J.-K. Cheng, H.-P. Dai, Talanta 49 (1999) 751.
[36] A.J. Baeumner, J. Pretz, S. Fang, Anal. Chem. 76 (2004) 888.
[37] F.F. Bier, F. Kleinjung, Fresen. J. Anal. Chem. 371 (2001) 151.
[38] T.-H. Wang, Y. Peng, C. Zhang, P.K. Wong, C.-M. Ho, J. Am. Chem. Soc. 127 (2005) 5354.
[39] P.S. Dittrich, K. Tachikawa, A. Manz, Anal. Chem. 78 (2006) 3887.
[40] H.H. Ruf, T. Knoll, K. Misiakos, R.B. Haupt, M. Denninger, L.B. Larsen, P.S. Petrou, S.E. Kakabakos, E. Ehrentreich-Förster, F. Bier, Microelectron. Eng. 83 (2006) 1677.
[41] A. Gulliksen, L.A. Solli, K.S. Drese, O. Sörensen, F. Karlsen, H. Rogne, E. Hovig, R. Sirevåg, Lab Chip 5 (2005) 416.
[42] C.-W. Wei, J.-Y. Cheng, C.-T. Huang, M.-H. Yen, T.-H. Young, Nucleic Acids Res. 33 (2005) e78.
[43] D. Ivnitski, D.J. O'Neil, A. Gattuso, R. Schlicht, M. Calidonna, R. Fisher, BioTechniques 35 (2003) 862.
[44] D. Erickson, X. Liu, R. Venditti, D. Li, U.J. Krull, Anal. Chem. 77 (2005) 4000.

[45] C.R. Yonzon, D.A. Stuart, X. Zhang, A.D. McFarland, C.L. Haynes, R.P. van Duyne, Talanta 67 (2005) 438.
[46] C.M. Niemeyer, Rev. Mol. Biotechnol. 82 (2001) 47.
[47] P.A.E. Piunno, U.J. Krull, R.H.E. Hudson, M.J. Damha, H. Cohen, Anal. Chem. 67 (1995) 2635.
[48] J.A. Ferguson, T. Boles, C. Adams, D. Walt, Nat. Biotechnol. 14 (1996) 1681.
[49] F.J. Steemers, J.A. Ferguson, D.R. Walt, Nat. Biotechnol. 18 (2000) 91.
[50] S.J. Wood, Microchem. J. 47 (1993) 330.
[51] P. Guedon, T. Livache, F. Martin, F. Lesbre, A. Roget, G. Bidan, Y. Levy, Anal. Chem. 72 (2000) 6003.
[52] A. Buhl, J.H. Metzger, N.H.H. Heegaard, P. von Landenberg, M. Fleck, P.B. Luppa, Clin. Chem. 53 (2007) 334.
[53] G. Feriotto, A. Ferlini, A. Ravani, E. Calzolari, C. Mischiati, N. Bianchi, R. Gambari, Hum. Mutat. 18 (2001) 70.
[54] E. Mariotti, M. Minunni, M. Mascini, Anal. Chim. Acta 453 (2002) 165.
[55] J.-K. Wen, X.-E. Zhang, Z. Cheng, H. Liu, Y.-F. Zhou, Z.-P. Zhang, J.-H. Yang, J.-Y. Deng, Biosens. Bioelectron. 19 (2004) 685.
[56] J.S. Chamberlain, R.A. Gibbs, J.E. Ranier, P.N. Nguyen, C.T. Caskey, Nucleic Acids Res. 16 (1988) 11141.
[57] W. Fritzsche, Rev. Mol. Biotechnol. 82 (2001) 37.
[58] R.A. Reynolds III, C.A. Mirkin, R.L. Letsinger, Pure Appl. Chem. 72 (2000) 229.
[59] K. Tamada, F. Nakamura, M. Ito, X. Li, A. Baba, Plasmonics 2 (2007) 185.
[60] D.-K. Kim, K. Kerman, M. Saito, R.R. Sathuluri, T. Endo, S. Yamamura, Y.-S. Kwon, E. Tamiya, Anal. Chem. 79 (2007) 1855.
[61] Y. Sato, K. Sato, K. Hosokawa, M. Maeda, Anal. Biochem. 355 (2006) 125.
[62] S. Hohng, T. Ha, Chem. Phys. Chem. 6 (2005) 956.
[63] A.P. Alivisatos, Sci. Am. 23 (2007) 73.
[64] G.M. Whitesides, J.C. Love, Sci. Am. 17 (2007) 13.
[65] R. Robelek, L. Niu, E.L. Schmid, W. Knoll, Anal. Chem. 76 (2004) 6160.
[66] S.F. Wuister, R. Koole, C.M. Donegá, A. Meijerink, J. Phys. Chem. B 109 (2005) 5504.
[67] C.-Y. Zhang, H.-C. Yeh, M.T. Kuroki, T.-W. Wang, Nat. Mater. 4 (2005) 826.
[68] C.-L. Feng, X. Zhong, M. Steinhart, A.-M. Caminade, J.-P. Majoral, W. Knoll, Adv. Mater. 19 (2007) 1933.
[69] P. Alivisatos, Nat. Biotechnol. 22 (2004) 47.
[70] J.-G. Lee, K. Yun, G.-S. Lim, S.E. Lee, S. Kim, J.-K. Park, Bioelectrochemistry 70 (2007) 228.
[71] X. Fang, X. Liu, S. Schuster, W. Tan, J. Am. Chem. Soc. 121 (1999) 2921.
[72] X. Liu, W. Farmerie, S. Schuster, W. Tan, Anal. Biochem. 283 (2000) 56.
[73] S.-W. Tam-Chang, T.D. Carson, L. Huang, N.G. Publicover, K.W. Hunter Jr., Anal. Biochem. 366 (2007) 126.
[74] A.J. Baeumner, N.A. Schlesinger, N.S. Slutzki, J. Romano, E.M. Lee, R.A. Montagna, Anal. Chem. 74 (2004) 1442.
[75] S. Kwakye, A. Baeumner, Anal. Bioanal. Chem. 376 (2003) 1062.
[76] N.V. Zaytseva, R.A. Montagna, E.M. Lee, A.J. Baeumner, Anal. Bioanal. Chem. 380 (2004) 46.
[77] J. Korlach, M. Levene, S.W. Turner, H.G. Craighhead, W.W. Webb, Biophys. J. 82 (2002) 507.
[78] B. Sepúlveda, J.S. del Río, M. Moreno, F.J. Blanco, K. Mayora, C. Domínguez, L.M. Lechuga, J. Opt. A: Pure Appl. Opt. 8 (2006) S561.
[79] J.C. Liao, M. Mastali, V. Gau, M.A. Suchard, A.K. Moller, D.A. Bruckner, J.T. Babbitt, Y. Li, J. Gornbein, E.M. Landaw, E.R.B. McCabe, B.M. Churchill, D.A. Haake, J. Clin. Microbiol. 44 (2006) 561.
[80] http://www.illumina.com.
[81] C.L. Baird, D.G. Myszka, J. Mol. Recognit. 14 (2001) 261.
[82] N.F. Campbell, J.A. Evans, N.C. Fawcett, Biochem. Biophys. Res. Commun. 196 (1993) 858.
[83] N. Lassalle, E. Vieil, J.P. Correia, L.M. Abrantes, Biosens. Bioelectron. 16 (2001) 295.
[84] X.C. Zhou, L.Q. Huang, S.F.Y. Li, Biosens. Bioelectron. 16 (2001) 85.
[85] D. Dell'Atti, S. Tombelli, M. Minunni, M. Mascini, Biosens. Bioelectron. 21 (2006) 1876.
[86] D. Dell'Atti, M. Zavaglia, S. Tombelli, G. Bertacca, A.O. Cavazzana, G. Bevilacqua, M. Minunni, M. Mascini, Clin. Chim. Acta 383 (2007) 140.
[87] M. Thompson, A.L. Kipling, Analyst 116 (1991) 881.
[88] J. Sakong, H. Roh, Y. Roh, Jpn. J. Appl. Phys. 46 (2007) 4729.
[89] H. Zhang, H. Tan, R. Wang, W. Wei, S. Yao, Anal. Chim. Acta 374 (1998) 31.
[90] Y. Okahata, Y. Matsunobu, I. Kunihara, M. Masayuki, A. Murukani, K. Makino, J. Am. Chem. Soc. 114 (1992) 8229.
[91] L.M. Furtado, M. Thompson, Analyst 123 (1998) 1937.
[92] A. Janshoff, H.-J. Galla, C. Steinem, Angew. Chem. Int. Ed. 39 (2000) 4004.
[93] M. Yang, W.C. Duncan-Hewitt, M. Thompson, Langmuir 9 (1993) 802.
[94] K.M. Hansen, T. Thundat, Methods 37 (2005) 57.
[95] Y. Lee, G. Lim, W. Moon, Sens. Actuator 130–131 (2006) 105.
[96] M. Nordström, D.A. Zauner, M. Calleja, J. Hübner, A. Boisen, Eleventh International Conference on Miniaturized Systems for Chemistry and Life Sciences, Paris, France, October 7–11, 2007.
[97] J. Koeser, P. Shahgaldian, M. Bammerlin, F.M. Battiston, U. Pieles, J. Phys.: Conf. Ser. 61 (2007) 612.
[98] L.M. Lechuga, J. Tamayo, M. Álvarez, L.G. Carrascosa, A. Yufera, R. Doldán, E. Peralías, A. Rueda, J.A. Plaza, K. Zinoviev, C. Domínguez, A. Zaballos, M. Moreno, C. Martínez-A, D. Wenn, N. Harris, C. Bringer, V. Bardinal, T. Camps, C. Vergnenègre, C. Fontaine, V. Díaz, A. Bernad, Sens. Actuator B 118 (2006) 2.
[99] T. de Lumley-Woodyear, C. Campbell, A. Heller, J. Am. Chem. Soc. 118 (1996) 5504.
[100] F. Patolsky, A. Lichtenstein, I. Willner, Nat. Biotechnol. 19 (2001) 253.
[101] L. Alfonta, A.K. Singh, Anal. Chem. 73 (2001) 91.
[102] F. Azek, C. Grossiord, M. Joannes, B. Limoges, P. Brossier, Anal. Biochem. 284 (2000) 107.
[103] M.I. Pividori, A. Merkoçi, S. Alegret, Analyst 126 (2001) 1551.
[104] E. Bakker, Y. Qin, Anal. Chem. 78 (2006) 3965.
[105] E. Domínguez, O. Rincón, A. Narváez, Anal. Chem. 76 (2004) 3132.
[106] K.M. Millan, S.R. Mikkelsen, Anal. Chem. 65 (1993) 2317.
[107] K. Millan, A. Saraullo, S.R. Mikkelsen, Anal. Chem. 66 (1994) 2943.
[108] J. Wang, X. Cai, G. Rivas, H. Shiraishi, P.A.M. Farias, N. Dontha, Anal. Chem. 68 (1996) 2629.
[109] A. Erdem, K. Kerman, B. Meric, U.S. Akarca, M. Ozsoz, Electroanalysis 11 (1999) 586.
[110] K. Kerman, D. Ozkan, P. Kara, B. Meric, J.J. Gooding, M. Ozsoz, Anal. Chim. Acta 462 (2002) 39.
[111] K. Hashimoto, K. Ito, Y. Ishimori, Anal. Chim. Acta 286 (1994) 219.
[112] Y. Jin, X. Yao, Q. Liu, J. Li, Biosens. Bioelectron. 22 (2007) 1126.
[113] H. Ju, B. Ye, J. Gu, Sensors 4 (2004) 71.
[114] F.R.R. Teles, D.M.F. Prazeres, J.L. Lima-Filho, Sensors 7 (2007) 2510.
[115] C. Xu, H. Cai, P. He, Y. Fang, Analyst 126 (2001) 62.
[116] S. Takenaka, K. Yamashita, M. Takagi, Y. Uto, H. Kondo, Anal. Chem. 72 (2000) 1334.
[117] K. Hashimoto, K. Ito, Y. Ishimori, U.S. Patent 5,972,692 (1999).
[118] K. Hashimoto, K. Ito, Y. Ishimori, Anal. Chem. 66 (1994) 3830.
[119] M.U. Ahmed, K. Idegami, M. Chikae, K. Kerman, P. Chaumpluk, S. Yamamura, E. Tamiya, Analyst 132 (2007) 431.
[120] F. Fixe, H.M. Branz, N. Louro, V. Chu, D.M.F. Prazeres, J.P. Conde, Biosens. Bioelectron. 19 (2004) 1591.
[121] C.F. Edman, D.E. Raymond, D.J. Wu, E. Tu, R.G. Sosnowski, W.F. Butler, M. Nerenberg, M.J. Heller, Nucleic Acids Res. 25 (1997) 4907.
[122] P. Bean, Am. Clin. Lab. (2001) 11.
[123] G. Gruner, Sci. Am. 17 (2007) 48.
[124] L. Nie, H. Guo, Q. He, J. Chen, Y. Miao, J. Nanosci. Nanotechnol. 7 (2007) 560.
[125] H. Chang, Y. Yuan, N. Shi, Y. Guan, Anal. Chem. 79 (2007) 5111.
[126] E. Paleček, Electroanalysis 8 (1996) 7.
[127] M.A. La-Scalea, S.H.P. Serrano, I.G.R. Gutz, Quim. Nova 22 (1999) 417.
[128] D.A. Skoog, F.J. Holler, T.A. Nieman, Principles of Instrumental Analysis, 5th ed., Harcourt College Publishers, USA, 1998, p. 666.
[129] J. Wang, X. Cai, C. Jonsson, M. Balakrishnan, Electroanalysis 8 (1996) 20.
[130] J.S. Daniels, N. Pourmand, Electroanalysis 19 (2007) 1239.
[131] C. Guiducci, C. Stagni, G. Zuccheri, A. Bogliolo, L. Benini, B. Samorì, B. Riccò, Euro. Solid-State Dev. Res. Conf. (2002) 479.
[132] J.-G. Guan, Y.-Q. Miao, Q.-J. Zhang, J. Biosci. Bioeng. 97 (2004) 219.
[133] K.S. Ma, H. Zhou, J. Zoval, M. Madou, Sens. Actuator B 11 (114) (2006) 58.
[134] T. Uno, H. Tabata, T. Hawai, Anal. Chem. 79 (2007) 52.
[135] J. Wang, E. Paleček, P.E. Nielsen, G. Rivas, X. Cai, H. Shiraishi, N. Dontha, D. Luo, P.A.M. Farias, J. Am. Chem. Soc. 118 (1996) 7667.
[136] F. Le-Floch, H.-A. Ho, P. Harding-Lepage, M. Bedard, R. Neagu-Plesu, M. Leclerc, Adv. Mater. 17 (2005) 1251.
[137] D.-S. Kim, Y.-T. Jeong, H.-J. Park, J.-K. Shin, P. Choi, J.-H. Lee, G. Lim, Biosens. Bioelectron. 20 (2004) 69.
[138] T. Sakata, Y. Miyahara, ChemBioChem 6 (2005) 703.
[139] J. Fritz, E.B. Cooper, S. Gaudet, P.K. Sorger, S.R. Manalis, Proc. Natl. Acad. Sci. U.S.A. 99 (2002) 14142.
[140] J. Wang, G. Rivas, X. Cai, N. Dontha, H. Shiraishi, D. Luo, F.S. Valera, Anal. Chim. Acta 337 (1997) 41.
[141] J. Wang, X. Cai, B. Tian, H. Shiraishi, Analyst 121 (1996) 965.
[142] M. Kamahori, Y. Ishige, M. Shimoda, Anal. Sci. 23 (2007) 75.
[143] A. Li, F. Yang, Y. Ma, X. Yang, Biosens. Bioelectron. 22 (2007) 1716.
[144] A. Lapicki, F. Sakamoto, A. Sandhu, Jpn. J. Appl. Phys. 46 (2007) L49.
[145] Z. Gao, N.C. Tansil, Nucleic Acids Res. 33 (2005) e123.
[146] P. Singhal, W.G. Kuhr, Anal. Chem. 69 (1997) 4828.
[147] K. Wu, J. Fei, W. Bai, S. Hu, Anal. Bioanal. Chem. 376 (2003) 205.
[148] K. Kerman, Y. Morita, Y. Takamura, M. Ozsoz, E. Tamiya, Electroanalysis 16 (2004) 1667.
[149] K. Kerman, Y. Morita, Y. Takamura, M. Ozsoz, E. Tamiya, Anal. Bioanal. Chem. 381 (2005) 1114.
[150] S.E. Henrickson, M. Misakian, B. Robertson, J.J. Kasianowicz, Phys. Rev. Lett. 85 (2000) 3057.
[151] S. Howorka, S. Cheley, H. Bayley, Nat. Biotechnol. 19 (2001) 636.
[152] A. Meller, L. Nivon, D. Branton, Phys. Rev. Lett. 86 (2001) 3435.
[153] H. Aoki, P. Bühlmann, Y. Umezawa, Electroanalysis 12 (2000) 1272.
[154] F. Patolsky, A. Lichtenstein, I. Willner, Angew. Chem. Int. Ed. 39 (2000) 940.
[155] D.L. Graham, H.A. Ferreira, P.P. Freitas, Trends Biotechnol. 22 (2004) 455.
[156] J.C. Rife, L.J. Whitman, US Patent Application Publication 2004-0253744.
[157] S.P. Mulvaney, C.L. Cole, M.D. Kniller, M. Malito, C.R. Tamanaha, J.C. Rife, M.W. Stanton, L.J. Whitman, Biosens. Bioelectron. 23 (2007) 191.
[158] A. Merkoçi, M. Aldavert, S. Marin, S. Alegret, Trends Anal. Chem. 24 (2005) 341.
[159] H. Xu, H. Wu, F. Huang, S. Song, W. Li, Y. Cao, C. Fan, Nucleic Acids Res. 33 (2005) e83/81.
[160] M. Gabig-Ciminska, A. Holmgren, H. Andresen, K.B. Barken, M. Wümpelmann, J. Albers, R. Hintsche, A. Breitenstein, P. Neubauer, M. Los, A. Czyz, G. Wegrzyn,

G. Silfversperre, B. Jürgen, T. Schweder, S.O. Enfors, Biosens. Bioelectron. 19 (2004) 537.
[161] J.-M. Nam, S.I. Stoeva, C.A. Mirkin, J. Am. Chem. Soc. 126 (2004) 5932.
[162] D. Pioch, B. Jürgen, S. Evers, K.-H. Maurer, M. Hecker, T. Schweder, Appl. Microbiol. Biotechnol. 78 (2008) 719.
[163] P. Yakovchuk, E. Protozanova, M.D. Frank-Kamenetskii, Nucleic Acids Res. 34 (2006) 564.
[164] S. Dubus, J.-F. Gravel, B. Le Drogoff, P. Norbert, T. Veres, D. Boudreau, Anal. Chem. 78 (2006) 4457.
[165] V. Martins, L.P. Fonseca, H.A. Ferreira, D.L. Graham, P.P. Freitas, J.S. Cabral, Technical Proceedings of the 2005 NSTI-Nanotech., vol. 1, 2005, p. 493.
[166] P.P. Freitas, H. Ferreira, D. Graham, L. Clarke, M. Amaral, V. Martins, L. Fonseca, J.S. Cabral, Europhys. News 34 (2003) 224.
[167] K. Smistrup, B.G. Kjeldsen, J.L. Reimers, M. Dufva, J. Petersen, M.F. Hansen, Lab Chip 5 (2005) 1315.
[168] M. Nilsson, H. Malmgren, M. Samiotaki, M. Kwiatkowski, B.P. Chowdhari, U. Landegren, Science 265 (1994) 2085.
[169] J. Jarvius, J. Melin, J. Göransson, J. Stenberg, S. Fredriksson, C. Gonzalez-Rey, S. Bertilsson, M. Nilsson, Nat. Methods 3 (2006) 725.
[170] J. Miao, Z. Cao, Y. Zhou, C. Lau, J. Lu, Anal. Chem. 80 (2008) 1606.
[171] W.-C. Lee, K.-Y. Lien, G.-B. Lee, H.-Y. Lei, Diag. Microbiol. Infect. Dis. 60 (2008) 51.
[172] G. Zheng, F. Patolsky, Y. Cui, W.U. Wang, C.M. Lieber, Nat. Biotechnol. 23 (2005) 1294.
[173] P.P. Freitas, H.A. Ferreira, F. Cardoso, S. Cardoso, R. Ferreira, J. Almeida, A. Guedes, V. Chu, J.P. Conde, V. Martins, L. Fonseca, J.S. Cabral, J. Germano, L. Sousa, M. Piedade, B. Silva, J.M. Lemos, L.A. Clarke, M.D. Amaral, in: M.S. Pereira (Ed.), Nanotechnology and the Detection of Biomolecular Recognition Using Magnetoresistive Transducers. A Portrait of State-of-the-art Research at the Technical University of Lisbon, Springer, Dordrecht, The Netherlands, 2007, pp. 3–22.
[174] IUPAC website (http://old.iupac.org/goldbook/L03540.pdf).
[175] F. Caruso, E. Rodda, D.N. Furlong, Anal. Chem. 69 (1997) 2043.
[176] S.A. Hofstadler, R. Sampath, L.B. Blyn, M.W. Eshoo, T.A. Hall, Y. Jiang, J.J. Drader, J.C. Hannis, K.A. Sannes-Lowery, L.L. Cummins, B. Libby, D.J. Walcott, A. Schink, C. Massire, R. Ranken, J. Gutierrez, S. Manalili, C. Ivy, R. Melton, H. Levene, G. Barrett-Wilt, F. Li, V. Zapp, N. White, V. Samant, J.A. McNeil, D. Knize, D. Robbins, K. Rudnick, A. Desai, E. Moradi, D.J. Ecker, Int. J. Mass Spectrom. 242 (2005) 23.
[177] D.C. Muddiman, G.A. Anderson, S.A. Hofstadler, R.D. Smith, Anal. Chem. 69 (1997) 1543.
[178] R. Sampath, S.A. Hofstadler, L. Blyn, M. Eshoo, T. Hall, C. Massire, H. Levene, J. Hannis, P.M. Harrell, B. Neuman, M.J. Buchmeier, Y. Jiang, R. Ranken, J. Drader, V. Samant, R.H. Griffey, J.A. McNeil, S.T. Crooke, D.J. Ecker, Emerg. Infect. Dis. 11 (2005) 373.
[179] R. Sampath, K.L. Russell, C. Massire, M.W. Eshoo, V. Harpin, L.B. Blyn, R. Melton, C. Ivy, T. Pennella, F. Li, H. Levene, T.A. Hall, B. Libby, N. Fan, D.J. Walcott, R. Ranken, M. Pear, A. Schink, J. Gutierrez, J. Drader, D. Moore, D. Metzgar, L. Addington, R. Rothman, C.A. Gaydos, S. Yang, K.S. George, M.E. Fuschino, A.B. Dean, D.E. Stallknecht, G. Goekjian, S. Yingst, M. Monteville, M.D. Saad, C.A. Whitehouse, C. Baldwin, K.H. Rudnick, S.A. Hofstadler, S.M. Lemon, D.J. Ecker, PLoS ONE 2 (2007) e489.
[180] F.R.R. Teles, D.M.F. Prazeres, J.L. Lima-Filho, Rev. Med. Virol. 15 (2005) 287.
[181] K.M. Black, N. Vats, Analyst 132 (2007) 1183.
[182] M.A. Dineva, L. Mahilum-Tapay, H. Lee, Analyst 132 (2007) 1193.
[183] M.J. Wolcott, Clin. Microbiol. Rev. 5 (1992) 370.
[184] P. Fortina, S. Surrey, L.J. Kricka, Trends Mol. Med. 8 (2002) 264.
[185] R.H.P. Peters, M.A. van Agtmael, S.A. Danner, P.H.M. Savelkoul, C.M.J.E. Vandenbroucke-Grauls, Lancet Infect. Dis. 4 (2004) 751.
[186] D. Griffiths, G. Hall, Trends Biotechnol. 11 (1993) 122.
[187] K. Cammann, U. Lemke, A. Rohen, J. Sander, H. Wilken, B. Winter, Angew. Chem. Int. Ed. 30 (1991) 516.
[188] S. Andreescu, O.A. Sadik, Pure Appl. Chem. 76 (2004) 861.
[189] J. Suter, M. White, H. Zhu, H. Shi, C.W. Caldwell, X. Fan, Biosens. Bioelectron. 23 (2008) 1003.
[190] M. Piliarik, H. Vaisocherová, J. Homila, Sens. Actuator B 121 (2007) 187.
[191] T. Endo, K. Kerman, N. Nagati, Y. Takamura, E. Tamiya, Anal. Chem. 77 (2005) 6976.
[192] F. Zezza, M. Pascale, G. Mule, A. Visconti, J. Microbiol. Methods 66 (2006) 529.
[193] S. Sawata, E. Kai, K. Ikebukuro, T. Iida, T. Honda, I. Karube, Biosens. Bioelectron. 14 (1999) 397.
[194] J. Zhang, H. Qi, Y. Li, J. Yang, Q. Gao, C. Zhang, Anal. Chem. 80 (2008) 2888.
[195] M. Cunha, D.L. Stokes, G.D. Griffin, T. Vo-Dinh, Biosens. Bioelectron. 19 (2004) 1007.
[196] T.H. Wang, S. Masset, C.M. Ho, 14th IEEE International Conference on Microelectro-Mechanical Systems, Technical Digest (MEMS 2001), 2001, p. 431.
[197] J. Li, W. Tan, K. Wang, D. Xiao, X. Yang, X. He, Z. Tang, Anal. Sci. 28 (2000) 3011.
[198] Q. Wang, X. Yang, K. Wang, Sens. Actuator B 123 (2007) 227.
[199] Y. Sato, A. Okumura, K. Suzuki, H. Kawaguchi, J. Biomater. Sci. Polym. Ed. 15 (2004) 297.
[200] K.S. Rao, S.U. Rani, D.K. Charyulu, K.N. Kumar, B.-K. Lee, H.-Y. Lee, Y. Kawai, Anal. Chim. Acta 576 (2006) 177.
[201] D. Caputo, G. de Cesare, A. Nascetti, R. Negri, J. Non-Cryst. Solids 352 (2006) 2004.
[202] F. Kleinjung, F.F. Bier, A. Warsinke, F.W. Seheller, Anal. Chim. Acta 350 (1997) 51.
[203] B.G. Healey, R.S. Matson, D.R. Walt, Anal. Biochem. 251 (1997) 270.
[204] A.J. Baeumner, R.N. Cohen, V. Miksic, J.H. Min, Biosens. Bioelectron. 18 (2003) 405.
[205] E.L. McCarthy, L.E. Bickerstaff, M.P. da Cunha, P.J. Millard, Biosens. Bioelectron. 22 (2007) 1236.
[206] D.F. Yao, F. Yu, J.Y. Kim, J. Scholz, P.E. Nielsen, E.K. Sinner, W. Knoll, Nucleic Acids Res. 32 (2004) e177.
[207] S.H. Chen, V.C.H. Wu, Y.C. Chuang, C.S. Lin, J. Microbiol. Methods 73 (2008) 7.
[208] M. Lazerges, H. Perrot, N. Zeghib, E. Antoine, C. Compere, Sens. Actuator B 120 (2006) 329.
[209] L. Nicu, M. Guirardel, F. Chambosse, P. Rougerie, S. Sinh, E. Trevisiol, J.M. Francois, J.P. Maioral, A.M. Caminade, E. Cattan, C. Bergaud, Sens. Actuator B 110 (2005) 125.
[210] V.C.H. Wu, S.H. Chen, C.S. Lin, Biosens. Bioelectron. 22 (2007) 2967.
[211] F. Mannelli, A. Minunni, S. Tombelli, R.H. Wang, M.M. Spiriti, M. Mascini, Bioelectrochemistry 66 (2005) 129.
[212] P. Skladal, C.D. Riccardi, H. Yamanaka, P.I. da Costa, J. Virol. Methods 117 (2004) 145.
[213] Y. Roh, J. Woo, Y. Hur, Y.E. Pak, Smart Structures and Materials 2005: Smart Electronics, MEMS, BIOMEMS, and Nanotechnology Conference, Proceedings of the Society of Photo-Optical Instrumentation Engineers (SPIE) 5763 (2005) 291.
[214] Y. Hur, J. Han, J. Seon, Y.E. Park, Y. Roh, Sens. Actuator A 120 (2005) 462.
[215] M. Duman, R. Saber, E. Piskin, Biosens. Bioelectron. 18 (2003) 1355.
[216] A. Bouchet, C. Chaix, C.A. Marquette, L.J. Blumb, B. Mandrand, Biosens. Bioelectron. 23 (2007) 735.
[217] K. Arora, N. Prabhakar, S. Chand, B.D. Malhotra, Sens. Actuator B 126 (2007) 655.
[218] Y. Xiao, A.A. Lubin, B.R. Baker, K.W. Plaxco, A.J. Heeger, Proceedings of the National Academy of Sciences of the USA 103, 2006, p. 16677.
[219] H. Korri-Youssoufi, A. Yassar, Biomacromolecules 2 (2001) 58.
[220] C.D.S. Riccardi, C. Kranz, J. Kowalik, H. Yamanaka, B. Mizaikoff, M. Josowicz, Anal. Chem. 80 (2008) 237.
[221] M. Mascini, M. Del Carlo, M. Minunni, B.N. Chen, D. Compagnone, Bioelectrochemistry 67 (2005) 163.
[222] J. Koehne, H. Chen, J. Li, A.M. Cassell, Q. Ye, H.T. Ng, J. Han, M. Meyyappan, Nanotechnology 14 (2003) 1239.
[223] G.J. Zhang, J.H. Chua, R.-E. Chee, A. Agarwal, S.M. Wong, K.D. Buddharaju, N. Balasubramanian, Biosens. Bioelectron. 23 (2008) 1701.
[224] Y. Fu, R. Yuan, Y. Chai, L. Zhou, Y. Zhang, Anal. Lett. 39 (2006) 467.
[225] F. Fu, R. Yuan, L. Xu, Y. Chai, X. Zhang, D. Tang, Biochem. Eng. J. 23 (2005) 37.
[226] Y. Fu, R. Yuan, L. Xu, Y. Chai, Y. Liu, D. Tang, Y. Zhang, J. Biochem. Biophys. Methods 62 (2005) 163.
[227] H. Berney, J. West, E. Haefele, J. Alderman, W. Lane, J.K. Collins, Sens. Actuator B 68 (2000) 100.
[228] T. Hianik, M. Fajkus, B. Sivak, I. Rosenberg, P. Kois, J. Wang, Electroanalysis 12 (2000) 495.
[229] M. Kamahori, Y. Ishige, M. Shimoda, Biosens. Bioelectron. 23 (2008) 1046.
[230] Z.Q. Gao, A. Agarwal, A.D. Trigg, N. Singh, C. Fang, C.H. Tung, Y. Fan, K.D. Buddharaju, J. Kong, Anal. Chem. 79 (2007) 3291.
[231] M. Díaz-González, A. Escosura-Muñiz, M.B. González-García, A. Costa-Garcia, Biosens. Bioelectron. 23 (2008) 1340.
[232] P. Abad-Valle, M.T. Fernandez-Abedul, A. Costa-Garcia, Biosens. Bioelectron. 20 (2005) 2251.
[233] G. Carpini, F. Lucarelli, G. Marrazza, M. Mascini, Biosens. Bioelectron. 20 (2004) 167.
[234] D.K. Xu, K. Huang, Z.H. Liu, Y.Q. Liu, L.R. Ma, Electroanalysis 13 (2001) 882.
[235] R. Miranda-Castro, P. De-Los-Santos-Alvarez, M.J. Lobo-Castanon, A.J. Miranda-Ordieres, P. Tunon-Blanco, Anal. Chem. 79 (2007) 4050.
[236] F. Lucarelli, G. Marrazza, M. Mascini, Biosens. Bioelectron. 20 (2005) 2001.
[237] F. Patolsky, A. Lichtenstein, I. Willner, Chem. A Euro. J. 9 (2003) 1137.
[238] X. Mao, J. Jiang, X. Xu, X. Chu, Y. Luo, G. Shen, R. Yu, Biosens. Bioelectron. 23 (2008) 1555.
[239] Y.C. Zhang, H.H. Kim, A. Heller, Anal. Chem. 75 (2003) 3267.
[240] M.J. LaGier, J.W. Fell, K.D. Goodwin, Mar. Pollut. Bull. 54 (2007) 757.
[241] S. Suye, T. Matsuura, T. Kimura, H. Zheng, T. hori, Y. Amano, H. Katavama, Microelectron. Eng. 81 (2005) 441.
[242] H. Xie, C.Y. Zhang, Z.Q. Gao, Anal. Chem. 76 (2004) 1611.
[243] M.I. Pividori, A. Merkoci, S. Alegret, Biosens. Bioelectron. 19 (2003) 473.
[244] X.Y. Du, M.Q. Wang, L.Y. Liu, W.L. Gonga, B.Z. Wang, Sensor Lett. 6 (2008) 226.
[245] C. Jiang, T. Yang, K. Jiao, H. Gao, Electrochim. Acta 53 (2008) 2917.
[246] Z. Chang, H. Pan, K. Zhao, K.M. Chen, P. He, Y. Fang, Electroanalysis 20 (2008) 131.
[247] K. Arora, N. Prabhakar, S. Chand, B.D. Malhotra, Biosens. Bioelectron. 23 (2007) 613.
[248] I.O. K'Owino, S.K. Mwilu, O.A. Sadik, Anal. Biochem. 369 (2007) 8.
[249] M. Revenga-Parra, T. Garcia, E. Lorenzo, F. Pariente, Biosens. Bioelectron. 22 (2008) 2675.
[250] X.-H. Lin, P. Wu, W. Chen, Y.-F. Zhang, X.-H. Xia, Talanta 72 (2007) 468.
[251] H. Peng, C. Soeller, J. Travas-Sejdic, Macromolecules 40 (2007) 909.
[252] N.N. Zhu, Z. Chang, P.G. He, Y.Z. Fang, Anal. Chim. Acta 545 (2005) 21.

[253] N.N. Zhu, A.P. Zhang, Q.J. Wang, P.G. He, Y.Z. Fang, Electroanalysis 16 (2004) 577.
[254] H. Aoki, Y. Umezawa, Electroanalysis 14 (2002) 1405.
[255] F. Yan, A. Erdem, B. Meric, K. Kerman, M. Ozsoz, O.A. Sadik, Electrochem. Commun. 3 (2001) 224.
[256] H. Cai, C. Xu, P. He, Y. Fang, J. Electroanal. Chem. 510 (2001) 78.
[257] M. Ozsoz, A. Erdem, K. Kerman, D. Ozkan, B. Tugrul, N. Topcuoglu, H. Ekren, M. Taylan, Anal. Chem. 75 (2003) 2181.
[258] D. Dell'Atti, M. Zavaglia, S. Tombelli, G. Bertacca, A.O. Cavazzana, G. Bevilacqua, M. Minunni, M. Mascini, Anal. Chem. 383 (2007) 140.
[259] C.A. Marquette, D. Thomas, A. Degiuli, L.J. Blum, Anal. Bioanal. Chem. 377 (2003) 922.
[260] S.A.M. Martins, G.A. Monteiro, L.P. Fonseca, D.M.F. Prazeres, Anal. Bioanal. Chem. 391 (2008) 2179.
[261] K. Kerman, Y. Matsubara, Y. Morita, Y. Takamura, E. Tamiya, Sci. Technol. Adv. Mater. 5 (2004) 351.
[262] J. Wang, G.D. Liu, R. Polsky, A. Merkoci, Electrochem. Commun. 4 (2002)722.
[263] A. Erdem, D.O. Ariksoysal, H. Karadeniz, P. Kara, A. Sengonul, A.A. Saviner, M. Ozsoz, Electrochem. Commun. 7 (2005) 815.
[264] V.C. Martins, F.A. Cardoso, J. Loureiro, M. Mercier, J. Germano, S. Cardoso, R. Ferreira, L.P. Fonseca, L. Sousa, M.S. Piedade, P.P. Freitas, in: Proceedings of the Biomagnetism and Magnetic Biosystems Based on Molecular Recognition Processes, San Feliu de Guixols, Spain, September 22–27, AIP Conference Proceedings 1025 (2008) 150.

Talanta 77 (2008) 514–517

Contents lists available at ScienceDirect

Talanta

journal homepage: www.elsevier.com/locate/talanta

Analysis of antioxidants by microchip capillary electrophoresis with chemiluminescence detection based on luminol reaction

Kazuhiko Tsukagoshi*, Takahiro Saito, Riichiro Nakajima

Department of Chemical Engineering and Materials Science, Faculty of Engineering, Doshisha University, Kyotanabe 610-0321, Japan

ARTICLE INFO

Article history:
Received 12 September 2007
Received in revised form 11 March 2008
Accepted 17 March 2008
Available online 26 March 2008

Keywords:
Microchip
Capillary electrophoresis
Chemiluminescence
Luminol
Antioxidant

ABSTRACT

A microchip including two micro-channels for electrophoretic flow and one micro-flow line for pumping flow was designed for the analysis of antioxidants by microchip capillary electrophoresis with a chemiluminescence detection system. The chemiluminescence reaction of luminol with hydrogen peroxide in the presence of Cu(II) catalyst was adopted in the present system, where active oxygen species, such as superoxide radical anions, generates. Nitroblue tetrazolium, superoxide dismutase, and catechin (catechin mixture from green tea) were analyzed as model analytes of antioxidants using the system. Negative peaks from baseline formed by the chemiluminescence reaction were observed based on reaction between active oxygen (superoxide radical anion) and antioxidants (analytes). The components of analytes mixture, nitroblue tetrazolium and superoxide dismutase, were well separated and detected within *ca.* 2 min. Catechin was also detected around 2 min, resulting in a response curve over the range of 0.1–1 mM. The amounts of catechin in the real samples of commercial green tea beverages were successfully determined.

1. Introduction

Capillary electrophoresis (CE) equipped with chemiluminescence (CL) detection has attracted a great attention as a high-performance analytical system for separation and detection of various kinds of analytes [1–5]. A CE with CL detection system was also integrated on a microchip; it is called microchip capillary electrophoresis with a chemiluminescence detection system [6,7]. This is matched to the concept of a micro-total analysis system (μ-TAS) or a lab-on-a-chip in comparison with fluorometry and spectrometry, because there is no light source or spectroscopy in CL detection. Other researchers also reported interesting microchip CE with CL detection systems. For example, Su et al. [8] developed and evaluated a glass electrophoresis microchip with an integrated flow-type CL detection cell. The chip has double-T-type electrophoretic sample injection and separation combined with a Y-type CL detector. Liu et al. [9] demonstrated chiral recognition using microchip electrophoresis coupled with CL detection; hydroxypropyl-β-cyclodextrin was chosen as an effective enantiomer selector to resolve chiral dansyl amino acids. Furthermore, in 2005 we successfully combined the microchip CE with CL detection system with an immunoassay using antibody-immobilized glass beads. A specific protein in human serum, a cancer marker, was analyzed by immune reaction, electrophoresis, and CL detection on the microchip within *ca.* 2 min [10]. We have been planning new applications of microchip CE with CL detection system.

Active oxygen and antioxidants are interesting from the point of view of not only specific chemical species in chemical reactions but also medical science with regard to disease factors, maintenance of health, and aging. As most of these species are related to CL reactions, they can be analyzed by CL analysis, *e.g.*, flow injection analysis [11–14], sequential injection analysis [15], liquid chromatography [16], CE [17], and microfluidic system [18]. In this study, we propose the analysis of antioxidants using a microchip CE with CL detection system based on the luminol reaction, taking advantage of the decrease in CL in the presence of antioxidants. That is, the suppression of CL from luminol in the presence of antioxidants to superoxide radical anions was, for the first time, introduced into the microchip CE with CL detection system as a principle for antioxidant detection. Antioxidant analytes showed negative peaks due to the quenching effect.

2. Experimental

2.1. Reagents

Water was purified by using a Millipore Elix 3 UV system (Millipore, Tokyo, Japan) for use. All reagents used were of commercially available special grade. They were purchased from the following sources: luminol, copper(II) sulfate, and nitroblue tetrazolium were from Nacalai Tesque (Kyoto, Japan); superoxide dismutase, catechin (catechin mixture from green tea), and hydrogen peroxide (30 wt.%)

* Corresponding author. Tel.: +81 774 65 6595; fax: +81 774 65 6803.
E-mail address: ktsukago@mail.doshisha.ac.jp (K. Tsukagoshi).

0039-9140/$ – see front matter © 2008 Elsevier B.V. All rights reserved.
doi:10.1016/j.talanta.2008.03.026

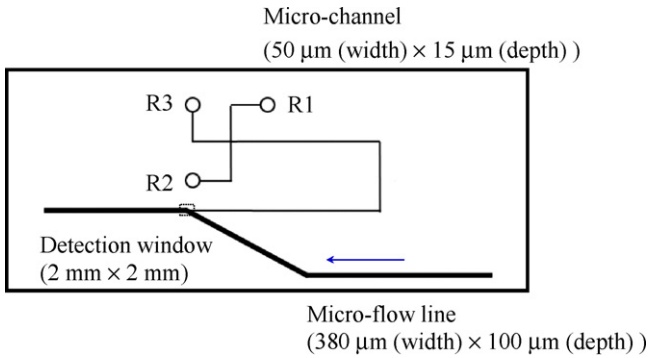

Fig. 1. Conceptual layout of the microchip. R1, analyte solution; R2 and R3, running buffers; and micro-flow line, reagent solution containing hydrogen peroxide.

were from Wako pure Chemical (Osaka, Japan). Three commercial green teas were also used: we called them A, B, and C, respectively, in this study.

2.2. Microchip

The conceptual layout of the microchip is shown in Fig. 1; it was made to order (Institute of Microchemical Technology, Kawasaki, Japan). The microchip was made of quartz glass and included two micro-channels (15 μm in depth and 50 μm in width) that crossed at the intersection. Three ends of the micro-channels accessed the reservoirs, R1–R3, which were holes of 2 mm in diameter. R1–R3 were located 10 mm from the intersection. The other end of the micro-channels was combined with a micro-flow line, *i.e.*, reagent flow line (100 μm in depth and 380 μm in width) as shown in Fig. 1. The detection window (2 mm × 2 mm) was made at the connecting point to the reagent line with black tape. The distance from the intersection to the detection window was 55 mm.

2.3. Analytical conditions and procedures

The microchip was set in a microchip-holder as shown in Fig. 2; the microchip was pinched between the upper and lower holders tightly through the four screws in order not to release solutions from connecting points between micro-channels and PEEK tubes. We have reported many papers concerning CE with CL detection systems including microchip CE with CL detection systems, more than *ca.* 50 papers. Analytical conditions in the present study were decided with reference to those reported in our previous papers [1,2,4,6,7,10,17], together with the results obtained in preliminary experiment of Section 3.1. The running buffer was prepared by dissolving 0.5 mM luminol, 0.1 mM Cu(II) (as copper(II) sulfate), and 20 mM potassium sodium tartrate in 20 mM carbonate buffer (pH 10.8). The sample solutions of antioxidants were prepared by

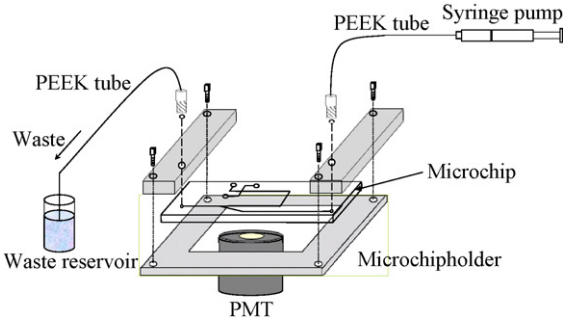

Fig. 2. Schematic diagram of the microchip and its surrounding equipment.

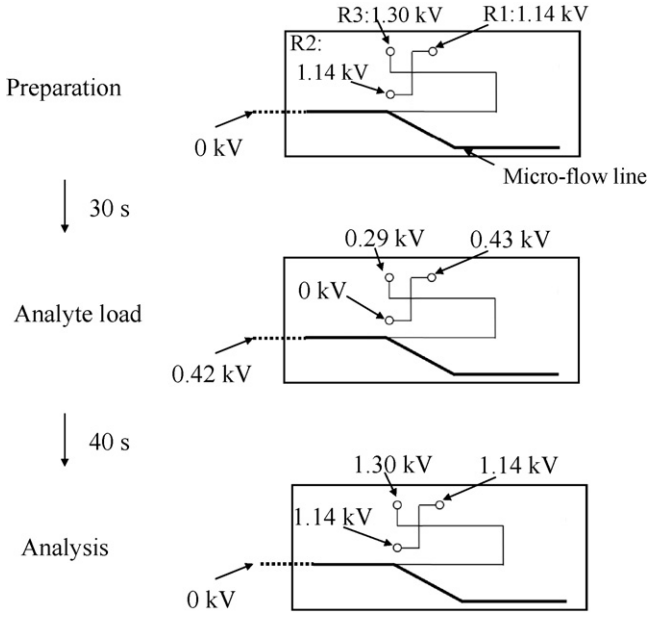

Fig. 3. Applied voltages.

dissolving antioxidants with 20 mM carbonate buffer (pH 10.8). The analyte solution was placed in R1 with the running buffers placed in R2 and R3. In addition, the micro-channels were filled with the running buffers. The reagent solution, 20 mM carbonate buffer (pH 10.8) containing 10 mM hydrogen peroxide, was fed into the micro-flow line by a micro-syringe pump at a flow rate of 0.5 μl min^{-1}, and then wasted in the vessel (5 ml volume) through a PEEK (polyetheretherketone) tube (260 μm i.d., 20 cm in length). Micro-syringe pump (MF-9090; Bioanalytical Systems, Indiana, USA) was used here; the flow rate was adjusted by the controller.

High voltages were applied to R1–R3 and the vessel as shown in Fig. 3 (preparation-analyte load-analysis). The high voltage equipment and the control were carried out by use of the related devices that were included in microchip capillary electrophoresis instrument (MCE 2010, Shimadzu Co. Ltd., Kyoto Japan). The running buffer was delivered electrophoretically into the separation channel through the preparation procedure. Next, in the analyte load procedure, the analyte solution was fed toward the intersection part. After the intersection part was filled with the analyte solution, the applied voltages were changed to the analysis procedure, leading to sample plug formation, component separation, and CL detection.

The CL in the detection window was detected with a photomultiplier tube (PM) (H6780; Hamamatsu Photonics Co. Ltd., Shizuoka, Japan). The baseline CL was formed based on the CL reaction of luminol with hydrogen peroxide in the presence of Cu(II) catalyst. The analytes, antioxidants, that migrated electrophoretically in the micro-channel were mixed with active oxygen generated with the reaction between hydrogen peroxide and Cu(II) catalyst in the detection area, leading to negative CL peak from the baseline.

3. Results and discussion

3.1. Detection of luminol on a microchip as a preliminary experiment

First, the CL that was generated with the reaction of luminol with hydrogen peroxide in the presence of Cu(II) catalyst was

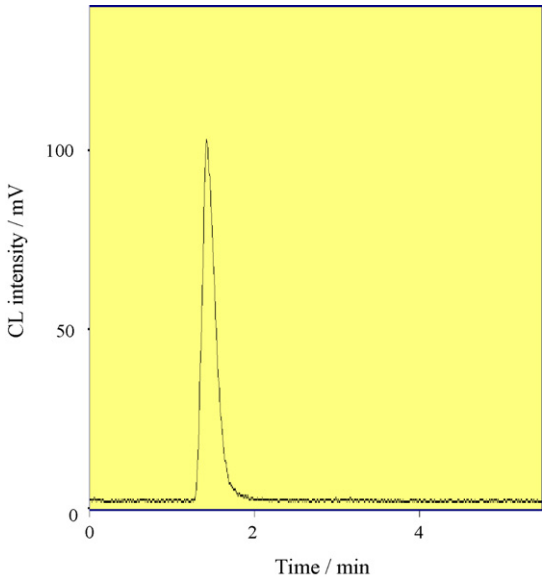

Fig. 4. Electropherogram of luminol. Conditions: running buffer, 20 mM carbonate buffer (pH 10.8) containing 0.1 mM Cu(II) and 20 mM potassium sodium tartrate; micro-flow line, 20 mM carbonate buffer (pH 10.8) containing 10 mM hydrogen peroxide at a flow rate of 0.5 μl min^{-1}; and analyte, 0.5 mM luminol.

confirmed on the microchip as follows. The running buffer was prepared by removing luminol from the running buffer described in the experimental section. Luminol solution was prepared by dissolving luminol in 20 mM carbonate buffer (pH 10.8) to give the analyte solution. Hydrogen peroxide solution was fed into the micro-flow line. The analyte solution of luminol was placed in R1, and analyzed using analytical procedures similar to those described in the experimental section. The obtained electropherogram of 0.5 mM luminol is shown in Fig. 4; the detailed analytical conditions are given in the figure caption. Luminol was detected at *ca.* 1.5 min with good reproducibility of CL intensities and migration times (RSD for both were less than 5%, $n = 7–10$). The analytical conditions for luminol detection, including reagent concentrations and flow rate, were taken into consideration for developing the present microchip CE–CL detection system for antioxidants analyses.

3.2. Separation and detection of antioxidants

The reaction between hydrogen peroxide and Cu(II) generates active oxygen species, such as superoxide radical anions. Nitroblue tetrazolium and sodium dismutase are well known as typical antioxidants or active oxygen trappers against superoxide radical anions. Analyte solutions of nitroblue tetrazolium, superoxide dismutase, and the mixture of nitroblue tetrazolium and superoxide dismutase were used as model analytes in analysis with the present microchip CE with CL detection system. Fig. 5 shows the corresponding electropherograms of the above analytes. The negative CL peaks from the baseline formed by the CL reaction of luminol with hydrogen peroxide in the presence of Cu(II) catalyst were observed based on the reaction between the antioxidants (analytes) and the active oxygen (superoxide radical anion). The negative CL peaks responded over the range of 0.1–1 mM nitroblue tetrazolium with the detection limit of 0.1 mM (S/N = 3) and 0.05–1 mM sodium dismutase with the detection limit of 0.05 mM (S/N = 3). The components of the mixture analyte, nitroblue tetrazolium and superoxide dismutase, were well separated and detected within *ca.* 2 min. Their CL peaks were identified from the detection time of each single CL peak obtained with each single analyte solution.

3.3. Catechin analysis

In addition, we examined catechin (catechin mixture from green tea) using the present system. Catechin is a well-known antioxidant; it is one of the polyphenol derivatives that react with radical species, such as hydroxyl radicals and superoxide radical anions. The most included species of catechin in green tea is epigallocatechin gallate, and it is usually included more than 40% to the total catechin amounts. Although the catechin mixture from green tea was not separated by the present system under the conditions used, the negative CL peak was observed on the electropherogram around 2 min.

Tentatively, we tried to estimate the total amounts of catechin in commercial green tea beverages using the present microchip CE–CL detection system. First, the relationship between the catechin concentration of the above catechin mixture from green tea and the percentage inhibition due to the negative CL peak was examined. The molecular weight of epigallocatechin gallate (458.37) was used

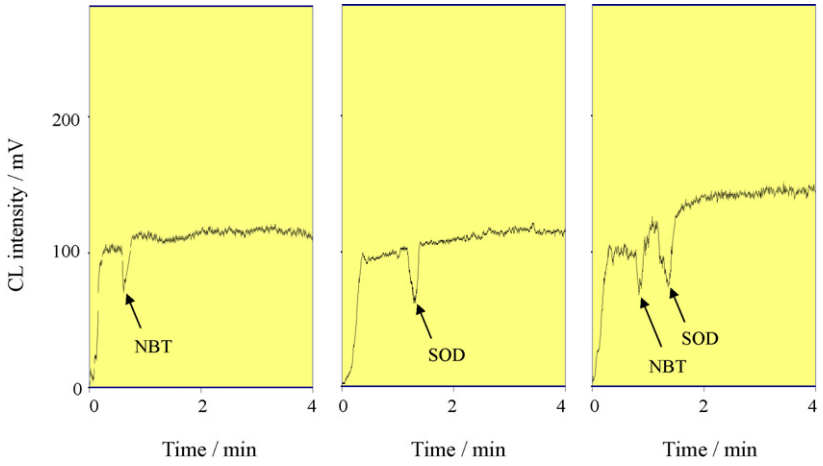

Fig. 5. Electropherograms of 1 mM nitroblue tetrazolium (NBT), 1 mM superoxide dismutase (SOD), and their mixture solution. Conditions: running buffer, 20 mM carbonate buffer (pH 10.8) containing 0.5 mM luminol, 0.1 mM Cu(II), and 20 mM potassium sodium tartrate; micro-flow line, 20 mM carbonate buffer (pH 10.8) containing 10 mM hydrogen peroxide at a flow rate of 0.5 μl min^{-1}; and analyte, 1 mM each.

as that of the mixture. The negative CL peak responded over the range of 0.1–1 mM catechin with the detection limit of 0.1 mM (S/N = 3). The linear relationship was observed for the concentration range of 0.1–0.5 mM (correlation coefficient, 0.999). Such a comparatively narrow responding range might be attributed to the detection principle based on negative peak formation from the baseline that shows high CL intensity. Ten-fold-diluted commercial green tea beverages were analyzed using this system. Negative CL peaks were also observed on the electropherograms at elution times of *ca.* 2 min. By use of the above-mentioned calibration curve, the commercial green teas, A, B, and C, were found to include catechin at concentrations of 510, 220, and 150 μM, (average values from 4–7 measurements), respectively. The data obtained with the present method were consistent with the manufacturers' reported catechin concentrations for A and C (530 and 170 μM, respectively; the concentration of catechin in B has not been reported).

4. Conclusion

The microchip CE with CL detection system is well known as one of the most interesting μ-TAS or a lab-on-a-chip devices; the range of its use must be increased in various ways. In this study, we introduced, for the first time, the suppression of CL from luminol in the presence of antioxidants into the microchip CE with CL detection system as a principle of antioxidant detection. Active oxygen and antioxidants are interesting from the point of view of specific chemical species as well as medical science. Several model antioxidants were subjected to the present microchip CE with CL detection system. They were analyzed showing the negative CL peaks on the electropherograms based on the interaction between active oxygen and antioxidants.

Acknowledgments

This work was supported by a Grant-in-Aid for Scientific Research (C) from the Ministry of Education, Culture, Sports, Science, and Technology, Japan. This study was also supported by the Academic Frontier Research Project on "New Frontier of Biomedical Engineering Research" of the Ministry of Education, Culture, Sports, Science, and Technology, Japan.

References

[1] K. Tsukagoshi, T. Nakamura, R. Nakajima, Anal. Chem. 74 (2002) 4109.
[2] K. Tsukagoshi, K. Nakahama, R. Nakajima, Anal. Chem. 76 (2004) 4410.
[3] J. Yuan, T. Li, X.-B. Yin, X. Jiang, W. Jin, X. Yang, E. Wang, Anal. Chem. 78 (2006) 2934.
[4] K. Tsukagoshi, K. Kyohei, F. Ueno, K. Noda, R. Nakajima, K. Araki, J. Chromatogr. A 1123 (2006) 106.
[5] J.C. Dumke, M.A. Nussbaum, Anal. Chem. 79 (2007) 1262.
[6] M. Hashimoto, K. Tsukagoshi, R. Nakajima, K. Kondo, Chem. Lett. (1999) 781.
[7] M. Hashimoto, K. Tsukagoshi, R. Nakajima, K. Kondo, A. Arai, J. Chromatogr. A 867 (2000) 271.
[8] R. Su, J.-M. Lin, K. Uchiyama, M. Yamada, Talanta 64 (2004) 1024.
[9] B.F. Liu, M. Ozaki, N. Matsubara, Y. Utsumi, T. Hattori, S. Terabe, Chromatogr. 23 (2002) 5.
[10] K. Tsukagoshi, N. Jinno, R. Nakajima, Anal. Chem. 77 (2005) 1684.
[11] A. Miyamoto, K. Nakamura, N. Kishikawa, Y. Ohba, K. Nakashima, N. Kuroda Naotaka, Anal. Bioanal. Chem. 388 (2007) 1809.
[12] L.M. Magalhaes, M.A. Segundo, S. Reis, J.L.F.C. Lima, J.M. Estela, V. Cerda, Anal. Chem. 79 (2007) 3933.
[13] D.L. Giokas, A.G. Vlessidis, N.P. Evmiridis, Anal. Chem. Acta 589 (2007) 59.
[14] M. Sariahmetoglu, R.A. Wheatley, I. Cakici, I. Kanzik, A. Townshend, Anal. Lett. 36 (2003) 749.
[15] K. Nakamura, Y. Ohba, N. Kishikawa, N. Kuroda, Naotaka, Bunsebi Kagaku 53 (2004) 925.
[16] T. Toyo'oka, T. Kashiwazaki, M. Kato, Talanta 60 (2003) 467.
[17] K. Tsukagoshi, T. Taniguchi, R. Nakajima, Anal. Chim. Acta 589 (2007) 66.
[18] M. Amatatongchai, O. Hofmann, D. Nacapricha, O. Chailapakul, A.J. de Mello, Anal. Bioanal. Chem. 387 (2007) 277.

Talanta 77 (2008) 839–843

Contents lists available at ScienceDirect

Talanta

journal homepage: www.elsevier.com/locate/talanta

Magnetic beads-based immunoassay as a sensitive alternative for atrazine analysis

Madalina Tudorache*, Anca Tencaliec, Camelia Bala

Laboratory of Quality Control and Process Monitoring, Department of Analytical Chemistry, University of Bucharest, 4-12 Regina Elisabeta, 030018 Bucharest, Romania

ARTICLE INFO

Article history:
Received 15 January 2008
Received in revised form 6 June 2008
Accepted 23 July 2008
Available online 31 July 2008

Keywords:
Immunoassay
Magnetic beads
Atrazine
Pesticides
Sensitivity
Hook effect

ABSTRACT

A new immunoassay strategy for sensitive atrazine determination based on magnetic beads is reported. The immuno-method is a competitive solid-phase immunoassay where the anti-atrazine antibody is immobilized on the magnetic beads surface and fixed at the reaction cell bottom using a simple magnet, which generates a magnetic field. Analyte and HRP (horseradish peroxidase) tracer compete for active sites of antibody. After the immunointeractions antibody-analyte and antibody-tracer, atrazine quantification from the sample is performed by injection of the chemiluminescence substrate (luminol, hydrogen peroxide and *p*-iodophenol). Different antibodies (polyIgG anti-atrazine Ab I and affinity purified polyIgG anti-atrazine AbI) were tested in this configuration. Also, optimum concentration of antibody-covered magnetic beads was set up (8 mg/l Ab II). Finally, the performance of magnetic beads-based immunoassay for atrazine determination was evaluated demonstrating that the magnetic beads-based immunoassay is one of the most sensitive method for atrazine determination (LoD = 3 pg/l, IC_{50} = 37 pg/l, DR = 10–1000 pg/l).

1. Introduction

Currently environmental immunoassay are facing an important diversification after an exponential development in the nineties [1]. Most of the papers published today in this field report new configurations of immunoassay dedicated to well-known pollutants, e.g. triazines (atrazine, simazine, propazine), coplanar polychlorinated biphenyls (PCBs), polycyclic aromatic hydrocarbons (PAHs), dioxins, trinitrotoluenes, etc. These new environmental immunoassays represent a valuable supplement to existing immunoassay techniques, since they are characterized by improved functional features such as high sensitivity and selectivity, rapid detection, simple analysis procedure and/or low influence of the effects of the matrix samples [2–4]. Triazines can be detected using an electrochemical/chemiluminescence competitive immuno strategy based on magnetic beads (LoD = 6 ppt and 12.90 ppn, respectively) [5,6], a lateral-flow-based dipstick immunoassay format with hapten-protein-gold conjugate (LoD = 1 ppb) [7] or an impedimetric immunosensor using interdigitated μ-electrodes (LoD = 8.34 ppb) [8]. Also, the PCBs can be monitored with a disposable immunomagnetic electrochemical sensor (LoD = 400 ppt) [9], while magnetic beads bioelectrochemical immunosystem have been developed for PAHs determination (LoD = 50 ppt) [10]. As it can be observed, most of these analysis methods are from the same immunoassay group called magnetic particles-based immunoassay, which represents a substantial evolution of the immunoassay technique in the last few years.

Magnetic particles-based immunoassay is a relatively new immunoassay configuration where the magnetic particles are the carriers/label of the biomolecules (antibodies). Magnetic particles as immobilizing materials are of great interest in the pursuit of increased stability of the surface-bound antibody, improved orientation of the immobilized antibody as well as increase in the protein loading [11]. Also, other advantages are more specific surface area obtained for the binding of larger amounts of biomolecules, lower mass transfer resistance, selective separation of the immobilized biomolecules from a reaction mixture by simple application of a magnetic field and/or sensitive detection based on variation of the magnetic permeability of superparamagnetic particles [12–15]. Magnetic particles are micro/nano-sized spheres of iron oxide (Fe_3O_4 or γ-Fe_2O_3) covered with a polymeric material which allows to attach, covalently/physically, usually the antibody onto the particle surface. Recently, the particles size was reduced from micro- to nano-scale, improving the possibility of handling the particles in suspension (avoiding the self-aggregation of magnetic

* Corresponding author at: Laboratory of Quality Control and Process Monitoring, Faculty of Chemistry, University of Bucharest, 4-12 Boulevard Regina Elisabeta, 030018 Bucharest-3, Romania. Fax: +40 21 4104888.
E-mail addresses: m.sandulescu@chem.unibuc.ro, madalina.sandulescu@gmail.com (M. Tudorache).

0039-9140/$ – see front matter © 2008 Published by Elsevier B.V.
doi:10.1016/j.talanta.2008.07.040

particles!) [16]. Despite of their name *magnetic particles*, many of the commercial beads are superparamagnetic, meaning that these can immediately be magnetised with an external magnetic field and resuspended immediately once the magnet is removed. There are many applications of this technique especially in the environmental analysis area, and the number of paper are still growing, demonstrating the current interest of the scientists in this area [5,9,10,17–24].

In this paper, we report a new format of magnetic particles-based immunoassay dedicated to atrazine determination. The method principle is similar with solid-phase competitive immunoassay using chemiluminescence detection and performed in a flow injection system. The antibody is directly immobilized on the magnetic beads surface and the obtained bioactive material is placed and kept in a reaction cell using a simple magnet, which generates a magnetic field strong enough to manipulate the antibody-coated particles. Samples containing the analyte and the enzyme tracer are added in the reaction cell, successively. Both of them compete for the same antibody active sites. After the immunoreaction antibody-analyte and antibody-tracer, the excess of analyte and tracer are removed by washing the reaction cell. Finally, specific enzyme substrate composed by luminol, hydrogen peroxide and *p*-iodophenol, is injected into the system. After substrate reaction a chemiluminescent product is generated. The analyte concentration in the sample is calculated considering the recorded chemiluminescence signal. Optimum conditions were selected for the flow injection immunoassay system (e.g. tracer concentration, nature of antibody, antibody-beads concentration). The magnetic beads-based immunoassay with chemiluminescence detection allowed the sensitive atrazine determination (LoD = 3 pg/l atrazine).

2. Experimental

2.1. Materials

Atrazine were purchased from the Institute of Organic Industrial Chemistry, Poland. Stock solution of atrazine (1 ppm) was prepared in distilled water and stored at room temperature. This solution was consecutively diluted with 10 mM PBS (phosphate buffer saline) pH 7.4 generating the proper standard solutions with different atrazine concentrations (e.g. 10^{-7} to 10^{-1} ppb atrazine) for further experiments. Atrazine derivative coupled to HRP (tracer) was synthesized according to Giersch's protocol [25]. A mixture of 1 mg of atrazine derivative (6-{{4-chloro-6[(1-methyl-ethyl)amino]-1,3,5-triazin-2-yl}amino}hexanoic acid), 1.7 mg *N*-hydroxy succimide (NHS) and 6.2 mg *N*,*N*′-dicyclohexyl carbodiimide (DCC) in 130 μl of dry dimethyl formamide (DMF) was incubated for 18 h at room temperature under stirring. 22 μl of the resulting activated ester solution was added slowly to 0.5 ml of 1 mg/ml HRP (peroxidase, type VI-A from horseradish, SIGMA, 1280 units/mg solid) in 130 mM $NaHCO_3$ under stirring conditions. The reaction mixture was centrifugated and the supernatant purified on PD-10 column using 10 mM PBS at pH 7.4 for elution. Stock solution of the enzyme tracer was used for daily preparation of the working solution diluting to 1:500 with PBS (10 mM, pH 7.4).

Polyclonal IgG anti-atrazine from rabbit (ARINA) (Lot-A_9) Ab I and affinity purified anti-atrazine antibodies from sheep Ab II were kindly provided by Prof. Sergei Eremin (Lomonosov Moscow State University, Russia) and Dr. Ram Abuknesha (Kings College, University of London, UK). Antibodies stock solutions were diluted properly with PBS (10 mM, pH 7.4). Both antibodies were immobilised on the magnetic beads surface (3 μm diameter, —COOH active groups on the surface, Micromod, Rostock, Germany) based on covalent attachment [26]. Therefore, the —COOH groups on the magnetic particles surface were activated with 4 mg EDAC (1-ethyl-3-(3-dimethylamino-propyl)carbodiimide) and 8 mg NHS dissolved in 1 ml MES (2-[*N*-morpholino]ethanesulfonic acid) buffer (pH 6.3). Then, 1 ml of 200 μg/ml Ab solution (dissolved in 0.1 MES buffer) was added to the particles performing the covalent attachment (—NH—CO—). Finally, Ab-modified beads were treated with glycine solution for avoiding the unspecific binding on the particles surface. All the time the particles were suspended and collected from the liquid phase using a magnetic field generated by permanent magnet [26].

Phosphate buffer saline (PBS) was prepared as stock solution of 100 mM concentration according to the following method: 80 g NaCl, 2 g KCl, 14.3 g $Na_2HPO_4 \times 2H_2O$ and 3.43 g KH_2PO_4 were dissolved in 1 l distilled water and the pH was adjusted with either NaOH or HCl. All the reagents were purchased from Merck, Darmstadt, Germany. The stock solution of PBS (100 mM) was diluted with distilled water until reached 10 mM PBS concentration (pH 7.4).

The chemiluminescence substrate solution contained 2.76 μM H_2O_2 (hydrogen peroxide) from a stock solution of 33% H_2O_2, 1.56 μM luminol (5-amino-2,3-dihydro-1,4-phthalazinedione) from a stock solution of 50 mM luminol in dimethyl sulphoxide (DMS) and 8.25 μM 4-iodophenol (PIP) from a stock solution of 150 mM in DMS. The reagents of the chemiluminescence substrate were from Sigma–Aldrich, Steinheim, Germany. Dilution of substrate reagents was performed in PBS buffer pH 10, in order to guarantee a proper environment for chemiluminescence reaction.

25% MeOH (Sigma–Aldrich, Steinheim, Germany) solution in distilled water acidified with five drops of 30% HCl solution was used to remove the antigen (atrazine) from the immunocomplex antibody-antigen on the magnetic beads surface in order to re-use the particle for new analysis.

3. Instruments

A flow injection system was set up for experiments, i.e. peristaltic pump with two channels (Minipuls 3, Gilson, Middleton, USA), manual injection valve (Rheodyne, USA) with two positions and six ports, reaction cell and chemiluminescence detector (Hamammatzu, Japan). The reaction cell was designed as 2 Plexiglas blocks clamped together by 10 screws. Inside of the cell, the reaction chamber looks like a channel of 100 μl volume, having a cylindrical shape. Here, the magnetic beads introduced by simple injection can be kept on the reaction cell bottom applying a magnetic field. Permanent neodymium magnet 12 cm × 2.5 cm × 0.5 cm (Hyab Magneter AB, Bromma, Sweden) placed outside of the reaction cell, very close to the bottom of the cell provided necessary magnetic field. Chemiluminescence detector is a photomultiplier tube (Hamamatzu, Japan) positioned together with the reaction cell in a black box in order to avoid the light interference on chemiluminescence detection. A computer PC records and prepares the analytical signal.

3.1. Method

Magnetic beads-based immunoassay method for atrazine determination is presented in Fig. 1. The immuno analysis was lunched by inserting the antibody-beads suspension in the reaction cell (step 1). The suspension was prepared in 10 mM PBS pH 7.4. A neodymium magnet, placed underneath the channel of the reaction cell, provided a magnetic field that fixed the beads at the bottom of the channel by its magnetic force during the experiments (step 2). To remove those beads that not hade been fixed, the cell chan-

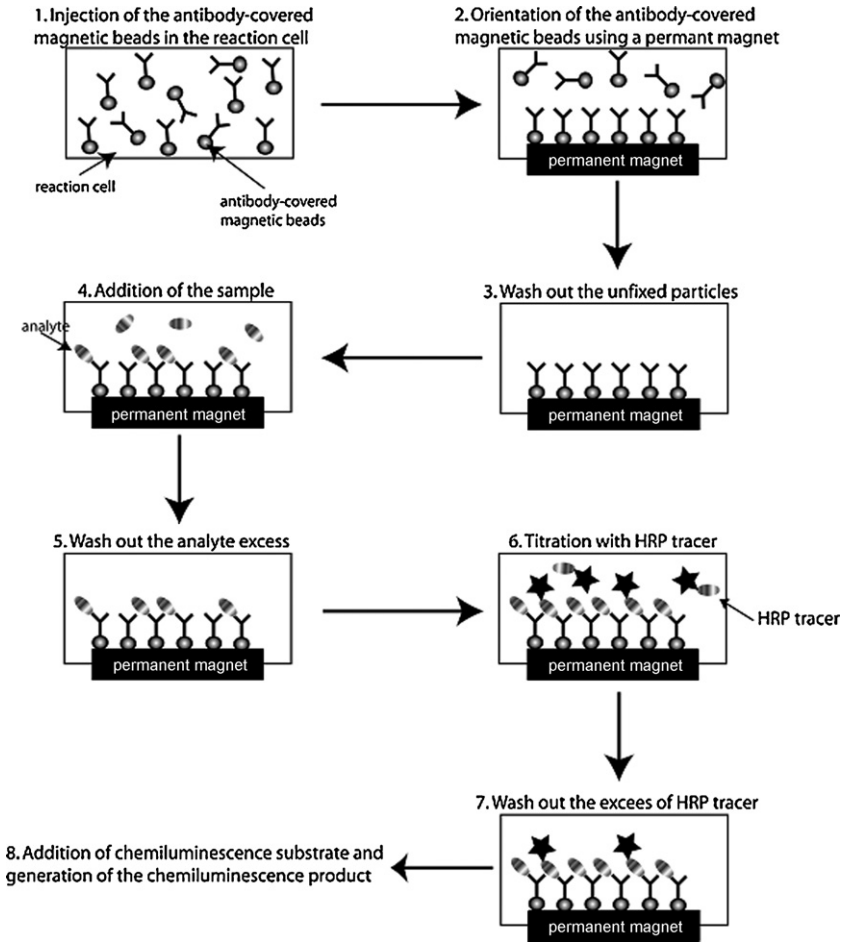

Fig. 1. Principle steps for performing the magnetic beads-based immunoassay.

nel was flushed with PBS solution (40 μl/min) for 10 min (step 3). Then, the analyte standard solution/sample containing the analyte (atrazine) was injected and was drive to the magnetic beads place (step 4). When the analyte comes in contact with the antibody, the flow was stopped for 3 min (incubation time for imunoreagents). After washing the excess of the analyte (step 5), tracer solution is added into the system for titration of the antibody free sites (step 6). Incubation of the tracer (3 min) was followed by washing step for elimination of tracer free fraction (unbound tracer) (step 7) and then injection of the chemiluminescence substrate in the reaction cell (step 8). The chemiluminescence signal indicates indirectly the analyte concentration in the sample, since that signal was proportional with bound fraction of the tracer.

Finally, the magnetic beads covered with antibody were regenerated using 25% MeOH solution, which allowed cutting antibody antigen bound removing the antigen and conserving the antibody active sites.

4. Results and discussions

The principle of magnetic beads-based immunoassay method developed for atrazine determination combines the features of a solid-phase competitive immunoassay with a sensitive chemiluminescence detection technique. The anti-atrazine antibody is covalently immobilized on the magnetic particles surface. The magnetic beads play a double role in this case. First, the particles are solid support for biomolecules. Also, they are carrier for the antibody allowing easily manipulation of the antibody for improving the kinetic of the immunointeraction antibody-antigen and increasing the immunoassay sensitivity. Therefore, the sensitivity of the magnetic beads-based immunoassay method is strongly influenced by the nature and concentration of the "complex" magnetic bead-antibody. We dedicated several experiments for choosing the right anti-atrazine antibody and also setting the proper antibody-beads concentration for our application. Also, other parameters influencing the immunoassay performances (e.g. tracer concentration, incubation time for immunointeraction antibody-tracer/antibody-antigen, flow rate, injection loop, chemiluminescence substrate composition, etc.) were set up at optimum value (the corresponding experimental data are not included in this paper).

4.1. Optimization of the immunoprocess

It is well known that the sensitivity of the competitive immunoassay can be easily improved if we chose the optimum combination of tracer and antibody, considering the nature and also the concentration of these immunoreagents [27]. According to this, several dilutions of the tracer (atrazine derivative-HRP) stock solution were tested having in mind to saturate the antibody active sites with tracer molecule for a good competition with the analyte. The obtained results indicated that lower dilution of tracer than 1:500 gave similar signals, which mean 1:500 dilution of tracer stock solution allowed blocking all the antibody affinity sites. Therefore, the following experiments were performed using tracer solution of 1:500 diluted tracer stock solution. The experimental results are

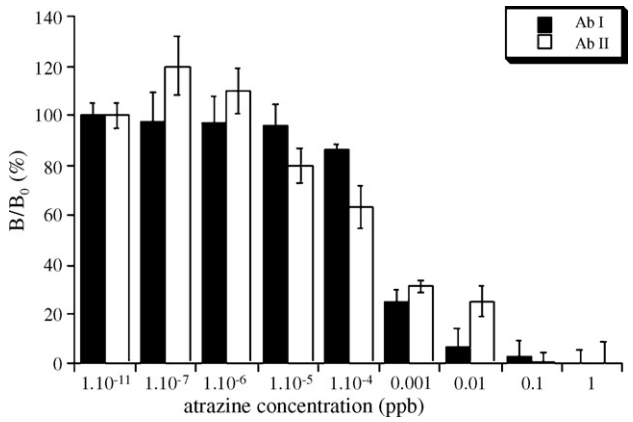

Fig. 2. Influence of antibody type on the magnetic beads-based immunoassay sensitivity (Ab I, polyIgG anti-atrazine; Ab II, affinity purified polyIgG anti-atrazine) ($n = 3$).

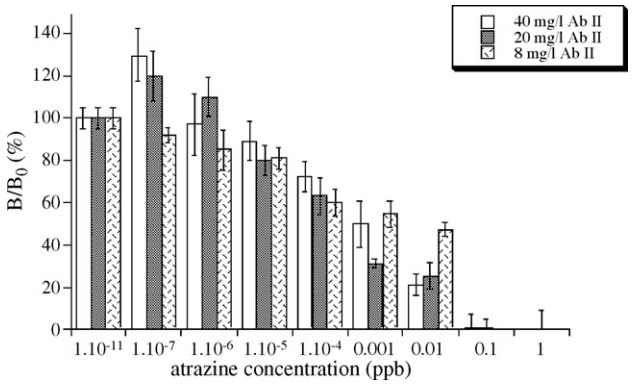

Fig. 3. Evaluation of the antibody concentration effect on the intensity of "low dose hook effect" ($n = 3$).

not presented in this paper. Then, experimental parameters such as flow rate, injection loop volume, incubation time for immunoreagents were set up at optimum value (i.e. 100 μl/min, 100 μl, 3 min, respectively). Since, those experiments are usual in immunoassay, we consider unnecessary to present the corresponding experimental data.

Further, we were looking for the best anti-atrazine antibody type in order to get a sensitive determination of atrazine using the magnetic beads-based immunoassay. Two different anti-atrazine antibodies were tested in the immunoassay configuration (see Fig. 2), polyclonal IgG anti-atrazine antibody (Ab I) and affinity purified anti-atrazine antibody (Ab II). Ab I is original antisera simple purified by ammonium phosphate precipitation and Ab II is affinity purified polyclonal antisera using an analyte affinity column. Therefore, Ab I contains a mixture of clones and only a fraction of them has affinity for our analyte (atrazine), while clones specific for atrazine can be found in Ab II solution. In both cases, the dilution curve of atrazine was performed (Fig. 2) and the characteristics of the analysis were compared. As we already expected according with the antibody composition, Ab II led to detect lower concentration of atrazine than Ab I (e.g. LoD = 0.54 and 0.027 ng/l for Ab I and Ab II, respectively). So that, Ab II was chosen to be used for futher experiments. The LoD values were calculated as analyte concentration generating 10% decrease of the maximum analytical signal (corresponding to zero dose). The calculation principle indicated previously was used for all the LoD values presented in this paper.

Unfortunately, the atrazine dilution curve for Ab II presented an apparent "low dose hook effect" [28–30] (see Fig. 2), which means the analytical signal increase little bit when lower analyte concentrations are added. The expectation was that the analytical signal decreased when the analyte was interacting with the Ab. We supposed that this "anomaly" is generated by an "apparent" increase of antibody activity in the presence of analyte at low concentrations. This is not a general behavior of antibody, but could be met sometimes for low and/or high concentration of analyte (low/high dose hook effect). Similar observations were reported previously for the same antibody, but in another immunoassay configuration [31], which means that "low dose hook effect" characterizes this affinity antibody activity for low atrazine concentration.

In order to elucidate this strength behavior, we made additional experiments varying the antibody concentration (e.g. 40, 20 and 8 mg/l Ab II). All other immunoassay parameters were kept constant (e.g. tracer concentration, analyte concentrations, etc.). The obtained results are plotted in Fig. 3. It is visible that the intensity of "low dose hook effect" is diminished by decreasing the Ab II concentration. For concentration of 8 mg/l Ab II, this effect is totally eliminated. Based on those experimental results, we demonstrated that "low dose hook effect" is a direct consequence of the antibody concentration vs. analyte/tracer concentration. A valuable explanation of this behavior could be that the antibody molecules are coupled together for solutions with high antibody concentration. In the presence of analyte molecules, the antibody–antibody interactions are cut off and more antibody molecules are able to bind analyte/tracer. Therefore, the bound fraction of the tracer increases leading to higher chemiluminescence signal.

Based on the previous experimental observations, concentration of 8 mg/l Ab II was set up as optimum antibody concentration for developing a sensitive magnetic beads-based immunoassay.

4.2. Characterization of the magnetic beads-based immunoassay

After a careful set up of the immunoassay parameters (e.g. tracer and antibody concentration), a calibration plot of the magnetic beads-based immunoassay method was performed in the range of $0–10^{-2}$ ppb atrazine concentration (Fig. 4). Three different injections were done for each atrazine concentration.

The sensitivity of this method was expressed as LoD = 3 pg/l calculated for 10% inhibition of the chemiluminescence signal corresponding to zero dose. Also, the method is characterized by IC_{50} = 37 pg/l and DR = 10–1000 pg/l. As we can observe, the developed magnetic beads-based immunoassay is a very sensitive method for atrazine analysis. This could be a cumulative effect due to high Ab II affinity for atrazine and also the use of magnetic beads as solid support/carrier for biomolecules.

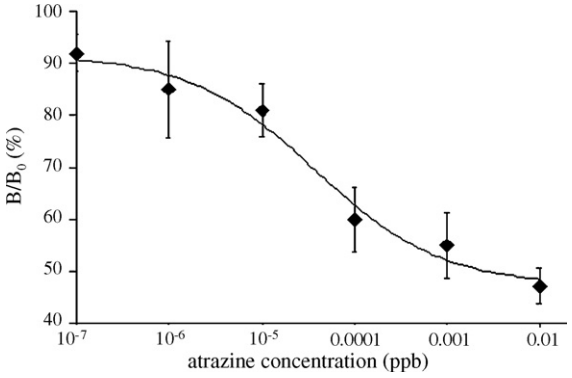

Fig. 4. Dilution curve of atrazine performing magnetic beads-based immunoassay for the optimum experimental conditions: 1:250 dilution grade of HRP tracer and 8 mg/l Ab II ($n = 3$).

The method is characterized by a good repeatability as well as reproducibility (7.35% and 15%, calculated for $n = 3$ replicates, respectively). The precision of the analysis for each atrazine concentration (repeatability) was calculated based on triplicates injections, while the inter-assay precision (reproducibility) was calculated based on three calibration curves performed in different days.

5. Conclusions

A very sensitive immunoassay method has been developed for atrazine determination allowing to detect atrazine at pg/l level. Based on our knowledge, this method seems to be one of the most sensitive one for atrazine determination at this time. This is due to the use of a high affinity antibody (affinity purified antibody) and also to a sensitive detection principle (e.g. chemiluminescence detection). Another important reason for high method sensitivity is the involvement of the magnetic beads as solid support/carrier for the antibody. In this way, low concentration of the antibody was used because the magnetic beads allowed to orientate the antibody in a favorable way for the immunointeraction. Also, an easy and efficient separation of bound and free fraction of tracer could be done, avoiding the most frequent errors introduced in this step for usual immunoassay procedure. The antibody-coated magnetic beads could be used for several analyses (after 10 analyses the binding capacity decreased with 2.4% and further after 20 analysis the binding capacity decreased with only 15%) if a regeneration step ended the immunoassay procedure. In this way, the problem of high antibody consumption was solved.

Acknowledgements

The authors kindly acknowledge Ministry of Education, Research and Youth Romania-CNCSIS, for financial support. Special thank to Dr. Jenny Emneus (Lund University, Sweden) for her scientific input. Also, we would like to thank to Prof. Sergei Eremin (Lomonosov Moscow State University, Russia) and Dr. Ram Abuknesha (Kings College, University of London, UK) for all the reagents.

References

[1] K. Dietmar, Anal. Bioanal. Chem. 385 (2006) 425.
[2] D.R. Shankaran, K.V. Gobi, N. Miura, Sens. Actuat. B 121 (2007) 158.
[3] S. Rodriguez-Mozaz, M.J.L. de Alda, D. Barcelo, Anal. Bioanal. Chem. 386 (2006) 1025.
[4] M. Diaz-Gonzalez, M.B. Gonzalez-Garcia, A. Costa-Garcia, Electroanalysis 17 (2005) 1901.
[5] E. Zacco, M.I. Pividori, S. Alegret, R. Galve, M.-P. Marco, Anal. Chem. 78 (2006) 1780.
[6] M. Tudorache, M. Co, H. Lifgren, J. Emneus, Anal. Chem. 77 (2005) 7156.
[7] J. Kaur, K.V. Singh, R. Boro, K.R. Thampi, M. Raje, G.C. Varshney, C.R. Suri, Environ. Sci. Technol. 41 (2007) 5028.
[8] E. Valera, J. Ramon-Azcon, A. Rodriguez, L.M. Castaner, F.-J. Sanchez, M.-P. Marco, Sens. Actuat. B 125 (2007) 526.
[9] S. Centi, S. Laschi, M. Franek, M. Mascini, Anal. Chim. Acta 538 (2005) 205.
[10] Y.-Y. Lin, G. Liu, C.M. Wai, Y. Lin, Electrochem. Commun. 9 (2007) 1547.
[11] S.-F. Wang, Y.-M. Tan, Anal. Bioanal. Chem. 387 (2007) 703.
[12] X. Zhao, S.A. Shippy, Anal. Chem. 76 (2004) 1871.
[13] S. Sole, A. Merkoci, S. Alegret, TrAC 20 (2001) 102.
[14] F. Ibraimi, D. Kriz, M. Lu, L.-O. Hansson, K. Kriz, Anal. Bioanal. Chem. 384 (2006) 651.
[15] A.Y. Rad, H. Yavuz, M. Kocakulak, A. Denizli, Macromol. Biosci. 3 (2003) 471.
[16] A.K. Gupta, M. Gupta, Biomaterials 26 (2005) 3995.
[17] H. Yu, J. Immunol. Meth. 218 (1998) 1.
[18] M. Dequaire, C. Degrand, B. Limoges, Anal. Chem. 71 (1999) 2571.
[19] G. Liu, S.L. Riechers, C. Timchalk, Y. Lin, Electrochem. Commun. 7 (2005) 1463.
[20] A.D. Wellman, M.J. Sepaniak, Anal. Chem. 78 (2006) 4450.
[21] G.D. Liu, C. Timchalk, Y.H. Lin, Electroanalysis 18 (2006) 1605.
[22] E. Zacco, J. Adrian, R. Galve, M.-P. Marco, S. Alegret, M.I. Pividori, Biosens. Bioelectron. 22 (2007) 2184.
[23] A. Agrawal, T. Sathe, S. Nie, J. Agric. Food Chem. 55 (2007) 3778.
[24] S. Centi, E. Silva, S. Laschi, I. Palchetti, M. Mascini, Anal. Chim. Acta 594 (2007) 9.
[25] T. Giersch, J. Agric. Food Chem. 41 (1993) 1006.
[26] M. Tudorache, I.A. Zdrojewska, J. Emneus, Biosens. Bioelectron. 22 (2006) 241.
[27] R. Ekins, in: C.P. Price, D.J. Newman (Eds.), Principles and Practice in Immunoassay, 1991, p. 96.
[28] Y.F. Xu, M. Velasco-Garcia, T.T. Mottram, Biosens. Bioelectron. 20 (2004) 533.
[29] A. Feltus, S. Ramanathan, S. Daunert, Anal. Biochem. 254 (1997) 62.
[30] M.S. Barbarakis, W.G. Qaisi, S. Daunert, L.G. Bachas, Anal. Chem. 65 (1993) 457.
[31] M. Tudorache, M. Rak, P.P. Wieczorek, J.-A. Jonsson, J. Emneus, J. Immunol. Meth. 284 (2004) 107.

Talanta 77 (2008) 494–499

Contents lists available at ScienceDirect

Talanta

journal homepage: www.elsevier.com/locate/talanta

Sequential injection-LOV format for peak height and kinetic measurement modes in the spectrophotometric enzymatic determination of ethanol: Application to different alcoholic beverages

Susana S.M.P. Vidigal, Ildikó V. Tóth, António O.S.S. Rangel*

Escola Superior de Biotecnologia, Universidade Católica Portuguesa, Rua Dr. António Bernardino de Almeida, 4200-072 Porto, Portugal

ARTICLE INFO

Article history:
Received 17 September 2007
Received in revised form 12 March 2008
Accepted 17 March 2008
Available online 1 April 2008

Keywords:
SI-LOV spectrophotometry
Ethanol
Alcohol dehydrogenase
Beverages
Initial rate measurement
Peak height measurement

ABSTRACT

The objective of this work was to make a contribution to study the potential of the sequential injection-lab-on-valve (SI-LOV) format for the miniaturization of enzymatic assays, by using different measurement modes (peak height and initialrate-based measurement). A LOV system was developed for the enzymatic assay of ethanol in beverages, based on the conversion of ethanol to acetaldehyde by alcohol dehydrogenase, using spectrophotometric detection. The use of the kinetic-based approach permits the applicability of the enzymatic determination to samples with intrinsic absorption, with a higher determination throughput.

A linear dynamic application range up to 0.040% (v/v) was achieved for both initial rate and for the peak height measurement, with good repeatability (R.S.D. < 5.0% and <1.0%, respectively). Enzyme, NAD^+, buffer and sample consumption per assay were 0.12 U, 0.066 mg, 150 and 15 μL, respectively. The determination rate achieved was 37 and 27 determinations h^{-1} for the initial rate and for the peak height measurement, respectively. The results obtained for several alcoholic beverages, including a certified sample material, were not statistically different from those obtained by the reference procedures.

1. Introduction

Flow analysis systems have been gaining an increased importance in wet analytical chemistry. This fact can be mainly explained by the possibility of automating analytical chemical procedures with a simultaneous dramatic decrease in reagents consumption. The trend for automation and miniaturization is particularly important for biochemical methods of analysis, due to the elevated costs of the reagents involved in enzymatic and immuno-assays, as well as by the often-limited amount of the samples available. Therefore, the possibility to perform the biochemical assays within small-integrated manifolds through flow-based automation of sample and reagent handling has received increased attention.

In this scenario, flow methods became widely popular among the scientific community, due to the possibility of automatic sample handing resorting to mostly simple and low cost apparatus. These approaches consist in the injection of a well-defined volume of sample solution into a carrier stream in a reproducible way [1]; one or more reagents can be added downstream and the product is measured in a suitable flow through detector.

Although these systems have proven to be an effective way of automating various biochemical methods, further downscaling would be important. In this context of downscaling and miniaturization one of the frequent objections to the micro- or nano-scale analytical circuits is their probable susceptibility to clogging when "real" samples are to be analyzed. In the sequential injection-lab-on-valve (SI-LOV) format the circuits are downsized only to the microlitre scale, being still easy to manipulate, but already in a compact format [2]. Like in sequential injection analysis (SIA), in a SI-LOV system, a well-defined volume of sample and reagents are sequentially aspirated to the holding coil and then propelled by reversed flow to the detector. In this equipment the manifold/detector is integrated on the top of the selection valve in a robust way, so the miniaturization is possible because of the proximity of the injection port to the flow cell [3]. Unlike traditional SIA, there is no need for the plugs to travel a distant path in the LOV format, since the volumes of sample and reagents involved are in a microliter scale. Therefore, an efficient overlapping of reagent zones is achieved in a repeatable way. The physical configurations of the flow channels are also designed to improve the mixing conditions. This way, one of the limitations attributed to SIA, the lack of efficient reagent/sample overlapping as a source of inaccuracy, especially when sample is contaminated by interfering species that also consume reagent in the overlapping zone, can be overcome.

* Corresponding author. Tel.: +351 225580064; fax: +351 225090351.
E-mail address: aorangel@esb.ucp.pt (A.O.S.S. Rangel).

0039-9140/$ – see front matter © 2008 Elsevier B.V. All rights reserved.
doi:10.1016/j.talanta.2008.03.034

The objective of this work was to study the potential of the SI-LOV format for the miniaturization of enzymatic assays. As a case study, we selected the enzymatic determination of ethanol in alcoholic beverages, an important parameter to define the quality and the stability of the product. The reference methods proposed by Office International de la Vigne et du Vin (OIV) are complex, laborious and most of them require distillation as sample pre-treatment [4–6]. To overcome these disadvantages enzymatic flow systems were developed for this determination [7–17]. Most of these methods exploit the reaction between the immobilized alcohol dehydrogenase with ethanol in the presence of NAD^+ to produce acetaldehyde and NADH. The detection is generally spectrophotometric of the produced NADH at 340 nm. The methods are fast, simple and do not require any other sample pre-treatment than dilution, however the process of enzyme immobilization frequently involves the manipulation of toxic reagents (glutaraldehyde), and the support material used for the immobilization process (controlled pore glass) can add to the cost of analysis.

In this scenario, our study comprised two main aspects: (i) the use of the SI-LOV format to further miniaturize the flow system and prevent the need for the enzyme immobilization; this study implied the assessment of the efficiency of the zones overlapping in LOV; (ii) comparison of two quantification methodologies, peak height based versus initial rate measurement; the latter one to cope with the possible interference of the sample intrinsic absorption [3,18].

2. Experimental

2.1. Reagent and solutions

All chemicals were of analytical reagent grade, and boiled Milli-Q water (resistivity 18 MΩ cm^{-1}) was used throughout the work. The buffer solution (pH 9.5) was prepared weekly by dissolving 5.58 g of $Na_4P_2O_7{\cdot}10H_2O$ in 250.0 mL of water. The pH of this solution was adjusted with phosphoric acid 8%, v/v. The buffer for the enzyme suspension (pH 7.5) was prepared by dissolving 0.178 g of $Na_2HPO_4{\cdot}2H_2O$ in 100.0 mL of water.

To daily prepare the working enzyme solution, 1 mg of lyophilized ADH (alcohol dehydrogenase, EC 1.1.1.1, from baker yeast, A7011, Sigma) was re-suspended in 1.00 mL of enzyme buffer pH 7.5, and this suspension was further diluted to 1.00 mL in the same buffer in a way to achieve the concentration of 24 U mL^{-1} in the working reagent solution. The cofactor solution was prepared daily by dissolving 0.0664 g of NAD^+ (NAD^+, free acid grade II, ~98%, 10621650001, Roche) in 5.00 mL of water.

The working standard solutions of ethanol were prepared daily from the stock standard solution (ethanol absolute pro analysis, 1210861212, UN1170, Panreac Quimica, SA) in a range between 0.010% and 0.040% (v/v).

For the zone overlapping study, a 24 mg L^{-1} bromothymol blue solution was prepared as described by Ruzicka and Hansen [1]. The carrier solution used for this study was borax 0.01 M.

2.2. Samples

Samples were purchased in a local supermarket. A total of 10 samples were analyzed, using the content of the same bottle for the reference and for the developed flow methods. For the table wine and spirit samples no other treatment than dilution was applied before sample analysis. Table wines were 350 times diluted, and the spirit samples were diluted 2500 times. The beer samples were filtered, degassed and 400 times diluted before analysis.

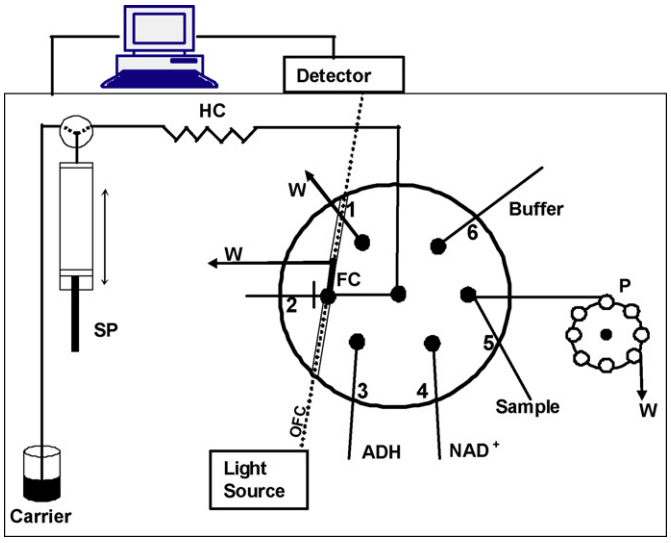

Fig. 1. Configuration of μSI-LOV system for the determination of ethanol; ADH, alcohol dehydrogenase 24 U mL^{-1}; NAD^+, cofactor 20 mM; Buffer, phosphate buffer pH 9.5; W, waste; Carrier, water; SP, syringe pump (2.5 mL); HC, holding coil; FC, flow cell; OFC, optical fibre cable; P, peristaltic pump; Detector, diode-array spectrophotometer.

A certified reference sample of low alcohol level wine was also analyzed (CRM 653, wine, nominal 0.5%, v/v). This sample was 20 times diluted before introduction into the SI-LOV system.

2.3. Apparatus

The SI-LOV system (FIAlab-3500, FIAlab Instruments, Medina, WA, USA) presented in Fig. 1 consisting of a bi-directional syringe pump (2500 μL of volume), a holding coil, a bi-directional variable speed peristaltic pump and a lab-on-valve manifold mounted on the top of a six-port multi-position valve, was used.

The USB 2000 Ocean Optics, a diode array spectrophotometer equipped with fiber optics (i.d.: 200 μm), and a DH-2000-BAL Mikropack, UV/Vis/NIR light source, was used. FIAlab for windows 5.0 software on an Intel Pentium III Computer (995 mHz, 128 MB) controlled the system.

2.4. Flow procedure

2.4.1. Peak height measurement

The initial steps (A–F) in Table 1 of the flow protocol were similar for the peak height and for the initial rate measurement. Those steps consisted in aspiration of carrier, buffer, sample and reagents to the holding coil: 1000 μL of carrier, then 50 μL of buffer, 15 μL of sample solution, 5 μL of ADH, 5 μL of NAD^+ and finally 100 μL of buffer. In the case of the peak height measurement, the following steps (G–J) consisted in reversing the flow and propelling the mixture, after 30 s of stop time in the holding coil, to the flow cell where the absorbance was measured.

2.4.2. Initial rate measurement

In this case, the stacked zones (steps K–M) were directed to the flow cell and the flow was stopped and the change in absorbance was monitored during 15 s. Afterwards, the reaction zone was dispensed.

2.4.3. Reference procedures

The reference methods used for beer and wine samples consisted in the distillation of the sample [4,5], and Anton Paar DMA

Table 1
Flow protocol

Step	Description	Volume (μL)	Flow rate (μL/s)	Selection valve position
A	Aspirate carrier to HC	1000	100	–
B	Aspirate buffer to HC	50	80	6
C	Aspirate sample to HC	15	25	5
D	Aspirate enzyme to HC	5	25	3
E	Aspirate cofactor to HC	5	25	4
F	Aspirate buffer to HC	100	25	6
Peak height measurement				
G	Reverse flow, reference scan	10	15	2
H	Stop period (30 s)	–	–	–
I	Dispense HC content, data acquisition	450	15	2
J	System washing, SP empty	–	100	2
Initial rate measurement				
K	Dispense selection of stacked zones	100	15	2
L	Stop period (15 s), data acquisition	–	–	–
M	System washing, SP empty	–	100	2

5000 Density meter was used for the measurement of the volumetric alcohol content of the distillates [4]. The spirit samples were diluted [6] before Density meter reading [4].

3. Results and discussion

3.1. Study of the overlapping of reagent zones

Enzymatic assays usually comprise the mixing of various solutions like sample, enzyme, buffer and frequently cofactor solutions. Therefore, when these assays are carried out in SIA, the number of plugs and the aspiration order are determined by the involved enzymatic reaction. In this work, the enzymatic assay is based on the reaction between ethanol and alcohol dehydrogenase in the presence of NAD^+ (cofactor), producing acetaldehyde and NADH. The formation of the reduced cofactor is measured spectrophotometrically at 340 nm. Additionally, the reaction occurs under controlled pH. Based on these conditions, the overlapping and mixing of the reagent zones is of great importance. Firstly the aspiration sequence was defined as buffer–sample–enzyme–cofactor–buffer; buffer solutions in the front and in the rear part of the sequence were used to sandwich the other reagents and assure the adjustment of the reaction pH. Within the sandwiched zone the sequence of the other reagents was selected to promote the penetration of the sample zone through the enzyme and cofactor sections [19,20]. In preliminary experiments, the aspiration flow rates were studied with the objective of using low sampling volumes with good repeatability. These preliminary studies were carried out using a bromothymol blue model solution (24 mg L^{-1}): when a combination of aspiration flow rate and volume uptaken fulfilled the criteria of R.S.D. < 5% (n = 10) for the absorbance values, it was applied in the enzymatic method. To assess the effect of the dimensions of the introduced reagent zones on the efficiency of the mixing, a study similar to Gübeli et al. [20] was carried out using also the model solution of bromothymol blue (24 mg L^{-1}). Using a borax solution (0.01 M) as carrier, the bromothymol blue solution was introduced sequentially in each port involved and the resulted peak profiles were recorded. The distance across the dispersed zone (W_t), the zone of total overlapping between the reagents (W_o) and the peak height absorbance (H) were measured. These parameters and the volumes studied are resumed in Table 2.

Table 2
Study of the overlapping of reagent zones using a model solution of bromothymol blue (24 mg L^{-1})

Aspiration sequence	Volume (μL)					
	A	B	C	D	E	F
Plug1: buffer	50	100	50	50	50	50
Plug2: sample	50	50	50	25	15	15
Plug3: enzyme	25	25	25	10	5	5
Plug4: cofactor	25	25	25	10	5	5
Plug5: buffer	50	50	100	100	100	50
W_t[a] (s)	25	32	34	28	20	15
W_o[b] (s)	13	9	16	17	16	8
H[c]	0.331	0.337	0.270	0.138	0.096	0.127

A–F correspond to different configuration and volumes tested.
[a] Total baseline width of the dispersed sample–enzyme–cofactor reagent zones.
[b] Baseline width of the sample–enzyme–cofactor reagent zone with total overlapping.
[c] Peak height absorbance of the enzyme zone.

In configurations A–C, the relative volumes of the buffer zones were studied maintaining the total volume of the other zones at 100 μL. In configuration C; although W_t was the largest, the zone of total overlapping between the reagents had also the largest extension, therefore this combination of the buffer solutions was maintained. To further improve the mixing conditions, the total volume of the sample–enzyme–cofactor sequence was reduced (configurations C–E); as expected, the dispersion of the enzyme zone increased (H decreased) with decreasing the total volume.

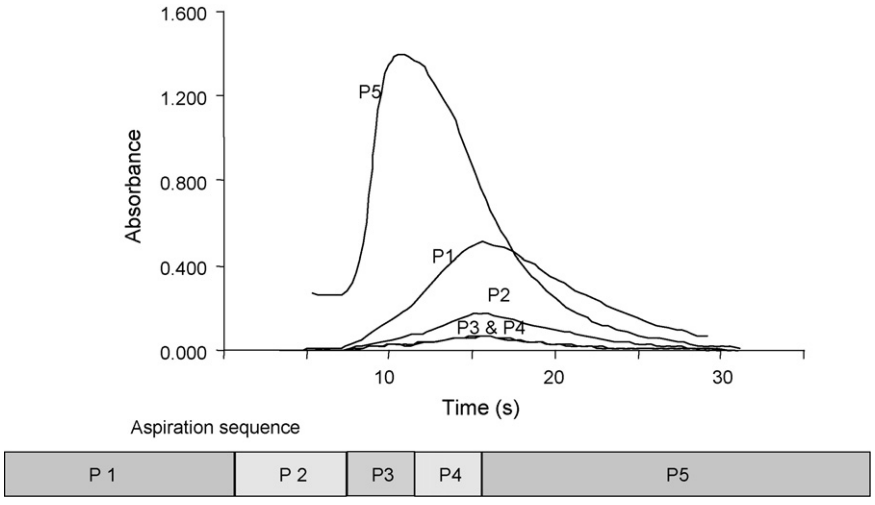

Fig. 2. Recorded peak profiles (P_i) obtained by the injection of 24 mg L^{-1} of bromothymol blue and corresponding aspiration sequence. P1 corresponds to 50 μL of buffer, P2 15 μL of sample, P3 5 μL of enzyme, P4 5 μL of cofactor and P5 100 μL of buffer.

Total overlapping between the sample, the enzyme and the cofactor zone was achieved in configuration E. With the objective of reducing the dispersion of the critical enzyme zone, while maintaining the low injection volumes, the last buffer zone was reduced to half (configuration F), the degree of overlapping of the zones deteriorated. Moreover, there is a need for a larger zone of the buffer solution to reach the flow cell before the reaction zone to perform a reference scan before the measurement. Therefore the configuration of E (Fig. 2) was maintained during the further studies. The repeatability of this aspiration sequence was also evaluated using the bromothymol blue solution. Good repeatability was found ($n = 10$) for all the volumes used in the sequence; 50 μL of buffer (R.S.D. < 0.7%), 15 μL sample (R.S.D. < 1.0%); 5 μL enzyme solution (R.S.D. < 2.9%); 5 μL cofactor solution (R.S.D. < 3.0%) and 100 μL of buffer (R.S.D. < 0.4%).

It can be also concluded from Fig. 2 that in this aspiration sequence the dispersion of the cofactor and the enzyme zone is equal; therefore the order of aspiration of these two zones would not affect the overlapping of the reagent zones.

3.2. Study of the enzymatic reaction for peak height measurement mode

After establishing the volume of the reagent zones, a study of the influence of the chemical parameters (pH, NAD^+ and ADH concentration) on the sensitivity of the enzymatic reaction was studied. Univariate procedure was applied and the sensitivity achieved in the range of 0.00–0.040% (v/v) of ethanol was monitored using the peak height measurement mode.

Initial conditions were established as diphosphate buffer pH 9.5 and 20 mM and 24 U mL^{-1} as NAD^+ and ADH concentrations, respectively, based on the previously published work [13] for the same determination using a SIA manifold.

The NAD^+ concentration was studied in a range between 10 and 30 mM. The sensitivity increased about 56% with the increase of the concentration from 10 to 20 mM. For higher concentrations the sensitivity decreased by 10%; therefore the concentration was set to 20 mM.

The effect of the enzyme concentration was studied for 14, 24 and 56 U mL^{-1}. The sensitivity increased 85% when the concentration was raised from 14 to 24 U mL^{-1}. By further increasing the concentration, the sensitivity did not show any further improvement, for that reason the concentration used was 24 U mL^{-1}.

The working pH is essential to assure the activity of the enzyme. This parameter was studied in a range between 8.5 and 10. The pH selected was 9.5 since it presented a higher sensitivity and was close to the reported optimum pH for this enzyme [21].

One way to enhance the sensitivity of enzymatic reactions is to increase the reaction time before detection. In a LOV system this approach is quite easily accomplished by introducing a stop period in the program sequence. A stop time (time elapsed between flow reversal of the stacked zones and propulsion to the detector) between 10 and 40 s was studied. The sensitivity increased with the stop time in the range of 10–30 s, but decreased about 57% when the stop time was 40 s. Thus the stop time selected was 30 s.

3.3. Initial rate measurement mode

When samples exhibit either an intrinsic absorption or potential interferents with reaction kinetics different from the analyte, the initial reaction rate measurement could be the most efficient way to overcome these difficulties. The LOV format is particularly suitable for kinetic-based measurements due to the easy manipulation of time sequences and the low volumes involved. In this case the stacked zones in the holding coil can be sent to the flow cell and the rate of product formation can be monitored during a pre-set time period. In this measurement mode, not only the length of the stop period is important for achieving adequate sensitivity and linearity, but also the volume used to propel the reagent zones to the flow cell. This volume will define what portion of the dispersed reagents/sample zone will be monitored during the initial rate measurement [18,19,22]. This volume will also define the relative concentrations of the reagents and the sample inside the flow cell. These flow reversal volumes were studied between 90 and 120 μL, with 5 μL increments. A higher initial rate ($\Delta A/\Delta t$) was achieved using a 100 μL volume; therefore this volume was set.

The stop time in the flow cell was studied in the range of 10–40 s. When this stop time was higher than 15 s the total number of recorded data (spectrophotometer specifications allow a reading frequency of 2 Hz) did not give a linear relationship. Therefore the results of the kinetic method were obtained from initial reaction rate using the data collected during the first 10 s of the stop period. Fig. 3 illustrates the increase of the initial rate with the increase of the ethanol concentration. It can be concluded that, besides the previously mentioned advantages concerning spectral and chemical interferences, the initial rate approach also presents a higher determination rate.

3.4. Figures of merit

The performance of the proposed methods was evaluated in terms of reagent consumption, application range, determination rate, repeatability and accuracy (Table 3). Both peak height mea-

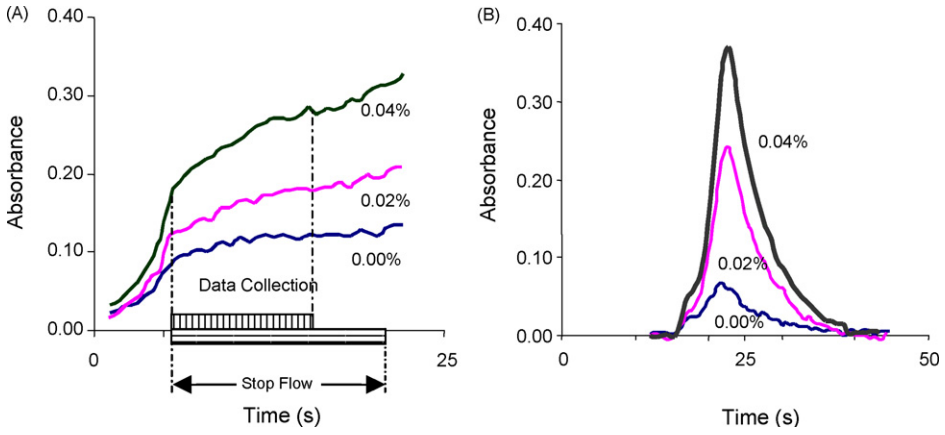

Fig. 3. Variation of the absorbance with the increase of the concentration of ethanol by (A) initial rate measurements and (B) peak height measurement.

Table 3
Figures of merit of the proposed methods

Parameter	Peak height measurement	Initial rate measurement
Reagent consumption per assay		
ADH	0.12 U	0.12 U
NAD^+	0.066 mg	0.066 mg
Sample solution	15 μL	15 μL
Buffer	150 μL	150 μL
Waste production per assay	1.2 mL	1.2 mL
Application range	Up to 0.04% (v/v)	Up to 0.04% (v/v)
Determination rate	27 h^{-1}	37 h^{-1}
LOD	0.003% (v/v)	0.004% (v/v)
LOQ	0.009% (v/v)	0.01% (v/v)
Repeatability (R.S.D.)	1.0% (9.1%, v/v) (n = 4)	5.0% (9.4%, v/v) (n = 6)
	0.7% (11.1%, v/v) (n = 4)	4.0% (11.0%, v/v) (n = 8)
	1.0% (10.4%, v/v) (n = 4)	4.0% (5.2%, v/v) (n = 7)
		2.5% (38.3%, v/v) (n = 10)
		4.6% (40.3%, v/v) (n = 10)

surement and initial rate measurement have the same reagent consumption, and they were linear up to 0.040%, v/v. The sampling rate was higher for the initial rate measurement. R.S.D.'s were below 5.0% in a range between 5.2% and 40.3% (v/v). The accepted precision for a reference method is established as ±0.1% (v/v) ethanol, referring to the measurement of different physical properties of the distilled samples. When looking at the results in Tables 3 and 4, the developed methods show worse repeatability, but it must be kept in mind that these assays were performed on the whole sample without distillation, and that the obtained precision is adequate for the control of the fermentation process [23]. The limit of detection and the limit of quantification were calculated as recommended by Miller and Miller [24].

The reproducibility of the initial rate measurement was evaluated by performing the calibration procedure under identical operation conditions during a working day. Applying a single factor

Table 4
Comparison of the results obtained for the analysis of different beverages according to the reference and the developed procedures

Sample	Reference methods %[a] ethanol (v/v)	%Ethanol (v/v)	
		Peak height measurement[b]	Initial rate measurement[b]
Red table wine	9.3 (±0.1)	9.1 (±0.1)	9.7 (±0.6)
Red table wine	12.4 (±0.1)	12.3 (±0.9)	12.3 (±0.2)
Red table wine	11.1 (±0.1)	11.1 (±0.1)	10.4 (±2.9)
White table wine	10.2 (±0.1)	10.4 (±0.1)	10.4 (±0.1)
Beer 1	5.2 (±0.1)	–	5.1 (±1.2)
Beer 2	4.6 (±0.1)	–	4.8 (±0.5)
Beer 3	4.7 (±0.1)	–	4.7 (±0.2)
Spirit 1	36.7 (±0.1)	–	36.7 (±3.7)
Spirit 2	36.6 (±0.1)	–	36.3 (±2.9)
Spirit 3	39.2 (±0.1)	–	39.8 (± 2.0)

[a] Mean and accepted precision for n = 3.
[b] Mean and standard deviation for n = 3.

Table 5
Results obtained in the analysis of the certified reference wine sample, CRM 653

Certified value, % ethanol (v/v)	0.539 ± 0.0095[a]
Peak height measurement, % ethanol (v/v)	0.537 ± 0.025[b]
t (α = 0.05)[c]	0.03
Initial rate measurement, % ethanol (v/v)	0.548 ± 0.026[b]
t (α = 0.05)[c]	0.15

[a] Laboratory mean and standard deviation of laboratory means.
[b] Mean and standard deviation for n = 7.
[c] t critical: 2.45.

Table 6
Comparison of some analytical figures of enzymatic (ADH) flow methodologies for ethanol determination in beverages

	Present work		FIA [7]	FIA[a] [10]	FIA[b] [12]	FIA[b] [14]	FIA [15]	SIA[a] [11]	SIA [13]	SIA [16]	Lab-on-valve [18]
Sample matrix	Table wine, beer and spirits		Beverages	Wine	Wine, saké	Wine, beer	Wine	Wine	Wine	Ferment. broth	No application
Measurement	Peak height	Initial rate	Peak height	Peak height	Initial rate	Peak height	Peak height	Peak height	Peak height	Peak height	Initial rate
Enzyme	Solution		Solution	Immobilized	Immobilized	Immobilized	Immobilized	Immobilized	Solution	Immobilized	Solution
Reagent consumptions											
ADH (U/assay)	0.12		225	Not given	16.7	0.5	≈0.4	Not given	1.1	Not given	48
NAD^+ (μmol/assay)	0.1		2.4	14	0.52	3.2	0.6	0.3	1	0.5	0.7
Sample (μL/assay)	15		30	3000	50	30	25	45	100	150	30
Waste production (mL/assay)	1.2		1	8.1	5.2	1.8	11	1.8	1.8	Not given	1
Range of applicability (%, v/v)	Up to 0.04	Up to 0.04	Up to 0.4	0.05–0.5	0.04–100 mM	Up to 50×10^{-3}	5–25	0.10–0.50	Up to 0.024	0.25–100 mM	50–250 mg L^{-1}
LOD (%, v/v)	0.003	0.004	Not given	2×10^{-3}	0.02 mM	2.5×10^{-3}	0.4	0.005	0.008	Not given	Not given
Determination rate (h^{-1})	27	37	120	20	10	40	30	45	25	26	120
R.S.D. (%)	<1	<5	Not given	<2.1	2	±0.3	<2.2	<3.4	<2.3	<6	<3

[a] With simultaneous determination of glycerol.
[b] With simultaneous determination of acetaldehyde.

ANOVA [24] treatment between and within day for the calibration curves revealed no significant differences for a 95% confidence level.

3.5. Application to beverage samples

To evaluate the accuracy of the proposed methods, a total of 10 beverage samples were analyzed. The reference procedure was also carried out using the same content of the bottle. The results obtained in the analysis are presented in Table 4.

The linear relationships ($C_{\text{peak height meas.}} = C_0 + SC_{\text{ref. meth.}}$) and ($C_{\text{initial rate meas.}} = C_0 + SC_{\text{ref. meth.}}$) were established ($n = 4$ and 10, respectively) and are described by the equations $C_{\text{peak height}} = -0.056\ (\pm 4.245) + 1.003\ (\pm 0.393) C_{\text{ref. meth.}}$, and $C_{\text{initial rate meas.}} = -0.037\ (\pm 0.446) + 1.003\ (\pm 0.021) C_{\text{ref. meth.}}$ [25]. Values presented in parentheses represent the limits of the 95% confidence intervals for the equation parameters. These values demonstrate that the obtained results were not statistically different.

A certified wine sample, CRM 653, with a low level alcohol (0.5%, v/v nominal value) was also analyzed. In this case the sample was 20 times diluted before introduction into the system, resulting in a much higher matrix to analyte ratio than in the case of the table wines. The results obtained for the peak height and the initial rate measurement presented in Table 5 show good agreement with the certified value [25].

4. Conclusions

The results obtained for the enzymatic determination of ethanol in beverages were comparable to those obtained by the reference method with good repeatability, minimum sample treatment and low reagent consumption. The low reagent consumption is an advantage when compared with some flow methodologies for the same determination (Table 6). The application range and the corresponding detection limits are comparable to those obtained by the other flow methodologies. The limit of detection for the proposed method is lower than the ones obtained with other flow methodologies using enzymes in solution.

The determination rate can be increased when the initial rate measurement is performed as only a 10 s period is used for data acquisition while in the peak height measurement the maximum absorbance must be achieved.

The easy manipulation of time sequences and the low volumes used in the LOV format system makes it proper for the kinetic-based assays. The initial rate measurement is the most efficient way when sample shows evidence of intrinsic absorption or contains potential interferents with a reaction rate different of the analyte. Additionally, the analytical response is not influenced by the schlieren effect in this type of measurement.

The use of a lab-on-valve format with reduced injection volumes, and strategic selected aspiration sequence proved to be an efficient way to overcome the deficient overlapping of sample and reagent zones frequently attributed to conventional SIA assays.

Acknowledgements

Susana Vidigal and Ildikó Tóth thank Fundação para a Ciência e a Tecnologia (FCT) and FSE (III Quadro Comunitário) for the grants SFRH/BD/23040/2005 and SFRH/BPD/5631/2001, respectively. We also thank the collaboration of the company Cockburn Smithes.

References

[1] J. Ruzicka, E.H. Hansen, Flow Injection Analysis, 2nd ed., Wiley, New York, 1988.
[2] J. Wang, E.H. Hansen, Trends Anal. Chem. 22 (4) (2003) 225.
[3] J. Ruzicka, Analyst 125 (2000) 1053.
[4] Office International de la Vigne et du Vin (OIV), Recueil des methodes internationales d'analyse des vins et des mouts, Titre alcoométrique volumique, OIV, Paris, France, 2005. MA-F-AS312-01-TALVOL.
[5] European Brewery Convention, Analytica-EBC, Fachverlag Hans Carl GmbH Nurenberg, Method 9.2.1, European Brewery Convention, Germany, 2005.
[6] Norma Portuguesa, Bebidas Alcoólicas e Espirituosas, Determinação do teor alcoólico em volume (grau alcoólico volumétrico), 1987. NP-2143.
[7] P.J. Worsfold, J. Ruzicka, E.H. Hansen, Analyst 106 (1981) 1309.
[8] I.L. Mattos, J.M. Fernandes-Romero, M.D. Luque De Castro, M. Valcárcel, Analyst 120 (1995) 179.
[9] W. Künnecke, J. Mohns, Anal. Chim. Acta 305 (1995) 241.
[10] A.O.S.S. Rangel, I.V. Tóth, Anal. Chim. Acta 416 (2000) 205.
[11] M.A. Segundo, A.O.S.S. Rangel, Anal. Chim. Acta 458 (2002) 131.
[12] H. Mori, Y. Sekine, Y. Takahashi, J. Health Sci. 49 (2003) 55.
[13] R.N.M.J. Páscoa, S.S.M.P. Vidigal, I.V. Tóth, A.O.S.S. Rangel, J. Agric. Food Chem. 54 (2006) 19.
[14] F. Lázaro, M.D. Luque de Castro, M. Valcárcel, Anal. Chem. 59 (1987) 1859.
[15] A.O.S.S. Rangel, I.V. Tóth, Am. J. Enol. Vitic. 50 (3) (1999) 259.
[16] M. Hedenfalk, B. Mattiason, Anal. Lett. 29 (7) (1996) 1109.
[17] R.A.S. Lapa, J.L.F.C. Lima, I.V.O.S. Pinto, Food Chem. 81 (2003) 141.
[18] Y. Chen, J. Ruzicka, Analyst 129 (2004) 597.
[19] J. Ruzicka, T. Gübeli, Anal. Chem. 63 (1991) 1680.
[20] T. Gübeli, G.D. Christian, J. Ruzicka, Anal. Chem. 63 (1991) 2407.
[21] www.sigma-aldrich.com, consulted in April of 2006.
[22] M.A. Segundo, A.O.S.S. Rangel, Anal. Chim. Acta 499 (2003) 99.
[23] M.D. Luque de Castro, J. González-Rodriguez, P. Pérez-Juan, Food Rev. Int. 21 (2005) 231.
[24] J.C. Miller, J.N. Miller, Statistics for Analytical Chemistry, 3rd ed., Ellis Horwood, New York, 1993, pp. 101–139.
[25] J.C. Miller, J.N. Miller, Statistics for Analytical Chemistry, 3rd ed., Ellis Horwood, New York, 1993, pp. 53–77.

Talanta 77 (2008) 815–821

Contents lists available at ScienceDirect

Talanta

journal homepage: www.elsevier.com/locate/talanta

Electrochemical immunoassay for α-fetoprotein through a phenylboronic acid monolayer on gold

Zhi Wang[a], Yifeng Tu[a,*], Songqin Liu[b,*]

[a] Institute of Analytical Chemistry, School of Chemistry and Chemical Engineering, Suzhou University, Suzhou 215123, PR China
[b] Jiangsu Provincial Key Laboratory of Biomaterials and Biodevices, School of Chemistry and Chemical Engineering, Southeast University, Jiangning, Nanjing 211189, PR China

ARTICLE INFO

Article history:
Received 23 April 2008
Received in revised form 10 July 2008
Accepted 16 July 2008
Available online 31 July 2008

Keywords:
Immunosensor
Self-assembled monolayer
Amperometry
α-Fetoprotein
Regeneration

ABSTRACT

A novel reusable electrochemical immunosensor for α-fetoprotein (AFP) based on phenylboronic acid monolayer on gold was proposed. The sensor was fabricated by immobilizing of 3-aminophenylboronic acid (APBA) conjugated thiol-mixed monolayer on gold through 2-(5-norbornene-2,3-dicarboximido)-1,1,3,3-tetramethyluronium tetrafluoroborate (TNTU) as linkage. AFP and enzyme-conjugated antibody were further trapped to the modified electrode surface through sugar–boronic acid and immunoaffinity interactions, respectively. The attached enzyme-conjugated antibody on the electrode surface could catalyze the reduction of hydrogen peroxide in the presence of thionine, which can be used to detect AFP in human serum by a competitive mechanism. Cyclic voltammetric, electrochemical impedance studies and photometric activity assays were used to probe the assembly and regeneration process of the immunosensor. The influences of the competitive ratio of antigen and antibody, pH value of the measuring solution, incubation temperature and time were explored for optimizing the analytical performance. The whole assay process including incubation, detection and regeneration of the electrode could be completed in 35 min. The detection of AFP in five serum samples provided from clinically diagnosed patients with liver cancer showed acceptable accuracy. The proposed immunosensor enabled fast, low-cost and would be valuable for clinical diagnosis.

1. Introduction

Recently, the reaction of boronic acid with sugars and/or glycoproteins has been extensively investigated for biosensor designs and recognition, separation and/or purification of glycoproteins [1–6]. For example, the immobilization of boronic acid in gels could be used for affinity chromatographic purification and detection of glycoproteins [2,7], especially for the separation and detection of glycated hemoglobin [8]. Copolymers containing boronic acid ligands, such as phenylboronic acid modified poly-*N*-vinyl-2-pyrrolidone [9], poly(*N*-isopropylacrylamide) derivatized phenylboronic acid [10], boronic acid functionalized poly(vinyl alcohol) membrane [11] and *m*-acrylamidophenylboronic acid–acrylamide copolymer [12], poly(aniline boronic acid) [4], have been widely used for saccharide sensing. Moreover, poly(aniline boronic acid) was used for the open tubular modification of capillary electrophoresis (CE) capillaries to separate diastereoisomers and proteins [2] and for molecular imprint technology to selectively recognize proteins [13], as well as for the development of DNA lectin mimics based on the PCR amplification of boronic acid-labeled DNA [14].

On the other hand, the immobilization of boronic acid on a solid matrix could be used for recognition, separation and purification of glycoproteins. For instances, boronic acid on magnetic microparticles could be used for enrichment of glycosylated human serum proteins, which could be further digested with trypsin and purified with magnetic MB-HIC C8 beads [15]. The boronic acid functionalized magnetic beads were also used for the separation of glycated hemoglobin, fibrinogen or RNase B [16]. This separation could be demonstrated by matrix-assisted laser desorption/ionization time of flight mass spectrometry. Moreover, the coupling of 3-aminophenylboronic acid (APBA) with dithiodialiphatic acids on either metallic colloids or gold electrodes [1], epoxy-boronate mixed monolayer [17], and phenylboronic acid monolayer [18–20] on gold has also been reported for the electrochemical sensing of sugars or glycoproteins. We demonstrated previously that the glycated molecules such as flavin adenine dinucleotide, horseradish peroxidase (HRP), glucose oxidase, and glycated antigen carcinoembryonic antigen (CEA) could bind specifically to phenylboronic acid monolayer on gold [20,21]

* Corresponding authors. Tel.: +86 25 52090613; fax: +86 25 52090616.
E-mail addresses: Tuyf_1@hotmail.com (Y. Tu), liusq@seu.edu.cn (S.Q. Liu).

0039-9140/$ – see front matter © 2008 Elsevier B.V. All rights reserved.
doi:10.1016/j.talanta.2008.07.039

or glassy carbon electrode [22]. The specific binding of these molecules to APBA interface was reversible and could be removed by sorbitol and acidic buffer. Based on this binding reversibility we successfully constructed a reusable immunosensor for the detection of CEA [21]. However, the analysis process including the binding of enzyme-conjugated CEA to APBA interface, the formation of the immunocomplex and the regeneration with sorbitol was complicated and time-consuming (approx. 1.5 h). To make the above method more practical, an improvement has been introduced in the present study by directly fixing the glycosylated antigen onto the boronic acid interface (Scheme 1). α-Fetoprotein (AFP), a 70 kDa glycoprotein with a single-chain alpha globulin composed of 590 amino acids and 3.4% carbohydrate that acts as an important tumor marker for the diagnosis of hepatocellular car-

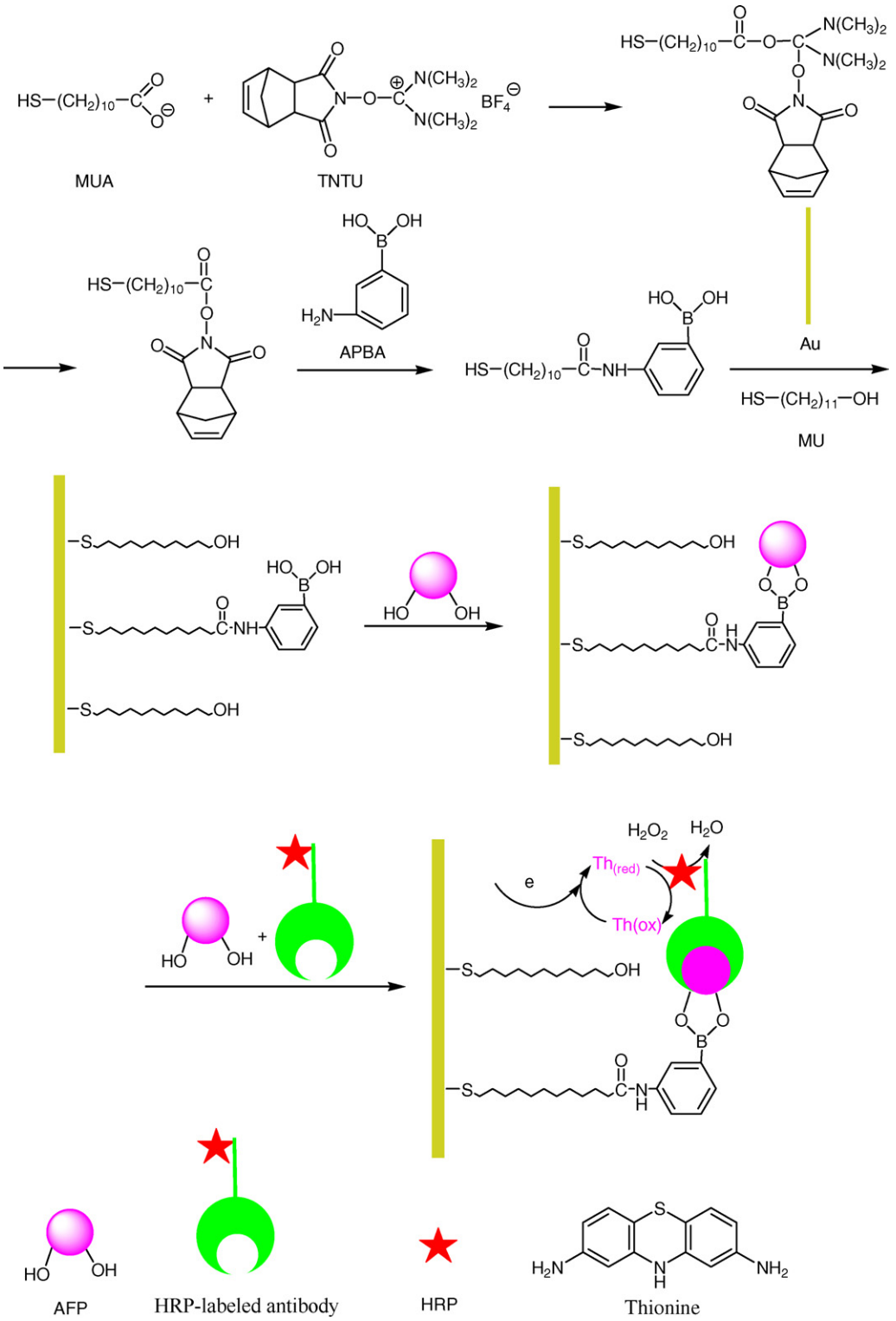

Scheme 1. Preparation of the immunosensor.

cinoma [23,24], was chosen to study this binding performances and the applications for reusable amperometric immunosensors. Our study demonstrated that glycoprotein AFP could be effectively bounded to the APBA interface on gold. The bound AFP could capture its HRP-labeled antibody from the analyte solution. This led to the increase of the charge-transfer impedance and the catalytical current to the reduction of H_2O_2 in the presence of thionine. The trapped HRP-labeled antibody by the immobilized AFP on gold could be easily regenerated with a basic solution, which produced a reusable immunosensor with R.S.D. of 2.5% for five times regeneration. Comparison with the previous work, the present work shortened the analysis time from 1.5 h to 35 min and facilitated the analysis processes.

2. Experimental

2.1. Chemicals

HRP-labeled carcinoembryonic antigen (HRP-anti-CEA), human AFP in a Tris–HCl buffered salt solution containing bovine serum albumin (BSA) and 0.01% methyl-isothiazolone as preservative, stock solution of HRP-labeled AFP monoclonal antibody (HRP-anti-AFP) from mouse (approx. 20 μg/mL) were purchased from CanAg Diagnostics AB and used as received. 3-Aminophenylboronic acid, 11-mercaptoundecanoic acid (MUA), 11-mercapto-1-undecanol (MU), BSA, thionine chloride and 2-(5-norbornene-2,3-dicarboximido)-1,1,3,3-tetramethyluronium tetrafluoroborate were obtained from Sigma–Aldrich Chemical Company (China). *N*-Methylmorpholine (NMM) was supplied by Fluka (China). Clinical serum samples were provided by Jiangsu Institute of Cancer Prevention and Cure (Nanjing, China). All other chemicals were of analytical grade and were used without further purification. Deionized water was used throughout the study. 0.1 mol L^{-1} phosphate buffer solution (PBS) at various pH values was prepared by mixing the stock solution of K_2HPO_4 and KH_2PO_4, which was used as the measuring buffer.

The conjugates of mercaptoundecanoic acid and phenylboronic acid (MUA–APBA) were obtained according to Liu's methods [21]. Briefly, MUA (8.0 μmol) and TNTU (7.9 μmol) were dissolved in 100 μL DMF containing 1 μL NMM (9.6 μmol) and incubated for 15 min at room temperature. APBA (0.05 mmol) was dissolved in 4 mL 0.1 mol L^{-1} carbonate buffer solution (pH 9.0) with a final concentration of 10 mmol L^{-1}. Then 11 μL MUA–TNTU solution and 100 μL APBA solution were mixed together and incubated for 2 h at room temperature. The MUA–APBA conjugate thus obtained was stored at 4 °C in a freezer.

2.2. Preparation of the protein-modified electrodes

To fabricate the protein-modified electrodes, the Au-wires were cleaned by boiling in 2 mol L^{-1} KOH for 2 h, rinsed with water and stored in piranha solution (3:1 concentrated H_2SO_4/H_2O_2, v/v). Prior to the modification, the electrodes were sequentially rinsed with water, ethanol and water. The clean Au-wire electrodes were immersed in a mixing solution of 111 μL MUA–APBA conjugates and 11 μL 0.24 mmol L^{-1} MU solution in ethanol at 4 °C overnight and then rinsed thoroughly with ethanol and PBS to remove the physically adsorbed material. Using MU to form the alkanethiols-mixed monolayer has been demonstrated to enhance the specific interface area and reduce the steric hindrance for the binding of protein [25–28]. The resulting APBA–MUA/MU-modified Au electrodes were further deposited in a 30 μL 60 ng mL^{-1} AFP solution for 1 h at 4 °C to generate the AFP-modified electrodes (AFP–APBA–MUA/MU–Au). After being rinsed thoroughly with PBS and soaked in 1% BSA for 30 min at 4 °C to block the possible remaining active site for non-specific binding, the modified electrodes were then stored in PBS for the following electrochemical measurements. The detail process for fabrication of the sensor was shown in Scheme 1.

2.3. Electrochemical measurements

Electrochemical measurements were performed with a CHI 660C electrochemical workstation (Shanghai, China). The three-electrode system was used for all electrochemical experiments, employing one of the above electrodes, platinum wire, and an Ag/AgCl electrode (saturated KCl) as the working, auxiliary, and reference electrodes, respectively. The cyclic voltammograms were recorded in 0.1 mol L^{-1} PBS solution containing 40 μmol L^{-1} thionine and 2.0 mmol L^{-1} H_2O_2. The AC impedance experiment was carried out with frequencies ranging from 100 kHz to 0.01 Hz in a 0.1 mol L^{-1} KCl solution containing 5 mmol L^{-1} 1:1 $K_3[Fe(CN)_6]/K_4[Fe(CN)_6]$. The data was recorded at the open circuit potential and fitted with an equivalent circuit Rs(RctCPE) for extraction of electrical parameters, such as resistance, from the impedance spectra [22,29].

A competitive method was used for the determination of AFP in samples [21,30–32]. Prior to measurement, the AFP–APBA–MUA/MU-modified electrode was incubated in a 1:9 (v/v) mixture solution of HRP-anti-AFP and AFP with different concentrations at 35 °C for 30 min to capture the free enzyme-conjugated antibody. In this case, the AFP on the modified Au-wires competed to bind specifically with free HRP-anti-AFP in the incubation solution with the AFP in the solution. The bound HRP-anti-AFP on the electrode surface led to the increase of the reduction current of H_2O_2 resulted from the enzymatic reaction in the presence of thionine. With the increase of AFP concentration, the free HRP-anti-AFP reduced in the incubation solution. This led to a decrease of the trapped HRP-anti-AFP by the surface-coated AFP and the current signal of the immunosensor. The decrease of the current signals was proportional with the increase of the AFP concentration in incubation solution, which is the basic for quantities detection of AFP in the presented work. After the measurements the electrode could be regenerated by simply immersing it in a NaOH solution (10 mmol L^{-1}) for 2 min to split the HRP-anti-AFP from AFP interface. For the control experiments, the AFP–APBA–MUA/MU-modified electrode was immersed in a HRP (0.2 mg mL^{-1}), AFP (20 ng mL^{-1}) and BSA (0.25 mg mL^{-1}) solution at 35 °C for 30 min and then recorded the electrocatalytic response of these electrodes in the same solution.

2.4. Spectra analysis

The photometric measurements were employed to probe the binding nature of the enzyme-conjugated antibody with the AFP–APBA-modified electrode and the bioactivity of the bound enzyme-conjugated antibody [21,22]. It was performed with a UV–NIR spectrophotometer (Varian 5000, USA). Ten AFP–APBA-modified electrodes were incubated in a HRP-anti-AFP and AFP solution to capture the free enzyme-conjugated antibody. After being rinsed thoroughly with PBS and water, they were immersed in 300 μL 10 mmol L^{-1} NaOH solution for 2 min to release the HRP-anti-AFP from the electrode surface. After being moved away from these electrodes, a mixture of 90 μL of 10 mmol mL^{-1} H_2O_2 and 2610 μL of 0.2 mg mL^{-1} TMB in pH 5.0 PBS was added to the above system, and solution absorption at 652 nm was measured for 10 min. HRP-free solutions were used as reference.

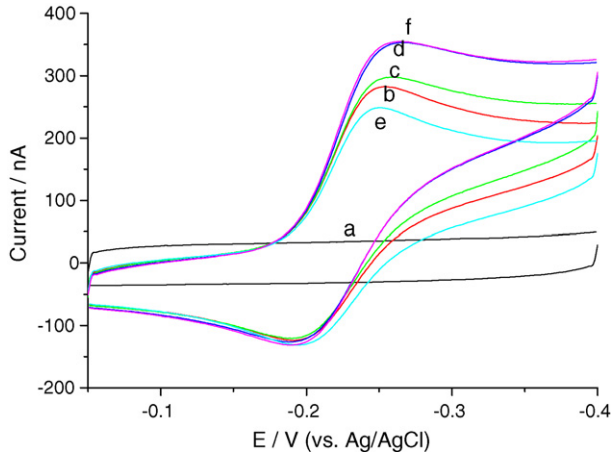

Fig. 1. CV of AFP-modified electrode in (a) 0.1 mol L^{-1} pH 8.5 PBS, (b) addition of 40 μmol L^{-1} thionine, (c) further addition of 2 mmol L^{-1} H_2O_2, (d) AFP-modified electrode incubated in HRP-anti-AFP for 30 min. (e) HRP-anti-AFP-modified electrode immersed in 10 mmol L^{-1} NaOH for 2 min (f) is (e) reincubated in HRP-anti-AFP solution for 30 min. The buffer solution is the same as (c) and the scan rate is 50 mV s^{-1}.

3. Results and discussion

3.1. Binding nature of the AFP–APBA–MUA/MU–Au

It has been reported that the thiol-mixed monolayer formed by immersing the cleaned Au-wire electrodes in a mixture solution containing 1:3 (mol ratio) of APBA–MUA conjugates and MU provides much more separated APBA sites than that of the MUA–APBA layer in the absence of MU on the gold electrode, and thus generates a better orientation for the binding of glycated proteins [25–28]. Therefore we chose the thiol-mixed monolayer to construct the immunosensor.

AFP with 3.4% carbohydrate [23] was expected to react with the APBA–MUA/MU-mixed monolayer through boronic acid–sugar interaction and thus affix the protein to the Au electrode. The AFP attachment and further formation of immunocomplex with its enzyme-conjugated antibody, HRP-anti-AFP, could be demonstrated by comparing the catalytic reduction of H_2O_2 in the presence of the electron-donor thionine. Fig. 1 shows the cyclic voltammograms of Au electrode with different coatings in 0.1 mol L^{-1} pH 8.5 PBS containing 40 μmol L^{-1} thionine and 2 mmol L^{-1} H_2O_2 at 50 mV s^{-1}. Upon addition of thionine and H_2O_2 to the buffer solution, a slightly increased reduction current could be observed from the AFP–APBA–MUA/MU–Au (Fig. 1a–c). After being incubated in HRP-anti-AFP solution for 30 min, the HRP-anti-AFP/AFP–APBA-modified electrode displayed an enhanced reduction current with the shape of a catalytic wave (Fig. 1d). The catalytic current of a HRP-anti-AFP-modified Au electrode was four times larger than that of an AFP–APBA–MUA/MU–Au electrode not exposed in HRP-anti-AFP solution (Fig. 1c). Control experiments using two proteins such as AFP or BSA instead of HRP-anti-AFP to react with the AFP–APBA interface showed that no detectable catalytic currents were observed (see supporting information). These results strongly suggested the successful trapping of HRP-anti-AFP to AFP–APBA interface and the electrocatalytic response came from the electrocatalytic property of HRP on the electrode surface [22,33,34]. As the HRP-anti-AFP was also a glycoprotein, two binding modes were thus possible: reaction with bound AFP to yield the immunocomplex or reaction with APBA interface to exchange AFP. Both, the antibody–antigen interaction and the exchange of AFP from the electrode surface, caused increase of the electrocatalytic response. To understand the binding mode of HRP-labeled AFP antibody to the AFP-modified electrode, glycoproteins such as HRP (glycosylation degree of 16–21%) [35] and HRP-anti-CEA (total of 28 asparagine-linked glycosylation sites) were employed for the control experiment. Using HRP and HRP-anti-CEA instead of HRP-labeled AFP antibody to react with AFP–APBA-modified electrode, no enhanced catalytically current was observed, respectively (see supporting information). These observations suggested (1) the presence of AFP on electrode surface blocked the HRP or HRP-anti-CEA to close and react with APBA interface; (2) HRP or HRP-anti-CEA could not replace AFP on the APBA-modified surface; (3) HRP or HRP-anti-CEA could not bind with AFP antigen on the electrode surface through an immunoreaction. Thus, the dominant interaction between HRP-labeled AFP antibody and AFP was specific formation of immunocomplex instead of competing binding of HRP-labeled AFP with APBA-binding sites. We speculated that HRP-labeled AFP antibody reacted with AFP before it diffused to the lower and more embedded APBA interface. The relatively large size of HRP-labeled AFP antibody also reduced its capability to bypass the AFP layer to reach the APBA interface.

The formation of immunocomplex was supported by its regeneration properties. It is well known that the antigen–antibody immunocomplex can be interrupted by using a strong acidic solution, e.g. 0.1 mol L^{-1} glycine–HCl (pH 2.2), or a strong basic solution, e.g. 0.1 mol L^{-1} NaOH [33]. Because of the low stability of sugar–boronic acid interaction in strong acidic solution [20,36], a 10 mmol L^{-1} NaOH was chosen as the regeneration solution. After immersing the HRP-anti-AFP/AFP–APBA-modified electrode in 10 mmol L^{-1} NaOH for 2 min, no clear catalytic current could be observed (Fig. 1e), indicating the release of HRP-anti-AFP from the AFP–APBA interface. Further incubation of this electrode in HRP-anti-AFP stock solution, the catalytic current recovered to its original state (Fig. 1f). The ^{11}B NMR spectra analysis indicated that some boronate complex was somewhat unstable at pH 11.0 [37]. In our case, the pH of regeneration solution (10 mM NaOH) is 12.0. Thus the binding of AFP and APBA might unstable at this pH and HRP-anti-AFP might bind directly with APBA interface (NaOH split AFP from APBA interface), which led to increase of catalytic current after a regeneration step. To illustrate this binding mode, the AFP-modified electrode after regeneration step was directly dipped into a 0.2 mg/mL HRP solution for 30 min, and then the catalytic response to the reduction of H_2O_2 in the presence of thionin was measured. If the AFP–APBA binding is not stable, it should be interrupted with NaOH. The resulting electrode should react with HRP and give a catalytic response. No enhanced catalytically current was observed in this measurement, suggesting that AFP–boronic acid complex was stable in this generation solution (see supporting information). This also indicated that the AFP on gold remained its immunoactivity to form the immunocomplex with HRP-labeled AFP after the regeneration procedure. Repetition this regeneration process, the sensor gave a good reproducibility with R.S.D. of 2.5% for five times regeneration.

The formation of immunocomplex was also supported by photometric measurements using TMB as the substrate. In this case, 10 AFP–APBA-modified electrodes were incubated in a HRP-anti-AFP and AFP solution to capture the free enzyme-conjugated antibody. After being washed thoroughly with PBS and water, they were immersed in 300 μL 10 mmol L^{-1} NaOH solution for 2 min. After moved away of these electrodes, H_2O_2 and TMB were added and solution absorption at 652 nm was measured for 10 min (Fig. 2b). The absorption peak suggested the presence of HRP-anti-AFP in the NaOH solution. Control experiments using HRP instead of HRP-anti-AFP in incubation solution, no clear absorption peak at 652 nm could be observed, indicating that the trapped of HRP-anti-AFP to

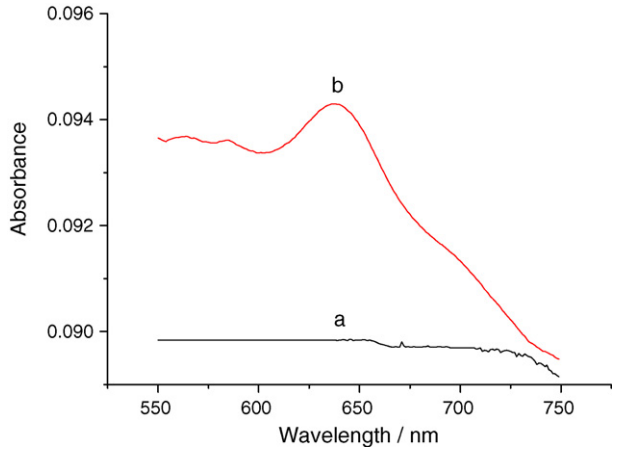

Fig. 2. UV–vis–NIR spectra. (a) is the mixture of 2.5 mL PBS (0.1 mol L^{-1}, pH 5.0), 490 μL TMB (0.2 mg mL^{-1}) and 10 μL H_2O_2 (10 mmol L^{-1}), and (b) is the mixture of (a) and the regeneration solution after immersing of the HRP-anti-AFP/AFP–APBA–MUA/MU–Au in 10 mmol L^{-1} NaOH for 2 min.

the electrode surface is due to the formation of the immunocomplex.

The attachment of AFP and the formation of immunocomplex could be further supported by the electrochemical impedance spectra analysis. The impedance measurements were carried out in 0.1 mol L^{-1} KCl containing 5 mmol L^{-1} 1:1 $K_3[Fe(CN)_6]/K_4[Fe(CN)_6]$ with an open circuit potential. The frequency was varied from 100 kHz to 10 mHz. Fig. 3 represents the Nyquist plots of the same electrode with different coatings. The charge-transfer resistance (R_{ct}) of the APBA-modified electrode in the absence of AFP (a) was much smaller than that of AFP–APBA–MUA/MU–Au (b). The increase of impedance from 16.8 to 50.9 kΩ of AFP–APBA–MUA/MU–Au to APBA–MUA/MU–Au was due to the immobilization of glycoprotein on the APBA interface, which significantly reduced the diffusion of the redox species through the film, making the redox process more difficult and causing the impedance to increase. After incubation of the AFP-modified electrode in a HRP-anti-AFP stock solution for 30 min, the impedance further increased from 50.9 to 93.6 kΩ (c) due to the formation of immunocomplex. These results were in agreement with the phenomena

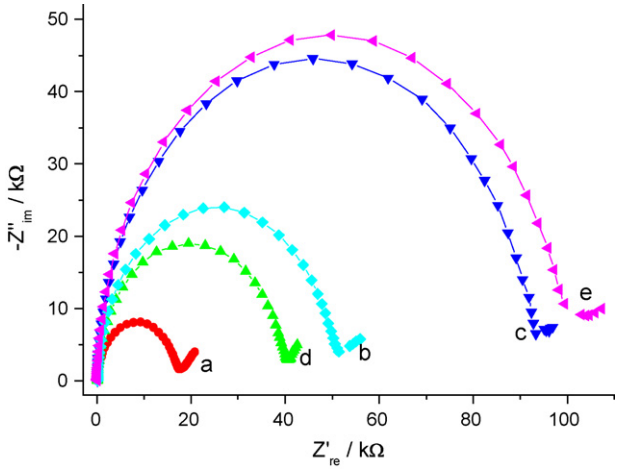

Fig. 3. Electrochemical impedance spectra: (a) APBA–MUA/MU-modified electrode, (b) immersed (a) in AFP for 1 h, (c) is (b) incubated in HRP-anti-AFP solution for 30 min, (d) is (c) immersed in 10 mmol L^{-1} NaOH for 2 min and (e) is (d) reincubated in HRP-anti-AFP solution for 30 min. The data were recorded in 0.1 M KCl containing 5 mM 1:1 $K_3[Fe(CN)_6]/K_4[Fe(CN)_6]$ with frequencies ranging from 100 kHz to 0.01 Hz.

observed from other electrochemical impedance immunosensors [33,38–40]. Subsequent immersion of the HRP-anti-AFP/AFP-modified electrode in 10 mmol L^{-1} NaOH for 2 min, the impedance decreased from 93.6 to 40.1 kΩ (d), slightly smaller than that of 50.9 kΩ for AFP first binding, indicating the release of the bounded HRP-anti-AFP from the AFP–APBA interface. Reincubation of this electrode in HRP-anti-PSA solution for 30 min, the impedance increased from 40.1 to 100.6 kΩ (e), slightly larger than 93.6 kΩ for HRP-anti-AFP/AFP-modified electrode (b), indicating the successful rebinding of HRP-anti-AFP with the AFP–APBA interface.

All these results illustrated that the resulted APBA–MUA/MU interface on gold can react with glycoprotein, AFP, based on the sugar–boronic acid interaction. The attached AFP on gold remained its immunoactivity by capturing its antibody to form the immunocomplex. The immunocomplex can be interrupted with a generation solution, which provides a possibility for rebinding HRP-labeled AFP antibody to the electrode surface. This can be used as the basic for AFP determination as shown as follows.

3.2. Optimization of immunoassay conditions

The analytical performance of the immunosensor was related to the ratio of HRP-anti-AFP and AFP, the incubation temperature and time in the incubation solution. The effects of the ratio of HRP-anti-AFP and AFP in the incubation solution on enzymatic reactions were examined as shown in Fig. 4A. In this case, a certain amount of HRP-anti-AFP stock standard solution (5 μL) mixed with different volume of AFP with a concentration of 2.5 ng mL^{-1}. At the mixture ratio of 1:5 and 1:7, the current response was similar to 1:0, no AFP in incubated solution. This suggested that the total binding sites of the surface-coated AFP on gold were occupied by the free HRP-anti-AFP in the incubation solution. When the ratio of HRP-anti-AFP:AFP increased to 1:9, the current signal of the immunosensor decreased, indicated that the free HRP-anti-AFP was not enough to saturate the surface-coated AFP on gold at this ratio. Thus the ratio of 1:9 was applied in the following competitive immunoassays.

The reaction of the antigen–antibody mostly depends on the incubation temperature and time in the incubation solution. By incubating AFP–APBA-modified electrode in HRP-anti-AFP standard stock solution for different periods of time, the catalytic current increased with increasing incubation time, approaching a maximum value at 30 min (Fig. 4B). Thus, the incubation time was controlled to be at 30 min. To test the optimal temperature for the incubation solution, the AFP-coated electrode was incubated in HRP-anti-AFP solution at different temperatures. The catalytic current of the immunosensor to H_2O_2 increased with the temperature in the incubation solution increasing from 10 to 35 °C, due to much faster formations of the immunocomplex in higher temperature. When the temperature reached above 35 °C, the catalytic current of the immunosensor to H_2O_2 decreased as a result of the lack of activity in the conjugated enzyme. Therefore, the temperature of the incubation solution was controlled to be at 35 °C.

The pH of the measuring solution affected the binding of AFP on the APBA interface and the conjugated enzyme activity. Given that an acidic solution with low pH also interfered with AFP:APBA interaction [20,36], a basic solution with pH 7.0–9.0 in the measuring solution was investigated. Fig. 4C shows the cyclic voltammograms of the AFP-modified electrode and the effect of pH on the catalytic current. The catalytic current increased with increasing pH from 7.0 to 8.5 because the boronate complex with cis-diol moiety was much more stable in alkaline conditions [20,36]. Further increasing of the pH the catalytic current decreased due to low activity of the conjugated enzyme. Thus the optimal pH value of the detection solution was pH 8.5.

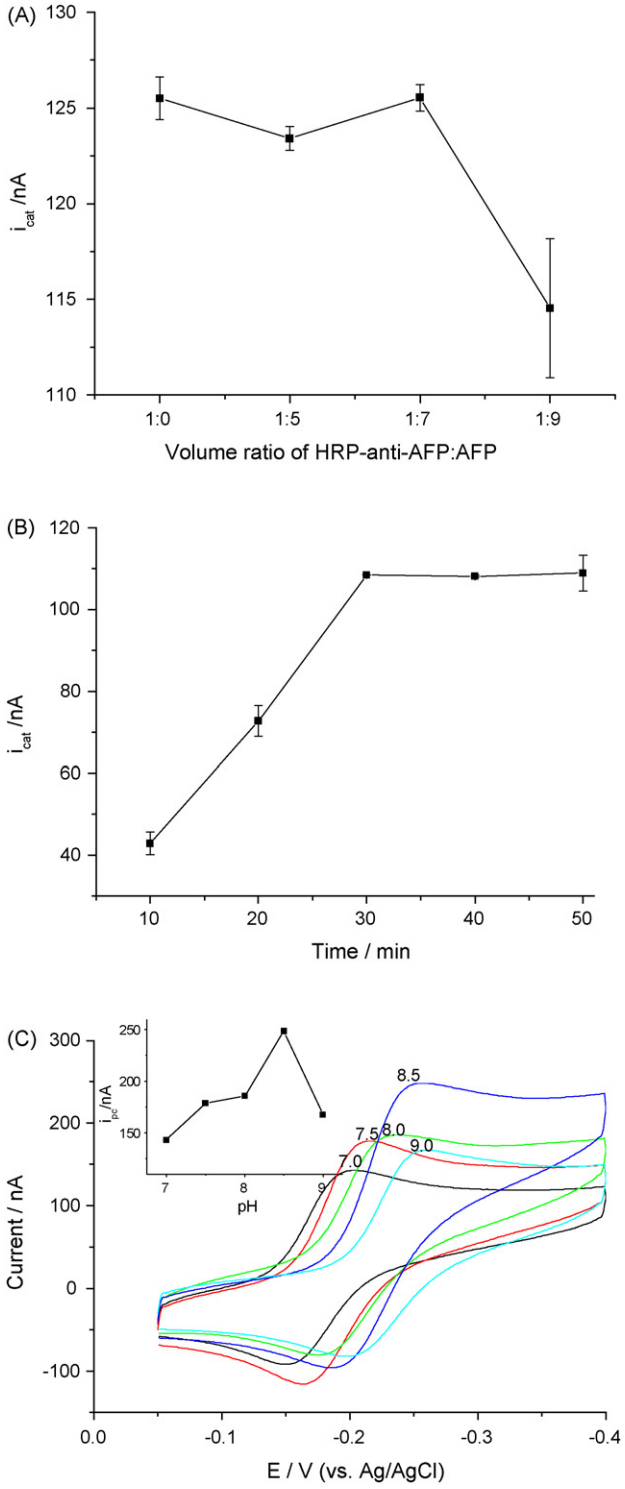

Fig. 4. Effect of the volume ratio of HRP-anti-AFP and AFP (A) and incubation time (B) in the incubation solution and pH of the measuring solution (C) on the electrocatalytic current of an HRP-anti-AFP-modified electrode. The electrocatalytic current was gained from CV in PBS (pH 8.5, 0.1 mol L^{-1}) containing thionine (40 μmol L^{-1}) and H_2O_2 (2 mmol L^{-1}) at −0.25 V.

3.3. Analysis of performances of the AFP immunosensor

Under the optimal conditions, the catalytical current of the immunosensor decreased with increasing AFP concentration in the incubation solutions as shown in Fig. 5. When the AFP-modified

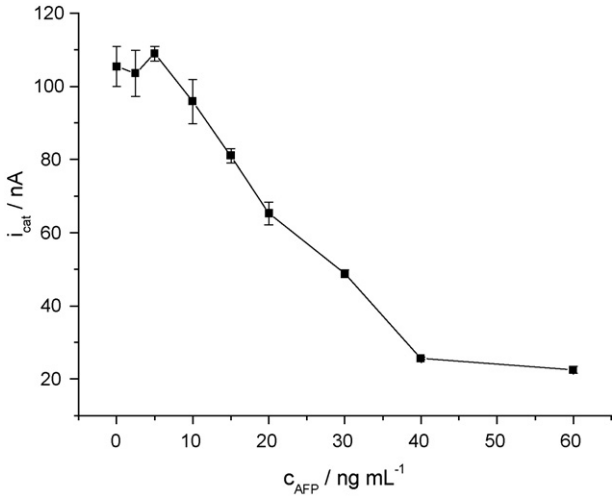

Fig. 5. Calibration curve of the current response *vs.* concentration of AFP in the incubation solution under optimal conditions. Inset shows linear calibration curves.

electrode was incubated in the mixture of 1:9 HRP-anti-AFP and AFP with different concentrations for 30 min, the cyclic voltammogram was recorded in 0.1 mol L^{-1} pH 8.5 PBS containing 40 μmol L^{-1} thionine and 2 mmol L^{-1} H_2O_2 and the catalytic current at −0.25 V was detected. The catalytic current decreased linearly at the AFP concentration range of 5–40 ng mL^{-1}. The regression equation was I (nA) = 117.5–2.3c (ng mL^{-1}) with a correlation coefficient of 0.9988 (insert in Fig. 5), where I is the catalytic current, and c is the AFP concentration in the incubation solution. When the AFP concentration exceeded to 40 ng mL^{-1}, a few HRP-labeled anti-AFP molecules were free to be captured by the immobilized AFP on gold and thus gave a low detection signal.

As we know that the presence of sugars interferes with the coupling of glycoprotein to boronic acid interface. Thus the effect of glucose in the incubation solution on detection was investigated. In this case, different amounts of glucose were added to the mixture of 1:9 HRP-labeled AFP antibody and 20 ng mL^{-1} AFP, followed by incubation of the AFP-modified electrode in this mixture solution for 30 min. The catalytical currents measured were shown in Fig. 6. It is noticed that the catalytical current was stable in the glucose concentration range from 1 to 10 mmol L^{-1}. It is known that the glucose concentration in the blood of a healthy adult is

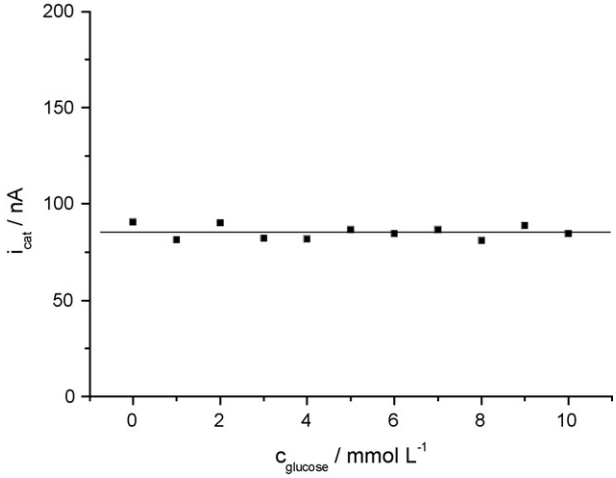

Fig. 6. The effect of different concentration of glucose in the incubation solution containing 1:9 HRP-anti-AFP and 20 ng mL^{-1} AFP from 1 to 10 mmol L^{-1}.

Table 1
Comparison of serum AFP levels in clinically determined using the proposed methods with immunoradiometric relative method (ng mL^{-1})

Sample	Proposed method (ng mL^{-1})	Immunoradiometric relative method (ng mL^{-1})	Deviation (%)
1	349.8 ± 8.2	339.6	−2.91
2	345.3 ± 16.7	346.8	0.434
3	1570 ± 18.9	1693.7	7.88
4	263.8 ± 5.4	259.4	−1.67
5	163.2 ± 10.2	149.7	−8.27

The data presents an average of the three independent measurements.

3.6–6.4 mmol L^{-1}, thus the presence of glucose in human blood should not interfere with the detection of AFP.

The accuracy of AFP immunosensor was examined by comparing the results obtained using the described method with those detected in clinic. Five AFP clinical serums were analyzed using the described method. The AFP concentrations in the clinical serum of some patients were beyond the linear range of the described method; thus proper dilution with 0.85% NaCl before assay was necessary. The results were compared with those obtained using a standard method provided by Jiangsu Institute of Cancer Prevention and Cure (Table 1). The relative deviation in the range from −8.27 to 7.88% between the two methods was considered as acceptable. The presence of glucose in blood did not seem to interfere with the binding of glycoproteins to the boronic acid interface; thus negligent effects on the detection of glycated antigen protein in blood were noticed.

4. Conclusions

A reusable and rapid immunoassay for the determination of AFP in human blood was obtained through the specific interaction between glycoprotein antigen and boronic acid monolayer on gold in combination with the competitive immunoreaction methods. Self-assembled APBA–MUA/MU-mixed monolayer on gold was suitable for the trapping of AFP based on the sugar–boronic acid interaction. The coated AFP could further capture its HRP-labeled antibody from the analyte solution. This led to the increase of the catalytical current to the reduction of H_2O_2 in the presence of thionine and the charge-transfer impedance. The trapped HRP-labeled antibody by the immobilized AFP on gold could be easily regenerated with a basic solution, which produced a reusable immunosensor with R.S.D. of 2.5% for five times regeneration. The whole assay process including regeneration of the electrode could be completed in 35 min. The glucose coexisted in blood known to interfere with the binding of glycoprotein to boronic acid interface did not affect the detection of glycated antigen protein in blood. In comparison with the traditional method, the described method showed acceptable reproducibility, and the results obtained from clinical sera were in acceptable agreement with those from parallel single-analyte tests.

Acknowledgments

The project is supported by the National Natural Science Foundation of China (Grant Nos. 20275025, 20675013, 20675055) and the Natural Science Foundation of Jiangsu (Grant No. BK2006090).

Appendix A. Supplementary data

Supplementary data associated with this article can be found, in the online version, at doi:10.1016/j.talanta.2008.07.039.

References

[1] N. Kanayama, H. Kitano, Langmuir 16 (2000) 577.
[2] A. Monzo, G.K. Bonn, A. Guttman, Anal. Bioanal. Chem. 389 (2007) 2097.
[3] T.D. James, K.R.A.S. Sandanayaka, S. Shikai, Nature 374 (1995) 345.
[4] E. Shohi, M.S. Freund, J. Am. Chem. Soc. 124 (2002) 12486.
[5] A. Kikuchi, K. Suzuki, O. Okabayashi, H. Hoshino, K. Kataoka, Y. Sakurai, T. Okano, Anal. Chem. 68 (1996) 823.
[6] N. Soh, M. Soneazki, T. Imato, Electroanalysis 12 (2003) 1281.
[7] Y.C. Li, E.L. Larsson, H. Jungvid, I.Y. Galaev, B. Mattiasson, Chromatographia 54 (2001) 213.
[8] A. Bossi, L. Castelletti, S.A. Piletsky, A.P.F. Turner, P.G. Righetti, J. Chromatogr. A 1023 (2004) 297.
[9] S. Kitano, Y. Koyama, K. Kataoka, T. Okano, Y. Sakurai, J. Control. Release 19 (1992) 162.
[10] K. Kataoka, H. Miyazaki, M. Bunya, T. Okano, Y. Sakurai, J. Am. Chem. Soc. 120 (1998) 12694.
[11] A. Kikuchi, K. Suzuki, O. Okabayashi, H. Hoshino, K. Kataoka, Y. Sakurai, T. Okano, Chem. Anal. 68 (1996) 823.
[12] R. Gabai, N. Sallacan, V. Chegel, T. Bourenko, E. Katz, I. Willner, J. Phys. Chem. B 105 (2001) 8196.
[13] A. Bossi, S.A. Piletsky, E.V. Piletska, P.G. Righetti, A.P.F. Turner, Anal. Chem. 73 (2001) 5281.
[14] N. Lin, J. Yan, Z. Huang, C. Altier, M.Y. Li, N. Carrasco, M. Suyemoto, L. Johnston, S.M. Wang, Q. Wang, H. Fang, J. Caton-Williams, B.H. Wang, Nucleic acids Res. 35 (2007) 1222–1229.
[15] K. Sparbier, T. Wenzel, M. Kostrzewa, J. Chromatogr. B 840 (2006) 29–36.
[16] J.H. Lee, Y.S. Kim, M.Y. Ha, E.K. Lee, J.B. Choo, J. Am. Soc. Mass Spectrom. 16 (2005) 1456–1460.
[17] J.M. Abad, M. Velez, C. Santamaria, J.M. Guisan, P.R. Matheus, L. Vazquez, I. Gazaryan, L. Gorton, T. Gibson, V.M. Fernandez, J. Am. Chem. Soc. 124 (2002) 12845.
[18] M. Zayats, E. Katz, I. Willner, J. Am. Chem. Soc. 124 (2002) 14724.
[19] J.C. Vidal, J. Espuelas, J.R. Castillo, Anal. Biochem. 333 (2004) 88.
[20] S.Q. Liu, U. Wollenberger, J. Halámek, E. Leupold, W. Stöcklein, A. Warsinke, F.W. Scheller, Chem. Eur. J. 11 (2005) 4239.
[21] X. Zhang, Y.F. Wu, Y.F. Tu, S.Q. Liu, Analyst 132 (2008) 485–492.
[22] S.Q. Liu, B. Miller, A. Chen, Electrochem. Commun. 7 (2005) 1232.
[23] C.G. Bergstrand, B. Czar, Scand. J. Clin. Lab. Invest. 8 (1956) 174.
[24] Y. Yamagata, H. Katoh, K. Nakamura, T. Tanaka, S. Satomura, S. Matsuura, J. Immunol. Meth. 212 (1998) 161.
[25] B. Ge, F. Lisdat, Anal. Chim. Acta 454 (2002) 53.
[26] A.E. Kasmi, J.M. Wallace, E.F. Bowden, S.M. Binet, R.J. Linderman, J. Am. Chem. Soc. 120 (1998) 225.
[27] C. Boozer, Q. Yu, S. Chen, C.Y. Lee, J. Homola, S.S. Yee, S. Jiang, Sens. Actuators B 90 (2003) 22.
[28] L. Hugo, D. Bernard, V. David, S. Christian, Biochemistry 41 (2002) 13424.
[29] S.Q. Liu, B.P. Lin, X.D. Yang, Q. Zhang, J. Phys. Chem. B 111 (2007) 1182.
[30] K. Inoue, P. Ferrante, Y. Hirano, T. Yasukawa, H. Shiku, T. Matsue, Talanta 73 (2007) 886.
[31] T. Kawaguchi, D.R. Shankaran, S.J. Kima, K.V. Gobi, K. Matsumoto, K. Toko, N. Miura, Talanta 72 (2007) 554.
[32] D. Du, X.X. Xu, S.F. Wang, A.D. Zhang, Talanta 71 (2007) 1257.
[33] Z. Dai, F. Yan, Y. Hua, X.Y. Hu, H.X. Ju, J. Immunol. Meth. 287 (2004) 13.
[34] Y. Zhuo, R. Yuan, Y.Q. Chai, D.P. Tang, Y. Zhang, N. Wang, X.L. Li, Q. Zhu, Electrochem. Commun. 7 (2005) 355.
[35] S. Aibara, H. Yamashita, E. Mori, M. Kato, Y. Morita, J. Biochem. 92 (1982) 531.
[36] M.F. Lappert, Chem. Rev. 56 (1956) 959.
[37] M.L. Stolowitz, C. Ahlem, K.A. Hughes, R.J. Kaiser, E.A. Kesicki, G. Li, K.P. Lund, S.M. Torkelson, J.P. Wiley, Bioconjug. Chem. 12 (2001) 229.
[38] C.M. Ruan, L.J. Yang, Y.B. Li, Anal. Chem. 74 (2002) 4814.
[39] L. Alfonta, I. Willner, D.J. Throckmorton, A.K. Singh, Anal. Chem. 73 (2001) 5287.
[40] S. Zhang, F. Huang, B.H. Liu, J.J. Ding, X. Xu, J.L. Kong, Talanta 71 (2007) 874.

Talanta 77 (2008) 628–634

Contents lists available at ScienceDirect

Talanta

journal homepage: www.elsevier.com/locate/talanta

Nanoparticle-amplified surface plasmon resonance study of protein conformational change at interface

Fuan Wang, Jianlong Wang, Xiaoqing Liu, Shaojun Dong*

State Key Laboratory of Electroanalytical Chemistry, Changchun Institute of Applied Chemistry, Graduate School of the Chinese Academy of Sciences, Chinese Academy of Sciences, Changchun 130022, China

ARTICLE INFO

Article history:
Received 11 April 2008
Received in revised form 7 June 2008
Accepted 15 June 2008
Available online 5 July 2008

Keywords:
Surface plasmon resonance
Gold nanoparticles
Protein folding
Layer-by-layer
Biosensors

ABSTRACT

This paper reports the study of protein conformational change by Au nanoparticles (AuNPs)-amplified surface plasmon resonance (SPR) spectroscopy. Taking cytochrome *c* (Cyt *c*) as an example, this paper gives a detailed description of the construction of metal–protein–metal sandwich nanostructure consisting of an Au film underlayer, a cytochrome *c* intermediate layer and an AuNPs upper layer. The incorporation of AuNPs into SPR biosensing results in increased SPR sensitivity to protein conformational change as demonstrated by acid denaturation of Cyt *c*. It suggests the conformational change of surface-confined Cyt *c* leads to the distance and electromagnetic coupling variations of Au film–AuNPs. The constructed Au film–Cyt *c*–AuNPs sandwich is stable to repeat acid treatment using solutions in the pH range of 2.0–10.0 and yields reproducible measurements. With high sensitivity and stability, nanoparticle-amplified SPR spectroscopy can be used as a supplement method to protein conformational study. It has potential for developing novel sensors and/or switching devices in response to protein conformational change.

1. Introduction

Surface plasmon resonance spectroscopy (SPRS) is a surface-sensitive technique based on the ability to detect dielectric constant change induced by molecular adsorption at a noble metal (usually gold) film. It is increasingly used as a unique and powerful analytical method for studies of biomolecular interaction and biosensing [1–4]. Because proteins folding state would affect their dielectric properties or thickness on Au film, it is possible to monitor the folding state or conformational change of protein by using SPRS. The conformational change of protein is resulted from the intrinsic flexibility of polypeptides structure and demonstrated to be very important in biological and engineered systems [5]. SPRS study of protein conformation was first carried out on dihydrofolate reductase (*Escherichia coli*) using acid as a denaturant [6]. Then, the conformational and electronic changes of redox protein were extensively studied by electrochemical SPRS [7]. SPRS, coupled with quartz crystal microbalance, has been used to investigate the ligand binding effects on the conformation of estrogen receptor–DNA complexes [8]. Recently, SPRS was used to monitor the ligand-induced conformational change of immobilized G-protein coupled receptor [9] and tissue transglutaminase [10]. In particular, several thermodynamics properties of the surface-confined protein could be quantified by using SPRS, as demonstrated separately by Zare's group [11,12] and Yi's group [13,14]. The quantification is based on the assumption that protein would change its structure under a certain denaturation environment, resulting in the variation of SPR curves, such as shifts of resonance angle at the reflectance minimum (θ_{SPR}) and reflectance (R/R_0) or change in width. In addition, these reports suggest that change in protein hydrodynamic volume, hydration state, and electronic state can sufficiently report upon the occurrence of a biochemical event at a SPR sensing surface. Accordingly, SPR measurements can contribute to our understanding of fundamental properties of biomolecules at solid–liquid interfaces.

Unfortunately, the inability of conventional SPRS to measure extremely small change in refractive index or dielectric constant hinders its application in ultrasensitive detection. To address this limitation, several ways have been developed. Among them, substantial interest has been focused on utilization of external labels with high molecular weight or high refractive index. Besides liposomes [15], latex particles [16] and certain protein [17], the most extensively studied and used amplification labels are Au nanoparticles (AuNPs), due to their superior properties including facile preparation, high density, large dielectric constant, and good biocompatibility [18–25]. There are several ways to integrate AuNPs for SPR measurements, for example, AuNPs can be used to label the analytes [19], fixed on the SPR-active substrates [20,21], embed-

* Corresponding author. Tel.: +86 431 85262101; fax: +86 431 85689711.
E-mail address: dongsj@ns.ciac.jl.cn (S. Dong).

0039-9140/$ – see front matter © 2008 Published by Elsevier B.V.
doi:10.1016/j.talanta.2008.06.042

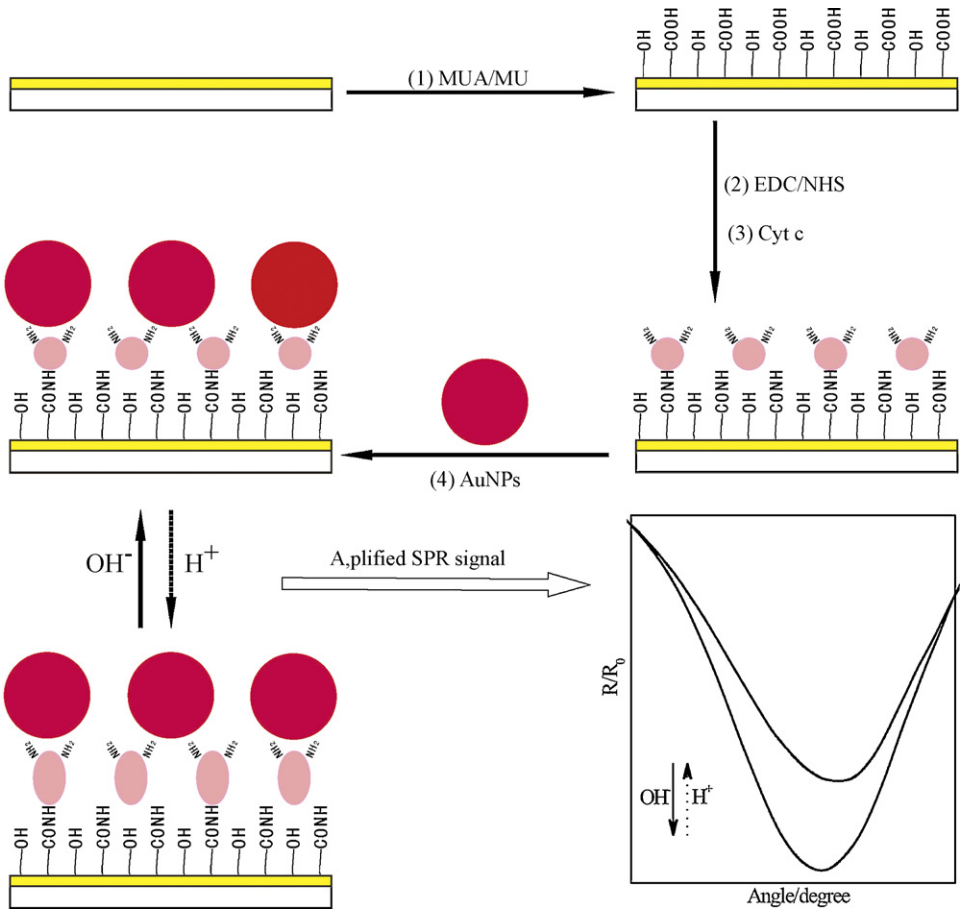

Fig. 1. Schematic illustration of the overall preparative procedure involved in the study, including the self-assembly of MUA/MU (1), immobilization of Cyt *c* (2 and 3) and AuNPs (4) (dimensions not to scale).

ded into molecularly imprinted polymers [22–24], or solubilized in aqueous solution [25]. All these reports demonstrate that SPR response can be dramatically enhanced by AuNPs and the amplification mechanisms of AuNPs amplified SPRS are mainly attributed to the coupling of the localized surface plasmons of AuNPs with the propagating plasmons of the Au film. Recently, the acid-induced swelling and shrinking of ultrathin polymer bush has been monitored by AuNPs amplified SPRS [26], implying that the protein conformational change could also be tracked by this method. Kang et al. constructed a surface-immobilized protein nanomachine by placing AuNPs atop the immobilized protein [13]. Heretofore, AuNPs amplified SPRS has been applied to highly sensitive detection of the antigen–antibody interaction and DNA hybridization, however, little attention has been given to its application in protein conformational research.

Cytochrome *c* (Cyt *c*) is a well-characterized globular protein both in the crystalline and in solution states and it represents the most common model for protein folding studies [27]. The acid-induced conformational change of Cyt *c* has been studied extensively by using various techniques, including SPRS [7,11,12]. The volume change and conformational transition of Cyt *c* with different pH have been determined, which is assigned to the hydration contribution from deprotonation of the protein, other hydration effects, and the formation and/or enlargement of packing defects in the protein tertiary structure during the steps of folding. The proposed denaturation mechanism is based on experiments both in bulk phase [12,28,29] and at interface [30,31]. As a surface-sensitive technique, SPRS had been successfully applied to study the conformational change of Cyt *c* at interface [7,11]. The reversible denaturation/renaturation of Cyt *c* on a solid surface might facilitate its further application as a sensor or a switch.

In this paper, we report the use of AuNPs amplified SPRS to study the denaturant induced conformational change of surface-confined Cyt *c*. Cyt *c* and AuNPs were successively immobilized onto the carboxylic acid terminated alkanethiol self-assembled monolayers (SAMs) modified Au film by consecutive adsorption from respective aqueous solution. SPRS was used to monitor the self-assembly process and investigate the denaturant-involved denaturation/renaturation of Cyt *c*. On the basis of this approach, we demonstrated that mounting AuNPs on Cyt *c* could dramatically enhance the SPR response of Cyt *c* denaturation/renaturation. As schematically shown in Fig. 1, the enhanced SPR response might be derived from the changing distance between AuNPs on the Cyt *c* and Au film on the sensor chip, which mirrors the conformational change of sandwiched Cyt *c*.

2. Experimental

2.1. Reagents

All aqueous solutions were made using deionized water, which was further purified with a Milli-Q system (Millipore). Horse heart cytochrome *c* (Cyt *c*, ≥95% (SDS-PAGE)), 11-mercaptoundecanoic acid (MUA), 11-mercaptoundecanol (MU), 1,6-hexanedithiol (HDT), *N*-hydroxysuccinimide (NHS) and *N*-(3-dimethylaminopropyl)-*N*′-ethylcarbodiimide hydrochloride (EDC) were obtained from

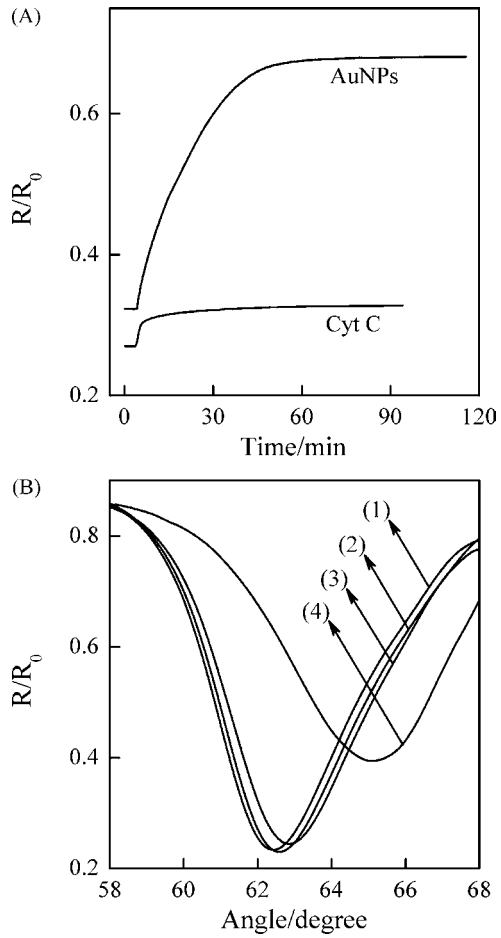

Fig. 2. (A) SPR *R–t* mode monitoring of in situ kinetics of Cyt *c* assembled onto the mixed MUA/MU SAMs modified Au film and the subsequent adsorption of AuNPs on Cyt *c* upon immersion of Au film into separate solutions. The reflectance change was measured at a fixed angle of incidence (θ_{SPR} = 62°). (B) In situ scanning SPR curves of MUA/MU (2), Cyt *c* (3), and AuNPs (4) sequential adsorption onto a bare Au film (1). All curves were recorded in pure water after washing.

Sigma–Aldrich. $HAuCl_4{\cdot}3H_2O$, trisodium citrate, phosphoric acid and sodium phosphate were purchased from Beijing Chemical Reagent Co. 20 mM phosphate buffer solutions (PBS) with different pH (2–10) were prepared by adjust the ratio of phosphoric acid to sodium phosphate. 5.0×10^{-5} mol L^{-1} Cyt *c* solution was prepared in 1 mM PBS (pH 6.03) and stored at a temperature of 4 °C. AuNPs with diameter of 16 nm were prepared by the conventional citrate reduction of $AuCl_4^-$ ions in water according to the conventional method [25].

2.2. Preparation of Cyt c modified SPR-active substrates and immobilization of AuNPs

The SPR-active substrate was cleaned prior to use by immersing it for 2 min in a freshly made piranha solution, followed by rinsing with doubly distilled deionized water and spectrophotometric grade ethanol. The overall assembly procedure of Cyt *c* and subsequent AuNPs immobilization were schematically shown in Fig. 1. For the preparation of Cyt *c* modified Au film (Au film–Cyt *c*), Au film was first incubated in a 1:3 mixture of MUA (5 mM) and MU (5 mM) ethanolic solution for 24 h, rinsed thoroughly with ethanol and water, and dried under a stream of N_2 (Step 1). Next, the carboxylic acid groups of MUA were activated by 30 min exposure to a 1:1 mixture of 0.4 M EDC and 0.1 M NHS aqueous solution (Step 2). After being rinsed carefully, this activated Au film was transferred to the as-prepared Cyt *c* solution and incubated for at least 30 min (Step 3). Cyt *c* was covalently immobilized on Au film surface via traditional carbodiimide coupling to protein-free amine moieties. After saturation, the surface was rinsed with copious amounts of water and buffer solution. At last, the immobilization of AuNPs was carried out on Au film–Cyt *c* via an exposure to aqueous dispersion of AuNPs (Step 4), resulting in Au film–Cyt *c*–AuNPs sandwich nanostructure.

2.3. In situ SPR measurement

SPR measurements were performed with a home-built SPR system [21], based on the Kretschmann configuration to achieve the resonant condition by attenuated total internal reflection spectroscope (ATR) [32]. The glass surface of the cleaned sensor chip was pressed onto the base of a half-cylindrical lens (ZK_7, n = 1.61) via an index matching oil (n = 1.61). Linearly p-polarized light having a wavelength of 670 nm from a diode laser was directed through the prism onto Au film. The intensity of the reflected light was measured as a function of the angle of incidence by using a photodiode with a chopper/lock-in amplifier technique. The gold surface of the sensor chip was mounted against the teflon cell by virtue of a Kalrez O-ring, which provided a liquid-tight seal and an electrolyte contact. Two approaches of SPRS were taken to monitor the construction of Au film–Cyt *c*–AuNPs sandwich nanostructure. First, Cyt *c* and AuNPs adsorption kinetics were followed by tracking the reflectance (R) at a fixed angle near the θ_{SPR} with time (R–t mode measurement), Cyt *c*/AuNPs adsorption giving rise to positive shifts in R. Second, after each assembly/water-rinsing step, angular reflectance curves (R–θ mode measurement) were recorded and fitted to a multilayer Fresnel model to obtain the optical film thickness (d) at the different construction intervals. Fresnel calculations were performed using the WINSPALL software (version 2.20) developed in the Max Planck Institute for Polymer Research in Germany.

3. Results and discussion

3.1. Assembly of Cyt c and AuNPs on Au film monitored in situ by SPRS

SPRS was used to follow the assembly procedures during the formation of MUA/MU, the attachment of Cyt *c* and the subsequently AuNPs immobilization. As shown in Fig. 2(A), the in situ R–t mode measurement was first used for study adsorption kinetics to establish the time of adsorption saturation. When the SPR instrument works at a fixed angle near the θ_{SPR}, the reflected light intensities change with the variation of organic film thickness or index of refraction that occurs at a certain condition. Since SPRS is surface-sensitive, making possible the monitor of adsorbates, especially biomolecules at extremely low quantities [33]. The in situ R–t mode measurement shows that the assembly rate is fast when Cyt *c* adsorbs on the activated Au film and then the AuNPs on Cyt *c*. The adsorption of Cyt *c* reaches equilibrium in about 30 min while that of AuNPs in about 1 h. After each assembly on Au film, SPR angular reflectance curves (R–θ) were collected and shown in Fig. 2(B). All the spectra were recorded in pure water after thorough rinsing to move weakly bound Cyt *c* and AuNPs. Upon formation of the mixed MUA/MU SAMs, the SPRS angle positively shifts for ca. 0.14° ($\Delta\theta_{SPR}$) in comparison with the basal surface. Upon saturation adsorption of the Cyt *c* to negative MUA/MU surface, another positive shift in $\Delta\theta_{SPR}$, 0.28°, occurs. A N-phase complex Fresnel calculation is used to determine these alkanethiol and protein films thickness, and a refractive index of 1.45 is assumed for both MUA/MUA and Cyt *c* lay-

ers measured here. This index of refraction is a typical value used previously to interpret SPRS and ellipsometry data from various ω-functionalized alkanethiol SAMs [34] and biomacromolecules [17]. Other refractive index values used for the SPR modeling calculations are 1.61 and 1.33, for ZK_7 lens and water, respectively. The permittivity and the thickness of the Au film are −0.114 + 3.71i and 40.9 nm, respectively. Thickness calculated from SPRS is reported as effective thickness at a particular refraction index since they measure an average thickness over the size of the incident beam. The values of effective thickness measured by R–θ mode measurements for MUA/MU and Cyt *c* monolayers are 1.5 ± 0.1 and 2.8 ± 0.1 nm, respectively. The thickness of the MUA/MU SAMs is consistent with the empirical formula reported by Bain et al. [35]. Mixed MUA/MU SAM is chosen as a protein matrix for two reasons. First, it can form dense packing of alkyl monolayers than MUA itself and immobilize more protein. Second, it can increase the conformational plasticity of surface-confined Cyt *c*. So an optimized value of 1:3 is accepted as the ratio of MUA to MU for the following experiments. Taking into account the crystallographic dimensions of Cyt *c* 3.0 nm × 3.4 nm × 3.4 nm and assuming that one molecule with the long axis parallel to the electrode surface [36], we conclude that the average surface coverage of Cyt *c* is 93% of its full packed monolayer.

Cyt *c* is a globular protein with 13 kDa molecular weight and contains a single heme cofactor. It is positively charged (+9) at neutral pH (p*I* 10.5) [37]. Based on the electrostatic and hydrophobic interactions between Cyt and AuNPs, thermal stable Cyt *c*-AuNPs superstructure biocomposite [12,30,31] and heme protein–AuNPs multilayers [38] have been successfully prepared and extensively studied. Here, AuNPs were successfully anchored on positively charged Cyt *c*, resulting the angle-resolved SPRS positively shifted by 2.23° (in $\Delta\theta_{SPR}$) and upward shifted by 0.116 (in $\Delta(R_{min}/R_0)$). The result is attributed to the coupling between the localized surface plasmon of AuNPs and surface plasmon polarization of Au film, according to a reported phenomenon that the adherence of AuNPs to Au film led to an increase in both the position of the SPRS angle and reflectance [13,39–41]. Considering the particles size and coverage (as determined by AFM), these results are in reasonable agreement with the literatures reported [41,42].

As a prerequisite to the nanoparticle-amplified SPRS study of Cyt *c* conformational change at interface, several criteria need to be met. First, Cyt *c* and AuNPs organizing at the interfaces is necessary, which has been successfully performed in our experimental procedure. Second, the physicochemical stability of tethered protein should be sufficiently high to retain their conformation/function upon combination with AuNPs. In this regard, Cyt *c* keeps its native conformation even in metal–protein–metal sandwiches [43,44] and the effects of AuNPs on Cyt *c* are related to the AuNPs size and the coverage of Cyt *c* on AuNPs. AuNPs with a diameter of 16 nm has little effect on the conformation of Cyt *c*. So, the response of Au film–Cyt *c*–AuNPs sandwich to denaturant solutions could be considered as an indirect reflection of the conformational change of surface-confined Cyt *c*. In addition, the behaviors of biomolecules at interfaces are often significantly different from that in bulk or in solution for biomolecules could not assume their full range of conformation and formed nonequilibrium structure [34]. Then we studied the conformational change of Cyt *c* at an interface by SPRS, especially the nanoparticle-amplified SPRS.

3.2. Denaturation and renaturation of Cyt c on Au film monitored in situ by SPRS

As a complementary of SPRS application in protein conformation study, AuNPs amplified SPRS was used to investigate the acid-induced conformational change of Cyt *c* by constructing Au

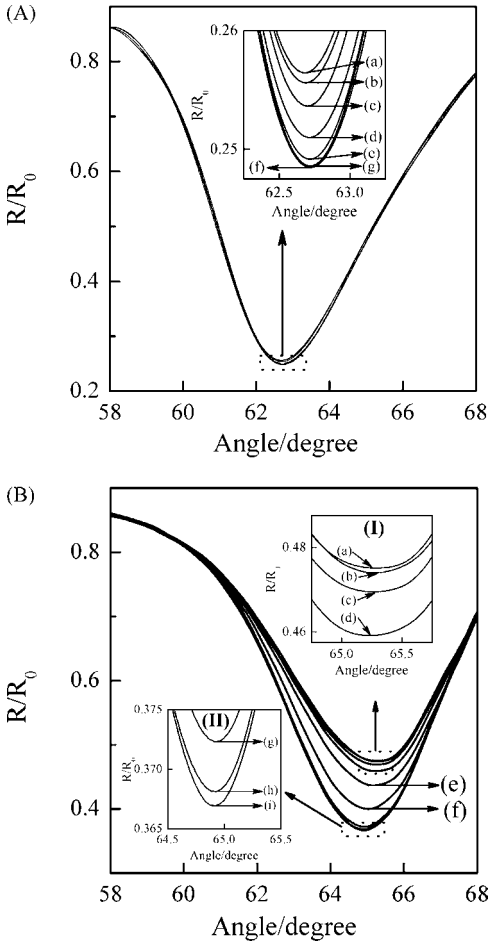

Fig. 3. SPR spectra measured for the Cyt *c*-modified Au film before (A) and after (B) the saturated assembly of AuNPs on Cyt *c* in PBS with different pH. Curve (a) to (i) were measured in PBS corresponding pH values of 2, 3, 4, 5, 6, 7, 8, 9 and 10. All curves were recorded after immerging the modified Au film in PBS with different pH for 30 min. The inset figures show the enlarged area corresponding separated rectangle area that cannot be discriminated.

film–Cyt *c*–AuNPs sandwich nanostructure. To check the effect of AuNPs on the acid-induced conformational change of Cyt *c*, angle-resolved SPR curves in PBS with different pH were obtained before (Fig. 3(A)) and after (Fig. 3(B)) the saturated assembly of AuNPs on Cyt *c*. All the spectra were recorded after changing pH of PBS for about 30 min. Concerning Au film–Cyt *c*–AuNPs sandwich, changing the pH of PBS from 2 to 10 produces a characteristic distinct SPR response. A noticeable reflectance upward shift and SPR angle positive shift is observed by gradually changing the pH of PBS from 10 to 2.

Most proteins seldom recover their activity once they are denatured, especially at a solid surface, but the ability to renature is an important factor when they are considered as catalysts or sensors. The stability and reversibility of Au film–Cyt *c*–AuNPs sandwich were checked by tracking the reflectance at a fixed resonance angle near the θ_{SPR} when pH of PBS was changed from 2 to 10 and reverse (Fig. 4). It is reported that Cyt *c* undergoes reversible denaturation at interface [11]. On the other hand, Cyt *c* could not renature on AuNPs when AuNPs are used as an indicator of protein conformational change [12,30,31]. Interestingly, the denaturation/renaturation process of Cyt *c* sandwiched in Au film–Cyt *c*–AuNPs nanostructure appeared to be highly reversible, as the reflectance at the fixed SPR angle increased when pH of PBS was changed from 10.0 to 2.0 but was fully recovered when the pH was

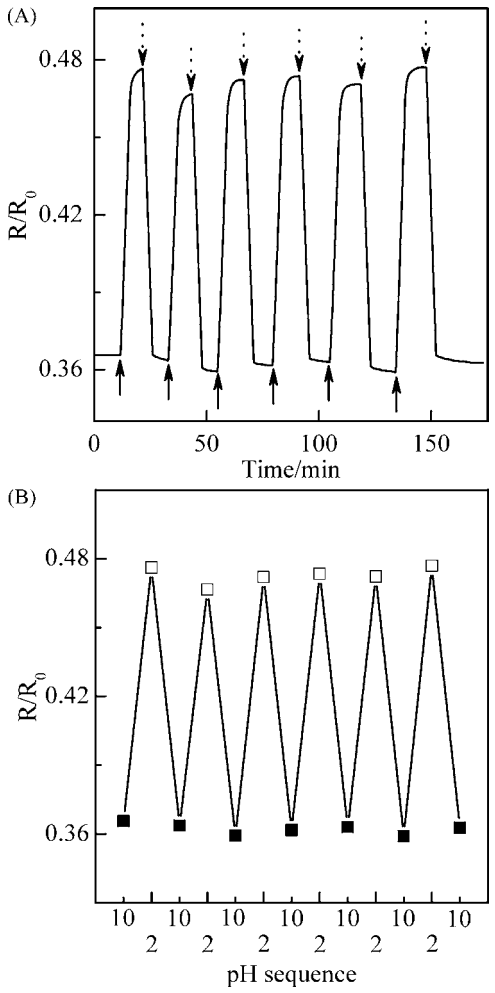

Fig. 4. (A) Time-dependent reflectance change measured at a fixed angle of incidence ($\theta_{SPR} = 65^{\circ}$) upon the multi-acid-induced conformational change of Cyt *c*. The arrows show the time of the cycling introduction of the acidic (pH 2, solid arrow) and alkaline (pH 10, dot arrow) PBS. (B) Summarized SPR experiment results of the acid/base induced conformational change of Cyt *c* suggest the good stability and reversibility of the Au film–Cyt *c*–AuNPs sandwich.

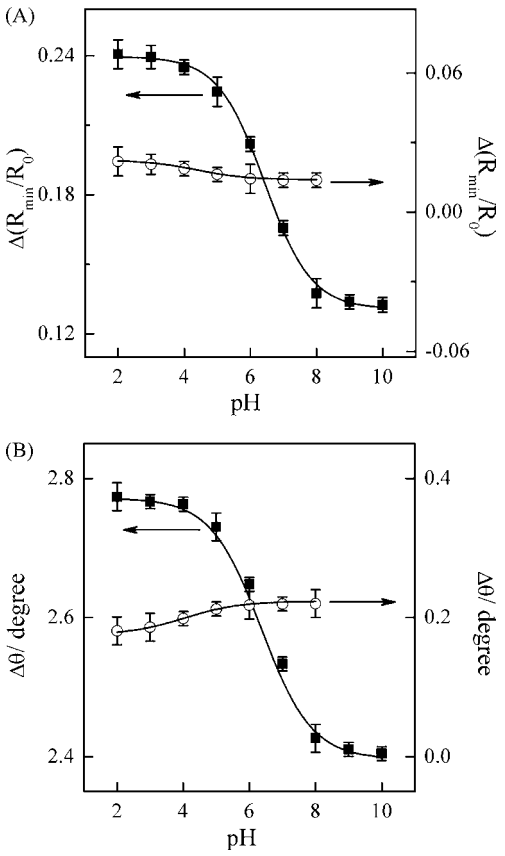

Fig. 5. The relative reflectivity (A) and SPR angle (B) plots of Au film with Cyt *c* in the absence (hollow circle) and presence (solid square) of adsorbed 16 nm diameter AuNPs as a function of pH. A sigmoidal fit to the titration curve is drawn as a solid line. Error bars show the standard deviation.

changed back to 10 (Fig. 4(A)). Noteworthy, the reflectance change was a collective representation of $\Delta\theta_{SPR}$ and $\Delta(R_{min}/R_0)$, so it could integrate all the SPR signal variations for the Au film–Cyt *c*–AuNPs sandwich as a function of pH. The results are summarized in Fig. 4(B) and demonstrate that the sandwiched Cyt *c* is quite robust to withstand multiple buffer washings, and its conformational change is highly reversible. No obvious decrease in reflectance ($\Delta\theta_{SPR}$ and $\Delta(R_{min}/R_0)$) is observed after six full cycles, indicating a firmly adsorbed AuNPs. The good stability is attributed to the high radius curvature of particles and their electrostatic/hydrophobic interactions with Cyt *c*. It is therefore envisioned that the combination of stimulus-responsive biomacromolecules (Cyt *c*) and AuNPs could afford a sensor chip for sensitive small-molecule detection (H^+) without requiring probe reagents.

The Au film–Cyt *c*–AuNPs sandwich responded immediately to the injection of acidic solution, and the signal of reflectance continued to climb slightly for a few minutes until reaching an equilibrium value in 30 min. When the pH of PBS changed from 2 to 10, the magnitude of the $\Delta(R_{min}/R_0)_{pH}$, $\Delta(R_{min}/R_0)_{pH} = (R_{min}/R_0)_{pH\,2} - (R_{min}/R_0)_{pH=10}$, increased with the prolonged exposure time of AuNPs solution until the adsorbed AuNPs reached saturation in 2 h, which also demonstrated the amplification effect of AuNPs on SPR signals. It is reported that the response of AuNPs amplified SPRS reaches a maximum value at a moderate coverage of AuNPs [13] on Au film and an appropriate distance [45] between AuNPs and Au film, and then decreases. In our case, we do not observe a "maximum" transition, which might be attributed to the different proteins and protein–AuNPs interactions. Here the electrostatic linked AuNPs are sub-monolayer and movable even under saturated adsorption [38], and thus may have little effect on the protein owned conformation as demonstrated by reversible denaturation/renaturation switching.

The variation of angle-resolved SPR curves for the acid-induced denaturation of Cyt *c* arises from the contributions of both the changes in bulk dielectric constant of the PBS and the conformational change in Cyt *c*. To differentiate between these two contributions, the SPR signal change at each pH of PBS for Au film–MUA is subtracted from the SPR signal change for Au film–Cyt *c* and Au film–Cyt *c*–AuNPs sandwich nanostructure ($\Delta S_{pH} = (S_{Cyt\,c})_{pH\,x} - (S_{MUA})_{pH\,y}$, where *S* represents SPR signal change, *x* and *y* represent the pH of PBS). For comparison, two of the signature SPR features ($\Delta\theta_{SPR}$ and $\Delta(R_{min}/R_0)$) are monitored as a function of the pH of PBS and shown in Fig. 5(A) and Fig. 5(B) respectively. As far as the reflectivity change $\Delta(R_{min}/R_0)$ is concerned, the $\Delta(R_{min}/R_0)$ at low pH versus high pH for Au film–Cyt *c*–AuNPs sandwich (solid squares in Fig. 5(A)) is amplified 12 times more than that for Au film–Cyt *c* system (hollow circles in Fig. 5(A)). However, the amplification of SPR angle shift ($\Delta\theta_{SPR}$) is 8 times more under the same circumstances (Fig. 5(B)). With increasing pH, the θ_{SPR} of Au film–Cyt *c*–AuNPs sandwich positively shifts while that of Au film–Cyt *c* system negatively shifts. It clearly shows the sub-

stantial improvement in the SPR response upon the combination of AuNPs with SPRS. The different enhancing efficiency for $\Delta(R_{min}/R_0)$ and $\Delta\theta_{SPR}$ is attributed to their distinct expression [46] that AuNPs has disparate impact. Moreover, increased extinction efficiency under acid environment for Cyt *c* could be deduced from Fig. 5(A), which is consistent with the literature [22,28]. Furthermore, to verify that these phenomena are derived from the conformational change of Cyt *c*, we replace Cyt *c* by 1,6-hexanedithiol (HDT) and construct Au film–HDT–AuNPs nanostructure for the same acid-induced denaturation/renaturation experiment. No SPR variation ($\Delta\theta_{SPR}$ and $\Delta(R_{min}/R_0)$) is found for PBS with different pH. Thus the distinct SPR variation of Au film–Cyt *c*–AuNPs sandwich might be an indirect reflection of the conformational change of surface-confined Cyt *c*. The acid-induced unfolding of Cyt *c* occurs around pH 2.6 in aqueous solution [47] while that of Au film–Cyt *c* system and Au film–Cyt *c*–AuNPs sandwich appears at pH 4.5 and pH 6, respectively. It suggests that surface-confined Cyt *c* lost parts of its bioactivity but immobilization on solid surface could improve its tolerance to the acid-induced denaturation [48].

As the thickness of an adsorbed molecular monolayer could be quantified by using SPRS, we tried to calculate the acid-induced protein volume or films thickness change via SPR theory. Hopefully, it could help us to acquire a deeper understanding of the nanoparticle-amplified SPRS. In this way, the SPR angle shift ($\Delta\theta_{SPR}$) originates from both the refractive index variation (Δn) and the average thickness change (Δd) of an adsorbed protein layer produced by the molecular reorientation or reorganization, as shown by Eq. (1) [7,49].

$$\Delta\theta = c_1\Delta n + c_2\Delta d \tag{1}$$

where c_1 and c_2 are constants ($c_1 = 2.2$ and $c_2 = 0.09$ from numerical calculations based on Fresnel optics model, other parameters are shown in the protein thickness calculation section). On the other hand, Lorentz–Lorenz relation could correlate the refractive index variation with the protein thickness change by Eq. (2), [7]

$$\Delta n = -\frac{1}{6n}(n^2+2)^2\left(\frac{n^2-1}{n^2+2} - \frac{{n_w}^2-1}{{n_w}^2+2}\frac{V_p}{V_p+V_w}\right)\frac{\Delta d}{d} \tag{2}$$

where n_w is the refractive index of water ($n_w = 1.33$), V_p and V_w are the volumes of the protein and water in the monolayer, respectively. From the above experiment results, we have $\Delta\theta = -0.044\Delta d$ and the decrease in the SPR angle (0.04) corresponds to an increase of ~0.9 nm in the protein thickness. This change is smaller than synchrotron small angle X-ray scattering [28,29] results (~2 nm) of acid denatured Cyt *c* in solution. However, it is reasonable considering that the protein is confined on Au film. The denatured protein decreases its effective dielectric constant, and explains why no SPR angle shift is observed for acid-induced denaturation of superoxide dismutase [13]. In addition, it lends credence to the assumption that AuNPs amplified SPRS is derived from a vertical movement of AuNPs, although minor contribution from horizontal movement cannot be ruled out [50]. The calculation is not suitable for Au film–Cyt *c*–AuNPs sandwich as the adsorbed AuNPs are absorbing dielectric with complicated refractive index. So, the inconsistency of opposite SPR angle shifts with increasing pH for Au film–Cyt *c*–AuNPs sandwich is acceptable. The underlying mechanism of the observed AuNPs amplified SPRS is governed by various interactions among and within the substrate-, protein-, and particle-layers of such a device [51]. However, details of these interactions are not fully understood at the present time.

4. Conclusions

In conclusion, AuNPs amplified SPRS was used to study the protein conformation by successive assembly of Cyt *c* and AuNPs on Au film. The amplified SPR signal ($\Delta\theta_{SPR}$, $\Delta(R_{min}/R_0)$) accompanying the acid-induced conformational change of Cyt *c* might be derived from the variation of vertical distance or coupling distance between AuNPs and Au film when the sandwiched Cyt *c* changed its conformation. This hypothesis was demonstrated by SPR calculation. The Au film–Cyt *c*–AuNPs sandwich nanostructure was stable for multiple pH switches and the acid-induced conformational change of Cyt *c* was quite reversible. We expect this work can expand the scope of SPRS for our understanding of fundamental properties of biomolecules at interfaces. Furthermore, the observation of AuNPs amplified SPR phenomenon had opened up the possibility of using SPRS as a probe of structural and optical properties of biomolecules and nanostructured composite materials in general.

Acknowledgements

This work was supported by special funds for major state basic research of China (no. 2002CB713803) and National Nature Science Foundation of China (no. 20675076).

References

[1] R. Advincula, E. Aust, W. Meyer, W. Knoll, Langmuir 12 (1996) 3536.
[2] A.W. Wark, H.J. Lee, A.J. Qavi, R.M. Corn, Anal. Chem. 79 (2007) 6697.
[3] M. Riskin, B. Basnar, E. Katz, I. Willner, Chem. Eur. J. 12 (2006) 8549.
[4] C. Gondran, M. Dubois, S. Fort, S. Cosnier, S. Szunerits, Analyst 133 (2008) 206.
[5] D. Eliezer, P.A. Jennings, P.E. Wright, S. Doniach, K.O. Hodgson, H. Tsuruta, Science 270 (1995) 487.
[6] H. Sota, Y. Hasegawa, M. Iwakura, Anal. Chem. 70 (1998) 2019.
[7] S. Boussaad, J. Pean, N.J. Tao, Anal. Chem. 72 (2000) 222.
[8] W.Y.X. Peh, E. Reimhult, H.F. Teh, J.S. Thomsen, X.D. Su, Biophys. J. 92 (2007) 4415.
[9] Z. Salamon, G. Lindblom, L. Rilfors, K. Linde, G. Tollin, Biophys. J. 78 (2000) 1400.
[10] J.E. Gestwicki, H.V. Hsieh, J.B. Pitner, Anal. Chem. 73 (2001) 5732.
[11] S. Chah, C.V. Kumar, M.R. Hammond, R.N. Zare, Anal. Chem. 76 (2004) 2112.
[12] S. Chah, M.R. Hammond, R.N. Zare, Chem. Biol. 12 (2005) 323.
[13] T. Kang, S. Hong, I. Choi, J.J. Sung, Y. Kim, J.S. Hahn, J. Yi, J. Am. Chem. Soc. 128 (2006) 12870.
[14] T. Kang, S. Hong, H.J. Kim, J. Moon, S. Oh, S.R. Paik, J. Yi, Langmuir 22 (2006) 13.
[15] T. Wink, S.J. van Zuilen, A. Bult, W.P. van Bennekom, Anal. Chem. 70 (1998) 827.
[16] E.F.A. Devries, R.B.M. Schasfoort, J. Vanderplas, J. Greve, Biosens. Bioelectron. 9 (1994) 509.
[17] J. Liu, L. Tiefenauer, S. Tian, P. Nielsen, W. Knoll, Anal. Chem. 78 (2006) 470.
[18] E. Katz, I. Willner, Angew. Chem. Int. Ed. 43 (2004) 6042.
[19] L. He, M.D. Musick, S.R. Nicewarner, F.G. Salinas, S.J. Benkovic, M.J. Natan, C.D. Keating, J. Am. Chem. Soc. 122 (2000) 9071.
[20] O. Lioubashevski, V.I. Chegel, F. Patolsky, E. Katz, I. Willner, J. Am. Chem. Soc. 126 (2004) 7133.
[21] J.L. Wang, F. Wang, X.Q. Zou, Z.A. Xu, S.J. Dong, Electrochem. Commun. 9 (2007) 343.
[22] J. Matsui, K. Akamatsu, S. Nishiguchi, D. Miyoshi, H. Nawafune, K. Tamaki, N. Sugimoto, Anal. Chem. 76 (2004) 1310.
[23] J. Matsui, K. Akamatsu, N. Hara, D. Miyoshi, H. Nawafune, K. Tamaki, N. Sugimoto, Anal. Chem. 77 (2005) 4282.
[24] I. Tokareva, I. Tokarev, S. Minko, E. Hutter, J.H. Fendler, Chem. Commun. (2006) 3343.
[25] M. Zayats, S.P. Pogorelova, A.B. Kharitonov, O. Lioubashevski, E. Katz, I. Willner, Chem. Eur. J. 9 (2003) 6108.
[26] I. Tokareva, S. Minko, J.H. Fendler, E. Hutter, J. Am. Chem. Soc. 126 (2004) 15950.
[27] H. Roder, G.A. Elove, S.W. Englander, Nature 335 (1988) 700.
[28] M. Kataoka, I. Nishii, T. Fujisawa, T. Ueki, F. Tokunaga, Y. Goto, J. Mol. Biol. 249 (1995) 215.
[29] S. Cinelli, F. Spinozzi, R. Itri, S. Finet, F. Carsughi, G. Onori, P. Mariani, Biophys. J. 81 (2001) 3522.
[30] X. Jiang, L. Shang, Y.L. Wang, S.J. Dong, Biomacromolecules 6 (2005) 3030.
[31] X. Jiang, U.G. Jiang, Y.D. Jin, E.K. Wang, S.J. Dong, Biomacromolecules 6 (2005) 46.
[32] H. Raetner, Surface Plasmon on Smooth and Rough Surfaces and on Gratings, Springer and Verlag, Berlin, 1988.
[33] T.T. Goodrich, H.J. Lee, R.M. Corn, J. Am. Chem. Soc. 126 (2004) 4086.
[34] C.E. Jordan, R.M. Corn, Anal. Chem. 69 (1997) 1449.
[35] C.D. Bain, E.B. Troughton, Y.T. Tao, J. Evall, G.M. Whitesides, R.G. Nuzzo, J. Am. Chem. Soc. 111 (1989) 321.

[36] G.W. Bushnell, G.V. Louie, G.D. Brayer, J. Mol. Biol. 214 (1990) 585.
[37] J.M. Pachence, J.K. Blasie, Biophys. J. 59 (1991) 894.
[38] Z.M. Qi, I. Honma, M. Ichihara, H.S. Zhou, Adv. Funct. Mater. 16 (2006) 377.
[39] G. Jiang, A. Baba, H. Ikarashi, R. Xu, J. Locklin, K.R. Kashif, K. Shinbo, K. Kato, F. Kaneko, R. Advincula, J. Phys. Chem. C 111 (2007) 18687.
[40] E. Hutter, S. Cha, J.F. Liu, J. Park, J. Yi, J.H. Fendler, D. Roy, J. Phys. Chem. B 105 (2001) 8.
[41] L.A. Lyon, M.D. Musick, M.J. Natan, Anal. Chem. 70 (1998) 5177.
[42] L.A. Lyon, D.J. Pena, M.J. Natan, J. Phys. Chem. B 103 (1999) 5826.
[43] C.D. Keating, K.M. Kovaleski, M.J. Natan, J. Phys. Chem. B 102 (1998) 9404.
[44] C.D. Keating, K.K. Kovaleski, M.J. Natan, J. Phys. Chem. B 102 (1998) 9414.
[45] L. He, E.A. Smith, M.J. Natan, C.D. Keating, J. Phys. Chem. B 108 (2004) 10973.
[46] S. Ekgasit, C. Thammacharoen, W. Knoll, Anal. Chem. 76 (2004) 561.
[47] R. Varhac, M. Antalik, Biochemistry 43 (2004) 3564.
[48] A. Bhambhani, C.V. Kumar, Adv. Mater. 18 (2006) 939.
[49] W.P. Chen, J.M. Chen, Surf. Sci. 91 (1980) 601.
[50] T. Okamoto, I. Yamaguchi, J. Phys. Chem. B 107 (2003) 10321.
[51] K.C. Grabar, R.G. Freeman, M.B. Hommer, M.J. Natan, Anal. Chem. 67 (1995) 735.

Talanta 77 (2008) 667–672

Contents lists available at ScienceDirect

Talanta

journal homepage: www.elsevier.com/locate/talanta

Highly sensitive spectrophotometric determination of cationic surfactants in ground waters as their Cu(II)–TPPS aggregates preceded by solid-phase fractionation

Yukio Yokoyama*, Hidetaka Kubo, Hisakuni Sato

Department of Analytical Chemistry, Faculty of Engineering, Yokohama National University, 79–5 Tokiwadai, Hodogaya, Yokohama 240-8501, Japan

ARTICLE INFO

Article history:
Received 4 April 2008
Received in revised form 4 July 2008
Accepted 4 July 2008
Available online 23 July 2008

Keywords:
Cationic surfactant
Spectrophotometric determination
Cu(II)–TPPS chromophore
PTFE-membrane filtration
Solid-phase extraction

ABSTRACT

A highly sensitive spectrophotometric determination of cationic surfactants in ground waters was established by forming their Cu(II)–TPPS aggregates, preceded by solid-phase extraction with an SCX cartridge. Cationic surfactants (CSs) were quantitatively trapped and isolated by the SCX solid phase. The use of Cu(II)–TPPS anionic chromophore could reduce the interference by unintentional metal ions coexisting in surrounding waters. The method was very sensitive in the determination of CSs less than 10^{-5} M levels with acceptable recovery and calibration data. The colorimetric sensitivity was very dependent on the alkyl-chain length of the surfactants, and a CS having 23 carbon atoms gave the highest sensitivity. Overall recoveries were 95–97% with R.S.Ds. less than 3% in the cases over 10^{-6} M levels. In the cases in 10^{-7} M levels, however, a portion of the analyte would be adsorbed by reservoir walls, which could seriously affect the trace determination. The preliminary addition of 4,4′-bipyridyl into the sample solution was effective in decreasing such unintentional analyte losses, leading up to 73% recovery. The developed method was applied to the analysis of river water at ppb levels of CSs with a fractional concentration through a SCX solid phase subjected by 500-mL aliquots of sample.

1. Introduction

Cationic surfactants (CSs), typically including long-chain alkyl quaternary ammonium salts, are industrially produced and consumed in our living environment, used as sanitizer, emulsifier, antifriction, antistatic agent. Although the production of CSs is relatively smaller comparing to anionic (AS) and nonionic (NS) surfactants, the quantification of CSs in ground waters at micro concentration levels is very important for assessment of our water environment. Since CSs can often present in ground waters together with ASs and NSs, fractional determination is necessary. In general, the spectrophotometric method is officially or often employed to determine total amounts of CSs in water samples, preceded by forming ion association precipitates with counter anionic agents such as Orange II [1,2], disulfine blue VN 150 [3,4], bromocresol green [5], and tetrabromophenolphthalein ethyl ester (TBPE) [6–8]. In general, these traditional methods are cumbersome and time-consuming in their procedures, furthermore including serious environmental problems to be solved, because of the solvent extraction process using halogenated solvent such as chloroform. In addition to this, it seems to be difficult to make it automatic.

Alternative to the use of such well-known coloring agents, more sensitive spectrophotometric method using tetraphenylporphinetetrasulfonic acid (TPPS) has been proposed [9–11] recently. In addition to the high sensitivity, the method can only require less harmful and toxic solvent, i.e. ethanol instead of chloroform, which can only dissolve the precipitates of ionic aggregates. However, the precipitates have been collected from the vessel inner wall where they adsorbed hydrophobically, which can give lower recovery and reproducibility from operator to operator [11].

This paper describes a highly sensitive spectrophotometric determination of cationic surfactants in ground waters after filtration of their Cu(II)–TPPS aggregates, which can reduce the influence of metal cations coexisting in the sample matrix. In addition to this, preliminary concentration and isolation procedures using solid-phase extraction techniques are also presented.

2. Experimental

2.1. Chemicals and materials

TPPS, *5,10,15,20*-tetraphenyl-*21H,23H*-porphinetetrasulfonic acid (H_6TPPS, Scheme 1), was purchased from Wako (Osaka,

* Corresponding author. Tel.: +81 45 339 3939; fax: +81 45 339 3939.
E-mail address: yokyuk@ynu.ac.jp (Y. Yokoyama).

0039-9140/$ – see front matter © 2008 Elsevier B.V. All rights reserved.
doi:10.1016/j.talanta.2008.07.021

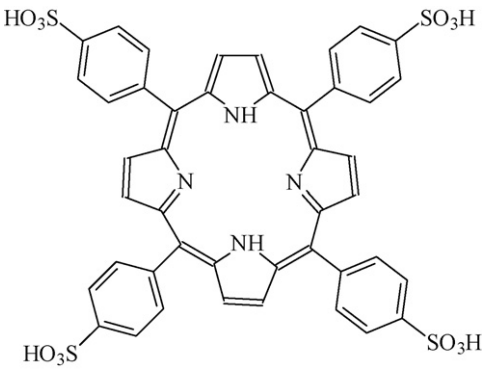

Scheme 1. Chemical structure of H_6TPPS.

Japan). Several quaternary alkylammonium chloride salts were purchased from Tokyo Kasei (Tokyo, Japan): tetradecyldimethylbenzylammonium (Zephiramine, Zeph, carbon number (cn): 23), hexadecyldimethylbenzylammonium (CDBA, cn: 25), octadecyldimethylbenzylammonium (SDBA, cn: 27), hexyltrimethylammonium (HTA, cn: 9), octyltrimethylammonium (OTA, cn: 11), decyltrimethylammonium (DTA, cn: 13), dodecyltrimethylammonium (LTA, cn: 15), tetradecyltrimethylammonium (TTA, cn: 17), hexadecyltrimethylammonium (CTA, cn: 19), hexadecyldimethylammonium (CDA, cn: 18), octadecyltrimethylammonium (STA, cn: 21), dodecylpyridinium (Lpy, cn: 17), and hexadecylpyridinium (Cpy, cn: 21). Acetic acid, sodium acetate, copper sulfate pentahydrate, sodium sulfate, 2-methoxyethanol, 4,4′-bipyridyl, and other chemicals were from Wako.

Orange II (sodium *p*-(2-hydroxy-1-naphthylazo)benzenesulfonate) and TBPE (tetrabromophenolphthalein ethyl ester) were purchased from Wako and disulfine blue VN 150 was from Merck (Tokyo, Japan).

All-plastic lab wares, such as volumetric flasks, graduated cylinders, and reservoir bottles, made of polyethylene (PE), polypropylene (PP), or polymethylpentene (PMP) were used throughout the experiments in place of glasswares to avoid unintentional adsorption of surfactants to the active glass surface.

2.2. Cation-exchange solid-phase cartridge

A Varian (Harbor City, CA) BondElut SCX (cation exchanger, 100 mg bed, 0.6 mequiv/g) of open-syringe type (5.7 mm i.d., 7.6 mm o.d., 57 mm in length) was used for the concentration and separation of CSs, which was conditioned by passing 5 mL of methanol, 5 mL of 50% (v/v) methanol/0.1 M hydrochloric acid, and 5 mL of water in order at a flow rate of ca. 1 mL/min.

2.3. Coloring agent

Equal volumes of 2.0×10^{-4} M TPPS and 2.0×10^{-4} M Cu(II) were mixed and allowed to stand for over 3 h at ambient temperature, which led to the 1.0×10^{-4} M Cu(II)–TPPS coloring agent.

2.4. Instrumentation

A JASCO (Tokyo, Japan) V-550 UV/VIS spectrophotometer with a set of narrow-width (4 mm) quartz cells of 1 cm in path length was used in all measurements.

2.5. Isolation procedure

A 5-mL aliquot of the standard surfactant mixture (stock solution) was loaded onto the conditioned SCX cartridge under a reduced pressure by aspirating, and subsequently the cartridge was rinsed by passing several 1-mL aliquots of water and then four 1-mL aliquots of 40% (v/v) methanol/water (total 4 mL) to wash NSs away from the cartridge. On this stage, all ASs (excess and associated with CSs) were removed from the SCX cartridge by only washing with water. The details have been described in a previous paper [12]. After passing a 2 mL of saturated sodium sulfate solution, the adsorbed CSs were desorbed and collected to a PTFE test tube by passing a subsequent 5 mL of 0.1 M hydrochloric acid–ethanol solution (60 v/v%). To remove ethanol, the solution was dried by heating at 70 °C using a block heater within a draft chamber. The residue was redissolved into a 5 mL of water and subjected to the measurement.

In the case of analyzing only CSs in real samples such as river water, 500-mL aliquot of the sample water was subjected to the SCX cartridge by means of the same procedure described as above, because about 100-hold concentration of sample water would be necessary.

In the case of analyzing CSs, ASs, and NSs simultaneously, the triple-stage solid-phase (TSS) cartridge, self-made by connecting SCX, SAX, and ODS cartridges in the order with the lowest dead volume, is available in place of the SCX cartridge. The TSS cartridge can fractionate and concentrate cationic, anionic, and nonionic surfactants through a pretreatment procedure described in our previous paper [12]. The individual analytes isolated should be subjected to the proper determination methods, such as Cu-TPPS method (this method) for CSs, Co(III)-5-Cl-PADAP method [13] for ASs, and ferric thiocyanate [12] method for NSs.

2.6. Spectrophotometric measurement

A 0.71 g of sodium sulfate (corresponding to 5 mmol) was dissolved in the resultant 5-mL CS aqueous solution, and then 1 mL of 1.0×10^{-4} M Cu(II)–TPPS and 2 mL of acetate buffer (pH 5) were added to the solution, allowing to form the ionic aggregates. The resulting precipitate was filtered through a hydrophilic PTFE-membrane filter (0.2 μm in pore size; 25 mm in diameter) (Advantec, Tokyo, Japan) by aspirating. After washing the precipitate with a 5 mL of supernatant of saturated sodium sulfate solution, the final chromatic substance on the filter was dissolved completely into 5 mL of 2-methoxyethanol, and the absorption spectrum for visible wavelength between 350 nm and 500 nm was measured. The determination was carried out based on the absorbance data at 413 nm.

3. Results and discussion

3.1. Cu(II)–TPPS complex as coloring agent

TPPS (H_2TPPS^{4-}) [9] (Scheme 1) is very useful complexing agent for transition metal ions such as Zn(II), Cu(II), Fe(II), Pd(II), etc.; and TPPS has been applied to the determination of trace metal ions [14–16]. Although TPPS has been successfully used for the determination of cationic surfactants [9–11], the TPPS colorimetric method may be influenced by unintentional metal ions such as Zn(II) and Cu(II) present in the environmental sample matrix. It seems, therefore, that the formation of CS–TPPS aggregates can be also affected by the presence of metal ions in the realistic water samples [11]. To eliminate the unintentional interference by such metal ions, probably causing the decrease in detectability or the shift in absorption maximum, we considered that a preliminary

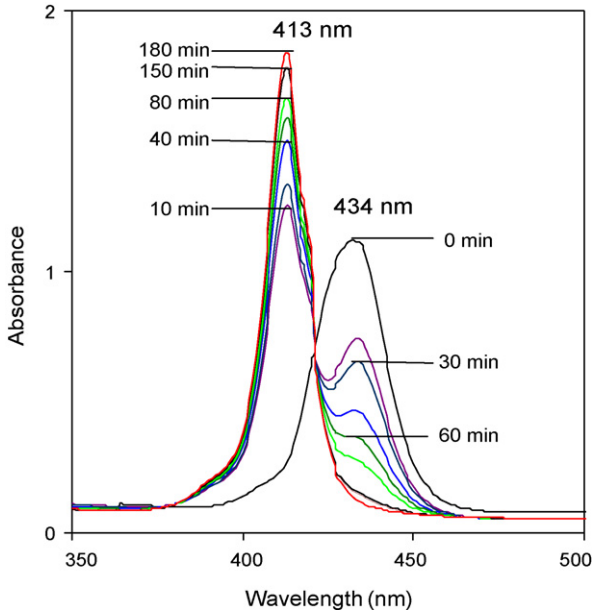

Fig. 1. Time dependence of the formation of Cu(II)–TPPS complex (1.25×10^{-5} M) on the visible-wavelength spectrum measured at pH 5 by acetate buffer.

formation of metal–TPPS complex should be useful and effective as the isolating and coloring agent for CSs. It is known that TPPS can form stable complexes with many metal ions. The stability of metal–TPPS complex is known for the formation constant *K*: Pd(II) > Cu(II) > Ni(II) > Co(II) > Fe(II) > Zn(II) > Mg(II) > and so on, and for the rate constant *k*: Cu(II) > Zn(II) > Co(II) > Fe(II) > Ni(II) > and so on [15]. Although TPPS is highly selective for copper(II), coexisting palladium(II) and zinc(II) can only interfere the formation of Cu(II)–TPPS due to their close *K* or *k* to Cu(II) [15]. However, Pd(II) is thought to be very minor minerals in the environmental waters comparing to other metal ions. The formation rate can suggest that Cu(II) is introduced into the TPPS cavity faster than other metal ions. In addition, these earlier papers have suggested that the Cu(II)–TPPS complex is stable for long period and will not be influenced by any other metal ions. Therefore, Cu(II)–TPPS anionic complex $[Cu(II)–TPPS]^{4-}$ [9], was chosen as the isolating and coloring agent for cationic surfactants.

Fig. 1 shows the time dependence of the formation of 1.25×10^{-5} M Cu(II)–TPPS chromophore in aqueous solution at pH 5 with acetate buffer on the visible-wavelength spectra. The peak maxima (λ_{max}) were shifted from 434 nm to 413 nm according to the degree of formation of Cu(II)–TPPS complex, in which the former λ_{max} (Soret band, 434 nm) is due to the free TPPS at pH 5 and the latter is due to the Cu(II)–TPPS complex. The superposed spectra clearly gave an isosbestic point at 421 nm, indicating that there is one-on-one equivalence between the free TPPS and the Cu(II)–TPPS. The formation of the complex was completed in 3 h at ambient temperature. Although the reaction rate seems to be slow, this is not so serious problem because such coloring agent is usually prepared as a stock solution. In addition, the presence of reduction species such as ascorbic acid can promote the complexation rate [17], but such fast reaction is not required in this method. Once Cu(II)–TPPS complexes completely formed, they are very stable for a long period in solution.

It is known that the Cu(II)–TPPS complex has the Soret band at the same wavelength of 413 nm as the CS–TPPS aggregates [9], and as the free TPPS at pH 6.5 [15]. In this study, however, the CS–TPPS gave peak maxima at 419 nm, probably due to pH. Such unsettledness in the peak maxima may cause the analytical results.

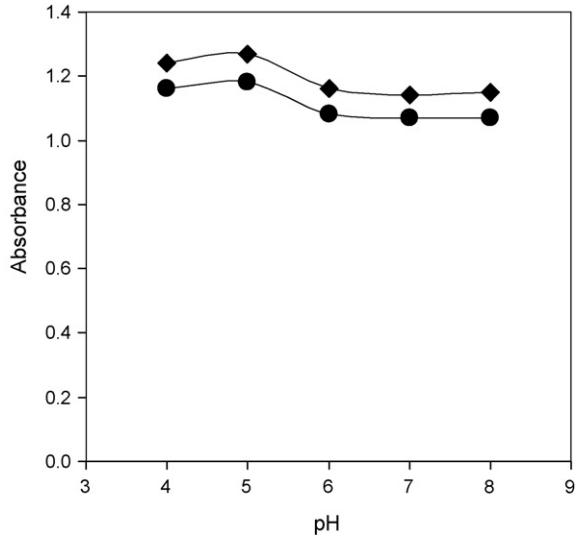

Fig. 2. pH Dependence of the formation of CS–Cu(II)–TPPS aggregates (1.0×10^{-5} M). CTMA and Zeph are denoted by (●) and (♦), respectively.

The optical sensitivity of CS–Cu(II)–TPPS aggregates slightly depended on pH of the solution. The changes in absorbability of CTMA–Cu(II)–TPPS and Zeph–Cu(II)–TPPS at several pH between pH 4 and 8 were within 5% relatively for both analytes, as shown in Fig. 2. Weakly acidic condition at pH 5.0 was selected for the quantification because of giving the highest absorbability with acceptable R.S.Ds. Although the visible-wavelength spectra of free TPPS strongly depend on the surrounding pH [15], those of Cu(II)–TPPS are almost independent of pH. Therefore, the use of Cu(II)–TPPS chromophore has a practical merit for the environmental analysis.

Fig. 3 shows the visible-wavelength spectra between 350 nm and 500 nm at pH 5 for several alkyltrimethylammonium– Cu(II)–TPPS aggregates dissolved in 2-methoxyethanol (1.0×10^{-5} M each), all giving their peak maxima at 413 nm. However, the colorimetric sensitivities for the analytes could depend on the alkyl-chain length or on their hydrophobicity, probably due to the difference in solubility constants of the precipitates. This fact has been known from earlier times, and there are various opinions for the reason, which is still unclear.

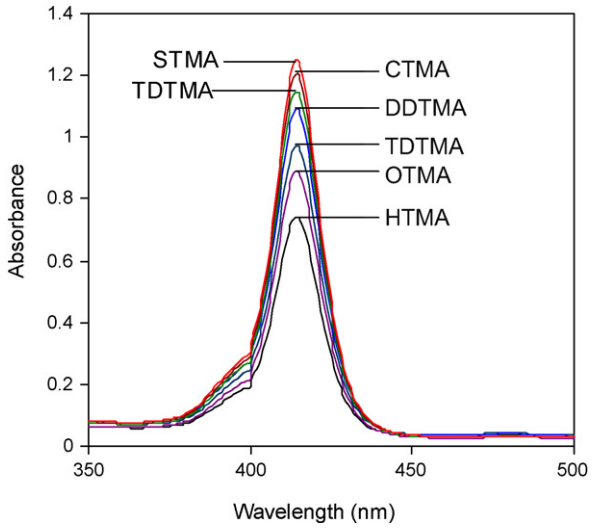

Fig. 3. Overwritten visible-wavelength spectra of alkyltrimethylammonium–Cu(II)–TPPS aggregates (1.0×10^{-5} M each) at pH 5.0.

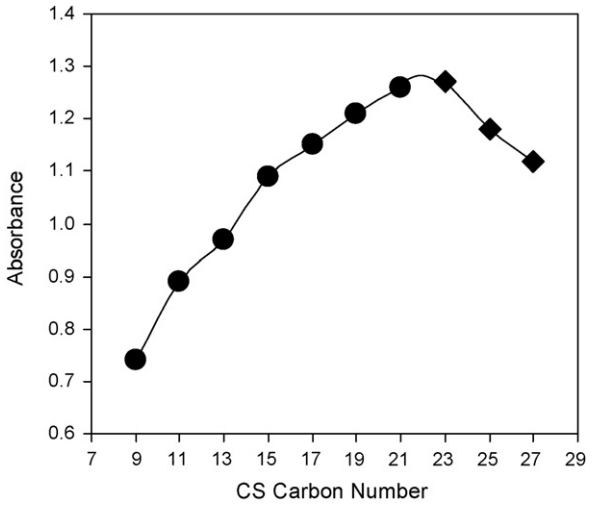

Fig. 4. Alkyl-chain length dependence of quaternary ammonium cationic surfactants on their optical sensitivity. Alkyltrimethylammonium and alkylbenzyldimethylammonium salts are denoted by (●) and (♦), respectively.

Fig. 4 shows the relationships between carbon numbers of CSs (alkyltrimethylammonium and alkyldimethylbenzylammonium) and their chromatic absorbabilities. The result indicated that Zeph (tetradecyldimethylbenzyl) having 23 carbon atoms could provide the highest molar absorptivity (ca.130,000 cm^{-1} M^{-1}) within the surfactants examined, which was relatively 5% higher than those obtained through CS–TPPS aggregates. The sensitivity was decreased according to both decrease and increase in the carbon numbers. Especially the discoloration was serious in short alkyl-chain CSs having less than six carbon atoms. This colorimetric method seems to be inapplicable for short-chain quaternary ammonium salts.

3.2. Recovery of CS–Cu(II)–TPPS aggregate from water samples

The recoveries for several CS–Cu(II)–TPPS aggregates collected from water system through the PTFE-membrane filtration (this method) were compared with those collected through an ODS solid-phase extraction (the present trial method) and PTFE-wall adsorption method [8,11]. Table 1 lists the overall recoveries of CSs obtained through the individual three methods, which were all based on the procedure described in Section 2.6. The recovery data through the PTFE-membrane filtration and through the ODS solid-phase extraction were closely the same both with acceptable R.S.Ds., but the PTFE-wall adsorption method could provide only poor recoveries less than 80% with R.S.Ds. exceeding 10% for the analytes. The analytical results obtained through the PTFE-membrane method were more reproducible than those through the ODS solid-phase extraction method. This indicates that the CS–Cu(II)–TPPS aggregates can be collected quantitatively on the hydrophilic-PTFE-membrane filter from the water samples, and subsequently the precipitate can be eluted quantitatively by 2-methoxyethanol. Ethanol was a choice for the solvent [11], but it could provide somewhat poor recovery due to the high volatility.

Table 1
Overall recoveries of several CS–Cu(II)–TPPS aggregates obtained through three different collecting methods, PTFE-membrane filtration (this method), ODS solid-phase extraction (present trial), and PTFE-wall adsorption method [11]; and those obtained by three different anionic chromophores, Orange II, disulfine blue, and TBPE

	Zeph	STMA	CDMBA	DDTMA	CTMA
Cu(II)–TPPS with: PTFE-membrane filtration					
%Recovery	96.5	93.8	96.7	95.7	95.8
%R.S.D. (n = 5)	0.87	1.00	1.38	1.34	1.42
ODS Solid-phase extraction					
%Recovery	95.9	93.4	96.7	94.6	95.4
%R.S.D. (n = 5)	1.86	1.97	2.40	2.22	2.16
PTFE-wall adsorption [11]					
%Recovery	65.9	72.4	78.6	75.3	78.4
%R.S.D. (n = 5)	11.4	12.1	10.7	14.7	11.1
% Recovery by other chromophores					
Orange II (485 nm)	90.1	94.5	85.1	79.7	85.9
Disulfine blue (631 nm)	95.2	97.2	93.7	79.3	88.4
TBPE (605 nm)	93.1	95.9	91.3	94.6	93.7

The addition of sodium sulfate to the sample solution was essential to form and collect the precipitate quantitatively; otherwise, the recovery would decrease considerably between 10% and 30%, which was dependent on the surfactants.

In addition to this, the analytical property of the Cu(II)–TPPS chromophore was also compared with those of more familiar anionic chromophores such as Orange II (485 nm), disulfine blue (631 nm), and TBPE (605 nm), which was based on the same analytical procedure as above. The recovery data indicated that the Cu(II)–TPPS chromophore, essentially the most sensitive among them, could provide the most reliable and acceptable results for the target cationic surfactants.

3.3. Quantification data

Table 2 lists the calibration data for the determination of several CSs. The linear relationships between CS concentration and the absorbance at 413 nm were obtained, in which the slope for Zeph corresponding to the effective molar absorptivity was the highest (ε = 131,000). This can lead to the upper limits of the sample concentration less than 1.0×10^{-5} M. However, in the case that the analyte concentration was around 10^{-7} M level, the quantification was seriously affected by some unintentional adsorption of CSs onto the reservoir wall. This may lead to somewhat poor r^2 values in Table 2.

Fig. 5 shows the wall-effect causing the decrease in CS recovery, which can depend on the analyte concentration. As might be expected, a glass-made sample reservoir seriously adsorbed cationic surfactants around 10^{-7} M levels showing 49% recovery, and even a polyethylene-made reservoir could give only 67% recovery. However, such serious wall-effect was somewhat reduced by adding (12.5 mg/L) 4,4′-bipyridyl in the subjected sample solution [18]. The use of PE or other plastic reservoir together with 4,4′-bipyridyl could improve the CS recovery at 10^{-7} M levels, giving ca. 73% recovery. The results can indicate that the wall-effect is negligible in the case over 10^{-6} M levels of the analyte concentration, but some *adsorption coefficient* (0.73 at 10^{-7} M in this case) has to

Table 2
Calibration data for CS determination through PTFE-membrane filtration of CS–Cu(II)–TPPS aggregates

	Zeph	STMA	CDMBA	DDTMA	CTMA
Linear range (mol/L)	$\sim 1.00 \times 10^{-5}$	$\sim 1.00 \times 10^{-5}$	$\sim 1.00 \times 10^{-5}$	$\sim 1.00 \times 10^{-5}$	$\sim 1.00 \times 10^{-5}$
Slope (AU/(mol/L $\times$ 10^5))	1.311	1.044	0.875	0.626	0.439
Intercept (AU)	0.009	0.012	0.001	0.005	0.008
r^2	0.9991	0.9992	0.9982	0.9989	0.9977

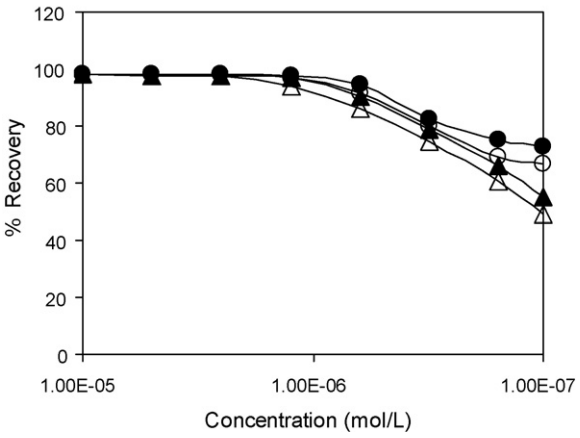

Fig. 5. Effects of 4,4′-bipyridyl additive to the sample solution on the recovery of cationic surfactants, in the cases using (△) glass bottle only; (▲) glass bottle with 4,4′-bipyridyl; (○) PE bottle only; (●) PE bottle with 4,4′-bipyridyl.

Table 3
Effects of ethanol content in the 0.1-M HCl eluting solvent on the recovery of Zeph and CTMA from the SCX solid phase expressed by percent recovery with R.S.D. ($n = 5$)

%Ethanol (v/v) in 0.1 M HCl	Zeph	CTMA
0	67.3 ± 1.6%	68.3 ± 1.2%
30	89.1 ± 1.2%	89.2 ± 1.3%
60	97.6 ± 1.2%	95.3 ± 1.7%
80	89.0 ± 1.1%	91.7 ± 1.1%

be considered in less than 10^{-6} M. In addition, the reservoir bottle should be thrown away after use.

3.4. Solid-phase extraction

This membrane filtration method may require the preceding isolation or clean-up process for the analytes before producing their Cu(II)–TPPS aggregates. A solid-phase extraction technique using an SCX cation-exchange cartridge was useful for this purpose [12]. Since complete adsorption and concentration of CSs onto the SCX solid-phase were observed, quantitative desorption and isolation of the analytes were examined using several acidified ethanol–water mixture. Table 3 shows the changes in percentage-recoveries of standard Zeph and of CTMA based on the *isolation procedure* described in Section 2. The result indicated that 60% (v/v) ethanol/0.1 M–HCl was adequate for the eluting solvent providing quantitative recovery with good R.S.D.

The CS analytes were quantitatively isolated from surfactant mixtures containing AS and NS by the SCX solid-phase extraction. Table 4 shows the overall recovery of Zeph and CTMA from several surfactant mixtures of different abundance ratios. Although

Table 4
Recoveries of Zeph and CTMA from three kinds of mixtures of cationic, anionic, and nonionic surfactants in different concentration ratios

	Zeph	CTMA
CS:AS:NS = 1:50:2		
%Recovery	97.7	95.3
%R.S.D. ($n = 5$)	1.14	1.36
CS:AS:NS = 1:10:10		
%Recovery	97.6	96.2
%R.S.D. ($n = 5$)	1.32	1.22
CS:AS:NS = 1:5:500		
%Recovery	97.6	97.0
%R.S.D. ($n = 5$)	1.30	1.17

Table 5
Analytical results of CS concentration found in river waters from Katabira River, Tsurumi River, and Oooka River

Rivers located in Yokohama City	Katabira River	Tsurumi River	Oooka River
Calibration curve method (μg/L as Zeph)	0.75	1.01	0.71
Standard addition method (μg/L as Zeph)	0.88	1.15	0.82

the environmental abundance of CS might be small comparing with those of AS and NS, the analytes could be collected quantitatively in excess of 95% recovery with acceptable R.S.D.

In addition, the triple-stage solid-phase extraction is very useful technique to separate and isolate CSs, ASs, and NSs individually from real water samples [12]. Since CSs are only trapped by the SCX cartridge, the subsequent isolation procedure is the same as above. The details are in the previous paper.

3.5. Application to river waters

Table 5 lists the analytical results of CS concentration in river waters collected from three different rivers in Yokohama City. Since the CS concentration might be μg/L levels (nearly 10^{-9} M) in the samples, a 500 mL of sample water was subjected to the SCX cartridge and the adsorbed substance was collected into a 5-mL fraction, corresponding to 100-fold concentration. In consideration with the *adsorption coefficient*, the results obtained by the calibration curve method and those by the standard addition method were well correlated with the correlation coefficient of 0.9964, giving the regression coefficient of 1.15. The standard addition method, giving approximately 15% higher values than the calibration method, is adequate for the determination because of reducing unintended matrix effects.

4. Conclusion

The developed spectrophotometric determination of trace amount of cationic surfactants in environmental waters based on the formation of CS–Cu(II)–TPPS aggregates is sensitive and practical. The quantitative extraction was successfully carried out using environmentally or ecologically mild solvent 2-methoxyethanol instead of harmful chloroform; and the overall recoveries were almost constant and satisfactorily high for the analytes. In addition, the probable interference by metal ions can be reduced by using Cu(II)–TPPS complex as the chromophore. Moreover, some fluorescent radiation of TPPS is also eliminated by the complexation.

Although the improved spectrophotometric method in combination with the solid-phase concentration and isolation technique is very powerful and sensitive for environmental analyses, some unintentional adsorption effects can arise in the determination of trace amount of CSs less than 10^{-6} M. Such adsorption of CSs onto reservoir walls or insoluble matrices in environmental waters is inevitable or serious from the trace-analysis viewpoint. The secondary adsorption of the analytes to reservoir walls can be suppressed to some extent by adding the cationic adsorbent, but the accurate determination of trace CSs is still in problem.

The developed method has not been verified using certified reference materials, because they are still unavailable probably due to the above reason. In addition, the dynamic range is not so wide due to the unavoidable adsorption. However, such disadvantages can arise in common in every method available for CS determination. Considering the above-mentioned technical merits, therefore, we

can conclude that the Cu(II)–TPPS method will be the first choice for the trace analysis of CS in environmental waters.

References

[1] G.V. Scott, Anal. Chem. 40 (1968) 768.
[2] E. Nakamura, H. Namiki, Bunseki Kagaku 33 (1984) 600.
[3] H.K. Biswas, B.M. Mandel, Anal. Chem. 44 (1972) 1636.
[4] J. Waters, W. Kupfer, Anal. Chim. Acta 85 (1990) 241.
[5] H.M.N.H. Irving, J.J. Markham, Anal. Chim. Acta 39 (1967) 7.
[6] M. Tsubouchi, Bull. Chem. Soc. Jpn. 44 (1971) 1560.
[7] S. Sakai, M. Tsubouchi, M. Nakagawa, M. Tanaka, Anal. Chim. Acta 93 (1977) 357.
[8] M. Kamaya, Y. Kaneko, K. Nagashima, Anal. Chim. Acta 384 (1999) 215.
[9] T. Tominaga, S. Endoh, H. Ishimaru, Bull. Chem. Soc. Jpn. 64 (1991) 942.
[10] N.C. Maiti, S. Mazumder, N. Periasamy, J. Phys. Chem. B 102 (1998) 1528.
[11] M. Kamaya, J. Takahashi, K. Nagashima, Microchim. Acta 144 (2004) 35.
[12] Y. Yokoyama, T. Okabe, H. Kubo, H. Sato, Microchim. Acta 149 (2005) 287.
[13] S. Taguchi, I. Kasahara, K. Goto, Bunseki Kagaku 30 (1981) 513.
[14] P. Hambright, P.B. Choch, J. Am. Chem. Soc. 96 (1974) 3123.
[15] J. Itoh, T. Yotsuyanagi, K. Aomura, Anal. Chim. Acta 74 (1975) 53.
[16] A. Corsini, O. Herrmann, Talanta 33 (1986) 335.
[17] S. Igarashi, T. Yotsuyanagi, K. Aomura, Bunseki Kagaku 27 (1978) 66.
[18] M. Shibukawa, R. Eto, A. Kira, F. Miura, K. Oguma, H. Tatsumoto, H. Ogura, A. Uchiumi, J. Chromatogr. A 830 (1999) 321.

Talanta 77 (2008) 809–814

Contents lists available at ScienceDirect

Talanta

journal homepage: www.elsevier.com/locate/talanta

An ultrasensitive chemiluminescence immunosensor for PSA based on the enzyme encapsulated liposome

Yue Zheng, Huan Chen, Xue-Ping Liu, Jian-Hui Jiang*, Yan Luo, Guo-Li Shen, Ru-Qin Yu*

State Key Laboratory for Chemo/Biosensing and Chemometrics, College of Chemistry and Chemical Engineering, Hunan University, Changsha 410082, PR China

ARTICLE INFO

Article history:
Received 11 April 2008
Received in revised form 5 July 2008
Accepted 16 July 2008
Available online 31 July 2008

Keywords:
Chemiluminescence immunosensor
Liposome
Prostate-specific antigen
Enhanced chemiluminescence reaction

ABSTRACT

A highly sensitive chemiluminescence immunosensor for the detection of prostate-specific antigen (PSA) was developed based on a novel amplification procedure with the application of enzyme encapsulated liposome. Horseradish peroxidase (HRP) encapsulated and antibody-modified liposome acts as the carrier of a large number of markers and specific recognition label for the amplified detection of PSA. In the detection of PSA, the analyte was first bound to the specific capture antibody immobilized on the microwell plates, and then sandwiched by the antibody-modified liposomes encapsulating HRP. The encapsulated markers, HRP molecules were released by the lysis of the specifically bound liposomes in the microwell with Triton X-100 solution. Then, the analyte PSA could be determined via the chemiluminescence signal of HRP-catalyzed luminol/peroxide/enhancer system. The "sandwich-type" immunoassay provides the amplification route for the PSA detection in ultratrace levels. The CL emission intensity exhibits dynamic correlation to PSA concentration in the range from 0.74 pg/ml to 0.74 μg/ml with readily achievable detection limit of 0.7 pg/ml.

1. Introduction

Prostate cancer (PCa) has become a most widespread and stubborn disease and a major cause of death in the old age male population nowadays [1]. It admits of no delay for the sensitive diagnosis and efficient treatment of PCa. Prostate-specific antigen (PSA), a 33-kDa single-chain glycoprotein with chymotrypsin-like protease activity, has been used as the most validated marker for the detection of PCa in screening, diagnosis and monitor of disease recurrence after surgical prostatectomy [2]. Several extracellular protease inhibitors such as α_1-antichymotrypsin (ACT) and α_2-macroglobulin (AMG), protein C inhibitor, and pregnancy zone protein could form complex with PSA [3,4], but the complex of PSA and AMG is unable to be detected by most immunoassays because of the formation of complexes between PSA and AMG masks all PSA epitopes for antibody recognition [5]. However, the combination with ACT allows PSA antigenicity to be retained on account of several PSA epitopes remaining unmasked. The complex of PSA and ACT is demonstrated to be the predominant form of the detectable total PSA (t-PSA) in serum by immunoassay, while the free PSA which was less than 30% of the t-PSA concentration coexists as the other form [6]. In clinic, the widely acknowledged PSA (t-PSA) cut point is 4.0 ng/ml for most patients and 2.5–3.0 ng/ml in younger men [7], but also there is a fact that about 14% of men with t-PSA levels less than 2.5 ng/ml have shown to have prostate cancer on biopsy and a considerable part of these cancers are of high grade [8]. In addition, the extremely small amount of PSA present in early stages of PCa recurrence after radical prostatectomy would be great challenge to the detection capabilities of existing immunoassays [9]. For these reasons, the development of a rapid, ultrasensitive t-PSA immunoassay with a broad linear range is promising in diagnostic tests.

Most of the current PSA detection methods are usually based on immunoassays. The more established approaches include enzyme-linked immunosorbent assays (ELISA) [10], time-resolved immunofluorometric assay [11], surface plasmon fluorescence immunoassay [12], bioluminescent immunoassay [13], electrochemical [14] and surface-enhanced Raman scattering (SERS) [15]. Lately, several new PSA detection methods employing the nanowire electrodes [16], the nanoparticle-based bio bar code [17], and the microcantilever method [18] are proposed. Although they all have their individual strengths, chemiluminescence (CL) is among the most widely used readout modality in virtue of undoubted advantages over other more widely used systems [19,20]. Owing to the light signal being generated by a chemical reaction in the dark, CL shows lower nonspecific signal and noninterference by

* Corresponding authors. Tel.: +86 731 8822577; fax: +86 731 8822782.
E-mail addresses: jianhuijiang@hnu.cn (J.-H. Jiang), rqyu@hnu.cn (R.-Q. Yu).

0039-9140/$ – see front matter © 2008 Elsevier B.V. All rights reserved.
doi:10.1016/j.talanta.2008.07.038

light scattering. CL presents excellent performance in the mode of sandwich-type assays, the sensitivity of which is determined primarily according to the detection limit of the label. In the most format of CL immunoassay, the bound sample constituents are usually separated by an immobilized immunoreagent on a solid phase, for example, microwell plates, assay tubes and microparticles, etc. In the same way, the bound and free tracers can also be separated and the separation step guarantees the low background signal of CL reaction.

Recently, the rapid development of materials with many improved properties for bioanalytical applications has led to a resurgence of interest in the development of particle-enhanced immunoassays, such as colloidal gold, latex particles and silica particles [21–26]. Among these particles, liposome exhibits outstanding features in easy preparation, high resistance to nonspecific adsorption and a versatile carrier of various functional molecules by interior entrapment or surface immobilization. Liposome is a spherical vesicle composed of a phospholipids bilayer surrounding an aqueous cavity [27]. In principle, the liposome can be prepared with ease as monodisperse nanoparticles and capable of showing high resistance to aggregation in aqueous solution. It can avoid nonspecific adsorption by taking advantage of the strong hydrophilic properties of the liposome membrane. In addition, Liposome also provides a very flexible, cell membrane-like environment where biological molecules can retain their structure and bioactivity [28,29]. Moreover, as a versatile immunoassay label, liposome has a large internal volume and outer surface area where thousands of reporter molecules can be entrapped or immobilized and the release of reporter molecules from liposome is controllable [30]. Enzyme molecules are also enclosed in liposome and the properties of HRP-trapped liposome have been thoroughly investigated using CL [31,32]. Thus, the development of liposome-based immunosorbent assays (LISA) has been widely studied [33].

In this paper, a sensitive chemiluminescence immunosensor was developed for the detection of PSA. A sandwich assay format was established by using a monoclonal antibody pair acting as the capture probe and detecting probe, respectively. The monoclonal antibody pair was comprised with two distinct antibodies against different epitopes of the PSA. The capture antibody specific to PSA was first immobilized on the microwell plates. After the specific combination of analyte, the detecting antibody-incorporated and HRP-encapsulated liposomes were introduced as a detection probe. The amount of analyte was corresponding with the number of bound liposomes and the HRP molecules released from them. Utilizing a luminol/peroxide/enhancer CL system, the measured CL intensity was exhibits dynamic correlation to PSA concentration in the sample solution.

2. Experimental

2.1. Materials

The PSA standard stock solution was purchased from National Institute for the Control of Pharmaceutical and Biological Products (Beijing, China). The antibody pair (capture antibody and detection antibody) consisted of PSA140 monoclonal antibody to t-PSA and PSA103 monoclonal antibody to t-PSA (immunoglobulins G, all developed in mouse) was obtained from Tianjian. Biotechnologies Company (Tianjin, China). Patient serums samples of varying PSA concentrations were supplied by Hunan Provincial Tumor Hospital (Changsha, China). Phosphoethanolamine (PE) and 1,2-dipalmitoyl-sn-glycero-3-phosphocholine (DPPC) were from Sigma. Bovine serum albumin (BSA), glycine, horseradish peroxidase (HRP), IgG, HSA, IgE, and thrombin were obtained from Beijing Dingguo Biotechnology Company (Beijing, China). Triton X-100, sodium dodecyl sulfate (SDS) and cetyltrimethylammonium bromide (CTAB) was purchased form Amresco. An enhanced (luminal/peroxide/enhancer) CL system (SuperSignal ELISA Femto; Pierce, Rockford, IL) was used for the measurement of HRP activity. All chemicals and reagents used in this study were of analytical grade quality. Solutions were prepared in deionized, distilled water (resistivity >18 MΩ cm).

2.2. Buffer and solutions

The Na_2CO_3–$NaHCO_3$ buffer solution (0.2 M, pH 9.6) was used as the coating buffer. The phosphate buffer saline (PBS, pH 7.4) was prepared using 1/15 M Na_2HPO_4 and 1/15 M KH_2PO_4. The glycine–NaOH solution (pH 7.2) was obtained by 3 M glycine and 3 M NaOH.

2.3. Apparatus

The chemiluminescence spectra were recorded on a fluorescence spectrophotometer (Jobin Yvon Fluorolog3, France). The 96-well microtiter plates (opaque white polystyrene plates with a Maxisorp surface, exhibiting low cross-talk between adjacent wells) were obtained from Nunc (Nalge Nunc, UK).

2.4. Preparation and functionalization of liposomes encapsulating HRP

The liposomes were prepared according to a documented procedure [34] with slight modifications described as follows: Stock solutions of DPPC and PE were prepared in a chloroform/methanol mixture (6:1, v/v). The solution of DPPC and PE (3 mg in total) were mixed in the molar ratio of 3:1 (DPPC/PE) in a 5-ml round-bottom flask. Then the organic solvent was removed by rotary evaporation under reduced pressure (0.09 MPa), leaving a thin lipid film on the inside wall of the flask. The film was dispersed in 1.5 ml of HRP solution and incubated in a water bath at 50 °C and then sonicated using a probe-type sonicator for 5–10 min at 100 W in ice bath to reduce the average size of the liposomes. The resulting liposome suspension was centrifuged at 3000 rpm (644 g) for 15 min to remove residual multilamellar vesicles and aggregated lipids. The unencapsulated enzymes were removed by sephadex G-100 column. The diameter of the resulting liposome was measured to be 120 ± 15 nm using a dynamic light scattering system (Zeta Plus, Brookhaven Instruments Corp.). The average volume of a single liposome was calculated to be 9.0×10^{-13} μl and the number of HRP molecules encapsulated in a single liposome was calculated to be 24.

2.5. Coupling of antibody to the HRP-encapsulated liposomes

Liposomal conjugates with mouse anti-tPSA monoclonal antibody (immunoliposomes) were prepared via glutaraldehyde coupling according to a documented method [35] with slight modifications: To 0.5 ml of 2.5% glutaraldehyde solution, 1.5 ml of liposomes encapsulating HRP (2 mg lipid ml^{-1}) were added in drops under gently stirring for 1 h at 25 °C. Excess glutaraldehyde solution was disposed by dialysis overnight in phosphate buffer (pH 7.2) at 4 °C. Then, 45 μl of 2.1 mg/ml PSA mouse anti-hIgG monoclonal antibody (detection antibody, PSA103) solution was added under gently stirring for 1 h at 25 °C. In order to block excess aldehyde groups on the liposome surface, 60 μl of 3 M glycine–NaOH (pH 7.2) was added followed by incubation overnight at 4 °C. The liposome-coupled and uncoupled antibody in the resulting solution were separated by sephadex G-100 column and kept at 4 °C until use.

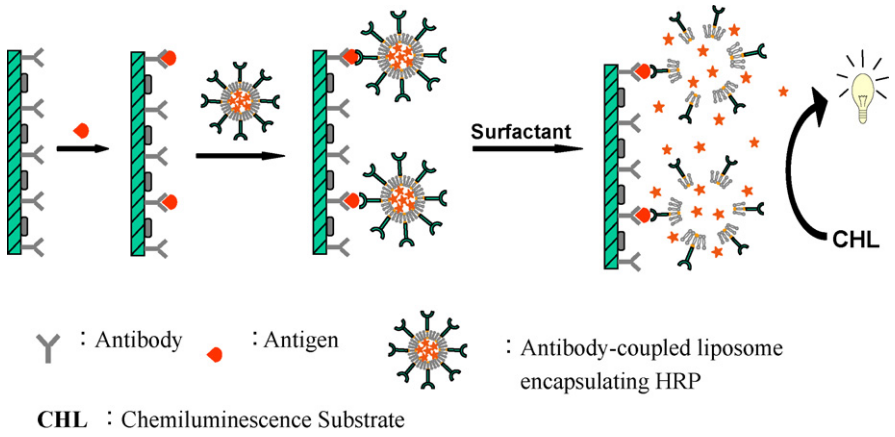

Scheme 1. Schematic diagram of the developed chemiluminescence immunosensing method for PSA.

2.6. Analytical protocol for chemiluminescence determination of PSA

The solid-phase antibody PSA140 Mab was immobilized on MaxiSorp microtitration wells by physical adsorption. The wells were coated overnight at 4 °C with antibody solution in Na_2CO_3–$NaHCO_3$ buffer. After thoroughly rinsing, the wells were blocked with 1% BSA for 1 h at 37 °C. After washing with PBS, the wells were exposed to the PSA standard solution or the serum sample with different PSA concentrations. After incubation at 37 °C for 0.5 h, wells were washed with PBS to remove the unbounded analyte. Then the Mab PSA103-functionalized liposomes encapsulating HRP were dispensed into the wells and incubated for 1 h at 37 °C. Wells were washed six times with PBS to remove the unbound and nonspecifically bound liposomes. Finally, surfactant solution was added to the wells and incubated for 30 min at room temperature to lyses the bound liposomes. The resulting solution was then transferred to an optical cuvette before chemiluminescence assay.

2.7. Light emission measurements

Light emission was measured using a fluorescence spectrophotometer (Jobin Yvon Fluorolog3, France), connected to a computer (F900 v. 6.3 software). 30 μl of stable peroxide solution was added to the cuvette and mixed well with the resulting solution. After luminescence background stabilized, 30 μl luminol/enhancer solution was injected immediately into the cuvette. The real-time output of luminescence intensity was monitored.

3. Results and discussion

3.1. Analytical principle of the chemiluminescence immunosensing method for PSA

A schematic representation of the detection principle of this chemiluminescence immunosensor was shown in Scheme 1. A typical "sandwich" type immunoassay was developed by the capture antibody fixed in the wells and the antibody-modified and HRP-encapsulated liposomes as detecting probes. First, the Mab PSA140 antibodies were fixed in the wells of the microtiter plate by physical adsorption. Due to the specific interaction of antigen–antibody, the PSA is captured on the inside surface of each well on interacting with the PSA sample solution, and then sandwiched by the liposome probe with Mab PSA103 and HRP. The lyses of liposomes were performed by the addition of surfactant and the released HRP molecules were measured through a HRP-catalyzed enhanced chemiluminescence reaction involving the oxidation of luminol by H_2O_2 with the enhancer.

The developed immunosensing method offered several unique advantages over conventional sandwiched immunoassay techniques in PSA detection. First, utilizing the immunoliposome, sensitivity is greatly increased through a multiplication effect. Second, liposome can be programmed to release these encapsulated substances. Third, liposome can avoid nonspecific adsorption by taking advantage of the strong hydrophilic properties of the liposome membrane. Also, the high sensitivity and lower nonspecific signal of CL technique make the developed immunosensing method more perfect when combined with immunoliposomes.

3.2. Optimization of Mab PSA140 immobilizing on the wells of microtiter plates

The immobilization of Mab PSA140 (capture antibody) on the solid phase is crucial to minimize the nonspecific adsorption would ultimately affect the analytical performance of the assay. For this reason, the concentration of Mab PSA140 in coating buffer was optimized. Fig. 1 shows the effect of concentration of Mab PSA140 on the chemiluminescence response at a fixed concentration of PSA. The

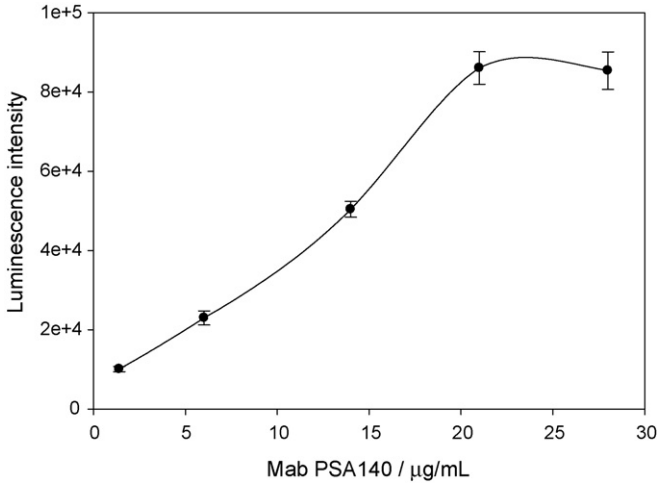

Fig. 1. Effects of concentration of PSA140 Mab immobilized on the wells of microtiter plates on chemiluminescence signal change. The assays for 74 ng/ml PSA using various concentrations of PSA140 Mab were carried out in the optimized buffer solution. The standard deviations obtained by three repeated measurements are shown as the error bars.

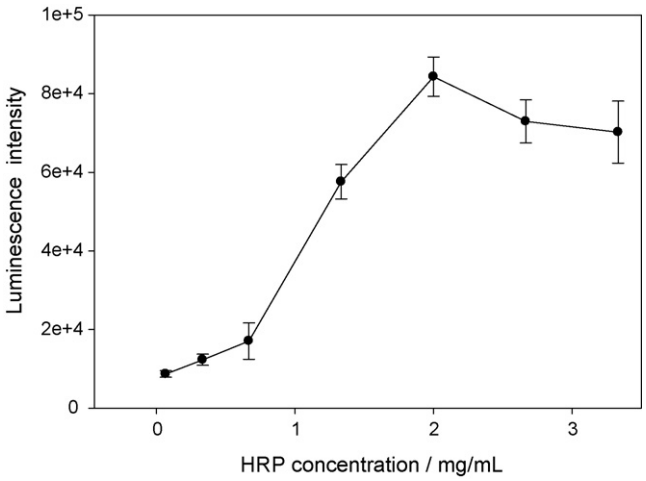

Fig. 2. Effect of amount of added enzyme (HRP) on the chemiluminescent intensity of the developed immunosensing method when the concentration of PSA was 74 ng/ml. Other experimental conditions kept unchanged in the optimized buffer solution. The standard deviations obtained by three repeated measurements are shown as the error bars.

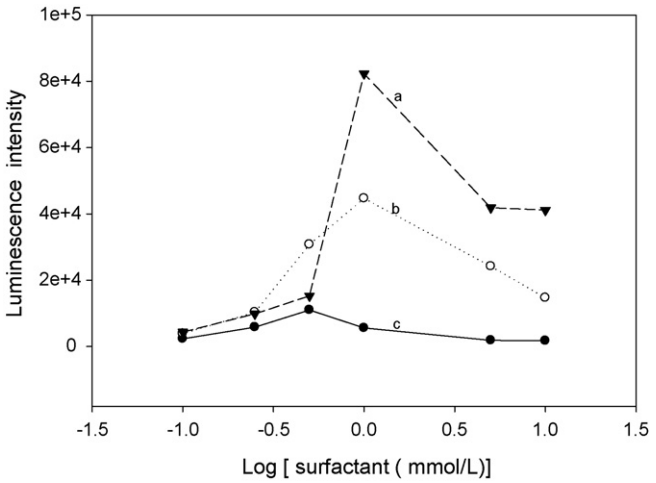

Fig. 3. Chemiluminescent intensity of the developed immunosensing method obtained from the lysis of antibody-modified liposomes encapsulating HPR using different surfactant with PSA concentration of 74 ng/ml: (a) varying concentration of Triton X-100 (b) varying concentration of SDS (c) varying concentration of CTAB. The standard deviations obtained by three repeated measurements are shown as the error bars.

chemiluminescence response varies gradually as the Mab PSA140 concentration changing in the range 1.4–35 μg/ml. The maximized response is obtained at the Mab PSA140 concentration of 28 μg/ml and then the signal levels off indicating that the immobilized antibodies were saturated when the Mab PSA140 concentration of 28 μg/ml.

3.3. Optimization of HRP encapsulation in liposomes

The chemiluminescence intensity is directly determined by the amount of the encapsulated HRP molecule, so the high efficiency of encapsulation should therefore guarantee the low detection limit and sensitivity enhancement in chemiluminescence detection. Therefore, the encapsulation efficiency of HRP within liposomes was optimized using HRP solution with HRP concentrations ranging from 1/15 to 10/3 mg/ml in the liposome preparation procedure. The effect of different concentrations of the HRP solution used in the liposome preparation procedure on the final chemiluminescence response is shown in Fig. 2. Chemiluminescence signal presents a waveform trend with increasing HRP concentrations at the uniform concentration of lipid solution. The largest luminescence intensity appears when the HRP concentration in the lipid solution is 2 mg/ml and then the number of HRP molecules encapsulated in a liposome was calculated to be 24. With higher HPR concentration, the capacity of the liposomes was observed to be reduced which is in good agreement with other works [36]. So the concentrations of the HRP solution used in the liposome preparation procedure was adopted to be 2 mg/ml in this experiments.

3.4. Optimization of the surfactant for the lyses of liposomes

An effective method to detect the marker encapsulated was crucial to the wide use of liposomes in future multiplex analyses. According to the literature, the released HRP marker was detected through the signal produced by catalyzing oxidation of luminol by H_2O_2 with the enhancer. Here, the effect of the character and concentration of three different surfactants were investigated. As shown in Fig. 3, a range of concentrations of surfactant (the nonionic surfactant Triton X-100, cationics CTAB and anionic surfactant SDS) were examined for the ability to lyse liposomes and release the HRP molecules into the solution. On the condition of the liposome encapsulating HRP concentration maintained constant, the surfactant concentration was increased from 0 to 10 mM and the optimal lysis occurred at 1 mM Triton X-100 solution concentration level. The initial increase in luminescence intensity upon surfactant addition is gradual until the critical micellar concentration (cmc) of Triton X-100 (1 mM) is reached. Lysis in a certain region results from the intercalation of surfactant monomers into liposomes. As the concentration of surfactant is increased beyond the cmc, liposomes begin to break apart to form micelles leading to the release of HRP molecules.

Surfactant commonly has a long-chain aliphatic group, and the hydrophobic tail (the dodecyl part of SDS) which binds to the hydrophobic backbone of the protein, breaks the hydrogen bond and hydrophobic interaction, resulting in the denaturation of protein. Therefore, as shown from Fig. 3, the chemiluminescence intensity increase gradually in the beginning with the increasing concentration, when the surfactant concentration further increases, the chemiluminescence intensity decreases quickly. This is an immediate evidence of the inactivation of the HRP as the concentration of surfactant reaches a certain value. So a Triton X-100 concentration of 1 mM was applied in subsequent experiments.

3.5. Determination of PSA

Fig. 4 depicts the chemiluminescence signal of the developed immunosensing method in response to PSA of varying concentration in the range from 0.74 pg/ml to 0.74 μg/ml. The luminescent intensity, as shown in Fig. 4A, was recorded real-time for 60 s, and the peak intensity was used as the measure for quantification. Fig. 4B depicts the dose–response curve of the peak intensity versus PSA concentration. It is clear that CL intensity exhibits dynamic correlation to PSA concentration through 6-decade range from 0.74 pg/ml to 0.74 μg/ml. This range covers the concentration on levels critical to prostate cancer diagnosis. According to the 3σ rule, a detection limit, which is defined as the concentration with signal three times standard deviation over the blank, is estimated to be 0.7 pg/ml.

We have investigated the chemiluminescence responses of the developed immunosensing method to common serum proteins. The technique gave mean (S.D.) chemiluminescence responses of

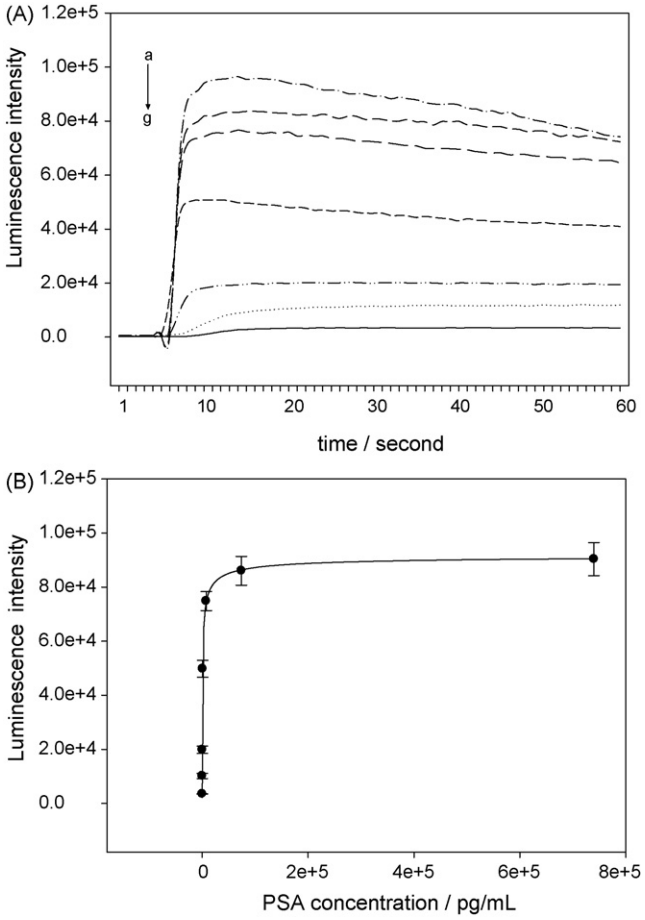

Fig. 4. (A) The chemiluminescent signals for different concentrations of PSA by the developed immunosensing method under the optimized conditions. (a) 0.74 μg/ml, (b) 74 ng/ml, (c) 7.4 ng/ml, (d) 0.74 ng/ml, (e) 74 pg/ml, (f) 7.4 pg/ml, (g) 0.74 pg/ml. (B) Calibration curve for PSA concentration. Conditions are the same as A. The standard deviations obtained by three repeated measurements are shown as the error bars.

3175 (111), 2895 (305), 2137 (64), 1984 (291), 2481 (59), 2171 (133), respectively, for BSA (50 μg/ml), HSA (50 μg/ml), human IgG (50 μg/ml), human IgE (50 μg/ml), thrombin (50 μg/ml) as well as whole serum negative for PSA (10-fold dilution). These responses were all much less than that, 49,766 (3102), obtained with 0.74 ng/ml PSA, indicating that the developed sensor demonstrates excellent selectivity for PSA detection. Therefore, the developed strategy was expected to hold promise for the detection of PSA in complicated serum specimens.

In order to investigate the feasibility of the developed to be applied for clinical analysis, four human serum specimens were collected from patients with prostate diseases and determined using the introduced method with reference to ELISA. The results of both methods are shown in Table 1. One observes that the biosensing method give concentration estimates comparable to ELISA, indicators of the feasibility of the developed method for real sample assay.

Table 1
Comparison of the results obtained by the ELISA method and the developed immunosensing method

Samples	PSA concentration determined by ELISA (ng/ml)	PSA concentration determined by the method (ng/ml)
1	1.88	1.95 ± 0.16
2	3.22	3.48 ± 0.32
3	13.00	11.95 ± 1.07
4	37.05	38.54 ± 2.00

4. Conclusion

The present study developed a novel CL for PSA detection using a sandwich assay format based on monoclonal antibodies pair, antibody-modified liposomes encapsulating HRP acting as highly specific recognition labels for the amplified detection of PSA. The liposome probe provided a biocompatible environment that was beneficial for the resistance of nonspecific adsorption of serum constituents, thus ensuring a low background signal in the assay, PSA first binds to anti-PSA monoclonal antibodies which were immobilized on the microwell plates and is then sandwiched by the antibody-modified liposomes encapsulating HRP. A high level of sensitivity is obtained with this approach in a concentration range that would enable PSA to be detected in clinical samples. The results demonstrated that the developed immunosensing method could allow sensitive, selective detection of PSA with highly resistance to nonspecific adsorption. It was expected that the developed strategy might furnish an ideal protocol for sensitive detection of various protein targets in clinic diagnosis and medical researches.

Acknowledgments

This work was supported by “973” National Key Basic Research Program (2007CB310500) and National Nature Science Foundation (Grant Nos. 20775023, 20675028, 20435010) of China.

References

[1] C.C. Boring, T.S. Suires, T. Tong, S. Montgomery, CA. Cancer J. Clin. 44 (1994) 7.
[2] T.J. Polascik, J.E. Oesterling, A.W. Partin, J. Urol. 162 (1999) 293.
[3] A. Christensson, C.B. Laurell, H. Lilja, Eur. J. Biochem. 194 (1990) 755.
[4] A. Christensson, H. Lilja, Eur. J. Biochem. 220 (1994) 45.
[5] J. Leinonen, W.M. Zhang, U.H. Stenman, J. Urol. 155 (1996) 1099.
[6] H. Lilja, A. Christensson, U. Dahlén, M.T. Matikainen, O. Nilsson, K. Pettersson, T. Lövgren, Clin. Chem. 37 (1991) 1618.
[7] G. Aus, C.C. Abbou, M. Bolla, A. Heidenreich, H.P. Schmid, H. van Poppel, J. Wolff, F. Zattoni, Eur. Urol. 48 (2005) 546.
[8] I.M. Thompson, D.K. Pauler, P.J. Goodman, C.M. Tangen, M. Scott Lucia, H.L. Parnes, L.M. Minasian, L.G. Ford, S.M. Lippman, E. David Crawford, J.J. Crowley, C.A. Coltman, N. Engl. J. Med. 350 (2004) 2239.
[9] A.M. Ward, J.W.F. Catto, F.C. Hamdy, Ann. Clin. Biochem. 38 (2001) 633.
[10] B. Acevedo, Y. Perera, M. Ruiz, G. Rojas, J. Benítez, M. Ayala, J. Gavilondo, Clin. Chim. Acta 317 (2002) 55.
[11] T. Soukka, J. Paukkunen, H. Härmä, S. Lönnberg, H. Lindroos, T. Lövgren, Clin. Chem. 47 (2001) 1269.
[12] Y. Fang, P. Björn, L. Stefan, K. Wolfgang, Anal. Chem. 76 (2004) 6765.
[13] Y. Seto, T. Iba, K. Abe, Luminescence 16 (2001) 285.
[14] C. Fernández-Sánchez, C.J. McNeil, K. Rawson, O. Nilsson, Anal. Chem. 76 (2004) 5649.
[15] D.S. Grubisha, R.J. Lipert, H.Y. Park, J. Driskell, M.D. Porter, Anal. Chem. 75 (2003) 5936.
[16] M.A. Roberts, S.O. Kelley, J. Am. Chem. Soc. 129 (2007) 11356.
[17] J.M. Nam, C.S. Thaxton, C.A. Mirkin, Science 301 (2003) 1884.
[18] G.H. Wu, R.H. Datar, K.M. Hansen, T. Thundat, R.J. Cote, A. Majumdar, Nat. Biotechnol. 19 (2001) 856.
[19] L.J. Kricka, Anal. Chim. Acta 500 (2003) 279.
[20] R.S. Chouhan, K. Vivek Babu, M.A. Kumar, N.S. Neeta, M.S. Thakur, B.E. Amitha Rani, A. Pasha, N.G.K. Karanth, N.G. Karanth, Biosens. Bioelectron. 21 (2006) 1264.
[21] N.T.K. Thanh, Z. Rosenzweig, Anal. Chem. 74 (2002) 1624.
[22] L. Tang, G.M. Zeng, G.L. Shen, Y.P. Li, Y. Zhang, D.L. Huang, Environ. Sci. Technol. 42 (2008) 1207.
[23] X.C. Zhou, J.Z. Zhou, Anal. Chem. 76 (2004) 5302.
[24] M.B. Medina, J. Agric. Food Chem. 52 (2004) 3231.
[25] M.B. Medina, J. Agric. Food Chem. 54 (2006) 4937.
[26] L.A. Dykman, V.A. Bogatyrev, B.N. Khlebtsov, N.G. Khlebtsov, Anal. Biochem. 341 (2005) 16.
[27] H.A.H. Rongen, A. Bult, W.P. van Bennekom, J. Immunol. Methods 204 (1997) 105.
[28] D. Rozema, S.H. Gellman, Biochemistry 35 (1996) 15760.
[29] M. Yoshimoto, T. Shimanouchi, H. Umakoshi, R. Kuboi, J. Chromatogr. B 743 (2000) 93.

[30] T. Imura, T. Gotoh, K. Otake, S. Yoda, Y. Takebayashi, S. Yokoyama, H. Takebayashi, H. Sakai, M. Yuasa, M. Abe, Langmuir 19 (2003) 2021.
[31] T. Kamidate, K. Komatsu, H. Tani, A. Ishida, Luminescence 22 (2007) 236.
[32] T. Kamidate, N. Kikuchi, A. Ishida, H. Tani, Anal. Sci. 21 (2005) 701.
[33] D. Monroe, J. Liposome Res. 1 (1990) 339.
[34] A.K. Singh, P.K. Kilpatrick, R.G. Carbonell, Biotechnol. Prog. 11 (1995) 333.
[35] Y. Nakano, M. Mori, S. Nishinohara, Y. Takita, S. Naito, H. Kato, M. Taneichi, K. Komuro, T. Uchida, Bioconjugate Chem. 12 (2001) 391.
[36] K. Koide, M. Karel, Int. J. Food Sci. Technol. 22 (1987) 707.

Talanta 77 (2008) 804–808

Contents lists available at ScienceDirect

Talanta

journal homepage: www.elsevier.com/locate/talanta

Accurately measuring respiratory activity of single living cells by scanning electrochemical microscopy

Lanlan Zhu, Ning Gao, Xiaoli Zhang*, Wenrui Jin*

School of Chemistry and Chemical Engineering, Shandong University, Jinan 250100, China

ARTICLE INFO

Article history:
Received 10 February 2008
Received in revised form 10 July 2008
Accepted 16 July 2008
Available online 3 August 2008

Keywords:
Scanning electrochemical microscopy
Single living cells
Respiratory activity

ABSTRACT

Scanning electrochemical microscopy (SECM) is a powerful tool to examine the respiratory activity of living cells. However, in SECM measurements of cell respiratory activity, the signal recorded usually also includes the signal corresponding to the cell topography. Therefore, measurements of cell respiratory activity using conventional SECM techniques are not accurate. In the present work, we develop a method for accurate measurement of the respiratory activity of single living cells using SECM. First, cells are immobilized on a glass substrate modified with collagen. Then, a Pt ultramicroelectrode tip of SECM held at −0.50 V is scanned along the central line across a living cell and a SECM scan curve, i.e., the relationship of the tip current versus the displacement (the first scan curve) is recorded with a negative peak. The peak current i_p on this first scan curve is composed of i_{p1}, which corresponds to the cell respiratory activity and i_{p2}, which corresponds to the cell topography. In order to isolate the i_{p2} component, the cell is killed by exposing it to 1.0×10^{-3} mol/L KCN for 10 min. The tip is then scanned again with the same trace over the dead cell, and a second SECM scan curve is recorded. Noting that the topography of the dead cell is the same as that of the living cell, this second scan curve with a negative peak corresponds now only to the cell topography. Thus, i_{p2} is obtained from the second SECM scan curve. Finally, i_{p1} corresponding to the respiratory activity of the living cell can be accurately calculated using $i_{p1} = i_p - i_{p2}$. This method can be used to monitor real-time change in the respiratory activity of single cells after exposing them to KBr, NaN_3 and KCN.

1. Introduction

Single-cell analysis has been through a rapid development in the last two decades. Measurements in living cells [1] are essential, because it is almost impossible to refabricate the cellular conditions in vitro. A variety of analytical techniques have been extended to living cells [2–4]. Scanning electrochemical microscopy (SECM) is first used to study processes occurring on chemical interfaces in 1989 [5]. The most important aspect of SECM is that it provides both structural and chemical information of the surface. Therefore, SECM has been considered as a powerful tool to characterize local bioelectrochemical nature of various biological surfaces such as enzymes [6–12], enzyme-labeled antigen–antibody complexes [13,14], plant tissues [15,16], mouse skin [17] and cells [18–20].

Over the past decade, there has been an increased interest in SECM of single living cells [21–35]. SECM as a useful tool for measuring oxygen concentration near a single cell has received attention because it is capable of providing real-time information on the cellular status and the metabolic activity at the single cell level. SECM has been used to examine in vivo photosynthetic electron transport of individual guard cells in plant leaf [21] and to detect respiratory activity of living cells [22,24,34,35], as well as photosynthetic activity of single protoplasts [23] by measuring the oxygen concentration over a living cell. Furthermore, the influence of benzoquinone on respiration and photosynthetic electron transport of a single protoplast [25], as well as the oxygen consumption of single bovine embryos [28] have been investigated using SECM.

In these SECM measurements, an ultramicroelectrode (UME) tip held at a negative potential is scanned over a living cell, which is immobilized on an insulating substrate, in order to record the localized distribution of oxygen by measuring the oxygen reduction current. The SECM scan curve with a negative peak, i.e., the relationship of the tip current versus the displacement, is obtained due to the oxygen uptake of the cell. A schematic diagram of how the oxygen concentration over a living cell is measured using SECM is shown in Fig. 1(A). It is noted that, besides its respiratory activity, the cell is also an insulator protruding from the substrate. When the tip is scanned above the cell, the cell as an insulator can block the diffusion of oxygen as mediator from the solution's interior to the cell surface. Oxygen reduction current over the substrate

* Corresponding authors. Fax: +86 531 8856 5167.
E-mail address: jwr@sdu.edu.cn (W. Jin).

0039-9140/$ – see front matter © 2008 Elsevier B.V. All rights reserved.
doi:10.1016/j.talanta.2008.07.050

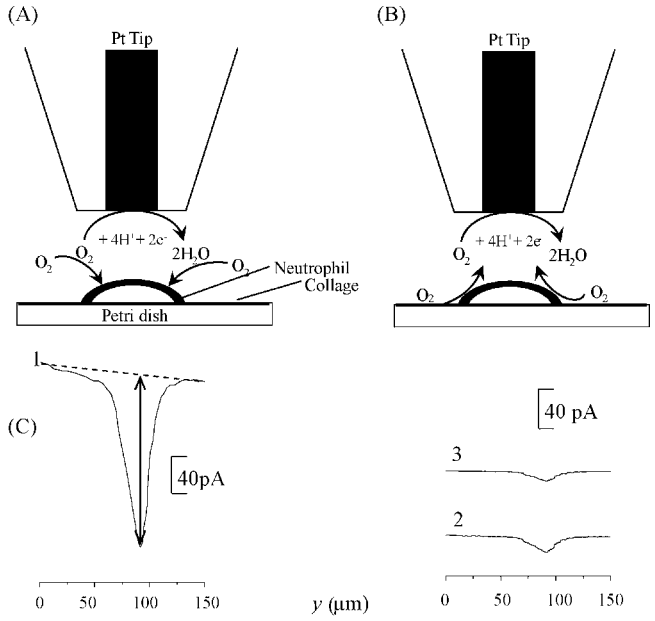

Fig. 1. Schematic representation of (A) measuring oxygen concentration due to cell respiration over a single living cell and (B) measuring SECM negative feedback current corresponding to the cell topography, as well as (C) SECM scan curves of a neutrophil (1) before and after exposing it to 1.0×10^{-3} mol/L KCN for (2) 10 min and (3) 30 min. Radius of Pt UME tip, 5 μm; tip potential, −0.5 V (vs. Ag/AgCl); scan rate, 7.5 μm/s; distance between the tip and the substrate surface, 10 μm.

containing a cell will decrease as compared to that over the substrate without the cell based on the SECM negative feedback mode [36]. The schematic diagram for recording the SECM scan curve of a living cell as an insulator at the negative feedback mode is shown in Fig. 1(B). This means that the scan curve (Fig. 1C, curve 1) with a negative peak corresponds not only to the cell respiration, but also to the cell topography. Therefore, the negative peak current on the SECM scan curve recorded for a living cell consists of two different kinds of currents, one corresponding to the cell respiratory activity and one corresponding to the cell topography. In this work, we describe a method for recording only the signal corresponding to the cell topography (Fig. 1C, curve 2), so that it becomes possible to accurately measure the respiratory activity of a living cell by SECM. Neutrophil is chosen as the model cell. This method can also be used to monitor real-time respiratory activity of single living cells after exposing them to chemical reagents.

2. Experimental

2.1. Reagents

4.5% dextran T-500 was prepared by dissolving appropriate dextran T-500 (Pharmacia Co., Uppsala, Sweden) in physiological buffer saline (PBS). The PBS consisted of 0.15 mol/L NaCl, 7.6×10^{-3} mol/L Na_2HPO_4 and 2.4×10^{-3} mol/L NaH_2PO_4 (pH 7.4). Lymphocyte separation medium was purchased from Shanghai Hengxin Chemical Reagents Co. Ltd. (Shanghai, China). Other chemicals (analytical grade) were purchased from standard reagent suppliers. All aqueous solutions were prepared with doubly distilled water. Several steps described in our previous work [37] were taken to minimize biological contamination. Collagen was prepared according to the following procedure: the tail from a ∼250 g rat was cleaned and immersed in 75% ethanol for 30 min before cutting it into pieces of ∼1.5 cm. Subsequently, the skin of the tailpieces was removed and the tail tendons were collected. The collected tail tendons were cut further into smaller pieces and kept in 150 mL of 0.1% acetic acid for 48 h at 4 °C with additional shaking in between. The mixture was centrifuged for 30 min at 4000 rpm. The supernatant was transferred to several 1.5 mL sterile tubes and stored at −20 °C.

2.2. Apparatus

A CHI900 scanning electrochemical microscope with a 5-μm-radius Pt UME tip (CH Instruments, Austin, TX, USA) was employed to accomplish SECM experiments. A FV500 Olympus confocal laser scanning fluorescence microscope with an excitation wavelength of 488 nm and a 40× objective was used in this work. The fluorescence images at >510 nm were acquired.

2.3. Preparation and immobilization of neutrophils

Preparation of human neutrophils was performed as described previously [38]. To immobilize neutrophils on the glass substrate of a Petri dish, we cleaned the substrate for 20 min with a solution containing 48% H_2SO_4, and 33% HNO_3, then washed it with distilled water for 15 min in an ultrasonicator. After drying, a drop of collagen was deposited onto the clean substrate. The Petri dish was placed in an airtight container with ammonia for 30 min to solidify the collagen. The collagen was rinsed with axenic PBS, dried and irradiated under ultraviolet ray for 12 h on a clean bench. Subsequently, ∼0.5 mL of neutrophil suspension was spread on the collagen. Three hours later, the neutrophils were immobilized on the collagen surface. Unfixed cells were removed by rinsing twice with axenic PBS. The cell density was ∼100 cells/cm^2. Four milliliters of axenic PBS as supporting electrolyte were added to perform the SECM experiment.

2.4. SECM scan curve

The SECM experiments were performed in a Petri dish acting as the electrochemical cell with a three-electrode system consisting of an Ag/AgCl reference electrode (1 mol/L KCl), a Pt wire as the auxiliary electrode, and a Pt UME tip as the working electrode. The Pt tip was polished with 0.05 μm γ-Al_2O_3 and cleaned with absolute ethyl alcohol, 1 mol/L NaOH, 1 mol/L HNO_3, and doubly distilled water, respectively, in an ultrasonicator. Then, the Pt UME tip was stabilized by scanning the tip several times in the range of 0 to −0.5 V in the PBS solution. Before the SECM scan curve was recorded, the central line of a neutrophil was found based on the profile of the oxygen concentration over a neutrophil, which is like a hill. The Pt tip potential was held at −0.50 V versus Ag/AgCl to detect the localized oxygen reduction current. The tip was moved slowly and vertically down to the glass substrate, and the tip current, i, was detected. When the tip was far away from the substrate, i was a constant value, meaning that the behavior of the tip did not change during the run. Then, i decreased with the distance due to negative feedback as the tip was close to the substrate. When i was at 80% of the steady-state current, the tip was stopped. In this case, the distance between the tip and the substrate could be estimated using the fit of the experimental normalized approach curve [39]. From this fitting, the distance was estimated to be ∼10 μm. Then, in order to find the central line of the cell, the tip was moved laterally toward a neutrophil immobilized on the substrate at a constant-height mode, according to the traces shown in Fig. 2. When the tip was moved along the x-axis above the neutrophil (solid line 1), i decreased, because the oxygen concentration above a neutrophil was lower than that over the substrate due to cell respiration and the effect of the negative feedback from the cell topography. When i increased, implying that the tip left the neutrophil, the tip was moved back (dashed line 2) and stopped at the

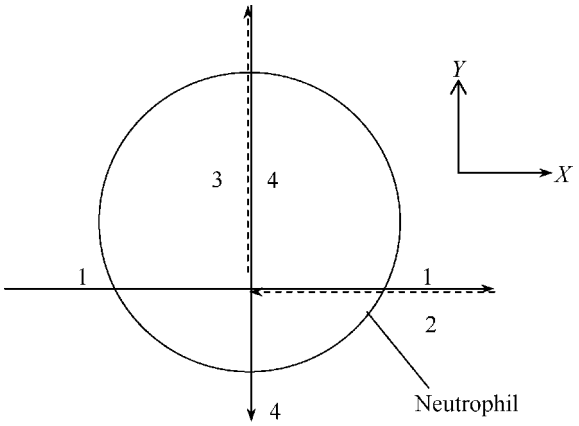

Fig. 2. Process of finding the central line of a cell by using SECM.

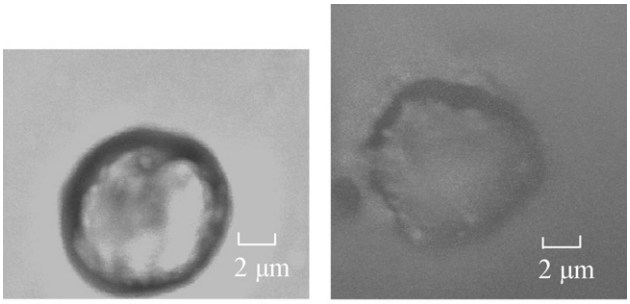

Fig. 3. Optical microscope images of a neutrophil after exposing it to 1.0×10^{-3} mol/L KCN for (A) 10 min and (B) 30 min.

position of minimum current. Then, the tip was moved along the *y*-axis (dashed line 3) across the whole neutrophil, which could be observed as *i* increased. Finally, the tip was scanned reversely along the same trace (solid line 4) and the two-dimensional SECM scan curve (*i*–*y* curve), i.e., the relationship of the tip current versus the displacement, was recorded. All measurements were performed at $25 \pm 2\,^{\circ}C$.

3. Results and discussion

3.1. Measurement of oxygen concentration over a cell

In PBS, oxygen was reduced at potentials more negative than 0 V versus Ag/AgCl. A steady-state reduction current was observed at −0.5 V. Therefore, the Pt tip potential was held at −0.50 V to detect localized oxygen reduction current over a cell. When the oxygen reduction current was used to monitor the respiratory activity of living cells, instability of this current at the Pt electrode with time was observed. This phenomenon is also reported by Bard's group [40]. In this case, the baseline current changes slightly during potential scanning (Fig. 1C) due to electrode deactivation. In order to eliminate the effect of the instability of the current recorded for oxygen reduction at the Pt electrode on the measurement of the peak currents, corresponding to the respiratory activity of the living cells, we used the peak current after subtracting the baseline current in the whole work, as shown in Fig. 1(C). In addition, in this work, since the cells are intact during the electrochemical measurement, chemical passivation and fouling of electrode surface caused by protein adsorption do not exist. This advantage allows an electrode to be scanned many times over and to record all scan curves for the measurements of cell respiratory activity and the exposure experiments of cells in chemical reagents, without losing reproducibility of the obtained results.

3.2. SECM scan curve of a dead neutrophil

To accurately measure the *i*–*y* curve corresponding to the cell respiratory activity over a living neutrophil, the *i*–*y* curve over a dead neutrophil corresponding to the cell topography should be measured first. For this purpose, a living neutrophil was killed by exposing it to 1.0×10^{-3} mol/L KCN. (*Caution*: KCN is very toxic! Care should be taken to avoid direct contact). At the same time, the cell topography was observed under an inverted microscope. Fig. 3 shows the optical microscope images of a neutrophil after exposing it to 1.0×10^{-3} mol/L KCN for 10 and 30 min, respectively. The cell membrane of the neutrophil was not damaged and the cell topography did no change until 10 min later (or longer depending on the cell situation). Moreover, neutrophils could be stained by trypan blue after exposing them to 1.0×10^{-3} mol/L KCN for 5 min, implying that the neutrophils were dead after 5 min. After ∼30 min, we could observe that the cell membrane was damaged. Thus, intact neutrophils without viability could be obtained after exposing it to KCN for ∼10 min.

Fig. 1(C) shows the *i*–*y* curves of a neutrophil before and after exposing it to 1.0×10^{-3} mol/L KCN for 10 min and 30 min, respectively. For a living neutrophil, the negative peak current, i_p, on the *i*–*y* curve (curve 1) was 185 ± 6 pA ($n = 3$). This includes the peak current corresponding to the respiratory activity of the neutrophil, i_{p1}, and the peak current corresponding to the cell topography, i_{p2}. i_{p2} of 18 ± 6 pA ($n = 3$) was obtained from the *i*–*y* curve (curve 2) after exposing the neutrophil to the KCN solution for 10 min. i_{p2} was ∼10% of i_p.

It is true that oxygen can permeate through the cell membrane, which enables an additional flux of oxygen through the cell to the SECM tip. In our previous work [41], however, we investigated the conversion reaction between hydroquinone (H_2Q) and benzoquinone (BQ) catalyzed by peroxidase (PO). In that experiment, H_2Q diffuses from a solution to a microwell containing PO through a nitrocellulose film with micropores covered on the microwell. The H_2Q is converted into BQ by PO and then the converted BQ diffuses from the microwell into the solution. That system is similar to a dead cell with oxygen diffusion. We found that the amount of BQ detected over the microwell with the nitrocellulose film is ∼3% of that obtained over the microwell without the nitrocellulose film. This means that the additional flux of oxygen through the cell to the SECM tip does not exceed ∼3% of that from the solution. This small deviation should be allowed.

Additionally, after the neutrophil was exposed to the KCN solution for 30 min, the profile of the neutrophil became fuzzy, implying that cell membrane was damaged. In this case, the peak current of 11 pA on the *i*–*y* curve (curve 3) could still be obtained. This value resulted from the height of the incomplete cell on the substrate. These results indicated that the peak current detected over a cell corresponding to the cell topography could not be neglected for measurement of respiratory activity of single living cells by SECM. So, to accurately measure cell respiratory activity, the peak current corresponding to cell topography should be considered. Additionally, the width of the scan curves in Fig. 1(C) was larger than the cell diameter. This is because the profile of the SCEM scan curves reflects the thickness of the diffusion layer of oxygen in the solution around the cell. Therefore, the tip-to-cell distance should be constant in SECM for accurate measurement of cell respiratory activity.

Confocal laser scanning fluorescence microscope (CLSFM) was also used to measure neutrophil topography. Neutrophils

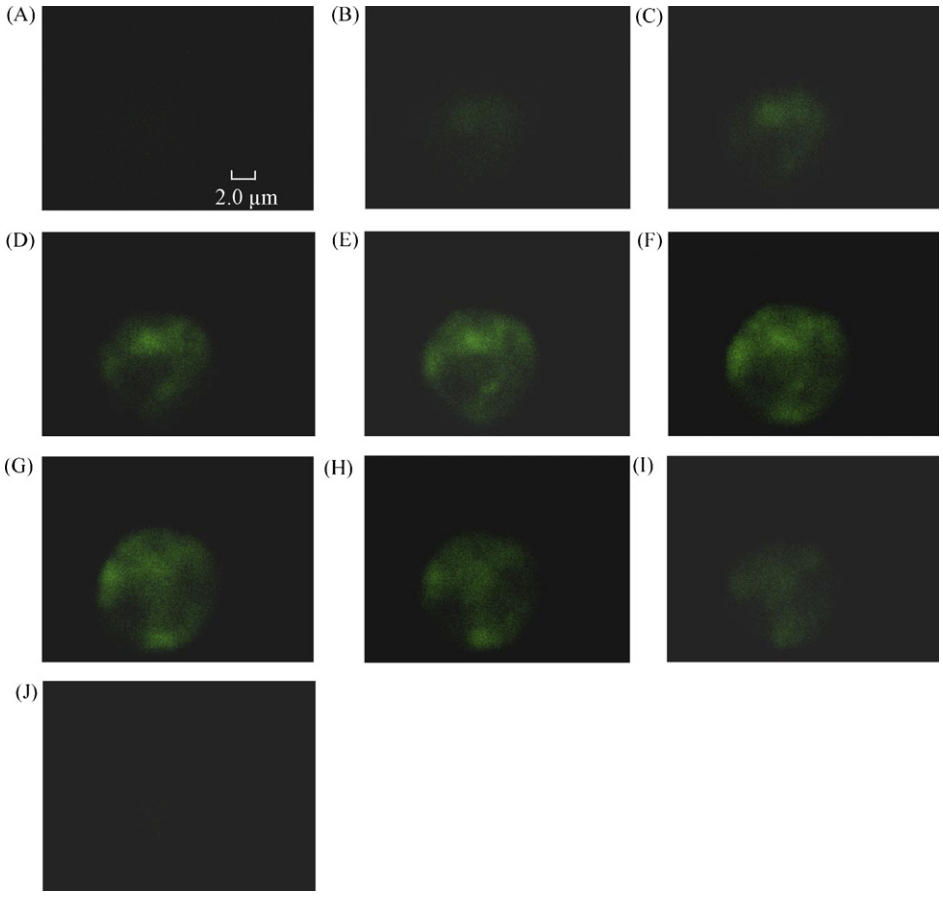

Fig. 4. Fluorescence images at different layers of a neutrophil taken by confocal laser scanning fluorescence microscope after incubation for 10 min with 2×10^{-4} mol/L NDA. The distance away from the basal surface of a neutrophil (μm): (A) 0; (B) 1.0; (C) 2.0; (D) 3.0; (E) 4.0; (F) 5.0; (G) 6.0; (H) 7.0; (I) 8.0 and (J) 9.0. 40× objective; 488 nm excitation and >510 nm emission.

immobilized on the substrate were first incubated with non-fluorescent naphthalene-2,3-dicarboxaldehyde (NDA). NDA is a derivatization reagent that is permeable to cell membrane and can form fluorescent complex with intracellular glutathione (GSH). The fluorescence emitted by NDA–GSH complex at 528 nm can be detected by excitation at 488 nm [42]. Since the NDA–GSH complex is impermeable to the cell membrane, fluorescence images can be acquired. Fig. 4 shows the fluorescence images of a neutrophil at different layers taken by CLSFM after incubation for 10 min with 2×10^{-4} mol/L NDA. Intracellular fluorescence could be detected from 1 to 8 μm from the basal surface of the neutrophil, indicating that the height of the neutrophil immobilized on the substrate was ~8 μm. When the neutrophil was exposed to 1.0×10^{-3} mol/L KCN for 30 min, fluorescence could no longer be detected, because the cellular membrane was seriously damaged, and the intracellular NDA–GSH complex leaked out into the solution. This phenomenon was in agreement with that observed using optical microscope shown in Fig. 3(B). The small height change of the cell could not be measured using CLSFM. It was found that with 1 μm of change in the gap between the tip and the cell, the peak current changed ~3%. Therefore, the deviation of i_{p2} between a living cell and a dead cell for the same cell should be less than this value.

3.3. Accurate measurement of respiratory activity of a living neutrophil

Respiratory activity of a living neutrophil could be accurately determined by measuring both the *i–y* curve of a living neutrophil and the *i–y* curve of a dead neutrophi. This last can be obtained by incubating the living neutrophil for 10 min in 1.0×10^{-3} mol/L KCN. From both *i–y* curves, i_p corresponding to the living neutrophil and i_{p2} corresponding to the dead neutrophil could be obtained. From these two values we can calculate i_{p1} ($i_{p1} = i_p - i_{p2}$), which corresponds only to the respiratory activity of the neutrophil. Using this method, one can accurately measure the change in respiratory activity of single neutrophils with and without chemical stimuli. Fig. 5 shows the normalized relationship between the cell respiratory activity and time, when stimulated by different chemical

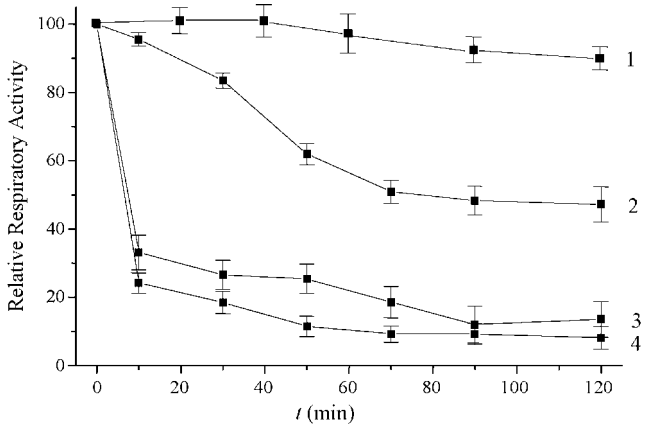

Fig. 5. Time course of relative respiratory activity of neutrophils (1) before and after exposing them to 7.70×10^{-5} mol/L (2) KBr, (3) NaN_3 and (4) KCN. Conditions as in Fig. 1C.

reagents ($n = 3$), i.e., the variation with time of the respiratory activity relative to the initial respiratory activity at time = 0. In Fig. 5, the relative respiratory activity was defined as the i_{p1} ratio versus that taken before exposure to chemical reagents. Curve 1 in Fig. 5 shows the time course of the relative respiratory activity of single neutrophils in PBS ($n = 3$). The relative respiratory activity of single neutrophils was almost constant during 40 min, then decreasing very slowly to ~90% at 120 min. When the neutrophils were exposed to PBS containing reagents such as KBr, NaN_3 and KCN, the relative respiratory activity decreased rapidly with exposure time. Curves 2–4 in Fig. 5 show the time course of the relative respiratory activity of single neutrophils, which were exposed to 7.70×10^{-5} mol/L KBr, NaN_3 and KCN, respectively ($n = 3$). The effect of different reagents on the cell respiratory activity was different. KCN exerted the most significant effect on the respiratory activity of neutrophils. The effect of KBr on the cell respiratory activity was the weakest.

4. Conclusions

The respiratory activity of a living cell can be accurately measured by recording both the SECM scan curves with a negative peak, for a living cell, which is immobilized on an insulating substrate and for the same cell after it is dead. The difference in peak current on both scan curves corresponds to the respiratory activity of the living cell. This method can be applied for other SECM experiments as well, where we want to determine the oxygen concentration near a living cell. This method can also monitor the real-time viability of living cells that suffer from chemical and physical stimuli.

Acknowledgments

This project was supported by the National Natural Science Foundation of China (Grant Nos. 20475033, 20675047, 90713016 and 20705016) and the National Basic Research Program of China (Grant No. 2007CB936602).

References

[1] M.R.H. Baltes, M. Hanocq, J.G. Dubois, Talanta 54 (2001) 893.
[2] J. Wu, Z. Ye, G. Wang, J. Yuan, Talanta 72 (2007) 1693.
[3] X. He, J. Chen, K. Wang, D. Qin, W. Tan, Talanta 72 (2007) 1519.
[4] J. Weng, X. Song, L. Li, H. Qian, K. Chen, X. Xu, C. Cao, J. Ren, Talanta 70 (2006) 397.
[5] A.J. Bard, F.R.-F. Fan, J. Kwak, O. Lev, Anal. Chem. 61 (1989) 132.
[6] D.T. Pierce, P.R. Unwin, A.J. Bard, Anal. Chem. 64 (1992) 1795.
[7] C. Kranz, G. Wittstock, H. Wohlschläger, W. Schuhmann, Electrochim. Acta 42 (1997) 3105.
[8] G. Wittstock, W. Schuhmann, Anal. Chem. 69 (1997) 5059.
[9] I. Turyan, T. Matsue, D. Mandler, Anal. Chem. 72 (2000) 3431.
[10] J. Zhou, C. Campbell, A. Heller, A.J. Bard, Anal. Chem. 74 (2002) 4007.
[11] D. Oyamatsu, Y. Hirano, N. Kanaya, Y. Mase, M. Nishizawa, T. Matsue, Bioelectrochemistry 60 (2003) 115.
[12] C. Zhao, G. Wittstock, Anal. Chem. 76 (2004) 3145.
[13] G. Wittstock, K.J. Yu, H.B. Halsall, T.H. Ridgway, W.R. Heineman, Anal. Chem. 67 (1995) 3578.
[14] H. Shiku, T. Matsue, I. Uchida, Anal. Chem. 68 (1996) 1276.
[15] C. Lee, J. Kwak, A.J. Bard, Proc. Natl. Acad. Sci. U.S.A. 87 (1990) 1740.
[16] H. Zhou, H. Shiku, S. Kasai, H. Noda, T. Matsue, H. Ohya-Nishiguchi, H. Kamada, Bioelectrochemistry 54 (2001) 151.
[17] E.R. Scott, H.S. White, J.B. Phipps, Anal. Chem. 65 (1993) 1537.
[18] T. Kaya, M. Nishizawa, T. Yasukawa, M. Nishiguchi, T. Onouchi, T. Matsue, Biotechnol. Bioeng. 76 (2001) 391.
[19] M. Nishizawa, K. Takoh, T. Matsue, Langmuir 18 (2002) 3645.
[20] Y.S. Torisawa, T. Kaya, Y. Takii, D. Oyamatsu, M. Nishizawa, T. Matsue, Anal. Chem. 75 (2003) 2154.
[21] M. Tsionsky, Z.G. Cardon, A.J. Bard, R.B. Jackson, Plant Physiol. 113 (1997) 895.
[22] T. Yasukawa, Y. Kondol, I. Uchida, T. Matsue, Chem. Lett. 27 (1998) 767.
[23] T. Yasukawa, T. Kaya, T. Matsue, Anal. Chem. 71 (1999) 4637.
[24] T. Yasukawa, T. Kaya, T. Matsue, Chem. Lett. 28 (1999) 975.
[25] T. Yasukawa, I. Uchida, T. Matsue, Biophys. J. 76 (1999) 1129.
[26] B. Liu, S.A. Rotenberg, M.V. Mirkin, Proc. Natl. Acad. Sci. U.S.A. 97 (2000) 9855.
[27] A. Hengstenberg, A. Blöchl, I.D. Dietzel, W. Schuhmann, Angew. Chem. Int. Ed. 40 (2001) 905.
[28] H. Shiku, T. Shiraishi, H. Ohya, T. Matsue, H. Abe, H. Hoshi, M. Kobayashi, Anal. Chem. 73 (2001) 3751.
[29] B. Liu, W. Cheng, S.A. Rotenberg, M.V. Mirkin, J. Electroanal. Chem. 500 (2001) 590.
[30] C. Cai, B. Liu, M.V. Mirkin, H.A. Frank, J.F. Rusling, Anal. Chem. 74 (2002) 114.
[31] B. Liu, S.A. Rotenberg, M.V. Mirkin, Anal. Chem. 74 (2002) 6340.
[32] J.M. Liebetrau, H.M. Miller, J.E. Baur, S.A. Takacs, V. Anupunpisit, P.A. Garris, D.O. Wipf, Anal. Chem. 75 (2003) 563.
[33] W. Feng, S.A. Rotenberg, M.V. Mirkin, Anal. Chem. 75 (2003) 4148.
[34] T. Kaya, Y.S. Torisawa, D. Oyamatsu, M. Nishizawa, T. Matsue, Biosens. Bioelectron. 18 (2003) 1379.
[35] Y. Takii, K. Takoh, M. Nishizawa, T. Matsue, Electrochim. Acta 48 (2003) 3381.
[36] M.V. Mirkin, B.R. Horrocks, Anal. Chim. Acta (2000) 119.
[37] X. Sun, W. Jin, Anal. Chem. 75 (2003) 6050.
[38] W. Jin, L. Jiang, Electrophoresis 23 (2002) 2471.
[39] Y. Shao, M.V. Mirkin, J. Phys. Chem. B 102 (1998) 9915.
[40] A.J. Bard, X. Li, W. Zhan, Biosens. Bioelectron. 22 (2006) 461.
[41] X. Zhang, F. Sun, X. Peng, W. Jin, Anal. Chem. 79 (2007) 1256.
[42] O. Orwar, H.A. Fishman, N.E. Ziv, R.H. Scheller, R.N. Zare, Anal. Chem. 67 (1995) 4261.

Talanta 77 (2008) 897–900

Contents lists available at ScienceDirect

Talanta

journal homepage: www.elsevier.com/locate/talanta

Calcium tungstate coprecipitation for removal of Sr interference with determination of Rb by ID-ICP-MS

Yanbei Zhu*, Kazumi Inagaki, Takashi Yarita, Koichi Chiba

National Metrology Institute of Japan (NMIJ), National Institute of Advanced Industrial Science and Technology (AIST), 1-1-1, Umezono, Tsukuba, Ibaraki 305-8563, Japan

ARTICLE INFO

Article history:
Received 2 July 2008
Accepted 22 July 2008
Available online 31 July 2008

Keywords:
Calcium tungstate
Coprecipitation
Sr
Rb
ID-ICP-MS
Rice flour

ABSTRACT

A coprecipitation method using calcium tungstate was developed to remove ^{87}Sr isobaric interference with ^{87}Rb prior to measurement of Rb by ID-ICP-MS. Precipitation of calcium tungstate was obtained by adding $Ca(NO_3)_2$ solution and $(NH_4)_2WO_4$ solution to the sample, where $(NH_4)_2WO_4$ was added more than the stoichiometric proportion to precipitate $Ca(NO_3)_2$ completely and remove Sr effectively. Furthermore, in order to reduce matrix burden to the ICP-MS instrument, the residual $(NH_4)_2WO_4$ was removed by adding conc. HNO_3. Prior to the application, thorough purification of coprecipitant reagent was carried out to reduce the blank. The effectiveness of the present method was verified by analyzing two brown rice flour certified reference materials (CRMs), NIES CRM 10a and NIES CRM 10b. Finally, the present method was applied to the measurement of Rb in a white rice flour RM sample being developed by National Institute of Metrology of Japan.

1. Introduction

Rubidium is one of the most common elements in the earth crust, animal/fish tissues, human blood and metabolites, and botanical samples [1–3]. The results of some researches indicate that Rb possibly contributes to the disturbance of nervous system of dialysis patients [4]. However, up to date, the biological role and the toxicity of Rb are still not clear. Studies on Rb are being challenged in various research fields [4–9].

Measurement of Rb could be carried out by a variety of analytical techniques, such as neutron activation analysis (NAA) [10], electrothermal atomic absorption spectrometry (ETAAS) [4,11,12], inductively coupled plasma atomic emission spectrometry (ICP-AES) [10], and inductively coupled plasma mass spectrometry (ICP-MS) [8,9,13]. Meanwhile, isotope dilution (ID) is a technique to increase the precision and accuracy of chemical analysis [14,15]. Because the measurant in ID analysis is the isotope ratio, when the reference isotope and the spike isotope were completely mixed, loss of substance and instrumental signal drift will not affect the analytical result [15]. However, isobaric interference of ^{87}Sr with ^{87}Rb is an obstacle to ID analysis of Rb, since there are only two stable Rb isotopes, i.e., ^{85}Rb and ^{87}Rb. A mass resolution of 300,000 is necessary for spectrometric separation of ^{87}Sr from ^{87}Rb, which is too difficult to realize. On the other hand, isobaric interference in ID-ICP-MS measurement of some elements might be corrected based on the isotope composition of the interfering element [16]. Unfortunately, application of such method to Rb is restricted by the fact that the radioactive decay of ^{87}Rb produces ^{87}Sr which results in the variation of Sr isotope composition among various samples [17]. Therefore, efficient separation of Rb from Sr is often indispensable for obtaining a reproducible data of Rb by ID-ICP-MS [18].

A number of works have been carried out to separate Sr from Rb before the ID analysis or isotopic ratio measurement [13,19–23]. In these researches, extraction and chromatographic separation using Sr-specific resin were almost the unique techniques. Recently, the work of Rowland et al. provided a novel technique for separation of Rb–Sr isobars based on electrothermal vaporization [13].

On the other hand, taking advantage of the simple operation and the convenience of batch processing, coprecipitation has been applied to the effective separation of various elements from different matrix [24–28]. However, coprecipitate-separation of Sr from Rb has not been reported, at least to our knowledge.

In the present experiment, we present a novel method for removal of Sr from the sample solution, so that the isobaric interference of ^{87}Sr with ^{87}Rb could be eliminated prior to the ID-ICP-MS measurement of Rb. Calcium tungstate was chosen as the coprecipitant, which was formed by adding $Ca(NO_3)_2$ and $(NH_4)_2WO_4$ solutions to the sample. The first reason for choosing calcium tungstate as the coprecipitant is that it is one of the most insoluble calcium compounds. The second reason is that the residual tungstate could be easily removed by adding acid solution, so that

* Corresponding author. Tel.: +81 29 861 4130; fax: +81 29 861 6889.
E-mail address: yb-zhu@aist.go.jp (Y. Zhu).

0039-9140/$ – see front matter © 2008 Elsevier B.V. All rights reserved.
doi:10.1016/j.talanta.2008.07.042

Table 1
Typical operating conditions of ICP-MS

ICP-MS (Agilent 7500c)	
Plasma conditions	
Incident power	1.5 kW
Coolant gas flow rate	Ar 15.0 L min^{-1}
Auxiliary gas flow rate	Ar 0.90 L min^{-1}
Sample gas flow rate	Ar 0.70 L min^{-1}
Make-up gas flow rate	Ar 0.40 L min^{-1}
Collision gas flow rate	He 3.00 L min^{-1}
Sampling conditions	
Sampling depth	7 mm from load coil
Nebulizer: MicroMist	
Sample uptake rate	0.1 mL min^{-1}
Spray chamber: Scott double path	
Wall temperature	2 °C
Data acquisition	
Scanning mode	Peak hopping
Data points	3 points per peak
Dwell time	1 ms
Sweeps	1000
Replicates	10

the burden to ICP-MS could be restrained effectively. The second reason is important, because an excess amount of ammonium tungstate is needed to remove Sr from the sample solution completely.

Effectiveness of the present method was verified by analysis of two certified reference materials (CRMs). Determination of Rb in a candidate white rice flour reference material was also carried out.

2. Experimental

2.1. Instrumentation

Measurement of Rb and Sr were carried out using an ICP-MS instrument (Agilent HP7500c, Yokogawa). The typical operating parameters of the ICP-MS are summarized in Table 1. A microwave digestion instrument (ETHOS 1, Milestone General K.K., Japan) and digestion vessels were utilized for the digestion of the samples. An automatic cleaning system (TraceClean system, Milestone General K.K.) was used for the cleaning of digestion vessels.

2.2. Materials, reagents, and samples

High purity calcium nitrate (99.995% as $Ca(NO_3)_2{\cdot}nH_2O$) and ammonium tungstate (99.999% as $(NH_4)_{10}W_{12}O_{41}{\cdot}5H_2O$) reagents used as coprecipitants were purchased from Wako Pure Chemical Industries, Ltd. (Japan). Calcium nitrate was dissolved in pure water to obtain a solution containing approximate 2% of Ca. Purified ammonium tungstate solution (approximate 5% of W) was obtained after the reagent was thoroughly purified using HNO_3.

The atomic absorption spectrometry grade single element standard solutions of Sr and Rb (1000 mg L^{-1}, guaranteed by the Japan Calibration Service System, JCSS) were also purchased from Wako Pure Chemical Industries, Ltd. Ultrapure grade (Ultrapur®) HNO_3, NH_4OH and H_2O_2 solutions were purchased from Kanto Chemical Co., Inc. (Japan). An ^{87}Rb enriched isotope spike was purchased from Oak Ridge National Laboratory (Oak Ridge, TN).

Polypropylene sample bottles, centrifuge tubes and single-use Eppendorf micropipette tips were used throughout the present experiment. Prior to the application in experiment, all sample bottles, tubes, and pipette tips were cleaned by soaking in 3 M nitric acid solution for 1 week followed by rinsing with pure water. Digestion vessels were cleaned with the TraceClean system employing 50% aqua regia followed by rinsing with pure water. Pure water used throughout the present experiment was prepared using a Millipore purification system (Element, Nihon Millipore Kogyo, Japan).

Rice flour CRMs purchased from National Institute for Environmental Studies (NIES, Japan; NIES 10a and NIES 10b) were analyzed to verify the effectiveness of the present method. Three bottles of candidate white rice flour RM sample being developed by National Metrology Institute of Japan (NMIJ) were randomly selected from the stocks and subjected to the digestion and measurement of Rb, too.

2.3. Microwave digestion procedure

An aliquot of 0.5 g of the sample was weighed and put into the digestion vessel. After adding 7 mL of nitric acid and 0.5 mL of hydrogen peroxide solution, the samples were subjected to the first step of microwave irradiation (ramp: 150 °C for 30 min, hold for 5 min). Furthermore, after cooling the vessels and adding 0.5 mL of hydrogen peroxide solution to each digestion vessel, the samples were subjected to the second step of microwave irradiation (ramp: 220 °C for 25 min, hold for 20 min). Finally, the residual acid was completely evaporated and the samples were dissolved to obtain approximate 20 mL of 2% nitric acid measurement solutions.

In the present experiment, digestion blank test was carried out using an empty digestion vessel, which was added with digestion reagents and subjected to microwave irradiation together with the samples. Test of moisture content was carried out according to the instruction of each CRMs.

2.4. Optimized procedure for coprecipitation

First, 40 μL of 10% $Ca(NO_3)_2$ solution and 1.6 mL of 10% $(NH_4)_2WO_4$ solution were added into each 1 mL of digested sample solution. After shaken for 5 min and laid for 30 min, the precipitate was separated by centrifugation (4000 rpm, 2 min), in which Sr was enriched. Furthermore, 2 mL of conc. HNO_3 was added to the supernatant solution. After shaken for 1 min and centrifuged (4000 rpm, 2 min), the residual tungstate was removed as precipitate of tungstic acid. Finally, the supernatant solution was properly diluted with pure water and measured with ICP-MS.

2.5. Calculation in the ID-ICP-MS method

Calculation of analytical results was based on Eq. (1) following the instruction of EURACHEM/CITAC Guide CG 4.

$$c_x = c_z \times r \times \frac{m_y}{w m_x} \times \frac{m_z}{m'_y} \times \frac{K_y \times R_y - K_b \times R_b}{K_b \times R_b - K_x \times R_x} \times \frac{K_{b'} \times R_{b'} - K_z \times R_z}{K_y \times R_y - K_{b'} \times R_{b'}} - c_{\text{blank}} \quad (1)$$

In Eq. (1), the subscripts of *x, y, z, b*, and *b′* represent the sample, the isotope enriched spike, the standard, the mixed solution of *x* and *y* for ID, and the mixed solution of *y* and *z* for reverse ID, respectively. The meaning of other symbols were as follows: m_x and m_y, mass of *x* and *y* in mixed *b* (g); m'_y and m_z, mass of *y* and *z* in mixed *b′* (g); c_x, c_y, and c_z, concentration of Rb [ng g^{-1}] in *x*, *y*, and *z*, respectively; c_{blank}, observed procedure blank [ng g^{-1}]; R_x, R_y, R_z, R_b and R_b', measured ratio of ^{85}Rb/^{87}Rb in *x, y, z, b* and *b′*, respectively; K_x, K_y, K_z, K_b, and K_b', mass bias correction factor of R_x, R_y, R_z, R_b, and R_b', respectively. The *w* and *r* are wet factor and repeatability factor, respectively.

3. Results and discussion

3.1. Purification of ammonium tungstate

Prior to the application to the samples, impurities in coprecipitant reagents were investigated. Because Sr impurity could be fully removed together with $CaWO_4$ in the coprecipitation process, purification was focused on Rb impurity. It was found that Rb in calcium nitrate was negligible, i.e., approximate 0.11 ng g^{-1} of Rb in a solution containing 2% Ca. However Rb in ammonium tungstate is significant, i.e., approximate 20 ng g^{-1} of Rb in a solution containing 5% of W. Therefore, ammonium tungstate was purified to reduce the reagent blank of Rb.

Firstly, approximate 10 g of $(NH_4)_2WO_4$ reagent was poured into 25 mL of 3 M HNO_3 solution to obtain a precipitate of H_2WO_4. After centrifuged separation, the H_2WO_4 precipitate was washed with another 25 mL of 3 M HNO_3 in an ultrasonic bath for 2 min. After that, the H_2WO_4 precipitate was centrifuged and collected again. The above washing procedure was repeated over 20-times until Rb signal in the supernatant became constant. Finally, the purified H_2WO_4 precipitate was dissolved with 100 mL of NH_4OH to obtain a purified ammonium tungstate, which was used as the coprecipitant. In order to check the washing efficiency, Rb in each supernatant solution was measured by ICP-MS. The signal intensity of ^{85}Rb in the 1st, 5th, 10th, 15th, 20th, and 21st supernatant solution was approximate 300 000, 50 000, 4000, 1500, 500 and 500 cps, respectively. It suggests that Rb was effectively removed after the washing procedure was performed for 20-times. After such purification, Rb concentration was reduced to approximate 0.8 ng g^{-1} in the purified ammonium tungstate solution which contained 5% of W.

3.2. Optimization of coprecipitant amounts

A digested solution of NMIJ candidate white rice flour RM sample was used as test solution to optimize the amount of coprecipitant, which is required to achieve a compromise of Sr removal efficiency and reagent blank control.

At first, 2 mL of the $(NH_4)_2WO_4$ solution (5% of W) was added into each 1 mL of the sample solution. Different amounts (20, 40, 60, and 80 μL, respectively) of the $Ca(NO_3)_2$ solution (2% of Ca) were added to the sample solutions. After coprecipitation and separation, the Sr content in the measurement solution was determined to assess the Sr removal efficiency. It was found that 40 μL of calcium nitrate solution was enough to remove Sr from the sample solution, where approximately 99% of Sr was removed.

Furthermore, 40 μL of the calcium nitrate solution was added into each 1 mL of the sample solution, into which different amounts of the ammonium tungstate solution were added to assess the Sr-removal efficiency. When 1.2, 1.4, 1.6, 1.8, and 2.0 mL was added, the Sr-removal efficiency was approximately 92, 93, 99, 99, and 99%, respectively.

As a result of the above optimization, 40 μL of the calcium nitrate solution and 1.6 mL of the purified ammonium tungstate solution were added to 1 mL of digested sample for coprecipitation to remove Sr. Under this condition, the concentration of Ca and W in the sample solution were approximate 0.03 and 3%, respectively, in which the mole ratio of (Ca:W) was approximate (1:22). The solubility of calcium tungstate at 20 °C is approximate 0.0024 g/100 mL (i.e., 24 μg/mL) [29]. Therefore, it is apparently that the Ca content could be fully precipitated. However, more than 90% of W content was left in the measurement solution after coprecipitation, in which the concentration of W was too high to be introduced into the ICP-MS. The residual W was removed as H_2WO_4 by adding 2 mL of conc. HNO_3. The concentration of W in the final measurement solution was reduced to approximate 30 μg g^{-1}.

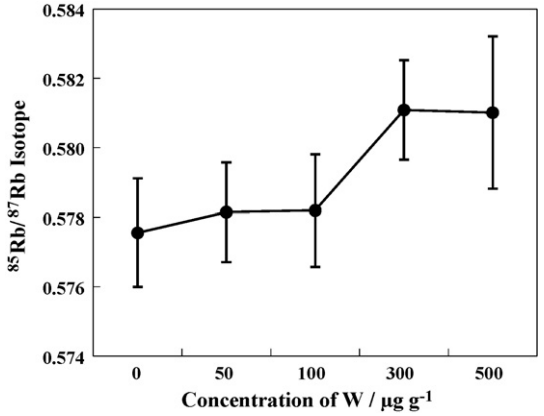

Fig. 1. Dependance of measured $^{85}Rb/^{87}Rb$ isotope ratio on the concentration of W in the sample.

In the present work, blank test was carried out by adding a small amount of isotope spike to a digestion vessel, in which the same amounts of digestion reagents as those used for the samples were also added. Blank test solution was also subjected to the coprecipitation separation in the same way as the sample. As a result, the blank was found to be 0.071 ± 0.001 μg g^{-1} (mean ± standard uncertainty, $n = 10$).

3.3. Effect of tungstate concentration on Rb isotopic ratio measurement

The solution for reverse ID was used as the matrix effect test solution for Rb isotopic ratio measurement. A proper amount of ammonium tungstate solution was added to the test solution so that the concentration of W was 50, 100, 300, and 500 μg g^{-1}, respectively. The results of Rb isotope ratio measurement are illustrated in Fig. 1. As is seen in Fig. 1, when the concentration of W exceeded 300 μg g^{-1}, the observed Rb isotopic ratio was slightly higher than that obtained in the test solution without ammonium tungstate. However, when the concentration of W in the solution was not more than 100 μg g^{-1}, it did not noticeably affect the measurement of Rb isotopic ratio. In the present work, because the concentration of W in final measurement solutions was approximate 30 μg g^{-1}, the analysis did not suffer from noticeable interference of W matrix.

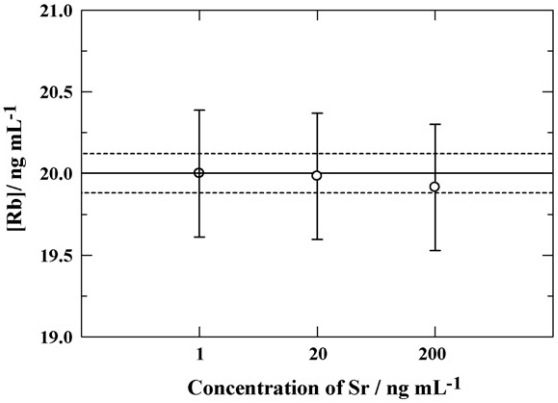

Fig. 2. Analytical results of Rb solution with different concentration of Sr (solid line: concentration calculated based on the solution preparation; dashed line: range of uncertainty; error bar: expanded uncertainty of measurement, $k = 2$).

Table 2
Analytical results of the samples ($\mu g\,g^{-1}$)

Sample	Present method[a]	Certified	ICP-MS[b]
NIES CRM 10a	4.41 ± 0.04	4.5 ± 0.3	
NIES CRM 10b	3.16 ± 0.05	3.3 ± 0.3	
NMIJ RM[c]	1.76 ± 0.03		1.75 ± 0.02

[a] Mean ± expanded uncertainty, $k = 2$.
[b] Analytical results obtained by ICP-MS with calibration method.
[c] NMIJ white rice flour candidate RM.

3.4. Analytical results of Rb solutions with various Sr concentrations

In order to confirm the effect of the present method, 20 ng mL^{-1} Rb standard solutions with 2, 20, and 200 ng mL^{-1} of Sr were determined by ID-ICP-MS after separation. The results are illustrated in Fig. 2. As is shown in Fig. 2, all the results agreed with the original concentration calculated based on the solution adjustment. Furthermore, the ratio $^{86}Sr/^{85}Rb$ in 20 ng mL^{-1} Rb standard solutions with 2, 20, and 200 ng mL^{-1} of Sr was 0.014, 0.140, and 1.402, respectively. After separation by coprecipitation, the ratio $^{86}Sr/^{85}Rb$ in all the obtained solutions decreased to less than 0.0001. These results confirmed the fact that the present coprecipitation method was effective to selectively remove Sr from the solution.

3.5. Analytical results of Rb in the samples

Two brown rice CRMs were analyzed to validate the present method. The results are summarized in Table 2, together with the certified values. All the results given in Table 2 were expressed as (mean ± expanded uncertainty ($k = 2$)), where the expanded uncertainty was estimated by spreadsheet calculation considering the standard uncertainty of each factor given in Eq. (1). It is seen in Table 2 that the analytical results of the CRMs agreed with the certified values very well, which indicate that the present method was effective for Rb measurement by ID-ICP-MS.

The present method was also applied to the measurement of Rb in white rice flour candidate RM being developed by NMIJ. It is seen in Table 2 that the analytical results obtained by the present method were coincident with that obtained by ICP-MS with calibration method.

4. Conclusion

A coprecipitation method with calcium tungstate was successfully applied to removal of Sr prior to the measurement of Rb by ID-ICP-MS. The blank could be controlled by purification of the coprecipitant reagent. The residual precipitant was effectively reduced by adding acid solutions to the sample solution. The results of CRMs indicate that the present method was effective as a candidate method for Rb measurement with ID-ICP-MS.

Besides, in order to confirm whether the coprecipitation of calcium tungstate could be used to separate other elements, a test was carried out for multielement mix solution. The results showed that coprecipitation with calcium tungstate could also effectively remove Sc, Mn, Fe, As, Y, Ba, lanthanides, Tl, Pb, and U from the solution. On the other hand, Li, Na, Mg, Al, V, Ag, and Th left in the measurement solution after precipitation of calcium tungstate. These results indicate that coprecipitation with calcium tungstate might be applied to not only the preconcentration of the former elements, but also the separation of the latter elements from the former ones. Further works using calcium tungstate coprecipitation are in progress.

Acknowledgement

This research was supported by the SME Intellectual Foundation Construction Project of the Japanese Ministry of Economy, Trade and Industry.

References

[1] B.S. Kamber, A. Greig, K.D. Collerson, Geochim. Cosmochim. Acta 69 (2005) 1041.
[2] H. Haraguchi, Bull. Chem. Soc. Jpn. 72 (1999) 1163.
[3] J.P. Goulle, L. Mahieu, J. Castermant, N. Neveu, L. Bonneau, G. Laine, D. Bouige, C. Lacroix, Forensic Sci. Int. 148 (2007) 281.
[4] J. Scancar, R. Milacic, M. Benedik, P. Bukovec, J. Pharm. Biomed. Anal. 21 (1999) 423.
[5] N. Milman, L.B. Jens, K.E. Byg, H.S. Pedersen, G. Mulvad, J. Trace Elem. Med. Biol. 20 (2006) 227.
[6] Y. Kanayama, S. Enomoto, T. Irie, R. Amano, Nucl. Med. Biol. 32 (2005) 505.
[7] H. Tamano, S. Enomoto, N. Oku, A. Takeda, Nucl. Med. Biol. 29 (2002) 505.
[8] D.B. Ward, M. Bell, Anal. Chim. Acta 229 (1990) 157.
[9] U. Ornemark, P.D.P. Taylor, P.D. Bievre, J. Anal. At. Spectrom. 12 (1997) 567.
[10] C. Belavaria, E. Andrasi, Z. Molnar, E. Bertalan, Microchem. J. 79 (2005) 367.
[11] K. Dash, S. Thangavel, S.C. Chaurasia, J. Arunachalam, Anal. Chim. Acta 584 (2007) 210.
[12] G. Gentscheva, A. Detcheva, I. Havezov, E. Ivanova, Microchim. Acta 144 (2004) 115.
[13] A. Rowland, T.B. Housh, J.A. Holcombe, J. Anal. At. Spectrom. 23 (2008) 167.
[14] P. Rodriguez-Gonzalez, J.M. Marchante-Gayon, J.I.G. Alonso, A. Sanz-Medel, Spectrochim. Acta 60B (2005) 151.
[15] K.G. Heumann, Int. J. Mass Spectrom. Ion Processes 11 (1992) 41.
[16] C.J. Park, K.H. Cho, J.K. Suh, M.S. Han, J. Anal. At. Spectrom. 15 (2000) 567.
[17] J.R. De Laeter, J.K. Bohlke, P. De Bievre, H. Hidaka, H.S. Peiser, K.J.R. Rosman, P.D.P. Taylor, Pure Appl. Chem. 75 (2003) 683.
[18] T. Waight, J. Baker, B. Willigers, Chem. Geol. 186 (2002) 99.
[19] P. Galler, A. Limbeck, S.F. Boulyga, G. Stingeder, T. Hirata, T. Prohaska, Anal. Chem. 79 (2007) 5023.
[20] C. Pin, S. Joannon, C. Bosq, B. Le Fevre, P.J. Gauthier, J. Anal. At. Spectrom. 18 (2003) 135.
[21] T. Prohaska, C. Latkoczy, G. Schultheis, M. Teschler-Nicola, G. Stingeder, J. Anal. At. Spectrom. 17 (2002) 887.
[22] L. Meynadier, C. Gorge, J.L. Birck, C. Allegre, J. Chem. Geol. 227 (2006) 26.
[23] M.V. Zoriy, D. Rashad, C. Pickhardt, H.T. Mohsen, H. Fostel, A.I. Helal, N.F. Zahran, J.S. Becker, At. Spectrosc. 24 (2004) 195.
[24] F.A. Aydin, M. Soylak, Talanta 73 (2007) 134.
[25] K. Inagaki, T. Narukawa, T. Yarita, A. Takatsu, K. Okamoto, K. Chiba, Anal. Bioanal. Chem. 389 (2007) 691.
[26] M. Tuzen, K.O. Saygi, M. Soylak, Talanta 71 (2007) 424.
[27] T. Yabutani, Y. Utsunomiya, Y. Kado, Y. Tani, H. Kishimoto, A. Fukuda, J. Motonaka, Anal. Sci. 22 (2006) 1021.
[28] S. Kagaya, Y. Araki, N. Hirai, K. Hasegawa, Talanta 67 (2005) 90.
[29] Solubility table, Wikipedia, the free encyclopedia, http://en.wikipedia.org/wiki/Solubility_table#R, March 2008.